

De-Shuang Huang
Yong Gan
Vitoantonio Bevilacqua
Juan Carlos Figueroa (Eds.)

LNCS 6838

Advanced Intelligent Computing

7th International Conference, ICIC 2011
Zhengzhou, China, August 2011
Revised Selected Papers



Springer

Commenced Publication in 1973

Founding and Former Series Editors:

Gerhard Goos, Juris Hartmanis, and Jan van Leeuwen

Editorial Board

David Hutchison

Lancaster University, UK

Takeo Kanade

Carnegie Mellon University, Pittsburgh, PA, USA

Josef Kittler

University of Surrey, Guildford, UK

Jon M. Kleinberg

Cornell University, Ithaca, NY, USA

Alfred Kobsa

University of California, Irvine, CA, USA

Friedemann Mattern

ETH Zurich, Switzerland

John C. Mitchell

Stanford University, CA, USA

Moni Naor

Weizmann Institute of Science, Rehovot, Israel

Oscar Nierstrasz

University of Bern, Switzerland

C. Pandu Rangan

Indian Institute of Technology, Madras, India

Bernhard Steffen

TU Dortmund University, Germany

Madhu Sudan

Microsoft Research, Cambridge, MA, USA

Demetri Terzopoulos

University of California, Los Angeles, CA, USA

Doug Tygar

University of California, Berkeley, CA, USA

Gerhard Weikum

Max Planck Institute for Informatics, Saarbruecken, Germany

De-Shuang Huang Yong Gan
Vitoantonio Bevilacqua
Juan Carlos Figueroa (Eds.)

Advanced Intelligent Computing

7th International Conference, ICIC 2011
Zhengzhou, China, August 11-14, 2011
Revised Selected Papers

Volume Editors

De-Shuang Huang

Tongji University, School of Electronics and Information Engineering

4800 Caoan Road, Shanghai 201804, China

E-mail: dshuang@tongji.edu.cn

Yong Gan

Zhengzhou University of Light Industry

School of Computer and Communication Engineering

No. 5, Dongfeng Road, Jinshui District, Zhengzhou Henan 450002, China

E-mail: ganyong@zzuli.edu.cn

Vitoantonio Bevilacqua

Polytechnic of Bari, Electrical and Electronics Department

Via Orabona 4, 70125 Bari, Italy

E-mail: vitoantonio.bevilacqua@gmail.com

Juan Carlos Figueroa

District University Francisco José de Caldas, Faculty of Engineering

Cra. 7a No. 40-53, Fifth Floor, Bogotá, Colombia

E-mail: jcfigueroag@udistrital.edu.co

ISSN 0302-9743

e-ISSN 1611-3349

ISBN 978-3-642-24727-9

e-ISBN 978-3-642-24728-6

DOI 10.1007/978-3-642-24728-6

Springer Heidelberg Dordrecht London New York

Library of Congress Control Number: 2011938014

CR Subject Classification (1998): I.2, I.4, I.5, F.1, H.3, H.4

LNCS Sublibrary: SL 1 – Theoretical Computer Science and General Issues

© Springer-Verlag Berlin Heidelberg 2011

This work is subject to copyright. All rights are reserved, whether the whole or part of the material is concerned, specifically the rights of translation, reprinting, re-use of illustrations, recitation, broadcasting, reproduction on microfilms or in any other way, and storage in data banks. Duplication of this publication or parts thereof is permitted only under the provisions of the German Copyright Law of September 9, 1965, in its current version, and permission for use must always be obtained from Springer. Violations are liable to prosecution under the German Copyright Law.

The use of general descriptive names, registered names, trademarks, etc. in this publication does not imply, even in the absence of a specific statement, that such names are exempt from the relevant protective laws and regulations and therefore free for general use.

Typesetting: Camera-ready by author, data conversion by Scientific Publishing Services, Chennai, India

Printed on acid-free paper

Springer is part of Springer Science+Business Media (www.springer.com)

Preface

The International Conference on Intelligent Computing (ICIC) was formed to provide an annual forum dedicated to the emerging and challenging topics in artificial intelligence, machine learning, pattern recognition, image processing, bioinformatics, and computational biology. It aims to bring together researchers and practitioners from both academia and industry to share ideas, problems, and solutions related to the multifaceted aspects of intelligent computing.

ICIC 2011, held in Zhengzhou, China, August 11-14, 2011, constituted the 7th International Conference on Intelligent Computing. It built upon the success of ICIC 2010, ICIC 2009, ICIC 2008, ICIC 2007, ICIC 2006, and ICIC 2005 that were held in Changsha, Ulsan/Korea, Shanghai, Qingdao, Kunming, and Hefei, China, respectively.

This year, the conference concentrated mainly on the theories and methodologies as well as the emerging applications of intelligent computing. Its aim was to unify the picture of contemporary intelligent computing techniques as an integral concept that highlights the trends in advanced computational intelligence and bridges theoretical research with applications. Therefore, the theme for this conference was “Advanced Intelligent Computing Technology and Applications”. Papers focusing on this theme were solicited, addressing theories, methodologies, and applications in science and technology.

ICIC 2011 received 832 submissions from 28 countries and regions. All papers went through a rigorous peer-review procedure and each paper received at least three review reports. Based on the review reports, the Program Committee finally selected 281 high-quality papers for presentation at ICIC 2011, which are included in three volumes of proceedings published by Springer: one volume of *Lecture Notes in Computer Science* (LNCS), one volume of *Lecture Notes in Artificial Intelligence* (LNAI), and one volume of *Lecture Notes in Bioinformatics* (LNBI). In addition, among them, the 10 and 44 high-quality papers have also, respectively, been recommended to *BMC Bioinformatics* and *Neurocomputing*.

This volume of *Lecture Notes in Computer Science* (LNCS) includes 94 papers.

The organizers of ICIC 2011, including Zhengzhou University of Light Industry, Institute of Intelligent Machines of Chinese Academy of Sciences, made an enormous effort to ensure the success of ICIC 2011. We hereby would like to thank the members of the Program Committee and the referees for their collective effort in reviewing and soliciting the papers. We would like to thank Alfred Hofmann, from Springer, for his frank and helpful advice and guidance throughout and for his continuous support in publishing the proceedings. In particular, we would like to thank all the authors for contributing their papers.

Without the high-quality submissions from the authors, the success of the conference would not have been possible. Finally, we are especially grateful to the IEEE Computational Intelligence Society, the International Neural Network Society, and the National Science Foundation of China for their sponsorship.

July 2011

De-Shuang Huang
Yong Gan
Vitoantonio Bevilacqua
Juan Carlos Figueroa

ICIC 2011 Organization

General Co-chairs	De-Shuang Huang, China DeLiang Wang, USA Yanli Lv, China
Program Committee Co-chairs	Zhongming Zhao, USA Kang-Hyun Jo, Korea Jianhua Ma, Japan
Organizing Committee Co-chairs	Yong Gan, China Sushi Zhang, China Hong-Qiang Wang, China Wei Jia, China
Award Committee Chair	Laurent Heutte, France
Publication Chair	Juan Carlos Figueroa, Colombia
Special Session Chair	Phalguni Gupta, India
Tutorial Chair	Vitoantonio Bevilacqua, Italy
International Liaison Chair	Prashan Premaratne, Australia
Publicity Co-chairs	Xiang Zhang, USA Kyungsook Han, Korea Lei Zhang, Hong Kong, China
Exhibition Chair	Xueling Li, China
Organizing Committee Members	Xunlin Zhu, China Shengli Song, China Haodong Zhu, China Xiaoke Su, China Xueling Li, China Jie Gui, China Zhi-Yang Chen, China
Conference Secretary	

Program Committee Members

Andrea Francesco Abate, Italy	Shih-Hsin Chen, China
Vasily Aristarkhov, Russian Federation	Wen-Sheng Chen, China
Costin Badica, Romania	Xiyuan Chen, China
Shuhui Bi, Japan	Yang Chen, China
David B. Bracewell, USA	Yuehui Chen, China
Martin Brown, UK	Ziping Chiang, China
Zhiming Cai, Macau, China	Michal Choras, Poland
Chin-chih Chang, Taiwan, China	Angelo Ciaramella, Italy
Pei-Chann Chang, China	Jose Alfredo F. Costa, Brazil
Guanling Chen, USA	Youping Deng, USA
Jack Chen, Canada	Eng. Salvatore Distefano, Italy

VIII ICIC 2011 Organization

Mariagrazia Dotoli, Italy
Meng Joo Er, Singapore
Ahmed Fadiel, USA
Karim Faez, Iran
Jianbo Fan, China
Minrui Fei, China
Wai-Keung Fung, Canada
Jun-Ying Gan, China
Liang Gao, China
Xiao-Zhi Gao, Finland
Carlos Alberto Reyes Garcia, Mexico
Dunwei Gong, China
Valeriya Gribova, Russia
M. Michael Gromiha, Japan
Kayhan Gulez, Turkey
Anyuan Guo, China
Phalguni Gupta, India
Sung Ho Ha, Korea
Fei Han, China
Kyungsook Han, Korea
Nojeong Heo, Korea
Laurent Heutte, France
Wei-Chiang Hong, Taiwan, China
Zeng-Guang Hou, China
Yuxian Hou, China
Kun Huang, USA
Peter Hung, Ireland
Sajid Hussain, USA
Peilin Jia, USA
Minghui Jiang, China
Zhenran Jiang, China
Kang-Hyun Jo, Korea
Yoshiaki Kakuda, Japan
Sanggil Kang, Korea
Muhammad Khurram Khan,
Saudi Arabia
Sungshin Kim, Korea
In-Soo Koo, Korea
Bora Kumova, Turkey
Yoshinori Kuno, Japan
Wen-Chung Kuo, Taiwan, China
Takashi Kuremoto, Japan
Vincent C.S. Lee, Australia
Guo-Zheng Li, China
Jing Li, USA
Kang Li, UK
Peihua Li, China
Ruidong Li, Japan
Shutao Li, China
Xiaoou Li, Mexico
Hualou Liang, USA
Honghuang Lin, USA
Chunmei Liu, USA
Liu Chun-Yu Liu, USA
Ju Liu, China
Van-Tsai Liu, Taiwan, China
Jinwen Ma, China
Tarik Veli Mumcu, Turkey
Igor V. Maslov, Japan
Filippo Menolascina, Italy
Primiano Di Nauta, Italy
Roman Neruda, Czech Republic
Ben Niu, China
Sim-Heng Ong, Singapore
Ali Özen, Turkey
Vincenzo Pacelli, Italy
Francesco Pappalardo, Italy
Witold Pedrycz, Canada
Caroline Petitjean, France
Pedro Melo-Pinto, Portugal
Susanna Pirttikangas, Finland
Prashan Premaratne, Australia
Daowen Qiu, China
Yuhua Qian, China
Seeja K. R., India
Marylyn Ritchie, USA
Ivan Vladimir Meza Ruiz, Mexico
Fariba Salehi, Iran
Angel Sappa, Spain
Jiatao Song, China
Stefano Squartini, Italy
Hao Tang, China
Antonio E. Uva, Italy
Jun Wan, USA
Bing Wang, USA
Ling Wang, China
Xue Wang, China
Xuesong Wang, China
Yong Wang, Japan
Yufeng Wang, Japan

Zhong Wang, USA	Xiang Zhang, USA
Wei Wei, Norway	Yanqing Zhang, USA
Zhi Wei, China	Zhaolei Zhang, Canada
Ling-Yun Wu, China	Lei Zhang, Hong Kong, China
Junfeng Xia, USA	Xing-Ming Zhao, China
Shunren Xia, China	Zhongming Zhao, USA
Hua Xu, USA	Chun-Hou Zheng, China
Jianhua Xu, China	Huiru Zheng, UK
Shao Xu, Singapore	Bo-Jin Zheng, China
Ching-Nung Yang, Taiwan, China	Fengfeng Zhou, USA
Wen Yu, Mexico	Mianlai Zhou, China
Zhi-Gang Zeng, China	Li Zhuo, China
Jun Zhang, China	

Reviewers

Ibrahim Sahin	Myriam Delgado	Song Zhu
Bora Kumova	Giuliana Rotunno	Lei Liu
Birol Soysal	Agostino Marcello	Feng Jiang
Yang Xiang	Mangini	Bo Liu
Gang Feng	Carson K. Leung	Ye Xu
Francesco Camastra	Gabriella Stecco	Gang Zhou
Antonino Staiano	Yaser Maddahai	Shengyao Wang
Alessio Ferone	Jun Wan	Yehu Shen
Surya Prakash	Jiajun Bracewell	Liya Ding
Badrinath Srinivas	Jing Huang	Hongjun Jia
Dakshina Ranjan Kisku	Kunikazu Kobayashi	Hong Fu
Zili Ying	Feng Liangbing	Tiantai Guo
Guohui He	Joaquin Torres-Sospedra	Liangxu Liu
Vincenzo Pacelli	Takashi Kuremoto	Dawen Xu
Pasqualedi Biase	Fabio Sciancalepore	Zhongjie Zhu
Federica Miglietta	Valentina Boschian	Jayasinha J.S.
Junying Zeng	Chuang Ma	Aravindan Chandrabose
Yibin Yu	Juan Xiao	Shanthi K.J.
Kaili Zhou	Lihua Jiang	Shih-Hsin Chen
Yikui Zhai	Changan Jiang	Wei-Hsiu Huang
Wen Qiang Yang	Ni Bu	Antonio Maratea
WenJu Zhou	Shengjun Wen	Sandra Venske
Dae-Nyeon Kim	Aihui Wang	Carolina Almeida
Ilmari Juutilainen	Peng Wang	Richard Goncalves
Alessandro Cincotti	Myriam Delgado	Ming Gao
Marzio Alfio Pennisi	Wei Ding	Feng Li
Carme Julià	Kurosh Zarei-nia	Yu Xue
Santo Motta	Li Zhu	Qin Ma
Nestor	Hoang-Hon Trinh	Ming Gao
Arana-Arexolaleiba	Alessia Albanese	Gang Xu

Yandong Zhang	Qiong Zhu	Jyun-Jie Lin
Benhuai Xie	Chi Zhou	Liang-Chih Yu
Ran Zhang	Qirong Mao	Richard Tzong-Han Tsai
Mingkun Li	Lingling Wang	Chin-Sheng Yang
Zhide Fang	WenYong Dong	Jheng-Long Wu
Xiaodong Yang	Wenwen Shen	Jun-Lin Lin
Lein Harn	Gang Bao	Chia-Yu Hsu
Wu-Chuan Yang	Shiping Wen	Wen-Jia Kuo
Bin Qian	Giorgio Iacobellis	Yi-Kuei Lin
Quan-ke Pan	Paolo Lino	K. Robert Lai
Junqing Li	Qi Jiang	Sumedha Gunewardena
Qiao Wei	Yan-Jie Li	Qian Xiang
Xinli Xu	Gurkan Tuna	Joe Song
Hongjun Song	Tomoyuki Ohta	Ryuzo Okada
Michael Gromiha	Jianfei Hu	Handel Cheng
Xueling Li	Xueping Yu	Chin-Huang Sun
Y.-h. Taguchi	Shinji Inoue	Tung-Chen Huang
Yu-Yen Ou	Eitaro Kohno	Bin Yang
Hong-Bin Shen	Rui-Wei Zhao	Changyan Xiao
Ximo Torres	Shixing Yan	Mingkui Tan
Weidong Yang	Jiaming Liu	Zhilgang Ling
Quanming Zhao	Wen-Chung Kuo	Lei Zhou
Chong Shen	Jukka Riekki	Hung-Chi Su
Xianfeng Rui	Jinhu Lu	Chyuan-Huei Yang
Phalguni Gupta	Qinglai Wei	Rey-Sern Lin
Yuan Xu	Michele Scarpiniti	Cheng-Hsiung Chiang
Yuefang Zhao	Simone Bassis	Chrisil Arackaparambil
Custiana Cucu	Zhilgang Liu	Valerio Bianchi
Xiaojuan Wang	Pei Wang	Zhi Xie
Guohui Zhang	Qianyu Feng	Ka-Chun Wong
Xinyu Li	Jingyi Qu	Zhou Yong
Yang Shi	Mario Foglia	Aimin Zhou
Hongcheng Liu	Michele Fiorentino	Yong Zhang
Lijun Xu	Luciano Lamberti	Yan Zhang
Xiaomin Liu	Lein Harn	Jihui Zhang
Tonghua Su	Kai Ye	Xiangjuan Yao
Junbiao Pang	Zhenyu Xuan	Jing Sun
Chun Nie	Francesco Napolitano	Jianyong Sun
Saihua Lin	Raphael Isokpehi	Yi-Nan Guo
Alfredo Pulvirenti	Vincent Agboto	Yongbin Zhang
Melo-Pinto Pedro	Ryan Delahanty	Vasily Aristarkhov
Armando Fernandes	Shaohui Liu	Hongyan Sang
Atsushi Yamashita	Ching-Jung Ting	Aboubekeur
Kazunori Onoguchi	Chuan-Kang Ting	Hamdi-Cherif
Liping Zhang	Chien-Lung Chan	Chen Bo

Min Li	Hong Wang	ZhengMao Zou
Linlin Shen	Fangmin Yao	Prashan Premaratne
Jianwei Yang	Angelo Ciaramella	Ibrahim Alishkan
Lihua Guo	Eric Hsu	Yusuf Altun
Manikandan Narayanan	Xiao-Feng Wang	Ali Ahmed Adam
Masoumeh Esfandiari	Jing Deng	Janset Dasdemir
Amin Yazdanpanah	Wanqing Zhao	Turker Turker
Ran Tao	Weihua Deng	Ibrahim Kucukdemiral
Weiming Yu	Xueqin Liu	JunSheng Zhou
Aditya Nigam	Sung Shin Kim	Yue Wang
Kamlesh Tiwari	Gyeongdong Baek	Yoshiaki Kakuda
Maria De Marsico	Seongpyo Cheon	Daqiang Zhang
Stefano R.	Bilal Khan	Min-Chih Chen
Wei Wei	Maqsood Mahmud	Aimin Zhou
Lvzhou Li	Pei-Wei Tsai	Shihong Ding
Haozhen Situ	Lin Zhang	Ziping Chiang
Bian Wu	Bo Peng	Xiaoyu Wen
Linhua Zhou	Jifeng Ning	Gao Liang
Shaojing Fan	Yongsheng Dong	Orion Reyes-Galaviz
Qingfeng Li	Chonglun Fang	Miguel Mora-Gonzalez
Rina Su	Yan Yang	Pilar Gomez-Gil
Hongjun Song	Hongyan Wang	Miguel Mora-Gonzalez
Bin Ye	Min Wang	Jida Huang
Jun Zhao	Rong-Xiang Hu	Insoo Koo
Yindi Zhao	Xiaoguang Li	Nhan Nguyen-Thanh
Kun Tan	Jing Zhang	ThucKieu Xuan
Chen Wei	Yue Jiao	Yang Zhao
Yuequan Yang	Hui Jing	Andreas Konstantinidis
Qian Zhang	Ruidong Li	Canyi Lu
Zhilgang Yan	Wei Xiong	Nobuo Funabiki
Jianhua Xu	Toshiaki Kondo	Yukikazu Nakamoto
Ju-Yin Cheng	Suresh Sundaram	Xin Zhou
Yu Gu	Hai Min	Qian Wang
Guang Zeng	Donghui Hu	Xiaoyan Yin
Xuezheng Liu	Xiaobin Tan	Juan Cui
Weirong Yuan	Stefano Dell'Attì	Francesco Polese
Ren Xinjun	Rafal Kozik	Sen Jia
Futian Yu	Michal Choras	Crescenzo Gallo
Mingjing Yang	R. Phan	Yu Sun
Chunjiang Zhang	Yuan-Fang Li	Xuewen Xia
Yinzhi Zhou	Tsung-Che Chiang	Chuan Peng
William Carswell	Ming Xia	Chen Jing-Yuan
Andrey Vavilin	Weimin Huang	Edison Yu
Sang-Hee Lee	Xinguo Yu	Petra Vidnerová
Yan Fan	Sabooth Ajaz	Klara Peskova

Martin Pilat	Guoping Lin	Wenlong Sun
Liu Zhaochen	Dun Liu	Xiaoli Wei
Jun Du	Changzhong Wang	Bing Wang
Ning Lv	Xiaoxiao Ma	Jun Zhang
Yoko Kamidoi	Xueyang Xiao	Peng Chen
Meng Wang	Wei Yu	Karim Faez
Hao Xin	Ming Yang	Xiaoyan Wang
Dingfei Ge	Francesca Nardone	Wei-Chiang Hong
Xin Gao	Kok-Leong Ong	Chien-Yuan Lai
Ivan Vladimir Meza Ruiz	David Taniar	Sugang Xu
Tsang-Yi Wang	Nali Zhu	Junfeng Xia
Sangyoon Oh	Hailei Zhang	Yi Xiong
Li Ruichang	My HaLe	Xuanfang Fei
Fan Jing	Haozhen Situ	Jingyan Wang
Lin Wang	Lvzhou Li	Zhongming Zhao
Chunlu Lai	Mianlai Zhou	Yonghui Wu
Hamide Cheraghchi	Chin-Chih Chang	Samir Abdelrahman
Wen-Tsai Sung	Carlos A. Reyes-Garcia	Mei Liu
Theanh Bui	Jack Chen	Fusheng Wang
Zhong Qishui	Wankou Yang	Shao-Lun Lee
Duyu Liu	Qijun Zhao	Wen Zhang
Keliang Jun	Jin Xie	Zhi-Ping Liu
Ying Qiu	Xian Chen	Qiang Huang
Huisen Wang	Gustavo Fontoura	Jiguang Wang
Maria Elena Valcher	Xiaoling Zhang	Rui Xue
Alex Muscar	Ondrej Kazik	Xiao Wang
SorinIlie	Bo Yan	Jibin Qu
Amelia Badica	Yun Zhu	Bojin Zheng
Guanghai Liu	B.Y. Lee	Susanna Pirttikangas
Changbin Du	Jianwen Hu	Ukasz Saganowski
Jianqing Li	Keling Chang	Chunhou Zheng
Hao Wang	Jianbo Fan	Zheng Chunho
Yurong Cheng	Chunming Tang	Mei Jun
Mingyi Wang	Hongwei Ma	Geir Solskinnsbakk
Claudio Franca	Valeria Gribova	Satu Tamminen
Jose Alfredo Ferreira Costa	Ailong Wu	Laurent Heutte
Tomasz Andrysiak	William-Chandra Tjhi	Mikko Perttunen
Ajay Kumar	Gongqing Wu	Renqiang Min
Lei Zhang	Yaohong Liang	Rong-Gui Wang
Zhoumian Wang	Bingjing Cai	Xinping Xie
Ji-Xiang Du	Lin Zhu	Horace Wang
Xibei Yang	Li Shang	Hong-Jie Yu
Junhong Wang	Bo Li	Wei Jia
Wei Wei	Jun Zhang	Huqing Wang
	Peng Chen	

Table of Contents

Neural Networks

Neural Network Ensemble Model Using PPR and LS-SVR for Stock Market Forecasting	1
<i>Lingzhi Wang and Jiansheng Wu</i>	
Stability Analysis of Neutral Systems with Distributed Delays	9
<i>Duyu Liu and Qinzhen Huang</i>	
Neural Network Model for Forecasting Balkan Stock Exchanges	17
<i>Miroslav Janeski and Slobodan Kalajdziski</i>	
A Robust Fault Detection and Isolation Scheme for Robot Manipulators Based on Neural Networks	25
<i>Mien Van, Hee-Jun Kang, and Young-Shick Ro</i>	
An Approach for High Resolution Radar Target Recognition Based on BP Neural Network	33
<i>Wei Cao, Hui Zhou, Zhimin Zhou, and Zuowei Fu</i>	

Machine Learning Theory and Methods

Hybrid Clustering Algorithm Based on the Artificial Immune Principle	40
<i>Yan Zhou and Zhifeng Hu</i>	
Succinct Initialization Methods for Clustering Algorithms	47
<i>Xueru Liang, Shangkun Ren, and Lei Yang</i>	
Variable Neighborhood Search for Drilling Operation Scheduling in PCB Industries	55
<i>Yun-Chia Liang and Chia-Yun Tien</i>	
Adaptive Weighted Fusion of Local Kernel Classifiers for Effective Pattern Classification	63
<i>Shixin Yang, Wangmeng Zuo, Lei Liu, Yanlai Li, and David Zhang</i>	
Improvement of LEACH Routing Algorithm Based on Use of Balanced Energy in Wireless Sensor Networks	71
<i>Jie Chen</i>	
Optimal Regularization Parameter Estimation for Regularized Discriminant Analysis	77
<i>Lin Zhu</i>	

Optimized Projection for Sparse Representation Based Classification ... <i>Can-Yi Lu</i>	83
Balanced-Sampling-Based Heterogeneous SVR Ensemble for Business Demand Forecasting..... <i>Yue Liu, Wang Wei, Kang Wang, Zhenjiang Liao, and Jun-jun Gao</i>	91

Fuzzy Theory and Models

CCC: Classifier Combination via Classifier <i>Can-Yi Lu</i>	100
Hybrid Reduction in Soft Set Decision Making..... <i>Ahmad Nazari Mohd Rose, Mohd Isa Awang, Hasni Hassan, Aznida Hayati Zakaria, Tutut Herawan, and Mustafa Mat Deris</i>	108

Fuzzy Systems and Soft Computing

A New Class of ε -Optimal Learning Automata..... <i>Wen Jiang</i>	116
Uncertainty Measures of Roughness Based on Interval Ordered Information Systems	122
<i>Jie Wang</i>	

Evolutionary Learning and Genetic Algorithms

A Differential Evolution Algorithm for the Extraction of Complex Natural Resonance Frequencies of Electromagnetic Targets	131
<i>Mustafa Secmen and M. Fatih Tasgetiren</i>	
A Novel Discrete League Championship Algorithm for Minimizing Earliness/Tardiness Penalties with Distinct Due Dates and Batch Delivery Consideration	139
<i>Zahra Pourali and Majid Aminnayeri</i>	

Local Meta-models for ASM-MOMA	147
<i>Martin Pilát and Roman Neruda</i>	

Swarm Intelligence and Optimization

Research on Vehicle Routing Problem with Stochastic Demand Based on Multi-objective Method	153
<i>Yanwei Zhao, Chuan Li, Jing-ling Zhang, Xingqiu Ren, and Wei Ren</i>	
A Stochastic Optimization Method for Solving the Machine-Part Cell Formation Problem	162
<i>Khoa Trinh, Jacques Ferland, and Tien Dinh</i>	

Fully Connected Multi-Objective Particle Swarm Optimizer Based on Neural Network	170
<i>Zenghui Wang and Yanxia Sun</i>	
Immune Gravitation Inspired Optimization Algorithm	178
<i>Yu Zhang, Lihua Wu, Ying Zhang, and Jianxin Wang</i>	
A Novel Multi Objective Genetic Algorithm for the Portfolio Optimization	186
<i>Vitoantonio Bevilacqua, Vincenzo Pacelli, and Stefano Saladino</i>	
Intelligent Computing in Computer Vision	
Tracking Multiple Feature in Infrared Image with Mean-Shift	194
<i>Ruiming Liu and Miao Yang</i>	
Research on Dynamic Human Object Tracking Algorithm	202
<i>Yongjian He, Qiong Wu, Shoupeng Feng, Rongkun Zhou, Yonghua Xing, and Fei Wang</i>	
Mobile Robot Navigation Using Reinforcement Learning Based on Neural Network with Short Term Memory	210
<i>Andrey V. Gavrilov and Artem Lenskiy</i>	
Histogram Based Color Object Classification by Multi-class Support Vector Machine	218
<i>Tarik Veli Mumcu, Ibrahim Aliskan, Kayhan Gulez, and Gurkan Tuna</i>	
Tracking Objects Using Orientation Covariance Matrices	226
<i>Peihua Li and Qi Sun</i>	
Action Recognition via an Improved Local Descriptor for Spatio-temporal Features	234
<i>Kai Yang, Ji-Xiang Du, and Chuan-Min Zhai</i>	
Event Recognition Based on a Local Space-Time Interest Points and Self-Organization Feature Map Method	242
<i>Yi-Lan Guo, Ji-Xiang Du, and Chuan-Min Zhai</i>	
Strategy of Statistics-Based Visualization for Segmented 3D Cardiac Volume Data Set	250
<i>Changqing Gai, Kuanquan Wang, Lei Zhang, and Wangmeng Zuo</i>	
Robust Gait Recognition Using Gait Energy Image and Band-Limited Phase-Only Correlation	257
<i>Min Wang, Wei Jia, Huanglin Zeng, and Xiao-Feng Wang</i>	

Implementation of Interactive Interview System Using Hand Gesture Recognition	264
<i>Yang Weon Lee</i>	
Integrated Real-Time Vision-Based Preceding Vehicle Detection in Urban Roads	270
<i>Yanwen Chong, Wu Chen, Zhilin Li, William H.K. Lam, and Qingquan Li</i>	
Real-Time Face Detection Using Integral Histogram of Multi-scale Local Binary Patterns	276
<i>Sébastien Paris, Hervé Glotin, and Zhong-Qiu Zhao</i>	
Study on UAV Video Reconnaissance Based Adaptively Tracking Algorithm for the Ground Moving Target	282
<i>Wen-Bo Zhao, Wei Chen, Guang-Zheng Zheng, Ke-Ming Huang, Kong-Jin Zhao, and Yu-Ge Li</i>	
Intelligent Computing in Image Processing	
Palm Print Image De-noising Based on BEMD and Wavelet Packet Transform-Wiener Filter	290
<i>Gui-Ping Dai</i>	
Pavement Crack Segmentation Algorithm Based on Local Optimal Threshold of Cracks Density Distribution	298
<i>Shengchun Wang and Wensheng Tang</i>	
Linear Pose Estimation Algorithm Based on Quaternion	303
<i>Yongjian He, Caigui Jiang, Chengwei Hu, Jingmin Xin, Qiong Wu, and Fei Wang</i>	
Image Enhancement Algorithm for Ink-on-Paper Fingerprints	311
<i>Raghav Agrawal, Badrinath Srinivas, and Phalguni Gupta</i>	
Multi-spectral Remote Sensing Images Classification Method Based on Adaptive Immune Clonal Selection Culture Algorithm	319
<i>Yi-nan Guo, Dawei Xiao, Shuguo Zhang, and Jian Cheng</i>	
Age Estimation Using Active Appearance Models and Ensemble of Classifiers with Dissimilarity-Based Classification	327
<i>Sharad Kohli, Surya Prakash, and Phalguni Gupta</i>	
Adaptive Variance Based Sharpness Computation for Low Contrast Images	335
<i>Xin Xu, Yinglin Wang, Jinshan Tang, Xiaolong Zhang, and Xiaoming Liu</i>	

Non-sampling Contourlet Based “Consistency Verification” Method of Image Fusion	342
<i>Shi-Bin Xuan, Gao-Li Sang, Bo Zhao, and Zeng-Guo Zheng</i>	
Understanding the Meaning of Shape Description for Interactive Object Recognition	350
<i>Satoshi Mori, Yoshinori Kobayashi, and Yoshinori Kuno</i>	
Gray Scale Potential Theory of Sparse Image	357
<i>Wen-Sheng Tang, Shao-Hua Jiang, and Shu-Lin Wang</i>	
Recognition of Leaf Image Based on Outline and Vein Fractal Dimension Feature	364
<i>Ji-Xiang Du, Chuan-Min Zhai, and Qing-Ping Wang</i>	
Weighted Multi Feature Based Image Retrieval with Orthogonal Polynomials Model and Genetic Algorithm	370
<i>Krishnamoorthi Ramasamy and Sathiya Devi Shanmugam</i>	
Automatic Context Analysis for Image Classification and Retrieval	377
<i>Andrey Vavilin, Kang-Hyun Jo, Moon-Ho Jeong, Jong-Eun Ha, and Dong-Joong Kang</i>	
Biometrics with Applications to Individual Security/Forensic Sciences	
Image Feature Extraction Using the Fusion Features of BEMD and WCB-NNSC	383
<i>Li Shang and Jie Chen</i>	
Palmprint Recognition with MEEMD and Statistically Independent Coefficients ICA	391
<i>Ting-Qin Yan, Shu-Fen Liu, and Chang-Xiong Zhou</i>	
A Palmprint Classification Method Based on Finite Ridgelet Transformation and SVM	398
<i>Wen-Jun Huai and Li Shang</i>	
Palmprint Recognition Based on Two-Dimensional Gabor Wavelet Transform and Two-Dimensional Principal Component Analysis	405
<i>Yu Zhang, Mei-Xing Qi, and Li Shang</i>	
Recognition Based on Fusion of Gait, Ear and Face Features Using KPCA Method	412
<i>Rohit Katiyar and Vinay Kumar Pathak</i>	
Face Recognition Using KFDA-LLE	420
<i>Guoqiang Wang and Guoqiang Ding</i>	

A Supervised Approach to Support the Analysis and the Classification of Non Verbal Humans Communications	426
--	-----

*Vitoantonio Bevilacqua, Marco Suma, Dario D'Ambruoso,
Giovanni Mandolino, Michele Caccia, Simone Tucci,
Emanuela De Tommaso, and Giuseppe Mastronardi*

Intelligent Image/Document Retrievals

A Text Classification Algorithm Based on Rocchio and Hierarchical Clustering	432
--	-----

Anping Zeng and Yongping Huang

Korean Documents Copy Detection Based on Ferret	440
---	-----

Byung Ryul Ahn, Won-gyum Kim, Won Young Yu, and Moon-Hyun Kim

Importance Weighted AdaRank	448
-----------------------------------	-----

Shangkun Ren, Yuexian Hou, Peng Zhang, and Xueru Liang

A Semantic Search Framework for Document Retrievals (Literature, Art and History) Based on Thesaurus Multiwordnet Like...	456
---	-----

*Vitoantonio Bevilacqua, Vito Santarcangelo, Alberto Magarelli,
Annalisa Bianco, Giuseppe Mastronardi, and Egidio Cascini*

Natural Language Processing and Computational Linguistics

A Novel Musical Synthesizer Embedded with Physical Modeling Sound Synthesis Algorithm	464
---	-----

Sangjin Cho, Myeongsu Kang, and Uipil Chong

Studies on the Automatic Recognition of Modern Chinese Conjunction Usages.....	472
--	-----

Hongying Zan, Lijuan Zhou, and Kunli Zhang

Implementation of High-Performance Sound Synthesis Engine for Plucked-String Instruments	480
--	-----

Myeongsu Kang, Jiwon Choi, Yongmin Kim, Cheol-Hong Kim, and Jong-Myon Kim

A Semantic Retrieval Framework for Engineering Domain Knowledge ...	488
---	-----

Xutang Zhang, Xiaofeng Chen, Xin Hou, and Ting Zhuang

Intelligent Data Fusion and Information Security

Forgeability Attack of Two Special Signature Schemes	494
--	-----

Jianhong Zhang, Yuanbo Cui, and Xi Wu

A Trojan Detector Generating Algorithm Based on Chaotic Theory	502
<i>Jie Qin, Qun Si, Huijuan Yan, and Fuliang Yan</i>	
Network Security Situation Assessment Based on Hidden Semi-Markov Model	509
<i>Boyun Zhang, Zhigang Chen, Xiai Yan, Shulin Wang, and Qiang Fan</i>	
Network Security Situation Assessment Based on Stochastic Game Model	517
<i>Boyun Zhang, Zhigang Chen, Wensheng Tang, Qiang Fan, Xiai Yan, and Shulin Wang</i>	

Intelligent Computing in Pattern Recognition

High Precision Detection of Infrared Energy Spectrum	526
<i>Xueguang Zhu</i>	
Using Heart Rate Variability Parameter-Based Feature Transformation Algorithm for Driving Stress Recognition	532
<i>Jeen-Shing Wang, Che-Wei Lin, and Ya-Ting C. Yang</i>	
An Online Self Gain Tuning Computed Torque Controller for a Five-Bar Manipulator	538
<i>Tien Dung Le, Hee-Jun Kang, and Young-Soo Suh</i>	

Intelligent Agent and Web Applications

Towards an Efficient Discovery Services in OPC Unified Architecture	544
<i>Mai Son and Myeong-Jae Yi</i>	
Asynchronous Modeling and Implementation of Web Services Based on JMS	553
<i>Jie Wang and Liang Tong</i>	

Intelligent Computing in Scheduling

An Effective Shuffled Frog Leaping Algorithm for Solving Hybrid Flow-Shop Scheduling Problem	560
<i>Ye Xu, Ling Wang, Gang Zhou, and Shengyao Wang</i>	
A Hybrid Algorithm Based on Simplex Search and Differential Evolution for Resource-Constrained Project Scheduling Problem	568
<i>Ling Wang, Ye Xu, and Chen Fang</i>	
A Differential Evolution Algorithm for Lot-Streaming Flow Shop Scheduling Problem	576
<i>Hongyan Sang, Liang Gao, and Xinyu Li</i>	

Flexible Job Shop Scheduling Problem by Chemical-Reaction Optimization Algorithm	584
<i>Junqing Li, Yuanzhen Li, Huaqing Yang, Kaizhou Gao, Yuting Wang, and Tao Sun</i>	
Discrete Harmony Search Algorithm for the No Wait Flow Shop Scheduling Problem with Makespan Criterion.....	592
<i>Kaizhou Gao, Shengxian Xie, Hua Jiang, and Junqing Li</i>	
Hybrid Differential Evolution Optimization for No-Wait Flow-Shop Scheduling with Sequence-Dependent Setup Times and Release Dates.....	600
<i>Bin Qian, Hua-Bin Zhou, Rong Hu, and Feng-Hong Xiang</i>	
An Improved Approximation Algorithm for a Class of Batch Scheduling Problems	612
<i>Jianwei Zhang, Baowei Zhang, Zengyu Cai, and Zhaoyang Li</i>	
Intelligent Control and Automation	
Exponential Stabilization for Takagi-Sugeno Fuzzy Systems with Time Delay via Impulsive Control	619
<i>Qishui Zhong and Shungang Xu</i>	
H_∞ Output Tracking Control for Neutral Delay System With Nonlinear Perturbations.....	626
<i>Cuihong Wang and Huijuan Cao</i>	
Chaotic Modeling of Time-Delay Memristive System	634
<i>Ju Jin, Yongbin Yu, Yijing Liu, Xiaorong Pu, and Xiaofeng Liao</i>	
Stability Analysis and Constrained Control of Positive Systems with Time-Varying Delays: A Linear Copositive Lyapunov-Krasovskii Functional Method	642
<i>Yulin Song</i>	
On Linear Co-Positive Lyapunov Functions for a Special of Switched Linear Positive Systems.....	650
<i>Xiuyong Ding, Lan Shu, and Changcheng Xiang</i>	
Induction Motor Speed-Regulating Control System Based on Nonlinear Kernel Ridge Regression	658
<i>Feng Wang, Jinlin Ding, and Zhifeng Hu</i>	
Parallel Robotics Control Strategy Study Based on Fuzzy-PID	664
<i>Caihong Zhu and Hongtao Zhang</i>	

Embedded Remote Controller with Two Cameras Intelligent Orientation and Bi-direction Wireless Communication	670
<i>Xueguang Zhu</i>	
Applying Answer Set Programming to Points-to Analysis of Object-Oriented Language	676
<i>Bo Yang, Mingyi Zhang, and Ying Zhang</i>	
Continuous Finite-Time Observer-Controller Based Speed Regulation of Permanent Magnet Synchronous Motors	686
<i>Yan Yan, Shuanghe Yu, Zhenqiang Yang, and Jialu Du</i>	
Observer-Based Exponential Stability Analysis for Networked Control Systems with Packet Dropout	694
<i>Xue Li, Jia-min Weng, Dajun Du, and Haoliang Bai</i>	
Modification Algorithm on Routh-Pade Model Reduction of Interval Systems	701
<i>Zhi-zhen Wang, Li Li, and Xiao-fang Wang</i>	
Author Index	705

Neural Network Ensemble Model Using PPR and LS-SVR for Stock Market Forecasting

Lingzhi Wang and Jiansheng Wu

Department of Mathematical and Computer Science, Liuzhou Teachers College
Liuzhou, Guangxi, 545004 China
{wlz1974,wjsh2002168}@163.com

Abstract. In this study, a novel Neural Network (NN) ensemble model using Projection Pursuit Regression (PPR) and Least Squares Support Vector Regression (LS-SVR) is developed for financial forecasting. In the process of ensemble modeling, the first stage some important economic factors are selected by the PPR technology as input feature for NN. In the second stage, the initial data set is divided into different training sets by used Bagging and Boosting technology. In the third stage, these training sets are input to the different individual NN models, and then various single NN predictors are produced based on diversity principle. In the fourth stage, the Partial Least Square (PLS) technology is used to choosing the appropriate number of neural network ensemble members. In the final stage, LS-SVR is used for ensemble of the NN to prediction purpose. For testing purposes, this study compare the new ensemble model's performance with some existing neural network ensemble approaches in terms of the Shanghai Stock Exchange index. Experimental results reveal that the predictions using the proposed approach are consistently better than those obtained using the other methods presented in this study in terms of the same measurements.

Keywords: Neural Network, Projection Pursuit Regression, Least Squares Support Vector Regression, Stock Market Forecasting.

1 Introduction

Stock market modeling and forecasting continues to be an important area in financial research and application. The financial market is complex, evolutionary, and non-linear dynamical system, which time series are inherently noisy and nonstationary [12]. Due to the high degrees of irregularity, dynamic manner and nonlinearity, it is extremely difficult to capture the irregularity and nonlinearity hidden in stock market by traditional linear models such as multiple regression, exponential smoothing, autoregressive integrated moving average, etc. Stock market is essential to the success of many businesses and financial institutions [34]. The main purpose of forecasting is to reduce the risk in decision making that is important for financial organizations, firm and private investors [5].

In recent years, Neural Network Ensemble (NNE), can remarkably enhance the forecasting ability and outperform any individual neural network. It is an

effective approach to the development of a high performance forecasting system [6]. The another main reason is that stock market data have tremendous noise and complex dimensionality. It make the performance of NNE become inconsistent and unpredictable. So the problems of dimensionality reduction and noise decrease are active research topics in the stock market forecasting.

Different from the previous work, this paper proposes a novel nonlinear neural network ensemble forecasting method in terms of Projection Pursuit Regression (PPR) and Least Square Support Vector Regression (LS-SVR), the PPR technology mainly aim that the high dimensional non-linear data which affects the stock market into the low dimensional space, and construct a neural network input matrix. Section 2 describes the building process of the neural network ensemble forecasting model in detail. For further illustration, this work employs the method set up a prediction model for Shanghai Stock Exchange (SSE) index in Section 3. Finally, some concluding remarks are drawn in Section 4.

2 The Building Process of the NN Ensemble Model

The scale of network is enlarged, the complexity of the model is increased because of high-dimensional data, The result can easily lead to neural network training time longer and slow convergence, which will lead to much time on the neural network training and slow in converge, and then to the reduce of the network's forecasting ability. For high-dimensional data this approach can be computationally intensive, especially if the involved covariance matrices should be estimated in a robust way. Moreover, if the sample size is lower than the dimension, additional problems with robust covariance estimation will arise. Therefore this paper is to reduce the original data of dimension by PPR under the premise of minimizing the loss of information.

2.1 Produce Input Sets Using Projection Pursuit Technology

The basic idea of PPR lies in: that the computer technology is used to project high-dimensional data into the low dimensional sub-space through some combination, and to find out the projection by minimizing the indicators, which can reflect the original data structure or characteristics, so as to achieve the goal of the study and analysis of high dimensional data [78].

Suppose $X_{n \times k}$ is the initial multivariate data set. A geometrical representation will imply that it is a set containing k data points in a N -dimensional space. $Y_{d \times k}$ is the resulting dimensionally reduced projection data. $A_{n \times d}$ is the parametric orthonormal matrix where $Y = A^T X$. The procedure of the projection pursuit is shown in Figure 1.

Projection pursuit regression model is as follows:

$$Y = f(X) = \sum_{m=1}^M G_m(a_m^T X) = \sum_{m=1}^M G_m \left[\sum_{j=1}^P a_{mj} x_j \right], \quad (1)$$

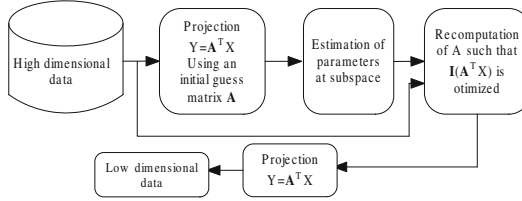


Fig. 1. A Flow Chart of Projection Pursuit Regression

where is $X \in R^P$, $a_m \in R^M$ and $M < P$, $G_m(\cdot)$ the ridge function, a_m is the direction of the projection. Projection pursuit regression model applies a least squares as the judging criteria of minimization, then the following formula becomes a very small:

$$L_2 = \min E[Y - \sum_{m=1}^M G_m[\sum_{j=1}^P a_{mj}x_j]]^2 \quad (2)$$

The simple algorithm is described as following

1. Let $m = 1$ and $Z_t^{(m)} = Y_t$.
2. Let $\sum_z^{(m)} = \frac{1}{n} \sum_{t=1}^n Z_t^{(m)} Z_t^{(m)'}$, and find V_m such that

$$V_m = \operatorname{argmax} \frac{1}{n} \sum_{t=1}^n (V_m' Z_t^{(m)})^4. \quad (3)$$

3. If $m = k$, then stop; otherwise, define $Z_t^{(m+1)} = (I - V_m V_m' \sum_{t=1}^n Z_t^m)$; that is, Z_t^{m+1} is the projection of the observations in an orthogonal direction to V_m . Let $m = m + 1$ and go to step 2.
4. Repeat the same procedure to minimize the objective function in (4), to obtain another set of k directions, namely $\{(V_t), t = 1, 2, \dots, k\}$.

A key step of the foregoing algorithm is to solve the optimization problem in (4). In this paper, we use a modified Newton method to solve the system given by the first-order optimality conditions, $\nabla \gamma_z(V) - 2\lambda \sum_z^{(m)} V = 0$ and $V' \sum_z^{(m)} V - 1 = 0$, by means of linear approximations. Readers interested in a more detailed introduction about PPR algorithm are referred to the related literature [9].

2.2 Generating Diverse Individual Ensemble

NN are one of the technologies soft computing. According to the principle of bias-variance trade-off, an neural network ensemble model consisting of diverse models with much disagreement is more likely to have a good generalization. Therefore, how to generate diverse models is a crucial factor. In this paper, there are three methods for generating diverse models.

(1) Using different training algorithms, such as the scaled conjugate gradient algorithm neural network (SCGA–NN), adaptive basis function neural network (ABF–NN), group method of data handling neural network (GMDH–NN), elman partial recurrent neural network (EPR–NN), radial basis function neural network (RBF–NN) and general regression neural network (GR–NN).

(2) Using different network architecture and starting connection weights, e.g., changing the different numbers of layers or different numbers of nodes in each layer.

(3) Training neural network with different training sets by Bagging and Boosting technology.

2.3 Selecting Appropriate Ensemble Members

After training, each individual neural predictor has generated its own result. However, if there are a great number of individual members, we need to select a subset of representatives in order to improve ensemble efficiency. In this paper, the Partial Least Square (PLS) regression technique [10] is adopted to select appropriate ensemble members. Interested readers can be referred to [10] for more details.

2.4 Least Squares Support Vector Regression

Least–Squares Support Vector Machines (LS–SVM) is a powerful nonlinear black–box regression method, which builds a linear model in the so–called feature space where the inputs have been transformed by means of a (possibly infinite dimensional) nonlinear mapping. When LS–SVM can be used for spectral regression purpose, it is called least squares support vector regression (LS–SVR). One of the advantages of LS–SVR is its ability to model nonlinear relationships [11]. In this section we will briefly discuss the LS–SVR method for a regression task. For more detailed information see [12].

Where $\{x_i, i = 1, 2, \dots, N\}$ are the output of linear and nonlinear forecasting predictors, $\{y_i, i = 1, 2, \dots, N\}$ are the aggregated output and the goal is to estimate a regression function f . Basically we define a N dimensional function space by defining the mappings $\varphi = [\varphi_1, \varphi_2, \dots, \varphi_N]^T$ according to the measured points. The LS–SVM model is of the form $f(x) = \omega^T \varphi(x) + b$ where ω is a weight vector and b is a bias term. The optimization problem is the following:

$$\begin{cases} \min J(\omega, \epsilon) = \frac{1}{2} \omega^T \omega + \gamma \frac{1}{2} \sum_{i=1}^N \epsilon_i^2 \\ s.t. \quad y_i = \omega^T \varphi(x_i) + b + \epsilon_i, i = 1, 2, \dots, N \end{cases} \quad (4)$$

where the fitting error is denoted by ϵ_i . Hyper-parameter γ controls the trade-off between the smoothness of the function and the accuracy of the fitting. This optimization problem leads to a solution by solving the linear Karush–Kuhn–Tucker (KKT) [13]:

$$\begin{bmatrix} 0 & \mathbf{I}_n^T \\ \mathbf{I}_n \mathbf{K} + \gamma^{-1} \mathbf{I} \end{bmatrix} \begin{bmatrix} b_0 \\ \mathbf{b} \end{bmatrix} = \begin{bmatrix} 0 \\ \mathbf{y} \end{bmatrix} \quad (5)$$

where \mathbf{I}_n is a $[n \times 1]$ vector of ones, \mathbf{T} means transpose of a matrix or vector, γ a weight vector, \mathbf{b} regression vector and b_0 is the model offset. \mathbf{K} is kernel function. A common choice for the kernel function is the Gaussian RBF:

$$K(x, x_i) = e^{\frac{\|x-x_i\|^2}{2\sigma^2}} \quad (6)$$

2.5 The Establishment of Ensemble Model

To summarize, the proposed NN ensemble model consists of four main steps. Generally speaking, firstly, the input factor of NN is selected by PPR from economic essential factor. Secondly, the initial data set is divided into different training sets by used Bagging and Boosting technology. Thirdly, these training sets are input to the different individual NN models, and then various single NN predictors are produced based on diversity principle. PLS model is used to select choose the appropriate number of neural network ensemble members. Finally, LS-SVR is used to aggregate the selected ensemble members. The basic flow diagram can be shown in Figure 2.

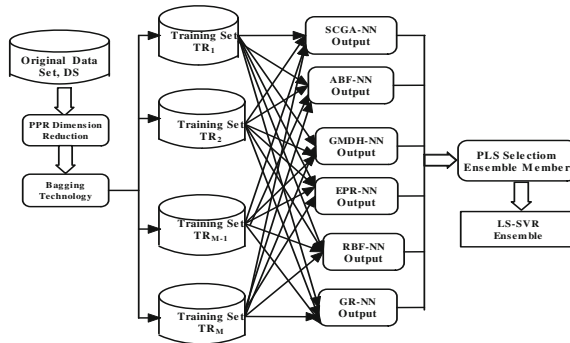


Fig. 2. A flow diagram of the proposed ensemble model

3 Experiment Study

The stock market is a complex system, influenced by various factors, such as politics, economy, society, people's life and so on, so the time series forecasting in stock market is characterized by data intensity, noise, non-stationary, unstructured nature, high degree of uncertainty, and hidden relationships. It is very difficult to extract information for forecasting model.

3.1 Data Description

In this section, the opening data-set of Shanghai Stock Exchange (SSE) is used to test the performance of the LS-SVR model. For comparison purposes, this paper is also established the Simple Regression Ensemble (SA) model. This paper take

daily opening data from February 4, 2005 to November 17, 2006. The training sample is 400 and testing sample is 30, which are used to evaluate the good or bad performance of and fitting and predictions.

In this paper, the established prediction model takes into account that the various technical indicators recorded the important act of the market, and in accordance with the conditions in China's stock market select 21 stock market technical indicators as input variables, that is, Open Price(p_1), Close Price (p_2), High Price (h_1), Low Price (h_2), Stochastic oscillator (SO), Moving stochastic oscillator (MSO), Slow stochastic oscillator (SSO), Rate of change (ROC), Momentum (M), Moving average (MA), Moving variance (MV), Moving variance ratio (MVR), Exponential moving average (EMA), Moving average convergence & divergence (MACD), Accumulation distribution oscillator (ADO), Disparity5 (D5), Disparity10 (D10), Price oscillator (OSCP), Commodity channel index (CCI), Relative strength index (RSI), Linear regression line (LRL), and makes them as variable factors which affect the stock market.

We can extract three variables used as neural network input by PPR. A triple-phase neural network ensemble model is proposed for SSE forecast, which has 3 input nodes and 3 hidden node. Training epochs are 1000. The learning rate is 0.75 and the momentum term is 0.60. The hidden nodes use sigmoid transfer function and the output node uses the linear transfer function.

3.2 Empirical Analysis

In this paper, four indicators are proposed for testing the effects of model fitting and prediction, such as, the mean average percentage error(MAPE), the root mean square error (RMSE), the trend accuracy (TC) and the correlation coefficient(CC). Details of indicators mathematical description can be seen the literature [9].

Figure 3 gives graphical representations of the fitting results for the 300 training samples using different models. Table 1 illustrates the fitting accuracy and efficiency of the model in terms of various evaluation indices for 30 training samples. Form the graphs and tables, the results show that learning ability of LS-SVR ensemble outperforms the other three models under the same network input. The more important factor to measure performance of a method is to check its forecasting ability of testing samples for actual SSE application.

Table 1 shows the fitting performance of 300 trading days and the prediction performances of 30 trading days of two models on the opening price on SSE. Figure 4 shows the forecasting results of opening price of 30 samples about the two models. From Table 1 and Figure 4, we can see that LS-SVR ensemble model is superior to SR ensemble model both in fitting and forecasting power.

Table 1 shows that the performance of training samples and testing samples of LS-SVR ensemble model are better than that of the SR model, which demonstrates that LS-SVR ensemble model has very strong learning and prediction capability, and higher prediction accuracy. It is hard to forecast the stock market in high numerical precision, however, the forecast of the trend of rising or falling is quite significant to investors F can describe the trend of the next trading day,

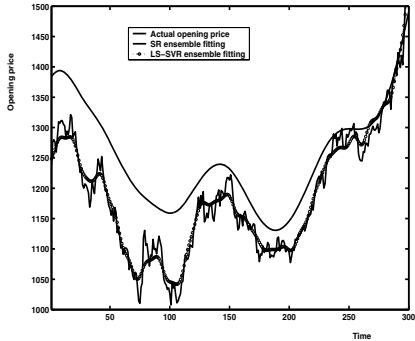


Fig. 3. The results fitting of 300 samples

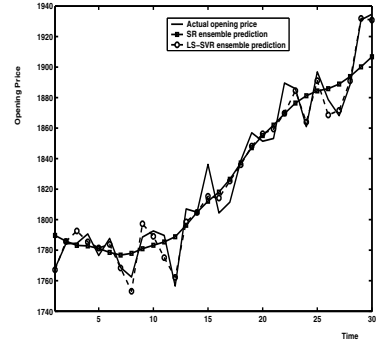


Fig. 4. The results forecasting of 30 samples

Table 1. The Evaluation of Fitting and Testing

Performance	Model	MAPE	RMSE	TC	CC
Fitting	SR ensemble	47.76%	78.33	26.67%(80)	0.4561
	LS-SLR ensemble	35.28%	26.10	66.67%(200)	0.8439
Testing	SR ensemble	79.94%	110.76	23.33%(7)	0.3420
	LS-SLR ensemble	26.71%	18.43	73.33%(22)	0.8975

we can see from Table 1 that the LS-SVR model fits correctly 200 times among the 300 trading days, with an accuracy rate of 66.67%, and predicts correctly 22 of the 30 trading days with an accuracy rate of 73.33%, and it also possesses good tracking ability of the future. While the SR ensemble model only possesses a fitting accuracy rate of 26.67%, and its prediction accuracy rate of 23.33%, which can only predict the basic trend. We can also see that from Figure 3 and Figure 4.

4 Conclusion

Accurate stock market modeling and forecasting is crucial for many businesses and financial institutions. The main purpose of forecasting is to reduce the risk in decision making that is important for financial organizations, firm and private investors. In this paper, a novel Neural Network ensemble model using Projection Pursuit Regression (PPR) and Least Squares Support Vector Regression (LS-SVR) is developed for stock market forecasting. In the process of ensemble modeling, some important economic factors are selected by the PPR technology as input feature for NN, the different individual NN models, the PLS technology is used to choosing the appropriate neural network ensemble members and LS-SVR is used for ensemble of the NN to prediction purpose. We establish the stock market prediction model and predict the SSE Index opening price, closing

price. Examples of calculation shows that the method can significantly improve the system's predictive ability, prediction accuracy, and with a high prediction accuracy of the rising and falling trend of the stock market. Empirical results obtained reveal that the proposed LS-SVR ensemble is a very promising approach to stock market forecasting.

Acknowledgment. The authors would like to express their sincere thanks to the editor and anonymous reviewer's comments and suggestions for the improvement of this paper. This work was supported by the Department of Guangxi Education under Grant No. 200707MS061.

References

1. Francis, E.H., Chao, L.J.: Modified Support Vector Machine in Financial Time Series Forecasting. *Neurocomputing* 48, 847–861 (2002)
2. Zhang, G.P., Berardi, V.L.: Time Series Forecasting with Neural Network Ensembles: an Application for Exchange Rate Prediction. *Journal of the Operational Research Society* 52, 652–664 (2001)
3. Huang, S.C., Wu, T.K.: Integrating GA-based Time-scale Feature Extractions with SVMs for Stock Index Forecasting. *Expert Systems with Applications* 35, 2080–2088 (2008)
4. Pai, P.F., Lin, C.S., Hong, W.C., Chen, C.T.: A Hybrid Support Vector Machine Regression for Exchange Rate Prediction. *International Journal of Information and Management Sciences* 17(2), 19–32 (2006)
5. Yu, L., Wang, S.Y., Lai, K.K.: A Novel Nonlinear Ensemble Forecasting Model Incorporating GLAR and ANN for Foreign Exchange Rates. *Computers & Operations Research* 32, 2523–2541 (2005)
6. Zhou, Z., Wu, J., Tang, W.: Ensembling Neural Networks: Many Could be Better Than All. *Artificial Intelligence* 137(1-2), 239–263 (2002)
7. Friedman, J.H., Tukey, J.W.: A Projection Pursuit Algorithm for Exploratory Data Analysis. *IEEE Transaction On Computers* 23(9), 881–889 (1974)
8. Wu, J., Zhou, J., Gao, Y.: Support Vector Regression Based on Particle Swarm Optimization and Projection Pursuit Technology for Rainfall Forecasting. In: Processing of 2009 International Conference on Computational Intelligence and Security, pp. 227–232 (2009)
9. Peña, D., Prieto, F.J.: Cluster Identification Using Projections. *Journal of the American Statistical Association* 96, 1425–1433 (2001)
10. Pirouz, D.M.: An Overview of Partial Least Square. Technical report, The Paul Merage School of Business, University of California, Irvine (2006)
11. Schölkopf, B., Smola, A.J.: Learning with Kernels: Support Vector Machines, Regularization, Optimization, and Beyond. The MIT Press, Cambridge (2002)
12. Suykens, J., Gestel, T.V., Brabanter, J.D.: Least Squares Support Vector Machines. The World Scientific Publishing, Singapore (2002)
13. Wang, H., Li, E., Yao, L.G.: The Least Square Support Vector Regression Coupled with Parallel Sampling Scheme Metamodeling Technique and Application in Sheet Forming Optimization. *Materials and Design* 30, 1468–1479 (2009)

Stability Analysis of Neutral Systems with Distributed Delays

Duyu Liu and Qinzheng Huang

College of Electrical and Information Engineering,

Southwest University for Nationalities

liuduyu10000@163.com

Abstract. The stability of linear neutral systems with distributed delays is studied in this paper. A new *neutral and discrete delays decomposition Lyapunov functional method* is proposed. Some stability conditions are derived. A numerical example illustrates that the stability criteria in this paper is less conservative than the existing ones. In addition, by using augmented Lyapunov functional, this method allows the coefficient matrix of the neutral term to have time-varying uncertainties.

Keywords: Lyapunov-Krasovskii functional, Neutral system, Stability Uncertainty, time-varying.

1 Introduction

Many practical processes can be modeled as general neutral systems, which contain delays in both its states and the derivatives of its states. During the past several years, the stability of neutral systems has received considerable attention, and many results have been developed (see [2–5, 7–12, 14, 15]). As an efficient tool, the Lyapunov-Krasovskii method is widely used (see [6]), and the stability criteria are often expressed in terms of linear matrix inequalities(LMIs)(see [1]).

To decrease conservatism of the conditions, the idea of discretized Lyapunov approach was applied to study neutral systems which led to much better stability criteria. Firstly, [12] applied the idea to investigate the stability of the systems and obtained discrete-delay-dependent stability criteria. Furthermore, [15] proposed a new discretized Lyapunov functional method and obtained both discrete- and neutral-delay-dependent stability criteria which are much less conservative than that in [12]. However, the discretized Lyapunov approach is complicated. Recently, [13] proposed a new delay decompositon approach to check the stability of neutral systems which was very simple, and obtained some less conservative result. However, both the discretized Lyapunov approach and the delay decomposition approach were only applied to the neutral systems with mixed delays.

Neutral systems with distributed delays are of importance both in practice and in theory. Much research has been done in the stability of the neutral systems. Recently, in [3] and [11], a descriptor system approach was used to investigate the stability of the neutral system. To reduce the conservatism of the stability conditions, in [14], free weighting matrices were employed, furthermore, a

new modified Lyapunov-Krasovskii functional was constructed. Stability criterion discrete-, distributed- and neutral-delay-dependent was proposed in [14]. To the best of our knowledge, the stability criterion in [14] is the least conservative among the existing ones.

The aim of this paper is to further reduce the conservatism of the stability conditions for the linear neutral system with distributed delays. To this end, the approach of delay decomposition is applied. The reduced conservatism is illustrated in a numerical example.

2 Problem Statement

Consider the following neutral system with discrete and distributed delays:

$$\begin{cases} \dot{x}(t) - C(t)\dot{x}(t-\tau) = A(t)x(t) + B(t)x(t-h) + D(t)\int_{t-r}^t x(s)ds, \\ x(t_0+\theta) = \phi(\theta), \forall\theta \in [-\max\{\tau, h, r\}, 0]. \end{cases} \quad (1)$$

where $x(t) \in \mathbb{R}^n$ is the state vector, the time delays $\tau > 0$, $h > 0$ and $r > 0$ are assumed to be known, the $\phi(t)$ is the initial condition, $A(t)$, $B(t)$, $C(t)$ and $D(t)$ are matrix functions with time-varying uncertainties, that is,

$$\begin{aligned} A(t) &= A + \Delta A(t), \quad B(t) = B + \Delta B(t), \\ C(t) &= C + \Delta C(t), \quad D(t) = D + \Delta D(t). \end{aligned}$$

where A, B, C, D are known real constant matrices, and $\Delta A(t)$, $\Delta B(t)$, $\Delta C(t)$, $\Delta D(t)$ are unknown matrices, which be described as

$$[\Delta A(t) \ \Delta B(t) \ \Delta C(t) \ \Delta D(t)] = LF(t) [E_a \ E_b \ E_c \ E_d],$$

where L , E_a , E_b , E_c , E_d are known real constant matrices, and $F(t)$ satisfies $\|F(t)\| \leq 1$ for any given t . Assume that the matrix $C(t)$ is Schur stable.

3 Main Results

In this section, we employ both the *delays bi-decomposition approach* and the *delays N-decomposition approach* to derive some new and less conservative stability criteria. We begin with the *discrete and neutral delays bi-composition approach*.

3.1 Stability Analysis for the System without Uncertainties

First, consider the nominal system of (1), that is the system

$$\begin{cases} \dot{x}(t) - C\dot{x}(t-\tau) = Ax(t) + Bx(t-h) + D\int_{t-r}^t x(s)ds, \\ x(t_0+\theta) = \phi(\theta), \forall\theta \in [-\max\{\tau, h, r\}, 0]. \end{cases} \quad (2)$$

For the stability of system (2), we have the following result.

Theorem 1. For given scalars $\tau, h, r > 0$, the neutral system (2) is asymptotically stable, if there exist symmetric matrices $P_{11}, P_{22}, P_{33}, P_{44}, L_\tau, L_h$, positive definition matrices $Q_\tau, Q_h, Q_r, R_\tau, R_h, R_r, W_\tau, W_h, U$, and any matrices

$P_{12}, P_{13}, P_{14}, P_{23}, P_{24}, P_{34}, S_{i,j}^{\tau}, S_{i,j}^h (i, j = 1, 2), M_i (i = 1, \dots, 10.)$ satisfying the following LMIs

$$\begin{pmatrix} P_{11} + \frac{L\tau}{\tau} + \frac{L_h}{h} P_{12} - \frac{L\tau}{\tau} P_{13} - \frac{L_h}{h} P_{14} \\ * & P_{22} + \frac{L\tau}{\tau} P_{23} & P_{24} \\ * & * & P_{33} + \frac{L_h}{h} P_{34} \\ * & * & * & P_{44} \end{pmatrix} > 0, \quad (3)$$

$$S_{\tau} = S_{\tau}^T = \begin{pmatrix} S_{1,1}^{\tau} & S_{1,2}^{\tau} \\ * & S_{2,2}^{\tau} \end{pmatrix} > 0, \quad (4)$$

$$S_h = S_h^T = \begin{pmatrix} S_{1,1}^h & S_{1,2}^h \\ * & S_{2,2}^h \end{pmatrix} > 0, \quad (5)$$

$$\Omega = \begin{pmatrix} \Omega_{1,1} & \Omega_{1,2} & \Omega_{1,3} & \Omega_{1,4} & \Omega_{1,5} & \Omega_{1,6} & \Omega_{1,7} & \Omega_{1,8} & \Omega_{1,9} & \Omega_{1,10} \\ * & \Omega_{2,2} & \Omega_{2,3} & \Omega_{2,4} & \Omega_{2,5} & \Omega_{2,6} & \Omega_{2,7} & \Omega_{2,8} & \Omega_{2,9} & 0 \\ * & * & \Omega_{3,3} & \Omega_{3,4} & \Omega_{3,5} & \Omega_{3,6} & \Omega_{3,7} & \Omega_{3,8} & \Omega_{3,9} & \Omega_{3,10} \\ * & * & * & \Omega_{4,4} & \Omega_{4,5} & \Omega_{4,6} & \Omega_{4,7} & \Omega_{4,8} & 0 & 0 \\ * & * & * & * & \Omega_{5,5} & \Omega_{5,6} & \Omega_{5,7} & \Omega_{5,8} & \Omega_{5,9} & \Omega_{5,10} \\ * & * & * & * & * & \Omega_{6,6} & \Omega_{6,7} & \Omega_{6,8} & \Omega_{6,9} & \Omega_{6,10} \\ * & * & * & * & * & * & \Omega_{7,7} & 0 & 0 & 0 \\ * & * & * & * & * & * & * & \Omega_{8,8} & 0 & 0 \\ * & * & * & * & * & * & * & * & \Omega_{9,9} & 0 \\ * & * & * & * & * & * & * & * & * & \Omega_{10,10} \end{pmatrix} < 0, \quad (6)$$

where

$$\begin{aligned} \Omega_{1,1} &= P_{14} + P_{14}^T + Q_{\tau} + Q_h + Q_r - \frac{R_{\tau}}{\tau} - \frac{R_h}{h} - \frac{R_r}{r} + S_{1,1}^{\tau} + S_{1,1}^h \\ &\quad - \frac{2W_{\tau}}{h} - \frac{2W_h}{h} + A^T M_1^T + M_1 A + rU, \\ \Omega_{1,2} &= P_{24}^T + \frac{R_{\tau}}{\tau} + A^T M_2^T, \quad \Omega_{1,3} = P_{34}^T + \frac{R_h}{h} + A^T M_3^T + M_1 B, \\ \Omega_{1,4} &= P_{44} + A^T M_4^T + M_1 D, \quad \Omega_{1,5} = P_{11} - M_1 + A^T M_5^T, \\ \Omega_{1,6} &= P_{12} + M_1 C + A^T M_6^T, \quad \Omega_{1,7} = P_{13} + A^T M_7^T, \\ \Omega_{1,8} &= -P_{14} + \frac{R_r}{r} + A^T M_8^T, \quad \Omega_{1,9} = S_{1,2}^{\tau} + \frac{2W_{\tau}}{\tau} + A^T M_9^T, \\ \Omega_{1,10} &= S_{1,2}^h + \frac{2W_h}{h} + A^T M_{10}^T, \quad \Omega_{2,2} = -Q_{\tau} - \frac{R_{\tau}}{\tau} - S_{2,2}^{\tau}, \\ \Omega_{2,3} &= M_2 B, \quad \Omega_{2,4} = M_2 D, \quad \Omega_{2,5} = P_{12}^T - M_2, \\ \Omega_{2,6} &= P_{22} + M_2 C, \quad \Omega_{2,7} = P_{23}, \quad \Omega_{2,8} = -P_{24}, \\ \Omega_{2,9} &= (-S_{1,2}^{\tau})^T, \quad \Omega_{3,3} = -\frac{R_h}{h} - S_{2,2}^h - Q_h + M_3 B + B^T M_3^T, \\ \Omega_{3,4} &= M_3 D + B^T M_4^T, \quad \Omega_{3,5} = P_{13}^T - M_3 + B^T M_5^T, \\ \Omega_{3,6} &= P_{23}^T + M_3 C + B^T M_6^T, \quad \Omega_{3,7} = P_{33} + B^T M_7^T, \\ \Omega_{3,8} &= -P_{34} + B^T M_8^T, \quad \Omega_{3,9} = B^T M_9^T, \quad \Omega_{3,10} = (-S_{1,2}^h)^T + B^T M_{10}^T, \\ \Omega_{4,4} &= -\frac{U}{r} + M_4 D + D^T M_4^T, \quad \Omega_{4,5} = P_{14}^T - M_4 + D^T M_5^T, \\ \Omega_{4,6} &= P_{24}^T + M_4 C, \quad \Omega_{4,7} = P_{34}^T, \quad \Omega_{4,8} = -P_{44}, \\ \Omega_{5,5} &= hR_h + \tau R_{\tau} + rR_r + \frac{\tau}{2}W_{\tau} + \frac{h}{2}W_h + L_{\tau} + L_h - M_5 - M_5^T, \\ \Omega_{5,6} &= M_5 C + M_6^T, \quad \Omega_{5,7} = -M_7^T, \quad \Omega_{5,8} = -M_8^T, \quad \Omega_{5,9} = -M_9^T, \\ \Omega_{5,10} &= -M_{10}^T, \quad \Omega_{6,6} = -L_{\tau} + M_6 C + C^T M_6^T, \quad \Omega_{6,7} = C^T M_7^T, \\ \Omega_{6,8} &= C^T M_8^T, \quad \Omega_{6,9} = C^T M_9^T, \quad \Omega_{6,10} = C^T M_{10}^T, \quad \Omega_{7,7} = -L_h, \\ \Omega_{8,8} &= -\frac{R_r}{r} - Q_r, \quad \Omega_{9,9} = S_{2,2}^{\tau} - S_{1,1}^{\tau} - \frac{2}{\tau}W_{\tau}, \quad \Omega_{10,10} = S_{2,2}^h - S_{1,1}^h - \frac{2}{h}W_h. \end{aligned}$$

Proof. Construct a Lyapunov-Krasovskii functional candidate as

$$V = V_1 + V_h + V_\tau + V_r, \quad (7)$$

where

$$\begin{aligned} V_1 &= \xi^T(t)P\xi(t), \quad \xi^T(t) = \left[x^T(t) \ x^T(t-\tau) \ x^T(t-h) \ \int_{t-r}^t x^T(s)ds \right], \\ P &= \begin{pmatrix} P_{11} & P_{12} & P_{13} & P_{14} \\ * & P_{22} & P_{23} & P_{24} \\ * & * & P_{33} & P_{34} \\ * & * & * & P_{44} \end{pmatrix}, \\ V_r &= \int_{t-r}^t x^T(s)Q_r x(s)ds + \int_{t-r}^0 \int_{t+\theta}^t x^T(s)Ux(s)ds \\ &\quad + \int_{t-r}^t (r-t+s)\dot{x}^T(s)R_r\dot{x}(s)ds, \\ V_h &= \int_{t-h}^t x^T(s)Q_h x(s)ds + \int_{t-\frac{h}{2}}^t y^T(s)S_h y(s)ds + \int_{t-h}^t \dot{x}^T(s)L_h\dot{x}(s)ds \\ &\quad + \int_{t-\frac{h}{2}}^t (\frac{h}{2}-t+s)\dot{x}^T(s)W_h\dot{x}(s)ds + \int_{t-h}^t (h-t+s)\dot{x}^T(s)R_h\dot{x}(s)ds, \\ V_\tau &= \int_{t-\tau}^t x^T(s)Q_\tau x(s)ds + \int_{t-\frac{\tau}{2}}^t z^T(s)S_\tau z(s)ds + \int_{t-h}^t \dot{x}^T(s)L_h\dot{x}(s)ds \\ &\quad + \int_{t-\frac{\tau}{2}}^t (\frac{\tau}{2}-t+s)\dot{x}^T(s)W_\tau\dot{x}(s)ds + \int_{t-\tau}^t (\tau-t+s)\dot{x}^T(s)R_\tau\dot{x}(s)ds, \\ y^T(s) &= [x^T(s) \ x^T(s-\frac{h}{2})], \quad z^T(s) = [x^T(s) \ x^T(s-\frac{\tau}{2})]. \end{aligned}$$

The time derivative of V along the trajectory of system (2) is given by

$$\dot{V} = \dot{V}_1 + \dot{V}_h + \dot{V}_\tau + \dot{V}_r + \gamma. \quad (8)$$

where

$$\begin{aligned} \gamma &= 2\zeta^T M \left(Ax(t) + Bx(t-h) + D \int_{t-r}^t x(s)ds - \dot{x}(t) + C\dot{x}(t-\tau) \right) = 0, \\ M^T &= [M_1^T \ M_2^T \ M_3^T \ M_4^T \ M_5^T \ M_6^T \ M_7^T \ M_8^T \ M_9^T \ M_{10}^T], \\ \zeta^T &= \begin{bmatrix} x^T(t) & x^T(t-\tau) & x^T(t-h) & \int_{t-r}^t x^T(s)ds & \dot{x}^T(t) \\ \dot{x}^T(t-\tau) & \dot{x}^T(t-h) & \dot{x}^T(t-r) & x^T(t-\frac{\tau}{2}) & x^T(t-\frac{h}{2}) \end{bmatrix}. \end{aligned}$$

When the LMI (6) is satisfied, we have $\dot{V} < 0$.

On the other hand, we have

$$\begin{aligned} V(x_t) &\geq \xi^T(t)\tilde{P}\xi(t) + V_r + \int_{t-h}^t x^T(s)Q_h x(s)ds \int_{t-\frac{h}{2}}^t y^T(s)S_h y(s)ds \\ &\quad + \int_{t-h}^t (h-t+s)\dot{x}^T(s)R_h\dot{x}(s)ds + \int_{t-\frac{h}{2}}^t (\frac{h}{2}-t+s)\dot{x}^T(s)W_h\dot{x}(s)ds \\ &\quad + \int_{t-\tau}^t x^T(s)Q_\tau x(s)ds + \int_{t-\frac{\tau}{2}}^t z^T(s)S_\tau z(s)ds \\ &\quad + \int_{t-\tau}^t (\tau-t+s)\dot{x}^T(s)R_\tau\dot{x}(s)ds + \int_{t-\frac{\tau}{2}}^t (\frac{\tau}{2}-t+s)\dot{x}^T(s)W_\tau\dot{x}(s)ds, \end{aligned} \quad (9)$$

where

$$\tilde{P} = \begin{pmatrix} P_{11} + \frac{L_\tau}{\tau} + \frac{L_h}{h} & P_{12} - \frac{L_\tau}{\tau} & P_{13} - \frac{L_h}{h} & P_{14} \\ * & P_{22} + \frac{L_\tau}{\tau} & P_{23} & P_{24} \\ * & * & P_{33} + \frac{L_h}{h} & P_{34} \\ * & * & * & P_{44} \end{pmatrix}.$$

The resulting inequalities are just the LMIs in (3)-(6). The proof is thus complete.

Next, we'll apply the approach of N-decomposition with N a given positive integer to derive more general result. Choose the following Lyapunov-Krasovskii functional for system (2)

$$V(x_t) = V_1 + V_r + \tilde{V}_h + \tilde{V}_\tau, \quad (10)$$

where

$$\begin{aligned}\tilde{V}_h &= \int_{t-h}^t x^T(s) Q_h x(s) ds + \int_{t-\frac{h}{N}}^t \tilde{y}^T(s) S_h \tilde{y}(s) ds + \int_{t-h}^t \dot{x}^T(s) L_h \dot{x}(s) ds \\ &\quad + \int_{t-h}^t (h-t+s) \dot{x}^T(s) R_h \dot{x}(s) ds + \int_{t-\frac{h}{N}}^t (\frac{h}{N}-t+s) \dot{x}^T(s) \dot{x}(s) ds, \\ \tilde{V}_\tau &= \int_{t-\tau}^t x^T(s) Q_\tau x(s) ds + \int_{t-\frac{\tau}{N}}^t \tilde{z}^T(s) S_\tau \tilde{z}(s) ds + \int_{t-\tau}^t \dot{x}^T(s) L_h \dot{x}(s) ds \\ &\quad + \int_{t-\tau}^t (\tau-t+s) \dot{x}^T(s) R_\tau \dot{x}(s) ds + \int_{t-\frac{\tau}{N}}^t (\frac{\tau}{N}-t+s) \dot{x}^T(s) W_\tau \dot{x}(s) ds, \\ \tilde{y}^T(\theta) &= \left(x^T(\theta) \ x^T(\theta - \frac{h}{N}) \cdots \ x^T(\theta - \frac{(N-1)h}{N}) \right), \\ \tilde{z}^T(\theta) &= \left(x^T(\theta) \ x^T(\theta - \frac{\tau}{N}) \cdots \ x^T(\theta - \frac{(N-1)\tau}{N}) \right).\end{aligned}$$

Similar to Theorem 1, we can obtain the following stability criterion.

Theorem 2. For given scalars $\tau, h, r > 0$, the neutral system (2) is asymptotically stable, if there exist symmetric matrices $P_{11}, P_{22}, P_{33}, P_{44}, L_\tau, L_h$, positive definition matrices $Q_\tau, Q_h, Q_r, R_\tau, R_h, R_r, W_h, W_\tau, U$, and any matrices $P_{12}, P_{13}, P_{14}, P_{23}, P_{24}, P_{34}, S_{i,j}^h, S_{i,j}^\tau (i < j; i = 1, 2, \dots, N-1; j = 2, \dots, N)$, $M_i (i = 1, \dots, 6 + 2N)$ satisfying (3) and the LMIs:

$$S_h = S_h^T = \begin{pmatrix} S_{1,1}^h & S_{1,2}^h & \cdots & S_{1,N}^h \\ * & S_{2,2}^h & \cdots & S_{2,N}^h \\ \vdots & \vdots & \ddots & \vdots \\ * & * & \cdots & S_{N,N}^h \end{pmatrix} \geq 0, \quad (11)$$

$$S_\tau = S_\tau^T = \begin{pmatrix} S_{1,1}^\tau & S_{1,2}^\tau & \cdots & S_{1,N}^\tau \\ * & S_{2,2}^\tau & \cdots & S_{2,N}^\tau \\ \vdots & \vdots & \ddots & \vdots \\ * & * & \cdots & S_{N,N}^\tau \end{pmatrix} \geq 0, \quad (12)$$

$$\Psi = \begin{pmatrix} \Psi_{11} & \Psi_{12} \\ * & \Psi_{22} \end{pmatrix} < 0, \quad (13)$$

where

$$\Psi_{12} = \begin{bmatrix} (1, 11) & (1, 12) & \cdots & (1, 2N+5) & (1, 2N+6) \\ (2, 11) & 0 & \cdots & (2, 2N+5) & 0 \\ (3, 11) & (3, 12) & \cdots & (3, 2N+5) & (3, 2N+6) \\ 0 & 0 & \cdots & 0 & 0 \\ (5, 11) & (5, 12) & \cdots & (5, 2N+5) & (5, 2N+6) \\ (6, 11) & (6, 12) & \cdots & (6, 2N+5) & (6, 2N+6) \\ 0 & 0 & \cdots & 0 & 0 \\ 0 & 0 & \cdots & 0 & 0 \\ (9, 11) & 0 & \cdots & (9, 2N+5) & 0 \\ 0 & (10, 12) & \cdots & 0 & (10, 2N+6) \end{bmatrix},$$

$$\Psi_{22} = \begin{bmatrix} (11, 11) & 0 & \cdots & 0 & 0 \\ * & (12, 12) & \cdots & 0 & 0 \\ \vdots & \vdots & \ddots & \vdots & \vdots \\ * & * & \cdots & (2N+5, 2N+5) & 0 \\ * & * & \cdots & * & (2N+6, 2N+6) \end{bmatrix},$$

where

$$\begin{aligned}
(1, 1) &= P_{14} + P_{14}^T + Q_\tau + Q_h + Q_r - \frac{R_\tau}{\tau} - \frac{R_h}{h} - \frac{R_r}{r} + S_{1,1}^\tau + S_{1,1}^h \\
&\quad - \frac{NW_\tau}{\tau} - \frac{NW_h}{h} + A^T M_1^T + M_1 A + rU, \\
(1, 9) &= S_{1,2}^\tau + \frac{NW_\tau}{\tau} + A^T M_9^T, \quad (1, 10) = S_{1,2}^h + \frac{NW_h}{h} + A^T M_{10}^T, \\
(1, 11) &= S_{1,3}^\tau - A^T M_{11}^T, \quad (1, 12) = S_{1,3}^h - A^T M_{12}^T, \\
(1, 2N+5) &= S_{1,N}^\tau - A^T M_{2N+5}^T, \quad (1, 2N+6) = S_{1,N}^h - A^T M_{2N+6}^T, \\
(2, 11) &= (-S_{2,N}^\tau)^T, \quad (2, 2N+5) = (-S_{N-1,N}^\tau)^T, \quad (3, 11) = B^T M_{11}^T, \\
(3, 12) &= (-S_{2,N}^h)^T + B^T M_{12}^T, \quad (3, 2N+5) = B^T M_{2N+5}^T, \\
(3, 2N+6) &= (-S_{N-1,N}^h)^T + B^T M_{2N+6}^T, \\
(5, 5) &= hR_h + \tau R_\tau + rR_r + \frac{\tau}{N}W_\tau + \frac{h}{N}W_h + L_\tau + L_h - M_5 - M_5^T, \\
(5, 11) &= -M_{11}^T, \quad (5, 12) = -M_{12}^T, \quad (5, 2N+5) = -M_{2N+5}^T, \\
(5, 2N+6) &= -M_{2N+6}^T, \quad (6, 11) = C^T M_{11}^T, \quad (6, 12) = C^T M_{12}^T, \\
(6, 2N+5) &= C^T M_{2N+5}^T, \quad (6, 2N+6) = C^T M_{2N+6}^T, \\
(9, 9) &= S_{2,2}^\tau - S_{1,1}^\tau - \frac{N}{\tau}W_\tau, \quad (9, 11) = S_{2,3}^\tau - S_{1,2}^\tau, \\
(9, 2N+5) &= S_{2,N}^\tau - S_{1,N-1}^\tau, \quad (10, 10) = S_{2,2}^h - S_{1,1}^h - \frac{N}{h}W_h, \\
(10, 12) &= S_{2,3}^h - S_{1,2}^h, \quad (10, 2N+6) = S_{2,N}^h - S_{1,N-1}^h, \\
(11, 11) &= S_{3,3}^\tau - S_{2,2}^\tau, \quad (12, 12) = S_{3,3}^h - S_{2,2}^h, \\
(2N+5, 2N+5) &= S_{N,N}^\tau - S_{N-1,N-1}^\tau, \quad (2N+6, 2N+6) = S_{N,N}^h - S_{N-1,N-1}^h.
\end{aligned}$$

3.2 Stability Analysis for the Uncertain System

In the following, we will give the robust stability condition of system (1).

Corollary 1. *For given scalars $\tau, h, r > 0$, the neutral system (2) is asymptotically stable, if there exist symmetric matrices $P_{11}, P_{22}, P_{33}, P_{44}, L_\tau, L_h$, positive definition matrices $Q_\tau, Q_h, Q_r, R_\tau, R_h, R_r, W_h, W_\tau, U$, any matrices $P_{12}, P_{13}, P_{14}, P_{23}, P_{24}, P_{34}, S_{i,j}^h, S_{i,j}^\tau (i < j; i = 1, 2, \dots, N-1; j = 2, \dots, N)$, $M_i (i = 1, \dots, 6+2N)$ and a scalar ε satisfying (3), (11), (12) and the following LMI:*

$$\begin{bmatrix} \Psi' & ML \\ * & -\varepsilon I \end{bmatrix} < 0, \quad (14)$$

where

$$\Psi' = \Psi + \varepsilon \begin{bmatrix} E_A^T E_A & 0 & E_A^T E_B & E_A^T E_D & 0 & E_A^T E_C & 0 & \cdots & 0 \\ * & 0 & 0 & 0 & 0 & 0 & 0 & \cdots & 0 \\ * & * & E_B^T E_B & E_B^T E_D & 0 & E_B^T E_C & 0 & \cdots & 0 \\ * & * & * & E_D^T E_D & 0 & E_D^T E_C & 0 & \cdots & 0 \\ * & * & * & * & 0 & 0 & 0 & \cdots & 0 \\ * & * & * & * & * & E_C^T E_C & 0 & \cdots & 0 \\ * & * & * & * & * & * & 0 & \cdots & 0 \\ \vdots & \ddots & 0 \\ * & * & * & * & * & * & * & \cdots & 0 \end{bmatrix}.$$

4 Numerical Example

In this section, we present a numerical example to illustrate the effectiveness and advantage of the proposed method. Consider system (II) with

$$A = \begin{bmatrix} -0.9 & 0.2 \\ 0.1 & -0.9 \end{bmatrix}, \quad B = \begin{bmatrix} -1.1 & -0.2 \\ -0.1 & -1.1 \end{bmatrix}, \quad C = \begin{bmatrix} -0.2 & 0 \\ 0.2 & -0.1 \end{bmatrix}, \quad D = \begin{bmatrix} -0.12 & -0.12 \\ -0.12 & -0.12 \end{bmatrix},$$

$$L = I, \quad E_A = E_B = E_C = E_D = 0.1I, \quad \tau = 0.1.$$

Let $N = 2$. When $r = 0.1$, the upper bounds of h that guarantee the stability of system computed by the methods in [3], [11] and [14] are 1.1, 1.2 and 1.3, respectively. By Theorem 3 in this paper, the upper bound of h is obtained as 1.9. When $h = 0.1$, the upper bounds of r that guarantee the stability of system (II) calculated by the methods [3], [11] and [14] are 6.2, 6.4 and 6.6, respectively. By our method, the upper bound of r is greater than 100. When taking $\tau = 1, h = 1$, by our method, the upper bound of r is obtained as 6.5. One can see that our method is less conservative than the previous ones. Applying

Table 1. the upper bound of h_{max} for different $N \geq 2$

N	2	3	4	5
h_{max}	1.9	2.3	2.6	2.9

Corollary 1, setting $r = 0.1$, we calculate the upper bounds of h for different N and list the results in Table 1.

5 Conclusions

The problem of the stability for linear neutral system with distributed delays has been investigated. A new *delays decomposition Lyapunov functional method* has been proposed for study the stability problem. First, we have employ the *neutral and discrete delays bi-decomposition Lyapunov functional method* and

neutral and discrete delays N-decomposition Lyapunov functional method to derive stability criteria for the neutral systems without uncertainties; second, we obtain the robust stability criteria for the neutral systems with time-varying uncertainties. A numerical example is given to show that our method is less than the existing ones.

Acknowledgements. This work was partially supported by National Nature Science Foundation under Grant No. 60974148, the Program for New Century Excellent Talents in University under Grant No. NCET-10-0097, and Sichuan Youth Science and Technology Fund under Grant No. 2011JQ0011.

References

1. Boyd, S., El Ghaoui, L., Feron, E., Balakrishnan, V.: Linear Matrix Inequalities in System and Control Theory. SIAM, Philadelphia (1994)
2. Chen, J.D., Lien, C.H., Fan, K.K., Chou, J.H.: Criteria for Asymptotic Stability of a Class of Neutral Systems via a LMI Approach. In: IEE Proceedings Control Theory and Applications, vol. 148, pp. 227–442 (2001)
3. Chen, W.H., Zheng, W.X.: Delay-dependent Robust Stabilization for Uncertain Neutral Systems with Distributed Delays. Automatica 43, 95–104 (2007)
4. Fridman, E.: New Lyapunov CKrasovskii Functionals for Stability of Linear Retarded and Neutral Type Systems. Systems and Control Letters 43, 309–319 (2001)
5. Fridman, E., Shaked, U.: A Descriptor System Approach to H Control of Linear Time-delay Systems. IEEE Transactions on Automatic Control 47, 253–270 (2002)
6. Gu, K., Kharitonov, V.L., Chen, J.: Stability of Time-delay Systems. Birkhäuser, Boston (2003)
7. Han, Q.L.: On Delay-dependent Stability for Neutral Delaydifferential Systems. International Journal of Applied Mathematics and Computer Science 11, 965–976 (2001)
8. Han, Q.L.: Robust Stability of Uncertain Delay-differential Systems of Neutral Type. Automatica 38, 719–723 (2002)
9. Han, Q.L.: Stability Criteria for a Class of Linear Neutral Systems with Time-varying Discrete and Distributed Delays. IMA Journal of Mathematical Control and Information 20, 371–386 (2003)
10. Han, Q.L., Yu, L.: Robust Stability of Linear Systems with Nonlinear Parameter Perturbations. In: IEE Proceedings Control Theory and Applications, vol. 151, pp. 539–546 (2004)
11. Han, Q.L.: A Descriptor System Approach to Robust Stability of Uncertain Neutral Systems with Discrete and Distributed Delays. Automatica 40, 1791–1796 (2004)
12. Han, Q.L.: On Stability of Linear Neutral Systems with Mixed Time Delays: A Discretized Lyapunov Functional Approach. Automatica 41, 1209–1218 (2005)
13. Han, Q.L.: A Discrete Delay Decomposition Approach to Stability of Linear Retarded and Neutral Systems. Automatica 45, 517–524 (2009)
14. Li, X.G., Zhu, X.J.: Stability Analysis of Neutral Systems with Distributed Delays. Automatica 44, 2197–2201 (2008)
15. Li, X.G., Zhu, X.J., Cela, A., Reama, A.: Stability Analysis of Neutral Systems with Mixed Delays. Automatica 44, 2968–2972 (2008)

Neural Network Model for Forecasting Balkan Stock Exchanges

Miroslav Janeski and Slobodan Kalajdziski

Ss. Cyril and Methodius University

Faculty of Computer Science and Engineering

Rugjer Boshkovik 16, 1000 Skopje

Republic of Macedonia

miroslav.janeski@gmail.com, skalaj@finki.ukim.mk

Abstract. Artificial neural networks (NN) can be used to model complex relations between inputs and outputs or to find patterns in data. When dealing with time series the process of prediction with NN has to be adopted to take into account the temporal characteristics of the data. A variety of different aspects of designing NN based forecasting models were introduced, and the most common way of dealing temporal data is by using sliding window. This paper presents a work where NNs are used to forecast stock market prices. We analyze which models are more adequate for different companies from Balkan stock exchanges and determine if there are possible relations among them. Unique aspect of our approach is that we experimentally determine optimal sliding window parameters and optimal number of hidden neurons for the appropriate companies. Also we try to emphasize the main reasons that influents on the forecasting stock market prices.

Keywords: artificial neural networks, forecasting financial time series, stock exchange, backpropagation, sliding-window, machine learning.

1 Introduction

In recent years artificial neural networks (NNs) have shown significant results in forecasting time series. Main reason for applying NNs in forecasting time series are their theoretical capabilities like nonlinear function approximation [1, 2]. Despite their theoretical capabilities and successful applications, NN are not yet established as a forecasting methods in business practice. In fact, forecasting with NN is a process of trial and error.

The stock movement prediction has been at focus for years since it can yield significant profits. Merging NNs like a powerful tool for time series data forecasting and stock market prediction as a target one can obtain interesting results. Forecasting stock market prices with NN based models was and still is a challenge for many researchers [3, 4, 5].

If we analyze the recent research of usage of NNs in forecasting financial time series, we can find interesting papers related with the NN best practices for forecasting financial time series. The state-of-the-art survey of NN applications in

forecasting is presented in [2]. According to [2] main unsolved mysteries in forecasting time series data with NNs are: how NNs model autocorrelated time series data, how to systematically build a NN based model for forecasting tasks, what is the best training method for forecasting tasks and what are the best pre- and post-processing techniques. Most significant recommendations of NN based financial time series forecasting are given in [6]. They propose and give detailed explanation of almost unified procedure in modeling NNs for forecasting financial time series. According to [7], NNs are suitable for financial forecasting and marketing analysis. One of their [7] main conclusions is that final forecasting model should not be one. There should be proposed several best models in order to provide more accurate and more precise forecast of the future. That is because only one case of success, one model on one time series, does not mean it will be successful in the future. A detailed presentation of applying NNs for stock market prices forecasting is given in [8]. There is provided theoretical background of modeling NNs and an attempt to build stock buying/selling alert systems is made. Besides the good application of sliding-window one disadvantage in this work is that NN models are only tested with one company from one stock market. These papers [2, 6, 7, 8] have a big influence on our work, especially on selecting the optimal procedure and parameters for modeling NNs for forecasting tasks. Our models are based upon the procedure in [6, 7] because is closest to some systematically modeling of NNs for forecasting and some of the parameters like selecting input variables and sliding –window sizes were adopted from [8].

The stock market time series data taken in row format are not much useful for forecasting purposes. In forecasting, attributes as a different time series data are highly correlated. Also they are autocorrelated with error and noise and is almost impossible to determine which attributes and preprocessing techniques give more suitable forecasting. Therefore when dealing with forecasting algorithms, a great amount of time should be spent for efficient data preprocessing. Data preprocessing techniques are one of the most explored in recent research [9, 10, 11]. Crone in his research [9] is stating that data preprocessing is still process of trial and error but his recommendations are that simpler techniques give better results than more complicated. When dealing with financial time series, data deseasoning and data detrending are two most used techniques, but there isn't a general rule which can be applied in general and in our model. Zhang in his research [10, 11] is stating that there are some improvements when using deseasoning and detrending but the process of defining the most adequate preprocessing technique is still process of trial and error.

From the related work one can conclude that NNs have good performances in forecasting tasks but there are still unsolved tasks like defining optimal NN topology, preprocessing techniques, training strategy and so on. In this paper we propose a NN based models for forecasting stock market prices evaluated on real time series from different Balkan stock markets. More specifically, we will experimentally evaluate NN models with various NN topologies and sliding-window sizes, and we will determine the best NN models for optimal forecasting Balkan stock exchanges. The experimental results will provide insights on models performance and the relationships among them.

This paper is organized as follows: section II presents the application of NN based model for forecasting several companies from Balkan stock exchanges. In section III

experimental design and the results are obtained. And finally, with section IV we conclude the paper and provide some directions for future work.

2 Application of NN Model for Forecasting Balkan Stock Exchanges

In the literature there is almost a unified procedure for designing NN model for forecasting stock prices. Kaastra in his paper [6] has elaborated the mayor issues in designing the NN model. There are several modifications of this procedure, but in general, the following issues need to be considered during the design of a NN model for stock prices forecasting:

- Defining the input and output data
- Determining the proper data preprocessing
- Choosing the network architecture and specifying the training algorithm
- Determining the training and testing strategy
- Determining the optimum network topology
- Evaluating the results

Some of them are problem related like output goal and input data, for some of them there are empiric recommendations like network architecture and training algorithm and some of them like determining the optimal network topology and training and testing strategy are still process of trial and error.

2.1 Input and Output Data

Success in designing a NN depends on a clear understanding of the problem. Knowing which input variables are important in the market being forecasted is critical. In forecasting stock market prices there are a lot of variables, but determining the proper input variables is always a hard issue. The input variables used in our model are the same as in [8].

Table 1. Input variables

Variable	Description
O_i	the opening price of day i
O_{i-1}	the opening price of day $i-1$
H_{i-1}	the daily high price of day $i-1$
L_{i-1}	the daily low price of day $i-1$
C_{i-1}	the closing price of day $i-1$
C_{i-2}	the closing price of day $i-2$
V_i	the trading volume of day i
M_{i-1}	the 5-day momentum of day $i-1$ ($C_{i-1}-C_{i-6}$)
O_i	the opening price of day i

There are several reasons for choosing these input variables. First of all, there are models that use these input variables and have very good performance [8]. Second, these variables are typical technical variables, which mean that can be easy

formalized for automated decision support. And third and most important is that these variables are available for every company from every stock exchange which makes the proposed model generic and suitable for forecasting stock prices from different companies from Macedonian and other Balkan stock exchanges. Input variables in the proposed model are shown in table 1. Among them there is only one derivative variable and that is 5 day momentum of the closing stock price of the previous day.

Like is mentioned above, defining the output data is problem related issue. Our target is to forecast stock price, so output data is presented by stock closing price of next day. There are also approaches where the output data is classified in mean of buy/sell signals. That signals are further used in trading strategies. Our model has regression task, to strictly determine the next day closing stock price.

2.2 Data Preprocessing

Once the attributes are selected they should be adequately preprocessed in order to achieve higher quality and reliable predictions. Data preprocessing refers to analyzing and transforming the input and output attributes to minimize noise, highlight important relationships, and detect trends and seasons of the variables to assist the neural network in learning the relevant patterns. In our model we are using linear scaling in range [-1, 1].

2.3 Network Architecture and Training Algorithm

In the literature, feed-forward multilayer perceptron and radial-based neural networks are the most used for forecasting stock market prices. Both of them have advantages and disadvantages. In our model we are using multilayer perceptron neural network. Backpropagation algorithm is used as training algorithm, which is one of the most used for tasks like this [2], besides his disadvantages like converge to any local minimum on the error surface, not guaranteed convergence and etc. The default values of the learning rate (0.35) and momentum (0.4) provided in [8] were adopted. These parameters can also be experimentally defined but theirs effect on the network generalization performance is already known and therefore were excluded from the experiments.

2.4 Training and Testing Strategy

The training and testing strategy is probably the most important issue in designing a NN. Choosing the appropriate size of the training set is task that has big influence on the generalization capabilities on the NN and is highly dependent on the nature of the observed time series. Moreover, even if the network can converge, it may have learned some historical patterns that may no longer be effective because the market conditions have already changed too drastically. The use of the sliding-window approach allows for the fact that the prediction model may change over time. That means the trained network that was optimal in the past may not be optimal any more.

In the experiment phase five companies from different Balkan stock exchanges where selected. Three of them “Komercijalna Banka” (KMB), “Makedonski

Telekom” (MTEL) and “Toplifikacija” (TPLF) are from Macedonian Stock Exchange, “Hrvatski Telekom” (HRT-H-A) from Zagreb Stock Exchange and “Magyar Telekom” (MTELEKOM) from Budapest Stock exchange. These companies were selected because they are one of the most successful in the appropriate stock exchanges and appropriate industries. Historical data was taken form official stock exchange’s web sites. The data sets are consisting of four year period, November 2006 – October 2010, expect for HRT-H-A were data set is consisted of three year period, November 2007 – October 2010, because HRT-H-A has started trading on the Zagreb Stock Exchange on October 5, 2007.

A sliding window approach [8,9,13] was adopted for training and testing. The most significant thing in our training – testing strategy is defining the optimal training and testing sliding window size. That means how many values one should look in the past to reasonable predict the future. The work presented in [8, 9] has similar practical use of sliding window where testing sliding window size is one month, while the training sliding window size is six months. In our case we adopted one month length for testing sliding window size. For defining the optimal training sliding window sizes several experiments were performed. Lack of recommendations in literature and different time series from different companies were the main reasons. Some time series are more stationary, other less and therefore different training sliding – window sizes are needed in order to proper train the NN.

2.5 Network Topology

Defining NN topology parameters is related with the problem of the observed domain. Network topology parameters are consisting of number of layers, number of hidden neurons number and the number of input and output neurons. Because the number of input and output variables are already defined with the attribute selection process the only thing remaining is the number of hidden layers and the number of hidden neurons. Theoretically, a neural network with one hidden layer with a sufficient number of hidden neurons is capable of approximating any continuous function. In practice [2], networks with one or two hidden layers are used in 90% of the cases. Large number of hidden layers than two can make the neural network time consuming and over fitted, which means that the network has too few degrees of freedom and memorize general patterns. In our system we used one hidden layer with different number of hidden neurons which was part of the experiments. Despites the lot of experiments in determining the optimal NN topology there is no magical formula for this task. In [8], there are several methods but most of them did not answer the problem in complete. We have used the following equation:

$$k = i * n - 1, i = 1, 2, 3\dots \quad (1)$$

where $i = 1, 2, 3\dots$ and n is the number of input neurons, to provide the initial topology for the experiments. We have tested with following NN topologies: 8-7-1, 8-10-1, 8-14-1 and 8-21-1.

2.6 Evaluating the Results

Results from the experiments will evaluated with two metrics: mean square error (MSE) and mean absolute error (MAE) in order to provide more appropriate analysis on the results.

3 Experiments and Results

In our experiments, we have tested with 4 different NN topologies and 5 different training sliding-window sizes, in total 20 different models for companies with four year data sets (KMB, MTEL and TPLF) and with 4 different NN topologies and 3 different training sliding-window sizes, in total 12 different models for HRT-H-A, due to lack of historical data.

Results with MSE and MAE are shown in Table 2 to Table 5, respectively. In general, there are two main trends that can be extracted from the results. First one is that for this kind of modeling, models with larger training sliding – window size have better performance than the ones with smaller training sliding-window size, but not the largest ones.

Table 2. TPLF MSE/MAE Errors

# hidden neutrons	3 months	6 months	12 months	18 months	24 months
7	0,009/0,047	0,003/0,028	0,002/0,029	0,001/0,026	0,001/0,025
10	0,008/0,044	0,003/0,029	0,002/0,031	0,001/0,026	0,002/0,029
14	0,01/0,047	0,003/0,028	0,007/0,032	0,008/0,031	0,002/0,029
21	0,008/0,046	0,006/0,036	0,002/0,03	0,004/0,034	0,002/0,03

Table 3. KMB MSE/MAE Errors

# hidden neutrons	3 months	6 months	12 months	18 months	24 months
7	0,065/0,009	0,072/0,076	0,007/0,039	0,036/0,056	0,007/0,045
10	0,113/0,12	0,037/0,078	0,005/0,044	0,05/0,06	0,032/0,066
14	0,101/0,11	0,491/0,167	0,009/0,047	0,011/0,062	0,033/0,069
21	0,07/0,105	0,512/0,16	0,014/0,053	0,331/0,053	0,079/0,076

Table 4. MTEL MSE/MAE Errors

# hidden neutrons	3 months	6 months	12 months	18 months	24 months
7	0,077/0,117	0,053/0,081	0,171/0,094	0,024/0,065	0,378/0,164
10	0,554/0,252	0,032/0,075	0,038/0,07	0,021/0,07	0,05/0,081
14	0,857/0,27	0,146/0,093	0,458/0,104	0,101/0,108	0,782/0,233
21	0,993/0,271	0,164/0,121	0,854/0,122	0,135/0,095	0,099/0,119

Table 5. MTELEKOM MSE/MAE Errors

# hidden neutrons	3 months	6 months	12 months	18 months	24 months
7	2,062/0,664	2,431/0,553	0,527/0,289	0,166/0,225	0,217/0,236
10	1,506/0,59	1,855/0,524	0,342/0,302	0,150/0,246	0,152/0,24
14	0,988/0,517	2,012/0,633	0,715/0,422	0,417/0,324	0,188/0,248
21	3,157/0,877	2,040/0,625	1,703/0,568	0,235/0,294	0,209/0,263

Second trend is that models with smaller number of hidden neurons have better performance than the ones with larger number of hidden neurons. These trends are mainly manifested at TPLF, MTEL and MTELEKOM. There are deviations from these rules. They are evident at KMB, where best model has 10 hidden neurons and 12 months training sliding-window size.

Additional thing that can be noticed from the results is the value of the MSE and MAE. Results from TPLF are significantly smaller than KMB, MTEL and MTELEKOM for the respective NN models. For example, the best TPLF model for MSE is 150 times better than the best MTELEKOM model. This situation is a result of the different stationary of the appropriate time series.

Original close prices of MTEL and MTELEKOM stocks are shown on Fig. 1. Different stationary of the time series is obvious. The effect of the noise in the data is also important thing that can be analyzed on appropriate figures. The world economic crisis (autumn 2009) is one of the main turnover points in the time series among the all companies. On MTEL time series (Fig. 1), the dividend payout days are also turnover points that add noise to the data which makes the appropriate time series more difficult to predict. Unlike the others MTELEKOM original price movement (Fig. 1) is fulfilled with daily deviations and is quite different from the others observed companies.

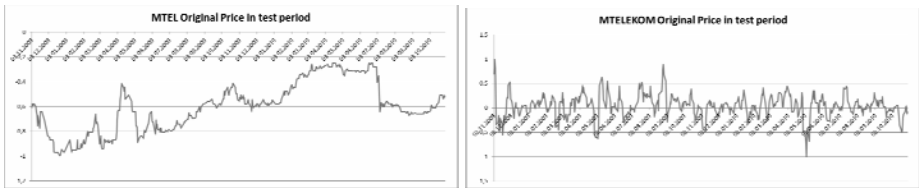


Fig. 1. MTEL and MTELEKOM original price in test period

Main motivation for this paper was to determine whether there are any relationships between the models of the observed companies. From the results on Table 4 and Table 5 and Fig. 1 one can conclude that besides the different stationary in the time series of MTEL and MTELEKOM same models have the best results. Actually, one can conclude that maybe there is a relation between these time series, but to extract rules of this kind there should be made additional experiments which will be part of the future work.

4 Conclusion and Future Work

In this paper we have presented design and implementation guidelines details of a NN based model for forecasting Balkan stock exchanges. Our work has been motivated by the theoretical properties of NNs in time series prediction and by challenge of the idea to predict stock prices. Our main contribution was to experimentally evaluate the optimal parameters of such a forecasting system like sliding window size and number of neurons in the hidden layer of the neural network.

We have evaluated our proposed model based on the historical data from Balkan stock exchanges in period of four years. Testing process included testing with different NN topologies and different sliding window sizes. The testing has shown interesting results. First of all there were extracted several trends that appeared in the results. Then MSE and MAE values were discussed and were selected main reasons for the obtained results. At the end were discussed possible relationships between related companies trading on different stock markets.

The future work will be focused on several targets. First of all, another more market related input variables will be considered, in order to provide more optimal models in a matter of shorter training sliding window size. For example, current input variables [8] are selected for dynamic stock markets with high daily deviations. Balkan stock markets are more static. Idea is that input variables that represent larger period of time will produce models with smaller training sliding window size. Second idea is to involve semantics in the models, which will provide semantic information to the neural network, and we expect that this will result in better generalization capabilities of the models.

References

1. Adya, M., Collopy, F.: How Effective are Neural Networks at Forecasting and Prediction? A Review and Evaluation. *Jour. of Forecasting* 17, 481–495 (1998)
2. Zhang, G.P., Patuwo, B.E., Hu, M.Y.: Forecasting with Artificial Neural Networks: The State of the Art. *Int. J. Forecast.* 14, 35–62 (1998)
3. Dase, D.D., Pawar, R.K.: Application of Artificial Neural Network for Stock Market Predictions: A Review of Literature. *Int. Journal of Machine Intelligence* 2 (2010)
4. Yamashita, T., Hirasawa, K., Jinglu, H.: Application of Multi-branch Neural Networks to Stock Market Prediction. In: *IEEE International Joint Conference on Neural Networks*, Montreal, Que (2005)
5. De Gooijer, J.G., Hyndman, R.J.: 25 Years of Time Series Forecasting. *International Journal of Forecasting* (2006)
6. Kaastra, L., Boyd, M.: Designing a Neural Network for Forecasting Financial and Economic Time Series. *Neurocomputing* 10(3), 215–236 (1996)
7. Yao, J.T., Tan, C.L.: Guidelines for Financial Forecasting with Neural Networks. In: *Proceedings of International Conference on Neural Information Processing*, Shanghai, China, pp. 757–761 (2001)
8. Philip, M.T., Paul, K., Choy, S.O., Kwan, R., Ng, S.C., Jacky, M., Tsang, J., Kai, K., TakLam, W.: Design and Implementation of NN5 for Hong Kong Stock Price Forecasting. *Engineering Applications of Artificial Intelligence* 20, 453–461 (2007)
9. Crone, S., Lessmann, S., Stahlbock, R.: The Impact of Preprocessing on Data Mining: An Evaluation of Support Vector Machines and Artificial Neural Networks. *European Journal of Operations Research* 173(3), 781–800 (2005)
10. Zhang, G.P., Qi, M.: Neural Network Forecasting for Seasonal and Trend Time Series. *European Journal of Operational Research* 160, 501–514 (2005)
11. Zhang, G.P., Kline, D.M.: Quarterly Time-series Forecasting with Neural Networks. *IEEE Transactions on Neural Networks* 18(6), 1800–1814 (2007)
12. Skabar, A., Cloete, I.: Neural Networks, Financial Trading and The Efficient Market Hypothesis. *Australian Computer Science Communications* 24(1), 241–249 (2002)
13. Dorffner, G.: Neural Networks for Time Series Processing. *Neural Network World* 4(96), 447–468 (1996)

A Robust Fault Detection and Isolation Scheme for Robot Manipulators Based on Neural Networks

Mien Van¹, Hee-Jun Kang², and Young-Shick Ro²

¹ Graduate School of Electrical Engineering, University of Ulsan, 680-749, Ulsan, South Korea

² School of Electrical Engineering, University of Ulsan, 680-749, Ulsan, South Korea

{hjkang, ysro}@ulsan.ac.kr, vanmien1@gmail.com

Abstract. This paper investigates an algorithm to the robust fault detection and isolation(FDI) in robot manipulators using Neural Networks(NNs). Two Neural Networks are utilized: the first NN (NN1) is employed to reproduce the robot's dynamic behavior, while the second NN (NN2) is used to achieve the online approximation for fault detection and isolation. This approach focused on detecting changes in the robot dynamics due to faults. An online monitoring is used not only to detect faults but also to provide estimates of the fault characteristics. A computer simulation example for a two link robot manipulator shows the effectiveness of the proposed algorithm in the fault detection and isolation design process.

Keywords: Neural Network, Fault Detection, Fault Diagnosis, Nonlinear Model.

1 Introduction

Various approaches to the fault detection and isolation in robot manipulators and nonlinear systems have been proposed recently. The nonlinear observer scheme is considered by using sliding mode[1], a differential-geometric approach to the fault diagnosis[2]. A residual generation for robot system based on unknown input or output have been considered [3-4], and the nonlinear observer are given [6-7,12]. The design and analysis of the fault detection and isolation in nonlinear system have been described [6,8]. Adaptive and online approximation has been given to approaches the nonlinear fault diagnosis [5-8,11-12]. In these techniques, an adaptive and online approximation is used to approach the fault function. Nowadays, with the advances of hardware and software, we can apply the high computation techniques such as neural network [5-12], adaptive fuzzy neural network [10] to fault diagnosis. In the robot system, the uses of neural network to diagnosis have been considered in [5,7,9,10,11]. The problem of identification for nonlinear systems using neural network are described in [18]. Moreover, robotic system faults often cause unpredictable nonlinear changes in the dynamics of the system; thus, this paper suggests a scheme for online detecting and approximating this type of fault.

In this paper, a model-based FDI scheme for robot manipulators using NN is proposed. We used NN for two purposes: first, a NN1 is trained to reproduce the

robot's dynamic behavior. Second, NN2 is used for online approximation the changes in the robot dynamics due to faults. They are used not only for fault detection but also for fault isolation.

The organization of this paper is as follows: in section 2, the robot dynamics and faults are investigated and problems are given. In section 3, the structure of the used NNs is described. The fault detection and isolation schemes are described in section 4. Simulation results on two link robot manipulator are used to check the effectiveness of algorithm given in section 5. Section 6 includes some conclusions.

2 Problem Formulation

Consider a robotic manipulator is described as follows:

$$\ddot{q}(t) = M^{-1}(q(t))[\tau(t) - V_m(q(t), \dot{q}(t))\dot{q}(t) - F(\dot{q}(t)) - G(q(t)) - \tau_d(t)] + \gamma(t-T)\phi(q, \dot{q}, \tau) \quad (1)$$

Where $q(t) = [q_1(t), q_2(t), \dots, q_n(t)]^T \in \Re^n$ are the joint coordinates, $M(q(t))$ is the inertia matrix of the robot manipulator, $V_m(q(t), \dot{q}(t))$ represents Coriolis and centripetal force, $F(\dot{q}(t))$ is the friction matrix, τ_d is a load disturbance matrix and $G(q(t))$ is the vector of gravity terms, the term $\phi(q, \dot{q}, \tau) \in R^n$ is a vector which represents the fault in robot manipulator, $\gamma(t-T) \in R$ represents the time profile of the faults, and T is the time of occurrence of the faults.

Let $v = \dot{q}^T$, we can rewrite (1) as:

$$\dot{v} = M^{-1}(q(t))[\tau(t) - V_m(q(t), \dot{q}(t))\dot{q}(t) - F(\dot{q}(t)) - G(q(t)) - \tau_d(t)] + \gamma(t-T)\phi(q, \dot{q}, \tau) \quad (2)$$

Changes in robot dynamic due to faults can be expressed as nonlinear functions of the positions and velocities of the joint and the torque inputs to the actuators. The following assumptions[5,7,9] are made in the construction of the robot manipulator estimation and learning throughout the paper.

Assumption 1: the robotic states and controls are bounded before and after the occurrence of a fault, i.e., $q(t), \dot{q}(t) \in L_\infty$.

Assumption 2: the modeling uncertainty is represented by friction component $F(\dot{q}(t))$ and load disturbance matrix τ_d is bounded:

$$|M^{-1}(q(t))[F(\dot{q}(t)) - \tau_d(t)]| \leq \bar{\mu}_i(q, \dot{q}, \tau, t) \quad \forall (q, \dot{q}, \tau) \in \bar{D}, \forall t \geq 0 \quad (3)$$

We let the time profile matrix be a diagonal matrix of the form:

$$\gamma(t-T) := \text{diag}\{\gamma_1(t-T), \dots, \gamma_n(t-T)\} \quad (4)$$

Each time profile component γ_i is assumed to be of the form:

$$\gamma_i(t-T) = \begin{cases} 0 & \text{if } t < T \\ 1 - e^{-\varphi_i(t-T)} & \text{if } t \geq T \end{cases} \quad (5)$$

Where $\varphi_i > 0$ is an unknown constant that represents the evolution rate.

3 Neural Network

Giving $x \in \mathbb{R}^{N_1}$ are the input, a three-layer NN has a net output given by[17] as follow:

$$y_i = \sum_{j=1}^{N_2} \left[w_{ij} \sigma \left[\sum_{k=1}^{N_1} v_{jk} x_k + \theta_{vj} \right] + \theta_{wi} \right] \quad (6)$$

where $\sigma(\cdot)$ the activation function, v_{jk} the first-to-second layer interconnection weights, and w_{ij} the second-to-third layer interconnection weights. The θ_{vm}, θ_{wm} , $m=1,2,\dots$, are threshold offsets and the number of neuron in layer l is N_l , with N_2 the number of hidden-layer neurons. The activation function $\sigma(\cdot)$ is selected:

$$\sigma(z) = \frac{1}{1 + e^{\alpha z}} \quad , \text{ sigmoid}$$

We denote $x = [x_0 x_1 x_2 \dots x_{N_1}]^T$ as the input, $y = [y_1 y_2 \dots y_{N_3}]^T$ as the output, the weights matrix $W^T = [w_{ij}]$, $V^T = [v_{jk}]$, the input x include the threshold vector $[\theta_{v1} \theta_{v2} \dots \theta_{vN_2}]^T$ as the first column of V^T , then:

$$y = W^T \sigma(V^T x) \quad (7)$$

4 Fault Detection and Isolation Architecture

4.1 Robot Dynamic Model

In this section, The NN1 is used to reproduce the robot's dynamic behavior; the procedure is performed when the robot is in normal operation.

When the robot is in normal operation, the dynamics of robot dynamic can be written:

$$\begin{aligned} \dot{V}^* &= M^{-1}(q(t))[\tau(t) - V_m(q(t), \dot{q}(t))\dot{q}(t) \\ &\quad - F(\dot{q}(t)) - G(q(t)) - \tau_d(t)] \end{aligned} \quad (8)$$

From (9), the input data x are chosen: q, \dot{q}, τ , and the output y is $\ddot{q} = \dot{v}^*$. Given input-output data (x_i, y_i) are obtained when robot is healthy, and then finding the best MLP network is formulated as a data fitting problem. The parameters to be determined are $(v_{ij}, w_{jk}, \theta_{vm}, \theta_{wm})$. The procedure is shown in [16]. After finding the best MLP network, we obtained NN1 is the estimated model of robot dynamic. The estimated model can be written:

$$\dot{\hat{v}}^* = W_1^T \sigma(V_1^T x) \quad (9)$$

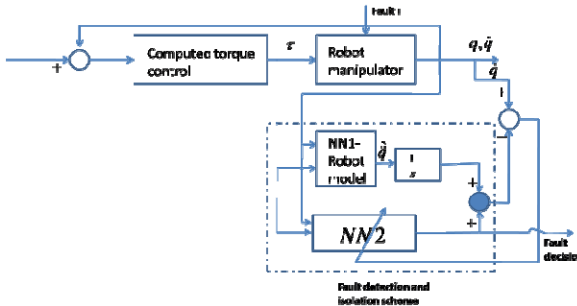


Fig. 1. Fault detection and isolation scheme

4.2 Fault Detection and Isolation Scheme

From (2) and (8), the formulation (2) can be rewritten:

$$\dot{v} = \dot{v}^* + \gamma(t-T)\phi(q, \dot{q}, \tau) \quad (10)$$

Based on (10) and (11), the observer is chosen as follow:

$$\dot{\hat{v}} = \dot{v}^* + \hat{\phi}(q, \dot{q}, \tau, \hat{W}_2, \hat{V}_2) \quad (11)$$

Where \hat{v} is the estimate of v , \hat{v}^* is the output of NN1, which is estimate of v^* , $\hat{\phi}$ is an online approximation model, \hat{W}_2, \hat{V}_2 represents a vector of adjustable weights of the online approximation. A key to online approximation $\hat{\phi}$ by using neural network, and \hat{W}_2, \hat{V}_2 are the weights of NN2.

From (10) and (11), the error dynamic can be described as below:

$$\tilde{v} = -\dot{\hat{v}}^* + \hat{\phi}(q, \dot{q}, \tau, \hat{W}_2, \hat{V}_2) - \gamma(t-T)\phi(q, \dot{q}, \tau) \quad (12)$$

Where $\tilde{v} = v - \hat{v}$ and $\tilde{v}^* = v^* - \hat{v}^*$ present the error between the nominal model and the estimated model (NN1). Corresponding to no-fault situation, the initial values of the adjustable weights \hat{W}_2, \hat{V}_2 are chosen in order to satisfy that:

$\hat{\phi}(q, \dot{q}, \tau, W_2^0, V_2^0) = 0$, from this initial condition, we need to adjust the neural weights to minimize the error between $\gamma(t-T)\phi(q, \dot{q}, \tau)$ and $\hat{\phi}(q, \dot{q}, \tau, \hat{W}_2, \hat{V}_2)$ over all input. The tuning weight and adaptation algorithm for NN2 are taken from[17]. From [17], the NN weight tuning is provided:

$$\dot{\hat{W}}_2 = F\hat{\sigma}\tilde{V}^T - F\hat{\sigma}'\hat{V}_2^T x\tilde{V}^T - kF\|\tilde{V}\|\hat{W}_2 \quad (13)$$

$$\dot{\hat{V}}_2 = Gx(\hat{\sigma}'^T \hat{W}_2 \tilde{V})^T = kG\|\tilde{V}\|\hat{V}_2 \quad (14)$$

With any constant matrices $F = F^T > 0, G = G^T > 0$ and scalar design parameter $k > 0$.

Fault Isolation policy: the NN1 is used in our work to reproduce the robot dynamic. The NN2 is employed to identify the unknown faults function, the output of NN2 is the model of faults function (Fig.1). When the robot normally operation, the output of the NN2 is small (approximate zero), and it is used to choose threshold. When the fault happens, the NN2 output is nonzero so that it overshoots the threshold. This will be used to detect, isolate and identify the type of faults function.

5 Simulation Results

In order to verify the performance of our proposed fault diagnosis scheme, the two link planar robot manipulator is given as an example to illustrate the FDI scheme for robot manipulator. Simulation results are presented in this section, the link parameters of the manipulator are given in table 1.

Table 1. Manipulator parameter

j=1,2	Link 1	Link 2
link's lengths $a_i(m)$	0.5	0.5
link's weight $m_i(Kg)$	10	7

The dynamic of robot manipulator:

$$\begin{bmatrix} \tau_1 \\ \tau_2 \end{bmatrix} = M \begin{bmatrix} \ddot{q}_1 \\ \ddot{q}_2 \end{bmatrix} + V_m + \begin{bmatrix} f_1 \\ f_2 \end{bmatrix} + \begin{bmatrix} \tau_{d_1} \\ \tau_{d_2} \end{bmatrix} \quad (15)$$

Where M is given by:

$$M = \begin{bmatrix} (m_1 + m_2)a_1^2 + m_2a_2^2 + 2m_2a_1a_2c_2 & m_2a_2^2 + m_2a_1a_2c_2 \\ m_2a_2^2 + m_2a_1a_2c_2 & m_2a_2^2 \end{bmatrix}$$

And V_m is given by

$$V_m = \begin{bmatrix} m_2 a_1 a_2 (2\dot{q}_1 \dot{q}_2 + \dot{q}_2^2) s_2 + (m_1 + m_2) g a_1 c_1 + m_2 g a_2 c_{12} \\ m_2 a_1 a_2 \dot{q}_1^2 s_2 + m_2 g a_2 c_{12} \end{bmatrix}$$

where $c_1 = \cos(q_1)$, $c_2 = \cos(q_2)$, $c_{12} = \cos(q_1 + q_2)$, $s_1 = \sin(q_1)$, $s_2 = \sin(q_2)$. We assumed that the robot has the following modeling uncertainties such that $f_1 = 1.3 \text{sgn}(\dot{q}_1) + 4\dot{q}_1$, $f_2 = 1.3 \sin(\dot{q}_2) + 4\dot{q}_2$, $\tau_{d_1} = \tau_{d_2} = \sin(30t)$

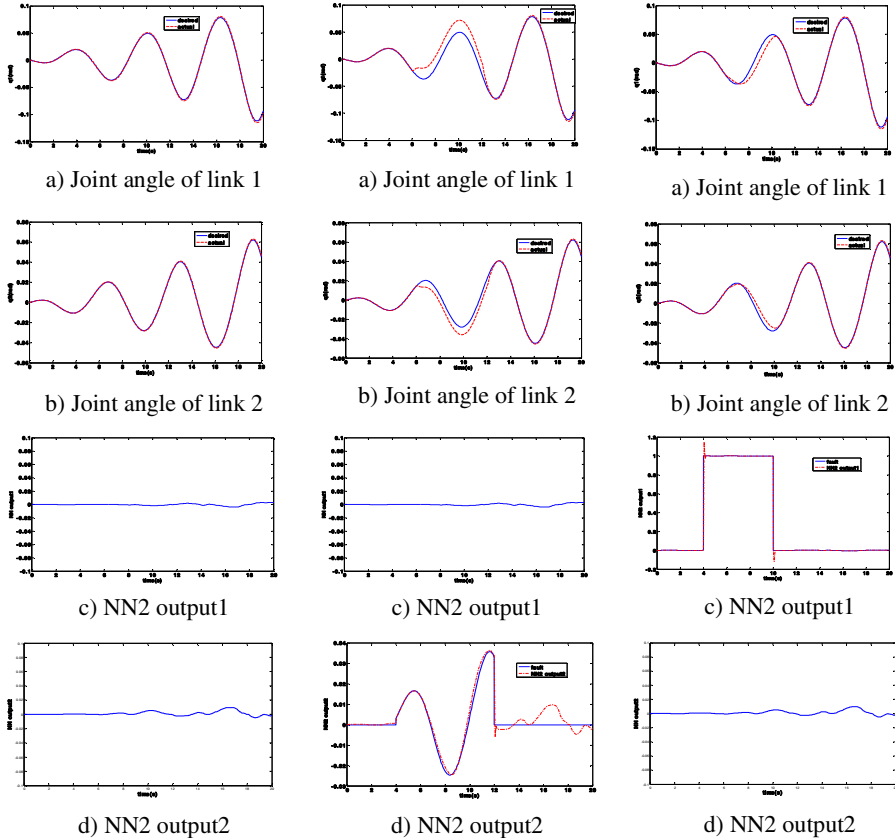


Fig. 2. Joint angles and NN2 outputs when nonfaulty

Fig. 3. Joint angles and NN2 outputs when F1 happened

Fig. 4. Joint angles and NN2 outputs when F2 happened

At first, robot in normal operation situation is considered, the simulation results for joint angles and NN outputs are shown in Fig.2. We can see that the NN2 outputs remain close to zero (Fig.2 c,d)), that demonstrate there is no fault in the system.

In order to check the identification capability of the proposed NN for some types of fault, we applied some types of fault. Firstly, we supply a fault

$F_1 = [0; 20\dot{q}_1^4 + \dot{q}_1^3 + \dot{q}_1^2 + \dot{q}_1]^T$ so that an abrupt fault happens at $t=4s$ and finishes at $t=12s$. The response of the joint angles and Neural Network outputs are shown in Fig.3. Fig.3 shows that the types of fault F_1 are detected and isolated. Secondly, when the fault $F_2 = [2\cos(\dot{q}_2); 0]^T$ happens, the joint angles and NN outputs are shown in Fig.4. Fig.4 verifies that the fault F_2 is detected and isolated. Thirdly, we generate a fault $F_3 = [20\dot{q}_1^4 + \dot{q}_1^3 + \dot{q}_1^2 + \dot{q}_1; 10\sin(\dot{q}_2)]^T$ happens, the joint angles and NN outputs are shown in Fig.5 that indicates the fault F_3 is detected and isolated from the proposed algorithm.

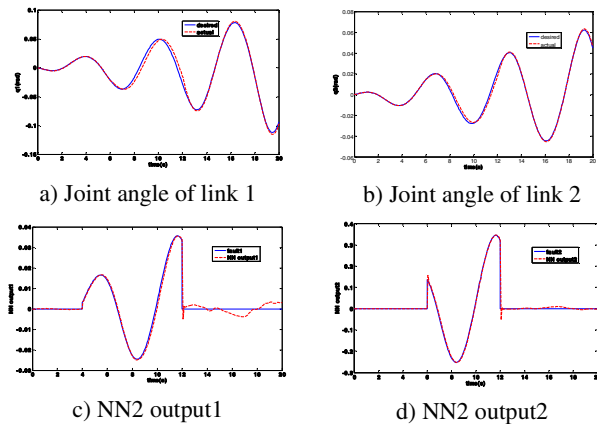


Fig. 5. Joint angles and outputs when F_3 happened

6 Conclusions

A model-based FDI scheme for robot manipulators using NN is presented in this paper. In this model, two functions of NN are proposed: the first reproduce the robot's dynamic behavior as the estimated robot dynamic model and other for online approximation the changes in robot dynamic due to faults as online monitoring, which is used not only for fault detection but also for determination of the fault characteristic. A computer simulation for a two link robot manipulator shows the effectiveness of the proposed algorithm in the fault detection and isolation process.

Acknowledgment. The authors would like to express financial supports from NARC (Network based Automation Research Center), and Ministry of Knowledge Economy under Human resources Development Program for Convergence Robot Specialists, respectively.

References

1. Brambilla, D., Capisani, L.M., Ferrara, A., Pisu, P.: Fault Detection for Robot Manipulators via Second-order Sliding Modes. IEEE Trans. Industrial Electronics 55, 3954–3963 (2008)

2. Persis, C.D., Isidori, A.: A Geometric Approach to Nonlinear Fault Detection and Isolation. *IEEE Trans. Autom. Control.* 46, 853–865 (2001)
3. Dixon, W.E., Walker, I.D., Dawson, D.M., Hartfranft, J.: Fault Detection for Robot Manipulators with Parametric Uncertainty: A Prediction-error-based Approach. *IEEE Trans. Robot.* 16, 689–699 (2000)
4. Intyre, M., Dixon, M.L., Dawson, W.E., Walker, D.M.: Fault Identification for Robot Manipulators. *IEEE Trans. Robotics.* 21, 1552–3098 (2005)
5. Huang, S.N., Tan, K.K.: Fault Detection, Isolation, and Accommodation Control in Robotic Systems. *IEEE Trans. Automation Science and Engineering.* 5, 1545–5955 (2008)
6. Polycarpou, M.M.: Fault Accommodation of A Class of Multivariable Nonlinear Dynamical Systems Using a Learning Approach. *IEEE Trans. Automat. Contr.* 46, 736–742 (2001)
7. Vemuri, A.T., Polycarpou, M.M.: Neural-network-based Robust Fault Diagnosis in Robotic Systems. *IEEE Trans. Neural Networks.* 8, 1410–1420 (1997)
8. Polycarpou, M.M., Trunov, A.B.: Learning Approach to Nonlinear Fault Diagnosis: Detectability Analysis. *IEEE Trans. Automat. Contr.* 45(4), 806–812 (2000)
9. Eski, I., Erkaya, S., Savas, S., Yildirim, S.: Fault Detection on Robot Manipulators Using Artificial Neural Networks. *Robotics and Computer-Integrated Manufacturing* 27, 115–123 (2011)
10. Yuksel, T., Sezgin, A.: Two Fault Detection and Isolation Schemes for Robot Manipulators Using Soft Computing Techniques. *Applied Soft Computing* 10, 125–134 (2009)
11. Huang, S.N., Tan, K.K., Lee, T.H.: Automated Fault Detection and Diagnosis in Mechanical Systems. *IEEE Transactions on Systems, Man, and Cybernetics, Part C: Applications and Reviews* 37, 1094–6977 (2007)
12. Trunov, A.B., Polycarpou, M.M.: Automated Fault Diagnosis in Nonlinear Multivariable Systems Using a Learning Methodology. *IEEE Trans. Neural Networks.* 11, 91–101 (2000)
13. John, J.C.: *Introduction to Robotics- mechanics and Control*, 3rd edn.
14. Iserman, R.: *Fault-Diagnosis Systems: An Introduction from Fault Detection to Fault Tolerance* (2005)
15. Demuth, H., Beale, M.: *Neural Network Toolbox for Use with Matlab User's Guide*. Version 4 (2002)
16. Heikki, N.K.: *Neural Networks: Basic Using Matlab Neural Network Toolbox* (2008)
17. Lewis, F.L., Yesildirek, A., Liu, K.: Multilayer Neural-Net Robot Controller with Guaranteed Tracking Performance. *IEEE Trans. Automat. Contr.* 7(2), 388–399 (1996)
18. Abdollahi, F., Talebi, A., Patel, R.V.: Stable Identification of Nonlinear Systems Using Neural Networks: Theory and Experiment. *IEEE Trans. Mechatronics* 11(4), 488–495 (2006)

An Approach for High Resolution Radar Target Recognition Based on BP Neural Network

Wei Cao^{1,2}, Hui Zhou³, Zhimin Zhou¹, and Zuowei Fu²

¹ College of Electronic Science& Engineering, National University of Defence Technology, Changsha, China

² College of Computer&Communication Engineering, Changsha University of Science&Technology, China

³ Hunan University of Chinese Medicine, Changsha, China

Abstract. The paper introduces an approach for high resolution radar target recognition by BP neural network. To solve the problem of sensitivity characteristics of HRRP, some preprocessing measures are taken, which enhances the signal-to-noise ratio effectively. Some features such as general central moments and distribution entropy of HRRP are extracted to form a new feature vector. A back-propagation (BP) neural network classifier is designed and trained to discriminate three kinds of target from each other, having as input the extracted features vector. Experiment results demonstrate that the method can improve the target classification performance efficiently and effectively.

Keywords: high resolution range profile (HRRP), target recognition, preprocessing, BP Neural Network, feature vector.

1 Introduction

High resolution range profile (HRRP) is based on the target scattering-center model. When the bandwidth is wide enough, the echo of target's backward electromagnetic dispersion forms a magnitude profile in the radial direction at radar sight which is called one-dimensional high resolution range profile. The range profile provides the distribution situation of target scattering-points in the range direction, which represents the potentially discriminative information on the geometry structure of target. HRRP is sensitive to the aspect angle. There exists phenomena of scattering-points' motion through range cell and flicker effect due to larger aspect variation[1]. Because HRRP is the sum of complex magnitude of echoes of target in certain range bin, when the targets' carrier frequency varies, the variation of echo phase will result in fluctuation of HRRP. To deal with the problem of aspect, translation and magnitude sensitivity of HRRP, preprocessing is the effective method generally used. Some feature extraction methods such as central moment property based one, average HRRPs based one and minimum entropy rule based one are used for RATR[2,3,4]. To improve recognition rate of RATR, several features are combined together to form a

feature vector. The new feature vector not only reflects the detailed structure property of target, but also enhances the identification rate of classification. The paper shows an approach for high resolution radar target recognition by BP neural network.

2 Process of BP Neural Network Based RATR

RATR is attributed to the process of deciding the category, type and property of a target according to certain decision criterion. Fig.1 shows the general processing flowchart of BP network based RATR. First, the radar echo signal is preprocessed, which consists of FFT, covering HRRP by a window in frequency domain, range profile aligning, power transformation, HRRP normalizing, etc. Then a set of target features are extracted. The feature vector sets are fed to a BP neural network. The BP neural network acts as a classifier and is trained to discriminate different kinds of target[4,5].



Fig. 1. The general processing flowchart of BP network based RATR

3 Target Features Extraction of HRRP

For a typical high resolution radar (HRR), the target echo energy is distributed across many range cells because of the physical target size compared with the radar resolution. In this case the target cannot be processed by point target detector[1].

Suppose the HRRP of target echo is:

$$X = [a(1), a(2), a(3), \dots, a(n), \dots, a(N)]^T \quad (1)$$

Where $a(n)$ is the complex magnitude of target echo in the n^{th} range cell. N is the length of range corridor.

3.1 Preprocessing

Suppose the pulse repetition frequency (prf) of HRR is f_r (Hz), 3db beamwidth of the antenna is θ_B ($^{\circ}$), the rotation speed of antenna is θ_s ($^{\circ}/\text{s}$). Then the number of pulses containing target echoes equals to

$$M = \frac{\theta_B f_r}{\theta_s} \quad (2)$$

The received signal is converted to digital samples with the sampling rate N. Suppose the number of the echoes is M, then we get the radar echo matrix A_{mn} . The HRRP of A_{mn} can be got by taking the FFT of the return signal.

$$A_{mn} = \begin{bmatrix} a_{11} & a_{12} & a_{13} & \cdots & a_{1N} \\ a_{21} & a_{22} & a_{23} & \cdots & a_{2N} \\ a_{31} & a_{32} & a_{33} & \cdots & a_{3N} \\ \vdots & \vdots & \vdots & \ddots & \vdots \\ a_{M1} & a_{M2} & a_{M3} & \cdots & a_{MN} \end{bmatrix} \quad (3)$$

To solve the problem of amplitude sensitivity, the HRRP is normalized to remove the influence of the gain of radar receiver amplifier. Normalizing A_{mn} , the HRRPs matrix P_{mn} is got, each row of the matrix represents one HRRP, that is the matrix X. Considering the problem of aspect and translation sensitivity, when the MTRC appears, motion compensation is executed on the echo of scattering-points falling in the same range cell. Then the HRRPs are made range-profile-aligning.

Power transformation is defined as

$$y(n) = a(n)^\alpha, 0.1 \leq \alpha \leq 0.4 \quad (4)$$

where $a(n)$ is the magnitude of target echo in the n^{th} range cell. After the nonlinear transformation, the HRRPs' distribution in feature space is better fitted by Gaussian-distribution. Therefore Gaussian classifiers can be used to make target recognition[3].

3.2 Feature Extraction

Considering the aspect sensitivity of HRRPs, we get range profiles in a small aspect angle to guarantee that the HRRPs remain relatively stable. After Preprocessing, some target features can be extracted. The average HRRPs will be got easily.

(1) Center Moment Feature

In digital image processing, region moment interprets a normalized grey-level image function as a probability density of a 2D random variable. Moments can be used for binary or grey-level region description. A moment is dependent on scaling, translation and rotation. As for RATR, center moments are translation invariant features which reflect the geometry shape information of target.

For the one-dimension normalized HRRP matrix X, its central moments of order k is given by

$$m_1 = \sum_{n=1}^N n a(n) \quad (5)$$

$$m_k = \sum_{n=1}^N (n - m_1)^k a(n) \quad (6)$$

where $k=2,3,\dots,K$. m_1 is the 1th origin moment, that is the centroid of HRRP. m_k denotes the kth central moments. Obviously the origin moment is associated with the shift of HRRP. The high order central moments play the role of compensating the shift influence of HRRP, but they are sensitive to the fluctuation of HRRP. Gentle undulation of echoes especially those in the range cell far away from the centroid of HRRP will lead to greater variation of the high order central moments[2,6]. To

guarantee the robust characteristics of central moments, we define a general high order central moments, which is expressed as

$$m_k = \left(\sum_{n=1}^N (n - m_1)^k a(n) \right)^{1/k} \quad (7)$$

where $k=2,3,\dots,K$. The general high order central moments can reduce the large dynamic range of previous one, thereby can fall its sensitivity resulted from the fluctuation of HRRP.

(2) Entropy Feature

In each HRRP, the echoes of scatters fall in several range cells. The change of elevation angle or azimuth of target as well as the interference of environment noise will result in the amplitude fluctuation of HRRPs in time domain. To describe the scattering property of target in every range cell, entropy feature is utilized.

In information theory, entropy can reflect the average randomness of a sample set of random variables, which is often used for measurement of uncertainty. The entropy of even distribution is the largest, whereas the entropy of concentrative distribution is smaller than that.

For each normalized HRRP $P(m, n)$, $n=1,2,\dots,N$ N is the dimension of the range profile, its distribution entropy is written as:

$$H(m) = - \sum_{n=1}^N p(m, n) * \log(p(m, n)) \quad (8)$$

where $m=1,2,\dots,M$ M is the number of HRRPs. $H(m)$ can reveal the distribution property of scattering-centers of the m^{th} HRRP. For different targets, larger entropy means the scattering-centers are distributed evenly in the range corridor. Smaller entropy reflects that the scattering-centers are of concentrative distribution in the range corridor. For a target within the same azimuth sector, its distribution entropy of HRRP is related with signal-to-noise ratio. The HRRP with larger distribution entropy means it is contaminated seriously by noise, so the signal-to-noise ratio of the echo is lower. Fig.2 and Fig.3 show separately the HRRPs with the largest and the smallest distribution entropy of jet J-8II when its azimuth sector is between 30° and 33° .

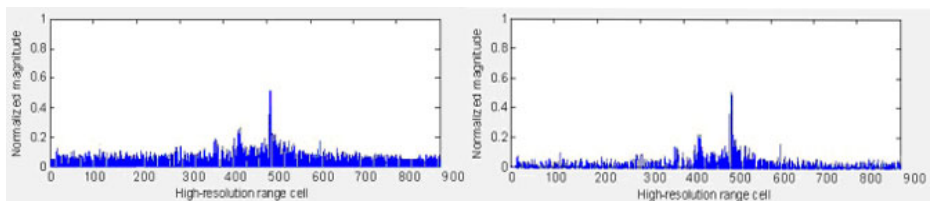


Fig. 2. The HRRP of J-8II with the largest entropy

Fig. 3. The HRRP of J-8II with the smallest entropy

It can be seen that the HRRPs of the same jet within the same azimuth sector change along with environment and the HRRP with larger distribution entropy is contaminated more seriously by noise. So we come to a conclusion that the distribution entropy feature of HRRP can reflect the scattering property of target well.

4 BP Neural Network Classifier

As for RATR, Classifier designing is a tough task, as well as an important step in pattern recognition. A back-propagation (BP) neural network is designed and trained to discriminate three kinds of jets from each other, having as input the extracted features vector.

The block diagram of the preprocessing, the feature extractor and the BP neural classifier is showed in Fig.4. The BP network classifier is of the multilayer perceptron architecture. The number of units in the input layer depends on the number of HRRPs, into which the extracted features of the HRRPs are fed. The number of hidden neurons is selected experimentally by means of training a set of networks with the number of hidden neurons varies from 4 to 10. The choice of output neurons is based on the type of targets identified.

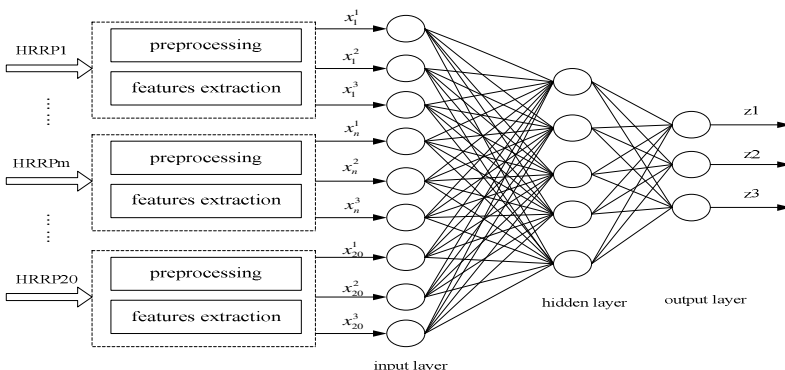


Fig. 4. Diagram of the BP neural network architecture

As concerns the input layer, the important work is deciding reasonable number of components for features vector to ensure effective classifying and to prevent overfitting of the network. For each HRRP, three features are extracted. Suppose the feature subunit of the m^{th} HRRP is $s(m) = [x_m^1, x_m^2, x_m^3]^T$, where x_m^1, x_m^2, x_m^3 represent three feature components separately which are the 1^{th} origin moment, the 2^{th} general central moment and the distribution entropy of the m^{th} HRRP. All feature components of HRRPs are taken as input of neurons in the input layer.

The hidden layer is composed of 4 to 10 nodes with sigmoidal activation. The output layer is made up of three nodes with sigmoidal activation to discriminate three different jets that are J-7G, J-8II, J-10S. We define z_1 , z_2 , z_3 as the outputs of the network. The weights in the network are adjusted by means of training procedure to make sure $[z_1, z_2, z_3] = [1,0,0]$, $[0,1,0]$, $[0,0,1]$ corresponding to target J-7G, J-8II, J-10S respectively.

5 Simulation Results

In the anechoic chamber, we measure the echoes of three target models. Assuming prf=900hz, $\theta_B = 3^\circ$, $\theta_s = 90^\circ/\text{s}$, elevation angle $\theta = 10^\circ$, azimuth angle $\Phi = 0^\circ:90^\circ$, we can get 30 HRRPs for each scan. Firstly, preprocessing is made sequentially for the HRRPs. Then for each HRRP, three feature components are extracted in turn, from which a feature vector is resulted. For every 3° azimuth interval, we choose randomly 20 feature vectors to form a training samples set and a testing sample set respectively. The 20 feature vectors are fed to the input layer of the BP neural network.

We trained separately the set of neural classifiers with 4-10 hidden nodes by the same data set. The simulation result is as Table 1:

Table 1. Recognition rate of BP neural network with different hidden nodes

Number of hidden nodes	Type of jet model		
	J-7G,	J-8II	J-10S
4	95.5%	95.3%	95.2%
5	95.8%	95.6%	95.4%
6	96.1%	95.8%	95.5%
7	96.8%	96.4%	95.8%
8	97.5%	96.8%	96.3%
9	97.2%	96.5%	95.9%
10	96.7%	96.2%	95.6%

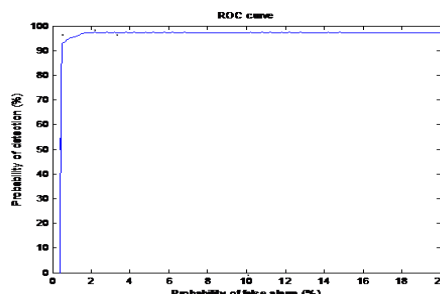


Fig. 5. ROC curve of the network with 8 hidden nodes

The results reveal that the BP network can provide a correct recognition rate of about 95.8%. And the network with 8 hidden neurons exhibits the best classification performance. The ROC curve of the network with 8 hidden nodes is shown in Fig.5. It can be seen that the probability of detection is very high and stable, exhibiting good classification accuracy.

6 Conclusion

To solve the problem of sensitivity characteristics of HRRP, sequential preprocessing are made, which enhances the signal-to-noise ratio effectively. Three feature components are extracted from each HRRP respectively. The BP neural classifier with three layers is tested by the measured data of three jet models. The recognition behaviour of different BP network with 4-10 hidden nodes is analyzed. The experimental results show the method proposed has excellent performance.

References

1. Huang, D.S.: Intelligent Signal Processing Technique for High Resolution Radars. China Machine Press, Beijing (2001)
2. Li, Y., Liu, H.W., Bao, Z.: Automatic Target Recognition of Radar HRRP Based on Central Moments Features. Chinese Journal of Electronics 32(12), 2078–2081 (2004)
3. Zhang, J.Y., Bai, X.H.: Study of The HRRP Feature Extraction in Radar Automatic Target Recognition. System Engineering and Electronics 29(12), 2047–2051 (2007)
4. Xu, H.L., Wang, Y., Yang, W.J., Wu, D.Q.: A Method of Establishing Template Database for High Resolution Radar Target Identification, pp. 1010–1013. IEEE, Los Alamitos (2008)
5. Wang, X.K., Zhang, X.F.: A New Architecture of Neural Network Array Replacing of A Multiple Outputs BP Model Network. Computer Science 28(10), 61–63 (2001)
6. Liu, H.W., Bao, Z.: Radar HRRP Recognition Based on Hybrid Features and Multi-Stage Feature Selection Scheme. System Engineering and Electronics 27(4), 596–599 (2005)
7. Khairnar, D., Merchant, S., Desai: Radial Basis Function Neural Network for Pulse Radar Detection. In: IEEE Proc., Radar, Sonar and Navigation, vol. 1, pp. 8–17 (2007)
8. Laura, P., Leonardo, B., Giuseppe, A., Dionisio, A.: Detection of Snow Clutter in ATC Ground Radar Signal, pp. 1340–1344. IEEE, Los Alamitos (2008)
9. Pham, T.D.: Combined Neural Networks For Radar Target Recognition from Radar Range Profiles, pp. 353–355. IEEE, Los Alamitos (2008)

Hybrid Clustering Algorithm Based on the Artificial Immune Principle

Yan Zhou and Zhifeng Hu

Department of Electronics & Information Engineering,
Suzhou Vocational University, Suzhou, 215104
Zhyan@jssvc.edu.cn

Abstract. A hybrid clustering algorithm based on the artificial immune theory is presented in this paper. The method is inspired by the clone selection and memory principle. The problem of local optimal can be avoided by introducing the differentiation of memory antibody and inhibition mechanism. In addition, the K-means algorithm is used as a search operator in order to improve the convergence speed. The proposed algorithm can obtain the better data convergence compared with the K-means algorithm based clustering approach and artificial immune based approach. Simulate experimental results indicate the hybrid algorithm has a faster convergence speed and the obtained clustering centers can get strong stability.

Keywords: immune principle, clustering algorithm, K-means, hybrid algorithm.

1 Introduction

Clustering analysis is a powerful information processing method. In all of the cluster analysis methods, C-means algorithm (HCM) and Fuzzy C-means algorithm (FCM) are most widely used. However, these two kinds of methods in clustering process are easy to fall into the local extreme value point and sensitive to initial data. Meanwhile, these two clustering analysis algorithms are only suitable for dealing with globular or ellipse data since their clustering validity depends on the distribution of samples. K-means algorithm[1-2] is also called hard C-means clustering algorithm. This clustering algorithm is a classical method for solving the problem of clustering which is simple, high speed, strong power of local search ability, etc. Although it has many advantages in dealing with clustering, it has the disadvantages like the C-means algorithm, such as the executing result of k-means algorithm is sensitive to initial conditions. Furthermore, this algorithm is normally based on objective function and gaining extremum value by adopting gradient method, so it is easy to drop into minimum value, even appearing degradation answer or no answer. The clustering algorithm [3] based on genetic algorithm(GA) can be used to solve the problem of initial value sensitive, consequently obtain the global optimal solution more likely. But when the sample number, category and dimension are too many, it is difficult to guarantee the genetic algorithm to obtain global optimal solution from each operation. In such situation, genetic algorithm usually gets into precocious phenomena.

Artificial immune system (AIS)[4-5] is a kind of computing paradigm which is inspired by the theoretical biology. The biological immune system function, principle and model are referenced in this system so that it has the strong learning ability, identification and distributed associative memory and feature extraction ability. In a word, it can be used to solve complex problems.

In order to settle the clustering shortcomings above, referenced the immune cells cloning and memory in the biological immune system [6-7], affinity maturation, and combined with the mechanism of k-means algorithm, a new hybrid clustering method based on the immune theory is proposed in this paper. The problem of local optimal can be successfully avoided through the memory cells inhibit the antibodies effectively. Compared with the K-means clustering algorithm approach, the proposed hybrid algorithm can make the convergence quicker and more effectively converge to the global optimal solution.

2 The Principle of Artificial Immune Algorithm

The immune system is an organization institute which has immune function. The so-called immune function is a physiological response, that is, the antigen material from own or outside body can be recognized by the organism and then cleared by the antibodies, as a result, the relatively stability of the organism can be retained. In the clustering analysis based on artificial immune theory, it is necessary to treat the objective data as antigens and the clustering centers as antibodies. The clustering process of the data is that immune system continuously produces antibodies, and the antibodies recognize the antigens, finally produce the best antibody to capture the antigens.

The thought of immune clustering algorithm is like this: every antibody can recognize near space antigens, it also means that whether the antigen can be recognized by the antibody is determined by the affinity of them. If the affinity of the antigen and antibody is bigger than a threshold, it means the success of recognition. Otherwise, it needs to select the best antibody to clone and mutate, then a new antibody sets is obtained. In fact, this approach aids to search the better center near the maximum affinity data to get the more optimal center. When the antigens still can not be recognized by the better antibody, the only way is to choose the best antibody to clone and mutate, preferential recognize and do circulation K times. In case, the antigen can not be recognized in the end, then the antigen should be regard as a new antibody directly. The immune clustering algorithm reaches end if all the input sample data sets have finished studied.

The proposed hybrid algorithm based on immune theory is an improvement of previous general immune algorithm. This paper adopts the mechanism of memory cell and inhibition cell differentiation and the producing of antibody is controlled by the inhibiting cell. It is effective to prevent the reproduce of memory cell and thereby improved the solution search efficiency.

3 K-means Clustering Algorithm

K-means clustering algorithm is a kind of mainstream iterative decline clustering method. The core thought of this algorithm is that the data objects are divided into different clusters through iterative computing, thus, the smallest object function can be got consequently, and the generated clusters can be compact and independence as possible.

This algorithm process can be described like that each cluster center is moved repeatedly to minimize the total measurement inner the cluster (e.g., distance and similarity). Specifically speaking, set a sample for x_i ($i = 1, 2, \dots, n$), given a group of initial center c_k ($i = 1, 2, \dots, n$), this initial center can be randomly chosen from the data samples. Afterwards, K-means algorithm executes the following steps alternatively: firstly, finding out the nearest clustering center for each sample x_i , secondly, computing the means of the cluster data and this new means vector become the new center of this cluster. This process continuously repeats until the objective function reaches convergence. In general, the objective function uses mean-square error principle, the definition is like this:

$$Q = 1 / \sum_k^K \sum_{p \in C_l} D_{ik}^2(c_k, x_i) \quad (1)$$

In Eq (1), the distance between data x_i to the clustering center c_k is expressed as $D_k(c_k, x_i)$, it is usually Euclidean norm. K-means algorithm is used as a search operator which is called K-means arithmetic operator. This design can accelerate the convergence speed of the hybrid algorithm.

4 The Description of Hybrid Algorithm

Assuming data set for the sample size as n , setting the dimension of the sample as l the clustering number as c . This algorithm can be described as following:

Step 1: Affinity value computation

In this algorithm, the individual data adopts float encoding based on clustering centers and each antibody S is consisted of c clustering centers, so the antibody can be expressed as float code string, the length is $c \times l$. The fitness function of antibody also means the affinity function of antigen and antibody. The affinity function β_i can be get from the objective function, it is expressed as this:

$$\beta_i = 1/Q = 1 / \sum_k^K \sum_{p \in C_l} D_{ik}^2(c_k, x_i) \quad (2)$$

In Eq(2), Q is the means square error function, as for the K-means algorithm, the individual with a small Q value(that is, the sum of discrete degree within class is small) has a big fitness value and has a good clustering effect.

The similarity degree between the antibodies is reflected by the affinity value between the antibodies. When the antibodies are more similar, and the affinity value between them is much larger, conversely, the affinity value is smaller. Set α_{ij} as the affinity value of the $i-th$ input data x_i between the $j-th$ data center c_j , α_{ij} is defined as:

$$\alpha_{ij} = \frac{1}{1 + \|x_i - c_j\|} \quad (i = 1, 2, \dots, N, j = 1, 2, \dots, H) \quad (3)$$

In Eq (3), the distance between two antibodies adopts Euclidean distance.

Step 2: Memory cells and the inhibition of cell differentiation

The antibody concentration γ_i can be calculated by the following formula:

$$\gamma_i = \frac{\sum_{n=1}^N S_{ij}}{N} \quad (4)$$

$$S_{ij} = \begin{cases} 1 & \alpha_{ij} \geq t \\ 0 & otherwise \end{cases} \quad (5)$$

In the Eq (4), t_1 is the threshold, N is the population size, that is the number of antibody in the antibody sets. In this way, if the concentration reaches a degree, the similar antibodies can be considered as the same antibody.

When the concentration γ_i of one antibody i exceeds the threshold t_1 , this indicates that this antibody has the absolute superiority in the antibody population size. In other way, this antibody reaches a relative optimal. The memory cell can be produced at this time which is used to record the optimal antibody in this local area. Because of the limited amount of memory cells, when the number of memory cell reaches the upper limit M , computing the affinity value between the preserved and differentiated antibodies. The memory cells with high affinity will be replaced by the new differentiated cells. At the same time, the memory cell can be seemed as inhibiting cell, and the antibody and inhibiting cell with high adhesion will be restrained by following antibody survival rate calculation.

The main idea of adopting memory cell as inhibiting cell is to ensure the new antibody no longer drop into the original local optimal.

Step 3: Antibody survival rate computation and survival choices

Survival choices can be come out by the method of Roulette law, that is, according the elimination rate, the antibodies which have low Survival rate may be eliminated. Therefore, the eliminated antibodies are replaced by some individuals that are randomly produced. This process is named immune complement. When the bonding force of antigens and antibodies is bigger, the Survival ability of antibody is stronger.

However, when the bonding force of antibodies and inhibiting cells is bigger, the Survival ability of antibody is weaker. As a result, the similar antibodies can inspire each other and improve Survival ability each other. In this way, the convergence property of the nearby optimal point can be improved.

$$e_j = A_j \frac{\prod_{w=1}^k (1 - L_{wj}^k)}{\gamma_j \sum_{i=1}^N A_i} \quad (6)$$

$$L_{ij} = \begin{cases} \beta_{ij} & \beta_{ij} \geq t_2 \\ 0 & otherwise \end{cases} \quad (7)$$

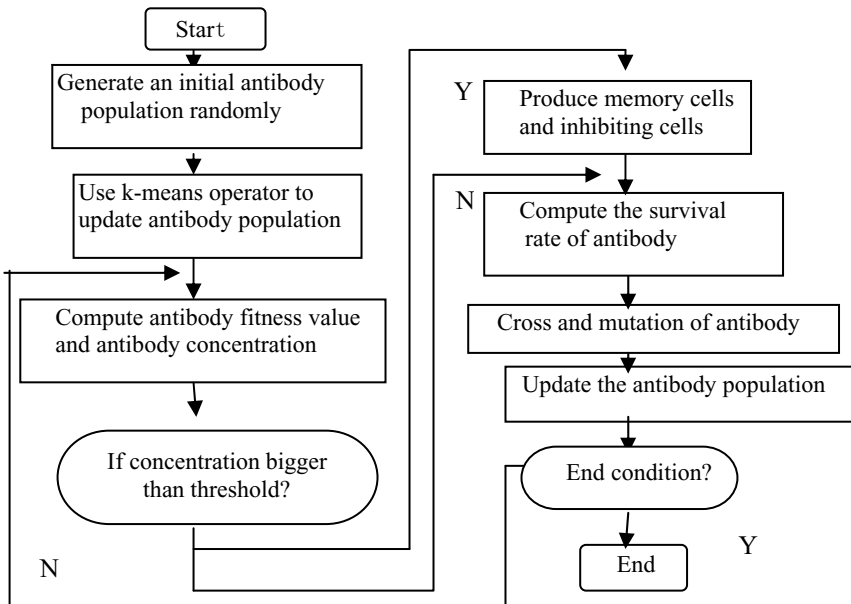
In Eq (6), e_j is the antibody survival rate, A_i is inhibiting cell number, k is the inhibition index, it can be taken for 1, in Eq(7), t_2 is the affinity threshold.

Step 4: Cross and mutation

The definition of gene matching cross operation based on most neighboring law is: set two Chromosomes as $l_1 = c_1^{(1)}c_2^{(1)}...c_k^{(1)}$ and $l_2 = c_1^{(2)}c_2^{(2)}...c_k^{(2)}$, these two Chromosomes are used to be crossed. Choosing each $c_i^{(1)}$ in l_1 cross with $c_j^{(2)}$ that is closest from $c_i^{(1)}$, this process is called $c_i^{(1)}$ and $c_j^{(2)}$ matching. During the genes matching, in order to keep the genes of l_1 and l_2 matching with each other, the pairing of gene would no longer take part in the Subsequent matching. Then the l_2 is given a new order l_2' according to the order of genes matching. Finally choosing the cross point randomly to carry out the single cross, and the new individuals l_1' and l_2' can be obtained.

The operation of mutation must follow the gene position. The float-point number in each gene position makes random mutation according to mutation probability, and the mutated gene position can be replaced by a random number which is evenly distributed in the mutation scale. However, the mutation scale is inversely proportional with the individual fitness value.

In this algorithm, the eliminated antibodies are replaced by some new produced antibodies that are randomly produced. In addition, for the surviving antibodies and the newly produced antibodies, copying quarter of the antibody sets, supposing the one with high expectance may be chosen, and the pairs of antibodies continue to cross and produce new antibodies. To the new antibodies, the genes are changed according to the pre-settable mutation rate and mutation operation approach. The flowchart for the hybrid clustering method is following:

**Fig. 1.** The flowchart for the hybrid clustering method

5 Simulation Experiment

Do simulation experiment under the environment of VC++ and MATLAB and based on the algorithm of K-means and hybrid clustering respectively. The parameters settings are: cross probability $P_c = 0.2$; mutation probability $P_m = 0.02$; mortality rate $P_e = 0.2$; concentration threshold $\gamma_c = 0.5$; Affinity threshold $t_1 = 0.9$; $t_2 = 0.5$, memory cells quantity $M = 30$, population size $N = 20$. Algorithm iterative 50 times is over. The experimental data adopts Iris3 Fisher with plant 150 sample data and does 20 times test, each of the samples for four dimension vector respectively represent four attributes plant. Two algorithms run separately 20 times, compute the maximum, minimum and average distance of within clusters E_k and the distance between clusters D_k . Experimental results are as following, the times in the table refer to the iteration times when the algorithm achieves optimal solution.

Table 1. The results of clustering based on different algorithms

Algorithm	$E_k \max$	$E_k \min$	$E_k \text{avg}$	$D_k \max$	$D_k \min$	$D_k \text{avg}$	T
K-means algorithm	11.569	6.387	8.987	6.097	3.625	4.861	32
Immune algorithm	11.402	6.186	8.532	6.465	3.896	5.153	26
Hybrid algorithm	11.013	5.943	8.483	7.032	4.072	5.602	19

The perfect result of clustering algorithm is to obtain the minimal distance within cluster and the maximal distance between clusters at the same time. From the data in the table above, it can be analyzed that the standard K-means algorithm is sensitive to the initial center, so that it is easy to drop into local optimal and converge too early and appear premature convergence if the center choose not correctly. The proposed hybrid clustering algorithm proposed in this paper is superior to K-means algorithm in global searching ability. Therefore, the obtained clustering results can get stronger stability, and the randomly distributed data clustering has obvious superiority. Meanwhile, from the solution of achieving optimal iteration times, the proposed algorithm with less average iteration times than K-means algorithm when obtaining the optimal value, obviously, the proposed algorithm has a faster convergence speed.

6 Conclusion

In this paper, the principle of artificial immune is applied for the data clustering and the proposed algorithm shows its superiority in acquiring global optimal solution. The hybrid clustering algorithm based on artificial immune is that considering K-means algorithm as a search operator, On the basis of simulating evolution algorithm, the immune memory, inhibiting cells and immune complement operator are added in the algorithm, as a result, this algorithm can search the global optimal quickly and effectively. The experimental tests indicate that the proposed hybrid algorithm is superior to the performance of k-means algorithm and artificial immune algorithm.

Acknowledgments. This paper is supported by the Natural Science Foundation of Jiangsu Province of China(No.BK2009131), and the foundation of innovative team of suzhou vocational university(No. 3100125).

References

1. Xu, Y., Chen, C., et al.: An Improved Clustering Algorithm For k-means. J. Computer Application and Software 25, 275–277 (2008)
2. Park, H.S., Jun, C.H.: A Simple and Fast Algorithm for K-means Clustering. J. Expert Systems with Applications 36, 3336–3341 (2009)
3. Yang, X.: Research of Key Techniques in Cluster Analysis. D. Hangzhou Zhejiang University (2005)
4. Yang, F.: Adaptive Clone and Suppression Artificial Immune Algorithm. J. Application Research of Computers 28, 481–484 (2011)
5. Mo, H.: Principle and Application of Artificial Immune System. Harbin industrial university press, Harbin (2002)
6. Liu, T., Wang, Y., et al.: A Cluster Algorithm Based on Artificial Immune System. J. Computer Project and Design 25, 2051–2053 (2004)
7. Ding, Y., Ren, L.: Artificial Immune System. J. Theory and Application Pattern Recognition and Artificial Intelligence 13, 12–14 (2000)

Succinct Initialization Methods for Clustering Algorithms

Xueru Liang¹, Shangkun Ren¹, and Lei Yang²

¹ School of Computer Sci. & Tec., Tianjin University, China

² College of Science, China University of Petroleum, China

liangsnowru@163.com, wronsky@tju.edu.cn, yang_lei_famous@126.com

Abstract. In this paper, we focus on the problem of unsupervised clustering of a data-set. We introduce the traditional K-Means (K-means) cluster analysis and fuzzy C-means (FCM) cluster analysis of the principles and algorithms process at first, then a novel method to initialize the cluster centers is proposed. The idea is that the cluster centers' distribution should be as evenly as possible within the input field. A “Two-step method” is used in our evolutionary models, with evolutionary algorithms to get the initialized centers, and traditional methods to get the final results. Experiment results show our initialization method can speed up the convergence, and in some cases, make the algorithm performs better.

Keywords: Clustering, K-means, fuzzy C-means, Genetic algorithm, Particle Swarm Optimization.

1 Introduction

We consider the general unsupervised clustering problem, i.e., given a set of data points, to find a method to classify all the data points into a number of clusters, say, k clusters.

As a main tool of unsupervised learning, cluster analysis has been widely used in data mining and pattern recognition. It is one of the most basic and common problems in fields like pattern analysis, data mining, document retrieval, image segmentation and decision making, etc. [1][2]

Former experts proposed some methods clearly to solve this problem, among which, K-means is the most celebrated and widely used clustering technique [1][2] while the Principal Direction Divisive Partitioning (PDDP) algorithm is a recently proposed technique [3][4][5][6].

In this paper, we propose a novel and simple method to initialize the cluster centers. In our experiment, this indeed make the convergence speed faster.

2 Related Work

There are many methods to do clustering, among which, K-means and FCM are the most classical methods. Some existing evolutionary algorithms can be used

for improving the precision of clustering. Although the traditional K-means and FCM are both simple and algorithms for fast convergence, they can be trapped in local optimum easily while Genetic algorithm and Particle Swarm Optimization algorithm have a strong universal, with the characteristics of global optimization.

2.1 Traditional Clustering Method

K-means is the most celebrated and widely used clustering technique [1] [2] [7] [8] [9] [10]. The basic steps of K-means are: initialize the k cluster centers, classify every object in the data set into the nearest cluster, then update the cluster centers by averaging the objects belonged to each cluster, do these again and again until convergence.

This algorithm aims at minimizing an objective function:

$$J = \sum_{i=1}^N \sum_{j=1}^k \|\mathbf{x}_i^{(j)} - \mathbf{c}_j\|^2 \quad (1)$$

where k stands for the number of clusters, N for the number of objects, \mathbf{c}_j is the center of the j th cluster. It can be proved that K-means will terminate after some steps, but it may not get the optimal solution. Sometimes it terminates in a local optimal point, for example, a saddle point.

Fuzzy c-means (FCM) [11] is a method of clustering which allows one piece of data to belong to two or more clusters. The relationship between objects and clusters can be described by the membership matrix:

$$\begin{pmatrix} r_{1,1}, & r_{1,2}, & \cdots, & r_{1,k} \\ r_{2,1}, & r_{2,2}, & \cdots, & r_{2,k} \\ \vdots & \vdots & \ddots & \vdots \\ r_{N,1}, & r_{N,2}, & \cdots, & r_{N,k} \end{pmatrix}$$

where r_{ij} denotes for the possibility that object i belongs to cluster j . It is based on minimization of the following objective function:

$$J_m = \sum_{i=1}^N \sum_{j=1}^k r_{ij}^m \|\mathbf{x}_i - \mathbf{c}_j\|^2, \quad 1 \leq m < \infty \quad (2)$$

where m is a fixed parameter.

2.2 Genetic Algorithm

Genetic algorithm (GA) [12] is a highly parallel, random and adaptive searching algorithm that is developed by drawing lessons from natural selection and evolution mechanism of nature. It can be divided into three steps: selection, crossover and mutation. To use a genetic algorithm, you must represent a solution to your problem as a genome (or chromosome). The genetic algorithm then creates a population of solutions and applies genetic operators such as mutation and crossover to evolve the solutions in order to find the best one(s).

2.3 Particle Swarm Optimization

Particle swarm optimization (PSO)[\[13\]](#) is a population based stochastic optimization technique developed by Dr. Eberhart and Dr. Kennedy in 1995, inspired by social behavior of bird flocking or fish schooling.

Each particle keeps track of its coordinates in the problem space which are associated with the best solution (fitness) it has achieved so far. (The fitness value is also stored.) This value is called *pbest*. Another “best” value that is tracked by the particle swarm optimizer is the best value, obtained so far by any particle in the neighbors of the particle, called *lbest*. When a particle takes all the population as its topological neighbors, the best value is a global best called *gbest*.

3 A Novel Method of Initializing Cluster Centers

We assume that every cluster follows a Gauss distribution, and the peaks distribute uniformly in the input domain. An example of 1-Dimensional data can be seen in Fig.1.

As K-means and FCM can be trapped by local optimal solution easily, it is very important to make a good initialization. Following the assumption we set the initialized centers uniformly distributed in the input domain. When we get the input data, the first step is to find the minimum and maximum value for each dimension. Formally, assume the input data is d -dimensional, firstly, we find two vectors: $\{min_i\}_{i=1}^d$ and $\{max_i\}_{i=1}^d$ standing for the minimum and maximum values for each dimension. This can be seen as the input domain. For example, for a 2-dimensional data set, we can get a squared area as the input domain. When we get the input domain, the initialized centers can be located uniformly in it. An example of 2-dimensional data of 4 clusters can be seen in Fig.2. Where the crosses stand for the initialized cluster centers, the dots for the data points and the square of dashed lines stand for the input domain.

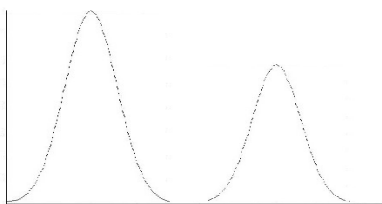


Fig. 1. Assumed Distribution of 1-Dimensional Data

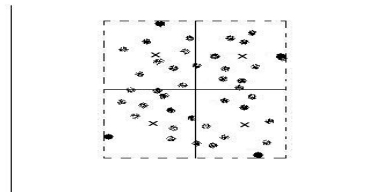


Fig. 2. Initialized centers of 2-Dimensional Input Data

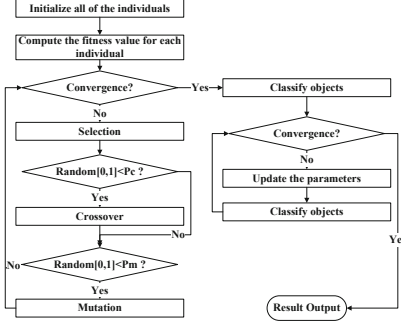


Fig. 3. Flowchart of the GA based clustering algorithm

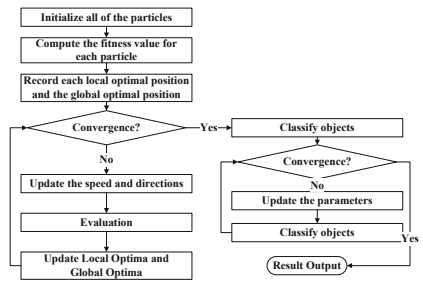


Fig. 4. Flowchart of the PSO based clustering algorithm

4 Evolutionary Clustering Models

Familiar with [14] and [15], we invite some evolutionary algorithms to help finding good initialized centers.

4.1 Clustering Model Inspired by GA

We treat each cluster as a chromosome, and the gene of individual can be represented by a $k \times d$ matrix:

$$ind_i \cdot gene = \begin{pmatrix} g_{1,1}, g_{1,2}, \dots, g_{1,d} \\ g_{2,1}, g_{2,2}, \dots, g_{2,d} \\ \vdots & \vdots & \ddots & \vdots \\ g_{k,1}, g_{k,2}, \dots, g_{k,d} \end{pmatrix}$$

where k is the number of clusters and the data is d -dimensional. As for the evaluation function, we can use the reciprocal of the objective function of K-means (or FCM):

$$f(\mathbf{x}) = \frac{1}{c(\mathbf{x})} = \frac{1}{\sum_{i=1}^N \sum_{j=1}^k \|\mathbf{x}_i^{(j)} - \mathbf{c}_j\|^2} \quad (3)$$

$$f(\mathbf{x}) = \frac{1}{c(\mathbf{x})} = \frac{1}{\sum_{i=1}^N \sum_{j=1}^k r_{ij}^m \|\mathbf{x}_i - \mathbf{c}_j\|^2} \quad (4)$$

The clustering model, which named “GA-K-means” and “GA-FCM”, can be described as the following flowchart Fig.3, where p_c is the probability of crossover while p_m is the probability of mutation.

4.2 Clustering Model Inspired by PSO

All the cluster centers are treated as a particle and each particle has its own position ($par_i.position$), direction ($par_i.direction$) and speed. What they are looking for is the best position for each cluster center. During searching, every particle exchanges information with other ones. The fitness functions can be set the same as GA-based model[16]. Fig.4. describes this algorithm clearly.

5 Experiment Results

5.1 Data and Experimental Setup

We use the Iris and Wine data set as our testing data set. Furthermore, we select some data points from “Checkerboard”, it is 2-dimensional, making it visualizable. Iris is perhaps the best known database to be found in the pattern recognition literature. The data set contains 3 classes of 50 instances each, where each class refers to a type of iris plant. One class is linearly separable from the other two; the latter are not linearly separable from each other. The Wine data are the results of a chemical analysis of wines grown in the same region in Italy but derived from three different cultivars. The analysis determined the quantities of 13 constituents found in each of the three types of wines.

The convergence speed of traditional algorithms with cluster centers initialized arbitrarily and the algorithms with cluster centers initialized by our method are compared with each other. The parameters in GA are also discussed, and different algorithms are compared with others.

5.2 Main Result

We choose C++ as the programming Language for the implementation for K-means and FCM, as well as the GA-based and PSO-based algorithms. The K-means algorithm with centers initialized randomly is denoted as *K-means* while the other one with centers initialized by our method is denoted as *Uniform-K-means*. The convergence speed of *K-means* and *Uniform-K-means* are compared. The comparison results can be seen in Fig.5 and Fig.6. In our first experiment, *K-means* terminates after 12 steps of iteration while *Uniform-K-means* terminates after only 5 steps; In the second trial, *K-means* terminates after 13 steps while *Uniform-K-means* terminates after 9 steps. In both experiments, they get the same clustering precision. We choose Checkerboard data as an intuitive example to show the clustering result of *FCM*, *GA*, *GA-K-means* and *PSO-K-means*. In the experiment, *GA-K-means* and *PSO-K-means* get the best result. When it comes to *GA-K-means* and *PSO-K-means* we use a “two-step” method: use *GA* or *PSO* to get initialized centers, then K-means is used to get the final result. The final results can be seen in Fig.7. FCM get the wrong result while GA get a better but not perfect result, however, both “Two-step method” get the perfect result.

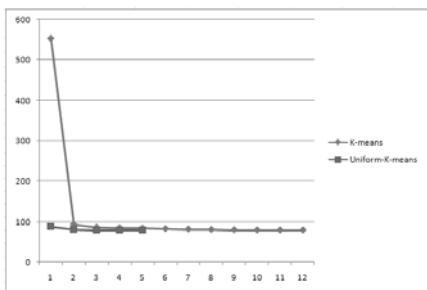


Fig. 5. Convergence Speed Comparison on Iris Data Set. K-means terminates after 12 steps of iteration while Uniform_K-means takes only 5 steps.

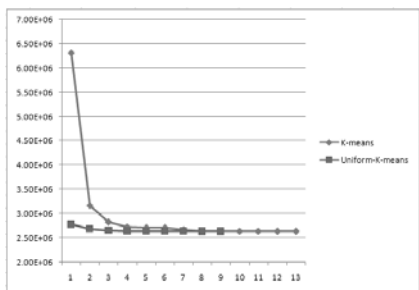


Fig. 6. Convergence Speed Comparison on Wine Data Set. K-means terminates after 13 steps while Uniform_K-means takes only 9 steps.

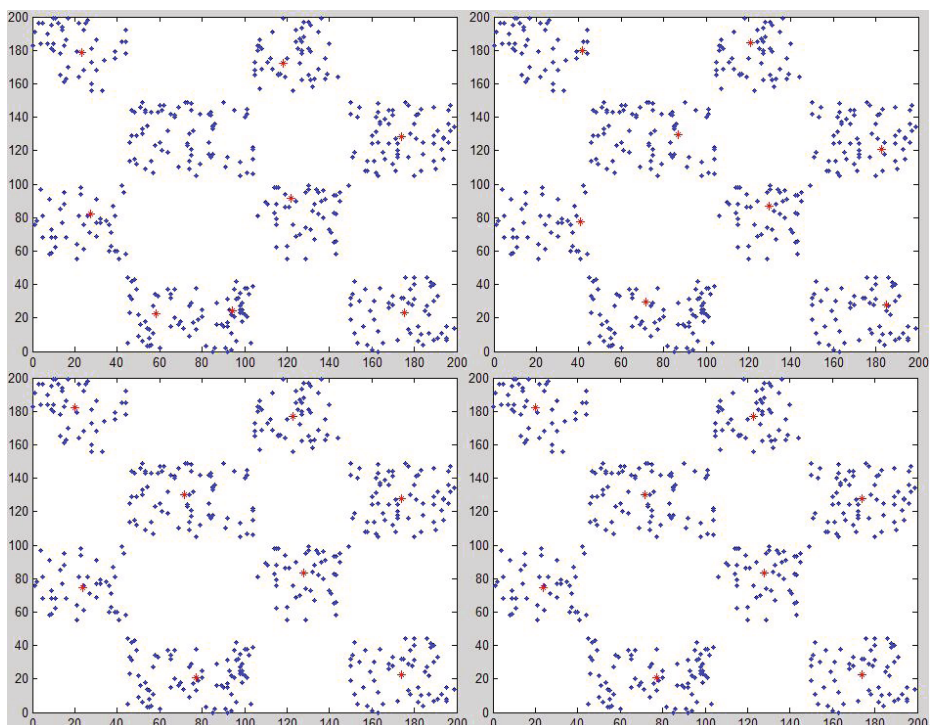


Fig. 7. CheckerBoard results comparison. Topleft-FCM, Topright-GA, Bottomleft-GA-K-means, Bottomright-PSO-K-means. The objects are shown as blue points while the cluster centers are shown as red stars.

When it comes to the clustering precision, we get the result shown in Table 1. The experiment result is obtained from the Wine data set. In this setting, the GA-based methods get the best result while only *Uniform_FCM* can compete with them.

Table 1. Clustering Precision on Wine Data Set

	Number of correct objects	Precision
<i>Uniform_K-means</i>	102	57.3034%
<i>Uniform_FCM</i>	123	69.1011%
<i>GA_K-means</i>	125	70.2247%
<i>GA_FCM</i>	124	69.6629%
<i>PSO_K-means</i>	117	65.7303%
<i>PSO_FCM</i>	122	68.5393%

5.3 Discussion of Parameters in GA

The mutation probability plays a very important role in GA. In our experiment, we set it from 0.1 to 0.3 and compare the results. The experiment results in Fig.8 indeed tell us something: with the larger mutation probability, the randomness of genetic algorithms gets larger, the local search capability would be weaker, and ultimately the optimal target value will be larger.

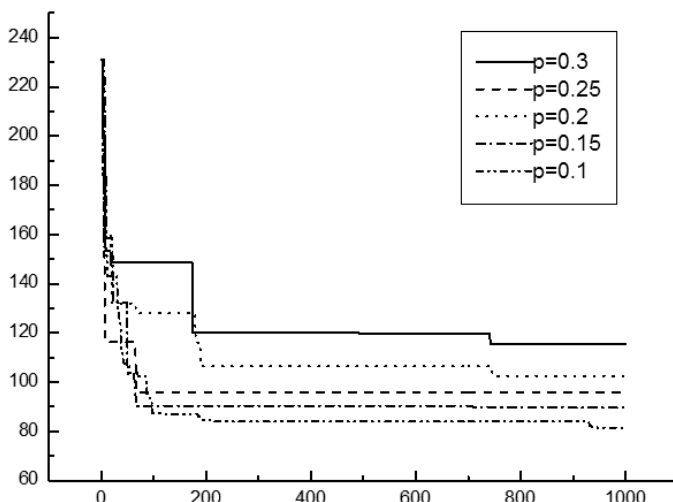


Fig. 8. Comparison of Different Mutation Probability. Horizontal axis stand for iteration steps while vertical axis stand for objective function values.

References

1. Gose, E., Johnsonbaugh, R., Jost, S.: Pattern Recognition and Image Analysis. Prentice-Hall, Englewood Cliffs (1996)
2. Jain, A.K., Murty, M.N., Flynn, P.J.: Data Clustering: a Review. ACM Computing Surveys 31(3), 264–323 (1999)
3. Boley, D.L.: Principal Direction Divisive Partitioning. Technical Report TR-97-056, Dept. of Computer Science, University of Minnesota, Minneapolis (1997)
4. Boley, D.L.: Principal Direction Divisive Partitioning. Data Mining and Knowledge Discovery 2(4), 325–344 (1998)
5. Boley, D.L., Gini, M., Gross, R., Han, S., Hastings, K., Karypis, G., Kumar, V., Mobasher, B., Moore, J.: Partitioning-Based Clustering for Web Document Categorization. Decision Support Systems 27(3), 329–341 (2000)
6. Boley, D.L., Gini, M., Gross, R., Han, S., Hastings, K., Karypis, G., Kumar, V., Mobasher, B., Moore, J.: Document Categorization and Query Generation on the World Wide Web Using WebACE. AI Review 13(5-6), 365–391 (2000)
7. Jim, Z.C.L., Tsung, J.H.: Fast global k-means clustering using cluster membership and inequality. Elsevier Science Inc., 655 Avenue of the Americas New York (2010)
8. Forgy, E.: Cluster Analysis of Multivariate Data: Efficiency versus Interpretability of Classification. Biometrics, 768–780 (1965)
9. Jain, A.K., Dubes, R.C.: Algorithms for Clustering Data. Prentice-Hall advance reference series. Prentice-Hall, Upper Saddle River (1988)
10. Selim, S.Z., Ismail, M.A.: K-means-type Algorithms: a Generalized Convergence Theorem and Characterization of Local Optimality. IEEE Trans. on Pattern Analysis and Machine Intelligence 6(1), 81–86 (1984)
11. Liu, X.Y., Liu, X., Wang, M.: Fuzzy Clustering Method and Application. Computer Knowledge and Technology (2011)
12. Ling, W.: Intelligent Optimization Algorithm and its Application. Tsinghua University Press, Beijing (2001)
13. Ling, W., Bo, L.: Particle Swarm Optimization and Scheduling. Tsinghua University Press, Beijing (2008)
14. Krishna, K., Narasimha Murty, M.: Genetic K-means Algorithm. IEEE Trans. Syst. Man Cybern B Cybern 29(3), 433–439 (1999)
15. Niknama, T., Amirib, B.: An Efficient Hybrid Approach Based on PSO, ACO and k-means for cluster analysis. Applied Soft Computing 10(1), 183–197 (2010)
16. Ye, J.X., Lin, Q.: Fuzzy K-means Document Clustering Analysis Based on PSO Algorithm. Computer Engineering and Design (2009)

Variable Neighborhood Search for Drilling Operation Scheduling in PCB Industries

Yun-Chia Liang and Chia-Yun Tien

No 135 Yuan-Tung Road, Chungli City,
Taoyuan County, 320 Taiwan

ycliang@saturn.yzu.edu.tw, s945423@mail.yzu.edu.tw

Abstract. Among all types of production environment, identical parallel machines are frequently used to increase the manufacturing capacity of the drilling operation in Taiwan printed circuit board (PCB) industries. So when a manager plans the production scheduling, multiple but conflicting objectives are often considered. Unlike the single objective problem, the multiple-objective version no longer looks for an individual optimal solution, but a Pareto front consisting of a set of non-dominated solutions. The manager then can select one of the alternatives from the set. For this matter, our research aims at applying a variable neighborhood search (VNS) algorithm in the identical parallel machine scheduling problem (IPMSP) with two conflicting objectives: makespan and total tardiness. In VNS, two neighborhoods are defined – insert a job to a different position or swap two jobs in the sequence. To save the computational expense, one of the neighborhoods is randomly selected for the target solution which is also arbitrarily chosen from the current Pareto front. The proposed VNS algorithm is tested on a set of real data collected from a leading PCB factory in Taiwan and its performance is compared with well-known methods in the literature. The computational results show that VNS outperforms all competing algorithms – SPGA, MOGA, NSGA-II, SPEA-II, and MACO in terms of solution quality and computational time.

Keywords: Variable Neighborhood Search, Identical Parallel Machine, Makespan, Total Tardiness.

1 Introduction

The scheduling of drilling operation, one of the key machining operations carried out in the PCB factories, is a classical type of the identical parallel machines problems. In order to expand the manufacturing capacity and improve the performance of the bottleneck workstation, parallel machines are common solutions among all types of production environment alternatives. For the number of machines greater than two in a single objective case, the identical parallel machine scheduling problem (IPMSP) belongs to the class of NP-Hard [1]. Needless to say, when multiple but conflicting objectives are often the case for a production planning, such problem becomes more complicated and challenged. Thus very often, a Pareto front consisting of a set of

non-dominated solutions will be needed so that the manager can select one of the alternatives from the set while preparing the production plan. Some recent applications of identical parallel machines problem with multiple objectives can be found in [2, 3].

Since the multi-objective IPMSP is considered more difficult to solve, metaheuristics become potential candidates for solving techniques. Variable neighborhood search (VNS), first introduced by Hansen and Mladenović [4], is one of the lately proposed metaheuristics. Its main idea is to explore search space based on the systematic change of neighborhoods, and has been successfully employed to solve single objective combinatorial problems [4, 5]. While its current applications in multi-objective problems are considered limited, publications of VNS on multiobjective optimization can be found in [6, 7]. Therefore, multi-objective scheduling problems are still fresh areas for VNS. For that, this study aims at extending the application of VNS to the identical parallel machine scheduling problems with bi-objective – makespan and total tardiness minimization.

The rest of the paper is organized as follows. Section 2 describes the problem definition and the basic assumptions of the IPMSP investigated. Section 3 introduces the detailed procedure of the proposed VNS algorithm while Section 4 discusses the computational results of case studies that are collected from a leading Taiwan PCB factory. Finally, the concluding remarks are summarized in Section 5.

2 Identical Parallel Machine Scheduling Problems

The scheduling of identical parallel machines involves the assignment of multiple jobs onto the system architecture's processing components – a bank of machines in parallel. While there are n jobs are scheduled for processing on m identical parallel machines, this study regards two conflicting objectives as the makespan and total tardiness to be optimized simultaneously. The objectives can be formulated as follows:

$$\text{Min } C_{\max} = \text{Max}(C_1, C_2, C_3, \dots, C_m) \quad (1)$$

$$\text{Min } T = \sum_{i=1}^n T_i \quad (2)$$

where n denotes the number of jobs and m represents the number of machines. C_i is the completion time of job i , $T_i = \max\{C_i - d_i, 0\}$ denotes the tardiness of job i , C_{\max} represents the makespan and T denotes the total tardiness over n jobs. In addition, some basic conditions of the problem are assumed as follows:

- (1) All jobs can be processed on any of the parallel machines.
- (2) Each of the parallel machines can process at most one job at a time.
- (3) Each job has to be processed without interruption on one of the machines, i.e., jobs are non-preemptive.
- (4) All jobs are independent and available at time zero.
- (5) The processing time and the due date of the jobs, the number of jobs, and the number of machines are given and fixed.
- (6) No downtime is considered, and set up time is included in processing time.

3 Variable Neighborhood Search Algorithm

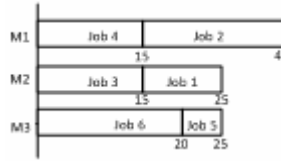
Hansen and Mladenović first proposed the VNS algorithm [4]. By employing the systematic change of neighborhoods, a local search-based VNS is able to avoid being trapped in the local optimum while attempts to reach to the global optimum. Thus, with such implementation of the VNS procedure, several issues have to be determined in advance; for instances (1) what neighborhood structure N_k and how many of them would be adopted; (2) the order of implementation among all N_k defined; (3) what search strategy should be adopted in changing neighborhoods. Lately, Geiger [6] developed a randomized variable neighborhood search to solve the multiple objective flow shop scheduling problem. Their VNS algorithm differs from the traditional single objective VNS algorithms on both random selection of neighborhoods and arbitrary selection of the base point among the unvisited non-dominated solutions. That is before conducting the neighborhood search, the base point is randomly picked from the set of non-dominated solutions not being performed in any neighborhood search yet. Next, one of the defined neighborhoods is arbitrarily selected and employed to the chosen solution. After the neighborhood search, the Pareto front is updated accordingly. This study is mainly based on Geiger's algorithm, but the detailed steps are designed according to the characteristics of the bi-objective IPMSP and will be justified in the following sections.

3.1 Initialization

During the initialization step, a set of neighborhood structures (N_k) and the stopping criterion are first determined. In the proposed VNS algorithm, two different neighborhood structures ($k = 1, 2$) are defined and the details will be introduced in Section 3.3. The stopping criterion in this study depends on the pre-determined maximum number of evaluations while the initial solution becomes the original member of the Pareto front. For that, the initial solution is generated by a two-phase approach, where a sequence of jobs is generated at random at the first phase, and a job-machine assignment rule - EAMF (Earliest Available Machine First) is used to assign jobs to the machines in the second phase. The principle of the EAMF rule is to assign the unscheduled jobs to the machine available at the earliest time among all others. For instance, suppose that a sequence of jobs is obtained accordingly as 4-3-6-2-1-5, with respect to their corresponding processing times shown in Table 1. Using the EAMF rule, the outcome will be illustrated in Figure 1 where six jobs are assigned to three machines at different timing.

Table 1. Numerical data of a 6-job example

Jobs	1	2	3	4	5	6
Processing Time	10	25	15	15	5	20

**Fig. 1.** An example of the initial solution

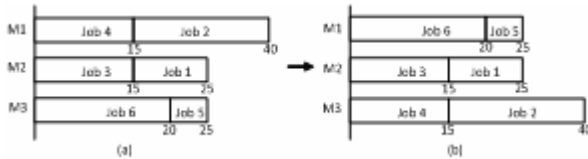
3.2 Shaking

The shaking operation, an important role of randomness in VNS, is implemented by randomly generating a neighboring solution of the current one based on the neighborhood structure presently visited. By doing this, VNS is able to extend itself from a purely deterministic local search technique to a stochastic one, i.e. provide a better chance to avoid trapping in local optima.

Furthermore, to offer a better starting point of neighborhood search in the proposed VNS algorithm, five neighboring solutions are randomly generated and then the best one is chosen as the base for the subsequent neighborhood search. Since this study considers two objectives simultaneously, the best solution here refers to the lowest values of both makespan and total tardiness among five neighboring solutions. If some of these five neighboring solutions are non-dominated to each other, one of them will be selected at random.

3.3 Neighboring Structure

This section depicts two types of neighborhood structures and illustrates each with an example. The neighborhood structures first involve the change in job sequence, and then employ the EAMF rule to determine the machine assignment.

**Fig. 2.** An example of neighborhood structure I

For neighborhood structure I (N_1), this structure exchanges positions of two jobs in the sequence and then assigns jobs to machines according to the EAMF rule. To avoid any possible redundant exchange causing no change in both objectives, the swap between both jobs located in the first position of different machines will not be considered. For instance, given the current job sequence as 4-3-6-2-1-5 as well *jobs* 4 and 6 swapped, the resulting sequence will become 6-3-4-2-1-5. Using the job processing times shown in Table 1, the current and new schedules are illustrated in Figures 2(a) and (b), respectively.

In neighborhood structure II (N_2), the procedure randomly selects a job from the sequence, and then inserts this job to a different position in the sequence. As a result,

jobs in the new sequence will also be assigned to machines based on the EAMF rule. Similar to N_1 , the insert moves may involve job transfer within a machine or between machines. For instance, given the current job sequence as 4-3-6-2-1-5, *job 1* is selected and inserted to the first position of the sequence which results in the new job order as such 1-4-3-6-2-5. Therefore, the current and new schedules will be illustrated in Figures 3(a) and (b), respectively. Although the makespan of the two schedules is identical, the total tardiness may change since the completion times of jobs 1, 5, and 6 have been changed.

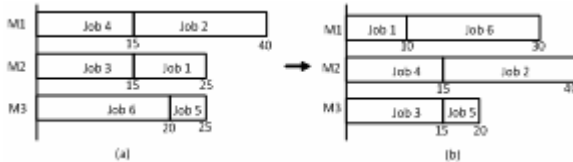


Fig. 3. An example of neighborhood structure II

3.4 Pareto Front Update

During the neighborhood search process, the approximated Pareto front, i.e. the set of non-dominated solutions, is updated using all the new neighboring solutions. To avoid ignoring or missing any potential solutions that could fit into the Pareto front, every solution being explored through the VNS procedure will be used to update the current Pareto front.

4 Case Study

This study implements the proposed VNS algorithm on a set of real data collected from the drilling operation in a Taiwan leading PCB factory. In this PCB application, the data are collected from three cases and each case consists of different combinations of jobs and machines in operation. Namely, Case one operates under 35 jobs and 10 machines, Case two under 50 jobs and 15 machines, and Case three under 65 jobs and 18 machines.

VNS is compared to several well-known multi-objective metaheuristics in the literature such as MOGA (multi-objective genetic algorithm), NSGA-II (non-dominated sorting genetic algorithm-II), and SPEA-II (strength Pareto evolutionary algorithm-II) [2]; some newly reported methods including SPGA (sub-population genetic algorithm) [2], and MACO (multi-objective ant colony optimization) [3]. To evaluate the performance of the competing algorithms, the measure $D1_R$ that considers both the convergence and diversification properties of a Pareto front is employed. $D1_R$ originally proposed by Ishibuchi et al. [8] computes the average value of minimum Euclidean distance formed by each non-dominated solution of the reference Pareto front to every non-dominated solution provided by a comparing algorithm. The details of $D1_R$ measure calculation can be found in [8]. For the comparison purpose, the objectives of each test problem are normalized so that minimum and maximum values of each objective among the reference solution are 0

and 100, respectively. In addition, the reference Pareto front is generated by the union of non-dominated solutions of SPGA, MOGA, NSGA-II, and SPEA-II that search five million solutions separately (provided by [2]).

To compare with competing algorithms, VNS is run 10 times for each case with different random number seeds and the stopping criterion for all algorithms is set to one million evaluations. Besides the $D1_R$ measures, the CPU time and the number of non-dominated solutions are also considered for evaluating the performance of each algorithm. Note that the number of non-dominated solutions obtained by each algorithm should be only considered as a secondary performance measure, since more non-dominated solutions don't necessarily guarantee the higher solution quality of the algorithm.

4.1 Solution Quality Comparison

Table 2 presents a statistical summary of performance measures for all 6 competing algorithms over 10 runs. The average (Avg), minimum (Min), and maximum (Max) values of $D1_R$, as well the average number of non-dominated solutions in the approximated Pareto front of the competing algorithm i (denoted by $|G_i|$) are evaluated among three cases. The best performance meaning the lowest $D1_R$ value and the highest $|G_i|$ value in each category is highlighted in bold.

In Case I, the smallest case with 35 jobs and 10 machines, VNS outperforms all competing algorithms in $D1_R$ statistics. Two latest algorithms in the literature SPGA and MACO perform comparably to traditional multi-objective evolutionary algorithms such as MOGA, NSGA-II, and SPEA-II. When the case size increases to the medium size of 50 jobs and 15 machines, similar performance can be found among algorithms. VNS is still superior to all other algorithms. The performance of MACO also improves and performs only next to VNS. In Case III, the largest case with 65 jobs and 18 machines, VNS once again shows its superiority in the competition. Moreover, the $D1_R$ values of most algorithms deteriorate quickly when the case size increases from the medium (Case II) to the large one (Case III); however, MACO is the only algorithm to keep the steady performance.

Table 2. Results of performance measures among competing algorithm over all three cases

Algorithm	Case I (35 jobs, 10 machines)				Case II (50 jobs, 15 machines)				Case III (65 jobs, 18 machines)			
	$D1_R$			$ G_i $	$D1_R$			$ G_i $	$D1_R$			$ G_i $
	Min	Avg	Max		Min	Avg	Max		Min	Avg	Max	
MOGA	8.1	16.4	29.8	20.5	17.1	18.9	20.7	32.6	26.7	28.5	30.4	31.9
NSGA-II	5.2	11.8	22.2	26.7	9.7	11.7	13.8	60.4	21.0	23.1	25.4	65.6
SPEA-II	4.8	10.4	22.5	26.8	7.7	10.3	12.9	41.7	17.0	18.9	20.9	47.8
SPGA	3.6	5.8	9.3	29.9	8.6	9.7	10.8	38.8	17.9	19.0	20.1	39.5
MACO	6.7	10.4	16.4	9.5	7.1	8.9	11.1	11.7	11.8	13.7	16.2	11.2
VNS	0.8	1.4	2.7	36.7	1.2	2.5	3.4	50.6	7.2	11.3	16.3	37.7

When considering the $|G_i|$ measure, NSGA-II provides the most number of non-dominated solutions among the competing algorithms. However, this advantage of NSGA-II has been offset by the inferiority of NSGA-II solution quality, i.e., the $D1_R$

value. On the other hand, VNS is able to offer quality and stable number of non-dominated solutions in all three cases, while MACO obtains the least number of non-dominated solutions in general.

4.2 Computational Effort Comparison

To evaluate the performance of algorithms, computational effort is another important measure next to the solution quality. In this study, to conduct a fair comparison, the stopping criterion of all algorithms is set to one million evaluations at maximum. Therefore, the computational effort of algorithms will be assessed on the basis of CPU time spent. The proposed VNS algorithm is coded in Borland 5.0 C++ Builder on a PC with Pentium4 2.8GB CPU and 512 MB RAM, and MACO is executed in a Pentium4 3.0GB PC with 512 MB RAM. SPGA, MOGA, NSGA-II, and SPEA-II are executed in the environment of Pentium4 2.4GB CPU with 512 MB memory. All algorithms are executed in similar settings.

Table 3 summarizes the average CPU time over 10 runs for all competing algorithms. VNS consumes the least computational expense while SPEA-II needs the most CPU time. MACO is the runner-up in the CPU time competition. In addition, with the increase of case size, VNS and MACO need the least CPU time and their changes are linearly flat. Meanwhile, SPEA-II is the least efficient algorithms and its CPU time increases tremendously when the case size increases.

Table 3. Comparison of average CPU time among all competing algorithms over three cases

Algorithm	Average CPU Time (seconds)		
	Case I (35 jobs, 10 machines)	Case II (50 jobs, 15 machines)	Case III (65 jobs, 18 machines)
MOGA	14.3	31.3	51.8
NSGA-II	30.9	60.2	97.3
SPEA-II	84.6	110.8	135.7
SPGA	22.6	51.8	88.6
MACO	12.7	21.7	29.5
VNS	11.4	19.4	27.9

5 Conclusions

The facts that multiple, yet conflicting, objectives are often encountered and, even more so, two conflicting objectives – makespan and total tardiness minimization have been identified in the PCB industries bring out the significance of this study. Although an identical parallel machine scheduling problem with multiple objectives has been discussed in several recent publications, few have implemented the variable neighborhood search algorithm to solve similar problems. More so, the VNS algorithm has accumulated some successful experiences on solving multi-objective problems. Thus, this study attempts to investigate on the VNS algorithm in a multiple-objective setting. In the VNS algorithm, two types of neighborhoods – insertion and swap of jobs are defined and random mechanisms are employed for neighborhood and the base solution selection. Three cases collected from a leading

PCB factory in Taiwan are used to evaluate the performance of VNS with leading multi-objective evolutionary algorithms MOGA, NSGA-II, SPEA-II, SPGA, and MACO in the literatures. Case studies show that VNS is able to provide stable and superior performance in both solution quality and computational expense. Furthermore, the simple structure and less number of parameters to be tuned up in VNS have accentuated its potential implementation in practice.

References

1. Garey, M.R., Johnson, D.S.: *Computers and Intractability: A Guide to the Theory of NP-Completeness*. W. H. Freeman, New York (1979)
2. Chang, P.C., Chen, S.H., Lin, K.L.: Two-phase Sub-population Genetic Algorithm for Parallel Machine Scheduling Problem. *Expert Syst. Appl.* 29(3), 705–712 (2005)
3. Liang, Y.C., Hsiao, Y.M.: A Multiple Ant Colony Optimization Algorithm for a Bi-objective Parallel Machine Scheduling Problem in Taiwan PCB Industries. In: The 3rd Annual Conference of the Operations Research Society of Taiwan, ORSTW074 (2006)
4. Hansen, P., Mladenović, N., Pérez, J.A.M.: Variable Neighborhood Search: Methods and Applications. *Ann. Oper. Res.* 175, 367–407 (2010)
5. Liang, Y.C., Chen, Y.C.: Redundancy Allocation of Series-parallel Systems Using a Variable Neighborhood Search Algorithm. *Reliab. Eng. Syst. Saf.* 92, 323–331 (2007)
6. Geiger, M.J.: Randomised Variable Neighbourhood Search for Multi Objective Optimisation. In: Proceedings of EU/ME Workshop: Design and Evaluation of Advanced Hybrid Meta-Heuristics, pp. 34–42 (2004)
7. Liang, Y.C., Lo, M.H.: Multi-objective Redundancy Allocation Optimization Using a Variable Neighborhood Search Algorithm. *J. Heuristics* 16(3), 511–535 (2010)
8. Ishibuchi, H., Yoshida, T., Murata, T.: Balance between Genetic Search and Local Search in Memetic Algorithms for Multiobjective Permutation Flowshop Scheduling. *IEEE Trans. Evol. Comput.* 7(2), 204–223 (2003)

Adaptive Weighted Fusion of Local Kernel Classifiers for Effective Pattern Classification

Shixin Yang¹, Wangmeng Zuo¹, Lei Liu¹, Yanlai Li¹, and David Zhang^{1,2}

¹ Biocomputing Research Centre, School of Computer Science and Technology,
Harbin Institute of Technology, Harbin 150001, China

² Department of Computing, The Hong Kong Polytechnic University,
Hung Hom, Kowloon, Hong Kong
shixyang@gmail.com

Abstract. The theoretical and practical virtual of local learning algorithms had been verified by the machine learning community. The selection of the proper local classifier, however, remains a challenging problem. Rather than selecting one single local classifier, in this paper, we propose to choose several local classifiers and use adaptive fusion strategy to alleviate the choice problem of the proper local classifier. Based on the fast and scalable local kernel support vector machine (FaLK-SVM), we adopt the self-adaptive weighting fusion method for combining local support vector machine classifiers (FaLK-SVMA), and provide two fusion methods, distance-based weighting (FaLK-SVMad) and rank-based weighting methods (FaLK-SVMar). Experimental results on fourteen UCI datasets and three large scale datasets show that FaLK-SVMA can achieve higher classification accuracy than FaLK-SVM.

Keywords: Kernel method, support vector machine, local learning, classifier fusion, nearest neighbors.

1 Introduction

Local learning algorithms (LLA) [1] are a class of learning algorithms to learn a local decision function for each test sample for classification. Compared with the global classifier, the generalization error could be further reduced by proper choice of the locality parameter in the local classifier [2]. Motivated by the virtues of LLA, several researchers independently extend support vector machine (SVM) [3] to its local formalization, local SVM [4, 5]. Local SVM is superior to SVM, and has been successfully applied to object recognition [4], remote sensing [5], and face recognition [6].

However, LLAs have several disadvantages. First, most LLAs are lazy learning methods. In the classification stage, intensive computational cost usually is required to determine the locality and to train a local classifier. Second, the choice of the proper locality parameter and local classifier remains a challenging problem. In order to enhance the computational efficiency, Cheng et al. [7] proposed a clustering method, MagKmeans. Recently, Segata and Blanzieri [8] developed a fast and scalable local kernel support vector machine (FaLK-SVM) method. Cover trees [9] are adopted to search the exact nearest neighbors, and a greedy method is used to solve

the minimum sphere set covering problem for the characterization of locality for the pre-computation of the local models [8, 10].

In this paper, we propose an adaptive fusion strategy to alleviate the difficulty in choosing appropriate local classifier of FaLK-SVM, named FaLK-SVMA hereafter. In FaLK-SVMA, we adopt a self-adaptive weighting fusion method for combining these local classifiers, and propose two fusion methods, distance-based weighting (FaLK-SVMA_d) and rank-based weighting methods (FaLK-SVMA_r). Experimental results show that FaLK-SVMA can achieve higher classification accuracy than FaLK-SVM.

The remainder of the paper is organized as follows: In Section 2, we first present a brief review of the FaLK-SVM method, and then discuss its disadvantages. In Section 3, we introduce our FaLK-SVMA methods. In Section 4, we give our experimental results on the fourteen UCI data sets and three large scale data sets. Finally, in Section 5, we conclude the paper by providing several concluding remarks.

2 FaLK-SVM

2.1 Brief Survey on FaLK-SVM

FaLK-SVM is a fast and scalable kernel method for pattern classification [8]. Conveniently, let χ be a training set $\{(\mathbf{x}_i, y_i) | i = 1, \dots, N\}$, where \mathbf{x}_i is the i th training sample, y_i is the class label of \mathbf{x}_i , and N is the number of training samples. Let the number of the nearest neighbors be k . In the training stage, FaLK-SVM chooses $k' \leq k$, and adopts a greedy method to obtain an (approximate) minimal k' -neighbourhood covering set of *centres* $\mathcal{C} \subseteq \chi$ [8, 10]. For each center $\mathbf{c} \in \mathcal{C}$, we train a local SVM classifier, using the k -nearest neighbors of \mathbf{c} . Thus $|\mathcal{C}|$ SVMs are trained and $|\cdot|$ is the cardinality of the set. In the test stage, given a sample \mathbf{x} , one can use cover trees [9] to search its nearest neighbors and the relevant model center located at \mathbf{c} with its k training samples $\{(\mathbf{x}_{r_c(i)}, y_{r_c(i)}) | i = 1, \dots, k\}$. Then the local SVM classifier in which \mathbf{c} is located can be used to classify the test sample \mathbf{x} ,

$$k\text{NN}\text{SVM}_{\mathbf{c}}(\mathbf{x}) = \text{sgn} \left(\sum_{i=1}^k \alpha_{r_c(i)} y_{r_c(i)} K(\mathbf{x}_{r_c(i)}, \mathbf{x}) + b_{\mathbf{c}} \right), \quad (1)$$

where $\mathbf{x}_{r_c(i)}$ denote the i th nearest neighbor of the center \mathbf{c} , $\alpha_{r_c(i)}$ denotes the local Lagrangian multiplier, and $b_{\mathbf{c}}$ denotes the local bias.

In the classification stage, there are two strategies to select the centre $\mathbf{c} \in \mathcal{C}$. For a test sample \mathbf{x} , one may select the local SVM classifier whose centre $\mathbf{c} \in \mathcal{C}$ is the nearest centre of the sample \mathbf{x} , $\mathbf{x}_{r_{\mathbf{x}}^{\mathcal{C}}(1)}$. Segata and Blanzieri named it as FaLK-SVMc,

$$\text{FaLK-SVMc}(\mathbf{x}) = k\text{NN}\text{SVM}_{\mathbf{c}}(\mathbf{x}), \quad \text{where } \mathbf{c} = \mathbf{x}_{r_{\mathbf{x}}^{\mathcal{C}}(1)}. \quad (2)$$

In addition, Segata and Blanzieri propose another strategy, FaLK-SVM, where we first find the nearest neighbor \mathbf{x}^{NN} of \mathbf{x} from the training set χ . If \mathbf{x}^{NN} is the j th nearest neighbor of the centre \mathbf{c}_l , then we choose the local classifier $k\text{NN}\text{SVM}_{cnt(\mathbf{x}^{NN})}(\mathbf{x})$ where $j_{cnt(\mathbf{x}_i)}$ is the minimal,

$$\begin{aligned} \text{cnt}(\mathbf{x}^{NN}) &= \text{choose}\left(\left\{\mathbf{c}_z \in \mathcal{C} \mid \mathbf{x}^{NN} = \mathbf{x}_{r_{\mathbf{c}_z}(h)}\right\}\right) \\ h &= \min\left(t \in \{1, \dots, k'\} \mid \mathbf{x}_{r_{\mathbf{c}_j}(t)} = \mathbf{x}^{NN}, \forall \mathbf{c}_j \in \mathcal{C}\right). \end{aligned} \quad (3)$$

The FaLK-SVM strategy can be written as,

$$\text{FaLK-SVM}(\mathbf{x}) = k\text{NSVM}_{\text{cnt}(\mathbf{t})}(\mathbf{x}), \quad \text{where } \mathbf{t} = \mathbf{x}^{NN}. \quad (4)$$

Based on the local risk minimization theory proposed by Vapnik and Bottou [2, 11], Segata and Blanzieri further discuss the generalization bounds for FaLK-SVM [8]. Moreover, the effectiveness of FaLK-SVM is also supported by recent theoretical results on consistency and localizability [12].

2.2 Discussion

Segata and Blanzieri [8] presented FaLK-SVMc and FaLK-SVM, for proper local classifier and each has own selection strategy for local classifiers. Although FaLK-SVM is superior to FaLK-SVMc in terms of the classification accuracy, one can not conclude that any of these assumptions are the optimal. Besides, the minimal k' -neighbourhood covering set may be only approximately optimal due to that the greedy method is adopted, and this would also make the selection of optimal local classifier more difficult.

On the other hand, for each centre \mathbf{c} , using its k -nearest neighbors we train a local SVM classifier $k\text{NSVM}_{\mathbf{c}}(\mathbf{x})$ to classify the test sample located in the k' -neighbourhood of the centre \mathbf{c} . Thus, if the test sample \mathbf{x} located in the k' -neighbourhood of several centres, maybe it is more appropriate to use all these local classifiers associated with the centres to classify \mathbf{x} .

3 Adaptive Fusion of Local SVM Classifiers

In this section, we first propose an improved FaLK-SVM method, FaLK-SVMA which select several local SVM classifiers and use a self-adaptive fusion method to classify the test samples. Then, several model selection issues related with FaLK-SVM and FaLK-SVMA, are provided.

3.1 The Adaptive Fusion Method

In FaLK-SVM and FaLK-SVMc, the local classifier $k\text{NSVM}_{\mathbf{c}}(\mathbf{x})$ is used to classify the test sample in the k' -neighbourhood of the centre \mathbf{c} . However, because the k' -neighbourhood covering set are overcomplete, one test sample may lie in the k' -neighbourhood of several centres $\{\mathbf{c}_1, \dots, \mathbf{c}_m\}$. In [8], two strategies select the local classifier corresponding to the proper one centre. We argue that proper combination of these local classifiers [13, 14, 15] could further enhance the classification accuracy.

In the classification stage, given the test sample \mathbf{x} , we first search the centres $\{\mathbf{c}_1, \dots, \mathbf{c}_m\}$ where \mathbf{x} lies in the k' -neighbourhood of the centre \mathbf{c}_i ($i = 1, \dots, m$). The classification result of the local classifier corresponding to the centre \mathbf{c}_i is,

$$y_{\mathbf{c}_i} = k\text{NSVM}_{\mathbf{c}_i}(\mathbf{x}). \quad (5)$$

We propose a self-adaptive weighted fusion method to combine the classification result $y_{\mathbf{c}_i}$. Let d_i be the distance between the sample \mathbf{x} and the centre \mathbf{c}_i . We assign the weight w_i to the classifier $k\text{NN}\text{SVM}_{\mathbf{c}_i}(\mathbf{x})$,

$$weight_i = (1/d_i)^a, \quad (6)$$

where $i = 1, \dots, m$, and a denotes the weight parameter with the default value 1.0. Moreover, the normalized weight of each model can be formed as follows,

$$w_i = \frac{weight_i}{\sum_{i=1}^m weight_i}. \quad (7)$$

Finally, we classify the test sample \mathbf{x} using the weighted fusion of the classifiers $k\text{NN}\text{SVM}_{\mathbf{c}_i}(\mathbf{x})$,

$$f(\mathbf{x}) = \sum_{i=1}^m w_i y_{\mathbf{c}_i}. \quad (8)$$

Hereafter we name the FaLK-SVMA with the weights defined in Eq. (7) as FaLK-SVMad.

Actually, there are other choices to determine the weight w_i . Let \mathbf{x}^{NN} be the nearest neighbor of \mathbf{x} from the training set. Suppose \mathbf{x}^{NN} be the k_i th nearest neighbor of the centre \mathbf{c}_i , one can define the weight w_i as,

$$w_i = \frac{(1/k_i)^a}{\sum_{j=1}^m (1/k_j)^a}, \quad (9)$$

where a denotes the weight parameter with the default value 1.0. Here we name the FaLK-SVMA with the weights defined in Eq. (9) as FaLK-SVMar. In [8], experimental results show that the FaLK-SVM strategy achieves higher accuracy than the FaLK-SVMc strategy. Thus we expect that FaLK-SVMar could also be effective to enhance the classification performance.

3.2 Model Selection

The choice of kernel function and the corresponding kernel parameter value is crucial for the performance of kernel methods. For both FaLK-SVM and FaLK-SVMA, we choose the Gaussian RBF kernel,

$$K(\mathbf{x}, \mathbf{x}') = \exp\left(-\frac{\|\mathbf{x} - \mathbf{x}'\|^2}{\sigma^2}\right) \quad (10)$$

where \mathbf{x} and \mathbf{x}' are two samples, σ is the parameter of the Gaussian RBF kernel.

One may choose the same σ value for all the local classifiers, and use the standard cross-validation method for model selection. In FaLK-SVM and FaLK-SVMA, we select the value of the parameter σ in an adaptive range determined by distances of samples. Besides, we set the k as a proportion of the size of the training set. Another parameter to be determined in the model selection of FaLK-SVMA is the soft margin regularization constant C . After choosing the range of each parameter, we use the κ -fold cross-validation method to determine the values of these parameters.

4 Experimental Results

In our experiments, we compare the classification performance of SVM, FaLK-SVM, and FaLK-SVMA. The source code of SVM is obtained from Lib-SVM library [16] and FaLK-SVM is obtained from [17]. We then implement the FaLK-SVMA code based on the FaLK-SVM source code. To evaluate the classification performance of FaLK-SVMA, we use fourteen data sets from the UCI machine learning repository [18], and three large scale data sets. For all the data sets, each of all the input characters is normalized to values within [-1, 1].

4.1 Experimental Results on the UCI Data Sets

Table 1 summarizes the information on the number of features d and the number of total instances N for each of the fourteen data sets.

The 10-fold cross validation (CV) method is adopted to determine the classifier parameters and to evaluate classification performance of the classifiers. For FaLK-SVM and FaLK-SVMA, there are three parameters to be determined, where C is chosen from $\{2^{-2}, 2^{-1}, \dots, 2^{10}\}$, the kernel parameter σ is chosen from $\sigma \in \{2^{-3}, 2^{-2}, \dots, 2^4, 2^5\}$ and the nearest neighbor parameter k is chosen from $k \in \{2^1, 2^2, \dots, 2^9, 2^{10}, N\}$. For the value of the k' parameter, we simply let $k' = k/2$.

Table 2 lists the classification accuracy of each method on the fourteen UCI data sets. One can see that, for eight of the fourteen data sets, FaLK-SVMA achieves higher or equal classification accuracy than FaLK-SVM. For eleven of the fourteen data sets, FaLK-SVMar achieves higher or equal classification accuracy than FaLK-SVM. Moreover, FaLK-SVMA achieves the highest classification accuracy on five of the fourteen data sets, while FaLK-SVM and Lib-SVM achieves the highest classification accuracy on two of fourteen and only one of fourteen, respectively. Thus, FaLK-SVMA can obtain more accurate classification performance.

Table 1. Summary of the fourteen Data Sets

Data set name	# of features	# of samples
Sonar	60	208
Heart	13	270
Haberman	3	306
Liver	6	345
Ionosphere	34	351
Hill	100	606
Breast	10	683
Australian	14	690
Transfusion	4	748
Diabetes	8	768
Fourclass	2	862
tic_tac_toe	9	958
Man	5	829
Numer	24	1000

Table 2. Classification accuracy (%) of Lib-SVM, FaLK-SVM, FaLK-SVMad, and FaLK-SVMar on the fourteen UCI Data Sets

Data set name	Lib-SVM	FaLK-SVM	FaLK-SVMad	FaLK-SVMar
Sonar	87.50	90.38	91.83	91.35
Heart	82.22	84.44	84.81	84.44
haberman	74.51	76.72	76.72	76.72
Liver	71.59	74.20	74.20	74.20
ionosphere	93.73	94.87	94.87	95.16
Hill	63.20	65.29	64.46	64.46
Breast	96.63	97.22	97.51	97.36
australian	86.23	87.39	86.96	87.25
transfusion	78.07	79.41	79.28	79.41
diabetes	76.43	78.26	78.78	78.39
fourclass	99.65	99.88	99.77	99.88
Tic_tac_toe	99.90	99.69	99.58	99.69
man	82.63	83.21	83.21	83.21
numer	75.30	75.90	76.00	75.90

4.2 Experimental Results on the Large Scale Data Sets

In this section, we use three large scale data sets to further evaluate the classification accuracy of FaLK-SVMA, FaLK-SVM and SVM. In Section 4.1, because the size of the data set is limited, we do not adopt an independent validation set to evaluate the classification. Thus, we further use three large scale data sets, and split each of them into a training set and a test set. Based on the training set, we determine the values of the model parameters using 10-fold standard cross validation. We evaluate the classification performance of each method based on the results obtained on the test set.

Table 3. Summary of the three large scale data sets

Data set name	# of features	# of training points	# of testing points
Splice	60	1000	2175
Astro	4	3089	4000
a1a	119	1605	30956

Table 4. Classification accuracy (%) of Lib-SVM, FaLK-SVM, FaLK-SVMad, and FaLK-SVMar on the three large scale data sets

Data set name	Lib-SVM	FaLK-SVM	FaLK-SVMad	FaLK-SVMar
splice	87.72	90.06	89.42	89.42
astro	95.50	96.25	96.05	96.40
a1a	80.81	84.27	83.72	84.38

From Table 4, one can see that, FaLK-SVMar achieve higher classification accuracy. Thus, FaLK-SVMA can obtain more accurate classification performance than FaLK-SVM. Moreover, although FaLK-SVMA is an improvement of FaLK-SVM, in the training stage FaLK-SVMA does not add any computational cost. In the test stage,

since the number of the local classifiers to be fused is limited, FaLK-SVMA would only add little computational cost than FaLK-SVM.

5 Conclusion

In this paper, we proposed an improved FaLK-SVM method, FaLK-SVMA. Considering that one test sample may lie in the k' -neighbourhood of several centres $\{\mathbf{c}_1, \dots, \mathbf{c}_m\}$, rather than choosing a proper centre \mathbf{c} to select the local classifier, we suggest that proper combination of these local classifiers would be more effective for enhancing the classification accuracy. Then we propose a self-adaptive weighted fusion method to combining the local SVM classifiers. Experimental results on fourteen UCI data sets and three large scale data sets show that FaLK-SVMA can achieve higher classification accuracy than FaLK-SVM.

In manifold learning [19, 20, 21], local learning algorithms have also been very promising in the construction of the global consistent dimensionality reduction model. Moreover, using the kernel trick, Bengio et al. [22] have proposed a method to build a kernel model for out-of-sample extension. In our future work, we will further improve the FaLK-SVM method, and study whether there is an individual global consistent model for representing the FaLK-SVM classifier.

Acknowledgments. The work is partially supported by the National S&T Major Project of China (Grant No. 2008ZXJ09004-035) and the Natural Science Foundation of China (Grant No.s 60871033, 60902099, 61001037 and 61071179).

References

1. Bottou, L., Vapnik, V.: Local Learning Algorithms. *Neural Computation* 4(6), 888–900 (1992)
2. Vapnik, V., Bottou, L.: Local Algorithms for Pattern Recognition and Dependencies Estimation. *Neural Computation* 5(6), 893–909 (1993)
3. Vapnik, V.: Statistical Learning Theory. Wiley- Interscience, Chichester (1998)
4. Zhang, H., Berg, A.C., Maire, M., Malik, J.: SVM- KNN: Discriminative Nearest Neighbour Classification for Visual Category Recognition. In: IEEE International Conference on Computer Vision and Pattern Recognition, vol. 2, pp. 2126–2136 (2006)
5. Blanzieri, E., Melgani, F.: Nearest Neighbor Classification of Remote Sensing Images with the Maximal Margin Principle. *IEEE Trans. Geoscience and Remote Sensing* 46(6), 1804–1811 (2008)
6. Yang, T., Kecman, V.: Face Recognition with Adaptive Local Hyperplane Algorithm. *Pattern Analysis and Applications* 13(1), 79–83 (2010)
7. Cheng, H., Tan, P.-N., Jin, R.: Localized Support Vector Machine and Its Efficient Algorithm. In: SIAM International Conference on Data Mining (2007)
8. Segata, N., Blanzieri, E.: Fast and Scalable Local Kernel Machines. *Journal of Machine Learning Research* 11, 1883–1926 (2010)
9. Beygelzimer, A., Kakade, S., Langford, J.: Cover Trees for Nearest Neighbor. In: 23rd International Conference on Machine Learning (ICML 2006), pp. 97–104 (2006)

10. Wang, J., Neskovic, P., Cooper, N.L.: A Minimum Sphere Covering Approach to Pattern Classification. In: International Conference on Pattern Recognition, vol. 3, pp. 433–436 (2006)
11. Vapnik, V.N.: The Nature of Statistical Learning Theory. Springer, Heidelberg (2000)
12. Zakai, A., Ritov, Y.: Consistency and Localizability. Journal of Machine Learning Research 10, 827–856 (2009)
13. Kittler, J., Hatef, M., Duin, R.P.W., Matas, J.: On Combining Classifiers. IEEE Trans. Pattern Analysis and Machine Intelligence. 20(3), 226–239 (1998)
14. Liu, C.L.: Classifier Combination Based on Confidence Transformation. Pattern Recognition 38(1), 11–28 (2005)
15. Zhang, L., Zhou, W.D.: Sparse Ensembles Using Weighted Combination Methods Based on Linear Programming. Pattern Recognition 44(1), 97–106 (2011)
16. Chang, C.-C., Lin, C.-J.: LIBSVM: a Library for Support Vector Machines,
<http://www.csie.ntu.edu.tw/~cjlin/libsvm/>
17. Segata, N.: FaLKM-lib: a Library for Fast Local Kernel Machines,
<http://disi.unitn.it/~segata/FaLKM-lib/>
18. Asuncion, A., Newman, D.: UCI Repository of Machine Learning Data Sets,
<http://www.ics.uci.edu.cn/~mlearn/mlrepository>
19. Tenenbaum, J.B., de Silva, V., Langford, J.C.: A Global Geometric Framework for Nonlinear Dimensionality Reduction. Science 290, 2319–2323 (2000)
20. Saul, L.K., Roweis, S.T.: Think Globally, Fit Locally: Unsupervised Learning of Low Dimensional Manifolds. Journal of Machine Learning Research 4, 119–155 (2003)
21. Roweis, S.T., Saul, L.K.: Nonlinear Dimensionality Reduction by Locally Linear Embedding. Science 290, 2323–2326 (2000)
22. Bengio, Y., Paiement, J.-F., Vincent, P., Delalleau, O., Roux, N.L., Ouimet, M.: Out-of-sample Extensions for LLE, Isomap, MDS, Eigenmaps, and spectral clustering. In: Advances in Neural Information Processing Systems (NIPS 2003), vol. 16 (2003)

Improvement of LEACH Routing Algorithm Based on Use of Balanced Energy in Wireless Sensor Networks

Jie Chen

Department of Electronic & Information Engineering, Suzhou Vocational University,
Suzhou 215104, Jiangsu, China
cj@jssvc.edu.cn

Abstract. Based on the analysis of LEACH routing algorithm, this paper proposes a novel clustering algorithm(I-LEACH) which selects cluster heads according to the node's residual energy and distance with other cluster heads. In addition, the clusters send data to the base station by means of combination of single hop and multi-hop manner for saving cluster heads' energy. Simulation results show that compared with LEACH and P-LEACH, the improved algorithm can balance energy consumption among nodes, reduce the energy consumption and prolong the lifetime of the networks.

Keywords: wireless sensor networks, LEACH, balanced energy, cluster.

1 Introduction

With outstanding real-time detection and transmission capacity, Wireless Sensor Networks (WSNs) have been extensively applied in many scenarios [1], such as smart home system and wildlife monitoring. Because of work environment and the own limitations, replacing the batteries on thousands of nodes is infeasible. Thus, energy is a scarce resource in wireless sensor networks. Therefore, in the design of WSNs routing protocols, energy efficiency has become the prime consideration.

LEACH algorithm(low energy adaptive clustering hierarchy) is more representative of the optimization of energy efficiency in the use of hierarchical routing algorithm [2]. Based on LEACH algorithm, this paper proposes a novel clustering algorithm. For balanced energy consumption, the residual energy is brought into electing cluster heads as a parameter. By calculating the distance among cluster heads it controls the distributing of cluster heads. And it sends data to the base station by means of combination of single hop and multi-hop manner for saving nodes' energy.

2 LEACH Routing Algorithm

In the LEACH proposed by Heinzelman et from the MIT, the concept of cluster is first proposed, and it is also the first sub-cluster data fusion routing algorithm [3]. The algorithm runs by round. Each round has two phases, initialization phase and stable phase. The initialization phase is the stages of cluster formation, and the stable phase is

stage of readiness phase in which data is transmitted. In order to minimize energy consumption, the initialization phase lasts longer than the stable phase.

The basic idea of LEACH is to randomly select cluster heads in each round, and evenly distributes the energy consumption of the entire networks to each sensor node in the networks, which can reduce energy consumption and improve the networks lifetime. In the initialization phase, each node generates a random between 0 and 1. If the random number generated by a node is less than the set threshold $T(n)$, the node broadcasts to all nodes that it's the cluster head [4]. When a node is elected to cluster head, it will set its own threshold to 0, so that the node will not be re-elected as cluster head. $T(n)$ can be given by

$$T(n) = \begin{cases} \frac{p}{1 - p(r \bmod(\frac{1}{p}))} & n \in G \\ 0 & n \notin G \end{cases} \quad (1)$$

here p is the desire cluster head probability, r is the number of rounds now, G is the set of nodes that have not been elected cluster head in the last $1/p$ rounds.

After the election of cluster heads, cluster heads broadcast to all the nodes in the networks. Based on the received signal power, non cluster head nodes choose which cluster to join and inform the appropriate cluster head. Cluster head node receives the data sent by the nodes in the cluster, and integrates the data, then sends the data to the base station. Over time, the network re-enters into the next round of work cycle.

In LEACH, the energy model is first order radio model. The model of wireless sensor networks makes the following assumptions:

- (1) The position of the base station is fixed and is far away from the sensor nodes.
- (2) All sensor nodes in the networks are same and energy is limited.
- (3) Radio transmission in all directions has the same amount of energy consumption.

The power consumption for a transmitting node:

$$E_{TX}(l, d) = \begin{cases} l(E_{elec} + \varepsilon_{fs}d^2) & d < d_0 \\ l(E_{elec} + \varepsilon_{mp}d^4) & d \geq d_0 \end{cases} \quad (2)$$

The power consumption for a receiving node:

$$E_{RX}(l, d) = lE_{elec} \quad (3)$$

here l is the size of data packets transmitted, d is transmission distance, E_{elec} is sending or receiving circuit's power, ε_{fs} and ε_{mp} are the energy consumption coefficient of the amplifier, d_0 is threshold distance. When the transmission distance is less than the threshold distance, free space channel model is used. On the contrary, Multi-path fading channel model is used.

Because of the thought of clustering and the dynamic cluster head rotation, the LEACH protocol evenly distributes energy consumption to all nodes. So the lifetime of the networks is effectively prolonged. But there are also some problems [5]:

- (1) Because cluster heads are randomly selected, it may causes that cluster heads are too dense or low in some regions.
- (2) Fixed number of cluster structure doesn't consider optimization of the number.
- (3) The single-hop communications between cluster heads and sink node will lead cluster heads far away from the sink to die early.

3 Improved Algorithm of LEACH

3.1 The Choice of Cluster Head

(1) For balancing energy consumption, the residual energy is brought into electing cluster heads as a parameter [6,7]. The average residual energy of all nodes is used as the reference point. If the node's energy is lower than the average energy, the probability of becoming the cluster head reduces.

In order to reduce energy consumption, each node adds its own residual energy information to the data packet. After receiving all of the data packets, the base station calculates the average energy, and broadcasts it.

(2) Considering the cluster head density, if there are cluster heads existing near the node, the node's probability of becoming cluster head will reduces. We set the distance threshold to $d_0/2$ [8]. Reducation is impacted by the distance.

Taking into (1)(2), $T(n)$ can be given by

$$T(n) = \begin{cases} \frac{p}{1 - p \left(r \bmod \left(\frac{1}{p} \right) \right)} \times \frac{E_{nc}}{E_{na}} \times \min\left(1, \frac{d_{nmin}}{d_0/2}\right) & n \in G \\ 0 & n \notin G \end{cases} \quad (5)$$

here E_{nc} is the residual energy of the node n , E_{na} is the average energy of all nodes those still exist. d_{nmin} is the distance between the node n and the nearest cluster head.

3.2 Data Communication

(1) Data communication between node and cluster head

At the beginning of each transmission round r , every node uses the equation (6) to elect the cluster head which the node will communicate with. The node will choose the cluster head whose $P(i,j)$ is the largest as its own cluster head.

$$P(i, j) = \begin{cases} \frac{E_{cc}(j)}{E_{ca} \times d(i, j) \times d_{sink}(j)} & d \leq d_o \\ \frac{E_{cc}(j)}{E_{ca} \times d(i, j)^2 \times d_{sink}(j)} & d > d_o \end{cases} \quad (6)$$

here $E_{cc}(j)$ is the residual energy of the cluster head j , E_{ca} is the average energy of all cluster heads, $d(i,j)$ is the distance between the node i and the cluster head j , $d_{sink}(j)$ is the distance between the cluster head j and the base station.

(2) Data communication among cluster heads

For reducing energy consumption, the cluster sends data to the base station by means of single hop and multi-hop manner. All the clusters calculate the parameter $C(i,j)$. Then some cluster heads will send data to the base station directly when they are near the base station or their neighboring cluster heads don't have enough energy. The other cluster heads will send the data to the cluster head j whose $C(i,j)$ is the largest.

$$C(i, j) = \begin{cases} \frac{E_{currnt}(i)^2}{d(i, j) \times d_{sink}(i)} & d_{sink}(i) < d_{sink}(j) \\ 0 & d_{sink}(i) \geq d_{sink}(j) \end{cases} \quad (7)$$

here $d(i,j)$ is the distance between the cluster heads i and the cluster head j .

4 Simulation and Results

4.1 Simulation Settings

To validate the performance of the proposed algorithm, we simulate it in MATLAB, using the parameters given in Table 1 [9]. The networks is an $M \times M$ square area where $M=200m$. The base station located at 50 m, 175m.

Table 1. Simulation parameters

Parameter	Value	Comments
N	200	Number of nodes
E0	0.5 J	Node initial energy
L	4,000 bits	Data packet
C	100 bits	Broadcast packet
p	0.05	Optimal probability
EDA	5 nJ/bit/message	Energy for data aggregation
Eelec	50 nJ/bit	Electronic energy
emp	0.0013 pJ/bit/m ⁴	Transmit amplifier for $d \geq d_0$
efs	10 pJ/bit/m ²	Transmit amplifier for $d < d_0$

4.2 Simulation Results

We start with comparing the effects of our algorithm(I-LEACH), the LEACH and P-LEACH proposed in 2010 [10].

Figure 1 shows the networks lifetime. As we can see, I-LEACH algorithm gives a large flat networks lifetime compared with LEACH and P-LEACH. From Figure 1, the first node died after the 388 rounds in LEACH, the 625 rounds in P-LEACH, but in

I-LEACH, the first node died after the 726 rounds. So the lifetime of the networks prolongs obviously. when we have to monitor the whole network, all the networks regions must be monitored. If a node dies, maybe the zone covered by this node will be out surveillance, which is not tolerable for some applications. I-LEACH balances the energy cost over every networks nodes, so the node deaths occur in a relatively short time.

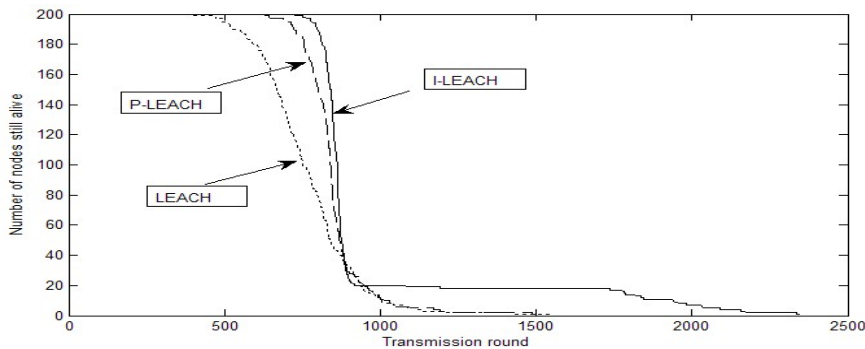


Fig. 1. Number of nodes still alive vs transmission rounds for network with 200 nodes

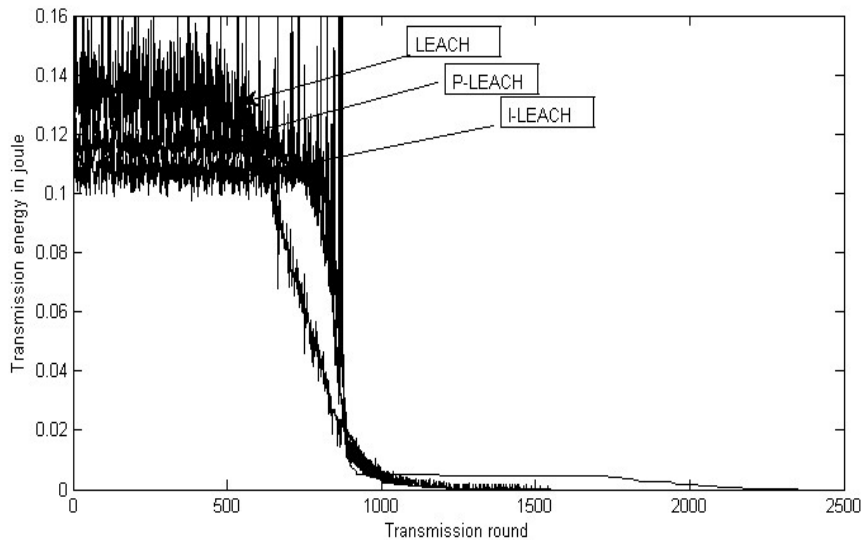


Fig. 2. Consumed energy per transmission round

Figure 2 shows the energy consumption per round. From the Figure2, we can see, at the beginning, I-LEACH algorithm costs the less energy than LEACH and P-LEACH. Then, after about 600 rounds, the energy consumed in I-LEACH becomes more than LEACH because the number of nodes still alive in I-LEACH is more than LEACH, so the transmission energy cost is greater in I-LEACH.

5 Conclusions

Routing algorithm in WSNs is an important part for which the goal is maximizing the system lifetime. In this paper, a novel clustering algorithm(I-LEACH) is proposed based on balanced and efficient energy. In the simulation results the networks lifetime, calculated until the first node dies prolongs, the entire networks will run for a long time. It means the new clustering algorithm can use the limited energy of the sensor nodes more efficiently.

Acknowledgments. This paper was supported by the Science Technology Foundation of Suzhou vocational university (No.SZD09L24).

References

1. Akyildiz, I.F., Su, W., Sankarasubramaniam, Y., Cayirci, E.: Wireless Sensor Network: A Survey. *Computer Networks* 38, 393–422 (2002)
2. Mingxia, G.U.: Provement and Simulation Research of Wireless Sensor Network LEACH Protocol. *Computer Simulation* 27, 139–141 (2010)
3. AlKarak, J.N., Kamal, A.E.: Routing Techniques in Wireless Sensor Network. *IEEE Wireless Communications* 11, 6–28 (2004)
4. Zhang, Q., Xiao, L.U., Chen, X.: Improvement of Low Energy Adaptive Clustering Hierarchy Routing Protocol based on Energy-efficient for Wireless Sensor Network. *Computer Engineering and Design* 32, 427–429 (2011)
5. Dai, S.J., Li, L.M.: High Energy-efficient Cluster-based Routing Protocol for WSN. *Application Research of Computers* 27, 2201–2203 (2010)
6. Li, C.Y., Shen, X.J., Chen, H.P., Sun, E.Y.: Research and Improvement of LEACH Routing Algorithm for Wireless Sensor Networks. *Chinese Journal of Sensor and Actuators* 23, 1163–1167 (2010)
7. Lin, N., Shi, W.H.: Simulation Research of Wireless Sensor Networks Based on LEACH Protocol. *Computer Simulation* 28, 178–181 (2011)
8. Zhang, X.X., Peng, J.: A Distributed Energy-efficient and Location-independent Coverage Clustering Protocol for Wireless Sensor Networks. *Journal of Sichuan University* 47, 1008–1014 (2010)
9. Bai, F., Kong, X.D., Mou, H.H.: An Improved Algorithm of LEACH Routing Protocol for Wireless Sensor Networks. *Computer & Digital Engineering* 39, 44–46 (2010)
10. Zheng, Z., Yan, L.S., Pan, W., Luo, B., Liu, J.T., Li, X.Y.: Routing Protocol Based on Cluster-Head-Chaining Incorporating LEACH and PEGASIS. *Chinese Journal of Sensor and Actuators* 23, 1173–1178 (2010)

Optimal Regularization Parameter Estimation for Regularized Discriminant Analysis

Lin Zhu

University of Science and Technology of China, Hefei, Anhui, 230027, China
zhomlynn@mail.ustc.edu.cn

Abstract. Regularized linear discriminant analysis (RLDA) is a popular LDA-based method for dimension reduction. Despite its good performance, how to choose the parameter of the regularizer efficiently is still unanswered, especially for multi-class situation. In this paper, we first prove that regularizing LDA is equivalent to augmenting the training set in a specific way and thereby propose an efficient model selection criterion based on the principle of maximum information preservation, extensive experiments prove the usefulness and efficiency of our method.

Keywords: Dimensionality Reduction, Linear Discriminant Analysis (LDA), Model Selection.

1 Introduction

With the advancements in data collection and storage technologies, there has been an exponential increase in the availability and usage of large, high-dimensional datasets. These data can directly be represented as vectors in high-dimensional vector spaces. Obviously, Operating directly on such high-dimensional vector space is ineffective and may lead to high computational and storage demands as well as poor performance. A typical way to circumvent the “curse of dimensionality” problem and other undesired properties of high dimensional spaces is to use dimensionality reduction techniques.

One of the most popular dimensionality reduction algorithms is linear discriminant analysis (LDA). It has been widely used in many applications such as microarray data classification; face recognition and gait recognition, etc. [1] - [5]. However, LDA still suffer from some drawbacks.

Computationally, LDA amounts to solving a generalized symmetric semi-definite eigenvalue decomposition (GEVD) problem. A straightforward implementation can thus be very instable for large datasets. So far a number of methods [1] - [6] have been explored to solve LDA with improved stability. Two seminal algorithms are uncorrelated linear discriminant analysis (ULDA) and regularized discriminant analysis (RDA). It can be further proven that ULDA is a special case of RDA.

In RDA, there is only one parameter i.e., the regularization parameter, which controls the smoothness of the estimator. Traditional methods like Cross-Validation

can be used to choose the parameter, however it becomes two resource-consuming for large datasets. In this paper, we propose an efficient method to estimate the regularization parameter for RDA. The results of experiments conducted on different databases demonstrate the efficiency and effectiveness of the proposed methods.

This paper is organized as follows. Section 2 outlines LDA, and RDA. Sections 3 describe the regularization parameter estimation for RDA. The experimental results will be presented in Section 5.

2 Background

If the given n D-dimensional training samples are grouped into c classes C_1, C_2, \dots, C_c , and there are n_j samples in C_j , let x_i^j denotes the i th sample from class C_j . The within-class scatter matrix S_w and between-class scatter matrix S_b and the total scatter matrix S_t are defined as:

$$\begin{aligned} S_w &= \frac{1}{n} \sum_{j=1}^c \sum_{i=1}^{n_j} (x_i^j - m_j)(x_i^j - m_j)^T \\ S_b &= \frac{1}{n} \sum_{j=1}^c n_j (m_j - m)(m_j - m)^T \\ S_t &= \frac{1}{n} \sum_{j=1}^c \sum_{i=1}^{n_j} (x_i^j - m)(x_i^j - m)^T = S_w + S_b \end{aligned} \quad (1)$$

m_j is the empirical mean of the j th class and m is the sample mean of the whole training set. After the samples are linearly projected into a d-dimensional space and the projection matrix are denoted as $W = [W_1, W_2, \dots, W_d]$, the new scatter matrices are:

$$\overline{S_w} = W^T S_w W, \quad \overline{S_b} = W^T S_b W, \quad \overline{S_t} = W^T S_t W \quad (2)$$

Therefore these matrixes could be seen as a measure of the between-class similarity and in-class similarity, and they can effectively describe spatial relationship between different classes. The LDA algorithm aims to get the optimal subspace that simultaneously minimize the between-class similarity and maximize the in-class similarity by solving the optimization problem

$$W = \arg \max_w \frac{\text{tr}(W^T S_b W)}{\text{tr}(W^T S_w W)} \quad (3)$$

Since $S_t = S_w + S_b$, we can use S_t instead of S_w . It can shown that the solution are the eigenvectors corresponding to the c largest eigenvalues of the matrix $S_t^{-1} S_b$.

One problem concerning the standard LDA method is that when all the training samples are just laying in a low-dimensional sub-space of the feature space, the total scatter matrix S_t are singular and we can't directly compute the eigenvectors

of $S_t^{-1}S_b$. In RLDA, a regularization term, usually an identity matrix multiplied by a shrinking factor λ is added to S_t and we solve the optimization problem instead

$$W = \arg \max_w \frac{\text{tr}(W^T S_b W)}{\text{tr}(W^T (S_t + \lambda I) w)} \quad (4)$$

We get the eigenvectors of $(S_t + \lambda I)^{-1} S_b$ as the optimal solution.

3 The Proposed Method

3.1 The Equivalent Form of RLDA

Since the generalization ability could be viewed as the trained model's ability to predict the true attributes of observations not available, so if more samples could be used for training, then the generalization ability of the model may be better. Sometimes, training set can even be extended by the samples already available based on the special properties of a certain kind of data.

For general data, if the Euclidean distance is a good enough measure of the similarity between two observations, which is the case in many areas where LDA can be used, then for every observation we already get, in the feature space at least every point within a very small Euclidean ball centered at this observation belongs to the same class as the observation. Furthermore, we don't really have to do this sampling job. When the sampling is extremely dense and uniform, the sum of the random sampled points becomes integral on the D-dimensional balls centered at every training sample, and we can compute the involved variables using the following definitions:

$$s_j = \bigcup_{i=1}^{n_j} \left\{ [v_1 \ v_2 \ \cdots \ v_D]^T \mid \| [v_1 \ v_2 \ \cdots \ v_D]^T - x_i^j \|_2 \leq R \right\}, j=1, 2, \dots, c \quad (5)$$

$$m_j = \left(\int_{s_j} dv_1 dv_2 \cdots dv_D \right)^{-1} \int_{s_j} \begin{bmatrix} v_1 \\ v_2 \\ \vdots \\ v_D \end{bmatrix} dv_1 dv_2 \cdots dv_D, j=1, 2, \dots, c \quad (6)$$

Note that these definitions are natural extensions of their corresponding definitions in the original LDA to the continuous set's case, since we simply use the integration on a domain instead of sum on a discrete set and volume of the integral domain instead of the number of training sample.

With these definitions we can finally develop the connection between the RLDA and the LDA variation we described above¹.

Theorem 1. *RLDA is equivalent to the extreme situation of performing LDA on n clusters uniformly sampled from n balls of radius R centered at n observed sample points. These newly sampled points' labels are the same as the centers of the balls*

¹ The proof of Theorem 3 is omitted due to space limitation.

they respectively come from. And the shrinking parameter λ and radius R satisfy this relationship: $\lambda = \frac{R^2}{D+2}$, D is the dimension of the feature space.

3.2 Model Evaluation Criterion

Based on the interpretation in 3.2, we can dissect RLDA into two steps. (1) Get infinite points uniformly sampled from D-dimensional balls of radius R centered at all observed sample points. (2) Perform LDA on the points we sampled. And we therefore transform the problem of choosing λ into the problem of choosing a proper R .

When designing the model selection criterion for R , we use the principle of maximum information preservation. Its main idea is that an optimal perceptual system should be designed to make the information maximally preserved when passing each layer or processing stage. It can be used in the parameter selection of an algorithm if we view an algorithm like RLDA as a perceptual system that accepts the input data and gives an output that preserves a specific kind of information as much as possible.

The information we try to preserve is also class-separability but defined in a different way. We want to make sure the class separability won't get worse than the original training set in step (1). Distance between two clusters is usually defined as the shortest path between them and in our case it become

$$\|x_{i_1}^{j_1} - x_{i_2}^{j_2}\|_2 - 2R \quad 1 \leq i_1 \leq n_{j_1}, 1 \leq i_2 \leq n_{j_2} \quad 1 \leq j_1, j_2 \leq c \quad (7)$$

$\|x_{i_1}^{j_1} - x_{i_2}^{j_2}\|_2$ is the Euclidian distance between two original samples $x_{i_1}^{j_1}$ and $x_{i_2}^{j_2}$.

As the radius increases, the distance between all pairs of clusters decreases. If the two clusters have the same class label, this means in-class measure ‘decreases’, in other words samples of the same class become ‘nearer’, which has a positive effect on class separability. But if they belong to different classes, this means the between-class variance measure decreases, in other words samples of different class become ‘nearer’, which has a negative effect on class separability. Based on this intuition, we define this parameter selection criterion

$$\lambda = \arg \max_R \frac{V_b}{V_w}, \lambda(R) = \frac{R^2}{\text{rank}(S_t) + 2}$$

$$V_b = \sum_{j_1=1}^c \sum_{j_2>j_1} \sum_{i_1=1}^{n_{j_1}} \sum_{i_2=1}^{n_{j_2}} d_b(x_{i_1}^{j_1}, x_{i_2}^{j_2}), V_w = \sum_{j=1}^c \sum_{i_1=1}^{n_j} \sum_{i_2>i_1}^{n_j} d_w(x_{i_1}^j, x_{i_2}^j)$$

$$d_b(x_{i_1}^{j_1}, x_{i_2}^{j_2}) = \|x_{i_1}^{j_1} - x_{i_2}^{j_2}\|_2 - 2R, d_w(x_{i_1}^j, x_{i_2}^j) = \max(\|x_{i_1}^j - x_{i_2}^j\|_2 - 2R, 0) \quad (8)$$

We choose the ‘true’ dimension of the feature space to be the rank of S_t because it has been proven that the regularized LDA works only in the range space of S_t and no information is gathered outside this space. When R becomes too large, V_w becomes zero, this means any pairs of clusters from the same classes become together and any further increment of R will only make two different classes mixed together. So we can define an upper bound on R as:

$$R < \max\left(\left\{\frac{\|x_{i_1}^j - x_{i_2}^j\|_2}{2} \mid j = 1, 2, \dots, c \quad 1 \leq i_1, i_2 \leq n_j\right\}\right) \quad (9)$$

We also define a lower bound on R as:

$$R > \min\left(\left\{\frac{\|x_{i_1}^{j_1} - x_{i_2}^{j_2}\|_2}{2} \mid 1 \leq j_1, j_2 \leq c \quad 1 \leq i_1, i_2 \leq n_j \quad j_1 \neq j_2 \quad i_1 \neq i_2\right\}\right) \quad (10)$$

The justification is that it is only when R is larger than the minimal distance between any pairs of clusters from different classes that confusion could be caused between two or more classes.

The optimization problem is not convex and hard to solve. Since this is only an estimation of the best parameter, in practice we can randomly select a few candidate parameters within the bound we proposed and output the one that maximize the object function.

4 Experiments

In this section we compare the performance of our method with the state-of-art speedup CV method proposed in [6]. All of our experiments have been performed on a P4 3.20GHz PC with 3GB memory.

4.1 Datasets

We test our method on two benchmark datasets. Their important properties are summarized in table 1.

Table 1. Statistics of the datasets

Dataset	Size	# of dimensions	# of classes
YALE	165	1024	15
Lung Cancer	203	12601	5

4.2 Results

The main observations from the performance comparisons include:

(1) In terms of time cost, our method has a considerable advantage over the speedup CV method proposed in [6] and therefore the original cross-validation and this advantage become even more significant for higher dimensional datasets. This property is preferable because high dimensional data but with a small sample size is common in practice.

(2) On the other hand, the parameter selected by our method can obtain a test result comparable with those by cross validation, especially when the given training set is small, this is because as a statistical method, cross validation can get a good prediction of a particular parameter's performance on the testing set only the samples available for training is enough to represent the whole set.

Table 2. Performance comparision

Dataset	Training set size	10-fold CV		Proposed method	
		Testing error (Mean \pm Std-Dev Percent)	Training time(s)	Testing error (Mean \pm Std-Dev Percent)	Training time(s)
YALE	30	48.7(6.8)	2.833	44.8(5.3)	0.009
	45	32.2(4.4)	3.560	31.6(3.8)	0.010
	60	24.5(4.7)	5.023	25.2(4.3)	0.014
	75	19.6(3.7)	5.905	20.7(3.5)	0.023
	90	17.3(4.2)	6.763	17.9(3.8)	0.028
	105	14.4(3.5)	8.216	15.2(3.6)	0.038
Lung Cancer	25	14.6(5.3)	14.137	13.8(5.0)	0.074
	50	9.6(3.1)	30.149	8.9(3.1)	0.167
	75	8.1(2.8)	44.835	7.5(2.3)	0.282
	100	7.2(3.1)	60.695	6.6(2.6)	0.406
	125	6.1(2.6)	75.390	5.9(2.2)	0.568
	150	6.7(3.7)	87.790	6.4(3.5)	0.732
	175	6.1(4.4)	102.189	5.9(4.3)	0.911

5 Conclusion

In this paper, we propose an efficient model selection criterion for RDA, based on the principle of maximum information preservation, extensive experiments prove the usefulness and efficiency of our method.

Acknowledgments. This work was supported by the grants of the National Science Foundation of China, Nos. 60975005, 61005010, 60873012, 60805021, 60905023, 31071168 & 30900321.

References

1. Belhumeur, P.N., Hespanha, J.P., Kriegman, D.J.: Eigenfaces vs. Fisherfaces: Recognition Using Class Specific Linear Projection. *IEEE Transactions on Pattern Analysis and Machine Intelligence* 19(7), 711–720 (1997)
2. Yang, J., Yang, J.Y.: Why Can LDA Be Performed in PCA Transformed Space. *Pattern Recognition* 36(2), 563–566 (2003)
3. Li, H.F., Jiang, T., Zhang, K.S.: Efficient and Robust Feature Extraction by Maximum Margin Criterion. *IEEE Transactions on Neural Networks* 17(1), 157–165 (2006)
4. Ye, J.P., Li, T., Xiong, T., et al.: Using Uncorrelated Discriminant Analysis for Tissue Classification with Gene Expression Data. *IEEE-ACM Transactions on Computational Biology and Bioinformatics* 1(4), 181–190 (2004)
5. Tao, D.C., Li, X.L., Wu, X.D., et al.: General Tensor Discriminant Analysis and Gabor Features for Gait Recognition. *IEEE Transactions on Pattern Analysis and Machine Intelligence* 29(10), 1700–1715 (2007)
6. Ji, S.W., Ye, J.P.: Generalized Linear Discriminant Analysis: A Unified Framework and Efficient Model Selection. *IEEE Transactions on Neural Networks* 19(10), 1768–1782 (2008)

Optimized Projection for Sparse Representation Based Classification

Can-Yi Lu^{1,2}

¹ Hefei Institute of Intelligent Machines, Chinese Academy of Sciences, Hefei, China

² Department of Automation, University of Science and Technology of China, Hefei, China
canyilu@mail.ustc.edu.cn

Abstract. Dimensionality reduction(DR) methods have commonly been used as a principled way to understand the high-dimensional data such as face images. In this paper, we propose a new supervised DR method called Optimized Projection for Sparse Representation based Classification(OP-SRC). SRC assumes that any new sample will approximately lie in the linear span of the training samples sharing the same class label. The decision of SRC is based on the reconstruction residual. OP-SRC aims to reduce the within-class reconstruction residual and simultaneously increases the between-class reconstruction residual. Therefore, SRC performs well in the OP-SRC transformed space. The feasibility and effectiveness of the proposed method is verified on Yale and ORL with promising results.

Keywords: Dimensionality Reduction, Sparse Representation, Face recognition.

1 Introduction

In many application domains, such as appearance-based object recognition, information retrieval and text categorization, the data are usually provided in high-dimensional form. Dimensionality reduction(DR) is an effective approach to deal with such data, due to its potential to mitigate the so-called “curse of dimensionality” [1] and improve the computational efficiency. A large family of algorithm has been designed to provide different solutions to the problem of DR. Among them, the linear algorithms Principal Component Analysis(PCA) [2] and Linear Discriminative Analysis(LDA) [3] have been the two most popular because of their relative simplicity and effectiveness. However, PCA and LDA consider only the global scatter of training samples and they fail to reveal the essential data structures nonlinearly embedded in high dimensional space. To overcome these limitations, the manifold learning methods were proposed by assuming that the data lie on a low dimensional manifold of the high dimensional space [4]. Locality Preserving Projection(LPP) [5] is one of the representative manifold learning methods.

The success of manifold learning implies that the high dimensional face images can be sparsely represented or coded by the representative samples on the manifold. Very recently, Writhe et al. presented a Sparse Representation based Classification(SRC) method [6]. The main idea of SRC is to represent a given test

sample as a sparse linear combination of all training samples, the sparse nonzero representation coefficients are supposed to concentrate on the training samples with the same class label as the test sample. SRC shows that the classification performance of most meaningful features converges when the feature dimension increases if a SRC classifier is used. Although this does provide some new insight into the role of feature extraction played in a pattern classification tasks, Qiao et al. argue that designing an effective and efficient feature extractor is still of great importance since the classification algorithm could become simple and tractable [7], and a unsupervised DR method called Sparsity Preserving Projections(SPP) is proposed, which aims to preserve the sparse reconstructive relationship of the data. In this paper, we propose a supervised DR method which is coined the Optimized Projection for Sparse Representation based Classification(OP-SRC). OP-SRC aims to gain a discriminative projection such that SRC achieves the optimum performance in the transformed low-dimensional space.

The remainder of this paper is organized as follows: Section 2 reviews the SRC algorithm. Section 3 presents the OP-SRC method. The experimental results are presented in Section 4. Finally, we conclude this paper in Section 5.

2 Sparse Representation Based Classification

Given sufficient c classes training samples, a basic problem in pattern recognition is to correctly determine the class which a new coming(test) sample belong to. We arrange the n_i training samples from the i th class as columns of a matrix $X_i = [x_{i1}, \dots, x_{in_i}] \in R^{m \times n_i}$ where m is the dimensionality. Then we obtain the training sample matrix $X = [X_1, \dots, X_c] \in R^{m \times n}$ where $n = \sum_{i=1}^c n_i$ is the total number of training samples. Under the assumption of linear representation, a test sample $y \in R^m$ will approximately lie on the linear subspace spanned by training samples

$$y = X\alpha \in R^m. \quad (1)$$

If $m < n$, the system of Eq.(1) is underdetermined, and also, its solution is not unique. This motivates us to seek the sparest solution to Eq.(1), solving the following ℓ^0 -minimization problem

$$(\ell^0): \quad \hat{\alpha}_0 = \arg \min \|\alpha\|_0 \text{ subject to } y = X\alpha, \quad (2)$$

where $\|\cdot\|_0$ denotes the ℓ^0 -norm, which counts the number of nonzero entries in a vector. However, the problem of finding the sparsest solution of an underdetermined system of linear equations is NP-hard and difficult even to approximate [8].

The theory of compressive sensing [9, 10] reveals that if the solution α is sparse enough, the solution of the ℓ^0 -minimization problem is equal to the following ℓ^1 -minimization problem

$$(\ell^1): \quad \hat{\alpha}_1 = \arg \min \|\alpha\|_1 \text{ subject to } y = X\alpha. \quad (3)$$

In order to deal with occlusion, the ℓ^1 -minimization problem (3) is extended to the following problem

$$(\ell_e^1): \quad \hat{\alpha}_i = \arg \min \| \alpha \|_1 \text{ subject to } \| y - X \alpha \| \leq \varepsilon, \quad (4)$$

where $\varepsilon > 0$ is a given tolerance.

For a given test sample y , SRC first computes its sparse representation coefficient α , then determines the class of this test sample from its reconstruction error between this test sample and the training samples of class i ,

$$r_i(\alpha) = \| y - X \delta_i(\alpha) \|_2. \quad (5)$$

For each class i , $\delta_i(\alpha): R^n \rightarrow R^n$ is the characteristic function which selects the coefficients associated with the i th class. Then the class $C(y)$ which test sample y belongs to is determined by

$$C(y) = \arg \min_i r_i(\alpha). \quad (6)$$

3 Optimized Projection for Sparse Representation Based Classification

In this paper, we consider the supervised DR problem. Considering a training sample x (belonging to the i th class) and its sparse representation coefficient α based on other training samples as dictionary. Ideally, the entries of α are zero except those associated with the i th class. In many practical face recognition scenarios, the training sample x could be partially corrupted or occluded. Or sometimes the training samples are not enough to represent the given sample. In these case, the residual associated with the i th class $r_i(x)$ may be not small enough, and may produce an erroneous predict. Thus, the Optimized Projection for Sparse Representation based Classification(OP-SRC) is proposed which aims to seek a linear projection matrix such that in the transformed low-dimensional space, the within-class reconstruction residual is as small as possible and simultaneously the between-class reconstruction residual is as large as possible.

Let $P \in R^{m \times d}$ be the optimized projection matrix with $d \ll m$. Each data point $x_{ij} \in X$ in the input space R^m is mapped into $y_{ij} = P^T x_{ij}$ in a d -dimensional space R^d . As a result, the data matrix in the original input space is converted into the one in R^d , that is, $Y = P^T X$.

For each training sample $y_{ij} \in Y$ in the transformed d -dimensional space R^d , by solving the extended ℓ^1 -minimization problem (4), we obtain its sparse representation coefficient α_{ij} using the remaining training samples as dictionary. Base on the decision rule of SRC, we define the within-class residual matrix as follows

$$\tilde{R}_W = \frac{1}{n} \sum_{i=1}^c \sum_{j=1}^{n_i} (y_{ij} - Y \delta_i(\alpha_{ij})) (y_{ij} - Y \delta_i(\alpha_{ij}))^T. \quad (7)$$

The between-class residual matrix is defined as follows

$$\tilde{R}_B = \frac{1}{n(c-1)} \sum_{i=1}^c \sum_{j=1}^{n_i} \sum_{l \neq i} (y_{ij} - Y\delta_l(\alpha_{ij}))(y_{ij} - Y\delta_l(\alpha_{ij}))^T. \quad (8)$$

The total residual matrix is defined as follows

$$\tilde{R}_T = \frac{n\tilde{R}_W + n(c-1)\tilde{R}_B}{nc} = \frac{1}{nc} \sum_{i=1}^c \sum_{j=1}^{n_i} \sum_{l=1}^c (y_{ij} - Y\delta_l(\alpha_{ij}))(y_{ij} - Y\delta_l(\alpha_{ij}))^T \quad (9)$$

To make SRC perform well on training data, we expect that the within-class residual is as small as possible and simultaneously the between-class residual is as large as possible. Therefore, we can choose to maximize the following criterion [11]

$$J(P) = \text{tr}(\beta\tilde{R}_B - \tilde{R}_W), \quad (10)$$

where β is the weight parameter balances the between-class and within-class residual information. Since P is a linear mapping, it is easy to show $\tilde{R}_W = P^T R_W P$ and $\tilde{R}_B = P^T R_B P$, where

$$R_W = \frac{1}{n} \sum_{i=1}^c \sum_{j=1}^{n_i} (x_{ij} - X\delta_i(\alpha_{ij}))(x_{ij} - X\delta_i(\alpha_{ij}))^T, \quad (11)$$

$$R_B = \frac{1}{n(c-1)} \sum_{i=1}^c \sum_{j=1}^{n_i} \sum_{l \neq i} (x_{ij} - X\delta_l(\alpha_{ij}))(x_{ij} - X\delta_l(\alpha_{ij}))^T. \quad (12)$$

So, we have

$$J(P) = \text{tr}(P^T (\beta R_B - R_W) P). \quad (13)$$

In this formulation, we have the freedom to multiply P with some nonzero constant. Thus, we additionally require that P is constituted by the unit vectors, i.e. $P = [p_1, \dots, p_d]$ and $p_k^T p_k = 1$. This means we need solve the following constrained optimization

$$\max \sum_{k=1}^d p_k^T (\beta R_B - R_W) p_k \quad \text{subject to} \quad p_k^T p_k = 1, k = 1, \dots, d. \quad (14)$$

We can use the Lagrange multipliers to transform the above objective function to include the constraint

$$L(p_k, \lambda_k) = \sum_{k=1}^d p_k^T (\beta R_B - R_W) p_k - \lambda_k (p_k^T p_k - 1). \quad (15)$$

The optimization is performed by setting the partial derivative of L with respect to p_k to zero

$$\frac{\partial L}{\partial p_k} = ((\beta R_B - R_W) - \lambda_k I) p_k = 0, \quad k = 1, \dots, d. \quad (16)$$

Now we obtain

$$(\beta R_B - R_W) p_k = \lambda_k p_k, \quad k = 1, \dots, d, \quad (17)$$

which means that the λ_k 's are the eigenvalues of $\beta R_B - R_W$ and the p_k 's are the corresponding eigenvectors. Thus

$$J(P) = \sum_{k=1}^d p_k^T (\beta R_B - R_W) p_k = \sum_{k=1}^d \lambda_k p_k^T p_k = \sum_{k=1}^d \lambda_k . \quad (18)$$

Therefore, P is composed of the first d largest eigenvectors of $\beta R_B - R_W$.

4 Experimental Verification

In this section, we investigate the performance of our proposed OP-SRC method for face representation and recognition. The system performance is compared with PCA [2], LDA [3], SPP [7] and SRC-DP [12]. PCA and LDA are two of the most popular linear methods in FR. SPP and SRC-DP are two new method corresponding to SRC. Similar to SPP and SRC-DP, we first perform PCA to reduce the dimension before implementing OP-SRC. Finally, SRC is employed for classification.

In our experiments, we experimentally set $\varepsilon = 0.05$ (refer to (4)) which usually leads SRC to better performance than other parameters. The SPGL1 toolbox [13, 14] is used for solving the extended ℓ^1 -minimization problem (4). We experimentally set $\beta = 0.25$ (refer to(17)) by searching in a large range of candidates.

A. Yale Database

The Yale face database [3] contains 165 gray scale images of 15 individuals. The images demonstrate variations in lighting condition, facial expression (normal, happy, sad, sleepy, surprised, and wink). A random subset with $l (=4, 5, 6, 7)$ images per individual is taken with labels to form the training set, and the rest of the database is considered to be the test set. For each given l , we average the results over 20 random splits. Notice that LDA is different from other methods because the maximal number of dimension is on less than the number of class c [3].

In general, the performance of all these methods varies with the number of dimensions. We show the best results and the optimal dimensionality obtained by PCA, LDA, SPP, SRC-DP and OP-SRC in Table 1, including the mean of accuracy as well as the standard deviation.

Table 1. Performance comparisons on the Yale database

Methods	4 Train	5 Train	6 Train	7 Train
PCA	0.6467±0.044(52)	0.671±0.029(64)	0.725±0.042(88)	0.721±0.055(64)
LDA	0.717±0.057(14)	0.752±0.039(14)	0.799±0.046(14)	0.814±0.046(14)
SPP	0.607±0.049(57)	0.638±0.045(72)	0.676±0.044(88)	0.702±0.046(104)
SRC-DP	0.706±0.049(29)	0.724±0.035(37)	0.771±0.042(34)	0.773±0.043(43)
OP-SRC	0.758±0.048(48)	0.794±0.036(62)	0.833±0.038(74)	0.853±0.048(88)

From Table 1, it can be found that OP-SRC obtains the highest recognition rates in all cases. Fig.1 shows the plots of accuracy rate versus dimensionality reduction. Note that, when the dimension of feature continues to increase, the performance of the OP-SRC algorithm decreases and has the same accuracy with PCA on the highest dimension. In this case, the obtained optimized projection matrix P is square and orthogonal, that is $P^T P = P P^T = I$. Thus, $\|P^T x - P^T X \alpha\| = \|x - X \alpha\|$. The sparse representation coefficient in the transformed space will be the same as in the subspace projected by PCA.

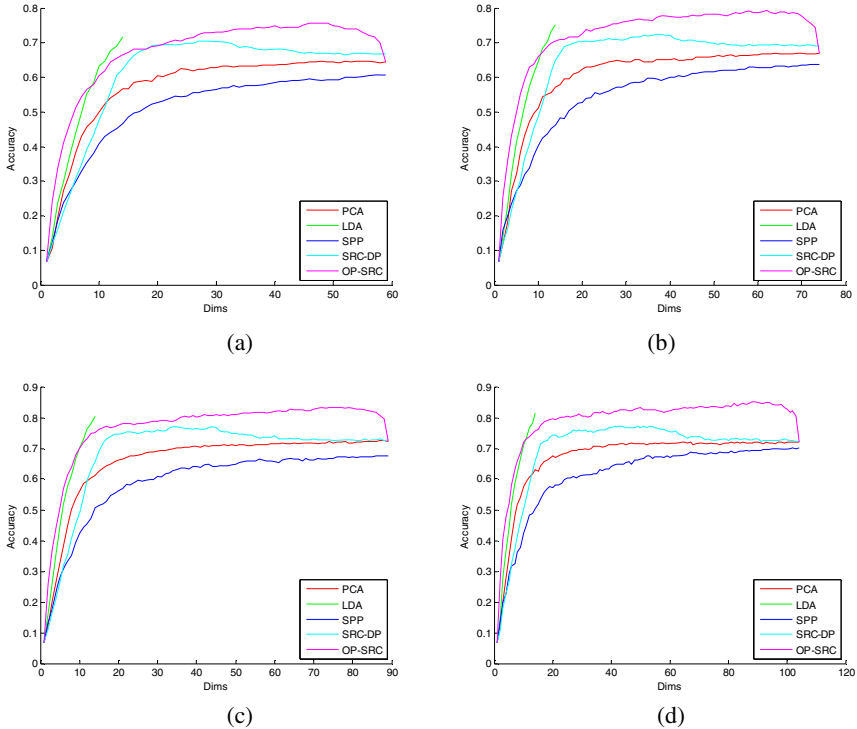


Fig. 1. Accuracy versus reduced dimensionality on Yale database: (a) 4 Train; (b) 5 Train; (c) 6 Train; (d) 7 Train

B. ORL Database

The ORL face database[15] is used for this test. It contains 400 images of 40 individuals. Some images were captured at different times and have different variations including expression (open or closed eyes, smiling or nonsmiling) and facial details (glasses or no glasses). The images were taken with a tolerance for some tilting and rotation of the face up to 20 degrees. A random subset with l ($=4, 5, 6, 7$) images per individual was taken with labels to form the training set. The rest of the database was considered to be the testing set. For each given l , we average the results over 20 random splits. The experimental protocol is the same as before. The recognition results are shown in Table 2 and Fig. 2. Our OP-SRC method outperforms all the other methods.

Table 2. Performance comparisons on the ORL database

Methods	4 Train	5 Train	6 Train	7 Train
PCA	$0.898 \pm 0.019(127)$	$0.921 \pm 0.018(183)$	$0.941 \pm 0.018(193)$	$0.954 \pm 0.023(134)$
LDA	$0.899 \pm 0.019(39)$	$0.930 \pm 0.017(39)$	$0.941 \pm 0.019(39)$	$0.950 \pm 0.023(39)$
SPP	$0.861 \pm 0.018(108)$	$0.887 \pm 0.026(170)$	$0.903 \pm 0.031(180)$	$0.922 \pm 0.026(202)$
SRC-DP	$0.888 \pm 0.018(124)$	$0.918 \pm 0.018(131)$	$0.929 \pm 0.028(221)$	$0.943 \pm 0.022(190)$
OP-SRC	$0.925 \pm 0.017(153)$	$0.950 \pm 0.017(195)$	$0.968 \pm 0.015(224)$	$0.975 \pm 0.013(255)$

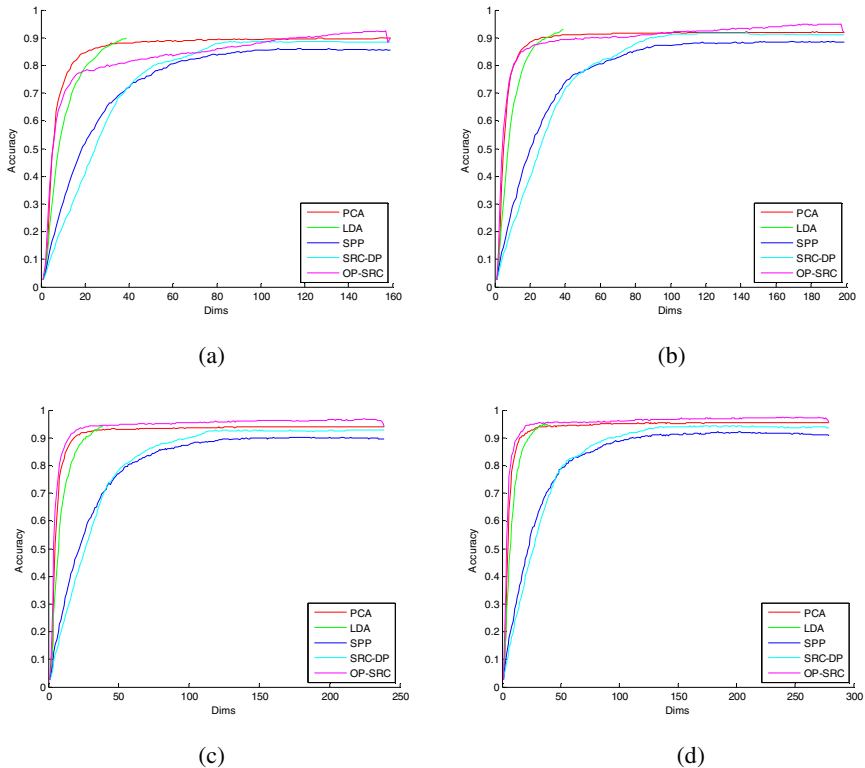


Fig. 2. Accuracy versus reduced dimensionality on ORL database: (a) 4 Train; (b) 5 Train; (c) 6 Train; (d) 7 Train

5 Conclusions

In this paper, based on sparse representation, we propose a new algorithm called Optimized projection for Sparse Representation based Classification(OP-SRC) for supervised dimensionality reduction. The optimized projection of OP-SRC decreases the within-class reconstruction residual and simultaneously increases the between-class reconstruction residual which matches SRC optimally in theory. The experimental results clearly demonstrate that the proposed OP-SRC has much better performance than PCA, LDA, SPP and SRC-DP, and also it is more effective with respect to the sparse representation based classification.

Acknowledgments. This work was supported by the grants of the National Science Foundation of China, Nos. 60975005, 61005010, 60873012, 60805021, 60905023, 31071168, 30900321, and the Knowledge Innovation Program of the Chinese Academy of Sciences, Y023A61121.

References

1. Jain, A.K., Duin, R.P.W., Mao, J.C.: Statistical Pattern Recognition: A Review. *IEEE Transactions on Pattern Analysis and Machine Intelligence* 22(1), 4–37 (2000)
2. Turk, M.A., Pentland, A.P.: Face Recognition Using Eigenfaces. In: *IEEE Computer Society Conference on Computer Vision and Pattern Recognition* (1991)
3. Belhumeur, P.N., Hespanha, J.P., Kriegman, D.J.: Eigenfaces vs. Fisherfaces: Recognition Using Class Specific Linear Projection. *IEEE Transactions on Pattern Analysis and Machine Intelligence* 19(7), 711–720 (1997)
4. Roweis, S.T., Saul, L.K.: Nonlinear Dimensionality Reduction by Locally Linear Embedding. *Science* 290(5500), 2323–2325 (2000)
5. He, X.F., et al.: Face Recognition Using Laplacianfaces. *IEEE Transactions on Pattern Analysis and Machine Intelligence* 27(3), 328–340 (2005)
6. Wright, J., et al.: Robust Face Recognition via Sparse Representation. *IEEE Transactions on Pattern Analysis and Machine Intelligence* 31(2), 210–227 (2009)
7. Qiao, L.S., Chen, S.C., Tan, X.Y.: Sparsity Preserving Projections with Applications to Face Recognition. *Pattern Recognition* 43(1), 331–341 (2010)
8. Amaldi, E., Kann, V.: On the Approximability of Minimizing Nonzero Variables or Unsatisfied Relations in Linear Systems. *Theoretical Computer Science* 209(1-2), 237–260 (1998)
9. Donoho, D.L.: For Most Large Underdetermined Systems of Linear Equations the Minimal L(1)-norm Solution Is also the Sparsest Solution. *Communications on Pure and Applied Mathematics* 59(6), 797–829 (2006)
10. Candes, E.J., Romberg, J.K., Tao, T.: Stable Signal Recovery from Incomplete and Inaccurate Measurements. *Communications on Pure and Applied Mathematics* 59(8), 1207–1223 (2006)
11. Li, H.F., Jiang, T., Zhang, K.S.: Efficient and Robust Feature Extraction by Maximum Margin Criterion. *IEEE Transactions on Neural Networks* 17(1), 157–165 (2006)
12. Yang, J., Chu, D.: Sparse Representation Classifier Steered Discriminative Projection. In: *20th International Conference on Pattern Recognition, ICPR* (2010)
13. Berg, E.V.D., Friedlander, M.P.: Probing the Pareto Frontier for Basis Pursuit Solutions. *SIAM Journal on Scientific Computing* 31(2), 890–912 (2008)
14. Berg, E.V.D., Friedlander, M.P.: SPGL1: A Solver for Large-scale Sparse Reconstruction (2007), <http://www.cs.ubc.ca/labs/scl/spgl1>
15. Samaria, F.S., Harter, A.C.: Parameterisation of A Stochastic Model for Human Face Identification. In: *2nd IEEE Workshop on Applications of Computer Vision* (1994)

Balanced-Sampling-Based Heterogeneous SVR Ensemble for Business Demand Forecasting

Yue Liu¹, Wang Wei¹, Kang Wang¹, Zhenjiang Liao¹, and Jun-jun Gao²

¹ School of Computer Engineering & Science, Shanghai University,
Shanghai, 200072, China

² Sydney Institute of Language and Commerce, Shanghai University,
Shanghai, 201800, China
yliu@staff.shu.edu.cn

Abstract. An accurate demand forecasting model has academic and practical significance to supply chain management. However, multi-source data and error data have great effect on the demand prediction accuracy. Therefore, a balanced-sampling-based ensemble of heterogeneous support vector regression forecasting method named BS-EnHSVR (Balanced-Sampling-based Ensemble of Heterogeneous SVR) is proposed in this paper to improve the prediction accuracy by employing balanced sampling and heterogeneous ensemble learning techniques. Training dataset is firstly classified to different clusters by using clustering algorithm, and then sample data from each cluster equally to generate training subset for training different individual SVR models with different training parameters for ensemble. Experimental results on beer sales show that the proposed method has good usability and generalization ability.

Keywords: Heterogeneous Ensemble, Support Vector Regression, Demand Forecasting.

1 Introduction

Demand forecasting as an important part of demand chain management, is also the basis for decision support of demand, and it will directly influence the inventory control and supply chain management[1][2]. Nowadays, retail competition is becoming increasingly fierce, inventory and supply chain have a direct impact on operating costs. Thus, a highly accurate demand forecasting model plays an important role of the retail industry. So far, there are many different demand forecasting methods were applied to different areas. In the early days, most demand forecasting adopted traditional statistical methods, such as independent judgment method, predict market method, Delphi method, structural analogy method, etc[3][4][5]. However, the relationship between supply and demand is always nonlinear, and also is chaotic. Both Support Vector Machine (SVM) [6] and ensemble learning [7] have good generalization ability. More and more researchers pay attention to apply SVM ensemble method to solve the real-world problems. A hybrid multiple models had presented to forecast short-term electricity demand [8], in which neural networks and SVM have been integrated to predict future electricity demand. Several neural

network prediction models were put forward for China's foreign trade and then SVM was employed to integrate the predictions of these models [9]. However, the determination of the parameters of individual SVM also involves a tedious trial-and-error process and depends on the users' prior knowledge and experience. And all the individual SVM's training parameters are fixed and same, which will reduce the accuracy and diversity of individual SVMs and then make the prediction accuracy of SVM ensemble model not satisfactory. Therefore, a selective and heterogeneous SVM ensemble was proposed for demand forecasting in paper [10]. Moreover, traditional ensemble methods are based on bootstrap sampling algorithm which chooses random samples with replacement from a data set and analyze each sample the same way. It is easy to cause the training dataset with unbalance data. In order to overcome the unbalance data problem, this paper proposed a novel method named BS-EnHSVR (Balanced-Sampling-based Ensemble of Heterogeneous SVR), in which balanced sampling method is employed to generate training dataset for the individual SVRs instead of bootstrap. Moreover, in order to improve the generalization ability of the individual SVRs and make the SVR ensemble model for demand forecasting easy to use, grid search method is also used to determine the training parameters for each individual SVRs. Finally, BS-EnHSVR is applied to forecast the demands for a beer retailer. The experimental results show that the proposed method has good usability and generalization ability.

The rest of this paper is organized as follows. In section 2, a model of sales demand is described to get the beer sales data. Section 3 details the algorithm of the new balance-sampling based SVR ensemble method for demand forecasting. The experiments are given in Section 4. Finally, conclusions are drawn.

2 Collection of Beer Sales Data

Retail industry has the characteristic of more products, more POS (Point Of Sale) data, and complex structures with multi-level of the supply chain, and uncertain customer needs, which makes it necessary to build a universal demand model. After investigation on a Tesco supermarket in Liaoning Province and interviewing with the category manager and food and beverage department head, a demand model for multi categories of beers, which is constructed based on the beer sales data in 2004, is described in paper [10]. In order to guarantee the intelligibility of this paper, the model is re-described here.

Assuming that the whole planning level is nT (the review period of general dealer and retailer are both T days), the demand value of this product of sales is generated by the demand function, shown as formula (1).

$$D_{it} = \left[\lambda * a_i * P_{it}^{-b_i} + (1 - \lambda) * \alpha_i * X_i^{\beta_i} \right] + S_{it} + \gamma_{it} * G_{it} - \theta_i * \sum_{j(j \neq i)} \gamma_{jt} * G_{jt} + n_i * \text{rand}(\bullet) . \quad (1)$$

$$(i = 1, 2, \dots, m; t = 1, 2, 3, \dots, n)$$

It assumes that the final demand of this product (including various brands) has uncertainty and seasonality. And there are twice demand peak in a year: spring festival and summer season. The demand of this product is formulated as a function of price, shelf-space allocated by retailer and promotional effecting factor. Where D_{it} is the demand of i th product in t th period of retailer. S_{it} is seasonal factor of i th product in t th period. P_{it} is the price of i th product in t th period. a_i and b_i ($a_i > 0, b_i < 1$) denote scale parameter and price elasticity factor respectively. X_i denotes shelf space allocated by retailer to i th product. α_i and β_i ($\alpha_i > 0, \beta_i < 1$) represent scale parameter and elastic factor of shelf-space; G_{it} represents whether retailer takes action of sales promotion for i th product in t th period or not, if it does, then let G_{it} be 1, else be 0. γ_{it} denotes the additional demand quantity of i th product caused by promotion at t th period. If retailer begins its promotion at $t = t^*$ period, $G_{it^*} = G_{i(t^*+1)} = \dots = G_{i(t^*+\tau)} = 1$, others are 0, where τ represents the number of weeks that promotion lasts, obviously the values of $\gamma_{it^*}, \gamma_{i(t^*+1)}, \dots, \gamma_{i(t^*+\tau)}$ are different when the beginning time of promotion is different. $\sum_{j(j \neq i)} \gamma_{jt} G_{jt}$ represents the additional sales of other brands caused by promotion, and θ_i denotes negative effecting factor to i th product realized by the additional sales of other brands caused by promotion. n_i is demand deviation factor (constant), $rand(\bullet)$ is random number generator that can generate numbers following standard normal probability distribution.

$$\text{Let } \rho_i = \begin{cases} 1, & \text{if } i\text{th product is selected} \\ 0, & \text{else} \end{cases}. \quad (2)$$

Thus, \hat{D}_{it} the demand of i th product in t th period can be described as follows:

$$\hat{D}_{it} = \rho * \left[D_{it} + \sum_{j \neq i} \pi_{ij} * D_{jt} * (1 - \rho_j) \right] \quad (3)$$

Where π_{ij} ($0 \leq \pi_{ij} \leq 1$) represents the substitution rate based on brand, which equals to the proportion of brand j customer who will switch to their second choice brand i if their first choice brand j is not included in the assortment. D_{jt} is the demand of j th product in t th period of retailer. There are three brands of bottled beers as the candidates, say brand 1 (a local brand), brand 2 (an adjacent region brand) and brand 3 (a national famous brand). The length of the whole planning level is one year, the ordering period of general dealer and retailer are both one week, namely $n=52$. The total shelf space of this product is $X=2205$. The demand of this product is seasonal

and there are twice demand peak in a year, $S_i = S_i * \sin(2 * 2\pi / 52 * t)$ is used to describe the seasonality. Assume that retailer only takes action of promotion for brand 1 and the type of promotion is not price-off. The length of promotion period is four weeks, and there is a gradually demand increasing in four weeks caused by promotion, use $(\gamma_i^1, \gamma_i^2, \gamma_i^3, \gamma_i^4)$ to denote the additional sales quantity, which means $(\gamma_i^1 > \gamma_i^2 > \gamma_i^3 > \gamma_i^4)$. And the negative effecting factor of the promotion of brand 1 to the sales of brand 2 and brand 3 are $\theta_2 = 0.2$ and $\theta_3 = 0.3$, respectively. The substitution rate π_{ij} ($0 \leq \pi_{ij} \leq I$) based on brand is

$$\pi_{ij} = \begin{bmatrix} 0 & 0.7 & 0.7 \\ 0.4 & 0 & 0.3 \\ 0.6 & 0.8 & 0 \end{bmatrix}$$

ss_{it} is the safety inventory of brand i in period t . It can be described as follows:

$$\begin{aligned} ss_{it} &= k_i \cdot MAD_{it} \\ MAD_{it} &= \frac{1}{t} \sum_{j=1}^t |\hat{D}_{ij} - D_{ij}| \end{aligned} \quad (4)$$

Where K_i is the safety inventory factor of brand i , MAD_{it} is the mean absolute deviation of brand i in the former t periods, D_{ij} is the real demand of brand i in period j and \hat{D}_{ij} is the forecast demand of brand i in period j .

Assuming the target service level is 98%, and then it should be known from the safety inventory factor table that the corresponding safety inventory factor is 2.56 from the safety inventory factor table. Thus the total gross profit of a year can be calculated as sales gross profit minus the cost of safety inventory cost:

$$TP_i = \sum_{t=1}^n D_{it} (P_{it} - W_{it}) - h_{it} ss_{it} . \quad (5)$$

Where W_{it} and P_{it} are respectively the wholesale price and retail price, h_{it} is the safety inventory cost of per piece (RMB/piece).

The parameters values for demand of these three brands are shown in table 1. Because brand 1 is a local brand, which should be selected by retailer anyhow, so brand 1 should be included in all the strategies of variant selection. Thus there are four strategies of variant selection.

Table 1. Parameters of demand model and profit model

Brand	a_i	b_i	P_i	W_i	α_i	β_i	s_i	X_i	h_i	λ_i	$(\gamma_i^1, \gamma_i^2, \gamma_i^3, \gamma_i^4)$	n_i
1	5900	2.5	2.80	2.3	17	0.5	170	$X/3$	0.12	0.5	(300,200,100,50)	13
2	3400	2.6	2.90	2.4	4	0.4	50	$X/3$	0.15	0.6	—	15
3	5900	2.3	3.20	2.6	28	0.6	130	$X/3$	0.17	0.4	—	10

3 Construction of Demand Forecasting Model of SVR Ensemble Based on Balanced-sampling

3.1 Introduction of Beer Sales Data

The most usual method retailers adopt is to simply use the average sales quantity of previous four weeks and last one to predict the sales quantity of this week, and other factors also are. Based on the reality of retail industry and expert knowledge, seven factors are collected as original features for our model: (1) price of current week, (2) seasonal factor, (3) execute sales promotion for current week or not, (4) the effect of sales quantity from promotion of other categories on current one, (5) and additional demand quantity of current category due to promotion, (6) average sales quantity of previous four weeks and (7) last week's sales quantity. The sales quantity of next week is used as the output. The original sales data used to construct models is generated by equation (1). Total 208 samples shown in table 2 are involved in the experiment.

Table 2. Samples of beer sales data

(1)	(2)	(3)	(4)	(5)	(6)	(7)	sales quantity of next week
2.6	158.9528	1	1	300	553	598	953
2.8	168.7605	0	0	0	668.5	953	626
2.8	168.7605	0	0	0	690.25	626	623
2.8	158.9528	0	0	0	700	623	597
2.8	139.9073	1	1	300	699.75	597	887

3.2 Algorithm Flow of the Demand Forecasting Model

BS-EnHSVR algorithm is proposed to reduce the generalization error, in which balance-sampling method is firstly used to sampling data as the training data for individual SVR, and then grid search algorithm is employed to get well-suited parameters to train individual SVR. Given the size of class best-selling = P, the size of class slow-moving = N, the expected size of training dataset for individual SVR of ensemble = Size, and the number of the individual SVRs of ensemble is Num. The process of BS-EnHSVR algorithm details as follows.

Step 1: Search several SVR parameters by training SVR model on the historical sales data used the Algorithm 1.

Step 2: Re-label the sales data by K-means clustering algorithm according to the sales quantity where K equals to 2. Then the sales records are clustered to two classes: best-selling and slow-moving.

Step 3: Sample equally from the relabeled data to train the individual SVRs of the ensemble. Select $\text{Size}/2$ from each of the two classes randomly, and then get a training dataset which size is Size. The selection process is repeated for Num times and Num training datasets are used to train Num individual SVRs.

Step 4: Train heterogeneous SVRs by using the Num training datasets generated in step 3 and the parameter generated in step 1.

Step 5: Combine of the results of all the Num individual SVRs by using simple average method.

The pseudo-code of algorithms is shown as follows.

```

Algorithm 1: Grid-Search Method for parameters
input: data=training set, gammas={parameter set of gamma},
Cs={parameter set of C}
output: (gamma2, C2) : pairs of parameters set,
size of set is 11

s1 = select 2/3*size sample from data randomly;
s2 = {data-s1};
for j = 1 to length(gammas)
    for k = 1:length(Cs)
        train SVR model with (gammas(j), Cs(k)) on
s1;
        test the SVR model on s2;
        if(model is better)
            //using insertion sort
            (gamma2 ,C2).add(gammas(j),Cs(k))

```

```

Algorithm 2: BS-EnHSVR
input: data=training set, num=11
output: preresult : Average of each model
{gammas, Cs} = Grid-Search()           //algorithem 1
result =k-means(data,K) // k is number of centers
// result is data sample with label
for i =1: num
    for j =1:K
        // S is sample assemble which are marked as j
        s= result[label==j]
        s1+= select size/k sample from s randomly
    train SVR model with (gammas(i),Cs(i)) on data s1
    //predictions of the model is recorded by pre(i)
    Preresult = preresult+ pre(i)
Preresult = preresult / num

```

4 Experiment

4.1 Experimental Setup

To verify the effectiveness of the model, an experiment on beer retail data is executed. The program is realized with Matlab 2009b, and Libsvm 2.89 toolkit developed by Chih-Jen Lin from Taiwan University is employed. RBF (Radial Basis Function) is chosen as kernel function in SVM model. The SVM model is Epsilon-SVR. In the experiment, the total number of individual SVRs is 11. Firstly, the data is normalized by maximum rule. And then the data is divided into training data and test

data according to 2:1. In practice, the retailer often analyses if the product is marketable. So, the data is divided into two classes—marketable and unmarketable by the sale quantity. The method is clustering the sale quantity data by K-means where $k=2$.

4.2 Experimental Results and Analysis

Models of SVR model, SVR Ensemble (SVRE) model, Support Vector Regression Ensemble based on Sampling Equally (SVRESE) are used for comparison with Heterogeneous Support Vector Regression Ensemble based on Sampling Equally (HSVRESE).

Table 3. Comparisons of each model on MAPE (100%)

	SVR	SVRE	SVRESE	HSVRESE
A	(4.87, 6.19, 3.03)	(4.93, 6.17, 3.09)	(6.81, 6.13, 3.08)	(3.75, 5.92, 2.34)
B	(6.16, 5.77)	(6.16, 5.80)	(6.86, 5.76)	(3.60, 5.07)
C	(5.75, 3.99)	(5.63, 3.99)	(6.19, 4.02)	(4.00, 3.07)
D	5.50	5.51	6.15	2.92

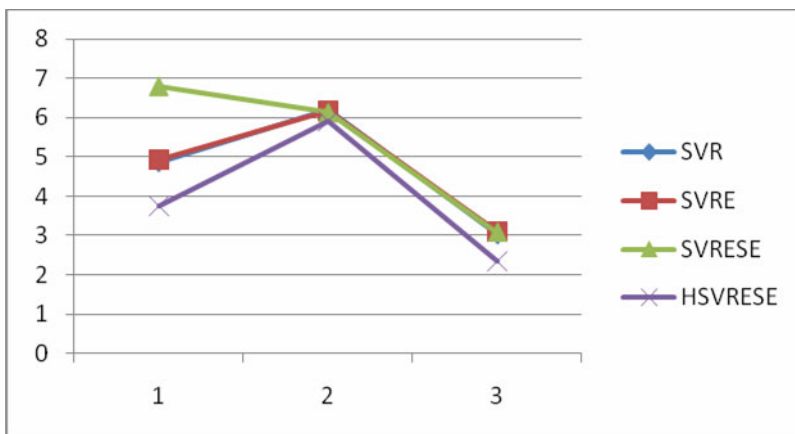


Fig. 1. MAPE (100%) index of each model when used sales plan A

Experiments are repeated 20 times. All the final results are the average values over the 20 iterations. Table 3 shows the results, where A, B, C, D are respectively the four different category planning strategies: A means all the three brands of beers, brand 1, brand 2 and brand 3, are selected by the beer retailer, B is brand 1 and brand 2 matched for sale, C is brand 1 and brand 3, while D means only brand 1 is considered by the retailer. The mean MAPEs (Mean Absolute Percentage Error) of HSVRESE, SVR, SVRE, and SVRESE are 3.83%, 5.53%, 5.16%, and 5.62% respectively. And the MAPE of HSVRESE is 1.79% lower than that of SVRESE, 1.33% lower than that of SVRE, 1.7% lower than that of SVR. As shown in Fig.1, there are four curves

representing every brand's MAPE indices for different models when sales plan A is executed, and it can be seen that HSVRESE has the lowest MAPE. Table 4 shows the MAPEs and their training parameters, gamma and penalty, of 11 individual SVRs of the ensemble. And the last line in table 4 indicates the MAPEs of the final ensemble. It is obviously that some individuals have lower MAPEs and some individuals have higher MAPEs than that of the ensemble. For example, the MAPE of the 10th individual SVR is lower than that of HSVRESE. But it depends on parameters selection. Parameters affect the results greatly. And in rapid business decision environment, seeking the most suitable learning parameters is costly, and experiments show that the heterogeneous can effectively reduce the generalization error after priority selection of the random parameters. Therefore, the conclusion can be drawn that HSVRESE can reduce MAPE when reduce dependence of parameter selection.

Table 4. MAPE and training parameters of 11 Individual SVMs

	A	B	C	D	gamma	penalty				
1	6.44	6.20	3.08	6.99	5.72	6.01	4.05	6.10	0.005	1100
2	2.42	5.98	2.34	2.05	4.60	2.17	2.62	1.93	0.005	2000
3	2.41	5.91	2.33	2.04	4.70	2.21	2.64	1.91	0.005	1500
4	6.74	6.10	3.12	6.57	5.78	6.63	4.09	6.32	0.005	500
5	2.51	5.92	2.41	2.01	5.07	2.38	2.62	2.09	0.090	1100
6	6.93	6.05	3.13	7.06	5.85	6.46	4.09	6.01	0.090	1500
7	2.41	5.96	2.27	2.06	4.67	2.28	2.67	1.91	1.000	2000
8	6.26	6.19	3.07	7.00	5.70	6.32	4.04	6.30	0.010	1100
9	2.45	6.01	2.34	2.21	4.93	2.29	2.68	2.03	0.010	1500
10	16.67	6.55	5.41	14.32	6.59	13.31	6.02	12.44	0.500	500
11	2.41	5.85	2.28	2.06	4.77	2.16	2.69	1.92	0.090	500
Ensemble	3.75	5.92	2.34	4.16	5.23	4.34	3.08	3.41		

In order to investigate the effect of forecasting precision on safety inventory and sales profit, table 5 shows the comparison of year's total safety inventory and gross profit among different models when target service level is 98%. It's clear that, the safety inventory of HSVRESE is 2863 lower than SVRE, 2844 lower than SVR, 2855 lower than SVRESE. And the sales profit of HSVRESE is 344 higher than SVRE, 341 higher than SVR, 307 higher than SVRESE. The results strongly prove the superiority of HSVRESE on reducing safety inventory and promote sales profit even under high services level, which will greatly enhance the competitive power of the retail company.

Table 5. Annual safety stock and gross margin of each model

	SVR	SVRE	SVRESE	HSVRESE
Year's total safety inventory(thousand piece)	5.510	5.529	5.221	2.666
Year's total gross profit(thousand RMB)	22.709	22.706	22.743	23.050

5 Conclusions

Demand forecasting is the basis of business operation in a company and the forecasting accuracy has a great effect on safety inventory, profit and competitive power of the company. This paper proposes a demand forecasting model of balanced-sampling-based SVR ensemble named BS-EnHSV to improve the sample's representativeness and the precision of the average individual SVR through using the balanced sampling. And then the model is applied to a beer demand forecasting. The experimental results show that, the generalization ability of BS-EnHSV is the best one than the other compared models, and then strongly prove the superiority of BS-EnHSV on reducing safety inventory and promote sales profit, which will greatly enhance the competitive power of the retail company.

Acknowledgments. This research is supported by the National Natural Science Foundation of China (Grant No. 70972106), National Natural Science Foundation of Shanghai, China (Grant No.09ZR1412600), Innovation Foundation of Shanghai University, China (Grant No.A.10010808904), Innovation Foundation of Graduations of Shanghai University, China (Grant No.SHUCX102177 and No.SHUCX112162), and Shanghai Leading Academic Discipline Project (Grant No. J50103).

References

1. Chopra, S., Meindl, P.: Supply Chain Management Strategy, Planning, and Operation. Tsinghua University Press, Beijing (2001)
2. Wang, Y.J.: Data Mining and Practical Modeling Methods for Supply Chain Management. Tsinghua University Press, Beijing (2001)
3. Joseph, P.M.: A Review of Selected Recent Advances in Technological Forecasting. Journal of Technological Forecasting & Social Change 70(8), 719–733 (2003)
4. Kesten, C.G.: Game Theory, Simulated Interaction, and Unaided Judgment for Forecasting Decisions in Conflicts: Further Evidence. Journal of Forecasting, 463–472 (2005)
5. Geoffrey, A.P., Bernard, J.M.: Twenty-five Years of Progress, Problems, and Conflicting Evidence in Econometric Forecasting. What about the next 25 years? International Journal of Forecasting 22(3), 475–492 (2006)
6. Cortes, C., Vapnik, V.: Support vector networks. Machine Learning 20, 273–297 (1995)
7. Hansen, L.K., Salamon, P.: Neural Network Ensembles. IEEE Trans. on Pattern Analysis and Machine Intelligence. 12, 993–1001 (1990)
8. Salgado, R.M., Pereira, J.J.F., Ohishi, T., Ballini, R., Lima, C.A.M., Zuben, F.J.V.: A Hybrid Ensemble Model Applied to the Short-term Load Forecasting Problem. In: International Joint Conference on Neural Networks, pp. 2627–2634 (2006)
9. Lean, Y.U., Wang, S.Y., Kin, K.L.: Forecasting China's Foreign Trade Volume With a Kernel-based Hybrid Econometrical Ensemble Learning Approach. Journal of Systems Science and Complexity 28, 1–19 (2007)
10. Liu, Y., Yin, Y.F., Gao, J.J., Tan, C.L.: Demand Forecasting by Using Support Vector Machine. In: The Third International Conference on Natural Computation (ICNC 2007), pp. 272–276 (2007)

CCC: Classifier Combination via Classifier

Can-Yi Lu^{1,2}

¹ Hefei Institute of Intelligent Machines, Chinese Academy of Sciences, Hefei, China

² Department of Automation, University of Science and Technology of China, Hefei, China

canyilu@mail.ustc.edu.cn

Abstract. The combination of classifier has long been proposed as a method to improve the accuracy achieved in isolation by a single classifier. Most of the extant works focus on how to generate a group of "good" base classifiers, such as AdaBoost and Bagging. We are interested in the method of combining multiple classifiers. In contrast to such popular used method as vote, we regard the classifier combination problem as a classification problem. From the perspective of pattern recognition, the base classifiers can also be regarded as a feature extraction method. In theory, any of classifiers can be used to combine the base classifiers as long as they are able to treat the outputs of base classifiers. More generally, the combination model is also able to deal with other machine learning problems including cluster and regression task, that is Learner Combination via Learner(LCL) model. A large empirical study shows that, comparing with majority vote(Bagging) and weighted majority vote(AdaBoost), CCC can significantly improve the performance.

Keywords: classifier combination, classifier, major vote.

1 Introduction

Classifier combination is a learning paradigm where a finite number of classifiers whose individual decisions are combined in some way(typically by weighted or unweighted vote) to classify new examples. It originates from Hansen and Salamon's work [1], which shows that the resulting classifiers can significantly improve the generalization ability. Due to its remarkable performance, classifier ensemble has been of the most active areas of research in supervised learning during the past twenty years. The technology has also been successfully applied to various areas, such as character recognition [2], speaker identification [3] and seismic signals classification [4].

Classifier combination includes two important aspects, i.e. generating a set of base classifiers and combining them.

As for generating base classifiers, Bagging [5] and Boosting [6] seem to be perceived as "classic" at present. They have been found to be accurate, computationally feasible across various data domains. Bagging is a bootstrap ensemble method that creates individuals for its ensemble by training each classifier on a random redistribution of the training set. Each classifier's training set is generated by randomly drawing with replacement. Boosting is a family of methods, the most prominent one of which is AdaBoost [7], it generates a series of base

classifiers whose training sets are determined by the performance of the earlier one in series. Examples that are incorrectly predicted by former classifier in the series are chosen more often than examples that were correctly predicted. AdaBoost attempts to produce new classifiers that are better able to predict examples for which the current ensemble's performance is poor. There are also many other methods for generating the base classifiers, representatives of which include Random Subspace [8], Random Forest [9] and Rotation Forest [10], etc.

As for the classifier combination methods, the most prevailing approach is weighted and unweighted majority vote. If the labels are available, majority vote is usually used. If the continuous outputs are supplied, an average, linear or nonlinear combination rules can be employed [11]. There are also some other approaches for combining predictions, representatives of which include Behavior Knowledge Space [12], Wernecke [13], SVD combination [14].

At present, most of ensemble approaches pay more attention on how to generate a “good” group of base classifiers. The combination methods are usually dependent on the generation procedure, such as Bagging. In this paper, differently from the traditional classifier combination methods, we regard the classifier combination problem not as a part of classifier ensemble, but a general classification problem. Many classifiers can be able to combine multiple classifiers. From this different point of view, some other problems about classifier ensemble could be converted into other topics in pattern recognition.

The rest of this paper is organized as follows. In section 2, we describe the CCC model. In section 3, the CCC model is extended to combine other machine problems. In section 4, a large empirical study is reported. Finally section 5 includes the conclusions and some future works.

2 Classifier Combination via Classifier

Consider the standard supervised learning problem. Let a training sample set be $X = \{(x_i, y_i) | x_i \in R^D, y_i \in \Omega, i=1, \dots, n\}$ where y_i is the label of x_i , D is the dimensionality of the sample space, n is the number of training samples, c is the number of classes. Assume m classifiers are generated using some method, such as AdaBoost and Bagging, denoted as $f = [f_1, \dots, f_m]^T$. For a given training sample x_j , $z_j = f(x_j)$ is the predicted vector of all the base classifiers on x_j . $z_{ij} = f_i(x_j)$, the element of z_j , could be the predicted label, or a c -dimensional vector $z_{ij} = [z_{ij}^{(1)}, \dots, z_{ij}^{(c)}]^T$, where the value $z_{ij}^{(l)}$ represents the support for the i -th classifier that vector x_j submitted for classification comes from class l . So the outputs of f could be discrete, continuous or even mixed.

2.1 The CCC Model

Fig.1 shows the CCC model. For classifier combination, the base learners and decision learner are all classifiers. We regard the base classifiers $f = [f_1, \dots, f_m]^T$

as a mapping from R^D to Ω^d , and Ω^d can be called as an intermediate feature space [15]. Thus the classifier combination aims to find a mapping $H : \Omega^d \rightarrow \Omega$, which actually can be solved as a classification problem. Then the traditional classifier combination methods can all be regarded as classifiers. Specially, the majority vote is similar to the nearest centroid method. Denote the centroid of l -th class as $C_l = [l, \dots, l]^T, l=1, \dots, c$. The predicted label of x_j using majority vote is $\arg \min_l d(f(x_j), C_l)$, where the distance between α and β is defined as

$$d(\alpha, \beta) = |\{i | \alpha_i \neq \beta_i\}|.$$

Differently from nearest centroid method, the centroid of the l -th class is not dependent on the training samples, thus majority vote does not employ the label information to help decision making. If the base classifiers are heterogeneous with different types of outputs, it's difficult to design a sophisticated method to combine them, but not for CCC as long as using a suitable decision classifier.

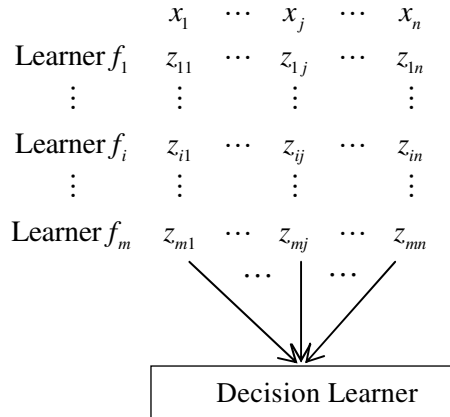


Fig. 1. The CCC model, where the learners are all classifiers

In detail, the whole procedure of the CCC model is as follow, firstly, the base learner is called to generate m base classifiers $f = [f_1, \dots, f_m]^T$ on the training set X . Secondly, the prediction of each training sample is regarded as its feature extraction, and the decision classifier is employed to provide the predicted label.

It is worth to mention that owing to the No Free Lunch Theorem [16], there is no guarantee some classifier will be always better than majority vote, and vice versa. But using the label information to help decision making is a reasonable direction.

2.2 A Pattern Recognition Perspective

Fig. 2 provides a pattern recognition perspective of CCC. Comparing traditional classifier combination system with CCC, the traditional combination methods are

special cases of classifier. Comparing the pattern recognition system with CCC, the generated multiple classifier f is only a special feature extraction method. Therefore, CCC is not only a classifier combination model, but also a pattern recognition system. In some case, such as for pattern recognition, the CCC model can be used as a dimensionality reduction method, the outputs of multiple classifiers is in low-dimensional space and is very discriminative even using majority vote which is a very simple classifier. The success of CCC will pave the way for dimensionality reduction using multiple classifiers.

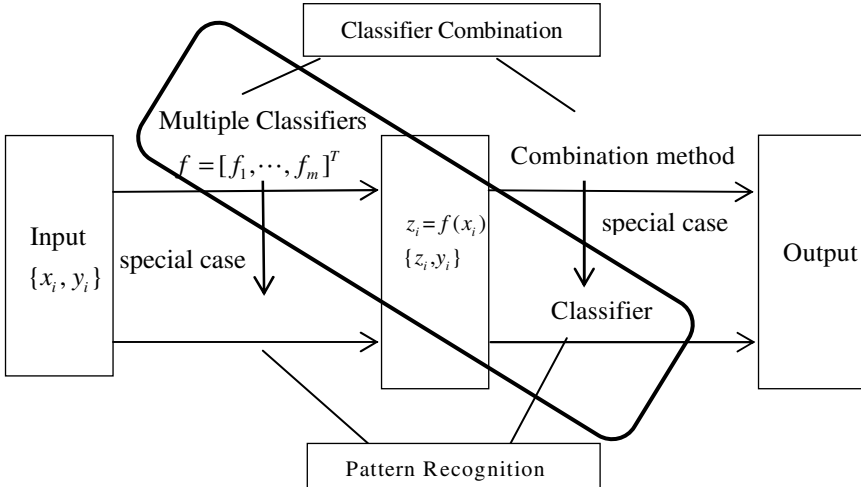


Fig. 2. The Relation among Classifier Combination, Pattern Recognition and the CCC model

2.3 Other Topics

Zhou et al. [17] proposed a selective ensemble method which shows that ensemble many instead of all classifiers can improve the generalization ability. It's time-consuming to select the optimal subset of classifiers(actually it's a NP-hard problem). But from the standpoint of CCC, the selective ensemble problem is actually a feature selection problem in pattern recognition. Some classifiers are able to select features such as decision tree.

Comprehensibility, i.e., understandability of the learned model to user, is desired in many real applications. Even when the base learners are comprehensible models such as small decision trees, the combination of them will lead to a black-box model. Improving the comprehensibility of ensemble methods is an important yet largely understudied direction [18]. If we use decision stump as the base classifier, and decision tree as the decision classifier, the resulting model is actually also a decision tree, which is also comprehensible. The more ideal model is to generate the decision tree at the same time as generating the based classifiers.

3 Learner Combination via Learner(LCL)

Aforementioned we focus on the classifier combination problems. Learner ensemble includes other problems, such as cluster ensemble, regression ensemble. We will show that the CCC model can be extended to LCL model which is able to tackle other learner combination problems.

- **Regression** is similar to classification with continuous outputs. In Fig. 1, we replace the base learners and decision learner as regression models, the resulting model will also very similar to CCC, it should be competitive enough.
- **Cluster ensemble** will be a little different from CCC, since no label information can be used. Similarly, we use a cluster model to replace the decision learner. The decision of each sample is independent from other samples when using majority vote, but not when using cluster model. Thus, using cluster to combine clusters seems to use more global information, which is a two-layer cluster model.
- **Other Machine Learning Problems** can also be tackled through LCL model, such as semi-supervised learning, transfer learning, multi-label learning. The base learners are all regarded as a mapping from the source space to the intermediate feature space. The outputs of LCL model is dependent on the decision learner which is corresponding to the machine learning problem.

LCL is an Algorithm-Independent model which will greatly expand the ensemble learning theory in more applications of machine learning problems.

4 Experimental Verification

An experiment is set up to compare CCC with AdaBoost and Bagging. We use the decision tree as base learner. The decision tree construction method was J48 from the WEKA library [19], a reimplementation of C4.5. Naïve Bayes(also implemented in WEKA) was used as the decision classifier. Note that other classifiers can also be used such as decision tree, kNN since they are suitable to mixed attribute. If the outputs of base classifiers are continuous, more classifiers can be used, i.e. SVM, Neural Network. We perform our experiments on 26 data sets from the UCI repository [20].

The experimental setting are as follows: the number of base classifiers was set to 25, other parameters of J48, AdaBoost and Bagging are kept at their default values in WEKA. For each data set, the experiments are repeated for 20 times. In each time, 10-fold cross validation is performed.

Table 1 shows the accuracies(mean \pm std). Since we focus on the classifier combination method, the decision classifier is performed on the base classifiers generated from AdaBoost and Bagging, respectively. In Table 1, AdaBoost+CCC indicates that we use the base classifiers from AdaBoost but use a classifier to combine them, and Bagging+CCC means similar. Fig. 3 gives a graphical overview of the results in Table 1. On the y-axis is the accuracy of the CCC model while on

the x-axis is the best accuracy between J48 and the competing ensemble method. If CCC is better than the other method for each data set, all the points on the graph would lie above the diagonal line which marks the equivalent scores. The data sets for which the differences are particularly large are labeled in the graphs. As most of the points in both subplots lie above the diagonal line, the figure demonstrates the advantage of CCC.

Table 1. Classification Accuracy and Standard Deviation of J48 and Ensemble Methods

Data	Base Learner C4.5	AdaBoost	AdaBoost+CCC	Bagging	Bagging+CCC
audiology	87.00±6.59	89.95±6.78	90.95±6.23	85.45±6.52	85.83±6.53
auto-mpg	54.60±12.11	56.60±12.91	62.03±12.22	39.53±11.91	43.97±12.09
autos	82.28±9.17	85.38±7.89	86.08±7.58	67.75±9.55	64.97±9.65
balance-scale	71.44±5.31	71.24±5.49	75.25±6.50	75.81±4.90	80.37±6.68
breast-cancer	25.22±12.09	36.22±15.76	41.11±15.87	14.17±11.63	42.44±16.40
breast-w	92.71±5.13	96.00±4.11	97.56±3.40	94.25±5.00	95.10±4.68
clean1	77.60±9.60	88.26±6.90	88.67±6.89	76.90±9.77	80.48±9.33
colic	70.75±10.92	72.14±12.02	74.54±11.91	71.11±10.98	71.54±11.01
credit-g	33.57±8.87	42.93±8.79	47.47±9.06	40.67±9.24	57.50±9.37
diabetes	57.24±11.31	56.24±10.99	60.94±10.00	57.09±10.00	65.78±8.77
flag	59.47±11.58	66.71±11.43	67.29±11.49	65.47±9.62	65.47±9.96
glass	63.60±11.84	73.83±10.59	74.10±10.94	67.27±11.31	70.30±11.95
hayes-roth	61.50±15.47	65.13±14.86	79.25±13.52	73.94±15.94	77.13±15.04
heart-c	72.39±12.44	75.04±11.43	76.11±11.20	73.57±11.70	76.93±11.54
heart-h	63.55±15.73	67.45±14.13	71.45±14.70	66.41±14.73	71.05±14.64
heart-statlog	70.83±12.72	74.29±13.12	75.25±12.91	75.00±12.89	78.00±12.34
hypothyroid	96.43±3.16	98.47±2.18	98.28±2.29	97.64±2.76	97.71±2.79
iris	93.25±8.44	92.65±8.24	93.00±7.83	91.30±8.52	91.40±8.51
labor	88.50±15.21	92.75±13.40	91.75±13.98	92.13±12.68	91.63±13.56
page-blocks	81.46±4.85	81.82±5.01	89.32±4.30	82.95±4.72	87.11±4.38
segment	96.47±1.43	98.27±0.97	98.19±0.98	96.53±1.32	96.64±1.30
sick	86.70±7.62	89.30±6.62	92.17±5.82	84.39±7.31	90.74±5.84
soybean	91.90±3.12	92.44±3.12	93.36±3.06	87.07±3.75	87.73±3.36
tic-tac-toe	72.48±7.58	96.73±2.97	97.39±2.91	78.70±7.39	88.61±5.95
vehicle	76.84±5.36	82.83±4.16	83.00±4.07	79.52±3.82	79.65±4.04
wine	91.42±9.34	95.17±6.96	95.00±7.09	93.67±8.11	94.25±7.81

5 Conclusions and Future Works

In this paper, we regard the classifier combination problem as a classification problem.

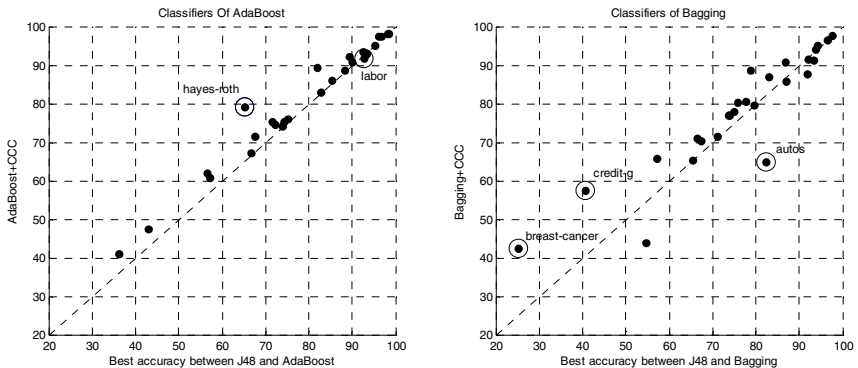


Fig. 3. Comparison of accuracy of CCC and best accuracy between J48 and the competing ensemble method

Using a classifier to combine classifiers is a reasonable choice since it can employ the label information. The CCC model can also be regarded as a special pattern recognition system, and the multiple classifiers can be employed as a feature extraction method, even a dimensionality reduction method. More generally, the LCL model is an Algorithm-Independent model which is appropriate for other machine learning algorithms and machine learning problems. This will further expand the influence and the scope of application of ensemble learning.

There are many works left to do in the future. Firstly, the CCC model provide a novel perspective for classifier combination, embedding the decision classifier into the classifier generating procedure will be a more ideal model like AdaBoost. Using decision tree to combine decision stump will lead to a comprehensible model. Secondly, since the LCL model is Algorithm-Independent, using it to tackle more machine learning problems will be an attractive direction. Thirdly, The success of CCC paves the way for dimensionality reduction using multiple classifiers. The traditional methods such as PCA and LDA can only handle the issue of continuous attributes, while multiple classifiers can handle different types of features. The outputs of multiple classifiers will be more discriminative due to the ensemble technology. At last, the theoretical analysis of LCL is also very important.

Acknowledgments. This work was supported by the grants of the National Science Foundation of China, Nos. 60975005, 61005010, 60873012, 60805021, 60905023, 31071168 & 30900321, and the grant of China Postdoctoral Science Foundation, No. 20100480708, the grant of the Key Scientific Research Foundation of Education Department of Anhui Province, No. KJ2010A289, the grant of Scientific Research Foundation for Talents of Hefei University, No. 11RC05..

References

1. Hansen, L.K.: Neural Network Ensembles. *IEE Transactions on Pattern Analysis and Machine Intelligence* 12, 993–1001 (1990)
2. Mao, J., Mohiuddin, K.M.: Improving OCR Performance Using Character Degradation Models and Boosting Algorithm. *Pattern Recognition Letters* 18, 1415–1419 (1997)

3. Chen, K., Wang, L., Chi, H.S.: Methods of Combining Multiple Classifiers with Different Features and Their Applications to Text-independent Speaker Identification. *International Journal of Pattern Recognition and Artificial Intelligence* 11(3), 417–445 (1997)
4. Shimshoni, Y., Intrator, N.: Classification of Seismic Signals by Integrating Ensembles of Neural Networks. *IEEE Transactions on Signal Processing* 46(5), 1194–1201 (1998)
5. Breiman, L.: Bagging Predictors. *Machine Learning* 24(2), 123–140 (1996)
6. Freund, Y.: Boosting a Weak Learning Algorithm by Majority. *Information and Computation* 121(2), 256–285 (1995)
7. Freund, Y., Schapire, R.E.: A Decision-theoretic Generalization of On-line Learning and an Application to Boosting. *Journal of Computer and System Sciences* 55(1), 119–139 (1997)
8. Ho, T.K.: The Random Subspace Method for Constructing Decision Forests. *IEEE Transactions on Pattern Analysis and Machine Intelligence* 20(8), 832–844 (1998)
9. Breiman, L.: Random forests. *Machine Learning* 45(1), 5–32 (2001)
10. Rodriguez, J.J., Kuncheva, L.I.: Rotation Forest: A New Classifier Ensemble Method. *IEEE Transactions on Pattern Analysis and Machine Intelligence* 28(10), 1619–1630 (2006)
11. Fumera, G., Roli, F.: A Theoretical and Experimental Analysis of Linear Combiners for Multiple Classifier Systems. *IEEE Transactions on Pattern Analysis and Machine Intelligence* 27(6), 942–956 (2005)
12. Huang, Y.S., Suen, C.Y.: Method of Combining Multiple Experts for the Recognition of Unconstrained Handwritten Numerals. *IEEE Transactions on Pattern Analysis and Machine Intelligence* 17(1), 90–94 (1995)
13. Wernecke, K.D.: A Coupling Procedure for the Discrimination of Mixed Data. *Biometrics* 48(2), 497–506 (1992)
14. Merz, C.J.: Using Correspondence Analysis to Combine Classifiers. *Machine Learning* 36(1-2), 33–58 (1999)
15. Kuncheva, L.I.: *Combining Pattern Classifiers: Methods and Algorithms*. Wiley, Hoboken (2004)
16. Duda, R.O., Hart, P.E., Stork, D.G.: *Pattern Classification*, 2nd edn. Wiley, Chichester (2000)
17. Zhou, Z.H., Wu, J.X., Tang, W.: Ensembling Neural Networks: Many Could Be Better Than All. *Artificial Intelligence* 137(1-2), 239–263 (2002)
18. Zhou, Z.H., Jiang, Y., Chen, S.F.: Extracting Symbolic Rules from Trained Neural Network Ensembles. *Ai Communications* 16(1), 3–15 (2003)
19. Witten, I., Frank, E.: *Data Mining: Practical Machine Learning Tools and Techniques*. Morgan Kaufmann, San Francisco (2005)
20. Blake, C.L., Merz, C.J.: UCI Repository of Machine Learning Databases (1998),
<http://www.ics.uci.edu/mlearn/MLRepository.html>

Hybrid Reduction in Soft Set Decision Making

Ahmad Nazari Mohd Rose¹, Mohd Isa Awang¹, Hasni Hassan¹,
Aznida Hayati Zakaria¹ Tutut Herawan², and Mustafa Mat Deris³

¹ FIT, Universiti Darul Iman Malaysia, Terengganu, Malaysia

{anm, hasni, isa, aznida}@unisza.edu.my

² FSKKP, Universiti Malaysia Pahang, Pahang, Malaysia

tutut81@uad.ac.id

³ FTMM, Universiti Tun Hussein Onn Malaysia, Johor, Malaysia

mmustafa@uthm.edu.my

Abstract. In this paper, we present an extended technique of decision making by implementing column reduction with reduction based on calculated maximal support objects. Using a Boolean valued information system, certain rows or objects can be defined as ultimate maximum support object, ultimate minimum support object and zero significance parameter. One can then reduce a table by eliminating the defined row or objects in what has been defined as hybrid reduction. As part of our paper, we have managed to show that our proposed model of hybrid reduction yielded a better data size reduction whilst still maintaining consistent results.

Keywords: Boolean-valued information system, Soft set theory, Hybrid Reduction, Maximal Supported Set, Decision Making.

1 Introduction

Handling uncertain data is very important because in reality, there are various kinds of real life problems that involve uncertain data such as in the field of engineering, medical, social, medical sciences and many others [1]. Fortunately, these predicaments can be solved using mathematical principles, and one of them is the Soft Set Theory [2]. The theory of soft set was proposed by Molodtsov in 1999 as a new way for managing uncertain data. As for standard soft set, it may be redefined as the classification of objects in two distinct classes, thus confirming that soft set can deal with a Boolean-valued information system.

The soft set theory has also been applied for data reduction; an area that supports decision making problems with less involvement of data by reducing the attributes of the original data. If excessive information governs the process of decision making, then issues of processing times and inefficiencies will be of primary concern.

Most of the researches in the soft set theories only focus in attribute reduction using several approaches as in [1,3,4,8]. Based on maximal supported set derived, we will demonstrate how column reduction will be complemented by row reduction; which we defined as hybrid reduction for the combined row and column reduction.

The rest of this paper is organized as follows. Section 2 describes the fundamental concept of soft set theory. Section 3 introduces the proposed technique of reduction and decision making using hybrid reduction based on supported sets. Section 4 outlines the results and finally, we conclude our works in section 5.

2 Soft Set Theory

Throughout this section U refers to an initial universe, E is a set of parameters, $P(U)$ is the power set of U .

Definition 2.1. (See [2].) A pair (F, E) is called a soft set over U , where F is a mapping given by $F : E \rightarrow P(U)$.

In other words, a soft set is a parameterized family of subsets of the universe U . For $e \in E$, $F(e)$ may be considered as the set of e -elements of the soft set (F, E) or as the set of e -approximate elements of the soft set, instead of a (crisp) set.

The relation between a soft set and a Boolean-valued information system is given as follows.

Proposition 2.2. If (F, E) is a soft set over the universe U , then (F, E) is a binary-valued information system $S = (U, A, V_{\{0,1\}}, f)$.

Proof. Let (F, E) be a soft set over the universe U , we define a mapping

$$f = \{f_1, f_2, \dots, f_n\},$$

where

$$f_i : U \rightarrow V_i \text{ and } f_i(x) = \begin{cases} 1, & x \in F(e_i) \\ 0, & x \notin F(e_i) \end{cases}, \text{ for } 1 \leq i \leq |A|.$$

Hence, if $A = E$, $V = \bigcup_{e_i \in A} V_{e_i}$, where $V_{e_i} = \{0,1\}$, then a soft set (F, E) can be considered as a binary-valued information system $S = (U, A, V_{\{0,1\}}, f)$.

From Proposition 2.2, it can be easily understood that a binary-valued information system can be represented as a soft set. Thus, we can make a one-to-one correspondence between (F, E) over U and $S = (U, A, V_{\{0,1\}}, f)$.

3 The Proposed Technique

In this section, we will introduce a new concept of reduction based on hybrid reduction. The main idea behind this object reduction is to further reduce the size of a database without having to store the values of sub optimal objects, or even next sub optimal objects and any other inferior objects.

Example 3.1. Let a soft set (F, E) represents a study on communication prowess among selected university students. Let's assume that eighteen students had been

surveyed in the universe $U = \{u_1, u_2, \dots, u_{18}\}$, and E is a set of parameters representing communication facilities used by the students, $E = \{e_1, e_2, e_3, e_4, e_5, e_6\}$. Consider the mapping $F : E \rightarrow P(U)$ given by “student communication prowess (\cdot) ”, where (\cdot) is to be filled in by one of the parameters in $p \in E$. Thus, the overall approximation can be represented as the following:

$$(F, E) = \left\{ \begin{array}{l} \text{email} = \{u_1, u_2, u_3, u_4, u_8, u_9, u_{10}, u_{11}, u_{13}, u_{14}, u_{15}, u_{16}, u_{17}\}, \\ \text{facebook} = \{u_2, u_3, u_4, u_5, u_8, u_9, u_{10}, u_{12}, u_{13}, u_{14}, u_{15}, u_{16}, u_{17}\}, \\ \text{blog} = \{u_1, u_2, u_3, u_4, u_6, u_8, u_9, u_{10}, u_{11}, u_{13}, u_{15}, u_{16}, u_{17}, u_{18}\}, \\ \text{friendsters} = \{u_2, u_3, u_4, u_8, u_9, u_{10}, u_{12}, u_{13}, u_{15}, u_{16}, u_{17}, u_{18}\}, \\ \text{ym} = \{u_2, u_3, u_4, u_5, u_6, u_7, u_8, u_9, u_{10}, u_{11}, u_{13}, u_{15}, u_{16}, u_{17}, u_{18}\}, \\ \text{sms} = \{u_2, u_3, u_4, u_8, u_9, u_{10}, u_{13}, u_{15}, u_{16}, u_{17}\} \end{array} \right\}$$

Fig. 1. The soft set

This example can be represented in the following Boolean-valued information system :

Table 1. Tabular representation of a soft set from Example 3.1

U/P	e_1	e_2	e_3	e_4	e_5	e_6	$f(\cdot)$	U/P	e_1	e_2	e_3	e_4	e_5	e_6	$f(\cdot)$
u_1	1	0	1	0	0	0	2	u_{10}	1	1	1	1	1	1	6
u_2	1	1	1	1	1	1	6	u_{11}	1	0	1	0	1	0	3
u_3	1	1	1	1	1	1	6	u_{12}	0	1	0	1	0	0	2
u_4	1	1	1	1	1	1	6	u_{13}	1	1	1	1	1	1	6
u_5	0	1	0	0	1	0	2	u_{14}	1	1	0	0	0	0	2
u_6	0	0	1	0	1	0	2	u_{15}	1	1	1	1	1	1	6
u_7	0	0	0	0	1	0	1	u_{16}	1	1	1	1	1	1	6
u_8	1	1	1	1	1	1	6	u_{17}	1	1	1	1	1	1	6
u_9	1	1	1	1	1	1	6	u_{18}	0	0	1	1	1	0	3

Definition 3.1. Let (F, E) be a soft set over the universe U and $u \in U$. A parameter co-occurrence set of an object u can be defined as $\text{coo}(u) = \{e \in E : f(u, e) = 1\}$.

Definition 3.2. Let (F, E) be a soft set over the universe U and $u \in U$. Support of an object u is defined by $\text{supp}(u) = \text{card}(\{e \in E : f(u, e) = 1\})$.

Definition 3.3. Let (F, E) be a soft set over the universe U and $u \in U$. An object u is said to be maximally supported by a set of all parameters E , denoted by $\text{Msupp}(u)$ if $\text{supp}(u) > \text{supp}(v) \quad \forall v \in U \setminus \{u\}$.

Based on Definition 3.3, we can make supported (ranked) ordered objects according their support value as $U_1 > U_2 > \dots > U_n$, where $U_i \subseteq U$ and $U_i = \{u \in U : u \text{ is } i\text{-th maximal supported by } E\}$, for $1 \leq i \leq n$. Thus, U_i is a collection of objects in U having the same support, i.e., objects of the same support are grouped into the same class. Obviously $U = \bigcup_{1 \leq i \leq n} U_i$ and $U_i \cap U_j = \emptyset$, for $i \neq j$. In other words, a collection of $U/E = \{U_1, U_2, \dots, U_n\}$ is a decision partition of U .

Definition 3.4. Let (F, E) be a soft set over the universe U and $A \subseteq E$. A is said to be indispensable if $U/A = U/E$. Otherwise, A is said to be dispensable.

According to Definition 3.4, we can reduce the number of parameters without changing the optimal and sub optimal decisions.

Definition 3.5. For soft set (F, E) over the universe U and $A \subseteq E$. A is reduction of E if only if A is indispensable and $\text{supp}_{E \setminus A}(u) =_{E \setminus A} \text{supp}(v)$, for every $u, v \in U$.

Definition 3.6. For soft set (F, E) over the universe U and $u \in U$. An object u will be the optimal decision if u is maximally supported by E .

Definition 3.7. For soft set (F, E) over the universe U and $u \in U$. The ultimate maximum support set is defined as of an object u , where

$$\text{Ultmax}(u) = \text{card}(\{e \in E : f(u, e) = 1\}) = n.$$

Referring to Definition 3.7, any object that has been regarded as part of the ultimate maximum support set and for any search result for optimal objects will definitely yield the object that belongs to the group of ultimate maximum support if there is any.

So in this case, since it is already confirmed that for any object that belongs to the group of ultimate maximum support set as the optimal object, then it is permissible to dispense such row which subscribe to the notion of ultimate maximum optimal object without compromising on the value of the optimal object.

Definition 3.8. For soft set (F, E) over the universe U and $u \in U$. The ultimate minimum support set is defined as an object u , where

$$\text{Ultmax}(u) = \text{card}(\{e \in E : f(u, e) = 0\}) = n.$$

Based on Definition 3.8, any object designated by the definition will be treated consistently as the ultimate minimum support set. Any object from the set of ultimate minimum support object will always be defined as the most inferior object hence can be considered as dispensable.

Definition 3.9. For soft set (F, E) over the universe U , the zero significant parameter is defined as $\text{Zerosig}(e) = \sum_j h_{ij} = 0$.

Definition 3.10. Any parameter with the notion as zero significant is an automated choice to be dispensed.

The pseudocode of hybrid reduction is as follows:

1. Input the soft set (F, E) over a universe U
2. Determine the co_occurrence of the parameters of each object.
3. Calculate its supported values
4. Determine the order of support by arranging it in decreasing order
5. Find the optimal, sub optimal , and next sub optimal until the inferior objects can be determined based on the ranking of supported values
6. Determine the cluster partition U / E
7. Determine $A \subset E$, such that $U / A = U / E$ and $\text{supp}(u) = \text{supp}(v)$ for every $u, v \in U$
8. If there is $A \subset E$, determine the reduced form
9. Determine any rows that had fulfilled the definition of the ultimate maximum support set
10. Delete/Partition the objects of ultimate maximum support set
11. If there is any ultimate minimum support set, delete/partition the row of the inferior object
12. If there is any ultimate minimum support set, mark the objects the inferior object.
13. If there is any zero significant parameter, delete the column
14. The newly formed subset of U is the product of hybrid reduction

Fig. 2. The pseudocode of hybrid reduction

4 The Results

As an example from Figure 1, the optimal objects are $\{u_2, u_3, u_4, u_8, u_9, u_{10}, u_{13}, u_{15}, u_{16}, u_{17}\}$. For these optimal objects, where $M_E = 6$, they can be categorised as the super optimal object.

$\text{Coo}(u_1) = \{e_1, e_3\}$,	$\text{Coo}(u_2) = \{e_1, e_2, e_3, e_4, e_5, e_6\}$,
$\text{Coo}(u_3) = \{e_1, e_2, e_3, e_4, e_5, e_6\}$,	
$\text{Coo}(u_4) = \{e_1, e_2, e_3, e_4, e_5, e_6\}$,	
$\text{Coo}(u_5) = \{e_2, e_5\}$,	
$\text{Coo}(u_6) = \{e_3, e_5\}$	$\text{Coo}(u_7) = \{e_5\}$,
$\text{Coo}(u_8) = \{e_1, e_2, e_3, e_4, e_5, e_6\}$,	

$\text{Coo}(u_{10}) = \{e_1, e_2, e_3, e_4, e_5, e_6\}$,
$\text{Coo}(u_{11}) = \{e_1, e_3, e_5\}$,
$\text{Coo}(u_{11}) = \{e_1, e_3, e_5\}$,
$\text{Coo}(u_{12}) = \{e_1, e_3\}$,
$\text{Coo}(u_{13}) = \{e_1, e_2, e_3, e_4, e_5, e_6\}$,
$\text{Coo}(u_{14}) = \{e_1, e_2\}$,
$\text{Coo}(u_{15}) = \{e_1, e_2, e_3, e_4, e_5, e_6\}$,
$\text{Coo}(u_{16}) = \{e_1, e_2, e_3, e_4, e_5, e_6\}$,
$\text{Coo}(u_{17}) = \{e_1, e_2, e_3, e_4, e_5, e_6\}$,
$\text{Coo}(u_{18}) = \{e_3, e_4, e_5\}$

Fig. 3. The parameters co-occurrence set of each object

The parameter's support derived from the each objects are as follows:

$\text{Supp}(u_i) = 6$, $i = 2, 3, 4, 8, 9, 10, 13, 15, 16, 17$
$\text{Supp}(u_j) = 3$, $j = 11, 18$
$\text{Supp}(u_k) = 2$, $k = 1, 5, 6, 12, 14$
$\text{Supp}(u_l) = 1$, $l = 7$

Fig. 4. The support of each parameter

The cluster partition formed is

$$U / E = \left\{ \underbrace{\{u_2, u_3, u_4, u_8, u_9, u_{10}, u_{13}, u_{15}, u_{16}, u_{17}\}}_{\max}, \{u_{11}, u_{18}\}, \{u_1, u_5, u_6, u_{12}, u_{14}\}, \{u_7\} \right\}$$

As in the above example, $\{u_2, u_3, u_4, u_8, u_9, u_{10}, u_{13}, u_{15}, u_{16}, u_{17}\}$ is the case of ultimate maximum support set because the number of parameter, $n = 6$. All the objects belong to the ultimate maximum support set are dispensable. This is known as row (object)

reduction. As object with attribute value is vital, therefore in this case, all objects belong to ultimate maximum support set are partitioned into separate data set consisting only optimal objects of ultimate maximum support set.

Table 2. The table after alienating the objects of Ultimate Maximum Support

U / P	e_1	e_2	e_3	e_4	e_5	e_6	$f(.)$
u_1	1	0	1	0	0	0	2
u_5	0	1	0	0	1	0	2
u_6	0	0	1	0	1	0	2
u_7	0	0	0	0	1	0	1
u_{11}	1	0	1	0	1	0	3
u_{12}	0	1	0	1	0	0	2
u_{14}	1	1	0	0	0	0	2
u_{18}	0	0	1	1	1	0	3

The cluster partition formed is still maintained with

$$U / E = \left\{ \begin{array}{l} \left\{ \underbrace{\{u_2, u_3, u_4, u_8, u_9, u_{10}, u_{13}, u_{15}, u_{16}, u_{17}\}}_{\max} \right\}, \\ \left\{ \{u_{11}, u_{18}\}, \{u_1, u_5, u_6, u_{12}, u_{14}\}, \{u_7\} \right\} \end{array} \right\}$$

In Table 2, the column representing e_6 can be considered as the zero significant column. Thus, it is conceivable to delete that column. As can be seen above, data size has been reduced to 37%. Yet, after the process of reduction by 63%, the optimal, sub-optimal, next sub-optimal until the inferior objects are all still maintained.

Table 3. The table after deleting parameter of zero significance e_6

U / P	e_1	e_2	e_3	e_4	e_5	$f(.)$
u_1	1	0	1	0	0	2
u_5	0	1	0	0	1	2
u_6	0	0	1	0	1	2
u_7	0	0	0	0	1	1
u_{11}	1	0	1	0	1	3
u_{12}	0	1	0	1	0	2
u_{14}	1	1	0	0	0	2
u_{18}	0	0	1	1	1	3

5 Conclusion

It has been argued that reduction by [1,3] are only successful at maintaining the same optimal object but not able to maintain consistencies for the sub-optimal objects. In our analysis, we had successfully reduced the data size to 37%, but still able to maintain consistency in optimal objects, and sub optimal objects until inferior objects. We have demonstrated that using our approach of hybrid reduction, data size can be reduced drastically without having to forego the aspect of consistency.

Acknowledgement. This work was supported by the FRGS of Ministry of Higher Education, Malaysia. Ref. No : FRGS/2/2010/SG/UDM/02/2.

References

1. Maji, P.K., Roy, A.R., Biswas, R.: An Application of Soft Sets in A Decision Making Problem. *Computer and Mathematics with Application* 44, 1077–1083 (2002)
2. Molodtsov, D.: Soft Set Theory - First Results. *Computers and Mathematics with Applications* 37, 19–31 (1999)
3. Chen, D., Tsang, E.C.C., Yeung, D.S., Wang, X.: The Parameterization Reduction of Soft Sets and Its Applications. *Computers and Mathematics with Applications* 49, 757–763 (2005)
4. Kong, Z., Gao, L., Wang, L., Li, S.: The Normal Parameter Reduction of Soft Sets and Its Algorithm. *Computers and Mathematics with Applications* 56, 3029–3037 (2008)
5. Zhao, Y., Luo, F., Wong, S.K.M., Yao, Y.Y.: A general definition of an attribute reduct. In: Yao, J., Lingras, P., Wu, W.-Z., Szczuka, M.S., Cercone, N.J., Ślezak, D. (eds.) RSCT 2007. LNCS (LNAI), vol. 4481, pp. 101–108. Springer, Heidelberg (2007)
6. Pawlak, Z., Skowron, A.: Rudiments of Rough Sets. *Information Sciences* 177(1), 3–27 (2007)
7. Jiawei, H., Micheline, K.: Data Mining, Concepts and Techniques, 2nd edn. Morgan Kaufmann Publishers, San Francisco (2006)
8. Mohd Rose, A.N., Herawan, T., Mat Deris, M.: A Framework of Decision Making Based on Maximal Supported Sets. In: Zhang, L., Lu, B.-L., Kwok, J. (eds.) ISNN 2010. LNCS, vol. 6063, pp. 473–482. Springer, Heidelberg (2010)
9. Hand, D., Mannila, H., Smyth, P.: Principles of Data Mining. The MIT Press, Cambridge
10. Pang, N.T., Michael, S., Vipin, K.: Introduction To Data Mining. Addison-Wesley, Reading (2006)
11. Fitsilis, P., Gerogiannis, V., Kameas, A., Pavlides, G.: Producing Relational Database Schemata from An Object Oriented. In: EUROMICRO 1994, System Architecture and Integration, Proceedings of the 20th EUROMICRO Conference, pp. 251–257 (1994)
12. Hadj, A.B., Boufares, F., Abdellatif, A.: Checking Constraints Consistency in UML class diagrams. In: The Proceeding of Information and Communication Technologies (ICTTA 2006), vol. 2, pp. 3599–3604 (2006)

A New Class of ε -Optimal Learning Automata

Wen Jiang

Intelligent Computing Laboratory, Hefei Institute of Intelligent Machines,
Chinese Academy of Sciences, P.O. Box 1130, Hefei Anhui 230031, China

Department of Automation, University of science and technology of China

wenjiang@mail.ustc.edu.cn

Abstract. New class of P-model absorbing ε -optimal learning automata was presented in this paper. The proposed learning automaton, Discretized Generalized Stochastic Estimator (DGSE) learning automaton, not only possesses the characteristics of the Stochastic Estimator Reward-inaction (SE_{RI}) learning automaton and the Discretized Generalized Pursuit Algorithm (DGPA) learning automaton, but also converges with a remarkable speed and accuracy. The asymptotic behavior of the DGSE algorithm is analyzed. Furthermore, we stick out the pitfalls in the proof of SE_{RI} algorithm, proved the proposed DGSE algorithm to be ε -optimal, and pointed out that this proof process could be applied to prove SE_{RI} algorithm. It's known that the SE_{RI} learning automaton is the fastest learning automaton up to now, whereas, the proposed DGSE learning automaton is much faster than the SE_{RI} learning automaton. A great number of experiments and simulations verified the propose DGSE learning algorithm is quite efficient when operating in P-model stationary environment.

Keywords: ε -optimal, learning automaton, stationary environment, P-model learning automaton.

1 Introduction

The theory of learning automata [1],[2],[3],[4],[5],[6],[7],[8],[12]and the applications of learning automats [9],[10],[11]have been widely studied in the half past century and it is a very efficient tool in the artificial intelligence. A learning automaton interacts with the environment, which feedback a response to the learning automaton, to select one optimal action provided by the environment. The learning system, as Fig.1 depicted, composed of a learning automaton and an environment. According to the characteristic of $b(t)$, the stochastic environment could be divided into three catalogs, P-model, Q-model, and S-model. If $b(t) \in \{0,1\}$, the corresponding learning automaton is P-model; if $b(t)$ is a finite set of distinct symbols, the corresponding learning automaton is Q-model; if $b(t)$ can take any value in the $[0,1]$ range, then the corresponding learning automaton is S-model. The environment is said to be stationary when the environment reward each action with a constant probability, and is non-stationary while the environment reward each action with probability varying with time.

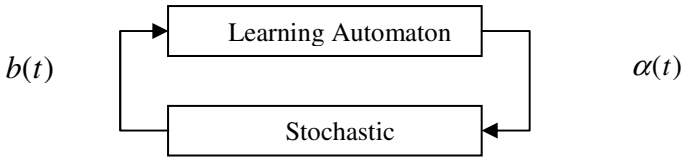


Fig. 1. Learning automaton interacts with environment

The Learning automaton randomly selects an action $\alpha(t)$ from an action vector which contains the probability of choosing each action. This action triggers a response from the stochastic environment. And this response will be used for updating the probability vector by learning algorithm. This cycle will be repeated till the optimal action, which the probability of selecting this action reaches “1”, is got.

The concept of learning automata was introduced by Tsetlin [3]. Since the probability of choosing every action is constant, this automaton belongs to the class of Fixed Structure Stochastic Automaton (FSSA). Some other similar Learning automatons belonging to this field are Krylov automaton [4], Krinsky automaton [4], Iraji-Jamalian Automaton (IJA) [5], and STack Architecture (STAR) automaton [6]. On the other side, the latter class of automaton is named as Variable Structure Stochastic Automaton (VSSA). Learning automaton in this class has been studied thoroughly. The basic form of learning automata of VSSA is non-estimator [7]. In an effort to make algorithm gets converged faster, deterministic estimator was introduced and studied [1]. Discretized learning algorithm was also brought in by Oommen to increase to convergence speed. It's important to notify that estimator algorithm and discretized learning automata always work together to improve the performance of an algorithm. For the deterministic estimator learning algorithm, some of them were used for handing the non-stationary environment. Latter, stochastic estimator schemes were introduced.. In stationary environment, the well known Stochastic Estimator Reward-inaction (SE_{RI}) algorithm [1] achieves the fastest algorithm among all other learning algorithm. This paper proposes an algorithm named Discretized Generalized Stochastic Estimator (DGSE) algorithm which falls in the field of stochastic estimator performs much better than SE_{RI} algorithm. In other words, as we known, the proposed DGSE algorithm is the fastest algorithm. Furthermore, pointing out there are some problems in the proof of [1], we prove the DGSE algorithm is ε -optimal in all random environments and the proof could also be applied to the proof of [1].

The above concerns the development of a single automaton. Nowadays, Structure of learning automaton, such as parallel structure and hierarchical structure, was introduced to improve the convergence speed [8].

This paper organized as follows. In section II, we present our DGSE algorithm. Experiments and simulations demonstrate that our algorithm is quite efficient in section III. The last section concludes this paper.

2 DGSE Learning Automaton

G. I. Papadimtriou and the coauthors of [1] introduced a new stochastic estimator learning automaton, SE_{RI} learning automaton, which is the fastest among the existing learning automatons operating in stationary environment. However, we make use of the advantages of this algorithm and discretized generalized pursuit algorithm (DGPA) [2] to create a new algorithm called discretized generalized stochastic estimator (DGSE) learning algorithm. The SE_{RI} learning automaton keeps estimates of the environmental characteristic to achieve a rapid and accurate convergence. The estimates of the reward probability are computed stochastically and not strictly depended on the feedback of the environment. The dependence between the stochastic estimates and the deterministic estimates is more relaxed when the latter are built on a few selections of the action. The SE_{RI} learning algorithm overcomes the two disadvantages of ε -greedy scheme [2] and the simulation results demonstrate that this algorithm is the fastest among existing learning algorithms. DGPA learning automaton converges slower than the SE_{RI} learning automaton, yet possessing a distinct characteristic pursuing all the actions that have higher estimates than the current chosen action. Lots of experiments show that this property makes the DGPA learning automaton converge faster than pursuit algorithms [2, 6]. So, it's quite easy to think about combining the advantage of DGPA and SE_{RI} , and this is DGSE learning automaton depicted as follows.

The learning system is made up with an environment and a learning automaton. The DGSE learning automaton is defined as a quintuple $\langle A, B, P, E, T \rangle$ where: $A = \{\alpha_1, \alpha_2, \dots, \alpha_r\}$ is the action vector contains r actions. We define $\alpha_i(t), i \in \{1, \dots, r\}$ denoting that the action α_i was selected at time instant t . The probability distribution is $P = \{p_1(t), p_2(t), \dots, p_r(t)\}$, and action $\alpha_i(t), i \in \{1, \dots, r\}$ is selected with probability $p_i(t)$ at time instant t . The set $B = \{0, 1\}$ is the feedback of the P-model environment and is inputted into the learning automaton. ‘1’ denotes a reward response and ‘0’ denotes a penalty response. E is the stochastic estimator, and we denotes the stochastic estimator at time instance t is $E(t) = (D(t), U(t))$, where $D(t) = \{d'_1(t), d'_2(t), \dots, d'_r(t)\}$. The deterministic estimate $d'_i(t)$ of the reward probability of each action $\alpha_i(t), i \in \{1, \dots, r\}$ is

$$d'_i(t) = \frac{H'_i}{G'_i} \quad (1)$$

where G'_i is the number of times that action α_i has been selected up to time t , and H'_i is the number of times that action α_i has been rewarded. $U(t) = \{U'_1(t), U'_2(t), \dots, U'_r(t)\}$ is the stochastic estimator vector at time instance t , and

$$U'_i(t) = d'_i(t) + R'_i \quad (2)$$

where R'_i is a random number which is uniformly distributed in the interval: $(-\gamma/G'_i, \gamma/G'_i)$, and γ is a designed parameter. T is the learning algorithm that listed below.

The environment in which the automaton operates is defined by a triple $\langle A, B, D \rangle$ where A and B are as defined above. The input of the environment is A and the output of the environment is B . The set $D = \{d_1, d_2, \dots, d_r\}$ contains the reward probability of each action provided by the environment and $d_i = \Pr\{b=1 | \alpha(t) = \alpha_i\}$. The environment is “stationary” when d_i is constant and is “nonstationary” when d_i is varying with time. We introduce the DGSE algorithm as follows.

Algorithm_DGSE

Parameters

N resolution parameter

$\Delta = 1/(rN)$ smallest step size

$K(t)$ the number of actions with higher estimates than current chosen action

G'_i the number of times that action α_i has been selected up to time t

H'_i the number of times that action α_i has been rewarded

Method

Initialization: $H'_i, G'_i, d'_i(0)$ and $p_i(0) = 1/r$.

Step 1: Select an action $\alpha(t) = \alpha_i$ according to the probability distribution $P(t)$.

Step 2: Update $P(t)$ with the following equations:

$$\begin{aligned} p_j(t+1) &= \min \left\{ p_j(t) + \frac{\Delta}{K(t)}, 1 \right\} && (\forall j, j \neq i) \text{ such that } u_j(t) > u_i(t) \\ p_j(t+1) &= \max \left\{ p_j(t) - \frac{\Delta}{r - K(t)}, 0 \right\} && (\forall j, j \neq i) \text{ such that } u_j(t) < u_i(t) \\ p_i(t+1) &= 1 - \sum_{j \neq i} p_j(t+1). \end{aligned} \quad (3)$$

Step 3: Update $U(t)$ according to the following equations for the chosen action:

$$G'_i = G'_i + 1; H'_i = H'_i + b(t); d'_i(t) = \frac{H'_i}{G'_i}; u_i(t) = d'_i(t) + R'_i \quad (4)$$

where R'_i is a random number which is uniformly distributed in the interval: $(-\gamma/G'_i, \gamma/G'_i)$.

Step 4: If $p_m(t+1) = 1$ then converge to action α_m else go to step 1.

End Repeat

END ALGORITHM_DGSE

3 Experimental Results

In this section, we evaluate the computational efficiencies of the proposed DGSE via comparing with the fastest learning automaton SE_{RI} . Although a more detailed comparison against the family of pursuit learning automata is also currently being complied, we reported here, in all brevity that the proposed DGSE is quite efficient.

In the experiments conducted, Configuration 1 to 2 forms the generally used benchmark of the test environment for Learning Automata [1]. For each configuration, we use the best parameters for SE_{RI} as [1] and with the parameters for themselves, SE_{RI} and DGSE runs 200 times separately. We can get the accuracy of each scheme and the probability evolution of the optimal action. In Table 1, the corresponding parameters for both algorithms and the accuracy among the 200 repeated experiments were reported. In addition, the parameters of each algorithm are set to make sure the accuracy of them is in the same level. Meanwhile, the environment E_1 is (0.65 0.5 0.45 0.4 0.35 0.3 0.25 0.2 0.15 0.1) and E_2 is (0.6 0.5 0.45 0.4 0.35 0.3 0.25 0.2 0.15 0.1) in which each element is the probability of feeding back correct response [9].

Table 1. Accuracy and parameters of the both above two algorithms

Environment	DGSE			SE_{RI}		
	n	γ	Acc.	n	γ	Acc.
E_1	4	6	198	16	8	199
E_2	5	6	193	32	12	199

Figure 1 and figure 2 are the evolution of the optimal action for SE_{RI} and DGSE with the configuration in E_1 to E_2 respectively. It clearly illustrates the power of DGSE.

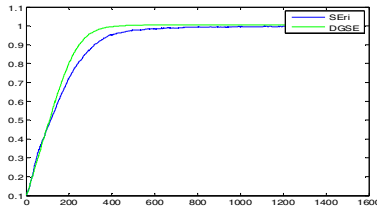


Fig. 1. The asymptotic value of the probability of choosing optimal action (Environment 1, average for 200 times)

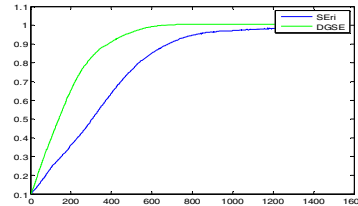


Fig. 2. The asymptotic value of the probability of choosing optimal action (Environment 2, average for 200 times)

The above two graph clearly demonstrate the proposed DGSE algorithm is comparable with the fastest learning automata algorithm up to now SE_{RI} .

3 Conclusions

In this paper, we proposed the first generalized stochastic learning automata. The learning algorithm makes use of the estimator to update the probability of selecting every action. The asymptotic behavior of the proposed scheme is analyzed and it is proved that the DGSE is ε -optimality in every stationary environment. Meanwhile, this proof is suitable for correcting that of the SE_{RI} algorithm [1]. Furthermore, different

experiments demonstrate our algorithm is quite efficient. The ε -optimality and the speed of convergence make the DGSE have broad application domains.

Acknowledgments. This work was supported by the grants of the National Science Foundation of China, Nos. 60975005, 61005010, 60873012, 60805021 & 60905023. 31071168, 30900321.

References

1. Papadimitriou, G.I., Sklira, M., Pomportsis, S.: A New Class of ε -optimal Learning Automata. *IEEE Trans. Syst., Man, Cybern. B* 34(1), 246–254 (2004)
2. Shutton, R.S., Barto, A.G.: Reinforcement Learning: An introduction. MIT Press, Cambridge (1998)
3. Tsetlin, M.L.: On the Behavior of Finite Automata in Random Media. *Avtomatika i Telemekhanika* 22(10), 1345–1354 (1961)
4. Thathachar, M.A.L., Oommen, B.J.: Automata Theory and the Modelling of Biological Systems. Academic, New York (1973)
5. Iraji, R., Manzuri-Shalmani, M.T., Jamalian, A.H., Beigy, H.: IJA Automaton: Expediency and ε optimality Properties. In: Proc. 5th IEEE Int. Conf. on Cognitive Informatics (ICCI 2006), pp. 617–622 (2006)
6. Econdomides, A.A., Kehagias, A.: The STAR automaton: Expediency and Optimality Properties. *IEEE Trans. Syst., Man, Cybern. B* 32(6), 723–737 (2002)
7. Oommen, B.J.: Absorbing and Ergodic Discretized Two-action Learning Autoamta. *IEEE Trans. Syst., Man, Cybern. SMC-16(2)*, 282–293 (1986)
8. Thathachar, M.A.L., Phansalkar, V.V.: Learning the Global Maximum with Parameterized Learning Automata. *IEEE Trans. Neural Networks* 6, 398–406 (1995)
9. Beigy, H., Meybodi, M.R., Menhaj, M.B.: Adaption of Learning Rate in Backpropagation Algorithm Using Fixed Structure Learning Automata. In: Proc. of ICEE 1998, Tehran Iran, vol. 3, pp. 117–123 (1998)
10. Beigy, H., Meybodi, M.R.: Adaption of Momentum Factor and Steepness Parameter in Backpropagation Algorithm Using Fixed Structure Learning Automata. In: Proc. of CSICC 1999 Conference Sharif University of Technology, Tehran, Iran, pp. 117–124 (1999)
11. Economides, A.A.: Learning Automata Routing in Connection-oriented Networks. *Int. J. Commun. Syst.* 8, 225–237 (1995)
12. Martin, R., Tilak, O.: on ε -optimality of the Pursuit Learning Algorithm (2011)

Uncertainty Measures of Roughness Based on Interval Ordered Information Systems

Jie Wang

College of Mathematics and Computer Science,
Shanxi Normal University, Linfen, Shanxi 041004, P.R. China
wjlkt@163.com

Abstract. Entropy theory is a useful measure of uncertainty about the information systems. In this paper, we address uncertainty roughness measures of knowledge and rough sets by introducing rough entropy, and some of its important properties are given, then we prove the rough entropy is more accurate than the rough degree to measure the roughness of rough sets in interval ordered information systems and through some examples are illustrated. These results will be very helpful for understanding the essence of knowledge content and uncertainty measurement in future research works of interval ordered information.

Keywords: Interval information systems, Dominance relation, Rough entropy, Rough degree.

1 Introduction

The rough set theory, proposed by Pawlak in the early 1980s [1], is an extension of the classical set theory for modeling uncertainty or imprecision information. It has important applications to intelligence decision, cognitive sciences, machine learning, pattern recognition, and so on.

The original rough set theory is mainly based on the indiscernibility relation. It does not consider attributes with preference-ordered domains, that is, criteria. However, in many real situations, we are often faced with the problems where the ordering of properties of the considered attributes plays a crucial role. One such problem is the ordering of objects. For this reason, Greco, Matarazzo, and Slowinski [2-4] proposed an extension of rough set theory, called the dominance-based rough set approach (DRSA) to take into account the ordering properties of criteria. In DRSA, where condition attributes are criteria and classes are preference ordered, the knowledge approximated is a collection of upward and downward unions of classes and the dominance classes are sets of objects defined by using a dominance relation. In recent years, many studies have been made in DRSA [5-7].

On the other hand, the concept of entropy, originally defined by Shannon in 1948 for communication theory, gives a measure of uncertainty about the structure of a system. It has been useful concept for characterizing information content in a great diversity of models and applications. Attempts have been

made to use *Shannon's* entropy to measure uncertainty in rough set theory [8]. Moreover, information entropy is introduced into incomplete information systems, and a kind of new rough entropy is defined to describe the incomplete information systems and roughness of rough set. Interval information systems are important type of data tables, which are generalized models of single-valued information systems. In recent years, some problems of decision making in the context of interval information systems have been studied [9]. Hence, consideration of the uncertain measure about entropy in interval ordered information systems is needed. This paper discussed the problem mainly.

In this paper, we address uncertainty measures of roughness of knowledge and rough sets by introducing rough entropy in interval ordered information systems. We prove that the rough entropy of rough sets is more accurate than the rough degree to measure the roughness of rough sets in interval ordered information systems, which is very helpful in future research works of interval ordered information systems.

2 Basic Notions Related to Interval Ordered Information Systems

The following recalls necessary concepts and preliminaries required in the sequel of our work. Detailed description of the theory can be found in [9].

An interval information system (IIS) is a quadruple $S = (U, AT, V, f)$, where U is a finite non-empty set of objects and AT is a finite non-empty set of attributes, $V = \bigcup_{a \in AT} V_a$ and V_a is a domain of attribute a , $f : U \times AT \rightarrow V$ is a total function such that $f(x, a) \in V_a$ for every $a \in AT$, $x \in U$, called an information function, where V_a is a set of interval numbers. Denote by

$$f(x, a) = [a^L(x), a^U(x)] = \{p | a^L(x) \leq p \leq a^U(x), a^L(x), a^U(x) \in R\}$$

we call it the interval number of x under the attribute a . In particular, $f(x, a)$ would degenerate into a real number if $a^L(x) = a^U(x)$. Under this consideration, we regard a single-valued information system as a special form of interval information systems.

In practical decision-making analysis, we always consider a binary dominance relation between objects that are possibly dominant in terms of values of an attributes set in an interval information system. In general, an increasing preference and a decreasing preference are considered by a decision maker. If the domain of an attribute is ordered according to a decreasing or increasing preference, then the attribute is a criterion.

Definition 2.1. An interval information system is called an interval ordered information system (IOIS) if all attributes are criterions.

It is assumed that the domain of a criterion $a \in AT$ is completely pre-ordered by an outranking relation \succeq_a ; $x \succeq_a y$ means that x is at least as good as y with respect to the criterion a . For a subset of attributes $A \subseteq AT$, we define $x \succeq_A y \Leftrightarrow \forall a \in A, x \succeq_a y$. In other words, x is at least as good as y with respect

to all attributes in A . In the following, we introduce a dominance relation that identifies dominance classes to an interval ordered information system. In a given IOIS, we say that x dominates y with respect to $A \subseteq AT$ if $x \succeq_A y$, and denoted by $xR_A^{\geq}y$. That is

$$R_A^{\geq} = \{(y, x) \in U \times U | y \succeq_A x\}$$

Obviously, if $(y, x) \in R_A^{\geq}$, then y dominates x with respect to A . In other words, y may have a better property than x with respect to A in reality.

Analogously, the relation R_A^{\leq} (called a dominated relation) can be defined as follows:

$$R_A^{\leq} = \{(y, x) \in U \times U | x \succeq_A y\}$$

Given $A \subseteq AT$ and $A = A_1 \cup A_2$, where the attributes set A_1 according to increasing preference and A_2 according to decreasing preference. Let us define these two binary relations more precisely as following:

$$\begin{aligned} R_A^{\geq} &= \{(y, x) \in U \times U | a_1^L(y) \geq a_1^L(x), a_1^U(y) \geq a_1^U(x) (\forall a_1 \in A_1); \\ &\quad a_2^L(y) \leq a_2^L(x), a_2^U(y) \leq a_2^U(x) (\forall a_2 \in A_2)\} \\ &= \{(y, x) \in U \times U | (y, x) \in R_A^{\geq}\} \\ R_A^{\leq} &= \{(y, x) \in U \times U | a_1^L(y) \leq a_1^L(x), a_1^U(y) \leq a_1^U(x) (\forall a_1 \in A_1); \\ &\quad a_2^L(y) \geq a_2^L(x), a_2^U(y) \geq a_2^U(x) (\forall a_2 \in A_2)\} \\ &= \{(y, x) \in U \times U | (y, x) \in R_A^{\leq}\} \end{aligned}$$

For simplicity, without any loss of generality, in the following we only consider attributes with increasing preference.

In general, we denote an interval ordered information system by $S = (U, AT, V, f)$. Thus the following definition can be obtained.

Definition 2.2. Let $S = (U, AT, V, f)$ be an interval ordered information system (IOIS), for $A \subseteq AT$, denote

$$\begin{aligned} R_A^{\geq} &= \{(y, x) \in U \times U | a_k^L(y) \geq a_k^L(x), a_k^U(y) \geq a_k^U(x), \forall a_k \in A\} \\ &= \{(y, x) \in U \times U | (y, x) \in R_A^{\geq}\} \end{aligned}$$

R_A^{\geq} are called dominance relations of information system S .

Let denote

$$\begin{aligned} [x]_A^{\geq} &= \{y \in U | a_k^L(y) \geq a_k^L(x), a_k^U(y) \geq a_k^U(x), (\forall a_k \in A)\} \\ &= \{y \in U | (y, x) \in R_A^{\geq}\} \\ U/R_A^{\geq} &= \{[x_i]_A^{\geq} | x_i \in U\} \end{aligned}$$

where $i \in \{1, 2, \dots, |U|\}$, then $[x]_A^{\geq}$ will be called a dominance class or the granularity of information, and U/R_A^{\geq} be called a classification of U about attribute set A .

The following properties of a dominance relation are trivial by the above definition.

Proposition 2.1. Let R_A^{\geq} be a dominance relation. The following hold.

(1) R_A^{\geq} is reflexive, transitive, but not symmetric, so it is not an equivalence relation.

(2) If $B \subseteq A \subseteq AT$, then $R_B^{\geq} \supseteq R_A^{\geq} \supseteq R_{AT}^{\geq}$.

- (3) If $B \subseteq A \subseteq AT$, then $[x]_B^{\geq} \supseteq [x]_A^{\geq} \supseteq [x]_{AT}^{\geq}$.
- (4) If $x_j \in [x_i]_A^{\geq}$, then $[x_j]_A^{\geq} \subseteq [x_i]_A^{\geq}$ and $[x_i]_A^{\geq} = \bigcup\{[x_j]_A^{\geq} : x_j \in [x_i]_A^{\geq}\}$.
- (5) $[x_i]_A^{\geq} = [x_j]_A^{\geq}$ iff $f(x_i, a) = f(x_j, a)$, ($\forall a \in A$).
- (6) $|[x_i]_B^{\geq}| \geq 1$ for any $x_i \in U$.

(7) U/R_B^{\geq} constitute a covering of U , i.e., for every $x \in U$ we have that $[x]_B^{\geq} \neq \emptyset$ and $\bigcup_{x \in U} [x]_B^{\geq} = U$.
where $|\cdot|$ denote cardinality of the set.

For any subset X of U , and AT of S , define

$$\begin{aligned} \underline{R}_A^{\geq}(X) &= \{x \in U \mid [x]_A^{\geq} \subseteq X\} \\ \overline{R}_A^{\geq}(X) &= \{x \in U \mid [x]_A^{\geq} \cap X \neq \emptyset\} \end{aligned}$$

$\underline{R}_A^{\geq}(X)$ and $\overline{R}_A^{\geq}(X)$ are said to be the lower and upper approximation of X with respect to a dominance relation R_{AT}^{\geq} . And the approximations have also some properties which are similar to those of Pawlak approximation spaces.

Proposition 2.2. Let $S = (U, AT \cup \{d\}, V, f, g)$ be an interval ordered information system and $X, Y \subseteq U$, $A \subseteq AT$, then its lower and upper approximations satisfy the following properties.

- (1) $\underline{R}_A^{\geq}(X) \subseteq X \subseteq \overline{R}_A^{\geq}(X)$.
- (2) $\underline{R}_A^{\geq}(X \cap Y) = \underline{R}_A^{\geq}(X) \cap \underline{R}_A^{\geq}(Y)$; $\overline{R}_A^{\geq}(X \cup Y) = \overline{R}_A^{\geq}(X) \cup \overline{R}_A^{\geq}(Y)$.
- (3) $\underline{R}_A^{\geq}(X \cup Y) \supseteq \underline{R}_A^{\geq}(X) \cup \underline{R}_A^{\geq}(Y)$; $\overline{R}_A^{\geq}(X \cap Y) \subseteq \overline{R}_A^{\geq}(X) \cap \overline{R}_A^{\geq}(Y)$.
- (4) $\underline{R}_A^{\geq}(X) = \sim \overline{R}_A^{\geq}(\sim X)$; $\overline{R}_A^{\geq}(X) = \sim \underline{R}_A^{\geq}(\sim X)$.
- (5) $\underline{R}_A^{\geq}(\emptyset) = \overline{R}_A^{\geq}(\emptyset) = \emptyset$; $\underline{R}_A^{\geq}(U) = \overline{R}_A^{\geq}(U) = U$.
- (6) $\underline{R}_A^{\geq}(\underline{R}_A^{\geq}(X)) = \underline{R}_A^{\geq}(X)$; $\overline{R}_A^{\geq}(\overline{R}_A^{\geq}(X)) = \overline{R}_A^{\geq}(X)$.
- (7) If $X \subseteq Y$, then $\underline{R}_A^{\geq}(X) \subseteq \underline{R}_A^{\geq}(Y)$, $\overline{R}_A^{\geq}(X) \subseteq \overline{R}_A^{\geq}(Y)$.
where $\sim X$ is the complement of X .

3 Rough Entropy of Knowledge in Interval Ordered Information Systems

In classical rough set theory, knowledge be regarded as partition of set of objects to an information system. However, it is known that equality relations is replaced by dominance relations in an interval ordered information system.

In this section, we will introduce rough entropy of knowledge and establish relationships between roughness of knowledge and rough entropy in interval ordered information systems.

Firstly, let give the concept of rough entropy of knowledge in interval ordered information systems.

Definition 3.1. Let $S = (U, AT, V, f)$ be an interval ordered information systems and $B \subseteq AT$. The rough entropy of knowledge B is defined as follows:

$$E(B) = \sum_{i=1}^{|U|} \frac{|[x_i]_B^\geq|}{|U|} \cdot \log_2 |[x_i]_B^\geq|$$

where $|\cdot|$ is the cardinality of sets.

Example 3.1. Given an interval ordered information system in Table 1.

Table 1. An interval ordered information system

U	a_1	a_2	a_3	a_4	a_5	a_6
x_1	[3,4]	[4,5]	[3,4]	[3,4]	[2,3]	[4,5]
x_2	[1,2]	[1,2]	[1,3]	[1,3]	[2,3]	[1,3]
x_3	[3,4]	[4,5]	[3,5]	[3,4]	[3,5]	[4,5]
x_4	[2,3]	[4,5]	[2,3]	[2,4]	[2,3]	[3,5]
x_5	[1,2]	[1,2]	[1,3]	[1,2]	[2,3]	[1,3]

The rough entropy of knowledge $AT = \{a_1, a_2, a_3, a_4, a_5, a_6\}$ can be calculated by above definition, which is

$$\begin{aligned} E(AT) &= \frac{2}{5} \log_2 2 + \frac{4}{5} \log_2 4 + \frac{1}{5} \log_2 1 + \frac{3}{5} \log_2 3 + \frac{5}{5} \log_2 5 \\ &= \frac{2}{5} + \frac{8}{5} + \frac{3}{5} \log_2 3 + \log_2 5 \\ &= 2 + \frac{3}{5} \log_2 3 + \log_2 5 \\ &= 5.27291 \end{aligned}$$

Proposition 3.1. Let $S = (U, AT, V, f)$ be an interval ordered information system and $B \subseteq AT$. The following hold.

- (1) $E(B)$ can obtain its maximum $|U| \cdot \log_2 |U|$, iff $U/R_B^\geq = U$;
- (2) $E(B)$ can obtain its minimum 0, iff $U/R_B^\geq = \{\{x_1\}, \{x_2\}, \dots, \{x_{|U|}\}\}$.

Proof. It follows directly from the Definitions 3.1.

Theorem 3.1. Let $S = (U, AT, V, f)$ be an interval ordered information system and $B_1, B_2 \subseteq AT$. If $U/R_{B_1}^\geq \subset U/R_{B_2}^\geq$, then $E(B_1) < E(B_2)$.

Proof. Because of $U/R_{B_1}^\geq \subset U/R_{B_2}^\geq$, we have that $[x_i]_{B_1}^\geq \subset [x_i]_{B_2}^\geq$ for every $\forall x_i \in U$. Thus there exists some $x_j \in U$ such that $|[x_j]_{B_1}^\geq| < |[x_j]_{B_2}^\geq|$. Hence, by the Proposition 2.1 and Definitions 3.1 we can obtain

$$\sum_{i=1}^{|U|} \frac{|[x_i]_{B_1}^\geq|}{|U|} \cdot \log_2 |[x_i]_{B_1}^\geq| < \sum_{i=1}^{|U|} \frac{|[x_i]_{B_2}^\geq|}{|U|} \cdot \log_2 |[x_i]_{B_2}^\geq|$$

i.e.,

$$E(B_1) < E(B_2)$$

Example 3.2. In Example 3.1, if denote $B = \{a_1, a_2, a_3\}$, from the table we have

$$\begin{aligned}[x_1]_B^{\geq} &= \{x_1, x_3\} \\ [x_2]_B^{\geq} &= \{x_1, x_2, x_3, x_4, x_5\} \\ [x_3]_B^{\geq} &= \{x_3\} \\ [x_4]_B^{\geq} &= \{x_1, x_3, x_4\} \\ [x_5]_B^{\geq} &= \{x_1, x_2, x_3, x_4, x_5\}\end{aligned}$$

Thus, it is obviously that $U/R_{AT}^{\geq} \subseteq U/R_B^{\geq}$, Moreover, $E(B)$ can be calculated easily, which is

$$\begin{aligned}E(B) &= \frac{2}{5} \log_2 2 + \frac{5}{5} \log_2 5 + \frac{1}{5} \log_2 1 + \frac{3}{5} \log_2 3 + \frac{5}{5} \log_2 5 \\ &= \frac{2}{5} + 2 \log_2 5 + \frac{3}{5} \log_2 3 \\ &= 5.99484\end{aligned}$$

On the other hand, by Example 3.1, we obtained $E(AT) = 5.27291$.

Thus, it is obviously that $E(AT) < E(B)$.

However, if denote $B' = \{a_2\}$ and $B'' = \{a_5\}$ in the system of Example 3.1, we have that

$$\begin{aligned}[x_1]_{B'}^{\geq} &= [x_3]_{B'}^{\geq} = [x_4]_{B'}^{\geq} = \{x_1, x_3, x_4\} \\ [x_2]_{B'}^{\geq} &= [x_5]_{B'}^{\geq} = \{x_1, x_2, x_3, x_4, x_5\}\end{aligned}$$

and

$$\begin{aligned}[x_1]_{B''}^{\geq} &= [x_2]_{B''}^{\geq} = [x_4]_{B''}^{\geq} = [x_5]_{B''}^{\geq} = \{x_1, x_2, x_3, x_4, x_5\} \\ [x_3]_{B''}^{\geq} &= \{x_3\}\end{aligned}$$

Furthermore, we can obtain that

$$\begin{aligned}E(B') &= 3 \times \frac{3}{5} \log_2 3 + 2 \times \frac{5}{5} \log_2 5 \\ &= \frac{9}{5} \log_2 3 + 2 \times \log_2 5 \\ &= 7.49679\end{aligned}$$

and

$$\begin{aligned}E(B'') &= \frac{5}{5} \times 4 \log_2 5 + \frac{1}{5} \times \log_2 1 \\ &= 4 \log_2 5 \\ &= 9.28771\end{aligned}$$

which show $E(B') < E(B'')$. While, $U/R_{B'}^{\geq} \subseteq U/R_{B''}^{\geq}$ does not hold. So, it can be conclude that the converse proposition of Theorem 3.1 does not hold.

Corollary 3.1. Let $S = (U, AT, V, f)$ be an interval ordered information system and $B_1, B_2 \subseteq AT$. If $U/R_{B_1}^{\geq} \subseteq U/R_{B_2}^{\geq}$, then $E(B_1) \leq E(B_2)$.

Theorem 3.2. Let $S = (U, AT, V, f)$ be an interval ordered information system and $B_1, B_2 \subseteq AT$. If $U/R_{B_1}^{\geq} = U/R_{B_2}^{\geq}$, then $E(B_1) = E(B_2)$.

Proof. Since $U/R_{B_1}^{\geq} = U/R_{B_2}^{\geq}$, we have that $[x_i]_{B_1}^{\geq} = [x_i]_{B_2}^{\geq}$ for every $\forall x_i \in U$. Thus, it is obtained $E(B_1) = E(B_2)$ directly.

Theorem 3.3. Let $S = (U, AT, V, f)$ be an interval ordered information system and $B_1, B_2 \subseteq AT$. If $U/R_{B_1}^{\geq} \subseteq U/R_{B_2}^{\geq}$ and $E(B_1) = E(B_2)$, then $U/R_{B_1}^{\geq} = U/R_{B_2}^{\geq}$.

Proof. Since $E(B_1) = E(B_2)$, it follows that

$$\sum_{i=1}^{|U|} \frac{|[x_i]_{B_1}^{\geq}|}{|U|} \cdot \log_2 |[x_i]_{B_1}^{\geq}| = \sum_{i=1}^{|U|} \frac{|[x_i]_{B_2}^{\geq}|}{|U|} \cdot \log_2 |[x_i]_{B_2}^{\geq}| \quad (*)$$

From $U/R_{B_1}^{\geq} \subseteq U/R_{B_2}^{\geq}$, we have that $[x_i]_{B_1}^{\geq} \subseteq [x_i]_{B_2}^{\geq}$ for every $x_i \in U$. This show that $1 \leq |[x_i]_{B_1}^{\geq}| \leq |[x_i]_{B_2}^{\geq}|$. Thus, it is true that

$$|[x_i]_{B_1}^{\geq}| \cdot \log_2 |[x_i]_{B_1}^{\geq}| \leq |[x_i]_{B_2}^{\geq}| \cdot \log_2 |[x_i]_{B_2}^{\geq}|$$

By the formula (*), it follows that

$$|[x_i]_{B_1}^{\geq}| \cdot \log_2 |[x_i]_{B_1}^{\geq}| = |[x_i]_{B_2}^{\geq}| \cdot \log_2 |[x_i]_{B_2}^{\geq}|$$

So, we easily obtain $|[x_i]_{B_1}^{\geq}| = |[x_i]_{B_2}^{\geq}|$, for every $x_i \in U$.

On the other hand, $[x_i]_{B_1}^{\geq} \subseteq [x_i]_{B_2}^{\geq}$, we get for every $x_i \in U$.

Hence, $U/R_{B_1}^{\geq} = U/R_{B_2}^{\geq}$

Corollary 3.2. Let $S = (U, AT, V, f)$ be an interval ordered information system and $B_1, B_2 \subseteq AT$. If $B_2 \subseteq B_1$ and $E(B_1) = E(B_2)$, then $U/R_{B_1}^{\geq} = U/R_{B_2}^{\geq}$.

4 Rough Entropy of Rough Sets in Interval Ordered Information Systems

In rough set theory, the roughness of a rough set can be measured by its rough degree. So we give the rough degree of a rough set in interval ordered information systems.

Definition 4.1. Let $S = (U, AT, V, f)$ be an interval ordered information system and $B \subseteq AT$. The rough degree of a rough set $X \subseteq U$ about B defined as follows:

$$\rho_B(X) = 1 - \frac{|R_B^{\geq}(X)|}{|R_B^{\geq}(X)|}$$

where $|\cdot|$ is the cardinality of sets.

From the above definition and Proposition 2.2, it is obvious to $0 \leq \rho_B(X) \leq 1$, and the following property can be obtained easily.

Theorem 4.1. Let $S = (U, AT, V, f)$ be an interval ordered information system and $B_1, B_2 \subseteq AT$. If $U/R_{B_1}^{\geq} \subseteq U/R_{B_2}^{\geq}$, then $\rho_{B_1}(X) \leq \rho_{B_2}(X)$, for any rough set $X \subseteq U$.

Proof. Since $U/R_{B_1}^{\geq} \subseteq U/R_{B_2}^{\geq}$, by the Proposition 2.1.4(5) we can obtain $R_{B_2}^{\geq}(X) \subseteq R_{B_1}^{\geq}(X)$, $R_{B_2}^{\geq}(X) \supseteq R_{B_1}^{\geq}(X)$, Thus

$$\frac{|R_{B_2}^{\geq}(X)|}{|R_{B_2}^{\geq}(X)|} \leq \frac{|R_{B_1}^{\geq}(X)|}{|R_{B_1}^{\geq}(X)|}$$

Hence, by Definition 4.2.1 we can have $\rho_{B_1}(X) \leq \rho_{B_2}(X)$.

From Theorem 4.1, we can get that coarser is the classification of interval ordered information systems, smaller is not the rough degree of a rough set of the system.

Furthermore, the following property can be obtained about the entropy of rough sets.

Theorem 4.2. Let $S = (U, AT, V, f)$ be an interval ordered information system and $B_1, B_2 \subseteq AT$. If $U/R_{B_1}^{\geq} \subset U/R_{B_2}^{\geq}$, then $E_{B_1}(X) < E_{B_2}(X)$, for any $X \subseteq U$.

Proof. Since $U/R_{B_1}^{\geq} \subset U/R_{B_2}^{\geq}$, by the Theorem 4.1.1 and Theorem 4.2.1 we can obtain that

$$\begin{aligned} E(B_1) &< E(B_2) \\ \rho_{B_1}(X) &< \rho_{B_2}(X) \end{aligned}$$

Hence, by the Definition 4.2.2 we have

$$E_{B_1}(X) < E_{B_2}(X)$$

5 Conclusion

Rough set theory is a new mathematical tool to deal with vagueness and uncertainty. Development of a rough computational method is one of the most important research tasks. While, in practise, ordered information system confines the applications of classical rough set theory. In this article, we address uncertainty measures of roughness of knowledge and rough sets by introducing rough entropy in interval ordered information systems. We prove that the rough entropy of rough sets is more accurate than the rough degree to measure the roughness of rough sets in interval ordered information systems, which is very helpful in future research works of interval ordered information systems.

Acknowledgements. This work is supported by the Natural Science Foundation of Shanxi Province in China (No. 2008011012), the Soft Science Project of Shanxi Province in China (No. 2011041021-03) and Shaanxi Provincial Department of Education on Natural Science Research Project(No. 2010JK887).

References

1. Pawlak, Z.: Rough Sets. *International Journal of Computer and Information Sciences* 11, 341–356 (1982)
2. Greco, S., Matarazzo, B., Slowiński, R.: A new rough set approach to multicriteria and multiattribute classification. In: Polkowski, L., Skowron, A. (eds.) RSCTC 1998. LNCS (LNAI), vol. 1424, pp. 60–67. Springer, Heidelberg (1998)
3. Greco, S., Matarazzo, B., Slowinski, R.: Rough set theory for multicriteria decision analysis. *European Journal of Operational Research* 129, 1–47 (2001)
4. Greco, S., Matarazzo, B., Slowinski, R.: Rough sets methodology for sorting problems in presence of multiple attributes and criteria. *European Journal of Operational Research* 138, 247–259 (2002)
5. Shao, M.W., Zhang, W.X.: Dominance relation and rules in an incomplete ordered information system. *International Journal of Intelligent Systems* 20, 13–27 (2005)
6. Xu, W.H., Zhang, W.X.: Knowledge reduction and matrix computation in inconsistent ordered information system. *Int. J. Business Intelligence and Data Mining* 3(4), 409–425 (2008)
7. Zhang, W.X., Xu, W.H.: Methods for knowledge reduction in inconsistent ordered information System. *J. Appl. Math. Comput.* 26, 313–323 (2008)
8. Xu, W.H., Yang, H.Z., Zhang, W.X.: Uncertainty measures of roughness of knowledge and rough sets in ordered information systems. In: Huang, D.-S., Heutte, L., Loog, M. (eds.) ICIC 2007. LNCS (LNAI), vol. 4682, pp. 759–769. Springer, Heidelberg (2007)
9. Qian, Y.H., Liang, J.Y., Dang, C.Y.: Interval ordered information systems. *Computers and Mathematics with Application* 23, 1–16 (2008)

A Differential Evolution Algorithm for the Extraction of Complex Natural Resonance Frequencies of Electromagnetic Targets

Mustafa Secmen¹ and M. Fatih Tasgetiren²

¹ Electrical & Electronics Engineering Department, Yasar University, 35100, Izmir, Turkey
mustafa.secmen@yaras.edu.tr

² Industrial Engineering Department, Yasar University, 35100, Izmir, Turkey
fatih.tasgetiren@yaras.edu.tr

Abstract. This paper presents a differential evolution algorithm in order to find unique resonance frequencies of an electromagnetic target in the resonance scattering region. These frequencies are estimated from the roots of Laplace transform of a specially designed incident signal. The parameters of the signal are computed with an intelligent differential evolution (DE) algorithm. The algorithm searches for minimization of the scattered signal's energy in late-time region, which is main fitness function in the algorithm. The proposed algorithm is demonstrated for a scattered signal of a dielectric sphere having several poles. The acquired pole results show very good agreement with theoretical expectations. Besides, the differential evolution algorithm has higher accuracy as compared to a similar method, which utilizes from genetic algorithm.

Keywords: Scattered signal, Resonance frequencies, Differential evolution.

1 Introduction

The discrimination of electromagnetic targets using scattered signals is very crucial in radar applications. The main aim in these applications is to find unique features for targets. According to scattered theory, an electromagnetic target has three scattering regions, which are Rayleigh, resonance and optical regions [1]. If the dimensions of the target are comparable to wavelength of incident signal ($d \sim \lambda$), the target is in resonance scattering region. In this region, the scattering phenomena from a target can be modeled by a linear and time-invariant (LTI) system, which is described in Fig. 1.

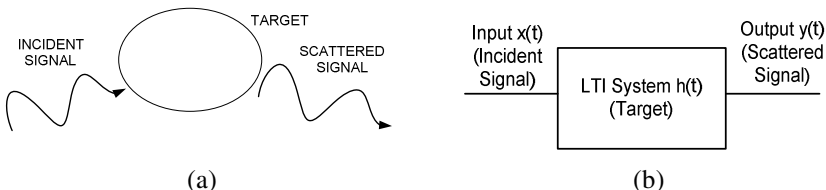


Fig. 1. (a) The scattering phenomena and (b) the modeling of the phenomena with a linear and time-invariant (LTI) system

According to Singularity Expansion Method (SEM) [2], the impulse response (for the case where $x(t)=\delta(t)$) for this system in this region is represented as the sum of time limited signal and superposition of damped exponential signals.

$$h(t) = g(t) + \sum_{n=1}^N a_n \exp(s_n t + \psi_n) \quad (1)$$

Here, $g(t)$ is the time-limited signal vanishing after a certain time interval, a_n is the amplitude of concerning damped exponential signal and N is the number of damped exponential signals. Correspondingly, the Laplace transform (response) of this signal is expressed with an entire function and a meromorphic function given as

$$H(s) = G(s) + \sum_{n=1}^N \frac{R_n}{(s - s_n)} \quad (2)$$

According to SEM theory, complex valued s_n parameters in (1) and (2) are constant for any aspect angle and polarization of incident and scattered electromagnetic signals. These parameters are called as complex natural resonances or equivalently, the poles of the target described in Fig. 1. Because, these poles are unique to target, the extraction of these resonances is usually essential to identify the targets.

Time limited signal part, $g(t)$ in (1), is usually dominant and suppresses the resonance part of time response, which contains target poles. Therefore, the natural resonance estimation methods try to keep away from time interval where $g(t)$ exists. Time interval where $g(t)$ vanishes is called as late-time region and the poles of the target is commonly computed by using this interval of the scattered signal.

There are several methods for the pole computation purpose, some of which can be categorized as pulse methods [3], [4]. The main in these methods is to find optimal incident pulse, which annihilates the effects of the resonances in the late-time interval. In other words, it is aimed to reach an optimal input signal for the target, which makes the energy of scattered signal minimum (ideally zero) after a certain time interval is passed. Then, the natural resonances of the target can be computed from the roots of Laplace transform of this optimal incident pulse as explained in [5].

The optimal incident pulse is usually constructed as the linear combination of some basis functions such as impulse, unit step or Legendre functions [4]-[6]. However, the coefficients of basis functions as well as the duration of the incident pulse are the variables needed to be optimized for minimizing the cost function to be explained in the following section. For this purpose, several optimization techniques such as gradient-descent algorithm [4] or genetic algorithm are used [6].

The differential evolution optimization used in this paper is a simple but powerful stochastic method. It has advantage over gradient type optimization that it may not be differentiable for the problem. Besides, it is superior to genetic algorithm by giving all parent individuals an equal chance and permitting the competition of offspring individual with its parent to qualify the proceeding generation.

In the following part of the paper, the theory and formulation for the optimization problem will be explained. Afterwards, the details of the differential evolution algorithm used in the method will be given. Finally, the application of the algorithm for a lossless dielectric sphere will be demonstrated and the results will be compared with theoretical values and the ones extracted with genetic algorithm in [6].

2 Theory and Formulation

The problem in this paper can be formulated with an optimization problem as

$$\min(J) = \min \left(\frac{\int_{T_L+T_p}^{\infty} y^2(t) dt}{\int_0^{T_p} x^2(t) dt} \right) = \min \left(\frac{\int_{T_L+T_p}^{\infty} (x(t) * h(t))^2 dt}{\int_0^{T_p} x^2(t) dt} \right) \quad (3)$$

where $*$ is the convolution operator, T_L is the beginning instant of the late-time interval where $g(t)$ in (1) vanishes and T_p is the width of the generated incident pulse. The resulting convolution should be zero in ideal case, which means zero energy in the late-time interval and by considering Laplace transform, it can be expressed as

$$y(t) = x(t) * h(t) = \sum_{n=1}^N |X(s_n)| \exp(s_n t + \phi_n) = 0 \quad \text{for } t > T_L + T_p \quad (4)$$

where $X(s)$ is the Laplace transform of $x(t)$. The expression (4) brings to the necessity of $X(s_n)=0$ that the roots of the Laplace transform of optimal incident pulse give the complex natural resonance frequencies of the target. In this paper, the incident pulse is considered to be constructed with unit step functions such that

$$x(t) = \sum_{j=1}^K x_j [u(t - (j-1)\Delta t) - u(t - j\Delta t)], \quad T_p = K\Delta t \quad (5)$$

where Δt is the sampling period when the continuous time-domain incident signal is converted to discrete time-domain signal as $x_j = x(j\Delta t - \Delta t)$. The Laplace transform of the expression in (5) is found to be

$$X(s) = \frac{1 - \exp(-s\Delta t)}{s} A(s) = \frac{1 - \exp(-s\Delta t)}{s} \sum_{j=1}^K x_j \exp[-s(j-1)\Delta t] \quad (6)$$

Therefore, once the variable x_j values are gathered, the target poles can be easily computed from the roots of $A(s)$ function in (6). When the known impulse response of the target is also converted to discrete-time domain as $h_j = h(j\Delta t - \Delta t)$, by using the definition of convolution operator, the continuous optimization problem can be rewritten in discrete-time domain as in (7).

$$\min \left(\frac{\sum_{j=D+K+1}^{U+K} y_j^2}{\sum_{j=1}^K x_j^2} \right) = \min \left(\frac{\sum_{m=D+K+1}^{U+K} \left(\sum_{j=1}^K x_j h_{m-j} \right)^2}{\sum_{j=1}^K x_j^2} \right), \quad D = \frac{T_L}{\Delta t}, \quad U = \frac{T_U}{\Delta t} \quad (7)$$

where D is beginning index of the late-time interval and T_U defines the predetermined upper time instant for impulse response that the response drops to a sufficiently small value after this instant. For impulse response, all h_j values after this time instant are assumed to be zero such that $h_j = 0$ for $j > U$. Besides, all nonpositive index are assumed to be zero that $h_j = 0$ for $j < 1$.

In the optimization problem given in (7), the parameters and values except x_j values and parameter K are all assumed to be known. Therefore, only parameter K and variables x_j 's are needed to be optimized. Here, parameter K can be considered as pulse width of the input signal and it should be integer number in the optimization; however, the variables x_j 's can be any real number. So, both pulse width and basis coefficients should be optimized to give the minimum energy in the late-time interval.

3 Differential Evolution Algorithm

Differential evolution (DE) is one of the latest evolutionary optimization methods proposed by Storn and Price [7]. Although DE was first introduced to solve the Chebychev polynomial fitting problem [7], it has been successfully applied in a variety of applications that an excellent review of applications of DE algorithms can be found in Das and Suganthan [8].

There exist several mutation variations in traditional DEs. We follow the *DE /rand/1/bin* scheme of Storn and Price [7] for a general description. By considering the fitness function in (7), the traditional DE algorithm starts with establishing the initial target population denoted by NP . Each individual in NP has a $K+1$ dimensional vector with parameter values determined randomly between predefined search ranges denoted by $x_{ij}^{\min} = -1$ and $x_{ij}^{\max} = 1$, respectively, such that

$$x_{ij}^t = x_{ij}^{\min} + (x_{ij}^{\max} - x_{ij}^{\min}) \times r \quad (8)$$

where x_{ij}^t is the i^{th} target individual with respect to j^{th} dimension at generation t ; and r is a uniform random number between 0 and 1.

Mutant individuals are generated in such a way that DE perturbs vectors from the target population by adding the weighted difference between two randomly selected target population members to a third member in the target population as follows:

$$v_{ij}^t = v_{aj}^{t-1} + F \times (v_{bj}^{t-1} - v_{cj}^{t-1}) \quad (9)$$

where a , b , and c are three randomly chosen individuals from the target population such that $(a \neq b \neq c \neq i \in (1, \dots, NP))$ and $j=1, 2, \dots, K+1$. $F > 0$ is a mutation scale factor which affects the differential variation between two individuals.

Mutation phase is followed by recombination of mutant individual with its corresponding target individual. For this purpose, a crossover operator is applied to obtain the trial individual such that

$$u_{ij}^t = \begin{cases} v_{ij}^t & \text{if } r_{ij}^t \leq CR \text{ or } j = n_j \\ x_{ij}^{t-1} & \text{otherwise} \end{cases} \quad (10)$$

where the index n_j refers to a randomly selected dimension $j=1,2,\dots,K+1$, which is used to ensure that at least one parameter of each trial individual u_i^t differs from its counterpart in previous generation u_i^{t-1} . CR is a user-defined crossover constant in the range of [0, 1] and r_{jj}^t is a uniform random number between 0 and 1. In other words, trial individual is made up with some parameters of mutant individual, or at least one of the parameters randomly selected.

As shown in the following part, during the crossover operator applied, we modified our DE to handle the first dimension K of our solution representation. For the first dimension of DE vector, we use an arithmetic crossover as follows.

$$u_{ij}^t = CR \times x_{ij}^{t-1} + (1 - CR) \times v_{ij}^t \quad (11)$$

During the reproduction of the trial population, it is possible to extend the search outside of the initial range of the search space. For this reason, parameter values violating the search range are restricted either to

$$u_{ij}^t = x_{ij}^{\min} + (x_{ij}^{\max} - x_{ij}^{\min}) \times r_1 \quad j = 1,2,\dots,K+1 \quad (12)$$

To decide whether or not the trial individual u_i^t should be a member of the target population for the next generation, it is compared to its counterpart target individual x_i^{t-1} at the previous generation. The selection is based on the survival of the fittest among the trial and target individuals such that

$$x_i^t = \begin{cases} u_i^t & \text{if } f(u_i^t) \leq f(x_i^{t-1}) \\ x_i^{t-1} & \text{otherwise} \end{cases} \quad (13)$$

The solution representation is given in Table 1 where each individual represents the decision variable K and x_j values, respectively. However, the DE algorithm works on a continuous domain. For this reason, floating point number K value is truncated to an integer value before computing the objective function value.

Table 1. Solution Representation

j	1	2	3	4	...	$K+1$
x_j	K	x_1	x_2	x_3	...	x_K

It is important to note here that once the value of the decision variable K is determined, K value is equal to the size of the DE vector x_K . For this reason, each individual in the population of the DE algorithm has a variable x_K size.

The initial population is constructed randomly with the lower bound as described before within the ranges of $[K^{LB}, K^{UB}]$ and $[x_{ij}^{LB}, x_{ij}^{UB}]$, respectively. Then, the first dimension and the rest of the dimensions are generated by

$$x_{il}^t = K^{LB} + (K^{UB} - K^{LB}) \times r, \quad x_{ij}^t = x_{ij}^{LB} + (x_{ij}^{UB} - x_{ij}^{LB}) \times r \quad (14)$$

where x_{ij}^t is the i^{th} target individual with respect to j^{th} dimension at generation t ; and r is a uniform random number between 0 and 1.

4 The Experimental Results for a Dielectric Sphere

The differential evolution algorithm described above is applied for a dielectric sphere with radius 1 meter and dielectric constant 5. The monostatic impulse response for the target is synthesized for frequency band of 0-0.5 GHz with analytical expressions [9]. In this frequency band, target is in resonance scattering region. Time response of this sphere is plotted in Fig. 2(a), where sampling period is selected as $\Delta t = 1$ nsec.

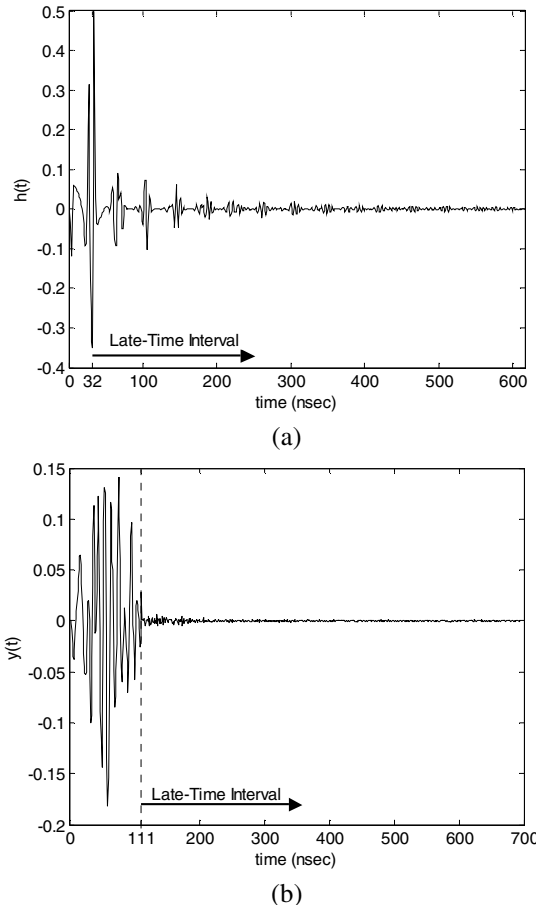


Fig. 2. (a) The impulse response of the dielectric sphere and (b) the scattered (output) signal for the optimized incident pulse of the dielectric sphere

For this dielectric sphere, constant parameters D and U are given as 32 and 616, respectively. The integer K is optimized in the integer range between $K^{LB}=10$ and $K^{UB}=90$ are x_i coefficients are searched in the continuous range [-1, 1]. The population size is selected as 100 and the number of iterations varies from 100 to 1000. However, due to limited space, the results only belonging to 1000 iterations are given. While time processing of method is 1 s for 100 iterations, it is 10 s for 1000 iterations.

As the results for 1000 iterations, the fitness value in (7) is evaluated as 0.000594 and K is found to be 79. The resulting scattered signal $y(t)$ is plotted in Fig. 2(b), where time index 111 corresponds to $U+K$ in (7). When these figures are compared, a considerable amount of energy exists in late-time interval of Fig. 2(a); however, this late-time energy is significantly reduced in Fig. 2(b). This is because the synthesized incident pulse has no cancellation effect on the part of scattered signal before late-time interval; therefore, a considerable scattered signal is available in this time region. However, this pulse causes an annihilation of effects of resonances in the late-time interval, which results in very little late-time scattered signal.

After the optimized x_j values are obtained, complex natural resonance frequencies are computed from the roots of the function $A(s)$ given in (6). The corresponding pole results of the dielectric sphere are tabulated in Table 2 by using a normalization of sr/c where r is the radius of the sphere and c is the speed of light. In the same table, the resonance frequencies extracted from theoretical expressions are also given. Both results show that although the selected application (target) has several distinct poles, the values computed by DE algorithm have very good agreement with the exact (theoretical) pole values especially in terms of imaginary parts of the poles.

Table 2. The extracted pole values in this study and in [6], and exact pole values for the selected lossless dielectric sphere where j represents imaginary part of complex number

Extracted Pole Values (Differential evolution algorithm)	Extracted Pole Values (Genetic algorithm)	Exact (Theoretical) Pole Values
-0.1488 \pm j1.2936	-0.1160 \pm j1.2399	-0.1479 \pm j1.2968
-0.1021 \pm j1.8798	-0.0949 \pm j1.9071	-0.0947 \pm j1.8740
-0.0603 \pm j2.4221	-0.0488 \pm j2.4873	-0.0571 \pm j2.4400
-0.1731 \pm j2.7459	-0.0292 \pm j2.8333	-0.1959 \pm j2.7431
-0.0264 \pm j3.0044		-0.0325 \pm j2.9952
-0.0793 \pm j3.3656		-0.0766 \pm j3.3555
-0.0343 \pm j3.5262		-0.0174 \pm j3.5398
-0.0491 \pm j3.9060		-0.0365 \pm j3.9178
-0.0066 \pm j4.0913		-0.0089 \pm j4.0745
-0.0196 \pm j4.4742		-0.0169 \pm j4.4653
-0.0431 \pm j4.5983		-0.0043 \pm j4.6002
-0.0235 \pm j5.6336		-0.0657 \pm j5.6387
-0.0543 \pm j6.0828		-0.0014 \pm j6.0385
-0.2173 \pm j6.1356		-0.2663 \pm j6.1188
-0.0108 \pm j6.7657		-0.0299 \pm j6.7528
-0.1358 \pm j7.4867		-0.1831 \pm j7.4630
-0.0710 \pm j8.8543		-0.0694 \pm j8.8551
-0.2048 \pm j9.1158		-0.2083 \pm j9.1101

A similar study, which uses the same dielectric sphere in the application part, is demonstrated in [6] by using genetic algorithm as the optimization tool. The incident pulse is constructed and optimized with Legendre polynomials as basis functions. The resulting pole results of the study in [6] mostly contain the complex resonance frequencies with relatively higher real parts. However, these signals attenuate very rapidly, which causes disappearing of these poles easily with a possible additional

noise. In that respect, the pole values extracted with DE algorithm in this paper are more stable to noise effects as their attenuation coefficients are relatively small. In Table 2, the pole values computed in this paper are also compared with the pole results of [6] having relatively small real parts. From the results in Table 2, it can be deducted that the pole values computed with DE algorithm show higher accuracy as compared to the poles estimated with genetic algorithm.

5 Conclusions

This paper has been demonstrated the extraction of poles of an electromagnetic target with an intelligent DE algorithm. This pole extraction method mainly attempts to solve an optimization problem, which is the minimization of the late-time energy of scattered signal of a target. For this purpose, an incident pulse is optimized and target specific pole values are extracted from the roots of the Laplace transform of this optimized incident pulse. The coefficients and length of the incident pulse are obtained with DE algorithm. This problem is applied to an electromagnetic target of a dielectric sphere. The pole results extracted after DE algorithm show high accuracy with the theoretical values. Besides, the method gathers the pole values with small damping coefficients, which are more robust to noise effects. The proposed method with DE algorithm is also compared with another method using genetic algorithm for the same application. According to the results, the proposed DE algorithm for this application is found to be more accurate than the method with genetic algorithm. Although the suggested method is demonstrated for a dielectric sphere, it can be applied for any target type in the resonance scattering region.

References

1. Barton, D.K.: Radar System Modeling and Analysis. Artech House, Boston (2005)
2. Baum, C.E.: The Singularity Expansion Method. In: Felsen, L.B. (ed.) Transient Electromagnetic Fields, pp. 129–179. Springer, New York (1976)
3. Lui, H.S., Shuley, N.V.Z.: Radar Target Identification Using a Banded E-pulse Technique. IEEE Trans. on Antennas and Propag. 54, 3874–3881 (2006)
4. Turhan-Sayan, G., Moffatt, D.L.: K-Pulse Estimation and Target Identification of Low-Q Radar Targets. Wave Motion 11, 453–461 (1989)
5. Rothwell, E.J., Chen, K.-M., Nyquist, D.P.: Extraction of the Natural Frequencies of a Radar Target from a Measured Response using E-Pulse Techniques. IEEE Trans. on Antennas and Propag. 35, 715–720 (1987)
6. Turhan-Sayan, G., Kuzuoglu, M.: Pole Estimation for Arbitrarily-Shaped Dielectric Targets using Genetic Algorithm-Based Resonance Annihilation Technique. Electronics Lett. 37, 380–381 (2001)
7. Storn, R., Price, K.: Differential Evolution - A Simple and Efficient Heuristic for Global Optimization over Continuous Space. Journal of Global Optimization 11, 341–359 (1997)
8. Das, S., Suganthan, N.: Differential Evolution: A survey of the State-of-the-Art. IEEE Trans. on Antennas and Propag. 15, 4–31 (2011)
9. Van Bladel, J.: Electromagnetic Fields. John Wiley & Sons Inc., New Jersey (2007)

A Novel Discrete League Championship Algorithm for Minimizing Earliness/Tardiness Penalties with Distinct Due Dates and Batch Delivery Consideration

Zahra Pourali and Majid Aminnayeri

Department of Industrial Engineering
Amirkabir University of Technology
Tehran, Iran

{z.pourali,mjnayeri}@aut.ac.ir

Abstract. In this paper, we develop a new evolutionary algorithm called League Championship Algorithm (LCA) to solve a new single machine scheduling nonlinear problem in JIT environment with batch delivery cost and distinct due dates. Despite its hardness, solving a non-convex function which minimizes earliness and tardiness costs simultaneously seems to be very useful and practical in industrial environments. In order to solve this complex problem, first we present a mathematical model and then design a new discrete nonlinear version of the LCA algorithm which is very efficient and helpful in combinatorial problems, either in terms of computational time or solution quality.

Keywords: just-in-time scheduling, batch delivery, League Championship algorithm, single machine.

1 Introduction

This paper addresses the single machine earliness tardiness batch scheduling problem with delivery cost consideration for each batch and distinct due dates. Traditionally, the earliness-tardiness scheduling problems are considered types of just in time scheduling problems. The JIT systems are so well known and important areas in manufacturing and production planning, because in this system all early and tardy penalties are undesirable and we want to achieve the schedule with zero penalty cost.

Since, in many cases, we should pay much money to deliver our finish goods to customers, it is important to think about models that can make a balance between early-tardy penalties and delivery costs. Nowadays, with respect to the growth in e-business competitions and the importance of logistics' role in this field, a new concept in JIT systems evolved that consider the transportation cost independent of number of jobs per batch and only according to the number of batches. Cheng and Kahlbacher [1] were the first ones that study the batch delivery scheduling problems. They worked on earliness penalties and batch delivery costs. Cheng and Gordon [2] solved this problem in general form, with processing times related to its batch, and obtained tow pseudo-polynomial time solutions for a special case with fixed upper bound for the number of batches.

Potts and Kovalyov [3] reviewed other groups of batch scheduling problems in which there are machines that can work on several jobs simultaneously. They also discussed about different aspects of batching problems. In this article, their main emphasize was on applying dynamic programming to solve batching problems. Because of interesting Relations between supply chain management and batching problems, some researchers studied batching problem considering this assumption. Pundoor et al. [4] studied a system with one supplier and one or more customers. Jobs are delivered in batches and all jobs that compose the batch belong to one customer. In recent years, some studies about batch delivery problems have been done by Mahdavi [5] and shabtay [6].

Due to the complexity of the non-convex objective functions, some meta-heuristic algorithms were applied. For example, Chang et al. [7] have been developed a new genetic procedure with injecting artificial chromosomes to solve single machine early-tardy problem. Tsai [8], Jou [9] employed genetic algorithms to solve their earliness-tardiness problems. In this paper a new meta-heuristic algorithm called League Championship Algorithm (LCA) proposed for finding best solutions in a reasonable computational time.

The remainder of the paper is organized as follows. Section 2, describes the basic definition of our combinatorial problem and represents a mathematical model. Section 3, explains the proposed League Championship Algorithm, in order to find an optimal or near optimal solution. Implementation issues and comparisons are investigated in Section 4. Finally, conclusions are given in Section 5.

2 Problem Definition

In this section, we define the non-linear earliness tardiness scheduling problem, with batch delivery consideration and distinct due dates. All of the parameters in this model are integers.

2.1 Notations

n : number of jobs

d_j : due date of job j

P_j : processing time of job j

α : earliness penalty of each job

β : tardiness penalty of each job

D : Delivery cost of each batch

σ : number of batches

C_i : completion time of all jobs in batch i

E_j : earliness of job j

T_j : tardiness of job j

2.2 Assumptions

1. All jobs are available for processing at time $t = 0$.
2. Delivery date of a batch equals the completion time of the last job in the batch.

3. All jobs are delivered in batches with unlimited capacity.
4. Delivery costs do not depend on the batch size and are the same for all batches.
5. The total delivery cost only depends on the number of delivered batches.
6. Our single machine is continuously available and can process at most one job at time.

$$TC = \sum_{j=1}^n \alpha E_j + \beta T_j + \sigma D \quad (1)$$

In this model, E_j and T_j are the difference between due date of job j and completion time of its batch. Positive value demonstrates earliness and negative is tardiness.

3 A League Championship Algorithm Solution Approach

Because of the hardness of our problem, in this section, we develop a league championship algorithm (LCA) to solve the problem. This algorithm is a new meta-heuristic algorithm to solve continuous optimization problems. In Sections 3.1 and 3.2, the general form of the LCA and the steps of the proposed solution algorithm are described respectively.

3.1 General League Championship Algorithm (LCA)

LCA method which was introduced by Husseinzadeh [10] is a new meta-heuristic algorithm to solve continuous optimization problems. Each individual (team) in the population (league size) represents a feasible solution to the problem being solved. The quality of each solution is measured by a fitness function and the search proceeds through a number of generations where each individual contribution to the next generation is proportional to its fitness.

Inspired by the competition of sport teams in a sport league, the League Championship algorithm (LCA) is presented for optimizing nonlinear continuous functions. A number of individuals as sport teams compete in an artificial league for several weeks (iterations). Based on the league schedule in each week, teams play in pairs and the outcome is determined in terms of win or loss, given known the team's playing strength (fitness value) resultant from a particular team formation (solution). In the recovery period, each team devises the required changes in the formation/playing style (a new solution) for the next week contest and the championship goes on for a number of seasons (stopping condition) [10].

3.2 The Proposed League Championship Algorithm

As described above, basic LCA is used for continuous problems, adopting the algorithm with our discrete problems, we added some new features to improve and appropriate the algorithm to solve our model efficiently. To do this, we generate discrete individuals instead of continuous ones. Following, we explain the main steps of the proposed LCA.

The Representation Scheme. One of the most important parts in our LCA method is the procedure in which we show the solution characteristics in the form of Teams.

In many papers which have been used meta-heuristics, one of the procedures to represent solutions in discrete models is implementing the algorithm with continues variables and at last convert them to integer numbers, but in this paper we used discrete values to generate our solutions from the beginning. This method would be much better than the former procedures.

In our model, the solutions are presented as a vector which its length is equal to the number of jobs and each bit shows the batch ID in which our job is assigned. For example, a sample solution is obtained as follows: $A=[1\ 3\ 4\ 4]$, That means the first job is assigned to batch 1, second job to batch 3, third job to batch 4 and fifth job to batch 4.

The Initial Population. Generating a set of initial solutions is the first step to implement LCA. There are two major decisions in LCA accomplishment. First, determine the appropriate population size which is not too small and not too large. This scheme causes to achieve appropriate solutions in reasonable time. Second, generate an initial population, containing primal sequences which generating randomly in our model. The quantity of the primal sequences is equal to the population size, determined in first step.

Fitness Evaluation. The aim of the fitness evaluation is to calculate the goodness of the candidate solutions (the team's playing strength). With respect to our objective function, the team's playing strength obtained by calculating jobs' earliness- tardiness and delivery costs.

Determining Winner/Loser. At the end of each competence, the outcome in terms of win, loss or tie is determined for each team. Based on this, each team is scored by 3 points for win, 0 for loss and 1 for tie. To determine winner and loser, in a certain competition, a tournament selection which is typically used in GA is used in LCAs [10].

Setting Up a New Team Formation. In LCA algorithm, each solution represents in form of a team formation. In order to achieve new solutions, we should update our team formations. The tow important factors in a team formation are the opponent status and the team status at previous week. Four different statuses should be take place according to the (lost or won) status for each job and its opponent. New formation is directly arranged by considering these statuses.

4 Computational Results

4.1 Data Generation

In this paper, we followed Abdul-Razaq and Potts [11] to generate our test problems.

The test problems were generated randomly in 4 sets of jobs ($n=6, 9, 18, 50$), each set consists of 12 subsets with 10 instances in each subset. The names of these 12

subsets are shown in Table1. Processing times were chosen to be randomly generated integers inside the [10,100]. Earliness and tardiness costs were also random integers between 1 and 10. For the due dates, we considered T (the tardiness factor) and ρ (the due date range) in the sets {0.3, 0.7} and {0.6, 1.2}, respectively. Our due dates generated uniformly over the integers $\{P \cdot (1 - T - \rho/2) \dots P \cdot (1 - T + \rho/2)\}$, where P is the total processing times of all the jobs. Due to the probable interactions between batch delivery costs and earliness-tardiness penalties which may lead to increase problem hardness, three different intervals for delivery cost were generated. For these intervals, delivery costs are generated randomly over integers inside [100, 4000], [4001, 12000] and [12001, 30000], respectively.

Table 1. Name of problems generated with variable parameters

n	Delivery Cost=rand(100,4000)				Delivery Cost=rand(4001,12000)				Delivery Cost=rand(12001,30000)			
	$T=0.3$		$T=0.6$		$T=0.3$		$T=0.6$		$T=0.3$		$T=0.6$	
	$\rho=0.5$	$\rho=1$	$\rho=0.5$	$\rho=1$	$\rho=0.5$	$\rho=1$	$\rho=0.5$	$\rho=1$	$\rho=0.5$	$\rho=1$	$\rho=0.5$	$\rho=1$
6	ETBD	ETBD	ETBD	ETB	ETB	ETB	ETB	ETB	ETB	ETB	ETB	ETB
	1	2	3	D4	D5	D6	D7	D8	D9	D10	D11	D12
9	ETBD	ETBD	ETBD	ETB	ETB	ETB	ETB	ETB	ETB	ETB	ETB	ETB
	13	14	15	D16	D17	D18	D19	D20	D21	D22	D23	D24
18	ETBD	ETBD	ETBD	ETB	ETB	ETB	ETB	ETB	ETB	ETB	ETB	ETB
	25	26	27	D28	D29	D30	D31	D32	D33	D34	D35	D36
50	ETBD	ETBD	ETBD	ETB	ETB	ETB	ETB	ETB	ETB	ETB	ETB	ETB
	37	38	39	D40	D41	D42	D43	D44	D45	D46	D47	D48

4.2 Experimental Results

Proposed LCA algorithm was coded in MATLAB 7 and was run on a Pentium 4 computer with 1.87 GHz CPU and 1 GB of RAM. Table 2 shows the results for 480 runs, the optimal solutions for each set of jobs in average and their computational times. As can be seen in table 2, the proposed algorithm obtained very suitable solutions in a reasonable time. Compared to the global solutions obtained by Lingo, our proposed algorithm reaches to global optimum for 13 sets out of 15. Also, in comparison with Lingo's best solutions in general, the proposed LCA reaches to better solutions about 32% more than Lingo.

Looking at the values depicted in Fig. 1, high performance of proposed LCA compared to Lingo's prolix CPU times (even for small sizes), reveals that a meta-heuristic is needed to solve the remained scenarios. With respect to Fig. 1 and 2, it can be proven that the proposed LCA method greatly overcomes the problem hardness both in objective values and computational times.

Table 2. Comparison of results of the model solved by Lingo 9 with the proposed LCA

Code	num of jobs	Lingo			LCA	
		Bestopt	Glob.opt	CPUtime(sec)	Best opt	CPUtime(sec)
ETBD1	6	4186.6	4186.6	5.40	4186.6	5.26
ETBD2	6	4435.5	4435.5	4.10	4435.5	5.07
ETBD3	6	7220.6	7220.6	6.5	7220.6	5.05
ETBD4	6	6094.2	--	6.7	6091.6	4.99
ETBD5	6	10833.3	10833.3	1.7	10833.3	5.08
ETBD6	6	11400.1	11400.1	1.5	11400.1	4.92
ETBD7	6	14654.1	14654.1	1.7	14654.1	4.97
ETBD8	6	14426.3	--	2.6	13735.8	4.96
ETBD9	6	24999.4	24999.4	1.5	24999.4	5.10
ETBD10	6	24837.2	24837.2	0.8	24837.2	5.06
ETBD11	6	24619.4	24619.4	1.5	24619.4	5.45
ETBD12	6	29319.5	29319.5	1	29319.5	5.08
ETBD13	9	5756.5	--	20.00	5756.3	5.78
ETBD14	9	7341.4	7341.4	13.10	7341.4	5.80
ETBD15	9	7156.5	--	24.9	6911.7	5.89
ETBD16	9	12102.7	--	24.8	11954.6	5.66
ETBD17	9	15143.2	15143.2	6.5	15143.2	5.81
ETBD18	9	15086.7	15086.7	8.1	15192.4	5.58
ETBD19	9	21405.1	21405.1	13.3	21405.1	5.64
ETBD20	9	17969.4	17969.4	16.7	18005.9	5.87
ETBD21	9	29623.6	--	2.3	15143.2	5.90
ETBD22	9	25708.7	--	2.5	15192.4	6.00
ETBD23	9	38621.6	--	5.6	21405.1	5.89
ETBD24	9	34305	--	3.7	17969.4	5.92
ETBD25	18	8967.2	--	478.80	8248.3	8.45
ETBD26	18	17946.4	--	212.00	17581.5	8.27
ETBD27	18	31786.3	--	8005.4	28859.2	8.28
ETBD28	18	32003.1	--	8965.3	17831.7	8.21
ETBD29	18	26538.2	--	409.7	25680.8	8.58
ETBD30	18	26996	--	154.7	27984.5	8.56
ETBD31	18	46872.9	--	3700.1	47761.4	8.37
ETBD32	18	43632.5	--	4540.8	43595.5	8.90
ETBD33	18	59594	--	128.6	55316.9	9.04
ETBD34	18	53696.9	--	39.2	56451.9	8.44
ETBD35	18	73459.9	--	488.6	78134.5	8.41
ETBD36	18	69671.4	--	458.1	63681.4	8.31
ETBD37	50	--	--	--	52645.8	25.56
ETBD38	50	--	--	--	72580.4	25.69
ETBD39	50	--	--	--	135305	25.51
ETBD40	50	--	--	--	75524.8	25.73
ETBD41	50	--	--	--	97688.4	26.01
ETBD42	50	--	--	--	81505.8	25.40
ETBD43	50	--	--	--	168457.4	26.15
ETBD44	50	--	--	--	159893.4	25.65
ETBD45	50	--	--	--	136743.4	26.15
ETBD46	50	--	--	--	193367.8	25.73
ETBD47	50	--	--	--	232108	26.02
ETBD48	50	--	--	--	227371.8	26.55

5 Conclusions

The expansion of single machine earliness–tardiness scheduling problem with batch delivery costs and distinct due dates were done using a new meta-heuristic algorithm. In this model we studied a general form of JIT – batch delivery problems with distinct due dates which increases the problem hardness and complexity verses common due dates. In order to present reliable solutions in reasonable time, we develop a new meta-heuristic algorithm called League Championship Algorithm. First, presenting a new mathematical model and then developing the new LCA algorithm to solve the mathematical model. 48 test problems were solved verifying the performance of our algorithm. Computational results strongly confirm the efficiency and potency of the proposed discrete LCA. As a feature work, it would be precious applying this method to solve other combinational optimization problems.

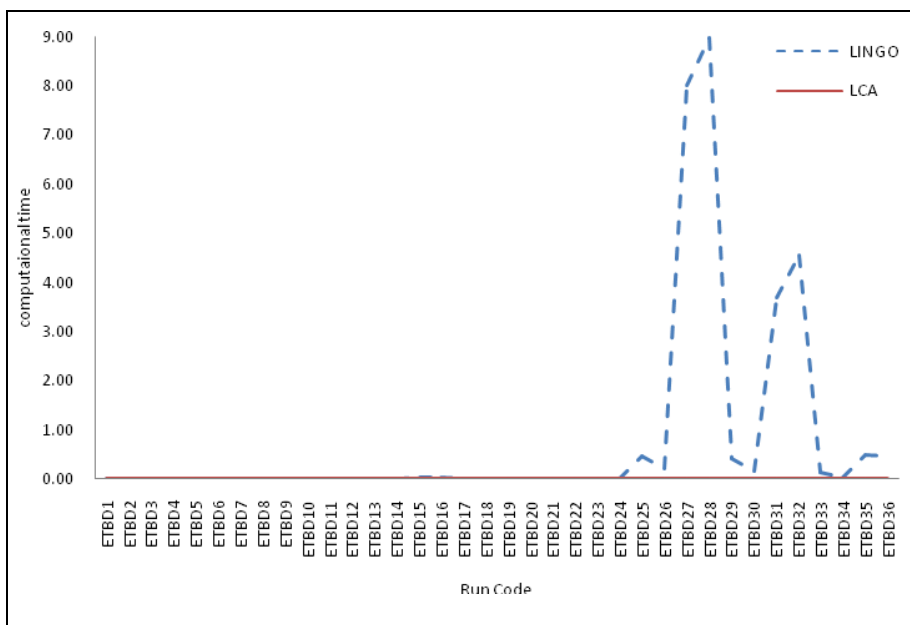


Fig. 1. Comparison between Computational results

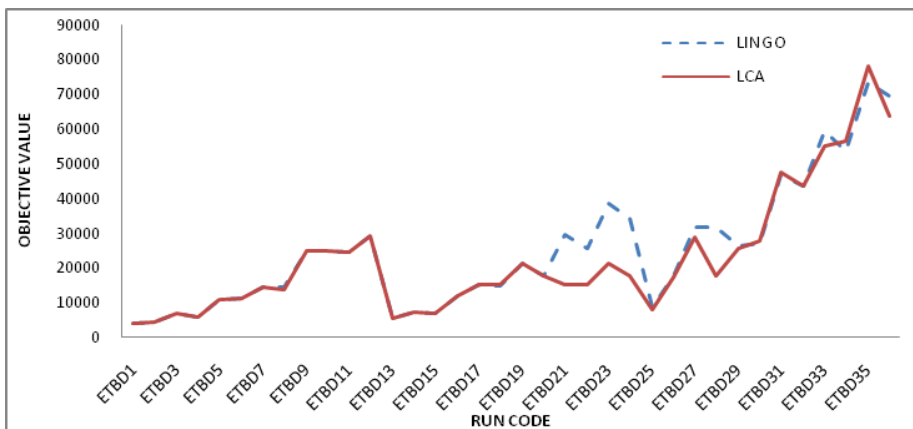


Fig. 2. Comparison between solution qualities

References

- Cheng, T.C.E., Kahlbacher, H.G.: Scheduling with Delivery and Earliness Penalties. *Asia-Pacific Journal of Operational Research* 10, 145–152 (1993)
- Cheng, T.C.E., Gordon, V.S.: Batch Delivery Scheduling on A Single Machine. *Journal of the Operational Research Society* 45, 121–1215 (1994)
- Chris, N.P., Mikhail, Y.K.: Scheduling with Batching: A Review. *European Journal of Operational Research* 120, 228–249 (2000)
- Guruprasad, P., Chen, Z.L.: Scheduling a Production–Distribution System To Optimize the Tradeoff between Delivery Tardiness and Distribution Cost. *Naval Research Logistics* 52, 571–589 (2005)
- Mohammad, M.M., Sara, S., Armin, A., Khalil, S.H.: Single-machine Batch Scheduling Minimizing Weighted Flow Times and Delivery Costs. *Applied Mathematical Modelling* 35, 563–570 (2011)
- Dvir, S.: Scheduling and Due Date Assignment to Minimize Earliness, Tardiness, Holding, Due Date Assignment and Batch Delivery Costs. *Int. J. Production Economics*. 123, 235–242 (2010)
- Chang, P.C., Chen, S.S., Fan, C.Y.: Mining gene structures to inject artificial chromosomes for genetic algorithm in single machine scheduling problems. *Applied Soft Computing* 8, 767–777 (2008)
- Tsai, T.I.: A Genetic Algorithm for Solving the Single Machine Earliness/Tardiness Problem with Distinct Due Dates and Ready Times. *Int. J. Adv. Manuf. Technol.* 31, 994–1000 (2007)
- Jou, C.: A Genetic Algorithm with Sub-indexed Partitioning Genes and Its Application to Production Scheduling of Parallel Machines. *Computers & Industrial Engineering* 48, 39–54 (2005)
- Ali, H.: League Championship Algorithm: A New Algorithm for Numerical Function Optimization. In: International Conference of Soft Computing and Pattern Recognition, pp. 43-48 (2009)
- Abdul, R., Potts, T.S.: Dynamic Programming State-space Relaxation for Single-machine Scheduling. *Journal of the Operational Research Society* 39, 141–152 (1988)

Local Meta-models for ASM-MOMA

Martin Pilát^{1,2} and Roman Neruda²

¹ Department of Theoretical Computer Science and Mathematical Logic,
Faculty of Mathematics and Physics, Charles University in Prague,
Malostranské náměstí 25, Prague, Czech Republic

² Institute of Computer Science, Academy of Sciences of the Czech Republic, Pod
Vodárenskou věží 2, Prague 8, Czech Republic
`Martin.Pilat@mff.cuni.cz, roman@cs.cas.cz`

Abstract. Evolutionary algorithms generally require a large number of objective function evaluations which can be costly in practice. These evaluations can be replaced by evaluations of a cheaper meta-model of the objective functions. In this paper we describe a multiobjective memetic algorithm utilizing local distance based meta-models. This algorithm is evaluated and compared to standard multiobjective evolutionary algorithms as well as a similar algorithm with a global meta-model. The number of objective function evaluations is considered, and also the conditions under which the algorithm actually helps to reduce the time needed to find a solution are analyzed.

Keywords: Multiobjective optimization, meta-model, evolutionary algorithm.

1 Introduction

Many real life optimization tasks require optimizing multiple conflicting objectives at once. It has been shown and widely accepted that multiobjective evolutionary algorithms (MOEA) are among the best methods for multiobjective optimization. In the past years several multiobjective evolutionary algorithms [3][12][1] were proposed and used to deal with these problems. However, most of them require lots of evaluations of each objective function, which makes them problematic to use for solving real life problems. These problems may have complex objective functions whose evaluations are expensive (either in terms of time or money).

The use of the meta-models aims at lowering the number of objective function evaluations which are needed to obtain the final solution. The meta-model is a simplified and cheaper approximation of the real objective function. Meta-models can be used in several ways to augment the multiobjective evolutionary algorithms. In one of the first approaches [10] its authors used the NSGA-II [3] and replaced the objective functions with their meta-models. In [7] and [8] authors describe an aggregate meta-model based on various SVM architectures. Although the memetic variant is also possible in multiobjective setting, only a few references were found in the literature which deal with meta-model assisted multiobjective memetic algorithms [5].

The paper is organized as follows: In the next section 2 The tests and their results are described in sections 3 and 4 Section 5 concludes the paper and provides ideas for future research.

2 Algorithm Description

In one of our previous papers [9] we proposed a multiobjective memetic algorithm with aggregate meta-model (ASM-MOMA). This algorithm was able to reduce the number of required evaluations of the objective functions by the factor of 5 to 10 on most problems. ASM-MOMA uses a single global meta-model trained after each generation as a fitness function during the local search.

In this paper, we propose a new variant of ASM-MOMA with local models instead of a single global one. We call this variant LAMM-MMA. The main difference between LAMM-MMA and other multiobjective evolutionary algorithms is the addition of a special memetic operator, which performs local search on some of the newly generated individuals (the generation of the new individuals is handled by the respective MOEA to which is this operator added). The operator uses the meta-model constructed based on previously evaluated points in the decision space, for which the values of objective functions are known. The meta-model is trained to predict the distance to the currently known Pareto front. Moreover, as an addition to ASM-MOMA, in LAMM-MMA the points do not have the same weight, as those that are closer to the locally optimized one are considered more important during the model building phase, see Equation 1 for details.

The main idea is that points closer to the known Pareto front are more interesting during the run of the algorithm and the memetic operator moves the individuals closer to the Pareto front. The purpose of the meta-model is not to precisely predict the value but rather provide a general direction in which the memetic search should proceed. To obtain a training set for the meta-models we also added an external archive of individuals with known objective values. This archive is updated after each generation when new individuals are added and at the same time the archive is truncated to ensure it does not grow indefinitely – random individuals are removed to match the limit on the number of individuals, see [9] for analysis of this approach.

The following sections detail the important parts of the algorithm. The main loop is essentially a generic MOEA with added memetic operator. We train a dedicated model for each individual I which shall be locally optimized by the memetic operator. For such an individual I we create a weighted training set

$$T_I = \left\{ \langle (x_i, y_i), w_i \rangle \mid y_i = -d(x_i, P), w_i = \frac{1}{1 + \lambda d(x_i, I)} \right\} \quad (1)$$

where $d(x, y)$ is the Euclidean distance of individuals x and y in the decision space, P is the set of non-dominated individuals in the archive and $d(x, P)$ is the distance of individual x to the closest point in the set P . λ is a parameter which controls the locality of the model, larger values of λ lead to more local model, whereas lower values lead to more global one.

The points which are closer to the individual I are more important during the training of the model. This distance weighting adds some locality to the models trained for each individual. The training set is constructed in such a way, that for the individuals closer to the currently known Pareto front the meta-model should return larger values. This fact is used during the local search phase (which uses the meta-model as a fitness function).

In the local search phase we use another evolutionary algorithm (this time it is only a single objective one) to find better points in the surroundings of each individual. The algorithm runs only for a few generations and it uses only meta-model evaluations. The newly found individuals are placed back to the population. During the initialization of the local search the individual which should be optimized is inserted in the initial population and its variables are perturbed to create the rest of the initial population.

The algorithm uses quite large number of meta-model evaluations and even trainings. This might lead to significant overhead. To find out how large this overhead is, we run a few benchmarks (archive size/training set size of 400 individuals, Intel Core i7 920 (2.87Ghz) processor and 6GB RAM). Table 2 shows the results. We can see that the evaluations are faster than the training by several orders of magnitude and that each training takes only a fraction of a second. Even if there are 100 trainings per generation, it would mean an overhead of roughly 15 to 30 seconds per generation, which still might be faster than a single evaluation of the real objective function. Therefore the overhead of the training and evaluation is easily compensated by the reduced evaluations of the objective functions.

Table 1. Times needed for training and evaluation of selected meta-models, in seconds

Model	Training (T_t)	Evaluation (T_m)
Linear regression	0.142	8.46×10^{-7}
Support vector regression	0.328	7.14×10^{-7}
Multilayer perceptron	3.75	1.80×10^{-5}

3 Test Setup

We tested our approach on the widely used ZDT [11] benchmark problems. These problems are all two dimensional, and we used 15 variables for each of them. In the local search phase we used various meta-models: namely multilayer perceptron, support vector regression, and linear regression. All the models use default parameters from the Weka framework [6] (which we used to run the experiments).

See Table 2 for the parameters of the main multiobjective algorithm and the internal single-objective algorithm.

As the base multiobjective evolutionary algorithm we used the NSGA-II and ϵ -IBEA with Simulated Binary Crossover [2] and Polynomial Mutation [4]. In the local search phase we used a simple single objective evolutionary algorithm with the same operators and the meta model as the fitness function.

To compare the results we use a measure we call H_{ratio} , it is defined as the $H_{ratio} = \frac{H_{real}}{H_{optimal}}$, where H_{real} is the hypervolume of the dominated space attained by the algorithm and $H_{optimal}$ is the hypervolume of the real Pareto set of the solutions. As the Pareto set is known for all the ZDT problems, we can compute this number directly. We use the vector $\mathbf{2} = (2, 2)$ as the reference point in the hypervolume computation. All points that do not dominate the reference point are excluded from the hypervolume computation. We compare the median number of function evaluations needed to attain the H_{ratio} of 0.5, 0.75, 0.9, 0.95, and 0.99 respectively.

Table 2. Parameters of the multiobjective algorithm

Parameter	MOEA value	Local search value
Stopping criterion	50,000 objective evaluations	30 generations
Population size	50	50
Crossover operator	SBX	SBX
Crossover probability	0.8	0.8
Mutation operator	Polynomial	Polynomial
Mutation probability	0.1	0.2
Archive size	400	—
Memetic operator probability	0.25	—
Meta-model locality parameter λ	—	1

4 Results

Table 3 shows the results of our algorithm compared to original ϵ -IBEA and ASM-MOMA. IBEA denotes the original ϵ -IBEA. LR, SVM, and MLP stands for the model used: linear regression, support vector regression and multilayer perceptron respectively. G denotes the single global model of ASM-MOMA and L stands for the local models as described in this paper.

The numbers in the table represent the median number of objective function evaluations needed to reach the specified H_{ratio} value. Twenty runs for each configuration were made.

From the results, we can see that the global models generally significantly decrease the number of required function evaluations, and the local models are even better than the global ones. Generally, linear regression gives better results than support vector regression and multilayer perceptrons. It probably creates simpler models which indicate the right general direction in which the local search should proceed. Moreover, we can see that the results of local models are almost always better than those of a single global model, thus we recommend using the faster models, i.e. linear regression or support vector regression instead of multilayer perceptrons.

On ZDT1 the global model was able to reduce the number of function evaluations to reach the $H_{ratio} = 0.95$ by a factor of 6.8 (LR) and the local model reduced it further, yielding the reduction factor of 7.3 for LR and even 7.7 with the SVM. For the $H_{ratio} = 0.99$ the reductions are not that large, but we can still see the number decreased by the factor of almost 4. In this case, local models did not improve the result.

On ZDT2 the results improved largely even for the $H_{ratio} = 0.99$. ASM-MOMA reduced the required number of objective function evaluations 8.4 times (SVM), while LAMM-MMA was able to reduce it almost 9 times with the same model and 9.6 times with the LR as the model.

Reaching the $H_{ratio} = 0.99$ was a problem for the original ϵ -IBEA on ZDT3, but both ASM-MOMA and LAMM-MMA were much more successful, both reducing the number of evaluations over 25 times. For the $H_{ratio} = 0.95$ (which is not that difficult for ϵ -IBEA) we can see again reduction factors of 8.5 and 9 for ASM-MOMA and LAMM-MMA respectively (LR in both cases).

Table 3. Median number of function evaluations needed to reach the specified H_{ratio} on ZDT1 test problem

H_{ratio}	ZDT1					ZDT2				
	0.5	0.75	0.9	0.95	0.99	0.5	0.75	0.9	0.95	0.99
IBEA	7400	13750	18200	20000	25550	750	2050	5150	7800	13000
IBEA-LR-G	1450	2500	2800	2950	7450	350	550	750	900	1650
IBEA-SVM-G	1400	2050	2700	3100	6850	350	550	850	1050	1550
IBEA-MLP-G	1800	2550	4000	4600	10100	450	650	950	1200	2700
IBEA-LR-L	1300	1900	2400	2750	7500	300	500	700	850	1350
IBEA-SVM-L	1350	1900	2350	2600	7100	350	550	800	1000	1450
IBEA-MLP-L	1400	1850	2450	3250	9650	350	550	750	900	1400
ZDT3						ZDT6				
H_{ratio}	0.5	0.75	0.9	0.95	0.99	0.5	0.75	0.9	0.95	0.99
	650	1550	5400	8150	33350	10300	13650	18400	23150	34050
IBEA	650	1550	5400	8150	33350	3050	6500	13400	17600	32100
IBEA-LR-G	350	550	850	950	1300	3000	7250	14100	19250	34150
IBEA-SVM-G	350	550	850	1000	1300	3500	7250	13250	18900	32450
IBEA-MLP-G	450	800	1100	1250	1800	3050	6850	13050	18750	31400
IBEA-LR-L	350	450	750	900	1300	3000	6500	12650	17850	32550
IBEA-SVM-L	400	650	850	1050	1450	3400	7050	13300	18200	32950
IBEA-MLP-L	400	650	950	1150	1600					

ZDT6, as in our previous paper [9], proved to be the most difficult problem. Although we can see reductions by the factor of 3.5 for the $H_{ratio} = 0.5$, this factor drops and there are only slight reductions of 6% for the $H_{ratio} = 0.99$. Note that LAMM-MMA again provided better reductions for this value, even though, the difference is not very large. Dealing with the difficulty of this problem is a motivation for further research.

5 Conclusions

In this paper we presented a memetic evolutionary algorithm for multiobjective optimization with local meta-models. We showed that the local models give better results than a single global model, usually reducing the number of needed function evaluations by another 10%. Although this difference may seem rather small it may greatly reduce the associated costs in practical tasks. We also showed that the algorithm is usable even for problems with quite simple objective functions, which take only milliseconds to evaluate, thus making it more widely usable. However, some problems are still difficult to solve with LAMM-MMA, and these provide the motivation for further research. Another open question is whether real life problems are among those easily solvable, or not.

We will continue the work on memetic multiobjective algorithms with aggregate meta-models. One of the goals is the reduction of the number of times the model is trained which is a problem especially for more expensive local models. These are trained multiple times in each generation. One possibility could be to cluster the individuals before the model is constructed and create a single local model for all the

individuals in the cluster. Another open question is the effect of the degree of locality (represented by the λ parameter) on the evolution convergence speed and the possibility to change this parameter adaptively.

Acknowledgments. This research has been supported by the Ministry of Education of the Czech Republic under project no. OC10047, and by Czech Science Foundation project no. 201/09/H057.

References

1. Bader, J., Zitzler, E.: HypE: An Algorithm for Fast Hypervolume-Based Many-Objective Optimization. TIK Report 286, Computer Engineering and Networks Laboratory (TIK), ETH Zurich (November 2008)
2. Deb, K., Agrawal, R.B.: Simulated binary crossover for continuous search space. *Complex Systems* 9, 115–148 (1995)
3. Deb, K., Agrawal, S., Pratap, A., Meyarivan, T.: A fast elitist non-dominated sorting genetic algorithm for multi-objective optimisation: NSGA-II. In: Schoenauer, M., Deb, K., Rudolph, G., Yao, X., Lutton, E., Guervós, J.J.M., Schwefel, H.P. (eds.) PPSN 2000. LNCS, vol. 1917, pp. 849–858. Springer, Heidelberg (2000)
4. Deb, K., Goyal, M.: A combined genetic adaptive search (geneas) for engineering design. *Computer Science and Informatics* 26, 30–45 (1996)
5. Georgopoulou, C., Giannakoglou, K.: Multiobjective metamodel-assisted memetic algorithms. *Multiobjective Memetic Algorithms*, 153–181 (2009)
6. Hall, M., Frank, E., Holmes, G., Pfahringer, B., Reutemann, P., Witten, I.H.: The WEKA data mining software: an update. *SIGKDD Explorations* 11(1), 10–18 (2009), <http://dx.doi.org/10.1145/1656274.1656278>
7. Loshchilov, I., Schoenauer, M., Sebag, M.: A mono surrogate for multiobjective optimization. In: Pelikan, M., Branke, J. (eds.) GECCO, pp. 471–478. ACM, New York (2010)
8. Loshchilov, I., Schoenauer, M., Sebag, M.: Dominance-based pareto-surrogate for multi-objective optimization. In: Deb, K., Bhattacharya, A., Chakraborti, N., Chakraborty, P., Das, S., Dutta, J., Gupta, S., Jain, A., Aggarwal, V., Branke, J., Louis, S.J., Tan, K. (eds.) SEAL 2010. LNCS, vol. 6457, pp. 230–239. Springer, Heidelberg (2010)
9. Pilát, M., Neruda, R.: ASM-MOMA: Multiobjective memetic algorithm with aggregate surrogate model. In: IEEE Congress on Evolutionary Computation. IEEE, Los Alamitos (to appear, 2011)
10. Voutchkov, I., Keane, A.: Multiobjective optimization using surrogates. Presented on Adaptive Computing in Design and Manufacture, ACDM 2006 (2006)
11. Zitzler, E., Deb, K., Thiele, L.: Comparison of Multiobjective Evolutionary Algorithms: Empirical Results. *Evolutionary Computation* 8(2), 173–195 (2000)
12. Zitzler, E., Künzli, S.: Indicator-Based Selection in Multiobjective Search. In: Yao, X., Burke, E.K., Lozano, J.A., Smith, J., Merelo-Guervós, J.J., Bullinaria, J.A., Rowe, J.E., Tiño, P., Kabán, A., Schwefel, H.-P. (eds.) PPSN 2004 Part VIII. LNCS, vol. 3242, pp. 832–842. Springer, Heidelberg (2004)

Research on Vehicle Routing Problem with Stochastic Demand Based on Multi-objective Method

Yanwei Zhao¹, Chuan Li², Jing-ling Zhang¹, Xingqiu Ren¹, and Wei Ren¹

¹ Key Laboratory of Special Equipment and Advanced Processing Technology Ministry of Education, Zhejiang Univ. of Tech., ZheJiang HangZhou 310012, China

² College of Computer Science & Technology, Zhejiang Univ. of Tech., ZheJiang Hangzhou 310023, China

zyw@zjut.edu.cn, lichuan726@gmail.com, jlzhang_zh@163.com

Abstract. This paper was targeted at minimizing the expectation of traveling distance maximizing the expectation of customers' degree satisfaction, a multi-objective vehicle routing problem with stochastic demand (VRPSD) model based on soft time window was proposed. In order to solve the problem, a hybrid PSO algorithm based on Pareto optimization method was designed in this paper. The paper made the standard PSO algorithm discrete by re-defining operators and employing swap recon, utilized challenge tournament method to construct Pareto optimal solution set, applied an external archive to keep the diversity of solutions. Ultimately, a standard example is used to verify the validity of the algorithm.

Keywords: Stochastic demand, multi-objective, degree of satisfaction, hybrid PSO algorithm, vehicle routing problem.

1 Introduction

Vehicle routing problem (VRP for short) has been a hot research field operations research, since VRP was first proposed by Dantzig and Ramser [1] in 1959. The importance of VRP is due to the strong impacts of its applications on the fields of transportsations, distributions, and logistics. As the VRPSD is one variant of VRP, it has the same importance of VRP, also it has several applications in the real life.

Many researchers have studied the VRPSD. In the existing literatures about it, and analyzed the asymptotic performance of its upper and lower bounds; Secomandi [2] combined neural dynamic programming and reinforcement learning method, proposed a NDP algorithm to solve VRPSD, and then, with the help of François Margot[3,4],made a research on the VRPSD with single vehicle under re-optimization strategy, introduced the finite-horizon Markov decision process(MDP), and proposed partial re-optimization heuristic algorithm; Alan L. Erera [5] had deeply studied VRPSD with time window constraints problem.

Presently, the research about VRP mainly focused on the single objective case. But for logistics companies, the short total traveling distance and less dispatchers lead to low cost, while favorable credit and good service is easy to form a fixed client base, that

will helpful for the company's long-term development. The actual need may be the solution with a set of multiple targets, rather than a single solution. In this paper, we considered the capacity constraint, joined the fuzzy time window, and established a multi-objective vehicle routing problem with stochastic demand.

The outline of this paper: Section 2 presented the description of the vehicle routing problem with stochastic demands (VRPSD) and the strategy used to solve the problem. Section 3 introduced the algorithm, discrete hybrid PSO, to solve the problem. Section 4 presented the simulation results and analysis. Finally, the conclusion was drawn in Section 5.

2 Problem Formulation

2.1 Problem Description

The multi-objective vehicle routing problem with stochastic demand (MOVRPSD) problem, involves m vehicles which start from depot 0 and provide commodity service to N customers whose demands are treated as independent stochastic variables with known distributions. $C = \{1, 2, \dots, N\}$ represents the set of Customers and $K = \{k_1, k_2, \dots, k_m\}$ vehicles set. P_i^C represents the probability of customer i need service, $P_i^D(k)$ stands for the probability of demand k . The distance between customer i and j is denoted by D_{ij} , where is symmetrical, i.e. $D_{ij}=D_{ji}$, and satisfies the triangular inequality, where $D_{ik}+D_{kj}>D_{ij}$. $[a_i, b_i]$ is the time window of customer i , where a_i is the earliest start time, b_i is the latest. At_i^k is the start time that vehicle k provides service for customer i , and μ_i is satisfaction degree of customer i , which is directly related with At_i^k . μ_i can be calculated by the equation (1):

$$\mu_i(t_i) = \begin{cases} 1 & 0 \leq t_i \leq b_i \\ e^{-(t_i - b_i)} & b_i < t_i \leq L_i \\ 0 & t_i > L_i \end{cases} \quad (1)$$

The objectives in this paper as follows:

- (1) Design a prior sequence, meet customers' time window, meanwhile, minimize the expectation of traveling distance;
- (2) Maximize expectation of customers' satisfaction degree μ ;

2.2 Strategy for VRPSD

We use a pre-optimization strategy[6], that is, when the demand of the customer is not clear, design a loop through all vertices and serve customers in term of the loop. When the demand state is definite, adjust the circuit using a certain rule. The specific adjustment rule as follows:

(1) If the remains of the vehicle is bigger than customer i demand: $D_i < Q_k^i$, the vehicle access the next customer directly;

(2) If the remain items meets customer i need exactly: $Q_k^i = D_i$, then the vehicle will serve the customer, return to the depot to upload, and then serve the next customer, so the distance will be exceeded: $\Delta = D_{i0} + D_{0j} - D_{ij}$;

(3) If the remains can not satisfy the customer i : $Q_k^i < D_i$, then the vehicle return to the depot to upload, and back to serve the current customer, the exceeded distance is $\Delta = D_{i0} + D_{0i} = 2 D_{i0}$.

2.3 Mathematical Model

Depending on the description and strategy above about VRPSD, we can define the objectives functions of MOVRPSD model as follows:

The first objective minimizes the expectation of total distance that is traveled by the vehicles, as the equation (2):

$$\min E(L(R)) = \min \sum_{i=1}^m E(L(R_i)) \quad (2)$$

And $E(L(R_i))$ is the distance expectation of sub-path R_i , which must satisfy the constraint (3),

$$C = \bigcup_{k=1,2,\dots,K} R_k \quad \text{且} \quad \forall i, j \in K, i \neq j \Rightarrow R_i \cap R_j = \emptyset \quad (3)$$

and it can be computed as the equation (4):

$$E(R_i) = \sum_{i=1}^n \sum_{j=i+1}^n d_{ij} p_i^c p_j^c \prod_{r=i+1}^n (1 - p_r^c) + \sum_{i=1}^n \delta_i s_{ii} + \sum_{i=1}^n \sum_{j=i+1}^n \gamma_i p_j^c s_{ij} \prod_{r=i+1}^{j-1} (1 - p_r^c) \quad (4)$$

It consists of three parts. Part I, the expectation of distance that the vehicle starts from depot, serves customers according to the prior sequence. Part II is the exceeded distance because that the remain can not satisfy the customer's demand, where δ_i , the probability that the vehicle can not meet customer i , is can be calculated by equation (5).

$$\delta_i = 0 \\ \delta_i = \sum_{h=1}^{i-1} \left\{ \sum_{k=1}^{K-1} \left(\sum_{r=k+1}^K p_i(k) f(h, i-1, Q-k) \right) \right\}, 2 \leq i \leq kn \quad (5)$$

Part III is the exceeded distance when the remains exactly meet the customer i , back to the depot to upload and serve the next customer j . And γ_i is the probability that the remains just satisfy customer i and it is described as equation (6). And $S(i,j)$, the exceeded distance, can be computed with formula (7).

$$\gamma_i = 0 \\ \gamma_i = \sum_{h=1}^{i-1} \left(\sum_{k=1}^K p_i(k) f(h, i-1, Q-k) \right), 2 \leq i \leq kn \quad (6)$$

$$S(i, j) = d_{i0} + d_{0j} - d_{ij} \quad (7)$$

The second objective maximizes the expectation of customers' satisfaction degree. For convenience purpose, maximizing problem equivalent to minimizing the problem in a sense. The second objective as follows:

$$\min \overline{E(S)} = \min(\Delta - \sum_{i=1}^N p_i(t_i) \mu_i(t_i)) \quad (8)$$

And $p_i(t_i)$ represents the probability when the serving time for customer i is t_i , we can get t_i using equation (9).

$$\begin{aligned} t_0 &= 0; \\ t_1 &= \max\{d_{v_1 v_0}, a_{v_1 v_0}\} \\ t_i^{(d)} &= \begin{cases} \max\{t_{i-1} + d_{v_{i-1} v_i}, a_{i0}\}, & d_i > 0 \\ t_{i-1}, & d_i = 0 \end{cases}, i = 2, 3, \dots, N \end{aligned} \quad (9)$$

3 Multi-objective Hybrid PSO Algorithm

3.1 Multi-objective Optimal Problem

Multi-objective optimization problems have several objectives to be handled. In order to solve the MOP, many methods have been proposed by scholars [7,8]. In this paper we apply the Pareto optimal solution to solve it. Some relevant definitions are shown as follows:

Definition 1: For a MOP composes of n decisive variables, r objective functions and multiple constraints. It can be described as formula (10):

$$\min y = \min(f(X)) = \min(f_1(X), f_2(X), \dots, f_r(X)) \quad (10)$$

Definition 2: For a given MOP $\min f(X)$, if $X^* \in D$ satisfies the constraint (11), we define X^* as a Pareto optimal solution.

$$\forall X \in D, f_i(X^*) \leq f_i(X) \quad (11)$$

Definition 3: Suppose x and y are two different individuals of the evolutionary population, if x and y satisfy the following two conditions, we say x dominate y , noted as $x \succ y$.

- 1) For all sub-objectives, x no worse than y ;
- 2) exist one sub-objective at least, x is better than y .

3.2 Hybrid PSO for MOVRPSD

For questions on the continuous space, PSO algorithm has higher search efficiency. However, the problem on the discrete domain, the standard PSO algorithm can not directly applicable. This paper based on the Literatures [9], [10] and [11], using operator redefinition method and the introduction of swap recon method to construct PSO algorithm for the problem. The reconstructed PSO algorithm could be performed by the following equations:

$$V_i^{t+1} = \omega \otimes V_i^t \oplus (c_1 * r_1) \otimes (P_{best_i} - X_i^t) \oplus (c_2 * r_2) \otimes (P_{gbest} - X_i^t) \quad (12)$$

$$X_i^{t+1} = X_i^t + V_i^{t+1} \quad (13)$$

where P_{best_i} and $gbest$ denote the best position of the i^{th} particle and the best position of the population, respectively. V is the particle's velocity, and X is the current position of the particle. In this paper, P_{best_i} , $gbest$ and X are random arrangement of one-dimensional array range from 1 to N, and $V = (s_1, s_2, \dots, s_m)$ is a set of switch sequences, where s_i is a swap recon. ω is the inertia coefficient which is a constant in interval $[0, 1]$, r_1, r_2 generated randomly in interval $[0, 1]$, c_1 is the rate of individual cognition that individuals learn from their own, while c_2 is the rate learning from the social, they are nonnegative constants.

In this paper, the operators in standard PSO algorithm have been re-defined: $\omega \otimes V$ represents the exchangers in V will be reserved depending on probability ω . The result of $P_{best_i} - X_i^t$ (or $P_{gbest} - X_i^t$) is a switching sequence v , that means X_i^t can become P_{best_i} (or P_{gbest}) changed with the sequence v ; V_1 and V_2 are both swap sequence, $V_1 \oplus V_2$ means that add V_2 to the tail of the V_1 , so that combined into a new swap sequences; $X + V$ represents X change itself to a new integer sequence according to the swap sequence in V .

3.3 Encoding and Decoding

According to the characteristics of vehicle routing problem, we use an integer encoding method in this paper. For a MOVRPSD with N customers, the particle could be represented as a random sort rang from 1 to N . For example, a Hamilton circuit $0 \rightarrow 1 \rightarrow 2 \rightarrow 3 \rightarrow 4 \rightarrow 5 \rightarrow 6 \rightarrow 0$ can be denoted by the particle $p = (1, 2, 3, 4, 5, 6)$, where 0 stands for the depot. The most important feature of this encoding method is simple, it never need mapping the binary code to integer as genetic algorithm.

3.4 Steps of MOPSO for VRPSD

Step 1. Initialize particle swarm pop , identify each particle's position, initial speed and previous best position $pbest$.

Step 2. Evaluate each particle $pop(i)$.

Step 3. In terms of the dominance-ship of particles, using challenge tournament method to construct a non-dominated solutions set [12]. In order to record the Pareto optimal solution, an external archive *ExArchive* with maximum capacity \bar{N} is added in this paper.

Step 4. Update position x and velocity v

- 1) Update $pbest$. Suppose x_i^k is the current position of particle i , if $pbest \succ x_i^k$, $pbest$ unchanged; if $x_i^k \succ pbest$, so $pbest = x_i^k$; if $pbest, x_i^k$ do not dominate each other, assign x_i^k to $pbest$ depend on the probability 0.5.
- 2) Update $gbest$. In this paper, a random selected Pareto optimal solution in *ExArchive* as global best solution $gbest$ each time.
- 3) Update velocity v . In this paper, v is a set of swap recons, which is decided by $pbest$ and $gbest$. According to the operators, we can calculate the new velocity v .

Step 5. If the termination conditions are satisfied or the iteration times up to maximum, then stop the search. Otherwise, go to **step 2**.

4 Simulation Results and Analysis

4.1 Data Sources

Up to present, there is no commonly used benchmark for the VRPSD in the literature. As such, many authors generated their own test problems. The data in this paper refers to Solomon's[13], which is a test for the deterministic VRP. In our work, the original data was adapted for the VRPSD. We worked on 3 instances C101, R101, RC101, which contains 50 customers. Supposed that all the demands were independent identically distributed, and these random demands were generated depending on the Poisson distribution $P(\lambda)$, where $\lambda=d_i$, there are 2λ stochastic demands for each customer. The original time window $[a_i, b_i]$ in Solomon benchmark was used in this paper, and the maximum delay time $\Delta\tau_i$ can be calculated by the formula $\Delta\tau_i=b_i+rand()*0.5*(b_i-a_i)$, so that the time range customers can tolerate is in the interval $[0, b_i+\Delta\tau_i]$.

The algorithm was programmed in Matlab, and simulations were performed on an Intel core quad CPU 2.66GHz computer. In the beginning, the size of population is 40, this capacity of the vehicles is 200, the size of external archive is 30, the maximum stagnation times is 20, maximum iteration time is 800.

4.2 Results and Analysis

For a multi-objective problem, the solution is usually not sole. In this paper, we select the third in C101 and the first in R101 from Table 1 as the solution, Figure 2 and Figure 3 shows the delivery routes of the solutions selected above. Figure 1 and Figure 2 shows the

distribution of vehicles in C101 and R101 respectively. In the figures, depot 0 was denoted by the solid square \blacksquare , and skipped customers by the red solid circle \bullet . The black dashed line represents the routes that the vehicles back to depot, reload, and serve the current customer because of the insufficient remains. And the red dashed line stands for that the vehicles back to depot, reload, and serve the next customer in the case of the remain empty. In C101, shown as Fig.1, the prior dispatcher number was 5, but 6 actually, that mean occurring once case of $Q_k^i < D_i$. In R101, the actual dispatcher number was 7 and the prior was 5, which occurring cases of $Q_k^i < D_i$ and $Q_k^i = D_i$ once each.

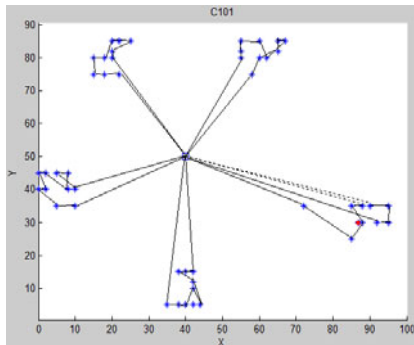


Fig. 1. Delivery paths of C101

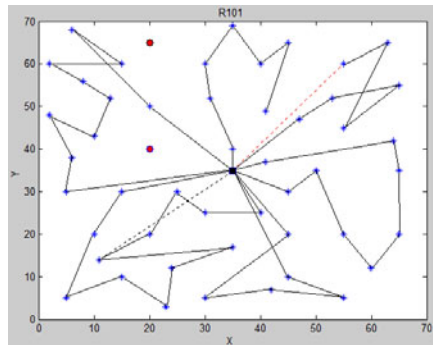


Fig. 2. Delivery paths of R101

Figure 3,4, 5 show the Pareto optimal solutions distribution of C101, R101 and RC101. In Solomon tests, C stands for clustering and R random, which is visible from Figure 2 and Figure 3. The result of C101 appeared sparsely compared with the result of R101. For the clustered case, it just needs to adjust the sub-paths to get a satisfactory result because of the customers' comparatively concentrated position. By contrast, R101, with larger search space, had more Pareto optimal solutions. And Figure 5, it was the consolidation of the former two cases. An adaptive grid method used enable to make the best solutions uniform distributed on the Pareto curve.

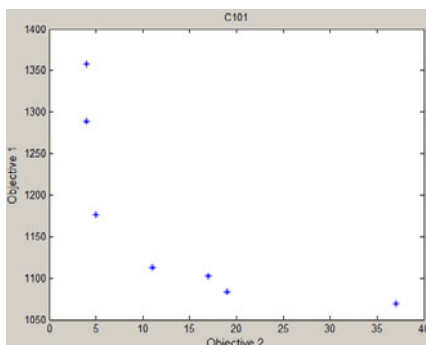


Fig. 3. The Pareto optimal solution of C101

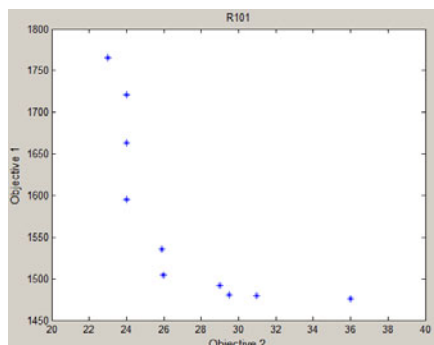


Fig. 4. The Pareto optimal solution of R101

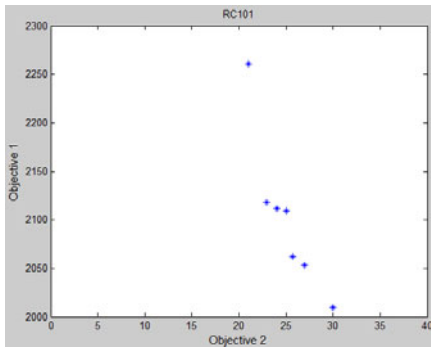


Fig. 5. The Pareto optimal solution of RC101

For C101, R101 and RC101, the convergence time was 398.7、450.6 and 537.4 respectively. It looks like the C101 tend to convergence. Their running time was 58.4s, 104.3s, and 87.7.s, so the algorithm proposed in this paper enable to get a feasible solution in limited time.

5 Conclusion

This paper mainly studied the multi-objective vehicle routing problem with stochastic demand (MOVRPSD), and established the mathematical model of the problem, which was targeted at minimizing the traveling distance expectations and customers' dissatisfaction expectation. A multi-objective discrete hybrid PSO algorithm based on Pareto optimal theory was designed. This article constructed Pareto optimal solutions set using the challenge tournament method. In order to maintain the diversity of the optimal solution, we introduced a external archive. Ultimately, the effectiveness of the algorithm was validated through three examples.

Acknowledgments. The authors would express sincere appreciation to the support from National Science Foundation of China, Grant No. 60970021.

Reference

1. Laporte, G.: Fifty Years of Vehicle Routing Problem. *J. Transportation Science*, 408–416 (2009)
2. Secomandi, N.: Comparing Neuro-dynamic Programming Algorithms for The Vehicle Routing Problem with Stochastic Demands. *J. Computers and Operations Research*, 1201–1225 (2000)
3. Secomandi, N., Margot, F.: Reoptimization Approaches for the Vehicle-Routing Problem with Stochastic Demands. *J. Operations Research*, 214–230 (2009)
4. Xie, B.L.: Research on Stochastic Vehicle Routing Problem. Southwest Jiaotong University (2003)

5. Erera, A.L., Morales, J.C., Savelsbergh, M.: The Vehicle Routing Problem with Stochastic Demand and Duration Constraints. *Transportation Science*, 1-19 (2010)
6. Bertsimas, D.J.: A Vehicle Routing Problem with Stochastic Demand. *Operations Research* 40(3), 574–585 (1992)
7. Cui, X.X.: Multiobjective Evolutionary Algorithm and Applications. National Defense Industry Press, BeiJing (2009)
8. Clerc, M.: Discrete Particle Swarm Optimization Illustrated by Traveling Salesman Problem. Springer, Berlin (2004)
9. Jie, X., De-xian, H.: Hybrid Particle Swarm Optimization for Vehicle Routing Problem with Multiple Objectives. *J. Computer Integrated Manufacturing Systems*, 573–584 (2007)
10. Huang, L., Wang, K.P., Zhou, C.G., et al.: A particle swarm optimization for Traveling Salesman Problem. *J. Journal of Jilin University (Science Edition)*, 477–480 (2003)
11. Lei, D.M., Yan, X.P.: Multiobjective Intelligent Optimization Algorithms and Applications. Science Press, BeiJing (2009)
12. Zheng, J.H.: Multiobjective Evolutionary Algorithm and Applications Science (2009)

A Stochastic Optimization Method for Solving the Machine–Part Cell Formation Problem

Khoa Trinh¹, Jacques Ferland², and Tien Dinh¹

¹ Faculty of Information Technology, University of Science, VNU-HCMC
227 Nguyen Van Cu, Ho Chi Minh City, Vietnam
ttdkhoa@acm.org, dbtien@fit.hcmus.edu.vn

² Interuniversity Research Center on Enterprise Networks, Logistics and Transportation, Université de Montréal,
C.P. 6228, Succ. Centre-Ville, Montréal (Québec)
ferland@iro.umontreal.ca

Abstract. In this paper, we study the machine–part cell formation problem. The problem is to assign the given machines and parts into cells so that the grouping efficacy, a measure of autonomy, is maximized. First, we introduce a new randomized local search algorithm which requires solving another subproblem for assigning optimally parts into cells on the basis of given groups of machines. Second, we propose an exact, polynomial-time algorithm to solve this subproblem. Finally, we provide the numerical results of our proposed algorithm, using a popular set of benchmark problems. Comparisons with other recent algorithms in the literature show that our algorithm can improve the current best-known solutions for some instances.

Keywords: Cell Formation Problem, Fractional Programming, Randomized Local Search Algorithm.

1 Introduction

The machine–part cell formation problem (CFP) is an important application of the group technology. The philosophy behind the problem is to decompose an entire manufacturing system, including machines and parts, into many subsystems in such a way that the number of interactions between machines and parts within a subsystem is maximized. In addition, we have to keep the number of interactions between machines and parts belonging to different subsystems as low as possible. By doing so, we reduce the handling cost, the setup cost, and the processing time of operating the whole system [1]. Ogoubi et al. also apply the CFP to design 3-D chip networks [2].

More specifically, in the CFP, we are given an incidence matrix that describes the relationships between machines and parts. We need to group them into several cells so that a certain measure of autonomy is maximized. A good survey of different autonomy measures can be found in [3]. In our study, we choose the popular grouping efficacy introduced in [4] as the measure of efficiency. Since

the CFP is known to be NP-hard [5], most of the methods are based on some heuristics or metaheuristics such as clustering methods [6], genetic algorithms [7], and tabu search [8]. An exact algorithm for this problem would require enormous computational effort, making it virtually impractical [9].

The rest of the paper is organized as follows. In Section 2, we formulate the CFP rigorously. We then present a randomized local search algorithm (RLSA) in Section 3. The most novel contribution of this paper is to develop an exact, polynomial-time algorithm for solving a subproblem of assigning parts to the cells once the assignment of machines into cells is known. Solving this subproblem efficiently is important since it has to be executed in each iteration of the RLSA. We will present this algorithm in Section 4. In Section 5, we provide the numerical results of our proposed algorithm to solve a set of 35 well-known benchmark problems. Finally, we conclude the paper in Section 6.

2 Problem Formulation and Preliminaries

The Cell Formation Problem is often defined as follows. Consider a set $I = \{1, 2, \dots, m\}$ of machines, and a set $J = \{1, 2, \dots, n\}$ of parts. An m -by- n incidence matrix A is also available, where $a_{i,j} = 1$ if machine i processes part j , and $a_{i,j} = 0$ otherwise. We refer to a subset of machines as a “machine group.” Similarly, we refer to a subset of parts as a “part family.” A production cell consists of a pair of a non-empty machine group and a non-empty part family (i.e. in our formulation, we assume that each production cell should contain at least one machine and one part). The objective is to find a solution of K production cells $(C, F) = \{(C_1, F_1), (C_2, F_2), \dots, (C_K, F_K)\}$ such that C_1, C_2, \dots, C_K form a partition of I , and F_1, F_2, \dots, F_K form a partition of J in order to maximize the grouping efficacy:

$$Eff(C, F) = \frac{a_1^{In}}{a + a_0^{In}},$$

where

$$a = \sum_{i=1}^m \sum_{j=1}^n a_{i,j}, \quad a_0^{In} = \sum_{k=1}^K \sum_{i \in C_k} \sum_{j \in F_k} 1 - a_{i,j}, \quad a_1^{In} = \sum_{k=1}^K \sum_{i \in C_k} \sum_{j \in F_k} a_{i,j}.$$

Note that a is the number of entries equal to 1 in A , and a_0^{In} and a_1^{In} are the number of entries equal to 0 and that of entries equal to 1 in all K cells, respectively.

3 A Randomized Local Search Algorithm

In this section, we propose a randomized local search algorithm (RLSA) based on the local search algorithm (LSA) introduced in [10]. Basically, the randomization of the LSA prevents a premature convergence to local optima. First, we modify

the stopping rule, allowing us to improve the current solution for a fixed number of iterations T .

Second, instead of using the greedy method to generate an initial feasible solution, we simply generate an initial solution randomly. In fact, the initial solution is not important compared to the procedure of modifying the current solution in each step.

Third, we change the “destroy&recover” strategy. Whenever we fail to improve the current solution, we simply reassign randomly p percent of parts (machines) to other random families (groups). Overall, the numerical results indicate that the random shuffle strategy seems to be better in that it diversifies the search space and prevents the algorithm from returning to some local extrema. However, we will not present numerical comparisons between these two strategies due to length limit of the paper.

Finally, our main contribution is to introduce a better way to improve the current solution in each iteration. To be precise, we are interested in the exact solution of the following subproblem.

Subproblem 1. Assume that K fixed machine groups C_1, C_2, \dots, C_K are specified for the CFP. Determine part families F_1, F_2, \dots, F_K that form a partition of the set J and maximize the grouping efficacy.

Proposition 1. The subproblem 1 can be solved in polynomial-time.

In the next section, we will introduce an exact, polynomial-time algorithm to solve the subproblem 1, based on Fractional Programming.

Note that the problem of finding machine groups on the basis of specified part families can be solved similarly by working on the transpose of the matrix A . Moreover, in the case that empty families or groups appear in the solution, we have to apply the “repair process” mentioned in [10] in order to deal with empty families or groups. In summary, the pseudo-code of the RLSA is described as follows.

Algorithm 1. Randomized Local Search Algorithm

```

1: Input  $\leftarrow m, n, K, A, T, p$ 
2: Randomly generate an initial feasible solution  $(C^0, F^0)$ 
3: Initialize  $(C, F) \leftarrow (C^0, F^0)$ ,  $(C_r, F_r) \leftarrow (C^0, F^0)$ 
4: for step  $\leftarrow 1$  to  $T$  do
5:   Find  $F_{opt} = (F_1, F_2, \dots, F_K)$  on the basis of machine groups in  $C$  to maximize
     the grouping efficacy and update  $F \leftarrow F_{opt}$ 
6:   if there is no improvement then
7:     Randomly take  $p$  percent of parts and reassign them to other random families.
8:   if the current solution  $(C, F)$  is better than  $(C_r, F_r)$  then
9:      $(C_r, F_r) \leftarrow (C, F)$ 
10:   $A \leftarrow A^T$ 
11: return  $(C_r, F_r)$ 
```

4 A Fractional-Programming-Based Algorithm for Subproblem 1

4.1 An Alternative 0–1 Fractional Programming Formulation

In this section, we formulate subproblem 1 as a mathematical optimization problem. First, we introduce the binary variables $y_{j,k}$,

$$y_{j,k} = \begin{cases} 1 & \text{if } j \in F_k \\ 0 & \text{otherwise} \end{cases},$$

for all pairs (j, k) , $j = 1, 2, \dots, n$, and $k = 1, 2, \dots, K$.

Now, for each valid assignment of parts to the K families, we have the relation

$$a_1^{In} = \sum_{j=1}^n \sum_{k=1}^K \sum_{i \in C_k} a_{i,j} y_{j,k}, \quad (1)$$

and

$$a_0^{In} = \sum_{j=1}^n \sum_{k=1}^K \sum_{i \in C_k} (1 - a_{i,j}) y_{j,k}. \quad (2)$$

Subproblem 1 can be written as the following 0–1 fractional programming problem $M(y)$

$$\max \quad Eff = \frac{a_1^{In}}{a + a_0^{In}} \quad (3)$$

$$\text{subject to } \sum_{k=1}^K y_{j,k} = 1 \quad j = 1, \dots, n, \quad (4)$$

$$y_{j,k} = 0 \text{ or } 1 \quad j = 1, \dots, n; k = 1, \dots, K.$$

Note that the constraints (3) and (4) make sure that each part is assigned to exactly one family.

4.2 A Subproblem of $M(y)$

Let Ω be the set of all feasible solutions y of the program $M(y)$. In order to solve $M(y)$ with the Dinkelbach algorithm, we have to solve a sequence of simpler problems, in which the fractional objective function is replaced by a linear function. In particular, the Dinkelbach algorithm specifies a sequence of values $\lambda \in \mathbb{R}$, and the following subproblem $M(\lambda, y)$ have to be solved.

$$\max \quad Eff(\lambda) = a_1^{In} - \lambda(a + a_0^{In}) \quad (5)$$

$$\text{subject to } y \in \Omega.$$

Substitute relations (1) and (2) into (5), we have

$$\begin{aligned}
Eff(\lambda) &= a_1^{In} - \lambda(a + a_0^{In}) \\
&= -\lambda a + \sum_{j=1}^n \sum_{k=1}^K \sum_{i \in C_k} a_{i,j} y_{j,k} - \lambda \sum_{j=1}^n \sum_{k=1}^K \sum_{i \in C_k} (1 - a_{i,j}) y_{j,k} \\
&= -\lambda a + \sum_{j=1}^n \left[\sum_{k=1}^K \left(\sum_{i \in C_k} a_{i,j} - \lambda \sum_{i \in C_k} (1 - a_{i,j}) \right) y_{j,k} \right].
\end{aligned}$$

Let

$$M_j = \sum_{k=1}^K \left(\sum_{i \in C_k} a_{i,j} - \lambda \sum_{i \in C_k} (1 - a_{i,j}) \right) y_{j,k},$$

we can write

$$Eff(\lambda) = -\lambda a + \sum_{j=1}^n M_j.$$

It follows that, to maximize the objective function $Eff(\lambda)$, all separate term M_j 's need to be maximized. Due to the constraints (3) and (4), for each part j , all but one value of y_{jk} are zero, which implies

$$M_{j \max} = \max_{k=1, \dots, K} \left(\sum_{i \in C_k} a_{i,j} - \lambda \sum_{i \in C_k} (1 - a_{i,j}) \right).$$

Therefore, we only need to assign each part j to the family $F_{\bar{k}}$ such that

$$\bar{k} = \arg \max_{k=1, \dots, K} \left(\sum_{i \in C_k} a_{i,j} - \lambda \sum_{i \in C_k} (1 - a_{i,j}) \right),$$

and the subproblem $M(\lambda, y)$ is now solved.

4.3 Applying the Dinkelbach's Algorithm to Solve the Problem $M(y)$

The details and analysis of the Dinkelbach algorithm can be found in [12]. The pseudo-code for the $M(y)$ problem is illustrated as follow.

Algorithm 2. Fractional-Programming-Based Algorithm

- 1: Input $\leftarrow m, n, A, K, C$
 - 2: Randomly generate some families $F^0 = (F_1^0, \dots, F_K^0)$ and initialize $\zeta \leftarrow 0$
 - 3: **repeat**
 - 4: $\zeta \leftarrow \zeta + 1$
 - 5: $\lambda_\zeta \leftarrow Eff(C, F^{\zeta-1})$
 - 6: Solve the subproblem $M(\lambda_\zeta, y)$ and let F^ζ be an optimal solution.
 - 7: **until** $Eff(\lambda_\zeta) = 0$
 - 8: **return** $(Eff(C, F) = \lambda_\zeta, F^\zeta = (F_1^\zeta, F_2^\zeta, \dots, F_K^\zeta))$
-

4.4 Running Time Analysis

The algorithm will terminate since the generated sequence $\{\lambda_\zeta\}$ is strictly increasing [12]. Moreover, it can be derived from the result in [11] that our algorithm will only have to solve at most $O(\log(mn))$ subproblems $M(\lambda_\zeta, y)$. Besides, the time complexity of solving each subproblem $M(\lambda, y)$ as shown in section 4.2 is $O(nK)$. Therefore, after taking into account the cost of precomputation, the FP-based algorithm runs in time $O(mn + \max(m, n)K \log(mn))$.

5 Empirical Study

In this section, we provide the numerical results of our algorithm as well as comparisons with other state-of-the-art approaches. All algorithms are tested on the 35 well-known benchmark problems for the CFP specified clearly in [17]. We have already collected the currently best-known solutions for these instances from various sources [10][13][14][15][16][17]. Besides, we compare our RLSA-FP with another recent algorithm introduced in [10]: a hybrid method combining LSA and a genetic algorithm (GA). Our algorithm will be tested with the parameters $T = 500$ and $p = 10$.

All algorithms are implemented in C++ using the compiler GCC 3.4.2. We conduct all experiments on a personal computer with the Intel-Quadcore 2.33GHz processor and 4GB RAM. The algorithms GA, and RLSA-FP are tested independently for 10 times, after which we record the average Eff , the average running-time, and the best solution. The results are summarized in Table 1, but to reduce its size, we only report the results for problems 15 to 35 in [10] since the results for other smaller problems are identical for the all methods.

Analysis: It can be seen in Table 1 that our proposed algorithm RLSA-FP is able to reach the best-known solutions for almost all cases, after 10 independent runs. Remarkably, it manages to improve the best-known solution for two instances: 29 and 33. The average Eff of the RLSA-FP is greater than that of the GA for 8 instances with an average gap about 0.4%. For another 5 instances, the GA have better average Eff to average gap only about 0.24%.

On average, it takes the RLSA-FP only about 2.3 seconds to solve the largest instance (with a 40x100 incidence matrix) on our computer. The GA runs very slowly on instances that have big values of K . Note that, although the original LSA runs as fast as the RLSA-FP, the quality of solutions by this algorithm is not very good. It fails to reach the best-known solution for 21/35 instances.

Indeed, if we increase the parameter T , the average Eff of our algorithm will be improved. However, we recommend to keep this parameter small, say, less than 2000, in order to take advantage of its very fast speed while the returned solution is as good as (and sometimes better than) the best solutions found by other current algorithms in the literature.

Table 1. The result of all algorithms

Instance	Size $m \times n$	Best-known Solution ^a	LSA		GA			RLSA-FP		
			Eff	Time	Max	Avg	Time	Max	Avg	Time
15	16×30	69.53 ([10])	66.42	0.27	69.53	69.53	22.14	69.53	69.53	0.34
16	16×43	57.53 ([13])	56.77	0.49	57.53	57.36	87.50	57.53	57.50	0.46
17	18×24	57.73 ([13])	53.61	0.35	57.73	57.53	52.06	57.73	57.73	0.33
18	20×20	43.17 ([10])	41.29	0.20	43.17	43.14	18.81	43.17	43.07	0.27
19	20×23	50.81 ([15])	50.00	0.30	50.81	50.81	40.02	50.81	50.81	0.33
20	20×35	77.91 ([13])	76.02	0.33	77.91	77.64	41.97	77.91	77.91	0.44
21	20×35	57.98 ([13])	56.08	0.33	57.98	57.39	35.81	57.98	57.98	0.42
22	24×40	100.00 ([13])	100.00	0.61	100.00	100.00	47.16	100.00	100.00	0.62
23	24×40	85.11 ([13])	85.11	0.59	85.11	85.11	78.86	85.11	85.11	0.61
24	24×40	73.51 ([13])	73.51	0.60	73.51	73.51	94.01	73.51	73.51	0.63
25	24×40	53.29 ([13])	52.94	0.92	53.29	53.29	222.95	53.29	53.29	0.61
26	24×40	48.95 ([13])	48.28	1.00	48.95	48.95	296.03	48.95	48.67	0.64
27	24×40	46.58 ([13])	45.58	0.99	46.58	46.58	280.81	46.58	46.37	0.62
28	27×27	54.82 ([13])	52.09	0.34	54.82	54.82	28.01	54.82	54.82	0.45
29	28×46	47.06 ([10])	45.49	1.10	47.06	46.91	328.76	47.08	47.06	0.79
30	30×41	63.31 ([10])	61.33	1.46	63.31	63.07	765.03	63.31	63.25	0.79
31	30×41	60.12 ([14])	60.12	1.65	60.12	60.12	617.88	60.12	60.10	0.90
32	30×41	50.83 ([15])	50.56	1.78	50.83	50.83	838.67	50.83	50.75	0.96
33	36×90	47.77 ([16])	43.83	3.81	47.77	47.74	2199.88	48.00	47.82	1.58
34	37×53	60.64 ([13])	60.34	0.53	60.63	60.39	68.68	60.64	60.64	1.04
35	40×100	84.03 ([17])	84.03	3.34	84.03	84.03	1021.55	84.03	84.03	2.23

^a Sources of the best-known solutions are shown in parentheses.

6 Conclusions

In this work, we have presented a randomized local search algorithm (RLSA) for the cell formation problem. The novel idea is to find a new, better way to improve the current solution in each iteration of the RLSA. To this end, we introduce an exact, polynomial-time algorithm to solve a special case of the CFP, in which an assignment of machines (or parts) is already known. We then experimentally show that our RLSA-FP outperforms other current algorithms in the literature in terms of the quality of solutions as well as the running time. It also improves the best-known solutions for two instances. The time complexity of RLSA-FP is only $O(mn + \max(m, n)K \log(mn))$ if we fix T as a constant, allowing us to solve very large inputs, say, with thousands of machines and parts, in just few minutes on a normal personal computer.

References

1. Wemmerlov, U., Hyer, N.: Research Issues in Cellular Manufacturing. *International Journal of Production Research* 25, 413–431 (1987)
2. Ogoubi, E., Ferland, J.A., Hafid, A., Turcotte, M., Bellemare, J.: A Multi-Constraint Cell Formation Problem for Large Scale Application Decomposition. Working paper, DIRO, Universit de Montral, Qubec, Canada (2010)

3. Papaioannou, G., Wilson, J.M.: The Evolution of Cell Formation Problem Methodologies Based on Recent Studies (1997–2008): Review and Directions for Future Research. *European Journal of Operational Research* 206, 509–521 (2010)
4. Sarker, B.R., Khan, M.: A Comparison of Existing Grouping Efficiency Measures and a New Weighted Grouping Efficiency Measure. *IIE Transactions* 33, 11–27 (2001)
5. Dimopoulos, C., Zalzala, A.M.S.: Recent Developments in Evolutionary Computation for Manufacturing Optimization: Problems, Solutions and Comparisons. *IEEE Transactions on Evolutionary Computation* 4(2), 93–113 (2000)
6. Srinivasana, G., Narendrana, T.T.: A Nonhierarchical Clustering Algorithm for Group Technology. *International Journal of Production Research* 29(3), 463–478 (1991)
7. Tunnuikij, T., Hicks, C.: An Enhanced Grouping Genetic Algorithm for solving the cell formation problem. *International Journal of Production Research* (2010)
8. Zolfaghari, S., Liang, M.: Comparative Study of Simulated Annealing, Genetic Algorithms and Tabu Search for Solving Binary and Comprehensive Machine–Grouping Problems. *International Journal of Production Research* 40(9), 2141–2158 (2002)
9. Elbenani, B., Ferland, J.A.: An Exact Method for Solving the Manufacturing Cell Formation Problem. Publication CIRRELT, Universit de Montral, Qubec, Canada (2010)
10. Elbenani, B., Ferland, J.A., Bellemare, J.: Genetic Algorithm and Large Neighborhood Search to Solve the Cell Formation Problem. Publication CIRRELT, Universit de Montral, Qubec, Canada (2010)
11. Matsui, T., Saruwatari, Y., Shigeno, M.: An Analysis of Dinkelbach’s Algorithm for 0–1 Fractional Programming Problems. Dept. Math. Eng. Inf. Phys., University of Tokyo (1992)
12. Crouzeix, J.P., Ferland, J.A., Hien, N.: Revisiting Dinkelbach–Type Algorithms for Generalized Fractional Programs. *Operational Research Society of India* 45 (2008)
13. Tunnuikij, T., Hicks, C.: An Enhanced Genetic Algorithm for Solving the Cell Formation Problem. *International Journal of Production research* 47 (2009)
14. Mahdavi, I., Paydar, M.M., Solimanpur, M., Heidarzade, A.: Genetic Algorithm Approach for Solving a Cell Formation Problem in Cellular Manufacturing. *Expert Systems with Applications* 36, 6598–6604 (2009)
15. James, T.J., Brown, E.C., Keeling, K.B.: A Hybrid Grouping Genetic Algorithm for the Cell Formation Problem. *Computers & Operations Research* 34, 2059–2079 (2007)
16. Luo, L., Tang, L.: A Hybrid Approach of Ordinal Optimization and Iterated Local Search for Manufacturing Cell Formation. *International Journal of Advance Manufacturing Technology* 40, 362–372 (2009)
17. Goncalves, J., Resende, M.G.C.: An Evolutionary Algorithm for Manufacturing Cell Formation. *Computers & Industrial Engineering* 47, 247–273 (2004)

Fully Connected Multi-Objective Particle Swarm Optimizer Based on Neural Network

Zenghui Wang¹ and Yanxia Sun²

¹School of Engineering, University of South Africa, Florida 1710, South Africa

²Department of Electrical Engineering & French South African Institute of Technology (F'SATI), Tshwane University of Technology, Pretoria 0001, South Africa
`{wangzengh, sunyanxia}@gmail.com`

Abstract. In this paper, a new model for multi-objective particle swarm optimization (MOPSO) is proposed. In this model, each particle's behavior is influenced by the best experience among its neighbors, its own best experience and all its components. The influence among different components of particles is implemented by the on-line training of a multi-input Multi-output back propagation (BP) neural network. The inputs and outputs of the BP neural network are the particle position and its the 'gradient descent' direction vector to the less objective value according to the definition of no-domination, respectively. Therefore, the new structured MOPSO model is called a fully connected multi-objective particle swarm optimizer (FCMOPSO). Simulation results and comparisons with exiting MOPSOs demonstrate that the proposed FCMOPSO is more stable and can improve the optimization performance.

Keywords: Multi-objective Optimization, Particle Swarm Optimization, Neural Network, Pareto Front, non-domination.

1 Introduction

The single-objective Particle Swarm Optimization (SOPSO), first introduced by [1], is a stochastic optimization technique that can be likened to the behavior of a flock of birds or the sociological behavior of a group of people. It has been used to solve a range of optimization problems, including neural network training [2] and function minimization [3]. In a particle swarm optimizer the individuals are evolved by cooperation among the individuals through generations. Every particle finds its personal best position and the group's best position through iteration, and then modifies their progressing direction and speed to rapidly reach optimum position. Particle swarm algorithms have been used to successfully optimize a wide range of problems [4]. Later, the SOPSO was extended to deal with multi-objective Optimization [5] [6]. The searching processes of the multi-objective PSO (MOPSO) are similar with SOPSO. During the search process, each particle can be regarded as an independent agent, which searches the problem space based on its own experience and the experiences of its peers. The former is the cognitive part of the particle update formula, while the latter is

the social part of the particle update formula. Both play crucial roles to guide the particle's search.

There are no connections among particle components for most PSOs. But the relationships among the variables of optimization problems can affect the optimization performance as the variables are coupled for most of the optimization problems. There are many classic optimization algorithms in the literature such as Quasi-Newton Methods [7], Gauss-Newton Method, Levenberg–Marquardt Method [8], and so on. In these optimization algorithms, the search direction is determined by all variables of the optimization function. Many intelligent optimization methods are proposed based on all components of the optimization problem such as Hopfield Neural Networks [9].

Moreover, the PSOs only use little information of past experience, such as the individual best position, the group's best position and so on. Most of the past information will be given up. The neural network is very powerful as it can memorize the information or characteristics of a complicated system. To improve the optimization performance of SOPSPO, Sun et al. proposed the full connected PSO for single-objective optimization problems [10] based on neural network which was used to memorize the tendency to a less value of fitness function at different positions which is the most important difference between the full connected PSO and other hybrid PSO-BP algorithms such as references [11], [12], and so on. It showed a good optimization performance. However, the full connected single-objective PSO cannot be directly used for multi-objective optimization problems as there are several optimization objectives, and the choices of the own experience and the swarm experience are different. The present paper aims at proposing a multi-objective version of full connected particle swarm optimization.

The remainder of this paper is organized as follows: Section 2 is an introduction of the multi-objective particle swarm optimization algorithm and BP neural network. Section 3 proposes the multi-objective version of full connected particle swarm optimization. Numerical results and comparisons are provided in Section 4. Finally, the concluding remarks appear in Section 5.

2 A Brief Introduction of Multi-Objective Particle Swarm Optimization

The canonical particle swarm algorithm works by iteratively searching in a region and is concerned with the best previous success of each particle, the best previous success of the particle swarm and the current position and velocity of each particle [1]. Every candidate solution is called a “particle”. A particle status on the search space is characterized by two factors: its position and velocity, which are updated by following equations.

$$V_i(t+1) = \omega V_i(t) + c_1 R_1(P_i - X_i(t)) + c_2 R_2(P_g - X_i(t)), \quad (1)$$

$$X_i(t+1) = X_i(t) + V_i(t+1), \quad (2)$$

where $V_i = [v_i^1, v_i^2, \dots, v_i^n]$ is the velocity vector of particle i ; $X_i = [x_i^1, x_i^2, \dots, x_i^n]$ represents the position of particle i ; P_i represents the best previous position of particle i (indicating the best discoveries or previous experience of particle i); P_g represents the best previous position among all particles (indicating the best discovery or previous experience of the social swarm); ω is the inertia weight that controls the impact of the previous velocity of the particle on its current velocity and is sometimes adaptive; R_1 and R_2 are two random weights whose components r_1^j and r_2^j ($j = 1, 2, \dots, n$) are chosen uniformly within the interval $[0, 1]$ which might not guarantee the convergence of the particle trajectory; c_1 and c_2 are positive constant parameters. Generally the value of each component in V_i should be clamped to the range $[-V_{max}, V_{max}]$ to control excessive roaming of particles outside the search space.

The difference between single-objective optimization and multi-objective optimization is that there are more than one objectives to be optimized for multi-objective optimization, that is, a multi-objective optimization problem can be described as:

$$\begin{aligned} \text{Find: } X^T &= [x_1, x_2, \dots, x_n], \\ \text{Minimize: } F(X) &= (f_1(X), \dots, f_m(X)), \\ \text{subject to: } X &\in \Omega. \end{aligned} \quad (3)$$

Here, R^m is the objective space, and $F : \Omega \rightarrow R^m$ consists of m real-valued objective functions. The analogy of PSO with evolutionary algorithms makes evident the notion that using a Pareto ranking scheme [6] could be the straightforward way to extend the approach to handle multiobjective optimization problems. The solution to the multi-objective optimization problem exists in the form of an alternate tradeoff known as a Pareto optimal set. Each objective component of any non-dominated solution in the Pareto optimal set can only be improved by degrading at least one of its other objective components. A vector F_a is said to dominate another vector F_b , denoted as

$$F_a < F_b, \text{ iff } f_{a,i} < f_{b,i} \forall i = \{1, 2, \dots, m\} \text{ and } \exists j \in \{1, 2, \dots, m\} \text{ where } f_{a,j} < f_{b,j} \quad (4)$$

For the more details about MMPSO, please refer to references [6] and [13].

3 Full Connected Multi-Objective Particle Swarm Optimization

As can be seen from equations (1) and (2), the position of a particle, the best experience among its neighbors and its own best experience are connected by fixed variables and random parameters. There exists a linear relationship between these elements. As every particle can be seen as the model of a single fish or a single bird, the position chosen by the particle can be regarded as a state of a neural network with a random synaptic connection. According to equations (1)–(2), the position components of particle i can be thought of as the output of a neural network as shown in Fig. 1(a) [10].

However, the relationship and influence only relies on the corresponding dimensional components of the particle swarm which is easily seen in Fig. 1(a). For example, the component $x_i^1(t+1)$ is only influenced by $x_i^1(t), v_i^1(t), p_i^1(t)$ and $p_g^1(t)$, but does not directly get information from the other components $x_i^2(t), x_i^3(t) \dots x_i^n(t), v_i^2(t), v_i^3(t), \dots v_i^n(t), p_i^2(t), p_i^3(t), \dots p_i^n(t)$ and $p_g^2(t), p_g^3(t), \dots p_g^n(t)$. To show the relationship among different components, neural networks can be used to model the characteristics of the gradient descent direction of the optimization problem. The inputs and outputs of the neural network are the positions of the particles and the gradient descent direction vector of the better experience of the particles, respectively. Here the back propagation neural network is used to learn the dynamics at different positions and the “Levenberg–Marquardt Method” [8] is chosen to train back propagation neural network.. The fully connected particle swarm structure based on multi-input multi-output BP neural network is therefore proposed which is shown in Fig. 1(b). In this structure, all the components of each particle are the inputs of the back propagation neural networks. The output of the back propagation neural network, $\nabla X_i = [\nabla x_i^1, \nabla x_i^2, \dots, \nabla x_i^n]$, reflects the gradient descent unit vector of the particle i . In order to take advantage of each component of the particle itself, the gradient descent unit vector $\nabla X_i(t)$ is added to equation (2). In our proposed fully connected particle swarm optimization, when the previous position was dominated by a position, a back propagation neural network is used to get the gradient descent unit vector at different position of the particle. The inputs of the training neural network are each component of the particle’s position, $X_i(t)$. The output of the training neural network is

$$\nabla x_i^j = \frac{X_i^j(t_1) - X_i^j(t_0)}{\|X_i(t_1) - X_i(t_0)\|}. \quad (5)$$

Here, $X_i^j(t_1)$ is the current position in problem space if the current position dominates the objective values related to $X_i(t_0)$ in objective space; $X_i(t_0)$ is updated with $X_i^j(t_0)$ when $X_i^j(t_1)$ is changed. For the improvement index $\Delta X_i^j(t)$, a random part is introduced to improve the search ability. Based on trial and error, the parameter α can be chosen in the range [0.01, 0.2], in this paper, 0.01 is used. When the particles get trapped into local minima, the random part helps the particles to escape from the local minima. The j^{th} component of particle i is described as

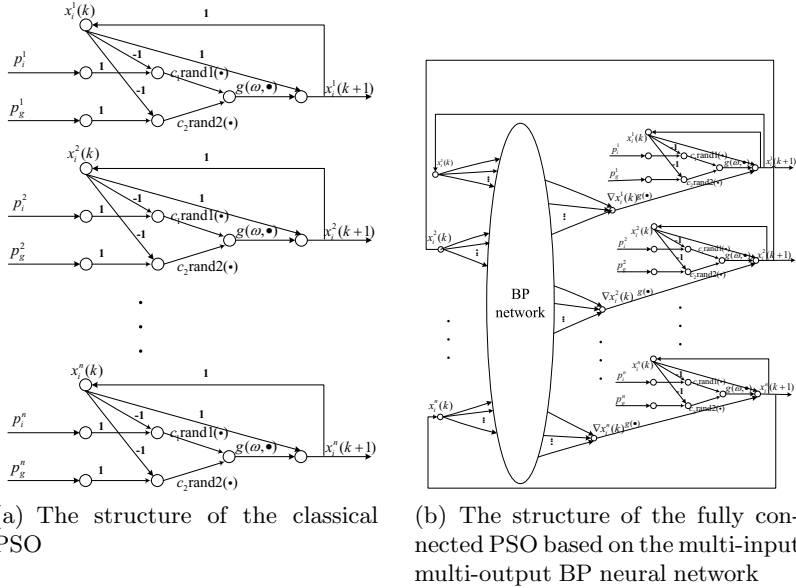
$$\Delta X_i^j(t) = g(\nabla x_i^j) = \frac{\alpha * \text{rand}(1) \nabla x_i^j}{\text{generations}}. \quad (6)$$

Equations (2) is therefore changed into the following equations:

$$X_i(t+1) = X_i(t) + V_i(t+1) + \Delta X_i(t), \quad (7)$$

The following procedure can be used for implementing the proposed particle swarm algorithm:

- 1) Initialize the BP neural network (the BP neural network can be trained using the existing data firstly), the swarm and assign a random position in

**Fig. 1.** Structures of Particle swarm optimization

the problem hyperspace to each particle and calculate the fitness function which is given by the optimization problem whose variables are corresponding to the elements of particle position coordinates.

- 2) Synchronously update the positions of all the particles according to equations (2), (8), and change the two states every iteration.
- 3) Evaluate the fitness function for each particle.
- 4) Find the non-dominated Pareto front and store it in the repository set. (The data from the first 50 iterations is used to train the neural network using 20 epochs before it is switched into the loop where it is trained online during each iteration using 5 epochs).
- 5) Repeat steps 2)–4) until a stopping criterion is met (e.g., maximum number of iterations).

4 Comparison between FCMOPSO and MOPSO

4.1 Test Problems

The test problems are Shaffer, Deb 2, ZDT1 and ZDT 4. For the Schaffer function [14] [13], the Pareto front is convex and connected. The Pareto front of Deb 2 [13] is disconnected and convex. The Pareto front of ZDT1 [14] [13] is convex. The Pareto front of ZDT4 [14] [13] is connected and non-convex. All of them are typical benchmark functions.

In this section, the performance of this proposed method is compared with multi-objective PSO [6]. In these examples, the total number of fitness function evaluations was set to 20 000. The particle number of particles is 100. A random initial population was created for each of the 20 runs on each test problem. The maximum number of external repository particles is 100.

Using the full connected multi-objective PSO and the multi-objective PSO in reference [6], the Pareto fronts are the 'o' symbols and the ' Δ ' symbols in Figs. 2(a)-2(d), respectively. From Figs. 2(a)-2(d), it can be seen that the proposed

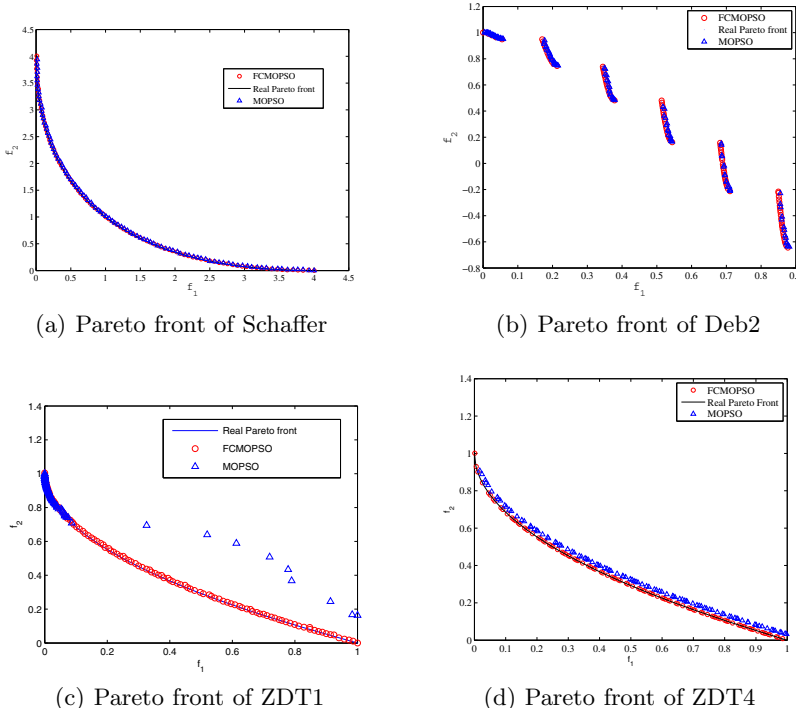


Fig. 2. Pareto fronts

method performs better than the algorithm in reference [6]. It would be better to use some performance metrics to find the comparison results other than just the figures as it is more convincing.

4.2 Performance Metrics

In order to provide a quantitative assessment for the performance of MO optimizer, two metrics are often taken into consideration, i.e., Generational Distance and Spacing metric [6] [13].

1)The metric of generational distance (GD) gives a good indication of the gap between the discovered Pareto front and the true Pareto front. The GD comparison of FCMOPSO and MOPSO [6] is shown in Table 1.

Table 1. GD comparison of FCMOPSO and MOPSO [6]

Problem	Method	Max	Mean	Min	std.dev
Schaffer	MOPSO	$2.194 * 10^{-4}$	$7.117 * 10^{-5}$	$3.244 * 10^{-5}$	$8.257 * 10^{-5}$
Schaffer	FCMOPSO	$2.210 * 10^{-5}$	$1.022 * 10^{-5}$	$2.792 * 10^{-6}$	$4.952 * 10^{-6}$
Deb2	MOPSO	$1.102 * 10^{-4}$	$9.817 * 10^{-5}$	$5.440 * 10^{-5}$	$9.510 * 10^{-6}$
Deb2	FCMOPSO	$9.412e-05$	$6.700 * 10^{-5}$	$4.170 * 10^{-5}$	$7.243 * 10^{-6}$
ZDT1	MOPSO	0.0048	0.0023	(Pareto front converges to a point)	
ZDT1	FCMOPSO	$1.927 * 10^{-4}$	$2.001 * 10^{-4}$	$2.054 * 10^{-4}$	$7.131 * 10^{-6}$
ZDT4	MOPSO	$2.177 * 10^{-4}$	$1.010 * 10^{-3}$	$2.177 * 10^{-4}$	$9.138 * 10^{-4}$
ZDT4	FCMOPSO	$3.127 * 10^{-4}$	$1.017 * 10^{-4}$	$4.950 * 10^{-5}$	$5.831 * 10^{-5}$

2)To measure the distribution of vectors throughout the non-dominated vectors found so far, the spacing metric is often used [6]. This metric can show how well the Pareto front found is if all the points are on or very close to the real Pareto front. At this situation, the smaller the spacing metric is, the better the particles are spread along the Pareto front. It would be better to use the spacing metric together with the Pareto front figure; otherwise it would be difficult to conclude the performance just according to the spacing metric. For example, all the Pareto front points converged to one point and the space metric is 0 in one simulation. The spacing metric comparison of FCMOPSO and MOPSO [6] is shown in Table 2.

Table 2. Spacing metric comparison of FCMOPSO and MOPSO [6]

Problem	Method	Max	Mean	Min	std.dev
Schaffer	MOPSO	0.0124	0.0071	0.0009	0.0044
Schaffer	FCMOPSO	$7.221 * 10^{-4}$	$3.267 * 10^{-4}$	$2.961 * 10^{-4}$	$1.249 * 10^{-4}$
Deb2	MOPSO	0.0175	0.0096	0.0044	0.0021
Deb2	FCMOPSO	0.0062	0.0045	0.0037	0.0016
ZDT1	MOPSO	0.0472	0.0230	(Pareto front converges to a point)	
ZDT1	FCMOPSO	0.0034	0.0033	0.0030	$3.1426 * 10^{-5}$
ZDT4	MOPSO	0.0349	0.0071	0.0068	0.0163
ZDT4	FCMOPSO	0.0141	0.0124	0.0112	0.0015

As can be seen from the statistic Tables 1 and 2, the proposed method can achieve better Pareto front than the classic MOPSO [6] for Schaffer, Deb2 and ZDT1 optimization problems. Although according to Table 2 the spacing metric of FCMOPSO is not better than the one of MOPSO, it can be shown that the obtained Pareto front is better than the one of MOPSO as shown in Fig. 2(d). The reason for the spacing metric of ZDT4 is that the Pareto front of MOPSO shrinks as it is away from the true Pareto front.

5 Conclusion

A fully connected multi-objective particle swarm optimization (FCMOPSO) model was proposed to improve the optimization performance of the MOPSO. For this new model, all components of each particle are directly participating in the evolutionary optimization process. The effect among different components of each particle was implemented via the back propagation (BP) neural network. Although the complexity is higher than the existing MOPSO algorithms, the performance of the proposed FCMOPSO is more stable and more accurate than the classic MOPSO.

References

1. Kennedy, J., Eberhart, R.: Particle Swarm Optimization. In: Proceeding of IEEE International Conference Neural Networks, Perth, Australia, pp. 1942–1948. IEEE Press, New York (1995)
2. van den Bergh, F., Engelbrecht, A.P.: Cooperative Learning in Neural Networks Using Particle Swarm Optimizers. *South African Computer Journal* 26, 84–90 (2000)
3. Shi, Y., Eberhart, R.: A Modified Particle Swarm Optimizer. In: IEEE International Conference on Evolutionary Computation, Piscataway, Alaska, USA, pp. 69–73. IEEE Press, New York (1998)
4. Kotinis, M.: A Particle Swarm Optimizer for Constrained Multi-objective Engineering Design Problems. *Engineering Optimization* (2010), doi:10.1080/0305052150903505877
5. Moore, J., Chapman, R.: Application of Particle Swarm to Multiobjective Optimization. Department of Computer Science and Software Engineering, Auburn University (1999)
6. Coello, C.A., Pulido, G.T., Lechuga, M.S.: Handling Multiple Objectives With Particle Swarm Optimization. *IEEE Trans. on Evolu. Comp.* 8, 256–279 (2004)
7. Fletcher, R., Powell, M.J.D.: A Rapidly Convergent Descent Method for Minimization. *Computer Journal* 6, 163–168 (1963)
8. More, J.J.: The Levenberg-Marquardt Algorithm: Implementation and Theory. In: Watson, G.A. (ed.) *Numerical Analysis*. Lecture Notes in Mathematics, pp. 105–116. Springer, Heidelberg (1977)
9. Hertz, J., Krogh, A., Palmer, R.G.: *Introduction to the Theory of Neural Computation*. Addison-Wesley, Reading (1991)
10. Sun, Y., Djouani, K., Qi, G., van Wyk, B.J., Wang, Z.: Fully Connected Particle Swarm Optimizer. *Engineering Optimization* 43, 801–812 (2011)
11. Liu, J., Qiu, X.: A Novel Hybrid PSO-BP Algorithm for Neural Network Training. In: Proceedings of the Second International Joint Conference on Computational Sciences and Optimization, pp. 300–303. IEEE Press, New York (2009)
12. Hu, J., Zeng, X.: A Hybrid PSO-BP Algorithm and Its Application. In: 2010 Sixth International Conference on Natural Computation, pp. 2520–2523. IEEE Press, New York (2010)
13. Coello Coello, C.A., Lamont, B.B., Van Veldhuizen, D.A.: *Evolutionary Algorithms for Solving Multi-Objective Problems*, 2nd edn. Springer, New York (2007)
14. Deb, K., Pratap, A., Agarwal, S., Meyarivan, T.: A Fast and Elitist Multiobjective Genetic Algorithm: NSGA-II. *IEEE Trans. on Evolu. Comp.* 6, 182–197 (2002)

Immune Gravitation Inspired Optimization Algorithm

Yu Zhang, Lihua Wu, Ying Zhang, and Jianxin Wang

College of Information Science and Technology, Hainan Normal University,
571158 Haikou, China
bullzhangyu@yahoo.com.cn

Abstract. The traditional Gravitational Search Algorithm (GSA) has the advantages of easy implementation, fast convergence and low computational cost. However, GSA driven by the gravity law is easy to fall into local optimum solution. The convergence speed slows down in the later search stage, and the solution precision is not good. Inspired by the biological immune system, we introduce the characteristics of antibody diversity and vaccination, and propose a novel immune gravitation optimization algorithm (IGOA) to help speed the convergence of evolutionary algorithms and improve the optimization capability. The comparison experiments of IGOA, GSA and PSO on some benchmark functions are carried out. The proposed algorithm shows competitive results with improved diversity and convergence. It provides new opportunities for solving previously intractable function optimization problems.

Keywords: Gravitational search algorithm, Optimization, Artificial immune system, Antibody diversity.

1 Introduction

Gravitational Search Algorithm (GSA) firstly proposed by Rashedi et al. [1-4] in 2009 is a new intelligent heuristic optimization algorithm, which is based on the metaphor of gravitational interaction between masses. GSA is inspired by the Newton's law of universal gravitation that states that every point mass in the universe attracts every other point mass with a force that is directly proportional to the product of their masses and inversely proportional to the square of the distance between them.

Like Particle Swarm Optimization (PSO) [5,6], GSA is an agent-based iterative optimization algorithm. In GSA, agents are considered as objects and their performance is measured by their masses. All these objects attract each other by a gravity force, and this force causes a movement of all objects globally towards the objects with heavier masses. The heavy masses correspond to good solutions of the problem. Specifically speaking, each mass (agent) in GSA has four specifications: its position, its inertial mass, its active gravitational mass, and its passive gravitational mass. The position of the mass corresponds to a solution of the problem, and its gravitational and inertial masses are determined using a fitness function. With time goes by, masses navigated by properly adjusting the gravitational and inertia masses are attracted by the heaviest mass that presents an optimum solution in the search space.

However, GSA driven by the gravity law is easy to fall into local optimum solution. The convergence speed slows down in the later search stage, and the solution precision is not good [7]. Therefore, to improve GSA performance, we should introduce other operators that can raise agent population diversity and solution accuracy.

Biological immune system (BIS) plays an important role in the defense of foreign invasion with a variety of antibodies, and thus keeps body healthy. BIS can quickly search for the best matching antibody when invaded by a known antigen. But when an unknown antigen enters the body, BIS can also generate the optimum antibody through the dynamic adaptive learning. This shows that BIS has internal mechanisms of immune memory and antibody diversity. Inspired by the immune mechanisms, we proposed an Immune Gravitation inspired Optimization Algorithm (IGOA) based on GSA. In IGOA, we use vaccination and memory antibody replacement to improve the convergence speed, and use antibody diversity mechanism to raise the diversity of agents. As a result, IGOA can avoid falling into local optimum solution and premature degradation, and therefore improves the global search capability and solution accuracy.

In the remaining sections of the paper, we first provide a brief review of GSA in Section 2. In Section 3, we introduce our IGOA in detail. Experiment and results are discussed in Section 4. Finally, a conclusion is stated in Section 5.

2 Gravity Search Algorithm

2.1 Newtonian Laws of Gravitation and Motion

Gravity Search Algorithm (GSA) could be considered as a closed system composed of a variety of masses obeying the Newtonian laws of gravitation and motion.

The Law of Gravity states that every particle of matter in the universe attracts every other particle with a force that is directly proportional to the product of the masses of the particles and inversely proportional to the square of the distance between them. Mathematically, this law can be translated into the equation shown below:

$$F = G \frac{M_1 M_2}{R^2} \quad (1)$$

Where F = the force of gravity, G = the gravitational constant, which adds the proper level of proportionality to the equation, M_1 & M_2 = the masses of the two particles, R = the straight-line distance between the two particles.

The law of Motion declares that the acceleration of an object produced by a total applied force is directly related to the magnitude of the force, the same direction as the force, and inversely related to the mass of the object. Mathematically, this law can be presented as following equation:

$$\Sigma F = Ma \quad (2)$$

The equations of motion are:

$$V = V_0 + at \quad (3)$$

$$S = V_0 t + \frac{1}{2} a t^2 \quad (4)$$

From equation (1), equation (2) and equation (3), we get

$$S = V_0 t + \frac{1}{2} \frac{GM_2}{R^2} t^2 \quad (5)$$

2.2 The Principle of GSA

In GSA, the isolated system with N agents (masses), the position of the i -th agent is defined by:

$$X_i = (x_i^1, \dots, x_i^d, \dots, x_i^n), i = 1, 2, \dots, N \quad (6)$$

where x_i^d presents the position of i -th agent in the d -th dimension and n is the space dimension.

At a specific time t , the force acting on mass i from mass j is defined as following:

$$F_{ij}^d = G(t) \frac{M_i(t) \times M_j(t)}{R_{ij}(t) + \epsilon} (x_j^d(t) - x_i^d(t)) \quad (7)$$

where M_j is the active gravitational mass related to agent j , M_i is the passive gravitational mass related to agent i , $G(t)$ is gravitational constant at time t , ϵ is a small constant, and $R_{ij}(t)$ is the Euclidian distance between two agents i and j .

The total force that acts on agent i in a dimension d is a randomly weighted sum of d -th component of the forces exerted from K agents:

$$F_i^d(t) = \sum_{j=1, j \neq i}^K rand_j F_j^d(t) \quad (8)$$

where $rand_j$ is a random number in the interval $[0, 1]$ and K is the set of first K agents with the best fitness value and biggest mass. K is a function of time, initialized to K_0 at the beginning and decreasing with time.

From the law of motion, the acceleration of the agent i at time t , and in direction d , $a_i^d(t)$, is given as follows:

$$a_i^d(t) = \frac{F_i^d(t)}{M_i(t)} \quad (9)$$

where $M_i(t)$ is the inertial mass of i -th agent.

The next velocity and position of an agent could be calculated as follows:

$$v_i^d(t+1) = rand_i \times v_i^d(t) + a_i^d(t) \quad (10)$$

$$x_i^d(t+1) = x_i^d(t) + v_i^d(t+1) \quad (11)$$

where $rand_i$ is an uniform random variable in the interval $[0, 1]$. This random number gives a randomized characteristic to the search.

The values of masses are calculated using the map of fitness. The gravitational and inertial masses are updated by the following equations:

$$m_i(t) = \frac{fit_i(t) - worst(t)}{best(t) - worst(t)} \quad (12)$$

$$M_i(t) = \frac{m_i(t)}{\sum_{j=1}^N m_j(t)} \quad (13)$$

where $fit_i(t)$ represent the fitness value of the agent i at time t , and, $worst(t)$ and $best(t)$ are defined as follows (for a minimization problem):

$$worst(t) = \max_{j \in N} fit_j(t) \quad (14)$$

$$best(t) = \min_{j \in N} fit_j(t) \quad (15)$$

The flow chart of GSA is shown in Figure 1.

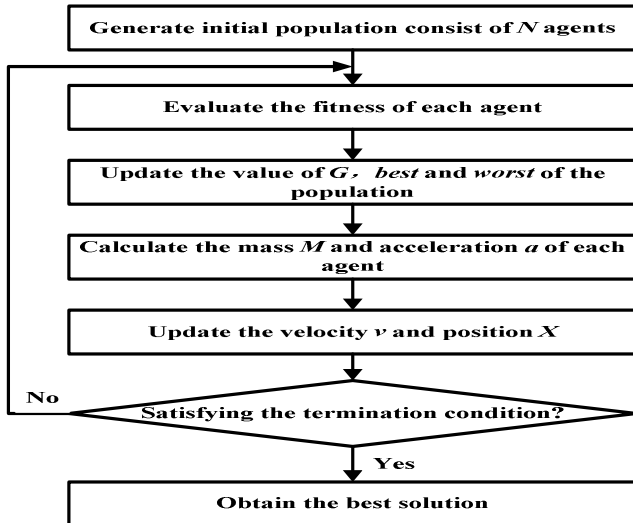


Fig. 1. The general flow chart of GSA

3 Immune Gravitation Inspired Optimization Algorithm (IGOA)

3.1 The Mechanism of Biological Immune System

Biological immune system is a system of biological structures and processes within an organism that protects against disease by identifying and killing pathogens and

tumor cells. It detects a wide variety of agents, from viruses to parasitic worms, and needs to distinguish them from the organism's own healthy cells and tissues in order to function properly.

The different aspects of immunity have been divided into two groups [8]:

①Innate immunity - is present from before birth, consisting of many non-specific factors and blood based immunity from the mother. They operate against almost any substance that threatens the body. Factors include physical barriers, some white blood cells and chemical barriers in the body.

②Acquired immunity - a more specialized form of immunity only found in the vertebrates. It is a result of an encounter with a new substance, which triggers events that induce an immune response specific against that particular substance. This involves B lymphocytes, T lymphocytes and macrophages, highlighting the importance of lymphatic tissue, the site of lymphocyte maturation and differentiation. Key characteristics of such acquired immune mechanism include:

- Recognition of Foreignness: The immune system must be able to recognize bacteria, viruses, fungi, parasites, and foreign materials in order to locate and destroy them.

- Specificity: Immunity to one foreign organism or substance does not necessarily provide resistance to different ones, even if the two are highly similar.

- Memory: The ability to develop an accelerated, enhanced, and long-lasting immune response after the initial attack by an infectious disease, or initial development of cancerous tissue.

3.2 Immune Gravitation Inspired Optimization Algorithm (IGOA)

In the design of artificial immune system, people generally consider an antibody as a candidate solution for the problem, antigen as the problem to be solved. The affinity between antibodies and antigens is calculated to evaluate the level how the antibody closes to the optimal solution to the problem. Some of prior knowledge and the characteristics of the problem be solved can be considered as vaccine [9,10]. Therefore, a novel Immune Gravitation inspired Optimization Algorithm (IGOA) that includes the mechanisms of antibodies diversity and immunity memory based on the GSA is proposed in this paper. The main idea of the proposed IGOA is that the characteristic of antibody diversity is to improve the solution space, and the characteristic of immunity memory is to enhance the solution quality. By taking these immune characteristics, IGOA will help to speed the convergence of evolutionary algorithms and improve the optimization capability.

The general flow chart of IGOA is as follows.

Step 1: Initialize parameters, including the gravitational constant G_0 , α , masses number N , and the maximum number of $Max_iteration$.

Step 2: Randomly generate the initial population A_k consisting of N masses with an initial velocity $V_0 = 0$.

Step 3: Extract the information to the problem be solved as vaccine V_a .

Step 4: Calculate the fitness of each mass in the current population A_k , and save the mass that has the best fitness as an immune memory mass M_i . Thereafter, determine whether the end conditions are met; if the termination conditions are met, the algorithm stops and returns the result, otherwise, continue.

Step 5: Vaccinate the mass in the initial population A_k with a certain probability to form new mass population B_k .

Step 6: Substitute a part of masses with poor fitness in the population B_k for an immune memory mass, thus to generate new mass population C_k .

Step 7: Select part of masses in the population C_k based on mass concentration and randomly generate an additional part of masses to form the next generation A_{k+1} .

Step 8: Update the gravitational constant G , *best*, *worst*, and M_i , $i = 1, 2, \dots, N$.

Step 9: Calculate the suffered gravity for each mass.

Step 10: Calculate the acceleration and velocity for each mass.

Step 11: Update the location of each mass in the population A_{k+1} .

Step 12: Go to *Step 4*.

4 Experiments and Results

To objectively evaluate the performance of the proposed algorithm IGOA, comparison experiments with the traditional gravity algorithm GSA and particle swarm optimization PSO are carried out, and the parameters of the three algorithms are the same as much as possible. Numerical function optimization problems are selected as benchmark problems to test the performance of the three algorithms.

4.1 Benchmark Functions

The benchmark functions used in our experiments are listed in Table 1 from literature [2,11,12,13]. In these tables, n is the dimension of function. The minimum value of the functions in Table 1 is zero.

Table 1. Benchmark functions

Benchmark function	Optimum value
$F_1(X) = \sum_{i=1}^n x_i^2, x \in [-100, 100]^n$	0
$F_2(X) = \sum_{i=1}^n x_i + \prod_{i=1}^n x_i , x \in [-10, 10]^n$	0
$F_3(X) = \sum_{i=1}^n \left(\sum_{j=1}^n x_j \right)^2, x \in [-100, 100]^n$	0
$F_4(X) = \max\{ x_i , 1 \leq i \leq n\}, x \in [-100, 100]^n$	0
$F_5(X) = \sum_{i=1}^{n-1} [100(x_{i+1} - x_i^2)^2 + (x_i - 1)^2], x \in [-30, 30]^n$	0
$F_6(X) = \sum_{i=1}^n [x_i^2 - 10\cos(2\pi x_i) + 10], x \in [-5.12, 5.12]^n$	0
$F_7(X) = \frac{1}{4000} \sum_{i=1}^n x_i^2 + \prod_{i=1}^n \cos(\frac{x_i}{\sqrt{i}}) + 1, x \in [-600, 600]^n$	0

4.2 Experimental Results

We compare IGOA with GSA as well as PSO on the benchmark functions above. In the cases, population size $N=50$, dimension size $n=30$, and iteration number is 1000.

The results for benchmark functions in Table 1 are listed in Table 2.

The better performance of IGOA benefits from the following features: (1) elitist antibody gene segments are retained, and inherited to offspring through vaccination, which will enhance local search capability and improve the convergence speed; (2) antibody population diversity is achieved by mutation that avoid the degenerative phenomenon and to enhance the global optimization capability.

In summary, from the test results of seven benchmark function problems, the performance of IGOA is superior to that of PSO and GSA.

Table 2. Experiment result of benchmark functions

		PSO	GSA	IGOA
F_1	Average best	1.8×10^{-3}	7.3×10^{-11}	2.6×10^{-12}
	Median best	1.2×10^{-3}	7.1×10^{-11}	2.2×10^{-12}
	Average mean fitness	5.0×10^{-3}	2.1×10^{-10}	7.6×10^{-11}
F_2	Average best	2.0	4.03×10^{-5}	2.13×10^{-5}
	Median best	1.9×10^{-3}	4.07×10^{-5}	2.47×10^{-5}
	Average mean fitness	2.0	6.9×10^{-5}	4.5×10^{-5}
F_3	Average best	$4.1 \times 10^{+3}$	$0.16 \times 10^{+3}$	$0.09 \times 10^{+3}$
	Median best	$2.2 \times 10^{+3}$	$0.15 \times 10^{+3}$	$0.11 \times 10^{+3}$
	Average mean fitness	$2.9 \times 10^{+3}$	$0.16 \times 10^{+3}$	$0.10 \times 10^{+3}$
F_4	Average best	8.1	3.7×10^{-6}	2.3×10^{-6}
	Median best	7.4	3.7×10^{-6}	2.7×10^{-6}
	Average mean fitness	23.6	8.5×10^{-6}	4.2×10^{-6}
F_5	Average best	$3.6 \times 10^{+4}$	25.16	19.87
	Median best	$1.7 \times 10^{+3}$	25.18	19.95
	Average mean fitness	$3.7 \times 10^{+4}$	25.16	19.89
F_6	Average best	55.1	15.32	12.75
	Median best	55.6	14.42	13.36
	Average mean fitness	72.8	15.32	13.29
F_7	Average best	0.01	0.29	0.01
	Median best	0.0081	0.04	0.002
	Average mean fitness	0.055	0.29	0.05

5 Conclusion

We propose a novel immune gravitation inspired optimization algorithm, IGOA. The proposed algorithm, which is based on the gravitational search algorithm (GSA), includes the mechanisms of antibodies diversity and immunity memory. The mechanism of antibodies diversity is to enhance the population diversity, and the mechanism of immunity memory is to save some optimum value of current

population. With these features, the proposed IGOA can help speed the convergence of evolutionary algorithms and improve the optimization capability. The comparison experiments of IGOA, GSA and PSO on some benchmark functions are carried out. The proposed algorithm shows competitive results with improved diversity and convergence. It provides new opportunities for solving previously intractable function optimization problems.

Acknowledgement. This work was supported by Hainan Natural Science Foundation (610220), Project of Zhejiang Key Laboratory of Information Security (2010ZISKL007), the Science and Technology Project of Hainan Normal University (00203020214) and the Key Project of Science and Technology of Haikou(2010071).

References

1. Rashedi, E.: Gravitational Search Algorithm. MS Thesis, Shahid Bahonar University of Kerman, Iran (2007)
2. Rashedi, E., Nezamabadi-pour, H., Saryazdi, S.: GSA: A Gravitational Search Algorithm. *Information Sciences* 179(13), 2232–2248 (2009)
3. Rashedi, E., Nezamabadi-pour, H., Saryazdi, S.: BGSA: binary gravitational search algorithm. *Natural Computing* (December 2009), <http://dx.doi.org/10.1007/s11047-009-9175-3>
4. Rashedi, E., Nezamabadi-pour, H., Saryazdi, S., et al.: Allocation of Static Var Compensator Using Gravitational Search Algorihm. First Joint Congress on Fuzzy and Intelligent Systems Ferdowsi University of Mashhad, Iran (2007)
5. Zhan, Z.H., Zhang, J., Li, Y., et al.: Adaptive Particle Swarm Optimization. *IEEE Transactions on Systems, Man, and Cybernetics, Part B: Cybernetics* 39(6), 1362–1381 (2009)
6. Chen, D.B., Zhao, C.X.: Particle swarm optimization with adaptive population size and its application. *Applied Soft Computing* 9(1), 39–48 (2009)
7. Gu, W.X., Li, X.T., Zhu, L., et al.: A gravitational search algorithm for flow shop scheduling. *CAAI Transaction on Intelligent Systems* 5(5), 411–418 (2010)
8. Hoffman, D.: A Brief Overview of the Biological Immune system (2011), <http://www.healthy.net/>
9. Dasgupta, D.: Advances in Artificial Immune Systems. *IEEE Computational Intelligence Magazine*, 40–49 (2006)
10. Forrest, S., Beauchemin, C.: Computer immunology. *Immunological Reviews* 216(1), 176–197 (2007)
11. Zhang, Y., Chen, X.M., Wu, L.H., et al.: MHC-inspired Antibody Clone Algorithm. *International Journal of Computational Methods* 7(2), 299–318 (2010)
12. Yao, X., Liu, Y., Lin, G.M.: Evolutionary Programming Made Faster. *IEEE Transactions on Evolutionary Computation* 3(2), 82–102 (1999)
13. Woldesenbet, Y.G., Yen, G.G.: Dynamic Evolutionary Algorithm with Variable Relocation. *IEEE Transactions on Evolutionary Computation* 13(3), 500–513 (2009)

A Novel Multi Objective Genetic Algorithm for the Portfolio Optimization

Vitoantonio Bevilacqua^{1,3,*}, Vincenzo Pacelli², and Stefano Saladino¹

¹ Dipartimento di Elettrotecnica ed Elettronica
Politecnico di Bari - Via Orabona, 4, Bari, 70125, Italy

² University of Foggia - Faculty of Economics
Via Caggese, 1 - 71100 - Foggia - Italy

³ e.B.I.S. s.r.l. (electronic Business in Security), Spin-Off of Polytechnic of Bari
Via Pavoncelli, 139 Bari – Italy
bevilacqua@poliba.it

Abstract. In this paper we propose a new implementation of a multi objective genetic algorithm that handles constrained problems to approach the financial problem of the portfolio optimization. The objective of the paper is to propose and empirically apply a new multi-objective genetic algorithm for portfolio optimization extending the Markowitz mean-variance model ([1,2] Markowitz, 1952 and 1959). At the end of the paper the obtained results are discussed and compared with non linear other different techniques.

Keywords: Multi-objective genetic algorithms, Pareto curves trade-off, constraints problems, portfolio optimization.

1 Introduction

The problem of portfolio selection is generally solved by the academicians and practitioners using linear and quadratic programming methods ([3] Lintner, 1965; [4,5] Michaud, 1989 and 1998; [6,7] Scherer, 2002 and 2004; [8] Satchell and Scowcroft, 2003; [9] Pomante, 2008). The efficiency of these methods has a limit, though, since considerable constraints are put on the problem formulation, that are the functional form of the optimisation criterion and the constraints. The analyst often has to shape the problem in a way that it can be solved by such methods. Thus, the answer that the linear model provides is a precise one, but often only to an approximate question ([10] Gilli and Schumann, 2009).

An alternative approach, less developed in the literature, that will be described in this paper is to use heuristic optimisation techniques like simulated annealing or genetic algorithms. Heuristic methods are a relatively new development in portfolio optimization theory as they have become practically relevant only in recent decades with the enormous growth in computing power. These methods have been shown to be capable to handle portfolio optimisation problems with all kinds of constraints and using alternative measures of risk ([11] Arnone, Loraschi and Tettamanzi, 1993; [12]

* Corresponding author.

Liu and Stefk, 1995; [13] Loraschi, Tettamanzi, Tomassini, Verda, 1995; [14] Rolland, 1997; [15] Ehrgott, Klamroth, Schewe, 2002; [16] Crama and Schyns, 2003; [17] Fernandez and Gomez, 2005; [18] Maringer, 2005; [19] Yu, Wang and Lai, 2006; [10] Gilli and Schumann, 2009).

In this framework the research aims to enrich the literature about the methodological tools for portfolio optimization through the development and empirical application of an innovative genetic algorithm.

2 The Problem Reformulation of the Portfolio Optimization

In the portfolio theory, an investor has to decide how to allocate his limited financial resources among a number of different assets and so he wants to know ex ante the optimal portfolio. In this situation, the investor has to face two problems: (*i*) he must evaluate and select different assets and then (*ii*) he must decide how to allocate his limited resources among the assets previously selected. In this paper, not treating the first problem, we try to solve the second one. Choosing an optimal portfolio weighting of assets when their future rate of return is uncertain may be seen as a problem of minimizing the uncertainty for a desirable level of the portfolio expected return. Modern Portfolio Theory calls this uncertainty risk and measures it as the standard deviation or the variance of the probability distribution of future returns. So choosing an optimal portfolio became a question of standard deviation minimization for a desirable level of expected return, because every investor wants to minimize risk and maximize the expected return. Markowitz (1959) [2] showed that as the level of risk increases, the expected return of optimal portfolios draws a convex non-decreasing curve called "efficient frontier", which represents the set of Pareto optimal portfolios and so the set of non-dominated portfolios. That is, the efficient frontier is characterized by the fact that higher expected returns correspond to greater risk.

The optimal portfolio selection problem lies in the selection of a combination of percentage weights to be attributed to the different assets selected and included in the portfolio, in order to obtain the optimal weight vector [$W=(w_1, w_2, w_3, w_i, \dots, w_n)$], such as to minimize a certain level of risk for a given level of expected return or vice versa. This can be expressed as a constraint multi objective optimization problem :

$$\max R_p = \sum_{i=1}^N x_i u_i \quad (2.1)$$

$$\min \sigma_p^2 = \sum_{i=1}^N x_i^2 u_i + 2 \sum_{i=1}^n \sum_{j=1}^n x_i x_j \rho_{ij} \sigma_i \sigma_j \quad \text{con}(i \neq j) \quad (2.2)$$

subject to:

$$\begin{aligned} \sum_{i=1}^N x_i &= 1 \\ x_i &\geq 0 \quad i = 1, 2, \dots, N \end{aligned}$$

where:

N denotes the number of the assets of the portfolio (securities, bonds, etc.);

x_i represents the percentage share of investment in the asset with $i \in \{1, 2, \dots, N\}$;

u_i denotes the expected return of the asset with $i \in \{1, 2, \dots, N\}$;

σ^2 denotes the variance of the asset $i \in \{1, 2, \dots, N\}$;

ρ_{ij} represents the correlation coefficient among the returns of assets $i \in \{1, 2, \dots, N\}$.

The first equation (2.2) states that all available wealth is allocated in the portfolio, so the sum of the different ratios of investments in the portfolio must necessarily be equal to 1, while the second first equation (2.2) ensures that the weights of the assets in the portfolio are not negative, in other words this constraint excludes the possibility of short selling.

The two-objective optimization problem can be parameterized to yield a convex combination parametric programming problem with objective:

$$\min \quad \lambda \sum_{i=1}^N \sum_{j=1}^N x_i x_j \sigma_{ij} - (1-\lambda) \sum_{i=1}^N x_i u_i \quad (i \neq j) \quad (2.3)$$

subject to:

$$\begin{aligned} \sum_{i=1}^N x_i &= 1 \\ x_i &\geq 0 \quad i = 1, 2, \dots, N \end{aligned} \quad (2.4)$$

where the parameter λ is the trade-off coefficient between risk and return ranging between 0 and 1:

- when $\lambda = 0$: the investor disregards risk and only seeks to maximize expected return;
- when $\lambda = 1$, the investor is extremely risk averse, therefore the risk alone is being minimized, whatever the expected return.

This new formulation of the problem is justified by the fact that, by introducing the trade-off coefficient (λ), there is not a general criterion to determine which trade-off between risk and return is considered the best, so solving the portfolio selection problem means finding a whole range of optimal portfolios for all the possible values of the trade-off coefficient (λ). The investor will thus be able to choose the most appropriate portfolio based on his or her requirements.

3 The New Constraints Like Multi-objective Approach (MOGACOP)

The multi-objective approach adopted in this paper is a new version of a previous algorithm [21] implemented and discussed in detail in [22]. In particular the potentialities of a Multi-Objective Genetic Algorithms (MOGAs) that are a relatively recent extension of Genetic Algorithms (GAs) reveal to be a good methods to search for trade-off solutions in several applications that spanning from finance to medicine [22]. In fact in nature stressed by selection only strong individuals have greater opportunity to pass their genes to future generations via reproduction by means a

particularly techniques coded in their chromosomes. Chromosomes are made of discrete units called genes where each gene controls one or more features of the problem to be solved. Being a population-based approach, GAs are well suited to solve multi-objective Optimization problems. GAs have been the most popular heuristic approach to multi-objective design and optimization problems and in literature it is reported that 90% of the approaches to multi objective optimization aimed to approximate the true Pareto front for the underlying problem. In previous works Bevilacqua et al presented a novel Pareto-Based multi-objective genetic algorithm (MOGA) for finding optimized trade-off solutions and addressed the problem of the design of an optimized topology of a feed-forward neural network that showed good results in terms of generalizations to support expert decision about malignant cells for breast cancer [21] and intelligent forecasting of exchange rate [23].

The algorithm used in this work is instead a novel MOGA algorithm that implements a checking of constraints verification to manage the possibility of searching for Pareto-Based solutions taking into account several domain constraints. Specifically, for each individual generated, the new procedure checks the satisfaction of the constraints and then only if satisfied the individual is placed in the Archive/Laboratory population otherwise it is discarded. Since the new proposed genetic algorithm adopts a Pareto- based approach strategy presented in [21] dividing individuals into three populations, and at the same time implements a specific constraints strategy to preserve the feasibility of the candidate solutions the authors in [22] refer to it namely as MOGACOP. The main strategy is based on the separation of three different populations and allows to operate at the same time, a local search on the best individuals, and a general search in the space of individuals who have relatively good behaviour, giving them more likely to reproduce using an approximation of roulette-wheel selection. This algorithm allows the seeding, so you can enter a number in the initial population of individuals that should speed up the evolutionary process. The three populations are:

1. an Archive population of variable size, which contains individuals closed to Pareto curve;
2. a Frontier population, which contains individuals that form the Pareto curve;
3. a Laboratory population, composed of individuals selected at each iteration from the previous two populations.

4 Description of the Data and the Empirical Results

In order to train and test the genetic algorithm developed, an empirical study was conducted for optimizing a portfolio of 54 assets belonging to different asset classes such as securities, financial indexes, commodities, currency and bonds. The statistical inputs needed to develop the Markowitz optimization will be estimated in a day, weekly and monthly holding period using a dataset of more than 150.000 daily prices surveys of the assets from January 1999 to December 2009.

Through the empirical application of the genetic algorithm developed to solve the optimization problem of a portfolio of 54 assets, it is obtained the optimal portfolios among the more efficient portfolios produced by the genetic algorithm for each holding period considered (table 1 and 2), that is the optimal weight vectors [$W=(w_1, w_2, w_3, w_i, \dots, w_{54})$] with the percentage of wealth to invest in each asset (table n. 1).

The table 1 represents the optimal weight vectors of the portfolios with minimum variance and maximum return in a day, weekly and monthly holding period, while table 2 represents the expected risk or variance and return of these optimal portfolios estimated using the classical method based on the historical data.

Table 1. The optimal weight vectors

ASSETS	MIN DAILY VARIANCE PORTFOLIO	MAX DAILY RETURN PORTFOLIO	MIN WEEKLY VARIANCE PORTFOLIO	MAX WEEKLY RETURN PORTFOLIO	MIN MONTHLY VARIANCE PORTFOLIO	MAX MONTHLY RETURN PORTFOLIO
Aegon	0,049%	2,150%	2,030%	0,055%	0,235%	1,060%
Air Liquid	2,230%	0,923%	3,190%	0,649%	4,710%	3,750%
Allianz	1,450%	0,266%	0,749%	0,040%	1,620%	2,420%
Alstom	1,290%	0,048%	0,460%	4,550%	0,243%	2,540%
Generali	2,750%	1,090%	1,850%	0,118%	0,869%	0,366%
Axa	2,010%	0,934%	1,500%	2,680%	0,062%	0,239%
Basf	2,100%	2,590%	2,150%	2,530%	4,570%	2,790%
Bayer	1,780%	3,490%	0,391%	1,780%	0,025%	4,270%
Banco Bilbao	4,730%	0,049%	2,260%	4,140%	1,260%	1,840%
Bnp Paribas	1,160%	3,250%	2,430%	0,570%	0,917%	4,420%
Carrefour	0,208%	0,967%	0,914%	0,969%	0,972%	1,180%
Crh	3,460%	0,104%	2,710%	4,280%	1,050%	1,080%
Daimler	0,290%	3,430%	1,300%	2,050%	1,410%	0,129%
Danone	0,595%	1,710%	2,040%	1,990%	2,980%	3,580%
Deutsche bank	1,750%	1,120%	3,090%	0,044%	1,000%	0,982%
Dt Telecom	1,390%	0,517%	2,370%	1,280%	2,930%	1,770%
E.On	1,390%	3,150%	2,330%	4,380%	3,130%	1,930%
Eni	4,130%	0,375%	3,750%	0,899%	2,490%	0,143%
Fr Telecom	0,824%	0,467%	0,837%	1,860%	2,370%	1,800%
Iberdrola	0,669%	3,770%	0,819%	2,590%	0,197%	1,610%
Ing Group	0,688%	1,040%	0,221%	0,303%	0,508%	0,009%
Intesa-San Paolo	1,240%	0,284%	1,740%	2,040%	2,270%	4,000%
L'oreal	4,810%	0,534%	2,690%	3,080%	0,385%	0,691%
Lvmh Moet	1,000%	0,634%	2,640%	0,344%	2,090%	4,220%

Table 1. (*continued*)

<i>Muenchener</i>	0,340%	0,005%	1,930%	0,223%	1,540%	2,440%
<i>Nokia</i>	0,278%	1,230%	0,876%	0,223%	0,777%	1,670%
<i>Philips</i>	1,860%	4,440%	1,050%	2,720%	0,996%	0,477%
<i>Repsol</i>	1,220%	0,370%	1,560%	3,950%	3,910%	2,340%
<i>Rwe</i>	4,490%	2,030%	1,920%	3,690%	1,420%	0,570%
<i>Saint Gobain</i>	0,925%	2,720%	1,210%	2,510%	1,950%	2,330%
<i>Sanofi-Aventis</i>	2,530%	1,740%	1,930%	0,283%	3,530%	1,680%
<i>Santander</i>	0,694%	0,030%	1,330%	3,170%	1,020%	2,100%
<i>Sap</i>	3,760%	1,120%	0,385%	2,110%	3,300%	1,780%
<i>Schneider</i>	0,850%	1,810%	4,610%	3,060%	2,920%	0,429%
<i>Siemens</i>	1,700%	4,510%	1,900%	1,490%	2,130%	3,340%
<i>Societe Generale</i>	1,330%	0,827%	4,100%	0,038%	2,620%	2,960%
<i>Telecom IT</i>	4,930%	0,094%	0,965%	0,123%	0,438%	0,561%
<i>Telefonica</i>	0,830%	0,547%	1,310%	1,820%	0,377%	0,604%
<i>Total</i>	0,300%	2,400%	1,210%	0,343%	0,255%	0,209%
<i>Unibail-Rodamco</i>	4,720%	4,300%	2,310%	2,240%	0,687%	0,783%
<i>Unicredit Group</i>	0,936%	3,760%	1,650%	1,300%	0,062%	0,123%
<i>Unilever</i>	0,261%	1,170%	2,250%	4,820%	2,260%	2,180%
<i>Vinci</i>	2,390%	4,810%	1,000%	3,220%	0,175%	9,080%
<i>Vivendi</i>	4,810%	2,850%	0,665%	1,340%	1,040%	1,260%
<i>Nasdaq Index</i>	0,403%	3,160%	0,846%	1,190%	1,610%	1,500%
<i>Dax Index</i>	0,821%	3,690%	4,980%	0,437%	0,150%	0,237%
<i>Dow Jones Index</i>	2,080%	3,000%	0,738%	0,790%	0,724%	0,675%
<i>S&P 500 Index</i>	1,690%	3,350%	1,120%	2,670%	4,360%	3,950%
<i>GBP</i>	3,440%	4,510%	1,660%	0,932%	2,670%	2,550%
<i>YEN</i>	2,970%	0,734%	0,985%	3,220%	2,190%	2,040%
<i>GOLD</i>	0,952%	2,430%	2,780%	2,320%	0,836%	1,090%
<i>Us Bonds 5 years</i>	0,497%	4,450%	0,436%	2,210%	0,229%	0,198%
<i>EU Bonds 5 years</i>	1,330%	0,750%	3,900%	1,090%	1,620%	1,550%
<i>USA Dollar</i>	4,660%	0,286%	3,900%	3,240%	15,900%	2,480%

Table 2. Risk and return of the optimal portfolios

	EXPECTED RISK	EXPECTED RETURN
<i>MIN DAILY VARIANCE PORTFOLIO</i>	59,44%	2,40%
<i>MAX DAILY RETURN PORTFOLIO</i>	76,30%	2,85%
<i>MIN WEEKLY VARIANCE PORTFOLIO</i>	18,80%	0,49%
<i>MAX WEEKLY RETURN PORTFOLIO</i>	28,00%	3,13%
<i>MIN MONTHLY VARIANCE PORTFOLIO</i>	1.110,00%	35,30%
<i>MAX MONTHLY RETURN PORTFOLIO</i>	1.780,00%	49,90%

5 Concluding Remarks

Unlike the quadratic programming methods which generally tend to generate optimal portfolios characterized by low diversification, the empirical analysis of the data seem to reveal that the genetic algorithm developed privileges the diversification as all assets are present in all portfolios and there is a substantial balance in assigning the percentage weights to the assets, with the exception of USA Dollar (weight of 15,90%) in the minimum variance portfolio of monthly returns and of the stock certificate of Vinci (weight of 9,08%) in the maximum return portfolio of monthly returns. The analysis of the data also reveals a great difference between the expected variance and return to vary of the holding period, although an higher expected return is always associated with an higher expected variance and this seems to confirm the good functionality of the algorithm developed. The good functionality of the algorithm is also confirmed by the analysis of the correlation coefficients among the returns of the assets as, in presence of high correlation coefficients between two assets, the algorithm clearly privileges in the allocation of the wealth the asset with lower variance in the minimum variance portfolios and the asset with higher return in the maximum return portfolios.

References

1. Markowitz, H.M.: Portfolio Selection. *Journal of Finance* 7 (1952)
2. Markowitz, H.M.: *Portfolio Selection: Efficient Diversification of Investments*. Wiley, Yale University Press (1959)
3. Lintner, J.: The Valuation of Risk Assets and the Selection of Risky Investments in Stock Portfolios and Capital Budgets. *Review of Economics and Statistics* 47, 13–37 (1965)
4. Michaud, R.O.: The Markowitz Optimization Enigma: Is ‘Optimized’ Optimal. *Financial Analysts Journal* 45(1), 31–42 (1989)
5. Michaud, R.O.: *Efficient Asset Management: A Practical Guide to Stock Portfolio Optimization and Asset Allocation*. Oxford University Press, Oxford (1998)
6. Scherer, B.: Portfolio Resampling: Review and Critique. *Financial Analysts Journal*, 99–109 (2002)
7. Scherer, B.: Asset Allocation: Implicit Versus Explicit Return Shrinkage. working paper (2004)

8. Satchell, S.E., Scowcroft, A.E.: Advances in Portfolio Construction Aand Implementation. Butterworth And Heinemann, Oxford (2003)
9. Pomante, U.: Il Market Timing Con il Modello Di Black e Litterman. Bancaria, n. 7-8 (2008)
10. Gilli, M., Schumann, E.: Robust Regression with Optimization Heuristics. Comisef Working Paper Series (2009)
11. Arnone, S., Loraschi, A., Tettamanzi, A.: A Genetic Approach to Portfolio selection. Neural Network World. International Journal on Neural and Mass-parallel Computing and Information System 3 (1993)
12. Liu, S., Stefek, D.: A Genetic Algorithm for The Asset Paring Problem in Portfolio Optimization. Operation Research and Its application, 441–449 (1995)
13. Loraschi, A., Tettamanzi, A., Tomassini, M., Verda, P.: Distributed Genetic Algorithms with An Application to Portfolio Selection Problems. In: Pearson, D.W., Steele, N.C., Albrecht, R.F. (eds.) Artificial Neural Networks and Genetic Algorithms, pp. 384–387 (1995)
14. Rolland, E.: A Tabu Search Method for Constrained Real Number Search: Applications to Portfolio Selection. Technical Report. Dept. of Accounting And Management Information Systems, Ohio State University. Columbus. U.S.A (1997)
15. Ehrgott, M., Klamroth, K., Schewe, C.: An MCDM Approach to Portfolio Optimization. European Journal of Operational Research, 155 (2004)
16. Crama, Y., Schyns, M.: Simulated Annealing for Complex Portfolio Selection Problems. European Journal of Operational Research 150, 546–557 (2003)
17. Fernandez, A., Gomez, S.: Portfolio Selection Using Neural Networks. Computers & Operations Research (2005)
18. Maringer, D.G.: Portfolio Management with Heuristic Optimization Advanced. Computational Management Science. Springer, Heidelberg (2005)
19. Yu, L., Wang, S., Lai, K.K.: An Intelligent-Agent-Based Fuzzy Group Decision Making Model for Financial Multicriteria Decision Support: The Case of Credit Scoring. European Journal OF Operational Research 195(3), 942–959 (2009)
20. Menolascina, F., Bevilacqua, V., Ciminelli, C., Armenise, M.N., Mastronardi, G.: A Multi-objective Genetic Algorithm Based Approach to the Optimization of Oligonucleotide Microarray Production Process. In: Huang, D.-S., Wunsch II, D.C., Levine, D.S., Jo, K.-H. (eds.) ICIC 2008. LNCS (LNAI), vol. 5227, pp. 1039–1046. Springer, Heidelberg (2008)
21. Bevilacqua, V., Mastronardi, G., Menolascina, F., Pedone, A., Pannarale, P.: A Novel Multi-Objective Genetic Algorithm Approach to Artificial Neural Network Topology Optimisation: The Breast Cancer Classification Problem. In: Proceedings of 2006 International Joint Conference on Neural Networks IEEE 06CH37726D, Vancouver, BC (1958-1965); ISBN/ISSN: 0-7803-9490-9 (2006)
22. Bevilacqua, V., Dotoli, M., Falagario, M., Sciancalepore, F., D'Ambruoso, D., Saladino, S., Scaramuzzi, R.: A Multi-Objective Genetic Optimization Technique for The Strategic Configuration of Distribution Networks. In: Huang, D.-S., et al. (eds.) ICIC 2011. LNCS, vol. 6839, pp. 243–250. Springer, Heidelberg (2011)
23. Pacelli, V., Bevilacqua, V., Azzolini, M.: An artificial neural network model to forecast exchange rate. Journal of Intelligent Systems and Applications 3(2), 57–69 (2011)

Tracking Multiple Feature in Infrared Image with Mean-Shift

Ruiming Liu and Miao Yang

School of Electronic Engineering, Huaihai Institute of Technology,
222005, No. 59 Cangwu Road, Lianyungang, P.R. China
{nanjue1975}@gmail.com

Abstract. Mean-shift algorithm with robust performance is one of the well-known tracking algorithms. Tracking targets with Mean-shift algorithm is tracking the statistical features of their pixels by the histograms. The classic Mean-shift for tracking targets based other features has not been developed. In this paper, we propose a strategy which can make Mean-shift track multiple types of features of targets. We first map the features into the pixel intensity and create the feature images. Then these feature images are used to construct multiple feature images (MFIs). The kernel density estimation algorithm tracks targets in MFIs can indirectly track these features.

Keywords: Mean-shift, Multiple feature image, Entropy, Gabor.

1 Introduction

The Mean-shift algorithm which is one of the well-known tracking algorithms, also known as kernel-based, uses the gradient-based search scheme [1][2][3]. Tracking moving targets in infrared (IR) closing sequences is a challenging research topic. Though a great deal of effort has been expended on this task, there has been only limited amount of work on thermal images in the computer vision community. A. Bal and M. S. Alam combined an intensity variation function with template model to track IR targets [4]. In [5], authors present an approach for real-time target tracking in the presence of high global motion, changes in target shape and intensity features. A decision fusion algorithm for target tracking in IR image sequences is proposed in [6]. Although Mean-shift can track all kinds of objects in color imagery, the performance of tracking objects in IR imagery is not satisfying.

2 Tracking Targets with Mean-Shift and Its Drawbacks in IR Target Tracking

For n data points x_i , $i = 1, 2, \dots, n$ in the d-dimensional space R^d , the kernel density estimation (KDE) of location $x(a, b)$ is defined as

$$\hat{f}_K(x) = \frac{1}{n} \sum_{i=1}^n \frac{1}{h_i^d} K\left(\left\|\frac{x - x_i}{h_i}\right\|^2\right) \quad (1)$$

where $h_i > 0$ is the bandwidth. The $K(\cdot)$ is so-called kernel and if satisfies:

$$K(x) = c_k k(\|x\|^2) > 0 \quad \|x\| \leq 1 \quad (2)$$

where $k(\cdot)$ is the profile of $K(\cdot)$. Employing the profile, Mean-shift can be rewritten as

$$\hat{f}_K(x) = \frac{c_k}{n} \sum_{i=1}^n \frac{1}{h_i^d} k\left(\left\|\frac{x - x_i}{h_i}\right\|^2\right) \quad (3)$$

If $h_i = h$, the density gradient estimation (DGE) is obtained by

$$\hat{\nabla}f_K(x) = \frac{2c_k}{nh^{d+2}} \sum_{i=1}^n (x - x_i) k'\left(\left\|\frac{x - x_i}{h}\right\|^2\right) \quad (4)$$

We can define another function by $k(x)$ as

$$g(x) = -k'(x) \quad (5)$$

Then the next position can be searched by the following iterative equation

$$y_{j+1} = \frac{\sum_{i=1}^n \frac{x_i}{h_i^{d+2}} g\left(\left\|\frac{y_j - x_i}{h}\right\|^2\right)}{\sum_{i=1}^n \frac{1}{h_i^{d+2}} g\left(\left\|\frac{y_j - x_i}{h}\right\|^2\right)} \quad j = 1, 2, \dots \quad (6)$$

For the IR targets, we can only depend on the probability density function (pdf) of image intensity. In the first frame, reference target model characterized by its intensity pdf p_0 for IR images is obtained by estimating from the data. We assume that the target model has been centered at the spatial location 0 and it is commonly estimated from the image data by m -bin histograms. The target model is defined by

$$\hat{p}_0 = \{\hat{p}_{0u}\}_{u=1,\dots,m} \quad \sum_{u=1}^m \hat{p}_{0u} = 1 \quad (7)$$

We assume that $\{x_k\}_{k=1,\dots,n}$ are the normalized locations in the mask centered at 0.

For improving the robustness of the pdf estimation, pixels in the target mask are weighted by an isotropic kernel which has a convex and monotonic decreasing kernel profile [2]. The probability of $u = 1, \dots, m$ in the mask can be denoted as

$$\hat{p}_{0u} = C \sum_{l=1}^n k(\|x_l\|^2) \delta[b(x_l) - u] \quad (8)$$

where $C = 1 / \sum_{l=1}^n k(\|x_l\|^2)$ is a normalization constant that guarantees $\sum_{u=1}^m \hat{p}_{0u} = 1$ and δ is the Kronecker delta function.

After getting the reference model of targets in the first frame, candidate targets can be tracked in the subsequent frame. In the i th frame, a candidate is defined at location z by

$$\hat{p}_i(z) = \{\hat{p}_{iu}(z)\}_{u=1,\dots,m} \quad \sum_{u=1}^m \hat{p}_{iu} = 1 \quad (9)$$

In the same way of representing the reference target model (9), the probability of $u = 1, \dots, m$ in the target candidate is denoted by

$$\hat{p}_{iu} = C_h \sum_{l=1}^{n_h} k\left(\frac{\|z - x_l\|^2}{h}\right) \delta[b(x_l) - u] \quad (10)$$

where $C_h = 1/\sum_{l=1}^{n_h} k(\|(z - x_l)/h\|^2)$ is a normalization constant. Mean-shift is a mode seeking algorithm. This can be achieved by optimizing a similarity function between the reference model and the target candidate. The Bhattacharyya coefficient $B[\hat{p}_{iu}(z), \hat{p}_{0u}]$ between the candidate target model and the reference model is set as the optimized function. It should be maximized as a function of z for finding the target position in the current frame. The location procedure in the current frame starts at the location z_0 of the target in the previous frame. Then the linear approximation of the Bhattacharyya coefficient in the current frame can be obtained by

$$B[\hat{p}_{iu}(z), \hat{p}_{0u}] \approx \frac{1}{2} \sum_{u=1}^m \sqrt{\hat{p}_{(i-1)u}(z_0) \hat{p}_{0u}} + \frac{1}{2} \sum_{u=1}^m \hat{p}_{iu}(z) \sqrt{\frac{\hat{p}_{0u}}{\hat{p}_{(i-1)u}(z_0)}} \quad (11)$$

Combining the above equation with (10), we have

$$B[\hat{p}_{iu}(z), \hat{p}_{0u}] \approx \frac{1}{2} \sum_{u=1}^m \sqrt{\hat{p}_{(i-1)u}(z_0) \hat{p}_{0u}} + \frac{C_h}{2} \sum_{u=1}^{n_h} w_l k\left(\frac{\|z - x_l\|^2}{h}\right) \delta[b(x_l) - u] \quad (12)$$

Where

$$w_l = \sum_{u=1}^m \sqrt{\frac{\hat{p}_{0u}}{\hat{p}_{(i-1)u}(z_0)}} \delta[b(x_l) - u] \quad (13)$$

To find the position of targets, we should maximize the second term of (13). According to the equation (6), the new target position should be

$$z_1^* = \frac{\sum_{l=1}^{n_h} x_l w_l g\left(\frac{\|z_0 - x_l\|^2}{h}\right)}{\sum_{l=1}^{n_h} w_l g\left(\frac{\|z_0 - x_l\|^2}{h}\right)} \quad (14)$$

where $g(x) = -k'(x)$. The convergence point z_1^* is just the target position sought by Mean-shift.

When color targets are tracked, Mean-shift takes advantage of three types of spectral information (RGB) to characterize them. The intensity information is the exclusive feature when it tracks IR targets [5]. It is deficient for representing targets. In this paper, multiple types of features are used to complete this task.

3 Tracking Targets in Multiple Feature Image

At present, the image is represented in 3D RGB space by

$$\mathbb{F}(x) \equiv (f_1, f_2, f_3) = (R, G, B) \quad (15)$$

or 1D intensity space by

$$\mathbb{F}(x) \equiv (f_1) = (I) \quad (16)$$

As a matter of fact, they denote three color features or intensity feature. Assuming there are d features, then we can represent an image in higher-dimensional space by

$$\mathbb{F}(x) = (f_1, f_2, \dots, f_d) \quad (17)$$

We call it multiple-features image. In our past work, the experiments validated that Gabor function value and entropy are practicable features for tracking task. They are also known as Gabor feature and entropy feature, and we simply review these two features.

(1) Gabor feature

Gabor feature has been demonstrated that the human visual system is sensitive to both orientations and spatial frequencies and Gabor filters have the strong ability to model the frequency and orientation sensitivity characteristic.

$$Gr(a, b, \theta, \sigma_a, \sigma_b) = \frac{1}{2\pi\sigma_a\sigma_b} e^{\left\{-\frac{1}{2}\left[\left(\frac{a}{\sigma_a}\right)^2 + \left(\frac{b}{\sigma_b}\right)^2\right] + j2\pi(a\cos\theta + b\sin\theta)\right\}} \quad (18)$$

where σ_a, σ_b are the standard deviations of Gaussian envelope along the $a-$ and $b-$ dimensions and θ represents the orientation. For an intensity image F , it is filtered with $Gr(a, b, \theta, \sigma_a, \sigma_b)$ by

$$FGr(a, b, \theta, \sigma_a, \sigma_b) = \sum_k \sum_l F(a-k, b-l) * Gr(a, b, \theta, \sigma_a, \sigma_b) \quad (19)$$

The Gabor feature just is the magnitude value of (19).

(2) Entropy feature:

In the development of information theory, Shannon stated that quantities of

$$E = -\sum_{i=0}^{N-1} p_i \log_2 p_i \quad (20)$$

plays an important role as measures of information, choice and uncertainty [7]. E is known as entropy which depends on the range and uniformity of the distribution. For discrete random variables, larger entropy means larger uncertainty. Now, we have three features, intensity, Gabor feature and entropy to construct a three-dimensional feature image for an IR image. Figure 1 shows the construction process of MFIs.

4 Experimental Results

In this section, we provide some experiments to validate the advantage of the proposed method over the classic method. We compare the tracking performance of Mean-shift tracker in IR images with in MFIs. For providing the impartial and objective comparison, experiments are run under the same conditions. Kernels with Gaussian profile $k(x) = \frac{1}{2\pi} \exp(-\frac{\|x\|}{2})$

were used for histogram computations. The feature

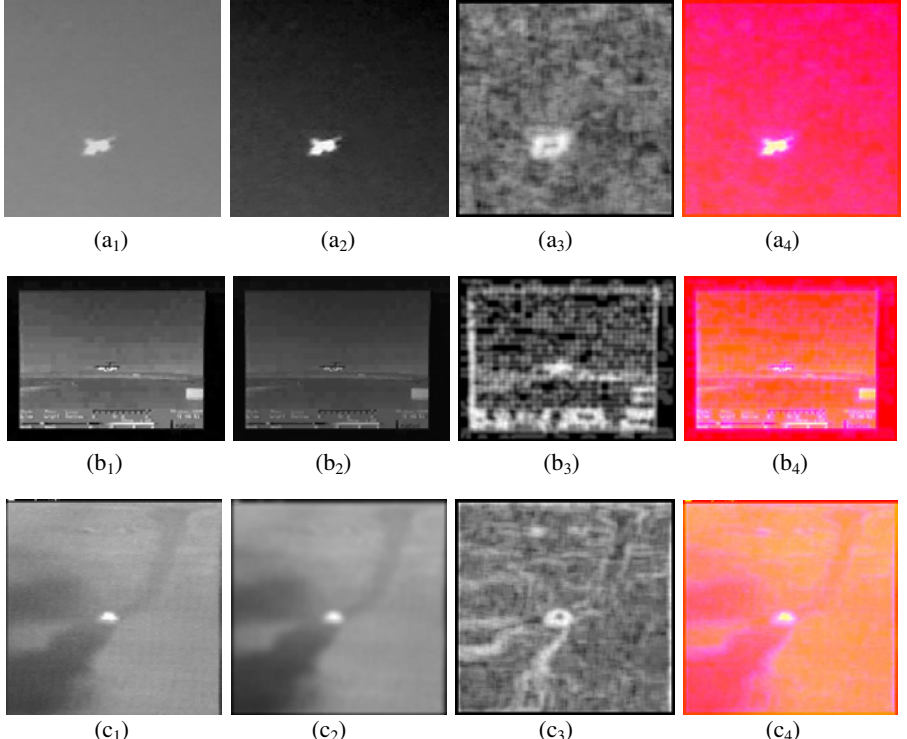


Fig. 1. The construction process of MFIs. (a₁), (b₁) and (c₁) are the original IR images of sequence 1, sequence 2 and sequence 3, respectively. (a₂), (b₂) and (c₂) are their corresponding Gabor feature images. (a₃), (b₃) and (c₃) are their corresponding entropy feature images. (a₄), (b₄) and (c₄) are the constructed MFIs.

space of MFI was quantized into $8 \times 8 \times 8$ bins and that of IR image was quantized into 8 bins. The entropy is computed from a 5×5 window centered at each pixel.

Figure 1(a₁), (b₁) and (c₁) present the first frames of three sequences for experiments. The first sequence has 20 frames of 128×128 pixels with one plane target. The second sequence has 20 frames of 120×160 pixels with another plane target in the night and the third sequence has 20 frames of 128×128 pixels with one tank target. From subsection 2.3, we can see the potential position of target just is the position which has a maximum Bhattacharyya coefficient value. The tracking process of Mean-shift-based methods is the process of searching the maximum Bhattacharyya coefficient. So the surface obtained by computing the Bhattacharyya coefficient is often used to evaluate the efficiency of tracking methods [2]. In Fig.2, the similarity surfaces (values of the Bhattacharyya coefficient around target centers) of the original IR images and the corresponding MFIs in Fig. 1 are shown.

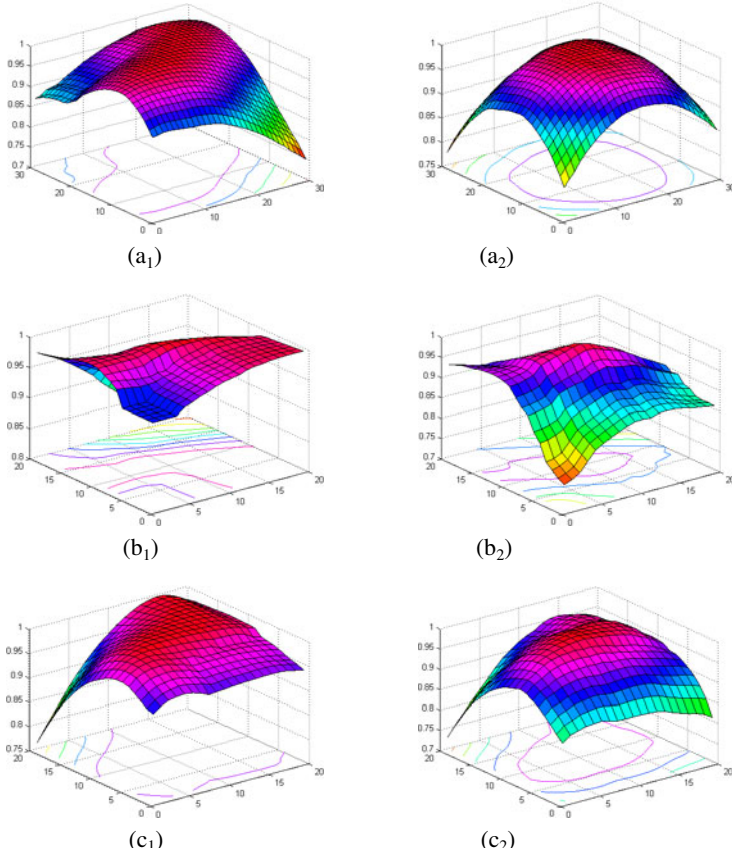


Fig. 2. The similarity surface of original IR images and MFIs of Fig. 1. (a₁), (b₁) and (c₁) are the similarity surfaces of original IR images of sequence 1, sequence 2 and sequence 3, respectively. (a₂), (b₂) and (c₂) are their similarity surfaces of corresponding MFIs.

From (a₁), (b₁) and (c₁) of Fig. 2, we can see the similarity surfaces around target centers are flat and smooth in IR images. That will result in a time-consuming tracking process and even will load to a sub-optimal convergence point. Therefore, it is difficult to search target positions from IR images by Mean-shift trackers. In contrast with IR images, the similarity surfaces of MFIs, shown in (a₂), (b₂) and (c₂) of Fig. 2, are bumpy and steep, which also is proved by the contours on the floor of every sub-image of Fig. 2. So there exists a gradient line which can make a fast and precise tracking process. From the comparison of the similarity surfaces in above subsection, we have every reason to expect that tracking targets in MFIs has better performance than in IR images. Fig. 3 shows the tracking error curves of the three experiment sequences in Fig. 1. The tracking errors in IR images and those in MFIs are presented with blue broken lines and red solid lines, respectively.

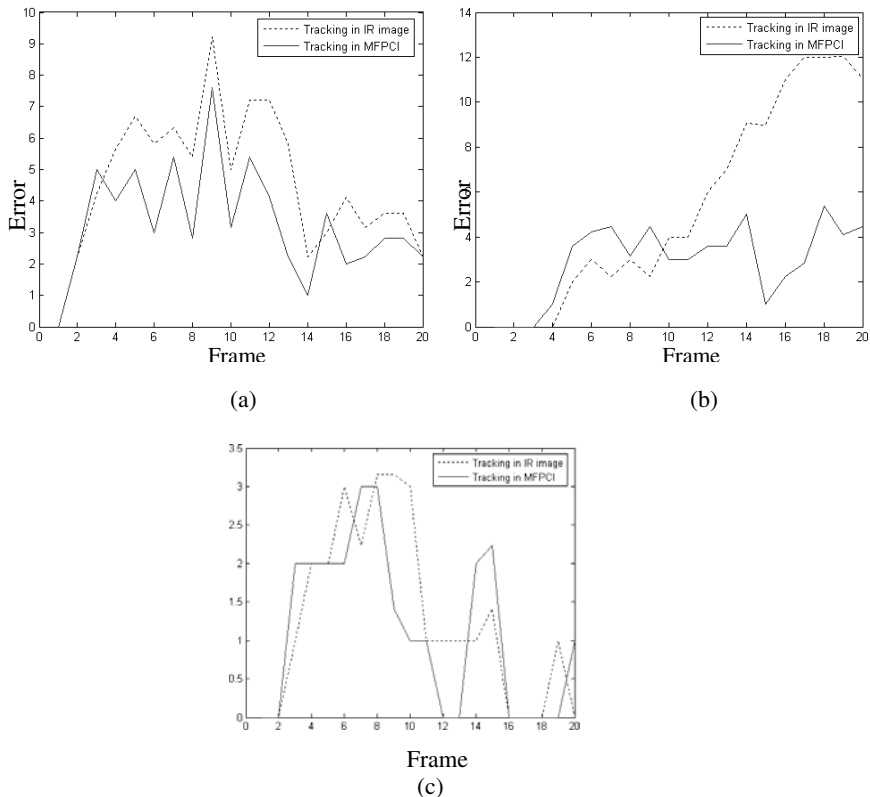


Fig. 3. The error curves of tracking three experiment sequences in Fig. 1. (a) the error curves of the first sequence of Fig. 1. (b) the error curves of the second sequence of Fig. 1. (c) the error curves of the third sequence of Fig. 1.

From Fig. 3, we can see the tracking errors in MFIs are smaller than those of tracking in IR images for most of frames of three sequences. The first sequence holds a plane target in calm sky background. It has a low contrast of target to background

and a stronger similarity between target and background. So it is not easy to track the target. The largest error of tracking in MFIs is smaller than that of tracking in IR images. The average errors of tracking in IR images and in MFIs are 4.64 pixels and 3.34 pixels, respectively. The improvement in tracking precision after adding Gabor feature and entropy feature is evident. The second sequence has a plane target in complex background. Tracking target in this sequence is very difficult because the target appearance has a violent change between two consecutive frames. The proposed method still has the smaller errors in most of frames than tracking target in IR images. Furthermore, the largest error of the proposed scheme is only 6 pixels while the largest error of tracking in IR images is even 12 pixels. The average errors of tracking in IR images and in MFIs are 5.48 pixels and 2.96 pixels, respectively. The third sequence holds a tank target embedded in dim background with a spot appearance. Tracking target in this sequence is more difficult. The average errors of tracking in IR images and in MFIs are 1.30 pixels and 1.13 pixels, respectively. The precision of tracking targets in MFIs is also higher. In conclusion, tracking MFIs has the smaller errors in most of frames than tracking target in IR images because the added features improve the distinguishability between target and background.

5 Conclusions and Acknowledgements

We propose a strategy which does not need to improve the kernel density estimation algorithm itself, but can make it track other features. Firstly, the features are mapped into the pixel intensity. Secondly, we construct MFI with the feature image. Then tracking targets is executed in MFI by Mean-shift. At present, the Gabor feature and entropy feature are developed in our framework. Finding other features to construct MFI and track targets is our future work.

This work is supported by Natural Science Fund for Colleges and Universities in Jiangsu Province under grant no. 09KJB510001 and no. 10KJB510002 through Huaihai Institute of Technology.

References

1. Comaniciu, D., Meer, P.: Mean Shift: A Robust Approach Toward Feature Space Analysis. *IEEE Transactions on Pattern Analysis and Machine Intelligence* 24(5), 603–619 (2002)
2. Comaniciu, D., Ramesh, V., Meer, P.: Kernel-Based Object tracking. *IEEE Transactions on Pattern Analysis and Machine Intelligence* 25(5), 564–577 (2003)
3. Fan, Z., Yang, M., Wu, Y.: Multiple Collaborative Kernel Tracking. *IEEE Transactions on Pattern Analysis and Machine Intelligence* 29(7), 1268–1273 (2007)
4. Bal, A., Alam, M.S.: Automatic Target Tracking in FLIR Image Sequences Using Intensity Variation Function and Template Model. *IEEE Transactions on Instrumentation and Measurement* 54(5), 1846–1852 (2005)
5. Yilmaz, A., Shafique, K., Alam, M.S.: Target Tracking in Airborne Forward Looking Infrared Imagery. *Image and Vision Computing* 21(7), 623–635 (2003)
6. Dawoud, A., Alam, M.S., Bal, A., Loo, C.: Target Tracking in Infrared Imagery Using Weighted Composite Reference Function-Based Decision Fusion. *IEEE Transactions on Image Processing* 15(2), 404–410 (2006)
7. Shannon, C.E.: A Mathematical Theory of Communication. *Bell System Technical Journal* 27, 379–423 (1948)

Research on Dynamic Human Object Tracking Algorithm

Yongjian He^{1,2,*}, Qiong Wu², Shoupeng Feng², Rongkun Zhou²,
Yonghua Xing², and Fei Wang¹

¹ Institute of Artificial Intelligence and Robotics, Xi'an Jiaotong University, Xi'an, China

² Xi'an Communication Institute, Xi'an, China

{heyj, qwu, spfeng, rkzhou, Yhxing, fwang}@aiar.xjtu.edu.cn

Abstract. This paper studies the dynamic human object tracking problem. Under the condition of both of the camera and the object being tracked simultaneously move, when the movement of the object is too fast and the speeds of the two do not match, the tracking of the moving object will have lag issues. This paper presents an improved particle-tracking method. The method, during the tracking process, can reduce the number of particles online according to the actual tracking situation, thereby reducing computation time, so that the computing speed can be adjusted in real time according to the velocity of the being-tracked object to form the best match of the speeds. Experimental results show that the improved algorithm well solves the lag problems of the moving object being tracked and the tracking performance is significantly improved.

Keywords: training human, dynamic tracking, particle tracking, motion model.

1 Introduction

As an important branch of computer version, the motion tracking technology of human video images has been receiving attention from researchers in fields of image processing and computer vision. In recent years, more and more researches are dedicated to different video tracks to get human joint motion[1]. In these algorithms, most of the basic ideas are based on Monte Carlo method, which represents the probability by particle collection and can be used in any form of state space models[2]. It simply refers to approximate the probability density function by finding a set of random sample propagating in state space using the sample mean instead of integral operation, thus getting the distribution process of the state minimum variance[3].

However, when the moving speed of the body in the video becomes faster, the tracking process cannot meet the real-time requirement causing tracking dislocation, delay, unsynchronization and so on[4]. This leads to a lot of computation time required in the tracking operation, resulting in the computation method itself is slow.

* Supported by National Natural Science Foundation of China (90820017), Basic Research and Business Subsidy of Central College. The corresponding author is Fei Wang.

In response to this problem, this paper improves the traditional particle tracking algorithm to solve the lag issues in the tracking process of human identification image. In the tracking process, according to the situation of human motion, dramatically reduce the number of particles involved in operations and use the tactful calculation of adaptive particle-tracking based on decision rules to achieve human motion tracking. This can in certain circumstances reduce the number of particles used making the tracking algorithm can have a real time adjustment based on the situation of human motion. Thus, even if the speed becomes faster, it can well meet the real-time match. Experiments show that this method takes short time and has high efficiency. This well solves the lag issues in the tracking process.

2 Human Motion Tracking Theories

The motion tracking theories in human video images are as follows: First, create a human motion model and then determine the space of human motion. In the human motion state space, it can randomly generate a set of samples according to the knowledge of prior distribution and the samples are called particles. Then, based on the observation, by adjusting the corresponding weights and the location of each sample, obtain a sample which submits to the actual distribution and take the mean of the sample as the estimate of system state. Finally, re-sample this group of particles to ensure uniform distribution of the weights[5].

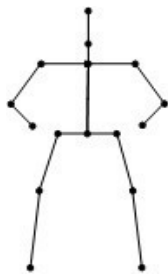


Fig. 1. Body Skeleton Model

Here present a simple introduction to the method of tracking the moving human by particles:

To track the moving body first is to build a human skeleton model. Because of simple structure, it has been widely used for a long time. Its principle is to take the body as a stick-shaped model which is a set of segments connected by points expressing joints or body features. These segments refer to human limbs, trunk or other important parts[6]. Each body segment can be expressed by a local coordinate frame and each joint includes translation and rotation degrees of freedom. As shown in Figure 1, it includes 16 joints with each joint has two rotation degrees of freedom.

Signal processing model used in particle tracking is expressed by the state equation and observation equation, that is:

$$x_k = f_k(x_{k-1}, w_k) \quad (1)$$

$$z_k = h_k(x_k, v_k) \quad (2)$$

Where, k refers to moment, x_k refers to vector state of the system at k , f_k means state transfer function, w_k refers to the process noise sequence, z_k means observation vector, h_k means observation function, and v_k means the observation noise sequence.

Recursion state prediction equation and state update equation are as follows:

$$p(x_k | Z_{k-1}) = p \int (x_k | x_{k-1}) p(x_{k-1} | Z_{k-1}) dx_{k-1} \quad (3)$$

$$z_k = h_k(x_k, v_k) \quad (4)$$

In order to facilitate the calculation, we can add a new probability calculation function for sampling.

$$p(x_k | Z_k) \approx \sum_{i=1}^N w_k^i \delta(X_k - X_k^i) \quad (5)$$

Through the above Equation, the important recursive equation can be observed.

$$\frac{w_{k-1}^i p(z_k | x_k^i) p(x_k^i | x_{k-1}^i)}{q(x_k^i | X_{k-1}^i, Z_k)} \quad (6)$$

The selection principle when the algorithm is applied is to meet the minimum variance of the important weight. To select a certain number of particles with weights to be involved in the operation, when the observed data is changed, update the weight of each particle in real time and carry out the recursive calculations.

To measure the tracking performance, the calculation equation of the error rate of the algorithm is given here. Use the pixel difference between the calibrated particles and the actual location of the human as a measure of the tracking performance. The lag rate of the tracking is set to r:

$$r = 1 - \frac{v_1}{v_2} = 1 - \frac{t_1}{t_2} = 1 - \frac{\frac{f_k(x) \bullet t'}{s}}{v_2} \quad (7)$$

Where, v_1 states the operation speed of the human being tracked, v_2 states the processing speed of the algorithm. It can be seen from the above Equation, v_1 is determined by the time that the human takes in certain moving distance. v_2 is determined by the processing time of the algorithm. If the value of the equation is close to one, the error rate is the lowest and the tracking performance is the best.

This paper proposes an algorithm based on the improved particle tracking, it can dynamically reduce the number of particles involved in operations, and thereby reducing the computation time, making the synchronization ratio achieve to be the same and reducing the lag rate in the tracking process.

3 Human Motion Tracking Based on Improved Particle Tracking Algorithm

This paper presents particle tracking method for object tracking and dynamic adjustment of the number of particles. This method can adjust the number of particles needs according to different situations in real time to avoid unnecessary waste and reduce the amount of the calculation to solve the over-high problem of the lag rate in the tracking process. The core of the algorithm is to dynamically adjust the operation speed, so that it can match with the speed of human motion.

3.1 Adjust the Number of Particles Online

Compared with Kalman Tracking and Unscented Kalman Tracking Algorithm, the precision of particle tracking algorithm is high. However, the particle tracking algorithm often takes more time, the primary cause is that the number of particles used in the process of tracking is large [7]. We can effectively reduce the number of particles involved in tracking. In this way, we can greatly reduce the tracking time and solve the problems that the tracking speed does not match with the movement speed and the lag rate is too high. In the improved algorithm, the normal distribution $N(\mu_i, p_k)$ that determined by the output tracking value μ_k at each stage and the variance of tracking error p_k can basically represent the distribution at k moment $\{X_i, i=1, \dots, N\}$. The basic idea is as follows:

First, define the evaluation index of algorithm:

$$IEI = \frac{1}{t \times RMSE} \quad (8)$$

In the above Equation, t stands for the time consumption for completing one simulation, $RMSE$ stands for the tracking error, IEI stands for the tracking function index which gives consideration to both arithmetic efficiency and evaluation precision. The higher the IEI value is, the higher combination property of algorithm is.

Define the function of tracking integrated performance cost (IPC)

$$C(\varepsilon_k, N_k) = m \int_{-\infty}^{\infty} \varepsilon_k^2 f(\varepsilon_k) d\varepsilon_k + \bar{c}_t \times N(k) \quad (9)$$

Among it, m is the scale factor, $f(\varepsilon_k)$ is probability density function for evaluated error, $\varepsilon_k \sim N(0, \frac{P_{k-1}}{N(k)})$; \bar{c}_t is the average time loss for processing a particle; $N(k)$

is the number of particles needing; $\varepsilon_k = \frac{1}{N(k)} \sum_{i=1}^{N(k)} x_k^i - \mu_{k-1}$ is the evaluation error brought during the evaluation of μ_{k-1} by particles' first order statistic (mean value).

First, calculate the IPC function at k moment:

$$C(\varepsilon_k, N_k) = m \int_{-\infty}^{\varepsilon_k} \frac{\sqrt{N(k)}}{\sqrt{2\pi P_{k-1}}} \exp\left(-\frac{\varepsilon_k^2}{2P_{k-1}/N(k)}\right) d\varepsilon_k + \bar{c}_t \times N(k) \quad (10)$$

From the above Equation, we can get:

$$C(\varepsilon_k, N_k) = m \frac{P_{k-1}}{N(k)^2} + \bar{c}_t \times N(k) \quad (11)$$

Calculate the derivative, we can get:

$$C'(\varepsilon_k, N_k) = -m \frac{P_{k-1}}{N(k)^3} + \bar{c}_t \quad (12)$$

Let $-m \frac{P_{k-1}}{N(k)^2} + \bar{c}_t = 0$, we can get:

$$N(k) = \sqrt{\frac{mP_{k-1}}{\bar{c}_t}} \quad (13)$$

$N(k)$ is the number of particles needing. From equation we can dynamically adjust the number of particles according to different moments. Therefore, compared with traditional particle tracking algorithm, the improved algorithm greatly reduces the arithmetic time in the progress of human tracking algorithm.

3.2 Operation Steps of Model Matching

Following, we use the second-order ARP kinetic model to process human motion tracking. Discrete-time second-order ARP model can be expressed as:

$$X_t = A_2 X_{t-2} + A_1 X_{t-1} + C_0 + B_0 W_t \quad (14)$$

In the Equation, X_t is the human motion vector, A_2 , A_1 and B_0 are coefficient matrix, A_2 and A_1 is the deterministic component of kinetic model, B_0 is random component, C_0 is offset vector, W_t is standard normality random component. equation 10 shows that the status at current moment t is forecasted by the status of the former two moments $t-1$ and $t-2$.

The second-order ARP model parameters used in this paper is obtained by the learning of motion model. The algorithm is as follows:

Giving a joint position training set $\{X_1, X_2, \dots, X_N\}$ which extracted from image sequence, calculate the parameters by following steps:

Step 1: Calculation

$$R_{-i} = \sum_{k=3}^N X_{k-i} \quad i = 0, 1, 2; \quad (15)$$

$$R_{ij} = \sum_{k=3}^N X_{k-i} X_{k-j}^T \quad i, j = 0, 1, 2; \quad (16)$$

$$R'_{ij} = R_{ij} - \frac{1}{N-2} R_i R_j^T \quad i, j = 0, 1, 2; \quad (17)$$

In the Equation, X_t is the human motion vector.

Step 2: According to the above three Equations, evaluate parameters A_2, A_1 and C_0 .

$$\begin{aligned} A_2 &= (R_{02}^t - R_{01}^t R_{11}^{t-1} R_{12}^t) (R_{22}^t - R_{21}^{t-1} R_{12}^t)^{-1} \\ A_1 &= (R_{01}^t - A_2 R_{21}^t) R_{11}^{t-1} \\ C_0 &= \frac{1}{N-2} (R_0 - A_2 R_2 - A_1 R_1) \end{aligned} \quad (18)$$

In the Equation, A_2 and A_1 is the deterministic component of kinetic model, C_0 is offset vector.

Step 3: Use coefficient matrix B_0 to evaluate the following matrix square root.

$$D = \frac{1}{N-2} (R_{00} - A_2 R_{20} - A_1 R_{10} - C_0 R_0^T) \quad B_0 = \sqrt{D} \quad (19)$$

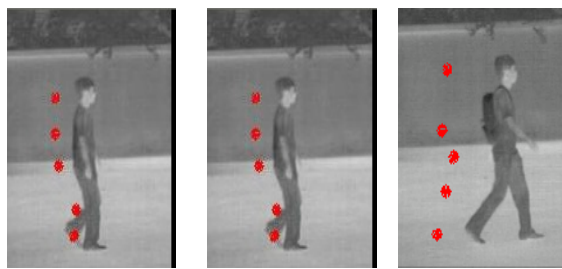
In the Equation, B_0 is coefficient matrix.

Finally, obtain the parameters and coordinate with the equation to track the human motion. In this way, we can dynamically adjust the particles' number and complete synchronous fast-track in the process of human motion.

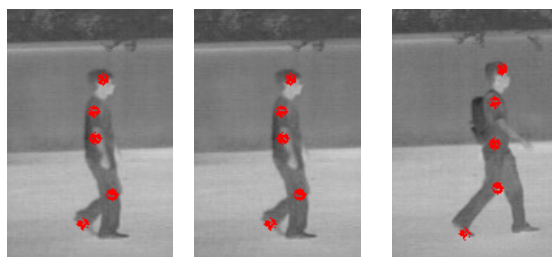
4 Simulation and Analysis of Experimental Results

Experimental data is obtained by ordinary digital cameras, the image resolution is 640×640 , camera shooting rate is 15 seconds / frame. The experimental results show in Figure 2.

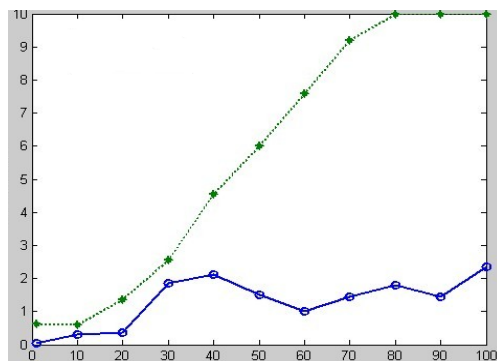
In the tracking experiments, the human walking speed is the key factor. This paper selects faster walking speed to carry out image acquisition and to compare experimental results. Experimenter's moving speed is 2 m / s ~ 5 m / s, for the particle tracking algorithm, this speed is fast enough. Comparing three groups of images, Figure 2 is the traditional particle tracking algorithm, Figure 3 is the improved particle tracking algorithm. The particles number N takes 100.



(a) the 7th frame (b) the 24 frame (c) the 67 frame

Fig. 2. The human tracking of traditional particle tracking algorithm

(a) the 7 frame (b) the 24 frame (c) the 67 frame

Fig. 3. The tracking results of the improved particle tracking algorithm**Fig. 4.** Algorithm lag rate comparison

Get the particles number and arithmetic time of the improved algorithm by statistics. In Figure4, the green line shows the lag rate of the traditional algorithm when the speed become faster; the blue line shows the lag rate of the proposed algorithm in this paper under the same condition.Statistical result shows as following table 1.

Table 1. The experimental contrast data of two algorithms

Experiment	Particle number (avg)	Time consumption	Lag rate
Traditional algorithm	100	4.75	65%
improved algorithm	67	2.45	22%

Through the image contrast, we can see when human speed become fast, the traditional tracking algorithm is not synchronized with the change. The red track point comes up pixels "dislocation", making the tracking lag. The algorithm proposed in this paper perfectly completes the human tracking when they walk fast which is shown in table I. By adjusting the number of particles online to increase the tracking performance, in the tracking progress, the speed of the proposed algorithm in this paper is quicker than traditional algorithm's. The synchronous ratio of tracking is greatly increased; the lag rate is significantly reduced. Therefore, we can believe that the proposed tracking algorithm can perfectly solve the lag problem of the tracking.

5 Conclusion

Apply the improved particle tracking algorithm proposed in this paper to human motion tracking. In the human motion progress, dynamically adjust particle's number. And use the human joint model and the motion model, which is obtained from learning, to track the human motion, greatly reducing the tracking time, so that we can handle the tracking errors of fast-moving targets. This paper does not need separate the human region in each frame and has no special requirements for the background. The experiment is only tracking simple human motion, so it has some limitations, and is not applied to other rigid objects, so these contents also need further researches.

References

1. Bregler, C., Malik, J.: Tracking People with and Exponential Maps. In: Proceedings of the IEEE Conference on Computer Vision and Pattern Recognition, Santa Barbara, CA, pp. 8–15 (1998)
2. Liu, X., Chuang, Y.T., Pan, Y.H.: The Human Motion Tracking Based on Model. Computer Research and Development 36(10), 1268–1273 (1999)
3. Dai, K., Liu, X.: The Human Motion Tracking Based on Image Sequence. Computer Simulation 17(9), 33–39 (2005)
4. Arulampalam, M.S., Maskell, S., Gordon, N.: A Tutorial on Particle Filters for Online Nonlinear/non-Gaussian Bayesian Tracking. IEEE Trans Signal Proceedings 50(2), 174–188 (2002)
5. Olivier, C., Simon, J.G.: An Overview of Existing Methods and Recent Advances in Sequential Monte Carlo. Proceedings of the IEEE 95(5), 899–924 (2007)
6. Gordon, N., Salmond, D., Smith, A.: Novel Approach to Nonlinear/non-Gaussian Bayesian State Estimation. IEEE Proceeding F Radar Signal Process 140, 107–113 (1993)
7. Julier, S.J., Uhlmann, J.K.: Unscented Filtering and Nonlinear Estimation. Proceedings of the IEEE 92(3), 401–403 (2004)

Mobile Robot Navigation Using Reinforcement Learning Based on Neural Network with Short Term Memory

Andrey V. Gavrilov¹ and Artem Lenskiy²

¹ Dept. of Production Automation in Machine Engineering
Novosibirsk State Technical University, Karl Marx av., 20,
Novosibirsk, 630092, Russia

Andr_gavrilov@yahoo.com

² School of Electrical, Electronics & Communication Engineering,
Korea University of Technology and Education,
1800 Chungjeol, Byeongcheon, Dongnam Cheonan, 330-708, Korea
a.a.lensky@gmail.com

Abstract. In this paper we propose a novel bio-inspired model of a mobile robot navigation system. The novelty of our work consists in combining short term memory and online neural network learning using history of events stored in this memory. The neural network is trained with a modified error back propagation algorithm that utilizes reward and punishment principal while interacting with the environment.

Keywords: neural networks, mobile robots, reinforcement learning.

1 Introduction

For the past decades a number of neural network based approaches have been suggested for mobile robots navigation. The early works are dated back to 1975, 1986 and were conducted by N.M.Amosov [1] and R.Brooks [2] correspondingly. Short review of this topic may be found in [3]. The key issue in mobile robot navigation is to design a system that allows robot to autonomously navigate in unstructured, dynamic, partially observable, and uncertain environments. The robot navigation problem can be divided into the following tasks: map building, localization, path planning, and obstacle avoidance. Some of these problems can be solved by applying approaches based on neural networks. One of the most popular approaches is based on a multilayer perceptrons (MLP) that is trained with the error back propagation (BP) learning algorithm. The disadvantages of approach based on the BP learning algorithm are in its complexity, slow training and orientation on supervised learning. Moreover, in the case when a part of MLP should be retrained, the whole training processes should be repeated. Janglova [4] attempted to overcome some of these shortcomings by proposing a multilayer hybrid neural network with preprocessing that utilize principle component analysis (PCA). His solution reduces the time needed for MLP training. However, it does not resolve the remaining disadvantages. A.Billard and G.Hayes [5] suggested a model for mobile robot navigation (DRAMA) that is based on recurrent neural network with delays. This is probably the first model

where an attempt to develop a universal neural network as a part of control system to navigate in uncertain dynamic environment was made. However, the model was mainly oriented on quite simple binary sensors for events detection.

An unsupervised learning model for map building based on adaptive resonance theory (ART) [7] was proposed by Araujo [6]. Another model for robot navigation was suggested in [8]. The robot model was able to receive commands on a natural language and analyze graphical image of the environment to take decisions for further movement. The system was extracting simple image features sensitive to spatial transformations. Therefore, the same object observed from different viewpoints generated distinct features. As a result the number of features representing the same object was too high, leading into a great number of neurons. To overcome this drawback a multi-channel cognitive model was proposed [9] and evaluated for solving a minefield navigation task. To classify objects it was proposed to create a separate ART models. However, similar problem affects this approach. With the increasing number of object groups the number of ART models increases slowing down the performance.

On other hand there are methods that are specifically designed for visual navigation. One recent approach [10-12] proposed to extract image features that are robust to spatial transformations. Thus, feature vectors remain the same for greater variations in a view angle, consequently keeping the number of neurons low.

Another way to reduce the number of neurons in ART model was proposed in [13-16]. The idea behind this method consist in preprocessing input vectors the multilayer perceptron which goal is to reduce the sensitivity of ART-2 model to spatial image transformations. However, the simulation experiments showed that this model (MLP-ART2) is more suitable for finding differences in image sequences. It also very depended on parameters of ART-2 and MLP, and selection of them is a complex and nontrivial task.

Gavrilov et. al [17] suggested to combine MLP-ART2 with the reinforcement learning which is based on modified error back propagation algorithm or Generalized Error Back Propagation (GEBP).

In this paper we propose a novel bio-inspired model of a mobile robot navigation system that combines MLP, short term memory and reinforcement learning with GEBP. The difference between the model presented in [17], and the proposed model is in the history of events that is used in learning of MLP when the robot gets either a reward or a punishment. Also the in the proposed model there is no ART-2 model that is associated with specific learning problems. It is also easier to train the proposed model. It may be seen as universal bio-inspired reinforcement learning in contrast to popular probabilistic approaches which are more abstract and mathematical based.

2 Proposed Architecture of Control System

The proposed control system for navigation of a mobile robot is shown in fig. 1. The proposed system consists of the following blocks: critic, short-term memory, FFNN trained with GEBP algorithm. The short-memory block store a few recent pairs of input and output vectors of the network. The critic block utilizes pairs of input and output vectors stored in short-term memory to train the network. Those vectors that represent collisions with obstacle are used as negative samples (punishment) and those that represent visible target are positive samples (reward).

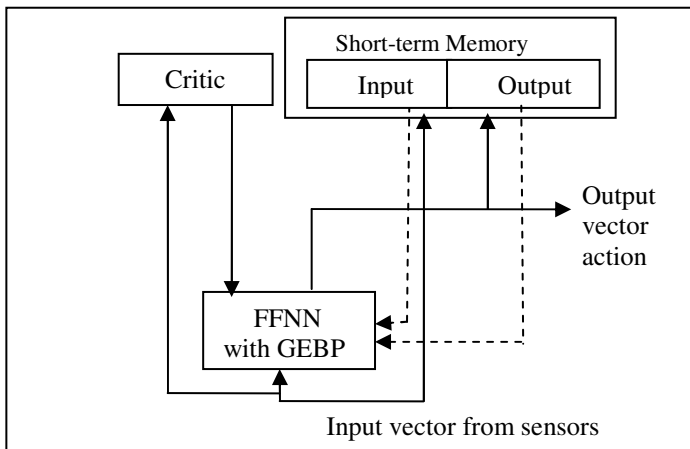


Fig. 1. Proposed Architecture

Below example of navigation algorithm learning to achieve target in unknown environment is shown using this architecture and generalized error back propagation algorithm. There *Estimation* is produced by critic as *none*, *reward* or *punishment*, *direction_to_turn* for control of motion is produced by neural network or simple logical algorithm (at short distance to obstacle). Functions WorkNN and LearnNN aims to produce *direction_to_turn* and to learn neural network with respect to *Estimation* correspondingly. Random behavior sometimes is needed to reduce possibility of cycling in motion, in particular, using untrained neural network in first time. Sensor vector and selected decision (randomly or by neural network) is stored in short-term memory and when critic generates reward or punishment this information is used for training of neural network. At that the influence of stored decisions depends on order in time. Procedure Move provides turn and one step of forward motion.

Algorithm of robot behavior

While *target_is_not_achieved*

 Get *values_from_sensors*;
 Calculate *distance_to_obstacle_in_front*;
 Assign *none* to *Estimation* ;

If *target_is_visible*

Then

 Assign *reward* to *Estimation*;
 Direction_to_turn := *Direction_to_target*;

End if

If *distance_to_obstacle_in_front < Threshold distance*

Then

 Assign *punishment* to *Estimation*;
 Calculate *direction_to_turn* from obstacle by simple
 logical algorithm;

```

Else
    Calculate random_value;
    If random_value < Probability of random behavior
    Then
        Assign random direction to Direction_to_turn;
    Else
        Direction_to_turn:=WorkNN(values_from_sensors);
    End if
    Storing of sensor vector and selected direction
        (input-output) in short-term memory;
    End if
    Move(Direction_to_turn);
    Current_situation := last situation in memory;
    r := 1;
    If Estimation is reward or punishment then
        While not_all_memory_is_tested
            LearnNN(Current_situation, Estimation);
            r := r/2;
            Current_situation := previous situation in memory;
        End while
    End if
End while
End of algorithm of robot behavior

```

The procedure LearnNN uses Generalized Error Back Propagation learning algorithm described below.

3 Generalized Error Back Propagation (GEBP) Algorithm Providing Learning Based on Positive and Negative Samples

Our Generalized Error Back Propagation (GEBP) is based on two modes of EBP – positive or negative respecting for attraction and repulsion of target output vector. Positive mode of this model is classic EBP. The negative mode provides update of weights with opposite sign. Thus updates of weights in GEBP are described as follows:

$$\Delta w_{ij} = ar\varphi_j x'_i, \quad (1)$$

where:

w_{ij} is weight of connection between i th neuron and j th neurons;

a is value of reward, 1 or -1;

r is a rate of learning;

φ_j is error propagation for j th neuron;

x'_i is derivative of active function of i th neuron.

Function φ_j for calculation of error propagation for output layer differs from same function in usual EBP algorithm. For case $a=1$ it is same as in EBP classic algorithm:

$$\varphi_j = y_j(1-y_j)(d_j - y_j), \quad (2)$$

where y_j and d_j are actual and desirable output of neuron respectively.

For case $a=-1$ the function φ_j is determined as

$$\varphi_j = ky_j(1-y_j) \exp\left[-\frac{1}{2\sigma^2}(d_j - y_j)^2\right] \quad (3)$$

The expression $y_j(1-y_j)$ of this formula represents the derivative of neuron's state like in usual error back propagation. The exponential function in this formula provides maximal value of φ_j at equality of actual and desirable states of j th neuron. Value σ represents the sensitivity in neighborhood of danger (undesirable) output vector. Coefficient k may be interpreted as a level of timidity and may be connected with simulation of emotions.

Another variant of calculation of φ_j is possible.

For $d_j \neq y_j$ function φ_j may be defined as

$$\varphi_j = \frac{ky_j(1-y_j)}{d_j - y_j} \quad (4)$$

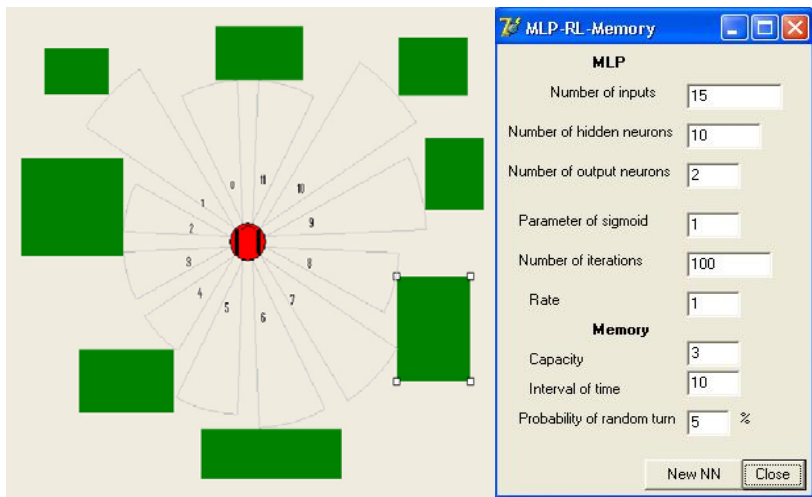
For $d_j = y_j$ φ_j may be determined as constant value k .

Unlike classical EBP with positive reward the punishment in GEBP provides adaptation of weights for repulsion of target output vector (the vector associated with any danger or collision). Particular case is learning to predict of events in time. In this case MLP may be replaced by recurrent neural network dealing with sequences of patterns, e.g. Elman model [18] with EBP through time.

4 Simulation

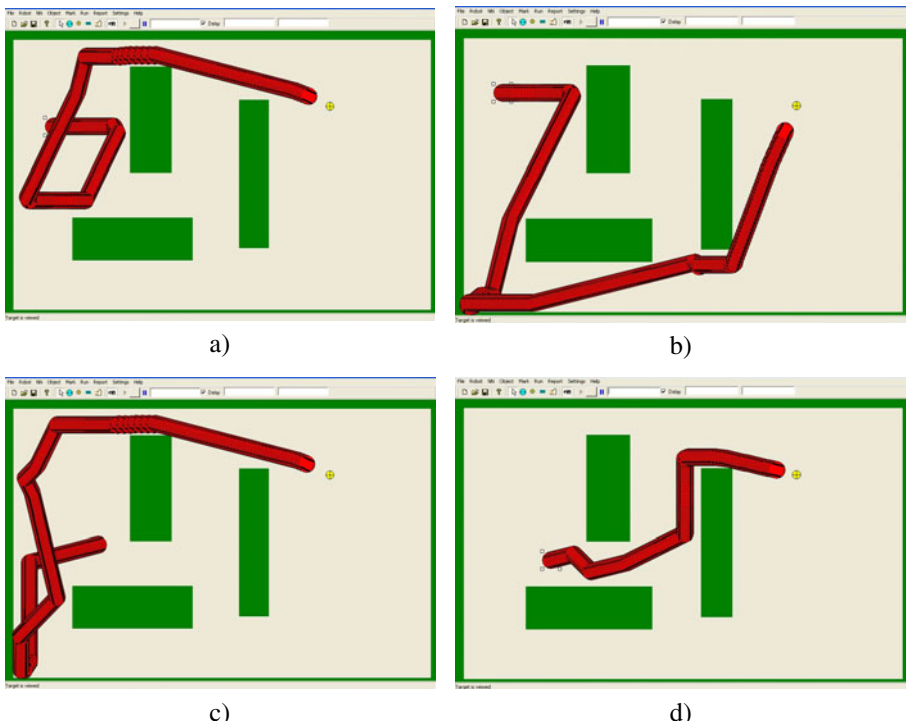
The simulation of the proposed algorithm and navigation system has been done using the Mobile Robot Simulator (MRS) developed for 2D-simulation of mobile robots in simplified environment with rectangles as obstacles, discrete time and step-type motion of robot [16]. Task solving by the robot is to find the path to a target without knowing the map.

In our experiments we use 12 range sensors (Fig. 2a) for estimating distances to surrounding obstacles. Besides them input of the neural network includes direction of robot motion and its coordinates. Therefore, input vector consists of 15 components. We use a neural network with two outputs. Direction of the robot movement is calculated as a difference between two outputs.



a)

b)

Fig. 2. a) Range sensors in MRS and b) parameters of simulation**Fig. 3.** Simulation examples, a),b),c) and d) are first, second, third and fourth series. The robot's trajectory is show in red, obstacles are green and the target is yellow.

In our previous simulations we used a network with one output, which often led to the problem of getting into a loop, especially in the beginning of the traverse when the network is untrained.

Fig. 2b shows a form with main parameters of the neural network and the short-term memory that are used in the experiments. The parameter “Interval of time” determines the number of steps of motion that is necessary to make a decision either by the neural network or using short-term memory that is limited by the parameter “Capacity”.

Some experiments are shown in Fig. 3. There are series of experiments with the same environment and same neural network that is trained once and permanently..

5 Conclusion

Conducted experiments show that based on the proposed navigation algorithm, robot behaves appropriately in an unknown indoor environment. The advantage of this model compared to classical reinforcement learning is the absence of a necessity of preliminary knowledge on the environment and discretization of space.

Our model is based on universal bio-inspired reinforcement learning in contrast to popular probabilistic approaches which are more abstract and mathematics based.

We are planning to test our model in real environment with different parameters. Besides we are planning to combine the proposed navigation algorithm with the algorithm suggested in [19, 20] that uses natural language to train and control a mobile robot.

References

1. Amosov, N.M., Kussul, E.M., Fomenko, V.D.: Transport Robot with A Neural Network Control System. In: Advance papers of the Fourth Intern. Joint Conference on Artificial intelligence, vol. 9, pp. 1–10 (1975)
2. Brooks, R.: A Robust System Layered Control System for A Mobile Robot. IEEE Trans. on Robotics and Automation RA-2, 14–23 (1986)
3. Zou, A., Hou, Z., et al.: Neural Network for Mobile Robot Navigation. A Survey. In: Wang, J., Yi, Z., Zurada, J.M., Lu, B.-L., Yin, H. (eds.) ISNN 2006. LNCS, vol. 3972, pp. 1218–1226. Springer, Heidelberg (2006)
4. Janglova, D.: Neural Networks in Mobile Robot Motion. Int. J. of Advanced Robotic Systems 1(1), 15–22 (2004)
5. Billard, A., Hayes, G.: DRAMA, A Connectionist Architecture for Control and Learning in Autonomous Robots. Adaptive Behavior 7(1), 35–63 (1999)
6. Rui, A.: Prune-able fuzzy ART Neural Architecture for Robot Map Learning and Navigation in Dynamic environment. IEEE Trans. on Neural Networks 17(5), 1235–1249 (2006)
7. Carpenter, G.A., Grossberg, S.: Pattern Recognition by Self-Organizing Neural Networks. MIT Press, Cambridge (1991)
8. Gavrilov, A.V., Gubarev, V.V., et al.: An Architecture of Hybrid Control System of Mobile Robot. Mechatronics, Automation, Control. 8, 30–37 (2004)

9. Tan, A.: FALCON: A Fusion Architecture for Learning, Cognition and Navigation. In: Proc. of IEEE Int. Joint Conf. on Neural Networks IJCNN 2004, vol. 4, pp. 3297–3302 (2004)
10. Lenskiy, A.A., Lee, J.-S.: Rugged Terrain Segmentation Based on Salient Features. In: International Conference on Control, Automation and Systems 2010, Gyeonggi-do, Korea (2010)
11. Lenskiy, A.A., Lee, J.-S.: Terrain Images Segmentation in Infra-red Spectrum for Autonomous Robot Navigation in IFOST 2010, Ulsan, Korea (2010)
12. Lenskiy, A.A., Lee, J.-S.: Machine Learning Algorithms for Visual Navigation of Unmanned Ground Vehicles. In: Igelnik, B. (ed.) Computational Modeling and Simulation of Intellect: Current State and Future Perspectives. IGI Global (2011)
13. Gavrilov, A.V.: Hybrid Neural Network Based on Models Multi-Layer Perceptron and Adaptive Resonance Theory. In: Proc. of 9th Int. Russian-Korean Symp. KORUS 2005, pp. 604–606. NSTU, Novosibirsk (2005)
14. Gavrilov, A.V., Lee, Y.-K., Lee, S.-Y.: Hybrid Neural Network Model based on Multi-Layer Perceptron and Adaptive Resonance Theory. In: Wang, J., Yi, Z., Žurada, J.M., Lu, B.-L., Yin, H. (eds.) ISNN 2006. LNCS, vol. 3971, pp. 707–713. Springer, Heidelberg (2006)
15. Gavrilov, A.V., Lee, S.-Y.: An Approach for Invariant Clustering and Recognition in Dynamic Environment. In: Elleithy, K. (ed.) Advances and Innovations in Systems, Computing Science and Software Engineering, pp. 47–52. Springer, Heidelberg (2007)
16. Gavrilov, A.V., Lee, S.-Y.: Usage of hybrid neural network model MLP-ART for navigation of mobile robot. In: Huang, D.-S., Heutte, L., Loog, M. (eds.) ICIC 2007. LNCS (LNAI), vol. 4682, pp. 182–191. Springer, Heidelberg (2007)
17. Gavrilov, A., Lee, S.-Y.: Unsupervised Hybrid Learning Model (UHLM) as Combination of Supervised and Supervised Models. In: IEEE Int. Conf. SMC UK&RI, Dublin (2007)
18. Elman, J.L.: Distributed Representations, Simple Recurrent Networks, and Grammatical Structure. Machine Learning 7(2/3), 195–226 (1991)
19. Gavrilov, A.V.: Context and Learning based Approach to Programming of Intelligent Equipment. In: The 8th Int. Conf. on Intelligent Systems Design and Applications ISDA 2008, Taiwan, pp. 578–582 (2008)
20. Gavrilov, A.V.: New Paradigm of Context based Programming-Learning of Intelligent Agent. In: Proc. of 1st Workshop on Networked Embedded and Control System Technologies. In: Conjunction with 6th Int. Conf. on Informatics in Control, Automation and Robotics ICINCO 2009, Milan, pp. 94–99 (2009)

Histogram Based Color Object Classification by Multi-class Support Vector Machine

Tarik Veli Mumcu¹, Ibrahim Aliskan¹, Kayhan Gulez¹, and Gurkan Tuna²

¹ Yildiz Technical University 34349 Istanbul/Turkey

{tmumcu, ialiskan, gulez}@yildiz.edu.tr

² Trakya University, Vocational College of Technical Sciences,

Department of Computer Programming, Edirne/ Turkey

gurkantuna@trakya.edu.tr

Abstract. This work presents a histogram based color object classification by SVM for laboratory automation. In the laboratory environment, existing problem is the classification of color objects which is understood as blob like pictures by the system via a camera. This automated system is located at hospitals, blood banks where we introduce the system different blood samples for different research purposes. The blood samples for different research purposes are realized with different colors of tube caps. These caps constitute the main problem here since their images are often blob like pictures. The segmented, multi color cap pictures are investigated in this paper by SVM for color object classification. To validate the performance of the system with SVM method, its output also compared to the other classification methods. In the future work different color spaces will be incorporated with SVM for better color classification.

Keywords: Support vector machine (SVM), Color object classification, Blob-like feature extraction.

1 Introduction

Automated robot vision systems have been the subject of intensive research, and successful applications have been realized for the last two decades. Today there are still many potential research subjects in automated vision robot systems where the automated design, design process, the choice of learning and optimization techniques still the challenges are.

Besides these increasing the reliability and productivity is another challenge. In the last decade particular efforts in which the industrial vision systems and the general multi sensor system design were the emphasis have been made.

Today color classification based on the Support Vector Machine Method is an application field with many examples. One of them is vehicle color classification based on the Support Vector Machine [10]. In this work the outdoor vehicle images are converted into HSV color model based image to eliminate distortions. A feature vector which based on a two dimensional histogram (hue-saturation pairs) is extracted and SVM is applied to classify the feature vectors to five different vehicle color

classes. Another application SVM for color Classification [11] is used for soccer robots. In this work one-class SVM is used for each color and interested in to treat each color without regard to the location and shape of the other colors.

Thus, the application [12] which is considered for face recognition and skin color is quite interesting since it uses directly the YCbCr color space, and this work considers SVM in terms of loop arranged, symmetrical divided classes furthermore independent component analysis is used for feature extraction. Moreover the work [13] based on lip color of a single person is quite attractive since it draws SVM-Histogram attention to the medical side like in our work. This study [13] concentrates on color of a lip to examine if stomach or spleen of a patient is healthy or not.[14] deals with eye detection problem uses YCbCr color space, PCA for dimensionality reduction, 2D haar wavelets to represent multi-scale image and finally SVM to point the center of an eye. [15] is the other interesting multi-class SVM work which examines the skin color information to detect and recognize the faces. This work uses Mahalanobis distance to extract the features and creates eigenfaces space.

In our work first data classes are constituted for different types of problems from easy to hard. These data sets can be seen below. Then we have computed the feature vector with using HSV color spaces and histogram are used as in the first reference. The application area, the different data sets, and using blob like pictures differs us from the most of the other works.

2 Data Sets

Today in automated medical labs where blood samples or different types of specimen are used for different purposes require reliable recognition process. In industrial environment different automated vision systems can be found for this purpose. The tubes used in labs containing blood samples or different specimen are need to be classified in a fast, reliable process. In order to realize this process the data sets used to illustrate different types of tube caps and different types of data classes are T, TT, SC, SH, GL, respectively.

T: Multi color caps with blob like color appearance, with obvious large variations of different color segment sizes, representing the same type.

TT: Multi color caps with blob like color appearance, with obvious large variations of different color segment sizes, representing the same type.

SC: Single color caps with blob like color appearance, with obvious large variations of different color segment sizes, representing the same type.

SH: Multi color caps with blob like color appearance, with obvious large variations of different color segment sizes, representing the same type.

GL: Single color caps with blob like color appearance, with obvious large variations of different color segment sizes, representing the same type.

All these data sets' samples have three features of the projected tube type in each class. These are minimum, maximum, and mean value of the picture which examples the tube on a numeric axis. Different color(s) tube caps with different sizes make one data set differ from the other one. The sets can be seen on Table.1.

Table 1. Data Sets

Data	#of data samples	#of classes	#of features
T	860	48	3
TT	860	43	3
SH	860	33	3
SC	360	15	3
GL	260	10	3

All the features represented in this data set are minimum, maximum, and mean values of the multi-colored blob like, color segmented tube pictures which are obtained via a camera from the automated system.

3 SVM and Other Methods Used in This Work

SVM which was developed by Vapnik [2] is one of the very popular methods which can be applied to many application fields. In the last decade, SVM is continuously receiving more attention both research and application with efficient outcomes. SVM uses the well-known structural risk minimization in statistical theory by introducing an optimal hyper plane in the feature space, and then forms the problem as a quadratic programming function to find a single solution. SVM has also been recently proposed as a very effective method for general purpose pattern recognition.

SVM is also the newest supervised machine learning technique. A detailed reference on SVM can be found in [8]. The structural risk minimization makes SVM different from the other supervised machine learning methods. For an unknown distribution function it is not possible to compute the expected the risk. Instead the empirical risk is computed. The key idea of the empirical risk is if empirical risk converges to the expected risk, then the minimum of the empirical risk may converge to the minimum of the expected risk, however a small value of the empirical risk expresses a small value of the expected risk in an indirectly way. That's why Structural Risk Minimization (SRM) [9] minimizes the empirical risk and the VC dimension at the same time. VC dimension provides bounds on error, which depend on both empirical risk and capacity of the function class.

Probabilistic Neural Networks (PNN) [3, 4] developed by Donald Specht provides a solution to classification problems using statistical Bayes strategy. This strategy primarily forms the problem based on a like-hood of events (input vectors) and combines it with a prior information to enhance the prediction. It is also possible to bring the learned pattern together with relative frequency (a prior probability) of each category to estimate and define the most likely class of an input vector. In implementation of PNN the sigmoid function is replaced with an exponential function to compute nonlinear decision boundaries. The network can also implement Parzen window as a different form of the activation function in pattern unit. Combining

Parzen window with PNN makes the user to define a classifier which minimizes the expected risk of wrongly classifying object.

Furthermore, instance based learning algorithms are also known as lazy learning algorithms. One of the most well known instance based learning algorithms is nearest neighbours. k-Nearest Neighbours (kNN) [6] and (RNN) [7] are two examples of this class of methods. Nearest Neighbour algorithms based on the instances in a data set which are close to each other have similar properties than the others. When instances are defined with a classification label, then the value of the label of a classified instance can be determined by observing the class of its nearest neighbours.

Once SVM is compared with kNN and other instance based learning algorithms as a classification method it has the following advantages. SVM as a supervised classifier suggest us more accuracy in general rather than kNN. The speed of classification in SVM is faster than kNN. It has more tolerance to missing values, more tolerance to irrelevant and highly interdependent features. It can deal with noise in a better way. However SVM has also the following disadvantages against kNN: The speed of learning is not faster, the attempt for incremental learning is not better than kNN. Detailed comparison between instance learning and support vector machines can be found in [2, 5].

Thus, the main advantage of SVM regard to PNN or Neural Networks (NN) in general is it can deal with irrelevant features better than NN. These both algorithms show similar performance in case of tolerance to noise, highly interdependent features, and speed of classification. In general accuracy SVM gives better results than Neural Networks [2, 5].

Thus, the new data sets are converted to the MATLAB environment and operated by data normalization and split process, later introduced to SVM classifier.

4 Results of the Data Classification

In data conversion, first data set (i.e. T) is converted from .txt file to .mat file for MATLAB. Data set is normalized and the numbers of classes inside the data set are found. Inside the classes, data is shuffled and splitted into two groups (train-test) for the given percentage ratio.

In SVM classifier, first the data is mapped into a higher dimensional space with RBF kernel and classified via soft margin optimization. Here σ is for the RBF kernel, C (penalty term) for the soft margin optimization. L_2 norm is used in the soft margin objective function. For each data set, the data is classified for fifteen times and the classification result is given as the mean value of these fifteen data classifications (Table 3).

In Table 2, the data sets are also processed with other classification methods to confirm the results of SVM classifier. Here k-NN represents k Nearest Neighbours classifier, RNN is for Reduced Nearest Neighbours classifier, PNN is for Probabilistic Neural Networks classifier, and SVM is for Support Vector Machine classifier.

More information about the process can be found in Section 5.

Table 2. Data Classification Rate (%) for Different Types of Data Classifiers

DATA	k-NN (k=5)	PNN T=1,σ= 0.1	RNN	SVM
T	64.33	67.84	69.74	74.61
TT	74.51	64.73	70.94	78.43
SH	93.42	89.78	92.28	94.66
SC	100	100	100	100
GL	100	100	100	100

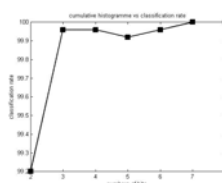
Table 3. Data Classification Rate (%) for SVM Classifier

Data	RBF (σ)	Penalty term (C)	Min-Max Cl. (%)	S.D.	Data split (%)	Cl. Rate (%)
T	0.006	14	68.43-77.64	10.3	50	74.61
TT	0.002	14	71.47-80.63	4.74	70	78.43
SH	0.002	14	89.45-95.66	4.4	70	94.66
SC	0.006-0.01	14-5	100-100	0	50	100
GL	0.006-4	14-1	100-100	0	50-20	100

On Table 3 the results are given for SVM data classification (the best classifier of the all methods used in this work). RBF column is for the RBF kernel to map the data set into a higher dimensional space. Penalty term (C) is for the soft margin optimization which is also be interpreted as the upper bound of the constraints in quadratic programming. Since each data classification is repeated for fifteen times in each data set, Min-Max classification rate represents the minimum and the maximum of these classifications. S.D. is for the standard deviation in statistical annotation, Data split is the percentage ratio of the training data among the whole data, and finally classification rate (Cl. Rate %) is the mean value of the fifteen data classifications for each data set. On some columns the parameter range shows the parameter sensitivity for the same classification rate. In other words between these ranges of the parameters the classification rate does not change.

Thus, as from the Table.2, it can easily be seen that multi-class SVM classifier is used in this method. This is realized with the help of error correct output codes. For this SVM classifier we have tried three different codes at the simulation stages (15-bit, 31-bit, 63-bit).

On the figures (Fig.1, Fig.2) examples of the data sets and example of the tube caps used in the data set can be seen. Fig.3 is used to explain that for low numbers of the multi SVM class classification, the bit numbers of the cumulative histograms does not play a vital role.

**Fig. 1. -2. -3.** An example to the tube caps in the data set SC. Single color tube- An example to the data set T. Multi color tube cap-Cumulative histogram bit sensitivity vs. classification rate.

5 Definitions of the Processes

On the figure 4 and 5 the three steps of the whole process can be seen. Here for the best classifier SVM multi class it is explained how we constitute the net and derive the annotations. The pictures taken by the camera are accepted as raw data.

Feature extraction: The data set is converted to the HSI space. Then the features are extracted by the cumulative histograms. Then we visualize the data set to understand to see how hard the problem is. The extracted features to the data set are recorded as a .txt file.

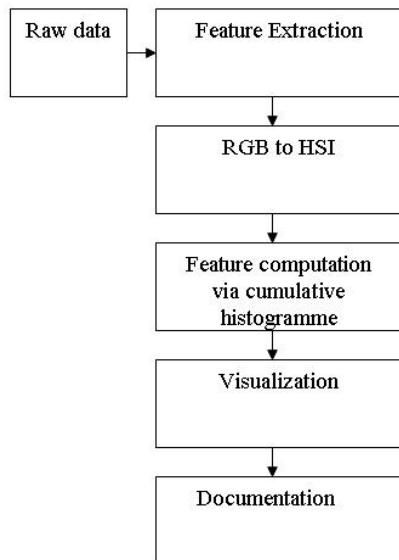


Fig. 4. Process-1. The picture taken from the tube cap via a camera is accepted as the raw data.

Data Conversion: Recorded .txt file is converted to a .mat file so that it can be processed in the MATLAB environment. Data is normalized to the (0-1) zone. All unique classes are found in the date set and they are processed with random permutation so that all data sets can be reorganized. Then the data sets are splitted in to the train and test so that it can be introduced forward to the multi class SVM classifier in order to first train the SVM net and then test it. This procedure can be seen on the figure 5.

Multi Class SVM Classifier: (Figure 5-second part) Net is constituted by the ECOC codes [1] for three different codes bits (15, 31, and 63) in order to validate the performance of the output. The net is trained with train data which is formerly splitted from the whole data.

Then it is tested by test data and the statistical annotations are derived in terms of kernel parameter for RBF kernel, standard deviation (S.D.), minimum and maximum classification rates inside the fifteen simulation process, the mean value of the fifteen different classification rates as the final classification rate (%Cl.).

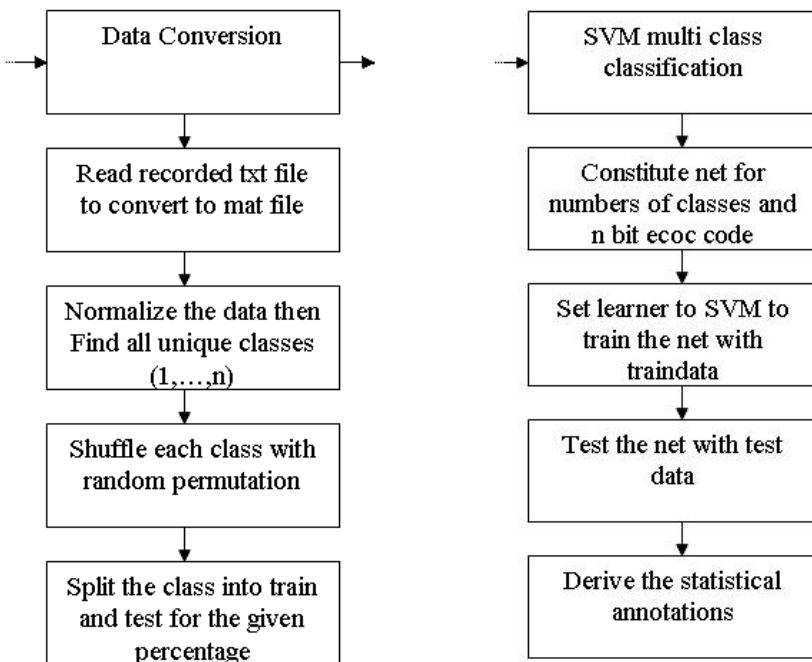


Fig. 5. Process-2. Data conversion. Process-3. The multi class SVM classifier.

6 Conclusion and Outlook

In this work a medical robot vision system, where the sample tube cap types and colors are still challenges, is enhanced with SVM method. The classifications are done for SVM for fifteen times for the each data set and the statistical annotations are also given to confirm SVM as a better classifier. SVM as a classifier is also compared to the other classifiers (k-NN, RNN, PNN). In the future our aim is to research these sample tube cap challenges with improved color features to reach better classification rate.

Acknowledgement. This study is supported by the Yildiz Technical University with the project number 2010-04-02-KAP05 and project number: 2010-04-02-ODAP1.

References

1. Thomas, G., Ghulum, B.: Solving multiclass learning problems via Error Correcting Output Codes (ECOC). *Journal of Artificial Intelligence Research* 2, 263–286 (1995)
2. Kotsiantis, S.B.: Supervised Machine Learning: A review of Classification Techniques. *Informatica International Journal of Computing and Informatics* (2007)
3. Donald, F.: Probabilistic Neural Networks for Classification, Mapping or Associative Memory. In: *IEEE International Conference on Neural Networks* (1988)

4. Donald, F.: Probabilistic Neural Networks And The Polynomial Adaline as Complementary Techniques for Classification. *IEEE Transactions on Neural Networks* I(I) (March 1990)
5. Kotsiantis, B., Zaharakis, I.D., et al.: A Review of Classification and Combining Techniques. *Artif. Intell. Rev.* 26, 159–190 (2006)
6. Cover, T., Hart, P.: Nearest Neighbor Pattern Classification. *IEEE Transactions on Information Theory* (1967)
7. Gates, G.: The Reduced Nearest Neighbour Rule. *IEEE Transactions on Information Theory* (May 1972)
8. Burges, C.: A Tutorial on Support Vector Machines for Pattern Recognition. *Data Mining and Knowledge Discovery* 2(2), 1–47
9. Vapnik, V.: *Statistical Learning Theory*. Wiley, Chichester (1998)
10. Vehicle, Color Classification Based on The Support Vector Machine Method
11. Quinlan, M.: Application of SVMs for Color Classification and Collision Detection with AIBO Robots. In: *Advances in Neural Information Processing Systems*, NIPS (2004)
12. Shu, S., Luo, J., et al.: Face Recognition Based on Skin Color Information and Support Vector Machine. In: *2010 Sixth International Conference on Natural Computation (ICNC)* (2010)
13. Zheng, L., Li, X., et al.: 2010 3rd International Congress on Lip Color Classification Based on Support Vector Machine and Histogram Image and Signal Processing (CISP) (2010)
14. Chen, S., Liu, C.: 2010 Fourth IEEE International Conference on Eye Detection Using Color Information and A New Efficient SVMBiometrics: Theory Applications and Systems, BTAS (2010)
15. Shu, S., Luo, J.: 2010 5th International Conference on Color Images Face Recognition Based on Multi-classification Support Vector Machine Computer Science and Education (ICCSE) (2010)

Tracking Objects Using Orientation Covariance Matrices

Peihua Li and Qi Sun

School of Computer Science and Technology, Heilongjiang University, Harbin, China

Abstract. This paper presents a novel model, called orientation covariance matrices, to represent the object region and introduces a steepest descent method for object tracking. This model partitions the gradient orientation space of joint color channels into subspaces (bins), and computes the covariance matrix of image features in every bin. In the model a feature point does not belong exclusively to one bin; instead, it makes contributions to several neighboring bins. This is accomplished by introducing the cosine function for weighting the gradient components of feature vectors. The weighting function helps to alleviate the effect of errors in the computation of gradients induced by noise and illumination change. We also introduce a spatial kernel for emphasizing the feature vectors which are nearer to the object center and for excluding more background information. Based on the orientation covariance matrices, we introduce a distance metric and develop a steepest descent algorithm for object tracking. Experiments show that the proposed method has better performance than the traditional covariance tracking method.

Keywords: Image processing, object tracking, orientation covariance matrices, steepest descent.

1 Introduction

Covariance tracking was first proposed by Porikli et al. [1]. One of its benefits is combination of spatial and appearance properties such as color and image gradients as well as their statistics. In addition, it is very compact to represent the object region by a covariance matrix of image features. Because the covariance matrices thus obtained are generally symmetric positive definite that produce a connected Riemannian manifold, theory of Lie group and Lie algebra is used to evaluate distances between these matrices and compute the matrices mean.

In the past years, the methodology of covariance tracking has gained interests of many researchers. Rather than using affine invariant Riemannian metric [2], Li et al. [3] adopted Log-Euclidean Riemannian metric [4] for measuring the distance between covariance matrices and presented an incremental subspace learning algorithm in Log-Euclidean Riemannian space for model representation and update. Computation of matrices mean in affine invariant Riemannian metric is time consuming, Wu et al. [5] addressed this problem by proposing an incremental covariance tensor learning. These matrices form a Lie group and the

corresponding theory is thus used for distance evaluation. Karasev et al. [6] presented a tracking method using kernel-based high-dimensional histogram, which estimated the first-order moment (mean vector) and second-order moment (covariance matrix) of features and used a weighted L2-norm as the distance metric. To describe the object region more effectively, Tuzel et al. [7] built five covariance matrices from overlapping regions of an object image for object detection. Representing an object region with both a mean vector and a covariance matrix, Gong et al. [8] developed a novel descriptor called shape of signal probability density (SOSPD). They constructed a novel matrix notation by considering both the mean vector and covariance matrix of image features.

Motivated by Histogram of Oriented Gradients (HoG) [9], we presented orientation covariance matrixes for region description. Specifically, we partition the joint gradient orientation space of color channels into subspaces (bins), construct a smooth function weighting the gradient components in the feature vectors, and compute the covariance matrix in every bin. Different from the orientation histogram, a feature point does not belong exclusively to one bin. Instead, it makes contributions to several neighboring bins by evaluating the difference between its orientation angle and bin centers. This helps alleviate the errors in computation of image gradient due to noise or illumination changes. We further introduce a distance metric between target and candidate covariance matrices and use a steepest descent method for object tracking.

2 Traditional Covariance Matrix Tracking

Let S be the target image of the width w and the height h . Let \mathbf{z} be the spatial coordinate of one point in S , and $\mathbf{D}(\mathbf{z}) = [R(\mathbf{z}) \ G(\mathbf{z}) \ B(\mathbf{z})]^T$ denotes the color vector of this pixel, where R, G, and B denote the component value of the three channels, respectively. The feature vector of this point is defined as

$$\mathbf{h}(\mathbf{z}) = \left[x \ y \ R(\mathbf{z}) \ G(\mathbf{z}) \ B(\mathbf{z}) \ R_x(\mathbf{z}) \ R_y(\mathbf{z}) \ G_x(\mathbf{z}) \ G_y(\mathbf{z}) \ B_x(\mathbf{z}) \ B_y(\mathbf{z}) \right]^T$$

where $R_x(\mathbf{z})$ and $R_y(\mathbf{z})$ represent the gradient in the direction x and y respectively in the R-channel, $G_x(\mathbf{z}), G_y(\mathbf{z})$ and $B_x(\mathbf{z}), B_y(\mathbf{z})$ have analogous meanings. In the rectangular region S , the covariance matrix of all the features can be computed as

$$\mathbf{M} = \frac{1}{wh} \sum_{\mathbf{z} \in S} (\mathbf{h}(\mathbf{z}) - \boldsymbol{\mu})(\mathbf{h}(\mathbf{z}) - \boldsymbol{\mu})^T \quad (1)$$

where $\boldsymbol{\mu}$ is the mean vector of the features. The covariance matrix \mathbf{M} is a symmetric, positive definite matrix. Its diagonal entries represent the variance of each component and the non-diagonal entries represent the correlations between different components.

Let $\mathbf{Y}_{\mathbf{u}}$ be the covariance matrix of the candidate region centered at \mathbf{u} . The distance between the two covariance matrices can be computed as [1]

$$\rho^2(\mathbf{M}, \mathbf{Y}_{\mathbf{u}}) = \sum_{k=1}^d \ln^2 \lambda_k(\mathbf{M}, \mathbf{Y}_{\mathbf{u}}) \quad (2)$$

The generalized eigenvalue $\lambda_k(\mathbf{M}, \mathbf{Y}_u)$ between \mathbf{M} and \mathbf{Y}_u satisfies $\lambda_k \mathbf{M} \mathbf{x}_k = \mathbf{Y}_u \mathbf{x}_k$, where \mathbf{x}_k denotes the generalized eigenvector and d is the dimension of feature vector. The matrices \mathbf{M} and \mathbf{Y}_u are generally symmetric and positive definite, and so the distance $\rho^2(\mathbf{M}, \mathbf{Y}_u)$ can be equivalently computed as [2]

$$\rho^2(\mathbf{M}, \mathbf{Y}_u) = \text{tr} \left[\log^2 (\mathbf{M}^{-\frac{1}{2}} \mathbf{Y}_u \mathbf{M}^{-\frac{1}{2}}) \right] \quad (3)$$

where tr denotes the matrix trace and \log denotes matrix logarithmic operation.

In [1], the exhaustive, local search is performed for object tracking. In each frame, a search window is first determined based on the tracking result of the last frame. Next, in the search window the covariance matrix of every possible position is computed and the one with the minimum distance is adopted as the tracking result in the current frame.

3 Orientation Covariance Matrices and Steepest Descent Method for Object Tracking

In this section we first introduce the spatial weight in the image feature representation. Then we present the novel covariance matrices based on orientation angle partition. Finally we give the corresponding tracking algorithm.

3.1 Spatial Weight in the Feature Vector

Instead of using the simple rectangle for representing the object region, we adopt the ellipse in describing the object shape. Let $\mathbf{u} = (x_c, y_c)$ be the object center, the object region is thus described by the following inequality:

$$\omega_{\mathbf{z}} = 1 - \frac{(x - x_c)^2}{(w/2)^2} - \frac{(y - y_c)^2}{(h/2)^2} \leq 1 \quad (4)$$

where w and h denote the width and height of the ellipse, respectively. This representation has the benefit of excluding more background information.

In practice the points nearer to the object center are often more credible and those farther become less reliable. Therefore, we introduce the spatial weight into the image feature that emphasizes the points nearer to the object center. The feature vector is thus defined as

$$\mathbf{h}(\mathbf{z}) = \omega_{\mathbf{z}} \begin{bmatrix} x & y & R(\mathbf{z}) & G(\mathbf{z}) & B(\mathbf{z}) & R_x(\mathbf{z}) & R_y(\mathbf{z}) & G_x(\mathbf{z}) & G_y(\mathbf{z}) & B_x(\mathbf{z}) & B_y(\mathbf{z}) \end{bmatrix}^T \quad (5)$$

Hence, in the computation of the covariance matrix the feature points do not play equal roles as in the traditional method. Rather, different feature points make varying contributions: the points nearer to the object center play more important roles than those farther.

3.2 Orientation Covariance Matrices

The joint gradient orientation space of R, G, and B channels is partitioned into small subspaces. By uniformly dividing the period $[0, 2\pi]$ of angle into n subintervals for each color channel, the orientation space is partitioned into n^3 bins. First we compute the gradient and orientation angles of every pixel in the three color channels. According to the orientation angles, we can determine to which bin the feature point belongs and then compute the covariance matrix corresponding to one bin. However, because of noises or illumination variation, the computed orientation angles may have errors, the above method can not deal with this case. Our idea is that a feature point does not contribute exclusively to one bin. Rather, it has contributions to several neighboring bins.

For clear illustration of the idea, we consider here only the joint orientation space of two color channels, say, R and G channels. Extension of the method to three channels is straightforward. Let \mathbf{z} be the spatial coordinate of one pixel in the image, and $\theta_R(\mathbf{z})$ and $\theta_G(\mathbf{z})$ be the orientation angles in the R- and G-Channel, respectively. Below we will explain how to determine to which bins this feature point will make contributions and what the contributions will be.

We divide the period $[0, 2\pi]$ into N subintervals and let $\theta_n = (2n+1)\pi/N$ be the centers of subinterval n , $n = 0, 1, \dots, N-1$. We determine the subintervals n for which

$$|\theta_R(\mathbf{z}) - \theta_n| < \pi/2 \quad (6)$$

There are a total of $N/2$ subintervals satisfying Eq. (6) which are denoted by $p_0, p_1, \dots, p_{N/2-1}$. Similarly, for the G-channel, we can determine the subintervals $q_0, q_1, \dots, q_{N/2-1}$ for which $|\theta_G(\mathbf{z}) - \theta_n| < \pi/2$. Then we get the final bins in the joint orientation spaces to which the point makes contributions as follows:

$$k_{p_i, q_j} = p_i * N + q_j \quad (7)$$

where $i, j = 0, 1, \dots, N/2 - 1$.

Fig. 1 illustrates how to determine the bins to which one point \mathbf{z} makes contributions when $N = 4$ and some θ_R and θ_G . In figure 1(a), the shaded subintervals are those to which the point makes contributions in the R-channel for the given θ_R . Likewise, the shaded subintervals in figure 1(b) show those that the point contributes to for the given θ_G in the G-channel. The figure 1(c) shows the bins to which the point contributes in the joint orientation space of the R- and G-channels.

We use the cosine function to measure the contribution values of the feature point to the corresponding bins. Define the weight function $\omega_{\theta_R(\mathbf{z})} = \cos(\theta_R(\mathbf{z}) - \theta_{p_i})$, $\omega_{\theta_G(\mathbf{z})} = \cos(\theta_G(\mathbf{z}) - \theta_{q_j})$. The novel feature vector that reflects the contribution of the point \mathbf{z} contributes to the bin k_{p_i, q_j} (k for short) has the following form:

$$\mathbf{g}_k(\mathbf{z}) = \omega_{\mathbf{z}} \left[x \ y \ R(\mathbf{z}) \ G(\mathbf{z}) \ B(\mathbf{z}) \ \omega_{\theta_R(\mathbf{z})} R_x(\mathbf{z}) \ \omega_{\theta_R(\mathbf{z})} R_y(\mathbf{z}) \right. \\ \left. \omega_{\theta_G(\mathbf{z})} G_x(\mathbf{z}) \ \omega_{\theta_G(\mathbf{z})} G_y(\mathbf{z}) \ B_x(\mathbf{z}) \ B_y(\mathbf{z}) \right]^T \quad (8)$$

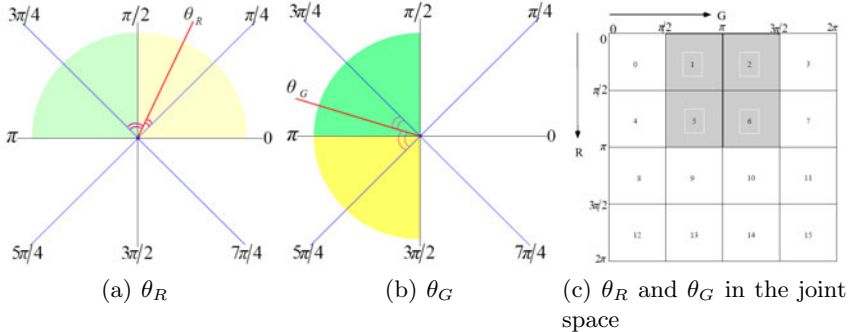


Fig. 1. Illustration of the bins to which the point \mathbf{z} makes contributions in the joint orientation space

Let $T_k, k = 0, 1, \dots, K - 1$, be the set of points for which

$$T_k = \{ \mathbf{z} \mid |\theta_R(\mathbf{z}) - \theta_k| < \pi/2 \text{ and } |\theta_G(\mathbf{z}) - \theta_k| < \pi/2 \} \quad (9)$$

where $K = N^2$ and k denotes the one dimensional index of the bins in the joint orientation space. Let $\mu_k = \sum_{\mathbf{z} \in T_k} \mathbf{g}_k / |T_k|$, where $|T_k|$ is the number of points in the set T_k . The covariance matrix corresponding to bin k is computed as

$$\mathbf{M}_k = \frac{1}{|T_k|} \sum_{\mathbf{z} \in T_k} (\mathbf{g}_k(\mathbf{z}) - \boldsymbol{\mu}_k)(\mathbf{g}_k(\mathbf{z}) - \boldsymbol{\mu}_k)^T \quad (10)$$

where $k = 0, 1, \dots, K - 1$.

3.3 Tracking with the Steepest Descent Method

We perform object tracking based on the steepest descent method proposed by Tyagi et al. [10]. In our method, the distance between the target and the candidate is defined as follows:

$$f(\mathbf{u}) = \frac{1}{K} \sum_{k=0}^{K-1} \text{tr} \left[\log^2 (\mathbf{M}_k^{-\frac{1}{2}} \mathbf{Y}_{\mathbf{u}}^k \mathbf{M}_k^{-\frac{1}{2}}) \right]$$

where \mathbf{M}_k , \mathbf{Y}_k^u denotes the covariance matrix corresponding to bin k in the target and candidate regions, respectively. Next we compute the gradient of $f(\mathbf{u})$

$$\nabla f(\mathbf{u}) = \frac{1}{K} \left[\sum_{k=0}^{K-1} \partial_x^k f(\mathbf{u}), \sum_{k=0}^{K-1} \partial_y^k f(\mathbf{u}) \right] \quad (11)$$

We follow [10] to calculate $\partial_x^k f(\mathbf{u})$ and $\partial_y^k f(\mathbf{u})$ as:

$$\begin{aligned}\partial_x^k f(\mathbf{u}) &= \text{tr}[2 \log P_{\mathbf{u}}^k (P_{\mathbf{u}}^k)^{-1} \mathbf{M}_k^{-\frac{1}{2}} \partial_x^k \mathbf{Y}_{\mathbf{u}} \mathbf{M}_k^{-\frac{1}{2}}] \\ \partial_u^k f(\mathbf{u}) &= \text{tr}[2 \log P_{\mathbf{u}}^k (P_{\mathbf{u}}^k)^{-1} \mathbf{M}_k^{-\frac{1}{2}} \partial_u^k \mathbf{Y}_{\mathbf{u}} \mathbf{M}_k^{-\frac{1}{2}}]\end{aligned}$$

where $P_{\mathbf{u}}^k = \mathbf{M}_k^{-\frac{1}{2}} \mathbf{Y}_{\mathbf{u}}^k \mathbf{M}_k^{-\frac{1}{2}}$, $\partial_x^k \mathbf{Y}_{\mathbf{u}} \approx 0.5 \log_{\mathbf{Y}_{\mathbf{u}}^k | x-dx, y} (\mathbf{Y}_{\mathbf{u}|x+dx,y}^k) / dx$, and $\partial_y^k \mathbf{Y}_{\mathbf{u}} \approx 0.5 \log_{\mathbf{Y}_{\mathbf{u}}^k | x, y-dy} (\mathbf{Y}_{\mathbf{u}|x,y+dy}^k) / dy$. Based on the steepest descent method, the new position \mathbf{u}^{j+1} can be computed by the following iterative equation:

$$\mathbf{u}^{j+1} = \mathbf{u}^j - \eta^j \nabla f(\mathbf{u}^j) \quad (12)$$

where η^j is the learning rate. The algorithm iterates until convergence. For details on how to select the parameter η^j refer to [10].

4 Experiments

The proposed covariance tracking method is implemented on a PC with Intel® Core™ 2 1.93GHz CPU and 1GB Memory. We use Visual C++ 2005 development environment for programming. The initialization is given manually which includes the center, height and width of the object. We partition the joint orientation space of R and G channels and set $n = 4$ in constructing the orientation covariance matrices. The proposed method is compared with the traditional covariance tracking method [1].

The first sequence, taxi sequence, was taken by a hand-held camera on the road (300 frames, size: 352×288 pixels). In the sequence, there are motion blurs because of camera motion and partial occlusion. Fig. 2 shows some typical tracking results, from left to right, frames 1, 63, 209 and 283. Table II gives the average distance errors and tracking time between the two approaches. We can see that the proposed method is significantly better than the traditional one in terms of tracking accuracy and time.

The second sequence, customer sequence, was taken in a shop lobby (383 frames, size: 384×288 pixels). In this sequence, there occurs occlusion around frame 102 and there are illumination changes along the lobby. Frames 1, 109, 127 and 383 are chosen to present the typical tracking results. As shown in Fig. 3 and Table II, the proposed method has smaller error and less tracking time than the traditional covariance tracking.

The last sequence, passenger sequence, was taken in the train station (90 frames, size: 720×526 pixels). In this sequence, the background has similar color with the object. The object is lost from frame 29 using the traditional covariance tracking. In contrary, the proposed approach can follow the object accurately. Some typical tracking results are shown in Fig. 4 and tracking error and time are given in Table II. The comparison shows that the orientation covariance matrices have better discriminative (representational) capability than the traditional covariance matrix.

Currently we only consider the joint orientation space of R and G channels. Note that the consideration of all three channels may be helpful for better discriminability of the model. However, it may lead to a larger number of covariance matrices and higher computational cost.



Fig. 2. Tracking results in the taxi sequence with the traditional covariance tracking method (top) and our proposed one (bottom)



Fig. 3. Tracking results in the customer sequence with the traditional covariance tracking method (top) and our proposed one (bottom)

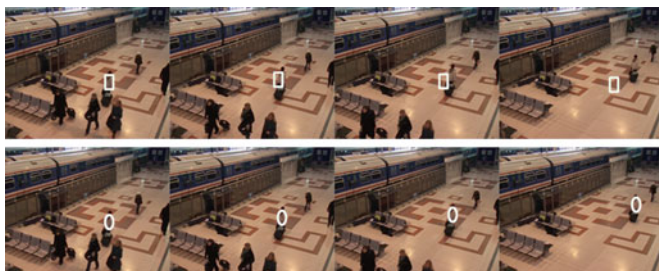


Fig. 4. Tracking results in the passenger sequence with the traditional covariance tracking method (top) and our proposed one (bottom)

Table 1. The average distance errors (mean \pm std) and tracking time

Image sequence	Method	Distance error (pixels)	Time (ms)
Taxi Sequence	Traditional method	10.93 ± 4.55	405.33
	Proposed method	5.39 ± 2.17	122.45
Customer Sequence	Traditional method	8.05 ± 5.46	178.94
	Proposed method	1.75 ± 0.89	130.71
Passenger Sequence	Traditional method	N/A	N/A
	Proposed method	4.01 ± 2.77	193.34

5 Conclusion

We present a model of orientation covariance matrices to represent image region and develop a steepest descent algorithm for object tracking. Experiments show that the proposed method has better tracking performance than the traditional method while having less tracking time thanks to the steepest descent algorithm. Future research concerns evaluation of the proposed method in extensive image sequences and comparisons with other state-of-the-art covariance tracking methods.

Acknowledgments. The research was supported by the National Natural Science Foundation of China (60973080, 61170149), Program for New Century Excellent Talents in University from Chinese Ministry of Education (NCET-10-0151), Key Project by Chinese Ministry of Education (No. 210063). It was also supported in part by the Program for New Century Excellent Talents of Heilongjiang Province (1153-NCET-002) and High-level professionals (innovative teams) of Heilongjiang University (Hdtd2010-07).

References

1. Porikli, F., Tuzel, O., Meer, P.: Covariance Tracking Using Model Update based on Lie Algebra. In: Proc. of IEEE Conf. on Computer Vision and Pattern Recognition, pp. 728–735 (2006)
2. Förstner, W., Moonen, B.: A Metric for Covariance Matrices. Technical Report. Dept. of Geodesy and Geoinformatics, Stuttgart University (1999)
3. Li, X., Hu, W., Zhang, Z., et al.: Real-time Visual Tracking via Incremental Covariance Tensor Learning. In: Proc. of IEEE Conf. on Computer Vision and Pattern Recognition, pp. 1–8 (2008)
4. Arsigny, V., Fillard, P., Pennec, X., Ayache, N.: Geometric Means in a Novel Vector Space Structure on Symmetric Positive-Definite Matrices. SIAM J. Matrix Analysis Applications 29(1), 328–347 (2006)
5. Wu, Y., Cheng, J., Wang, J.Q., Lu, H.Q.: Visual Tracking via Incremental Log-Euclidean Riemannian Subspace Learning. In: Proc. of Int. Conf. on Computer Vision, pp. 1631–1638 (2009)
6. Karasev, P., Malcolm, J.G., Tannenbaum, A.: Kernel-based High-dimensional Histogram Estimation for Visual Tracking. In: Proc. of Int. Conf. on Image Processing, pp. 2728–2731 (2008)
7. Tuzel, O., Porikli, F., Meer, P.: Region Covariance: A Fast Descriptor for Detection and Classification. In: Leonardis, A., Bischof, H., Pinz, A. (eds.) ECCV 2006. LNCS, vol. 3952, pp. 589–600. Springer, Heidelberg (2006)
8. Gong, L., Wang, T., Liu, F.: Shape of Gaussians as Feature Descriptors. In: Proc. of IEEE Conf. on Computer Vision and Pattern Recognition, pp. 2366–2371 (2009)
9. Dalal, N., Triggs, B.: Histograms of Oriented Gradients for Human Detection. In: Proc. of IEEE Conf. on Computer Vision and Pattern Recognition, pp. 886–893 (2005)
10. Tyagi, A., Davis, J.W., Potamianos, G.: Steepest Descent for Efficient Covariance Tracking. In: IEEE Workshop on Motion and Video Computing, pp. 1–6 (2008)

Action Recognition via an Improved Local Descriptor for Spatio-temporal Features

Kai Yang¹, Ji-Xiang Du^{1,2}, and Chuan-Min Zhai¹

¹ Department of Computer Science and Technology, Huaqiao University, Xiamen 361021

² Institute of Intelligent Machines, Chinese Academy of Sciences, Hefei, Anhui 230031

{beyondyangkai, jxdu77, cmzhai}@gmail.com

Abstract. This paper presents and investigates an improved local descriptor for spatio-temporal features on action recognition. Follow the idea of local spatio-temporal interest points on human action recognition, we develop a memory-efficient algorithm based on integral videos. The contribution of our job is we use the SURF descriptors on cuboids to speed up the computation especially for the integral video and improve the recognition rate. We present recognition results on a variety of dataset such as YouTube and KTH, compared to previous work, the results showed that our algorithm is more efficient and accurate compared with the previous work.

Keywords: action recognition, spatio-temporal features, cuboids, SURF.

1 Introduction

It's a challenging job to learning actions in uncontrolled video data such as movies or internet videos. Too much variation such as the camera ego-motion, shot boundaries, motion blur and interlacing have a bad effect on the detection and recognition. More and more growing amount of video data has increased from 6h in 2007 to 20h in 2009(+330%)[2] , but many work still use simplistic video data, no clutter, simple background, artificial actions etc. For the future application in our life such as video surveillance, human-computer interfaces, we should learn the action from the uncontrolled video. In this work, we develop a general framework for describe the detected interest points based on cuboids and SURF, which was proposed by Piotr Dollar[3] and Herbert Bay[4]. Consider some obvious difficulties faced in the action recognition, the cuboids inspired by the object recognition which relays on sparsely detected features. It has proved that such approaches can be robust to pose variation, image clutter and some imprecise nature of the feature detectors.

We propose to characterize the action in a single image and location in 3D space (Fig.1). The interest points are detected by cuboids on the crucial parts. A behavior can be fully described in terms of the cuboids type and locations of the interest points. And we can discriminate the different actions by the type of the description of the rich features.

The difference between object recognition[5] and video analysis is the dimensions form 2D to 3D. The additional dimensional is time, so we can deal with it independently. According to Piotr Dollar's[3] idea, direct 3D counterparts are inadequate for detection of

spatio-temporal feature points, we extracted the cuboids from the video (Fig.2), and cluster them in some prototypes. So the information of the behavior is characterized by the location and the prototypes of cuboids.

Though such a representation is sufficient for recognition and robust with the variations, but the computation of extracting cuboids is time consuming.



Fig. 1. (a)The interest points detected shown on a single image. (b)Visualization in the 3D space of the behavior handclapping on KTH. Because of the big mount points of the uncontrolled video, it's difficult to see the details of the points very clearly. The distribution of the interest points depends on different behaviors.

1.1 A Brief Introduction of Related Works

We have explained the difficulty in action recognition in section 1. There is no prior knowledge about human positioning nor any of its limbs is given in a video. Some surveys on action recognition and analysis include Weinland[6], Poppe[7] recently.

For the traditional methods, most of them based on the holistic human model, such as time templates[8], it uses the human shape masks and silhouette information to represent the body, and optical flow[9] formed a good tracking framework, people want to track the person first based a pre-defined feature. It needs to extract the contours of the person in video first, such as background subtract, and the time series of the features provides a descriptor that can be used in a general recognition framework.

There are some faults by this method in an uncontrolled video. First, it's not an easy job to extract the person especially on the confused background. Second, it's very difficult to know the location of the person. So the local space-time features[2] are applied on the video to character the shape and motion information on a local region. Local features provide an independent way to represent the events by the spatio-temporal shifts and scales which can be good at dealing with the confused background.

1.2 Spatio-temporal Interest Points

The spatio-temporal interest points[10] methods was applied on human action recognition for the last few years. Laptev use sparsely detected spatio-temporal features for recognition used the feature detector by harris3D[11]. He extends the harris2D detect on image to 3D videos, and the recognition result made a good performance.

In Piotr's paper, the interest point can be detected by the Gauss filter on the spatial dimensions and Gabor filter on the temporal dimension. And the descriptor of the cuboids can be gradient and optical flow, PCA-SIFT[12] etc.

1.3 Structure of the Paper

The structure of the paper is as follows. In section 2 we describe the interest detector proposed by Piotr[3], we talk about the improved cuboids description compared to cuboids. We showed the types of the improved cuboids. In section 3, we do some experiments on the various datasets. And in last section part, we present a detailed comparison of the various datasets with the state-of-art level on the efficiency and accuracy.

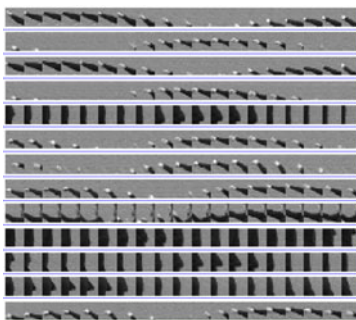


Fig. 2. The cuboids extracted from the video clips. It shows that analogous interest points are clustered together.

2 Improved Algorithm

We use the interest points detector proposed by Piotr. A method is using a response function, which is calculated at every location in the image and feature points correspond to local maxima. A general way to get the interest points in spatial domain is the detection of corners. Another common way is to get the response of the value by the filter, such as the Laplacian of Gaussian(LOG). The response of the function is showed in Fig.4.

Feature Detector. A lot of approaches for interest point detection[13], such as harris corners, LOG, SIFT. Gradient vectors are detected by taking the first order derivatives of a smoothed image which is showed in formula 1.

$$L(x, y, \sigma) = I(x, y) * g(x, y, \sigma) \quad (1)$$

g is the Gaussian smoothing kernel and σ controls the spatial scale at each point. Another common approach of the detector is the LOG of the response function. It is improved by Lowe to use for SIFT descriptor, called DOG, show in formula 2.

$$D = (g(.;k\sigma) - g(.;\sigma)) * I = L(.,k\sigma) - L(.;\sigma) \quad (2)$$

k is a parameter controls accuracy of the approximation. when k goes to 1, the DOG will similar with the LOG.

The harris2D detector is extends to 3D by Laptev and Lindeberg. The idea is based on the 3D Gradients, not only on x and y but also on t . In the spatial domain, showed in formula 3 and 4.

$$L^{\text{sp}}(x, y; \sigma_l^2) = g^{\text{sp}}(x, y; \sigma_l^2) * f^{\text{sp}}(x, y) \quad \mu^{\text{sp}}(\cdot; \sigma_l^2, \sigma_i^2) = g^{\text{sp}}(\cdot; \sigma_i^2) * \begin{pmatrix} (L_x^{\text{sp}})^2 & L_x^{\text{sp}} L_y^{\text{sp}} \\ L_x^{\text{sp}} L_y^{\text{sp}} & (L_y^{\text{sp}})^2 \end{pmatrix} \quad (3)$$

The g^{sp} is the Gaussian kernels with the variance σ_l^2 , given the observation σ_l^2 , the points can be found using a second moment matrix integrated over a Gaussian window. The spatio-temporal corner is an image region containing a spatial corner and the velocity is reversing its direction.

We extend the detection on image $I(x, y)$ to image series $I(x, y, t)$. So the detection is not only on the spatial x and y but on the temporal t . Because of the rarity of spatio-temporal corners, the useful features for object recognition may useless. Similar to the cuboids interest detector, we use the response function calculated by application of separable linear filters. We use the Gaussian smooth filter on the spatial domain and Gabor filter on the temporal domain which is proposed by Piotr. The response of the function can be seen in Fig. 2. The response function is as follows.

$$R = (I * g * h_{ev})^2 + (I * g * h_{od})^2 \quad (4)$$

Where g is the 2D Gaussian smoothing kernel applied only on the spatial dimensions, h_{ev} and h_{od} are a quadrature pair of 1D Gabor filters and applied only on temporally.

$$h_{ev}(t; \tau, \omega) = -\cos(2\pi\omega)e^{-t^2/\tau^2} \quad h_{ev}(t; \tau, \omega) = -\sin(2\pi\omega)e^{-t^2/\tau^2} \quad (5)$$

The experiments shows the detector can adapt variations in human pose, different environments and so on. But if the action is translating the response function will not detect the interesting points successfully.

2.1 Improved Cuboids Descriptor

After detecting the interest points we should design a good descriptor for the cuboids. In the previous work, a PCA-SIFT and optical flow are used in describe the detected points. But the computation speed is slow and the memory consumed is often out of memory. It is a restriction for the application on real-time in the future. So we proposed a speeded up method for the descriptor. Similar to the SIFT, SURF[4] is slightly different with SIFT. SIFT builds an image pyramids, filtering each layer with Gaussians of increasing sigma values and taking the difference. And the SURF creates a “stack” without two to one down sampling for higher levels in the pyramid resulting in images on the same resolution, it filters the stack using a box computation of rectangular box in near constant time.

First we also should do some transformations similar with the previous work. We normalization of the pixel values so that the descriptor can be robust to the invariance

of the appearance, changes in illumination and so on. And we also calculated the gradients and optical flow at every spatio-temporal location (x, y, t) , and then we established a local histogram using the Herbert's[4]SURF descriptor, which was extended to videos by Willem[14]. Like the previous approaches, the 3D patches are divided into a grid of local $M \times M \times M$ histograms. Each cell is represented by a vector of weighted sums of uniformly sampled responses of Haar-wavelets along the three axes. Fig.3 shows the haar-wavelets filter on the x and y directions.

At each interest point detected by the cuboids, it's spatial scale and temporal scale is defined as σ and τ . A rectangular volume can be defined with the dimensions $s\sigma \times s\sigma \times s\tau$, s is a magnification factor. So the volume can be subsequently divided into $M \times M \times N$ bins, M is the number of bins in the spatial and N is the temporal direction. We can sum the responses of the 3 axis-aligned Harr-wavelets d_x, d_y, d_z in the form of vector $v = (\sum d_x, \sum d_y, \sum d_z)$. According to Williems's[14]suggestion, it's no significant benefit to include the sums over the absolute values while doubling the descriptor size.



Fig. 3. The haar-wavelets filter on the x and y directions to computer the response. The time dimension is similar to x.

2.2 Types of the Improved Cuboids

Even though the number of interest points detected and described in histograms, the types of the cuboids are essential small and limited. We can use the k means to cluster the types of the descriptors for the points.

After the interests points are clustered in some types, the points can vote for the type, so each cuboids can be assigned a type, because the point contain all the information necessary to characterize a behavior, so the results is a histogram vector for an action. And the distance between the behavior histograms can be calculated by using the Euclidean distance.

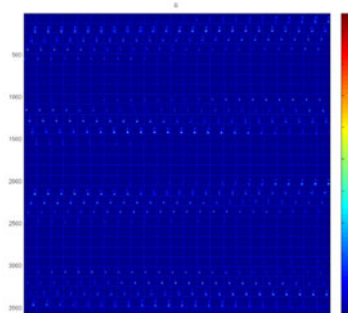


Fig. 4. The response of the function of the behavior walking. We can see that the bigger response is at the knee and the hand, where is the important part for action recognition.

3 Experiments

We do our experiments on three datasets: KTH, weizmann, and YouTobe. The KTH and Weizmann is simple datasets and the YouTobe is the uncontrolled data on the internet. Some frames are show in Fig. 5.

We describe each dataset in detail in this section and show the results, we do some experiments to verify our method's efficiency and accuracy. Finally we made a brief conclusion of our improved methods.

3.1 Datasets

The KTH datasets containing six types of human actions(walking, jogging, running, boxing, hand waving and handclapping) performed several times by 25 subjects in four different scenarios.

The Weizmann datasets includes nine persons and ten behaviors. The background is very simple and the action is simple. We can compared with the results of the state-of-art between our algorithm on this datasets.

The YouTobe datasets is some videos download from the internet. Its background is confused and the actions are varied unusually. The videos belong to the uncontrolled videos.



Fig. 5. Frames from the videos in each datasets: the first line, KTH, the second line Weizmann, and the last is the YouTobe

3.2 Computation Time

Video analysis consumes a lot of time because of the mount of the frames. Table 1 gives an overview of the time consuming on some video sequences. A Pentium(R) Dual-core CPU @ 2.70GHz, RAM is 4.00GB are used for processing. The needed computation time for feature detection and recognition is independent on the number of the features. The second volume is the data length of the datasets which depends on the frames per second, we calculated the frames in each video on the third volume. In the forth volume we show the time consuming by Williems and the last volume is ours. From the table we can see that our method uses less time than Williems's except the last dataset YouTobe. Next we will try to improve the method further.

Table 1. Comparison on the computation time

Datasets	Data length	Frames	Willem's[14]	ours
Mouse	70min	95650	1h43min	1h21min
KTH	1h10min	181576	2h20min	2h08min
Weizmann	45min	65720	1h15min	1h10min
YouTobe	1h20min	224823	2h46min	2h55min

3.3 Action Classification Results

According to the large size of the dataset, we used leave one out cross validation to classify the action. We extract 4 datasets from each database named set00, set01, set 02, set03. In each datasets we set 5 small datasets for each behavior. Four of them are used for training and the left one for testing. The results of the three datasets are show in Fig. 6 and 7.

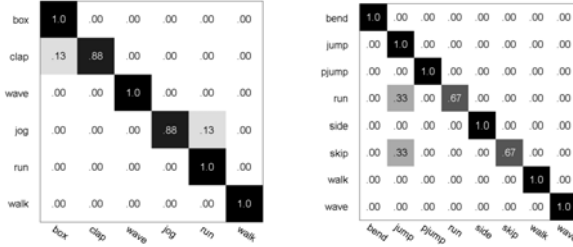


Fig. 6. The recognition results for the datasets KTH and Weizmann. It shows that the algorithm performs well.

The above tow datasets is very simple and the actions are behaviors by conduction. The confuse matrix show our algorithm performs very well on them. And the classification of the error is less than 4% and 9%. Our goal is applied the algorithm on the uncontrolled datasets. The next we show the result on YouTobe datasets, which is realistic videos.

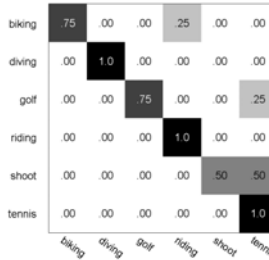


Fig. 7. Our algorithm on the uncontrolled video YouTobe

4 Compare with the State-of-Art Level

The comparison of our algorithm and the current state-of-art is in table 2.

Table 2. Comparison with the state-of-art-level

methods	KTH	Weizmann	YouTobe
Cuboids[2]	78.5%	88.5%	62.5%
Harris3D[10]	92.1%	90.7%	69.2%
HOG3D[13]	91.8%	91.2%	72.4%
Ours	96%	91.75%	83.33%

Conclusion from Table. The results shows that our algorithm performs good recognition rate and time consuming on the same datasets especially the uncontrolled video data YouTobe, which has a potential application in the future.

Acknowledgments. This work was supported by the grants of the National Science Foundation of China (Nos. 60805021, 60905023, 60975005, 60873012 & 61005010), the Program for New Century Excellent Talents in University (No.NCET-10-0117), the Program for Excellent Youth Talents in University of Fujian Province (No.JA10006), the Fundamental Research Funds for the Central Universities of Huaqiao University (No.JB-SJ1003), the Scientific Research Foundation of Huaqiao University (No.09HZR15), the grant of China Postdoctoral Science Foundation (No.20100480708), the grant of the Key Scientific Research Foundation of Education Department of Anhui Province (No.KJ2010A289), the grant of Scientific Research Foundation for Talents of Hefei University (No.11RC05).

References

1. Klaser, A., Marszalek, M., Schmid, C.: A Spatio-temporal Descriptor Based on 3D-gradients. In: BMVC (2008)
2. Klaser, A.: Learning Human Actions in Videos. University De Grenoble, pp. 26–30 (2010)
3. Dollar, P., Rabaud, V., Cottrell, G., Belongie, S.: Behavior Recognition via Sparse Spatio-Temporal Features. In: Visual Surveillance and Performance Evaluation of Tracking and Surveillance, pp. 65–72 (2005)
4. Bay, H., Tuytelaars, T., Van Gool, L.: SURF: Speed up Robust Features. In: Leonardis, A., Bischof, H., Pinz, A. (eds.) ECCV 2006 Part I. LNCS, vol. 3951, pp. 404–417. Springer, Heidelberg (2006)
5. Fergus, R., Perona, P., Zisserman, A.: Object Class Recognition by Unsupervised Scale-invariant Learning. In: CVPR (2003)
6. Weinland, D., Ronfard, R., Boyer, E.: A Survey of Vision-based Methods for Action Representation, Segmentation and Recognition. Technical report, INRIA (2010)
7. Poppe, R.: A Survey on Vision-based Human Action Recognition. Image and Vision Computing 28, 976–990 (2010)
8. Davis, J.W., Bobick, A.F.: The Representation and Recognition of Action Using Temporal Templates. In: CVPR, pp. 928–934 (1997)
9. Efros, A.A., Berg, A.C., Mori, G., Malik, J.: Recognizing Action at a Distance. In: ICCV (2003)
10. Laptev, I.: On Space-time Interest Points. IJCV 64, 107–123 (2005)
11. Laptev, I., Schudlt, C., Caputo, B.: Recognizing Human Actions: A local SVM approach. In: ICPR (2004)
12. Ke, Y., Sukthankar, R.: PCA-SIFT: A More Distinctive Representation for Local Image Descriptors. In: CVPR, pp. 506–513 (2004)
13. Wang, H., Ullah, M.M., Klaser, A., Laptev, I.: Evaluation of Local Spatio-temporal Features for Action Recognition. In: BMVC (2009)
14. Willems, G., Tuytelaars, T., Van Gool, L.: An Efficient Dense and Scale-Invariant Spatio-Temporal Interest Point Detector. In: Forsyth, D., Torr, P., Zisserman, A. (eds.) ECCV 2008, Part II. LNCS, vol. 5303, pp. 650–663. Springer, Heidelberg (2008)

Event Recognition Based on a Local Space-Time Interest Points and Self-Organization Feature Map Method

Yi-Lan Guo¹, Ji-Xiang Du^{1,2}, and Chuan-Min Zhai¹

¹ Department of Computer Science and Technology, Huaqiao University, Xiamen 361021

² Institute of Intelligent Machines, Chinese Academy of Sciences, Hefei, Anhui 230031

{jxdu77, cmzhai}@gmail.com, yeyongqing1986@163.com

{gylwerlove, jxdu77, cmzhai}@gmail.com

Abstract. This paper proposes a novel method based on local space-time interest points and self-organization feature map to recognize and retrieval complex events in real movies. In this method, an individual video sequence is represented as a SOFM density map then we integrate such density map with SVM for recognition events. Local space-time features are introduced to capture the local events in video and can be adapted to size and velocity of the pattern of the event. To evaluate effectiveness of this method, this paper uses the public Hollywood dataset, in this dataset the shot sequences has collected from 32 different Hollywood movies and it includes 8 event classes. The presented result justify the proposed method explicitly improve the average accuracy and average precision compared to other relative approaches.

Keywords: Local space-time interest points, Local space-time features, self-organization feature map, event recognition.

1 Introduction

Video becomes an easily created and widely spread media serving entertainment, education, communication and other purposes. The associated demand for mining large collections of realistic video data or retrieving interesting videos and so on motivates further research in automatic video understanding. Now a lot of research about video event detection depends strongly on specific domain knowledge and prior model result in it is difficult to apply to other domain or even other database. For example the method proposed by [1] can only used in detecting smoking event and similar events, such as drinking and eating. To develop a general event detection framework applies to different domain, reducing the need of domain knowledge is a necessary step.

Formulating a generalized event detection solution for real world video stream is a challenging problem due to scene variations (e.g., indoor and outdoor), viewing direction variations (e.g., from view, side view etc.), type and size variability of scene entities (e.g., pedestrian, vehicle, point object, large object etc.), and varying environmental conditions (e.g., illumination change, background motion etc.).

Event recognition methods can be roughly categorized into model-based methods and appearance-based techniques. Model-based approaches relied on various models

including HMM, coupled HMM, and Dynamic Bayesian Network to model the temporal evolution. But HMM cannot recognize events contain multiple objects. First, this model must detect the object, and then construct appropriate model, so a similar event class would have to make a model. It is inevitable to limit popularity of this method, and Bayesian Network also has the problem of learning parameter difficultly.

Appearance-based approaches employed space-time features extracted from salient regions with significant local variations in both spatial and temporal dimensions. Many different space-time feature detectors [2][3][4][5][6][7] and descriptors [6][8][9][10][11][12] have been proposed in the past few years. Local space-time features capture characteristic shape and motion in video and provide relatively independent representation of events with respect to their spatio-temporal shifts and scales as well as background clutter and multiple motions in the scene. Such features are usually extracted directly from video and therefore avoid possible failure of other pre-processing methods such as motion segmentation and tracking.

To delimit the problem, many previous research used a number of simplifying assumptions for example (a) restricted camera motion; (b) specific scene context, e.g. in field sports or surveillance scenes; (c) reliable spatial segmentation; and (d) restricted variation of viewpoints. Notably, event recognition has not yet been addressed in unrestricted scenarios such as in feature films.

In order to provide a common framework for recognizing event in real film scenarios, in our experiment, Harris3D detector proposed by [2] is introduced to capture local space-time interest points, and we use jet response of interest points as their feature which can be adapted to size and velocity of the pattern of the event. The number of frames of each video clip is different and the quantity of the space-time interest points of each frame is also diverse, so in order to unify the representation of video sequence, we adopt the idea of Self-Organizing Feature Map. For every event class local spatio-temporal features used for training were first trained to construct a neural map which was a 2D plane with a lattice on it, and a video is then represented as SOM density map. In our proposed framework of event recognition, there is no object detection and tracking, no need to build model, and also without making a distinction between single person and multi-person interactions or person-vehicle interactions and others. The presented result justify the proposed method explicitly improve the average accuracy and average precision compared to other relative approaches.

2 Feature Representation and Classification

2.1 Local Space-Time Features

In the spatio-temporal domain, points with a significant local variation of image intensities are referred to as “interest points” and are attractive due to their high information contents and relative stability with respect to perspective transformations of the data.

To represent a video sequence, we use local space-time features [2]. The local space-time features often correspond to interesting events in video data. To

detect local features in video sequence $f(x, y, t)$, we construct its scale-space representation $L(\cdot; \sigma^2, \tau^2) = f * g(\sigma^2, \tau^2)$ using Gaussian convolution kernel $g = \exp(-(x^2 + y^2)/2\sigma_l^2 - t^2/2\tau_l^2)/\sqrt{(2\pi)^3 \sigma_l^4 \tau_l^2}$. We compute the second-moment matrix using spatio-temporal image gradients L_x, L_y, L_t with a Gaussian neighborhood of each point

$$\mu = g(\cdot; \sigma_l^2, \tau_l^2) * \begin{pmatrix} L_x^2 & L_x L_y & L_x L_t \\ L_x L_y & L_y^2 & L_y L_t \\ L_x L_t & L_y L_t & L_t^2 \end{pmatrix} \quad (1)$$

L_x, L_y, L_t was defined as

$$\begin{aligned} L_x(\cdot; \sigma_l^2, \tau_l^2) &= \partial_x(g * f) \\ L_y(\cdot; \sigma_l^2, \tau_l^2) &= \partial_y(g * f) \\ L_t(\cdot; \sigma_l^2, \tau_l^2) &= \partial_t(g * f) \end{aligned} \quad (2)$$

And define positions of features by local maxima of spatio-temporal corner functions (3).

$$H = \det(\mu) - k \operatorname{trace}^3(\mu) \quad (3)$$

Second-order derivatives of L normalized by the scale parameters as follows

$$\begin{aligned} L_{xx,norm} &= \sigma^{2a} \tau^{2b} L_{xx} \\ L_{yy,norm} &= \sigma^{2a} \tau^{2b} L_{yy} \\ L_{tt,norm} &= \sigma^{2c} \tau^{2d} L_{tt} \end{aligned} \quad (4)$$

All of these entities assume local extreme over space and time. To find such extreme, we differentiate the expressions in (4) with respect to the spatial and the temporal scale parameters. By setting difference expressions to zero, we obtain $a = 1, b = 1/4, c = 1/2, d = 4/3$. In order to adapt to different scales of space and time, normalized Laplace operator defined by second-order derivatives of L is adopted

$$\begin{aligned} \nabla_{norm}^2 L &= L_{xx,norm} + L_{yy,norm} + L_{tt,norm} \\ &= \sigma^2 \tau^{1/2} (L_{xx} + L_{yy}) + \sigma \tau^{3/2} L_{tt} \end{aligned} \quad (5)$$

We detect interest points that are simultaneous maxima of the spatio-temporal corner function (3) over space and time (x, y, t) as well as extreme of the normalized spatio-temporal Laplace operator (5) over scales (σ^2, τ^2) . The detected interest points are shown in Fig.1.



Fig.1. Space-time interest points. These six frames come from a video sequence belong to answer phone event class. Yellow circle show the detected interest points.

Spatio-temporal neighborhoods of local features contain information about the motion and the spatial appearance of events in image sequences. To capture this information, we compute spatio-temporal jets

$$j = (L_x, L_y, L_t, L_{xx}, \dots, L_{ttt}) \quad (6)$$

For every detected interest points was represented by jet response.

2.2 Self-Organization Feature Map and SOFM Analysis

This section presents our approach for feature classification. It builds on existing Self-organization Feature Map. The number of frames of each video clip is different

and the quantity of the space-time interest points of each frame is also diverse, so in order to unify the representation of video sequence, we adopt the idea of Self-Organizing Feature Map. For every event class local spatio-temporal features used for training were first trained to construct a neural map which was a 2D plane with a lattice on it, and a video is then represented as SOFM[13] density map.

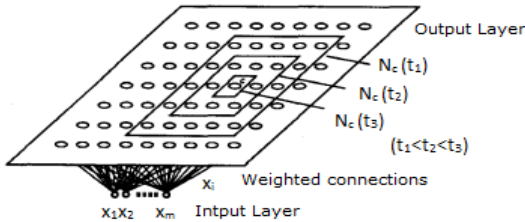


Fig.2. The structure of SOFM network. The n input neurons are connected to each neuron in the map lattice. The neurons in the map layer are also connected to each other.

SOFM neural networks (Fig.2) defines a mapping from the input data space R^n onto a regular two-dimensional array of nodes R^2 . After adequate self-learning steps, the network will tend to be spatially “organized” according to the structure of the input data set. Similar input vectors that are close together in the n -dimensional input space will be assigned to neurons that are close to together on the flat feature map. According to this property, SOFM can provide a clustering analysis for raw data set.

For a given video sequence sample $S = (j_1, j_2, \dots, j_m)$, it contains m features, namely m space-time interest points. If cell i responds to input vector j_i , we call cell i or the location of cell i on the map as the image of vector j_i . Every feature vector j_i in the input set has and only has one image on the neural map, but one cell can be the image of many vectors. If we use a plane with a lattice on it to represent the neural map, one square representing one neuron, and write the number h_i of input features whose image is this cell in the corresponding square, we get a map $H = (h_1, h_2, \dots, h_n)$ as shown in Fig.3. This map tells us how the images of input patterns are distributed on the neural map, thus we call it SOFM density map or SOFM image distribution map. So, finally each video sequence was represented by a map $H = (h_1, h_2, \dots, h_n)$.

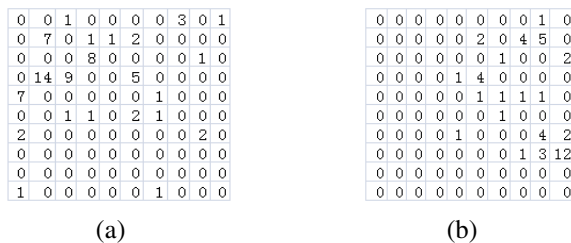


Fig.3. Examples of SOFM density map.(a)and(b)come from different event classes’ samples answerphone and getoutcar respectively. The neural map used above is trained by the positive samples come from answerphone event class.

3 Experiment

Support Vector Machines^[14] are state-of-the art large margin classifiers which have recently gained popularity within visual pattern recognition, so our experience use SVM as a classifier.

In our experiment, we use the public Hollywood dataset^[15]. This dataset is the subset of samples originates from 32 movies, where the training samples come from 12 movies and the testing samples are from another 20 movies. There are 8 event classes: answering the phone, getting out of the car, hand shaking, hugging, kissing, sitting down, sitting up and standing up. In our experiments, we used the clean training dataset.

Table 1. The result of our experiments

event	Average Accuracy	Average Precision	Average Recall
Answerphone	0.5565	0.5264	0.5429
Getoutcar	0.6722	0.3865	0.3265
Handshake	0.5908	0.4858	0.5357
Hugperson	0.5968	0.5445	0.6111
Kiss	0.6025	0.7019	0.6641
Sitdown	0.5644	0.5541	0.6803
Situp	0.6156	0.3493	0.4127
Standup	0.6092	0.6903	0.7529
Total average	0.601	0.52985	0.5658

Table 2. The result of contrastive papers. (a) is the average precision of the 8 event classes in [10]. (b) is the average precision in [16] use different methods.

event	Average precision	event	SIFT	HoG	SIFT
			HoF	HoG	HoF
Answerphone	0.321	Answerphone	0.105	0.088	0.107
Getoutcar	0.415	Getoutcar	0.191	0.090	0.116
Handshake	0.323	Handshake	0.123	0.116	0.141
Hugperson	0.406	Hugperson	0.129	0.135	0.138
Kiss	0.533	Kiss	0.348	0.496	0.556
Sitdown	0.386	Sitdown	0.161	0.316	0.278
Situp	0.182	Situp	0.142	0.072	0.078
Standup	0.505	Standup	0.262	0.350	0.325
Total average	0.384	Total precision	0.183	0.208	0.0217

(a)

(b)

For each event classes, we use the positive training samples to get neural map respectively. The number of neurons of map layer is 10*10. There are 7 group tests in every event class, the samples of every group come from the positive samples and one of another seven kind of negative samples. By these tests, we obtain mean average accuracy, mean average precision and mean average recall is 0.601, 0.52985 and 0.5658. The result is show in Table.1, and the accuracy of the standup event class is shown in Fig.4.

By comparing our result with the result of papers [10] and [16] was show in Table.2, we can get conclusion that the average precision improved. In [17] author adopted four local features detector and six descriptors for recognizing events, and the best average accuracy is only 45.8%.

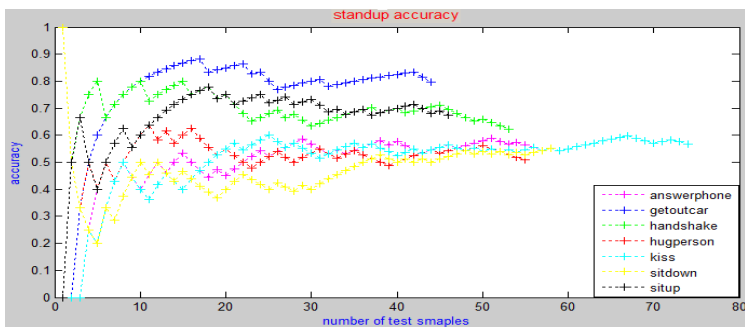


Fig. 4. The accuracy of the standup event class. Seven curves represent the accuracy comes from seven combined test. The test is formed by the combination of positive samples and another seven negative samples. Because of the number of testing samples is different, the maxima of horizontal ordinate of every curve is different. On the basis of seven group tests, the average accuracy of the standup event class is 0.6092.

4 Conclusion

In our proposed framework of event recognition, there is no object detection and tracking, no need to build model, and also without making a distinction between single person and multi-person interactions or person-vehicle interactions and others, so it can provide a relatively common framework used in real video scenarios, and Harris3D detector can solve the problem of multiple scales, moreover, the local space-time features can be adapted to size and velocity of the pattern of the event. In addition, jet responses of the space-time interest points capture characteristic shape and motion in video and provide relatively independent representation of events. The presented result justify the proposed framework explicitly improve the average accuracy and average precision compared to other relative approaches. The correct rate has improved, but the speed of extraction of the space-time feature is very low, it needs to be further improved.

Acknowledgments. This work was supported by the grants of the National Science Foundation of China (Nos. 60805021, 60905023, 60975005, 60873012 & 61005010), the Program for New Century Excellent Talents in University (No.NCET-10-0117), the Program for Excellent Youth Talents in University of Fujian Province (No.JA10006), the Fundamental Research Funds for the Central Universities of Huaqiao University (No.JB-SJ1003), the Scientific Research Foundation of Huaqiao University (No.09HZR15), the grant of China Postdoctoral Science Foundation (No.20100480708), the grant of the Key Scientific Research Foundation of Education Department of Anhui Province (No.KJ2010A289), the grant of Scientific Research Foundation for Talents of Hefei University (No.11RC05).

References

1. Pin, W., Jun-Wei, H., Jin-Cheng, C., Shyi-Chyi, C., Shau-Yin, T.: Human Smoking Event Detection Using Visual Interaction Clues. In: ICPR, pp. 4344–4347 (2010)
2. Laptev, I., Lindeberg, T.: Space-time Interest Points. In: ICCV, pp. 432–439 (2003)
3. Dollar, P., Rabaud, V., Cottrell, G., Belongie, S.: Behavior Recognition Via Sparse Spatio-temporal Features. In: Joint IEEE International Workshop on Visual Surveillance and Performance Evaluation of Tracking and Surveillance, pp. 65–72 (2005)
4. Jhuang, H., Serre, T., Wolf, L., Poggio, T.: Abiologically Inspired System for Action Recognition. In: ICCV, pp.1–8 (2007)
5. Oikonomopoulos, A., Patras, I., Pantic, M.: Spatio-temporal Salient Points for Visual Recognition of Human Actions. IEEE Transactions on Systems, Man, and Cybernetics, Part B: Cybernetics, pp. 710–719 (2006)
6. Willems, G., Tuytelaars, T., Van Gool, L.: An Efficient Dense and Scale-invariant Spatio-temporal Interest Point Detector. In: Forsyth, D., Torr, P., Zisserman, A. (eds.) ECCV 2008, Part II. LNCS, vol. 5303, pp. 650–663. Springer, Heidelberg (2008)
7. Wong, S.F., Cipolla, R.: Extracting Spatio-temporal Interest Points Using Global Information. In: ICCV, pp.1–8 (2007)
8. Kläser, A., Marszałek, M., Schmid, C.: A Spatio-temporal Descriptor Based on 3D-gradients. In: BMVC (2008)
9. Laptev, I., Lindeberg, T.: Local Descriptors for Spatio-temporal Recognition. In: MacLean, W.J. (ed.) SCVMA 2004. LNCS, vol. 3667, pp. 91–103. Springer, Heidelberg (2006)
10. Laptev, I., Marszałek, M., Schmid, C., Rozenfeld, B.: Learning Realistic Human Actions from Movies. In: CVPR, pp.1–8 (2008)
11. Scovanner, P., Ali, S., Shah, M.: A 3-dimensional SIFT Descriptor and Its Application to Action Recognition. In: ACM International Conference on Multimedia (2007)
12. Laptev, I., Pérez, P.: Retrieving Actions in Movies. In: ICCV, pp.1–8 (2007)
13. Xuegong, Z., Yanda, L.: Self-organizing Map as a New Method for Clustering and Data Analysis. In: Proceeding of 1993 International Joint Conference on Neural Networks, pp. 2448–2451 (1993)
14. Schuldt, C., Laptev, I., Caputo, B.: Recognizing Human Actions: a local SVM approach. In: ICPR, pp. 32–36 (2004)
15. <http://www.irisa.fr/vista/Equipe/People/Laptev/download.html>
16. Marszałek, M., Laptev, I., Schmid, C.: Actions in Context. In: CVPR, pp. 2929–2936 (2009)
17. Wang, H., Muneeb Ullah, M., Klaser, A., Laptev, I., Schmid, C.: Evaluation of Local Spatio-temporal Features for Action Recognition. In: BMVC (2009)

Strategy of Statistics-Based Visualization for Segmented 3D Cardiac Volume Data Set

Changqing Gai¹, Kuanquan Wang¹, Lei Zhang^{1,2}, and Wangmeng Zuo¹

¹ Biocomputing Research Center, School of Computer Science and Technology,
Harbin Institute of Technology, Harbin 150001, China,

² School of Art and Design, Harbin University, Harbin 150086, China
wangkq@hit.edu.cn

Abstract. In this paper, we propose a method to design the transfer function of segmented cardiac volume data set by using statistical information of the cardiac tissues. To explore the interior subtle tissues of heart, visualization strategy is provided to guide the user to a satisfied rendering result with the help of opacity and gradient magnitude modulation. Using the visible human cardiac data set segmented from the CT data, experimental results indicate that our method can provide high quality rendering result and multi-level visualization effect.

Keywords: Statistics, Volume Rendering, Transfer function, 3D Cardiac Volume Data Set.

1 Introduction

Heart is one of the most important organs of the human being. Coronary heart disease has become one of the world's leading causes of death [1]. Therefore, medical imaging technology related with anatomical structure of heart developed quickly in recent years.

Due to the layered structure, the interior structures of the heart are hard to explore, thus it is helpful to visualize the three dimensional cardiac anatomical data in diagnosis and treatment of the heart diseases. Goodyer et al. [2] proposed an advanced visualization method for high-resolution MRI data, and designed a high definition multi-panel display wall. Hurmusiadiis Vassilios [3] developed a heart simulation platform for education and medical training, which demonstrated the cells, tissues and organs of heart. Yang et al. [4] designed an accelerated visualization algorithm and tested on the MRI data of sheep heart and sliced data set of human heart from the Visible Human Project.

Volume rendering is the main method of visualizing volume data. It can not only provide contour information but also reveal the interior structures of the volume data. Popular volume rendering algorithms including ray casting [5] and texture slicing [6] are effectively making use of the hardware characteristics of the GPU so as to improve the rendering speed [7-9]. Transfer function is used to assign the optical property for each voxel. It is essential to volume visualization, directly affects the

final rendering results [10]. Kniss et al. [10, 11] proposed a multi-dimensional transfer function, using the voxel density, gradient and two-dimensional derivative to design the optical property. Bruckner et al. [12] designed a style transfer function, which integrated different styles of non-photorealistic rendering and effectively highlighted the important regions. Maciejewsk et al. [13] described a non-parametric method based on clustering in the structuring feature space to generate volume transfer function. Although researchers have made intensive study on the transfer function design, there is still lack of a method for the design of transfer function of complicated layered structure and strategy to direct users to interactively visualize the volume data.

In this paper, we propose a novel method for designing transfer function with the statistical information of segmented 3D cardiac volume data set, and provide a strategy of visualization to guide the users to adjust the rendering result, finally realize multi-level visualization of the heart.

The rest of the paper is organized as follows. In Section 2, we introduce the design method of transfer function for the cardiac volume data set. In Section 3, we provide the proposed visualization strategy, and describe how to modify the opacity with the statistical information and gradient magnitude. In Section 4, we conclude the paper.

2 Statistics-Based Algorithm for Designing Transfer Function

A reasonable transfer function can reveal the important spatial information inside the volume data set. For the segmented cardiac volume data set, different gray levels represent different kinds of tissue. According to the statistical information, we can know the proportion of each gray level, and determine the tissue represented by it based on the prior knowledge.

2.1 Statistics of the 3D Cardiac Volume Data Set

We make a histogram for the volume data set:

$$p(u_r) = \frac{n_r}{MNL} \quad r = 0, 1, 2, \dots, K - 1 \quad (1)$$

where u_r is the gray level, $p(u_r)$ is the frequency of u_r , n_r is the number of voxels in the data set with gray level u_r , MNL is the total number of voxels in the data set, and $[0, K-1]$ is the range of gray level.

Fig. 1 shows the statistical result using Eq. (1), where the horizontal axis corresponds to gray level; the vertical axis corresponds to the frequency of each gray level. From Fig. 1, one can see that gray levels related with the cardiac tissues are in the range of [30, 70].

2.2 Transfer Function Design

In the segmented 3D cardiac data set, each cardiac tissue is assigned with a specific gray level. Thus, we can determine which tissue is represented by a gray level with

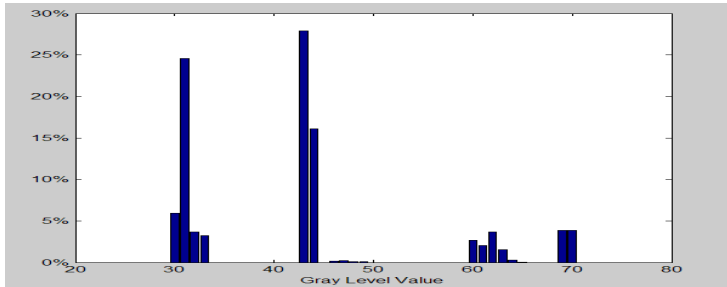


Fig. 1. The histogram of the 3D cardiac volume data set

the histogram. For clearly demonstrating the anatomical structures of the heart, different colors are employed to represent different tissues according to the relative location of tissues in the cardiac anatomical model, and the doctor will be familiar with the rendering result. Opacity for each voxel is another important factor in transfer function design. Considering the spatial position of the tissues, the opacity of interior tissues is larger than that of exterior tissues, and the optical property of transition is different from that of the tissues. For example, gray level 30 represents the right ventricle, belonging to exterior tissues, so its opacity is smaller. We design the transfer function as a lookup table which is shown in Fig. 2.

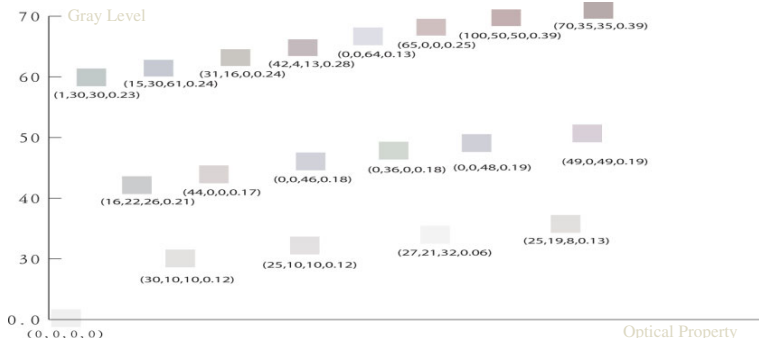


Fig. 2. The lookup table for the 3D cardiac volume data set

In Fig. 2, the vertical axis corresponds to gray level; the squares correspond to the optical property of the voxels. The optical property of a voxel is represented by the quaternion (R, G, B, A) , where R means red, G means green, B means Blue, and A means opacity.

In the rendering process, we use gray level as index to fetch the optical property of each voxel from the lookup table. The mapping equation is described as:

$$Col_{rgba} = F(g) \quad (2)$$

where Col_{rgba} is the optical property, g is the gray level in the volume data set, and F is the mapping function implemented in the lookup table. Fig. 3 shows the rendering results with the transfer function described in Fig. 2.

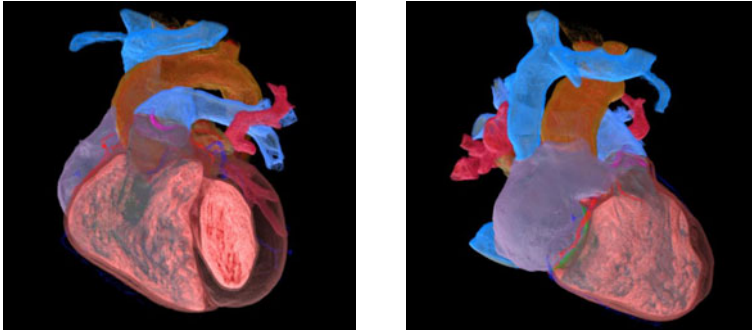


Fig. 3. The rendering result of the 3D cardiac volume data set from different point of view

As can be seen in Fig. 3, the rendering results, obtained from different point of view, not only keep the exterior silhouette, but also show the interior structures. In the left of Fig. 3, the silhouette of ventricles is preserved and papillary muscles inside the ventricles are unfolded. From the right of Fig. 3, one can see the coronary in red between the right ventricle and the right atrium. Behind the coronary one can see the valve in green, but we cannot get the whole picture of the valve because of the occlusion.

3 Strategy of Visualization

Due to the complicated layered structure, it is difficult to observe the interior subtle tissues of the heart. The mitral valve is located between the left atrium and the left ventricle. When the blood flows through, the mitral valve closes, preventing the blood backflows. Doctor estimates whether the heart is healthy according to the occlusion of the mitral valve. But it is occluded by the exterior tissues. To solve the problem, we design a visualization strategy to provide an interactive guide for users. The statistic result of the segmented cardiac volume data and the gradient magnitude are integrated into the visualization strategy.

3.1 Opacity Modulation Based on the Statistics

We design an opacity modulation scheme by use of the statistical data from the volume data set. The opacity of the voxel is modulated as below:

$$\alpha_s = (\alpha_o \times \gamma_k)^{k_s} \quad (3)$$

where α_s is the shaded opacity, α_o is the original opacity, k_s is the exponential coefficient, and γ_k is defined as follows,

$$\gamma_k = \beta / p(k) \quad (4)$$

where β is a constant value, $p(k)$ is the frequency of gray level k .

The volume rendering result contains much information that can be obtained through reasonable parameters adjustment. Here our visualization strategy is to tune parameters of β and k_s . β is in charge of minor adjustment of image rendering and k_s controls the basic skeleton of rendering result. Initially, β and k_s are set to 1.0. When adjusting the parameters, the user should initiate transfer function searches along individual directions, i.e., changing one parameter every time. In this method, the user can explore the evolution of the result as other parameters do not change. We first adjust the k_s parameter. When k_s increases, the whole image is fading, then we tune the β parameter, the subtle tissues such as the mitral valve will be enhanced when β increases. Fig. 4 shows the rendering results.

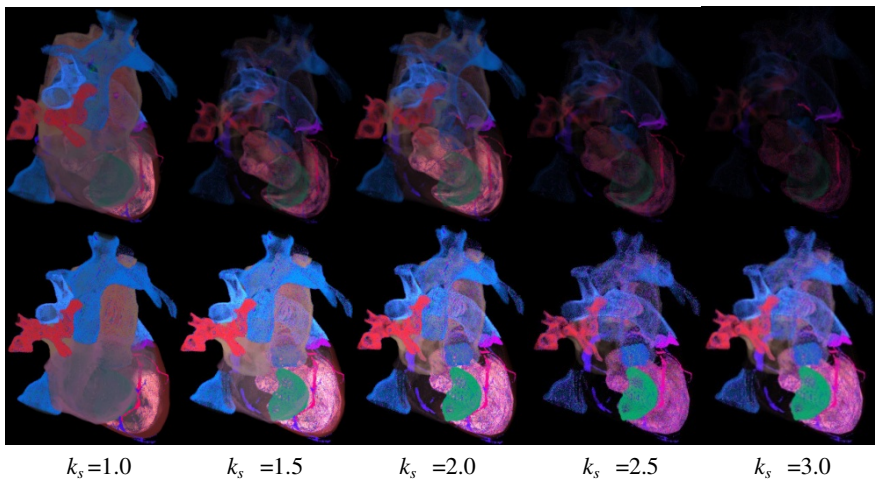


Fig. 4. The rendering results of the 3D cardiac volume dataset using the statistics. β is set to 1.0 in the first row and 2.0 in the second row respectively.

To observe the mitral valve, the green tissue in Fig. 4, a reference search path of (β, k_s) is: $(1.0, 1.0) \rightarrow (1.0, 1.5) \rightarrow (1.0, 2.0) \rightarrow (2.0, 2.0) \rightarrow (2.0, 2.5) \rightarrow (2.0, 3.0)$. As can be seen in Fig. 4, the contour fades away when k_s increases, then the mitral valve is obviously enhanced when β increases.

3.2 Gradient Modulation

The silhouette is incompatible with the interior subtle tissues, as seen in Fig. 4, when the contour is clear, the subtle tissues are fading out, and vice versa. To get a balance between them, gradient magnitude modulation is taken into account. The gradient magnitude modulation is designed to enhance material boundaries. The Eq. (4) is modified as:

$$\gamma_k = \frac{\|g_{k,p}\|}{g_{\max}} \beta / p(k) \quad (5)$$

where $\|g_{kp}\|$ is the gradient magnitude of gray level k at point p , g_{\max} is the maximal gradient magnitude of the volume data set. When the point p is the interior part of a subtle tissue, it is not rendered because $\|g_{kp}\|$ is zero. So we do a transformation for $\|g_{kp}\|/g_{\max}$:

$$\gamma_k = \frac{\|g_{kp}\| + N}{g_{\max} + N} \beta / p(k) \quad (6)$$

where N is a nonnegative number. If $N = 0$, $(\|g_{\max}\| + N)/(g_{\max} + N) = \|g_{kp}\|/g_{\max}$; if $N = \infty$, $(\|g_{kp}\| + N)/(g_{\max} + N) = 1$, so Eq. (6) is the same as Eq. (4). We choose $N = g_{\max}$, the result will be a balance of $N = 0$ and $N = \infty$. After the transformation, $(\|g_{kp}\| + N)/(g_{\max} + N)$ is in the range of [0.5, 1.0].

In practice, g_{\max} can be pre-computed or set to the theoretical maximal gradient magnitude of the data set. The rendering results using the gradient magnitude are shown in Fig. 5:

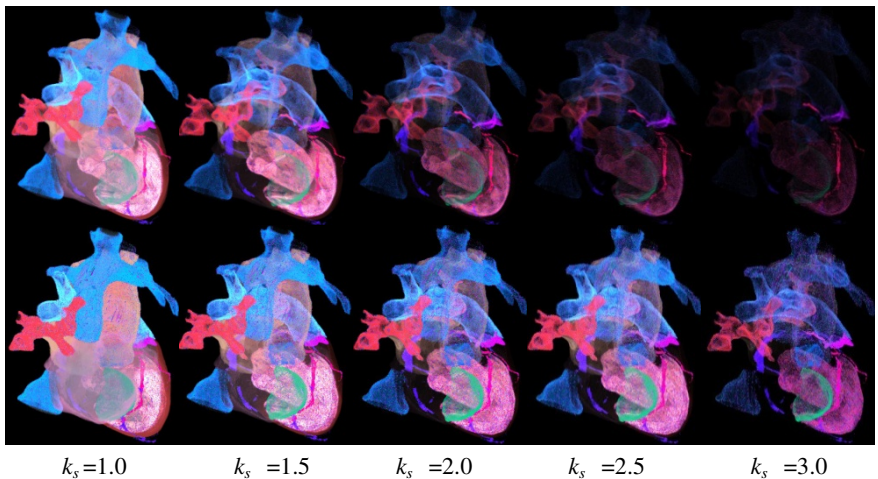


Fig. 5. The rendering result of the 3D cardiac volume data set using the gradient magnitude. β is set to 1.0 in the first row and 2.0 in the second row respectively.

The opacity of each voxel decreases using Eq. (6), because the range of gradient magnitude has been transformed to [0.5, 1.0]. When β and k_s are fixed, the rendering result in Fig. 5 is more transparent than that in Fig. 4. When β is small, the rendering result is not as clear as that in Fig. 4, such as the images in Fig. 4 and Fig. 5 where β is 1.0 and k_s is 1.0. But when β increases, rendering result gets a good balance between the contour and the interior subtle tissues, as the image in Fig. 5 where β is 2.0 and k_s is 1.0 and the two images in Fig. 4 where k_s is 1.0.

4 Conclusion

Our contributions are two-fold. On one hand, we present a method for designing the transfer function based on the statistical result. On the other hand, we show how frequency of gray level and gradient magnitude can be used to adjust the opacity to reveal multi-level visualization of heart. Besides, we design the visualization strategy according to the statistical characteristics of the cardiac data set. The proposed method is also expected to be applicable to other layered medical data sets. Moreover, it can be incorporated into the existing volume rendering platform without too much effort.

References

1. Elisa, T., Barbara, V.: Prediction of Coronary Heart Disease in a Population with High Prevalence of Diabetes and Albuminuria: The Strong Heart Study. *Circulation* 113, 2897–2905 (2006)
2. Goodyer, C.E., Grau, V., Mansoori, T., Schneider, J.E., Brodlie, K.W., Kohl, P.: 3D Visualization of Cardiac Anatomical MRI Data with Para-Cellular Resolution. In: 29th Annual International Conference of the IEEE 2007, pp. 147–151. IEEE Press, Lyon (2007)
3. Hurmisiadis, V.: Virtual heart: Simulation-based cardiac physiology for education. In: Computer in Cardiology 2007, pp. 65–68. IEEE Press, Durham (2007)
4. Yang, F., Zuo, W., Wang, K., Zhang, H.: Visualization of Segmented Cardiac Anatomy with Accelerated Rendering Method. In: Computer in Cardiology 2009, pp. 789–792. IEEE Press, Park City (2009)
5. Gobbetti, E., Marton, F., Guitián, J.: A single-pass GPU ray casting framework for interactive out-of-core rendering of massive volumetric datasets. *The Visual Computer: International Journal of Computer Graphics* 24(7), 797–806 (2008)
6. Abellán, P., Tost, D.: Multimodal volume rendering with 3D textures. *Computers and Graphics* 32(4), 412–419 (2008)
7. Krüeger, A., Kubisch, C., Straub, G., et al.: Sinus endoscopy-application of advanced GPU volume rendering for virtual endoscopy. *IEEE Transactions on Visualization and Computer Graphics* 14(6), 1491–1498 (2008)
8. Liang, R., Pan, Z., et al.: Fast Hardware-Accelerated Volume Rendering of CT Scans. *Journal of Display Technology* 4(4), 431–436 (2008)
9. Rößler, F., Botchen, R.P., et al.: Dynamic Shader Generation for GPU-based Multi-Volume Ray Casting. *Computer Graphics and Applications* 28(5), 66–77 (2008)
10. Kniss, J., Kindlmann, G., Hansen, C.: Multidimensional Transfer Functions for Interactive Volume Rendering. *IEEE Transactions on Visualization and Computer Graphics* 8(3), 270–285 (2002)
11. Kniss, J., Kindlmann, G., Hansen, C.: Interactive volume rendering using multi-dimensional transfer functions and direct manipulation widgets. In: Proceedings of the IEEE Conference on Visualization, pp. 255–262. IEEE Press, Los Alamitos (2001)
12. Bruckner, S., Gröller, M.E.: Style transfer functions for illustrative volume rendering. *Computer Graphics Forum* 26(3), 715–724 (2007)
13. Maciejewski, R., Woo, I., Chen, W., Ebert, S.: Structuring Feature Space: A Non-Parametric Method for Volumetric Transfer Function Generation. *IEEE Transactions on Visualization and Computer Graphics* 15(6), 1473–1480 (2009)

Robust Gait Recognition Using Gait Energy Image and Band-Limited Phase-Only Correlation

Min Wang^{1,2}, Wei Jia², Huanglin Zeng¹, and Xiao-Feng Wang³

¹ College of auto.& inf. Eng., Sichuan University of Science and Technology,
Sichuan, 643000, China

² Hefei Institute of Intelligent Machines, Chinese Academy of Science,
P.O. Box 1130, Hefei 230031, China

³ Department of Computer Science and Technology,
Hefei University, Hefei, 230601, China
wangmin0118@gmail.com

Abstract. Variations in clothing or taking something during walking change a walker's appearance, making the problem of gait recognition much more difficult. In this paper, we exploit Band-Limited Phase-Only Correlation (BLPOC) method combine Gait Energy Image (GEI) for gait recognition. We use BLPOC method for feature extraction and matching in GEI. The results of experiments conducted on gait dataset CASIA_B show that BLPOC based method is significant robust on the walker's appearance change compare to Principal Component Analysis (PCA) in GEI.

Keywords: Gait Recognition, GEI, BLPOC, PCA.

1 Introduction

Gait recognition, which aims essentially to discriminate individuals by the way they walk, has been widely researched during the past decade. Gait has the unique advantage of being noninvasive compare to other biometrics such as fingerprint and iris, and it is easily acquired at a distance. These advantages are important to video-based intelligent security surveillance system in which gait recognition is the key technique.

Gait recognition techniques can be roughly divided into two different approaches: model-based and model-free. Model-based approaches use the human body structure and kinematic information gathered from the walking body. This information is then used to construct a recognition model or directly be used as feature. Though model-based approaches are view invariant and reflect the kinematic characteristics of walking, it is hard to accurately locate the joints' position due to the highly flexible structure of non-rigid human body and self-occlusion. Therefore, current research focuses on model-free approaches, in which the proposed approaches directly operate on the gait image sequences.

Among model-free approaches, gait energy image (GEI) [1] has been proved to be the most effective one. GEI is obtained by averaging the binary silhouettes of a

pedestrian over one gait cycle. It is the time-normalized accumulative energy image of human walking in a complete cycle. The intensity of a pixel in GEI reflects the frequency (i.e. the energy) of body occurrence at the position of this pixel for a complete walking cycle. GEI is a robust feature since random noise has been reduced in the average process, and it saves storage space and computation time. GEI has inspired many of other gait recognition techniques. Yu et al. [2] used GEI for gender classification, and achieved impressive result. Yang et al. [3] proposed an enhanced GEI (EGEI) gait representation method to apply dynamic region analysis to improve dynamic information of the features extracted. Zhang et al. [4] proposed an active energy image (AEI) method for gait recognition. The basic idea of AEI is to extract the active regions of a gait sequence by calculating the difference between two adjacent silhouette images in a gait sequence. T.H.W. Lam et al. [5] proposed gait flow image (GFI) for gait recognition. The optical flow field is adopted to construct the GFI. Tao et al. [6] applied Gabor filter and its variations on GEI and used general tensor discriminant analysis (GTDA) to perform the feature selection task and to reduce the size of tensor gait. To overcome the effect of walker's appearance change, many methods have been proposed. The most effective method is the part-based approach use GEI. Md. Altab Hossain et al. [7] collected a gait dataset in the light of substantial clothing variations, and exploited part-based approach to gait recognition.

In this paper we exploit Band-Limited Phase-Only Correlation (BLPOC) [8] method for feature extraction and matching in GEI. BLPOC based method has been successfully applied to iris [9] and palmprint [10,11] recognition. It's effective and efficient method to match images which contain plenty low contrast line, direction and texture feature.

The rest of the paper is organized as follows. In Section 2, we describe the details of GEI and BLPOC method. The experiments are carried out to evaluate the proposed approach in Section 3. Finally, Section 4 concludes the paper.

2 Method Details

2.1 Gait Energy Image

Fig. 1 shows the preprocessing of gait sequences. Firstly, the silhouette is extracted from the original gait sequence by using the simple background subtraction. Then, the binarization process renders the image in black and white by thresholding.

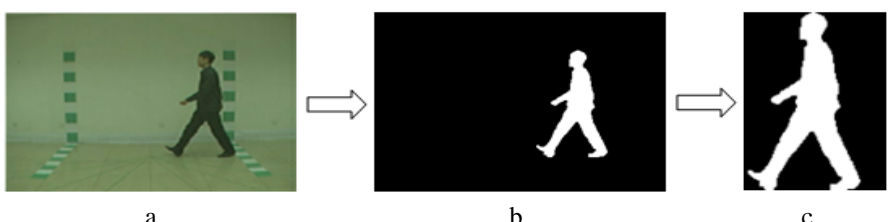


Fig. 1. A example of silhouette extraction in CASIA B: (a) original image, (b) after background subtraction and thresholding, (c) normalized silhouette image

Finally, the silhouette image can be obtained by computing the bounding box of the silhouette image in the binarized image. The silhouette image is cropped according to the position and size of the bounding box and normalized to a fixed size to eliminate the scaling effect by camera. The normalized silhouette image then be used to gait period estimation.

Human gait show distinct periodicity. The period can be estimated by the number of foreground pixels in the silhouette image. However, sharp changes in the gait cycle are more obvious in the lower part of the body, gait period can be estimated more stability only use of the lower half of the silhouette image.



Fig. 2. Gait sequence and GEI

After estimation of the gait period, GEI can be obtained by averaging the binary silhouettes over one gait cycle. Fig. 2 shows silhouette images in one period and their GEI. The intensity of a pixel in GEI reflects the frequency of body occurrence at the position of this pixel for a complete walking cycle. GEI is a robust feature since random noise has been reduced in the average process, and it saves storage space and computation time.

2.2 Fundamentals of Band-Limited Phase-Only Correlation

Band-Limited Phase-Only Correlation (BLPOC) based method has been successfully applied to iris and palmprint recognition. It's effective and efficient method to match images which contain plenty low contrast line, direction and texture feature.

Firstly, the definition of POC is described as follows:

Consider two $N_1 \times N_2$ images, $f(n_1, n_2)$ and $g(n_1, n_2)$. Let $F(k_1, k_2)$ and $G(k_1, k_2)$ denote the 2D DFTs of the two images. Here, $F(k_1, k_2)$ is given by:

$$F(k_1, k_2) = \sum_{n_1=0}^{N_1} \sum_{n_2=0}^{N_2} f(n_1, n_2) e^{-j2\pi(\frac{n_1 k_1}{N_1} + \frac{n_2 k_2}{N_2})} = A_F(k_1, k_2) e^{j\theta_F(k_1, k_2)}. \quad (1)$$

where $A_F(k_1, k_2)$ is amplitude and $\theta_F(k_1, k_2)$ is phase. $G(k_1, k_2)$ can be defined in the same way. The cross-phase spectrum $R_{FG}(k_1, k_2)$ is give by:

$$R_{FG}(k_1, k_2) = \frac{F(k_1, k_2) \overline{G(k_1, k_2)}}{|F(k_1, k_2) \overline{G(k_1, k_2)}|} = e^{j\theta(k_1, k_2)} \quad (2)$$

where $\overline{G(k_1, k_2)}$ is the complex conjugate of $G(k_1, k_2)$ and $\theta(k_1, k_2)$ denotes the phase difference $\theta_F(k_1, k_2) - \theta_G(k_1, k_2)$. The POC function $r_{fg}(n_1, n_2)$ is the 2D Inverse DFT (2D IDFT) of $R_{FG}(k_1, k_2)$ and is given by:

$$r_{fg}(n_1, n_2) = \frac{1}{N_1 N_2} \sum_{k_1 k_2} e^{j\theta(k_1, k_2)} e^{j2\pi(\frac{n_1 k_1}{N_1} + \frac{n_2 k_2}{N_2})} \quad (3)$$

From formulas (2) and (3), we can see that original POC exploits all components of image's 2D DFT to generate the out plane. In [10], ITO et al., found that BLPOC can achieve better recognition performance by removing the high frequency components and only using the inherent frequency band for matching.

Here we denote the center area of $\theta_F(k_1, k_2)$ and $\theta_G(k_1, k_2)$ as $\theta_F(k_1, k_2)_{BL}$ and $\theta_G(k_1, k_2)_{BL}$, whose size is $J_1 \times J_2$. Thus, the BLPOC function is given by:

$$r_{fg}(n_1, n_2)_{BL} = \frac{1}{J_1 J_2} \sum_{k_1 k_2} e^{j(\theta_F(k_1, k_2)_{BL} - \theta_G(k_1, k_2)_{BL})} e^{j2\pi(\frac{n_1 k_1}{J_1} + \frac{n_2 k_2}{J_2})} \quad (4)$$

3 Experiments and Results

The proposed method was tested on the CASIA gait dataset B [12] to evaluate its effectiveness and robustness. The CASIA_B dataset contains 124 subjects' gait sequences collected under different views, clothing and carrying conditions. There are 11 views ($0^\circ, 18^\circ, \dots, 180^\circ$) for each subject and 10 sequences per view. Among all the 10 sequences, two sequences are walking with bag, two on coat, and the rest are normal walking. We used the sequences collected at the 90° view to test our proposed method. In our experiments, first four normal sequences use for training, the rest of sequences use for test. The test sequences are divided into three conditions: two normal sequences, two with bag and two on coat. The experiments were conducted on a personal computer with an Intel Core 2 Duo E4600 processor (2.39GHz) and 2.0G RAM configured with Microsoft Windows XP and Matlab R2010a.

3.1 Experiment 1

In this experiment, we try to determine suitable values of J_1 and J_2 in formula (4). For convenience, we let J_1 equal to J_2 . That is to say, the selected center area of the 2D DFT spectrum is a square, whose size is $J_1 \times J_2$. Furthermore, in order to choose the best J_1 , we conduct the tests exploiting different values of J_1 . Here, the

value of J_1 is set to an even number, and changes from 10 to 80 with an interval of 2. In experiment, we consider four situations, three conditions use for test respectively, and all conditions use for test. Fig. 3 shows the result of experiment, when the value of J_1 is 50, all situations get the almost best CCR. Therefore, we set the value of J_1 to 50.

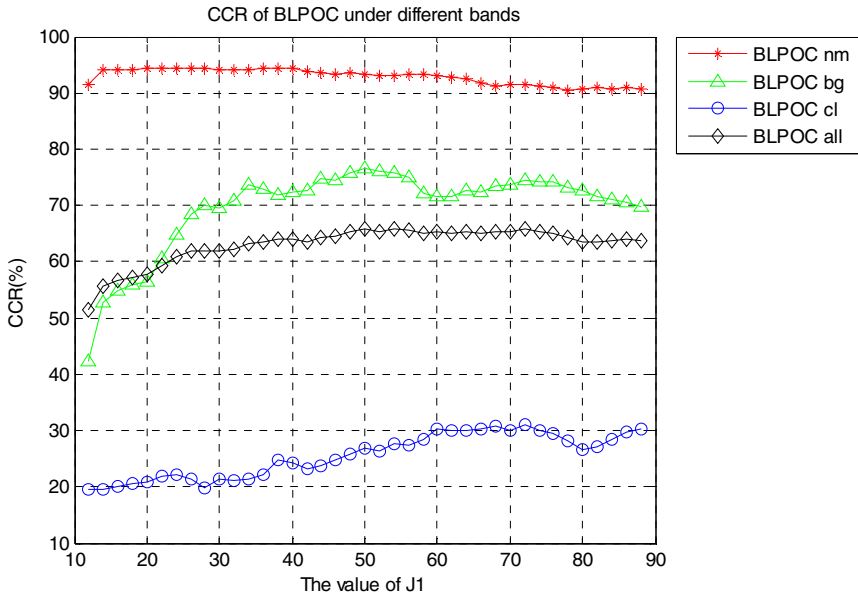


Fig. 3. The Correct Classification Rate (CCR) of BLPOC under different bands (J_1)

3.2 Experiment 2

In this experiment, we test PCA and BLPOC on three conditions, respectively. Fig. 4 shows the result. In normal walking condition, BLPOC almost has the same recognition rate compare to PCA. But, in other two conditions, BLPOC has significantly outperform PCA. Table 1 shows recognition rate of BLPOC and PCA in rank 1.

Table 1. Recognition Rate in rank 1

Condition	CCR of PCA	CCR of BLPOC
normal	95.69%	93.30%
bag	35.02%	76.57%
coat	14.99%	26.78%

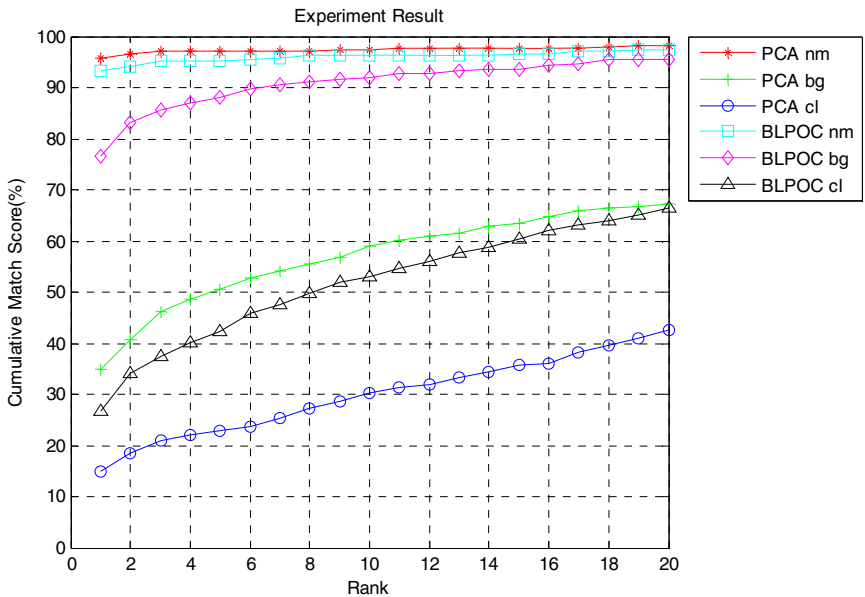


Fig. 4. Experiment Result

4 Conclusions and Future Works

In this paper, we exploited Band-Limited Phase-Only Correlation (BLPOC) method combine Gait Energy Image GEI for gait recognition. We first obtained the GEI of gait sequences, and then we used BLPOC method for feature extraction and matching in GEI. The results of experiments conducted on gait dataset CASIA_B showed that BLPOC based method were significant robust on the walker's appearance change compare to Principal Component Analysis (PCA) in GEI. Our future work will be concentrated on improving BLPOC method and doing more experiments on challenging gait dataset.

Acknowledgments. This work was supported by the grants of the National Science Foundation of China, Nos. 60705007 & 61005010 , the grant of the Knowledge Innovation Program of the Chinese Academy of Sciences Y023A61121 and Y023A11292, the grant of China Postdoctoral Science Foundation, No. 20100480708, the grant of the Key Scientific Research Foundation of Education Department of Anhui Province, No. KJ2010A289, and the grant of Scientific Research Foundation for Talents of Hefei University, No. 11RC05.

References

1. Han, J., Bhanu, B.: Individual Recognition Using Gait Energy Image. *IEEE Transactions on Pattern Analysis and Machine Intelligence* 28, 316–322 (2006)
2. Yu, S., Tan, T., Huang, K., Jia, K., Wu, X.: A Study on Gait-based Gender Classification. *IEEE Transactions on Image Processing* 18, 1905–1910 (2009)

3. Yang, X., Zhou, Y., Zhang, T., Shu, G., Yang, J.: Gait Recognition Based on Dynamic Region Analysis. *Signal Processing* 88, 2350–2356 (2008)
4. Zhang, E., Zhao, Y., Xiong, W.: Active Energy Image Plus 2DLPP for Gait Recognition. *Signal Processing* 90, 2295–2302 (2010)
5. Lam, T.H.W., Cheung, K.H., Liu, J.N.K.: Gait flow image: A Silhouette-based Gait Representation for Human Identification. *Pattern Recognition* 44, 973–987 (2011)
6. Tao, D., Li, X., Wu, X., Maybank, S.J.: Tensor Discriminant Analysis and Gabor Features for Gait recognition. *IEEE Transactions on Pattern Analysis and Machine Intelligence* 29, 1700–1715 (2007)
7. Hossain, M.A., Makihara, Y., Wang, J.Q., Yagi, Y.: Clothing-invariant Gait Identification Using Part-based Clothing Categorization and Adaptive Weight Control. *Pattern Recognition* 43, 2281–2291 (2010)
8. Jia, W., Hu, R.X., Gui, J., Lei, Y.K.: Newborn Footprint Recognition Using Band-Limited Phase-Only Correlation. *Neural Computing & Applications* 20, 643–941 (2011)
9. Miyazawa, K., Ito, K., Aoki, T., Kobayashi, K., Nakajima, H.: An Effective Approach for Iris Recognition Using Phase-Based Image Matching. *IEEE Transactions on Pattern Analysis and Machine Intelligence* 30, 1741–1756 (2008)
10. ItO, K., Aoki, T., Nakajima, H.: A Palmprint Recognition Algorithm using Phase-Only Correlation. *IEICE Transactions on Fundamentals* 91, 1023–1030 (2008)
11. Litsuka, S., ItO, K., Aoki, T.: A Practical Palmprint Recognition Algorithm Using Phase Information. In: *Proceedings of International Conference on Pattern Recognition*, pp.8–11 (2008)
12. Yu, S., Tan, D., Tan, T.: A Framework for Evaluating the Effect of View Angle, Clothing and Carrying Condition on Gait Recognition. In: *Proceedings of International Conference on Pattern Recognition*, pp. 441–444 (2006)

Implementation of Interactive Interview System Using Hand Gesture Recognition

Yang Weon Lee

Department of Information and Communication Engineering, Honam University,
Seobongdong, Gwangsangu, Gwangju, 506-714, South Korea

Abstract. This paper describes a implementation of virtual interactive interview system. A hand motion recognition algorithm based on the particle filters is applied for this system. The particle filter is well operated for human hand motion recognition than any other recognition algorithm. Through the experiments, we show that the proposed scheme is stable and works well in virtual interview system's environments.

1 Introduction

Gestures and gesture recognition are terms increasingly encountered in discussions of human-computer interaction. The gestural equivalent of direct manipulation interfaces are those which use gesture alone. These can range from interfaces that recognize a few symbolic gestures to those that implement fully fledged sign language interpretation. Similiary interfaces may recognize static hand poses, or dynamic hand motion, or a combination of both. In this paper, we focused into the development of hand gesture recognition using particle filter to apply the virtual interview system. As shown in Figure 1, the virtual interview system is designed for interviewee to make a practice before facing real interview. But this

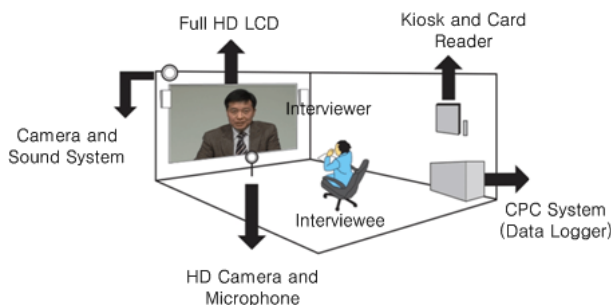


Fig. 1. Overall hand motion recognition operation diagram

system is not automatically interactive system between interviewee and its system. So, it is needed to revise the system as a fully automated mode. We applied particle filter for hand motion recognition and tracking. Particle filter [1] is based

on the Bayesian conditional probability such as *prior* distribution and *posterior* distribution. First of all, we expanded the existing algorithm [2] to derive the CONDENSATION-based particle filter for hand motion recognition. Also, we adopt the nine hand motion model to confirm the algorithm performance such as leftover and paddle. The overall scheme for the hand motion recognition system is shown in Figure 2.

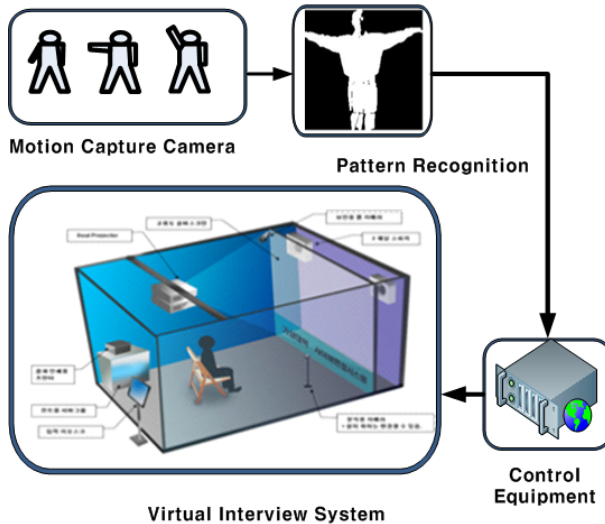


Fig. 2. Overall System Operation Diagram

2 CONDENSATION Algorithm

2.1 Particle Filter Algorithm

The particle filter approach to track motion, also known as the condensation algorithm [1] and Monte Carlo localisation , uses a large number of particles to explore the state space. Each particle represents a hypothesised target location in state space. Initially the particles are uniformly randomly distributed across the state space, and each subsequent frame the algorithm cycles through the steps illustrated in Figure 3.

1. Deterministic drift: particles are moved according to a deterministic motion model (a damped constant velocity motion model was used).
2. Update probability density function (PDF): Determine the probability for every new particle location.
3. Resample particles: 90 percent of the particles are resampled with replacement, such that the probability of choosing a particular sample is equal to the PDF at that point; the remaining 10 percent of particles are distributed randomly throughout the state space.

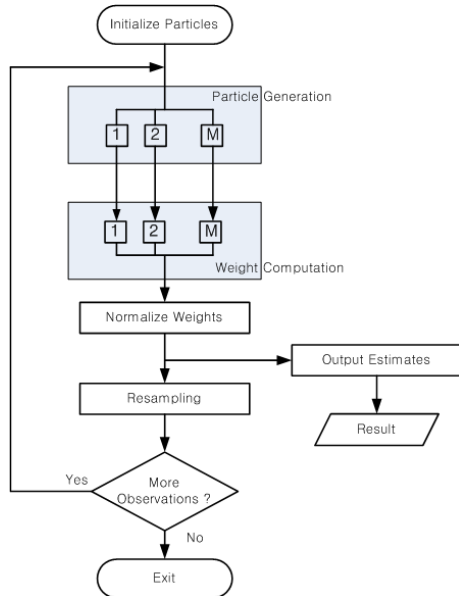


Fig. 3. Process of particle filter calculation

4. Diffuse particles: particles are moved a small distance in state space under Brownian motion.

This results in particles congregating in regions of high probability and dispersing from other regions, thus the particle density indicates the most likely target states. See [3] for a comprehensive discussion of this method. The key strengths of the particle filter approach to localisation and tracking are its scalability (computational requirement varies linearly with the number of particles), and its ability to deal with multiple hypotheses (and thus more readily recover from tracking errors). However, the particle filter was applied here for several additional reasons:

- it provides an efficient means of searching for a target in a multi-dimensional state space.
- reduces the search problem to a verification problem, ie. is a given hypothesis face-like according to the sensor information?
- allows fusion of cues running at different frequencies.

2.2 Application of Particle Filter for the Hand Motion Recognition

In order to apply the particle filter algorithm to hand motion recognition, we extend the methods described by Black and Jepson [2]. Specifically, a state at time t is described as a parameter vector: $s_t = (\mu, \phi^i, \alpha^i, \rho^i)$ where: μ is the integer index of the predictive model, ϕ^i indicates the current position in the

model, α^i refers to an amplitudal scaling factor and ρ^i is a scale factor in the time dimension. Note that i indicates which hand's motion trajectory this ϕ^* , α^* , or ρ^* refers to left and right hand where $i \in \{l, r\}$. My models contain data about the motion trajectory of both the left hand and the right hand; by allowing two sets of parameters, I allow the motion trajectory of the left hand to be scaled and shifted separately from the motion trajectory of the right hand (so, for example, ϕ^l refers to the current position in the model for the left hand's trajectory, while ϕ^r refers to the position in the model for the right hand's trajectory). In summary, there are 7 parameters that describe each state.

Initialization. The sample set is initialized with N samples distributed over possible starting states and each assigned a weight of $\frac{1}{N}$. Specifically, the initial parameters are picked uniformly according to:

$$\begin{aligned}\mu &\in [1, \mu_{max}] \\ \phi^i &= \frac{1 - \sqrt{y}}{\sqrt{y}}, y \in [0, 1] \\ \alpha^i &= [\alpha_{min}, \alpha_{max}] \\ \rho^i &\in [\rho_{min}, \rho_{max}]\end{aligned}\tag{1}$$

Prediction. In the prediction step, each parameter of a randomly sampled s_t is used to s_{t+1} determine based on the parameters of that particular s_t . Each old state, s_t , is randomly chosen from the sample set, based on the weight of each sample. That is, the weight of each sample determines the probability of its being chosen. This is done efficiently by creating a cumulative probability table, choosing a uniform random number on $[0, 1]$, and then using binary search to pull out a sample (see Isard and Blake for details [1]). The following equations are used to choose the new state :

$$\begin{aligned}\mu_{t+1} &= \mu_t \\ \phi_{t+1}^i &= \phi_t^i + \rho_t^i + N(\sigma_\phi) \\ \alpha_{t+1}^i &= \alpha_t^i + N(\sigma_\alpha) \\ \rho_{t+1} &= \rho_t + N(\sigma_\rho)\end{aligned}\tag{2}$$

where $N(\sigma_*)$ refers to a number chosen randomly according to the normal distribution with standard deviation σ_* . This adds an element of uncertainty to each prediction, which keeps the sample set diffuse enough to deal with noisy data. For a given drawn sample, predictions are generated until all of the parameters are within the accepted range. If, after, a set number of attempts it is still impossible to generate a valid prediction, a new sample is created according to the initialization procedure above.

Updating. After the Prediction step above, there exists a new set of N predicted samples which need to be assigned weights. The weight of each sample is

a measure of its likelihood given the observed data $Z_t = (z_t, z_{t_1}, \dots)$. We define $Z_{t,i} = (z_{t,i}, z_{(t-1),i}, \dots)$ as a sequence of observations for the i th coefficient over time; specifically, let $Z_{(t,1)}, Z_{(t,2)}, Z_{(t,3)}, Z_{(t,4)}$ be the sequence of observations of the horizontal velocity of the left hand, the vertical velocity of the left hand, the horizontal velocity of the right hand, and the vertical velocity of the right hand respectively. Extending Black and Jepson [2], we then calculate the weight by the following equation:

$$p(z_t|s_t) = \prod_{i=1}^4 p(Z_{t,i}|s_t) \quad (3)$$

where $p(z_{t,i}|s_t) = \frac{1}{\sqrt{2\pi}} \exp^{-\frac{\sum_{j=0}^{\omega-1} (z_{(t-j),i} - \alpha^* m_{(\phi^* - \rho^* j),i}^\mu)^2}{2(\omega-1)}}$ and where ω is the size of a temporal window that spans back in time. Note that ϕ^* , α^* and ρ^* refer to the appropriate parameters of the model for the blob in question and that $\alpha^* m_{(\phi^* - \rho^* j),i}^\mu$ refers to the value given to the i th coefficient of the model μ interpolated at time $\phi^* - \rho^* j$ and scaled by α^* .

3 Experiment Result

To test the proposed particle filter scheme, we used two gesture model which is shown in Figure 4 in this paper. The coefficient of particle filter are $\mu_{max} = 2$, $\alpha_{min} = 0.5$, $\alpha_{max} = 1.5$, $\rho_{min} = 0.5$, $\rho_{max} = 1.5$ to maintain the 50Also, the other parameters are settled by $\sigma_\phi = \sigma_\alpha = \sigma_\rho = 0.1$. The variable of ω equation 3 is 10.

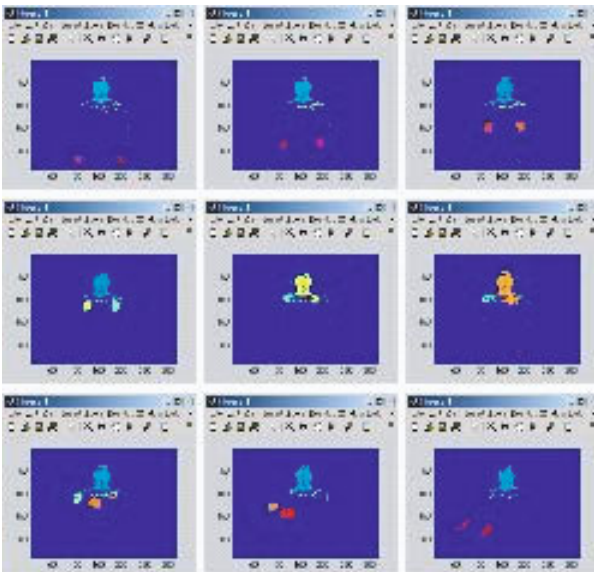


Fig. 4. The Tracking process of particle filter for the model 1(From left to right, top to down)

4 Conclusions

In this paper, we have developed the particle filter for the hand motion recognition. This scheme is important in providing a computationally feasible alternative to classify the hand motion in real interview system. We have proved that given an image, particle filter scheme classify the hand motion recognition in real time.

References

1. Isard, M., Blake, A.: CONDENSATION-conditional Density Propagation for Visual Tracking. *International Journal of Computer Vision* 29(1), 5–28 (1998)
2. Black, M.J., Jepson, A.D.: A Probabilistic Framework for Matching Temporal Trajectories: Condensation-based Recognition of Gestures and Expressions. In: Burkhardt, H.-J., Neumann, B. (eds.) *ECCV 1998. LNCS*, vol. 1406, pp. 909–924. Springer, Heidelberg (1998)
3. Isard, M., Blake, A.: A Mixed-state Condensation Tracker with Automatic Model-switching. In: *Proceedings 6th International Conference of Computer Vision*, pp. 107–112 (1998)
4. Lee, Y.W.: Adaptive Data Association for Multi-target Tracking Using Relaxation. In: Huang, D.-S., Zhang, X.-P., Huang, G.-B. (eds.) *ICIC 2005. LNCS*, vol. 3644, pp. 552–561. Springer, Heidelberg (2005)
5. Lee, Y.W., Seo, J.H., Lee, J.G.: A Study on the TWS Tracking Filter for Multi-Target Tracking. *Journal of KIEE* 41(4), 411–421 (2004)

Integrated Real-Time Vision-Based Preceding Vehicle Detection in Urban Roads

Yanwen Chong¹, Wu Chen², Zhilin Li², William H.K. Lam³, and Qingquan Li¹

¹ State Key Laboratory for Information Engineering in Surveying,
Mapping and Remote Sensing, Wuhan University, 129 Luoyu Road,
Wuhan 430079, China

lmarschongyw@gmail.com, qqli@whu.edu.cn

² Department of Land Surveying and Geoinformatics,
Hong Kong Polytechnic University, Kowloon, Hong Kong, China

{lswuchen, lslzli}@inet.polyu.edu.hk

³ Department of Civil and Structural Engineering,
Hong Kong Polytechnic University, Kowloon, Hong Kong, China

cehklam@polyu.edu.hk

Abstract. This paper presents a real-time algorithm for a vision-based preceding vehicle detection system. The algorithm contains two main components: vehicle detection with various vehicle features, and vehicle detection verification with dynamic tracking. Vehicle detection is achieved using vehicle shadow features to define a region of interest (ROI). After utilizing methods such as histogram equalization, ROI entropy and mean of edge image, the exact vehicle rear box is determined. In the vehicle tracking process, the predicted box is verified and updated. Test results demonstrate that the new system possesses good detection accuracy and can be implemented in real-time operation.

Keywords: Feature extraction, Shadow boundary, Vision tracking, Vehicle detection.

1 Introduction

Real-time vision-based preceding vehicle detection systems have many applications. They can be used to assist drivers in perceiving any dangerous situations earlier to avoid accidents through sensing and understanding of the environment around the vehicle [1]-[2].

The vehicle detection process can be carried out in the road triangle. To detect the preceding vehicle using a feature-based method, the use of 2D features, such as shadow, rear lights, symmetry, texture, edge and shape has been widely studied[3]–[5]. Betke [3] developed a real-time vision system that analyzed color videos taken from a forward-looking video camera in a car driving on a highway. The system used a combination of color, edge and motion information to recognize and track the road boundaries, lane markings and other vehicles on the road. Huang [5] used shadow information underneath a vehicle as a sign pattern for the preceding vehicle detection and a classic Sobel edge operator was used to detect the horizontal shadow points.

Detection verification with tracking is a common vision-based approach, which predicts the vehicle location in the following frames [3], [6], [7]. Vehicle detection can be improved considerably, both in terms of accuracy and time, by taking advantage of the temporal continuity present in the data. Shen [7] proposed a position prediction mechanism to track the vehicle based on a constant speed model. In this paper, we propose a more general vehicle position prediction formula, which is suitable for not only the constant velocity situation but also for when the vehicle accelerates or decelerates. In this way, the detected vehicle in the following frame will be located more precisely.

2 Vehicle Detection with Shadow Feature

We assume that the road triangle includes all our objects of interest (roads and vehicles) is gotten. The following vehicle detection process will be carried out in the road triangle. Using shadow information as a sign pattern for vehicle detection has been discussed by many authors [5], [8], but there is no systematic way to select appropriate threshold values. The intensity of the vehicle shadow depends on the illumination of the captured image, which in turn depends on the weather and road conditions. In our approach, instead of taking the absolute threshold of the image, we extract the underneath candidates by checking the gradient of intensity as a local feature of vehicle shadow in the image. Because the vehicle shadow is spatially continuous, a gradient mask can be used to detect the underneath shadow line. The Sobel operator is a classic first order edge detection operator that finds gradient in a direction [5], [7], [9] and Fig. 1(a) shows the Sobel operator matrix. Huang [5] adopted the values with $a=1$, $b=2$ to extract vehicle shadows and the result of Fig. 1(b) after the Sobel operator is given in Fig. 1(c). To further highlight the horizontal edge of vehicle shadows, the Scharr Sobel operator with $a=3$, $b=10$ was adopted in our algorithm [10]. With the Scharr Sobel operator, the result of the original image (Fig. 1(b)) is shown in Fig. 1(d). Comparing Fig. 1(c) and Fig. 1(d), the horizontal edges obtained with the Scharr operator are much clearer and therefore the vehicle shadows will be easier to detect.

After the vehicle shadow lines are extracted from an image, we try to form initial ROIs based on the shadow information. Firstly, the shadow image (i.e., Fig. 1(d)) is scanned from bottom to top and only those horizontal edge pixels with an intensity greater than T_1 and a continuous pixel number greater than $f \times T_2$ (f is a scale parameter proportional to the distance to the host vehicle) are retained and are considered as the width of a vehicle ROI. The height of the ROI is set as $4/3$ times the width. Fig. 1(e) shows the potential vehicle ROIs in the image.

Although the Scharr operator enhances the horizontal lines in the image, some non-vehicle interferences such as tree shadows, building shadows, or road irregularities can cause false positives (as shown in Fig. 1(e)). To remove these false positives, the initial ROI generated based on the shadow feature is further examined by the ROI entropy and mean of edge image.

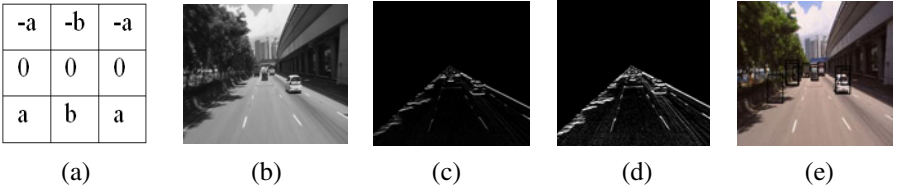


Fig. 1. The horizontal edge operators and the resulting ROI in the road triangle

2.1 ROI Entropy

A ROI entropy reflects the variation of pixel luminance value in a selected area. Given the pixel intensity range $[0, 1, 2, \dots, L-1]$ in a ROI, with the corresponding frequencies of probability $P_0, P_1, P_2, \dots, P_{L-1}$, the ROI entropy is defined as follows:

$$E_{ROI} = - \sum_0^{L-1} P_n \log P_n \quad (1)$$

The more diverse the pixel luminance value in a ROI, the greater is the entropy value of the ROI. Generally the variations in pixel luminance values in the vehicle area are larger than those in the road background; therefore the ROI entropy can be used to distinguish vehicles from road background.

In our approach, each ROI entropy is calculated and the mean image entropy E_{image} , defined as the mean value of all the ROI entropies, is used as the threshold. If E_{ROI} is less than E_{image} , the ROI is considered as an interference.

2.2 Mean of Edge Image

The Roberts edge operator is designed to extract edges in an image. In the ROI including the vehicle, the edge information is richer than that in other areas. Thus, we also apply the Roberts operator to obtain the edge information in the initial ROI for the purpose of removing false positives. Defining the mean value of the edge pixel in a ROI as ME_{ROI} , and the average value of all the ME_{ROI} in the image as ME_{image} , if

ME_{ROI} is less than ME_{image} , the initial ROI is considered as an interference.

After applying the ROI entropy and the mean of edge criteria, the false positive ROIs using shadow features are removed. Also the edge information can help us to refine the size of ROI. In every ROI, the Roberts edge image is examined. The region enclosed by a pair of vertical edges and a pair of horizontal edges will be taken as a vehicle candidate. The exact vehicle rear rectangle limited by the horizontal edges and vertical edges in the ROI is obtained.

3 Vehicle Detection with Prediction and Verification

The accuracy and efficiency of vehicle detection can be further improved by taking advantage of the temporal continuity of a vehicle presented in continuous images [3].

This tracking process can be divided into a two step approach: prediction and verification. The prediction uses a kinematic model to predict the position of ROI in the next image, while the verification checks if in the predicted location we can find the same object as in the previous image.

Shen [7] proposed a ROI prediction algorithm based on the constant velocity model. When we applied Shen's method in the testing images, significant prediction errors were found, particularly when the front vehicles had accelerations. Based on a constant acceleration model, we derived new ROI prediction formulae:

$$x(t+1) = 3[x(t) - x(t-1)] + x(t-2) \quad (2)$$

$$y(t+1) = 3[y(t) - y(t-1)] + y(t-2) \quad (3)$$

where (x, y) are the coordinates of the upper-left and bottom-right corner point of the prediction region, t is time.

Fig. 2 shows the prediction results with Shen's method and the new prediction method. In this example, a truck is detected and a ROI box is determined, then the tracking process begins. The black box in the image shows the predictions in the subsequent images. With Shen's prediction approach (the top row), the predicted ROI gradually moved away from the real truck location. When the new prediction algorithm is applied (the bottom row in Fig. 2), the predicted ROI is well matched with the vehicle.

In the verification process, the following criteria is used [7]:

$$|R(t+1) - R(t)| < T \text{ and } |G(t+1) - G(t)| < T \text{ and } |B(t+1) - B(t)| < T \quad (4)$$

where $R(t+1)$, $G(t+1)$, and $B(t+1)$ are Red, Green, Blue color mean values of the detected box, respectively, at time $t+1$. $R(t)$, $G(t)$, and $B(t)$ are the Red, Green and Blue color mean values of the detected box, respectively, at time t , and T is a threshold value. The T value will be changed based on experimental data. If the R , G , B mean values of a predicted box satisfy the criteria, the predicted box is valid for tracking.

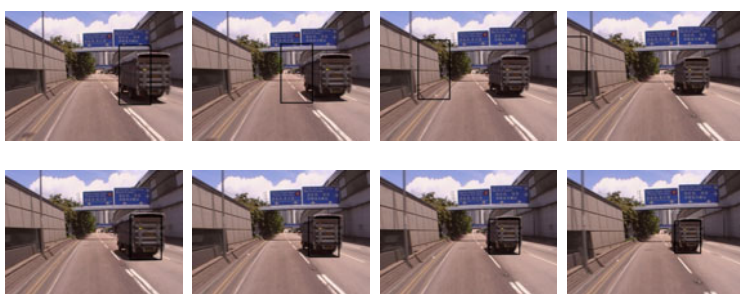


Fig. 2. The prediction of vehicle location using different prediction methods. Shen's algorithm (top row), New algorithm (the bottom row).

4 Experiment Results

To evaluate the performance of the proposed vehicle detection system, tests were carried out under different driving conditions in Hong Kong. The system includes a normal video camera and a standard PC (core 2 Duo GPU 2.5 G). It can process approximately 20 fps, which is sufficient for real-time applications.

Fig. 3 show detection results in typical Hong Kong urban roads. The bounding box superimposed on the original images shows the final detection results. In Fig. 3, the four vehicles are far away from the host vehicle. Once a vehicle is detected then the tracking process will be carried out.

To evaluate the performance of our system, we carried out a test on different roads in Hong Kong for 2 hours. The total number of vehicles in the video images was 1856, of which 1747 vehicles were automatically detected (or a detection rate of 94.1%). This is compatible with other studies by Shen [7] and Huang [5], with detection rates of 98.9% and 87.8%, respectively, although the road conditions are different in different tests. There were some cases of mis-detections and false detections. The main reasons for mis-detections are either the vehicle shadows were too weak to extract or the front vehicles were too close to the host vehicle. The false positives are mainly due to the interference of environmental noise, such as trees, buildings or stains on the road.



Fig. 3. Vehicle detection and tracking example in the urban main road where the four vehicles are far away from the host vehicle

5 Discussions and Conclusions

Robust and reliable vehicle detection in images is vital to driver assistance systems or autonomous vehicles. It can also be used to monitor traffic conditions. In this paper, we proposed a new method to detect vehicles in front using moving video images, employing various vehicle features, such as vehicle shadows, luminance entropy, edges and multiple images tracking. This system can be used to extract traffic information on roads (i.e., number of vehicles, road occupation rate, and vehicle density), to estimate the relative positions and speeds among vehicles, and to classify vehicle types.

The main limitation of the proposed method is that the vehicle shadow or the rear lights must be clear in the images. Therefore, vehicles that are too close or too far away cannot be detected by the system.

Acknowledgments. This paper was supported by an internal research grant J-BB7Q from the research committee of the Hong Kong Polytechnic University, LIESMARS Special Research Funding and the National Natural Science Foundation of China (40721001,40830530).

References

1. Darms, M.S., Rybski, P.E., Baker, C., Urmson, C.: Obstacle Detection and Tracking for the Urban Challenge. *IEEE T. Intell. Transp.* 10, 475–485 (2009)
2. Heimes, F., Nagel, H.: Towards Active Machine-Vision-Based Driver Assistance for Urban Areas. *Int. J. Comput. Vision.* 50, 5–34 (2002)
3. Betke, M., Haritaoglu, E., Davis, L.: Real-time Multiple Vehicle Detection and Tracking from A Moving Vehicle. *Mach. Vision Appl.* 12, 69–83 (2000)
4. Hoffman, C., Dang, T., Stiller, C.: Vehicle Detection Fusing 2D Visual Features. In: Proc. IEEE Intelligent Vehicles Symp., pp. 280–285. IEEE Press, Parma (2004)
5. Huang, S., Chen, C., Hsiao, P., Fu, L.: On-board Vision System for Lane Recognition and Front-vehicle Detection to Enhance Driver's Awareness. In: Proc. 2004 IEEE Int. Conf. Robotics and Automation, pp. 2456–2461. IEEE Press, New Orleans (2004)
6. Lefaix, G., Marchand, T., Bouthemy, P.: Motion-based Obstacle Detection and Tracking for Car Driving Assistance. In: Proc. 16th Int. Conf. Pattern Recognition, pp. 74–77. IEEE Computer Society Press, Los Alamitos (2002)
7. Shen, X.L.: Vision Detection of Lanes and Vehicles for Advanced Safety Vehicles. National Central University, Chung-li (2007)
8. Mori, H., Charkai, N.: Shadow and Rhythm as Sign Patterns of Obstacle Detection. In: Proc. Int'l Symp. Industrial Electronics, pp. 271–277. IEEE Press, Budapest (1993)
9. Wang, C., Thorpe, C., Suppe, A.: Radar-Based Detection and Tracking of Moving Objects from a Ground Vehicle at High Speeds. In: Proc. IEEE Intelligent Vehicles Symp., pp. 416–421. IEEE Press, Columbus (2003)
10. Zhang, L., Zhang, L., Mou, X.Q., Zhang, D.: FSIM: a Feature Similarity Index for Image Quality Assessment. *IEEE Trans. Image Processing* (to appear)

Real-Time Face Detection Using Integral Histogram of Multi-scale Local Binary Patterns

Sébastien Paris¹, Hervé Glotin¹, and Zhong-Qiu Zhao²

¹ LSIS/DYNI, Université Aix-Marseille,
Avenue Escadrille Normandie Niemen,
13397 MARSEILLE Cedex 20, France

sebastien.paris@lsis.org, glotin@univ-tln.fr

² Laboratory of Image Information Processing,
Hefei University of Technology
Tunxi Road No.193, Hefei, Anhui, China (230009)
zhongqiuzhao@gmail.com

Abstract. This paper introduces a novel fast and efficient method for face detection using integral histogram of multi-scale local binary patterns (HMSLBP). Histogram of LBP and its variants are among the state-of-the-art descriptors in vision systems and is very competitive compared to well known Bag-of-SIFT. HMSLBP has the property to be mainly linearly separable and can be trained efficiently with a fast large-scale support vector machine (SVM) solver. The new proposed detector offers a framerate superior to 20 fps in VGA mode with modern computers.

Keywords: Face detection, LBP, Integral Histogram, Large-Scale SVM.

1 Introduction

Supervised patterns recognition, especially for face detection applications have received a lot of attention during the last two decades. For real-time systems, several thousand of sub-windows must be scanned in a fraction of seconds per frame. At least two major bottlenecks are encountered: i) the feature extraction processing and ii) the model prediction for classifying each sub-window input. In order to tackle such problems, [9] had first introduced 3 basic ingredients for building an efficient real-time machine: i) Haar's rectangle features with their fast computation thanks to the integral image technique, ii) boosting methods by providing a strong linear predictor using only a small subset of available features and iii) a cascade procedure in order to reject as soon as possible a non-face candidate.

Histograms of LBP are competitive features widely used in face recognition, texture classification and scene categorization [6][10]. Each LBP can be seen as a visual micro-pattern encoding mainly contours and differential excitation informations of the 8 neighbors surrounding a central pixel. The final visual descriptor HLBP is built by counting occurrences of each LBP in a region of interest (ROI).

Variants of LBP can improve accuracy and/or reduce the number of histogram bins. Center-Symmetric LBP [2] uses a 4 neighborhood topology limiting dictionary size to 16 elements, whereas multi-scale LBP [4][6] encodes relations between blocks of $(s \times s)$ pixels in order to capture information at different scales. For real-time face detection, computing several thousand of histograms consumes the major amount of time spent in the detection process.

2 Histogram of Multi-scale Local Binary Pattern with Spatial Pyramid Architecture

In this section, we present two multi-scale versions of LBP for an image \mathbf{I} ($n_y \times n_x$), *i.e.* the MSLBP and the center-symmetric variant CSMSLBP. Basically MSLBP encodes the relationship between a central block of $(s \times s)$ pixels located in (y_c, x_c) with its 8 neighbors blocks whereas center-symmetric MSLBP encodes the relationship between symmetric blocks of the central one. These 2 micro-patterns are defined as follows:

$$\begin{cases} MSLBP(y_c, x_c, s) = \sum_{i=0}^{i=7} \mathbb{1}_{\{A_i \geq A_c\}} 2^i \in \{0, 255\} \\ CSMSLBP(y_c, x_c, s) = \sum_{i=0}^{i=3} \mathbb{1}_{\{A_i \geq A_{i+4}\}} 2^i \in \{0, 15\}, \end{cases} \quad (1)$$

where $A_c, \{A_i\}_{i=0,\dots,7}$ design area of the central block and areas of its 8 neighbors respectively and $\mathbb{1}_{\{x\}} = 1$ if event x is true, 0 otherwise. The different areas in eq.(1) can be computed efficiently thanks to the image integral technique. Let's define \mathbf{II} the image integral of \mathbf{I} by $\mathbf{II}(y, x) \triangleq \sum_{y'=0}^{y' < y} \sum_{x'=0}^{x' < x} \mathbf{I}(y', x')$.

Any square area $A(y, x, s)$ with upper-left corner located in (y, x) and side length s can be computed with only 4 values and 3 operations, $A(y, x, s) = \mathbf{II}(y + s, x + s) + \mathbf{II}(y, x) - (\mathbf{II}(y, x + s) + \mathbf{II}(y + s, x))$. For any scale s , MSLBP requires $(8 + 1) \times 3$ operations whereas CSMSLBP only 8×3 for computing $A_c = A(y_c, x_c, s)$ and $\{A_i\}_{i=0,\dots,8}$ areas in eq.(1). For the sequel, we will use the unique notation LBP for both MSLBP or CSMSLBP. The histogram of LBP for the current scale s , computed on the entire image \mathbf{I} and denoted $\mathbf{x}_{LBP}(\mathbf{I}, s)$ is defined by concatenation of the b bins $h_{LBP}(\mathbf{I}, j, s)$ such $\mathbf{x}_{LBP}(\mathbf{I}, s) \triangleq [h_{LBP}(\mathbf{I}, 0, s), \dots, h_{LBP}(\mathbf{I}, b - 1, s)]^T$, $s = 0, \dots, S - 1$ where S denotes number of scales used (S is the cardinal of the set \mathcal{S}) and $b = \{256, 16\}$ for MSLBP or CSMSLBP respectively. Each bin $h_{LBP}(\mathbf{I}, j, s)$ is calculated by summing LBP over the image \mathbf{I} such as $h_{LBP}(\mathbf{I}, j, s) = \sum_{y_c=s-1}^{y_c=n_y-s-1} \sum_{x_c=s-1}^{x_c=n_x-s-1} \mathbb{1}_{\{LBP(y_c, x_c, s) = j\}}$. Most computation time of the detector is spent during the last equation especially when a spatial pyramid is used to retrieve several local histograms at a time (associated with each sub-windows of the spatial pyramid). Fortunately, following the work of [7], integral histogram framework can be used to accelerate this process. This approach is equivalent to build b integral images of LBP. From eq.(1), we construct the two

following 4D-tensors of size $(n_y \times n_x \times b \times S)$: $\mathbf{I}_{LBP}(y, x, j, s) = \mathbb{1}_{\{LBP(y, x, s)=j\}}$ and $\mathbf{II}_{LBP}(y, x, j, s) = \sum_{y'=0}^{y' \leq y} \sum_{x'=0}^{x' \leq x} \mathbf{I}_{LBP}(y', x', j, s)$ where $\mathbf{I}_{LBP}(y, x, j, s) \in \{0, 1\}$

is in practice deeply sparse. \mathbf{II}_{LBP} represents all images integral for each LBP value. Now each bin $h_{LBP}(\mathbf{I}, j, s)$ can be efficiently retrieved from \mathbf{II}_{LBP} tensor by $h_{LBP}(\mathbf{I}, j, s) = \mathbf{II}_{LBP}(n_y, n_x, j, s) + \mathbf{II}_{LBP}(0, 0, j, s) - (\mathbf{II}_{LBP}(0, n_x, j, s) + \mathbf{II}_{LBP}(n_y, 0, j, s))$. According to last equation, only 4 values and 3 computations are required to compute each bin histogram. Moreover, for any rectangle $\mathbf{R}(y, x, h, w) \subseteq \mathbf{I}$ with upper-left corner located in (y, x) , with height h and width w , we can compute each bin histogram $h_{LBP}(\mathbf{R}, j, s)$ for $\mathbf{x}_{LBP}(\mathbf{R}, s)$ in the same way $h_{LBP}(\mathbf{R}, j, s) = \mathbf{II}_{LBP}(y+h, x+w, j, s) + \mathbf{II}_{LBP}(y, x, j, s) - (\mathbf{II}_{LBP}(y, x+w, j, s) + \mathbf{II}_{LBP}(y+h, x, j, s))$. The last equation will be useful when \mathbf{R} will represent one of the W sub-windows associated with the spatial pyramid introduced in the next section. For all the S scales, the final full histogram is built by concatenated all histograms $\mathbf{x}_{LBP}(\mathbf{R}, s)$ as $\mathbf{x}_{LBP}(\mathbf{R}) \triangleq [\mathbf{x}_{LBP}(\mathbf{R}, 0), \dots, \mathbf{x}_{LBP}(\mathbf{R}, S-1)]^T$. The histogram $\mathbf{x}_{LBP}(\mathbf{I}, s)$ captures global information of the entire image \mathbf{I} at scale s . In order to be more discriminative, we propose to use a L levels spatial pyramid dividing \mathbf{I} in W sub-windows. It permits to capture local informations through the W local histograms $\{\mathbf{x}_{LBP}(\mathbf{R}_p, s)\}$, $p = 0, \dots, W-1$, $s = 0, \dots, S-1$. More precisely, the L levels pyramid is defined through the matrix $\Lambda \triangleq [\mathbf{r}_y, \mathbf{r}_x, \mathbf{d}_y, \mathbf{d}_x]$ of size $(L \times 4)$. For a level $l \in \{0, \dots, L-1\}$, image \mathbf{I} is divided into possibly overlapping sub-windows $\mathbf{R}_{l,v}$ of size $(h_l \times w_l)$. In our implementation, $h_l \triangleq \lfloor n_y r_{y,l} \rfloor$ and $w_l \triangleq \lfloor n_x r_{x,l} \rfloor$ where $r_{y,l}$ and $r_{x,l}$ are the l^{th} element of \mathbf{r}_y and \mathbf{r}_x respectively. Sub-windows shifts in x-y axis are defined by integers $\delta_{y,l} \triangleq \lfloor n_y d_{y,l} \rfloor$ and $\delta_{x,l} \triangleq \lfloor n_x d_{x,l} \rfloor$ where $d_{y,l}$ and $d_{x,l}$ are element of \mathbf{d}_y and \mathbf{d}_x respectively. Overlapping can be performed if $d_{y,l} \leq r_{y,l}$ and/or $d_{x,l} \leq r_{x,l}$. Full histogram vector $\mathbf{x}_{LBP}^{spyr}(\mathbf{I}, \Lambda)$ is obtained by concatenating all $\mathbf{H}_{LBP}(\mathbf{R}_{l,v}, s)$ such as

$$\begin{aligned} \mathbf{x}_{LBP}^{spyr}(\mathbf{I}, \Lambda) &\triangleq [\lambda_0 \mathbf{x}_{LBP}(\mathbf{R}_{0,0}, 0), \dots, \lambda_0 \mathbf{x}_{LBP}(\mathbf{R}_{0,W_0-1}, 0), \dots, \\ &\quad \lambda_{L-1} \mathbf{x}_{LBP}(\mathbf{R}_{L-1,0}, 0), \dots, \lambda_{L-1} \mathbf{x}_{LBP}(\mathbf{R}_{L-1,W_{L-1}-1}, 0), \dots, \\ &\quad \lambda_0 \mathbf{x}_{LBP}(\mathbf{R}_{0,0}, S-1), \dots, \lambda_0 \mathbf{x}_{LBP}(\mathbf{R}_{0,W_0-1}, S-1), \dots, \\ &\quad \lambda_{L-1} \mathbf{x}_{LBP}(\mathbf{R}_{L-1,0}, S-1), \dots, \lambda_{L-1} \mathbf{x}_{LBP}(\mathbf{R}_{L-1,W_{L-1}-1}, S-1)]^T, \end{aligned} \quad (2)$$

where $\lambda_l = \left(\frac{\max_{j=0, \dots, L-1} \{h_j\}}{h_l} \right) \cdot \left(\frac{\max_{j=0, \dots, L-1} \{w_j\}}{w_l} \right)$ represents the weight associated with the l^{th} pyramid level and is proportional to the ratio of the current area $\mathbf{R}_{l,v}$ versus the biggest area found in the set of rectangles. Total size of histogram $\mathbf{x}_{LBP}^{spyr}(\mathbf{I}, \Lambda)$ is equal to $d = b.W.S.$

3 Large-Scale Linear Support-Vector Machine

For training model efficiently, according to the Vapnik theory, we aim to minimize the structural error in order to generalize performances on unseen data.

A finer analyse indicates that the second error term of the total risk'upper bound is increasing when the VC dimension \hbar is also increasing. This later is directly linked with the particular choice of the kernel, $\hbar = 2d + 1$ for linear kernel and $\hbar = \infty$ for RBF kernel for examples. In other words, one may prefer a simple linear separator especially when input feature dimension d is high. This conducts to large-scale linear SVM solvers based on efficient Newton optimizers [3]. Complexity of such large-scale solver is reduced to $O(dN)$. For the rest of this section, we will use the notation \mathbf{x} for \mathbf{x}_{LBP}^{spyr} . Let's define the set of LBP histograms by $\mathbf{X} \triangleq \{\mathbf{x}_1, \dots, \mathbf{x}_N\}$ and their corresponding labels $\mathbf{y} \triangleq \{y_1, \dots, y_N\}$ where $\mathbf{x}_i \in \mathcal{X} \subseteq \mathbb{R}^d$ and $y_i \in \{-1, 1\}$. We assume that $\mathbf{X} = \mathbf{P} \cup \mathbf{N}$ i.e. the union of a positive (face) and negative (non-face) sets. $N = N^+ + N^-$ where N^+ , N^- design number of positives and negatives examples respectively. The linear SVM problem consists to find the hyperplane parameter $\hat{\mathbf{w}}$ minimizing the sum of a ℓ_2 loss function and a ℓ_2 regulation term such that $\hat{\mathbf{w}}^T = \arg \min_{\mathbf{w}} \left\{ \frac{1}{2} \mathbf{w}^T \mathbf{w} + C \sum_{i=1}^N \max(1 - y_i \mathbf{w}^T \mathbf{x}_i, 0)^2 \right\}$. To solve this problem, we use a modified version of the liblinear package [1] accepting dense input vectors and available from [5]. The procedure to train full model is described as follows: we sample with replacement an initial pool of N^+ positive examples to form \mathbf{P} . Moreover, in order to introduce more diversity and robustness in the model, we apply according the probabilities p_θ and p_s a rotation $\theta \sim \mathcal{N}(0, \sigma_\theta^2)$ and a scaling factor $r_p \sim U_{[r_{p,l}, r_{p,u}]}$ to each drawn positive image. The size of positive example will be $(n_y r_p \times n_x r_p)$. For negatives, we randomly select an image from the set of collected pictures then extract uniformly inside it a patch of size $(n_y r_n \times n_x r_n)$ where $r_n \sim U_{[r_{n,l}, r_{n,u}]}$. We repeat this operation until to have N^- images to form \mathbf{N} . We solve SVM with $\mathbf{X} = \mathbf{P} \cup \mathbf{N}$ (and corresponding labels vector \mathbf{y}) to obtain the initial parameter $\hat{\mathbf{w}}_0^T$. In order to decrease false alarms rate, we add to \mathbf{N} , ΔN^- new examples defining the set $\Delta \mathbf{N}_1$ (and extracted by the same way described previously) whom are predicted as positives by applying current model $\hat{\mathbf{w}}_0^T$. The set \mathbf{N} is augmented and becomes $\mathbf{N} \cup \Delta \mathbf{N}_1$ and we learn a new model $\hat{\mathbf{w}}_1^T$. We repeat this procedure a maximum of K times and/or until false alarme rate is below a fixed threshold.

4 Results

The associated detector scans a full image \mathbf{Y} of $(N_y \times N_x)$ pixels over multiple shifting windows \mathbf{I} with increasing size $(n_y \times n_x)$. The 3 main parameters control these windows and typically for a VGA image of (640×480) pixels wise approximatively $M = 30000$ windows are used with size starting from (24×24) to (320×240) . Our detector demands a total of $O(N_y N_x (1 + 27S + bS) + 6M d)$ operations. We illustrate performances of our approach¹ for several parameter choices: HCSMSLBP/HMSLBP feature, scaling set \mathcal{S} , spatial pyramid \mathbf{A} .

¹ Results can be retrieved by using our face detection toolbox for Matlab available in <http://www.mathworks.com/matlabcentral/fileexchange/24092-face-detection-toolbox>

Positive examples are retrieved from the LFWcrop Face Dataset [8] with 13233 grey images and size resolution equal to (64×64) . Negative examples are extracted from pictures collected from the web. We fix the following parameters to train models $N^+ = 9000$, $N^- = 15000$, $\Delta N^- = 1000$, $K = 5$, $p_\theta = 0.05$, $p_s = 1$, $\sigma_\theta^2 = 7^2$ deg, $r_{p,l} = 0.8$, $r_{p,u} = 1.5$, $r_{n,l} = 0.7$, $r_{n,u} = 3$, $C = 2$. For testing, positive examples are retrieved from our collection of 4920 frontal images with equal proportion of men and women aged from 20 to 79 and with size resolution approximately equal to (128×128) (publishing agreement is actually pending). These positives capture more hair and ears parts compared to the LFWcrop'ones. This is introducing more diversity/difficulties in the test set. Negative test examples are also retrieved from web. We use the following parameters for generating testing data: $N^+ = 3000$, $N^- = 7000$, $p_\theta = 0.05$, $p_s = 1$, $\sigma_\theta^2 = 5^2$ deg, $r_{p,l} = 0.7$, $r_{p,u} = 1.3$, $r_{n,l} = 0.7$, $r_{n,u} = 3$. Performances will be given by ROC, area under the curve (AUC), training time and detector time. A comparaison with Haar's features (horizontal and vertical patterns) trained with adaboosting is given for a fair comparaison. No cascading is performed, decelerating detection process but reaching the maximum detection rate. In Fig. 1, ROC are given for 7 parameters configuration given in Table. II. With these particular choice for Δ_1 , Δ_2 , Δ_3 , we have $W_1 = 1$, $W_2 = 5$ and $W_3 = 17$ respectively. Performances of Haar+adaboosting are considerably decreasing when model is trained with LFWcrop dataset and tested with our frontal dataset compared to model trained with the frontal MIT+CMU dataset. As expected, HLBP performs better than HCSBBP for a common Δ , when the dictionary size b is increasing. Scaling factor s shows more influence for HMSLBP than for HCSMLBP. The spatial pyramid have a great impact: HLBP(Δ_2), HMCSLBP(Δ_3) and HCSMSLBP(Δ_3) clearly outperform Haar+adaboosting (MIT+CMU). Moreover, according to table II, the HCSLBP(Δ_3) reaches a framerate close to 20 fps in VGA format² and is $\frac{256}{16}$ faster and less memory consuming than its HLBP(Δ_1) counterpart.

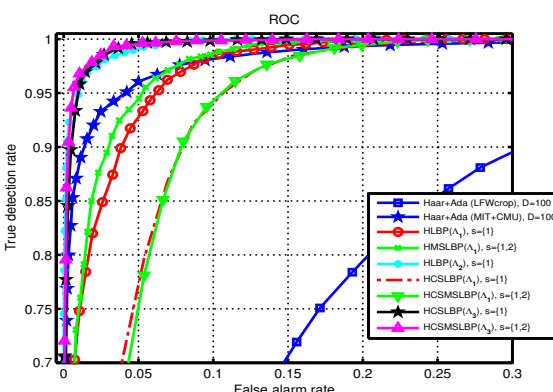


Fig. 1. ROC for linear kernel

² Test have been performed on a core I7@1600Mhz/4 cores/HT off/16Gb laptop with win64 system.

Table 1. AUC, training time (TT) and detection rate (DR)

Parameters	AUC	TT (s)	DR (fps)
$b = 256, \mathcal{S} = \{1\}, \mathbf{A}_1 = [1, 1, 1, 1], d = 256$	0.98810	1391	3.30
$b = 256, \mathcal{S} = \{1, 2\}, \mathbf{A}_1 = [1, 1, 1, 1], d = 512$	0.9900	18230	1.62
$b = 256, \mathcal{S} = \{1\}, \mathbf{A}_2 = \begin{bmatrix} 1 & 1 & 1 & 1 \\ 1 & 1 & 1 & 1 \\ 2 & 2 & 2 & 2 \end{bmatrix}, d = 1280$	0.9981	1991	1.47
$b = 16, \mathcal{S} = \{1\}, \mathbf{A}_1 = [1, 1, 1, 1], d = 16$	0.9674	721	38.57
$b = 16, \mathcal{S} = \{1, 2\}, \mathbf{A}_1 = [1, 1, 1, 1], d = 32$	0.9636	733	21.81
$b = 16, \mathcal{S} = \{1\}, \mathbf{A}_3 = \begin{bmatrix} 1 & 1 & 1 & 1 \\ 1 & 1 & 1 & 1 \\ 4 & 4 & 4 & 4 \end{bmatrix}, d = 272$	0.9977	2007	18.80
$b = 16, \mathcal{S} = \{1, 2\}, \mathbf{A}_3 = \begin{bmatrix} 1 & 1 & 1 & 1 \\ 1 & 1 & 1 & 1 \\ 4 & 4 & 4 & 4 \end{bmatrix}, d = 544$	0.9982	2896	9.51

5 Conclusions and Future Work

We present a novel real-time face detector based on fast histograms features coupled with feature map based additive homogeneous kernel approximation. Both the LBP codes and histograms computation are accelerated with the image integral technic. Our detector achieves approximatively 20 fps with modern computers and outperforms methods based on boosting framework. The fast histogram technic (with integral histograms) can be extended to any features using integral image.

References

1. Fan, R.E., Chang, K.W., Hsieh, C.J., Wang, X.R., Lin, C.J.: LIBLINEAR: A library for large linear classification. *JMLR* 9, 1871–1874 (2008)
2. Heikkilä, M., Pietikäinen, M., Schmid, C.: Description of interest regions with center-symmetric local binary patterns
3. jui Hsieh, C., wei Chang, K., jen Lin, C., Keerthi, S.S.: A dual coordinate descent method for large-scale linear svm (2008)
4. Liao, S., Zhu, X., Lei, Z., Zhang, L., Li, S.Z.: Learning multi-scale block local binary patterns for face recognition. In: Lee, S.-W., Li, S.Z. (eds.) ICB 2007. LNCS, vol. 4642, pp. 828–837. Springer, Heidelberg (2007)
5. Maji, S.: Dense version of liblinear,
<http://www.cs.berkeley.edu/~smaji/projects/digits/>
6. Paris, S., Glotin, H.: Pyramidal multi-level features for the robot vision@icpr 2010 challenge. In: ICPR, pp. 2949–2952 (2010)
7. Pereira, E., Gomes, H., de Carvalho, J.: Integral local binary patterns: A novel approach suitable for texture-based object detection tasks. In: SIBGRAPI, August 30–September 3, pp. 201–208 (2010)
8. Sanderson, C., Lovell, B.C.: Multi-region probabilistic histograms for robust and scalable identity inference. In: Tistarelli, M., Nixon, M.S. (eds.) ICB 2009. LNCS, vol. 5558, pp. 199–208. Springer, Heidelberg (2009),
<http://itee.uq.edu.au/~conrad/lfwcrop/>
9. Viola, P., Jones, M.: Robust real-time face detection. *International Journal of Computer Vision* 57, 137–154 (2004)
10. Wu, J., Rehg, J.M.: Where am i: Place instance and category recognition using spatial pact. In: CVPR (2008)

Study on UAV Video Reconnaissance Based Adaptively Tracking Algorithm for the Ground Moving Target

Wen-Bo Zhao, Wei Chen , Guang-Zheng Zheng, Ke-Ming Huang ,
Kong-Jin Zhao, and Yu-Ge Li

New Star Research Institute of Applied technology, Hefei 230031 China
zhaowenbo@ustc.edu

Abstract. In this paper, the problem of adaptive tracking for the Ground Moving Target (GMT) based on Unmanned Aerial Vehicle (UAV) reconnaissance video is addressed. More specifically, motion model and observation model of GMT are proposed, a novel Kalman Filter (KF) initialization strategy is introduced, and Interacting Multiple Model Kalman Filter (IMMKF) algorithm is adopted for tracking GMT purpose. Simulation results indicate the promising future of our proposed strategies on the area of moving target tracking domain compared to traditional methods.

Keywords: UAV, Target tracking, Kalman filter, Interacting multiple model.

1 Introduction

Recently the study of the battle application of UAV has been became the important development domain for many countries. Based on UAV the study of video reconnaissance of GMT is the hot-point in current for UAV battle application. Many UAV applications, such as, civil application, anti-terrorism, military strike, etc., has been widely concerned. Although the military UAV with the video reconnaissance can give a GMT location by means of using the analysis positioning method (APM), with the affair of cumulative errors existing in the video reconnaissance procedure, the positioning errors for GMT is more largely. And APM can not directly provide the state information of the GMT, i.e., velocity, acceleration, direction, etc. For transacting purpose of the noised measure data, the state estimation method, can accomplish the smooth of past motion state, estimation of the current motion state, and prediction of the next moment, of the GMT. The common estimation method include maximum likelihood(ML) estimation, maximum posterior(MP) estimation, the minimum variance(MV) estimation and minimum least square(MLS) estimation, etc. Kalman filter algorithm(KFA) was proposed in the sixties of the 20th Century by Kalman in Ref.[1]. Under the conditions of the line model and Gaussian noise distribution, by KFA,

the optimal estimation of a tracked target can be obtained. KEA can afford not only the accurate position, the velocity, the acceleration,etc.,of the tracked target, but also the information of the next moment of the tracked target by means of the prediction technology, which can help enhance the rate and accurate of the control system.In this paper, KEA will be used to estimate the motion position, motion velocity, motion direction of GMT with real-time and high accurate, utilizing UAV video reconnaissance information, including video tracking information, UAV carrier attitude and positioning information, the attitude measurement information of the airborne reconnaissance equipment and the target ranging information. The high accurate and real-time motion information of GMT, can be used for military purpose, for example, which can be provided for artillery force to shot a GMT with block shooting manner.

2 KFA Modeling to Track the GMT

2.1 Motion Modeling of the GMT

In this paper the constant velocity motion (CVM) model and turn model will be adopted to used for describing the constant velocity GMT and maneuvering GMT. The Cartesian coordinate system (CCS) of UAV grand station will selected as tracking coordinate system(TCS) of KFA.

The CV Modeling of GMT. It is assumed that the tracked GMT moving with CVM in the xy plane of CCS of UAV grand station, that UAV video reconnaissance equipment axis align the center of GMT, that output interval of measurement information be T seconds.Therefore, the CVM model of GMT can be described as the Eq.(1).

$$X_k = \Phi_{k/k-1} X_{k-1} + \Gamma_k W_k \quad (1)$$

Where X_k is a state vector of GMT , include x -axis position & velocity , y -axis position & velocity, i.e., $X_k = [x_k \dot{x}_k y_k \dot{y}_k]^T$,at Time k . And W_k is a state noise vector, composed of independent noise components of x -axis and y -axis. And $\Phi_{k/k-1}$ and Γ_k is respectively a state transition matrix and an instigate matrix, which can be expressed as the Eq.(2).

$$\Phi_{k/k-1} = \begin{bmatrix} 1 & T & 0 & 0 \\ 0 & 1 & 0 & 0 \\ 0 & 0 & 1 & T \\ 0 & 0 & 0 & 1 \end{bmatrix} \quad \Gamma_k = \begin{bmatrix} T^2/2 & 0 \\ T & 0 \\ 0 & T^2/2 \\ 0 & T \end{bmatrix} \quad (2)$$

The Maneuver Modeling of GMT. While a GMT do move with maneuver motion in xy plan of CCS of UAV grand station, a turn model can be applied to describe its state. At this time, the state model is the same as the Eq.(1), but

its form of the state transition matrix $\Phi_{k/k-1}$ is different from one of Eq.(2), which is given as Eq.(3)

$$\Phi_{k/k-1} = \begin{bmatrix} 1 & \frac{\sin(\omega_k T)}{\omega_k} & 0 & \frac{\cos(\omega_k T)-1}{\omega_k} \\ 0 & \cos(\omega_k T) & 0 & -\sin(\omega_k T) \\ 0 & \frac{1-\cos(\omega_k T)}{\omega_k} & 1 & \frac{\sin(\omega_k T)}{\omega_k} \\ 0 & \sin(\omega_k T) & 0 & \cos(\omega_k T) \end{bmatrix} \quad (3)$$

2.2 Measurement Modeling for a GMT by UAV Video Reconnaissance

In general, UAV video reconnaissance measurement is fulfilled in the coordinate system of the airborne video equipment, meanwhile, also considers the position & attitude data of UAV carrier, attitude data of airborne video equipment and target ranging data in real time. Obviously, the state vector and measurement vector of a tracked GMT have the nonlinear function relationship. Therefore, this measure model does not satisfy the linearization requirement of a measure model of KFA. For this reason, a CCS of UAV grand station is selected as the measurement coordinate system of KFA. In this way, a "measure vector" and a state vector have a simple linear relationship. Generally, in KFA implement procedure, a measurement covariance matrix can be essential, need pre-computing. Based on the real application procedure, a measurement covariance matrix is a diagonal matrix, made up of the diagonal elements as the covariance of the measurement component and non-diagonal elements as zeros. However, as selecting CCS of UAV grand station as "measurement coordinate system" of KFA, this measurement covariance matrix can not be constructed according to the above means. Construction of the novel covariance matrix requires considering the distribution property of measurement noise of UAV video reconnaissance, combining the coordinate transition relationship, by using statistics methods, to analyze and solve. Beyond the discussion focus, the measurement covariance construction will not be analyzed in emphasis in this paper. Based on the above analysis, the measurement model of a GMT and covariance matrix can be expressed as Eq.(4) and Eq.(5).

$$Z_k = H_k X_k + V_k \quad (4)$$

$$R_k = \begin{bmatrix} E[(\Delta x)^2] & E[\Delta x \Delta y] \\ E[\Delta x \Delta y] & E[(\Delta y)^2] \end{bmatrix} \quad (5)$$

Where, H_k is the measurement matrix, Δx and Δy is respectively x -axis & y -axis errors, produced in CCS of UAV grand station by measurement noise of UAV video reconnaissance. $E[\cdot]$ is a mathematical expectation operator.

2.3 Initialization Strategy for KFA

The initialization method is an important content of KFA application. As this paper main discuss focus on the motion position & velocity of GMT in xy plane of

CCS of UAV grand station, initialization realization of KFA can make use of the two-point-difference method. In other words, according to the measurement data at time 1 and time 2, an estimation & covariance of a initial state for GMT can be calculated. It is assumed that $Z_1 = [z_{11}, z_{12}]^T$ and $Z_2 = [z_{21}, z_{22}]^T$ respectively means the 1st measure vector and the 2nd measure vector. According to theory of the coordination system selection talked in this above for KFA, Z_1 and Z_2 can be expressed as x -axis & y -axis component of coordination transition of video reconnaissance data of GMT, from the video reconnaissance coordination system to UAV grand station coordination system. Then, at Time 2, the estimation of GMT can be given as Eq.(6).

$$\hat{X}_2 = \left[z_{21} \frac{z_{21}-z_{11}}{T} z_{22} \frac{z_{22}-z_{12}}{T} \right] \quad (6)$$

Then the estimation covariance at time 2 can be given as Eq.(7).

$$E \left[\left(X_2 - \hat{X}_2 \right) \left(X_2 - \hat{X}_2 \right)^T \right] = \begin{bmatrix} E[\Delta x^2] & \frac{E[(\Delta x)^2]}{T} & E[\Delta x \Delta y] & \frac{E[\Delta x \Delta y]}{T} \\ \frac{E[(\Delta x)^2]}{T} & Q_x T^2 + \frac{2E[(\Delta x)^2]}{T^2} & \frac{E[\Delta x \Delta y]}{T} & \frac{2E[\Delta x \Delta y]}{T^2} \\ E[\Delta x \Delta y] & \frac{E[\Delta x \Delta y]}{T} & E[(\Delta y)^2] & \frac{E[(\Delta y)^2]}{T} \\ \frac{E[\Delta x \Delta y]}{T} & \frac{2E[\Delta x \Delta y]}{T^2} & \frac{E[(\Delta y)^2]}{T} & Q_y T^2 + \frac{2E[(\Delta y)^2]}{T^2} \end{bmatrix} \quad (7)$$

Where meanings of $E[\Delta x^2]$, $E[\Delta x \Delta y]$ and $E[\Delta y^2]$ are equivalent to the ones of Eq.(5).

3 The Interacted Procedure of Multiple Models KFA

For the tracking problem of maneuver targets, if a single state model will be merely used into KFA, it is difficultly suitable to all cases of the maneuver targets. The interaction multiple models (IMM) algorithm is integrated to describe possible maneuver cases of a GMT. It can be known that IMM algorithm will be the best applicable to track the maneuver targets Ref.[5].

The Interaction Procedure of Models

$$\hat{X}_{k-1}^{oj} = \sum_{i=1}^r \hat{X}_{k-1}^i \mu_{k-1}^{ij} \quad (8)$$

$$P_{k-1}^{oj} = \sum_{i=1}^r \mu_{k-1}^{ij} \left\{ P_{k-1}^i + \left[\hat{X}_{k-1}^i - \hat{X}_{k-1}^{oj} \right] \left[\hat{X}_{k-1}^i - \hat{X}_{k-1}^{oj} \right]^T \right\} \quad (9)$$

$$\mu_{k-1}^{ij} = P \left\{ M_{k-1}^i / M_{k-1}^j, Z^{k-1} \right\} = p_{ij} \mu_{k-1}^i / \sum_{i=1}^r p_{ij} \mu_{k-1}^i \quad (10)$$

For Model $M_k^j, \hat{X}_{k-1}^{oj}, P_{k-1}^{oj}$,and Z_k are Input to KFA

① Sate step prediction $\hat{X}_{k/k-1}^j$

$$\hat{X}_{k/k-1}^j = \Phi_k^j \hat{X}_{k-1}^{0j} \quad (11)$$

② Prediction covariance matrix $P_{k/k-1}^j$

$$P_{k/k-1}^j = \Phi_k^j P_{k-1}^{0j} (\Phi_k^j)' + \Gamma_{k-1}^j Q_k^j \Gamma_{k-1}^j \quad (12)$$

③KFA Gain K_k^j

$$K_k^j = P_{k/k-1}^j (H_k)' \left[H_k P_{k/k-1}^j (H_k)' + R_k \right]^{-1} \quad (13)$$

④Update estimation \hat{X}_k^j

$$\hat{X}_k^j = \hat{X}_{k/k-1}^j + K_k^j [Z_k - H_k \hat{X}_{k/k-1}^j] \quad (14)$$

$$P_k^j = [I - K_k^j H_k] P_{k/k-1}^j \quad (15)$$

Computing Update Probability of Models

$$\begin{aligned} \mu_k^j &= P\{M_k^j/Z^k\} = P\{Z_k/M_k^j, Z^{k-1}\} P\{M_k^j/Z^{k-1}\} \\ &= \frac{1}{c} \Lambda_k^j \sum_{i=1}^r p_{ij} \mu_{k-1}^i = \Lambda_k^j \bar{c}_j / c \end{aligned} \quad (16)$$

Where c is a normalized constant,i.e., $c = \sum_{j=1}^r \Lambda_k^j \bar{c}_j$, Λ_k^j is the likelihood function of Measurement Z_k .

$$\Lambda_k^j = P\{Z_k/M_k^j, Z^{k-1}\} = \frac{1}{(2\pi)^{n/2} |S_k^j|^{1/2}} \exp \left\{ -\frac{1}{2} v_j^T (S_k^j)^{-1} v_j \right\} \quad (17)$$

Where v_k^i is the measure innovation, which can expressed as $v_k^j = Z_k - H_k \hat{X}_{k/k-1}^j$,
 S_k^j is covariance matrix of v_k^i , which can be expressed as $S_k^j = H_k P_{k/k-1}^j (H_k)' + R_k$.

Output Interaction

$$\hat{X}_k = \sum_{j=1}^r \hat{X}_k^j \mu_k^j \quad (18)$$

$$P_k = \sum_{j=1}^r \mu_k^j \left\{ P_k^j + [\hat{X}_k^j - \hat{X}_k] [\hat{X}_k^j - \hat{X}_k]^T \right\} \quad (19)$$

Where \hat{X}_k and P_k represent the GMT state estimation and covariance based on IMMKFA.

4 Simulation and Conclusion

It is assumed that there is a video reconnaissance UAV, at 1,000 meter altitude, tracking the vehicle moving on ground by video reconnaissance. In order to stably tracking the vehicle, simulated UAV is controlled to flight by the snakelike line, keeping the reconnaissance axis aligned at the center of the tracked vehicle. It is assumed that initial state of the simulated UAV is $[100 \ 22 \ 250 \ 4]^T$, and the out interval of video reconnaissance information is one second, and state noise sequence and measure noise sequence are both Gaussian white noise distribute, and the standard deviation of target ranging is X meter, and suppose the standard deviation of the attitude angles for both UAV carrier and video reconnaissance system are supposed as X degrees. In order to test the performance of proposed algorithm, it is assumed that simulated GMT do move with complex maneuvering manner. The simulated results are depicted as Fig.1 Fig.6.

Seen from the simulated result, the proposed IMM-KFA is able to reduce the video reconnaissance noises greatly. The proposed algorithm can adaptively track the GMT, without manual intervention.

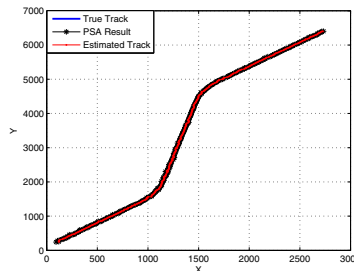


Fig. 1. IMM-KFA Estimated Tracks Vs PSA Results

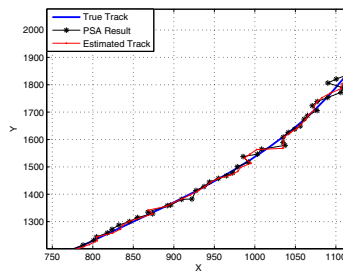


Fig. 2. Zoom Out of Fig.1

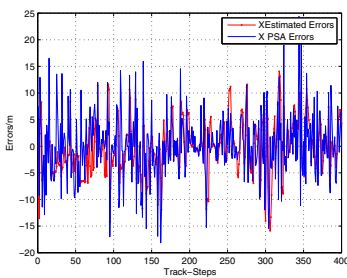


Fig. 3. Estimated Velocity Vs True Velocity in X -Axis

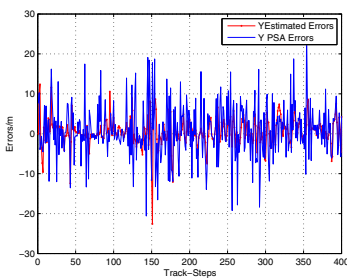


Fig. 4. Estimated Velocity Vs True Velocity in Y -Axis

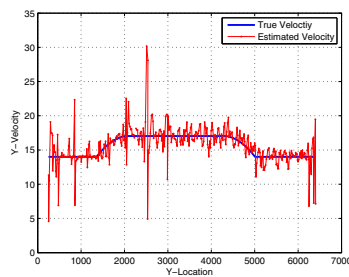


Fig. 5. Estimated Errors Vs PSA Errors in X -Axis

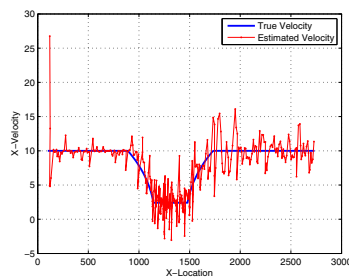


Fig. 6. Estimated Errors Vs PSA Errors in Y -Axis

In this paper, based on the video reconnaissance information of UAV, the IMMKFA adopted, the initialization strategy built up, adaptively tracking a GMT is accomplished. The simulation demonstrates that the proposed algorithm effectively fulfill tracking a maneuvering GMT without manual intervention. On contrast to the traditional PA method of UAV video reconnaissance, the proposed IMMKFA, can effectively decrease the error margin of PA, greatly enhance the tracking performance for the GMT. The future application of the proposed algorithm has good prospects.

Acknowledgements. This work was supported by National Natural Foundation of China(61070218) and Anhui Provincial Natural Science Foundation (11040606M130).

References

1. Madison, R., DeBitetto, P., Olean, A.R., Peebles, M.: Target Geo-location from a Small Unmanned Aircraft System (2008)
2. Yang, W.H.: Multi-sensor Data Fusion and Application. Xidan University Publish House, Xian (2006)
3. Simon, H.: (Zheng, B.Y. translated) Adaptively Filter Theory. Electronics Industry Publish House, Beijing (2003)
4. Yang, L.J., Geng, B.Y.: Multi-sensor Data Fusion Handbook. Electronics Industry Publish House, Beijing (2008)
5. Knorn, F., Leithd, J.: Adaptive Kalman Filtering for Anomaly Detection in Software Appliances. In: IEEE Conference on Computer Communications Workshops INFOCOM 2008, April 13-18, pp. 1–6 (2008)

Palm Print Image De-noising Based on BEMD and Wavelet Packet Transform-Wiener Filter

Gui-Ping Dai

Department of Electronic & Information Engineering,
Suzhou Vocational University, Suzhou 215104, Jiangsu, China
luiping_0127@163.com

Abstract. A novel de-noising method based on BEMD (Bi-dimensional Empirical Mode Decomposition) and wavelet packet transform-wiener filter was proposed. Firstly, BEMD was applied to decompose the preprocessed palm print image including noise into a group of IMFs (Intrinsic Mode Functions) with different intrinsic time scales, and then the first several IMFs corresponding to high frequency information and noise were de-noised by means of wavelet packet decomposition integrated with wiener filter; finally, the image was reconstructed through adding the processed IMFs and the residual component. Simulation results show that compared with BEMD, wavelet packet threshold de-noising and BEMD integrated with wavelet threshold de-noising, this proposed method can achieve more superior de-noising performance with the lowest MSE and the highest PSNR, which provides a basis for the accurate extraction of palm print features.

Keywords: Bi-dimensional empirical mode decomposition, Wavelet packet transform, Wiener filter, Palm print image de-noising.

1 Introduction

Palm print recognition is a new recognition technology in the field of biological authentication, which is applied to the identity automatic confirmation according to the palm texture characteristics as biological characteristics. The process is roughly divided into four parts: image collection, pretreatment, feature extraction, classification decision-making. And the comprehensive and accurate extraction of the palm print features is the key of the rapid and accurate identity recognition [1]. However, due to the effect of exterior environment, some important detail information of palm print is usually polluted by noise in the process of collection and transmission, while detail information is the basis of feature extraction. Therefore, the elimination of noise has become an important issue in the field of palm print recognition [2].

The traditional image de-noising method mostly includes filtering method on the basis of Fourier transform and the wavelet packed de-noising method. The former demands that the analyzed image is linear, periodic or stationary and thereby cannot

extract the time-frequency characteristics. Therefore, the marginal and detailed information of analyzed image will be lost, which makes the image has become blurred [3]. However, the wavelet packet de-noising method can carry out the time-frequency analysis of image with the characteristic of low entropy, multi-resolution, and flexible selection of wavelet base. Therefore, the abrupt information and noise of image can be effectively distinguished, which can keep the good resolution of abrupt information while improving the signal-to-noise ratio. Although the wavelet packet transform has more elaborate frequency resolution and more superior time-frequency properties, but still not get rid of the defects of Fourier transformation. De-noising effects depend on the selection of priori wavelet basis, which results in lack of adaptability [4].

BEMD is an adaptive time-frequency localized and multi-scale analysis method. Compared to Fourier transform and wavelet packet analysis based on priori function basis, BEMD can adaptively break down image and noise into a group of IMF (Intrinsic Mode Function) sub images with different intrinsic time scales according to the image inherent characteristics. Each of IMFs not only can reveal the intrinsic real physical information of image including noise, but also can reduce the interference or coupling between the image characteristic information, and thus provides a more effective and novel method for the follow-up image processing [5].

In this paper, combining with the adaptive decomposition characteristics of BEMD, multi-resolution analysis of wavelet packet de-noising and Wiener filtering, a novel palm print image de-noising method based on BEMD and wavelet packet transform-Wiener filter was proposed. As a result, the marginal and detailed information of palm print image can be remained as more as possible while de-noising.

2 Algorithm Description of BEMD

BEMD algorithm is the expansion of one-dimensional EMD, which can extract the details of image on different characteristic scales through the auto-merging sifting process. For the two-dimensional image $f(x, y)$, $x = 1, \dots, M$, $y = 1, \dots, N$, The algorithm of BEMD is described as follows:

(1) External initialization: Assume i is the number of IMF decomposition layers, and its value is initialized into $i = 1$. The processed image is given as follows:

$$r_0(x, y) = f(x, y). \quad (1)$$

(2) Extracting i th IMF sub image through sifting process

① Internal initialization: $h_0(x, y) = r_{i-1}(x, y)$. Assume j is the number of Iterations while extracting each IMF and its value is initialized into $j = 1$.

② Find out the local maximum and minimum points of $h_{j-1}(x, y)$ through Morphological algorithm or 8 neighborhood pixels algorithm.

③ Select the appropriate surface interpolation algorithm for envelopment fitting, so that the maximum and minimum points of $h_{j-1}(x, y)$ were respectively interpolated to form the upper and lower 2-D envelopment surface $u_{\min}(x, y)$ and $u_{\max}(x, y)$.

④ Compute the mean value matrix of the upper and lower envelopment surface:

$$m_{j-1}(x, y) = [u_{\min}(x, y) + u_{\max}(x, y)] / 2. \quad (2)$$

⑤ Subtract the mean value matrix from $h_{j-1}(x, y)$:

$$h_j(x, y) = h_{j-1}(x, y) - m_{j-1}(x, y). \quad (3)$$

⑥ Increment j by 1, which results in $j = j + 1$. Repeat steps ② to ⑤ and calculate the sifting termination conditions until $h_j(x, y)$ meets the IMF requirement, when ith IMF sub image can be obtained which is defined as $I_{imfi}(x, y) = h_j(x, y)$.

(3) Compute the residual component: $r_i(x, y) = r_{i-1}(x, y) - I_{imfi}(x, y)$.

If the number of extreme value points of $r_i(x, y)$ is not less than 2 or the decomposed IMF number failed to meet the requirement, then $i = i + 1$, switch to step (2) and denote $r_i(x, y)$ as processed image; Otherwise the decomposition is completed, $r_i(x, y)$ is the final residual component.

(4) Finally, BEMD decomposition with N layers of image $f(x, y)$ can be described as follows:

$$f(x, y) = \sum_{i=1}^N I_{imfi}(x, y) + r_N(x, y). \quad (4)$$

In which $I_{imfi}(x, y)$ is decomposed ith IMF sub image and $r_N(x, y)$ is the final residual component. Denote the sifting termination conditions in step ⑥ as follows:

$$SD = \sum_{x=0}^X \sum_{y=0}^Y \left[\left| h_j(x, y) - h_{j-1}(x, y) \right|^2 / h_{j-1}^2(x, y) \right] \leq r. \quad (5)$$

In which r stands for the iterative termination parameter, and experiments indicate that the selection of r will directly affect the number and quality of decomposed IMFs. In order to ensure that IMF can more effectively reflect the details of image, the value of r generally lies between 0.2 and 0.3. In this paper, r is taken as 0.2.

In conclusion, the key point of BEMD lies in the search algorithm for local extreme points of image and the envelopment surface fitting algorithm, especially the latter one, namely that is extreme value point interpolation algorithm. Thus the following will optimize the algorithm from this aspect.

3 De-noising Algorithm of IMF Sub Images Based on Wavelet Packed Transform and Wiener Filter

3.1 Principle of Image De-noising Based on Wavelet Packed Transform and Wiener Filter

Wavelet packet transform is the promotion of wavelet multi-resolution analysis, which not only can carry out multi-layers decomposition of low-frequency coefficients, but also for high-frequency coefficients can carry out the further subdivision. Therefore, wavelet packet transform has the excellent properties of further divided elaborate spectrum window as scale increases. Hence compared with wavelet analysis, wavelet packet transform has more elaborate frequency resolution and more superior time-frequency properties [6]. On the other hand, Wiener filter is a local adaptive linear filter based on least mean-square error principles. It can adjust the output according to local variance, thereby has excellent de-noising property for noise with known probability distribution [7].

In this paper, in view of the above advantages of wavelet packet transform and Wiener filter, a novel image de-noising method based on wavelet packet transform integrated with Wiener filter is proposed. Firstly, the wavelet packet transform was carried out to break down the IMF sub images including noise in order to form wavelet packet tree with four forks. The most energy of noise included in IMF images is mainly concentrated on the decomposition layer with high frequency after wavelet packet decomposition. Therefore, the high frequency part's variance of wavelet packet decomposition coefficient on the first layer was computed by means of the median absolute variance estimation method, in order to estimate the variance of noise. Secondly, Wiener filter algorithm is adopted to carry out the de-noising processing of wavelet packet coefficients with high frequency on each layer, thus to estimate IMFs 's wavelet packet high frequency coefficient. Finally, by means of the wavelet packet reconstruction algorithm, making a second de-noising processing, the de-noised high-frequency coefficients and low frequency coefficients of wavelet packet decomposition were processed to reconstruct the original IMF sub images.

4 De-noising Algorithm of IMF Sub Images Based on Wavelet Packed Transform and Wiener Filter

Assume $f(x, y)$ is an original palm print image without noise, while $g(x, y)$ is an image including $f(x, y)$ mixed with noise, and $I_{imfi}(x, y)$ is ith IMF obtained by BEMD decomposition of $g(x, y)$. As a result, the de-noising algorithm of IMF sub images based on wavelet packet transform and Wiener filter is described as follows:

- (1) BEMD decomposition: BEMD algorithm is carried out to decompose the palm print image including noise $g(x, y)$ into a set of IMF sub images $I_{imfi}(x, y)$ with different characteristic scales which size is from small to large (accordingly the instantaneous frequency of IMFs is from high to low).

- (2) Wavelet packet decomposition: wavelet packet analysis is carried out to break down sub images with high frequency such as IMF1 and IMF2, in order to obtain the wavelet packet coefficients on each layer.
- (3) Estimation of the variance of noise: by means of the median absolute variance estimation method, the high frequency part's variance of wavelet packet decomposition coefficient on the first layer was computed, in order to estimate the variance of noise included in IMF sub images.
- (4) Wiener filtering of wavelet packet coefficients with high frequency: Wiener filtering algorithm is used to de-noise the wavelet packet coefficients with high frequency on each layer.
- (5) Wavelet packet reconstruction: the de-noised high-frequency coefficients and low frequency coefficients of wavelet packet decomposition were processed to reconstruct the original IMF sub image $\hat{I}_{imf_i}(x, y)$.
- (6) BEMD reconstruction: the final residual component $r_N(x, y)$ is added up with each de-noised IMF sub image $\hat{I}_{imf_i}(x, y)$, thus to obtain the final de-noised palm print image $\hat{f}(x, y)$.

4 Simulation Verification

The palm print image analyzed in the simulation comes from the PolyU palm print image database provided by the Hong Kong polytechnic university. The size of the image in pixel is 384×284 . The image preprocessing method proposed in literature [8] is adopted to detect the corner, establish the coordinate system, then locate and segment the palm print image. As a result, the ROI area with size of 128×128 is obtained, as shown in Fig. 2(a). Then Gaussian noise with mean zero and variance 0.1 was superposed on the image shown in Fig. 2(a). The compound image is as shown in figure 1(a).

BEMD algorithm is carried out to break down the palm print image including noise shown in Fig.1 on five lays, in order to obtain five IMF sub images with different characteristics scales which size is from small to large (accordingly the instantaneous frequency of IMFs is from high to low).The decomposition results are as shown in Fig.1 (b)-(f). Within this BEMD decomposition, the morphological algorithm is adopted to acquire the local extreme points of image and the CSRBF interpolation based on the conjugate gradient method is used to carry out the envelope curve surface fitting. According to the essence of BEMD, IMF1 and IMF2 with smaller scales are the main distribution layer of noise, which also contains the most detailed structural and marginal information, while the remaining IMFs with larger scales reflects the basic structure and change trend information of image. If the noise is eliminated simply through removing IMF1, IMF2 and then adding the remaining IMFs with larger scales, as a result of which the important details of palm print image will be lost, especially the marginal information. The de-noised palm print image merely by means of BEMD is shown in Fig.2 (b). It can be seen that the de-noising effect is not ideal and the texture and detailed features are blurred.

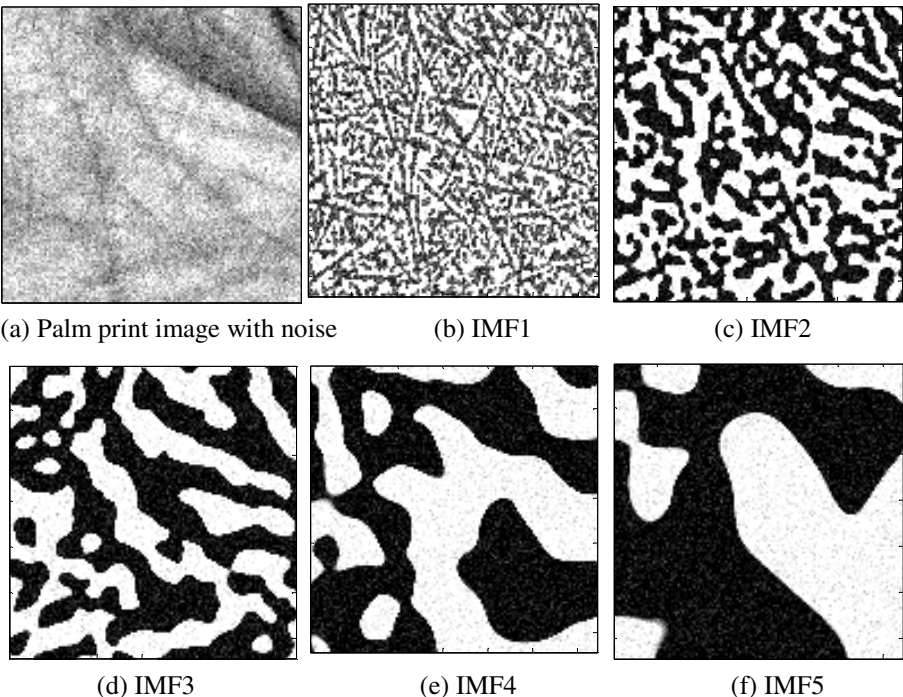


Fig. 1. BEMD decomposition of the palm print image with noise. Obtain five IMF sub images with different instantaneous frequency from high to low.

Therefore, on the basis of BEMD decomposition, wavelet packet transform-Wiener filtering algorithm is adopted to de-noise the IMF1 and IMF2 sub images. In experiment, ‘sym8’ is selected as the orthogonal wavelet basis function, and the number of decomposition layers is 2. The size of Wiener filtering window is 3x3. The finally de-noised palm print image is shown in Fig.2 (c). Compared with BEMD filtering, the de-noising effect of this integrated method is more excellent, the loss of palm print texture information is less and thus the palm lines and detailed features extracted are clearer. The de-noised palm print image merely by means of the wavelet packet threshold de-noising is shown in Fig.2 (d). It can be seen that although this method can keep good resolution of details while improving the SNR of image, but the de-noising result depends on selection of a priori wavelet basis function, which results in lacking certain adaptability. Therefore, the loss of texture information is more and the distortion is larger.

In order to quantitatively reflect the de-noising performance of the algorithm proposed in this paper, the mean square error (MSE) and the peak value signal-to-noise ratio (PSNR) are adopted as indicators measuring the de-noising quality. Meanwhile the proposed method is respectively compared with BEMD de-noising, wavelet packet threshold de-noising and BEMD integrated with wavelet threshold de-noising method. The comparison results are shown in Table 1. In the simulation experiment, Gaussian noise with different variances was superposed on the image

shown in Fig. 2(a), and the four de-noising methods were compared with each other on the aspects of MSE and PSNR. It can be seen that compared with BEMD and wavelet packet threshold de-noising, the integrated de-noising algorithm proposed in this paper can achieve more superior de-noising performance with the lowest MSE and the highest PSNR, which provides a basis for the accurate extraction of palm print features.

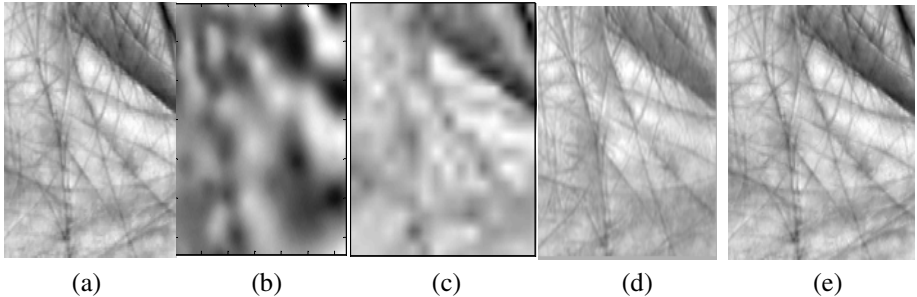


Fig. 2. Comparison of de-noising results through three methods. (a) palm print image without noise, (b) BEMD de-noising, (c) wavelet packet threshold de-noising, (d) BEMD integrated with wavelet threshold de-noising, (e) BEMD integrated with wavelet packet transform-Wiener filter de-noising.

Table 1. De-noising results comparison between the three de-noising methods

De-noising Algorithms	Noise variances	MSE	PSNR/dB
BEMD de-noising	0.02	1035.3	17.98
	0.1	1091.6	17.75
Wavelet packet threshold de-noising	0.02	217.3	24.76
	0.1	240.5	24.32
BEMD integrated with wavelet threshold de-noising	0.02	112.2	27.63
	0.1	116.4	27.47
Method proposed in this paper	0.02	84.3	28.87
	0.1	91.6	28.51

5 Conclusion

In this paper, a novel image de-noising method based on BEMD integrated with wavelet packet transform- Wiener filter is proposed. In this algorithm, wavelet packet transform is carried out to break down the IMF sub images with higher-frequency which is obtained by BEMD decomposition. And then by means of Wiener filtering, the details of palm print and noise can be thoroughly separated, in order that the marginal and detailed information of palm print image can be remained as more as possible while de-noising. Therefore, the loss of palm print texture information is less and thus the palm lines and detailed features extracted are clearer. Simulation results

show that compared with BEMD and wavelet packet threshold de-noising, the integrated de-noising method proposed in this paper can achieve more superior de-noising performance with the lowest MSE and the highest PSNR, which provides a basis for the accurate extraction of palm print features.

Acknowledgements. This paper was supported by the National Nature Science Foundation of Jiangsu Province (No. BK2009131).

References

1. Huang, S., Xu, C.: Principle Line Extraction and Restoration Based on Wavelet Theory. *Journal of Image and Graphics* 11(8), 1139–1149 (2006)
2. Lian, Q.S., Chen, S.Z.: Palm print Identification Algorithm Based on Energy and Direction Feature Fusion of Gabor Wavelet. *Chinese Journal of Scientific Instrument* 29(3), 556–561 (2008)
3. Guo, J.Y., Yuan, W.Q.: Palm print Recognition Based on Two-dimensional Fisher Linear Discriminant. *Computer Engineering* 34(6), 212–213 (2008)
4. Zhao, H.H., Zhou, D.J.: SMT Solder Joint Image De-noising Based on Wavelet Packet Transform and Wiener Filter. *Computer Science* 37(9), 279–282 (2010)
5. Nunes, J.C., Guyot, S.: Texture Analysis Based on Local Analysis of The Bidimensional Empirical Mode Decomposition. *Machine Vision and Application* 16(8), 177–188 (2005)
6. Jorge, S., Shrikanth, S.: Discriminative Wavelet Packet Filter Bank Selection for Pattern Recognition. *IEEE Transactions on Signal Processing* 57(5), 1796–1810 (2009)
7. Ercelebi, E., Koc, S.: Lifting Based Wavelet Domain Adaptive Wiener Filter for Image Enhancement. *IEEE Proceedings Vision, Image and Signal Processing* 153(1), 312–316 (2006)
8. Huan, R.H., Yang, R.L.: SAR Images Feature Extraction and Target Recognition Based on ICA and SVM. *Computer Engineering* 34(13), 24–28 (2008)

Pavement Crack Segmentation Algorithm Based on Local Optimal Threshold of Cracks Density Distribution

Shengchun Wang and Wensheng Tang*

Department of Computer Teaching, Hunan Normal University, Changsha, China
chuyf@qq.com, tangws@hunnu.edu.cn

Abstract. Asphalt pavement distress is very important for road maintenance and rehabilitation decisions. The traditional manual pavement crack detection by human eyes is expensive, labor intensive, time consuming, and subjective. Automatic pavement distress detection algorithms are developed quickly in recent years. Segmentation is one of important step in automated pavement crack detect system. In this paper, a new segmentation algorithm by multi-scale and local optimum threshold is developed. The algorithm was shown to be more effective and robust than conventional segmentation algorithms.

Keywords: Image segmentation, Multi-scale, Image processing.

1 Introduction

Highways and roads are a major public asset in all counties. And highway has been developing very quickly in China in recent years. It takes hard maintenance and rehabilitation work. The maintenance and rehabilitation of highway pavements in the united state requires over 17 billion dollars per year [1]. But the traditional pavement

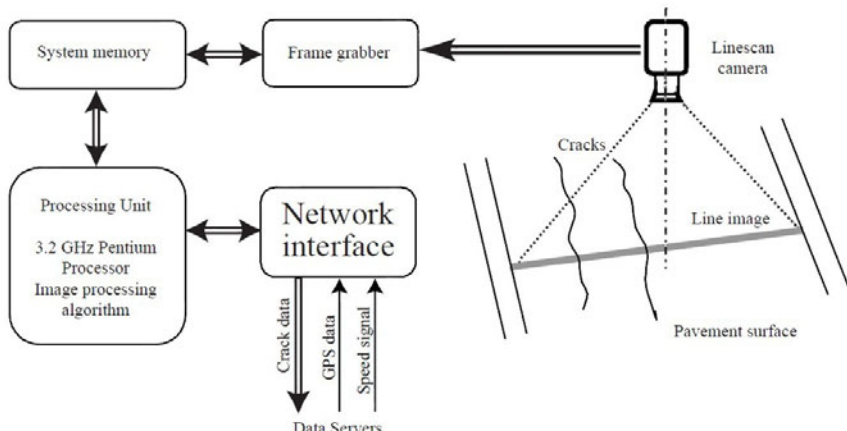


Fig. 1. Pavement image acquisition and processing system [2]

* Corresponding author.

crack detect system by human eyes is very costly, labor intensive, time consuming, and subjective. Because of high demands for intelligent pavement management strategies the development of automated pavement detect system has been gaining a lot of attention in last decade.

The typical automated pavement crack detect system always include a line-camera, a high-speed frame grabber, and a high performance computer. It is shown in figure 1.

2 Related Works

Many researchers have focused their efforts into developing effective algorithms to automate the process of pavement distress detection using pavement images. The current algorithms could be classified into five types: (1) threshold segmentation-based algorithm [3][4]; (2) edge detection-based algorithm [5]; (3) fractal geometric theory-based algorithm[6]; (4) neural network-based algorithms [7]; (5)Other algorithms[9].

E. Teomete et al [3] proposed the use of histogram projection to identify cracks within a cropped image. Cheng et al [4] approached a real-time thresholding based on sample space reduction and interpolation approach. T. C. Hutchinson et al [5] proposed the Fast haar wavelet transform is used to detect crack edges on the surfaces. Wang et al. [6] proposed texture analysis to classification the pavement crack. Sam Owusu-Abatio [7] proposed the problem of pavement crack classification using neural networks. After thresholding into binary images, they calculated Hu, bamieh, and Zemike moments. Using these moments as an input vector is to multiplayer perceptron with seven nodes indicating the output. They reported an 100% classification accuracy. Chen et al [8] proposed a method to pavement crack detection based on fuzzy set theory.

3 Methodology and Experiments

There are lots of white noises presented in the pavement images because of the nature of road surface. The most noises are based on pixel level scale. Another common phenomenon is that the illumination and reflectance of the pavement image are not uniformity. So some one global threshold segmentation algorithms such as OTSU [9] can't get satisfactory result. And the global detection algorithms are also time consuming and noneffective. To improve this, GCA (Grid Cell Analysis) method is proposed [10]. Pavement source images are first divided into non-overlapping blocks. Then it realizes the local optimal threshold in every block images. Its result is better than global threshold one. But it still doesn't consider about the crack density distribution in the pavement image.

The proposed method is focus on finding a local optimal threshold value by crack density distribution. Compare with background and noises, the crack shows darker and more continuous. And the noises show more independently. When we execute pyramid structure scale transform shown as figure 2. The scaled image shows low noises. And cracks are more distinct than the large image.

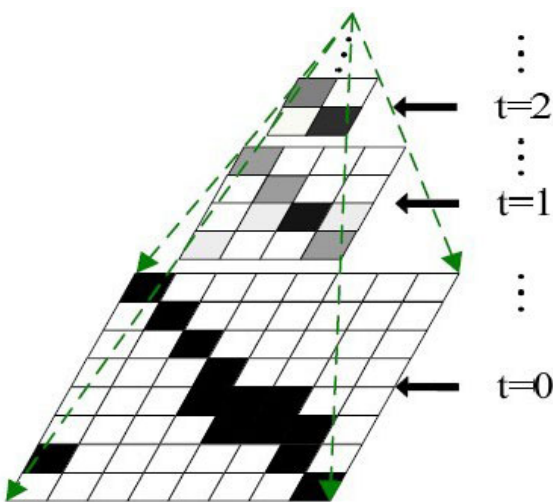


Fig. 2. Scale transformation of pyramid structure [11]

But it still has problem. The real edges of crack are lost. It can't get accuracy edge from scaled image. So the proposed method only gets rough edges of crack from scaled image. The more important is get potential crack areas.

The proposed method as follow:

Step 1: Low pass filter;

Step 2: Enhance the pavement crack image;

Step 3: Split the image into non-overlapping areas (it shown as figure 3 (a)).

Step 4: Scale the image to 1/2 and 1/4 size (it shown as figure 3 (b), (c));

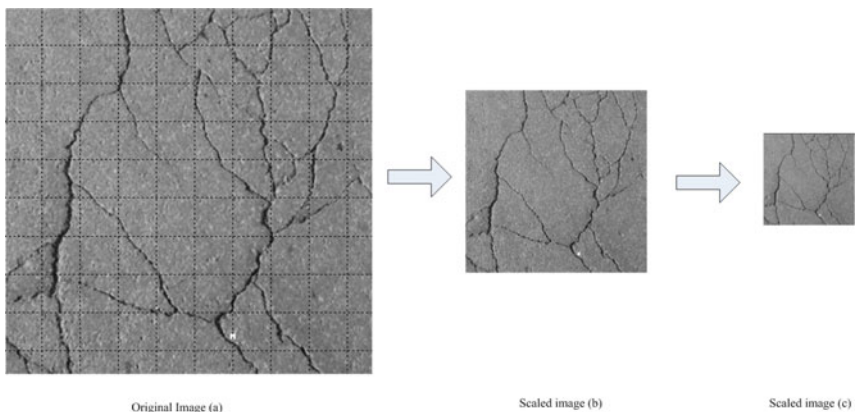


Fig. 3. Pyramid structure scale transform

Step 5: Use OTSU segmentation algorithm in scaled image (c) and change the image into binary image.

Step 6: Split the binary image as same count as original image in Step 3. And we defined $Area_p$ as

$$Area_p = \frac{P_{dark}}{P_{count}} \quad (1)$$

P_{dark} is the number of dark points in one split area. And P_{count} is the points count in the same area. When $Area_p \geq 0.05$. The area is defined as optional crack area.

Step 7: Compare with scaled image and original image, find all potential crack areas in original image (it shown as figure 4 (b) which red points marked areas).

Step 8: Merge the marked potential crack areas into unique one. Then use OTSU algorithm in this unique potential area to segment the crack. And clear other rest background areas.

The result image shown as figure 4 (c)

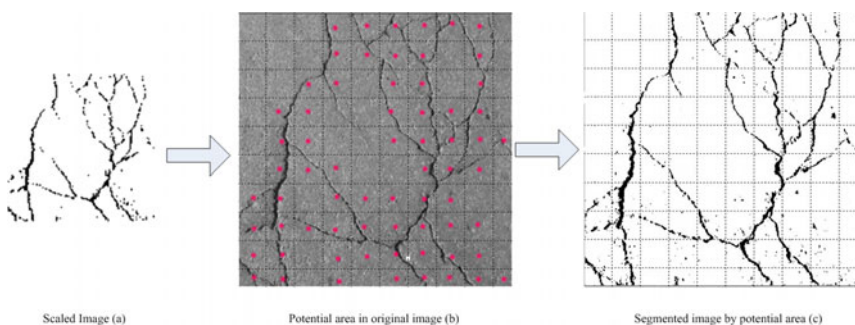


Fig. 4. Proposed method processing

Compare with global threshold value algorithm and local optimal threshold value algorithm. The proposed method focuses on potential crack areas. And the method finds optimal threshold value in unique potential area. It gets better result than traditional threshold algorithm. The result is shown as figure 5. It clearly shows that the image (c) has less noises and distinct cracks.

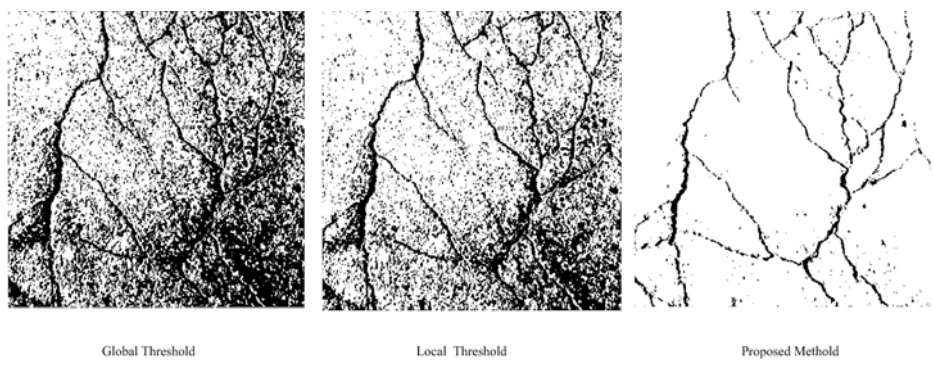


Fig. 5. Compare with other segmentation algorithms

4 Conclusion and Future Work

This paper presents a new method to segment the pavement crack images. Compare with global threshold value algorithm and local optimal threshold value algorithm, the proposed method in this paper segments pavement crack image by crack density distribution. The method show better segmentation result than conventional global threshold value algorithm and optimal threshold value algorithm.

We also can see some tiny branch cracks lost in the result image. How to get balance between scale size and accuracy edge will be focused in future work.

Acknowledgements. This project supported by Youth Foundation of Human Normal University (No.60907), and supported by program for excellent talents in Hunan Normal University (No.ET61008), and supported by Hunan Provincial Natural Science Foundation of China Under Grant (No.07JJ3129).

Reference

1. McGhee, K.H.: Automated Pavement Distress Collection Techniques. NCHRP: Transportation Research Board, National Research Council (2004)
2. Bugao, X., Huang, X.: Automated Pavement Cracking Rating System A Summary, http://www.utexas.edu/research/ctr/pdf_reports/7_4975_S.pdf
3. Teomete, E., Amin, V.: Digital Image Processing for Pavement Distress Analyses. In: Proc. of the 2005 Mid-Continent Transportation Research Symposium, Ames, Iowa (2005)
4. Cheng, D., Shi: Real-Time Image Thresholding Based Sample Space Reduction and Interpolation Approach. Journal of Transportation Engineering 17(4), 264–272 (2003)
5. Hutchinson, T.C., Chen, Z.: Improved Image Analysis for Evaluating Concrete Damage. Journal of civil engineering 20, 210 (2006)
6. Wang, H., Zhu, N., Wang, Q.: Fractal Features Analysis and Classification for Texture of Pavement Surfaces. Journal of Harbin Institute of Technology 37(6), 816–818 (2005)
7. Sam, O.: Effect of Neural Network topology on Flexible Pavement Cracking Prediction. Computer-Aided Civil and Infrastructure Engineering 13(5), 349–355 (1998)
8. Cheng, H.D., Chen, J., et al.: Novel Approach to Pavement Cracking Detection Based on Fuzzy Set Theory. Journal of Computing in Civil Engineering 13(4), 270–280 (1999)
9. Otsu, N.: Threshold Selection Method from Gray-Level Histograms. IEEE Transactions on Systems, Man, and Cybernetics 1(9), 62–66 (1979)
10. Siwaporn, Sorncharean, Suebskul, P.: Crack Detection on Asphalt Surface Image Using Enhanced Grid Cell Analysis. In: 4th IEEE International Symposium on Electronic Design, Test and Applications, Hong Kong, pp. 49–54 (2008)
11. Li, D., Liu, X.: A Model for Segmentation and Distress Statistic of Massive Pavement Images Based on Multi-Scale Strategies. In: ISPRS Congress, Vol. XXXVII, pp. 63–68 (2008)

Linear Pose Estimation Algorithm Based on Quaternion

Yongjian He^{1,2,*}, Caigui Jiang¹, Chengwei Hu³, Jingmin Xin¹,
Qiong Wu², and Fei Wang^{1,**}

¹ Institute of Artificial Intelligence and Robotics, Xi'an Jiaotong University, Xi'an, China

² Xi'an Communication Institute, Xi'an, China

³ China Academy of Space Technology, Beijing, China

{heyj, cgjiang, cwhu, jmxin, Qwu, fwang}@aiar.xjtu.edu.cn

Abstract. A novel linear camera pose estimation algorithm is presented using known 3D to 2D line correspondences and point correspondences. The rotation parameters are represented by unit quaternion. For n ($n \geq 4$) correspondences, we establish an equation system with $2n$ quadratic equations in thirteen variables and apply the “relinearization” method to obtain the rotation parameters and translation parameters simultaneously. We compare our algorithm with Ansar’s NLL algorithm for line correspondences by some synthetic experiments. Our algorithm performs better on the aspect of running time and accuracy of determined pose parameters. Some real experiments are produced by 1 point-3 lines, 2 points-2 lines, 3 points- 1 line correspondences. The projection of a 3D model is applied to estimate the performance of our algorithm.

Keywords: pose estimation, quaternion, relinearization.

1 Introduction

Camera pose estimation from 3D to 2D feature correspondences has received a lot of attention in the past two decades. It has been widely used in the field of computer vision, robot navigation, photogrammetry, augmented reality (AR) and so on.

An immense number of pose estimation methods based on feature correspondences are proposed. The most popular features are points, lines and higher order entities (conics, kinematic chains or higher order 3D curves). A class of point based pose estimation methods[1,5,9,10,11] and line based pose estimation methods [1,2,3,4,5,6,7] have been developed. Qiang et al. [15] had proposed the liner pose estimation algorithm with at least 6 points, 6 lines or 2 circle-ellipse correspondences. Andreas Ess et al. [14] had presented the generalized linear pose estimation algorithm with at least four point or five line correspondences. Both the above two algorithm apply the direct rotation matrix with nine elements and six constraint equations about the rotation matrix elements. In this paper, we propose a new linear algorithm based on n ($n \geq 4$) correspondences combined with line and point correspondences. This algorithm represents the rotation matrix with a unit quaternion. We obtain $2n$ quadratic equations in thirteen variables which are represented as the quadratic terms of

* Supported by National Natural Science Foundation of China (90820017), Basic Research and Business Subsidy of Central College.

** Corresponding author.

four elements from the quaternion and solve these equations using “relinearization” algorithm. At least four 3D-2D correspondences are needed. We can use four lines, three lines-one point, two lines- two points, one line- three points and four points for the pose estimation. Compare with Ansar’s algorithm, due to the advantage of the expression of rotation matrix by a unit quaternion, our algorithm guarantee the orthonormality of rotation matrix and the algorithm’s computational complexity is less. The real model are projected using the pose estimated by 1 point-3 lines, 2 points-2 lines, 3 points- 1 line 3D-2D correspondences.

2 Pose Estimation Algorithm

2.1 Notation

The camera pose can be parameterized by translation vector T and rotation matrix R . The notation of translation is

$$T = \begin{bmatrix} t_x & t_y & t_z \end{bmatrix}^T \quad (1)$$

But the representation of rotation matrix is difficult and has different forms, involving direct rotation matrix, Euler angle and unit quaternion.

A quaternion representation of rotation is written as a normalized four-dimensional vector $\hat{q} = [q_0 \ q_1 \ q_2 \ q_3]^T$, where

$$q_0^2 + q_1^2 + q_2^2 + q_3^2 = 1 \quad (2)$$

The rotation can be denoted as

$$R = \begin{bmatrix} q_0^2 + q_1^2 - q_2^2 - q_3^2 & 2(q_1q_2 - q_0q_3) & 2(q_3q_1 + q_0q_2) \\ 2(q_1q_2 + q_0q_3) & q_0^2 - q_1^2 + q_2^2 - q_3^2 & 2(q_3q_2 - q_0q_1) \\ 2(q_3q_1 - q_0q_2) & 2(q_3q_2 + q_0q_1) & q_0^2 - q_1^2 - q_2^2 + q_3^2 \end{bmatrix} \quad (3)$$

Unit quaternion provides a convenient mathematical notation for representing rotation matrix. We use this kind of representation in our method.

We assume the camera is calibrated, and then the camera intrinsic matrix $A = \begin{bmatrix} f_u & 0 & u_0 \\ 0 & f_v & v_0 \\ 0 & 0 & 1 \end{bmatrix}$ is known. A 3D point in world coordinate is denote

as $p_{wi} = [X_{wi} \ Y_{wi} \ Z_{wi}]^T$. The corresponding 3D coordinate in camera coordinate is $p_{ci} = [X_{ci} \ Y_{ci} \ Z_{ci}]^T$. The projective 2D image point is denoted as $p_h = [u_i \ v_i]^T$. A 3D line in Cartesian coordinate can be represented by $L_i = \{p_i \ v_i\}$, where $\{p_i\}$ is a point on the line and $\{v_i\}$ is normalized vectors represented the direction of the line. The representation of the corresponding projected line L_{hi} on 2D image coordinate is

$$A_i u + B_i v + C_i = 0 \quad (4)$$

where A_i, B_i, C_i are line parameters.

2.2 Constraint Equations

(1) Point constraint

The constraint of 3D-2D points can be expressed as the following Eq.(5) and Eq.(6)

$$P_{Ci} = RP_{Wi} + T \quad (5)$$

$$\begin{aligned} u_i &= u_0 + f_u \frac{X_{c_i}}{Z_{c_i}} \\ v_i &= v_0 + f_v \frac{Y_{c_i}}{Z_{c_i}} \end{aligned} \quad (6)$$

According to Eq.(3),(5),(6),then

$$\begin{aligned} h_{i1}q_0q_1 + h_{i2}q_0q_2 + h_{i3}q_0q_3 + h_{i4}q_1q_2 + h_{i5}q_1q_3 + h_{i6}q_2q_3 + h_{i7}q_0^2 \\ + h_{i8}q_1^2 + h_{i9}q_2^2 + h_{i10}q_3^2 + h_{i11}t_x + h_{i12}t_y + h_{i13}t_z = 0 \\ w_{i1}q_0q_1 + w_{i2}q_0q_2 + w_{i3}q_0q_3 + w_{i4}q_1q_2 + w_{i5}q_1q_3 + w_{i6}q_2q_3 \\ + w_{i7}q_0^2 + w_{i8}q_1^2 + w_{i9}q_2^2 + w_{i10}q_3^2 + w_{i11}t_x + w_{i12}t_y + w_{i13}t_z = 0 \end{aligned} \quad (7)$$

Let $s_u = (u - u_0)/f_u$, $s_v = (v - v_0)/f_v$. The weight parameters of Eq.(7) is denoted as following

$$\begin{aligned} h_{i1} &= -2Y_{Wi}s_u & h_{i2} &= 2Z_{Wi} + 2X_{Wi}s_u & h_{i3} &= -2Y_{Wi} & h_{i4} &= 2Y_{Wi} \\ h_{i5} &= 2Z_{Wi} - 2X_{Wi}s_u & h_{i6} &= -2Y_{Wi}s_u & h_{i7} &= X_{Wi} - Z_{Wi}s_u & h_{i8} &= X_{Wi} + Z_{Wi}s_u \\ h_{i9} &= -X_{Wi} + Z_{Wi}s_u & h_{i10} &= -X_{Wi} - Z_{Wi}s_u & h_{i11} &= 1 & h_{i12} &= 0 \\ h_{i13} &= -s_u & w_{i1} &= -2Z_{Wi} - 2Y_{Wi}s_v & w_{i2} &= 2X_{Wi}s_v & w_{i3} &= 2X_{Wi} \\ w_{i4} &= 2X_{Wi} & w_{i5} &= -2X_{Wi}s_v & w_{i6} &= 2Z_{Wi} - 2Y_{Wi}s_v & w_{i7} &= Y_{Wi} - Z_{Wi}s_v \\ w_{i8} &= Z_{Wi}s_v - Y_{Wi} & w_{i9} &= Y_{Wi} + Z_{Wi}s_v & w_{i10} &= -Y_{Wi} - Z_{Wi}s_v & w_{i11} &= 0 \\ w_{i12} &= 1 & w_{i13} &= -s_v \end{aligned}$$

(2) Line constraint

L_{Ci} represents a line in camera coordinate. Its corresponding 2D image line is L_{qi} . We denoted the plane which crosses L_{Ci} and L_{qi} as O_i . The normal vector of plane O_i is defined as N_i , where

$$N_i = [A_i f_u \quad B_i f_v \quad C_i + A_i u_0 + B_i v_0]^T \quad (8)$$

There are two major geometric constraints of 3D to 2D line correspondence. One constraint is that N_i is orthogonal to the direct vector v_{Ci} . The other is that the point p_{Ci} located on the plane O_i . The two constraints can be represented as

$$\begin{aligned} N_i^T v_{Ci} &= N_i^T R v_{Wi} = 0 \\ N_i^T p_{Ci} &= N_i^T (R p_{Wi} + T) = 0 \end{aligned} \quad (9)$$

where $v_{wi} = [v_{i1} \ v_{i2} \ v_{i3}]^T$, $p_{wi} = [p_{i1} \ p_{i2} \ p_{i3}]^T$ and $N_i = [N_{i1} \ N_{i2} \ N_{i3}]^T$ can be obtained from known 3D to 2D line correspondences. Substitute Eq. (3) into Eq. (9), we establish the equations:

$$\begin{aligned} & a_{i1}q_0q_1 + a_{i2}q_0q_2 + a_{i3}q_0q_3 + a_{i4}q_1q_2 + a_{i5}q_1q_3 \\ & + a_{i6}q_2q_3 + a_{i7}q_0^2 + a_{i8}q_1^2 + a_{i9}q_2^2 + a_{i10}q_3^2 = 0 \\ & b_{i1}q_0q_1 + b_{i2}q_0q_2 + b_{i3}q_0q_3 + b_{i4}q_1q_2 + b_{i5}q_1q_3 \\ & + b_{i6}q_2q_3 + b_{i7}q_0^2 + b_{i8}q_1^2 + b_{i9}q_2^2 + b_{i10}q_3^2 + b_{i11}t_x + b_{i12}t_y + b_{i13}t_z = 0 \end{aligned} \quad (10)$$

The weight parameters are known and denoted as following

$$\begin{aligned} a_{i1} &= 2N_{i3}v_{i2} - 2N_{i2}v_{i3} & a_{i2} &= 2N_{i1}v_{i3} - 2N_{i3}v_{i1} & a_{i3} &= 2N_{i2}v_{i1} - 2N_{i1}v_{i2} \\ a_{i4} &= 2N_{i2}v_{i1} + 2N_{i1}v_{i2} & a_{i5} &= 2N_{i3}v_{i1} + 2N_{i1}v_{i3} & a_{i6} &= 2N_{i2}v_{i3} + 2N_{i3}v_{i2} \\ a_{i7} &= N_{i1}v_{i1} + N_{i2}v_{i2} + N_{i3}v_{i3} & a_{i8} &= N_{i1}v_{i1} - N_{i2}v_{i2} - N_{i3}v_{i3} & a_{i9} &= -N_{i1}v_{i1} + N_{i2}v_{i2} - N_{i3}v_{i3} \\ a_{i10} &= -N_{i1}v_{i1} - N_{i2}v_{i2} + N_{i3}v_{i3} & b_{i1} &= 2N_{i3}p_{i2} - 2N_{i2}p_{i3} & b_{i2} &= 2N_{i1}v_{i3} - 2N_{i3}p_{i1} \\ b_{i3} &= 2N_{i2}p_{i1} - 2N_{i1}p_{i2} & b_{i4} &= 2N_{i2}p_{i1} + 2N_{i1}p_{i2} & b_{i5} &= 2N_{i3}p_{i1} + 2N_{i1}p_{i3} \\ b_{i6} &= 2N_{i2}p_{i3} + 2N_{i3}p_{i2} & b_{i7} &= N_{i1}p_{i1} + N_{i2}p_{i2} + N_{i3}p_{i3} & b_{i8} &= N_{i1}p_{i1} - N_{i2}p_{i2} - N_{i3}p_{i3} \\ b_{i9} &= -N_{i1}p_{i1} + N_{i2}p_{i2} - N_{i3}p_{i3} & b_{i10} &= -N_{i1}p_{i1} - N_{i2}p_{i2} + N_{i3}p_{i3} & b_{i11} &= N_{i1} \\ b_{i12} &= N_{i2} & b_{i13} &= N_{i3} \end{aligned}$$

2.3 Linear Pose Estimation Algorithm

For n line and m point correspondences, Let

$$L = [q_0q_1 \ q_0q_2 \ q_0q_3 \ q_1q_2 \ q_1q_3 \ q_2q_3 \ q_0^2 \ q_1^2 \ q_2^2 \ q_3^2 \ t_x \ t_y \ t_z]^T \quad (11)$$

Combined the constraint equation Eq.(0) and Eq.(0), we can derive the constraint equation system as

$$M_{2(n+m)}L = 0 \quad (12)$$

We first consider the each element in L as independent variable. Eq. (13) can be considered as a linear system of $2n$ equation in 13 variables. The solution of the system is sum weighted basic solution of the homogeneous linear system. The solution can be represent as

$$L = \sum_{i=1}^m \lambda_i v_i \quad (13)$$

where $v_i (i = 1 \dots m)$ is basic solution of the linear system which can be obtained by the SVD method. We apply $L(1:10)$ to denote the first 10 elements in L which are quadratic terms of four quaternion elements and $v_i(1:10)$ to denote the first 10 elements in each basic solution. Then we can derive

$$L(1:10) = \sum_{i=1}^m \lambda_i v_i(1:10) \quad (14)$$

λ_i ($i = 1 \dots m$) is the weight of each basic solution. m is the number of basic solution. For $2n$ dependent equation in 10 variables, $m=13-2n$.

Actually, the variables in $L(1:10)$ are correlated. We can produce the constraint equations of λ_i ($i = 1 \dots m$) according to the correlations of these variables. For example, we have $(q_a q_b)(q_c q_d) = (q_a q_c)(q_b q_d)$, and then the constraint Eq. (15) can be deduced.

$$\sum_{i=1}^m \lambda_{ii} (v_i^{ab} v_i^{cd} - v_i^{ac} v_i^{bd}) + \sum_{i=1}^m \left(\sum_{j=i+1}^m \lambda_{ij} (v_i^{ab} v_j^{cd} + v_j^{ab} v_i^{cd} - v_i^{ac} v_j^{bd} - v_j^{ac} v_i^{bd}) \right) = 0 \quad (15)$$

We define $\lambda_{ij} = \lambda_i \lambda_j$ ($i = 1 \dots m, j = 1 \dots m$). And we can produce a set of equations because of the correlations of variables in $L(1:10)$. The detail algorithm for solving this kind of equation can be found at the reference [8].

3 Experiments

3.1 Synthetic Experiments

In our synthetic experiments, the synthetic data is created as follows: we randomly produce n line parameters $L_{Ci} = \{p_{Ci} \ v_{Ci}\}$ under the camera coordinate and create translation vector T and rotation matrix R from random Euler angles. We then calculate the line parameter $L_{Wi} = \{p_{Wi} \ v_{Wi}\}$ in 3D world coordinates. Applying the pin-hole camera model, we can obtain the 2D line parameters L_{Hi} . For each 2D image line, we choose 100 points on the line and add the Gaussian noise whose variance is σ for each point and establish the noisy line parameter L'_{Hi} using least-square estimation method. We use $L_{Wi} = \{p_{Wi} \ v_{Wi}\}$ and L'_{Hi} as the input of the algorithm and determine the camera pose R^* and T^* , then compare with the ground true pose R and T .

We define the rotation error E_R and translation error E_T as

$$E_T = \frac{\|T - T^*\|}{\|T\|} \quad (16)$$

$$E_R = \frac{\|R - R^*\|}{\|R\|} \quad (17)$$

Where $\| \ \|$ represents the matrix norm.

We denote our algorithm as LQL (linear algorithm based on quaternion for line correspondences) and compare our algorithm with Ansar's NLL (n line linear algorithm), in which rotation matrix was directly represented by nine elements and $n(2n-1)+12$ equations with 46 variables were applied.

Experiment 1: Compare the estimation errors vary the number of line correspondence.

For the number of line correspondence from 4 to 12 with Gaussian noise of 2×2 pixels, we create the synthetic data using the method above. For each condition, we

do the experiments 1000 times for each algorithm and calculate the mean rotation error and mean translation error which are showed in figure 2. For our algorithm LQL and Ansar's NLL, the rotation error and translation error both decrease as the increasing of line correspondences number. The performance of LQL is better than NLL in both rotation and translation demonstrated in figure 1.

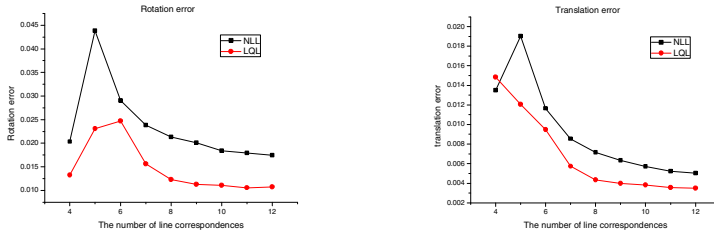


Fig. 1. The mean rotation error and translation error of 1000 trails versus number of line correspondences for LQL and NLL

Experiment 2: Compare the estimation errors vary image noise.

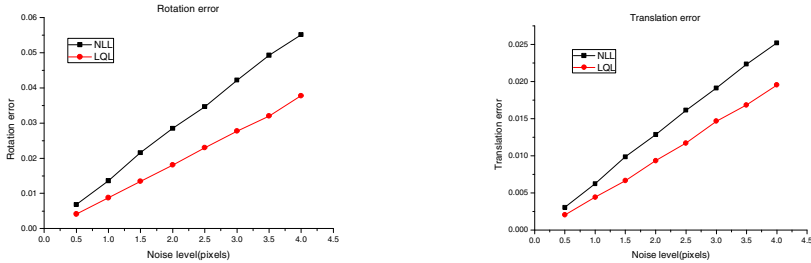


Fig. 2. The mean rotation error and translation error of 1000 trails versus noise level for LQL and NLL

For the image Gaussian noise's variance vary form 0.5 to 4 pixels, we compare the rotation error and translation error for the algorithm LQL and NLL using five lines. We also do the experiments 1000 times for each algorithm under the same noise level and calculate the mean rotation error and mean translation error. For the algorithm LQL and NLL, the rotation error and translation error both increase as the increasing of image Gaussian noise. The experiments demonstrate LQL has better accuracy for rotation and translation than NLL demonstrated in figure 2.

Experiment 3: Compare the running time for different algorithms.

We do the all simulation experiment offline using matlab on a 2.3GHz AMD personal computer and compare LQL and NLL for line correspondence form 4 to 12. The

running time is the average of 1000 trails. The result is show in table 1 which demonstrates that LQL is faster than NLL.

Table 1. Running times(in second) for algorithm NLL and LQL under matlab on a 2.3G AMD

algorithm	4 lines	5 lines	6 lines	7 lines	8 lines	9 lines	10 lines	11 lines	12 lines
NLL	0.2579	0.0514	0.0718	0.0976	0.1267	0.1612	0.1994	0.2439	0.2984
LQL	0.0065	0.0042	0.0034	0.0035	0.0036	0.0038	0.0038	0.0041	0.0042

3.2 Real Images

The real images were captured by a Besler 1400-gc CCD camera with 1390×1038 resolution and a Computar camera lens with 8mm physical length. The camera was calibrated using MATLAB calibration toolbox [13] and the calibrated efficient focal lengths are $(f_u, f_v) = (1302.98, 1300.93)$ and the optical center on the image are $(u_0, v_0) = (712.04, 513.19)$. The experiments were test by projection of 3D model on the 2D image. We applied 3 lines- 1 point, 2 lines- 2 points, 1 line- 3 points to calculate the camera pose. The projection well covered the real model which indicated the effectiveness of our pose estimation algorithm. The real images experiment results were shown in figure 3.

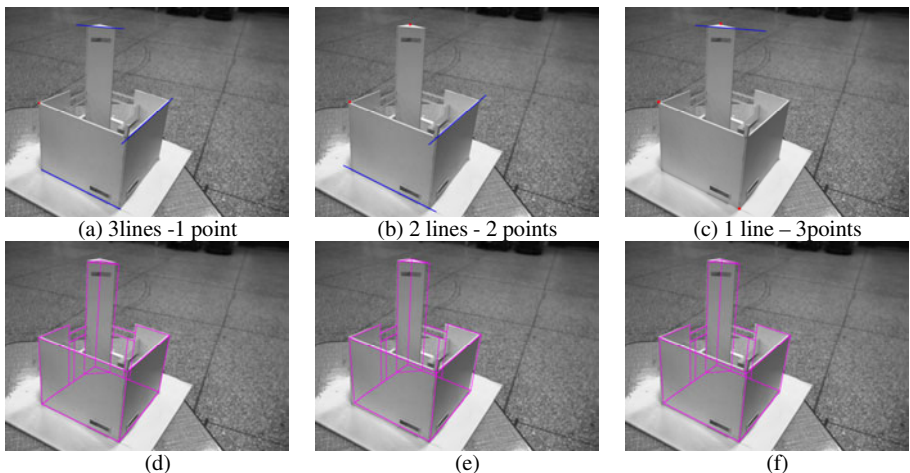


Fig. 3. (a), (b), (c) are respectively represent the geometric features which were applied for pose estimation. (d), (e), (f) are corresponding projection results.

4 Summary

An efficient linear camera pose estimation algorithm is presented for 3D to 2D line and point correspondences. In our algorithm, the rotation matrix is represented by a unit

quaternion which can guarantee the orthonormality of rotation matrix. For n ($n \geq 4$) correspondence, the algorithm can determine the rotation and translation parameters simultaneously. The synthetic experiments show less running time and more accurate pose estimation result of our algorithm compared with Ansar's NLL algorithm. The projection of a special model was conducted by the pose estimated by 1 point-3 lines, 2 points-2 lines, 3 points- 1 line correspondences. The projection was well registered with real model image.

Acknowledgements. Supported by National Natural Science Foundation of China (90820017), Basic Research and Business Subsidy of Central College. The corresponding author is Fei Wang.

References

1. Ansar, A., Daniilidis, K.: Linear Pose Estimation from Points or Lines. *IEEE Trans. Pattern Analysis Machine Intell.* 25(5), 578–589 (2003)
2. Dhorne, M., Richetin, M., Lapreste, J.T., Rives, G.: Determination of the Attitude of 3D Objects from a Single Perspective View. *IEEE Trans. Pattern Analysis Machine Intell.* 11(12), 1265–1278 (1989)
3. Chen, H.: Pose Determination from Line-to-plane Correspondences: Existence Solutions and Closed-form Solutions. *IEEE Trans. Pattern Analysis Machine Intell.* 13(6), 530–541 (1991)
4. Horaud, R., Conio, B., Leboulleux, O., Lacolle, B.: Ananalytic Solution for the Perspective 4-point Problem. *Computer Vision Graphics Image Process* 47, 33–44 (1989)
5. Liu, Y., Huang, T.S., Faugeras, O.D.: Determination of Camera Location from 2-d to 3-d Line and Point Correspondences. *IEEE Trans. Pattern Analysis Machine Intell.* 12(1), 28–37 (1990)
6. Phong, T.Q., Horaud, R., Yassine, A., Pham, D.T.: Object Pose from 2-D to 3-D Point and Line Correspondences. *International Journal of Computer Vision* 15(3), 225–243 (1995)
7. Christy, S., Horaud, R.: Iterative Pose Computation from Line Correspondences. *Computer Vision and Image Understanding* 73(1), 137–144 (1999)
8. Kipnis, A., Shamir, A.: Cryptanalysis of the HFE Public Key Cryptosystem by Relinearization. In: Wiener, M. (ed.) CRYPTO 1999. LNCS, vol. 1666, pp. 19–30. Springer, Heidelberg (1999)
9. Quan, L., Lan, Z.D.: Linear N-point Camera Pose Determination. *IEEE Trans. Pattern Analysis Machine Intell.* 21(8), 774–780 (1990)
10. Fiore, P.D.: Efficient Linear Solution of Exterior Orientation. *IEEE Trans. Pattern Analysis Machine Intell.* 23(2), 140–148 (2001)
11. Moreno-Noguer, F., Lepetit, V., Fua, P.: Accurate Non-iterative on Solution to the PnP Problem. In: Proc. IEEE Conf. on Computer Vision (2007)
12. Kuipers, J.B.: Quaternions and Rotation Sequences: a Primer with Applications to Orbits, Aerospace, and Virtual Reality. Princeton University Press, Princeton (1999)
13. Camera calibration toolbox for matlab,
http://www.vision.caltech.edu/bouguetj/calib_doc/
14. Ess, A., Neubeck, A., Van Gool, L.: Generalized linear pose estimation. In: British Machine Vision Conference, BMVC (2007)
15. Ji, Q., Costa, M.S., Haralick, R.M., Shapiro, L.G.: International Journal of Pattern Recognition and Artificial Intelligence 13(5), 705–733 (1999)

Image Enhancement Algorithm for Ink-on-Paper Fingerprints

Raghav Agrawal, Badrinath Srinivas, and Phalguni Gupta

Department of Computer Science & Engineering
Indian Institute of Technology Kanpur
Kanpur - 208016, India
{raghavag,badri,pg}@iitk.ac.in

Abstract. Quality of a scanned ink-on-paper fingerprint (or offline fingerprint) is generally poorer than that of online fingerprint and therefore, it requires an efficient enhancement method. This paper presents an algorithm to enhance the offline fingerprints using adaptive techniques. The algorithm handles certain problems that are specific to this type of fingerprints. It involves fingerprint extraction, intra-image classification followed by adaptive region enhancement of classified regions. It has been tested on IIT Kanpur database. The results show that the proposed algorithm performs well in enhancing ink-on-paper fingerprints.

Keywords: Biometrics, Fingerprint, Enhancement, Offline Fingerprint, Ink-on-paper Fingerprint.

1 Introduction

Fingerprint of a person is believed to be unique, has a lot of entropy and is easy to acquire. These characteristics make it the most widely used biometric trait in the world. Fingerprint matching is an important area of research in the field of biometrics. However, fingerprint acquisition methods may not provide acceptable images for fingerprint matching. Therefore, automatic fingerprint matching requires the acquired image to be enhanced to a certain level so that the matching has minimum error.

Ink-on-paper fingerprints are those fingerprint impression which are obtained by application of a coloured liquid (ink) on the finger and then pressing/rolling the inked finger on a paper. It is the most prominent method for fingerprint acquisition. Most of the government offices have fingerprint records in this format and therefore, to computerize these offices would require conversion of those fingerprint records into useful digital fingerprints. The proposed algorithm can enable to successfully convert large volumes of ink-on-paper fingerprints into *good quality* digital fingerprints which can then be used by a fingerprint matching system.

In offline fingerprints, the general factors of quality degradation *e.g.* dirt, scars, moisture etc. are present as are in the case of online fingerprints. But the uneven application of ink on finger and the uneven pressure applied while

pressing/rolling the finger on paper may degrade the quality further. Some of the problems that arise due to these factors are:

1. In some regions of the finger, the valleys get filled up with ink, which leads to narrowing of valleys formed on paper in the impression. These regions appear as dark regions. We call them as *wet regions*.
2. On the other hand, some regions do not acquire ample amount of ink and the corresponding impression is very *dry*. In these regions, the ridges appear broken, typical to a *dry* fingerprint. We address them as *dry regions*.

This paper attempts to enhance such images which comprise of both *wet* and *dry* regions in the same image. It is organized as follows. Section 2 briefly discusses some of the most common techniques used in fingerprint image enhancement. Section 3 describes the proposed algorithm. Experimental results have been analysed in Section 4. Conclusions are given in the last section.

2 Literature Review

There exist several fingerprint image enhancement methods such as Gabor filtering, directional median filtering, wavelet based methods. These methods can be classified into two broad categories: enhancement in spatial domain and enhancement in frequency domain.

2.1 Enhancement in Spacial Domain

In spacial domain, fingerprints have a well defined local ridge orientation and local ridge frequency. Therefore, the method uses this regularity and employs the directional filters or bandpass filters. The most popular method in this domain for fingerprint enhancement is due to Hong et. al.^[1]. They have used Gabor filters as the bandpass filters. Gabor filters are both frequency-selective and orientation-selective bandpass filters, which means, the filters can be effectively tuned to specific frequency and orientation values. In this method the image has been normalized and local ridge orientation and local ridge frequency has been computed at each pixel of the image. The image is convolved with Gabor filters tuned to the local ridge orientation and local ridge frequency. As an effect, ridges oriented in the local orientation direction are enhanced while those in other direction are suppressed. This reduces noise while increasing the contrast between the foreground ridges and the background. The TGF (Traditional Gabor Filter) is given by:

$$G(x, y; \theta, f) = e^{-1/2\left(\frac{x_\theta^2}{\sigma_x^2} + \frac{y_\theta^2}{\sigma_y^2}\right)} \cos(2\pi f x_\theta), \quad (1)$$

$$x_\theta = x \cos \theta + y \sin \theta, \quad (2)$$

$$y_\theta = -x \sin \theta + y \cos \theta \quad (3)$$

where θ is the ridge orientation, f is the local ridge frequency and σ_x and σ_y are the space constants of the Gaussian envelope along x -axis and y -axis axis, respectively. The 2-D Gabor filter can also be written as

$$G(x, y; T, \phi) = h_x(x; T, \phi)h_y(y; \phi) \quad (4)$$

where $h_x(x; T, \phi)$ is the bandpass filter in the direction perpendicular to the ridge orientation , and $h_y(y; \phi)$ is the low-pass filter in the direction of the ridges [4]. In traditional Gabor filtering method (TGF), only one frequency is used to estimate the variation in ridges and valleys. In [4], two frequencies are used corresponding to the local ridges and valleys.

A common drawback of enhancement methods in spatial domain is their dependence on ridge orientation and frequency. These parameters are highly distorted in poor quality regions of the image. Therefore, the enhancement is not effective in the poor quality regions.

2.2 Enhancement in Frequency Domain

In frequency domain, the enhancement methods are mainly based on Fourier transform. The most popular method in this domain is directional Fourier filtering [5]. In this method, 16 images are formed corresponding to 16 different directions using a band pass filter. Then inverse Fourier transform is applied on each image to obtain the final enhanced image. A common drawback of Fourier transform based enhancement is that the short ridges are filtered out. Therefore, this method does not give good result for *dry* images which may be seen as formed of small or broken ridges.

Apart from these two broad classifications, there are others which try to reap benefits of both the techniques. For example, in [7], the fingerprint is divided into non-overlapping blocks and the Fourier transform of each block is computed. The spatial benefit of constant local ridge orientation and frequency is used along with the fact that frequency based enhancement does not depend on calculation of ridge orientation and frequency which is often the source of error in spatial domain.

3 Proposed Algorithm

In ink-on-paper images both *wet* and *dry* regions coexist in the same image. So, using the same algorithm for the whole image may not produce good results. This is because of the fact that the degradation in the *wet* regions is of different nature compared to that in the *dry* region. In *dry* regions, the ridges are broken up and the algorithm needs to join such broken parts of ridges. On the other hand, in *wet* regions, due to extra ink inside the valleys, these valleys get narrow and so the algorithm should separate the ridges i.e. widen the valleys. These two tasks are of entirely different nature and it is difficult for a single algorithm to cater to both of these.

In this paper we propose an algorithm to deal with this specific problem. In our algorithm, we first perform the background separation, then divide the image into *dry* and *wet* regions using a segmentation algorithm. We carry on the enhancement of these regions separately using specific algorithms that perform better with such classification [2].

Any fingerprint enhancement would require to separate the background from the fingerprint. While this task is simple in case of online fingerprints, the same is not true for offline fingerprints as the background of offline fingerprints is not as uniform as that of online fingerprints. Also, it may contain some small patches of fingerprints along with the major fingerprint. Sometimes, a part of the major fingerprint is so *dry* that it separates the fingerprint into two parts. We first perform the background separation to extract out the fingerprint image from the scanned input image. We calculate the various parameters required for the clustering of sub-blocks and also for the enhancement algorithms used over the clusters. The mean and variance of the extracted fingerprint image is calculated and using these values, the fingerprint image is normalized to a desired mean and variance [1]. This reduces the effect of different ink shades used for fingerprint acquisition, the colour shade of background paper *etc.* Fig. 1 shows a normalized image from original image. Local ridge orientation [6] and local ridge frequency [1] are calculated. Fig. 2 shows the quiver plot of the orientation for 2 different fingerprints. This is followed by calculation of local ridge valley thickness ratio, which we consider as the most important parameter for clustering purposes. In a sub-block, the ridges and valleys should ideally be of same size. But as in case of *wet* regions, the ridges tend to be thicker than the valleys and so the number of pixels that correspond to ridges is more than that corresponding to the valleys. The ridge valley thickness ratio for a sub-block is a measure of this variation. The higher the ratio, more is the sub-block *wet*. If this ratio is infinity for some sub-block, it would mean that the region has no valleys. This usually happens when the finger slides on paper while rolling or the finger is excessively inked. Such regions cannot be enhanced and should be discarded. Similarly, regions where this ratio is zero would mean a no ridge region and may correspond to background region. Since, we have already separated out the background from our image, zero value for ridge valley thickness ratio may only occur at the fingerprint boundary.

Image sub-blocks are clustered using k-means algorithm with $k = 2$ with the help of mean, variance and ridge valley thickness ratio in the clusters to get the *dry* and *wet* regions. Small discrete regions are reduced using connected component analysis. The idea is that if an image sub-block identified as *dry* is surrounded by *wet* blocks on all sides then it should be treated as a *wet* block and vice versa. This is followed by identification of clusters. These clusters are enhanced separately and then merged to obtain the final enhanced image. Some steps of the algorithm are described below.

Calculation of Ridge Valley Thickness Ratio for Image Blocks. We take an image window in the direction of the image block orientation, centred at the center of the block, and calculate the number of pixels that form ridges

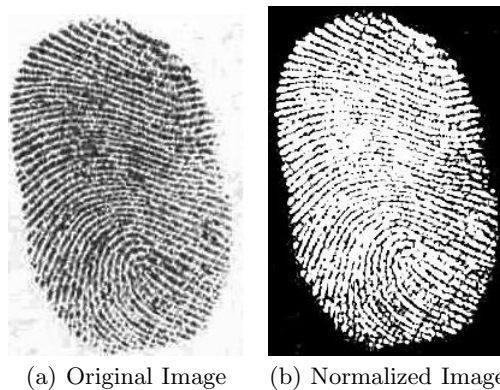


Fig. 1. Normalization

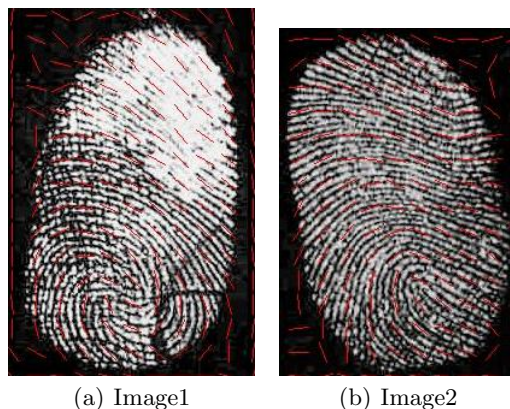
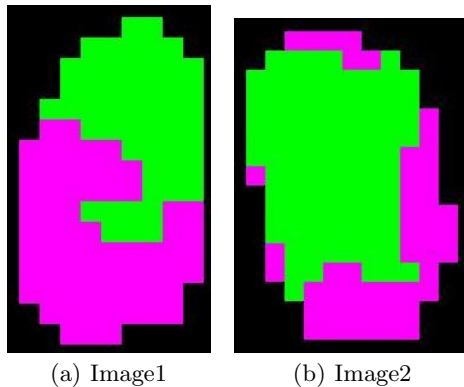


Fig. 2. Orientation

and number of pixels that form valleys. We also count the number of ridges and valleys in the window. Sum of ridges or valleys is reduced such that pixel counts of both of them are in equal numbers. For example, if for a sub-block, 500 pixels contribute to ridges and 400 pixels to valleys and the number of ridges are one more than the number of valleys then the last ridge pixels (say 100 pixels were in the last ridge of the window) are subtracted from the ridge pixel count. Therefore, the final pixel count of ridges and valleys becomes 400 and 400 respectively. Pixel count is divided to get the ridge valley thickness ratio, which is 1 in the given example. Note that we consider only complete ridges and complete valleys and leave the partial ridges and valleys at the start and end of the window.

**Fig. 3.** Clustering

Identify *dry* Region Cluster from above Two Clusters. The k-means algorithm gives two clusters but does not give information about which cluster is *dry* and which is *wet*. We identify the clusters using the fact that since the *wet* regions are regions in which more ink has been applied on paper, these would correspond to lower mean value (considering ridges as black coloured imprint on white background) compared to *dry* regions. So, the cluster with lower average mean value is classified as *wet* region. The other stands as *dry* region. Fig. 3 shows image clusters for two images where green sub-blocks correspond to *wet* region and pink sub-blocks correspond to *dry* region.

Enhancing *dry* Image Cluster. In enhancing the *dry* image cluster, we first skeletonize it and then apply directional motion blurring, in the direction of ridges (to join the broken ridges).

Enhancing *wet* Image Cluster. To enhance the *wet* image cluster, modified Gabor filter [4] is applied to increase valley width and to enhance image in the direction of the ridges. This is followed by skeletonization and motion blurring.

Merge the Two Clusters to Form Final Image. When the enhanced clustered subimages are merged, one may get misaligned in terms of ridge continuities. This is avoided by applying morphological operations to the image clusters before merging them to ensure seamless blocks in the final image.

It can be noted that all parameters that are needed to enhance the image are adaptive. Thus, the algorithm is invariant to overall orientation, size of the fingerprint and the size of the image.

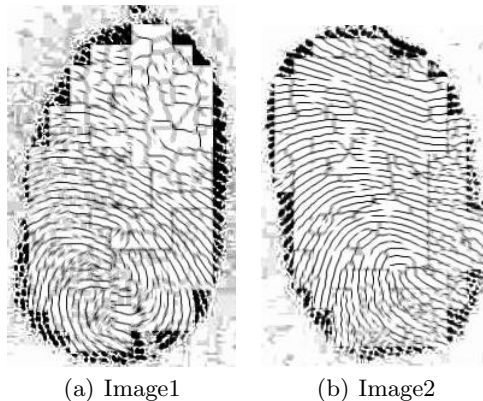


Fig. 4. Final Enhanced Images

4 Experiments and Results

The algorithm has been tested on IIT Kanpur database which consists of 2500 scanned ink-on-paper fingerprint images of Indian villagers who are supposed to have very poor quality fingerprints due to the nature of their trade. The database images are at 300 dpi both, horizontal and vertical with bit depth of 24 but are of variable size varying between 150x300 and 350x300.

The enhancement process sets the block size and various other parameters based on the image size. The Gabor filter is set to size 7. The clustering algorithm has been used only in the blocks that correspond to the fingerprint and not to the blocks that belong to the background, as those blocks seriously affect the clustering. The fingerprint region is segmented out of the full image. Among the sub-blocks that belong to the fingerprint, the blocks that are at the boundary are not passed to the algorithm. This is because, these regions also contain some part of the background which can again adversely affect the classification.

The performance of the enhancement algorithm is judged using the fingerprint image quality algorithm [8]. It ranks an input image from 1 (best) to 5 (worst). It has been observed that the image quality algorithm [8] has ranked most of the images in the IITK database as level 5. Out of these 2500 images the proposed algorithm could enhance 537 images to level 3 or level 4. Fig. 4 shows two images enhanced by our algorithm.

5 Conclusion

Offline fingerprints pose a different problem than the online fingerprints which make the state-of-the-art algorithms available for online fingerprints less effective when they are applied to these fingerprints. We have presented a novel algorithm for enhancing fingerprint images using adaptive techniques which cater to the specific problem of offline fingerprints.

Acknowledgements. This work has been supported by the Department of Information Technology, Government of India, Delhi, India. Authors are thankful to all reviewers for their valuable comments which have helped us to improve the quality of the paper.

References

1. Hong, L., Wan, Y., Jain, A.: Fingerprint Image Enhancement: Algorithm and Performance Evaluation. *IEEE Transactions on Pattern Analysis and Machine Intelligence* 20(8), 777–789 (1998)
2. Yun, E.K., Cho, S.B.: Adaptive fingerprint image enhancement with fingerprint image quality analysis. *Image and Vision Computing* 24(1), 101–110 (2006)
3. Kanungo, T., Mount, D.M., Netanyahu, N.S., Piatko, C.D., Silverman, R., Wu, A.Y.: An efficient k-means clustering algorithm: analysis and implementation. *IEEE Transactions on Pattern Analysis and Machine Intelligence* 24(7), 881–892 (2002)
4. Yang, J., Liu, L., Jiang, T., Fan, Y.: A modified Gabor filter design method for fingerprint image enhancement. *Pattern Recognition Letters* 24(12), 1805–1817 (2003)
5. Sherlock, B.G., Monro, D.M., Millard, K.: Fingerprint enhancement by directional Fourier filtering. *IEE Proceedings on Vision, Image and Signal Processing* 141(2), 87–94 (1994)
6. Thai, R.: Fingerprint Image Enhancement and Minutiae Extraction. Technical Report, The University of Western Australia (2003)
7. Willis, A.J., Myers, L.: A cost-effective fingerprint recognition system for use with low-quality prints and damaged fingertips. *Pattern Recognition* 34(2), 255–270 (2001)
8. Tabassi, E., Wilson, C.L., Watson, C.: NIST fingerprint image quality. Technical Report NISTIR 7151, NIST (2004)

Multi-spectral Remote Sensing Images Classification Method Based on Adaptive Immune Clonal Selection Culture Algorithm

Yi-Nan Guo¹, Dawei Xiao¹, Shuguo Zhang, and Jian Cheng^{1,2}

¹ School of Information and Electrical Engineering, China University of Mining and Technology, Xuzhou, Jiangsu 221116, China

² Department of Automation, Tsinghua University, Beijing 100084, China
nanfly@126.com

Abstract. In immune clonal selection algorithm for remote sensing images classification problem, only clonal selection mechanism is adopted. It makes the exploitation and exploration of the algorithm limited. To solve above problem, adaptive immune clonal selection culture algorithm is introduced in the paper. It fully uses the dual evolution mechanism of culture algorithm to extract implicit knowledge in belief space. According to the evolution situation noted in topological knowledge, a hybrid selection strategy integrating clonal selection and $(\mu+\lambda)$ selection are proposed in population space. Simulation results indicate that the classification method based on adaptive immune clonal selection culture algorithm can improve the classifier performance better.

Keywords: Immune clonal selection, remote sensing images classification, culture algorithm.

1 Introduction

Aiming at remote sensing images classification problem, two kinds of classification method are considered. They are supervised methods and unsupervised methods. Unsupervised methods can be self-organization and independent on prior knowledge. However, the classification accuracy is always not satisfied. Supervised methods depending on prior knowledge have the better classification accuracy. However, they just consider the local characteristics of the classification problems. The global characteristics are ignored. So they are easy to fall into local optimal[1,2]. Because the traditional classification methods need to consider more conditions for use, such as the parameters, the distribution of samples, they have limited classification performances.

Compared with the traditional classification methods, the artificial immune algorithm is a kind of nonparametric classification method. It doesn't require the data to obey normal distribution. So how to select the training samples is not an important issue which directly influences the classification. Immune clonal selection algorithm(ICS) is a kind of artificial immune algorithm. The selection mechanism used in ICS plays an important role in algorithm performances. It usually makes the evolution falling into prematuration because only antibodies with large affinity are

preserved. Aiming at solving this problem, the simulated annealing algorithm is introduced. However, this algorithm needs enough model disturbance and iteration combining with rigorous annealing plan to ensure obtaining the optimal solutions. So its efficiency is lower, which makes it applied limitedly[3,4]. The largest resource threshold[5] is defined to control the individual selection. The worst individual is eliminated so as to make the total resource less than the largest resource threshold. So it is in fact to only preserve the individual with large affinity. Moreover, the largest resource threshold is determined subjectivity. Besides, whether the ICSA is satisfied the diversity and whether it can avoid prematuration largely depend on the selection mechanism.

Therefore, considering the exploration and exploitation, a novel remote sensing images classification algorithm based on adaptive immune clonal selection culture algorithm(AICSCA)[6] is proposed. It adopts the dual evolution mechanism of culture algorithm[7]. Valuable information embodied in the evolution is extracted as knowledge in belief space, which reflects the evolution situation. A novel hybrid selection strategy is given in population space. According to the evolution situation memorized in knowledge, three kinds of selection strategy integrating clonal selection and $(\mu+\lambda)$ selection are adaptively chosen so as to avoid converging in the local optimal solutions and improve the diversity.

2 Remote Sensing Images Classification Method Based on Adaptive Immune Clonal Selection Culture Algorithm

In remote sensing images, the culture is reflected by multi-band gray values. Gray values in each band vary between 0 and 255. In order to improve the classification performances, an optimal characteristics center of gray values for each class of the culture is obtained by continuously training the training samples which are form the selected training areas. These centers are used to classify the whole remote sensing images[8]. In this paper, the antigen is denoted by the cluster center of each class. The initial population consists of the training samples from selected training area.

In AICSCA, ISCA is introduced in population space. Clonal selection or $(\mu+\lambda)$ selection are normally adopted in ISCA. The population is expanded and compressed repeatedly by clonal selection. It is in fact a kind of local selection mechanism, which affects the global convergence speed. $(\mu+\lambda)$ selection is a global selection mechanism, which is easy to make the evolution converged to local optimal solutions[6]. Obviously, pure selection strategy can not satisfy the needs. So hybrid selection mechanism is done. In order to reasonably choose selection strategies, the evolution situation is extracted as knowledge in belief space. Here, three kinds of selection strategy including clonal selection, $(\mu+\lambda)$ selection and $(\mu+\lambda)$ selection with random substitute mechanism are adopted. The details algorithm steps are shown as follows:

Step1: Population space and belief space are initialized. The training samples are taken as the initial population. Their mean values are made as the initial center. The antibodies which have the largest affinity and the variable range in each dimension are memorized as the initial knowledge in belief space.

Step2: The affinities of all antibodies are calculated. And the number of their clonal antibodies is computed in terms of the affinities.

Step3: The offspring population is obtained via clonal expansion operation and mutation operation. And it is combined with the population in last generation..

Step4: According to the knowledge, the dominant antibodies are selected by hybrid selection strategy. The antibody population in next generation is obtained.

Step5: The knowledge in belief space is updated.

Step6: The termination condition is judged. If the difference between the sum affinities of all training samples to the center in adjacent generation is lower than a certain threshold or the maximum generation is achieved, the evolution process is stopped. Otherwise, it jumps to step3.

Step7: The remote sensing images are classified by the optimal classifying centers.

Obviously, how to define the antibody for this kind of classification problem and how to reasonably describe and utilize implicit knowledge are two key issues.

2.1 Definition of Antigen and Antibody

Above all, the number of the culture is determined. Then the areas for training samples of each class are selected. The mean gray value in each band of all antibodies in each class is taken as the initial clustering center, which is the initial antigen. It varies along with the antibody population. The training samples in each class are chosen as the initial antibody population. The antigen and antibody shall be normalized.

2.2 Main Operations in Population Space

In population space, the population is proliferated via cloning antibody. And the affinity between antigen and antibody is improved by mutation operation.

A) Immune Clonal operation

The clonal size is affected by the affinity between antigen and antibody. The larger the affinity is, the clonal size is less. So the clonal size $c_i(t)$ of the antibody ab_i is:

$$c_i(t) = \text{round}(n_c \cdot \text{affinity}(ag, ab_i)) \quad (1)$$

$$\text{affinity}(ag, ab_i) = \text{norm}(\exp(-\|ag - ab_i\|)) \quad (2)$$

Here, n_c is a constant. $\text{affinity}(ag, ab_i)$ is the affinity between antigen ag and antibody ab_i , which is normalized to reflect the similarity among them. The key of clonal operation is to extend the antibody ab_i to a sub-antibody population $ab_i^C(t)$, whose size is $c_i(t)$. All sub-antibody populations are composed of the offspring population. And population size is $\sum_{i=1}^m c_i(t)$.

B) The Mutation Operation

In order to avoid falling into prematuration, the mutation operation is done for the antibodies after the clone operation $ab_i^C(t)$. We know that if the affinity of a antibody is larger, this antibody embodies better evolution information. It shall be saved into

offspring population. So the scale of mutation operator is smaller. Here, Gaussian mutation operator is used. Let $N(0,1)$ be a random vector satisfied normal distribution.

$$ab_i^M(t) = ab_i^C(t) + \sqrt{|f(ab_i^C(t))|} \times N(0,1) \quad (3)$$

C) The Selection operation

Clonal selection or $(\mu+\lambda)$ selection are normally adopted.

Clonal Selection Strategy. In clonal selection, the dominant antibodies are chosen from combined population. Here, combined population consists of the father population and offspring population after clonal operation. Assume $ab^M(t) \in AB_i^M(t)$ is the dominant antibodies obtained by clonal selection operation from antibody $ab_i(t)$. It is selected into offspring population in next generation $AB(t+1)$ in terms of following probability[6].

$$p(ab_i(t+1) \in AB(t+1)) = \begin{cases} 1 & f(ab_i(t)) < f(ab^M(t)) \\ \exp(-\frac{f(ab_i(t)) - f(ab^M(t))}{\sigma}) & [f(ab_i(t)) \geq f(ab^M(t))] \wedge [f(ab_i(t)) < f(ab_j(t)), \exists ab_j(t) \in AB(t)] \\ 0 & [f(ab_i(t)) \geq f(ab^M(t))] \wedge [f(ab_i(t)) > f(ab_j(t)), \forall ab_j(t) \in AB(t)] \end{cases} \quad (4)$$

where σ is the diversity coefficient of population.

$$\sigma = \frac{1}{m} \sum_{i=1}^m (ab_i(t) - \frac{1}{m} \sum_{i=1}^m ab_i(t))^2 \quad (5)$$

It is obvious that two factors influence the possibility of a antibody selected into offspring population. One is the affinity between antibodies in offspring population and antigen. The other is the distribution of population in last generation. Clonal selection is done only in the combined population. This ignores the competition among antibodies. Therefore, it is good for the diversity of population, whereas the global convergence ability is decreased.

$(\mu+\lambda)$ Selection Strategy $(\mu+\lambda)$ selection is to select m antibodies with larger affinity from the combined population to offspring population in next generation. So it easily lead to prematurity.

2.3 Extraction and Utilization of Implicit Knowledge

At present, there are five kinds of knowledge[7] are introduced in belief space of cultural algorithms. In AICSCA, normative knowledge and topographical knowledge are adopted. The distribution of dominant antibodies' fitness values are recorded as topographical knowledge. It is used to adaptively choose the selection strategy so as to avoid falling into prematurity.

In topographical knowledge, three kinds of indexes are introduced. They are the evolutionary degree, the coverage degree of antibodies and the dispersion degree of antibodies, respectively expressed by $ED^q(t)$, $CD^q(t)$ and $SD^q(t)$ [6]. The evolutionary degree notes the evolution situation of the antibodies in sub-space $R^q(t)$ to the whole

population. The coverage degree of antibodies is the span of this sub-space. The dispersion degree of antibodies describes relative convergence extent of $R^q(t)$.

$$ED^q(t) = \frac{\bar{f}^q(t)}{\bar{f}(t)} \quad (6)$$

$$CD^q(t) = \min_{j=1,\dots,n} \left[\frac{\max_{k=1,\dots,m_q} ab_{kj}^q(t) - \min_{k=1,\dots,m_q} ab_{kj}^q(t)}{u_j^q - l_j^q} \right] \quad (7)$$

$$SD^q(t) = \min_{j=1,\dots,n} \sigma_j^q(t) \quad (8)$$

Here, $\bar{f}^q(t)$ denotes the average affinity between antigen and antibodies in the sub-space. $\bar{f}(t)$ is the average affinity of combining population. u_j^q and l_j^q are the upper and lower bound of j -th variable in $R^q(t)$. $\sigma_j^q(t)$ is the dispersion degree of antibodies in j -th dimension of $R^q(t)$.

$$\sigma_j^q(t) = \frac{1}{m_q} \sum_{k=1}^{m_q} (ab_{kj}^q(t) - \frac{1}{m_q} \sum_{k=1}^{m_q} ab_{kj}^q(t))^2 \quad (9)$$

Obviously, larger $ED^q(t)$ shows that the affinity of antibodies are better. The dominant antibodies are more possible to be appeared in $R^q(t)$. Larger $CD^q(t)$ indicates that the antibodies cover $R^q(t)$ more. Less $SD^q(t)$ shows that the antibodies in $R^q(t)$ are centralized more.

In order to maintain the exploration ability in the search space and avoid falling into prematurity, knowledge-inducing hybrid selection strategy[6] is proposed. If the diversity of antibodies in a sub-space is good, the clonal selection strategy is adopted. In the dominant sub-space with more antibodies, $(\mu+\lambda)$ selection strategy is used. According to the indexes memorized in topographical knowledge, the selection mechanism for the antibodies in $R^q(t)$ is obtained.

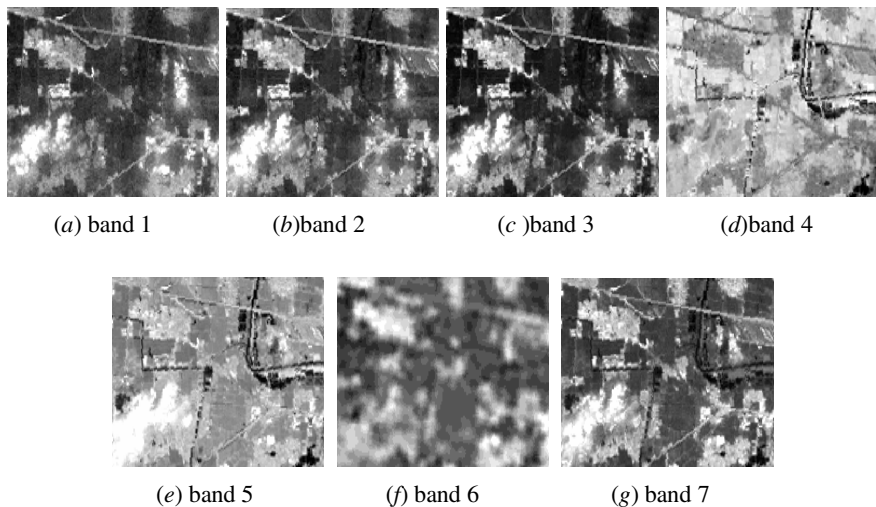
Rule1:If $CD^q(t) < \alpha$, $SD^q(t) < \beta$ and $ED^q(t) \geq \gamma$, the selection strategy by combining the elitist preserved strategy with $(\mu+\lambda)$ selection strategy is adopted.

Rule2:If $CD^q(t) \geq \alpha$ or $SD^q(t) \geq \beta$, the clonal selection strategy is adopted.

Rule3:If $CD^q(t) < \alpha$, $SD^q(t) < \beta$ and $ED^q(t) < \gamma$, the selection strategy by combining $(\mu+\lambda)$ selection strategy with random substitute mechanism is adopted.

3 Simulation and Analysis

In order to validate the rationality of the AICSCA classification method for remote sensing images, simulation experiments are done by matlab7.0. In multi-spectral remote sensing images, massive data information is contained. So the cultures are easy to be recognized. However, the redundant data increases the difficulty for image processing. Therefore, they need to be pre-processed. The processed original remote sensing images used in experiments are shown in Fig.1. Here, the size of each picture is 197×119.

**Fig. 1.** 7 bands of original remote sensing images

In the paper, the proposed AICSCA classification method is compared with maximum likelihood(ML) classification method and minimum distance(MD) classification method. Aiming at classification problem for above 7-band remote sensing images, the detailed classification results are shown by the confusion matrices, as shown in Table.1. And the algorithms' performances are compared in terms of two indexes. They are classification accuracy and Kappa coefficient. The classification results in simulation are shown in Table.2.

Table 1. Comparison of the confusion matrices with different classification methods

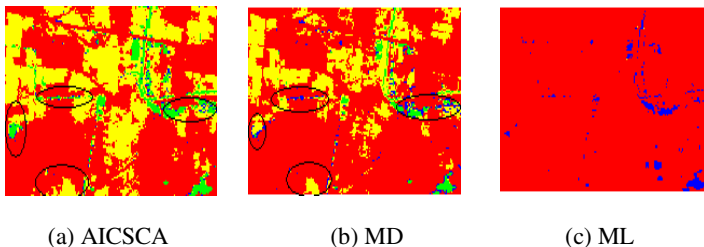
Methods	Class1	Class2	Class3	Class4	Total
ML method	Class1	100	0	53	0
	Class2	0	100	0	0
	Class3	0	0	47	0
	Class4	0	0	0	100
	Total	100	100	100	100
	Class1	92	0	0	0
MD method	Class2	0	100	0	0
	Class3	8	0	100	0
	Class4	0	0	0	100
	Total	100	100	100	16
	Class1	99	0	0	0
	Class2	0	100	0	0
AICSCA method	Class3	1	0	100	0
	Class4	0	0	0	100
	Total	100	100	100	2

Table 2. Comparison of the performances with different classification methods

Methods	ML method	MD method	AICSCA method
Accuracy	0.8675	0.98	0.9975
Kappa coefficient	0.8233	0.9733	0.9967

From above classification results, we know that the performance of AICSCA classification method is better than other two classification methods. Its accuracy and Kappa coefficient are both better. Therefore, AICSCA classification method is feasible to be used in remote sensing images classification problem. Here, the classification effect for maximum likelihood classification method is worse. The reason for this is that the data used in ML classification method are needed to satisfy the normal distribution. However, this is impossible to be satisfied in practice.

The classification results of 7-band remote sensing images adopting above three classification methods are shown in Fig.2.

**Fig. 2.** Classification result based on different classification methods

Compared with Fig.1, it is obvious that the classification effect based on AICSCA classification method is better than ML and MD classification methods as shown in Fig.2. Although in maximum likelihood classification method, some class of the culture are partitioned, corresponding class labels are wrong in certain class. So the classification performance of this method is bad. In minimum distance classification method, the cultures are classified in better accuracy. However, the parts with wrong class label still exists as marked by black circle in Fig.2. Besides, the classes which has the similar spectral are classified into the same class. The reason for this is the Euclidean distance is adopted in MD classification method. So the cultures in each band to the corresponding center can be distinguished well. However, it is bare to distinguish the sum distance in all bands, which leads to the wrong classification. In AICSCA classification method, the mean of the training samples is replaced by the optimal center to classify. So it does not need the data satisfied normal distribution. But there exists the wrong classification among the similar spectral in AICSCA. The reason for this is it adopts the same measure method like Euclidean distance as minimum distance classification method.

4 Conclusions

In immune clonal selection algorithm, only one kind of selection mechanism is usually adopted. It makes the evolution easily falling into prematurity. So the dual evolution mechanism of culture algorithm is introduced into ICSA. Adaptive immune clonal selection culture algorithm for remote sensing images classification is proposed in the paper. Implicit knowledge reflecting the evolution situation is extracted in belief space. ICSA with knowledge-inducing hybrid selection strategy is given in population space. It integrates clonal selection and $(\mu+\lambda)$ selection. Simulation results aiming at 7-band remote sensing images classification indicate that the classification method based on adaptive immune clonal selection culture algorithm can improve the classifier performances. Its accuracy and Kappa coefficient are both better than the traditional classification methods.

Acknowledgment. This work was supported by National Natural Science Foundation of China under Grant 60805025, Natural Science Foundation of Jiangsu under Grant BK2010183, the China Postdoctoral Science Foundation Funded Project under Grant 20090460328 and Qinglan Project of Jiangsu.

References

1. Zhang, L., Chen, X.H., Weng, Y.: Remote Sensing Image Classification Using Clonal Selection Algorithm Based on AIS. *Geography and Geo-Information Science* 24, 37–40 (2008)
2. Zhong, Y.F., Zhang, L.P., Li, P.X.: Multispectral Remote Sensing Image Classification Based on Simulated Annealing Clonal Selection Algorithm. In: IEEE Proceedings of Geoscience and Remote Sensing Symposium, pp. 3745–3748 (2005)
3. Chen, H.G., Li, L.H., Xu, H.P., et al.: Modified Very Fast Simulated Annealing Algorithm. *Tongji University (natural science)* 34(8), 1121–1125 (2006)
4. Chen, H.G., Wu, J.S., Wang, J.H., et al.: Mechanism Study of Simulated Annealing Algorithm. *Tongji University (natural science)* 32, 802–805 (2004)
5. Zhang, C.M., Liang, Y., Wan, S.J., et al.: Research on Image Classification Algorithm Based on Artificial Immune Learning. In: Li, D., Liu, Y., Chen, Y. (eds.) CCTA 2010, Part III. IFIP AICT, vol. 346, pp. 403–412. Springer, Heidelberg (2011)
6. Guo, Y.N., Wang, H., Cheng, J.: Adaptive Immune Clonal Selection Cultural Algorithm. *Chinese Journal of Electronics* 38(4), 966–972 (2010)
7. Guo, Y.N., Wang, H.: Overview of cultural algorithms. *Computer Engineering and Applications* 45(9), 41–46 (2009)
8. Zhong, Y.F., Zhang, L.P., Gong, J.Y., et al.: Remote Sensing Image Classification Based on Artificial Immune System. *Journal of Remote Sensing* 9(4), 374–380 (2005)

Age Estimation Using Active Appearance Models and Ensemble of Classifiers with Dissimilarity-Based Classification

Sharad Kohli, Surya Prakash, and Phalguni Gupta

Department of Computer Science and Engineering,
Indian Institute of Technology Kanpur
Kanpur 208016, India
{ksharad,psurya,pg}@cse.iitk.ac.in

Abstract. This paper proposes a novel technique that uses Active Appearance Models (AAMs) and Ensemble of classifiers for age estimation. In this technique, features are extracted from face images by AAMs and a global classifier is then used to obtain an idea about the age by distinguishing between child/teen-hood and adulthood, before age estimation. This is done by an ensemble containing various classifiers trained on multiple dissimilarities and thereby which reduces misclassification error. Different aging functions are considered for the classified images to estimate age more accurately. Experiments are performed on the publicly available FG-NET database. The method is found to be a good age estimator.

1 Introduction

Human face is an abundant information source and conveys information about the identity, gender, ethnicity, emotional state, age etc of the subject shown in the face image. Human beings are able to continuously extract this information and use it in face to face communication [1]. Automatic interpretation and extraction of such information has been extensively studied [2][3][4] for its applications in Human Computer Interaction(HCI). Age plays a vital role in any interaction, but research in the field of automatic age estimation has been constrained because of several reasons. Different people age in different ways, depending on factors such as genetics, race, external conditions such as weather, living styles, eating and drinking habits, and also idiosyncratic features, such as extent and frequency of facial expressions [5]. Moreover, makeup and attempts to artificially slow down the aging process through the use of anti-aging products also effect age prediction accuracy. Aging is also ethnicity specific, so a technique designed to work on faces of one region might not do well on faces of other region.

There is a great amount of variation that occurs in the face during child/teen-hood and adulthood [6]. Over the course of the lifespan there are certain noticeable skeletal and soft tissue age-related shape, size, and configuration changes in individuals [5]. During childhood and adolescence, the changes in facial structure are due to stretching of cranial complex. For adults, facial structure is affected by some cranial changes but the most important noticeable changes are due to lines, wrinkles, creases and sagging of skin [5].

1.1 Motivation

We are motivated by various real life applications of automatic age estimation. It has applications in the field of forensic science for the purpose of age progression. Since age progression systems generally need the age of the person in the presented image, hence an accurate facial age estimator can be useful in making automatic age progression systems. Further, age estimation would also help in improving age invariant person identification [9]. Automatic age estimation would also enable the machine interface and computing environment to be adjusted based on the age of the user and thereby improving HCI. It can also be used to restrict the access of certain items, such as websites with unsuitable material or cigarettes and alcohol, to under-age individuals. It can further be used in age based indexing of face images, thereby allowing age based retrieval of face images as per need.

1.2 Overview of Proposed Approach

This paper presents a hierarchical age estimation method to make unique aging functions for the two different age classes. Feature vectors extracted from AAMs [8] are used first to get a rough estimate on the age of the subject by classifying them into the age category that it belongs. We use an ensemble of various diverse classifiers trained on different dissimilarities to take the decision. In order to get an accurate estimate of age, faces classified as child/teen-hood are passed to a specific child/teen-hood age determination function and the rest to the specific adult age estimation function.

1.3 Organisation of Paper

The rest of the paper is organised as follows: In Section 2 we provide a brief overview of the various approaches used for age estimation. Section 3 discusses the various methods used in our age estimation technique. Section 4 proposes a hierarchical age estimation method using ensemble of diverse classifiers. The experimental results are reported in Section 5. Finally in Section 6 future work and conclusions are presented.

2 Related Work

Most of the work in age estimation can be broadly categorized in three different categories [10], such as anthropometric model [11], aging pattern subspace [12] and regression functions [10][11]. Anthropometric models study the craniofacial changes and facial skin wrinkle patterns to classify faces as babies, young adults and senior adults. AGing pattErn Subspace(AGES) [12] uses EM-like iterative learning algorithm to learn a representative subspace using Principal Component Analysis (PCA). The age of a test face is determined by the projection in the subspace that can reconstruct the face image with minimum error. Lanitis *et al.* [1] have approached the problem of age estimation in a regression way. They have used quadratic “aging functions” to model the effects of aging. They have further proposed hierarchical age estimation techniques where first an idea about the age of subjects is obtained using a global aging function, and then age

specific functions or appearance specific functions or weighted combination of both are used to further estimate the age in this rough range. Luu *et al.* [7] have proposed an age estimation technique where different aging functions are used for different age groups, based on their carno-facial development.

3 Background

This section provides an overview of the various techniques that have been used in the paper. Section 3.1 introduces Active Appearance Models which are used to extract features from a face image. Section 3.2 provides an overview of various ensemble creating methods and discusses the criteria required for an ensemble to be an effective classifier.

3.1 Active Appearance Model(AAM)

Cootes *et al.* [13] have proposed a statistical approach to model facial appearance. AAMs have been successfully used in various areas involving image interpretation such as face recognition [14], facial expression recognition [15], age estimation and progression [1] and various other fields. Basically AAMs involve a combination of statistical shape and appearance model to form a combined appearance model. A set of landmark points

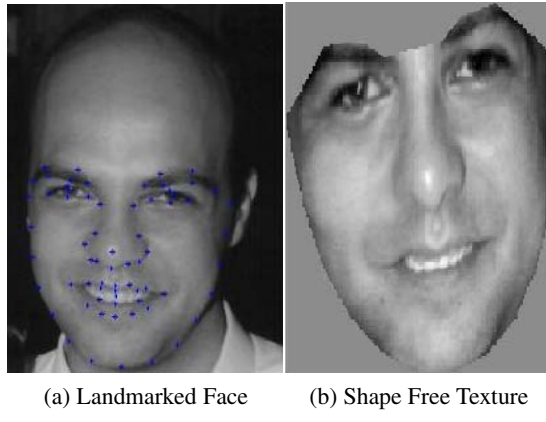


Fig. 1. Landmarked Face and Shape Free Texture of an Image from FG-NET Database

representing a shape is used to build a shape model by applying Principal Component Analysis (PCA) as follows:

$$x = \bar{x} + P_s b_s \quad (1)$$

where \bar{x} represents the mean shape, P_s is the eigen-vector matrix and b_s is a set of shape parameters. Similarly, a texture model is obtained by wrapping each shape to a mean shape and then a statistical model is extracted from this shape free patch using PCA as:

$$g = \bar{g} + P_g b_g \quad (2)$$

where \bar{g} represents the mean normalised grey-level vector, P_g is the eigen-vector matrix and b_g is a set of grey-level model parameters. Both models are combined with appropriate weights to account for the difference in the units of shape and texture models as:

$$b = \begin{pmatrix} W_s b_s \\ b_g \end{pmatrix} \quad (3)$$

where W_s is the diagonal matrix of weights and a final model is built through PCA as:

$$b = Qc \quad (4)$$

where Q is the matrix of eigenvectors of b and c is a vector having parameters controlling both shape and appearance.

3.2 Classification Using Ensemble of Classifiers

Diversity is a key factor which drives accuracy in ensemble learning i.e. individual classifiers do not always agree, but measuring diversity is not straightforward [16]. Common ensemble methods such as Boosting, Random Subspace, etc work by introducing certain perturbations in training sample, most of these methods achieve the desired result for unstable classifiers (eg. decision trees) where as only some work well for stable classifiers (eg. Support Vector Machines).

A different approach of ensuring diversity in the classifiers is by using different dissimilarities. Different dissimilarity measures reflect different features of the dataset [18]. But selection of the type of dissimilarity to be used for the present classification problem is no easy task as there does not exist any dissimilarity measure that outperforms the rest. Therefore, it makes sense to use an ensemble of classifiers trained on different dissimilarities, as they miss-classify different samples depending on different features and thus ensuring high degree of diversity.

4 Proposed Age Estimation Technique

Feature vector $X = [x_1, x_2, \dots, x_n]^T \in R^{n \times m}$ are extracted from the face images using AAM. A global classifier trained on this entire set is used to get an initial rough estimate of the age of the subject in the image. This global classifier is actually an ensemble of various diverse classifiers. These classifiers vary in their decision taking process as they have been trained on different dissimilarities and also with different weights for the 2 classes, i.e. child/teen-hood and adulthood. As the data is highly unbalanced (Table 1), so certain classifiers are trained by placing a higher penalty or higher weight for the adult class.

Classifiers such as SVMs fail to work directly from a distance matrix. To enable classifiers to work on different dissimilarity measures the approach of [18] is followed, as discussed in the next section.

4.1 Classifiers Based on Different Dissimilarities

Let $D \in R^{n \times n}$ denote a distance matrix of all the n subjects in training data. Using a metric multidimensional scaling algorithm [19] a projection of D in low dimensional Euclidean space can be found, such that the original distances are preserved. Define B as the matrix of inner products of training data X , i.e. $B = XX^T$ and $X = [x_1, x_2, \dots, x_n]^T$ is the matrix of the training data. B can also be expressed in terms of the distance matrix as:

$$B = -\frac{1}{2}JD^{(2)}J \quad (5)$$

where J is the centering matrix, i.e. $J = I - \frac{1}{n}O \in R^{n \times n}$, $D^{(2)}$ is the matrix of square of distances, I is the identity matrix and O is the $n \times n$ matrix of all ones. If B is positive semidefinite, a $k(\leq n)$ dimensional representation of X , i.e. X' can be found by eigen decomposition of B , giving X' as :

$$X' = Q\Lambda^{\frac{1}{2}} \quad (6)$$

where $Q \in R^{n \times k}$ is an orthogonal matrix of the first k eigen-vectors of B and $\Lambda^{\frac{1}{2}} \in R^{k \times k}$ is a diagonal matrix consisting of the square root of the corresponding eigenvalues. Having found a low dimensional representation of X , test samples can be added to this space via a linear projection [17]. Let $X'' \in R^{s \times k}$ be the matrix of the test samples to be determined. Further, let $D'^{(2)} \in R^{s \times n}$ be a square distance matrix, expressing square of distances between the s test samples and the n training samples that have already been projected. The matrix $B' \in R^{s \times n}$, of inner products, relating test data to training data can be found as:

$$B' = -\frac{1}{2}(D'^{(2)}J - UD^{(2)}J) \quad (7)$$

where $U = \frac{1}{n}1^T1 \in R^{s \times n}$. Since B' is related to X' and X'' as:

$$B' = X''X'^T \quad (8)$$

X'' can be found as a least mean-square error solution to Equation (8). Moreover, certain dissimilarities may generate a non positive semi-definite inner product matrix B (as in Equation 5), but as these values are very small in this case, so they can be safely neglected.

Final decision is taken by majority voting of each of the classifier. Depending on the final class label an image is either sent to a child/teen-hood aging function or the adult aging function for further accurate age estimation.

4.2 Age Estimation Functions

In each class, regression is used to interpret the aging process, as described by Lanitis *et al.* [1]. But instead of using a simple quadratic function to model the aging function, we have used a variety of regression functions to model the aging process. Regression

functions are trained on the data for that particular class and a mean of value estimated by various functions is taken to give the final estimate. Since aging process varies in child/teen-hood and adulthood, so different regression functions, such as Support Vector Regression [21], PLS Regression [22] and OLS Regression, have been used for the two different classes.

For the training stage, the child/teen-hood aging function is trained with face images of subjects with known ages, ranging from 1 to 21 years, while adult aging function is trained with images of subjects having ages ≥ 21 years.

5 Experimental Results

We have used the publicly available FG-NET [20] aging database for our experiments. FG-NET database contains scanned 1001 images of 82 subjects, varying in pose, expression and illumination. Each face image has 68 landmarked points as shown in Fig. 11. For training we have used 848 images with ages ranging from 0-69, rest of the images are used for testing. The performance is evaluated by using the standard Mean Absolute Error(*MAE*), which can be defined by:

Table 1. Experimental Results of on FG-NET Database

Age Range	1–13	13–21	21–35	35–69
Images	481	8	170	102
Training Images	623		225	
Test Images	108		45	
MAE	2.467		6.53	
Overall MAE		4.35		

$$MAE = \frac{\sum_{i=1}^N |\widehat{age}_i - age_i|}{N} \quad (9)$$

where N is the number of test images, age_i is the real age of the i^{th} subject, and \widehat{age}_i is the estimated age of the i^{th} subject. Another measure to evaluate performance is the Cumulative Score, defined as:

$$CumScore(l) = \frac{N_{e \leq l}}{N} \times 100\% \quad (10)$$

where $N_{e \leq l}$ is the number of images where the absolute age estimation error is not less than l . For our experiments the overall *MAE* is 4.35 and Cumulative Score at various error levels is given in Fig. 2. We have been able to achieve the lowest *MAE* and the highest Cumulative Score as compared to other published results on the FG-NET database.

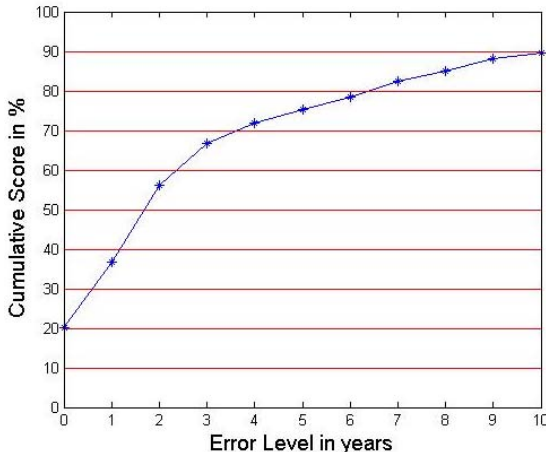


Fig. 2. Cumulative Score of our Age Estimation method at error levels from 0 to 10 years in FG-NET database

6 Conclusions and Future Work

The paper has presented a novel age estimation technique taking into account the degree of variation that occurs in the face during child/teen-hood and adult hood. Experiments have been conducted on the FG-NET database using AAMs and ensemble of diverse classifiers based on different dissimilarities resulted in the lowest possible *MAE* and the highest possible Cumulative Score to the best of our knowledge. One can also compare the performance of the proposed approach with results obtained by other published methods. To check the robustness of the proposed approach, it is required to check it on larger databases. Further, the contribution of each of the individual classifiers to the overall accuracy and how it can be improved also need to be critically studied.

Acknowledgment. This work has been supported by the Department of Information Technology, Government of India, Delhi, India. Authors are thankful to all reviewers for their valuable comments which have helped us to improve the quality of the paper.

References

1. Lanitis, A., Taylor, C.J., Cootes, T.F.: Toward automatic simulation of aging effects on face images. *IEEE Transactions on Pattern Analysis and Machine Intelligence* 24(4), 442–455 (2002)
2. Chellappa, R., Wilson, C.L., Sirohey, S.: Human and machine recognition of faces: a survey. *Proceedings of the IEEE* 83(5), 705–741 (1995)
3. Fasel, B., Luettin, J.: Automatic facial expression analysis: a survey. *Pattern Recognition* 36(1), 259–275 (2003)

4. O'toole, A.J., Deffenbacher, K.A., Valentin, D., McKee, K., Huff, D., Abdi, H.: The Perception of Face Gender: The Role of Stimulus Structure in Recognition and Classification. *Memory and Cognition* 26, 146–160 (1997)
5. Albert, M., Ricanek, K., Patterson, E.: A review of the literature on the aging adult skull and face: Implications for forensic science research and applications. *Forensic Science International* 172(1), 1–9 (2007)
6. Magnus, C., Forsberg: Facial morphology and ageing: a longitudinal cephalometric investigation of young adults. *European Journal of Orthodontics* 1(1), 15–23 (1979)
7. Luu, K., Ricanek, K., Bui, T.D., Suen, C.Y.: Age estimation using active appearance models and support vector machine regression. In: Proceedings of the 3rd IEEE International Conference on Biometrics: Theory, Applications and systems, pp. 314–318 (2010)
8. Edwards, G.J., Lanitis, A., Taylor, C.J., Cootes, T.F.: Statistical models of face images – improving specificity. *Image and Vision Computing* 16(3), 203–211 (1998)
9. Ramanathan, N., Chellappa, R.: Face Verification across Age Progression. In: Proceeding of IEEE Conference of Computer Vision and Pattern Recognition, pp. 462–469 (2005)
10. Fu, Y., Huang, T.S.: Human Age Estimation With Regression on Discriminative Aging Manifold. *IEEE Transactions on Multimedia* 10(4), 578–584 (2008)
11. Kwon, Y.H., da Vitoria Lobo, N.: Age Classification from Facial Images. *Computer Vision and Image Understanding* 74(1), 1–21 (1999)
12. Geng, X., Zhou, Z.-H., Zhang, Y., Li, G., Dai, H.: Learning from facial aging patterns for automatic age estimation. *ACM Multimedia*, 307–316 (2006)
13. Cootes, T.F., Edwards, G.J., Taylor, C.J.: Active Appearance Models. *IEEE Transactions on Pattern Analysis and Machine Intelligence* 23(6), 681–685 (2001)
14. Kang, H., Cootes, T.F., Taylor, C.J.: A Comparison of Face Verification Algorithms using Appearance Models. In: British Machine Vision Conference, vol. 2, pp. 477–486 (2002)
15. Tang, F., Deng, B.: Facial Expression Recognition using AAM and Local Facial Features. In: Proceedings of the Third International Conference on Natural Computation ICNC 2007, vol. 02, pp. 632–635 (2007)
16. Kuncheva, L.I., Whitaker, C.J.: Measures of Diversity in Classifier Ensembles and Their Relationship with the Ensemble Accuracy. *Machine Learning* 51(2), 181–207 (2003)
17. Pekalska, E., Paclík, P., Duin, R.P.W.: A Generalized Kernel Approach to Dissimilarity-based Classification. *Journal of Machine Learning Research* 2, 175–211 (2001)
18. Blanco, Á., Martín-Merino, M., De Las Rivas, J.: Ensemble of Support Vector Machines to Improve the Cancer Class Prediction Based on the Gene Expression Profiles. *Innovations in Hybrid Intelligent Systems* 44, 393–400 (2008)
19. Chen, Chun-houh, Wolfgang, Unwin, A., Cox, M.A.A., Cox, T.F.: Multidimensional Scaling Handbook of Data Visualization, pp. 315–347 (2008)
20. The FG-NET Aging Database, <http://www.fgnet.rsunit.com/>
21. Smola, A.J., Scholkopf, B.: A tutorial on support vector regression Statistics and Computing, vol. 14(3), pp. 199–222 (2004)
22. Wold, S., Eriksson, L., Kettaneh, N.: PLS in Data Mining and Data Integration. *Handbook of Partial Least Squares*, pp. 327–357 (2010)

Adaptive Variance Based Sharpness Computation for Low Contrast Images

Xin Xu^{1,2}, Yinglin Wang², Jinshan Tang¹, Xiaolong Zhang¹, and Xiaoming Liu¹

¹ School of Computer Science and Technology, Wuhan University of Science and Technology,
Wuhan 430081, China

² Department of Computer Science and Engineering, School of Electronic, Information and
Electrical Engineering, Shanghai Jiao Tong University, Shanghai 200240, China
xuxin@wust.edu.cn, dadaotang@yahoo.com,
dragon2zhang2005@yahoo.com.cn, lxmzju@gmail.com,
wang-y1@cs.sjtu.edu.cn

Abstract. Low contrast images are easily suffering from noise effect. As a result, it can witness many local false peaks in the graph of sharpness function. However, the presence of many local false peaks hinders the camera's passive auto-focus system to perform its function in locating the focused peak. This paper presents an improved variance based sharpness computation which can adapt to various degrees of noise. The proposed sharpness computation can bring in the local false peaks generated by noise influence, and therefore produce a well defined focused peak standing for the best focused image. The experimental results from several image sequences validate the effectiveness of our proposed method.

Keywords: auto-focus, low contrast, sharpness computation, noise reduction.

1 Introduction

The obtaining of high quality imaging is one of a key requirement for most image-related applications. Auto-focus (AF) provides a means of achieving this objective. The basic idea of AF is automatic adjusting on lens of camera to the right position, ensuring the image is well positioned at the focal plane [1]. Focus is normally defined in terms of sharpness; and AF is a key factor affecting the sharpness of a final captured image. Thus, the most high quality imaging is obtained in large part by how the lens is adjusted by camera's AF system to bring an image into focus where sharpness is maximized [2].

Many AF systems were developed in the past, which can be classified into two types of systems. One is active AF and the other is passive AF [3]. The active AF systems are generally costive and thus passive AF systems have attracted more attention now. A passive AF system generally includes three components: focusing region selection, sharpness computation, and peak search [3]. Focusing region selection procedure determines the region of captured image for sharpness computation. Then a sharpness function is used to this region to calculate a fitness

value. And the maximum fitness value can be obtained through a peak search step. In this paper, we just focus on the sharpness computation and thus we select the whole region of image and perform an exhaustive search.

Unfortunately, most sharpness function does not always work well for low contrast images obtained under dim lighting conditions. Low contrast images, suffering from a lack of sharpness, are easily influenced by noise. As a result, many local false peaks may be generated in the graph of sharpness function, making it difficult for the camera's passive auto-focus system to perform its function in locating the focused peak. Poor ambient lighting conditions include low levels of natural light, incandescent electric light, dimly lighting clubs/restaurants, street lighting, or even the complete absence of light. Attempting to enhance the sharpness of images, especially video images, captured under such low light conditions can be very frustrating. According to [4], passive AF extracts a measure of sharpness from the image itself, and treats a defocus image as the image generated by convolving a focused image with a low-pass filter whose bandwidth is proportional to the degree of focus. In other words, sharpness computation in passive AF assigns more weight to the high frequency content when evaluating the degree of focusing. However, in low light conditions, there are few content in the high frequency range. It is difficult to extract adequate sharpness information. The improvement of low-light AF performance is important for capturing high-quality images to meet consumers' demand in undesired lighting conditions. The goal of our work described in this paper is to overcome this weakness for most passive AF systems, and propose a robust sharpness computation which is capable of handling low contrast images in noisy environment.

2 Related Works

Sharpness function is a quantitative description of the image sharpness in mathematics, and it is a numerical measure that provides a value indicating the degree of focus for an out-of-focus image [5]. Because the sharpness is related to the contrast of an image and thus we can use contrast measure as the sharpness computation. Many contrast measures have been used for passive AF. In [3] and [4], comparison of different AF algorithms is made to explore their relative merits through examining them in a variety of scene. Results indicate 2D spatial measurement methods yield best performance in terms of accuracy and unimodality. However, they are very sensitive to noise, and not robust to different scene conditions such as low light conditions.

On the contrary, variance based methods are fast and robust. The basic idea of this method is to calculate the variance of image intensity, assuming image is best focused when the variance reaches a maximum [4]. A typical variance based method is performing the computation in discrete cosine transform (DCT) domain, where AC coefficients of image can be used to represent the variance of luminance [6]. However, low light conditions pose a major problem for traditional variance based methods of its poor discrimination power. In low light conditions, contrast measure becomes fluctuant, and non-uniformity in image intensity seems to be not distinct when the focus changes. As a result, it is quite difficult to locate the peak.

In order to make the contrast measure works well for low contrast images, Shen et al. tried to compensate and give rise to the homologous region [7]. They not only calculate AC coefficients, but also compute DC coefficients of image. And the ratio between AC coefficients and DC coefficients is defined as contrast measure. Lee et al [8] further improved the Shen's method, which can avoid the iterative moving of step motor during the contrast computation procedure. The nonlinear regression routine is used to quickly predict the location of the maximum focus value through a Gaussian profile fitting. Afterwards, Kristan et al. [9] proposed a focus measure based on the Bayes spectral entropy of the image spectrum. DCT was used to map between the spatial and spectral domains. The image was divided into non-overlapping sub-images of 8*8 pixels, where sharpness values are calculated separately. And the mean of sharpness values is taken as a measure of overall focus. However, this measure needed to establish some predefined threshold, which varied with the content of an image. In [10], ratio of the AC and DC components in DCT domain were also used as the measure of focus. Differently, they found that the lowest five AC components and a DC component coefficient contained the most energy (information) of an image as well as the detailed edge and base edge information. Thus the ratio was adjusted in their method.

However, due to the neglect of existing correlations among adjacent blocks pixels in DCT computation, it may incur an undesired effect called "blocking artifact" [11]. In addition, the DCT based methods require much computation time as a lot of processing is involved in conversion to and from the DCT coefficients. Aiming to address this problem, Lin [12] proposed to use regional monotones of focus value variation to attenuate the influence of noise generated false peaks. And the inconsistency in the motion direction of lens caused by image disturbances can be checked and corrected using these monotonous properties. However, low illumination could induce a problem of low signal-to-noise (S/N) ratio for focus value measure, which makes it difficult to obtain the monotonous properties because of the noise influence. Afterwards, Gamadia et al. [2] process the low contrast image in a different way. They attempt to reduce the effect of the additive white Gaussian noise through introducing image enhancement preprocessing steps. This method is computationally simple, and can make improvement in low light AF performance. However, the discrimination power of their proposed contrast measure is not robust. For a raw image corrupted by another kind of noise except for the additive white Gaussian noise, their method may fail to work well.

In this paper, we propose a new contrast measure which is capable of handling low contrast images in noisy environment. The proposed contrast measure can carry more information about the image discontinuities, and thus has more discrimination power. Our method was tested on a number of low contrast image sequences captured by an actual digital camera, and result validated the effectiveness of this contrast measure.

3 Proposed Contrast Measure

As stated previously, various contrast measures have been introduced and investigated in passive AF system. And the Contrast Measure based on Squared Laplacian

(CMSL) yields good performance in terms of accuracy and unimodality [3], [4]. It can be expressed as follows

$$L(x, y) = \frac{1}{J * K} \sum_{x=1}^J \sum_{y=1}^K G(x, y)^2 \quad (1)$$

where $G(x, y)$ is computed by

$$G(x, y) = \sum_{i=x-1}^{x+1} |I(x, y) - I(i, y)| + \sum_{j=y-1}^{y+1} |I(x, y) - I(x, j)| \quad (2)$$

where $I(x, y)$ is the intensity value of an image pixel at location (x, y) , the parameters J and K are the height and width of focusing region in the image over which the contrast is evaluated.

However, in low light conditions, the higher frequency content in a focused image is just a little more than that in the corresponding defocused or blurred image. A focused image obtained from low light conditions possesses a small sharpness value which may be easily influenced by noise. As a result, CMSL may generate a fluctuant curve with many local false peaks. In this case, it is difficult to distinguish a well-defined peak, and thus hinders the following peak search procedure to perform its function in locating the best focused contrast peak.

As we know, the sharper the focus peak is, the easier it is to find the best focused lens position. Thus bringing in the local false peaks can decrease the noise contribution, and help locating the best focused contrast peak. According to [4], the second-order function gives better results than higher orders, because of the increase in noise effects. And it is better suited than the first-order difference, as the width of the top of the extremum of the focus function is smaller. Thus we wonder whether an order between first and second variance can be effective. In order to cope with noise and low light conditions, we introduce a Contrast Measure Adaptive to Noise influence (CMAN). Our contrast measure is defined based on CMSL, which can be expressed as follows

$$F(x, y) = \frac{1}{J * K} \sum_{x=1}^J \sum_{y=1}^K G(x, y) (\sqrt[n]{G(x, y) + 1} - 1) \quad (3)$$

where n is computed by

$$n = \begin{cases} 1 & m \leq T1 \\ 2 & T1 < m < T2 \\ 3 & m \geq T2 \end{cases} \quad (4)$$

where the parameter m is the number of local maximums with value bigger than a predefined threshold T . When m is not more than the parameter T_1 , it means that the noise have little influence on image. And it can observe a well defined peak standing for the best focused image. CMSL can work well on this image. In this case, the parameter n is equal to 1, and (3) is equal to (1). If m is more than the parameter T_1 and less than the parameter T_2 , the noise adds a little bias to the contrast measure. At this time, the shape of the curve becomes a little fluctuant due to the noise. It becomes difficult to locate the focus peak due to the absence of a well defined peak. Decrease the order of contrast measure can help alleviating the noise effects, and bringing in the local false peaks. As the number of local maximum with big value increases to a certain extent T_2 , the shape of the curve becomes more fluctuant. And it becomes more difficult to locate the best focused image. In this case, further decrease of the order of contrast measure is necessary.

4 Experimental Results

Three different image sequences were used in the experiments to investigate the performance of CMAN. Each image sequence was composed of the same objects obtained in different lens position, from defocusing to focusing and from focusing to defocusing. The three image sequences are representative for a certain class of image types, including low contrast image with little noise influence, low contrast image with adequate noise and low contrast image corrupted by much noise. The noise is not restricted to additive white Gaussian noise. CMAN and CMSL were tested in the experiments, where T is set to half value of the focused peak in CMSL, T_1 is set to 1 indicating just one well defined peak, and T_2 is set to 9 standing for the presence of adequate noise. In order to gauge the performance of CMAN and CMSL, noise reduction preprocessing and peak search procedure were implemented in all of the tests. From the previous discussion, it can be expected that CMAN and CMSL would response differently towards these image sequences.

In the first experiment, the resulting contrast value is plotted against 70 different lens positions in a consumer level digital camera, from near to far. When the image is little influenced by noise, the contrast measurements in CMSL and CMAN are the same. Thus, CMSL and CMAN have the same contrast value in all the 70 lens positions when the image is little influenced by noise.

In the second experiment, the low contrast image with adequate noise influence acquired at 70 different lens positions from near to far is used for experiment. The results are shown in Fig. 1, where the 57th lens position is the one with the best contrast. As we can see, when noise adds a little influence on image, the curve generated by CMSL is more fluctuant than CMAN. And we can observe a local false peak with big value in the 50th lens position of the curve produced by CMSL. In this case, it is difficult to distinguish the focus peak from this local false peak. Differently, CMAN can decrease the value of local false peak and work well in this image. As illustrated in Fig. 1, although there are still a number of local false peaks, their value is relatively small and can be distinguished from the focus peak. In other words, CMAN brings in the peak of local maximum caused by the noise influence, and produces a well-defined focus peak.

In the last experiment, the low contrast image is corrupted by much noise. We also capture the image sequence at 70 different lens positions from near to far. The 68th lens position is the one with the best contrast. The results shown in Fig. 2 clearly indicate that CMAN has more robust performance than CMSL. While CMSL fail, CMAN is still able to determine correctly the focus position.

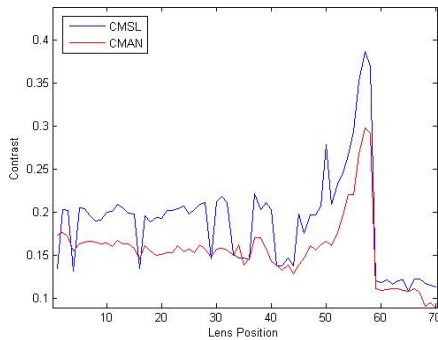


Fig. 1. Influence of adequate noise on image shape obtained by CMSL and CMAN

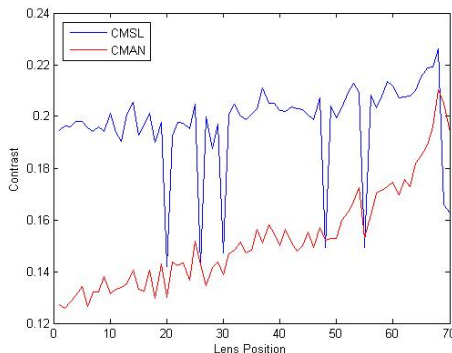


Fig. 2. Influence of much noise on image shape obtained by CMSL and CMAN

5 Conclusions

This paper has described an adaptive sharpness computation which can provide a noticeable improvement in discrimination performance under low light conditions. The experimental results from an actual digital camera deployment validate this method developed to distinguish the focus peak from local false peaks.

Acknowledgments. This work was supported in part by the Program of Wuhan Subject Chief Scientist (201150530152), the Open Foundation (2010D11) of State Key Laboratory of Bioelectronics, the Educational Commission of Hubei Province

(NO.Q20101101), the Educational Commission of Hubei Province (NO. D20091102), the project (2009CDA034) from Hubei Provincial Natural Science Foundation, the project (2008CDB345) from Hubei Provincial Natural Science Foundation, and the Project (2008TD04) from Science Foundation of Wuhan University of Science and Technology, as well as National Natural Science Foundation of China (60975031).

References

1. Li, J.: Autofocus Searching Algorithm Considering Human Visual System Limitations. *Optical Engineering* 44 art. no. 113201 (2005)
2. Gamadia, M., Kehtarnavaz, K., Roberts-Hoffman, K.: Low-light Auto-focus Enhancement for Digital and Cell-phone Camera Image Pipelines. *IEEE Transactions on Consumer Electronics* 53, 249–257 (2007)
3. Shih, L.: Autofocus Survey: A Comparison of Algorithms. In: 2007 Proc. of SPIE - The International Society for Optical Engineering, art. no. 65020B (2007)
4. Groen, F.C.A., Young, I.T., Ligthart, G.: A Comparison of Different Autofocus Algorithms. *Cytometry* 6, 81–91 (1985)
5. Kehtarnavaz, N., Oh, H.J.: Development and Real-time Implementation of a Rule-based Auto-focus Algorithm. *Real-Time Imaging* 9, 197–203 (2003)
6. Bain, J., Dublet, J.: Automatic Focus and Iris Control for Cameras. In: 1995 Proc. of IEEE Fifth International Conference on Image Processing and its Applications, pp. 232–235 (1995)
7. Shen, C.H., Chen, H.H.: Robust Focus Measure for Low-contrast Images. In: 2006 Proc. of IEEE International Conference on Consumer Electronics, art. no. 1598314, pp. 69–70 (2006)
8. Lee, M.E., Chen, C.F., Lin, T.N., Chen, C.N.: The Application of Discrete Cosine Transform (DCT) Combined with the Nonlinear Regression Routine on Optical Auto-Focusing. In: 2009 Proc. of IEEE International Conference on Consumer Electronics, pp. 1–2 (2009)
9. Kristan, M., Pers, J., Perse, M., Kovacic, S.: A Bayes-spectral-entropy-based Measure of Camera Focus Using a Discrete Cosine Transform. *Pattern Recognition Letters* 27, 1431–1439 (2006)
10. Lee, S.Y., Yoo, J.T., Kumar, Y., Kim, S.W.: Reduced Energy-ratio Measure for Robust Autofocusing in Digital Camera. *IEEE Signal Processing Letters* 16, 133–136 (2009)
11. Luo, Y., Ward, R.K.: Removing the Blocking Artifacts of Block-based DCT Compressed Images. *IEEE Transactions on Image Processing* 12, 838–842 (2003)
12. Lin, K.C.: Microscopic Autofocusing Using Regional Monotonous Variations of Multiple Focal Value Measures. *Journal of Electronic Imaging* 19 art. no. 023012 (2010)

Non-sampling Contourlet Based “Consistency Verification” Method of Image Fusion

Shi-Bin Xuan, Gao-Li Sang, Bo Zhao, and Zeng-Guo Zheng

School of Mathematics and Computer Science,
Guangxi University for nationalities, nanning, China
sanggao1i@126.com

Abstract. The image fusion is one of the important research areas of data fusion. The wavelet-based fusion is the most popular image fusion methods at present. To remove "block" appeared in the results of wavelet-based fusion, the paper proposes a window-based "consistency verification" which is used to deal with the fusion result image obtained through Non-sampling contourlet transform (NSCT). Within the window scope, the algorithm takes the current coefficient as the centre point of the window, and statistics the coefficients derived from each source image. Then the weights are assigned according to each source image occupy the proportional in the window. At last the value of the window center can be automatically determined by re-weighting. Experimental results show proposed algorithm is feasible and effective.

Keywords: Contourlet transform, Image fusion, Coefficients of low-frequency, Coefficient of high-frequency, Consistency verification.

1 Introduction

Image fusion technology has been earliest proposed in the late 1970s of 20th century. By processing two or many source images coming from the same object, image fusion extracts the information of each channel, and outputs the more accurate, comprehensive and reliable uniformed image in the output side finally. Therefore, the fused image can obtain the quite rich message, and is more suitable for human visual observation than source images. It has been widely applied in military region, such as remote sensing satellite images, visible images, infrared images, medical images, multi-sensor image fusion and so on. It has been becoming the important research field of the computer vision, including the target identification, robot as well as military already [1].

Although there has been a considerable number of image fusion articles, the most of their research are multi-scale decomposition on variety of fusion rules, the work on the fused images "consistency" is still relatively little. Considering the pixels in image have stronger relativity, we introduce the concept of region in image fusion in this paper. More recently, Yong Yang [2] proposed the method of synthesizing the region and the weighting in medical image fusion. Although this method has improved in the consistency of the fusion results, the way of selecting weight is too simple.

The main reasons causing the “inconsistency” of image can be listed as follows: First, It cannot obtain quite comprehensive details in each direction to decompose image using wavelet multi-scale tool. Second, many methods only considered the fusion rule for low frequency and high frequency coefficients, and neglected the relations between high frequency and low frequency coefficients. Third, even if some algorithms consider “consistency” of the image [2], because the idea of the algorithm is not mature, it is hard to get satisfactory results.

The remainder of the paper is organized as follows. The Non-Sampling contourlet-based image fusion technique is reviewed in Section 2. The specific description of the proposed method is described in Section 3. Experimental results and analysis are presented in Section 4 and the conclusions are given in Section 5.

2 NSCT Based Image Fusion

The Contourlet transform is a method of "real" two-dimensional image representation. It is a sparse representation method of two-dimensional piecewise smooth signal. Wavelet transformation approximates the curve with the points finally, but Contourlet transformation approximates the curve with line. Therefore Contourlet transformation needs fewer coefficients to express the smooth curve compared to wavelet transformation [3]. The NSCT has the characteristic of multi-resolution, multi-criteria and multi-directions decompose comparing to the classical wavelet transformation.

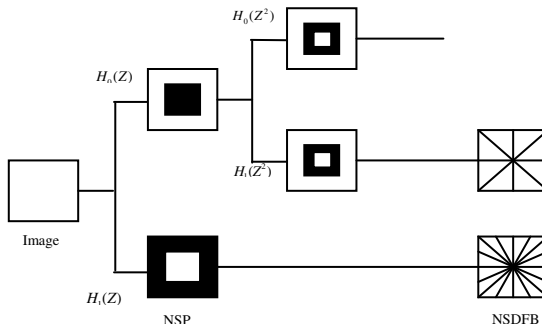


Fig. 1. Multi-criterion decomposition of NSCT

3 NSCT Based the New Method of "Consistency Verification"

First, the source image is decomposed by NSCT. Then the coefficients of both low-frequency and high-frequency are fused using different fusion rules. Finally, in order to reduce the contrast between low-frequency and the high-frequency coefficients, and to strengthen the relation between low-frequency and the high-frequency coefficients, the “consistency verification” is used to process all the coefficients.

3.1 Low-Frequency Band Fusion

In this paper, to simplify the description of fusion rule, we assumed that there are only two source images, X and Y , and a fused image Z . The method can be easily extended to more than two images. Generally, the multi-scale decomposition (MSD) of an image I can be denoted as D_I . Hence we will encounter D_X , D_Y and D_Z . Let $p = (m, n, k, l)$ indicate the index corresponding to a particular MSD coefficient. Where m and n indicate the spatial position in a given frequency band, k is the decomposition level, and l is the frequency band of the MSD. Therefore, $D_I(p)$ denotes the MSD value of the corresponding coefficient at the position (m, n) with decomposition level k and frequency band l .

Based on the preceding analysis, for the low-frequency band, selecting the highest local visibility can be used as a fusion rule. This approach is derived from literature [4], and is motivated by the fact that the HVS is sensitive to the contrast. Hence, this method can be likely to provide better details to the human.

The algorithm first calculates the window-based visibility of all coefficients in the low-frequency band. The visibility of wavelet coefficients is defined as [5]:

$$VI(p) = \frac{1}{w^2} \sum_{(i, j) \in B_w} \Lambda(\bar{D}(p)) \frac{|D(m+i, n+j, k, l) - \bar{D}(p)|}{\bar{D}(p)} \quad (1)$$

$$\bar{D}(p) = \frac{1}{w^2} \sum_{(i, j) \in B_w} D(m+i, n+j, k, l) \quad (2)$$

$$\Lambda(\bar{D}(p)) = \left(\frac{1}{\bar{D}(p)} \right)^\alpha \quad (3)$$

Where B_w is a $w \times w$ block, $\Lambda(\bar{D}(p))$ is the weighting factor, $VI(p)$ denotes the visibility of the block, α is a visual constant obtained by perceptual experiment, and its range is from 0.6 to 0.7. After calculating the visibility of all the coefficients in the low-frequency band, the corresponding coefficients of higher visibility are then chosen into the fused image according to formula (4).

$$D_Z(p) = \begin{cases} D_X(p) & , VI_X(p) \geq VI_Y(p) \\ D_Y(p) & , VI_X(p) < VI_Y(p) \end{cases} \quad (4)$$

3.2 High-Frequency Bands Fusion

It is generally believed that the details of an image are mainly included in the high-frequency bands of the image. We compute the variance in a local neighborhood to

select the high-frequency coefficients according to above analysis. The procedure can be formulated as follows [2, 8]:

$$\sigma_I(p) = \frac{1}{S \times T} \sum_{s=-S/2}^{S/2} \sum_{t=-T/2}^{T/2} (D_I(m+s, n+t, k, l) - MEAN_I(p))^2 \quad (5)$$

$$MEAN_I(p) = \frac{1}{S \times T} \sum_{s=-S/2}^{S/2} \sum_{t=-T/2}^{T/2} D_I(m+s, n+t, k, l) \quad (6)$$

where $S \times T$ is the neighboring size, and $MEAN_I(p)$, $\sigma_I(p)$ denote the mean value and variance value of the coefficients centered at (m, n) in the window of $S \times T$ respectively. Then, the fusion scheme for the high-frequency bands can be illustrated as follows:

$$D_Z(p) = \begin{cases} D_X(p), & \sigma_X(p) \geq \sigma_Y(p) \\ D_Y(p), & \sigma_Y(p) \geq \sigma_X(p) \end{cases} \quad (7)$$

3.3 Improved Consistency Verification

In the above analysis, all the coefficients of both low-frequency and high-frequency bands are selected by the maximum selection schemes. But as we know the maximum selection technique will bring unnecessary noise into images. Moreover, since we cope with the low-frequency and high-frequency coefficients separately, this method cannot guarantee the consistency of the fused image. Therefore, a consistency verification scheme is must performed to ensure the integrity of the regional characteristics of the fused image.

This paper has improved the way of “consistency verification” by means of the method of selecting weights based on window [2]. Considering the various information of the source images, the algorithm automatically determine the weights according to the proportion of each source image in the window. For example, within the 3×3 window, If the number of coefficients from image X is 4, and the number of coefficients from image Y is 5, Then we set the corresponding weight value of the image X to $4 / (3 \times 3)$, while set the corresponding weight value of the image Y to $5 / (3 \times 3)$. Obviously, the method delicate balances the two source images, and avoids losing information.

The calculation process can be detailed as bellows:

$$D'_X(p) = \max_{w \in W} (|D_X(p, w)|), \quad (8)$$

$$D'_Y(p) = \max_{w \in W} (|D_Y(p, w)|), \quad (9)$$

$$q_X(p) = \begin{cases} 1, & D'_X(p) > D'_Y(p), \\ 0, & \text{otherwise,} \end{cases} \quad (10)$$

$$q_Y(p) = \begin{cases} 1, & D_Y(p) > D_X(p), \\ 0, & \text{otherwise,} \end{cases} \quad (11)$$

$$q_X^*(p) = 1/(w \times w) \times \sum q_X(p) \quad (12)$$

$$q_Y^*(p) = 1/(w \times w) \times \sum q_Y(p) \quad (13)$$

$$D_Z(p) = q_X^*(p)D_X(p) + q_Y^*(p)D_Y(p), \quad (14)$$

Equations (12) and (13) are the concrete expression of weight selection in this paper, $w \times w$ is the window size, $\sum q_X(p)$ and $\sum q_Y(p)$ expresses the number of coefficients coming from the image X and Y in the window separately. $q_X^*(p)$ and $q_Y^*(p)$ are the weighting factors of image X and image Y respectively. $D_Z(p)$ is obtained by automatic weighting for coefficient of both image X and image Y.

Then the fused image can be obtained by an inverse NSCT transform for all the coefficients. Therefore, the algorithm can be simply expressed as follows:

Step 1. Register the multi-mode source images.

Step 2. Decompose the images to 3-4 levels by NSCT.

Step 3. The coefficients of the low-frequency are processed by (1) to (4), and the coefficients of the high-frequency are selected by (5) to (7).

Step 4. The consistency verification are used to deal with the coefficients of both the low-frequency and high-frequency using formulae from (8) to (14).

Step 5. The inverse NSCT transform is used to the combined coefficients obtained from Step 4.

4 Experimental Results and Analysis

In this section, in order to show the superiority of the proposed method, the proposed method is compared with those of pixel averaging method, and the classic DWT method [2]. In all test cases we assume the source images to be in perfect registration. In order to achieve the ideal fusion effect, and to sacrifice the smallest storage space and the computation load, this paper selects three layer decompositions. A 3×3 window is considered for calculating the variance in this paper, which has been proved to be more effective by many researchers [5, 6]. After a great deal of experiments, the default value of parameter α can be chosen to be 0.7.

4.1 Multi-focus Image Fusion Experiments Results and Analysis

There are two multi-focus images which have been registered perfectly as shown in Figures 2(a) and 2(b). The images are the size of 255 x 255. Figure 2(a) is the image blurred on the left, while Figure 2(b) is the image blurred on the right. Figures 2(c)-2(e) are the fused results obtained by fusing Figure 2(a) and Figure 2(b) with the pixel averaging method, the classic DWT method [2], and the proposed method, respectively.

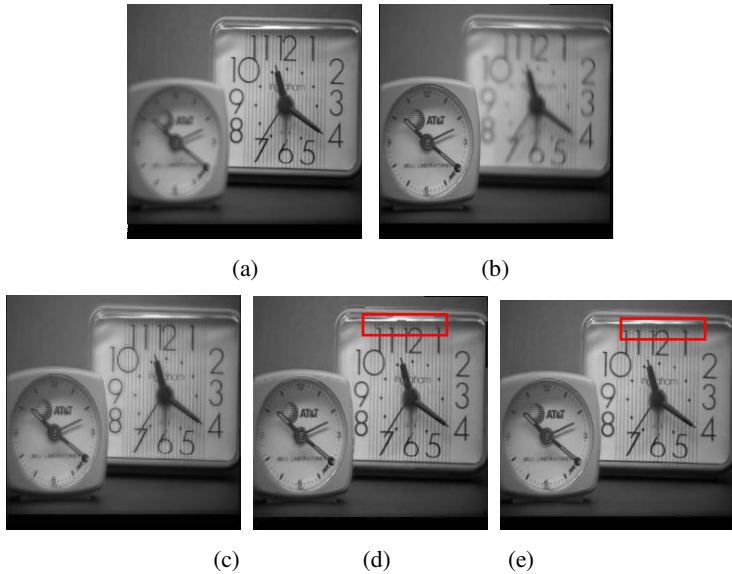


Fig. 2. Fused results of the Multi-focus images with different methods

Judged by the visual effect, the clarity of Figure 2 (c) is insufficient obviously, and quite dim. Although the clarity of the Figure 2 (d) is significant improvement comparing with the Figure 2 (c), there are evident “block” phenomenon in figure marks. Figure 2 (e) is obtained by the proposed the method in this paper. It has obviously improved the “block” phenomenon and clarity of fusion image comparing to Figure 2 (c) and Figure 2 (d).

Table 1. Quantitative evaluation results of the three different fusion methods

Fusion methods	Information entropy	Standard deviation	Mutual information	Cross entropy
Pixel averaging	5.8245	15.3265	1.0656	2.8216
Classic DWT method	5.8723	15.3342	1.0743	2.6338
Proposed method	5.8827	15.3359	1.0795	2.5900

However, it is insufficient only to depend on the visual observation, because it does not have the strict mathematical model, and the visual observation is mainly depending on the vision which may be doped some uncertain factors. Considering the lack of subjective evaluation methods, we need further quantitative evaluation of fused image. It will be more objective and more effective than visual observation. We take entropy, standard deviation, cross entropy and mutual information as objective evaluation criteria [7]. Fusion performance evaluation criteria: For each group of fusion experiments, if the fused image's entropy, the standard deviation and the mutual information value is

relatively big, while the cross entropy is relatively small, then the performance of corresponding fusion method is relatively better. The effects of different fused methods are shown in table 1. Comparing with other two methods, we can see the proposed method has higher information entropy, standard deviation and average gradient, but cross entropy obviously is lower than other two methods actually.

4.2 The Infrared Image Fusion Experiments and Analysis

Figure 3 lists two medicine images, Figure 3 (a) is the nuclear MR image, Figure 3 (b) is the X-ray CT image. The size of the images is for 305 x 305. Figures 3(c)–3(e) are the fused results obtained by fusing Figure 3(a) and Figure 3(b) with the pixel averaging method, the classic DWT method [2], and the proposed method respectively.

Observing images obtained by three methods carefully, Figure 3 (c) is quite gloomy, fuzzy. Although the clarity of the Figure 3 (d) get significant improvement comparing to the Figure 3 (c), but there are “block” phenomenon in the image edge part (e.g. chart mark). Just you see that the same edges in figure 3 (e) have no “block” existed, moreover the clarity is also quite satisfying.

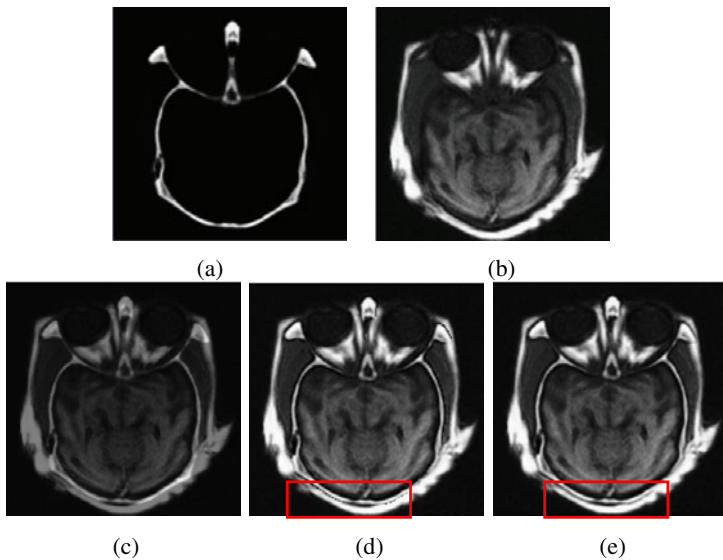


Fig. 3. Fused results of the CT and MR images with different methods

We use the same objective evaluation criteria to test the fused images obtained by the three methods. The result of experience is shown in Table 2. From the table 2, in evaluation parameters: information entropy, standard deviation and mutual information, the proposed method can get higher value than the pixel average obviously. For example, the information entropy of pixel average method is 4.7831, while the corresponding values of other two methods are 5.2998 5.2983 respectively. Therefore, based on these examples, we can conclude that all the effect of quantitative evaluation is consistent with the visual observation basically. Therefore, the performance of proposed method is better than the existing other two fusion methods.

Table 2. Quantitative evaluation results of the three different fusion methods

Fusion methods	Information entropy	Standard deviation	Mutual information	Cross entropy
Pixel averaging	4.7831	16.1732	0.1462	3.0368
Classic DWT method	5.2983	18.2563	0.2905	1.9537
Proposed method	5.2998	18.2934	0.2951	1.9530

5 Conclusions

Based on previous image fusion often result in the “inconsistent” phenomenon, this paper proposes the NSCT based “consistency verification” method of image fusion. According to the different multi-scale decomposition frequency domain, the different fusion rules are adopted for high-frequency coefficients and low-frequency coefficients respectively. For the low-frequency band, we take the highest local visibility as the fusion ruler. And for the high-frequency bands, we use a scheme which selects the highest variance in a neighborhood. Finally, all the combined coefficients are dealt by a window based consistency verification. The “block” problem is effectively reduced which often exists in the fused image. Experimental results further indicates that the proposed fused image can reflect the more clear details, and more abundant information, and more small distortion. “Block” phenomenon also get significant improvement.

References

1. Chai, Q., Yang, W.: Improved Fusion Algorithm for Infrared and Visual Images. *Infrared Technology* 30(2) (2008)
2. Yang, Y.: Medical Image Fusion via an Effective Wavelet-Based Approach. *EURASIP Journal on Advances in Signal Processing* (2010)
3. He, G.D., Liang, D.: Fusion of Infrared and Visible Light Images Based on Nonsubsampled Contourlet Transform. *Microel Ectrronics & Computer* 26(2) (2009)
4. Huang, J.W., Yun, Q.S., Dai, X.H.: A Segmentation-based Image Coding Algorithm Using the Features of Human Vision System. *Journal of Image and Graphics* 4(5), 400–404 (1999)
5. Liu, G.X., Yang, W.H.: A Wavelet-decomposition-based Image Fusion Scheme and Its Performance Evaluation. *Acta Automatica Sinica* 28(6), 927–934 (2002)
6. Li, M., Zhang, X.Y., Mao, J.: Neighboring Region Variance Weighted Mean Image Fusion Based on Wavelet Transform. *Foreign Electronic Measurement Technology* 27(1), 5–6 (2008)
7. Li, X., Zhan, Y.: A New EPMA Image Fusion Algorithm based on Contourlet-lifting Wavelet Transform and Regional Variance. *Jounal of Software* 5(11), 1200–1207 (2010)

Understanding the Meaning of Shape Description for Interactive Object Recognition

Satoshi Mori, Yoshinori Kobayashi, and Yoshinori Kuno

Department of Information and Computer Sciences, Saitama University,
Saitama city, Saitama 338-8570, Japan
{tree3miki,yosinori,kuno}@cv.ics.saitama-u.ac.jp

Abstract. Service robots need to be able to recognize objects located in complex environments. Although there has been recent progress in this area, it remains difficult for autonomous vision systems to recognize objects in natural conditions. Thus we propose an interactive object recognition system, which asks the user to verbally provide information about the objects that it cannot recognize. However, humans may use various expressions to describe objects. Meanwhile, the same verbal expression may indicate different meanings depending on the situation. Thus we have examined human descriptions of object shapes through experiments using human participants. This paper presents the findings from the experiments useful in designing interactive object recognition systems.

Keywords: Interactive Object Recognition, Service Robot, Ontology.

1 Introduction

Service robots have attracted the attention of researchers for their potential use with handicapped and elderly persons. In order to make service robots user-friendly, we are currently developing a robot that can recognize user's speech and locate and bring objects that have been requested. Such robots need to have a vision system that can recognize the objects requested. Object recognition has been an active area of research in computer vision. Recently, much progress has been made due to data representations using invariant semi-local features such as SIFT [1] and classification procedures developed in the field of statistical machine learning [2]. Yet, it remains difficult for vision systems to recognize objects in various natural conditions. In addressing this problem, we are currently working on an interactive object recognition system [3][4][5]. Here the robot asks the user to verbally provide information about the object it cannot detect such as color and spatial relationship to other objects.

Dating back to the work by Winograd [6], there has been a great deal of research inquiring into the ways robot systems understand the scene or task through interaction with the user [7][8][9]. These studies, however, have dealt with objects that can be described by simple word combinations such as 'blue box' or 'red ball'. In our application domain, objects are often more complex. For example, we may want the robot to bring a bag of potato chips that has various colors. In order to develop an

effective interactive object recognition system, we need to know how humans describe such complex objects. We may not seem to use complex expressions even for such complex objects. Thus we performed observation experiments on human-human interactions [4]. We examined how humans get other humans to understand and retrieve an object they want when the others are not supplied with the name of the object. We found two main ways. One is to describe attributes of the object, such as color and shape. The other is to mention the spatial relationships of the object in relation to other objects. We obtained 227 utterances to describe the attributes of objects. We found that color is most often mentioned followed by shape. In [4], we further examined how humans describe object colors to find that they usually use one major color to describe multi-colored objects. In order to be user-friendly, the robotic system should be able to understand such human expressions and locate objects without fail. For this, we proposed a vision system that identifies multicolored objects even when the user mentions one color. In [5], we addressed the spatial relation issue. Since shape descriptions are used second most often after color, we consider shape in this paper. We examine how humans describe object shapes and propose an interactive object recognition system based on the examination results.

2 Experiments on Shape Descriptions Used by Humans

We performed experiments to examine what expressions humans use to describe object shapes and what shapes those expressions actually indicate.

2.1 Expressions Used for Describing Shapes

In order to carry out our observation experiments of human-human interaction, we assembled 26 objects that we may want a service robot to bring, such as food and stationery as shown in Fig. 1. We examined how humans describe object shapes when they were only allowed to mention expressions about shapes.

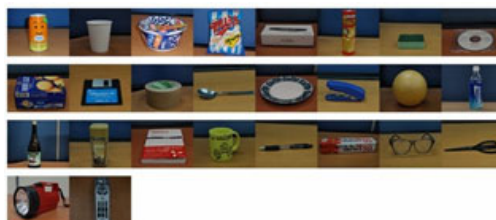


Fig. 1. Objects used in the experiment

Fig. 2 is a representation of the experimental setting. Five pairs of participants took part in the experiment. They were Japanese students at Saitama University. Japanese was used for communication. We placed several objects (among those shown in Fig. 1) on top of a table on participant B's side. We also placed one of the same objects on participant A's side. We asked participant A to describe the object shape to

participant B without naming the object and mentioning other attributes, and asked participant B to choose the correct object. Participant A continued with the description until participant B selected the correct object. We obtained 143 utterances that described object shape.

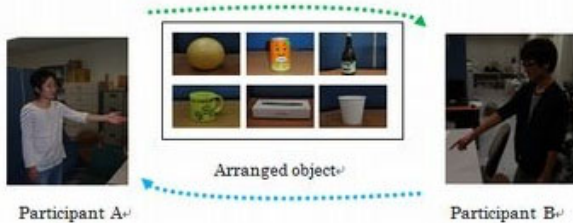


Fig. 2. Experimental setting

Fig. 3 shows the classification results of collected expressions. The upper bar graph indicates the classification results by what part of objects are mentioned. ‘Whole shape’ indicates expressions about the whole object shape, such as a sphere for a ball. ‘Front, upper, or side surface shape’ includes expressions that describe the shape viewed from the front, upper, or side. ‘Component shape’ indicates expressions that describe a shape of a part of the object. ‘Surface pattern shape’ means expressions about shapes of patterns on the object surface. The whole shape expressions are further classified as shown in the lower bar graph in Fig. 3. In addition to geometrical terms such as sphere, cylinder, and cube, there are various expressions such as mentioning object names that have such shapes, such as V-shaped and doughnut-like shape.

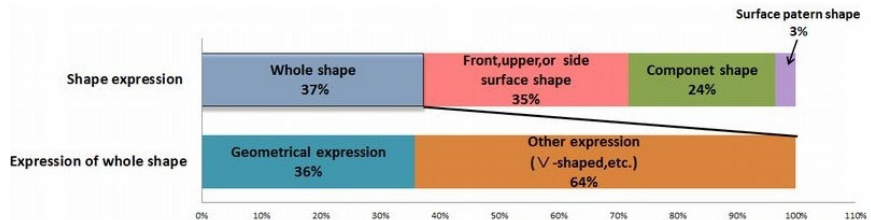


Fig. 3. Classification of shape expressions

2.2 Experiment on Round Objects

We noticed that some expressions are used for describing variety of object shapes through the experiment described above. This certainly depends on the language. However, we think that the same can be true in various languages although each usage of expression may vary depending on the language. In this paper, we do not discuss such language issues, concentrating on the Japanese language case.

A typical expression example that we noticed is ‘Marui’ in Japanese. ‘Maru’ is the Japanese for circle and ‘Marui’ is its adjective form. ‘Marui’ is also used for describing a sphere. ‘Marui’ may be used for 2-D circle, 3-D sphere and sometimes various curved objects in Japanese. ‘Shikakui’ the Japanese for quadrangle in a narrow sense is another example. It may be used for mentioning a rectangular parallelepiped (box) as well. In order to examine more details about the expression ‘Marui’, we performed an experiment. Hereafter, we use ‘round’ as the corresponding English for ‘Marui’ (‘round’ in English may not be used in the same way).

We performed an experiment to know the degree of roundness of various possible round objects. We adopted Thurstone’s method of paired comparisons [10] to make the scale of roundness. We generated 10 objects by computer graphics as shown in Fig. 4. We prepared 45 cards, each showing one of the possible 45 pairs from these 10 objects. We used 57 participants. All of them were Japanese students at Saitama University and Japanese was their native language. We showed them these 45 cards and asked to indicate which they think more round for each card.

Fig. 5 shows the roundness scale computed from the result. In Japanese, ‘Marui’ is used to indicate both 2-D circle and 3-D sphere. However, 3-D objects are felt rounder than 2-D objects.

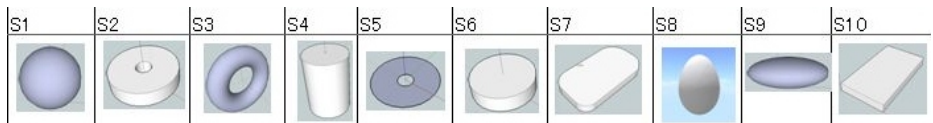


Fig. 4. Objects used for making a roundness scale

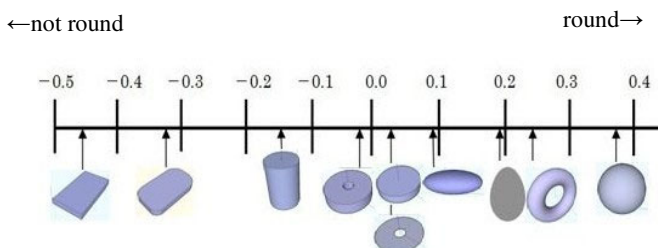


Fig. 5. Roundness scale

3 Shape-Based Interactive System Design

3.1 Design Implications Obtained through the Experiments

From the experimental results in the previous section, we have found that we need to consider the followings in designing an interactive object recognition system.

- (1) 2-D shape expressions may indicate the shapes of objects seen from a certain direction. The vision system needs to take such cases into account when the user mentions 2-D shapes.
- (2) Names of objects with a distinctive shape are used to describe shapes. The system needs to detect such shape objects.
- (3) Shape expressions may not necessarily indicate the whole object shapes. They may show the shapes of components of the object or those of patterns on the object surface. The system considers this possibility.
- (4) There are such shape expressions that may indicate various shapes. Also the meaning may depend on the situation such as other objects existing in the scene.

We should consider these factors to construct the object shape ontology, and develop image processing methods to detect objects with the desired shapes. We are now working on these. The next section describes our preliminary study toward the shape-based interactive object recognition.

3.2 Preliminary System Implementation

We are planning to integrate the shape-based interaction system that we are currently working on with our previous color and spatial-relation based interaction system [11]. The integrated system will first try to recognize ordered objects by the autonomous recognition method. If it cannot recognize them, it turns into the interactive mode. The system tries to recognize the object through interactions about color, shape, and spatial relationship.

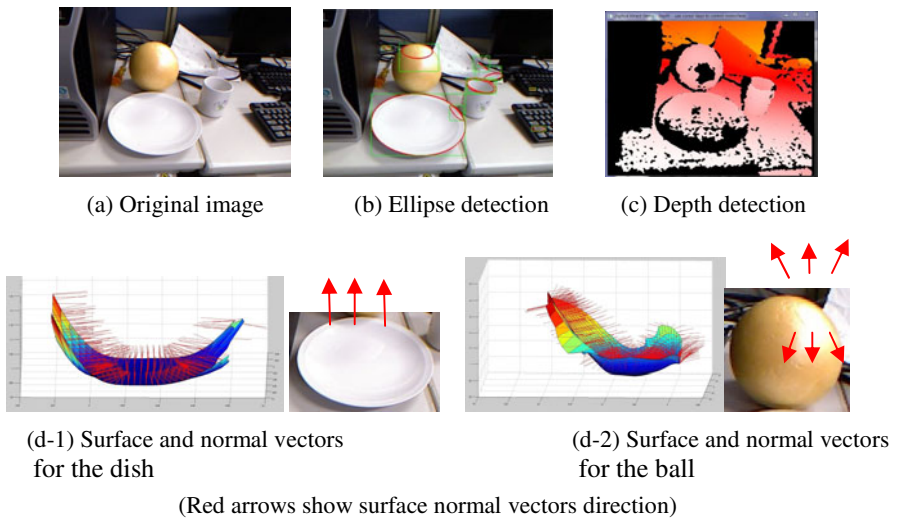


Fig. 6. Scene with multiple different round objects

We need to detect 2-D shapes such as patterns on surfaces as well as 3-D shapes. Thus we have adopted Kinect [12] that provides both color and depth images.

In 2.1, we have found that shapes related to circle and quadrangle are most frequently mentioned. Thus we first developed image processing modules to detect ellipses and quadrangles.

Then we developed a 3D shape detection module. We divide each object surface into small patches and compute the surface normal orientation for each patch to obtain the orientation histogram of the surface. We roughly classify surfaces into flat, cylindrical and spherical based on their orientation histograms.

We can deal with the situation examined in 2.2 by using these modules. Fig. 6 shows a scene with a dish (close to a 2-D circle), a cup (cylinder), and a ball (3-D sphere). All three objects might be mentioned as round objects. However, if a person asks to bring the round object in this scene, the first candidate should be the sphere according to the findings in 2.2. The 3-D shape detection module can recognize these objects as a circle, a cylinder, and a sphere, and pick the sphere as the first candidate.

4 Conclusion

It remains difficult for autonomous vision systems to recognize objects in natural conditions although there has been recent progress. Thus we have proposed an interactive object recognition system, which asks the user to verbally provide information about the objects that it cannot recognize. In this paper, we have considered interactions about shape. Through observation experiments of human-human interaction, we have found what parts of objects are described how. We have also found that there are cases that the same expression is used to describe different shapes depending on the situation. As we have revealed in this paper, humans use various expressions to describe object shapes as well as use a small number of expressions for various object shapes. This makes it difficult to understand the meaning of shape expressions. We need to construct the object shape ontology by considering these issues, and to develop image processing modules to detect various shapes.

Acknowledgment. This work was supported in part by the Japan Society for the Promotion of Science under the Grant-in-Aid for Scientific Research (KAKENHI 19300055, 23300065).

References

1. Lowe, D.G.: Distinctive Image Features from Scale-invariant Keypoints. *International Journal on Computer Vision* 20(2), 91–110 (2004)
2. Ponce, J., Hebert, M., Schmid, C., Zisserman, A. (eds.): *Toward Category-Level Object Recognition*. LNCS, vol. 4170. Springer, Heidelberg (2006)
3. Kurnia, R., Hossain, M.A., Nakamura, A., Kuno, Y.: Generation of Efficient and User-Friendly Queries for Helper Robots to Detect Target Objects. *Advanced Robotics* 20(5), 499–517 (2006)
4. Mansur, A., Sakata, K., Kobayashi, Y., Kuno, Y.: Human Robot Interaction through Simple Expressions for Object Recognition. In: Proc. 17th IEEE RO-MAN, pp. 647–652 (2008)

5. Cao, L., Kobayashi, Y., Kuno, Y.: Spatial Relation Model for Object Recognition in Human-robot Interaction. In: Huang, D.-S., Jo, K.-H., Lee, H.-H., Kang, H.-J., Bevilacqua, V. (eds.) ICIC 2009. LNCS, vol. 5754, pp. 574–584. Springer, Heidelberg (2009)
6. Winograd, T.: Understanding Natural Language. Academic Press, New York (1972)
7. Kawaji, T., Okada, K., Inaba, M., Inoue, H.: Human Robot Interaction through Integrating Visual Auditory Information with Relaxation Method. In: IEEE Int. Conf. Multisensor Fusion on Integration for Intelligent Systems, pp. 323–328 (2003)
8. McGuire, P., Fritsch, J., Steil, J.J., Roothling, F., Fink, G.A., Wachsmuth, S., Sagerer, G., Ritter, H.: Multi-modal Human Machine Communication for Instruction Robot Grasping Tasks. In: Proc. IROS 2002, pp. 1082–1089 (2002)
9. Takizawa, M., Makihara, Y., Shimada, N., Miura, J., Shirai, Y.: A Service Robot with Interactive Vision- objects Recognition Using Dialog with User. In: Proc. First Int. Workshop Language Understanding and Agents for Real World Interaction (2003)
10. Thurstone, L.L.: The Method of Paired Comparisons for Social Values. Journal of Abnormal and Social Psychology 21, 384–400 (1927)
11. Kuno, Y., Sakata, K., Kobayashi, Y.: Object recognition in Service Robots: Conducting Verbal Interaction on Color and Spatial Relationship. In: Proc. IEEE 12th ICCV Workshops (Human-Computer Interaction), pp. 2025–2031 (2009)
12. Kinect, <http://www.xbox.com/en-US/kinect>

Gray Scale Potential Theory of Sparse Image^{*}

Wen-Sheng Tang¹, Shao-Hua Jiang^{1, **}, and Shu-Lin Wang²

¹ Instructional Division for Computer Technology, Hunan Normal University

² School of Computer and Communication, Hunan University

(410006, Changsha, China)

tangws@hunnu.edu.cn, itwxf@msn.com

Abstract. According to the relative position among the pixels of sparse image, we proposed the Gray Scale Potential of image. By taking the example of the binary images, this paper highlighted the definition of gray scale potential and the extraction of gray scale potential. Then we pointed out that the gray scale potential was an intrinsic feature of image. As for binary image, it reflects the relative distances of pixels to a baseline or to a reference point, and if the image is gray image, it reflects not only the distances but also the gray level feature. The gray scale potential has obvious advantage in representing the sparse image, because it can reduce the computational work and storage. Even two-dimensional image can be simplified to one-dimensional curve. Finally, some experimental data were given to illustrate the concept of gray scale potential. It shows that the gray scale potential of image is a steady feature and can be used in object recognition.

Keywords: Gray Scale Potential, Sparse Image, Image Feature, Feature Extraction.

1 Introduction

In the field of computer vision and image processing, image features [1] are very important concepts. Image feature is the properties of image which can be used to identify the image itself. Such as texture [2], edge [3], shape[4-5], histogram [6-7] and so on. Usually they are classified as statistical features and visual features. Statistical characteristics are man-made features, they can be used only after transformation, such as histogram, spectrum [8] and moments [9], etc.; the visual features were the natural features which can be feel, such as the brightness of object region, texture and edge contour, etc. [1]. These features can be used for image registration, fusion, object recognition and object tracking [10] and so on. The relative position of the pixels in image is an important feature. It has a clearly significance, and easy to be processed [11] when it is used in registration, fusion and object recognition.

* A Project Supported by Scientific Research Fund of Hunan Provincial Education Department (No. 10C0945), Hunan Provincial Natural Science Foundation of China (Grant NO.07JJ3129), Program for Excellent Talents in Hunan Normal University(No ET61008), The National Science Foundation of China (Grant NO. 60973153).

** Corresponding author.

Based on the relative position of pixels in sparse image, this paper proposed the theory of gray scale potential feature. And by the example of the binary images, it introduced the definition of gray scale potential feature, and illustrated how to extract the gray scale potential feature. Finally, some experimental data were given to demonstrate that the gray scale potential of image was a steady feature and can be used in object recognition.

2 Definition of Gray Scale Potential

In the field of image processing, there are some concepts which have some relation to gray scale potential:

Gray histogram[6-7], histogram is a statistical feature of image. For a gray image, the histogram reflects the distribution of different gray level in statistics. The statistical characteristics of gray histogram can be very well applied on image processing. For instance, if the histogram shows that the image was too bright or too dark, then we can enhance the image by histogram equalization.

Projection [12], projection is the shadow of object in the projective space which was projected by a pointlike or parallel light source. Projection can show the characteristics of 3-d objects in the form of two-dimension characteristics. Now, projection has been widely used in the 2-d image and 3-d visualization, especially in the field of medical imaging, it has made a considerable progress, such as X-ray imaging, CT imaging, etc.

A. Definition of Gray Scale Potential

Sparse images are often used in the field of image processing, such as the contour, skeleton, etc. Sparse image is the image which has some large regions with a fixed gray or color. And those regions can be viewed as background of image. In some cases, they may be ignored and does not affect the result of image processing. For instance, the black or white background of a contour image can be ignored, the image processing results are not affected.

Usually, a sparse image can be represented by a sparse matrix, which was filled with a large number of zeros as background. These large amounts of useless information will greatly influence the processing speed and the memory utilization.

The projections of image *f* on the 2-d space are the shadows on *x*-axis and *y*-axis of all nonzero pixels, namely, the background pixels of sparse image. When the projective values are the sums of multiple original pixels, it is called the cumulative projection. Even though the projection and the cumulative projection can reduce dimension, the information distortion is very serious. When $N > 2$, they both are impossible to restore the image itself.

We put the concept of *Gray Scale Potential* by using the electric potential in physics for reference. It generates a sequence of weight values according to the distance of nonzero pixels to the reference point. For instance, start from the centroid, we generate a sequence of weight values along the direction of radius, e.g. w_1, w_2, \dots, w_n . Then the sequence of weight values (w_1, w_2, \dots, w_n) constitutes a vector $W = (w_1, w_2, \dots, w_n)$, which is named as weight vector. We denote the pixels matrix of image by

$$f = \begin{pmatrix} a_{11} & a_{12} & \cdots & a_{1n} \\ a_{21} & a_{22} & \cdots & a_{2n} \\ \vdots & \vdots & \ddots & \vdots \\ a_{m1} & a_{m2} & \cdots & a_{mn} \end{pmatrix} \quad (1)$$

Take the point a_{rc} as the reference point, and (r, c) are the coordinates. Then the distance between a random point a_{ij} to the reference point is $D = \sqrt{(i - r)^2 + (j - c)^2}$. And now take another point (r, w) , let $w > c$, namely (r, c) and (r, w) are the same horizontal line, then the random point $a_{i,j}$ of image, (r, c) and (r, w) can constitute a triangle ($i \neq r$) or a straight line ($i = r$), where (r, c) and (r, w) may be the pixels of image or not, strictly speaking, it is a reference point only. For the convenient of expression, we denote them by a_{rc} and a_{rw} , such a representation will never affect the result.

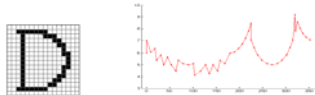
When $i \neq r$, by these three points we can get three lines

$$\begin{cases} D((i, j), (r, c)) = \sqrt{(i - r)^2 + (j - c)^2} \\ D((i, j), (r, w)) = \sqrt{(i - r)^2 + (j - 2)^2} \\ D((r, c), (r, w)) = \sqrt{(r - r)^2 + (c - w)^2} = (w - c) \end{cases}. \quad (2)$$

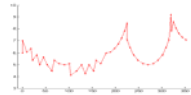
Then it can be calculated that

$$\theta = \arccos\left(\frac{D((i, j), (r, c))^2 + D((r, c), (r, w))^2 - D((i, j), (r, w))^2}{2D((i, j), (r, c))D((r, c), (r, w))}\right). \quad (3)$$

If $i = r$ and $j > 0$, then $\theta = 0$, and if $j < 0$, then $\theta = 180^\circ$. Or it can denote by radian, as shown in Figure 1.



(a) Only one pixel wide of the letter D



(b) gray scale potential of (a)

Fig. 1. single pixel wide letter D and gray scale potential

So then, each nonzero pixels of image, namely not background, can be denoted by the pairs of numbers (r, θ) , then sort them by θ gradually increasing. Now, we got some pairs of points in rapid sequence called as gray scale potential. If we connect these pairs of points in sequence, we got a polygonal line graph called as gray scale potential graph. As for the more common case which is not a single ring, we can denote it by a sequence of polygonal lines according certain strategy. This notation which denoted the nonzero points of a sparse image by a sequence of coordinates as (r, θ) is called gray scale potential of the image.

Take Figure 1(a) as an example, suppose the coordinate of the reference point is $(8, 9)$, and take the point $(14, 9)$ as the second reference point, and then we can link the second reference point $(14, 9)$ to the reference point $(8, 9)$ and get a line, which is viewed as the ray with an angle of $\theta = 0$. After this, we can get a sequence of coordinates as $P = \{(6, 0), (7, 0), (6, 10), (6, 18), (5, 22), (6, 31), (5, 37), (6, 45), (5, 53), (5, 63), (5, 68), (5, 79), (5, 90), (5, 101), (4, 104), (5, 117), (5, 127), (4, 135), (5, 143), (5, 153), (5, 158), (5, 169), (6, 180), (6, 190), (6, 198), (7, 207), (7, 214), (8,$

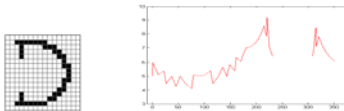
$(220), (9, 225), (7, 225), (6, 231), (6, 239), (5, 248), (5, 259), (5, 270), (5, 281), (5, 292), (6, 301), (6, 309), (7, 315), (9, 319), (8, 320), (9, 325), (8, 330), (8, 337), (7, 344), (7, 352)\}$, and the figure 1(b) is the polygonal lines graph of gray scale potential which is called gray scale potential graph.

B. The determination of reference points

It can be inferred from the definition of gray scale potential that the location of reference point has an effect on the sequence of coordinates, namely, the gray scale potential. If we link the sequence of coordinates to produce gray scale potential graph, it will be influenced by the relocation of reference point. In order to make the gray scale potential graph remained relatively stable, it is the key that to select a relatively stable reference points. In view of the centroid of sparse image is a stable feature point, we take the centroid as the reference point. If we generate the gray scale potential sequence with the reference point mentioned above, then this sequence will has a reasonable numerical size, and be insensitive to error. So we can take the centroid as the reference point. After this, we need to determine another reference point for calibrate the direction of $\theta = 0$. We usually give an appropriate increment to the coordinate x_c of centroid. Namely, $(x_c + \delta, y_c)$ is the auxiliary reference point to calibrate the direction of $\theta = 0$. Where the value of δ should be determine elaborately, because of a too big or too small δ will cause a big error. According to our experiments, we can add the width to the height of image, and the δ usually can be a quarter of the sum. By this way, the θ will be more stable and small error.

If there is a gap in the graphic, as shown in figure 2 (a), then the gray scale potential graph will appear a gap also, just as shown in figure 2 (b). Of course, we can connect it directly and get a continuous graph, but the original gray scale potential graph is divided into two sections. It will cause inconvenience to the image registration and object recognition. In this case, we can connect the head and the tail of the polygonal lines graph, and then give a shift to the graph, so we can get a continuous polygonal lines graph which is similar to the original polygonal lines graph.

In the above discussion, we can, of course, take the other point as the reference point. Here we only provide a relatively reasonable method to determinate the reference point.



(a) Letter D with a gap (b) gray scale potential of the semi-closed image (a)

Fig. 2. Letter D with a gap and the gray scale potential graph of it

The stability of gray scale potential.

A proper conclusion can be draw from the definition of gray scale potential that, if we rotate the image around the axis which is parallel to the line of sight, and finally, the gray scale potential graph will has a shift θ_o along the x -axis. And the scaling of image will cause a shift along the y axis.

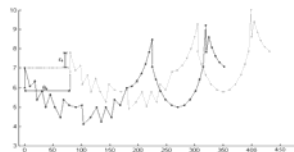


Fig. 3. A comparison of gray scale potential graph between original image and the image after a rotation and a scaling. Where the dark one is original image, and the light one is the image after a rotation θ_0 and a scaling of $(r + r_0)/r$ times.

Obviously, it can be drawn from the definition of gray scale potential and the experiments that the gray scale potential graph is an invariant to shift, rotation and scaling.

3 Experimental and Results

In order to inspect the effect while the gray scale potential was used to identify the image, our experiments take Arabic numbers which font name are Microsoft Sans Serif, and extract the gray scale potential respectively by 32×32 , and generate the gray scale potential graph. Figure 4 list the gray scale potential graph of letters 1, 2, 3 and 4.

As shown in Figure 4, the gray scale potential graph of each letter has a completely different characteristic curve. These letters can be distinguished very well by using the gray scale potential. It is suitable for feature extraction and object recognition.

In addition, the gray scale potential of the curlicue font letter D which is shown in Figure 1 was calculated, and the gray scale potential graph was shown in Figure 5.

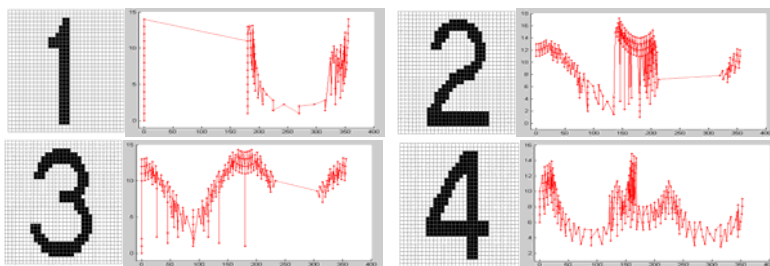
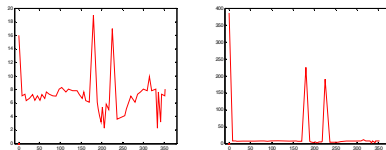


Fig. 4. the lattice diagram and gray scale potential graph of letter A, B, C, D, E and F

It can be seen from Figure 5 that the details will be more clearly if the weight value sequence was generated according the distance, and if the weight value sequence was generated by n -th power of 2, then the details of image will be poor, and noise immunity significantly be worse. Therefore, the weight value sequence needs an aborative selection. A better approach is extended the range of θ and spread out the graph as spiral. Here no longer expatiatory.

Compared with the cumulative projection, we can find the latter has some disadvantages: First, the original image can not resume from the cumulative projection. Second, there are two projection images which are projection on x -axis and projection on y -axis, if there is a slight rotation, there is a great change to the cumulative projection, so it is no an invariant to rotation. Finally, the cumulative projection does not save the relative position between the pixels, lack a global view of image.



(a) generate weight value by distance (b) generate weight value by n -th power of 2

Fig. 5. two kind of gray scale potential of curlicue fonts letter D which is show in Figure 1

4 Conclusion

The gray scale potential is an intrinsic characteristic of image, as for binary image, the gray scale potential reflects the relative distances of pixels to a baseline or to a reference point, and if the image is gray image, it reflects not only the distances but also the gray level feature. Since the gray scale potential processed only a small amount of pixels which are the non background of sparse images. It can reduce the computational work and storage, and easy to use and has an intuitional meaning. Even two-dimensional image can be simplified to one-dimensional curve. So we can process the image with the traditional signal processing techniques and methods, and expand the processing technology of 2d graphics with the existing knowledge and experience.

The gray scale potential well reserve the relative position between pixels of the sparse image, although only small amounts of data take part in the calculation, we can obtain the whole result. Even we can resume the whole image by using the gray scale potential, Theoretical analysis and experimental data has strong evidence for our conclusion.

Although the above discussion are for the sparse image, but as for the non-sparse image, we can extract their contour or skeleton in some cases, then use the relevant research results to process it. And how to expand the application field of gray scale potential, enrich and perfect the gray scale potential theory is the next work.

Acknowledgment. The authors would like to thank the anonymous reviewers for their helpful and constructive comments.

References

1. Liu, H., Zhang, S.F., Zhang, Y.X.: Infrared Imaging Fuze. *Aero Weaponry* 36, 12–15 (2005)
2. Wen, S., Yang, J.P., Liu, J., et al.: A New Texture Analysis Approach Based on Statistics of Texture Primitive's Gray Pattern. *Acta Electronica Sinica* 28(4), 73–75 (2000)
3. Ge, J.G., Zhu, Z.Q., He, D.F., Chen, L.G.: A Vision-based Algorithm for Seam Detection in A PAW Process for Large-diameter Stainless Steel Pipes. *The International Journal of Advanced Manufacturing Technology*, 9–10, 1006–1011 (2005)
4. Duan, Y., Hua, J., Qin, H.: Interactive Shape Modeling Using Lagrangian Surface Flow. *The Visual Computer* 21(5), 279–288 (2005)
5. Goldenshluger, V.S.: On the Shape-From-moments Problem and Recovering Edges from Noisy Radon Data. *Probability Theory and Related Fields* 128(1), 123–140 (2004)
6. Belozerskii, L.A., Oreshkina, L.V.: Estimation of the Informative Content of Histograms of Satellite Images inThe Recognition of Changes in Local Objects. *Pattern Recognition and Image Analysis* 20(1), 65–72 (2010)
7. Viitaniemi, V., Laaksonen, J.: Representing Images with χ^2 Distance Based Histograms of SIFT Descriptors. In: Alippi, C., Polycarpou, M., Panayiotou, C., Ellinas, G. (eds.) ICANN 2009. LNCS, vol. 5769, pp. 694–703. Springer, Heidelberg (2009)
8. Li, P.C., Cheng, J., Yuan, R.F., Zhao, W.V.: Robust 3D Marker Localization Using Multi-spectrum Sequences. In: Bebis, G., Boyle, R., Parvin, B., Koracin, D., Kuno, Y., Wang, J., Pajarola, R., Lindstrom, P., Hinkenjann, A., Encarnação, M.L., Silva, C.T., Coming, D. (eds.) ISVC 2009. LNCS, vol. 5876, pp. 529–537. Springer, Heidelberg (2009)
9. Cheong, M., Loke, K.-S.: Textile Recognition Using Tchebichef Moments of Co-occurrence Matrices. In: Huang, D.-S., Wunsch II, D.C., Levine, D.S., Jo, K.-H. (eds.) ICIC 2008. LNCS, vol. 5226, pp. 1017–1024. Springer, Heidelberg (2008)
10. Xu, P.Q., Xu, G.X., Tang, X.H., Yao, S.: A Visual Seam Tracking System for Robotic Arc Welding. *The International Journal of Advanced Manufacturing Technology* 37(1-2), 70–75 (2008)
11. Wu, X.J., Yang, J.Y., Wang, S.T., Liu, T.M.: A Study on a New Method of Feature Extraction. *Journal of Image and Graphics* 9(2), 129–133 (2004)
12. Askar, Chen, Y., Jia, Z.H.: A Probabilistic Weighted Summation Projection Technique for Multidimensional Signal Detection. *Acta Electronica Sinica* 33(7), 1331–1333 (2005)
13. Olshausen, B.A., Field, D.J.: Emergence of Simple-Cell Receptive Field Properties by Learning A Sparse Code for Natural Images. *Nature* 381, 607–609 (1996)

Recognition of Leaf Image Based on Outline and Vein Fractal Dimension Feature

Ji-Xiang Du^{1,2}, Chuan-Min Zhai¹, and Qing-Ping Wang¹

¹ Department of Computer Science and Technology, Huaqiao University, Xiamen 361021

² Institute of Intelligent Machines, Chinese Academy of Sciences, Hefei, Anhui 230031

{jxd77, cmzhai}@gmail.com, wqp86@126.com

Abstract. This article discussed a method of describing the characteristics of plant leaves based on the outline fractal dimension and venation fractal dimension. The method first separated leaf edge and vein .According to multiple threshold edge detection, we get multiple vein. Then, the two-dimensional fractal dimension of the leaf edge image and multiple vein images will be calculated, which as the basis of plant leaves classification and recognition.

Keywords: plant leaves classification, fractal dimension, venation.

1 Introduction

Plant taxonomy is the oldest plant discipline and most comprehensive a foreign branch discipline. Plant classification is not only the basis of botany, also be a plant geography, plant ecology, plant genetics, plant biochemistry, plant physiology, Chinese herbal medicine study and even the entire life science foundation, which plays an important role in the development and utilization of plant resources. Plant taxonomy based on plant leaves image is a very important research topic.

Plant identification usually involves the analysis of many parts of the specimen. such as edge, vein, the number of split tablets, leaves deep cleft, skeleton etc. The characteristics of the leaf margin generally reflect the leaf edge information, with or without teeth, the number of teeth, etc. It is one of the main shape characteristics of a plant that the context of distribution of leaves. Compared with outline, though the context of distribution of leaves is very complicated, contain more information. The main vein and secondary veins are often associated with the distribution of plant structure is similar to. Therefore, we can carry on more details through the analysis of the vein.

Fractal theory as a new cross-sectional discipline is non-linear cutting edge and important branch of science, as well as the rise in recent years, a shape data description method. And because the fractal dimension can effectively measure the characteristics of complexity object has penetrated into the biological, chemical, the information such as the image and graphic each branch, which become one of the most popular data processing tools on image analysis and processing and related field. We explore and study the fractal of the leaf edge ant the vein, which will be finally applied in the field of plant leaf classification.

2 Fractal Dimension

Fractal geometry was born and developed in the development of modern mathematics. French scientist B. Mandelbrot [1] put forward the concept of fractal in 1975. And he proposed defining fractal as the whole and some symmetry set in a certain meaning, have a certain meaning since similar to assemble. Our usually said dimension is all to space. In Euclidean geometry, the dimension is a natural number, i.e., a point possesses a dimension 0, a straight line has a dimension 1, a plane has a dimension 2, and a solid, therefore, possesses a dimension 3. This kind of dimension accorded with the dimension of the topological definition proposed by Jules Henri Poincaré in 1912, and the dimension got according to this definition very rationally was always nonnegative integers. However, lots of phenomenon of nature which many people are familiar and very unpredictable filled with, such as the coastline of the complicated form, the cloud, the rolling hills, beautiful snow ice, thunderous lightning form, the outer profile of the forest, tree crown structure, the distribution of blood vessel in the human body, etc. These geometric figures involved are unable to describe using such 1, 2, 3 integer value.

2.1 The Box Dimension

Fractal dimension as an important characteristic quantity is a mathematical measure to describe the complexity of fractal sets, which have been widespread attention in theoretical research and practical applications. Fractal geometry involves various approaches to define fractional dimension, the most common of which is Hausdorff's dimension, also known as the similarity dimension [2]. Hausdorff's study provided the basis for important fractal concepts. But Hausdorff's dimension is inconvenient in real calculation, often adopt the box dimension [3] in practical application. This algorithm was adopted extensively for which is easy to achieve through the program, and the method is most extensive to employ in each field so far.

We fill the entire area of an image F with boxes of size δ . Changing the size of δ means that the number of boxes $N(\delta, F)$ also changes, in other words, the smaller the size of δ , the greater the number of boxes. The box-counting method defines the fractal dimension of an object by the expression

$$D_F = \lim_{\delta \rightarrow 0} \left(\frac{\ln(N(\delta, F))}{\ln(1/\delta)} \right) \quad (1)$$

According to the formula (1), when δ_k tends to 0, then $\ln N_{\delta_k} / \ln(1/\delta_k)$ tends to 0, we can get the fractal dimension D. Narrow δ_k gradually, and fit data some

$(-\ln \delta_k, \ln N_{\delta_k})$ in $-\ln \delta_k, \ln N_{\delta_k}$ pairs of logarithm system of coordinates. Then, in this system of coordinates, the slop of the curve is estimation value of F .

Regard an image of size $w \times h$ as a matrix of size $w \times h$, each element in matrix is correspondent to a pixel, its value is equivalent to the color of pixels of the image. As to binary image, the element value is 0 or 1 respectively in corresponding matrix. According to the dispersed characteristic of such pixels, we are very apt to determine whether the area is covered. If the matrix that the box encloses is a zero matrix, indicate that has not covered the Region of Interest of the image. Therefore, we traverse the matrix to calculate the number of nonzero matrix. The fractal dimension can be obtained according to the formula (1)[4].

3 Extraction of Leaf Outline and Venation

Before the fractal dimension feature of leaf outline and venation segmentation is extracted, we need to separate leave outline and venation at first. Then we calculate respectively the fractal dimension of the leave outline and venation, and regard as the characteristic parameter of plant leaves.

Extraction of leaf outline is the most basic content in the computer vision. In fact the edge extraction process can be attributed to the classification or segmentation of the edge point and non-edge points, so we can extract the outline based on threshold value. The image used in the experiment are single leaf images, there are obvious differences in leaves and the background image. The distribution about gray level histogram of these images is a bimodal, can get binary image based on overall threshold value. Here we use the iterative threshold selection segmentation method [5] to compute the threshold. The leaf outline by the following figure:



Fig. 1. Extraction of leaf outline

3.1 Extraction of Leaf Venation

The leaf venation system segmentation was a complex task, because of the low contrast and changeable venation. There is actually few research about how to extract venation at present, the traditional one is the method based on threshold value or edge detection. The method based on the threshold value distinguishes the pixel set according to the distinction of gray level, which is very suitable for the image that there are obvious differences in leaves and the background image. A method of extracting venation information based on ANN (Artificial Nerve Network) was proposed by Fu Hong [6], etc, who proposed adopting a lot of characteristics as the parameter to distinguish the venation from the background, for the single feature as the parameter is difficult to extract venation information.

Taking into account that there are the larger number of experimental samples in the experiment, and the the artificial neural network method needs training, which is relatively slow to extract the venation. Therefore, in this article, edge detection will be used to extract venation. We will set multiple threshold values and combine multiple characteristic at the same time. Then we will get multiple venation images with corresponding multiple threshold values based on edge detection according to each threshold value established. These venation images are regarded as the sub characteristic under the single blade, which are regarded as the following basis for classification. Have the venation image under a lot of threshold values of blade in Fig. 2 as follows:

threshold value original image	1 ^φ	10 ^φ	20 ^φ	30 ^φ	40 ^φ	50 ^φ	60 ^φ
							

Fig. 2. The venation images under a lot of threshold value

4 The Experiment Verifies and Analysis Result

4.1 Plant Samples

The database used in the text was set up by laboratory ourselves. We has chosen 30 kinds of plant leaves among them as the experimental data, each kind of plant blade includes 30 samples at least. The total sample was 2422. These blades have single

backgrounds, no occlusion, which form is relatively intact, which were suitable for shape analysis. As following picture 4:

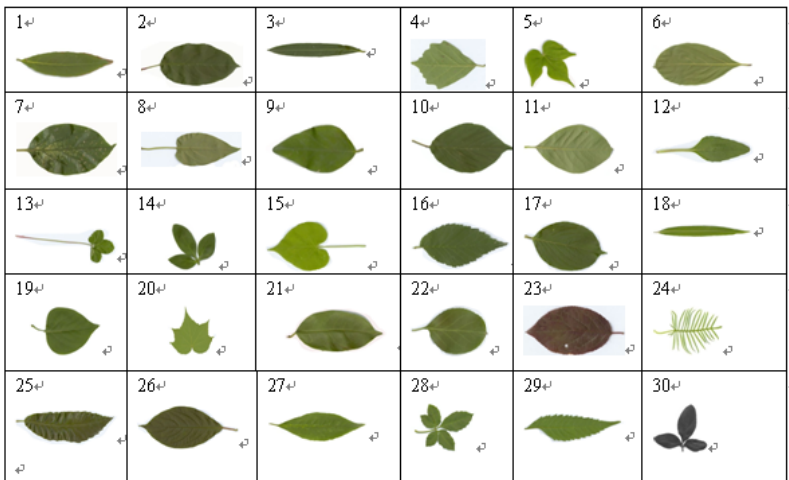


Fig. 3. Plant samples

4.2 Classification

According to calculating the box dimension method above, we have extracted the box-dimension of leave outline and the venation under different threshold value to each blade through the experiment.

In order to verify the validity of classification method, we will divide the train samples and the test samples into 7 to 3. Thirty percent is randomly selected as the test samples and the rest as the training samples.

We will get in front of the leaf margin and the veins of leaf fractal image as a feature vector, this feature vector as the basis for classification of plant leaves. In this study, the relatively simple K-nearest neighbor classifier was used to identify, which is known for simple classification does not require learning .

To improve the recognition rate, our traditional method of seven Hu [7] moment invariants combined with other literature to compare the proposed method, classifying the results as follows:

Table 1. Comparison of classification

Method of feature extraction	K nearest average recognition rate
Seven Hu moment invariants[7]	67.731%
Six outline and venation fractal dimension features	74.332%
Eight area geometric features of leaves[8]	73.168%
7 Hu moments +6 fractal dimensions	84.19%

5 Conclusions

This article discussed a method of describing the characteristics of plant leaves based on the outline fractal dimension and venation fractal dimension. We have verified that the method was valid through the experiment. Although they did not identify 100% of the clusters, the method has already classified and recognized most samples correctly, and the fractal dimension method is rotation-invariant.

Acknowledgments. This work was supported by the grants of the National Science Foundation of China (Nos. 60805021, 60905023, 60975005, 60873012 & 61005010), the Program for New Century Excellent Talents in University (No.NCET-10-0117), the Program for Excellent Youth Talents in University of Fujian Province (No.JA10006), the Fundamental Research Funds for the Central Universities of Huaqiao University (No.JB-SJ1003), the Scientific Research Foundation of Huaqiao University (No.09HZR15), the grant of China Postdoctoral Science Foundation (No.20100480708), the grant of the Key Scientific Research Foundation of Education Department of Anhui Province (No.KJ2010A289), the grant of Scientific Research Foundation for Talents of Hefei University (No.11RC05).

References

1. Mandelbrot, B.B.: *Fractals: Form, Chance, and Dimension*. W.H. Freeman, San Francisco (1977)
2. Schroeder, M.R.: *Fractals, Chaos, Power Laws: Minutes from An Infinite Paradise*. Freeman W.H., New York (1991)
3. Voss, R.F.: Fractals in nature: from characterization to simulation. In: Peitgen, H.-O., Saupe, D. (eds.) *The Science of Fractal Images*, pp. 21–70. Springer, New York (1988)
4. Dong, R.P., Xie, H.P.: Computation Method of Fractal Dimension for 2-D Digital Image. China University of Mining & Technology (2004)
5. Ridler, T.W., Calvard, S.: Picture Threshold Using An Iterative Selection Method. *IEEE Transaction on System, Man and Cybernetics* 8(8), 630–632 (1978)
6. Fu, H., Chi, Z.R.: Extraction of Leaf Vein FeaturesBased on Artificial Neural Network. *Chinese Bulletin of Botany* 21(4), 429–436 (2004)
7. Chen, C.-C.: Improved Moment Invariants for Shape Discrimination. *Pattern Recognition* 26(5), 683–686 (1993)
8. Xiao, F., Wang, Huang, D.-S.: Feature Extraction and Recognition for Leaf Images. *Computer Engineering and Applications* (2006)

Weighted Multi Feature Based Image Retrieval with Orthogonal Polynomials Model and Genetic Algorithm

Krishnamoorthi Ramasamy and Sathiya Devi Shanmugam

Vision Lab, Department of Computer Science and Engineering, Anna University of Technology, Thiruchirappalli, Tamilnadu, India
rkrish26@hotmail.com, sathyadevi_s@yahoo.com

Abstract. This paper proposes a new image retrieval method with weighted multi feature in multi resolution enhanced orthogonal polynomials model and genetic algorithm. In the proposed method, initially the orthogonal polynomials model coefficients are computed and reordered into multiresolution subband like structure. Then the statistical and invariant texture and shape features such as mean, standard deviation and moments are directly extracted from the subband coefficients. The extracted texture and shape features are integrated into linear multi feature set and the significance of each feature in the multi feature set is determined by assigning appropriate weight. This paper also proposes a method to compute the optimized weight for each feature in the integrated linear multi feature set using genetic algorithm. Then the obtained optimized weight is multiplied with the corresponding features in the multi feature set and the weighted Manhattan distance metric is used for retrieving similar images. The efficiency of the proposed method is experimented on the standard subset of COREL database images and yields promising results.

Keywords: Orthogonal Polynomials, Shape, Texture, Genetic Algorithm.

1 Introduction

Advances in data storage and image acquisition technologies have allowed for creating large multimedia data sets. In order to deal with this huge volume of data, it is necessary to develop appropriate information systems or tools, which can support different services such as searching, retrieving, browsing and indexing. One such information system that provides the above-mentioned services is called Content Based Image Retrieval (CBIR) system. Basically, CBIR systems try to retrieve images similar to a user defined specification or pattern based on low level content properties such as shape, texture and color. Though some of the image retrieval applications are implemented based on single feature, but the single feature is found to be insufficient for natural, web based image retrieval applications as it affects the retrieval performance. Hence recently general-purpose CBIR systems concentrate on multiple features along with some domain specific features for improving the performance of image retrieval. The combination of structure, color, shape and texture called mutifeatures for image retrieval is presented in [1-2]. Wavelet transform based multi feature extraction for image retrieval is reported in [3-4]. Since the physical meaning, importance and value ranges of each feature are different in the

linear combination of multi feature set, the similarity score computation with single distance metric becomes a series problem and degrades the retrieval accuracy. This problem can be solved using two methods viz., (i) relevance feedback and (ii) appropriate weight generation. Relevance feedback is computationally high demanding and difficult to incorporate human into the loop. The latter method can be viewed as an optimization problem and a suitable optimization technique has to be incorporated to generate the weight in an adaptive manner for effective discrimination and retrieval with less computational cost. Hence this paper proposes a method for optimized weight generation using genetic algorithm for multi feature representation with multi resolution enhanced orthogonal polynomials model for efficient image retrieval. This paper is organized as follows. The multi feature extraction from orthogonal polynomials enhanced multiresolution subband is presented in section 2. The genetic algorithm based optimized weight generation process is presented in section 3. The performance metric and experiments and results are discussed in section 4. Conclusion is drawn in section 5.

2 Proposed Feature Vector Extraction

In this section, texture and shape feature extraction processes for the image under analysis with orthogonal polynomials model coefficients are presented. The orthogonal polynomials model based transformation and reordering of the model coefficients into multiresolution subband like structure is presented in [5].

2.1 Texture Feature Extraction

The texture feature extraction process from the orthogonal polynomials enhanced multiresolution reordered subbands is presented in this sub section. The statistical property of the texture is characterized by the well known second order measures. In the orthogonal polynomials model, it is observed that when the block of an image is rotated the coefficient's magnitude remain unaltered but their position and the sign vary. At the same time the absolute difference between the corresponding coefficients of the original and the rotated block in the zig - zag sequence is zero. Hence the feature extraction considers the absolute value of the subband coefficients for extracting rotation invariant texture feature. Since most of the signal energy is contained in the low frequency coefficients of the reordered logarithmically spaced subbands, the texture features are extracted from them. In the proposed work, the image is reordered into four multi resolution subbands and the statistical texture features viz mean (μ_k), standard deviation (σ_k) and energy (E_k) are extracted from them. The obtained feature vector F_s of dimension 12 (i.e 4 subbands ($4 \times 3 = 12$)) as

$$F_s = (E_0, \mu_0, \sigma_0, E_1, \mu_1, \sigma_1, \dots, E_{3 \log_2 N+1}, \mu_{3 \log_2 N+1}, \sigma_{3 \log_2 N+1}) \quad (1)$$

2.2 Shape Feature Extraction

The shape features are extracted based on salient points. The salient points are extracted from edges and are used for extracting important shape feature for rough shape modeling. The shape feature extraction consists of two stages. (i) Salient point extraction with gradient and (ii) Moment feature computation.

(i) *Salient Point Extraction with Gradient*: The salient points are extracted in two steps: (i) Non-maximum suppression and (ii) Adaptive threshold. Conventionally, the non maximum suppression is performed in high computational cost. In order to avoid this, this paper proposes a simple method for non maximum suppression performed either horizontal (x) or vertical (y) direction depending on the magnitude of the gradient points. The coefficients of S_2 and S_3 subband posses the gradient information in horizontal (x) and vertical (y) directions and are used in non maximum suppression process. If the gradient magnitude of S_2 subband is larger and not greater than its neighbors on both the sides of x direction, then the coefficients of S_2 and S_3 are suppressed. Similar comparisons and suppressions are performed in the y direction if the coefficients of S_3 has larger magnitude. After performing the non maximum suppression on the coefficients of S_2 and S_3 subbands, the gradient magnitude G_{ij} is computed and is defined as:

$$G_{ij} = \sum_{i=0}^X \sum_{j=0}^Y (|\beta_{ij}^{S_2}| + |\beta_{ij}^{S_3}|) \quad (2)$$

where X and Y are the size of the subbands and $\beta_{ij}^{S_2}, \beta_{ij}^{S_3}$ are the coefficients of S_2 and S_3 subbands respectively. The adaptive threshold T , which is a sum of the mean of pixel values and the gradient magnitude is used to extract the salient points and is defined as:

$$T = \frac{1}{MN} \left(\sum_{i=0}^M \sum_{j=0}^N \beta_{ij}^{S_1} \right) + \frac{1}{XY} \left(\sum_{i=0}^X \sum_{j=0}^Y G_{ij} \right) \quad (3)$$

where M and N are the row and column values of the S_1 subband. In the proposed method, the salient points s_i are extracted from the gradient magnitude G_{ij} based on the adaptive threshold T . Thus the adaptive threshold is effectively applied to the gradient magnitude which removes the majority of non edge responses and the salient points (s_1, s_2, \dots, s_n) are extracted. These salient points form the salient map for extracting the shape features.

(ii) *Moment Feature Computation*: The image shape features are directly extracted from the salient map to characterize the shape information with Hu moment [6] which is invariant to scaling, rotation and translation. From the salient points, the seven invariant Hu's moments are computed resulting in the feature vector FV of dimension seven. The extracted feature vector FV and texture feature vector F_s both requires normalization so as to avoid domination of features having high magnitude over the others. Hence this paper uses the min-max normalization and the new maximum and minimum value of the features, which are 1 and 0 respectively in this proposed work.

2.3 Proposed GA Based Weight Generation

In this section, GA based feature weight generation process using texture and shape is presented. In the proposed weight generation method, initially the database (DB) images are subjected to two portions: (i) Training and (ii) Testing. In the training portion, training pair (TP) is generated as: A *training Pair* (TP) is the pair which consists of query image I_Q and the user defined best matched image I_M and is denoted as:

$$TP = (I_Q, I_M) \quad (4)$$

where $I_Q, I_M \in DB$. During experimentation, m training pairs are considered and each of this training pair the appropriate weight is generated iteratively (generation) using

integrated weighted dissimilarity function Dt , uniform order based crossover and order based mutation with genetic algorithm. The Dt is defined below: *The Integrated Weighted Dissimilarity Function $Dt(I_1, I_2)$* between two images I_1 and I_2 is defined as

$$Dt(I_1, I_2) = \frac{\sum_{i=1}^n diff(FV_{I_1}, FV_{I_2})}{\sum_{i=1}^n w_i} \quad (5)$$

where $diff(FV_{I_1}, FV_{I_2})$ is the Manhattan distance between the features of the query image I_1 and the target image I_2 and w_i is the weight associated with the features and n is the number of features. For each iteration or generation, the uniform order based crossover, order based mutation and roulette wheel selection are used. At the end of the final iteration, the chromosome that gives optimal weight in which the dissimilarity value Dt is minimum, is considered as the optimal weight. By utilizing this weight the similarity is computed with the query image and the images in the testing database including the user defined best matched image in the training pair TP based on weighted Manhattan distance. Then the obtained distances are sorted in ascending order and the rank of the best user defined image is identified.

The ranking score is computed as per *score function $S(r)$* , which is defined as: The *ranking score function $S(r)$* for the given training pair $TP = (I_Q, I_M)$ is defined as:

$$S(r) = \begin{cases} (k + 1 - r)/k & \text{if } r \leq k \\ 0 & \text{otherwise} \end{cases} \quad (6)$$

where r is the ranking of the target and k is the lowest ranking that has a score. The same process is repeated for m training pair and total count $TC(w)$ is computed as defined below: *Total Count*: The total count $TC(w)$ is the number of correct hits given by an integrated weighted dissimilarity function Dt with the set of weights w for searching in DB against training pair and is given below.

$$TC(w) = \sum_{i=1}^m S(r_i) \quad (7)$$

where S is the ranking score function, m is the number of training pairs, r_i is the ranking for the target i using Dt and w is the set of weight in Dt . The optimal weight for each feature is obtained in such a way that, in which training pair, the set of weight will give the maximum $TC(W)$ value. In other words, the optimal weight w is obtained when $TC(W)$ is maximized and is defined as:

$$\operatorname{argmax}_w TC(w) \quad (8)$$

4 Experiments and Results

The retrieval efficiency of the proposed method is experimented with a subset of popular image database COREL [7] and the experimental results are presented in this section. We have considered five classes of images such as Dinosaur, Elephant, Rose, Bus and Waterfall, each class containing 100 images. The images in the Corel database are of color images and hence are converted into gray scale. These images are of size (256 x 256) with the pixel values in the range 0 – 255. During experimentation, the image under analysis is divided into (2 x 2) non overlapping blocks and each block is subjected to the orthogonal polynomials transformation. The transformed coefficients

Table 1. Weight for all the features using GA

Texture + Shape Features	Optimized Weight value	Texture + Shape Features	Optimized Weight value	Texture + Shape Features	Optimized Weight value	Texture + Shape Features	Optimized Weight value	Texture + Shape Features	Optimized Weight value
μ_0	0.264	σ_I	0.623	E_2	0.491	Φ_1	0.787	Φ_6	0.220
σ_0	0.003	E_I	0.220	μ_3	0.264	Φ_2	0.003	Φ_7	0.230
E_0	0.623	μ_2	0.538	σ_3	0.268	Φ_3	0.787		
μ_1	0.264	σ_2	0.003	E_3	0.220	Φ_4	0.538		

are reordered into multi resolution subband like structure and the same process is repeated for all the blocks in the image. The image is then decomposed into one level and each subband is named as S_1 , S_2 , S_3 and S_4 . The statistical texture features are extracted from these subbands resulting in the feature vector F_s . The S_2 and S_3 subband coefficients posses the first order derivative information in horizontal and vertical directions and are used to extract edge information with non maximum suppression. After the non maximum suppression process, gradient magnitude G_{ij} is obtained using equation (2) and adaptive threshold is applied on G_{ij} to extract the salient map. The moment feature is extracted from the salient map so as to result a rough shape feature vector of dimension 7. Then the global multi feature vector of dimension 19 is obtained by combining texture and shape feature vector and is normalized. These features are stored in the feature database. The same process is repeated for all the images in the database and the corresponding multifeatures are stored in the feature database. Then from each class fifty percentage of images are taken for training to compute the optimized weight using GA. The weight assignment process with genetic algorithm is performed as described in section 3. During the weight generation process, the following parameters are used: (i) $PopSize (P) = 50$ (ii) $Training Pair (TP) = 35$ (iii) $Cross over Probability = 0.7$ (iv) $Mutation Probability = 0.02$ (v) $Maximum no. iterations = 100$ (vi) $Database size (D) = 500$ and (vii) $k = 50$. The genes in the population take the value between 0 and 1. (i.e., the weights are assigned between 0 and 1). The value of k in the ranking score function is set to 50, because the total number of images considered in this experiment is 500 and 10% of total number of images is 50. Therefore, if the target is ranked in the first position, total count $TC(w)$ is increased by 1. If the target is ranked in the second position, $TC(w)$ is increased by 49 / 50 and so on. The above mentioned process is repeated for the all training image pairs. The experiments are repeated 10 times with different random seeds. The optimized weights for all the 19 features are computed and are shown in the table 1. The weights are converged in the 135th iterations and the weights also exhibit human visual perception. All the training pairs are ranked between 3rd and 16th places in the ranked retrieval except the waterfall pair.

In order to strengthen the experimental result of the proposed weighted multi feature set, the experiment is conducted with four categories of features (i) multi feature with optimized weight ($(W(S+T))$, (ii) multi feature ($S+T$) (Combination of shape and texture features), (iii) Shape feature (S) and (iv) Texture feature (T). The

performance of the proposed method is measured in terms Average Retrieval Ratio (ARR) which is defined as:

$$ARR = \frac{1}{N} \sum_{i=1}^N \frac{m_i}{N} \quad (9)$$

where N is the total number of similar images in one category and m_i is the number of retrieved relevant images. The retrieval accuracy of each class with the weighted multi feature set is obtained by considering each image in the database as query image and the above mentioned process is repeated to extract the shape and texture features. Then the obtained multifeature set is multiplied by optimized weight as shown in table 2. The similarity is computed with integrated weighted dissimilarity function as described in the equation (5) between the query image and the images in the database. Then the performance is evaluated using average precision. The obtained retrieval accuracy of all the five classes are plotted as a graph with the categories in X axis and the retrieval accuracy in Y axis and the same is presented in figure 1(a). Then the overall retrieval accuracy of all the five classes are computed. The obtained result is plotted as a graph and is shown in the figure 1(b). The overall accuracy for the

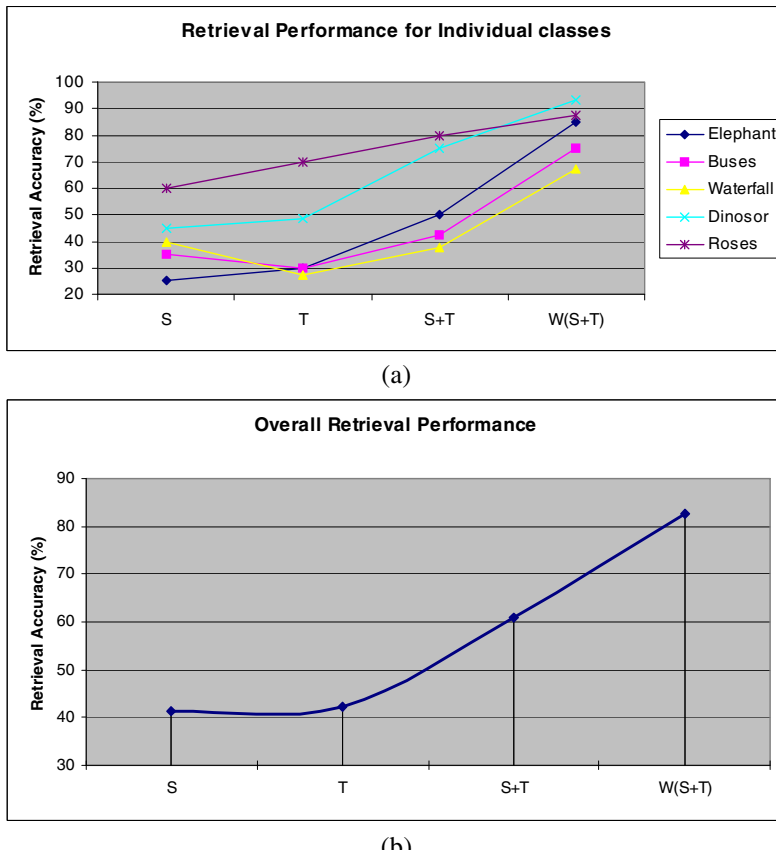


Fig. 1. (a) Retrieval Accuracy of individual classes with five categories. (b) Overall Retrieval Accuracy of individual classes with four categories.

proposed weighted multi feature set is 82.73%. In order to strengthen the experimental result of the proposed method, the experiment is conducted with multi feature set without assigning weight for the features. Similarly the retrieval accuracy of each class using the multi feature set is obtained and the results are incorporated in the same figure 1(a). The overall retrieval accuracy is presented in figure 1(b). From the result we inferred that, the retrieval performance increases sharply for the multi feature set with optimized weight category than multi feature set alone. The experiments are performed by considering the shape and texture features individually and the retrieval accuracy is measured. The obtained retrieval result for all the classes are incorporated in the same figure 1(a). From the figure, it is observed that texture feature outperforms compared to shape feature. The overall retrieval accuracy for these two categories are 41.36% and 42.28% respectively and the same are also plotted as a graph and is shown in figure 1(b). From the graph, it can be observed that the multi feature set with weight yields 82.73% of retrieval accuracy compared with other categories. Hence from the various categories of experimental result, it is inferred that, considering more than one feature with appropriate weight yield better retrieval result. The multifeature is the more discriminative power than single feature in general purpose image retrieval system.

5 Conclusion

In this paper a new image retrieval method with weighted multi feature in multi resolution enhanced orthogonal polynomials model and genetic algorithm is proposed. The transformed coefficients are reordered into multiresolution subband like structure and the statistical and invariant texture and shape features are directly extracted from them. The extracted features are integrated into linear multi feature set and the significance of each feature in the multi feature set is determined by assigning appropriate weight with genetic algorithm. The proposed method gives promising result.

References

1. Iqbal, Q., Aggarwal, J.K.: Combining Structure, Color and Texture for Image Retrieval: A Performance Evaluation. In: 16th International Conference on Pattern Recognition, vol. 2, pp. 438–443 (2002)
2. Howe, N.R., Huttenlocher, D.P.: Integrating Color, Texture, and Geometry for Image Retrieval. In: IEEE Conference on Computer Vision and Pattern Recognition, vol. 2, pp. 239–246 (2000)
3. Yumin, T., Lixia, M.: Image Retrieval Based on Multiple Features Using Wavelet. In: Fifth International Conference on Computational Intelligence and Multimedia Applications, pp. 137–142 (2003)
4. Huang, R.B., Du, M.H.: Object Region Based Color Image Retrieval Integrating Multi features. In: Proceedings of the 2007 International Conference on Wavelet Analysis and Pattern Recognition, pp. 1729–1734 (2007)
5. Krishnamoorthy, R., Sathiya Devi, S.: Design of Fusion Texture Feature with Orthogonal Polynomials Model and Co-occurrence Property for Content Based Image Retrieval. Lecture Notes in Engineering and Computer Science, vol. 2173(1), pp. 1172–1177 (2008)
6. Hu, M.K.: Visual Pattern Recognition by Moment Invariants. IRE Transactions on Information Theory 8(2), 179–187 (1962)
7. <http://www.corel.com>

Automatic Context Analysis for Image Classification and Retrieval

Andrey Vavilin¹, Kang-Hyun Jo¹, Moon-Ho Jeong², Jong-Eun Ha³,
and Dong-Joong Kang⁴

¹ Electrical Engineering Department, University of Ulsan

{andy, jkh2011}@islab.ulsan.ac.kr

² Kwangwoon University

mhjeong@kw.ac.kr

³ Seoul National University of Science

jeha@snu.ac.kr

⁴ Pusan National University

djkang@pusan.ac.kr

Abstract. This paper describes a method for image classification and retrieval for natural and urban scenes. The proposed algorithm is based on hierarchical image contents analysis. First image is classified as urban or natural according to color and edge distribution properties. Additionally scene is classified according to its conditions: illumination, weather, season and daytime based on contrast, saturation and color properties of the image. Then image content is analyzed in order to detect specific object classes: buildings, cars, trees, sky, road etc. To do so, image recursively divided into rectangular blocks. For each block probabilities of membership in the specific class is computed. This probability computed as a distance in a feature space defined by optimal feature subset selected on the training step. Blocks which can not be assigned to any class using computed features are separated into 4 sub-blocks which analyzed recursively. Process stopped then all blocks are classified or size of block is smaller then predefined value. Training process is used to select optimal feature subset for object classification. Training set contains images with manually labeled objects of different classes. Each image additionally tagged with scene parameters (illumination, weather etc.).

Keywords: Image retrieval, image classification, optimal feature subset selection.

1 Introduction

The explosive growth in digital imaging during last decade caused the huge collection of images to be created in many areas. Usually, the only way to search in these collections was by keyword indexing or by manual browsing. Digital image databases, however, open the way to more effective image retrieval: content-based searching. In this paper we propose an algorithm for image retrieval which is based on context analysis of several semantic layers of the scene.

For effective image retrieval a scene classification method is required. The main goal of scene classification is automatically labeling of image among a set of semantic categories (street, forest, seashore etc). From an application viewpoint, scene classification is relevant in systems for organization of personal and professional imaging collections, and has been widely explored in content based image retrieval systems [1].

One of general approach for scene classification is based on low-level image analysis [3]. This approach classifies scenes based on the set of low level features which describes color, texture and shapes presented in image combined with supervised learning technique. Recently, several studies classifying scenes using global cues (such as color histograms, power spectrums etc) as indoor vs. outdoor, or urban vs. natural were presented. Among them it is possible to distinguish two main trends. In *global-based* approach the scene is analyzed using set of low-level features computed for whole image [4,5]. In *local-based* the image is separated into several blocks and features are extracted from all of them [6,7].

Another technique used for classification is based on scene context analysis. It uses scene content (people, buildings, trees etc) as additional cues to improve the classification performance obtained by low-level features. A scene is described as a set of semantic objects presented in image.

Among the semantic methods, three different categories could be distinguished according to the meaning they give to the semantic of scenes, and hence which is the representation they build: techniques which describe the image by the objects and those that build the semantic representation from local information, and proposals which describe the image by semantic properties.

More detailed description of image classification techniques is given in [8,9].

2 Algorithm Description

In this work we consider a scene to consist of three semantic layers. First layer contains ground and sky information, second layer contain buildings and trees, last layer contains moving objects. Objects of different layers separated into classes as follows.

- Layer 1: *sky, clouds, grass, road and pavement.*
- Layer 2: *buildings and trees.*
- Layer 3: *cars, buses, trucks.*

Furthermore, each class may contain subclasses which are automatically detected during the training process. For example buildings usually contain windows which typically have different properties with walls. Taking this into account, we can separate class *buildings* into two subclasses: *walls* and *windows*. Additionally, we can define two rules useful for classification: *building* should contain *walls* and *windows* and *windows* must be inside of *wall* regions. Subclasses are detected automatically during the training step [10].

Urban and natural scene typically contains different objects. Thus, knowing the scene type makes further analysis easier. In this work 3 types of scenes were considered: *natural* (contains only natural objects such as trees, sky, mountains,

rivers, etc), *urban* (contains human-made objects such as buildings, roads, vehicles etc) and *mixed* (contains both natural and human-made objects). This classification is based on a very low dimensional representation on the scene referred as a Spatial Envelope [11,12]. It consists of five perceptual qualities: naturalness (vs man-made), openness (presence of a horizon line), roughness (fractal complexity), expansion (perspective in man-made scenes), and ruggedness (deviation from the horizon in natural scenes). However, the contribution of each feature cannot be understood as they stand, and more importantly, they are not directly meaningful to human observers. Each feature corresponds to a dimension in the spatial envelope space, and together represents the dominant spatial structure of a scene.

2.1 Scene Condition Evaluation

Appearance of scene is strongly affected by lighting and weather conditions. Furthermore, natural objects in scene may look different depending on season. In this work initially we considered the following factors to be most influential: *daytime* (morning, evening, day and night), *lighting conditions* (normal, underexposed, overexposed, HDR), *weather conditions* (good, rain, snow), and *season* (winter, spring, summer and autumn). Each image is classified according to these categories. Some categories are strongly related. For example, images taken in morning or evening are more likely contains overexposed or underexposed regions due to dynamic range limitations of cameras. We considered a part of image as overexposed when it has a loss of highlight detail, that is, when important bright parts of an image are “washed out” and underexposed when it has a loss of shadow detail, that is, when important dark areas are “muddy” or indistinguishable from black. Image was considered to be over- or underexposed if more than 30% of its area was over- or underexposed. By lighting conditions, scene could also be classified as a HDR if both over and under exposed regions are presented or normally exposed, if none of them could be found in image. One of the main goals of training step was to find dependences between scene conditions and object appearance.

2.2 Image Retrieval

On retrieval step input image is first classified according to the scene conditions. It is very difficult to recognize exact scene conditions. For example, pictures taken in evening and morning time will have very similar color distributions. However, the goal of condition estimation is to improve classification performance, by minimizing the effect of scene conditions to object appearance. Thus, morning and evening images could be grouped in a same class due to the similar effect to object appearance.

Scene conditions described as a probabilities vector $P^C = (P^L, P^D, P^W, P^S)$ where P^L , P^D , P^W and P^S are vectors which describes probabilities of scene to belong a particular class. For example, $P^L = (p^{LN}, p^{LO}, p^{LU}, p^{LH})$ shows probabilities of scene to be normally exposed (p^{LN}), overexposed (p^{LO}), underexposed (p^{LU}) and HDR (p^{LH}). Using computed probabilities the most probable scene conditions $P_{\max}^C = (P_{\max}^L, P_{\max}^D, P_{\max}^W, P_{\max}^S)$ are selected.

On the next step image is divided into 64 rectangular blocks (8 blocks in horizontal and vertical directions) of the same size. For each block descriptive feature vector is computed. A set of computed features was automatically selected on training process (refer to [13] for details). If the block can not be classified according to selected scene conditions with probability higher than 60% it is divided into 4 sub-blocks and classification repeated recursively. Process is stopped when all blocks are classified or size of block is less than 1000 pixels. Blocks which can not be classified with probability higher than 30% are marked as *unknown*. These blocks have no effect to image search process.

Finally, the scene description is generated based on amount of presented objects in the scene. Furthermore, for each class of presented objects, feature vector is recalculated using information from all blocks of the same class. This description vector is used to retrieve images from the database. First, we search images with respect to objects, presented in scene. Then the most similar are selected using distance in feature space as the matching measure. Main idea of proposed image retrieval method is shown in Fig.1.

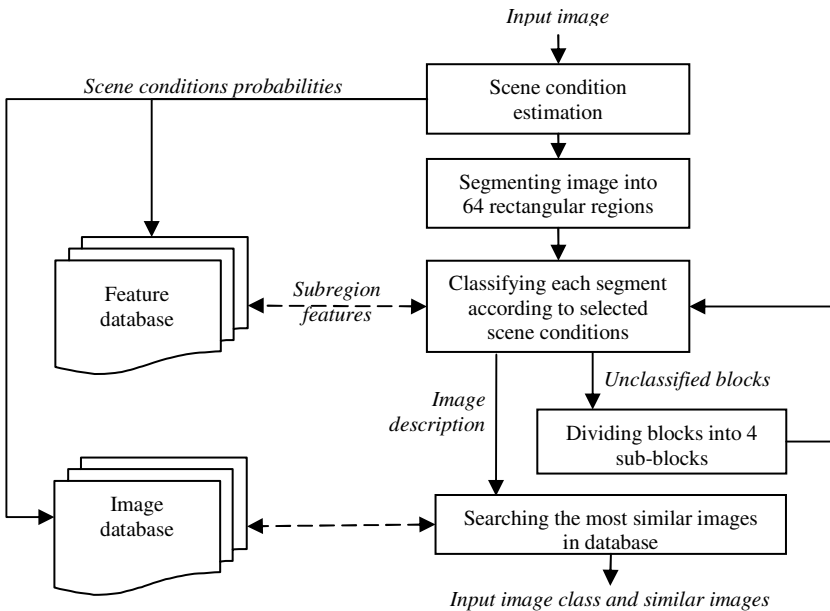


Fig. 1. Image retrieval process

3 Experimental Results

The training set consists of 1000 labeled images of outdoor scenes with resolution from 1024x768 up to 3000x2000. Test set consists of 295 unlabeled images.

First group of tests was made to evaluate the performance of scene condition estimation. Input images were automatically classified using the proposed method and compared with ground truth. Results are shown in Table 1. It is easy to see that the

most difficult problem is image classification according to weather conditions (66.6%). Time of the day can be correctly estimated with a probability 87% and urban vs natural scene classification has 94.5% rate. Second group of tests was made to evaluate the performance of retrieval method. Results are shown in Fig.2. In this work the precision and recall are defined as follows:

$$precision = \frac{\# \text{of relevant images retrieved}}{\text{Total } \# \text{of retrieved images}} \quad (1)$$

$$recall = \frac{\# \text{of relevant images retrieved}}{\text{Total } \# \text{of relevant images in base}} \quad (2)$$

Table 1. Scene conditions evaluation

Class	Number of images	Correct classification
<i>Scene class</i>		
Natural	150	140
Urban	103	101
Mixed	42	38
Total	295	279 (94.5%)
<i>Daytime classes</i>		
Day	40	29
Evening and morning	80	71
Night	40	40
Total	160	140 (87.5%)
<i>Weather conditions classes</i>		
Normal conditions	30	25
Fog	15	10
Rain or snow	30	15
Total	75	50 (66.6%)
<i>Lighting conditions classes</i>		
Normal lighting conditions	100	100
HDR scene	100	98
Total	200	198 (99%)

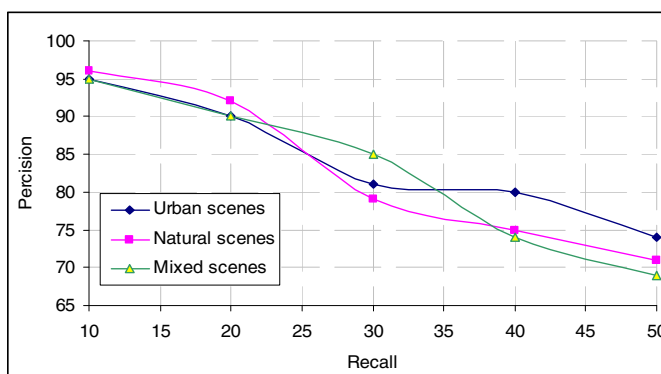


Fig. 2. Image retrieval results

4 Conclusions

Image classification and retrieval method based on scene condition estimation and recursive segmentation is proposed. Training process is used for selecting optimal features for classification and for subclass detection. In addition, dependences between scene conditions and object appearance are analyzed during the training process. Image retrieval is based on three main parameters: scene conditions, objects presented in a scene and their properties. Using scene condition hypothesis allows minimize the effect of different lighting and weather conditions on object appearance.

Acknowledgments. This research was supported by the MKE(The Ministry of Knowledge Economy), Korea, under the Human Resources Development Program for Convergence Robot Specialists support program supervised by the NIPA(National IT Industry Promotion Agency) (NIPA-2010-C7000-1001-0007) and post-BK21 at University of Ulsan.

References

1. Adams, W.H., Iyengar, G., Lin, C., Naphade, M.R., Neti, C., Nock, H.J., Smith, J.R.: Semantic Indexing of Multimedia Content Using Visual, Audio, and Text Cues. *Journal on Applied Signal Processing* 2, 1–16 (2003)
2. Wang, J., Li, J., Wiederhold, G.: Simplicity: Semantics-sensitive Integrated Matching for Picture Libraries. *IEEE Transactions on Pattern Analysis and Machine Intelligence* 23(9), 947–963 (2001)
3. Chang, E., Goh, K., Sychay, G., Wu, G.: Cbsa: Content-based Soft Annotation for Multimodal Image Retrieval Using Bayes Point Machines. *IEEE Transactions on Circuits and Systems for Video Technology Special Issue on Conceptual and Dynamical Aspects of Multimedia Content Description* 13(1), 26–38 (2003)
4. Shen, J., Shepherd, J., Ngu, A.H.H.: Semantic-sensitive Classification for Large Image Libraries. In: *International Multimedia Modelling Conference*, Melbourne, Australia, pp. 340–345 (2005)
5. Paek, S., Chang, S.F.: A Knowledge Engineering Approach for Image Classification Based on Probabilistic Reasoning Systems. In: *IEEE International Conference on Multimedia and Expo.*, New York, vol. II, pp. 1133–1136 (2000)
6. Serrano, N., Savakis, A., Luo, J.: Improved Scene Classification Using Efficient Low-level Features and Semantic Cues. *Pattern Recognition* 37, 1773–1784 (2004)
7. Shandilya, S.K., Singhai, N.: A Survey On: Content Based Image Retrieval Systems. *International Journal of Computer Applications* 4(2), 22–26 (2010)
8. Bosch, A., Muñoz, X., Martí, R.: Review: Which Is the Best Way to Organize/Classify Images by Content? *Image and Vision Computing* 25(6), 778–791 (2007)
9. Vavilin,A., Ha,L.M., Jo,K.H.: Optimal Feature Subset Selection for Urban Scenes Understanding. In: *URAI 2010 Busan*, Korea (2010)
10. Torralba, Q.A.: Modeling the Shape of the Scene: A Holistic Representation of the Spatial Envelope. *International Journal of Computer Vision* 42(3), 145–175 (2001)
11. Oliva, A., Torralba, A.: Scene-centered Description from Spatial Envelope Properties. In: *BMCV 2002. LNCS*, vol. 2525, pp. 263–272. Springer, Heidelberg (2002)

Image Feature Extraction Using the Fusion Features of BEMD and WCB-NNSC

Li Shang and Jie Chen

Department of Electronic Information Engineering, Suzhou Vocational University,
Suzhou 215104, Jiangsu, China
{sl0930,cj}@jssvc.edu.cn

Abstract. A novel image feature extraction method, using the fusion features obtained by the algorithms of Bidimensional Empirical Mode Decomposition (BEMD) and Weight Coding Based Non-negative Sparse Coding (WCB-NNSC), is proposed in this paper. This BEMD algorithm is on the basis of EMD, and is especially adaptive for non-linear and non-stationary 2D-data analysis. And the weight coding based NNSC algorithm includes more class information. Utilizing Intrinsic Mode Functions (IMF) extracted by BEMD to be the training set of the weight coding based NNSC algorithm, the feature basis vectors of natural images can be successfully learned, and these features behave locality, orientation, and spatial selection. Further, using extracted features, the image reconstruction task is implemented successfully. Moreover, compared with other feature extraction methods, such as FastICA, basic NNSC, WCB-NNSC and so on, simulation results show that our method proposed here is indeed efficient and effective in performing image feature extraction task.

Keywords: BEMD, Weight coding, NNSC, Image, Feature extraction.

1 Introduction

Transforming the input data into the set of features is called feature extraction. For natural images, image feature extraction is an important content in pattern recognition and image processing, and it is also a special form of dimensionality reduction. Using features extracted, the desired task of image processing, such as image denoising, image restore, image retrieval and so on, can be implemented successfully. Currently, there are many image feature methods that have been developed, for example, wavelet-based transform method [1], Fisher Linear Discriminant (FLD) [2], Principal Component Analysis (PCA) method [3], Independent Component Analysis (ICA)[4], Sparse Coding (SC) [5], Non-negative Sparse Coding (NNSC) [6], etc., and all these methods can successfully extract image features by using different skills and strategies. Especially, the methods of ICA, SC and NNSC are based on statistical measures and are very fit to extract the higher order information of images. However, the image feature extraction task is a challenging title to this day, and many research workers in image processing field are concentrating on exploring valid feature extraction methods. Moreover, the NNSC method is proposed in recent years and is very valid in

modeling the receptive fields in the mammalian primary visual cortex in the brain. In order to extract the optimal features of images, in this paper, on the basis of NNSC, we proposed the weight coding based NNSC. At the same time, in order to save information in the high frequency and the low frequency, the Bidimensional Empirical Mode Decomposition (BEMD) [7] is used to preprocess natural images. Using pre-processed data by BEMD as the training set of the Weight Based NNSC (WCB-NNSC) algorithm, the image features can be extracted successfully. Further, using the features extracted, the image restore task can be implemented efficiently. Otherwise, compared with other image feature extraction methods of Basic NNSC (BNNSC), Standard Sparse Coding (SSC), WCB-NNSC and the fixed point fast Independent Component Analysis (FastICA), simulation results also show that our image feature extraction method indeed outperforms any other above-mentioned.

2 The BEMD Algorithm

The EMD approach was proposed by Huang in 1998, which is a signal analysis method behaving the discriminating capacity of high time-frequency [9]. This decomposition technique is adaptive and appears to be a suitable for nonlinear, non-stationary data analysis. But EMD method is fit to process 1D signal. In order to apply EMD on images, Nunes proposed a new multi-scale decomposition method called BEMD for image analysis in 2003 [8]. The BEMD method extracts zero-mean 2D AM-FM components called Intrinsic Mode Functions (IMF). Each IMF has the same number of zero crossings and extrema, at the same time, each IMF is symmetric with respect to the zero mean. For each mode, the algorithm, extracting locally the highest frequency oscillations from original signal, is called “sifting process”. The bidimensional sifting process is defined here as follows [7-8]:

- (1) Let $I_r = I_{ori}$ and $I_{res} = I_{ori}$. I_{ori} is the original 2D signal $f(x, y)$, I_r denotes the residual components, and I_{res} is the reconstruction image.
- (2) Search all extrema of I_{res} using the morphological method.
- (3) Compute the 2D upper and lower envelope by connecting extrema points with radial basis functions, and then the maximum and minimal envelope extrema, denoted by S_{upper} and S_{lower} respectively, are obtained;
- (4) Determine the mean envelope E_m of upper an lower envelopes:

$$E_m = (S_{upper} + S_{lower})/2;$$
- (5) Extract the details $I_{res} = I_{res} - E_m$;
- (6) Repeat steps 2 to 5 until I_{res} can be considered as zero mean and $SD < \varepsilon$. Then, let $I_{res} = IMF_i$, i is the sequence number of IMFs. Here ε is the threshold value setted in advance. SD is the criterion of 2D-sifting process to stop, which is written as follows:

$$SD = \sum_{k=0}^K \sum_{l=0}^L \left| I_{resi(j-1)}^{(k,l)} - I_{resij}^{(k,l)} \right|^2 / \sum_{k=0}^K \sum_{l=0}^L \left(I_{resi(j-1)}^{(k,l)} \right)^2 . \quad (1)$$

where K is the number of 2D IMFs, j is the repeat time of steps 2 to 5. (k,l) is the pixel coordinate of images.

(7) Let $I_r = I_r - I_{res}$ and $I_{res} = I_r$.

(8) Repeat steps 2 to 7 until the extrema number of I_r is less than 2.

Thus, the i 2D IMFs and the residual term I_r can be obtained. The factorization representation of 2D image signal $I(x,y)$ is written as follows:

$$I(x,y) = \sum_{i=1}^K IMF_i(x,y) + I_r(x,y) . \quad (2)$$

3 The Algorithm of WCB-NNSC

3.1 The Cost Function

The basic NNSC (BNNSC) algorithm is proposed by Hoper early [6]. This BNNSC method adopts the idea of a parts-based representation for Sparse Coding (SC), by also putting positive constraints on the weights and the coefficients. It is similar to NMF with sparseness constraints [9], whereas NMF methods apply multiplicative update rules that don't require the definition of a learning rate. However, NMF, SC and NNSC don't care about the existence of different classes, and they produce features that are useful for general image reconstruction but lack the property of being class-specific. As to the above problems, referring to the document [9], we defined the following object function of the WCB-NNSC algorithm:

$$E_w = \frac{1}{2} \sum_i \left\| \mathbf{x}_i - \sum_m \mathbf{w}_m s_{mi} \right\|_2^2 + \gamma \sum_{i,m} f(s_{mi}) + \beta \sum_m \sum_{\substack{i,\tilde{i} \\ q(i)=q(\tilde{i})}} \frac{\mathbf{w}_m^T \mathbf{x}_i \mathbf{w}_m^T \mathbf{x}_{\tilde{i}}}{n_{q(i)} n_{q(\tilde{i})}} . \quad (3)$$

where the samples $\mathbf{x}_i = (x_{i1}, x_{i2}, \dots, x_{iN})^T$ ($i=1,2,\dots,L$), $\mathbf{x}_{\tilde{i}}$ denotes another labeled sample column vector, the coefficients $s_{mi} = (s_{1i}, s_{2i}, \dots, s_{Mi})$ ($m=1,2,\dots,M$), and the weights (column vectors) $\mathbf{w}_m = (w_{m1}, w_{m2}, \dots, w_{mN})^T$. $q(i)$ and $q(\tilde{i})$ are the label of \mathbf{x}_i and $\mathbf{x}_{\tilde{i}}$, respectively. $n_{q(i)}$ and $n_{q(\tilde{i})}$ are the number of samples corresponding to the class of \mathbf{x}_i and $\mathbf{x}_{\tilde{i}}$. The weights have the same dimension N with the samples. Otherwise, noted that the column vector \mathbf{x}_i , \mathbf{w}_m and row vector \mathbf{s}_m subject to the non-negative constraints.

In Eqn. (3), The first term is the reconstruction error of \mathbf{x}_i , which is approximated by a linear combination $\sum_m \mathbf{w}_m s_{mi}$. The coefficients s_{mi} specify how much the $m-th$ weight is involved in the reconstruction of the $i-th$ data vector. The second term is

sparse punitive function $f(s_{mi})$, which is defined the negative logarithm of coefficients' sparse density, namely $f(s_{mi}) = -\log(p(s_{mi}))$. The density $p(\cdot)$ is selected as follows:

$$p(s) = \frac{1}{2b} \frac{(d+2)[0.5d(d+1)]^{(0.5d+1)}}{\left[\sqrt{0.5d(d+1)} + |s/b|\right]^{(d+3)}}. \quad (4)$$

where parameters $d, b > 0$, d is a sparsity parameter and b is a scale parameter. Parameters d and b are estimated by the following equations:

$$b = \sqrt{E\{s^2\}}, \quad d = \frac{2 - k + \sqrt{k(k+4)}}{2k-1}, \quad k = b^2 p_s(0)^2. \quad (5)$$

The sparsity term increase the cost, the more the activation is spread over different s_{mi} , and so many of them become zero while few are highly activated. The influence of the sparsity term is scaled with the positive constant γ . The last term is weight coding term, which causes cost if a w_m has a large inner product with differently labeled samples x_i and $x_{\tilde{i}}$. The influence of the weight term is scaled with the positive constant β .

3.2 The Learning Rules

The minimization of the cost functions of sparse coefficient and weight coding can be done in turn by applying coefficient and weight steps. The updating rule of coefficient vectors s_m is implemented by using an asynchronous fixed-point search, at the same keeping the w_m constant. In the same way, when updating weight vectors w_m , sparse coefficient vectors s_m are kept constant. The updating formula of sparse vectors s_m is defined as follows:

$$s_m = \lambda \left(w_m^T x_i - \sum_{\tilde{m} \neq m} s_{\tilde{m}} w_{\tilde{m}}^T w_m - \gamma f'(s_{mi}) \right) (w_m^T w_m)^{-1}. \quad (6)$$

where $\lambda > 0$, it ensures the positivity of the coefficients. This update rule is applied to randomly chosen s_{mi} until convergence. The weight step is a single gradient step with a fixed step size η in the weight vectors w_m , keeping the s_{mi} constant:

$$w_m = \lambda \left[w_m - \eta \left(\sum_i \sum_{\tilde{m}} s_{\tilde{m}} w_{\tilde{m}} s_{mi} - \sum_i x_i s_{mi} + \beta \sum_{\substack{i, \tilde{i} \\ q(i) \neq q(\tilde{i})}} \frac{x_i (w_m^T x_{\tilde{i}})}{n_{q(i)} n_{q(\tilde{i})}} \right) \right]. \quad (7)$$

The weight step is executed for each w_m at the same time and the parameter λ is applied component wise. Before the next coefficient step, the weights are normalized using the formula $w_m = / \|w_m\|_2$.

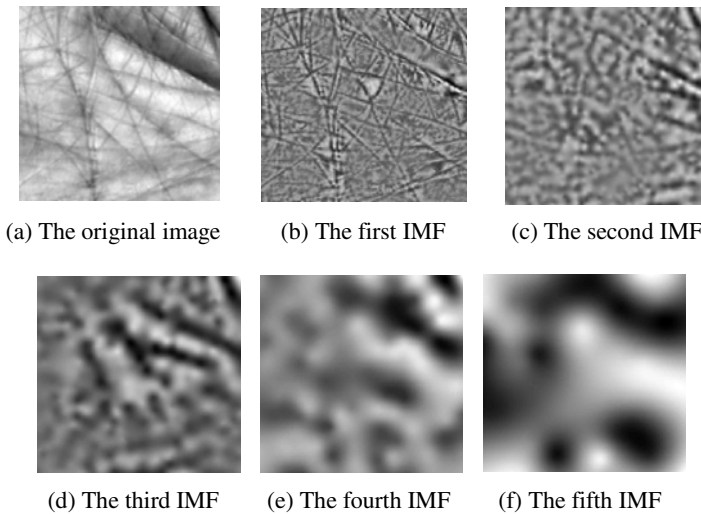


Fig. 1. The original image and its five Intrinsic Mode Functions (IMFs) obtained by BEMD algorithm

4 Experiment Results

4.1 Image Feature Extraction

In simulation experiment, we selected 60 palmprint images of the first 10 persons from the Hong Kong Polytechnic University (PolyU) palmprint database to test. First, each image is decomposed into five IMF components from high frequency to low frequency by BEMD algorithm, thus, 300 images composed of IMFs are obtained. As an example of using BEMD, Figure 1 shows an original palmprint image and its corresponding five IMFs, here, noted that the residue of each IMF is ignored. On the basis of BEMD, for each IMF image, an 8×8 pixel patch is used to sample randomly 100 times, and the data set with the size of 64×30000 is obtained. Then, using the set as the input training set of our WCB-NNSC algorithm, the feature vectors of palmprint images, obtained by the combination features of BEMD and WCB-NNSC (denoted by BEMD-WCB-NNSC here), can be learned, which is shown in Fig. 2 (a)~(c). At the same time, without considering the BEMD method, for 60 original images, an 8×8 pixel patch is also used to sample each image randomly 1000 times, the obtained matrix set with the size of 64×60000 is used as the input set of WCB-NNSC. The learned features of WCB-NNSC are shown in Fig. 2 (d)~(f). In Figure (2), the white represents the positive pixels, the gray denotes the zero pixels, and the black shows the negative pixels. Clearly, feature vectors obtained by BEMD-WCB-NNSC have more distinct sparseness and locality than those obtained by WCB-NNSC. Then, using the weighted average method for those features learned, the fusion features can be obtained. Further, using these fusion features, the image restore task can be discussed.

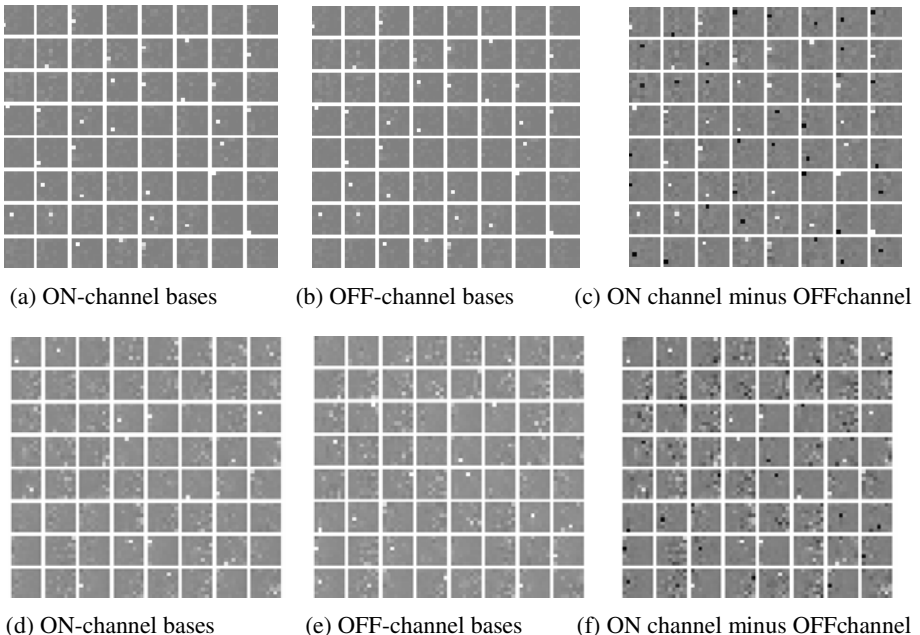


Fig. 2. Feature basis vectors obtained by different algorithms. The first line is obtained by BEMD-WCB-NNSC algorithm. The second line is obtained by WCB-NNSC algorithm.

4.2 Testifying Image Features

To testify the validity of our feature extraction method, using the feature bases extracted, we implemented the image reconstruction task of palmprint images. A test image shown in Fig. 3 was randomly selected from the PolyU palmprint database. Assume that the number of image patches with 8×8 pixels sampled from this selected image was 100, 300, 500, ..., 10000, etc., respectively. Then, corresponding to different image patches, some of reconstruction images obtained by our method were shown in Fig. 3. Note that the larger the number of image patches is, the clearer the reconstructed image is, and the visual efficiency is better. When the number of image patches is 50000, it is difficult to tell it from the original images only with naked eyes. This experimental result further testifies that the features extracted by the BEMD-NNSC method are indeed effective.

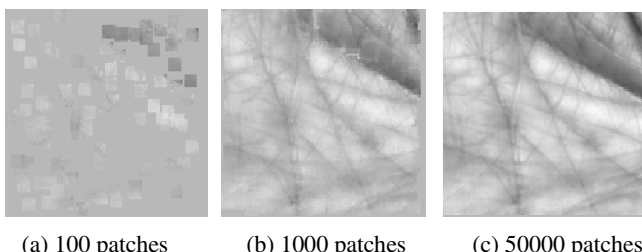


Fig. 3. The reconstructed results obtained by our SC algorithm corresponding to image patches

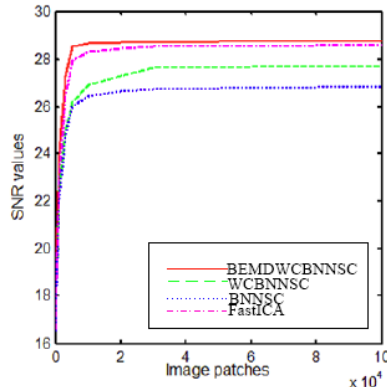


Fig. 4. The SNR values of different algorithm. Solid line: BEMD-WCB-NNSC algorithm; Dashed line: WCB-NNSC algorithm; Dotted line: BNNSC algorithm; Dash dotted line: FastICA algorithm.

Otherwise, in order to measure the quality of restored images, the signal to noise ratio (SNR) values of the reconstruction images obtained by different algorithms, such as basic NNSC (BNNSC), WCB-NNSC and FastICA, were also calculated and plotted in Fig.4. Noted that in test the number of image patches of an appointed image is 100, 300, 500, 1000, 3000, 5000, 10000, 20000, 30000, 50000, 60000, 80000 and 100000. And the SNR curves of BEMD-WCB-NNSC, WCB-NNSC, BNNSC and FastICA are plotted in solid line, dashed line, dotted line and dash dotted line respectively. According to Fig.4, it is easy to see that the values of the BNNSC algorithm are the least, and those of the BEMD-NNSC are the largest. The values of the WCB-NNSC algorithm are somewhat larger than those of BNNSC, but lower than those of FastICA and BEMD-WBNNSC. However, the SNR values of FastICA are very close to ones of BEMD-WCB-NNSC. Thus, the conclusion can be obtained that the BEMD-WCB-NNSC algorithm is indeed efficient in image feature extraction task.

5 Conclusions

In this paper, a novel natural image feature extraction method using the weighted average fusion features obtained by BEMD-WCB-NNSC and WCB-NNSC is proposed. Features obtained by WCB-NNSC lose much detailed information, and the features obtained by BEMD lose much contour information. While the BEMD-WCB-NNSC method combined the advantages of BEMD and WCB-NNSC, features obtained by BEMD-NNSC contain both the detailed information and the contour of a natural image. And using these features extracted, a natural image can be successfully reconstructed. At the same time, using the image measure criterion of SNR, the efficiency of image reconstruction is proved. Further, compared with feature extraction methods of BNNSC, WCB-NNSC and FastICA, experimental results of SNR obtained by different algorithm also show that our algorithm is indeed efficient and useful in practice.

Acknowledgments. This work was supported by the National Natural Science Foundation of China (Grant No. 60970058), the Natural Science Foundation of Jiangsu Province of China (Grant No. BK2009131), the Innovative Team Foundation of Suzhou Vocational University (Grant No. 3100125) and the “Qing Lan Project” of Jiangsu Province.

References

1. Jain, A.K., Ross, A., Prabhakar, S.: An Introduction to Biometric Recognition. *IEEE Transactions on Circuits and Systems for Video Technology* 14(1), 4–40 (2004)
2. Wu, X.Q., Zhang, D., Wang, K.Q.: Fisherpalms Based Palmprint Recognition. *Pattern Recognition Letters* 24(15), 2829–2838 (2003)
3. Connie, T., Teoh, A., Goh, M.: Palmprint Recognition with PCA and ICA. *Image and Vision Computing NZ* 3, 227–232 (2003)
4. Bell, A.J., Sejnowski, T.J.: The Independent Components of Natural Scenes Are Edge Filters. *Vision Research* 37, 3327–3338 (1997)
5. Olshausen, B.A., Field, D.J.: Emergence of Simple-cell Receptive Field Properties by Learning A Sparse Code for Natural Images. *Nature* 381, 607–609 (1996)
6. Hoyer, P.O.: Modeling Receptive Fields with Non-negative Sparse Coding. *Neurocomputing* 52(54), 547–552 (2003)
7. Nunes, J.C., Niang, O., Bouaoune, Y., Delechelle, E., Bunel, P.: Bidimensional empirical mode decomposition modified for texture analysis. In: Bigun, J., Gustavsson, T. (eds.) *SCIA 2003. LNCS*, vol. 2749, pp. 171–177. Springer, Heidelberg (2003)
8. Hoyer, P.: Non-negative Matrix Factorization with Sparseness Constraints. *Journal of Machine Learning Research* 5, 1427–1469 (2004)
9. Hasler, S., Wersing, H., Kömere, E.: Combining Reconstruction and Discrimination with Class-specific Sparse Coding. *Neural Computation* 19(7), 1897–1918 (2007)

Palmpoint Recognition with MEEMD and Statistically Independent Coefficients ICA

Ting-Qin Yan, Shu-Fen Liu, and Chang-Xiong Zhou

Depart of Electronic Information Engineering, Suzhou Vocational University,
Suzhou, Jiangsu 215104, China
maxytz@tom.com

Abstract. A palmpoint recognition method based on multi-dimensional ensemble empirical mode decomposition (MEEMD) and statistically independent coefficients independent components analysis (ICAII) is proposed in this article. Palmpoint images are decomposed with MEEMD to get high frequency IMF components and low frequency IMF components, then reconstruct palmpoint images with the high frequency IMF components to get palmpoint images set which can be used for recognition. When all processes above are finished, the next step is to extract ICAII feature from the reconstructed palmpoints and recognize the reconstructed palmpoints. The palmpoint database of Hong Kong Polytechnic University is used in experiments, the results of the experiments convincingly indicate that the recognition rate of this method is higher than ICAII and the speed of recognition is also faster.

Keywords: Palmpoint recognition, MEEMD, ICA.

1 Introduction

Personal identification has been an important issue now. Conventional means for personal identification include passports, keys, tokens, ID cards, personal identification number(PIN) [1]. All these means can be easily changed and therefore are unreliable. For that reason, biometric identification is emerging. Iris [2], retina [3], face [4], voice [5], signature [6] and DNA [7] have been using for biometric authentication. With the development of our information society, the importance of biometric identification is growing. Among these biometric techniques, palmpoint recognition is one of the most reliable approaches. Palmpoints are abundant of such features as creases, palm lines, texture, ridges, delta points and minutiae, these features of palmpoints have the critical properties of universality, uniqueness, permanence and collectibility for personal authentication[8]. With creases and palm lines, low-resolution images can be used in the palmpoint recognition.

Much work have been done on the palmpoint recognition [1,8-10]. Independent Component Analysis(ICA) is the most important one among all of these methods[10]. ICA has been regarded as an efficient tool for understanding the hidden factors that underlie sets of random variable. In ICA model, a palmpoint image can expressed as a

linear superposition of basis functions, these basis functions are able to capture inherent features of the palmprint, so we can employ ICA to finish the objective of palmprint recognition. Two different frameworks of ICA are adopted to recognise palmprints. Framework I observed images as random variables and the pixels as outcome while framework II treated pixels as random variables and the images as outcome. The result shows that ICA framework II yields the better performance.

To get better recognition rates, multi-dimensional ensemble empirical mode decomposition(MEEMD) [11] is incorporated into palmprint recognition. During the course of precessing, a palmprint image is decomposed into intrinsic mode functions (IMFs), then reconstruct palmprint image with corresponding higher frequency parts of IMFs, we can get a distinct palmprint with more detail, which used as inputs of ICA. In this paper, framework II of ICA is performed on the reconstructed palmprint images. Compared with framework II of ICA without MEEMD, the result of experiments shows a higher recognition rate and a faster test speed.

2 Multi-dimensional Ensemble Empirical Mode Decomposition (MEEMD)

Empirical Mode Decomposition(EMD) is an important method for data analysis, it can decompose a complex signal into a set of intrinsic mode functions (IMFs), so that more detail information of signal can be extracted. But EMD has its own drawbacks, for example mode mixing, To overcome some drawbacks of EMD, Zhaohua Wu proposed a new noise assisted data analysis method named multi-dimensional ensemble empirical mode decomposition (MEEMD) in 2009[11], that can complete EEMD for multi-dimensional data.

The algorithm of EEMD can be described as follow: a series of white noise is added to the targeted data, then decompose the data with white noise into IMFs, repeat these steps with different white noise series each time, so the ensemble means of corresponding IMFs of the decompositions can be extracted.

For image, EEMD is applied in one dimension, then applied in the second dimension to the results of the decompositions of the first dimension, decompositions of image could be gotten by combining the components with appropriate strategy. In this paper, MEEMD is applied for palmprint images. The number of IMFs is 4, we can get 4 IMFs and a remainder component, and palmprint image is reconstructed from 4 IMFs with formula (1). Fig.1 shows the decompositions and reconstructions of a palmprint.

$$f_{rec}(x, y) = \sum_{j=1}^4 IMF_j(x, y) \quad (1)$$

We can see from the result that the reconstructed palmprint image with high frequency IMF components (i) without the remainder (f) spotlights the high frequency details of palmprint, and remove the influence of background. In this paper, ICAII is applied on such reconstructed palmprint images to extract palmprint feature and recognize it.

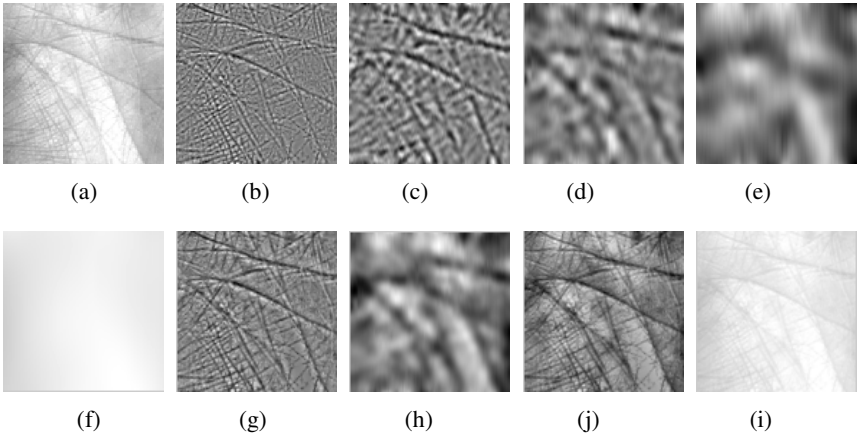


Fig. 1. The decompositions and reconstructions of a palmprint with MEEMD. (a)original palmprint. (b)-(e) IMF components 1-4. (f) the remainder after 4 components are extracted. (g) reconstructed palmprint with two high frequency IMF components(b)- (c). (h) reconstructed palmprint with two low frequency IMF components(d)- (e). (i) reconstructed palmprint with four IMF components(b)- (e). (j) reconstructed palmprint with four IMF components(b)- (e) and the remainder component(f).

3 Statistically Independent Coefficients ICA (ICA II)

ICA is a very general-purpose statistical technique. In the model of ICA, a vector of observed mixtures x is regard as a linear combination of unknown independent signals s . Let A be the unknown mixing matrix, the mixing model can be written as

$$x = As . \quad (2)$$

It is assumed that the source signals are independent of each other and the mixing matrix A is invertible. The purpose of Independent Components Analysis (ICA) is to find a separating matrix W , and to extract a set of independent singals u from the vector of observed mixtures x , so that

$$u = Wx . \quad (3)$$

is an estimation of the independent source signals.

There are many methods which can be used to estimate independent components, such as fastICA, informax, and so on. Regardless of which algorithm is used to compute ICA, there are two frameworks for ICA in palmprint recognition. In framework I, the input palmprint images in x are considered to be a linear mixture of statistically independent basis images s combined by an unknown mixing matrix A . In framework II, pixels are treated as random variables and mages as observations. In this paper, framework II of ICA is performed on the PCA coefficients to reduce the dimensionality, so the statistically independent coefficients ICA is named for it.

Take the input of ICA II is matrix C ($m \times p$), where p represents the number of pixels in the train images, and m be the number of the train images. Calculate the eigenvalues E and the eigenvectors V , then project the zero-mean images D into the space of eigenvectors V to get PCA coefficients R :

$$R = DV . \quad (4)$$

Reduce the dimensionality of PCA coefficients set to get PCA coefficients set $R(m, h)$ corresponding to the first m eigenvectors. ICA II is performed on the PCA coefficients $R^T(m, h)$ to get ICA coefficients, so the statistically independent coefficients can be computed as

$$F = WR^T . \quad (5)$$

Basis vectors U can be obtained as

$$U = VW^{-1} . \quad (6)$$

The basis images generated by ICA II and MEEMD-ICAII is shown in fig.2. (a) is the basis vectors of ICA II, (b) is the basis vectors of MEEMD-ICAII. The basis shows more globalized features.

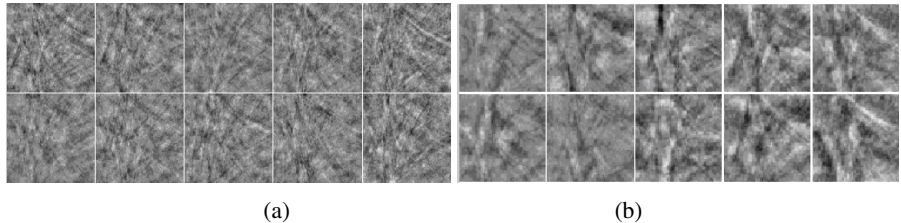


Fig. 2. The first 10 basis images generated by each technique. (a) shows 10 non-localized ICA basis vectors for ICA framework II. (b) depicts 10 basis vectors for MEEMD-ICAII.

4 Palmpoint Recognition Algorithm Based on MEEMD and ICA II (MEEMD-ICAII)

Based on the discussion above, a new algorithm based on multi-dimensional ensemble empirical mode decomposition(MEEMD) and architecture II independent components analysis(ICA II) is presented in this paper. Palmprint images are decomposed into 4 intrinsic mode functions (IMFs) and a remainder component with MEEMD algorithm, reconstruct palmprint images from 4 intrinsic mode functions (IMFs), get rid of the remainder component from palmprint images to reduce the influence of low frequency signal, such as illumination. Divide reconstruct palmprint images into train set and test set, ICA II is performed on the train set of palmprint images.

MEEMD is performed on an original palmprint image(128×128), 4 IMFs(111×111) and a remainder(111×111) component can be gotten, as shown in Fig.1. we can see from Fig.1(i) that the reconstructed palmprint image get rid of the influence of illumination which act on the original palmprint image. Detail characteristics of palmprints in fig.1(i) are more prominent than in fig.1(a), and these characteristics are important information for recognition. The recognition algorithm with reconstruct palmprint images is as follow:

1. MEEMD is performed on the original palmprint images, then reconstruct palmprints with IMFs, as fig.1(i). Divide reconstructed palmprint images into train set and test set.
2. PCA is performed on the reconstructed palmprint images, the space of eigenvectors V will be gotten. The zero-mean images set D is projected into the space of eigenvectors V to get PCA coefficients R .
3. Reduce the dimensionality of PCA coefficients V , then input it into ICA to get basis vectors space.
4. Projecting the train set into the basis vectors space.
5. Projecting the test set into the basis vectors space, then matching and recognizing with appropriate algorithm, such as cosine, Euclidean, and so on.

5 Experimental Results

The experimental operating system is microsoft windows vista, with platform of Intel(R) Core(TM)2 Duo CPU(1.5GHZ), and 1014M RAM. The algorithm was programmed with MATLAB 7.0.

Our experiments make use of Hong Kong Polytechnic University (PolyU) palmprint database. This database contains 100 classes, with 6 images from each class. For each class, the first three images are used as training data while the remaining three are treated as testing data. The average interval between the training samples and the testing samples is two months. The resolution of the original palmprint images is 384×284 pixels, and the size of the region of interest (ROI) is 128×128 pixels. MEEMD is performed on the ROI, the reconstructed palmprint images with high frequency IMFs is 111×111 pixels. Each image is scaled to the size of 55×55 pixels to reduce the computational cost. Thus, the size of the training matrix is 300×3025 , and the testing matrix is also 300×3025 . The InfoMax algorithm is employed in ICA, and the cosine algorithm and the Euclidean algorithm are used in recognition, respectively. Contrastively, we experimented ICA II with original palmprint images. Each image is scaled to the size of 64×64 pixels, the size of the training set and the testing set is 300×4096 . The interval between the training samples and the testing samples is also two months.

The recognition rate of MEEMD-ICAII and ICA II with cosine algorithm is shown in fig.3. The number of basis images is in x , and the recognition rate is in y label.

The solid line displays the recognition rate of MEEMD-ICAII and the dot line displays the recognition rate of ICA II. The rising speed of MEEMD-ICAII is faster than ICA II while m is small. The maximum recognition rate of MEEMD-ICAII is

98.67%, while the maximum of ICA II is 98.34%. we can see from fig.1(i) and (a) that the reconstructed palmprints get rid of the influence of low frequency information, the high frequency information is employed thoroughly in recognition, so the recognition rate of MEEMD-ICAII is higher than ICA II.

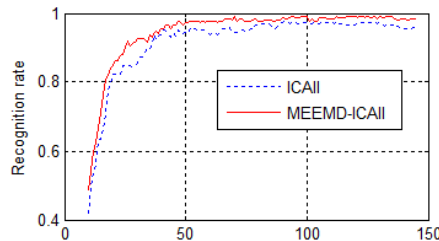


Fig. 3. The recognition rate of MEEMD-ICAII and ICA II with cosine algorithm. MEEMD-ICAII is solid while ICA II is dot.

Table 1 show the recognition rate of Euclidean and cosine distance, we can see that the conclusion in Euclidean is the same as in cosine algorithm, the recognition rate of MEEMD-ICAII is higher than ICA II. The recognition rate with cosine algorithm is higher than that in Euclidean algorithm.

Table 1. Recognition rate with cosine and Euclidean algorithm

	MEEMD-ICAII	ICA II
Euclidean	0.9400	0.9367
Cosine	0.9867	0.9834

Compressed reconstructed palmprint images are employed in MEEMD-ICAII, each with 55×55 pixels. Compressed palmprint images are also used in ICA II, each with 64×64 pixels. The cost of MEEMD-ICAII is smaller, so the speed is faster. Table 2 shows the testing time. When cosine algorithm is employed, the testing speed of MEEMD-ICAII is faster 28.10% than ICA II, and when Euclidean algorithm is employed, the testing speed of MEEMD-ICAII is faster 14.87% .

Table 2. Testing time of ICA (seconds)

	MEEMD-ICAII	ICA II
Euclidean	0.2286	0.2626
Cosine	0.5936	0.7604

6 Conclusions

In this paper, we proposed a new palmprint recognition algorithm with MEEMD and ICAII. The high frequency information of palmprints can be extracted with MEEMD,

so MEEMD is introduced into recognition. We reconstructed palmprint images with high frequency IMFs of MEEMD, and take these reconstructed palmprint images as the input of ICAII to finish the task of recognition. The results of experiments show that the recognition rate of MEEMD-ICAII is higher than ICA II, and the testing speed is also faster. The recognition rate of MEEMD-ICAII is higher than ICAII 0.34% in cosine, and 0.35% in Euclidean. The testing speed in MEEMD-ICAII is faster than ICA II 28.10% in cosine, and 14.87% in Euclidean.

Acknowledgements. This research was sponsored by the grants of Natural Science Foundation of China (No. 60970058), the grants of Natural Science Foundation of Jiangsu Province of Suzhou Vocational China (No.BK2009131).

References

- Panigrahy, S.K., Jena, D., Jena, S.K.: A Rotational and Translational-Invariant Palmprint Recognition System. In: First International Conference on Data Engineering and Management, ICDEM 2008, Bishop Heber College, Tiruchirapalli, pp. 380–383 (2008)
- Feng, G., Wu, Y.Q.: An Iris Recognition Algorithm Based on DCT and GLCM. In: Proceedings of the SPIE (S0277-786X). 7000, pp. 1–8 (2007)
- Chen, J., Theodore, S.R., Tian, J., Laine, A.F.: A Novel Registration Method for Retinal Images Based on Local Features. In: 30th Annual International Conference of the IEEE Engineering in Medicine and Biology Society, EMBS 2008, pp. 2242–2245. The University of British Columbia, Vancouver (2008)
- Karima, O., Ben, A.: 3D Face Recognition Using RICP and Geodesic Coupled Approach. In: IEEE International Multimedia Modeling, University of Nice Sophia Antipolis, France, pp. 390–400 (2009)
- Rabaoui, A., Lachiri, Z., Ellouze, N.: Using HMM-based Classifier Adapted to Background Noises with Improved Sounds Features for Audio Surveillance Application. International Journal of Signal Processing 5(1), 46–55 (2008)
- Ozaki, M., Adachi, Y., Ishii, N.: Writer Recognition by Means of Fuzzy Similarity Evaluation Function. In: 4th International Conference on Knowledge Based Intelligent Engineering Systems& Allied Tech2nologies, pp. 287–291 (2000)
- Fazekas, A.J., Burgess, K.S., Kesanakurti, P.R.: Multiple Multilocus DNA Barcodes from the Plastid Genome Discriminate Plant Species Equally Well. Proc. Natl. Acad. Sci. USA. 105(8), 2923–2928 (2008)
- Jia, W., Huang, D.S., Zhang, D.: Palmprint Verification Based on Robust Line Orientation Code. Pattern Recognition 41(5), 1504–1513 (2008)
- Satoshi, I., Koichi, I., Takafumi, A.: A Practical Palmprint Recognition Algorithm Using Phase Information. In: Proc of the19th International Conference on Pattern Recognition, pp. 1–4 (2008)
- Shang, L., Huang, D.S., Du, J.X., Zheng, C.H.: Palmprint Recognition Using FastICA Algorithm and Radial Basis Probabilistic Neural Network. Neurocomputing 69, 1782–1786 (2006)
- Wu, Z.H., Huang, N., Chen, X.Y.: The Multi-dimensional Ensemble Empirical Mode Decomposition Method. World Scientific 1(3), 339–372 (2009)

A Palmprint Classification Method Based on Finite Ridgelet Transformation and SVM

Wen-Jun Huai and Li Shang

Department of Electronic & Information Engineering, Suzhou Vocational University,
Suzhou 215104, Jiangsu, China
{hwj,s10930}@jssvc.edu.cn

Abstract. A multi-scale palm print classification method based on FRIT (finite ridgelet transform) and SVM (support vector machine) was proposed. First, palm image with preprocessing was decomposed by using FRIT. As a result, ridgelet coefficients in different scales and various angels were obtained. The important linear feature of palmprint was included in the low frequency coefficients of FRIT decomposition coefficients. After the decomposition coefficients were transformed into feature vectors, SVM was chosen as a classifier. These feature vectors were regarded as feature parameters of palm print and sent into SVM to training. Two kernel functions are used as a discriminant function. Finally, SVM trained was used for classification of palmprint. The experiments were performed in PolyU Palmprint Database. The results indicate that proposed method has better performance than wavelet with SVM method, and classification accuracy used RBF (radial basis function) as kernel is higher than the use of polynomial kernel function.

Keywords: Finite ridgelet transform (FRIT), Support vector machine (SVM), Palmprint classification.

1 Introduction

Biometric recognition technology has been paid more and more attention as a new method for identity authentication. Palmprint recognition has become a research hotspot due to the fact that palm is unique in many domestic and foreign researchers, the details are permanent, the information is rich and the collection of palm is convenient. In the palmprint identification process, the recognition rate is largely determined by the uniqueness and robustness of feature extracted. According to the analysis and description method of the palm, the feature extraction method can be classified into the following four categories: feature extraction based on structure [1], feature extraction based on the time-frequency analysis [2, 3], feature extraction based on statistics and feature extraction based on sub-space approach [4]. Zhang and shu proposed SLS method, using 12 templates to do line feature extraction. Then some sections of the straight line are used to approximate each line feature of palmprint, and finally to match the whole palmprint by matching these line segments [1]. But this approach ignores many of detailed information can be used to distinguish the palmprint, so that some palm of the structure similarity can not be distinguished

effectively. The typical feature extraction is a line feature extraction method for online palmprint images based on morphological median wavelet which proposed by Dai Qingyun, Yu Yinglin [5], the algorithm proposes to do nonlinear multi-resolution analysis to original image using morphological median wavelet, and then take one low-frequency component to do orientation template matching. It overcomes double-edge effect caused by edge extraction algorithm. As improved, ridgelet transform was proposed by E.Candès [6] and D.L.Donoho [7] professor. Ridgelet transform is a new kind of multi-scale analysis technique after Wavelet transform. Ridgelet get more sparse than the wavelet representation in some aspects of image processing. The palmprint recognition based on ridgelet transform was first proposed in Literature [8]. It used ridgelet transform and threshold method to extract palmprint feature information. Experiments in the PolyU Palmprint Database, obtained 95.25% recognition rate.

A multi-scale palmprint classification method based on FRIT and SVM was proposed. The image classification results show that the method can extract the palmprint features, and recognition accuracy is higher than classical Wavelet method in a large number of palmprint.

2 Basic Principle

2.1 Finite Ridgelet Transformation and the Converse

Suppose the image is composed of $p \times p$ matrix, p is a prime number. Defined set $Z_p = \{1, 1, \dots, p-1\}$, Z_p^2 is a finite region that generated by template p . Thus, the FRAT (finite radon transform) that a discrete picture on finite mesh, is defined as follow:

$$r_k[l] = FRAT(k, l) = p^{-1/2} \sum_{(i, j) \in L_{k,l}}^p f(i, j) \quad (1)$$

Where: $L_{k,l}$ representation a dot set in linear, it composed between slope k and intercede l on mesh Z_p^2 .

Transform by using FRAT for specific size of the discrete finite grid Z_p^2 , will produce a FRAT sequence in each direction, corresponding to a column of the output matrix. Then 1-D DWT (one-dimensional discrete wavelets transform) can be executed in each column of Radon coefficient. Finally, ridgelet coefficient matrix can be obtained. The whole process is called discrete FRIT [9].

Based on FRIT, we can obtain 2-D image of the main linear features. By the way of inverse transform on the ridgelet coefficient matrix. The inverse transformation of FRAT can be expressed as flow.

$$IFRAT(i, j) = FBP_r(i, j) - \frac{1}{p} \sum_{(i', j') \in Z_p^2} f(i', j') \quad (2)$$

Where: the minuend is an average of all pixel gray value on the original discrete finite mesh Z_p^2 , when it is zero, then $f(i,j) = FBP_r(i,j)$. FBP is finite back projection.

Therefore, every pixel on the original discrete finite mesh Z_p^2 should subtract the mean of pixel before making FRAT, as the pending discrete finite grid. Finally, using the result between the pixel value of FBP and the mean, image restoration can be done.

2.2 SVM Classification Algorithm

SVM has been used successfully in many object recognition applications [10, 11]. It uses linear model to implement nonlinear class boundaries through some nonlinear mapping the input vectors x into the high-dimensional feature space. The optimal separating hyperplane is determined by giving the largest margin of separation between different classes. For the two-class case, this optimal hyperplane bisects the shortest line between the convex hulls of the two classes. An optimal hyperplane is required to satisfy the following constrained minimization as

$$\min \{1/2 \|W\|^2\} \text{ with } y_i(W \cdot x_i + b) \geq 1, i = 1, 2, \dots, n. \quad (3)$$

Where n is the number of training sets.

For a linearly non-separable case, the above formula can be extended by introducing a regularization parameter C as the measurement of violation of the constraints as follows:

$$\max \left\{ \sum_{i=1}^n \lambda_i - \frac{1}{2} \sum_{i,j=1}^n \lambda_i \lambda_j y_i y_j (x_i \cdot x_j) \right\} \text{ with } \sum_{i=1}^n y_i \lambda_i = 0, 0 \leq \lambda_i \leq C, i = 1, 2, \dots, n. \quad (4)$$

Where, the λ_i are the Lagrangian multipliers and nonzero only for the support vectors. Thus, hyperplane parameters (w, b) and the classifier function $f(x; w, b)$ can be computed by optimization process. The decision function is obtained as follows:

$$f(x) = \operatorname{sgn} \left\{ \sum_{i=1}^n y_i \lambda_i (x_i \cdot x) + b \right\}. \quad (5)$$

A kernel can be used to perform this transformation and the dot product in a single step which provided the transformation can be replaced by an equivalent kernel function. This helps in reducing the computational load and at the same time retaining the effect of higher-dimensional transformation. There are usually some used kernels, such as polynomial, radial basis and sigmoid.

In this paper, one-to-many approach is used to finish the palm classify, which is converted to two kinds problems. There need to construct hyperplane between the first k classes and other $k-1$ classes. In this way, the system only need to build k classes SVM classifiers, each classifier will identify a class of data from other classes.

In order to construct SVM network, Firstly, we select someone's ten palmprints and ten other different people palm image. Secondly, these palmprints was divided into two groups, each group include five of the same palm prints and five different people palm. A group as training sample set, another group and other 110 palmprint images from database as a test sample set. So the test set contains 120 palmprint images.

3 Palmprint Recognition Based on FRIT and SVM

The algorithm based on FRIT and SVM is summarized below:

Step1: ROI (region of interest) extraction. The approach of extraction the area of ROI in palm refers to Shu Wei's ideas for training sample and test image. First, hand image should be binarization after grayscale variation. Second, contour extracting for hand image. Third, locate the key points, and establish the coordinate system by directional projection algorithm. Finally, select and divide the appropriate ROI regional. The size of palm is transformed into 128×128 .

Step2: Image preprocessing. The study sample image and test image should be geometric normalization and gray level normalization, the gray scale range of image is $[0, 1]$. To reduce the computational complexity, we divide the ROI region into 16 blocks.

Step3: Feature extraction. In this step, using FRIT to extract features for each sub-blocks of 16 training images respectively. First, we transform each block palm print, including training images and test images, into radon domain. Second, obtain the ridgelet transform coefficients by DWT [12].

Step4: Constitute feature vector. The low-frequency coefficients of FRIT contain much important information about palm line, which can be used as feature vectors to training and classification in SVM. The feature coefficients in the previous step combined to constitute feature vector. Coefficient matrix is the $l \times l$, the feature vector size is $1 \times l^2$.

Step5: Construction of k -class SVM, the number of support vector is l^2 .

Step6: To learn and train for k class SVM respectively. All transform coefficients matrix after learning samples will be input to the k classes SVM alone.

Step7: Palmprint classification test. The feature coefficients, obtained through FRIT from test image, be input to the trained SVM in proper order, the results can be obtained according to the output about palmprint classification.

4 Experimental Results

4.1 Data Preprocessing

This work is carried on the PolyU Palmprint Database in order to verify the effectiveness of the proposed method. The database includes 100 different palms, and each of these palms has twenty images. The samples for each palm were collected in two sessions, which means that the first ten samples were captured in one session and the other ten samples in another session. After preprocessing of palmprint image, we got the ROI region of some palms that size is 128×128 . Some of these are shown in fig.1.

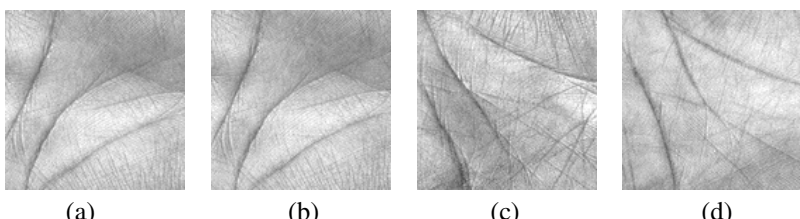


Fig. 1. Some samples after preprocessing. (a) and (b) from same palm. (c) and (d) from different people

After FRIT, some palm line features from one palm is shown in fig.2, which from different directions in training sample set.

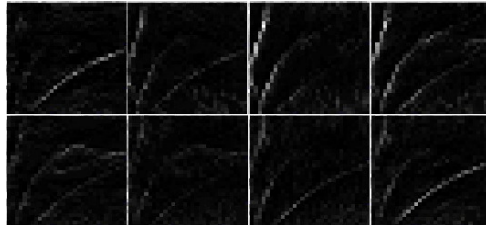


Fig. 2. Palm images formed by low-frequency coefficients in different directions

4.2 Palm Classification Performances

In finishing the classification mission, the features of palmprint were extracted well by using FRIT algorithm. The SVM was used to testing feature extraction method based on the kernel of RBF and polynomial function. For comparison, the features was obtained by using Wavelet algorithm has also been tested. The experiment results are shown in Table 1.

Table 1. The classification accuracy of FRIT + SVM and Wavelet + SVM

Methods	Kernel function	Testing samples	Correct number	Recognition rate (%)
FRIT + SVM	polynomial	120	111	92.5
	radial basis	120	115	95.83
Wavelet + SVM (Daubechies2)	polynomial	120	107	89.3
	radial basis	120	112	93.34

Regarding to Table 1, our proposed method has improved the palmprint recognition accuracy than using Wavelet with SVM. Classification results of the proposed method are slightly higher recognition accuracy than the latter, its best recognition rate can reach up to 95.83% that is only slightly above the result from ridgelet transform and threshold method to extract palmprint feature information [8], and only around to 93.34% using Wavelet which is almost close to 93.75% in literature [13]. Along with the increase of sample size and training, recognition rate will be more stable. Both polynomial and radial basis kernel were chosen as the discriminate function to train and classify in the experiment. SVM net with RBF kernel has higher accuracy than use polynomial kernel. It can be seen, RBF kernel is the better choice in SVM because of the given palm without priori knowledge.

Further analysis the data in fig.3, parameter σ has great effect on classification accuracy. It is found that, with the increase of σ , the classified accuracy increase obviously while it keeps almost constant when the value σ up to 20. For the test image with considerable variation in illumination, the proposed method can also correctly identify. Several palmprint images, which does not correctly identify, has too large

position deviation. It can consider to improve the palmprint preprocess algorithm to find all image with weak point as early as possible, further improve the classification accuracy.

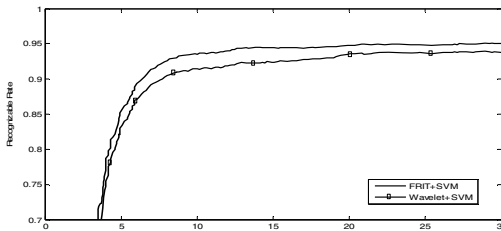


Fig. 3. Recognition rates for test sample set. σ is the width of RBF.

5 Conclusion and Future Work

In this paper, a novel method about palm classification is proposed which combines FRIT and SVM. We can see from the experiment that the proposed method has a good performance. According to the tests palm set which applied, the classification results of FRIT with SVM are better than Wavelet with SVM on palmprint classification, radial base kernel is used on SVM that has higher accuracy and stability than used polynomial kernel. The experimental results show that the feature information has a strong discriminate ability and still have potential to be improved. In the future work, we will investigate the classification method based on the fusion with other features in palm and the classifier optimization will be investigated as well.

Acknowledgments. The authors would like to express their sincere thanks to Biometric Research Center at the Hong Kong Polytechnic University for providing us the PolyU Palmprint Database. This work was supported by the grants of National Nature Science Foundation of Jiangsu Province of China (No. BK2009131), and Startup Foundation Research for Young Researchers of Suzhou vocational university (No. 2010SZDQ03).

References

1. Shu, W., Zhang, D.: Two Novel Characteristics in Palm-print Verification. *Datum point invariance. Pattern Recognition* 32, 691–702 (1999)
2. Zhang, D., Kong, W.K., You, J.: Online Palmprint Identification. *IEEE Tran. on Pattern Analysis And Machine Intelligence* 25, 1041–1050 (2003)
3. Han, C.C.: A Hand-based Personal Authentication Using A Coarse-to-fine Strategy. *Image and Vision Computing* 22, 909–918 (2004)
4. Su, X.S., Lin, X.R., Ding, T.H.: Palmprint Feature Extraction Based on Wavelet Transform. *Journal of Tsinghua University (Science and Technology)* 43, 1049–1055 (2003)
5. Dai, Q.Y., Yu, Y.L.: A Line Feature Extraction Method for Online Palmprint Images Based on Morphological Median Wavelet. *Journal of Computer* 26, 234–239 (2003)

6. Candes, E.J.: Harmonic Analysis of Neural Networks. *Applied and Computational Harmonic Analysis* 6, 197–218 (1999)
7. Donoho, D.L.: Orthonormal Ridgelets and Linear Singularities. *SIAM Journal on Mathematical Analysis* 31, 1062–1099 (2000)
8. Dong, K.F., Feng, G.Y., Hu, D.W.: Digital curvelet transform for palmprint recognition. In: Li, S.Z., Lai, J.-H., Tan, T., Feng, G.-C., Wang, Y. (eds.) *SINOBIOMETRICS 2004. LNCS*, vol. 3338, pp. 639–645. Springer, Heidelberg (2004)
9. Yuan, X.G., Zhang, A.: Ridgelet Transform and Its Application to Image Denoising. *Computer Engineering and Application* 40, 83–85 (2004)
10. Dumais, S.: Using SVMs for Text Categorization. *IEEE Intelligent Systems* 13, 21–23 (1998)
11. Pontil, M., Verri, A.: Support Vector Machines for 3D Object Recognition. *IEEE Trans. on Pattern Analysis & Machine Intelligence*. 20, 637–646 (1998)
12. Huai, W.J., Shang, L.: Palm line extraction using FRIT. In: Huang, D.-S., McGinnity, M., Heutte, L., Zhang, X.-P. (eds.) *ICIC 2010. CCIS*, vol. 93, pp. 499–506. Springer, Heidelberg (2010)
13. Xu, X.B., Zhang, D.Y., Zhang, X.M., Cao, Y.J.: Palmprint Recognition Based on Discrete Curvelet Transform and Support Vector Machine. *J. Infrared Millim. Wave*. 28, 456–460 (2009)

Palmprint Recognition Based on Two-Dimensional Gabor Wavelet Transform and Two-Dimensional Principal Component Analysis

Yu Zhang¹, Mei-Xing Qi², and Li Shang¹

¹ Depart of Electronic information engineering, Suzhou Vocational University, Suzhou International Educational Park, Road 106, Zheneng Dadao, Suzhou 215104, Jiangsu, China
Zhixin331@163.com

² Department of Mechanical Engineering, Suzhou Industrial Park Institute of Vocational Technology, 68 Sugian Road , Suzhou Industrial Park,Suzhou 215021, Jiangsu, China
qimeixing@163.com

Abstract. A method of palmprint recognition based on Two-Dimensional Gabor(2DGabor) Wavelet Transform and Two-Dimensional Principal Component Analysis(2DPCA) is proposed. This method firstly carries out 2DGabor wavelet transform for the palmprint image, so that the amplitude of the filtered image can be used as the eigenvector for the palmprint image. And the 2DPCA is used to decrease the dimension of the eigenvector, and the nearest neighbor classifier is employed for palmprint classification.Finally, simulation experiment to compare the method of palmprint recognition based on 2DGabor wavelet and 2DPCA with the method based on Gabor wavelet and PCA is conducted with the assistance of the palmprint image database provided by Hongkong Polytechnic University. The experiment shows that the palmprint recognition method based on 2DGabor wavelet transform and 2DPCA is more effective.

Keywords: Two-Dimensional Gabor Wavelet Transform, Two-Dimensional Principal Component Analysis, eigenvector, The nearest neighbor classifier, Palmprint recognition.

1 Introduction

Palmprint recognition method is one of the biometrics identification technologies. This method uses computers to analyse the image of palmprint,extract useful recognition information and identify palmprint automatically.Characterized with simple sampling, rich images, high customer acceptability, this method has become one of the most potential biometrics identification technologies.

Feature extraction is a basic and important part of palmprint recognition technology.2DGabor wavelet is multi-scale and directional, and has favorable capacity in distinguishing the signal in the time domain and frequency domain [1].

But using the 2DGabor wavelet to express images will result in higher dimensions of the metrixes.To solve this problem, the dimensions of the matrixes need to be reduced.

2DPCA directly uses matrixes to calculate covariance matrix and can get relatively small covariance[2].Therefore, this article puts forward a palmprint recognition method which combines the 2DGabor wavelet and 2DPCA method, and has proved the effectiveness of this method with experiments.

2 Feature Extracting of Palmprint Images Based on 2DGabor Wavelet

2.1 2DGabor Filter Function

2DGabor filter function can be in the form of[3]:

$$\psi_j(\bar{x}) = \frac{\|\bar{k}_j\|^2}{\sigma^2} \exp\left(-\frac{\|\bar{k}_j\|^2 \|\bar{x}\|^2}{2\sigma^2}\right) (\exp(i\bar{k}_j \bar{x}) - \exp(-\frac{\sigma^2}{2})) \quad (1)$$

$$\bar{k}_j = \begin{pmatrix} k_{jx} \\ k_{jy} \end{pmatrix} = \begin{pmatrix} k_v \cos \varphi_u \\ k_v \sin \varphi_u \end{pmatrix} \quad (2)$$

In the above formula, \bar{x} is the image coordinate with a given position; \bar{k}_j is the centre frequency of the filter; φ_u represents the directional selectivity of the filter; $\|\bullet\|$ represents modular arithmetic. In natural images.

It can be seen from formula (1) that the 2DGabor wavelet is a set of filters generated through stretching and revolving the scale of the 2DGabor filter.To sample the entire frequency domain of a image, Gabor filter with multiple central frequencies and directions can be used to describe the image.

The different choice of parameter k_v or φ_u respectively represents the sampling method of 2DGabor wavelet in the frequency domain and directional space. Parameter σ determines the bandwidth of the filter. The experiment of Lades[3] indicates that for images with the scale of 128×128 , the best experimental effect can be attained when the maximum central frequency of the filter is $\frac{\pi}{2}$ and its bandwidth is half of its frequency interval.

As the texture of the image is randomly distributed, the real numeric range of φ_u is from 0 to 2π . Considering the symmetry of the Gabor filter, the real numeric of φ_u ranges from 0 to π . To effectively describe the local features of the palmprint image, this article uses 20 Gabor filters k_j composed of 5 central frequencies and 4 directions to express the palmprint image. The numerical values of k_v and φ_u are as the follows:

$$k_v = 2^{\frac{v+2}{2}} \pi, \varphi_u = \mu \frac{\pi}{4} \quad (3)$$

In the formula, $v = 0, \dots, 4$, $\mu = 0, \dots, 3$, $j = \mu + 4v$.

2.2 Feature Extraction of Palmpoint with 2DGabor Method

Evaluate the convolution of the palmpoint images with the 2DGabor filter. After preprocessing, the palmpoint image is $I(\bar{x})$ with a scale of 128×128 . The filtered result is:

$$O_j(\bar{x}) = I(\bar{x}) * \psi_j(\bar{x}) \quad (4)$$

The amplitude of the filtered palmpoint image is served as the feature vector of the image:

$$S = \left\{ O_j : j = \mu + 4v, v \in \{0, \dots, 4\}, \mu \in \{0, \dots, 3\} \right\} \quad (5)$$

In order to reduce the dimension of the extracted features, the formula $\rho = 64$ (8×8) is used to sample the eigenvector. $S = \left\{ O_j^{(\rho)} \right\}$, Transform $|O_j|^{(\rho)}$ into column vector, S becomes 256×20 and is used to express the features of the palmpoint image.

3 The Dimension Reduction of 2DPCA[4]

3.1 Calculation of 2DPCA

The main calculating process of 2DPCA[2] is: suppose x is an n-dimensional normalized vector, A is a $m \times n$ image matrix, then the image matrix can be directly projected on X . Thus we can get a m-dimensional projected column vector $Y = AX$, which is the projection feature column vector of image A . This paper introduces the method of using the overall dispersion of the training samples to measure the judgement of X towards the samples. The overall dispersion of the projected samples can be described by the trace of the eigenvector covariance matrix. The following standard of judgement can be applied:

$$J(X) = \text{tr}(S_x) \quad (6)$$

In this formula, S_x represents the covariance matrix of the projected eigenvector of the training sample. The physical significance of finding out the maximum among the judgement standards is to find out the projection direction X which involves all samples. This can maximize the overall dispersion of the projected samples. Covariance matrix S_x can be expressed as:

$$\begin{aligned} S_x &= E(Y - EY)(Y - EY)^T = E[AX - E(AX)][AX - E(AX)]^T \\ &= E[(A - EA)X][(A - EA)X]^T \end{aligned} \quad (7)$$

To simplify, G_t is defined as:

$$G_t = E[(A - EA)^T(A - EA)] \quad (8)$$

Matrix G_t is the covariance matrix. According to the above definition of G_t , it is easy to prove that G_t is a positive definite matrix. G_t can be directly calculated from the original training image matrix.

3.2 Dimension Reduction of the Features

Suppose there are M palmprint images A_j (j is the integer from 1 to M) in the training set, each with the scale of $m \times n$. The average image of the training samples is represented by \bar{A} , $\bar{A} = \frac{1}{M} \sum_{j=1}^M A_j$. Therefore, G_t can be defined as:

$$G_t = \frac{1}{M} \sum_{j=1}^M [(A_j - \bar{A})^T(A_j - \bar{A})] \quad (9)$$

The standard of judgement can be written as:

$$J(X) = X^T G_t X \quad (10)$$

In the above formula, X is an n -dimensional normalized column vector. The linear vector X which maximizes the criteria $J(X)$ is called the optimal projection axis, namely the eigenvector that corresponds to the maximum feature value of G_t .

Normally, the d largest orthogonal eigenvectors $\{X_1, X_2, \dots, X_d\}$ are selected as the optimal projection axis:

$$\begin{cases} \{X_1, X_2, \dots, X_d\} = \arg \max J(X) \\ X_i^T X_j = 0, i \neq j, i, j = 1, 2, \dots, d \end{cases} \quad (11)$$

$d < n$. Suppose $y_k = AX_k$, $k = 1, 2, \dots, d$, y_1, y_2, \dots, y_d are called the main component vectors of A of the given palmpoint image. After projecting on the optimal projection axis, an $m \times d$ matrix is obtained. $Y = [y_1, y_2, \dots, y_d] = A[X_1, X_2, \dots, X_d]$ is the feature matrix of image A .

4 Nearest Neighbour Classifier

Nearest neighbour classifier[5] is one of the most important nonparametric pattern recognition methods. The basic rules are:

Suppose there are C categories of the pattern recognition problems: w_1, w_2, \dots, w_c , each category has N_i samples which indicate its category, w_i categories of discrimination functions can be made:

$g_i(x) = \min \|x - x_i^k\|$, $k = 1, 2, \dots, N_i$, x_i^k indicates there are $k = 1, 2, \dots, N_i$ samples in category i ($i = 1, 2, \dots, c$) $k = 1, 2, \dots, N_i$. If $g_i(x) = \min g_i(x), i = 1, 2, \dots, c$, $x \in w_j$.

The Euclidean distance between the feature matrixes $Y_i = [y_1^{(i)}, y_2^{(i)}, \dots, y_d^{(i)}]$ and $Y_j = [y_1^{(j)}, y_2^{(j)}, \dots, y_d^{(j)}]$ can be defined as:

$$d(Y_i, Y_j) = \sum_{k=1}^d \|y_k^{(i)} - y_k^{(j)}\|^2 \quad (12)$$

$y_k^{(i)}$ represents the k th pivot element of the feature matrix Y_i , $\|y_k^{(i)} - y_k^{(j)}\|^2$

represents the Euclidean distance between the vectors of pivot elements $y_k^{(i)}$ and $y_k^{(j)}$. Suppose the training samples are Y_1, Y_2, \dots, Y_M , each sample belongs to a given

category w_k , testing sample is Y , if $d(Y_i, Y_j) = \min\{d(Y_i, Y_j) | j = 1, 2, \dots, M\}$ and $Y_j \in w_k$, then $Y \in w_k$.

5 Simulation Experiment

The experiment uses the palmprint image database provided by the Hongkong Polytechnic University. The database includes 100 persons, each palmprint image has the pixel of 128×128. There are 600 images, 6 images per person. In the experiment, the first 1 (2, 3, 4, 5) images of each person are taken out to constitute 100(200,300,400,500) training sample set of the palmprint images, and the rest 500(400,300,200,100) sample images are used for tests. The experimental results of comparing the method of 2DGabor+2DPCA and Gabor+PCA are shown in the following table1.

Table 1. Recognition rate of two calculation methods with different numbers of training samples

Numbers of training samples	1	2	3	4	5
2DGabor+2DPCA	97.28	97.20	97.60	98.20	98.90
Gabor+PCA	96.04	96.15	96.06	97.50	98.00

As can be seen in table1, with different numbers of training samples, the correct recognition rates of the method of 2DGabor+2DPCA are all higher than the method of Gabor+PCA.

The experiment also compares the correct recognition rate with different lengths of different eigenvectors of the two methods. The results are shown in table2.

Table 2. The recognition rate with different eigenvector lengths of the two calculating methods

Length of the vector	15	25	35	45	55
2DGabor+2DPCA	95.65	96.98	97.99	98.88	98.92
Gabor+PCA	94.95	95.30	96.59	97.21	98.10

As can be seen from table2, as the length of the eigenvectors grows, the recognition rate improves. The recognition rates of the method of 2DGabor+2DPCA are slightly better than the method of Gabor+PCA in all lengths.

6 Conclusion

This paper combines the method of 2DGabor wavelet and 2DPCA to recognize palmpint images. The simulation results show that in different sampling numbers, the recognition rate improves as the length of the vectors increases. Moreover, the recognition rate of both methods are slightly improved in different vectors with different lengths. Therefore, the combined method of palmpint recognition proposed by this paper is proved to be effective through experiments.

Acknowledgments. This work was supported by the grants of National Nature Science Foundation of Jiangsu Province of China (No. BK2009131).

References

1. Li, F., Chen, T.: Wavelet Conversion Method Used in the Feature Analysis of the Model of Visual Cortex Simple Cells. *Journal of Mathematical Medicine* 21, 134–136 (2008)
2. Yang, J., Zhang, D.: Two-Dimensional PCA: A New Approach to Appearance-Based Face Representation and Recognition. *IEEE transactions on pattern analysis and machine intelligence* 26, 131–137 (2004)
3. Lades, M., Vorbruggen, J.C., Buhmann, J.: Distortion Invariant Object Recognition in the Dynamic Link Architecture. *IEEE Transactions on Computers* 42, 300–311 (1993)
4. Wu, Q., Zhou, X.: A Face Recognition Method Based on 2DDWT and 2DPCA. *Computer Application* 26, 2089–2091 (2006)
5. Rao, X., Yang, S.: Nearest Neighbour Classifier of the Nucleus and Its Simulation. *System Engineering and Electronic Technique* 29, 470–472 (2007)

Recognition Based on Fusion of Gait, Ear and Face Features Using KPCA Method

Rohit Katiyar¹ and Vinay Kumar Pathak²

¹ Teacher Fellow, CSE Deptt, HBTI, Kanpur

rohit.katiyar@rediffmail.com

² Vice Chancellor, Uttarakhand Open University, Haldwani

vinaypathakhbt@gmail.com

Abstract. In this paper, a simple multimodal biometrics recognition system having three modalities i.e. Gait, Ear and Face is used and for different biometric traits features Kernel Principal Component method is used for fusion. Because of these biometric traits, our proposed method requires no significant user co-operation and also work from a long distance. The method has been successfully tested on 300 images corresponding to 30 subjects from three databases including ORL face database, USTB ear database and CASIA gait database. The experimental results exhibit excellent recognition performance than Gait, Ear and Face unimodal biometric recognition. As, the every database contain the data of different persons so we can use them only for testing for the given subject.

Keywords: Multimodal Biometrics, Gait Biometrics, Ear Biometrics, Face biometrics, Kernel PCA.

1 Introduction

In today's scenario multimodal biometrics is becoming a hot research topic in biometric area. As any unimodal biometric may not be acceptable to a particular group or situation in the case of any personal identity authentication system so, somehow multimodal biometrics technology is used to alleviate the problem's intrinsic to unimodal biometrics systems. Multimodal biometric systems are expected to be more reliable due to the presence of multiple pieces of evidence and also able to meet the stringent performance requirements imposed by various applications. By asking the user to present a random subset of biometric traits, the system ensures that a live-user is indeed present at the point of acquisition. However, an integration scheme is required to fuse the information presented by the individual modalities. In additional, multimodal biometric system takes more than one single feature into account [1, 2]. This helps in identifying and verifying the person with more accuracy even if one of the features gives less matching scores [3]. In a multimodal biometric system that uses different biometric modalities, different fusion levels are possible: fusion at feature extraction level, fusion at matching score level or fusion at decision level. Fusion at feature extraction level is difficult because feature vectors which are

used by different biometric traits may be inaccessible or incompatible. Hence, due to easily accessing and easily integrating, fusion at matching score level are generally preferred.

In this paper, multimodal biometric identification system which is based on features extracted from three biometrics modalities including face, ear and gait using Kernel Principal Component Analysis method is proposed. The main reason of using these three biometric traits is that, our system requires no significant user co-operation and also because of the gait biometric feature, our system can work from a long distance. In this method, the fusion of the unimodal systems into a multimodal one has been carried out at a matching score level and the decision of the multi modal system will come from the fusion of the different unimodal scores. We applied our proposed method on the face images from ORL face database [4] and ear images from USTB ear database [5] and gait silhouette images from CASIA Gait Database [6]. The rest of the paper is organized as follows. Section 2 describes the feature extraction and fusion method based on KPCA and applies it to the fusion feature extraction and classification experiments and Section 4 draws a conclusion.

2 Feature Fusion Method Based on KPCA

A. Fusion Method of Kernel Matrices

The block diagram of multimodal biometrics system is given in fig.1 through which you can see that how multiple biometrics traits are combined and features taken from different traits are fused and combined into one feature vector. Given training samples of gait $\{x_i\}$, ear $\{y_i\}$ and face $\{z_i\}$, map them into a high-dimensional feature space F respectively via $\Phi_x(\cdot)$, $\Phi_y(\cdot)$ and $\Phi_z(\cdot)$. With kernel method, we can acquire the corresponding kernel matrices of gait, ear and face as follows:

$$(K_x)_{ij} = k_x (x_i, x_j) \quad (1)$$

$$(K_y)_{ij} = k_y (y_i, y_j) \quad (2)$$

$$(K_z)_{ij} = k_z (z_i, z_j) \quad (3)$$

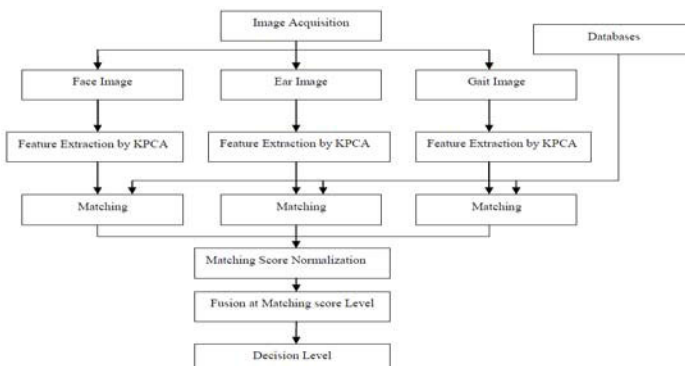


Fig. 1. Block-diagram of the multimodal biometric system based on matching score fusion

By using the idea of decision level fusion, we present the multiple classifier fusion as feature fusion rule. According to the decision template method proposed by Kuncheva et al. [7], the matrices could be fused reasonably. So we define the following fusion rules in our fusion feature extraction method based on KPCA. Fusing K_x of gait, K_y of ear and K_z of face with different rules:

Product rule:

$$(K_{f-prd})_{ij} = (K_x)_{ij} \cdot (K_y)_{ij} \cdot (K_z)_{ij} \quad (4)$$

Average rule:

$$(K_{f-avg})_{ij} = ((K_x)_{ij} + (K_y)_{ij} + (K_z)_{ij})/3 \quad (5)$$

Weighted-sum rule:

For Average rule, considering the different weights of different features, we present the weighted-sum rule as follows:

$$(K_{f-wsum})_{ij} = \alpha(K_x)_{ij} + \beta(K_y)_{ij} + \gamma(K_z)_{ij} \quad (6)$$

Where $\alpha + \beta + \gamma = 1$

After fusing the kernel matrices by different rule, the new kernel matrix K_f for fusion could be got. K_f is the correlation matrix of samples in high dimensional space F .

Then we can prove the kernel matrices acquired with different fusion rules are still valid kernel.

According to the definition of Mercer kernel, we have

$$\sum_{i,j=1}^n C_i C_j K_x(x_i, x_j) \geq 0, \quad \forall C_i \in R \quad (7)$$

$$\sum_{i,j=1}^n C_i C_j K_y(y_i, y_j) \geq 0, \quad \forall C_i \in R \quad (8)$$

$$\sum_{i,j=1}^n C_i C_j K_z(z_i, z_j) \geq 0, \quad \forall C_i \in R \quad (9)$$

The kernel matrix K_f after fusion is named as $K_r(r_i, r_j)$.

For Average rule, we have

$$\sum_{i,j=1}^n C_i C_j K_r(r_i, r_j) = \sum_{i,j=1}^n C_i C_j (K_x(x_i, x_j) + K_y(y_i, y_j) + K_z(z_i, z_j))/3 \geq 0 \quad (10)$$

So K_{f-avg} is still a positive definite matrix.

For Average rule, we define $K = K_x \otimes K_y \otimes K_z$ is the tensor product of K_x , K_y and K_z . K_r is the main sub-matrix of K . So $\forall C_i \in R$, such that

$$\sum_{i,j=1}^n C_i C_j K_r(r_i, r_j) \geq 0 \quad (11)$$

So, K_{f-prd} is still a positive definite matrix.

For weighted-sum rule, we have

$$\begin{aligned} \sum_{i,j=1}^n C_i C_j K_r(r_i, r_j) &= \sum_{i,j=1}^n C_i C_j (\alpha K_x(x_i, x_j) + \beta K_y(y_i, y_j) + \gamma K_z(z_i, z_j)) \\ &= \alpha \sum_{i,j=1}^n C_i C_j K_x(x_i, x_j) + \beta \sum_{i,j=1}^n C_i C_j K_y(y_i, y_j) + \gamma \sum_{i,j=1}^n C_i C_j K_z(z_i, z_j) \geq 0 \end{aligned} \quad (12)$$

So, $K_{f\text{-wsum}}$ is still a positive definite matrix.

B. KPCA Algorithm

Kernel principal component analysis algorithm has been proposed by Scholkopf [8] in 1998. It is the combination of kernel projection and PCA dimension reduction method.

The PCA linear transformation is based on second order statistics, which is commonly used due to their simplicity in manipulation. With second order methods, a representation with minimum reconstruction error of the data is found using the information contained in the covariance matrix of the data. It is assumed that all the information of Gaussian variables (zero mean) is contained in the covariance matrix.

However, most data sets such as face images are characterized by non-Gaussian and high order features. Therefore higher order methods are required to provide meaningful representations of these data. KPCA provides a good way to find the optimal projection direction of image in a high-dimensional feature space of the input data.

Define a nonlinear mapping ϕ . Firstly, the samples x_i are mapped into a high dimensional feature space F via ϕ considering the zero-mean training samples x , which the number of the samples is M , the covariance matrix of the projected data in the high-dimensional feature space F can be written as:

$$C^\phi = \frac{1}{M} \sum_{i=1}^M \phi(x_i) \phi(x_i)^T \quad (13)$$

According to the idea of PCA, our goal is to find an eigenvector v such that

$$\lambda v = C^\phi v \quad (14)$$

Since

$$\lambda v = C^\phi v = \frac{1}{M} \sum_{i=1}^M (\phi(x_i) \cdot v) \phi(x_i) \quad (15)$$

all the eigenvectors v correspond to the eigenvalues λ exist in the spanning space of $\phi(x_i)$ ($i = 1, 2, \dots, M$) This means

$$\lambda (\phi(x_i) \cdot v) = (\phi(x_i) \cdot C^\phi v), \quad i=1, \dots, M \quad (16)$$

And there exist α_i ($i = 1, 2, \dots, M$) such that

$$v = \sum_{i=1}^M \alpha_i \phi(x_i) \quad (17)$$

According to the two equations above, we have

$$\lambda \sum_{j=1}^M \alpha_i (\phi(x_i) \cdot \phi(x_j)) = \frac{1}{M} \sum_{j=1}^M \alpha_j \sum_{k=1}^M (\phi(x_i) \cdot \phi(x_k)) (\phi(x_k) \cdot \phi(x_j)) \quad (18)$$

($i = 1, 2, \dots, M$)

Defined a $M \times M$ matrix

$$K = (K_{ij})_{M \times M} \text{ Where } K = (\phi(x_i) \cdot \phi(x_j)) \text{ and } \alpha = (\alpha_1, \dots, \alpha_M)^T.$$

The eq.(18) can be simplified as

$$M\lambda K\alpha = K^2\alpha \quad (19)$$

To find the solution of eq. (19), It is sufficient to solve the eigenvalues problem:

$$M\lambda\alpha = K\alpha \quad (20)$$

Suppose the eigenvalues of K are $\lambda_1 \geq \lambda_2 \geq \dots \geq \lambda_M$ the corresponding eigenvectors are $\alpha_1, \alpha_2, \dots, \alpha_M$. After discarding the eigenvectors correspond to the zero eigenvalues, the remaining eigenvectors correspond to the non-zero eigenvalues must to be normalized so that the following equation is satisfied in the feature space R^F .

$$(\alpha_k \cdot \alpha_k) = 1, k = 1, \dots, M \quad (21)$$

According to eq.(17), the equation can be written as :

$$\begin{aligned} 1 &= \sum_{i=1}^M \sum_{j=1}^M \alpha_i^k \alpha_j^k (\phi(x_i) \cdot \phi(x_j)) = (\alpha^k \cdot K \alpha^k) = \lambda_k (\alpha^k \cdot \alpha^k), k \\ &= 1, 2, \dots, m \end{aligned} \quad (22)$$

That is, the eigenvector α^k need satisfy.

$$(\alpha^k \cdot \alpha^k) = \frac{1}{\lambda_k}, k = 1, \dots, m \quad (23)$$

To carry out the feature measurement, we need to implement projection twice for the original samples. The first projection is mapping the samples into the high-dimensional feature space, that is:

$$\phi = x \in R^n \rightarrow \phi(x) \in R^F \quad F > N$$

The second one is mapping the high dimensional samples on the principal components in the feature space, that is:

$$(v_k, \phi(x)) = \sum_{i=1}^M \alpha_i^k (\phi(x_i) \cdot \phi(x)) \quad k = 1, 2, \dots, m$$

We can substitute the computation of $(\phi(x) \cdot \phi(y) \cdot \phi(z))$ in the high dimensional space by kernel function as follows according to the kernel theory.

$$k(x, y, z) = (\phi(x) \cdot \phi(y) \cdot \phi(z))$$

Thus we can use the kernel trick to find the kernel matrix K we need not carry out the first mapping $\phi(\cdot)$, finally, we should discuss the Centering problem of the high-dimensional projection. So far we have ignored one detail for the sake of simplicity. While in general case $\phi(x_i)$ dose not satisfy the assumption that $\phi(x_i)$ are centered in R^F , the kernel matrix need to be modified. When computing

$C^\emptyset = \frac{1}{M} \sum_{i=1}^M \emptyset(x_i) \emptyset(x_i)^T$, $\phi(x_i)$, are substituted by $\tilde{\emptyset}(x_i) \phi(x_i) - \frac{1}{M} \sum_{i=1}^M \emptyset(x_k)$ and we can get

$$\begin{aligned}\tilde{K}_{i,j} &= (\tilde{\emptyset}(x_i) \cdot \tilde{\emptyset}(x_j)) = \left(\left(\phi(x_i) - \frac{1}{M} \sum_{k=1}^M \emptyset(x_k) \right) \cdot \left(\phi(x_j) - \frac{1}{M} \sum_{l=1}^M \emptyset(x_l) \right) \right) \\ &= K_{ij} - \frac{1}{M} \sum_{k=1}^M K_{kj} - \frac{1}{M} \sum_{l=1}^M K_{il} + \frac{1}{M^2} \sum_{k=1}^M \sum_{l=1}^M K_{kl}\end{aligned}\quad (24)$$

that is,

$$\tilde{K} = (\tilde{K}_{ij})_{M \times M} = K - I_M K - K I_M + I_M K I_M \quad (25)$$

Where $(I_M)_{ij} = \frac{1}{M}$ ($i, j = 1, 2, \dots, M$).

C. Feature Fusion Method Based on KPCA

The principal components of K_f span the gait, ear and face fusion feature space, namely gait plus ear-plus-face space. We centralize K_f through equation (25) and acquire . Then solve the eigenvalues problem $m\tilde{\lambda}\tilde{\alpha} = \tilde{K}_{fusion}$ discussed before. After the training stage, the final fusion feature vectors $\tilde{w}^k \cdot \phi(t) = \tilde{\alpha}$ can be calculated, by using the feature fusion rule and the algorithm of Kernel PCA, all the probe and gallery samples are projected in the gait-plus-ear-plus-face space to extract gait-ear-plus-face features for classification and recognition.

We summarize our fusion feature extraction method based on KPCA in multimodal biometrics as follows:

1. Computing the kernel matrices K_x , K_y and K_z of x , y and z respectively with equation (1), (2) and (3).
2. Computing the fusion matrix K_f via different fusion rule;
3. Centralizing the fusion K_f through equation (25) and getting.
4. Solve $m\tilde{\lambda}\tilde{\alpha} = \tilde{K}_f \tilde{\alpha}$, getting the eigenvalues of and the corresponding eigenvectors, and extracting the principal components $\tilde{\alpha}^k$. ($k = p, \dots, m$);
5. For the input samples, computing the projection to the eigenvectors \tilde{w}^k ($k = p, \dots, m$) and forming the fusion feature vector $\tilde{w}^k \cdot \phi(t) = \tilde{\alpha} K_f$.

3 Experiments and Results

Before performing multimodal recognition based on fusion of gait, ear and face, input images should be preprocessed and normalized. Firstly the video sequences of gait databases are interpret as the silhouette then we calculate the MGEI corresponding to all those silhouette images then pure ear images in the profile face images are cropped. Both ear and profile face images are filtered with Wiener filtering to

emphasize the features. Then the ear images are transformed into the size of 40×25 pixels, and the profile face images are into the size of 100×100 pixels. Here the proportion of normalized scales is decided by the image area proportion between ear and profile face. Finally, the redistribution of intensity values of the images is carried out using histogram equalization, thereby producing an image with equally distributed intensity value.



Fig. 2. Multimodal image example of ear and face from different angles

For unimodal biometrics of gait, ear or profile face, we apply KFDA to extract the discriminant features. For feature-level fusion of multimodal biometrics based on gait, ear and profile face, we apply the feature-level fusion method based KFDA with Average rule, Product rule and Weighted-sum rule respectively.

Typical kernels include polynomial kernel $(x_i, x_j)^d$, sigmoid kernel $(a(x_i, x_j) + b)$ and Gaussian kernel $\exp(-\|x - y\|^2 / \sigma^2)$, all of which satisfy Mercer's theorem. The choice of kernel is always decided by experiment. Here, we have adopted Gaussian kernel for gait, ear and face feature extraction in our system and the kernel parameter σ is set to a 10000.

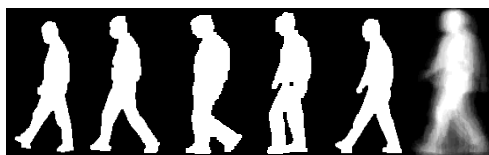


Fig. 3. MGEI of the corresponding Silhouette images

From previous research work we know that 84.69% persons are correctly recognized by gait, 90.08% persons are correctly recognized by ear and 92.19% persons are correctly recognized by face, respectively. For the feature fusion method, the best performance is achieved by the Weighted-sum rule at 94.52% accuracy. The Average rule obtain recognition rate at 93.88% and the Product rule obtain recognition rate at 93.25%. The experimental results show that the recognition rate of multimodal recognition based on fusion of gait, ear and profile face is higher than that of the recognition adopting the unimodality. Moreover, comparing the different feature fusion rule, the Weighted-sum rule got the best performance, and Average rule and Product rule follow it. The result testifies that the method is efficient for feature fusion and could get better fusion feature description.

4 Conclusion

In this paper a new method of feature fusion method based on kernel principle component analysis is proposed and applied to multimodal biometrics based on fusion of gait, ear and face. The experimental results show that the method is efficient for fusion feature extraction, and the multimodal recognition based on gait, ear and profile face performs better than gait, ear or profile face unimodal biometric recognition and expands the recognition range. The work provides a new effective approach of non-intrusive biometric recognition. But still a lot is remaining to do as the whole approach is assumed on indoor conditions. So, for outdoor environment where multiple subjects are there this algorithm did not perform well and we are looking towards some alternative approach.

References

1. Jain, A.K., Hong, L., Pankanti, S.: Can Multibiometrics Improve Performance? In: Proc. AutoID 1999, Summit, NJ, USA, pp. 59–64 (1999)
2. Jain, A.K., Hong, L., Kulkarni, Y.: Amultimodal Biometric System Using Fingerprint, Face and Speech. In: Second Internat. Con. on AVBPA, Washington, DC, USA, pp. 182–187 (1999)
3. Xu, L., Kryzak, A., et al.: Ethods of Combining Multiple Classifiers and Their Application to Handwriting Recognition. IEEE Trans. on Systems, Man and Cybernetics 22(3), 418–435 (1992)
4. Samaria, F., Harter, A.: Parameterisation of a Stochastic Model for Human Face Identification. In: Proc. of the 2nd IEEE Workshop on App. of Com. Vision, USA (1994)
5. Li, Y., Mu, Z., Xu, Z.: Using Ear Biometrics for Personal Recognition. In: Li, S.Z., Sun, Z., Tan, T., Pankanti, S., Chollet, G., Zhang, D. (eds.) IWBRS 2005. LNCS, vol. 3781, pp. 221–228. Springer, Heidelberg (2005)
6. Chinese Academy of Sciences, Institute of Automation Gait Database,
<http://www.sinobiometrics.com/>
7. Kuncheva, L.I., Vezdek, J.C., Duin, R.P.W.: Decision Templates for Multiple Classifier Fusion: An Experimental Comparison. Pattern Recognition 34, 299–314 (2001)
8. Scholkopf, B., Smola, A., Muller, K.: Nonlinear Component Analysis as a Kernel Eigenvalue Problem. Neural Computation 10(5), 1299–1319 (1998)

Face Recognition Using KFDA-LLE

Guoqiang Wang and Guoqiang Ding

Department of Computer and Information Engineering, Luoyang Institute of Science and Technology, 471023 Luoyang, Henan, P.R. China
`{wgq2211, ding}@163.com`

Abstract. Locally Linear Embedding (LLE) is a recently proposed algorithm for non-linear dimensionality reduction and manifold learning. However, since LLE aims to discover the intrinsical low dimensional variables from high dimensional nonlinear data, it may not be optimal for classification problem. In this paper, an improved version of LLE, namely KFDA-LLE, is proposed using kernel Fisher discriminant analysis (KFDA) method for face recognition task. First, the input training samples are projected into the low-dimensional space by LLE. Then KFDA is introduced for finding the optimal projection direction. Experimental results on face database demonstrate that the proposed method excels the other methods.

Keywords: Face Recognition, Manifold learning, Locally Linear Embedding, Kernel Fisher Discriminant Analysis (KFDA).

1 Introduction

Over the past two decades, face recognition has become an active research topic in computer vision and pattern recognition, owing to its wide and potential application in many areas such as information security, surveillance, and human-computer interaction [1]. And much progress has been made in the past few years. Since the 1990s, subspace-based face recognition has been extensively studied, and many algorithms have been proposed. Among them, eigenface and fisherface are the most popular algorithms, the underlying ideas of which are principal component analysis (PCA) [2] and linear discriminant analysis (LDA) [3] respectively. However, recently, a number of research efforts have shown that the face images possibly reside in a nonlinear submanifold. But both PCA and LDA effectively see only the Euclidean structure. They fail to discover the underlying structure, if the face images lie on a nonlinear submanifold hidden in the image space. Some nonlinear techniques have been proposed to discover the nonlinear structure of the manifold, i.e. Isomap [4], Locally Linear Embedding [5] and Laplacian Eigenmaps [6]. These nonlinear methods do yield impressive results on some benchmark artificial data sets. However, these methods are developed based on reconstruction and are not optimal for classification viewpoint.

Recently, there has been some interest in the problem of developing low dimensional representations through kernel based techniques for face recognition [7], [8]. These methods can discover the nonlinear structure of the face images. However,

they are computationally. Moreover, none of them explicitly considers the structure of the manifold on which the face images possibly reside.

In this paper, we propose method for face recognition by extending the LLE with Kernel Fisher Discriminant Analysis (KFDA). Firstly, the input training samples are projected into the low-dimensional space. Then KFDA is introduced for finding the optimal projection direction. Finally, nearest neighbor classifiers are used for face recognition. Experimental results demonstrate the effectiveness and robust of the proposed recognition approach.

2 KFDA-LLE

LLE maps its inputs into a single global coordinate system of lower dimension, attempting to discover nonlinear structure in high dimensional data by exploiting the local symmetries of linear reconstructions. Its optimizations do not involve local minima though capable of generating highly nonlinear embeddings.

The LLE transformation algorithm is based on simple geometric intuitions, where the input data consist of N points x_i , $x_i \in R^D$, $i \in [1, N]$, each of dimensionality D , which obtained by sampling an underlying manifold. Provide there is sufficient data (such that the manifold is well sampled), each data point and its neighbors are expected to lie on or near a locally linear patch of the manifold. Linear coefficients that reconstruct each data point from its neighbors are used to characterize the local geometry of these patches. As an output, it provides N points y_i , $y_i \in R^d$, $i \in [1, N]$ where $d < D$. A brief description of LLE algorithm is as follows:

Stage I, the cost function to be minimized is defined as:

$$\epsilon(W) = \sum_{i=1}^N \left\| x_i - \sum_{j=1}^N W_{ij} x_{ij} \right\|^2 \quad (1)$$

Given $X = [x_1, x_2, \dots, x_N]$, the dimension of x_i is D . For one vector x_i and weights W_{ij} that sum up to 1, this gives a contribution:

$$\epsilon^i(W) = \left\| \sum_{j=1}^K W_{ij} (x_i - x_j) \right\|^2 = \sum_{j=1}^K \sum_{m=1}^K W_{ij} W_{im} C_{jm}^i \quad (2)$$

where C^i is the $K \times K$ matrix:

$$C_{jm}^i = (x_i - x_{ij})^T (x_i - x_{im}) \quad (3)$$

Stage II, the weight matrix W is fixed and new m -dimensional vectors y_i are sought which minimizes another cost function:

$$\epsilon(Y) = \sum_{i=1}^N \left\| y_i - \sum_{j=1}^N W_{ij} y_{ij} \right\|^2 \quad (4)$$

The W_{ij} can be stored in an $n \times n$ sparse matrix M, then re-writing equation (4) gives:

$$\epsilon(Y) = \sum_{i=1}^N \sum_{j=1}^N M_{ij} y_i^T y_j \quad (5)$$

To improve the LLE standalone classification performance, one needs to combine LLE with some discrimination criterion. The KFDA-LLE is similar to the original LLE in the first two steps. The original facial vector $x \in R^D$ is transformed into the feature vector $y \in R^d$ with $d < D$. The main different between them is that in our algorithm, the feature vector y is nonlinearly mapped into a high dimensional space, and then a FLD method is utilized, globally forming a nonlinear mapping, i.e. KFDA. The computation in high dimension space can be facilitated by the Mercer kernel function.

The main ideal of KFDA first maps the feature vectors y into a high dimension space F by a nonlinear mapping ϕ . Fisher linear discriminant analysis (FLD) can then be performed in F . Thus, we define the within-class scatter matrix S_w^ϕ , the between-class scatter matrix S_b^ϕ for the mapped training samples respectively as follows:

$$S_w^\phi = \sum_{i=1}^c \sum_{j=1}^{n_i} (\phi(g_j - \mu_i^\phi)(\phi(g_j) - \mu_i^\phi)^T \quad (6)$$

$$S_b^\phi = \sum_{i=1}^c n_i (\mu_i^\phi - \mu^\phi)(\mu_i^\phi - \mu^\phi)^T \quad (7)$$

where μ_i^ϕ is mean vector of class i and μ^ϕ is the total mean vector in the mapped space respectively. If S_w^ϕ is nonsingular, the optimal projection W_{opt} is chosen as the matrix with orthonormal columns which maximizes the ratio of the determinant of the between-class scatter matrix to that of the within-class scatter matrix, i.e.,

$$W_{opt} = \arg \max_W \frac{|W^T S_b^\phi W|}{|W^T S_w^\phi W|} \quad (8)$$

According to the theory of reproducing kernel [6], any solution w must lie in the space which is spanned by $\{\phi(x_1), \dots, \phi(x_N)\}$, i.e,

$$w = \sum_{i=1}^n \alpha_i \phi(g_i) = \Phi \alpha \quad (9)$$

where we define Φ as $[\phi(g_1), \phi(g_2), \dots, \phi(g_n)]$ and a coefficient vector α as $[\alpha_1, \alpha_2, \dots, \alpha_n]^T$. After substituting Eq. (6), Eq. (7), Eq. (9) into Eq. (8), it follows

$$w^T S_b^\phi w = \alpha^T K_b \alpha . \quad (10)$$

$$w^T S_w^\phi w = \alpha^T K_w \alpha . \quad (11)$$

where,

$$\xi_j = [k(g_1, g_j), \dots, k(g_n, g_j)]^T \quad (12)$$

$$K_b = \sum_{i=1}^c n_i (m_i - m)(m_i - m)^T \quad (13)$$

$$K_w = \sum_{i=1}^c \sum_{j=1}^{n_i} n_i (\xi_j - m_i)(\xi_j - m)^T \quad (14)$$

$$m_j = \frac{1}{n_j} \left[\sum_{i=1}^{n_j} k(g_1, g_i), \dots, \sum_{i=1}^{n_j} k(g_n, g_i) \right]^T \quad (15)$$

$$m = \frac{1}{n} \left[\sum_{i=1}^n k(g_1, g_i), \dots, \sum_{i=1}^n k(g_n, g_i) \right]^T \quad (16)$$

Then, the following eigenvalues problem is obtained:

$$A = \arg \max_A = \frac{|A^T K_b A|}{|A^T K_w A|} = [\alpha_1, \dots, \alpha_{c-1}] \quad (17)$$

To deal with the singularity of with-scatter matrix K_w that one often encounters in classification problems, we can use a regulation strategy with adding a multiple of the identity matrix to the within-scatter matrix, i.e., $K_w = K_w + \epsilon I$ where ϵ is a small number). This also makes the eigenvalue problem numerically more stable. Another

viable approach for singularity problem by using PCA could also be adopted [3]. This method performs a linear dimensionality reduction removing the null space to obtain a matrix of full rank.

For a new testing sample z , whose projection onto the optimal discriminant vector w of the feature F is

$$\begin{aligned} w^T \phi(z) &= \sum_{k=1}^n \alpha_k \phi^T(x_k) \phi(z) = \sum_{k=1}^n \alpha_k k(x_k, z) \\ &= \alpha^T [k(g_1, z), \dots, k(g_n, z)]^T \end{aligned} \quad (18)$$

3 Experimental Results

To verify the effectiveness of the proposed algorithm, we have carried out experiment on the ORL face database [9]. The ORL database contains ten different images of 40 distinct subjects in up-right, frontal position with tolerance for some tilting and rotation of up to 20%. Moreover, the most variation of some image scale is close to 10%. Therefore, it is expected that this is a more difficult database to work with. All images were grayscale and normalized such that the two eyes were aligned at the same position. For the purpose of computation efficiency, all images are resized to 32×32 pixels.

In this experiment, Five face images per person are chosen randomly as training images while the remaining five images are set as test images. To reduce the fluctuation of results caused by the randomness of data sets, the experiment was performed 10 times and the results are averaged. For simplicity, we applied the nearest neighbor classifier for classification. Table 1 contains a comparative analysis for the obtained recognition rates. From Table 1, it can be seen that the performance of the KFDA-LLE algorithm outperforms other methods such as Eigenface, Fisherface, LLE. It demonstrates that the performance is improved because KFDA-LLE preserves the local structure and kernel methods could effectively extract the nonlinear feature for further classification.

Table 1. The experimental results on test database using the different methods

Method	Reduced Space	Face Recognition Rate
Eigenface	199	86.63%
Fisherface	39	93.02%
LLE	44	89.74%
KFDA-LLE	35	97.86%

4 Conclusion

In this paper, we propose KFDA-LLE algorithm for face recognition. First, training set is projected into the intrinsic low-dimensional space. Then KFDA is used to find

an optimal projection direction for classification. In face recognition experiments, KFD-LLE serves as a feature extraction process compared with LLE, and two other well-established subspace methods combined with Nearest Neighbor classifier. Experimental results on face databases show that the proposed algorithm excels LLE and is highly competitive with those two baseline methods for face recognition.

References

1. Zhao, W., Chellappa, R., Rosenfeld, A., Phillips, P.J.: Face Recognition: A Literature Survey. Technical Report CAR-TR-948, University of Maryland, College Park (2000)
2. Turk, M., Pentland, A.: Eigenfaces for Recognition. *Journal of Cognitive Neuroscience* 3(1), 71–86 (1991)
3. Belhumeur, P.N., Hespanha, J.P., Kriegman, D.J.: Eigenfaces vs. Fisherfaces: Recognition Using Class Specific Linear Projection. *IEEE Trans. Pattern Analysis and Machine Intelligence* 19(7), 711–720 (1997)
4. Tenenbaum, J.B., de Silva, V., Langford, J.C.: A Global Geometric Framework for Nonlinear Dimensionality Reduction. *Science* 290, 2319–2323 (2000)
5. Roweis, S., Saul, L.: Nonlinear Dimensionality Reduction by Locally Linear Embedding. *Science* 290, 2323–2326 (2000)
6. Belkin, M., Niyogi, P.: Laplacian Eigenmaps and Spectral Techniques for Embedding and Clustering. In: *Advances in Neural Information Processing Systems*, Vancouver, British Columbia, Canada, vol. 14 (2002)
7. Liu, Q., Huang, R., Lu, H., Ma, S.: Face Recognition Using Kernel Based Fisher Discriminant Analysis. In: *Proceedings of the Fifth International Conference on Automatic Face and Gesture Recognition* (2002)
8. Yang, M.H.: Kernel Eigenfaces vs. Kernel Fisherfaces: Face Recognition Using Kernel methods. In: *Proceedings of the Fifth International Conference on Automatic Face and Gesture Recognition* (2002)
9. <http://www.uk.research.att.com/facedatabase.html>

A Supervised Approach to Support the Analysis and the Classification of Non Verbal Humans Communications

Vitoantonio Bevilacqua^{1,2,*}, Marco Suma¹, Dario D'Ambruoso¹,
Giovanni Mandolino¹, Michele Caccia¹, Simone Tucci¹,
Emanuela De Tommaso¹, and Giuseppe Mastronardi^{1,2}

¹ Dipartimento di Elettrotecnica ed Elettronica, Polytechnic of Bari, Italy

² e.B.I.S. s.r.l. (electronic Business in Security), Spin-Off of Polytechnic of Bari, Italy

bevilacqua@deemail.poliba.it

Abstract. It is well known that non verbal communication is sometimes more useful and robust than verbal one in understanding sincere emotions by means of spontaneous body gestures and facial expressions analysis acquired from video sequences. At the same time, the automatic or semi-automatic procedure to segment a human from a video stream and then figure out several features to address a robust supervised classification is still a relevant field of interest in computer vision and intelligent data analysis algorithms. We obtained data from four datasets and we used supervised methods to train the proposed classifiers and, in particular, three different EBP Neural-Network architectures for humans templates, mouths and noses and J48 algorithm for gestures. We obtained on average of correct classification equal to a: 80% for binary classifier of humans templates, 90% for happy/non happy, 85% of binary disgust/non disgust and 80% related to the 4 different gestures.

Keywords: Neural Network, Emotions Recognition, Humans Silhouettes, Gesture Recognition, Facial Expressions Recognition, Human Detection, Hands, Action Units, Centre of Gravity, Pose Estimation.

1 Introduction

Good communication is the foundation of successful relationships, both personally and professionally. But we communicate with much more than words. In fact, many researches show that the majority of our communication is nonverbal. Nonverbal communication, or body language, includes facial expressions, gestures, eye contact, posture and even the tone of our voice. Although the details of his theory have evolved substantially since the 1960's, Ekman remains the most vocal proponent of the idea that emotions are discrete entities [1]. Unlike some forms of nonverbal communication, facial expressions are universal. About gestures recognition we consider how the way we move communicates a wealth of information to the world. This type of nonverbal communication includes our posture, stance, and subtle movements. Gestures are omnipresent in our daily lives. However, the meaning of

* Corresponding author.

gestures can be very different across cultures and regions, so it is important being careful to avoid misinterpretation. Using these ideas, we want to provide an automatic system which is able to evaluate emotions in particular situations (videoconference, meetings, neurological examination, investigation).

2 Materials

Materials for all the four datasets have been collected with the goal of increasing the variance of their samples and then supporting the amount of information in the training examples necessary for the proposed supervised classifiers.

2.1 Humans Silhouettes

The humans silhouettes used in this paper comes from those walking in a video stream dataset where the training examples consist of only 20 different silhouettes binary images obtained after a pre-processing phase of background subtraction. By this methods the training examples consist in each of a number of different and several human silhouettes extracted from each frame.



Fig. 1. a) and b) samples frames and c) 4 different examples of humans silhouettes with their several dimensions and behaviours

2.2 Facial Expressions

First of all we explain the concept of Action Units (AUs) as minimal facial actions not separable, elements for the construction of facial expressions. Combination of these, with different intensities, generate facial expression. According to our previous work [2] we can assert that, generally, prescinding other AUs, the presence of AU-10 discriminates unequivocally disgust emotion; the presence of AU-12 or AU-13 discriminates unequivocally happy emotion. For this reason we are able to recognize two of the six primary emotions declared by Paul Ekman: happy and disgust emotions. To extract middle and lower part of the face we have used our tool; moreover we have used public databases of faces [3] and then we have taken our regions of interest.

2.3 Gestures

Each frame of the video has a resolution of 640x480 pixel. As for the automatic classification of gestures, the research has been based on different studies by psychologist David McNeill [4], who divides them into four main categories:

- *deictic gestures*: typical indicating movements, usually emphasized by the movement of fingers or by other parts of the body that can be used for this purpose.
- *iconic gestures*: gestures that express formal relation in respect to the semantic content of discourse. They mainly occur in the area occupied by the torso of the prototype being focused;
- *metaphoric gestures*: they represent real figures. These refer to abstract concepts, as moods or language. The density of such gestures is concentrated in the lower part of the torso;
- *beat gestures*: these may be recognized by only focusing the attention on the characteristics of their movements.

It has been decided to monitor the movement of the center of gravity (CG) of the hands in each frame so as to be able to calculate various parameters of evaluation, such as the velocity with which gestures are made.

3 Methods

The application of supervised neural network using Error Back Propagation algorithm gives easier solution to complex problems such as in correct classification of silhouettes shapes, facial expression and gestures. Advantages of neural networks include their high tolerance to noise as well as their ability to classify patterns not used for training. In particular we implemented neural networks supervised classifier for the classification of silhouettes, mouths and noses emotions features and the J48 classifier for gestures.

3.1 Silhouettes Classification

The neural network classifier is a two layers feed-forward with 396 inputs (corresponding to 33*12 dimensions of the smallest figure previously resized to contain the smallest human silhouette) with 6 logistic neurons in the first layer and 1 neuron as output. The images passed to the neural networks have the following characteristics: the height bigger than the width, the ratio between height and width ranging 1.9 and 4, the height bigger than 33 pixels and the width bigger than 12 pixels. All images are divided in more images and then each image contains a singular human silhouette always resized to 33*12 pixels in order to have the same number of inputs for each neural network classification sample. This procedure guarantee a constant number of neural network's input. In any case to achieve good performance in terms of generalization the training set is selected with large variability in terms of positive poses and movements that are people not staring the cameras (not frontal images), people with their arms far or closed to the body, people not very well identified owing of the presence of just one arm and negative ones that are objects similar to people used as contrary examples.

3.2 Facial Expression Classification

We have realized two NNs, that work in parallel; the first one receives the form of the mouth: in happy expressions the mouth should be open, the teeth should be visible and its shape is curved (AU-12, AU-13); the second one receives the nose: in disgust expressions nasolabial furrows are visible (AU-10).

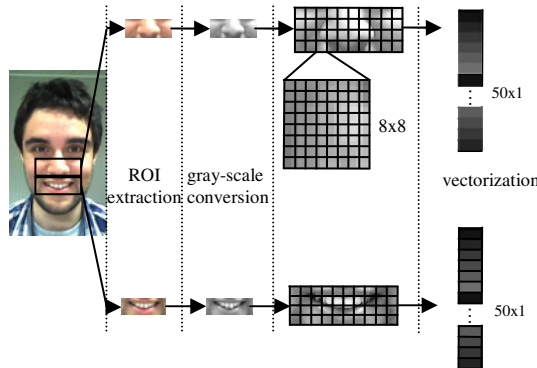


Fig. 2. Segmentation and vectorization of the face

Each bitmap gray-scale image is a band of 40×80 pixels which contains respectively the lower and the middle part of the face; to use it as input for the neural network they have been arranged in an array and then normalized, obtaining a 1×50 vector (a function calculates a mean value each 8×8 pixels). In case of no happy and no disgust expressions, the network returns 0 (zero); in the other case the network returns 1. To train the NN for the mouth, we have used a training set of 200 photos that are composed of 100 negative and 100 of positive examples in 20000 epochs. The NN comes with a structure of the first layer of 300 neurons, the second layer of 200 neurons, the third layer of 10 neurons and 1 output neuron ($300 \times 200 \times 10 \times 1$). To train the NN for the nose, we have used a training set of 100 examples that are composed of 50 negative and 50 positive examples in 20000 epochs. The NN comes with a structure of the first layer of 400 neurons, the second layer of 80 neurons, the third layer of 10 neurons and 1 output neuron ($400 \times 80 \times 10 \times 1$).



Fig. 3. mouths and noses from our tool (the first four images) and from public databases

3.3 Gestures

For gestures analysis the supervised classifier is implemented by means of J48 algorithm instead of using a EBP NN classifier. Rule induction systems are currently

employed in several different environments ranging from loan request evaluation to fraud detection, bioinformatics and medicine [5]. In particular the main goal of this scheme is to minimize the number of tree levels and tree nodes, thereby maximizing data generalization. The input is a 10 elements array where the features are the x coordinate of the right hand CG, the y coordinate of the right hand CG, the x coordinate of the left hand CG; the y coordinate of the left hand CG, the position of the right hand (respect to the torso of the prototype being shot), the position of the left hand, the right/left hands slant (measured in radiant), the velocity of the movement of the right/left hand. To find CG, frames have been processed according to the follow workflow consisting of skin detection by color-space conversion from RGB to HSV, background subtraction technique to exalt only the hands region, image smoothing and binarization, tracing of rectangles that contain hands, CG identification, edge and features detection; template matching to notice resting position of hands; gestures classification and storing data on .csv file.

4 Experimental Results

In this paper we have presented a system that recognizes separately shapes, two of six primary emotions and analyzes information derived from gestures. The complete project expects to recognize all primary emotions. In particular in the following we show, separately, results related to facial expressions, gestures and silhouettes.

About facial processing, using about 150 test images, the results of NNs have achieved about 90% for happy/no-happy emotion and 85% for disgust/no-disgust emotion of success rate. We can assert that the results are reliable, also because in some particular cases nor human beings can distinguish exactly emotions.

About gestures, the confusion matrix is shown in Table 1. The NN has correctly classified approximately 80% of gestures. The network has specifically been able to label “metaphoric gestures” in a precise way. Performances are not optimal as for the recognition of “deictic gestures” and “beat gestures”. “Iconic gestures” are not present in the preregistered video.

Table 1. Confusion matrix of data set for gestures. Deictic (A); Spontaneous (B); Beat (C); not recognized (D); Metaphoric (E).

	A	B	C	D	E
A	53	71	3	0	0
B	6	280	10	3	1
C	1	9	54	1	0
D	1	2	1	20	0
E	0	1	1	0	25

Neural network shows on average good results in terms of false positives and then in the following figure are reported detected Vs total humans per each frame.



Fig. 4. Detected Vs total humans number per each tested frame

5 Conclusions

The goal of this paper is to investigate emotion-related and realize a system to recognize separately emotional patterns of the body and face using Neural Networks. The research aims at developing an intelligent system that can interpret intellectual conversation between human beings. When we interact with others, we continuously give and receive countless wordless signals. The nonverbal signals we send either produce a sense of interest, trust, and desire for connection, or they generate disinterest, distrust, and confusion. The analyzed gestures and facial emotions represent non-verbal communication; they provide the user to what the speaker is saying, thus helping the listener to interpret the meaning of words. Future works forecast the design of a new multimodal system performing at the same time emotion recognition by means other several facial bands (eyebrows band eyes bands), gestures recognition and human silhouettes.

References

- [1] Ekman, P.: FACS: Facial Action Coding System, Research Nexus division of Network Information Research Corporation, Salt Lake City, UT 84107 (2002)
- [2] Bevilacqua, V., D'Ambruoso, D., Mandolino, G., Suma, M.: A New Tool to Support Diagnosis of Neurological Disorders by Means of Facial Expressions. In: IEEE Proc. of MeMeA, pp. 544–549
- [3] <http://www.emotional-face.org>
- [4] <http://mcneilllab.uchicago.edu>
- [5] Menolascina, F., Bevilacqua, V., et al.: Novel Data Mining Techniques in ACGH Based Breast Cancer Subtypes Profiling: the Biological Perspective. In: Proc. of IEEE Symp. on Comp. Intelligence in Bioinformatics and Comp. Biology (CIBCB 2007), pp. 9–16 (2007)

A Text Classification Algorithm Based on Rocchio and Hierarchical Clustering

Anping Zeng¹ and Yongping Huang²

¹ School of Computer and Information Engineering,
Yibin University, Yibin, Sichuan 644007, China

² Computational Physics Key Laboratory of Sichuan Province,
Yibin University, Yibin, Sichuan 644007, China
Zengap@126.com

Abstract. The disadvantages of traditional classification algorithms are firstly discussed. Then, a new algorithm called HI-Rocchio is proposed. The HI-Rocchio algorithm includes two parts. The first part is an incremental Rocchio algorithm based on Rocchio algorithm, and the second is an improved Hierarchical clustering algorithm. The HI-Rocchio algorithm not only can generate new classes incrementally but also get multi hierarchical relationship between classes. Experiments verified the effectiveness of the algorithm.

Keywords: Rocchio algorithm, Text classification, Incrementally, Hierarchical clustering.

1 Introduction

As an information filtering, information retrieval, search engine, Web page automatic classification, text databases, digital libraries and other areas of technology infrastructure, Text classification has a wide range of application, and has become a hot research topic. Currently, text classification techniques include Rocchio algorithm [1], K-Nearest Neighbor algorithm [2], Bayesian method [3], support vector machine [4] and neural networks [5] methods, etc. However, these methods have some disadvantages as follow:

- They ignore the contradiction between the relatively fixed features of the training set and the continued changing of new document's themes. When new documents are added to the system quickly, the ability of matching the new documents to the original classification rules and the classification accuracy rate will become less.
- Every sample of the training set belongs to one class only, and there is no hierarchical relationship in the classes. A good Classification process is to achieve the merging from a similar result, but also realizes the dividing from not similar result. Classes and their concept have big and small, some concepts can be sub-concepts of other concepts, which lead to hierarchical relationship between the concepts [6]. However, the traditional classification algorithms can not deal with the hierarchical relationship.

For the first disadvantage, the traditional algorithms generally re-train the classification rules regularly or irregularly. To continue to receive the new classification rules, they must update the whole training set. It not only increases the training time but also leads to the inconsistencies of classification rules between each classification processes. Based the previous work, this paper proposes an incremental Rocchio algorithm, which can generate a new class incrementally. For the second disadvantage, the hierarchy is generated by hand generally. This paper proposes an improved hierarchical clustering to generate hierarchy.

2 An Introduction of Rocchio Algorithm

In 1971, Rocchio presented a classical Rocchio algorithm, which is an important method for text classification based vector space model [1]. The main idea of the algorithm is as follows:

Step 1: The algorithm gives a benchmark data set and the division of the initial classes, labels all samples of the data set for the initial classes.

Step 2: The data set is divided into training set and test set.

Step 3: The algorithm selects a class C_i (initially, each class only includes a sample), and Wc_i is the representative vector. In the training set, every sample which belongs to C_i , its weight vector's weight expresses by positive, and is added to vector Wc_i . To these samples which do not belong to C_i , their weight vector's weight expresses by negative, and is added to vector Wc_i . Formula 1 defines the representative vector Wc_i :

$$Wc_i = \alpha \times \sum_{d_i \in c_i} \frac{\overrightarrow{Wd_i}}{|\overrightarrow{Wd_i}|} - \beta \times \sum_{d_j \notin c_i} \frac{\overrightarrow{Wd_j}}{|\overrightarrow{Wd_j}|} \quad (1)$$

α, β are two parameters.

Step 4: Repeat Step 3 until all classes are selected.

Step 5: The algorithm selects a document D_i from test set, and the document has not been classified. The similarities between D_i and all class vectors will be computed using the cosine method, and then D_i is labeled to the class C_{max} whose similarity is the maximum.

Step 6: Using Formula 1, the algorithm adds vector D_i into representative vector of the class C_{max} , and gets a new vector to represent the class C_{max} . To other classes, the vector D_i is subtracted from their representative vector.

Step 7: Repeat Step 5 and Step 6.

3 An Introduction of Hierarchical Clustering Algorithm

Hierarchical clustering algorithm [2] is a hierarchical merging or splitting based on a given data set. Figure 1 shows the produce process of a set of nested clusters organized as a hierarchical tree. There are two main types of Hierarchical

clustering algorithm, agglomerative (bottom-up) and divisive (top-down) Hierarchical clustering. The agglomerative algorithm starts with the bottom points and each document is an individual class (or cluster) at first. At each step, the algorithm merges the closest pair of classes to a parent class until only one class (or k classes) left. In figure 11, there are six individual classes ($C_1, C_2, C_3, C_4, C_5, C_6$) and four merging steps. But the divisive algorithm starts with a top class (or k classes). At each step, the farthest one point is divided from its parent class until each class contains a point.

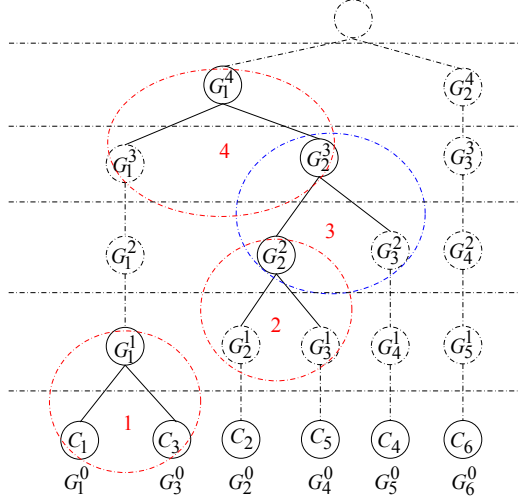


Fig. 1. Hierarchical clustering tree

In this paper, the agglomerative method is proposed, and a six classes' example is given to illustrate the algorithm. The algorithm are summarized as follows:

Step 1: The initial classification. The figure 1 shows that there are N ($N = 6$) samples, and each sample is a class. The classes are labeled as: $G_1^0, G_2^0, G_3^0, G_4^0, G_5^0, G_6^0$. *Min_Sim* is the minimum similarity threshold.

Step 2: The algorithm calculates the distance (similarity) between the each classes, and then generates a 6×6 -dimensional distance matrix D^0 .

Step 3: In figure 1, G_1^0 and G_3^0 are the closest pair in D^0 , and they will be merged into one group G_1^1 . So, the new classification $(G_1^1, G_2^1, G_3^1, G_4^1, G_5^1)$ is generated ($G_2^1 = G_2^0$, $G_3^1 = G_4^0$, $G_4^1 = G_5^0$ and $G_5^1 = G_6^0$). If the number of classification is less than two, the algorithm stops.

Step 4: We calculate the 5×5 -dimensional distance matrix D^1 .

Step 5: G_2^1 and G_3^1 is the closest pair in D^1 , if the closest pair's similarity is less than Min_Sim , the algorithm stops, else G_2^1 and G_3^1 will be merged into

one group G_2^2 . So, the new classification $(G_1^2, G_2^2, G_3^2, G_4^2)$ is generated ($G_1^2 = G_1^1$, $G_3^2 = G_4^1$ and $G_4^2 = G_5^1$).

Step 6: Calculate the 4×4 -dimensional distance matrix D^2 .

Step 7: G_2^2 and G_3^2 is the closest pair in D^2 , if the closest pair's similarity is less than Min_Sim , the algorithm stops. Else, G_2^2 and G_3^2 are merged into one group G_2^3 . So, the new classification (G_1^3, G_2^3, G_2^3) is generated ($G_1^3 = G_1^2$ and $G_3^3 = G_4^2$).

Step 8: Calculate the 3×3 -dimensional distance matrix D^3 .

Step 9: G_1^3 and G_2^3 is the closest pair in D^3 . If the closest pair's similarity is less than Min_Sim , the algorithm stops, else G_1^3 and G_2^3 will be merged into one group G_1^4 . So, the new classification (G_1^4, G_2^4) is generated ($G_2^4 = G_3^3$). The classification only has two elements, so the algorithm stops. Table I shows the result of the algorithm.

Table 1. Hierarchical clustering classification result

Parent class	Child class	threshold
G_1^4	C_1	closest
G_1^4	C_2	closest
G_1^4	C_3	closest
G_1^4	C_4	closest
G_1^4	C_5	closest
G_2^4	C_6	null

The Hierarchical clustering method is the most commonly used clustering method. However, in every merging, you must compute the overall similarity between all the classes to select the minimum pair to merge, so the speed is relatively slow, and the algorithm is not suitable for large document sets.

4 HI-Rocchio Algorithm

This paper proposes an improved algorithm, named as HI-Rocchio. The algorithm is divided into two steps: first, new classes are incremental generated by the improved Rocchio algorithm; second, hierarchical tree is generated by the improved hierarchical clustering methods.

4.1 Incremental Rocchio Algorithm

The main idea of incremental Rocchio algorithm is as follows:

Step 1: The data set is divided into training set and test set, the training set is labeled and test set is not.

Step 2: In the training set, we use Rocchio algorithm to calculate the center of each class as the representative vector.

Step 3: An unlabeled document is selected to be calculated similarities with all candidate classes. If all similarities are less than a certain threshold, a new class will be generated, and its vector equals the document's vector.

Step 4: Otherwise, the document is labeled as the class corresponding to the maximum similarity, and this class's new representative vector will be calculated using Rocchio algorithm.

Step 5: If there are not labeled samples, the algorithm goes to step 3.

4.2 Improved Hierarchical Clustering Algorithm

The number of classes generated by the incremental Rocchio Algorithm is small, which is suitable for realizing hierarchical clustering. However, the classes of traditional Hierarchical clustering have no hierarchy. The process of merging in each new class will also remove the old two. In addition, the algorithm is merging only two classes one time but not more classes, the merger speed is slow.

The improved hierarchical clustering can merge several similar classes into a parent class simultaneously, not remove the old classes. The idea of the algorithm is described as follows:

Step 1: The system initializes classification and sets the minimum similarity threshold w.r.t. min_sim .

Step 2: The algorithm calculates the distance between the each class, and then generates an $m \times m$ -dimensional similarity matrix D^k .

Step 3: The maximum similarity threshold w.r.t. max_sim is set. If the similarities between G_i^k, \dots, G_j^k are greater than max_sim , a new parent class G_l^{k+1} will be generated and G_i^k, \dots, G_j^k are its child classes. At the same time, if there are some other classes' similarities are greater than max_sim , another parent class G_m^{k+1} will be generated.

Step 4: The new similarity matrix D^{k+1} are generated on the parent classes. If the minimum similarity in D^{k+1} is less than the minimum similarity threshold min_sim , the algorithm stops, and the classification is the result. (Or, if there are only two parent classes, then the algorithm stops). Go to step 3.

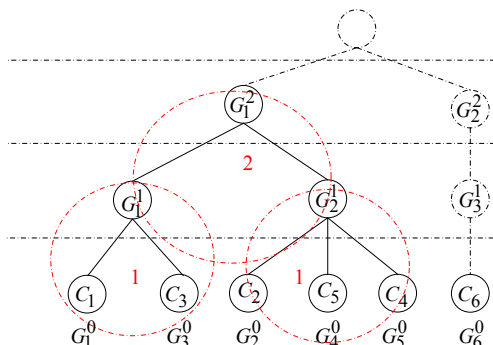


Fig. 2. Improved Hierarchical clustering tree

The six classes' example of last section is given to illustrate the improved hierarchical clustering algorithm. Figure 2 is the improved hierarchical clustering tree, and the processing steps are summarized as follows:

Step 1: The initial classification. The classes are labeled as: $G_1^0, G_2^0, G_3^0, G_4^0, G_5^0, G_6^0$.

Step 2: The algorithm Calculates the distance (similarity) between the each classes, and then generates a 6×6 -dimensional distance matrix D^0 .

Step 3: In D^0 , the similarity between G_1^0 and G_3^0 is greater than max_sim , the similarities between G_2^0, G_4^0 and G_5^0 are greater than max_sim . So, G_1^0 and G_3^0 will generate their parent class G_1^1 , and G_2^0, G_4^0, G_5^0 will generate their parent class G_2^1 . The new classification (G_1^1, G_2^1, G_3^1) is generated ($G_3^1 = G_6^0$). If the number of classification is less than two, the algorithm stops.

Step 4: We calculate the 3×3 -dimensional distance matrix D^1 .

Step 5: In D^1 , the similarity between G_1^1 and G_2^1 is greater than max_sim_i , so, G_1^1 and G_2^1 will be merged into one group G_1^2 . The new classification (G_1^2, G_3^1) is generated ($G_2^2 = G_3^1$). The classification only has two elements, so the algorithm stops. Table 2 shows the result of the algorithm.

Table 2. Improved Hierarchical clustering classification result

Parent class	Child class	Similarity threshold
G_1^2	G_1^1	max_sim_1
G_1^2	G_2^1	max_sim_1
G_2^2	G_3^1	null
G_1^1	C_1	max_sim
G_1^1	C_3	max_sim
G_2^1	C_2	max_sim
G_2^1	C_4	max_sim
G_2^1	C_5	max_sim
G_3^1	C_6	null

4.3 Classification

The process of HI-Rocchio algorithm's classification is described as follows:

Step 1: First, min_sim is the similarity threshold, and top parent classes are stored in array $pc[]$.

Step 2: A document is pre-processed, broken down into words, extracts feature, and a vector D_i is used to represent the document.

Step 3: The similarities between D_i and the classes in $pc[]$ are calculated, sim_max is the max similarity of them, and C_i is the corresponding class to sim_max .

Step 4: If sim_max is less than min_sim , a new class is created and D_i is labeled as it. Then, the algorithm stops.

Step 5: Otherwise, if the child classes of C_i are null, D_i is labeled C_i , and the algorithm stops. Else, the child classes of C_i are stored in array $pc[]$, and go to step 3.

5 Experiments

To validate the efficiency of the algorithm, we run Rocchio algorithm, HI-Rocchio algorithm and Hierarchical clustering in the TanCorp dataset [9]. The TanCorp dataset is a commonly used benchmark in the field of text categorization. The collection includes 14150 documents, which are nearly distributed into 60 classes.

(1) Comparing the micro-F1 between HI-Rocchio and Rocchio algorithm To compare the HI-Rocchio and Rocchio algorithm, we divided the documents corpus into two parts (training part and test part), and do twice experiments. The micro-F1 is very suitable for comparing the merits of the two algorithms under different feature dimensions(x-axis in figure 3 and figure 4). So, the first experiment compares the micro-F1 between the two algorithms in the Non-incremental case, and the second compares the micro-F1 between the two algorithms in the incremental case.

In the first experiment, respectively, all the classes' documents are divided according to the ratio of 7:3. Both the training set and test set contain 60 classes. The figure 3 shows the result of the first experiment. We can see that HI-Rocchio and Rocchio algorithm are almost the same efficiency.

In the second experiment, all documents are divided according to the ratio of 7:3 too. The training set contains only 58 classes, the other 2 classes is incremental classes. The figure 4 shows the result of the second experiment. We can see that the efficiency of Rocchio algorithm descends, but HI-Rocchio keeps high efficiency.

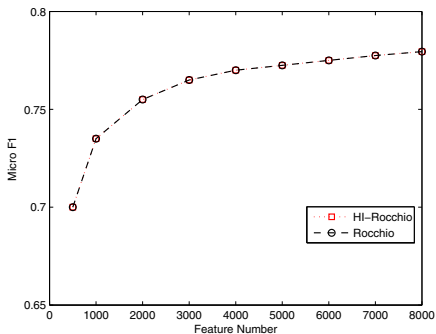


Fig. 3. The first experiment

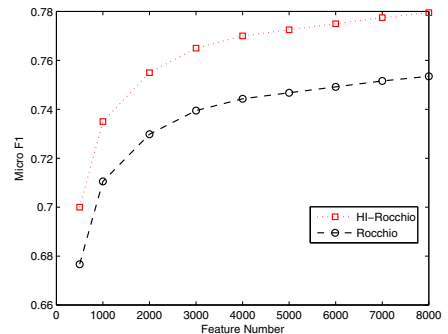


Fig. 4. The second experiment

(2) Comparing the runtime HI-Rocchio and Hierarchical clustering First, Rocchio algorithm is used to calculate the center vectors of the 60 classes in corpus. Then, we cluster on the 60 classes directly rather than on the 14510 documents. The time spent on Hierarchical clustering is the HI-Rocchio's log60 times.

6 Conclusions

This paper proposes a HI-Rocchio algorithm based on the Rocchio algorithm and Hierarchical clustering algorithm. The experimental results showed the advantages of HI-Rocchio algorithm as follows:

- The HI-Rocchio algorithm can generate new class to handle the contradiction between the relatively fixed features of the training set and the continued changing of new document's themes, but the Rocchio can't.
- The HI-Rocchio algorithm has multi hierarchical relationship to descript the text documents, but the Rocchio algorithm and hierarchical relationship have not.
- The HI-Rocchio algorithm runs much faster than Hierarchical clustering in the process of text cluster.

In addition, the more levels of Hierarchical tree, the more thresholds need to set in HI-Rocchio algorithm. How to set the similarity thresholds is one of future works. In [10], Y.Q. Miao proposed a pairwise optimized Rocchio algorithm, how to improve it is the next work too.

Acknowledgment. This work is partially supported by Scientific Research Fund of Sichuan Provincial Education Department No.10ZB049; and the Foundation of Yibin Technical Bureau under Grant No.20072036.

References

1. Rocchio, J.J.: Relevance Feedback in Information Retrieval. *The SMART Retrieval System*, 313–323 (1971)
2. Tan, S.: Neighbor-Weighted k-Nearest Neighbor for Unbalanced Text Corpus. *Expert Systems with Applications* 28(4), 667–671 (2005)
3. Li, J.M., Sun, L.H., Zhang, Q.R.: Application of Native Bayes Classifier to Text Classification. *Journal of Harbin Engineering University* 24(1), 71–74 (2003)
4. Kim, H., Howland, P., Park, H.: Dimension Reduction in Text Classification with Support Vector Machines. *Journal of Machine Learning Research* 6(1), 37–53 (2005)
5. Ruiz, M.E., Srinivasan, P.: Hierarchical Text Classification Using Neural Networks. *Information Retrieval* 5(1), 87–118 (2002)
6. Zhang, Y.P.: *Commercial Space and Granular Computing: Structured Problem Solving Theory and Methods*, pp. 116–117. Science Press, Beijing (2010)
7. Li, B.C., Shao, M.Z., Huang, H.: *Pattern Recognition Theory and Application*, pp. 106–107. Xidian University Press (2008)
8. Ma, H.F., Fan, X.H., Chen, J.: An Incremental Chinese Text Classification Algorithm Based on Quick Clustering. In: *International Symposiums on Information Processing*, pp. 308–312 (2008)
9. Tan, S.B., Cheng, X.Q., Ghanem, M.M.: A Novel Refinement Approach for Text Categorization. In: *CIKM*. ACM, New York (2005)
10. Miao, Y.Q., Kamel, M.: Pairwise Optimized Rocchio Algorithm for Text Categorization. *Pattern Recognition Letters* 32, 375–382 (2011)

Korean Documents Copy Detection Based on Ferret

Byung Ryul Ahn¹, Won-gy whole Kim², Won Young Yu³, and Moon-Hyun Kim¹

¹ Artificial Intelligence Lab, School of Computer Engineering, SungKyunKwan Univ., 300 Chunchun-Dong, Jangan-Ku, Suwon-si 440-746, South Korea

² Copyright Protection Center, Sangam-Dong, Mapo-Gu, Seoul 121-270, South Korea

³ Contents Research Division, ETRI, 161 Gajeong-dong, Yuseong-gu, Daejon, South Korea
anbr0305@skku.edu, wgkim@cpcmail.or.kr,
zero2@etri.re.kr, mhkim@ece.skku.ac.kr

Abstract. With the development of electronic documents, plagiarism is rapidly increasing and, given the difficulty of manual detection, need for plagiarism detection systems to help protect intellectual property has emerged. Many content-based detection systems have been developed and are actually used in some foreign countries, but they are still insufficient for documents in Korean. In particular, the high variance of Hangul makes the development of detection systems more difficult. This study proposes a Hangul document detection method based on Ferret's trigrams. Ferret only considered the frequency of trigram matches as a way to detect similarity, but in this study the system is developed further by weighting results depending on the degree of trigram match, thereby improving the accuracy of similarity detection.

Keywords: Intelligent Computing in Pattern Recognition.

1 Introduction

Document plagiarism means the unauthorized use of the original documents of another author without recognition of the source, as if the plagiarist had created them. Examples of document plagiarism include the arbitrary use of information obtained from the media and the unauthorized reuse of the program source codes of another author without references.

Detection of plagiarism is essential for copyright protection. However, with the development of the Internet, the volume of digital information available and easily accessible has increased massively, and manually detecting plagiarism is expensive in both time and effort. Therefore, we need programs that can automatically detect document plagiarism. Although many document copy detection programs have been released, their performance is unsatisfactory. This paper proposes an algorithm to improve the detection accuracy of existing programs. The key is to use two elements of the algorithm to identify plagiarism: firstly the number of matching trigrams in the original document, and secondly weighting the trigrams where they match sequentially.

Chapter 2 briefly reviews previous studies related to plagiarism detection. Chapter 3 examines the Hangul document plagiarism detection system proposed in this paper. Chapter 4 evaluates the performance of the recommended algorithm through example cases. Chapter 5 presents conclusions.

2 Related Works

Many existing plagiarism detection systems work on the basis of content. Thus, the comparison unit of the system compares documents and calculates the similarity between them. Representative plagiarism detection systems include

- COPS : Detects plagiarism by sentence-unit examinations [1]
- SCAM : Detects plagiarism by word-unit examinations [2]
- SSK(Semantic Sequence Kernel) : Detects plagiarism by finding the semantic sequences in a document and comparing them [3][4]
- PPChecker : Uses synonym information in plagiarism detection and presents plagiarism patterns [5]
- Ferret : Uses trigrams as the unit of comparison to solve the problems of many errors in the comparison of words and duplicated detections of partial sentences in the comparison of sentences[6][7]

Because COPS performs comparisons in sentence units, its detection performance is greatly lowered by even minor variations. SCAM performs word-unit examinations and may falsely detect plagiarism for documents on similar subjects. SSK produces fewer detection errors than these above two systems, but its algorithm, necessitating the discovery of semantic systems, is complex. PPChecker exhibits weakness in the discrimination of sentence structure variations. Lastly, the English language based Ferret system only checks the number of trigram matches.

3 Proposed System

This chapter proposes a plagiarism detection system, based on the Ferret system, that compares trigrams but with added algorithms. Because the target of detection is Hangul documents, we need to isolate morphemes before hand, since Hangul has many word-ending variations. The isolated morphemes comprise the units of comparison in each trigram unit; the trigram units are then used for comparison between documents. The following sections describe in detail the architecture and comparative analysis process of this system

3.1 System Architecture

- Morphemic Parser : Receives the queried document and the original document, and breaks them down into morphemes.
- Trigram Generator : Organizes a set of trigrams from the set of morphemes of each document by grouping three morphemes into one trigram.
- Trigram Comparison Analyzer : Compares trigrams, one by one, between the two documents. A set of all trigrams and a set of trigrams common to both documents are obtained. This system gives different weights to the matches based on the number of sequentially matched trigrams, and then determines the number of matches.

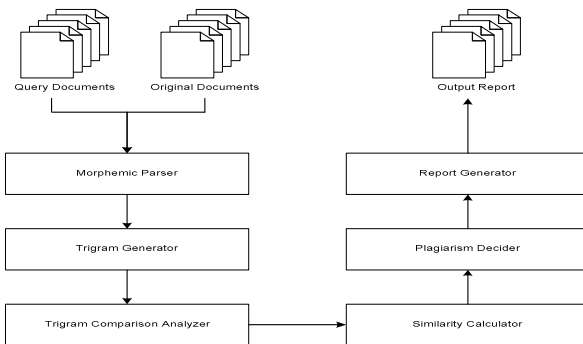


Fig. 1. Basic architecture of the proposed system

- Similarity Calculator : Similarity is calculated from the values produced by the Trigram Comparison Analyzer. The similarity value 1 is obtained for a perfect match; and the more similar the documents are, the closer the similarity value is to 1.
- Plagiarism Decider : Whether Plagiarism has been detected is decided based on the value produced by the Similarity Calculator being above an agreed reference value.
- Report Generator : A report is generated, which summarizes the matching trigrams and provides information regarding the plagiarism outcome.

As in this heading, they should be Times 11-point boldface, initially capitalized, flush left, with one blank line before, and one after.

3.2 Morphemic Parser

3.2.1 Concept of Morpheme. The general definition of a morpheme is the smallest unit of meaning. Morphemes can be classified into grammar morphemes and word morphemes by their meanings or functions. Word morphemes are morphemes that have word meanings and indicate or describe objects, statuses or actions. Typically, nouns, verbs, adjectives, and adverbs belong to them. For example, in the Hangeul sentence, “pyojeol tamjineun geunjeol doieoyahanda,” “pyojeol,” “tamji,” “geunjeol,” “doi,” and “ha” are examples of word morphemes.

Grammar morphemes are those that have grammatical meanings. They are used together with word morphemes and show their relationships. In Korean they are generally suffixes. In the above example, “neun,” “eoya,” and “da” are examples of grammar morphemes.

3.2.2 Implementation of Morphemic Parser. We did not develop a new morphemic parser, as the existing one was adequate. This was the Intelligent Morphemic Parser v1.0, developed by 21st Century Sejong Plan.[9] Using this we extracted morphemes from a document, removing the grammar morphemes to leave only word morphemes in order to exclude the highly variable character of Hangul grammar morphemes to

improve detection of plagiarism. In the example sentence given above only the five word morphemes, “pyojeol, tamji, geunjeol, doi, and ha” would be used for plagiarism detection.

3.3 Trigram Comparison Analyzer Algorithms

3.3.1 Basic Steps

1. Receive documents for comparison.
 2. Use the words in each document as tokens, but with the endings removed.
 3. Organize each document into a set of trigram units.
 4. If there are M trigrams in the original document, number the trigrams from 1 to M , and compare each of them with each of the trigrams in the queried document.
 5. When the trigrams of the two documents match, update the intersection until a pair of trigrams in the sequence does not match, and add 1 to the count variable (perform the counter (i, j) reflexive statement). If a sequence of five trigrams matches in a row, by the repetitive matching of i and j , the value $\sum_{k=1}^5 k$ becomes 15. Thus, the higher the number of the sequential matches, the greater the weight in proportion to k^2 .
 6. Calculate similarity, as follows:

If: $x = \frac{n(A \cap B)}{n(A \cup B)}$ (rate of discovered trigrams), and $y = \frac{\sum_{i=1}^n \sum_{j=1}^{constM} t[i][j]}{\sum_i^n}$

where $tblockNum$ is the number of matching trigram groups, and $contNum$ is the number of sequentially matching trigram groups, (in the second equation, the numerator is the final value of the variable count, and the denominator corresponds to the perfect match. The higher the number of sequential matches and the more the matching trigrams there are, the greater the y value.), the geometric mean $\sqrt[2]{\frac{xy}{x+y}}$ will be deemed the degree of similarity.

3.3.2 Algorithm Steps

The basic function of this algorithm is to compare each trigram in the original document with each trigram in the queried document. If the identical trigram is

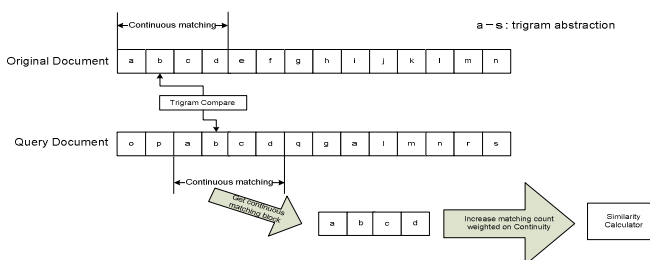


Fig. 2. Algorithm steps based on the continuity of matching trigrams

discovered, the next trigrams are compared until the trigrams do not match, and the count value is increased by $\sum_{k=1}^{\alpha}$ (α is the number of sequentially matching trigrams). When a pair of trigrams does not match, comparison of separate pairs resumes until the next matching pair of trigrams from each document is found. Even if the number of matching trigrams is identical, a document with a higher continuity of matching trigrams is considered more similar to the original document than one with lower continuity, and the accuracy of plagiarism detection is thus improved.

4 Experiments and Evaluation

The performance of the proposed algorithm was tested as follows. Parts of the poems of Kim Soweol were used as the first original document and the author's own poem, containing some parts of Soweol's original poems, both changed and unchanged, together with a simple explanation of the poem "Azalea" were used as the two queried documents. The second original document contained a simple explanation of data mining, and the two queried documents consisted of a plagiarized version of the original with some changes and a non-plagiarized document about the same subject. Thus, three of the queried documents contain plagiarism or quotations, and one was a non-plagiarized document on the same subject.

First, each document was reorganized into sets of morphemes. These were mechanically classified using the existing "Intelligent Morphemic Parser." Then, three morphemes from the set of morphemes were grouped in a duplicated manner to create trigram sets. After that, the union and intersection of the two documents being tested were obtained and continuity weights were measured in accordance with the proposed algorithm. They were then put into the similarity calculator to determine similarity.

The following shows the original documents and trigram sets used in this test.

<Original text of the poems by Kim Soweol>

어제도 하루 밤 나그네 집에 가마귀 가와기와 울며 새었소. 오늘은 또 몇 섭 리 어디로 갈까. 산으로 올라갈까 들로 갈까
오라는 끗이 없어 나는 뜻 가요. 말 마소, 내 집도 정주 광산 차 가고 배가는 끗이라오. 어 보소, 공중에 저 기러기 공중엔 길
있어서 잘 가는가? 어 보소, 공중에 저 기러기 열 섭자 북판에 내가 셨소. 나 보기가 역겨워 가실 때에는 말없이 고이 보내
드리오리다.

<Author's own poem that quotes the poems by Kim Soweol>

들에는 꽃 피네 꽃이 피네 봄 여름 가을 없이 꽃이 피네 나는 방황하는 나그네 오늘은 또 어디로 갈까. 항상 곁에 있을 줄
알았던 사랑하는 그 사람이여. 가실 때에는 말없이 고이 보내 드리려 했는데 왜 그냥 떠나 버렸소. 선 체로 이 자리에 돌이
되어도 부르다가 내가 죽을 이름이여! 그대를 찾아 오늘도 나는 방황하는 나그네

<Explanation of "Azalea" the poem by Kim Soweol>

Understanding and impression of "Azalea" the poem by Kim Soweol

나 보기가 역겨워 가실 때에는 말없이 고이 보내 드리오리다. 영변에 악산 전달래 풋 아름따나 가실 길에 뿌리오리다.
가시는 걸음걸음 놓인 그 꽃을 사뿐이 즈레 밟고 가시옵소서. 나 보기가 역겨워 가실 때에는 죽어도 아니 눈물 흘리오리다.

This poem is the essence of Soweol's poems. It artistically sublimates the traditional "affection and regret" through a woman who overcomes the sadness of separation through her will for resignation. This "affection and regret" is in line with the traditional emotions of Korean people, which has been expressed ceaselessly through such poems as "Gongmudohaga," "Gasiri," "Seogyeongbyeolgok," and "Arirang."

As we all know, the traditional Korean emotions of "regret and grief" and the traditional rhythms of Korean folk songs are the two main elements of, and inspirations for Soweol's poems. Over 150 poems left by Soweol, who is regarded as the greatest Korean poet, were published in the collection "Azalea", before his death. Another collection of his poems "Soweolsicho" was published after his death by Kim Eok and numerous others have been published since and become best sellers.

< Data mining - original text >

Summary: 많은 데이터 가운데 숨겨져 있는 유용한 상관관계를 발견하는 것. <데이터 웨어하우스와 데이터 마트가 사용자가 원하는 데이터들을 미리 만들어 놓고 이를 꺼내 볼 수 있도록 하는 개념인 반면, 각 데이터의 상관관계를 인공 지능 기법을 통해 자동적으로 밝혀 주는 것. 예를 들면... 비를 좋아하는 사람에 대한 데이터가 있고 색깔에 대한 선호도와 관계된 데이터가 있다면 이 둘의 관계를 밝혀 내는 기능을 수행한다. 즉 정확히 수치화하기 힘든 데이터 간의 연관을 찾아내는 역할을 한다.> 데이터베이스로부터 과거에는 알지 못했지만 데이터 속에서 유도된 새로운 데이터 모델을 발견하여 미래에 실행 가능한 정보를 추출해 내고 의사 결정에 이용하는 과정을 말한다

< Data mining - plagiarized text >

데이터베이스에서 말하는 데이터마이닝이란 많은 데이터 가운데 숨겨진 유용한 상관관계를 발견하는 것이다. 데이터의 상관관계를 인공 지능 기법을 통해 자동으로 밝혀 주게 된다. 예를 들면 상점에서 고객이 빵을 사는 경우의 데이터와 고객이 우유를 사는 경우의 데이터가 있다고 할 때 이 둘간의 관계성을 밝힐 수 있고 이를 마케팅에 반영할 수 있다.

< Data mining - non-plagiarized text >

데이터마이닝이란? 1. 정보 추출 작업 : 데이터마이닝은 데이터 웨어하우스를 구축한 다음 정보분석 과정을 거쳐 경영전략을 지원하는 정보를 추출하는 것이다. 즉 데이터 웨어하우스에 숨겨져 있는 데이터 간의 유형과 관계를 탐색하고 이를 분석하여 업무에 적용 할 수 있는 정보로 변환함으로써 기업의 의사결정에 적용하는 일종의 데이터베이스 분석기법이다. 데이터 변수간의 통계적인 유용한 상관관계 발견이나, 시계열성 분석 등이 이루어지는 다양한 통계처리 과정을 데이터 마이닝이라고 한다....

The procedures for similarity calculations using the above trigram sets are described below.

4.1.1 Original Document 1 vs. Queried Document 1-1

Number of trigrams in the intersection of the two documents = 16

Number of trigrams in the union of the two documents = 51 (number of trigrams in queried document) + 216 (number of trigrams in original document) – 16 (number of trigrams in the intersection between the two documents) – 14 (number of identical trigrams in original document) = 237 , Because $x = 16/237 = 0.0675$ and

$$y = \frac{\sum_{i=1}^2 i + \sum_{i=1}^3 i + \sum_{i=1}^4 i + \sum_{i=1}^5 i}{\sum_{i=1}^5 i} = 0.0385, \text{ Similarity} = 0.0490.$$

4.1.2 Original Document 1 vs. Queried Document 1-2

Number of trigram intersections between the two documents = 33

Number of trigrams in the union of the two documents = 120 (number of trigrams in queried document) + 216 (number trigrams in original document) – 33 (number of trigrams in the intersection of the two documents) – 14 (number of identical trigrams in original document) - 3 (number of identical trigrams in queried document) + 3 (number of identical trigrams in the intersection of the two documents) = 289, Because $x = 33 / 289 = 0.1142$ and $y = 561 / 7260 = 0.0773$, Similarity = 0.0922.

4.1.3 Original Document 2 vs. Queried Document 2-1

Number of trigrams in the intersection of the two documents = 1

Number of trigrams in the union of the two documents = 120 (number of trigrams in queried document) + 188 (number of trigrams in original document) – 1 (number of trigrams in the intersection of the two documents) = 307, Because $x = 1 / 307 = 325.7329 * 10^{-5}$ (approx.0.0033) and $y = 1 / 7260 = 1.3774 * 10^{-4}$, Similarity = 2.6431^{-4} (approx. 0.00264).

4.1.4 Original Document 2 vs. Queried Document 2-2

Number of trigrams in the intersection of the two documents = 15

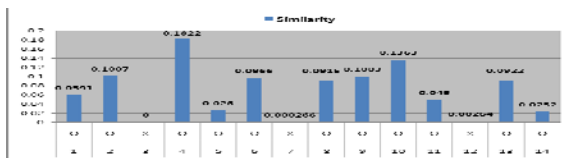
Number of trigrams in the union of the two documents = 84 (number of trigrams in queried document) + 216 (number of trigrams in original document) – 15 (number of trigrams in the intersection of the two documents) = 285, Because $x = 15 / 285 = 0.0526$ and $y = 120 / 7260 = 0.0165$, Similarity = 0.0252.

4.2 Evaluation

In the four tests, the similarity values of the plagiarized documents ranged from 0.0252 to 0.0922 and the similarity value of the non-plagiarized document was 0.00264. Thus, the tests demonstrated that the higher the degree of plagiarism, the higher the similarity value. The similarity was the highest between original document 1 and queried document 1-2, which had the longest sequences of matching trigrams. Between queried documents 1-1 and 1-2, 1-1 had a slightly higher trigram matching rate, but document 1-2 had longer sequences of matching trigrams because it copied the whole poem as it was; the similarity of document 1-2 to the original was thus greater. The plagiarism of document 1-2 from the original is more conspicuous, which shows the validity of this algorithm taking sequences of matched trigrams into account.

What, then, is the minimum value of similarity that a document must have to be regarded as plagiarism? There is no absolute standard for this: it varies according to the type, size, subject, and other features of the documents. To get more accurate data, this study conducted more tests similar to those described above.

As a result, the following statistics were obtained.



algorithm, to Hangul documents. To do this, we needed an additional step of parsing the document into morphemes. Advancing from the evaluation of similarity by the number of matching trigrams based on the Ferret algorithm, this study improved the performance by considering the length of sequences of matching trigrams, and demonstrated the effectiveness of this new technique. Although the threshold of similarity for deciding plagiarism has occurred varies according to the characteristics of the documents under review, we could estimate a generally applicable threshold through tests. The accuracy of this estimate could be improved through comparing a range of sample types. To create a perfect plagiarism detection program, we need to take other considerations into account, such as the exchange of similar words, and more research is necessary in this regard.

References

1. Brin, S., Davis, J., et al.: Copy Detection Mechanisms for Digital Documents. In: Proceedings of the ACM SIGMOD Annual Conference (1995)
2. Shivakumar, Garcia-Molina: SCAM: A Copy Detection Mechanisms for Digital Documents. In: Proceedings of International Conference on Theory and Practice of Digital Libraries (1995)
3. Bao, J.P., Shen, J.Y., et al.: Document Copy Detection Based On Kernel Method. In: International Conference on Natural, pp. 250–255 (2003)
4. Bao, J.-P., Shen, J.-Y., Liu, X.-D., Liu, H.-Y., Zhang, X.-D.: Semantic Sequence Kin: A Method of Document Copy Detection. In: Dai, H., Srikant, R., Zhang, C. (eds.) PAKDD 2004. LNCS (LNAI), vol. 3056, pp. 529–538. Springer, Heidelberg (2004)
5. Kang, N., Gelbukh, A., Han, S.-Y.: PPChecker: Plagiarism Pattern Checker in Document Copy Detection. In: Sojka, P., Kopeček, I., Pala, K. (eds.) TSD 2006. LNCS (LNAI), vol. 4188, pp. 661–667. Springer, Heidelberg (2006)
6. Lyon, C., Barret, R., et al.: A Theoretical Basis to the Automated Detection of Copying Between Texts, and Its Practical Implementation in the Ferret Plagiarism and Collusion Detector (2004)
7. Bao, J.P., Lyon, C., et al.: Copy detection in Chinese Documents Using the Ferret: a Report on Experiments. Technical Report 456 (2006)
8. <http://ko.wikipedia.org>
9. <http://www.sejong.or.kr>

Importance Weighted AdaRank

Shangkun Ren¹, Yuexian Hou¹, Peng Zhang², and Xueru Liang¹

¹ School of Computer Sci. & Tec., Tianjin University, China

² School of Computing, The Robert Gordon University, UK

{wronsky,yxhou}@tju.edu.cn, p.zhang1@rgu.ac.uk, liangsnowru@163.com

Abstract. Learning to rank for information retrieval needs some domain experts to label the documents used in the training step. It is costly to label documents for different research areas. In this paper, we propose a novel method which can be used as a cross-domain adaptive model based on importance weighting, a common technique used for correcting the bias or discrepancy. Here we use “cross-domain” to mean that the input distribution is different in the training and testing phases. Firstly, we use Kullback-Leibler Importance Estimation Procedure (KLIEP), a typical method in importance weighing, to do importance estimation. Then we modify AdaRank so that it becomes a transductive model. Experiments on OHSUMED show that our method performs better than some other state-of-the-art methods.

Keywords: Learning to Rank, importance weighting, transductive learning, AdaRank, AdaBoost.

1 Introduction

We consider the general ranking problem, i.e., given a query as the information need of the user, to find a function to order the retrieved documents.

With the development of information retrieval, ranking has become a very important branch of supervised learning and semi-supervised learning. Many exiting machine learning methods have been applied to this area, this is the so-called “Learning to Rank”.

Learning to Rank is an important problem of learning a ranking or ordering on instances, which has attracted a lot of attention in information retrieval and machine learning recently [1] [2] [3] [4].

Since it is costly to label all the search domains and there are already many labeled data in some domains, researchers wonder whether there exist an approach to use the labeled data in one domain to make prediction for unlabeled domains. That’s just the thing we care about in this paper. Fortunately, we indeed find a novel method for this problem.

We denote the domain which has many labeled data as related domain D_r , and the domain which we want to predict as target domain D_t . As there is no labeled data in D_t , we can take D_r as training data and D_t as test data, denote their distributions as $P_{tr}(\mathbf{x})$ and $P_{te}(\mathbf{x})$, respectively. A situation where

the input distribution $P(\mathbf{x})$ is different in the training and testing phases but the conditional distribution of output values, $P(\mathbf{y}|\mathbf{x})$, remains unchanged is called covariate shift[5], where \mathbf{x} is the explanatory variable, and \mathbf{y} is the response variable. The influence of covariate shift could be alleviated by weighting the training data in maximizing the log-likelihood function, the optimal choice of the weight function is asymptotically shown to be the ratio of the density function of the explanatory variable in the training set to that in the test set [6]:

$$w(\mathbf{x}) := \frac{p_{te}(\mathbf{x})}{p_{tr}(\mathbf{x})} \quad (1)$$

This can be viewed as the importance of training data from a different domain. We can use this to correct the bias or discrepancy between the training data and the test data. We propose a novel method based on this, at the same time, boosting is used in our model.

2 Related Work

In learning to rank, there are two steps, training and testing. In the first step, we are given a set of queries(to be exactly, m queries), a list of documents for each query, and a relevant level for the document to denote the similarity between the document and the corresponding query. Formally, we can denote the training set as $D_{tr} = \{q_i, \mathbf{x}_i, \mathbf{y}_i\}_{i=1}^m$, where q_i denotes for the i th query, \mathbf{x}_i denotes for the document list for the i th query, \mathbf{y}_i for the labels, which means the real rankings. We aim to learn a rank function $F(q_i, x_{ij})$ such that, for two documents: x_{ij} and x_{ik} , document x_{ij} should be ranked higher than document x_{ik} iff $F(q_i, x_{ij}) > F(q_i, x_{ik})$. Then, in the second step, we are given another set of queries(to be exactly, n queries), also a list of documents for each query but without labels, $D_{te} = \{q_i, \mathbf{x}_i\}_{i=m+1}^{m+n}$. We use the function F learned from the first step to calculate a score for each document, and rank them according to their scores. So what we want to do is to find a prediction function that makes as little error as possible in the test set.

Ranking learning, in which the training data are collected in the form of pairwise instance preference, is known as preference learning. Many approaches arose based on this, for example, RankSVM [1][2], RankBoost [3], etc. However, in these approaches, only the pair document dependence is considered, which means that dependence between each document in the whole rank can't be fully considered. From this perspective, listwise models do better and some models are proposed by other experts. For example, AdaRank[7] inspired by AdaBoost, RankCosine[8] inspired by RankBoost model and Vector Space model to improve the precision. In these models, more dependence between documents is considered.

It seems that it's difficult to create a new approach to gain better rank performance. Researchers turn their attention to find some method to improve the performance of the existing models. Many works have been done. Chen, D. et al.[9] gave the definition of the cross domain learning to rank problem. Algorithms are proposed by conducting feature level and instance level knowledge

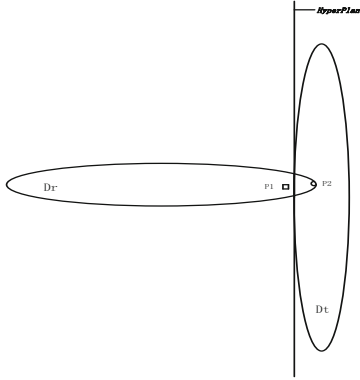


Fig. 1. A special case of Related domain(D_r) and Target domain(D_t)

transfer. Geng, X. et al.^[10] proposed a more efficient method in which KNN was used. Gao, W. et al.^[11] proposed a method to measure the extent, to which query-document instance in the related domain is similar to the target domain. Firstly, they conduct a hyperplane H_{rt} to separate the related domain data D_r from the target domain data D_t . Then, they calculate the importance of each related-domain document using its distance to the hyperplane. There is an apparent disadvantage of this method. As shown in Fig. 1, intuitively, the document P_2 of related domain which is mixed in the target domain should be more important than the document P_1 . But since P_2 is far from the classification hyperplane while P_1 is near the hyperplane, the importance values calculated by the above method will violate our intuition. The method we use avoids this problem by directly estimate the ratio between $P_{te}(\mathbf{x})$ and $P_{tr}(\mathbf{x})$, where $P_{tr}(\mathbf{x})$ denotes the density function of training data while $P_{te}(\mathbf{x})$ denotes the density function of test data.

3 Kullback-Leibler Importance Estimation Procedure

Kullback-Leibler Importance Estimation Procedure (KLIEP)^[5] is currently a state-of-the-art method in importance weighting. Its main advantages being its automatic model selection procedure and proven convergence properties.

In calculating importance, density estimation is a difficult work, especially for high-dimension situations. Sugiyama, M. et al. got an approach to estimate $w(\mathbf{x})$, at the same time, avoiding estimating densities.

The main idea is to minimize the K-L divergence of $p_{te}(\mathbf{x})$ and its estimate: $\hat{w}(\mathbf{x}) \cdot p_{tr}(\mathbf{x})$

$$\begin{aligned} KL[p_{te}(\mathbf{x}) || \hat{p}_{te}(\mathbf{x})] &= \int_D p_{te}(\mathbf{x}) \log \frac{p_{te}(\mathbf{x})}{\hat{w}(\mathbf{x})p_{tr}(\mathbf{x})} d\mathbf{x} \\ &= \int_D p_{te}(\mathbf{x}) \log \frac{p_{te}(\mathbf{x})}{p_{tr}(\mathbf{x})} d\mathbf{x} - \int_D p_{te}(\mathbf{x}) \log \hat{w}(\mathbf{x}) d\mathbf{x} \end{aligned} \quad (2)$$

where $p_{tr}(\mathbf{x})$ denotes for the density function of the training data, $p_{te}(\mathbf{x})$ denotes for the density function of the test data, $\hat{w}(\mathbf{x})$ is a linear approximation of $w(\mathbf{x})$. Since the first term has nothing with $w(\mathbf{x})$, we focus on the second term and define the objective function as follows:

$$J := \int_D p_{te}(\mathbf{x}) \log \hat{w}(\mathbf{x}) d\mathbf{x} \approx \frac{1}{n_{te}} \sum_{j=1}^{n_{te}} \log \hat{w}(\mathbf{x}_j^{te}) = \frac{1}{n_{te}} \sum_{j=1}^{n_{te}} \log \left(\sum_{l=1}^b \alpha_l \varphi_l(\mathbf{x}_j^{te}) \right) \quad (3)$$

To make the weights $\hat{w}(\mathbf{x})$ positive, we must restrict $\alpha_l \geq 0$ for $l = 1, 2, \dots, b$, and $\hat{p}_{te}(\mathbf{x})$ should be a probability density function:

$$\begin{aligned} 1 &= \int_D \hat{p}_{te}(\mathbf{x}) d\mathbf{x} = \int_D \hat{w}(\mathbf{x}) p_{tr}(\mathbf{x}) d\mathbf{x} \\ &\approx \frac{1}{n_{tr}} \sum_{i=1}^{n_{tr}} \hat{w}(\mathbf{x}_i^{tr}) = \frac{1}{n_{tr}} \sum_{i=1}^{n_{tr}} \sum_{l=1}^b \alpha_l \varphi_l(\mathbf{x}_i^{tr}) \end{aligned} \quad (4)$$

Gauss kernels are used as the basis function: $\varphi_l(\mathbf{x}) = \mathbf{K}_\sigma(\mathbf{x}, \mathbf{x}_l^{te})$ and this can be solved easily then we get our importance $w(\mathbf{x})$.

4 A Boosting Model with Importance Weighting

4.1 General Model

In a ranked retrieval context, appropriate sets of retrieved documents are naturally given by the top L retrieved documents. Many approaches arose to measure the goodness of a ranker. An approach that has seen increasing adoption, especially when employed with machine learning approaches to ranking is measures of cumulative gain, and in particular normalized discounted cumulative gain (NDCG) [12]. NDCG is evaluated over L top search results. Let $R(j, d)$ be the relevance score assessors gave to the d th document for query j . Then,

$$\text{NDCG}(Q, L) = \frac{1}{|Q|} \sum_{j=1}^{|Q|} Z_k \sum_{m=1}^L \frac{2^{R(j,m)} - 1}{\log(1 + m)} \quad (5)$$

where Z_k is a normalization factor calculated to make sure that a perfect ranking's NDCG at L is 1. For a query q_i , whose total number of retrieved documents is less than L , i.e. $n_{q_i} < L$, the last summation is done up to n_{q_i} .

L denotes for the truncation level. The advantage of NDCG is that it is a non-binary measurement, and it does help to separate “Good” from “Perfect”, since we usually use more than 2 kinds of labels for a set of documents. Another important reason for this is Ping, L. et al. [13] have proven that the DCG error can be bounded by the square root of the classification error.

4.2 Importance Weighted AdaRank

Given a test query, we can calculate the importance for each document in the training set using KLIEP. For each document \mathbf{x}_i , calculate a weight $w(\mathbf{x}_i)$ using equation(1), by summing up and normalizing, we can get a weight for each training query, namely, $\{w(q_i)\}_{i=1}^m$. This can be seen as the importance of each training query. As the test data is used in the training step, our method becomes a transductive model.

Inspired by AdaBoost[4] and AdaRank[7], we could train a set of weak rankers and combine them to make better prediction:

$$F = \sum_{t=1}^T \alpha_t f_t \quad (6)$$

where f_t is the weak ranker gotten from the t th round, and T is the total number of rounds we have done. We could fix T or make the loop terminate automatically when the performance stops going better.

In each round, we get a weak ranker, and we should calculate a weight for it. The magnitude of this weight will base on the performance of the weak ranker. Actually, a good ranker will get a large weight. At the same time, we maintain a distribution of weights over the queries in the training data. We denote the distribution of weights at round t as \mathbf{P}_t , and $\mathbf{P}_t = \{P_t(i)\}_{i=1}^m$, each element standing for the weight of a training query. We can initialize \mathbf{P}_1 with $\{w(q_i)\}_{i=1}^m$ we have gotten from KLIEP or we can set $\mathbf{P}_1 = \{\frac{1}{m}, \frac{1}{m}, \dots, \frac{1}{m}\}$. At the end of each round, we update this distribution according to the rank performance in this query and the weights $\{w(q_i)\}_{i=1}^m$ from KLIEP. We define a cost function positively correlated to $\{w(q_i)\}_{i=1}^m$: $C(w(q_i))$. Intuitively, when $w(q_i)$ is large (i.e. $C(w(q_i))$ is large) and query i is ranked poorly, we should increase our attention on it(query i) significantly. When $w(q_i)$ is small (i.e. $C(w(q_i))$ is small) and query i is ranked poorly, we should increase our attention on it slightly. If $w(q_i)$ is large (i.e. $C(w(q_i))$ is large) and query i is ranked nicely, we should decrease our attention on it slightly. The last case, if $w(q_i)$ is small (i.e. $C(w(q_i))$ is small) and query i is ranked nicely, we could decrease our attention on it significantly. This makes our method a cost-sensitive method, we call it “IW-AdaRank”.

The weak rankers are constructed based on training data and the weight distribution \mathbf{P}_t . The goodness of a ranker f_t is measured as follows:

$$\text{Goodness}(f_t) = \sum_{i=1}^m P_t(i) \cdot \text{NDCG}(\pi(q_i, \mathbf{d}_i, f_t), \mathbf{y}_i, L) \quad (7)$$

where $\pi(q_i, \mathbf{d}_i, f_t)$ denotes for the rank results for query $i(q_i)$ with the weak ranker f_t .

Our algorithm can be described as follows:

Input: The training set \mathbf{X}_{tr} , i.e. $\{q_i, \mathbf{d}_i, \mathbf{y}_i\}_{i=1}^m$

The test set \mathbf{X}_{te} , i.e. $\{q_i, \mathbf{d}_i\}_{i=m+1}^{m+n}$

The truncation level L

Output: The Rank function F

1 For the training set \mathbf{X}_{tr} and test set \mathbf{X}_{te} , calculate the importance:

$$w(\mathbf{x}) = \text{KLIEP}(\mathbf{X}_{tr}, \mathbf{X}_{te}) \approx \frac{P_{te}(\mathbf{x})}{P_{tr}(\mathbf{x})}$$

2 Calculate the importance for each training query $\{C(q_i)\}_{i=1}^m$;

3 Initialize the distribution for each training query $\{P_1(i)\}_{i=1}^m$;

4 for $t = 1:T$

 4.1 Train a weak ranker f_t according to \mathbf{P}_t and \mathbf{X}_{tr} ;

 4.2 Calculate α_t for ranker f_t :

$$\alpha_t = \frac{1}{2} \cdot \ln \frac{1 + \sum_{i=1}^m P_t(i) \cdot \text{NDCG}(\pi(q_i, \mathbf{d}_i, f_t), \mathbf{y}_i, L)}{1 - \sum_{i=1}^m P_t(i) \cdot \text{NDCG}(\pi(q_i, \mathbf{d}_i, f_t), \mathbf{y}_i, L)}$$

 4.3 Update the rank function:

$$F_t(\mathbf{x}) = \sum_{k=1}^t \alpha_k f_k(\mathbf{x})$$

 4.4 Update the distribution:

$$P_{t+1}(i) = \frac{\exp(-\text{NDCG}(\pi(q_i, \mathbf{d}_i, F_t), \mathbf{y}_i, L)) \cdot C(w_i)}{\sum_{j=1}^m \exp(-\text{NDCG}(\pi(q_j, \mathbf{d}_j, F_t), \mathbf{y}_j, L)) \cdot C(w_j)}$$

End for

5 The rank function $F = F_T$.

As the test data is used in our training step and our method is trained by documents lists, our method becomes a transductive listwise model. The deviation between training set and test set can be corrected by our importance estimating step. That's why we believe that our method can perform better than AdaRank.

As for the weak ranker, we could use a single feature as a weak ranker. As described by Xu, J. and Li, H. [7] we choose the single feature that has the optimal performance among all of the features:

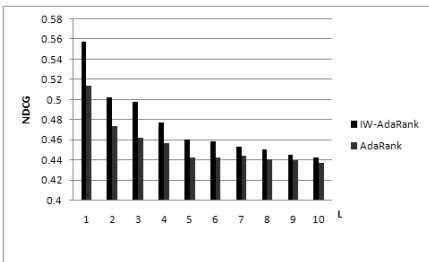
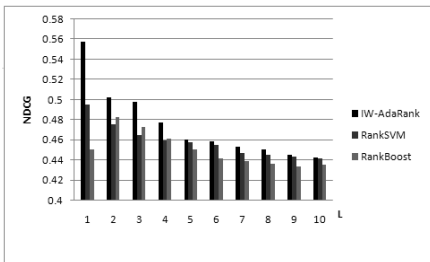
$$\max_k \sum_{i=1}^m P_t(i) \cdot \text{NDCG}(\pi(q_i, \mathbf{d}_i, x_k), \mathbf{y}_i, L)$$

where x_k stands for the k th feature.

As an alternative, we can also choose Cohen's RIPPER [15] as the weak learner. When using it, we must transform it into a cost-sensitive rank model.

5 Experimental Setup and Main Results

We use the document retrieval data: OHSUMED in LETOR dataset. This is a re-ranking (subset ranking) problem, where an initial set of documents have been retrieved and the goal is to sort the set in an order that can reflect the relevance

**Fig. 2.** V.S. AdaRank on OHSUMED**Fig. 3.** V.S. RankSVM and RankBoost on OHSUMED

between documents and the query [16]. The original OHSUMED collection was created for information retrieval research. It is a subset of MEDLINE, a database on medical publications. There are 106 queries. For each query, there are a number of documents associated [17]. Each query is about a medical search need, and thus is also associated with patient information and topic information. There are three relevance levels: definitely, possibly, or not relevant. There are a total of 16,140 query-document pairs with relevance judgments.

The OHSUMED dataset is divided into five subsets and conducted 5-fold cross-validation experiments. The results reported below are those averaged over five trials. As a baseline, we use the results of AdaRank in OHSUMED dataset. It's available in [18].

From Fig. 2, you can see that we make a great improvement in the performance. In addition, we make some other comparisons. In OHSUMED, we are given two baseline results using RankSVM and RankBoost respectively. The comparison between our method and theirs can be seen in Fig. 3.

The results indicate that all the improvements in terms of NDCG are statistically significant. It is evident from these results that IW-AdaRank gives an improved performance compared to original AdaRank. Furthermore, the performance of IW-AdaRank is seen to be better than RankSVM and RankBoost.

Acknowledgement. The authors would like to thank anonymous reviewers for their constructive comments. This work is supported in part by the Natural Science Foundation of China (NSFC, grant 61070044); Natural Science Foundation of Tianjin (grant 09JCYBJC00200); the NSFC-RSE (Royal Society of Edinburgh) International Joint Project Scheme; the European Union Framework Programme 7 through its Marie Curie International Research Staff Exchange Scheme (grant 247590); and the United Kingdom's Engineering and Physical Sciences Research Council (grant EP/F014708/2).

References

1. Joachims, T.: Optimizing Search Engine using Clickthrough Data. In: Proceedings of the ACM Conference on Knowledge, Discovery and Data Mining, Edmonton, Alberta, Canada, pp. 133–142 (2002)

2. Herbrich, R., Graepel, T., Obermayer, K.: Large margin rank boundaries for ordinal regression. In: Smola, A., Bartlett, P., Schlkopf, B., Schuurmans, D. (eds.) Advances in Large Margin Classifiers, pp. 115–132 (2000)
3. Freund, Y., Iyer, R., Schapire, R., Singer, Y.: An efficient boosting algorithm for combining preferences. Journal of Machine Learning Research 4, 933–969 (2003)
4. Xishuang, D., Xiaodong, C., Yi, G., Zhiming, X., Sheng, L.: An Overview of Learning to Rank for Information Retrieval. In: CSIE, vol. 03 (2009)
5. Sugiyama, M., Suzuki, T., Nakajima, S., Kashima, H., von Bnau, P., Kawanabe, M.: Direct importance estimation for covariate shift adaptation. Annals of the Institute of Statistical Mathematics 60(4), 699–746 (2008)
6. Shimodaira: Improving predictive inference under covariate shift by weighting the log-likelihood function. Journal of Statistical Planning and Inference 90(2), 227–244 (2000)
7. Xu, J., Li, H.: AdaRank: A boosting algorithm for information retrieval. In: SIGIR, Amsterdam, Netherlands, pp. 391–398 (2007)
8. Qin, T., Liu, T.Y., Tsai, M.F., Zhang, X.D., Li, H.: Learning to search web pages with query-level loss functions. Technical Report MSR-TR (2006)
9. Depin, C., Yan, X., Jun, Y., Gui, R.X., Gang, W., Zheng, C.: Knowledge transfer for cross domain learning to rank. Information Retrieval 13, 236–253 (2009)
10. Xiubo, G., Yan, T.L., Tao, Q., Andrew, A., Hang, L., Heung, Y.S.: Query dependent ranking using k-nearest neighbor. In: SIGIR, Singapore (2008)
11. Wei, G., Peng, C., Kam, F.W., Aoying, Z.: Learning to rank only using training data from related domain. In: SIGIR, Geneva, Switzerland (2010)
12. Christopher, D.M., Prabhakar, R., Hinrich, S.: An Introduction to Information Retrieval. Cambridge University Press, Cambridge (2008)
13. Ping, L., Christopher, J.C.B., Qiang, W.: McRank: Learning to Rank Using Classification and Gradient Boosting. In: Proceedings of the International Conference on Advances in Neural Information Processing Systems, Vancouver, B.C., Canada (2007)
14. Robert, E.S., Yoram, S.: Improved boosting algorithms using confidence-rated predictions. Machine Learning 37(3), 297–336 (1999)
15. William, W.C.: Fast Effective Rule Induction. In: Proc. Twelfth Int'l. Conf. on Machine Learning, pp. 115–123. Morgan Kaufman, San Francisco (1995)
16. Kevin, D., Katrin, K.: Semi-supervised ranking for document retrieval. Computer Speech and Language 25, 261–281 (2011)
17. Jun, Xu., Yan, T.L. and Hang, L.: The OHSUMED Dataset in LETOR. Microsoft Research Asia (2007)
18. AdaRank on LETOR,
[http://research.microsoft.com/en-us/um/beijing/projects/letor/
baselines/adarank.html](http://research.microsoft.com/en-us/um/beijing/projects/letor/baselines/adarank.html)

A Semantic Search Framework for Document Retrievals (Literature, Art and History) Based on Thesaurus Multiwordnet Like

Vitoantonio Bevilacqua^{1,2,*}, Vito Santarcangelo^{1,2}, Alberto Magarelli¹,
Annalisa Bianco³, Giuseppe Mastronardi^{1,2}, and Egidio Cascini⁴

¹ Department of Electrical and Electronics, Polytechnic of Bari,
Via E. Orabona, 4 – 70125 Bari – Italy

² e.B.I.S. s.r.l. (electronic Business in Security), Spin-Off of Polytechnic of Bari,
Via Pavoncelli, 139 Bari – Italy
bevilacqua@poliba.it

³ Gius. Laterza & Figli S.p.A., piazza Umberto I 54, 70121, Bari

⁴ Accademia Italiana del Sei Sigma - c/o Università degli Studi Guglielmo Marconi,
Via Giusti 7, 50121 Firenze

Abstract. The aim of this paper is to show the application of a Thesaurus based approach to several issues of interest for an Italian Publishing House. Final experimental results reveal good performance in terms of rate of retrieval and recall and then encourage the prosecution of the multidisciplinary research.

Keywords: Thesaurus, Multi-Wordnet, Monte Carlo Method, retrieval.

1 Introduction

This paper introduces the work carried out by the University Politecnico of Bari in collaboration with the Gius. Laterza and Figli publishing house, as part of the project Diderot: Data Oriented Integrated System for the Rapid Definition of Multimedial Object and Texts. Diderot is a research project held in the area of the National Innovation Founding of the Italian Government in which the editorial sector, ICT industries and research institutions have been working together to design and develop a system able to govern all the steps related to the production of education content, content to be delivered with different outputs through different channels of distributions (printed books, e.books, learning objects for the web or the interactive whiteboard, etc.). New educational products could be created on the basis of pre-existent raw material that could be reshaped and modified to satisfy the requirements of a specific output and target or on the basis of a new content to be written. But the real goal for a XXI Century publishing house is to be able to re-use the wide and pre-existent catalogue in order to give shape to new contents and to adapt or re-create the original material to give birth to innovative products. The new ways of teaching, the increasing use of interactive whiteboards and computers in the classroom and at

* Corresponding author.

home, the new ways of learning that the new media and the habit to use them boost in the new generation, makes for a publisher a *must* rethink its content and innovate its production process. Therefore, Diderot had to deal with two different priorities necessarily intertwined: implementing a new production system and together an information and retrieval system, able to store and research raw material from published books. This second objective implies to deal and solve different problems we came across along the research work. First of all, a published book is not just a set of self-contained assets ready to be used, but a linear structured work, where style and content are normally associated in a single body. The shape of the product is correlated to the content [6] and this implies that different products are released in different shapes, more often not marked up according to a standard set of indexing keys. This feature results from the production process of an educational book: every single book has its own graphic design, the shape is part *and* expression of the content and the final product is released after having been processed in authoring systems like InDesign. The lack of a separation between content and shape creates not a few problems when the goal is to store and research the content inside the book. The first problem that the Diderot team had to face was therefore finding a way to index content already produced according to a set of standard keys. The research of the editorial standards and the analysis of the Laterza education books led to choose Docbook as an XML markup language useful to index published work. The team has then created a table of correspondence among the styles as set in the books (chapters – paragraphs – indexes – notes – exercises – etc.) and the Docbook tags. Two more problems came so ahead. Which kind of content could represent the raw material to be converted into DocBook files? InDesign XML files, final result of the production process, or Word revised files, the final content after revision before a graphic designer has given to the book its own final shape? The answer to this question required not a simple task, as we will explain in the following part of this paper. The second problem was given by the need to index the content with keywords that will make possible to store and retrieve it through semantic keys. We had therefore to design a semantic engine which allowed retrieval thanks to indexing keys. But how should these keys been assigned? The process of creating new entries every time we had to index a book without referring to a structured vocabulary was not approachable, because we will have encountered a wide number of variations and similar expressions that would have made difficult and burdensome the system, the more it would have been populated with new material. The solution was to turn to a structured vocabulary to be optimized with terms appropriate to classify the Laterza educational content. Therefore, two new fields of research were undertaken: searching for a multilingual lexical database that could be the basis for future expansion and detecting the areas of classification that could result suitable to index the educational products published by Laterza. The original material was related to different fields of study (language and literature, history, history of art), that implied that a multilingual thesaurus related to a specific cultural domain would not have satisfied the purpose. We needed just a multilingual lexical database that could be expanded with terms related to our material. The investigation led us to select Multiwordnet, a multilingual lexicon database in which the Italian Wordnet is strictly aligned with the original project developed by the Princeton University: WordNet. This lexicon had to be extended with terms related to the specific domains and with the key-values that could

result useful to set a semantic query. Therefore, for every single domain the set of data directly related to the field has been identified and for each of them a set of Italian keywords has been defined and uploaded to the system. This methodology has the advantage to maintain the consistency and integrity of the Lexicon and to finalize a system that is possible to enhance in time adding new terms.

2 Background [1]

A semantic search engine [4] is a retrieval system that allows to conduct research expressing the questions in the same way that humans request information to each other. Through the network of the meanings of words (Knowledge based of the semantic search engine) it is possible to correctly identify the meaning of the speech, so the search engine is able to return all the content related to the initial question. If the query is precise the performance of the engine increases. A query as “the Italian poetry in romanticism” can be hard to understand for a classical search engine (it would consider the occurrences of each term but would not consider the meaning of the sentence , but it is very simple for a semantic search engine that would consider the set of meanings that exist between the words of the query. Examples of semantic search engine are www.hakia.com and <http://www.sensebot.net>. Hakia returns results from Web, Blogs, Images and Video, Sensebot shows us the concepts of its Knowledge Base. The different dimension of concepts in this graphical representation relates to the rank of matching relevance with the input query.

3 Analysis of the Problem and Materials

As previously said, in order to populate the Diderot database it was necessary to find a way for conferring the raw material of Laterza school books to the system. A possible file-format considered initially for the scope of indexing books has been the IDML (In Design Mark-up Language) format. The inability to index texts in this format by PhpDig moved us to create an algorithm that converts such books into Docbook files. Docbook format is a XML standard widely used that counters the hierarchical structure of a book ready to be published. Docbook linear structure indexes chapters, paragraphs, notes of the book: this indexing allows to release the book in multiple outputs: volumes to be printed, e-books, content to be delivered on a web site, and so on. Indexing has not yielded, at first, significant results for the complexity of the IDML standard. The first step has been to understand the correspondence between the IDML tag and Docbook tags. In this regard, we have considered conversion tables. IDML is the XML result of a book produced using InDesign. In order to convert the raw material in a text ready to be published, specific styles are assigned to the content, each of them defines a part of the work (chapter title – chapter number – and so on). The same styles are marked up in Docbook: in theory, it would be therefore possible to set a table of correspondence between the IDML and Docbook XML. As a matter of fact, we realized that the resulting table could not be applied to every occurrence, because each designer uses InDesign with a different scheme that cannot be represented in a single conversion table. In addition to

this, IDML spreads the linear content in single sub-units not understandable as self-contained assets, but just as part of a major referenced structure: many of these sub-units do not contain any content, but just information about it. This makes it difficult to reconstruct the original chapter as viewed in separated multiple files. For all these reasons, the final analysis led to choose the .doc format as a proper content source suitable to be converted into Docbook files. The conversion process has been realized as follows. .doc files have been converted, first of all, in HTML pages as to be quickly indexed by a search engine. For this action the “Word to HTML Converter” has been used. The operation is simple: we enter the location of the source file to convert, and the folder in which we want to allocate the resulting HTML file. At this point, after invoking a script that removes the head generated by the Converter, we create hyperlinks to each paragraph of a chapter, so as to obtain maximum benefit from indexing. It is possible to do it manually (with an html/text editor) or with a script that binds the tag <h1> for chapter titles and the tag <h2> only for paragraph titles. In this way, we can identify these paragraph titles and create hyperlinks between them (with the tag). Finally, the resulting file is uploaded on the server after logging in with administrator credentials. At this point, when the procedure of indexing is ended, semantic searches within documents are possible through the knowledge base, the thesaurus, which is properly populated.

4 Methods: Thesaurus and Retrieval

The thesaurus is based on the MultiWordnet structure [2]. MultiWordnet is an international lexical database with a simple structure (indexes and relational database). As part of the Diderot project a thesaurus has been implemented that is based on three index databases and a database of relationships. The index databases refer to three semantic areas: “History”, “Art History” and “Literature”, whose relationships have been saved in the “Common Relation” database. In order to preserve the integration and the consistency within the research project Multiwordnet, the structure of the index fields has been maintained and we used the same type of notation on the letter of id#. To avoid id# overlapping with those already present in MultiWordNet, different letters have been chosen as id# related to the specific domains: the letter “S” has been used as id# for historical terms, the “L” for id# for literature’s vocabularies, and the “K” as id# for words referred to the History of Art.

The semantic search engine [5] can be represented by a simple block diagram as showed in figure 2 . The INPUT data is the sentence to be (characterized by word, punctuation, prepositions and conjunctions) written by the user in the INPUT FORM. The sentence is filtered by the FILTERING block (this block removes stop words) and the output of this one is a VECTOR OF WORDS. These words are the input of the THESAURUS QUERIES block, which calls the thesaurus through each word and obtains the associated ENTITIES. These ones are the input of the LOGICS block, that elaborates them and considers the related ones, which are the inputs of the DOCS QUERIES block. This block queries the file server and obtains the relevant docs with relative score. The DOCS QUERIES block is the PhpDig web spider and search engine.

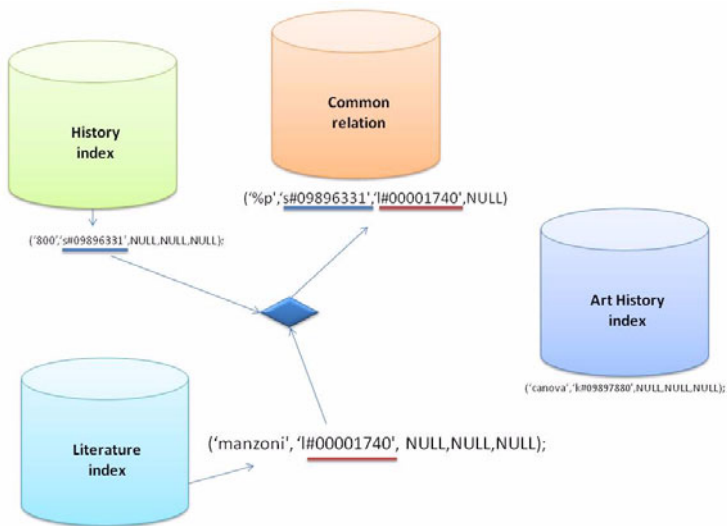


Fig. 1. The figure shows the relation between the lemmas “Manzoni” (Literature) and “800” (History) in the Relation Database with the type “%p” (has part in)

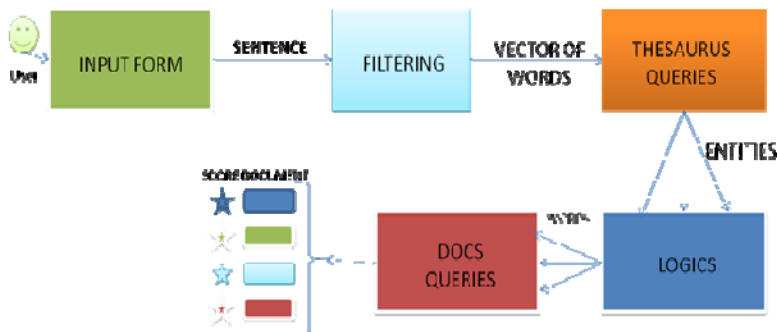


Fig. 2. System Block Diagram

An example can be useful to show the data flow on this block diagram. The user writes the sentence “the Italian romanticism in poetry”, so the FILTERING block returns the vector of words [Italian, romanticism, poetry]. The system queries the THESAURUS with these words and obtained for the “Italian” word the names of Italian events, authors and artists set in the thesaurus [Boccaccio, Manzoni, Leopardi], for the “romanticism” word the names of international events, authors and artists related [800, Manzoni, Leopardi, VanGogh], for the “poetry” the words generalized by this term and the international poets and authors [lyrics, rhymes, Leopardi]. Matching these results is possible to invoke the PhpDig with the logic words obtained from the thesaurus [Leopardi].

5 Experimental Results and Validation

For the validation of the system has been considered a bandwidth validation and a classical parametric validation for the retrieval system. The first is based on a statistical tool based on Monte Carlo method, the second on the measure of the parameters precision and recall of the system.

5.1 Statistical Bandwidth Validation

Monte Carlo method is based on a simulated sampling, representing the cumulated probability distribution of X . The procedure to choose an element x of X is: 1) a random decimal number included between 0 and 1 is taken, by means of a random numbers generator; 2) the obtained number is put on the y axis; 3) this number is projected on the curve $y = F(x)$; 4) the x value, determined in this way, is an element of a sample extracted by X . This procedure is adequate, in fact, to assign to the x value determined as illustrated above, the meaning of an element of a sample extracted from X . In fact, we can write:

$$P(x_1 < x_{\text{campione}} < x_1 + dx) = dy_1 = \frac{dF(x_1)}{dx_1} dx = f(x_1)dx \quad (1)$$

in order to consider x an element of a sample from X . For further news about the Monte Carlo method it is useful to read the paper [3]. Obviously, the way to apply the method depends on the specific problem under consideration. An important statistical tool to help the control of the upload bandwidth request of the server, based on Monte Carlo method, has been implemented. The input variables of the system are X1 (number of users) and X2 (average number of requests per user), detected for 15 days. For example, the first day the number of users that has been connected on the system is 30, then $X1=30$ and the total number of request is 300 ($X2=300/30=10$). The 15 X1 numbers are ordered in increasing mode and for each of them is associated a value between 0 and 1. 1000 random numbers are then generated and a value of X1 is associated to each of them. The same procedure is followed for X2, and the 1000 X1*X2 products are calculated. After that, the mean value of these results is calculated and this value is compared with that of upload bandwidth of the server. The analysis of this bias value is the output of this system. Once obtained the result it is possible to draw the cumulative probability distribution of the bandwidth, from which it is possible to obtain all kinds of needed information.

5.2 Comparison between Semantic Search Engines

We have considered some queries about literature for testing the performances of our semantic web search engine with those of www.hakia.com and www.sensebot.net. Hakia supports only English language while the second supports English, French, German e Spanish languages. The queries used are “the Italian poetry of 1300”, “the Italian satire in the Renaissance” and “the Sculpture in the Baroque”. For the first query **our system** returns documents about “Landini, Sacchetti, Petrarca”, **Hakia** “Cavalcanti, Petrarca, Giacomo da Lentini”, **Sensebot** returns a meaning map that

shows Dante and Petrarch as right results. Our system as output of the query “the Italian satire in the Renaissance” produces “Ariosto”, Hakia produces “William Baldwin, Ariosto”, Sensebot produces the semantic map in the figure 3, in which we can see that the meaning is wrong.



Fig. 3. Sensebot map of the query "The italian satire in the Renaissance"

The output of our system for the query “the Italian sculpture in the Baroque” is “Bernini” with its relative documents scored as shown in figure 4.

100.00	<u>19.1 GIAN LORENZO BERNINI.html</u>	26.39	<u>19.3 PIETRO DA CORTONA.html</u>
41.34	<u>19.2 FRANCESCO BORROMINI.html</u>	13.78	<u>19 IL BAROCCO.html</u>
37.31	<u>19.4 BAROCCO.html</u>	7.96	<u>18 NATURALISMO E CLASSICISMO.html</u>

Fig. 4. Output of our system for the query "The italian sculpure in the Baroque"

The output of Hakia is general but in those results we can see the word “Bernini”, the map returns by SensBot is shown in the following figure 5.



Fig. 5. Sensebot map of the query "The italian sculpe in the Baroque"

Our system is highly performing thanks to a thesaurus dedicated to Literature, Art and History, but this has been made possible thanks to the implementation of words and to the process of stemming data. Hakia returns very good results also if the historical period isn't correct in some outputs, Sensebot has a very innovative graphical representation of the semantic map, but the results sometimes are wrongs.

6 Conclusions

This paper shows the features and the potentialities of a semantic search engine used for the context of literature, history of art and history. The search engine implemented can be adapted for other semantic contexts by the realization of a related thesaurus. The limits of our search engine are the use of single words of the sentence and a poor graphical interface for the results of the query. Good features of our system is the possibility of fully control of the thesaurus, of the implementation of new relations and the good performances of relevance on the document retrieval.

References

1. Tumer, D., Shah, M.A., Bitirim, Y.: An Empirical Evaluation on Semantic Search Performance of Keyword-Based and Semantic Search Engines. Google, Yahoo, Msn and Hakia, Internet Monitoring and Protection. In: ICIMP 2009, pp. 51–55 (2009)
2. Pianta, E., et al.: Multiwordnet Developing an Aligned Multilingual Database. In: Proceedings of the 1st International WordNet Conf., pp. 293–302 (2002)
3. Cascini, E.: Considerazioni Sulla Variabilità Di Un Processo Di Misura Con Una Applicazione Nell’area Della Customer Satisfaction. *Sei Sigma & Qualità* 1(2), 18–210 (2006)
4. Kassim, J., et al.: Introduction to Semantic Search Engine. In: International Conference on Electrical Engineering and Informatics, pp. 380–385 (2009)
5. Loganathanraj, R., et al.: An Ontology Based Semantic Literature Retrieval System. In: Proc. of the 19th IEEE Symp. on Computer-Based Medical Systems (2006)
6. He, R., Liu, L.: Educational Resource Sharing Model Based on Semantic Grid. Computational Intelligence and Software Engineering (2009)

A Novel Musical Synthesizer Embedded with Physical Modeling Sound Synthesis Algorithm

Sangjin Cho, Myeongsu Kang, and Uipil Chong^{*}

School of Electrical Engineering, University of Ulsan, 93,
Daehak-ro, Nam-gu, Ulsan, 680-749, Korea
`{sjcho75, ilmareboy, upchong}@ulsan.ac.kr`

Abstract. This paper describes a novel synthesizer that can generate sounds of two plucked string and one woodwind instrument. This consists of laser strings, frets, physical modeling sound engine. Laser strings constructed by pairs of a laser module and a photodiode describe plucking, strumming and blowing. Frets are implemented by using voltage divider and they enable the player to represent various playing styles such as guitar solos. Each fret has different voltage values to adjust intonation on the synthesizer. These values are converted into 12-bit data and served as an argument of the sound engine based on digital waveguide model with time-varying propagation speed (DWTVPS). Sound synthesis algorithm is embedded onto the digital signal processor. Consequently, the synthesized sounds are played through a speaker in real-time.

Keywords: Musical synthesizer, Laser string, Fret, Voltage divider, Physical modeling, Sound synthesis, Digital signal processor.

1 Introduction

The high developed acoustic technology provides a variety of sensitive cultural contents to the public. It has been recently provided that a number of novel interfaces cross boundaries that are inherent to the conventional techniques/shapes of instruments. Moreover, these interfaces combine with musical sound synthesis algorithm based on the musical acoustics. This combination supports a creative music environment that makes the user stimulate his/her senses and sensitivity.

D. Overholt introduced the 'Overtone Violin' which has gestural controllers via embedded sensors [1]. It allows the instrument to be extended/enhanced to new methods of expression that are not inherent to the conventional technique. In addition to these, many novel interfaces for music performance were designed, such as 'Mountain Guitar' [2] which is allowed to adjust intonation by detecting the movement of the guitar body, 'GXtar' [3] using techniques of the guitar, and T-stick [4] which is a family of digital musical instruments for performance with orchestras. 'Musicpole' [5] and 'Sweatstick' [6] are similar to T-stick in shape.

In this paper, a novel musical synthesizer based on acoustics and digital signal processing techniques is introduced. The organization of this paper is as follows. The

* Corresponding Author.

proposed synthesizer and sound synthesis algorithm are described in Section 2, and Section 3 shows the results of synthesized sounds and gives a demonstration how to play the proposed synthesizer. Finally, conclusions are mentioned in Section 4.

2 A Novel Musical Synthesizer

In this paper, two plucked string instruments (guitar and Gayageum) and a woodwind instrument (Taepyeongso) were targets of the proposed synthesizer. The Gayageum and Taepyeongso are Korean traditional instruments. The Gayageum has twelve silk strings supported by twelve movable bridges, which are called Anjok, and is able to be tuned up by moving the Anjok to the left/right [7, 8]. The Taepyeongso is a Korean double reed wind instrument in the shawm or oboe family. It has a conical wooden body having eight tone-holes, with a metal mouthpiece and cup-shaped metal bell.

2.1 Laser Strings

Laser strings are to depict plucking the guitar and Gayageum strings and consist of pairs of a laser module and a photodiode [9]. Each photodiode is arranged to detect a light signal from the corresponding laser module at all time. While each photodiode is detecting the signal from each corresponding laser module, sound is not produced because this is the same phenomenon that string is not plucked yet. In contrast, the moment that each photodiode does not detect each laser signal means the string is held, so sound is generated when the photodiode detect the signal again.

2.2 Frets

Frets are metal strips embedded along the fret board and located at exact points that divide the scale length in accordance with a specific mathematical formula. Pitch of each consecutive fret is defined at a half-step interval on the chromatic scale. For the wind instrument in this paper, frets are applied to eight tone-holes. Frets are implemented by resistive voltage dividers that produce a fraction of its input voltage only with resistors. Each resistor value which corresponds to the specific fret is able to be computed by using voltage difference, V_f , between the adjacent frets and expressed as

$$R_n = \frac{R_s^2 V_f}{R_0 V_{in} - R_s V_f} \quad (1)$$

where, $R_s = \sum_{i=0}^n R_i$, V_{in} is an input voltage.

2.3 Sound Synthesis Algorithm

In the first-order bidirectional linear digital waveguide proposed by J. O. Smith, the waveguide output for a discrete time constant n at position k is expressed as

$$y(n, k) = y_r(n - k) + y_l(n + k) \quad (2)$$

where $y_r(n)$ and $y_l(n)$ are right/left-going traveling waves, respectively [10]. The digital waveguide model is a kind of physical modeling. In this model, a distance between discrete time index n and $n+1$ is denoted by $X = cT$ and it is represented as a unit delay in digital domain when the fixed propagation speed is uniformly distributed in space. If the propagation speed relatively varies in time, the wave moves a distance $\tilde{X} = c(n)T$. Figure 1 implies the propagation distance for two cases of propagation speeds, respectively. For the case of $c(n) > c$, the traveling waves move further than a unit delay. In contrast, the traveling waves move shorter than a unit delay for the case of $c(n) < c$. It represents a physical string that unit delays are connected in cascade.

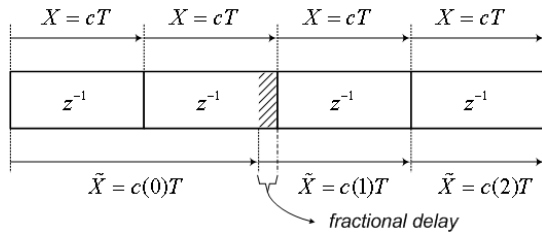


Fig. 1. Propagation distance corresponding to wave speed

It is impossible to be existed any time index between n and $n+1$ in digital domain, such as $n+0.7$. Thus, there is no way to directly express the propagation distance of traveling waves that is shorter than a unit delay. In order to represent this fractional distance, a fractional delay filter has been used [11]. The right-going traveling wave, which is expressed $y(n, m) = y_r(n, m)$, is only considerable to explain the digital waveguide model with time-varying propagation speed. The left-going traveling wave is able to be applied as the right-going traveling wave. In this case, we assume there is no loss. When an initial distribution is given as $y(0, m)$, $m = -\infty, \dots, \infty$, the output at an observation point k at $n = 1$ is expressed by $y(1, k) = y(0, k - c(0)T)$, and then the output at $n = 2$ is given as $y(2, k) = y(0, k - c(0)T - c(1)T)$ and so on. If the time-varying velocity is defined as $c(n) = i(n)c + c_d(n)$ where $i(n) \geq 0$ and $0 \leq c_d(n) \leq c$, the output can be generalized as

$$\begin{aligned} y(n, k) &= y(0, k - \sum_{l=0}^{n-1} c(l)T) \\ &= y(0, k + M(n) + d(n)), \quad n > 0 \end{aligned} \quad (3)$$

where $M(n) = -\sum_{l=0}^{n-1} i(l)$ and $d(n) = -T \sum_{l=0}^{n-1} c_d(l)$. $M(n)$ is a parameter related to the position of the delay line which means the position of the traveling-wave in the digital waveguide and $d(n)$ is able to be implemented with the fractional delay filter [11]. The final output of the DWTWPS is given as

$$y(n, k) = y_r(0, k + M(n) + d(n)) + y_l(0, k - M(n) - d(n)), \quad n > 0. \quad (4)$$

A remarkable characteristic of the DWTVPS is to synthesize pitch-shifting sounds.

In order to simulate a complete plucked string instrument, it is required to represent frequency-dependent damping of the sound and characteristics of the body. Figure 2(a) shows a plucked string instrument model. In this model, waveguide is equivalent to a physical string and excitation corresponds to the plucking string. The plucked string instrument model can be merged and rearranged as Fig. 2(b) because of linearity. Therefore, it is possible to record a body “impulse response” and use it as the string excitation. For the wind instrument, characteristics of the bore are commuted as the excitation. This technique is referred to as commuted waveguide synthesis (CWS) [12].

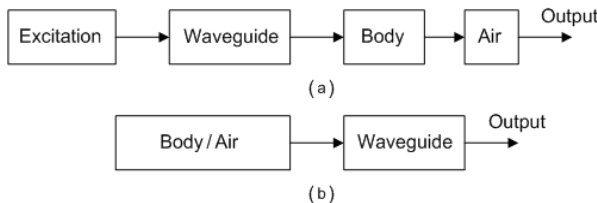


Fig. 2. Schematic diagram of the plucked string instrument: (a) Classic model and (b) Commuted synthesis model

2.4 Processor and Sound Engine

The TMS320F2812, which is a high-performed digital signal processor [13], is used for the proposed synthesizer. Figure 3 shows a schematic diagram describing how the TMS320F2812 works for the proposed synthesizer.

As shown in Fig. 3, a potentiometer is connected to an ADCINA0 pin on the processor to choose an instrument. The 12-bit ADC on the TMS320F2812 has 0V to 3V analog input range. Then, the maximum digital value must be 4095 and the minimum is 0 after conversion. Table 1 shows three operating modes corresponding to a threshold value between 0 and 4095.

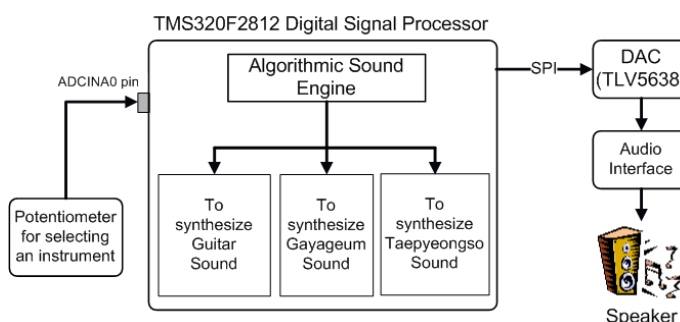


Fig. 3. Schematic diagram showing how the TMS320F2812 works for the proposed synthesizer

The sound synthesis algorithm is embedded onto the processor, and synthesized sound samples are transmitted to the DAC using SPI communication. Finally, sounds are played through a speaker via an audio interface in real-time and three main steps are as follows:

Table 1. Three operating modes of the proposed synthesizer

Threshold value	Operating Modes
0 ~ 1000	Guitar Mode
1001 ~ 2000	Gayageum Mode
2001 ~ 4095	Taepyeongso Mode

Step1. System initialization. As soon as power is supplied to the TMS320F2812, system initialization is occurred. For instance, it is required that an operating system clock is set up to derive the processor and the system clock is divided down for the peripheral devices in this first step.

Step2. Initializing and setting up peripheral devices. It is necessary to initialize and set up peripheral devices. For instance, the ADC module must be initialized and set up by the user to select an instrument. For the proposed synthesizer, a sound sample of the instruments is synthesized and transmitted to the DAC using SPI communication in an interrupt service routine (ISR). The ISR is called at every 62us (for the guitar and Gayageum) or 21us (for the Taepyeongso) which is a critical time for generating and transmitting the sound sample. The DAC TLV5638 is a dual 12-bit voltage output DAC and programmed with a 16-bit serial string containing 4 control and 12 data bits [14].

Step3. Infinite Loop (While loop). After all initializations and configurations of the processor, an infinite while loop is repeating until power is off. Three important tasks are dealt with in the while loop: continuous A/D conversion of the potentiometer, initialization of parameters to synthesize desired sounds and calling the ISR at every certain time.

3 Results and Demonstration

The DWTVPS is based on the commuted synthesis. It is focused on that whether it is possible to synthesize pitch-shifting sounds and to describe realistic playing with the proposed synthesizer or not. Although there may be a variety of different tunings for the guitar, the most common by far is known as "Standard Tuning." which has the strings turned from a low E(82.41Hz), to a high E(329.63Hz), traversing a two octave range – E2, A2, D3, G3, B3 and E4 [15]. The first string E4 is an example to be synthesized when slide, hammer-on and pull-off from the 1st fret to the 3rd fret are occurred. Figure 4 shows the spectra of sounds by sliding, hammer-on and pull-off of the example sound. Vibrato is a musical effect, produced in singing and on musical instruments by a regular pulsating change of pitch. Bending is exactly as it sounds: bending the string to the side by pushing it (towards the sixth string) or pulling it

(towards the first string), often while a fretted note is ringing. As vibrato and bending are played at 3rd fret on the first string (its pitch is 391.96Hz, G) using the proposed synthesis algorithm, the result is shown as in Fig. 5.

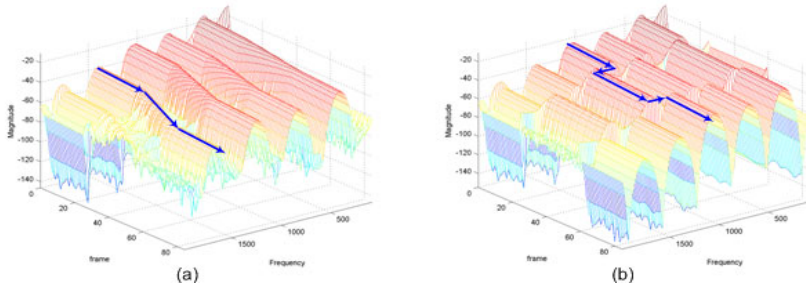


Fig. 4. Spectra of sounds by (a) sliding and (b) hammer-on and pull-off

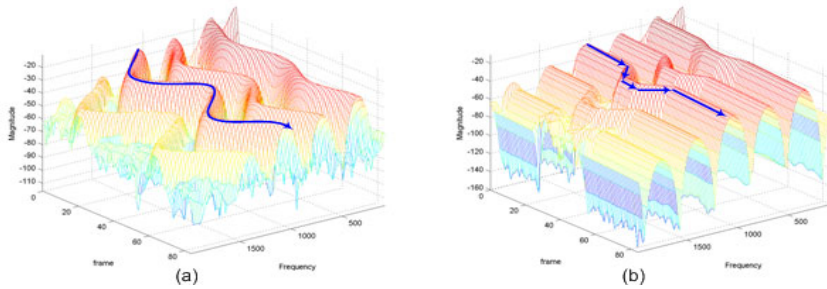


Fig. 5. Spectra of sounds by (a) vibrato and (b) bend and release

As shown in Fig. 4 and 5, the proposed synthesizer plays a role as the real acoustic guitar by applying the DWTVPs algorithm to the synthesizer. Similarly, Gayageum sounds are easily able to be synthesized with some modifications of the DWTVPs model such as changing the excitation signal and parameters. However, there are some differences between original sounds and recorded sounds. The difference may be caused by the experimental environment. To verify this assumption, a noise profile of the 11th Gayageum string is analyzed as illustrated in Fig. 6(a). In the case of the 11th Gayageum string, it is said that the timbre of the sound is directly affected by from the first harmonic to the 8th harmonic (around 3500Hz) because the magnitude of the noise (-40dB) is generally bigger than the harmonics of the Gayageum sound after the 8th harmonic. Namely, this noise affects to the high-frequency band of the recorded sound, and it makes a little different sound when compared with the original sound. To solve this problem, a second-order low-pass Butterworth filter ($f_c=3500\text{Hz}$, $f_s=1/43.35 \times 10^{-6}\text{Hz}$) is designed to the output. Figure 6(b) describes that the noise at high-frequency band is reduced. More high-order low-pass filter may have a good result for reducing the noise, but it takes more time to run the algorithm. The running

time of the algorithm is very relative to the delay line length of the proposed model. If it takes more time due to adding the low-pass filter, the delay line length will be down and the quality of the recorded sound will be poor as well. Therefore, it is necessary to design an analog low-pass filter.

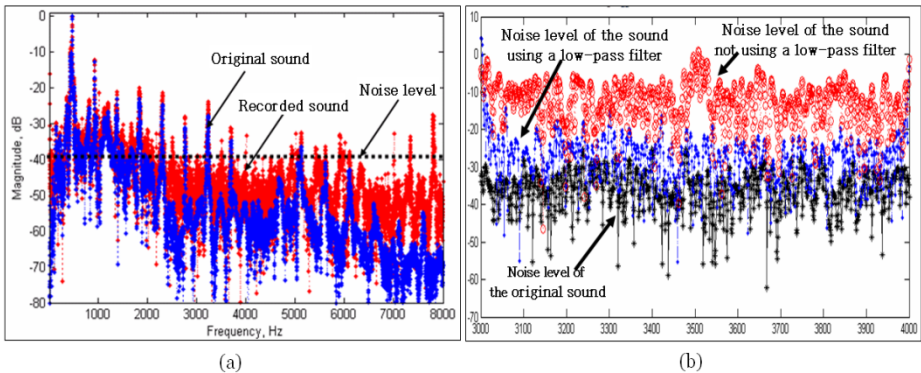


Fig. 6. (a) Noise profile of the 11th Gayageum string and (b) Comparison of the recorded sound by the low-pass filter

A demonstration gives an example how to play the proposed synthesizer. Arirang is arguably the most popular and best-known Korean folk song, both inside and outside Korea. In this demonstration, the most famous version of Arirang in Korea called Gyeonggi Arirang has been played in guitar mode including hammer-on and pull-off. Moreover, the proposed synthesizer has been played in the Taepyeongso mode with the same song. The demonstration has been recorded in author's laboratory so that many noise signals were included. It is possible to see the demonstration on the website at http://signal.ulsan.ac.kr/elekto/documents/ICIC2011_demo.htm as well as sound files. (The first is original sound, the second is synthesized on the computer by using MATLAB and the third is recorded sounds from the output of the proposed synthesizer).

4 Conclusions

In this paper, a novel musical synthesizer embedded with physical modeling sound synthesis algorithm is introduced. The proposed synthesizer gives possibility to develop a novel interface for additional musical instruments. In addition, the proposed synthesis algorithm is able to generate pitch-shifting sounds so that it is possible to represent a variety of playing styles, such as strumming the guitar and playing solos. For the future works, it is required that we should enhance the synthesizer to expand to other instruments, such as violin, cello and so on. Moreover, we need to upgrade the proposed synthesizer to be played easily for novice and go hand in hand with the development of interfaces based on human tactile to represent senses and sensitivity of players.

Acknowledgments. This research was supported by Basic Science Research Program through the National Research Foundation of Korea(NRF) funded by the Ministry of Education, Science and Technology(2011-0014539).

References

1. Overholt, D.: The Overtone Violin. In: Proceeding of the 2005 International Conference on New Interfaces for Musical Expression (NIME 2005), Vancouver, pp. 34–37 (2005)
2. Kanebako, J., Gibson, J., et al.: Mountain Guitar: A Musical Instrument for Everyone. In: Proceeding of the 2007 International Conference on new Interfaces for Musical Expression (NIME 2007), New York, pp. 396–397 (2007)
3. Kessous, K., Castet, J.: An Interface Using Guitar Techniques. In: Proceeding of the 2006 International Conference on new Interfaces for Musical Expression (NIME 2006), Paris, pp. 192–195 (2006)
4. Malloch, J., Wanderley, M.: The T-stick: from Musical Interface to Musical Instrument. In: Proceeding of the 2007 International Conference on New Interfaces for Musical Expression (NIME 2007), New York, pp. 66–69 (2007)
5. MUSICPOLE MIDI controller,
http://www.themusicpole.com/the_MUSICPOLE.pdf
6. Sweatstick alternative MIDI controller,
<http://www.rayedgar.com/sweatstick.html>
7. National Center for Korean Traditional Performing Arts,
<http://www.ncktpa.go.kr/>
8. Cho, S., Chong, U.: Development of Improved String Model for Instruments with Anjok. The Acoustical Society of Korea 26(7), 328–333 (2007)
9. Cho, S., Chong, U.: Implementation of Non-stringed Instruments Without Bodies. In: Proceedings of Meetings on Acoustics, vol. 2, p. 35001 (2008)
10. Smith, J.O.: Physical Modeling using Digital Waveguides. Computer Music Journal 16(4), 74–91 (1992)
11. Laakso, I., Vlimki, V.: Splitting the Unit Delay - Tools for Fractional Delay Filter Design. IEEE Signal Processing Magazine 13, 30–60 (1996)
12. Commuted Waveguide Synthesis,
http://www.music.mcgill.ca/~gary/618/week5/string_model.html
13. TMS320F2812 Digital Signal Processor datasheet,
<http://focus.ti.com/lit/ds/symlink/tms320c2812.pdf>
14. TLV5638 DAC datasheet,
<http://focus.ti.com/lit/ds/symlink/tlv5638.pdf>
15. Guitar tunings, http://en.wikipedia.org/wiki/Guitar_tunings

Studies on the Automatic Recognition of Modern Chinese Conjunction Usages

Hongying Zan, Lijuan Zhou, and Kunli Zhang

School of Information Engineering, Zhengzhou University, 450001, Zhengzhou, China
{iehyzan, ieklzhang}@zzu.edu.cn, zhlijuan1018@126.com

Abstract. The conjunctions can connect words, sentences and even paragraphs. They have special connection functions and their usages are complex and diverse. At present, the studies on conjunctions are mostly human-oriented. These descriptions can not avoid such limitations as subjectivity and illegibility, and are not easy to be applied directly to natural language processing (NLP). This paper studies the automatic recognition of conjunction usages in the background of NLP. It designs a rule-based method and several statistical methods for conjunction usages recognition. Results are compared and analyzed and turns out that rule-based method and statistical methods have advantages and disadvantages.

Keywords: Conjunction Usages, Rule-Based, Usages Recognition.

1 Introduction

Conjunction usages refer to where conjunction with some meaning can be used. The same conjunction may indicate different meanings in different contexts and have different usages. Only if we investigate different conjunction usages comprehensively, can we understand their semantic information better and realize NLP. Through recognizing conjunction usages automatically, conjunction structure phrases and unknown polar words can be detected better. Also, automatic recognition of conjunction usages would involve multiple sentences because of the connective function of conjunctions, which is different from the automatic recognition of usages of other functional words which involve only one sentence. Therefore, the studies on automatic recognition of conjunction usages are of great importance.

2 Related Work

Yu et al. [1] initially put forward the thoughts of building the “Trinity” knowledge base of modern Chinese functional words and defined functional words as adverb, preposition, conjunction, auxiliary, modality and position words. Zan et al. [2] constructed modern Chinese functional words knowledge base which contains usage dictionary, usage rule base and usage corpora of functional words. Liu et al. [3] discussed automatic recognition of adverb usages based on rules preliminarily. Zhang [4] studied automatic recognition of common Chinese adverb usages based on statistics. These studies mainly aim at constructing knowledge base of functional words or automatic

recognition of adverb usages. However, studies on conjunctions usages which are used by machine are limited, such as recognition of conjunction usages.

This paper firstly researches automatic recognition of conjunction usages based on rules according to conjunction usage dictionary and usage rules base. In addition, it uses Conditional Random Fields (CRF), Maximum Entropy (ME) and support vector machine (SVM) to realize automatic recognition of conjunction usages based on statistics for minority conjunctions.

3 Knowledge-Bases for Conjunction Usages

3.1 Dictionary of Conjunction Usages

Dictionary of conjunction usages, which adopts usage —attribute as corresponding relationship, establishes usage dictionary using the form of relational database and describes the specific attribute character of each conjunction usage in detail.

Dictionary of conjunction usages covers all conjunctions in Modern Chinese Grammar Information Dictionary [5], as well as conjunctions appear in Modern Chinese Functional Words Dictionary [6], Modern Chinese Dictionary [7] and Modern Chinese Eight Hundred Words [8]. In addition, we adjust entry and modify usages according to participle and pos tagging corpus of People's Daily (1998.1) which is offered by computational linguistics institute of Beijing University. At present, dictionary of conjunction usages were recorded 321 conjunctions and 701 usages, entries and usages distribution are shown in Fig.1.

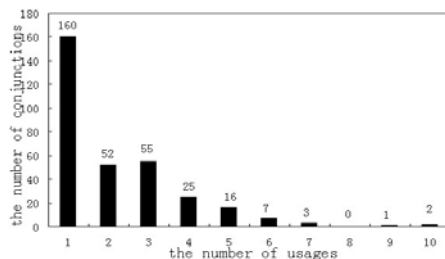


Fig. 1. Entries and usages distribution of conjunctions

3.2 Rule Base of Conjunction Usages

On the basis of dictionary of conjunction usages, each conjunction usage was investigated in dictionary example corpus, the operable judgment conditions character was extracted with description conjunction usage rules with orderly BNF paradigm. Then the paper constructed conjunction usages rule base to provide formalized basis for automatic recognition of modern Chinese conjunction usages. Rules contain 6 usage features: F, M, L, R, N, E. F stands for head of the sentence contains target conjunction, M stands for before target conjunction but not contiguous, L stands for before target conjunction and contiguous, R stands for behind target conjunction and contiguous, N stands for behind target conjunction but not contiguous, E stands for the end of the

sentence contains target conjunction. The presentation of other symbols can refer to Yuan et al. [9] and usage rules description to Zan et al. [2].

4 Automatic Recognition of Conjunction Usages

4.1 Automatic Recognition of Conjunction Usages Based on Rules

Automatic recognition of conjunction usages based on rules is developed on the base of automatic tagging system of functional words usages based on rules. The specific steps of automatic tagging system of functional words usages are:

- (1) Initialize tagging corpus and usage rule base. Split corpus into paragraphs which are read into memory with dynamic array when reading corpus. Usage rules are read into memory with hash table.
- (2) Read the whole sentence which needs to be tagged, find all functional words which need to be tagged and corresponding rules and dispose the entire sentence to get corresponding dictionary and original sentence, as well as the location of functional words which need tagging in dictionary and original sentence.
- (3) Search the rules of functional words which need to be tagged, read their usage rules in sequence. Then determine the kind of verifier to analyse and match usage rules and to determine the tagging result. At last, output the entire sentence and read the next sentence when all the functional words of the current sentence are tagged. The tagging program is over when there is no a whole sentence which needs tagging.

Conjunctions can connect words, small clauses, sentences and paragraphs. The above system introduces large noise data for conjunctions with connecting words and small clauses when it splits corpus into paragraphs. Therefore, the system needs to cut sentence again after above step (1) to only withhold sentences besides conjunction which needs to be tagged. The particular way is: summarizing conjunctions which connect sentences and paragraphs according to the usages of conjunctions artificially and putting these conjunctions in a text file "cword.txt ". The program first looks for whether this conjunction is in the file when it tags each conjunction. If the conjunction is not in the file, the program only needs to keep the sentence which contains the conjunction and ignores other sentences in current paragraph.

Automatic tagging system used six types of verifier to satisfy different requirements of feature attributing from finding ranges of dictionary and matching result. Yuan et al. [9] introduced design requirements of all kinds of verifier and realization of automatic tagging system functional words usages based on rules.

4.2 Automatic Recognition of Conjunction Usages Based on Statistics

Empirical method based on the statistics obtains language knowledge from training data automatically or semi-automatically, sets up effectively statistical language model and optimize according to the actual situation of training data constantly. On the contrary, rationalism method based on rules is difficult to adjust according to actual data. So rule method is worse than empirical method based on statistics in some ways. Considering usages of conjunction are related to context sequence, this paper chooses three statistical models with wide applications and good effect in Machine learning.

CRF is an undirected graph model which calculates conditional probability of output node under the condition of giving input node. It inspects conditional probability of tagging sequence corresponding to input sequence. Its training target is that maximizing conditional probability [10]. ME is a statistical model which is widely used in classification problem. Its basic thought is that excavating potential constraint conditions in a known event set, then selecting a model which must satisfy known constraint conditions and distribute unknown events which may happen as evenly as possible [11]. SVM is a study method based on statistical learning theory which maximizes the middle line of data with different characters by using some strategies and judges category of this data aimed at characters of data [12]. This paper adopts CRF++ toolkit¹, maxent (Zhang)² and LibSVM toolkit³ as automatic tagging tools.

5 Experiments and Results Analysis

5.1 Automatic Recognition Results of Conjunction Usages Based on Rules

Seven months participle and pos tagging corpus of People's Daily (1998.1, 2000.1-2000.6) were adopted in this paper as automatic recognition corpora of conjunction usages based on rules. First, automatic tagging system was used to tag all conjunctions in experimental corpora to get machine tagging results. Then the corpora were artificially proofread with one more people cross to form standard corpora of recognition of conjunction usages. If machine tagging results and standard corpus after artificially proofreading were same, machine tagging results would be considered as correct ones. The experiment counted on tagging results of all conjunctions in corpus of every month and used precision rate (P), recall rate(R) and F-measure to measure automatic recognition results of conjunction usages based on rules, the experiment results are show in Table 1(the left table).

Main reasons of incorrect identification results were summarized through analysing machine tagging results which were inconsistent with artificially tagging results. The rules were done some modification to improve identification precision.

(1) Perfection of enumeration words in rules.

Conjunction usage rules are formed on the basis of dictionary of conjunction usages which only contains few example sentences. Therefore, it is hard to avoid appearing enumeration words are not full or do not appear in large-scale corpus, such as following examples with “不仅(not only)” extracted from the corpora:

- 搞好/v 薄弱/a 学校/n , /wd 不仅/c<?FAIL> 要/vu 加强/v 硬件/n 建设/vn , /wd 更/dc 重要/a 的/ud 是/vl 要/vu 加强/v 学校/n 领导班子/n 建设/vn 。 /wj
- 不仅/c<?FAIL> 要/vu 养成/v 良好/a 的/ud 师德/n 师风/n , /wd 同时/c 要/vu 加强/v 对/p 教师/n 进行/vx 继续/vn 教育/vn , /wd 实现/v 知识/n 更新/vn 。 /wj

¹ CRF++: Yet Another Toolkit[CP/OL].<http://www.chasen.org/~taku/software/CRF++>

² http://homepages.inf.ed.ac.uk/s0450736/maxent_toolkit.html

³ <http://www.csie.ntu.edu.tw/~cjlin/libsvm>

Table 1. Usages recognition results rule-based. The left table is result before rules revise. The right table is result after rules revise.

	S ₁	P	R	F		S ₂	P	R	F
1998.1	25364	0.7919	0.7833	0.7876	1998.1	301	0.8373	0.8347	0.836
2000.1	28975	0.7897	0.7806	0.7851	2000.1	33	0.8397	0.8372	0.8384
2000.2	25645	0.7954	0.786	0.7907	2000.2	71	0.8283	0.8256	0.8269
2000.3	33793	0.7875	0.7785	0.783	2000.3	103	0.8453	0.8429	0.8441
2000.4	31552	0.7998	0.7904	0.7951	2000.4	74	0.8476	0.8449	0.8462
2000.5	27941	0.7979	0.7878	0.7928	2000.5	86	0.8343	0.8318	0.833
2000.6	32215	0.8062	0.7962	0.8012	2000.6	96	0.859	0.8568	0.8579

S1: the number of conjunctions, S2: the number of wrong part-of-speech conjunctions

Usages of “不仅(Not only)” are “<c_bu4jin3_1a>” in above two examples, while they are tagged “<?FAIL>” by machine. The reason of first example is that rule “<c_bu4jin3_1a>” does not contain enumeration word “更(the more)”, the reason of second example is that there is no enumeration words in the sentence. So we change rule “@<c_bu4jin3_1a>→N ^N→(vla)*[{w}]*([也|还|而且|并且|又])” to “@<c_bu4jin3_1a>→N ^N→(vla)*[{w}]*[也|还|而|并且|又|更|亦|而且]”.

(2) Dispose of connective problems of conjunctions

Because conjunctions can connect small clauses, context feature usually does not appear in the small clause which contains conjunction needed to be tagged, but it appears in other clause that there are more punctuation between other clause and conjunction. Rule needs to be increased braces to let small clauses or punctuation appear more times, such as the following examples with “但(but)” extracted from the corpora:

● 我/rr 的/ud 家乡/n 虽然/c 地处/v [豫南/ns 平原/n]ns , /wd 平畴沃野/i , /wd 但/c<?c_dan4_1> 发展/v 并/d 不/df 快/a 。/wj

Usages of “但(but)” are “c_dan4_1a” in above example and there are two commas between “但(but)” and “虽然(although)”. So we change rule“@<c_dan4_1a>→M ^M→(虽|尽管|固然)”, ” to “@<c_dan4_1a>→M ^M→(虽|尽管|固然){*, }”.

(3) Adjustment of rules order

To ensure high precision, independent rules, rules which are easy to identify accurately or rules with high appearing frequency should be endowed with higher priority according to mutual containing or covering relations between rules. Namely these rules are put in previous position to make them be used in recognition of conjunction usages early. For example, conjunction “和(and)” appear 10579 times in January 1998 corpus, the number of tagged “<c_he2_1a>” and “<c_he2_1c>” by machine respectively are 1506 times and 756 times, while tagged “<c_he2_1b>” are only 95 times. So we put rule of usage “<c_he2_1b>” after rules of usage “<c_he2_1a>” and “<c_he2_1c>”.

(4) Modification of wrong part-of-speech

Because participle precision is not 100%, it is hard to avoid appearing wrong part-of-speech. Some words are not conjunctions, but their pos tagging are conjunctions, such as "并(and)" and "才(only if)", "首先(first)", "由于(because)", "只是(just)" and "只有(only)". They will affect automatic recognition precision rate of conjunction usages. The number of conjunctions is 25364 including 301 wrong part-of-speech conjunctions in January 1998 corpus.

Rules were revised and perfected and wrong part-of-speech conjunctions were removed according to the above four suggestions. The experiment results are shown in Table 1 (the right table) which improves compared to the result of the left table.

5.2 Automatic Recognition Results of Conjunction Usages Based on Statistics

Six common conjunctions "和(and)", "而(while)", "或(or)", "因为(because)", "那么(then)" and "而且(but also)" were chosen from the paper to do experiment according to the connection relations. The experiment corpus was participle and pos tagging corpus of People's Daily (1998.1), and the experiments evenly divided the sentences that contain six conjunctions into four data sets by the usage category and used four fold cross-validation to obtain average cross-validation results of each word. Because statistical method identified usages for all appearance of the six words in corpus, precision rate and recall rate were the same, so this paper only used precision rate as evaluating standard of statistical method. The method based on statistics was concerned to features template, statistical methods and selection of context window, so the following experiments were carried out according to the three aspects.

Firstly, the experiment selects the context window as 2 and uses CRF model to investigate experimental results of the six words in three features template according to the context character of conjunction usages, and the results are shown in Fig.2.(the left figure). Template T_1 is word, T_2 is parts of speech and T_3 is words, parts of speech and their combinations. From Macro Average of the six conjunctions, the conclusion can be drawn that T_3 is superior to the other two templates. Because conjunctions are of connective function and they often possess connectives of collocation, but parts of speech of connectives is uncertainty, so words and parts of speech information are very necessary.

Then the experiment selects context window as 2, uses T_3 template and three statistical methods to get the results and compares to results based on rules, the results are shown in Table 2. Experiment results show that, when the conjunctions whose results based on rules are bad use methods based on statistics, their results have improved. In addition, SVM method is better than the method of CRF and ME except "或(or)", the reason is usages distribution of "或(or)" is not very average. However, statistical recognition results of "而且(but also)" are obviously lower than rules results, this is because it is easier to distinguish from their different usages. So rule method should be adopted for conjunctions whose different usages are easily distinguished formally, while statistical methods should be used for conjunctions whose rule effect are bad.

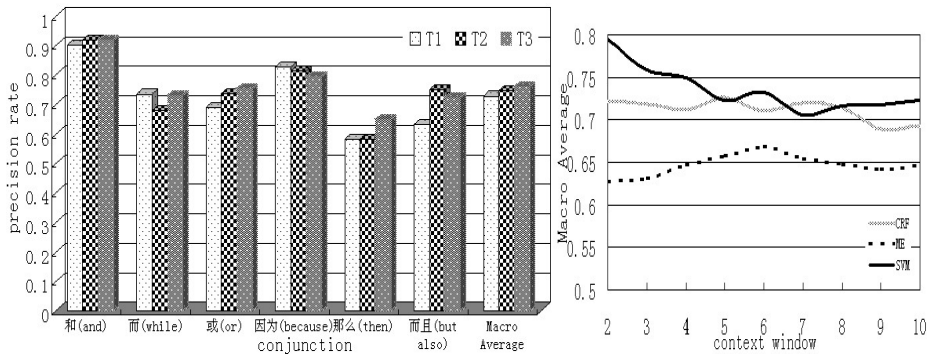


Fig. 2. Usages recognition results based on statistics. The left figure is result with different feature templates. The right figure is results with different window sizes.

Table 2. Usages recognition results with different models

	rule-based	CRF	ME	SVM
和(and)	0.8197	0.9179	0.8822	0.9729
而(while)	0.4921	0.7324	0.6007	0.742
或(or)	0.6036	0.7387	0.6626	0.6383
因为(because)	0.6034	0.7923	0.7094	0.9787
那么(then)	0.5	0.645	0.4831	0.6715
而且.(but also)	0.9662	0.7056	0.6815	0.9435
Macro Average	0.6642	0.7553	0.6699	0.8245

Finally, effects of experimental results in different context windows are inspected. Fig. 2.(the right figure) shows that three statistical models average experimental results of the rest of five conjunctions except “和(and)” in T3 template, the abscissa stands context window, while the ordinate stands Macro Average of five conjunctions. As can be seen from the line graph, Macro Average of SVM model decline intensively with the increase of context window, while Macro Average of CRF and ME model is relatively stable. CRF and ME model reach the maximum when window is respectively 5 and 6. So recognition of conjunction usages is not better when context window is bigger, it may bring more noise with the increase of window size.

6 Conclusions

The paper adopted the thoughts of building the “Trinity” knowledge base of modern Chinese functional words to realize automatic recognition of conjunction usages based on rules according to conjunction usage dictionary and usage rule base. In addition, it also realized automatic recognition of conjunction usages based on statistics for minority conjunctions through using CRF, ME and SVM model. Results showed that the methods of rule and statistics possessed advantages and disadvantages.

In the future, more efforts will continue to be made to improve conjunction usage dictionary and usage rule base and build a comprehensive accurate knowledge base of modern Chinese functional words face to NLP. Besides we will try to process weighted rules and adopt combination method of rules and statistics to improve automatic recognition precision rate of conjunction usages according to relative frequency of conjunction usage distribution. Meanwhile, much more studies on automatic recognition of conjunction usage will be applied to other fields of NLP, such as automatic detection of conjunction structure phrases and unknown polar words. We expect improve the effect of machine translation and save manpower devotion for constructing basic polar resources.

Acknowledgements. The work in this paper is supported by a grant from the Natural Science Foundation of China (No.60970083), the Open Projects Program of Key Laboratory of Computational Linguistics (Peking University), Ministry of Education and the Outstanding Young Talents Technology Innovation Foundation of Henan Province (No.104100510026).

References

1. Yu, S.W., Zhu, X.F., Liu, Y.: Knowledge-base of Generalized Functional Words of Contemporary Chinese. *Journal of Chinese Language and Computing* 13(1), 89–98 (2003)
2. Zan, H.Y., Chai, Y.M., Zhang, K.L., Yu, S.W.: Studies on the Functional Word Knowledge Base of Contemporary Chinese. *Journal of Chinese Information Processing* 21(5), 107–111 (2007) (in Chinese)
3. Liu, R., Zan, H.Y., Zhang, K.L.: The Automatic Recognition Research on Contemporary Chinese Language. *Computer Science* 8(A), 172–174 (2008) (in Chinese)
4. Zhang, J.H.: Studies on Automatic Recognition of Common Chinese Adverb's Usages Based on Statistics. Zhengzhou University, Zhengzhou (2010) (in Chinese)
5. Yu, S.W., Zhu, X.F., Wang, H., Zhang, Y.Y.: Modern Chinese Grammar Information Dictionary. Tsinghua university press, Beijing (2003) (in Chinese)
6. Zhang, B.: Modern Chinese Functional Words Dictionary. Commercial Press, Beijing (2006) (in Chinese)
7. Chinese Social Sciences Language Institute Dictionary Editorial Office.: Modern Chinese Dictionary. Commercial Press, Beijing (2007) (in Chinese)
8. Lv, S.X.: Modern Chinese Eight Hundred words. Commercial Press, Beijing (2009) (in Chinese)
9. Yuan, Y.C., Zan, H.Y., Zhang, K.L., Zhou, Y.H.: The Automatic Annotation Algorithm Design and System Implementation Rule-base Function Word Usage. In: The 11th Chinese Lexical Semantics Workshop, Suzhou, pp. 163–169 (2010) (in Chinese)
10. Lafferty, J., McCallum, A., Pereira, F.: Conditional Random Fields: Probabilistic Models for Segmenting and Labeling Sequence Data. In: Proceedings of the 18th ICML 2001, Montreal, pp. 282–289 (2001)
11. Berger, A.L., Della Pietra, V.J., Della Pietra, S.A.: A Maximum Entropy Approach to Natural Language Processing. *Computational Linguistics* 22(1), 39–71 (1996)
12. Vapnik, V.N.: The Nature of Statistical Learning Theory. Springer-Verlag New York, Inc., Secaucus (2000)

Implementation of High-Performance Sound Synthesis Engine for Plucked-String Instruments

Myeongsu Kang¹, Jiwon Choi¹, Yongmin Kim¹,
Cheol-Hong Kim² and Jong-Myon Kim^{1,*}

¹ School of Electrical Engineering, University of Ulsan, Ulsan, South Korea
^{{ilmareboy, regular912, jafstar, jmkim07}@ulsan.ac.kr}

² School of Electronics and Computer Engineering,
Chonnam National University, Kwangju, South Korea
^{cheolhong@gmail.com}

Abstract. This paper implements a high-performance sound synthesis engine for plucked-string instruments. To do this, we evaluate the impact of sample-per-processing-element (SPE) ratios on system performance, area efficiency, and energy efficiency. Experimental results for the sound synthesis algorithm of acoustic and classical guitars indicate that the highest area efficiency and energy efficiency are achieved at SPE ratio=5,513 (PES=48) and 2,756 (PES=96), respectively, for the acoustic guitar. For the classical guitar, the maximum area efficiency and energy efficiency are achieved at SPE ratio=22,050 (PES=12) and 5,513 (PES=48), respectively. The synthetic sounds using the reference multi-core processor were very similar to original sounds sampled at 44.1 kHz.

Keywords: Multi-core processors, design space exploration, area efficiency, energy efficiency, sound synthesis, plucked-string instruments.

1 Introduction

Many sound synthesis techniques support a creative musical environment that allows the user to simulate sounds according to individual senses and sensitivity. The *Virtual Air Guitar* and *Overtone Violin* are good examples for that [1, 2]. Recently, mobile phones have also been explored as new interfaces for controlling musical parameters as part of locative performances. *iPhone ocarina* and *Stanford Mobile Phone Orchestra* are representative examples of this trend [3, 4]. To develop musical interfaces using sensors or mobile phones, physics-based methods of musical sound synthesis have received increasing attention. Physics-based sound synthesis recreates natural and rich musical sounds. However, the computational complexity in this sound synthesis model by many numerical integrations of the wave equation has limited its use in real-time applications.

Single instructions multiple data (SIMD) processor array architectures are promising candidates for sound synthesis applications based on physical modeling.

* Corresponding author.

While it is evident that the overall performance improvement is achieved with increasing the number of PEs (or parallelism), no general consensus has been reached that what granularity of processors and memories on the array system provides the most efficient operation of such sound synthesis algorithms on performance and both area efficiency and energy efficiency for variable PEs (or varying sample-per-processing element (SPE) ratio).

This paper implements a high-performance sound synthesis engine yielding the most efficient PE architecture. To do this, this paper quantitatively evaluates the impact of SPE ratios on system performance, area efficiency, and energy efficiency for the multi-core array architectures. In addition, this paper illustrates the correlation between SPE ratio and PE architecture for a target implementation in 130nm technology. To identify the most efficient SPE ratio, seven different PE configurations are simulated for the sound synthesis algorithm of target instruments (acoustic guitar and classical guitar). The analytical results indicate that the most efficient operation is achieved at a SPE ratio in the range of 2,756 to 22,050 for target instruments.

The rest of this paper is organized as follows. Section 2 introduces the synthesis model, and Section 3 presents the reference multi-core processor and Section 4 introduces the process of extracting parameters for evaluating system performance and efficiency as well as evaluation metrics. Section 5 analyzes execution performance, area efficiency, and energy efficiency for each SPE configuration. Finally, Section 6 concludes this paper.

2 Sound Synthesis of Plucked-String Instruments

As mentioned in Section 1, there are many sound synthesis techniques. Among them, PM synthesis is based on mathematical descriptions of acoustic musical instruments, and it is useful to synthesize the plucked instruments [5]. Consequently, PM synthesis is used to generate single notes of target instruments in this paper. In this study, we commute the body response as an excitation of the plucked-string model. Consequently, we are only to implement the string model as shown in Fig. 1.

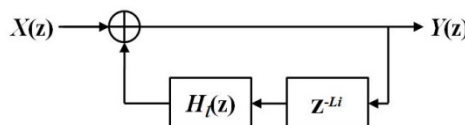


Fig. 1. String model of the plucked-string instruments

In this string model, the delay length determines the fundamental frequency of the synthesized sound and can be computed as $L=f_s/f_0$, where f_s and f_0 are the sampling rate and the desired fundamental frequency. It is possible to synthesize musical sounds with desired fundamental frequencies, whereas we are not able to describe the frequency-dependent damping of a physical string. To represent the frequency-damping, the loop filter can be introduced [5]. We use a first-order all-pole filter:

$$H_l(z) = g \frac{1 + a_1}{1 + a_1 z^{-1}}, \quad (1)$$

where g is the gain of the filter at 0Hz and a_1 is the filter coefficient that determines the cutoff frequency of the filter. For stability, $-1 < a_1 < 0$ and $|g| \ll 1$ are required.

3 Multi-core Processor Array and Design Space Exploration

3.1 The Reference Multi-core Processor Array

Fig. 2 shows a block diagram of the reference multi-core array and a signal processing element. It consists of 2-dimensional processing element (PE) array, local memory, and array control unit (ACU). Each PE for the sound engine has a reduced instruction set computer (RISC) datapath with the following characteristics:

- Small amount of 32-bit word local storage,
- Three-ported general-purpose register (16 32-bit words)
- ALU: computes basic arithmetic and logic operations,
- Barrel shifter: performs multi-bit logic/arithmetic shift operations,
- MACC: multiplies 32-bit values and accumulates into a 64-bit accumulator,
- Sleep: activates or deactivates a PE based on local information, and
- Nearest neighbor communications through a north-east-west-south (NEWS) network and serial I/O unit.

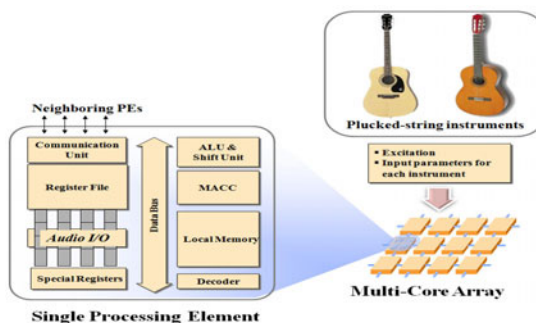


Fig. 2. Block diagram of a multi-core array and a single processing element

3.2 Determination of Optimal Grain Size

A key design issue for portable musical devices such as *iPhone ocarina* is to determine the processor grain size. To determine the effect of grain size on the reference multi-core processor architecture, sample-per-processing-element (SPE) variation is the selected design variable in this paper. The SPE ratio is the amount of sample data

directly mapped to each processing element. The local memory size is varied according to SPE ratios. As the SPE ratio increases, additional local memory is needed to store synthetic information such as filter coefficients and delay lengths and temporary data produced during processing. The local memory size is defined as

$$MEM_{PE} = \frac{MAX_{DL}}{PE_{STR}} + 4 \quad [words], \quad (2)$$

where ‘ MAX_{DL} ’ is the maximum delay length of desired sounds, which is set to 535 because the lowest fundamental frequency of target instruments is 82.41Hz ($MAX_{DL} = 44,100\text{Hz}/82.41\text{Hz} = 535$), and PE_{STR} is the number of PEs per each string of the target instrument. In addition, an additional 4-words memory space is required to store synthetic information: filter coefficients of the loop filter (a_1 and g), all-pass filter (C), and a delay length. Then, an overall system memory is calculated by $MEM_{SYS} = MEM_{PE} \times N_{PE}$ [words], where N_{PE} is the number of PEs. Table 1 summarizes seven different multi-core configurations based on the SPE variations.

Table 1. Modeled multi-core processor paramters

Parameters	Values						
N_{PE}	6	12	24	48	96	192	384
SPE ratio	44,100	22,050	11,025	5,513	2,756	1,378	689
MEM_{PE} [words]	540	273	139	72	39	22	14
MEM_{SYS} [KB]	12.96	13.11	13.35	13.83	14.38	16.90	21.51

4 Experimental Environment

4.1 Parameter Extraction for Performance Evaluation

Fig. 3 shows a methodology infrastructure that consists of three levels: application, architecture, and technology. At the application level, an instruction-level multi-core simulator is used to profile execution statistics, such as cycle count, dynamic instruction frequency, and PE utilization for seven different PE configurations; this is accomplished by retargeting and optimizing the sound synthesis algorithm for each configuration based on the architecture and its execution properties. At the architectural level, the heterogeneous architectural modeling (HAM) [6] of functional units for multi-core arrays is used to calculate the design parameters of each PE configuration. The design parameters are then passed to the technology level. At the technology level, the Generic System Simulator (GENESYS) [7], an analytical technology modeling tool with macro cell capability, is used to calculate technology parameters, such as latency, area, power, and clock frequency, for each PE configuration. The Design Space Explorer then calculates the throughput, area, and energy, and determines the execution times, area efficiency, and energy efficiency for each PE configuration. Optimal design points for delivering real-time execution of the workload while maintaining high area efficiency and energy efficiency are explored among the configurations.

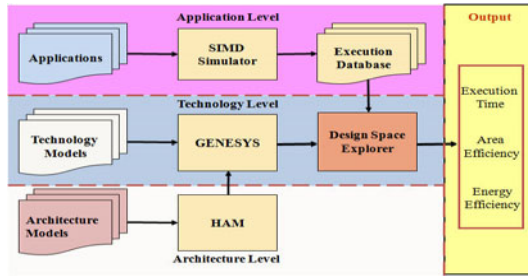


Fig. 3. Methodology infrastructure for the multi-core processor architecture

4.2 Evaluation Metrics

Table 2 summarizes evaluation metrics for the sound synthesis algorithm using the several different multi-core processors. Execution time is running time of the sound synthesis algorithm, area efficiency is the amount of task throughput per unit of area, and energy efficiency is the task throughput achieved per Joules.

Table 2. Summary of evaluation metrics

Execution Time	Area Efficiency	Energy Efficiency
$t_{exec} = C / f_{clk}$	$\eta_A = \frac{1}{t_{exec} \times Area} \left[\frac{1}{s \cdot mm^2} \right]$	$\eta_E = \frac{1}{t_{exec} \times Energy} \left[\frac{1}{s \cdot Joules} \right]$

C is the cycle count, f_{clk} is the clock frequency, t_{exec} is the cycle time, $Area$ is the PE array (mm^2), and $Energy$ is the system energy required to complete the sound synthesis algorithm in 130nm technology.

5 Experimental Results

5.1 Synthetic Sounds

Fig. 4 shows spectra comparisons between synthesized sounds using the multi-core processor and original sounds, and they are very similar. Moreover, synthetic sound samples are available at: <http://eucs.ulsan.ac.kr/ICIC/soundengine>.

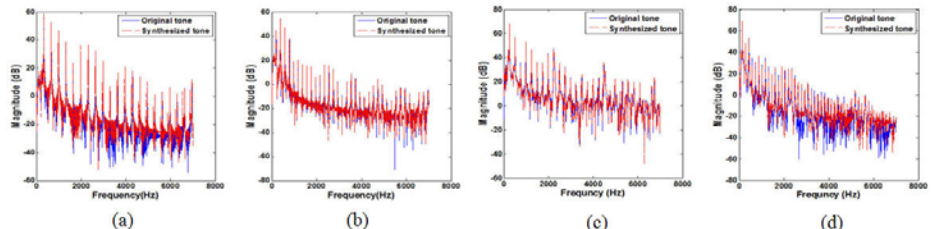


Fig. 4. Spectra of the original sounds (solid line) and synthesized sounds using the multi-core processor architecture (dotted line). (a) acoustic guitar (E4, 329.63Hz), (b) acoustic guitar (G3, 196.00Hz), (c) classical guitar (B3, 246.94Hz), and (d) classical guitar (D3, 146.83Hz).

5.2 Execution Time

Fig. 5 depicts execution times for different SPE configurations. The execution time decreases when the number of PEs increases (or SPE ratios decrease). The slopes indicate the speedup efficiency, and the decreasing ratios of them are not equal for each SPE configuration. For the acoustic guitar, the execution time reduction dramatically decreases at SPE values below 5,513. In the case of the classical guitar for SPE values below 22,050, the execution time reduction is less than those of other PE configurations.

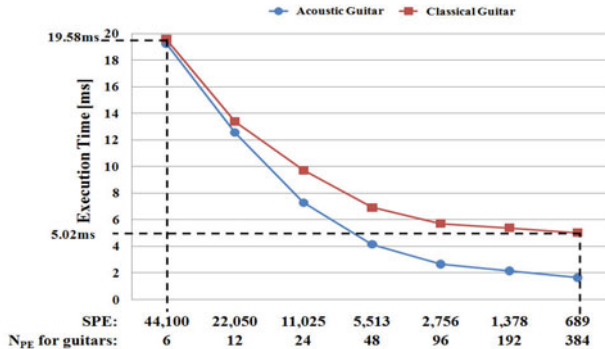


Fig. 5. Execution time for different numbers of PEs

The execution time of the sound synthesis algorithm closely correlates with sampling rate of synthetic sounds. To meet CD-quality sound (or sampling rate of 44.1 kHz), a sound sample must be synthesized within 1/44,100 seconds (0.2ms). As shown in Fig. 5, all of the PE configurations are fast enough to guarantee CD-quality sound.

5.3 System Utilization

Fig. 6 presents system utilization for different SPE configurations. The system utilization converges to around 80% for SPE ratio below 22,050 because more PEs are put to sleep in order to map irregular delay lengths. Additionally, the classical guitar has lower system utilization than the acoustic guitar.

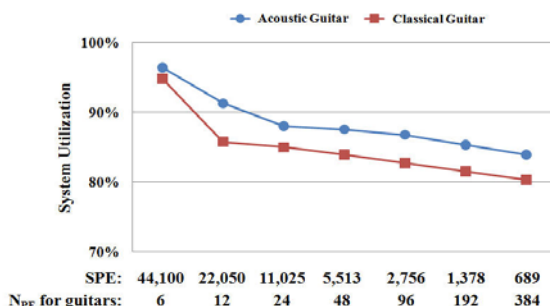


Fig. 6. System utilization for PE configurations

5.4 Area and Energy Efficiencies

Area and energy efficiencies for each SPE ratio are shown in Fig. 7. The efficiencies have been normalized to the task average to allow comparisons of different musical instruments across the sound synthesis algorithm. Therefore, the horizontal axis is not significant. In other words, the shape of the curve is significant. Experimental results indicate that the maximum area efficiency and energy efficiency are achieved at SPE ratios=5,513 (PEs=48) and 2,756 (PEs=96), respectively, for the acoustic guitar. In the case of the classical guitar, the highest area efficiency and energy efficiency are achieved at SPE ratios=22,050 (PEs=12) and 5,513 (PEs=48), respectively.

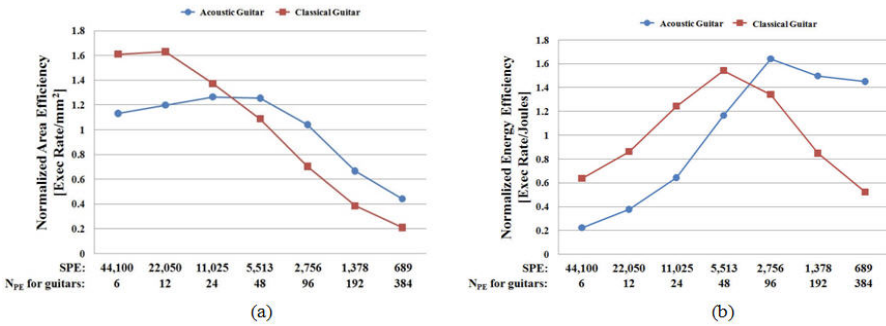


Fig. 7. Area and energy efficiencies for different PE configurations. (a) area efficiency, and (b) energy efficiency.

6 Conclusions

The demand for real-time sound synthesis for portable, hand-held musical devices has grown in recent years, and it is considerably related to power consumption and system area. In this paper, we explored the design space of multi-core processors for sound synthesis of plucked-string instruments including acoustic and classical guitars. To explore the design space of multi-core processors, we selected SPE ratio as a design variable and evaluated the impact of SPE ratio on system performance, area efficiency and energy efficiency. Experimental results indicate that the maximum area efficiency and energy efficiency are achieved at SPE ratios=5,513 (PEs=48) and 2,756 (PEs=96), respectively, for the acoustic guitar. In the case of the classical guitar, the highest area efficiency and energy efficiency are achieved at SPE ratios=22,050 (PEs=12) and 5,513 (PEs=48), respectively. In addition, the synthetic sounds using the reference multi-core architecture are very similar to original sounds in their spectra.

Acknowledgement. This work was supported by the National Research Foundation of Korea (NRF) grant funded by the Korea government (MEST) (No. R01-2008-000-20493-0) and (No. 2010-0010863).

References

1. Karjalainen, M., Maki-Patola, T., Kanerva, A., Huovilainen, A., Janis, P.: Virtual Air Guitar. *J. Audio Eng. Soc.* 54(10), 964–980 (2006)
2. Overholt, D.: The Overtone Violin. In: 2005 International Conference on New Interfaces for Musical Expression, Vancouver, pp. 34–37 (2005)
3. Wang, G.: Designing Smule's Ocarina: the iPhone's Magic Flute. In: International Conference on New Interfaces for Musical Expression, Pittsburgh, pp. 202–209 (2009)
4. Oh, J., Herrera, J., Bryan, J.N., Dahl, L., Wang, G.: Evolving the Mobile Phone Orchestra. In: International Conference on New Interfaces form Musical Expression, Sydney, pp. 82–87 (2010)
5. Valimaki, V., Juopaniemi, J., Karjalainen, M., Janosy, Z.: Physical Modeling of Plucked String Instruments with Application to Real-time Sound Synthesis. *J. Audio Eng. Soc.* 44(5), 331–353 (1996)
6. Chai, S.M., Taha, T., Wills, D.S., Meindl, J.D.: Heterogeneous Architecture Models for Interconnect-Motivated System Design. *IEEE Trans. VLSI Systems* 8(6), 660–670 (2000)
7. Nugent, S., Wills, D.S., Meindl, J.D.: A Hierarchical Block-based Modeling Methodology for SoC in GENESYS. In: 15th Annual IEEE International AISC/SOC Conference, New York, pp. 239–243 (2002)

A Semantic Retrieval Framework for Engineering Domain Knowledge

Xutang Zhang¹, Xiaofeng Chen¹, Xin Hou², and Ting Zhuang¹

¹ School of Mechatronics Engineering, Harbin Institute of Technology Harbin,
150001, Heilongjiang, China

² Science and Technology on Electromagnetic Scattering Laboratory,
100854, Beijing, China

{zxt,cxf}@hit.edu.cn, houxinhit@gmail.com, zhuangt2000@163.com

Abstract. In this paper, we propose a knowledge retrieval framework based on semantically annotated engineering ontology generated from domain documents. Particularly, we propose a scheme for build relations between ontology and domain documents. First, we build anthologies in engineering domain. Next, we transform the keywords into domain ontology concepts, and then find the synonyms of these keywords which are used as real queries to directly input into the query system. The semantic-based knowledge search and retrieval is then performed by ontology mapping and comparison. Using the semantic network of ontology, this system not only can conduct keyword-based retrieval, but also can understand the queries and answer questions by fuzzy inference based on domain ontology.

Keywords: Ontology, Knowledge retrieval, Query semantic retrieval, Query semantic extension.

1 Introduction

Knowledge retrieval (KR) is a new information retrieval (IR) method, which is being developed based on traditional information retrieval techniques and models. KR seeks to return information in a structured form, consistent with human cognitive processes as opposed to simple lists of data items[1]. Compared to traditional information retrieval, knowledge retrieval discovers the internal meanings of articles and concentrates on semantics of queries and knowledge rather than only rigidly literal matching as IR does [2].

Traditional IR models include Boolean model, vector space model and probabilistic model, which are all keyword-based retrieval, i.e. user query is searched through accurate or partial word matching. This method is simple to use, but cannot meet the demands of knowledge retrieval due to the lack of semantic labeled information. As engineering development and design are knowledge-intensive, lots of experience and knowledge is involved during this process. It is necessary to develop a search mechanism that can effectively and efficiently get the information and knowledge needed in engineering activities.

2 Knowledge Retrieval Framework

This section proposed an ontology-based knowledge retrieval framework, as shown in Fig. 1. Semantic processing, semantic recognition and semantic matching are the basis of this framework.

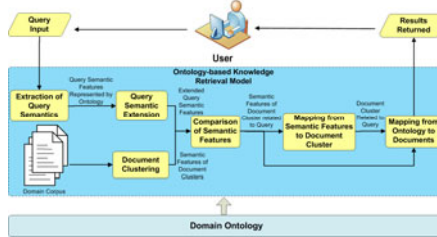


Fig. 1. Proposed ontology-based knowledge retrieval framework

First, the user's query input is analyzed to extract the semantic features, which would be mapped into ontology semantic features to determine the query semantic features. As the limitations of query, it is hard to guarantee that the query intention can be completely depicted only by the limited input, so through the query semantic expansion, other potential semantic features related to the query would be identified and included in the query to improve search effectiveness. On the other hand, domain documents would be clustered to get the representative semantic features of each cluster. Thus the cluster semantic features closest to the query semantics features can be obtained by the comparison of cluster semantic features and query semantic features, and then the document cluster that most represent the query semantic features can be found. Finally, the parts in document cluster most relevant to the query would be returned to users by mapping from ontology to domain corpus.

Domain ontology, describing domain concepts and the relationships between these concepts, embodies domain knowledge and has been incorporated into IR system [2-4]; therefore, constructing domain ontology is the basis of authors' work. the GRAONTO algorithm proposed by Xin et.al was used to construct ontology from domain text corpus[5]. GRAONTO is a graph-based approach for automatic ontology construction. Based on the concept extraction phase in GRAONTO, let $C = \{C_1, C_2, \dots, C_n\}$ be the set of ontology concepts, for $\forall C_i \in C$, there must exist a set of terms $T_j = \{T_{j1}, T_{j2}, \dots, T_{jm}\}$ that corresponds to the concept C_i , denoting by $T_j \mapsto C_i$. Therefore, if the term T_{jm} is included in the query, then its corresponding ontology concept is C_i , and its set of synonym is $\{T_{j1}, T_{j2}, \dots, T_{jm-1}\}$. Document can be regarded as a set of terms $D = \{t_1, t_2, \dots, t_p\}$, if $t_p \in T_j$, then the term t_p would be labeled with C_i .

3 Ontology-Based Knowledge Retrieval Mechanisms

In this section, the details of the proposed framework are addressed, including two main methods, i.e. Query Semantic Extension and Query Semantic Retrieval.

The Latent Semantic Analysis (LSA) was used in this paper to determine the internal semantic relations between the query and the domain content [6]. LSA assumes that there are some latent semantic structures in data, but they have been weakened due to the randomness and incomplete of the query. LSA employs algebraic statistical methods to discover and rebuild these semantic structures. It projects term frequency information to the vector space through the singular value decomposition (SVD) to express relationships between words and documents[7].

The Query Semantic Extension inputs domain corpus and outputs extended query semantic features, which consists of the following three steps:

Step1: Generation of Semantic Matrix: In order to mine the latent semantics, the domain document is transformed into semantic matrix, which describes not only ontology concepts but also the distribution of these concepts.

The semantic matrix $W(w_{i,j})_{M \times N}$ is defined as below:

$$w_{i,j} = \sum_{t_m \in \Omega_{c_i}} t_{m,j} \quad (1)$$

$$t_{m,j} = (1 - \varepsilon_m) \frac{\kappa_{m,j}}{\lambda_j} \quad (2)$$

$$\varepsilon_m = -\frac{1}{\log N} \sum_{j=1}^N \frac{\kappa_{m,j}}{\tau_m} \log(\frac{\kappa_{m,j}}{\tau_m}) \quad (3)$$

$$\tau_m = \sum_j \kappa_{m,j} \quad (4)$$

where Ω_{c_i} denotes the set of terms that corresponds to ontology concept c_i ; $t_{m,j}$ is the value of term t_m in document d_j ; $\kappa_{m,j}$ represents how many times that term t_m appears in document d_j ; λ_j is the total number of terms in in document d_j ; ε_m denotes the normalized entropy of t_m in d_j ; N is the total number of documents; τ_m describes the total number of t_m in all documents.

The structure of semantic matrix is as follows:

$$W(w_{i,j})_{M \times N} = \begin{pmatrix} d_1 & d_2 & d_3 & \dots & d_N \\ c_1 & w_{1,1} & w_{1,2} & w_{1,3} & \dots & w_{1,N} \\ c_2 & w_{2,1} & w_{2,2} & w_{2,3} & \dots & w_{2,N} \\ c_3 & w_{3,1} & w_{3,2} & w_{3,3} & \dots & w_{3,N} \\ \dots & \dots & \dots & \dots & \dots & \dots \\ c_M & w_{M,1} & w_{M,2} & w_{M,3} & \dots & w_{M,N} \end{pmatrix} \quad (5)$$

Since ontology concepts are relatively stable, the query can be regarded as a document d_{N+1}^* in the query process. We add d_{N+1}^* to the semantic matrix as a column, forming a query semantic matrix $QW(w_{i,j})_{M \times (N+1)}$. Its definition is

$$QW(w_{i,j})_{M \times (N+1)} = \begin{pmatrix} d_1 & d_2 & d_3 & \dots & d_N & d_{N+1}^* \\ c_1 & w_{1,1} & w_{1,2} & w_{1,3} & \dots & w_{1,N} & w_{1,N+1} \\ c_2 & w_{2,1} & w_{2,2} & w_{2,3} & \dots & w_{2,N} & w_{2,N+1} \\ c_3 & w_{3,1} & w_{3,2} & w_{3,3} & \dots & w_{3,N} & w_{3,N+1} \\ \dots & \dots & \dots & \dots & \dots & \dots & \dots \\ c_M & w_{M,1} & w_{M,2} & w_{M,3} & \dots & w_{M,N} & w_{M,N+1} \end{pmatrix} \quad (6)$$

Step2: SVD & Feature Reduction of Semantic Matrix, Query semantic matrix $QW(w_{i,j})_{M \times (N+1)}$ defined the vector representation of domain ontology concept and domain corpus, where each concept c_i is expressed as a $(N+1)$ -dimensional row vector, while each document d_j is represented as an M -dimensional column vector. However, these vectors are not suitable to be used in knowledge retrieval directly because: (1) N and M are generally large; (2) c_i and d_j are generally sparse; (3) Ontology concept and domain corpus lie in two different and independent vector spaces. Therefore, SVD is used to solve these problems by decomposing semantic matrix into weighted matrices with practical meanings. Through SVD, the Matrix QW^* is decomposed into U (an M -by- A unitary matrix), S (is A -by- A diagonal matrix) and V (($N+1$)-by- A unitary matrix).

During the process of SVD, each concept c_i and each domain document d_j are mapped to the vector $\bar{u}_i = u_i S$ and $\bar{v}_j = v_j S$ in vector space L . Vector space L is decomposed into ontology concept space U and domain corpus space V . After SVD, there might exist noisy semantic features in matrices, hence, feature reduction is needed to discard these meaningless features. QW^* reserves the main semantic information of QW , filtering the high-order noisy semantic features in QW and hence will be used in the selection of latent semantics.

Step3: Selection of Latent Semantics, Selection of latent semantics can discover those semantic features that are related with the query but do not appear in the query explicitly.

Let QW^* be the matrix after feature reduction of QW . Suppose the column vector corresponding to the query d_{N+1}^* in QW and QW^* is respectively $v_{N+1} = (w_{1,N+1}, w_{2,N+1}, \dots, w_{M,N+1})^T$ and $v_{N+1}^* = (w_{1,N+1}^*, w_{2,N+1}^*, \dots, w_{M,N+1}^*)^T$. Let $w = \{w_{i,N+1} \mid w_{i,N+1} > 0, i=1\dots M\}$ be the set of non-zero elements in v_{N+1} , Let $w^* = \{w_{i,N+1}^* \mid w_{i,N+1}^* > 0 \cap w_{i,N+1} > 0, i=1\dots M\}$ be the set of elements corresponding to w in v_{N+1}^* . Then, the elements $w_{i,N+1}^* \in w_E^*$ in column vector d_{N+1}^* corresponding to the concepts that would be extended as the latent semantics should meet:

$$w_E^* = \{w_{i,N+1}^* \mid w_{i,N+1}^* > \min(w^*) \cap w_{i,N+1}^* \notin w^*, i=1\dots M\} \quad (7)$$

3.1 Query Semantic Retrieval

The ideas of this algorithm and its basic processes are as follows:

- (1) The terms in document graph are replaced with ontology concepts, and then the nodes with the same labels are merged into a new node, but the relationships between nodes still remain.
- (2) Each document in domain corpus corresponds to an ontology semantic graph. Domain documents are clustered based on ontology semantic graphs. Meanwhile, the median graph for each cluster is then calculated to represent this cluster.

- (3) In the retrieval process, the extended query semantic features can be regarded as a new domain document that will be represented as ontology semantic graph. Then the median graph closest to new median graph can be found by comparing this graph with every median graph of documents. Hence, the cluster corresponding to the closest median graph is the set of documents that are most relevant with the query.
- (4) Finding the contents most relevant to the query by comparing the query ontology semantic graph with ontology semantic graph of each document.

4 Experiments

This section designs an experiment to measure the performance of the ontology-based knowledge retrieval proposed in this paper. Meanwhile, comparisons with semantics-enable retrieval method[8] and keyword-based retrieval approach [9] were also conducted to demonstrate the benefits of this approach.

In this experiment, the 15 groups of queries were input in the ontology-based knowledge retrieval system, semantics-enable information retrieval system and keyword-based information retrieval system respectively to check whether the retrieved results were compliable to the benchmark that was set up by domain experts.

The Precision-Recall measure commonly used in data mining was used in this research to assess the performance of information retrieval.

Fig. 2 illustrates the precision-recall curves for Query 1, Query 3, Query 5, Query 7 and the overall results after 15 queries, and the Precision-Recall curve. From these curves, we can see that semantic-enable approaches outperformed the keyword-based method, and especially, the ontology-based knowledge retrieval algorithm proposed in this paper performed the best.

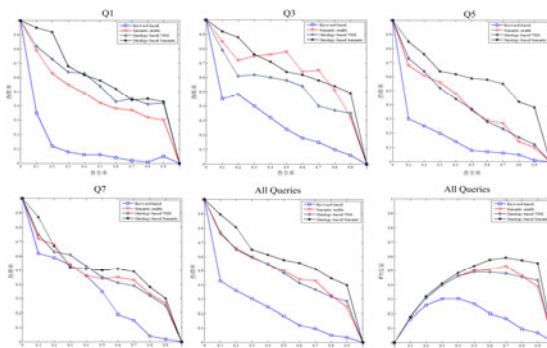


Fig. 2. P-R Curves of Different Information Retrieval Algorithms

5 Conclusions

An ontology-based engineering knowledge retrieval framework has been proposed. The semantics of the queries are first analyzed, and then converted into domain

ontology concepts. Subsequently, the corresponding semantic features with regards to query semantics are expanded by ontology-based query expansion, and thus the retrieval system can understand the query intention of the users more clearly. The domain corpus are labeled with ontology concepts and the document clustering is performed based on ontology semantic graph during query retrieval process to find the proper document collection semantically closest to the queries, and finally the sorted domain documents related to the query semantics are obtained and returned to users. The experimental results show that this approach outperforms the keyword-based and the existing semantic-enable information retrieval methods.

Acknowledgments. This research is supported by the National Natural Science Foundation of China (No. 51001121).

References

1. Chen, M.Y., Chu, H.C., Chen, Y.M.: Developing A Semantic-enable Information Retrieval Mechanism. *Expert Systems with Applications* 37(1), 322–340 (2010)
2. Zhou, L.: Ontology Learning: State of the Art and Open Issues. *Information Technology & Management* 8(3), 241–252 (2007)
3. Gu, N., Xu, J., Wu, X.Y., Yang, J.M., Ye, W.: Ontology Based Semantic Conflicts Resolution in Collaborative Editing of Design Documents. *Advanced Engineering Informatics* 19(2), 103–111 (2005)
4. Niaraki, A.S., Kim, K.: Ontology Based Personalized Route Planning System Using a Multi-Criteria Decision Making Approach. *Expert Systems with Applications* 36(2), 2250–2259 (2009)
5. Hou, X., Ong, S.K., Nee, A.Y.C., Zhang, X.T., Liu, W.J.: Graonto: A Graph-based Approach for Automatic Construction of Domain Ontology. *Expert Systems with Applications* (2010), accepted manuscript,
<http://dx.doi.org/10.1016/j.eswa.03.090>
6. Wei, C.P., Yang, C.C., Lin, C.M.: A Latent Semantic Indexing-based Approach to Multilingual Document Clustering. *Decision Support Systems* 45(3), 606–620 (2008)
7. Gao, J., Zhang, J.: Clustered SVD Strategies in Latent Semantic Indexing. *Information Processing & Management* 41(5), 1051–1063 (2005)
8. Chen, M.Y., Chu, H.C., Chen, Y.M.: Developing a Semantic-Enable Information Retrieval Mechanism. *Expert Systems with Applications* 37(1), 322–340 (2010)
9. Castells, P., Fernandez, M., Vallet, D.: An Adaptation of the Vector-Space Model for Ontology-Based Information Retrieval. *IEEE Transactions on Knowledge and Data Engineering* 19(2), 261–272 (2007)

Forgeability Attack of Two Special Signature Schemes

Jianhong Zhang, Yuanbo Cui, and Xi Wu

College of Science, North China University of Technology,
Beijing 100144, P.R. China
jhzhangs@163.com
<http://cs.ncut.edu.cn>

Abstract. Unforgeability is a primitive property of a secure digital signature. As two extensions of digital signature, proxy signature and certificateless blind signature play an important role in the sensitive transmission. In this work, we analyze the security of two signature schemes, one is the certificateless proxy blind signature scheme [6] which was proposed by Tso *et al* in NSS2010, the other is an efficient proxy signature scheme [8] which was proposed by Hu *et al* in NSWCTC 2010. Then, we show that the two schemes were insecure, meanwhile, we also show that Tso et al's basic certificateless proxy signature is insecure. In Tso *et al*'s scheme, any one can forge a signature on an arbitrary message. Finally, we give the corresponding attack method and analyze the reason to produce such the attack, respectively.

Keywords: unforgeability, proxy signature, certificateless proxy blind signature, proxy signature.

1 Introduction

Digital signature is an important cryptographic tool, it can provide the authenticity of a digital message. A valid digital signature gives a recipient reason to believe that the message was created by a known sender, and that it was not altered in transit. Digital signatures are commonly used for software distribution, financial transactions, and in other cases where it is important to detect forgery or tampering. A digital signature system is said to be secure if it is existentially unforgeable under a chosen-message attack [7]. Roughly speaking, it means that an adversary who is given a signature for a few messages of his adaptive choice should not be able to produce a signature on a new message. If a signature system is insecure, then it means that it cannot be against chosen-message attack.

In 1996, Mambo introduced the concept of proxy signature [5]. In a proxy signature scheme, an original signer delegates his signing authority to another (proxy) signer in such a way that the proxy signer can sign any message on behalf of the original signer. In addition, any verifier can verify and distinguish a normal signature from a proxy signature. Proxy signature schemes have been shown to be useful in many applications such as in electronics transaction [3] and/or mobile agent environments [5].

Recently, Tso *et al* gave a certificateless proxy signature scheme[6] and extended it to the blind signature in NSS2010, And Hu *et al* also gave an efficient proxy signature scheme[8] in NSWCTC 2010. They claimed that their scheme were secure. Unfortunately, in the work, by analyzing the two signature schemes, we show that the two schemes were insecure, then we analyze the reason to produce these insecure factors and gave the corresponding attacks.

2 Reviews of Hu *et al*'s Proxy Signature Scheme

Recently, Hu *et al*'s proposed a novel proxy signature scheme[8] from bilinear maps and claimed that their scheme was secure. In the following, we will review the scheme.

2.1 System Setup

Let \mathbb{G}_1 and \mathbb{G}_2 be two cyclic multiplicative groups of the same prime order p . $g \in \mathbb{G}_1$ is a random generator of \mathbb{G}_1 . Let $\mathbb{G}_1 \times \mathbb{G}_1 \rightarrow \mathbb{G}_2$ be a bilinear map and $H : \{0, 1\}^* \rightarrow \mathbb{G}_1$ be a cryptographic hash function. The system parameters are

$$\{\mathbb{G}_1, \mathbb{G}_2, p, e, g, H\}$$

2.2 Key Generation

For this algorithm, it takes as input the system parameters, selects a random element $x \in Z_p^*$ to compute $X = g^x$, then it outputs the public-private key pair (x, X) .

2.3 Signing Algorithm

Given a secret key x of the user , and a signed message $M \in \{0, 1\}^*$, it computes a standard BBS signature

$$\delta = H(00||X||M)^x$$

the resultant signature on message M is $\delta \in \mathbb{G}_1$.

2.4 Verification

Given a public key X , a message M and the corresponding signature δ , a verifier can check as follows.

$$e(\delta, g) = e(H(00||X||M), X)$$

If so, then the verifier returns 1; otherwise it returns 0.

2.5 Delegation Algorithm

Assume that the user j is a proxy signer, the user i is the original signer. To produce a delegation, the user i chooses an appropriate warrant W_{ij} , and computes

$$D_{ij} = H(01||X_i||X_j||W_{ij})^{x_i}$$

and give the warrant certificate (W_{ij}, D_{ij}) to the user j . The user j accepts the warrant certificate if and only if the following equation holds

$$e(D_{ij}, g) = e(H(01||X_i||X_j||W_{ij}), X_i)$$

2.6 Proxy Signing

Given a signed message M , the proxy signer j with private key x_j and warrant certificate (W_{ij}, D_{ij}) . The proxy signer j computes

$$\delta_{ij} = D_{ij}H(11||X_j||M)^{x_j}$$

as the proxy signature on message M on behalf of the original signer i .

2.7 Proxy Signature Verification

For a proxy signature δ_{ij} on message M , a verifier can check if the following equation holds.

$$e(\delta_{ij}, g) = e(H(01||X_i||X_j||W_{ij}), X_i)e(H(11||X_j||M), X_j)$$

If so, it returns 1 and we say that (W_{ij}, M, δ_{ij}) is a valid proxy signature of user j on behalf of user i under the warrant W_{ij} ; otherwise, it returns 0.

3 Security Analysis on Hu *et al.*'s Scheme

In [8], Hu *et al* claimed that their scheme was secure since they think that their scheme was based on a secure digital signature scheme BBS [1]. However, by analyzing the security of their scheme, we show that the scheme cannot be against the original signer's attack. According the above proxy signature generation, we know that the above proxy signature δ_{ij} is essentially an aggregate BBS signature, and D_{ij} and δ_{ij}/D_{ij} are two independent BBS signatures. In the following , we will the proxy signature can not be against the original signer's attack. The detail attack is done as follows:

1. Assume that the original signer is an attacker.
2. Given a proxy signature δ_{ij} on message M .
3. The attacker computes as follows:
 - (a) Firstly, it chooses a warrant W' to compute $h_1 = H(01, ||X_i||X_j||W')$.
 - (b) Then it computes $U = x_i h_2$
 - (c) Finally, it sets $\delta'_{ij} = \delta_{ij} - x_i(h_1 - H(01||X_i||X_j||W_{ij}))$

Obviously, the forged proxy signature δ'_{ij} is a valid proxy signature under the warrant W' . It means that δ'_{ij} is a proxy signature on message M under a novel warrant. Thus, the forge is valid.

The reason to produce such an attack is that the scheme is essentially an aggregate BBS signature. The two BBS signatures are merged into a signature. At the same time, the merged signature doesn't include message each other.

4 Reviews of TSo *et al*'s Certificateless Proxy Blind Signature Scheme

In [6], Tso *et al* proposed a certificate proxy signature, then they extend it to a certificateless proxy blind signature scheme. Please the interested reader refer to [6] for the detail. In the following, we review Tso et al's Certificateless Proxy Blind Signature Scheme.

4.1 Setup

This algorithm is run by the KGC. On input the system's parameter λ , the algorithm generates a bilinear group \mathbb{G}_1 of prime order $q(q \geq 2)$ such that CDH problem is hard in \mathbb{G}_1 . Let $e : \mathbb{G}_1 \times \mathbb{G}_1 \rightarrow \mathbb{G}_2$ be the bilinear pairing. The generator of \mathbb{G}_1 is P . Pick a random number $s \in Z_q$ as KGC's master secret key and set $P_{pub} = sP$. Q is another generator of group \mathbb{G}_1 which is generated and the DL-problem of P and Q is unknown to all users. It also chooses three distinct cryptographic hash functions $H_0 : \{0, 1\}^* \rightarrow \mathbb{G}_1$, $H_1 : \{0, 1\}^* \rightarrow \mathbb{G}_1$ and $H_2 : \{0, 1\}^* \rightarrow Z_q$. It outputs the system parameter as

$$\text{Param} = \{\lambda, \mathbb{G}_1, \mathbb{G}_2, q, e, P, Q, P_{pub}, H_0, H_1, H_2\}$$

4.2 Partial-Private-Key-Extract

Assume the original signer's identity information is ID_A and the proxy signer's identity information is ID_B , respectively. For this algorithm, the KGC computes firstly $Q_A = H_0(ID_A)$, $Q_B = H_0(ID_B)$, then it computes partial private key

$$D_A = sQ_A, D_B = sQ_B$$

by the KGC's master secret key. Finally, D_A is sent to ID_A and D_B is sent to ID_B securely as their partial private keys via a secure channel.

4.3 Set-Secret-Value

The original signer A runs this algorithm to choose a random number $x_A \in Z_q$ and compute $S_A = x_A Q_A$ as its secret value, where $Q_A = H_0(ID_A)$. Similarly, the proxy signer B runs the algorithm to get a random number $x_B \in Z_q$ and computes $S_B = x_B Q_B$ as its secret value.

4.4 Set-Private-Key

In the algorithm, the original signer A sets $sk_A = (D_A, S_A)$ as private key. At the same time, proxy signer B sets $sk_B = (D_B, S_B)$ as his private key.

4.5 Set Public Key

In this algorithm, the original signer A sets its public key $PK_A = x_A P$ and the proxy signer B sets its public key $PK_B = x_B P$.

4.6 Delegation-Generation

Let m_w be the warrant to be signed by the original signer A who wants to delegate its signing right to B . The original signer A picks $k_Z \in_R Z_q$, and computes $r_A = e(P, P)^{k_A}$, $h_A = H_2(m_w, r_A, ID_A, ID_B, PK_A)$ and $\delta_d = h_A(D_A + S_A) + k_A P$. Then A sends the warrant m_w together with the delegation (r_A, δ_d) to the proxy signer B via a secure channel.

4.7 Delegation-Verification

Upon receiving warrant certificate (m_w, r_A, δ_d) , the proxy signer B computes $h_A = H_2(m_w, r_A, ID_A, ID_B, PK_A)$, $Q_A = H_0(ID_A)$ and accept the delegation if and only if

$$e(\delta_d, P) = e(Q_A, PK_A + P_{pub})^{h_A} r_A$$

4.8 Proxy-Key-Generation

If the delegation verification is passed. The proxy signer B generates the following proxy key by the warrant certificate (m_w, r_A, δ_d)

$$d_p = h_A(S_B + D_B) + \delta_d$$

4.9 Proxy Blind Signing

It is an interactive protocol between a receiver and a proxy signer. Given a message M , the receiver picks four random numbers $t_0, t_1, t_2, t_3 \in Z_q$ and blinds the original message M by computing

$$T_1 = t_1^{-1} P, T_2 = t_2 Q \quad \text{and} \quad M' = t_0 H_1(M, T1, T2, PK_B) + t_2 P$$

The receiver then sends the new version M' of M to the proxy signer. The proxy signer chooses $k_0, k_1 \in_R Z_q$, computes $U' = k_0 P + k_1 Q$, $V_B = k_0 M'$, $S' = d_p + V_B$, $K' = k_1 P$ and then returns (S', U', K') to the receiver. The receiver unblind the message by computing $S = t_1(S' - t_2(U' + t_3 Q))$, $U = t_0 U'$, $K = K' + t_3 P$ and outputs the proxy signature on M as

$$\delta = (r_A, m_w, S, U, T_1, T_2, K)$$

4.10 Proxy-Signature-Verification

Given the identities (ID_A, ID_B) of original signer and proxy signer, a warrant m_w , a message M and a proxy blind signature $\delta = (r_A, m_w, S, U, T_1, T_2, K)$, any verifier accepts the proxy blind signature on M if and only if

$$\begin{aligned} e(S, T_1) &= (e(Q_A, PK_A + P_{pub})e(Q_B, PK_B + P_{pub}))^{h_A} \cdot \\ &\quad r_A \cdot e(H_1(M, T_1, T_2, PK_B), U)e(T_2, K) \end{aligned}$$

where $h_A = H_2(m_w, r_A, ID_A, ID_B, PK_A)$.

5 Security Analysis

In [6], Tso et al claimed that their scheme was secure. The scheme can satisfy unforgeability of the proxy blind scheme. Then they also gave the corresponding security analysis and show that the security of the scheme was based on the CDH Problem. In the following, we will show that the scheme is insecure. It is universally forgeable, that is to say, anyone can produce a proxy blind signature on arbitrary a message m .

Let C be an attacker, to produce a forgeable attack, C executes the following steps:

1. Let m'_w be a warrant message.
2. Let M' be a forged message.
3. C randomly chooses a number $r \in Z_q$ to compute $r'_A = e(rP, PK_A + P_{pub})^{-1}$, note that r'_A is an element of group \mathbb{G}_2 .
4. Then C computes $h'_A = H_2(m'_w, r'_A, ID_A, ID_B, PK_A)$
5. C sets $T'_2 = (PK_A + P_{pub})$ and $K' = -h'_A Q_A + rP$
6. C randomly chooses $t \in Z_p$ to compute $T'_1 = t(PK_B + P_{pub})$.
7. C sets $S' = t^{-1}(h'_A Q_B + H_1(M', T_1, T_2, PK_B))$.
8. C sets $U' = PK_B + P_{pub}$.

Finally, the forged proxy blind signature on message M' under the warrant m'_w is $\delta' = (S', U', K', T'_1, T'_2, r'_A)$.

5.1 Correctness

In the subsection, we will show that our forgery is valid. Since

$$\begin{aligned} &(e(Q_A, PK_A + P_{pub}) \cdot e(Q_B, PK_B + P_{pub})^{h'_A} \cdot r'_A \cdot \\ &\quad e(H_1(M', T'_1, T'_2, PK_B), U')e(T'_2, K')) \\ &= (e(Q_A, PK_A + P_{pub}) \cdot e(Q_B, PK_B + P_{pub})^{h'_A} \cdot e(rP, PK_A + P_{pub})^{-1} \cdot \\ &\quad e(H_1(M', T'_1, T'_2, PK_B), U')e(T'_2, K')) \\ &= (e(Q_A, PK_A + P_{pub}) \cdot e(Q_B, PK_B + P_{pub})^{h'_A} \cdot e(rP, PK_A + P_{pub})^{-1} \cdot \\ &\quad e(H_1(M', T'_1, T'_2, PK_B), U')e((PK_A + P_{pub}), -h'_A Q_A + rP)) \end{aligned}$$

$$\begin{aligned}
&= (e(Q_B, PK_B + P_{pub})^{h'_A} \cdot e(H_1(M', T'_1, T'_2, PK_B), U')) \\
&= (e(Q_B, PK_B + P_{pub})^{h'_A} \cdot e(H_1(M', T'_1, T'_2, PK_B), PK_B + P_{pub})) \\
&= (e(h'_A Q_B, PK_B + P_{pub}) \cdot e(H_1(M', T'_1, T'_2, PK_B), PK_B + P_{pub}))
\end{aligned}$$

where $h'_A = H_2(m'_w, r'_A, ID_A, ID_B, PK_A)$

$$\begin{aligned}
e(S', T'_1) &= e(t^{-1}(h'_A Q_B + H_1(M', T_1, T_2, PK_B)), t(PK_B + P_{pub})) \\
&= e(h'_A Q_B + H_1(M', T_1, T_2, PK_B), (PK_B + P_{pub}))
\end{aligned}$$

It means that the forged proxy blind signature $\delta' = (S', U', K', T'_1, T'_2, r'_A)$ satisfies the verification equation

$$\begin{aligned}
e(S', T'_1) &= (e(Q_A, PK_A + P_{pub}) \cdot e(Q_B, PK_B + P_{pub})^{h'_A} \cdot r'_A \cdot \\
&\quad e(H_1(M', T'_1, T'_2, PK_B), U') e(T'_2, K'))
\end{aligned}$$

Thus, our forged attack is successful. The reason to produce such attack is many free elements of proxy blind signature (S, U, K, T_1, T_2, r_A) . The relation among U, S, T_1, T_2 and K is not restricted, therefore, it results in attack.

5.2 Tso et al's Basic Proxy Signature and Its Attack

In the subsection, we show that Tso et al's proxy signature scheme is also insecure. The difference of Tso et al's proxy blind signature with Tso et al's basic proxy signature is only proxy signing and proxy signature verification. We briefly review it.

Proxy Sign: Given a message M , the proxy signer chooses $k_B \in Z_q$ to compute $U = k_B P$, $V_B = k_B H_1(M, U, PK_B)$ and $S = d_p + V_B$. The proxy signature on message M is $\delta = (r_A, m_w, S, U)$.

Proxy Signature Verification: Given the identities (ID_A, ID_B) of original signer and proxy signer, a warrant m_w , a message M and a proxy signature $\delta = (r_A, m_w, S, U)$, any verifier checks the following equation

$$\begin{aligned}
&e(S, P) \\
&= (e(Q_A, PK_A + P_{pub}) \cdot e(Q_B, PK_B + P_{pub})^{h_A} \cdot r_A \cdot e(H_1(M, U, PK_B), U))
\end{aligned}$$

where $h_A = H_2(m_w, r_A, ID_A, ID_B, PK_A)$.

Attack: We will show if the original signer colludes the proxy signer, then they can attack the certificateless proxy signature scheme in the case that the partial-private-keys of proxy signer and the original signer is not produced by the KGC. If they collude, it means that the attacker has the private keys (x_B, x_A) of the proxy signer and the original signer. Then it can compute as follows:

1. Let M' and m'_w be the signed message and warrant, respectively.
2. The attacker randomly chooses $r \in Z_q$ to compute $r'_A = e(rP, P)$.

3. Then, the attacker computes $h'_A = H_2(m'_w, r'_A, ID_A, ID_B, PK_A)$.
4. Next, the attacker randomly chooses $l_A, l_B \in Z_q$ to set the public keys of the original signer and the proxy signer as $PK_A = -P_{pub} + l_A P$ and $PK_B = -P_{pub} + l_B P$.
5. And the attacker randomly chooses $t \in Z_q$ to compute $U' = tP$.
6. Finally, it sets $S' = h_A(l_A Q_A + l_B Q_B) + rP + tH_1(M', U', PK_B)$.

The forged certificateless proxy signature is (r'_A, m'_w, U', S') on message M' under the warrant m'_w . According to the above forging process, we know the forged certificateless proxy signature is valid, it can pass proxy signature verification equation.

6 Conclusion

In a digital signature, unforgeability is a primitive property which can ensure the integrality of message and authenticity of identity. Recently, two special signature schemes: proxy signature and certificateless proxy blind signature, were proposed in 2010. They were claimed to be secure. However, in this work, by analyzing the security of the two schemes, we show that the two schemes were insecure. And Tso *et al*'s scheme was universally forgeable, any one can forge a signature on arbitrary message in the name of the others. Finally, we give the corresponding attack and analyze the reason to produce such attack.

Acknowledgments. I thank the anonymous referees for their very valuable comments on this paper. This work is supported by the National Natural Science Foundation of China (No: 60703044), the Nova Programma (No:2007B-001).

References

1. Boneh, D., Lynn, B., Shacham, H.: Short Signatures From the Weil Pairing. In: Boyd, C. (ed.) ASIACRYPT 2001. LNCS, vol. 2248, pp. 514–532. Springer, Heidelberg (2001)
2. Yap, W., Heng, S., Goi, B.: An Efficient Certificateless signature scheme. In: Zhou, X., Sokolsky, O., Yan, L., Jung, E.-S., Shao, Z., Mu, Y., Lee, D.C., Kim, D.Y., Jeong, Y.-S., Xu, C.-Z. (eds.) EUC Workshops 2006. LNCS, vol. 4097, pp. 322–331. Springer, Heidelberg (2006)
3. Park, H.U., Lee, L.Y.: A Digital Nominative Proxy Signature Scheme for Mobile Communications. In: Qing, S., Okamoto, T., Zhou, J. (eds.) ICICS 2001. LNCS, vol. 2229, pp. 451–455. Springer, Heidelberg (2001)
4. Gamage, C., Leiwo, J., Zheng, Y.: An Efficient Scheme for Secure Message Transmission Using Proxy-signcryption. IEEE society, 420–431 (1999)
5. Mambo, M., Usuda, K., Okamoto, E.: Proxy Signatures: Delegation of the Power to Sign Message. IEICE Transaction Functional E79-A(9), 1338–1354 (1996)
6. Tso, R., Yi, X.: Certificateless Proxy Signature and Its Extension to Blind Signature. Network and System Security, 542–547 (2010)
7. Goldwasser, S., Micali, S., Rivest, R.: A digital Signature Scheme Secure Against Adaptive Chosen-Message Attacks. SIAM J. Computing 17(2), 281–308 (1988)
8. Hu, G.Z., Han, L.S.: Proxy Signature Scheme Secure against Chosen Key and Chosen Warrant Attacks. In: 2010 Second International Conference on Networks Security, Wireless Communications and Trusted Computing, pp. 325–328 (2010)

A Trojan Detector Generating Algorithm Based on Chaotic Theory

Jie Qin, Qun Si, Huijuan Yan, and Fuliang Yan

College of Information Science and Engineering,
Henan University of Technology, Zhengzhou, China
qinjie0160@163.com

Abstract. After studying the existing detector generating algorithms used in the intrusion detection systems, we improves the lacks of the algorithms and use them into Trojan detection system, and propose a new approach of detector generating based on chaotic theory. The over-spread character of chaos sequence combined the concept of weighted Euclidean distance was used to generate set of detector with better distribution, and chaos initial value sensitivity was used to enlarge the searching space. The experiment indicates that the algorithm not only remains the diversity of population but also has fast astringency speed.

Keywords: chaos, Trojan, weighted Euclidean, detector.

1 Introduction

The biological immune principle is applied in Trojan detecting filed of network security, which is to sum up the computer security question as the recognition of “self” and “not self”, and it can make the system detect Trojan intrusion rapidly and accurately, then do the alarm [1]. In order to reach these objectives above, the effective detector generation algorithm is the key and difficult point of Trojan detection system based on biological immune. First S.Forrest proposed the negative selection algorithm based on immune theory to generate detectors[2], the algorithm is also called exhaustive random detector generating algorithm[3]. Following the algorithm there are linear time detector algorithm and greed detector algorithm, but the above algorithms exist system larger systematic expenses problem, then, Castro and TIInlnis proposed negative selection algorithm with variation to improve the above problems, introducing variation to the algorithm expands the cover space[4]. The reference [1] integrates the negative selection algorithm and cloning algorithm, and proposes the mode coding algorithm to reduce spending. It the other research on the generation of antibody uses the vaccination injection principle[5] and encodes the intrusion to the system by human, but reduces its automatism. The system expenses mainly focus on the formulation of antibody, so how to produce detector set directly and effectively is the point of Trojan detection filed [3-5].

The detector generating algorithm based on chaotic theory [7] overcomes the restrict of the difficult of random detector generating algorithm increases exponentially along with the increase of self set scale, additionally, compared with linear time detector generating algorithm and greed detector generating algorithm, it is not only applicable to r-continuous bit matching rules, but also suitable for any kind of matching rules[8]. At present, the algorithms based on chaotic theory mostly use Logistic model[9] to produce chaotic sequences, and then create initial detector or add chaotic and random disturbance, although the property of algorithm improves to some extent, but still exists the problems of large search blind and slow convergence speed[10]. In order to overcome the defects, some scholars combine chaotic mechanics characteristics to entropy of information theory[11], the algorithm change and control the distribution situation of initial detector in solution space, but it also has the defect of fault charge. According to the above defects this paper will introduce chaotic theory to the Trojan detector generating algorithm and proposes a method based on chaotic theory combined with weighted Euclidean of math to generate uniform detectors, this method can well solve the problem. The following contents of the paper is: in the second part it will introduce the chaotic characteristics of system; in the third part it will introduce the detector generating algorithm based on chaotic theory combined weighted Euclidean; in fourth part it will show the experiment results, and finally it shows paper working summary and the next work direction.

2 Chaotic Character of Immune System

Chaos is a cyclic behavior which has not regular period and generated by continuous or discrete dynamical system, and widely used in engineering, physical, mathematical, biology and other fields[8][11]. Also chaos has initial values sensitivity, over-spread character and randomness etc[12].

The immune system is needed to constantly absorb and consume the energy and materials, and it is a dissipative system. Investigating the change of antigens cell concentration in immune system, and the following equation (1) shows its value-added approach:

$$Ag(t+1) = k(1 - \frac{Ag(t)}{Ag_{\max}})Ag(t) - k'Ag(t) \quad (1)$$

In the above equation, function $Ag(t)$ indicates the antigens cell concentration at t, the antigens cell concentration of $t+1$ can be calculated by t moment. The k reflects appreciation rate of antigen and shows the death rate of cell, for example we take initial value $Ag(0)$ equal 0.3. when the value of $\mu = k-k'$ is less than 3.0, the function is stable; When the value of μ is more than 3.1 and is not more than 3.4, the function tends oscillation; And when the value of μ is not less than 3.4 and is less than 4.0, the function presents chaos phenomenon[12].

3 The Detector Generating Algorithm Based on Chaotic Theory Combined Weighted Euclidean

Due to the sensitivity for initial value of chaos, that is even slight change of initial state can cause the great differences of the system state, thus it can increase the space range. By using this character of chaos, it produced individual evenly distribute in individual solution space, and won't have gathered phenomenon, so this can effectively avoid possible data redundancy. The individual which will not adapt to the solution space can conduct "variation" by using the chaos disturbance to get more optimal individuals[12].

In this paper it generates candidate set of detectors mainly by using chaotic sequence, then construct the initial set of detector according to knowledge of mathematical Euclidean, thus generate qualified detector set. Detector generating algorithm process is shown in below as figure 1.

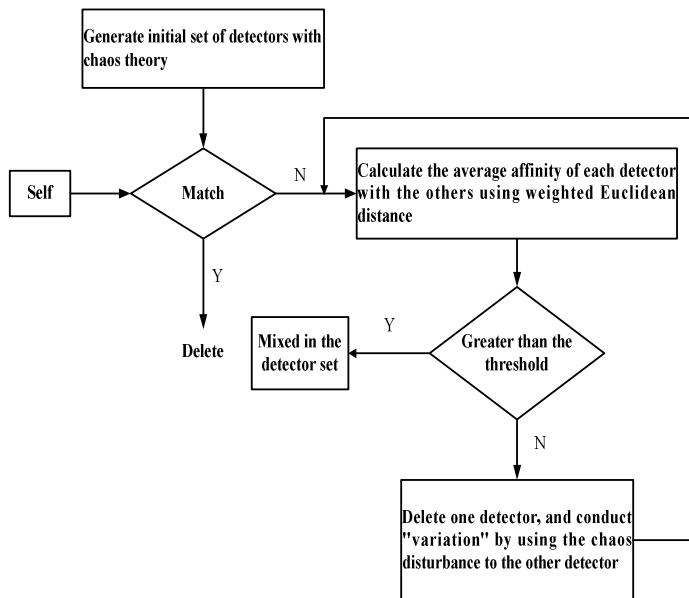


Fig. 1. Detector generating algorithm based on chaotic theory combined weighted Euclidean

3.1 The Initialization of Initial Detector

Detector initialization directly affect the generation efficiency and quality of mature detector[14]. Because the properties that the chaotic sequence has good over-spread and randomness character and also has uniform distribution of individual solution space, so in this paper the algorithm uses the chaotic sequence to produce initial detector.

Generating the first individual as x_0 randomly in detector set, and then maps x_0 to $[0,1]$ region, and get y_0 as the initial value to generate chaotic sequence, later, it uses Logistic chaotic iterative equations to produce chaotic sequences as y_i , and then maps the y_i to individual solution space, and thus generate the initial set of detector as y_i ($i = 1, 2, 3 \dots$). And for each detector it randomly generated the weights $w_1 w_2 \dots w_n$ ($0 < w_i < 1$) which represents the importance.

3.2 The Construction of Fitness Function

In the artificial immune algorithm based on information entropy, because it needs to calculate information entropy of each individual in each generation population, so it makes the speed of the algorithm slows greatly[11]. The fitness of detector x_1 represents the average affinity with the other detectors, and reserves the detector which has high fitness in the select process. The fitness function is constructed as following function (2):

$$a(\vec{x}_i) = \frac{\sum_{j=1, j \neq i}^M w_j \sqrt{\sum_{k=1}^N (y_i^k - y_j^k)^2}}{M-1} \quad (2)$$

The y_i^k in the function means the value of k bit of detector I, M means the number of all the initial detectors, w_j means the important level which is weight value of detector j, and each detector is N binary coding.

3.3 Chaos Disturbance

The detector that not more than the specified value is marched the chaos disturbance as function (3):

$$y'_r = (1-\eta)\hat{y} + \eta y_r \quad (3)$$

\hat{y} is the current optimal value, η is the parameter in $[0,1]$ and change adaptively with the change of algebraic r. y_r is the chaos vector after iterating r times. y'_r is the one after imposing disturbance. The function it shows us that because the sensitivity of initial value the slight change of it can cause great difference, and then get the aim of increasing scope of variation, optimizing individual and enriching population, also accelerates the speed to generate detector.

4 Test Comparing

To prove the actual effect of this method by comparing to the detector generating algorithm based on chaotic theory and information entropy[3-7]. Because the

computation of Logistic chaos iteration function is smaller and convenient to use, so in the test we use function (4) to get chaotic sequence:

$$x_{n+1} = \mu x_n (1 - x_n) \quad (4)$$

In test, μ equals 3.7, x is the chaotic vector, $0 < x_n < 1$, and its chaotic space is $[0,1]$. Take the self set size for 40, that is generating 40 individuals randomly, and operates on the detector according to the fitness of it to get the next generation detector set, and this reduces the time spending than the detector generating algorithm based on chaotic theory and information entropy. Under the same conditions, we carry out comparison test with the two detector generating algorithms, in the following fig.2. it shows the relationship of evolution generation number and the detector number.

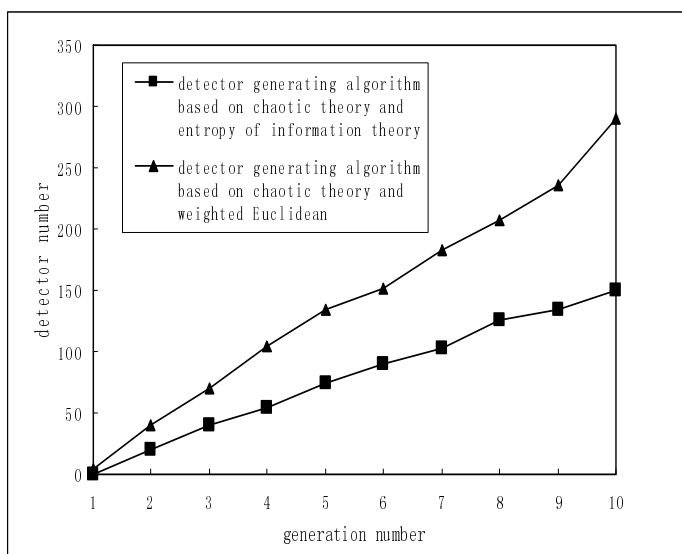


Fig. 2. The relationship of generation number and detector number

Table 1 gives the comparison result of tow algorithm performance.

In the experiment the number of repeat operation of the algorithm is 50, and the time-consuming is the sum of running 50. From the table 1 we can see that in the detector generating algorithm based on chaotic theory and information entropy, because of calculating the information entropy of each population and it reduces the algorithm speed. At the same time we find that with the increase of populations the computation of information entropy growth explosively, and this hinders the efficiency of above algorithm. By contrast, the advantage of the algorithm mentioned in this paper is displayed.

Table 1. Comparison result of two algorithm performance

algorithm \ performance	Number of algorithm runs	Evolution number of every time	Time-consuming	Optimal number of each converge to global
Detector generating algorithm based on chaotic theory and information entropy	50	400	25.6	44
The algorithm in this paper	50	400	4.0	45

5 Conclusion and Prospect

In this paper the chaotic theory is applied in Trojan detection filed, and it proposes a detector generating algorithm based on chaotic theory combined weighted Euclidean distance, also through experiment verifying the validity of this method. The method has much higher efficiency than traditional Trojan detector generating algorithm based on information entropy. Combining chaotic theory can generate uniform Trojan detector, then ensure the diversity of population. The next step of this paper is using the algorithm to Trojan detection system, and further step is to verify the effectiveness of the algorithm by setting up the appropriate weight of weighted Euclidean distance.

References

1. Paul, K., Williams, D., et al.: An Artificial Immune System Architecture for Computer Security Applications. *IEEE Transaction on Evolutionary Computation*, 6–3 (2002)
2. Forrest, S., Alan, S., Allen, L.: Self-Nonself Discrimination in a Computer. In: Proceedings of the 1994 IEEE Symposium on Security and Privacy, pp. 202–212 (1994)
3. Zhang, H.: The Research and Implementation of Unknown Trojan Detection System Based on Artificial Immune. Master thesis of Xian University of electronic science and technology (2009)
4. Zhang, J.: A Network Intrusion Detection System Model Based on Immune Principle. Lanzhou: The master's degree thesis of Lanzhou University of technology (2008)
5. Chen, L., Zhang, L.: The Research on The Application of Artificial Immune Mechanism on Trojan Detection System. University of electronic science and technology journal 34(2), 221–224 (2005)
6. Yan, X.: Immune Intrusion Detection Model Using Vaccination Strategies. Electronic journal 37(4), 221–224 (2009)
7. Zhang, N., Li, Z., et al.: The Immune Generating Algorithm Based on Chaotic Theory. Computer application (May 2006)

8. Wang, H., He, C.: The Public Water-marking Based on Robustness of Chaos Mapping. *Journal of software* 15(8), 1245–1251 (2004)
9. Tavazoei, M., Haeri, M.: An Optimization Algorithm Based on Chaotic Behavior and Fractal Nature. *J. Compute. Applied Math.* 206, 1070–1081 (2007)
10. Zuo, X.Q., Fan, Y.S.: A Chaos Search Immune Algorithm with Its Application to Neuro-fuzzy Controller Design. *Chaos, Solitons and Fractals* 30, 94–109 (2006)
11. Shu, H., You, Z.: Application of Decision Attribute Classification and Mining Algorithm Based on Information Entropy. *Computer engineering and application* 01, 186–189 (2004)
12. Hrycej, T.: Identifying Chaotic Attractors with Neural Networks. In: *Proceedings of IEEE International Conference on Neural Network*, pp. 2664–2668 (1995)
13. Castro, L., Timmis, J.: Artificial Immune System. A Novel Computational Intelligence Approach. Springer, London (2002)
14. Li, T.: A Dynamic Intrusion Detection Model Based on Immune. *Science bulletin* 50, 17 (2005)

Network Security Situation Assessment Based on Hidden Semi-Markov Model

Boyun Zhang^{1,2}, Zhigang Chen², Xiai Yan¹, Shulin Wang³, and Qiang Fan¹

¹ Department of Computer Science and Technology, Hunan Police Academy,
Changsha, Hunan 410138, China
hnjxzby@yahoo.com.cn

² School of Information Science and Engineering,
Central South University, Changsha, Hunan 410086, China

³ School of Computer and Communication,
Hunan University, Changsha, 410082, China

Abstract. This paper takes use of the hidden semi-Markov model to evaluate network security situation. HsMM modifies HMM model on the presumption that certain system status dwell time abides with exponential distribution, which is more suitable to describe the actual situation of network system operation. We propose the HsMM system status prediction algorithm under partial observation conditions, and applies it into network security situation assessment. The experiment result shows that HsMM could model system status dwell time, so it is very propitious to make network system security assessment under complicated and changeable attacks.

Keywords: Network security, Network security state assessment, hidden semi-Markov model.

1 Introduction

With the rapid development of Internet, network security issues are also increasingly serious. Corresponding, security technologies should shift its focus from solving single security problem to studying the security situation and trends of the whole network. Network security situation awareness may acquire, comprehend, evaluate and predict future development trend on many factors which influence network security, and it becomes security technology focus of the next generation[1]. Network security situation assessment is the core of situation awareness as well as the qualitative and quantitative description of network security situation.

In this paper we use hidden semi-Markov model to simulate network system actual operation, take alarm data from network defense system as data source, and then evaluate network security situation with HsMM modeling..

This paper begins with the basic algorithm of HsMM, and then proposes correspondent solutions for HsMM application problems; at last it gives more attention on the network security assessment method based on HsMM.

2 System Status Prediction Algorithm Based on HsMM

HsMM is extracted from the comprehensive thoughts of discrete HMM and continuous HMM, it was first proposed and systematically studied by Huang[2] and his fellow scholars. HsMM modified HMM model assumption that system dwell time at certain status complies with exponential distribution, which is more suitable to describe computer system actual operation[3]. Three basic issues should be solved[4] in order to apply given HsMM better in practical operation: issue 1: HsMM probability reasoning (forward-backward algorithm in broad sense). Issue 2: HsMM decoding (improve Viterbi algorithm). Issue3 HsMM training (improve Baum-Welch algorithm). In this paper we focus on issue 1.

The goal of status prediction is to acquire observation information of a certain period of time and predict the future status based on certain observation data. But the current algorithm of HsMM requires all known observation records then it can make system status prediction, therefore it needs to develop a HsMM status prediction algorithm when there is only partial observation.

Granted a period of observation signal before $t-1$, predict certain system status probability at time t , that is

$$P(q_t = s_m | o_{t-d}^{d-1}) \quad (1)$$

where d is constant, which represents observation duration. Mark prediction sequence fragment as o_a^b , namely $o_a^b = (o_a, o_{a+1}, \dots, o_b)$, $1 \leq a \leq b \leq T$.

Because there is no similar metric algorithm of HsMM as HMM to prevent underflow, it tests and iterate over the probability after using the model to prevent underflow. The following are some variables defined in the algorithm.

Variable $\alpha_{tlx}(m, d)$, shown as equation (2), x value could be $t-1$ or t , which correspondingly represent given observation sequence o_1^{t-1} or o_1^t prediction or system status s_m at time t , status duration probability is d .

$$\alpha_{tlx}(m, d) \triangleq P(q_t = s_m, \tau_t = d | o_1^x) \quad (2)$$

Status q_t Marginal probability distribution, definition is variable $\gamma_{tlx}(m)$:

$$\gamma_{tlx}(m) \triangleq \sum_d \alpha_{tlx}(m, d) \quad (3)$$

This section focuses on status prediction, so it only discuss when $x=t-1$. Its main concern is $\alpha_{tlx-1}(m, d) \triangleq P(q_t = s_m, \tau_t = d | o_1^{t-1})$.

$$\text{Variable } b_m^* \text{ is marked as : } b_m^* \triangleq \frac{\alpha_{t|t}(m, d)}{\alpha_{t|t-1}(m, d)} \quad (4)$$

The calculation process of variable b_m^* is :

$$\begin{aligned} b_m^* &\triangleq \frac{\alpha_{t|t}(m, d)}{\alpha_{t|t-1}(m, d)} = \frac{P(q_t = s_m, \tau_t = d, o_1^{t-1}, o_t) \cdot P(o_1^{t-1})}{P(q_t = s_m, \tau_t = d, o_1^{t-1}) \cdot P(o_1^{t-1}, o_t)} \\ &= \frac{P(o_t | q_t = s_m, \tau_t = d, o_1^{t-1})}{P(o_t | o_1^{t-1})} = \frac{b_m(o_t)}{P(o_t | o_1^{t-1})} \end{aligned} \quad (5)$$

$\because \forall d$ with its Markov property, there is $P(o_t | q_t = s_m, \tau_t = d, o_1^{t-1}) = b_m(o_t)$,

Denominator calculation of equation (5) is calculated as:

$$P(o_t | o_1^{t-1}) = \sum_{m,d} \alpha_{t|t-1}(m, d) \cdot b_m(o_t) = \sum_m \gamma_{t|t-1}(m) \cdot b_m(o_t)$$

Given observation sequence o_1^t , the condition probability of one status m ends at time t , marked as $\mathcal{E}_t(m)$, that is $\mathcal{E}_t(m) \triangleq P(q_t = s_m, \tau_t = 1 | o_1^t) = \alpha_{t|t-1}(m, 1) b_m^*(o_t)$

Given observation sequence o_1^t , the condition probability of one status m start time $t+1$, marked as $\mathbb{S}_t(m)$, that is $\mathbb{S}_t(m) \triangleq P(\tau_t = 1, q_{t+1} = s_m | o_1^t) = \sum_n \mathcal{E}_t(n) \cdot a_{nm}$

Because status $(q_t, \tau_t) = (s_m, d)$ maybe transferred from other status, or persist the previous status, that is $(q_{t-1}, \tau_{t-1}) = (s_m, d+1)$, then get the following forward recurrence formula : $\alpha_{t|t-1}(m, d) = \mathbb{S}_{t-1}(m) \cdot p_m(d) + b_m^*(o_{t-1}) \cdot \alpha_{t-1|t-2}(m, d+1)$

Its initial value is : $\alpha_{t=1|t=0}(m, d) = \pi_m \cdot p_m(d)$

Add $\alpha_{t|t-1}$ with respect to d to get q_t marginal distribution:

$$\gamma_{t|t-1}(m) \triangleq \sum_d \alpha_{t|t-1}(m, d)$$

With known observation sequence o_1^{t-1} , this value is the probability of observing system in status q_t at time t .

3 Network Security Situation Assessment Process Based on HsMM

3.1 Situation Assessment Procedure

The network security situation assessment procedure described as follows:

(1) Make feature extraction of life-cycle historical data, we select the alarm information with prediction information number as Snort IDS. Classify and assign numbers on alarm number as prediction sequence.

(2) Take the first half-year data from Honeynet as training set, train HsMM model and get model parameters $\{\pi, A, B, p_j(d)\}$.

(3) Preprocessing security alarm information which needs to be assessed then get correspondent prediction information sequence vector O .

(4) Take use of HsMM status prediction method in certain observation conditions which is introduced at section 2.3 to predict system status probabilities at the very next moment, as $P_i^t = \{p_{normal}^t, p_{probed}^t, p_{attacked}^t, p_{compromised}^t\}$

(5) Make quantitative disposal of risk value when system is in different security state, as $C_{risk} = \{C_{normal}, C_{probed}, C_{attacked}, C_{compromised}\}$.

(6) Based on different system status probability distribution at time t and risk quantitative value, calculates system security state value $\gamma' = C_{risk} \cdot P_i^t$

3.2 Discussions about Status Dwell Time in HsMM

The most disadvantage of traditional HMM model is its presumption of system duration at certain status. Markov chain implies the fact: when system is in status S_i , if the probability of its status transferring to itself is a_{ii} , then the probability density $p_i(d)$ of system in status S_i duration time is $p_i(d) = (a_{ii})^{d-1}(1-a_{ii})$, which is in exponential distribution. But it is an inappropriate presumption for some issues in real world; Markov Process also meets *Memory less Property* of exponential distribution. This conclusion indicates that system in any status i dwell time d is Non - memory Property, that the probabilities are the same between known system dwell in status i for s time units, then dwell in status i for another t time, and system get into i status in the first place then dwell for t time units. This conclusion is inconsistent with the system status dwell time distribution of network security state evaluation. So we decide to utilize HsMM to model network security defense system.

This paper makes expended research on system status dwell time distribution, it evaluates system security state when $p_i(d)$ is under Logarithmic distribution, negative binomial, geometric distribution and Poisson distribution[5].

4 Experiment Results

HoneyNet dataset is collected by HoneyNet.org[6] from hacker attack data and composed of 11 months attacks information (April, 2000- February, 2001). We take the data of December, 2000 as an example to evaluate and predict security threat status, and analyze system security threat status evolution within the month.

Select four kinds of system security state in this experiment: Normal- the host is in a normal status, without any suspicious incidents; Probed- the host is probed or scanned, when the host is in this state, the system's availability will be affected, which may also increase the likelihood of attack; Attacked- the host is under attacks from outside, the system performance will be seriously affected in this state, and system is likely to be broken; Compromised- the host is controlled by malicious program or hackers.

First we train HsMM model parameters, take HoneyNet data of first half of the year (May-November) as training set to train HsMM. Iterations are 40 and convergence threshold is 0.0001. The log/iteration convergent after 28 iterations.

The initial probability distribution of HsMM model is {0.7, 0.1, 0.1, and 0.1}. The initial value and the value after training of state transfer matrix are shown in table 1:

Table 1. HsMM model parameter

HsMM initial probability transfer matrix	State transfer matrix after HsMM training
[N] [P] [A] [C]	[N] [P] [A] [C]
[N] 0.00 0.55 0.225 0.225	[N] 0.000 0.613 0.363 0.024
[P] 0.15 0.00 0.500 0.350	[A] 0.116 0.000 0.863 0.021
[A] 0.20 0.35 0.000 0.450	[P] 0.119 0.458 0.000 0.423
[C] 0.25 0.25 0.500 0.000	[C] 0.039 0.110 0.851 0.000

Pre-process December data and get correspondent prediction information sequence vector O , and calculate the probability distribution of system in different status, then combine it with risk quantitative value to calculate system security state value. Experiment assigns the risk value of system in different status as {10, 20, 30, and 40}.

Table 2. System state dwell time probability distribution

Dwell time probability distribution type	parameter value	System status
geometric distribution	$p=\{0.3,0.4,0.5,0.35\}$	{N,P,A,C}
negative binomial distribution	$(r=3,p=0.4),(r=4,p=0.5),(r=5,p=0.45),$ $(r=6,p=0.55)$	{N,P,A,C}
logarithmic distribution	$p=\{0.9,0.5,0.6,0.8\}$	{N,P,A,C}
Poisson distribution	$\lambda=\{4,6,8,5\}$	{N,P,A,C}

For system dwell time probability distribution, it tests logarithmic distribution, negative binomial, geometric distribution and Poisson distribution. Parameters used in the experiment are shown in Table 2.

Evaluate system security state under various types of system dwell time probability distribution and results are shown in figure1 and figure 4. We can see from experiment results that when system is under certain status for a period of time (see the black hollow circles in figures), and then it transfers into next different status. This indicates that hackers could not attack network system by only one bugle blast, but with the deepening of attacks, system security state gradually deteriorated.

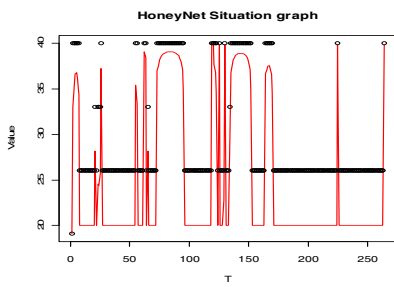


Fig. 1. The situation graph of state dwell time in geometric distribution

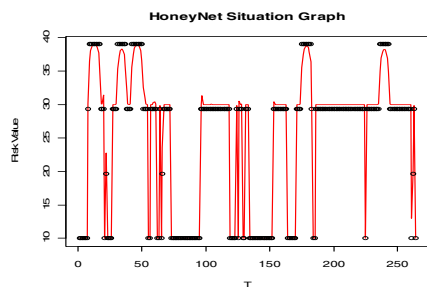


Fig. 2. The situation graph of state dwell time in negative binomial distribution

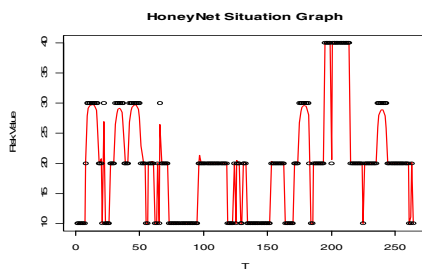


Fig. 3. The situation graph of state dwell time in Poisson distribution

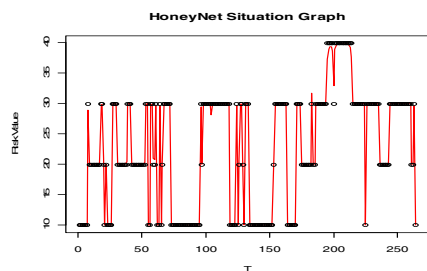


Fig. 4. The situation graph of State Dwell time in logarithmic distribution

Figure 1 is the experiment result when system stratus duration assumption is in geometric distribution. The results are very sensitive to network attacks, it upgrades network security threat status into Compromised State when attacks just begin, and therefore it is little value.

Figure 2 is the security state evaluation result when system status dwell time is in negative binomial distribution, which reflects that the system is under attacks by hackers ($T = 15$) in the first few days, after a period of attempts, system is broken ($T=175$). But its evaluation values is too high, such as when $T=15$ and attacks just happens, the system is not broken yet, it is inappropriate to assess its status as Compromised state.

Figure 3 is the security state evaluation result when system status dwell time is in Poisson distribution, which reflects the actual situation of network attacks. Hackers start attack at $T=15$, after a period of truce, then attack again, the system is broken at $T=175$ with the continuous attacks. Correspondingly, HsMM evaluation model classifies system as *Attacked* state and the compromised state, which is consistent with the actual observations.

Figure 4 is the security state evaluation result when system status dwell time is in logarithmic distribution, which gives a high risk evaluation for network security state. For example, the attack process is intermittent, and hackers do not continuously attack throughout the whole period, but detect, rest and then find security vulnerabilities to infiltrate again. Its evaluation result is more pessimistic than actual security situations.

From above analysis, we believe that the security state evaluation result is more objective when system status dwell time is in Poisson distribution, and it is more consistent with actual results.

5 Conclusion

In this paper we use hidden semi-Markov model to simulate the actual network system operation, take network defense system captured alarm data as source data, and modeling with HsMM to assess network security situation. Because the actual observation data collected in the same status may occur irregular dwell, and it cannot be accurately described by HMM model. HsMM modifies HMM model presumption that system dwell time in certain status complies with exponential distribution, which is more suitable to describe the actual situation of network system operation. With the different probability distribution of system dwell time, we select and test logarithmic distribution, negative binomial, geometric distribution and Poisson distribution, among which the security evaluation result of system status time in Poisson distribution reflects the actual situation of network attracts, hackers detect before attacking, then attempt to attack again after a period of truce, at last the system is broken with the continuous attacks, the experiment result is consistent with observations. In the mean while, it combines HsMM forward-backward algorithm and proposes HsMM system status prediction algorithm under partial observation conditions, then applies it to Honeynet network security situation assessment and get favorable evaluation effects. Experiment results show that HsMM can model for system status dwell time, and it is very suitable for network system security evaluation with complicated and changeable attacks.

Acknowledgments. This work was partially supported by the National Natural Science Foundation of China under Grant No.60973153, the Application of

Innovation Plan Fund of the Ministry of Public Security under grand No. 2007YYCXHNST072, the Postdoctoral Science Foundation of Central South University, the Hunan Postdoctoral Scientific Program under Grant No. 2009RS3037 and the Science and Technology Planning Project of Hunan Province, China.

References

1. Bass, T., Roger, R.: Defense-in-Depth Revisited: Qualitative Risk Analysis Methodology for Complex Network-Centric Operations. In: Proceedings of IEEE Military Communications Conference, vol. 1, pp. 64–70 (2001)
2. Huang, X.D.: Phoneme Classification Using Semicontinuous Hidden Markov Models. *IEEE Trans. SP* 40(5), 1062–1067 (1992)
3. Yu, S.Z.: Hidden semi-Markov models. *Artificial Intelligence* 174, 215–243 (2010)
4. Yao, T.R.: Digital Signal Processing, pp. 316–346. Huazhong University of Science and Technology Press, Wuhan (1991)
5. Johnson, M.T.: Capacity and Complexity of HMM Duration Modeling Techniques. *IEEE Signal Processing Letters* 12(5), 407–410 (2005)
6. Project H.Scan 17 (2002), <http://www.honeynet.org/scans/scan17>

Network Security Situation Assessment Based on Stochastic Game Model

Boyun Zhang^{1,2}, Zhigang Chen², Wensheng Tang⁴, Qiang Fan¹,
Xiai Yan¹, and Shulin Wang³

¹ Department of Computer Science and Technology, Hunan Police Academy,
Changsha, Hunan 410138, China
hnjxzby@yahoo.com.cn

² School of Information Science and Engineering, Central South University,
Changsha, Hunan 410086, China

³ School of Computer and Communication, Hunan University, Changsha, 410082, China

⁴ Department of Computer Teaching, Hunan Normal University, Changsha, 410081, China

Abstract. From the perspective of game theory, this paper studies the information security problem, establishes an offense and defense game model of information security, and puts forward a quantitative evaluation algorithm of network security based on stochastic game model. It makes use of the network administrator's evaluation of network equipment's importance to determine the game parameters, analyze Nash equilibrium and work out Nash strategy of the attacker and the defender so as to obtain the probability distribution when network is in different secure states and finally get the evaluation results of network security situation through quantitative analysis. The game model of the attacker and the defender put forward in this paper provides a new idea for solving information security problem in reality.

Keywords: network security, network security situation assessment, stochastic game theory, risk evaluation.

1 Introduction

The essence of offense and defense in information security can be abstracted as the strategy dependency of the attacker and the defender. Whether the defensive strategy adopted by the defender is valid or not should not only depend on his own behavior but also depend on the strategies adopted by the attacker and defense system. Therefore the game theory can be used to study the offense and defense contradiction and the optimal defense decision and other information security offense and defense challenges[1]. Samuel N Hamilton points out[2] that the game theory will play a key role in network offense and defense field, and it is a quite promising research field for information security in the future.

In 1997, Syverson P. E [3] put forward an idea that dynamic game should be used to rationally analyze normal nodes and malicious nodes in network. LyeKong-wei et al[4] regarded the attacker and the defender as the two players in a non-zero-sum dynamic game, and calculated the optimal response strategy of both sides. Sun Wei

et al[5] studies the offense and defense problem of information security with the use of evolutionary game theory, establishes the game model of information security offense and defense, and analyzes the replication dynamic and evolutionary stable strategy of the attacker and the defender. These studies all regard information security problem as the dynamic game between the attacker and the defender, and study it respectively from the perspectives of strategies and interaction between the attacker and the defender.

From the perspective of game theory, this paper studies the information security problem, establishes an offense and defense game model of information security, and puts forward a quantitative evaluation algorithm of network security based on stochastic game model.

2 Offense and Defense Game Model

In 1950 and 1951, John Nash published two important articles about non-cooperative game[6] [7], which defined non-cooperative game and its equilibrium solution in a very general sense, and proved the existence of the equilibrium solution. It basically laid the foundation of modern non-cooperative game theory. The basic terms of game theory include: participant, action, strategy, information, and payoff function (payoff), result and equilibrium[8]. Among these terms, participant, strategy and payoff function are the most basic elements needed to describe a game. Nash equilibrium is a strategy combination composed of the optimal strategies of all the participants. In this strategy combination, the strategies of other participants are given, no single participant has positivity to choose other strategies, and nobody will take the initiative to break the equilibrium: this is the philosophy of Nash equilibrium.

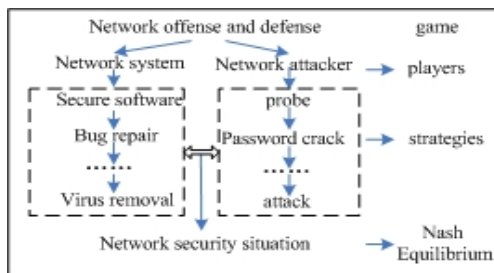


Fig. 1. Offense and defense game model of network security

Offense and defense game model of information security refers to the process that describes how the attacker and the defender start the game by controlling the related offense and defense technologies and management. What they game is the vulnerability of information systems. The mutual influence and interaction between the strategies of the attacker and the defender is the basic hypothesis of the offense and defense model. According to the above game process between the attacker and the defender, the offense and defense game model of information security is to be built as shown in Figure 1. The offense and defense process is the game process

between the attacker and the defender. For the attacker, regardless of what protection strategies the defender adopts, he always wants to adopt a suitable strategy to achieve the goal of attacking; meanwhile, the defender is always looking for a suitable strategy to protect against the attacker.

3 The Evaluation System Framework

According to the need for network security quantitative evaluation, we establish the stochastic game model of network security. Based on the follow hypotheses, then we introduce the stochastic game theory.

Hypothesis 1: Both of the network administrator and attacker know the overall information of the network, including network topology, network bugs existing on each host and so on.

Hypothesis 2: The network administrator will evaluate the importance of his own network equipment, and it is expressed as $\tilde{I} = (i_1, i_2, \dots, i_n)$, in which n is the number of network equipment; $i_j \in (0, 1)$ and $\sum_{j=1}^n i_j = 1$.

Hypothesis 3: Scoring of all equipment on the network forms a vector $\tilde{V} = (v_1, \dots, v_n)$, in which n is the number of network equipment. The attacker with permission may cause damage to the network; the network administrator can modify the score based on the severity of destruction of the network.

Hypothesis 4: State i 's network risk score V_i is the inner product of the importance vector \tilde{I} of network equipment and the score vector of network equipment in this state: $V_i = \tilde{V}_i \cdot \tilde{I}$.

Hypothesis 5: Both of the network administrator and attacker are rational. The former's goal is to avoid the reduction of the security score V of the entire network, while the latter's goal is to reduce the security score V of the entire network.

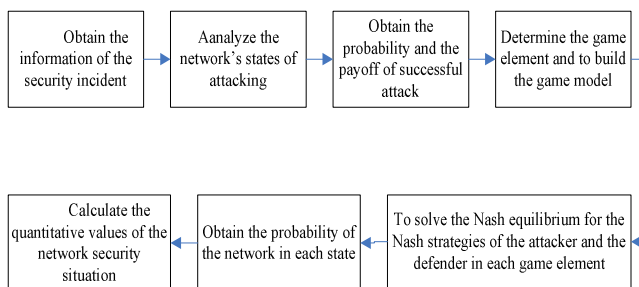


Fig. 2. The evaluation process of the network security situation

The network administrator and the attacker being considered as the two players in the stochastic game model, the network administrator's goal is to protect the network from being attacked, while the attacker hopes to achieve his purpose of attacking at a small cost. The process during which the network administrator resists attacks from

the attacker being regarded as the process of stochastic games, this game process is composed of multiple stage games[9], and each stage game with adoptable action set and payoff function corresponds to a network state. Through the exploitable bugs existing in the network, we can generate the action set of the network administrator and the attacker and calculate scores of all possible states of the network, using Nash equilibrium to compute the expected behaviors of both sides for the probability of the network in each state, so as to analyze the synthetical evaluation results of the entire network.

The entire situation evaluation process is shown in Figure 2, and is described in details as follows:

(1) *The information extraction* The network information needed to be used includes: the network topology, the type of each host in the network, bugs existing on each host in the network, the operating system and software of each host, a list of disabled ports,etc. Such information can be obtained through the relevant security tool software.

(2) *To establish the attack database* The attack template stands for the attacker's meta attack in the process of attack.

(3) *The process of the stochastic game of the network security* According to the results of the previous two steps, we match the states of each host to the conditions in the attack template library so as to obtain the network's possible states of being attacked, among which the state of possibly being continued to be attacked is the stage game in the stochastic game called as game elements[10].Under the attack template library and the host's state in the network, we find out the action set of these game elements, and then calculate the payoff of these actions and the transition probabilities between game elements by the probability of the successful attack q_{ij}^{kl} .

If the attacker's attack action is discovered by the administrator or the attacker chooses to give up the attack, then the game comes to the end. By solving the Nash equilibrium in the entire process of the stochastic game, we obtain the Nash strategies of the attacker and the defender in each game element.

(4) *To calculate the integrated score* of the network security situation after obtaining the Nash strategy of the attacker and the defender, we can obtain the probability of the network in each state in conjunction with the transition probability between the game elements.

If the network is in state k , and the attacker adopts the attack action i and succeeds, then the system is in state l , and if the Nash strategies of the attacker and the administrator are respectively $(x_1, x_2, \dots, x_{m_k}), (y_1, y_2)$, then the probability Q^{kl} of the system's successfully converting to the state l is:

$$Q^{kl} = q_{ij}^{kl} \times x_i \times y_2 \quad (1)$$

The probability P_l of the system's being in the state l :

$$P_l = P_k \times Q^{kl} \quad (2)$$

According to the score of each state of the network and the importance vector of the network equipment, we can calculate the score V_i (i stands for the state the network is in) of each state of the network. If n is the number of all states of being possibly

attacked of the network, then we can calculate out the quantitative evaluation result V of the integrated security situation of the entire network:

$$V = \sum_{i=1}^n P_i V_i \quad (3)$$

4 Experiments and Discussion

We use HoneyNet data set[11] to do experiments in order to find the trend and the law of the security situation. Taking the data of November 2000 as an example, we evaluate the security threat situation and analyze the evolution of the security threat state of the network service level within one month.

The network security situation in the each element is described as follows:

1) *The security state of the system* Provided that there are three categories of network services are running in the network, then the state of the network equipment at the time t can be expressed as $S_t = \{S_{ftp}, S_{rpc}, S_{www}, S_{attacker}\}$, if $X \in \{ftp, www, rpc\}$, then $S_x = \{\text{normal, probed, attacked, compromised}\}$, which stands for the state value of each network service. For consistency, the state of the attacking side will also be included and is expressed as: $S_{attacker} = \{\text{detect, undetected}\}$.

2) *The action set of the attacker and the defender*. In allusion to different network services, the action set of the attacking side will be various. For simplicity, we uniformly express it as: $A^1 = \{\text{attack } i^{\text{th}} \text{ service}, \emptyset\}$, in which, i stands for the type i network service, namely, referring to ftp, www and rpc, and \emptyset stands for not attacking temporarily.

The action plans of the defending side are: service network restart, virus killing, security patch installation and suspicious accounts remove and so on. Of course, the number of the action set of the attacker and the defender is large, for simplicity, we will only simplify it into two actions as preventing the attacks and not taking any measures, and it is expressed as: $A^2 = \{\text{Defend}, \emptyset\}$.

3) *The transition probability of the security state*. According to experts' advice or the network security administrators' experience, we can determine it. For example, the probability of from being attacked to being breached of the RPC service in the network can be defined as 0.5 and is expressed as: $\Pr(RPC_attacked | RPC_compromised) = 0.5$. In order to reduce the impact of human factors on the experimental results, we can obtain the distribution matrix of the state transition probability by training the HMM model.

The parameters in the experiment list follow:

The importance of the network service is $\tilde{I} = \{ftp, www, rpc\} = \{45, 60, 90\}$; The score of the network service state $\tilde{V}_i = (v_{ftp}, v_{www}, v_{rpc})$ are: $\tilde{V}_{Normal} = \{1.0, 1.0, 1.0\}$, $\tilde{V}_{Probed} = \{0.6, 0.6, 0.6\}$, $\tilde{V}_{Attacked} = \{0.4, 0.4, 0.4\}$, $\tilde{V}_{Compromised} = \{0.2, 0.2, 0.2\}$.

Taking the network services of ftp, www and rpc supplied by the host 172.16.1.107 as an example, we carry out the test. Taking the data at 22:00 on November 30 for an

example, we, through analysis, can draw out the transition graph of the security state shown in Figure 3. The network's states of being attacked continuously in the graph are ②, ⑤, ⑥, and these three states correspond to the action set score of the attacker corresponding to game elements Γ_1 , Γ_2 , Γ_3 . The attacker's action sets are $\{attack_{www}, attack_{rpc}, attack_{ftp}, \emptyset\}$, and the administrator's action sets in each state are $\{\emptyset, \text{defend}\}$.

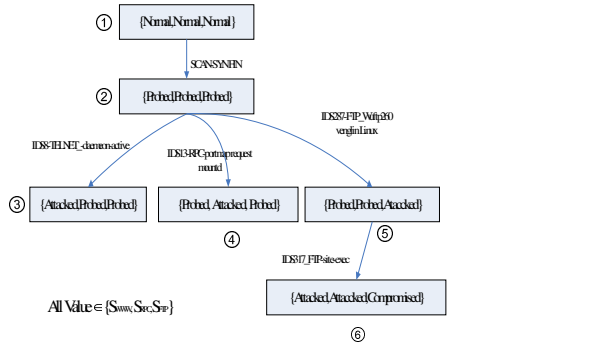


Fig. 3. The transition graph of the network security state of HoneyNet data set

According the stochastic game theory, we can obtain game elements Γ_1 , Γ_2 , Γ_3 , and under the state to which game elements Γ_1 , Γ_2 , Γ_3 correspond, the attacker's Nash strategy and the administrator's can be obtained by simultaneous equations. The results are shown in Table 1. At the same time, we can calculate out the Nash equilibrium of the attacker and the defender of November and the payoff of both sides, and the results are shown in Figure 4.

Table 1. The Nash equilibrium of the attacker and the defender

state of the system	strategy of the attacker	strategy of the defender	payoff of the attacker	payoff of the defender
WWW_normal	0.00, 0.00, 0.00, 1.00	0.00, 1.00	76.90	-76.90
WWW_attacked	0.25, 0.40, 0.30, 0.05	0.35, 0.65	77.98	-77.98
WWW_compromised	0.28, 0.68, 0.10, 0.04	0.20, 0.50	73.45	-73.45
RPC_normal	0.00, 0.00, 0.00, 1.00	0.00, 1.00	73.70	-73.70
RPC_attacked	0.20, 0.20, 0.50, 0.10	0.20, 0.80	77.32	-77.32
RPC_compromised	0.15, 0.15, 0.60, 0.01	0.50, 0.50	80.06	-80.06
FTP_normal	0.00, 0.00, 0.00, 1.00	0.00, 1.00	73.07	-73.07
FTP_attacked	0.5, 0.25, 0.25, 0.00	0.60, 0.40	73.87	-73.87
FTP_compromised	0.65, 0.15, 0.15, 0.05	0.50, 0.50	76.41	-76.41

Meanwhile, according to formula (1) and (2), we can calculate out the probability distribution value of the network in each state, and through formula (3), we can obtain

the quantitative value of the entire network's security situation. We have respectively calculated out the security situation value of the three categories of services—ftp, www and rpc on the host 172.16.1.107 in November, for ease of comparison, the calculation result values are normalized, and the results are respectively shown in Figure 5 - Figure 7.

1) The rpc service opened in the system is frequently attacked, which indicates that there may be many bugs or bugs easily to be breached in the rpc service, and the set of this service is worth inspecting by the administrator;

2) The attack power which Services of ftp and www are exposed to is small, which indicates that security bugs of them are less and the security is high; or the attacker's objectives are not here;

3) November 3 - 4, November 6 - 7, November 10 -13 and November 19 -22, 2000 are periods of time during which services are intensively attacked, and these periods are around the weekend. This aspect shows that the weekend, compared to ordinary times, is the period during which services are more easily to be attacked by hackers, and needs more cares and precautions.

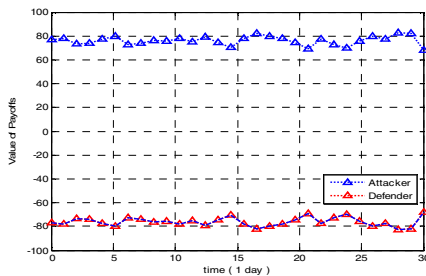


Fig. 4. Chart of the comparison of the attacker and the defender's payoff

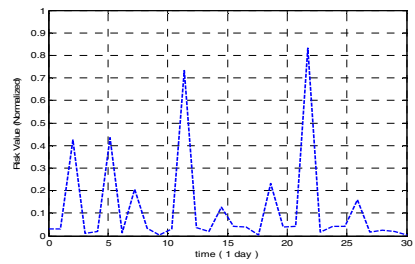


Fig. 5. The security situation graph of the RPC service of the host 172.16.1.107

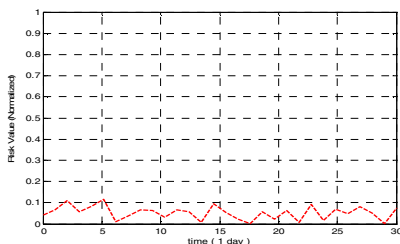


Fig. 6. The security situation graph of the www service of the host 172.16.1.107

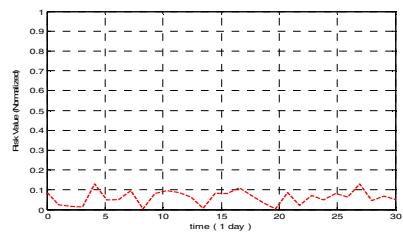


Fig. 7. The security situation graph of the FTP service of the host 172.16.1.107

5 Conclusion

From the standpoint of game theory, information security is in fact a game between the information protector and the intruder. From the perspective of game theory, this paper studies the information security problem, establishes an offense and defense game model of information security, and puts forward a quantitative evaluation algorithm of network security based on stochastic game model. It makes use of the network administrator's evaluation of network equipment's importance to determine the game parameters, analyze Nash equilibrium and work out Nash strategy of the attacker and the defender so as to obtain the probability distribution when network is in different secure states and finally get the evaluation results of network security situation through quantitative analysis.

Although the use of game theory has shown a great advantage in the network security situation evaluation, there are still some problems. For example, one of the biggest flaws is that we assume that the attacker is rational and they determine their own behaviors based only on acquired compensation and cost. We also assume that the attacker and the defender always have a very comprehensive understanding of the game stage which has been completed, which is not easy to achieve in reality. In addition, there is certain subjectivity from the aspect of the setting of related parameters. It is hoped that related parameters can be set more objectively and definitely through the study of the actual data set in the future.

Acknowledgments. This work was partially supported by the National Natural Science Foundation of China under Grant No.60973153, the Application of Innovation Plan Fund of the Ministry of Public Security under grant No. 2007YYCXHNST072, the Postdoctoral Science Foundation of Central South University, the Hunan Postdoctoral Scientific Program under Grant No. 2009RS3037 and the Science and Technology Planning Project of Hunan Province,China.

References

1. Jiang, W., Fang, B.X., Tian, H.Z.: Evaluating Network Security and Optimal Active Defense Based on Offense and Defense Game Model. Chinese Journal of Computers 4, 817–826 (2009)
2. Hamilton, S.N., Miler, W.L., OttA, A.: The Role of Game Theory in Information Warfare. In: Proceedings of 4th Information Survivability Workshop, Vancouver, Canada, pp. 45–46. IEEE Computer Society Press, Washington, DC, USA (2002)
3. Syverson, P.E.: A different Look at Secure Distributed Computation. In: Proceedings of the 1997 IEEE Computer Security Foundations Workshop, vol. I3(2), pp. 109–115. Computer Society, Washington (1997)
4. Lye, K.W., Jeannette, M.W.: Game strategies in network security. International Journal of Information Security 4(1-2), 71–86 (2005)
5. Sun, W., Kong, X.W., He, D.Q.: Study of Information Security Offense and Defense Problem Based on Evolutionary Game Theory. Information Science 9, 1408–1412 (2008)
6. Nash, J.F.: Equilibrium Points in N-Person Games. Proceedings of the National Academy of Sciences of the United States of America 36, 48–49 (1950)

7. Nash, J.F.: Non-Cooperative Games. *Annals of Mathematics* 54, 286–295 (1951)
8. Xie, S.Y.: Economic Game Theory, 2nd edn., pp. 20–41. Fudan University Press, Shanghai (2002)
9. Harold, W.K.: Classics in Game Theory. China Renmin University Press, Beijing (2002)
10. Owen, G.: Game Theory. Academic Press, London (1982)
11. Project Honeynet. Scan 17 (2002), <http://www.honeynet.org/scans/scan17/>

High Precision Detection of Infrared Energy Spectrum

Xueguang Zhu

The Institute of Mechanical & Electrical Engineering of Anhui Institute of Architecture & Industry, Hefei, Anhui, China
Zhuxg_00@126.com

Abstract. Infrared energy spectrum has unique absorption properties for different gas. The complexity of the gas molecules determines the number of absorption peaks. The amount of absorption and the specific character of the absorption curve are unique to each gas. That the infrared absorption is different between carbon isotope's oxides can be used for medical treatment, provided detection precision is high enough. In order to implement high precision, refer measurement cell is introduced in this paper, which is in swing way periodically switched with the main measurement sample cell to come true channel consistency, and the modulation frequency is selected by the maximum detection rate of the detector.

Keywords: infrared energy spectrum, carbon isotope, unique absorption selectivity, high precision detection.

1 Introduction

Infrared (IR) gas detection is a well-developed measurement technology. The main advantage of infrared instruments is that the detector does not directly interact with the gas to be detected. The major functional components of the analyzer are protected with optical parts. Gas molecules interact only with a light beam. The infrared sensor itself is directly exposed to the gas, often causing the sensor to drift. In the old days, infrared gas analyzers have a reputation for being complicated, cumbersome, and expensive, for poor element performance and limited technology means. However, recent technical advancements, including the availability of powerful amplifiers and associated electronic components, have opened a new frontier for infrared gas analysis.

The mechanism of IR detection is directly or indirectly transforming electromagnetic waves' energy into electric signal. Here we are only interested in 2~6 microns wavelength. The more atoms that form a molecule have the more absorption bands that will occur. Unique gas absorption "fingerprints" is determined by the molecule structure. The structure of the gas molecules determines the number of absorption peaks. The region and the amount of absorption are unique to each gas, so gas molecules can be fingerprinted. For instance methane gas has a strong absorption peak at 3.4 microns, while carbon dioxide has a peak at 4.26 microns, as a matter of

fact, for isotope ^{13}C there is a slight difference. In gas monitoring applications, only one specific absorption region is used to quantitatively determine the gas concentration.

The IR energy spectrum detection technology is applied into medical treatment[1,8], which traces back to 1983. That year an Australia doctor discovered a kind of gastricism which is caused by a germina called Hp. This stomach illness infects among crowds in an easy way. A great number of medical researches indicate that the main reason of infecting gastricism is by Hp. In 1994, Hp is listed into the first causing cancer gene by international sanitation organization. Presently the methods to diagnose Hp are stomach mirror and ^{13}C marker. The stomach mirror method brings a great affliction to the detected, so it is hard to be accepted widely. On the contrary, the latter which is detected by ^{13}C marker expiration examination, and doesn't need invasion, is generally welcomed. ^{13}C marker is safe, and has no radiativity. It is recognized authority detection method. How does it work? Let the detected take medicine, a kind of carbamide which is made from ^{13}C . If his stomach really has Hp, then the Hp will decompose the carbamide into Carbon dioxide and others. Whether does the carbon dioxide breathed out by a certain detected consist of a definite concentration ^{13}C oxide? If has, he probably has Hp. By this mean, the accurate diagnosis is achieved. Now the key problem is how to upgrade the detection precision of infrared energy spectrum. Due to extremely low ^{13}C concentration, if detection accuracy is not very high, it is hard to ensure right diagnosis rate.

For the purpose to attain high accuracy, Refer measurement cell is introduced in this paper, which is in swing way periodically switched with the main measurement sample cell to come true channel consistency, and the modulation frequency is selected by the maximum detection rate of the detector. Therefore detection precision is obviously improved.

2 The System Structure

The main implement graph in fig.1, and it includes chopper motor, swing motor, reflection mirrors, IR filter, IR source, Infrared detectors, reference cell and sample cell, air pumps, power unit, temperature control unit, advanced micro process unit (MPU), and so on. Each part is combined organically together by the MPU which is the control centre.

IR source needs a regular incandescent light bulb. Of course it depends on the type of detector used. The bulb radiates sufficient energy in the 3~5 micron range for the detection of carbon dioxide. The detector's sensitivity is limited, so the larger the light bulb's power the better. However, too large power will bring trouble to temperature control unit, so the bulb type should be carefully selected.

Two reflection mirrors are used on both sides to upgrade detection sensitivity and to focus the light energy to the detectors.

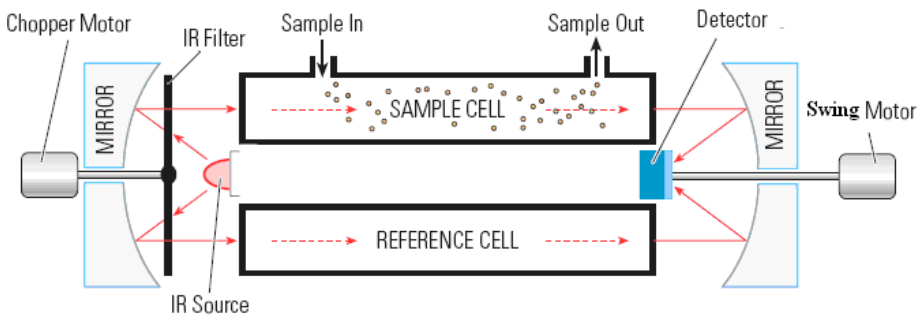


Fig. 1. Infrared energy spectrum detection system plot

The measurement process needs about one minute. First wipe out the remainder gas in sample cell, after that, open input gas valve. The gas from the bag is certainly dried by desiccant having been put inside the tube, next it comes into the sample cell. The gas flow is driven by air pump. The reference cell has changeless carbon dioxide concentration with fixed proportion between ^{12}C and ^{13}C .

The motors adopt step motors, for it is easy to control accurately and to implement synchronization between step motors. The detecting process requires the MPU of controlling the modulation frequency in order to improve signal to noise ratio (SNR).

3 Technical Measures

Whether is the infrared energy spectrum technology for ^{13}C marker able to apply to medical treatment? It greatly depends on measurement means in addition to advanced electronic components.

At first, it may be necessary to modulate the light source according to maximum detection rate from (12) for high signal to noise ratio (SNR). When the modulation disk is rotating, equivalently the infrared light is turning on and off at a specific frequency. The modulation frequency depends on rotation speed, so the rotation speed is determined by maximum SNR.

Secondly refer measurement cell is in swing way periodically switched with the main measurement sample cell, to come true channel consistency, so precision is obviously improved. The choppers are synchronously driven. In addition the phase can be changed as in phase or out of phase. The aim is also to ensure the detecting channel consistency.

Thirdly the IR filter in Fig.2 is installed on the chopper. Bandwidth determines the selectivity of the filter. Center wavelength determines the gas that will be detected. The filters with different central wavelengths are mounted in a symmetric arrangement. By exposing the gas mixture to a filter window, the corresponding central wavelength infrared light will pass through to sense the absorptivity so as to deduce the gas concentration. From Fig.2, we can see that there are four different central wavelengths. The resolution factor of IR detection equipment depends on the filter selectivity. The

peaks of ^{12}C and ^{13}C carbon dioxide are extremely near. Carbon dioxide ^{12}C is absorbed strongly at 4.26 microns, while carbon dioxide ^{13}C absorbs strongly at 4.412 microns. The filter windows must be very narrow, and the spectrum outside the window should be suppressed as much as possible.

At last, the detectors' selection and consistency are fatal. The discreet filtration for the detectors is a must. The same type has slight different performance between two elements. The slight difference makes channel inconsistency, possibly gives rise to large error. After filtration channel consistency is easy to be ensured.

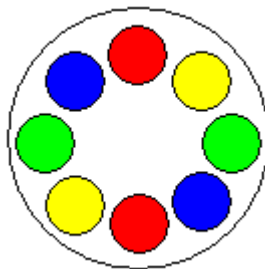


Fig. 2. Modulation disk also for infrared filter

4 Infrared Detection Principle

We adopt thermoelectric infrared detector for the consideration of cost and property. In infrared detection domain, the normalized detector rate^[7-8] is defined as

$$D^* = \frac{(A \cdot \Delta f)^{1/2}}{P_N} \quad (1)$$

Where A is the detector's area, Δf is detector signal process channel bandwidth, and P_N is noise effective power. For the thermoelectric infrared detector, thermal resistor' temperature goes up after being radiated by infrared light, and we have

$$H \frac{d(\Delta T)}{dt} + K' \Delta T = \alpha P \quad (2)$$

in which, H is the thermal capacity of thermal resistor, α is the absorptivity of the detector's surface to the eradiation, and P is incidence power, ΔT is temperature varying, the K' is

$$K' = K - K_0(T_0 - T_a)\eta \frac{R_L - R}{R_L + R} \quad (3)$$

Where η is resistance temperature factor, R is semi-conductor thermal resistor, R_L is load resistor, T_a is environment temperature, T_0 is sensor operation temperature. When incidence power P is indicated as a time-varying complex variable

$$P = P_0 \exp(j\omega t) \quad (4)$$

Then the temperature varying is the function of time

$$\Delta T = \Delta T_0 \exp\left(-\frac{K'}{H} t\right) + \frac{\alpha P_0}{K' + j\omega H} \exp(j\omega t) \quad (5)$$

Suppose $H/K'=0.5\text{ms}$, $\Delta T=10^0\text{C}$, $\alpha P_0/K'=5^0\text{C}$, the temporary component of temperature change shown in Fig. 3 is the solid line, and the steady part is dashed line. The signal voltage amplitude is

$$|U_s| = \frac{\eta I R R_L \alpha P_0}{(R + R_L)(K'^2 + \omega^2 H^2)^{1/2}} \quad (6)$$

The voltage response of the thermal resistor is defined as

$$\mathfrak{R} = \frac{|U_s|}{P_0} = \frac{\eta I R R_L \alpha}{(R + R_L)(K'^2 + \omega^2 H^2)^{1/2}} \quad (7)$$

When $R_L \gg R$ and let $\tau = \frac{H}{K'}$, one obtains

$$\mathfrak{R} = \frac{\eta I R^{1/2} K_0^{1/2} (T_0 - T_a)^{1/2}}{K'(1 + \omega^2 \tau^2)^{1/2}} \quad (8)$$

The thermo-noise voltage mean square value is

$$\bar{U}_{n,t}^2 = 4kT_0 R \Delta f \quad (9)$$

That of current noise

$$\bar{U}_{n,f}^2 = \frac{CI^\alpha R \Delta f}{l A f^\beta} \quad (10)$$

That of temperature noise

$$\bar{U}_{n,T}^2 = 4kT_0^2 G \left(\frac{\mathfrak{R}}{\alpha} \right)^2 \Delta f \quad (11)$$

Generally, temperature noise is very small, when modulation frequency is high enough, the normalized detector rate is

$$D^* = \frac{\eta A_0^{1/2} \kappa_0^{1/2} (T_0 - T_a)^{1/2}}{(4kT_0)^{1/2} (K'^2 + \omega^2 H^2)^{1/2}} \quad (12)$$

A_0 is detector effective area, κ_0 is substrate thermo-conductivity. We select the modulation frequency from (12), to get maximum SNR. The temperature control circuit[6] is also very important, and we get a constant environment temperature by temperature controlling unit. We suppose that $\beta=1.5$, and when current noise equals thermo-noise, the operation frequency is 1.5kHz, the normalized detector rate is shown

as in Fig. 4. In this case, the modulation frequency should be selected near and less than 500Hz, the SNR reaches maximum.

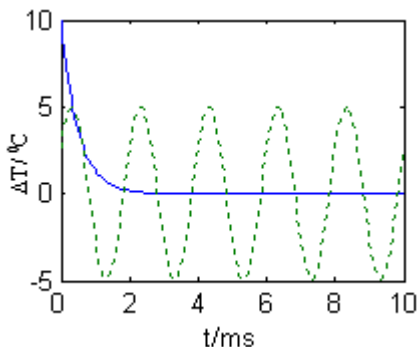


Fig. 3. Temperature evolvement characteristics

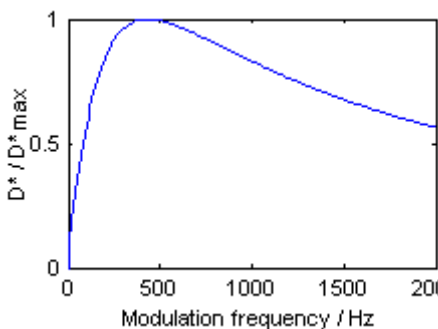


Fig. 4. Normalized detector rate frequency characteristics

5 Conclusion

Carbon isotope marker technology can be used for medical treatment by means of high accuracy and excellent detectivity of infrared energy spectrum, for IR spectrum has unique absorption properties for different gas. The new technology in swing way periodically switched for the measurement is adopted in this paper to ensure the channel consistency so as to implement high accuracy.

References

- [1] McManna, N.: Camera Detects Faulty Cells. *Photonics Spectra* 11, 123 (1999)
- [2] Staff, R.: Anthropological Information. *Photonics Spectra* 9, 91–98 (1998)
- [3] Hand, A.J.: Photonics Analyze Food Quickly, Effectively. *Photonics Spectra* 10, 114–119 (1998)
- [4] Han, T., Zhu, X.G.: Synthetic Interference to Infrared Imaging Missile. *Spaceflight Electronic Countermeasure in Chinese* 5, 26 (2002)
- [5] Hallader, M.: Research into Coil Systems Advances Remediation of Nuclear Reactors. *Society of Photo-Optical Engineering* 1, 1–6, 23–29 (1999)
- [6] Robinson, K.: Photodynamic Therapy Offers New Medical Treatments. *Photonics Spectra* 5, 219 (1998)
- [7] Appel, D.: Laser Application in DNA Analysis. *Laser Focus World* 4, 46 (1998)
- [8] Kincade, K.: Raman Spectroscopy Enhances in Vivo Diagnosis. *Laser Focus World* 7, 83 (1998)

Using Heart Rate Variability Parameter-Based Feature Transformation Algorithm for Driving Stress Recognition

Jeen-Shing Wang¹, Che-Wei Lin¹, and Ya-Ting C. Yang²

¹ Department of Electrical Engineering,

² Institute of Education & Center for Teacher Education,

National Cheng Kung University

Tainan 701, Taiwan, R.O.C.

jeenshin@mail.ncku.edu.tw

Abstract. This paper presents a heart rate variability (HRV) parameter-based feature transformation algorithm for driving stress recognition. The proposed parameter-based transformation algorithm consists of feature generation, feature selection, and feature dimension reduction. In order to generate significant features from ECG signals, parameter-based feature generation method is proposed in this study. The parameter-based method calculates features from five-minute HRV analysis. The kernel-based class separability (KBCS) is employed as the selection criterion for feature selection. To reduce computational load of the algorithm, principal component analysis (PCA) and linear discriminant analysis (LDA) are adopted for feature dimension reduction. Our experimental results show that the combination of KBCS, LDA, and PCA can achieve satisfactory recognition rates for the features generated by parameter-based feature generation method. The main contribution of this study is that our proposed approach can use only ECG signals to effectively recognize driving stress conditions with very good recognition performance.

Keywords: Heart rate variability, driving stress, k-nearest neighbor algorithm.

1 Introduction

Physiological signal analysis has been validated as an effective method for recognizing physiological conditions of a person [1]. Among diverse physiological signals, heart rate variability (HRV) analysis based on electrocardiogram (ECG) is a noninvasive and effective technique to reflect the autonomic nervous system (ANS) regulation of the heart [2]. In general, HRV analysis includes time-domain analysis, frequency-domain analysis, and nonlinear-domain analysis. Various parameters or indices extracted from time, frequency, or nonlinear analyses can be used to represent the functions or conditions of the cardiovascular and autonomic nervous systems [2]. Because of the associations between HRV parameters and ANS, many researchers have employed HRV parameters for monitoring variations or conditions in various problem domains such as: 1) ANS function evaluation of chronic diseases with different severity levels [3], 2) physiological conditions recognition such as stress, depression and emotion

recognition [4]. Recently, many research papers have focused on detecting stress level through biosignals [5, 6]. Setz *et al.* focused on electrodermal activity (EDA) for detecting stress stimulus from cognitive load. Several classifiers were evaluated, and one of them achieved the stress recognition accuracy of 82.8% [5]. Healey and Picard conducted a comprehensive research for detecting various driving stress (low, medium, and high driving stress). Physiological signals including ECG, electromyogram (EMG), EDA, and respiration were collected. With the aid of a Fisher projection and a linear discriminant, they achieved the recognition accuracy of 97% [6].

From a review of literature, we found that there are still two main problems in using physiological signals for stress condition detection. The first problem is the numbers of sensors for collecting different physiological signals. In real-world applications, it's difficult if not impossible to wear different kinds of sensors simultaneously. The other one is the effectiveness of detection for a single sensor. Since the effectiveness of HRV obtained from ECG has been validated for diverse physiological conditions by many research papers, to develop an efficient driving stress recognition strategy with HRV parameters would be a worthwhile research topic for further investigation. In this paper, we develop a k -nearest neighbor classifier with a HRV-based feature transformation algorithm to distinguish physiological conditions under the following three situations: rest before driving (low stress), rest after driving (low stress), and during driving (medium/high stress).

The rest of this paper is organized as follows. The detailed description of HRV parameter-based feature transformation algorithm for driving stress recognition, including the proposed parameter-based feature generation method, feature selection, and feature dimension reduction are introduced in Section 2. The simulation results are presented in Section 3. Finally, conclusions are presented in the last section.

2 HRV Parameter-Based Feature Transformation Algorithm

Before introducing the proposed HRV parameter-based feature transformation algorithm, we will present the driving conditions with different driving stress level that we want to recognize, and the idea of our recognition strategy. The ECG signals used in the study were downloaded from the MIT Media Lab [7]. The measured signals include three different driving conditions: the periods of 1) rest before driving (low stress) (15 minutes), 2) rest after driving (low stress) (15 minutes), and 3) during driving (medium/high stress) (20~60 minutes). In [6], the driving conditions are categorized into low, medium, and high driving stress. However, due to insufficient labels of the measured signals, we combine the medium and high stress levels into one group denoted as “medium/high” stress in the period of during driving condition. According to the research finding in [8], the LF band power and the LF/HF ratio increase when a person is under stress. In addition, from our analysis and observation on a large amount of ECG signals from the database, we found that the trend variations of the LF power increases as the driving time increases, while the LF power decreases as the time of rest increases. Therefore, observing the variation on a physiological parameter can obtain significant information for physiological condition detection.

Fig. 1 shows the block diagram of the proposed HRV parameter-based feature transformation algorithm for driving stress recognition. The proposed HRV parameter-based feature transformation algorithm consists of the following procedures: feature generation, feature selection, and feature dimension reduction. In this study, driving stress recognition is based on HRV parameters derived from ECG in a five-minute interval, which is named “parameter-based” feature generation method. The procedures of the proposed HRV parameter-based feature transformation algorithm and the k-NN classifier used for driving stress recognition will be explained in this section.

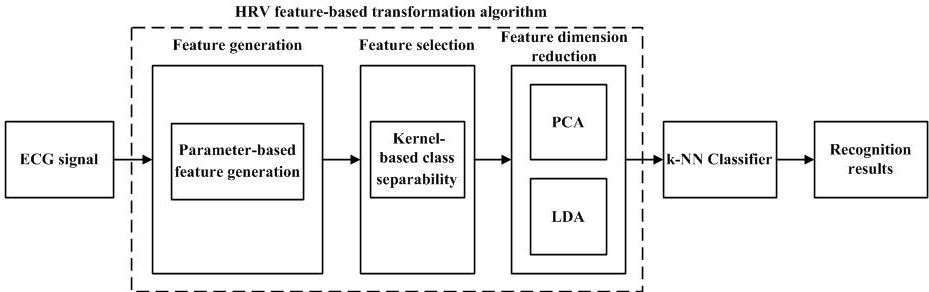


Fig. 1. The block diagram of the proposed HRV parameter-based feature transformation algorithm for driving stress recognition

Feature Generation. In the feature generation process, the first step is to segment ECG signals into a series of five-minute windows with 50% overlap, and then perform the QRS detection algorithm to obtain the RR tachogram for computing the eight HRV parameters of each window. These HRV parameters include: 1) time-domain parameters: SDNN, RMSSD, NN50, pNN50, and 2) frequency-domain parameters: the powers of VLF band, LF band, HF band, and the LF to HF ratio. The detailed procedures of these two steps can be found in our previous work [9]. With the eight HRV parameters, we produce the following sixteen features. The first eight features are composed of the eight HRV parameters minus their respective averages of each five-minute HRV parameter in the 15-minute rest periods occurred at the beginning of the test. The remaining eight features are formed by the eight HRV parameters minus their corresponding HRV parameters in the previous window. Therefore, besides the first window, every five-minute window of the ECG data can be transferred into a 16-dimensional feature vector. Afterward, this process executes two normalization procedures. In the first normalization, all HRV parameters obtained from all time intervals of each subject are normalized to the range of [0, 1] using a max-min normalization. Since a subject may have similar HRV representations in different driving conditions with different driving stress levels, the purpose of the first normalization is to make the feature vectors as separate as possible for the above situation. The second normalization carries out the max-min normalization to all the data samples collected from the subjects. The objective of the second normalization is to eliminate the individual differences.

Feature Selection. A feature selection process intends to pick p features out of the original d features. This process is expected to produce low classification errors when the selected features are used by a classifier. We adopt the feature selection method developed by [10]. The feature selection method comprises a search strategy and a selection criterion. We adopt the best individual N (BIN) as the search strategy. In the BIN, a selection criterion is individually applied to each of the features. The features giving larger criterion values are selected. The adopted selection criterion is the kernel-based class separability (KBCS).

Feature Dimension Reduction. The feature dimension reduction process aims at projecting the p -dimensional feature vector on a t -dimensional subspace. Hence, the combination of the feature selection and feature dimension reduction processes can reduce the feature dimensionality by projecting the original d -dimensional feature space onto a t -dimensional subspace, where $d > t$. Both processes are expected to obtain high between-class separability and low within-class separability. Principal component analysis (PCA) [11] and linear discriminant analysis (LDA) [12] are employed in our feature dimension reduction process.

Classifier for Recognition. Finally, a k -nearest neighbor (k -NN) classifier is used to evaluate the reduced feature vectors for the proposed HRV parameter-based feature generation approach. A k -NN algorithm is one of the low-computation complexity methods for pattern recognition, and the principle of k -NN is based on an intuitive concept that data points of the same class should be closer in the feature space. Given a training dataset of n points with their desired class is specified as $\{(\mathbf{X}_1, \mathbf{y}_1), (\mathbf{X}_2, \mathbf{y}_2), \dots, (\mathbf{X}_n, \mathbf{y}_n)\}$, where $(\mathbf{X}_i, \mathbf{y}_i)$ represents data pair i , \mathbf{X}_i is the feature vector, and \mathbf{y}_i is the corresponding target class. Subsequently, for a new data point \mathbf{x} , the most likely class should be determined by k -NN ($k = 3$ in this study).

3 Experimental Results

The ECG signals downloaded from the MIT Media Lab [17] are used to validate the effectiveness of the proposed HRV parameter-based feature transformation algorithm and the k -NN classifier. Because the proposed parameter-based feature transformation algorithm consists of three procedures: feature generation, feature selection, and feature dimension reduction, different combinations of these procedures may result in different recognition performance. In order to identify an optimal combination of these procedures for the k -NN classifier, we conduct the experiment of using the proposed parameter-based features, feature selection method, and feature extraction method in the recognition of driving stress conditions. KBCS is utilized to select important features from the original feature sets (parameter-based features). In addition, the effect of using PCA and LDA for feature dimension reduction will be evaluated in the experiment. Finally, with the optimal feature transformation combination, cross-validations of 5-fold, 10-fold, and leave-one-out are performed for the training process of the k -NN classifier to achieve the best recognition accuracy.

The number of features generated by the parameter-based feature generation (PBFG) method is 16. The number of features is reduced to 14 after KBCS is applied. Table 1 shows the recognition rates of three combinations of feature transformation methods by a 5-fold cross-validation. From Table 1, we can see that the recognition rate of the feature transformation method with the combination of PBFG, KBCS, LDA, and PCA (denoted as PBFG+KBCS+LDA+PCA) is 81.06% which outperforms those of two other combinations, PBFG+KBCS and PBFG+KBCS+LDA whose recognition rates are the same at accuracy 78.28%. LDA does not provide any improvement in this experiment. Table 2 demonstrates the average recognition rates of the feature transformation method, PBFG+KBCS+LDA+PCA, for 5-fold, 10-fold, and leave-one-out cross-validations. From Table 2, only the method, PBFG+KBCS+LDA+PCA, with leave-one-out cross-validation can achieve a perfect recognition performance. The recognition accuracy by leave-one-out outperforms 5-fold and 10-fold cross-validations. This can be attributed to the amount of training samples because leave-one-out cross-validation only use a single observation from the original samples as the validation data, and the remaining observations as the training data. Hence, the optimal recognition accuracy is obtained by the leave-one-out cross-validation.

Table 1. Average recognition rates of three combinations of feature transformation methods by a 5-fold cross-validation

Methods	PBFG+KBCS	PBFG+KBCS+LD A	PBFG+KBCS+LDA+PC A
Average recognition rate	78.28 %	78.28 %	81.06 %

Table 2. Average recognition rates of PBFG+KBCS+LDA+PCA for 5-fold, 10-fold, and leave-one-out cross-validations

Methods	5-fold cross- validation	10-fold cross- validation	Leave-one-out cross-validation
Average recognition rates	81.06 %	88.28 %	100 %

4 Conclusions

We have developed an effective k -NN classifier with HRV parameter-based feature transformation algorithm for driving stress detection under different conditions. The proposed parameter-based feature transformation algorithm consists of feature generation, feature selection, and feature dimension reduction. In order to generate significant features from ECG signals, parameter-based feature generation method is proposed in this study. The parameter-based feature generation method generates features from the HRV analysis of each five-minute window of the ECG signal. With the features generated by the parameter-based feature generation, feature selection based on KBCS and feature dimension reduction by PCA and LDA are employed to

reduce the feature dimension and select the most important features. A k -NN classifier is then trained for driving stress recognition. According to our experimental results, the optimal combination of feature transformation methods is KBCS+LDA+PCA with leave-one-out cross-validation. Unlike most of research papers employed diverse physiological signals (ECG, EMG, GSR, and respiration) to recognize the driving stress, our proposed approach using only ECG signals can effectively recognize driving stress conditions with very good recognition performance. Our experimental results have successfully validated the effectiveness of the k -NN classifier with the proposed HRV parameter-based feature transformation algorithm. In the future, we will realize the proposed approach in a wearable embedded system for driving fatigue detection.

References

1. Picard, R.W., Vyzas, E., Healey, J.: Toward Machine Emotional Intelligence: Analysis of Affective Physiological State. *IEEE Trans. Pattern Analysis and Machine Intelligence* 23, 1175–1191 (2001)
2. Malik, M., Camm, A.J., Kleiger, R.E., Malliani, A., Moss, A.J., Schwartz, P.J.: Heart rate variability: Standards of Measurement, Physiological Interpretation, and Clinical Use. *European Heart Journal* 17, 354–381 (1996)
3. Kallio, M., Suominen, K., Bianchi, A.M., Makikallio, T., Haapaniemi, T., Astafiev, S., Sotaniemi, K.A., Myllylä, V.V., Tolonen, U.: Comparison of Heart Rate Variability Analysis Methods in Patients with Parkinson's Disease. *Medical and Biological Engineering and Computing* 40, 408–414 (2002)
4. Kim, K.H., Bang, S.W., Kim, S.R.: Emotion Recognition System Using Short-Term Monitoring of Physiological Signals. *Medical and Biological Engineering and Computing* 42, 419–427 (2004)
5. Setz, C., Arnrich, B., Schumm, J., Marca, R.L., Tröster, G., Ehlert, U.: Discriminating Stress from Cognitive Load Using a Wearable EDA Device. *IEEE Trans on Information Technology in Biomedicine* 14, 410–417 (2010)
6. Healey, J.A., Picard, R.W.: Detecting Stress during Real-world Driving Tasks using Physiological Sensors. *IEEE Trans. Intelligent Transportation Systems* 6, 156–166 (2005)
7. PhysioBank,
<http://www.physionet.org/physiobank/database/drivedb/>
8. Castro, M.N., Vigob, D.E., Chu, E.M., Fahrer, R.D., Achával, D., Costanzo, E.Y., Leiguarda, R.C., Noguésa, M., Cardinali, D.P., Guinjoan, S.M.: Heart Rate Variability Response to Mental Arithmetic Stress Is Abnormal in First-degree Relatives of Individuals with Schizophrenia. *Schizophrenia Research* 109, 134–140 (2009)
9. Lin, C.W., Wang, J.S., Chung, P.C.: Mining Physiological Conditions from Heart Rate Variability Analysis. *IEEE Computational Intelligence Magazine* 5, 50–58 (2010)
10. Wang, L.: Feature Selection with Kernel Class Separability. *IEEE Trans. Pattern Analysis and Machine Intelligence* 30, 1534–1546 (2008)
11. Jackson, J.E.: *A User's Guide to Principal Components*. John Wiley and Sons, New York (1991)
12. Martinez, A.M., Kak, A.C.: PCA versus LDA. *IEEE Trans. Pattern Analysis and Machine Intelligence* 23, 228–233 (2001)

An Online Self Gain Tuning Computed Torque Controller for A Five-Bar Manipulator

Tien Dung Le¹, Hee-Jun Kang^{2,*}, and Young-Soo Suh²

¹ Graduate School of Electrical Engineering, University of Ulsan,
680-749, Ulsan, South Korea

ltdung@mail.ulsan.ac.kr

² School of Electrical Engineering, University of Ulsan,
680-749, Ulsan, South Korea
{jkang, yssuh}@ulsan.ac.kr

Abstract. Parallel manipulators have advantages like high accuracy, high stiffness, high payload capability, low moving inertia, and so on. This paper presents the problems of control the five-bar manipulators using computed torque control method. In order to improve the control performance, an online self gain tuning method using neural networks is proposed for gain tuning of computed torque controller. Simulation results show the effectiveness of the proposed method in comparison with the traditional computed torque control method.

Keywords: Five-bar manipulator, Computed torque controller, Online self gain tuning, Neural network.

1 Introduction

The parallel manipulators have potential advantages in terms of stiffness, accuracy and high speed. The parallel manipulators have wide applications such as flight simulators, photonics alignment, pick and place operation. In literature, there are many studies taken up in order to realize the potential performances in motion control of parallel manipulators [1-8]. The conventional Computed Torque Control (here are abbreviated as CTC) law is a linear control method to combine the PD control term and the feedback dynamic compensation term. The CTC method has been proposed in [3-8] for parallel manipulators. One of the disadvantages of the conventional CTC method is that the linear PD with the proportional and derivative constant which is used to reduce tracking errors sometimes can not bring about a satisfied tracking accuracy. This is due to nonlinear factors such as modeling error and friction in the dynamic model of the parallel manipulators. Thus, some new algorithms are used to tune the PD gains in the CTC method. In [9, 10] the intelligent methods are used to optimized the PD gains in computed torque controller. However, it is not easy to carry out these types of controller in practice because of the complicated structure and innumerable calculations.

* Corresponding author.

The main contribution of this paper is proposing a new method for tuning the computed torque gains using neural networks. Compared with other tuning methods, the proposed method in our paper has simple structure but leads to get good performance in tracking trajectories.

The paper is organized as follows. In section 2, the dynamic model of a planar five-bar manipulator is formulated in the active joint space following the results in [7], and a traditional computed torque controller is applied based on this dynamic model. The proposed method for tuning the PD gains of computed torque controller using neural networks is presented in section 3. In section 4, the trajectory tracking simulations are carried out, and the results are compared to the conventional computed torque controller. Finally, several important remarks are concluded in section 6.

2 Dynamic Modeling and Computed Torque Control

A five-bar manipulator is depicted in Fig.1. It consists of two active joints q_{a1} , q_{a2} and two passive joints q_{p1} , q_{p2} . $E(x, y)$ is the end-effector and L_1 , L_2 , L_3 , L_4 and L_5 are the links length of manipulator.

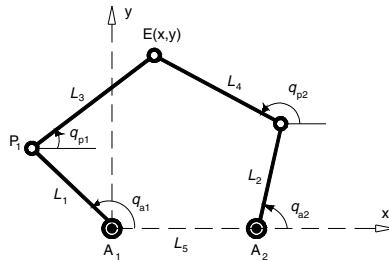


Fig. 1. The planar five-bar mechanism

To implement CTC method for planar five-bar manipulator, it is necessary to develop the dynamic model in the active joint space. In [7], Hongnian Yu already developed a full dynamic model for five-bar mechanism based on Lagrangian formulation. By applying the results of this paper to the planar case, the dynamic model of the planar five-bar mechanism can be formulated as:

$$\mathbf{M}\ddot{\mathbf{Q}}_{12} + \mathbf{C}\dot{\mathbf{Q}}_{12} = \boldsymbol{\tau}_{12} \quad (1)$$

Where $\mathbf{Q}_{12} = [q_{a1} \ q_{a2}]^T$ is a vector which represents two independent active joints (input). And $\dot{\mathbf{Q}}_{12} = [\dot{q}_{a1} \ \dot{q}_{a2}]^T$, $\ddot{\mathbf{Q}}_{12} = [\ddot{q}_{a1} \ \ddot{q}_{a2}]^T$ are velocity vector and acceleration vector respectively. \mathbf{M} is the generalized inertia matrix, \mathbf{C} is the vector containing the effects of the Coriolis and centripetal torque, and $\boldsymbol{\tau}_{12} = [\tau_1 \ \tau_2]^T$ is a vector of the generalized torque of active joints A_1 and A_2 respectively. The detail computation of components in equation (1) can be found in [7].

The dynamic equation (1) of five-bar manipulator has highly nonlinear nature. The traditional CTC law applied to this robot manipulator is:

$$\tau_{12} = \hat{\mathbf{M}}(\mathbf{Q}_{12}).\mathbf{Q}_{12}^* + \hat{\mathbf{C}}(\mathbf{Q}_{12}).\dot{\mathbf{Q}}_{12} \quad (2)$$

In which $\hat{\mathbf{M}}(\mathbf{Q}_{12})$ and $\hat{\mathbf{C}}(\mathbf{Q}_{12})$ are estimation of $\mathbf{M}(\mathbf{Q}_{12})$ and $\mathbf{C}(\mathbf{Q}_{12})$ and:

$$\mathbf{Q}_{12}^* = \ddot{\mathbf{Q}}_{d12} + \mathbf{K}_v \dot{\mathbf{e}}_{12} + \mathbf{K}_p \mathbf{e}_{12} \quad (3)$$

where $\ddot{\mathbf{Q}}_{d12}$ denotes the reference of acceleration of two active joints. $\mathbf{e}_{12} = [e_1 \ e_2]^T$, $\dot{\mathbf{e}}_{12} = [\dot{e}_1 \ \dot{e}_2]^T$ respectively denotes the tracking error which is defined by: $e_i(t) = q_{dai}(t) - q_{ai}(t)$, $\dot{e}_i(t) = \dot{q}_{dai}(t) - \dot{q}_{ai}(t)$, $i=1,2$. $\mathbf{K}_p \in \mathbf{R}^{2 \times 2}$, $\mathbf{K}_v \in \mathbf{R}^{2 \times 2}$ are diagonal matrices with positive K_{pi} and K_{vi} on the diagonals. If the gain matrices \mathbf{K}_p and \mathbf{K}_v are chosen with positive elements, then the closed-loop system is linear, decoupled, and exponentially stable. In the conventional CTC method, elements of the gain matrices \mathbf{K}_p and \mathbf{K}_v are constant.

3 Online Self Gain Tuning Using Neural Networks

The structure of the proposed online self gain tuning using neural networks in the computed torque controller is shown in figure 2. The output of the neural network is the input to the computed torque controller (inverse dynamics):

$$\mathbf{Q}_{12}^* = f(x) \quad (4)$$

Function $f(x)$ is the sigmoid function which has a nonlinear relationship as presented in the equation (5), and x is the input of sigmoid function.

$$f(x) = \frac{1 - e^{-2xY_G}}{Y_G(1 + e^{-2xY_G})} \quad (5)$$

where Y_G is the parameter determining sigmoid function's shape.

The input of the sigmoid function in the output layer is:

$$x(t) = \ddot{q}_{da}(t) + K_v(t)\dot{e}(t) + K_p(t)e(t) \quad (6)$$

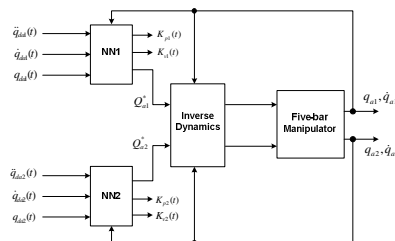


Fig. 2. Online self tuning computed torque gains using neural network

To tune the gains $K_p(t)$ and $K_v(t)$, the steepest descent method using following equation was applied:

$$K_p(t+1) = K_p(t) - \eta_p \frac{\partial J(t)}{\partial K_p} \quad (7)$$

$$K_v(t+1) = K_v(t) - \eta_v \frac{\partial J(t)}{\partial K_v} \quad (8)$$

In which η_p and η_v are learning rates determining the convergence speed. And $J(t)$ is the cost function error:

$$J(t) = \frac{1}{2} (q_{da}(t) - q_a(t))^2 \quad (9)$$

Using the chain rule, the following equations are derived:

$$\frac{\partial J}{\partial K_p} = \frac{\partial J}{\partial q_a} \frac{\partial q_a}{\partial Q^*} \frac{\partial Q^*}{\partial x} \frac{\partial x}{\partial K_p} ; \quad \frac{\partial J}{\partial K_v} = \frac{\partial J}{\partial q_a} \frac{\partial q_a}{\partial Q^*} \frac{\partial Q^*}{\partial x} \frac{\partial x}{\partial K_v}$$

As done by Yamada [11] and T.D.C. Thanh [12], for convenience $\frac{\partial q_a}{\partial Q^*} = 1$ is assumed. Finally the equations (7) and (8) are expressed as follows:

$$K_p(t+1) = K_p(t) + \eta_p e_p(t) e_p(t) \frac{4e^{-2xY_G}}{(1+e^{-2xY_G})^2} \quad (10)$$

$$K_v(t+1) = K_v(t) + \eta_v e_v(t) e_p(t) \frac{4e^{-2xY_G}}{(1+e^{-2xY_G})^2} \quad (11)$$

4 Simulations and Results

Simulation studies were conducted on Matlab-Simulink with respect to the case when five-bar manipulator tracks a linear trajectory. The link parameters of five-bar manipulator used in simulations were as shown in table 1. Where L_i is the length of link i^{th} , L_{ci} is the distance from the joint to the center of mass for the i^{th} link, m_i is the mass of the link i^{th} , and I_i is the inertia of link i^{th} .

Table 1. Parameter for five-bar manipulator

Link i	L_i (m)	L_{ci} (m)	m_i (kg)	$I_i(kg.m^2)$
1	0.102	0.05	0.8	0.0027
2	0.102	0.055	0.8	0.0031
3	0.18	0.09	1.2	0.0013
4	0.18	0.09	1.2	0.0013
5	0.132	-	-	-

Figure 3 shows the results of tracking of robot. The parameters of conventional computed torque controller was set to be: $K_{p1} = K_{p2} = 600$, $K_{v1} = K_{v2} = 40$. These parameters of conventional computed torque controller were obtained by trial-and error method.

The tracking error curves of the end-effector controlled by conventional method and proposed method are showed in the figure 4. It can be seen that the tracking accuracy of the proposed method is better than the tracking errors of the conventional CTC method. Figure 5 shows the results of online self gain tuning CTC using neural networks. The initial values of K_{pi} , K_{vi} , $i=1,2$ are set to be the same as the conventional computed torque controller.

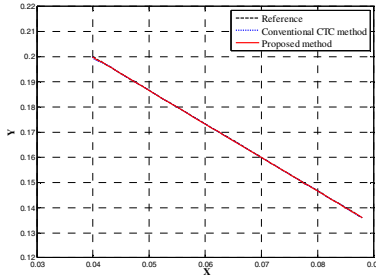


Fig. 3. The desired trajectory and the real trajectory of the end-effector

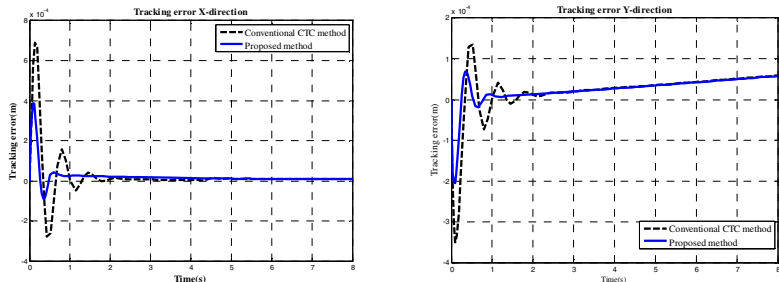


Fig. 4. Linear trajectory tracking errors of the end-effector for X-direction and Y-direction

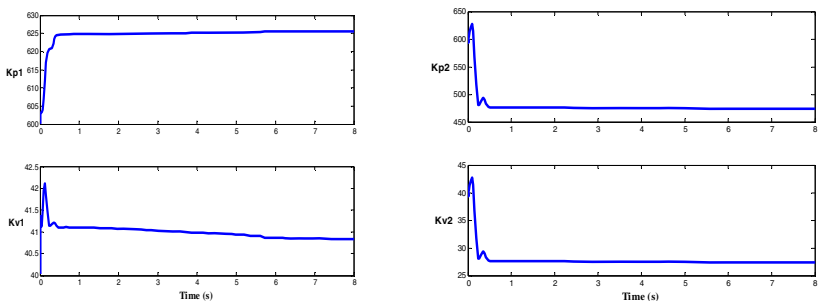


Fig. 5. Online self gains tuning of computed torque controller for joint 1 and joint 2

From the simulation results above, the proposed online self gain tuning method of computed torque controller using neural networks was verified to be very effective in the control of five-bar manipulator and showed the adaptability of gains K_{pi} , K_{vi} , $i=1,2$ tuning to minimize the position control performance.

5 Conclusion

In this paper, the problems of control the five-bar manipulators using computed torque control method is presented. In order to improve the control performance, an online self gain tuning method using neural networks is proposed for gain tuning of computed torque controller of a five-bar manipulator. Through the control simulation of the five-bar manipulator tracking a circular trajectory, it could be seen that the proposed method has a simple structure but delivers better performances in comparison with traditional computed torque control method.

Acknowledgement. The authors would like to express financial supports from NARC (Network based Automation Research Center), and Ministry of Knowledge Economy under Human Resources Development Program for Convergence Robot Specialists, respectively.

References

1. Ghorbel, F.H., et al.: Modeling and Set Point Control of Closed-chain Mechanisms: Theory and Experiment. *IEEE Transactions on Control Systems Technology* 8, 801–815 (2000)
2. Ouyang, P.R., et al.: Nonlinear PD Control for Trajectory Tracking with Consideration of The Design for Control Methodology. In: *Proceedings of IEEE International Conference on Robotics and Automation, ICRA 2002*, vol. 4, pp. 4126–4131 (2002)
3. Shang, W., Cong, S.: Nonlinear Computed Torque Control for A High-speed Planar Parallel Manipulator. *Mechatronics* 19, 987–992 (2009)
4. Shang, W., et al.: Active Joint Synchronization Control for A 2-DOF Redundantly Actuated Parallel Manipulator. *IEEE Transactions on Control Systems Technology* 17, 416–423 (2009)
5. Hui, C., et al.: Dynamics and Control of Redundantly Actuated Parallel Manipulators. *IEEE/ASME Transactions on Mechatronics* 8, 483–491 (2003)
6. Codourey, A.: Dynamic Modeling of Parallel Robots for Computed-Torque Control Implementation. *The International Journal of Robotics Research* 17, 1325–1336 (1998)
7. Yu, H.: Modeling and Control of Hybrid Machine Systems — A Five-bar Mechanism Case. *International Journal of Automation and Computing* 3, 235–243 (2006)
8. Yiu, Y.K., Li, Z.X.: PID and Adaptive Robust Control of A 2-DOF Over-actuated Parallel Manipulator for Tracking Different Trajectory. In: *Proceedings of IEEE International Symposium on Computational Intelligence in Robotics and Automation, 2003*, vol. 3, pp. 1052–1057 (2003)
9. Yang, Z., et al.: Motor-mechanism Dynamic Model Based Neural Network Optimized Computed Torque Control of A High Speed Parallel Manipulator. *Mechatronics* 17, 381–390 (2007)
10. Llama, M.A., et al.: Stable Computed-torque Control of Robot Manipulators Via Fuzzy Self-tuning. *IEEE Transactions on Systems, Man, and Cybernetics, Part B: Cybernetics* 30, 143–150 (2000)
11. Yamada, T., Yabuta, T.: Neural Network Controller Using Autotuning Method for Nonlinear Functions. *IEEE Transactions on Neural Networks* 3, 595–601 (1992)
12. Thanh, T.U.D.C., Ahn, K.K.: Nonlinear PID Control to Improve The Control Performance of 2 axes Pneumatic Artificial Muscle Manipulator Using Neural Network. *Mechatronics* 16, 577–587 (2006)

Towards an Efficient Discovery Services in OPC Unified Architecture

Mai Son and Myeong-Jae Yi*

School of Computer Engineering and Information Technology
University of Ulsan, San-29, Moogu-2 Dong, Namgu, Ulsan 680-749, South Korea
sonm9285@yahoo.com, ymj@mail.ulsan.ac.kr

Abstract. The OPC Unified Architecture, simply abbreviated to OPC UA, is the new generation of well-known and globally successful OPC standards. The OPC UA has totally thirteen parts which comprise specifications to ensure high performance communication, independent platform, and unified data model in enterprise systems. Discovery part, one of OPC UA parts, specifies a set of discovery services by which OPC UA Client perform discovery process to obtain information about OPC UA servers, including endpoint and security information. Unfortunately, the key part is still being developed, which leads to the limitation in development of OPC UA components. In this paper, we not only enrich the discovery concept by using WS-Discovery and extend it for global discovery case but also give readers an approach of how to implement discovery services in practice. The implementation will be deployed on Microsoft WCF Framework.

Keywords: OPC UA, OPC UA Discovery, Service Discovery, Discovery Service Set, WS-Discovery.

1 Introduction

In enterprise systems, a number of servers at different levels of the plan architecture will be available. Servers expose different information, while the unknown of the server organization is current challenge, especially in OPC UA systems.

An OPC UA server (UA Server) provides particular endpoints with some kinds of configuration regarding communication, encoding, and even security information, which an OPC UA client (UA client) needs to communicate with the UA server.

In order to support discovery process, OPC UA specifies a set of abstract services and three basic concepts such as *simple discovery*, *normal discovery*, and *hierarchical discovery* [2]. Those define *local discovery server* and *global discovery server* as two medium components to store server records and even endpoint records. Local discovery server resides on the same computer with the UA server and many UA servers on a single machine can share the same local discovery server. On the other hand, global discovery server exists in a network with a well-known address. Unfortunately, the implementation of these concepts has currently limitations. It

* Corresponding author.

doesn't indicate how a client can find endpoints of a server and how a server can publish its endpoints which have different configurations. These problems become more complex in case UA servers locate in different network segments or sites.

In this paper, we will try to enrich the discovery concept by using WS-Discovery specification. The remainder of this paper is structured as follows: After discussing related work in section 2, we will introduce our design of the proposed discovery services in detail in section 3. Section 4 then proposed the implementation in aspect of a principle. Finally, we come to conclusion in section 5.

2 Related Work

Discovery server is a server that needs to support suitable mechanism for discovery process. Some earlier service discovery protocols such as SLP (Service Location Protocol), Bluetooth SDP, describe various services and queries through predefined templates. However, the templates restrict the capability of description and make it difficult to adapt to the diversity and heterogeneity of services [6].

Recently, Universal Description, Discovery and Integration (UDDI) specification has been presented as a specification which defines a standard way of registering, deregistering, and looking up services [7]. Nevertheless, UDDI used centralized approach that is conflict with SOA paradigm and it is currently used as an in-house technology rather than a global service registry [8].

To overcome the lack of decentralized management capabilities, Web Services Dynamic Discovery (WS-Discovery) specification was developed [5]. WS-Discovery supports a multicast discovery protocol to locate services. By default, probes are sent to a multicast group, and target services that match return a response directly to the requester. If the number of endpoint is large, a discovery proxy will be used. WS-Discovery has been being potential specification which many research based on.

Pohlseni et la. [9] applied WS-Discovery for searches across different subnets with discovery proxies. However, this approach didn't indicate how to find out global directory.

Using other deployment, Hwang et la. [10] tried to apply WS-Discovery for Universal Service Discovery Protocol in ubiquitous environment. This approach used ubiquitous web service broker (UWS-Broker) to support the dynamic service discovery. Nonetheless, the UWS-Broker had many components unnecessary for OPC UA discovery process.

Some other approaches used semantic web technologies to solve the problem of service discovery such as using web ontology language to build community-based service discovery [11] or building ontology architecture for integrating information among different OPC UA servers [12]. However, the semantic discovery does not fully function without developer support. Hence, a lot further research has to be done to make these approaches viable for all application.

The following sections will exploit WS-Discovery to design components enhancing OPC UA discovery process. The implementation in practice is based on Window Communication Framework and ensures the flexibility and reliability.

3 Design of the Proposed Discovery Services

This section will give a brief mechanism of the discovery service set then apply WS-Discovery to enhance this one.

3.1 OPC UA Discovery Service Set

OPC UA standard presents the *Discovery Service Set* which contains basically three services that used to discover endpoints and to read the security configuration for those endpoints such as *Register Server service*, *Find Server service*, and *Get Endpoint service* [3].

UA Servers use *Register Server service* to register themselves with *Discovery Server*. Discovery Server contains the UA server information records that describe them. However, discovery servers shall reject registrations if they find out that the candidate information does not match the information in server certificate used to create secure channel, secure channel is created before establishing the session between client and server. In some cases, UA server doesn't want to work after installing, so register method should support offline mode.

UA Clients call *Find Server service* to discover any registered servers. This service runs on the server called Discovery Server. To reduce the results returned, this service specifies *filter criteria*. The parameters of filter criteria may be scope or timeout value. This service shall not require any message security.

After finding the desired UA server, UA client read the security information necessary to establish a secure channel by calling *Get Endpoint service*. Once a client retrieves the information about the Endpoints, the client can save this information and use it to connect directly to the servers again without going through the discovery process. Of course, if the server configuration may have changed after that, then the client finds that it cannot connect to the server and the client needs to go through the discovery process again. To reduce the results returned, Get Endpoint service specifies filter criteria as well.

3.2 Discovery Mechanism with WS-Discovery

Local Discovery Server, a quickly proposed solution, seems to be a good solution. However, in large-scale environments, using many local discovery servers leads to the complexity and waste of bandwidth. Instead, *dedicated discovery server*, simply called discovery server, is considered as a better solution. Unfortunately, dedicated discovery servers also lead to a new challenge that is how to locate those servers in network environment. To do it, there are two solutions based on Web Service Discovery specification (WS-Discovery).

The first solution is using a *well-known address* for discovery server and extended address parts for services. At the beginning, UA clients send a unicast *Probe* message to this address, if the discovery server has a desired service it answers through a unicast *ProbeMatch* message. If ProbeMatch information is sufficient, UA clients can connect to the service published by the discovery server. The discovery server with the information of service addresses can be sent out in variety ways e.g. an administrator sends users by email or SMS, or users could learn from DNS. The

well-known address of discovery server, called the base address, and extended parts are used to connect to the desired services. For instance, if a base address of a discovery server is “*opc.tcp://localdiscovery:4840*”, the address of register service and find server service will be as follows:

“*opc.tcp://localdiscovery:4840/register*”
 “*opc.tcp://localdiscovery:4840/discovery*”

The second solution is based on the *multicast feature* presented by WS-Discovery specification. In case either UA servers or clients don’t know the location of discovery server, they search for services by sending Probe messages in a multicast manner. If there are matches, the discovery server sends a ProbeMatch response back to the source. Using the service information returned from the discovery server, UA clients and servers can then contact the services directly. When multiple compatible endpoints are discovered, filter criteria is used to distinguish them by the scope of services. The developer can provide the criteria for finding operation to reduce the total number of services the developer is looking for e.g. MaxResult. The duration time which specifies how long the client waits for responses is used as well.

3.3 Discovery Server Components

A discovery server not only hosts Find Server and Register Server services but also enables to host extended services if necessary. To ensure the flexibility, a message router component will be presented as a message routing and dispatch component. Besides that, to extend global discovery process over the internet, a global router component is proposed as well. Because UDP messages are packed into SOAP messages, it is easy to send them from a discovery server to each other over HTTP protocol. The global router component has an UDP Discovery Endpoint which is used to send UDP discovery messages to discover servers located in other networks and to receive UDP discovery messages from discovery servers outside.

Discovery server described in Fig. 1, has two key components, message router and global router.

A message router component is proposed with three main functions:

- *Message routing*. Message router component works as a routing service which can deliver each message to a dedicated service by using a message filter. All coming messages will be stored in a *message queue*. The message router takes each message from the message queue and sends it to related service.
- *Protocol bridging*. Message router component can use HTTP protocol to retrieve messages, convert them, and transfer them to dedicated service by using other protocol.
- *Error handling*. If dedicated service has a backup version, message router component can be used to redirect messages to backup service in case the main service has shut down.

Discovery servers have an ability of exchanging server information record by using *global router* component. In other words, global router component can work as a client which can connect to the other discovery server and get its server information records. Whereas, it also plays a role of a service which receives the server information records returned from other discovery servers. This component sends

UDP discovery messages in a multicast way over the internet by using discovery server information records stored in the cache file.

In our concept, we choose using cache files to store the server information records. There are two kinds of cache file. One is a cache file that contains the OPC UA description records. One or more records are returned to a client when receiving Find Server request from the client. The other cache file contains the information that is required in global discovery e.g. well-known addresses of discovery servers located on other network segments or sites. It can be configured manually by administrators or be learned from DNS.

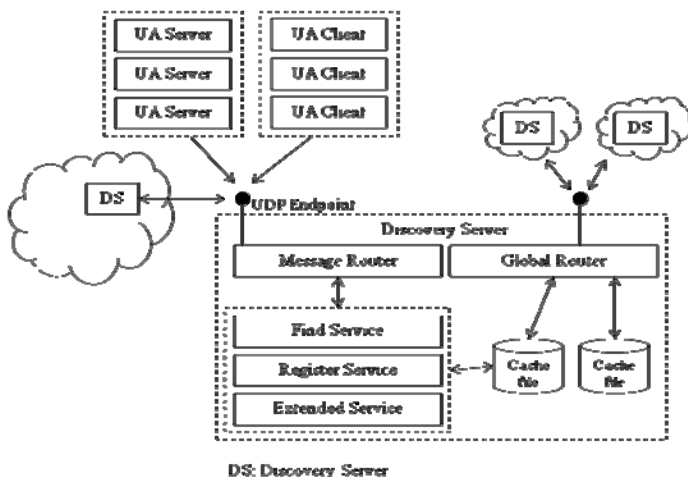


Fig. 1. OPC UA Discovery Server Components

3.4 Discussion

The design concept is evaluated in some aspects such as security, performance, reliability, and extension ability:

- *Security*. Because the information returned from a Get Endpoints service has no security, a client should compare them to the information returned in the create session process such as host name, server certificate, endpoint description
- *Performance*. Sending messages in a broadcast manner has a disadvantage of network communication overload but it reduces the management cost. Otherwise, using well-known address is better way in case of large-scale network. For the purpose of decreasing the response time between a discovery server and a UA client, the number of returned records will be reduced by using filter criteria.
- *Reliability*. Primary discovery server exchanges request message and information with backup discovery server. When something happens with the primary server, the backup server will detect this failure and immediately switches itself to the primary server by registering its address to the DNS.

- *Extension and Replacement.* Using message router that uses a routing service that dispatches messages to dedicated service brings the ability of extension and replacement. Programmers can develop any service and connect it to the message router easily by adding some information into the configuration file of the message router.

4 Implementation Concept

Because OPC UA SDK and stack source codes are not open, programmers and developers are difficult to extend mechanism. Consequently, our components are being developed with the support of Microsoft WCF, Window Communication Foundation. In this section, we will briefly describe the overall discovery server implementation on the WCF 4 version that supports APIs for WS-Discovery standard.

4.1 Network Topology

In OPC UA environment, discovery server plays an important role. If something not good happens e.g. a discovery server suddenly fails, our network will lost all server records and data stored in it. Therefore, a redundancy mechanism is required to increase the efficiency and reliability of the server.

Basically, the network topology with redundancy feature is indicated in Fig. 2. This topology only focuses on the principle of discovery server redundancy, other redundancy mechanisms for UA servers and clients are not considered.

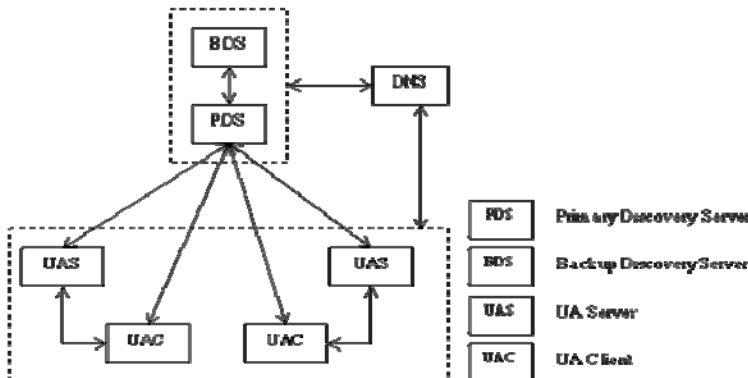


Fig. 2. Network Topology for Discovery Redundancy

Three components used as the most important ones in discovery process include:

- *PDS (Primary Discovery Server).* A main server has a well-known address that used in discovery process. When a UA server begins working after completely installing, it informs PDS about the appearance by one of two methods: broadcasting UDP messages or using the well-known address.

- **BDS (Backup Discovery Server)**. This server is a mirror of a PDS. A backup server will be used to replace main server as long as the primary server stops
- **DNS (Domain Name System)**. A DNS server exposed discovery server address that UA servers and UA clients use to connect to discovery server. In addition, it plays role in switching between primary server and backup server.

4.2 Discovery Process

The discovery process is show in Fig. 3 divided into sub-processes including:

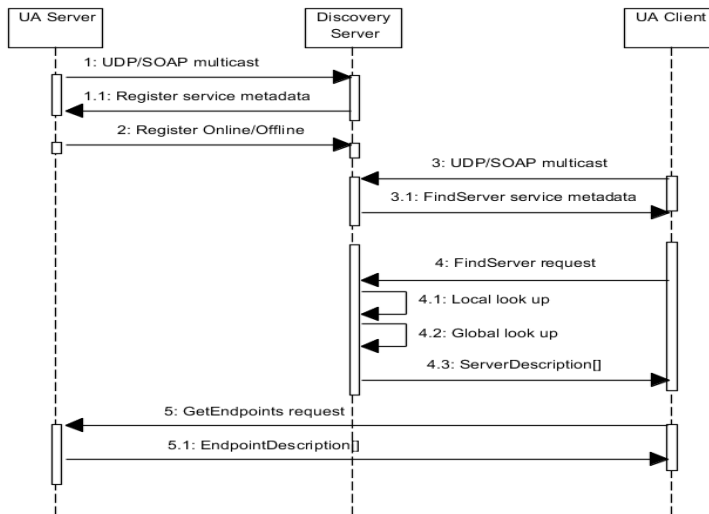


Fig. 3. Discovery Process Overview

Discovery Server Search. This process focuses on how to locate discovery server in local network like step 1 and 3 in Fig. 3. To solve that, message router component implements an endpoints called UDP Discovery Endpoint, which is the new feature of WCF 4 for service discovery. With the UDP Discovery Endpoint, the message router can retrieve the UDP multicast message sent from UA servers or UA clients.

When UA servers or UA clients look for any discovery server, they send Probe messages by using a Multicast IP Address. Each service that receives the request determines whether it matches the criteria in the Probe message and responds directly to the client with a ProbeMatch message if the service matches the criteria specified in the Probe message. The number of result can be decreased by using some parameters of a filter criteria object such as Scope, MaxResult, and Timeout.

Register Process. After handling the endpoint address of discovery server, UA server can register itself with discovery server by using the endpoint like step 2 in Fig. 3. Register messages will be sent to the message router. Then the message router transfers them to register server service. Register service in OPC UA specification proposed a register method which has two online and offline modes.

Find Server Process. The UA server records can be stored in the discovery server at the same network segment with demand machine or in other network segment. So, the find server process has two sub-processes: local look up process and global look up process (step 4 in Fig. 3). As long as a Find Server service receives a find request from a client, it searches the server information in the cache file. If required servers exist in the cache file, discovery server will send server description records back to the client. Depending on the scope specified in Filter Criteria object, discovery server makes a decision for searching process only in the local or global network. Searching in global network requires the discovery server use a cache file that stores the well-known addresses of discovery server of other segments. At the discovery server side, tasks of find server process include the followings:

```

function find_server(filter_criteria)
    local_db_look_up(filter_criteria);
    if (found = true)
        send(client,server_description_list)
    else
        global_ds_list = get_global_server_list();
        new_filter = create_new_filter_criteria();
        send_request (global_ds_list,new_filter);
        wait();
    end
end function

```

If discovery server located on other segment has required server information, it sends server description list back to source discovery server by calling callback function. Afterward, the discovery server will send the list to the client.

```

callback function global_ds_lookup(server_list)
    send(client,server_list)
end function

```

Get Endpoint Process. After getting server description records, a client uses discovery addresses specified in each record to connect to the Get Endpoint service. The Endpoint service return UA Endpoint Description list to the client like step 5.

5 Conclusion

In this paper, we proposed a discovery approach based on WS-Discovery to solve these two discovery problems: how to locate the discovery server on the network and how to perform discovery process over the internet.

We applied WS-Discovery specification to enhance OPC UA discovery process for both local and global discovery case, and proposed the implementation in real situation as well.

Discovery server contains two key components, message router component is used to retrieve message from UA servers and clients and global router component is used to exchange server information with other discovery server locating in other network segments. Our network topology also uses backup discovery server and DNS as a redundancy strategy to ensure the reliability.

The discovery service set can be used without security and it is therefore vulnerable to DOS attacks. In the future, a discovery server should minimize the amount of processing required to send the response. To overcome the problem, we intend to apply one of two solutions. The first solution is using semantic technology to manage efficiently server information. The client can get the result fast and more exactly. The second solution is applying some database management systems instead of storing in cache file.

Acknowledgements. This work was supported in part by the Korean Ministry of Knowledge Economy and Ulsan Metropolitan City through the Network-based Automation Research Center (NARC) at the University of Ulsan and by the National Research Foundation of Korea (NRF) grant funded by the Korean Government (MEST) (NRF-2011-0002953). The authors also would like to thank the anonymous referees for their valuable comments and suggestions.

References

1. Lange, J., Iwanitz, F., Burke, T.J.: OPC From Data Access to Unified Architecture 4th. VDE VERLAG GMBH, Berlin (2010)
2. Mahnke, W., Leitner, S.H., Damm, M.: OPC Unified Architecture. Springer, Heidelberg (2009)
3. The OPC Foundation: The OPC Unified Architecture Specifications: Part 1–11. Version 1.xx (2009), <http://www.opcfoundation.org/Downloads.aspx>
4. Lowy, J.: Programming WCF Services 3rd. O'Reilly Media, Sebastopol (2010)
5. Web Services Dynamic Discovery (WS-Discovery) Specification, <http://docs.oasis-open.org/ws-dd/ns/discovery/2009/01>
6. Jin, B., Zhang, L., Zang, Z.: A Unified Service Discovery Framework. In: Proceedings of the 6th IEEE Conference on Grid and Cooperative Computing, pp. 203–209. IEEE Press, Los Alamitos (2007)
7. UDDI Specification, <http://www.oasis-open.org/committees/uddi-spec/doc/spec/v3/uddi-v3.0.2-20041019.htm>
8. Pohlsen, S., Buschmann, C., Werner, C.: Integrating a Decentralized Web Service Discovery System into the Internet Infrastructure. In: Proceedings of the IEEE 6th European Conference on Web Services, pp. 13–20. IEEE Press, Los Alamitos (2008)
9. Pohlsen, S., Werner, C.: Robust Web Service Discovery in Large Networks. In: Proceedings of the IEEE International Conference on Services Computing, pp. 512–524. IEEE Press, Los Alamitos (2008)
10. Hwang, Y.Y., Oh, I.H., Im, H.J., Lee, K.C., Lee, K.: Lee. S.: Universal Service Discovery Protocol. In: Proceedings of the IEEE International on Convergence Information Technology, pp. 2380–2385. IEEE Press, Los Alamitos (2007)
11. Perryea, C.A., Chung, S.: Community-based Service Discovery. In: Proceedings of the IEEE International on Web Services, pp. 903–906. IEEE Press, Los Alamitos (2006)
12. Hadlich, T., Muehlhause, M., Diedrich, C.: Discovery and Integration of Information in a Heterogeneous Environment. In: Proceedings of the 2010 IEEE International on Emerging Technologies and Factory Automation, pp. 1–8. IEEE Press, Los Alamitos (2010)

Asynchronous Modeling and Implementation of Web Services Based on JMS

Jie Wang¹ and Liang Tong²

¹ Zhengzhou University of Light Industry,
School of Computer and Communication engineering,
ZhengZhou, China

² Yellow River Engineering Consulting Co.,Ltd,
ZhengZhou, China
lemon_dream_jie@yahoo.com.cn

Abstract. A solution of asynchronous Web Services is proposed through the analysis of Web Services' concept and architecture. And on this basis, some further discussions on how to implement the WebLogic JMS-based Asynchronous Web Services with several specific examples. It is proved that asynchronous Web Services can improve performance of application in particular case, but it is not always applicable. In practice, appropriate Web Services should be adopted according to actual situation.

Keywords: Web Services, Asynchronous Web Services, JMS.

1 A Brief Introduction of Web Services

1.1 Web Services Concepts

Web Services can be defined from multiple perspectives. From the technical level, a Web Service is one of the application software that can be identified by URI. XML describes its interface and binding, and it is interactive with other applications based on XML messages[1]. From the functional point of view, Web Services is a new Web application, with self-contained, self-describing and modular characteristics that can be released, searched and called through the Web [2]. Its implementation can be a simple response to customer's requests or to complete a complex business processes. With the proper configuration, a Web service can directly be monitored and invoked by other applications.

1.2 Web Service Architecture

Web Services Architecture is within application layer architecture of the top layer of TCP/IP. It is built on three basic agreements of XML [3]: Web Services Description Language (WSDL); Simple Object Access Protocol (SOAP) and Universal Description, Discovery and Integration (UDDI). A typical Web Services architecture is shown in Fig.1 [4]. In this architecture, service requester, provider and registration

center interact between these three entities to complete the service transfer. The complete system of Web Service shall be composed of one or more of the above entities. These different entities provide a complete Web Services function by publishing, finding and binding the three operations.

First of all, Contract Providers supply the description of the services, and the Web Service Registration center registers the contract as the definition of the Web Services. Secondly, the service provider locates the contract through the Web service registration center, accomplishes the services as described in the contract, and then registers this service. Please pay attention here, the contract providers and service providers can be the same entity or different entities. Finally, through the Web service registration center the service requester finds the needed definition of the services, which is the contract, thus accessing to Web services by binding it to the Web Services implementation. In the whole process of the interaction, Web service registration center is the key to accomplish the publication and searches. In essence, from the point of view of the Web Services, the registration center is a Web service itself. The contract is a medium between the service requester and the service provider. The service requester and provider are bound by the contract.

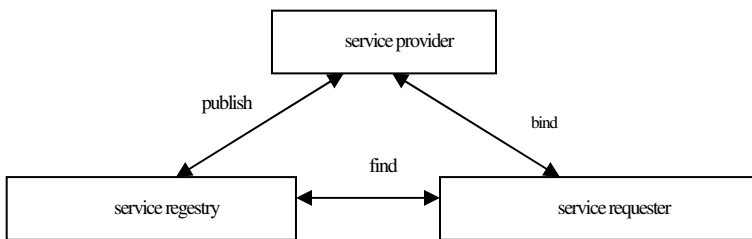


Fig. 1. Web Services Architecture

2 Differences between Asynchronous Web Services and Synchronous Web Services

In the Web Service architecture, there are two models in the interaction between the service requester and the service provider, synchronous and asynchronous. In the synchronous model, the interaction is bi-directional; the service requester sends a request to the service provider and then waits for response. The provider receives the request, processes it, then sends the response back to the requester. During the provider handling the request, the service requester stays in a blocked state and cannot perform other work. In this interaction model, if the provider responses immediately, it causes no problem to the requester. If the provider is busy or takes a long time to process the request, the requester has to be in waiting state. For example, if the Web Services query large databases, the current thread of the client will have to wait for the call completion. The thread has nothing to do but wait till the query returns. Another example, when waiting for other threads to complete the TCP socket or the backend Web service call, there will be a similar problem. When the client program runs on the server and the

server is with a huge load, it's not a good option to keep the thread in a waiting state. The asynchronous model can solve this problem. In the asynchronous interaction model, the interaction is in one way, it does not require an immediate response, which permits the requester to continue other work after sending the request. The service provider will notice the requester in some acceptable way after the request is processed.

3 Asynchronous Web Services Modeling Based on JMS

3.1 General of JMS

JMS is a group of Java API, it contains a common set of enterprise message concept to support the asynchronous messages. In an asynchronous message mode, a JMS message provider sends a message to the client and the client receives it without any response. In a synchronous message mode, such as SOAP messages sent by HTTP, an application (service requester) sends a message to another application (service provider) to ask for a service, the requester will be blocked and cannot do any other work before the arrival of the response.

JMS has two message models: point-to-point message queue mode and publishing/subscribing model. All the news message queues are kept till all messages are consumed or expired. The typical message queue mode has only one consumer. Publishing/subscribing model has a sender (releaser) and a receiver (subscriber/client). A client subscribes a topic and when the message is sent to a topic, the publisher will send a message to all subscribers. Publishing/subscribing model usually has many consumers.

In the distributed enterprise, communication is needed between the enterprise system and J2EE application. JMS is usually used in this case. You can use JMS to visit Web services in the system or to communicate with the web service directly. A web service in the J2EE can be accessed with JMS message or message-driven Bean. Web services and Message-Driven Bean are also in the J2EE application server. They can also accept and process the JMS messages sent by the client.

3.2 Creating Asynchronous Web Services with JMS Asynchronous Messages

WebLogic component supports the development of Web services by the use of asynchronous message. In the asynchronous message mode, JMS is used as a message frame; the message-driven Bean sends messages to the JMS message destinations, or receives messages from JMS message destination. Using asynchronous messages, the client can send a message containing the data to a one-way Web service without response from the Web service, which looks like sending a message to the database. The client can maneuver other Web service operation to receive information.

WebLogic components use the queue-message mode in JMS to create asynchronous Web services. In JMS realization, JMS server is used to save message queues. A JMS message-driven Bean processes messages, and also a JMS message type is used to deliver messages between the client and the server. A destination queue has to be configured in the JMS server. If the message requires a response, a reception queue is needed. As the asynchronous message doesn't need response, the receiving queues of

message are optional. Message-driven Bean must be configured to listen to any incoming messages in the target queue. Then the Web Service Designer will import the message-driven Bean of the project, and create a Web service of JMS to send data to the destination. If necessary, the messages can also be received from the receiving queue. Fig. 2 shows a typical asynchronous message queue using the Web service model.

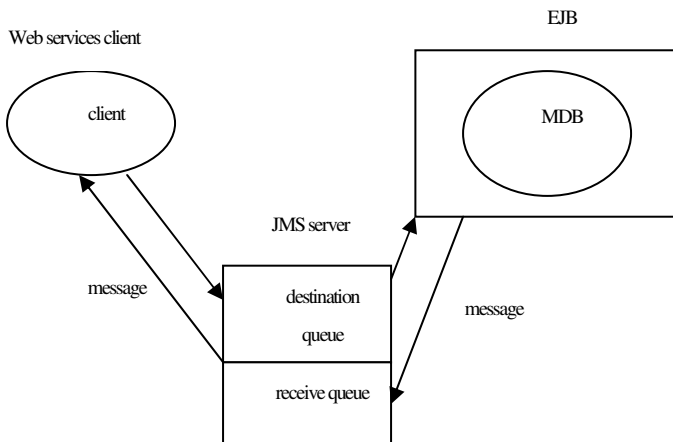


Fig.2. Asynchronous Web Services Model

4 Example to Create Asynchronous Web Services with WebLogic

From the above, you know, WebLogic can use JMS to create asynchronous Web services. To realize JMS needs a JMS server to store messages, a JMS message-driven Bean to deal with JMS messages and a JMS message (i.e. data) to transfer messages between the client and the server.

In a J2EE student information management system, there is a query module to number the students and to feed back all the relative information of the students. This function is implemented with a dialog Bean named StuSession. The relative information of the students is shown by a noumenon Bean - Student corresponding to the students' information in the database table. The dialog Bean will transfer the noumenon Bean according to the student serial number transferred from the client and the noumenon Bean will feed back the relative student information to the dialog Bean, and then the dialog Bean will send the results back to the client. According to the actual demands, now we need to pack this query functionality as Web Services. From the analysis of the above Asynchronous Web Services and Synchronous Web Services, it's reasonable to encapsulate this functionality as an asynchronous Web Service.

In this case, we will create a Message Driven Bean in the EJB module and an asynchronous Web service to modify the business logic in the message-driven Bean, and a request shall be sent to the Web service. during response, the server will feed back the information from the database to the client asynchronously through MDB.

This process involves the following steps:

First a project shall be created.

JMS will be configured in the WebLogic Server. A JMS connection factory will be created first, the JNDI is named as StudentJMSFactory. Then a JMS service and two JMS queues will be created. The JNDI will be respectively named as StudentRequestQueue and StudentResponseQueue.

A message-driven Bean will be created and named as StuMdb to receive and respond to the messages sent to the JMS server.

An asynchronous Web service shall be created. The Web service will be first configured in the project, then StuMdb will be encapsulated as a Web service with the Web Services Designer and finally the appropriate settings will be made for the JMS sending and receiving services. Information type will be set up in sending services, which is a JavaBean, i.e. StudentNumber, and the name for operation is stuRequest; In receiving services, the receiving queue is set up as StudentResponseQueue, information type as StudentInfo, which is also a JavaBean and the receiving operation is stuResponse. The project will be compiled when the setup is completed.

The business logic will be implemented in Message-Driven Bean. The appropriate business logic has to be accomplished within the onMessage () method of StuMdb, and thus the incoming JMS messages can be dealt with. Prior to this, two variables need to be defined and the setMessageDrivenContext () method will be modified. In StuMdb the dialog Bean StuSession will be referred to, which can be set up in the DD Editor. Then two variables will be declared in the StuMdb: private StuSessionHome stuSessionHome and private StuSession stuSession; The modified method of setMessageDrivenContext () is shown as follows:

```
public void
setMessageDrivenContext(MessageDrivenContext
messageDrivenContext) {
    this.messageDrivenContext = messageDrivenContext;
    Context context = new InitialContext();
    Object object = =
context.lookup("java:comp/env/ejb/StuSession");
    stuSessionHome = (StuSessionHome)
javax.rmi.PortableRemoteObject.narrow(
        object, StuSessionHome.class);
}
```

After the business logic is realized the onMessage () method is as follows (exceptions ignored):

```
public void onMessage(Message msg) {
    StudentNumber StudentNumber = null;
    StudentInfo StudentInfo = null;
    if (msg instanceof ObjectMessage) {
        StudentNumber = (StudentNumber)((ObjectMessage)
msg).
getObject();
    }
    stuSession = stuSessionHome.create();
```

```

StudentInfo = new StudentInfo();
StudentInfo
stuSession.getByStuNo(StudentNumber.getEmpNo());
Jms1 jms1 = new Jms1();
jms1.sendObject(StudentInfo);
}

```

=

A program from the client is written to initiate the request to the server. The client will first obtain the port of the Web service. Because it is an asynchronous transfer, a pair of methods will be used to complete the request and response. The beginning method feedback FutureResult data type, and later on, the system will put the result into this data type. FutureResult type has a `isCompleted()` method, which can determine whether the method is completed. For asynchronous transfer, two different modes can be adopted - polling and callbacks, and here the first model will be used. The corresponding transfer program is as follows:

```

private static void pollingMethod() {
    try {
        StuMdbPort          port      = new
        StuMdb_Impl().getStuMdbPort();
        FutureResult         futureResult = =
        port.startStuRequest(newStudentNumber(
            new java.lang.Short((short)2)), null);
        while( !futureResult.isCompleted() ){
            Thread.sleep( 300 );
        }
        port.endStuRequest(futureResult);
        futureResult = port.startStuResponse(null);
        while( !futureResult.isCompleted() ){
            Thread.sleep( 300 );
        }
        StudentInfo          StudentInfo = =
        port.endStuResponse(futureResult);
        System.out.println("StudentInfo: " +
        StudentInfo.getFullName());
        System.out.println(" ");
    }
    catch (Exception ex) {
    }
}

```

=

+

Web services will be deployed and tested. In the JB the corresponding applications and Web modules are published to the WebLogic server, and to be tested through the test page. Here the development, deployment and test of an asynchronous Web service are completed.

5 Conclusion

From the above example, we know that asynchronous Web Services based on JMS are implemented essentially with the message-driven Bean and two message queues. The message-driven Bean asynchronously receives and processes requests from the client and server-side response, to achieve service Asynchronous transfers. In some particular case, Asynchronous Web Services can improve the application performance, however. But it is not all cases which are suitable to asynchronous Web Services. In practical operation, synchronous and asynchronous Web Services transfers will be respectively adopted as per the length of time required based on the implementation of Web Services.

References

1. Castro Leon, E.: A Perspective on Web Services (EB/OL)
<http://www.webservices.org/index.php/article/113/1/61/> (2004)
2. Tsalgatidou, A., Pilloura, T.: An Overview of Standards and Related Technology in Web Services. Distributed and Parallel Databases 12(2-3), 135–162 (2002)
3. Web Services Architecture. W3C Working Draft (EB/OL) (2003),
<http://www.w3.org/TR/ws-arch/>
4. Web Services: Concepts and Definitions. Herzum Software Version 0.7 (2002)

An Effective Shuffled Frog Leaping Algorithm for Solving Hybrid Flow-Shop Scheduling Problem

Ye Xu, Ling Wang, Gang Zhou, and Shengyao Wang

Tsinghua National Laboratory for Information Science and Technology (TNList),

Department of Automation, Tsinghua University, Beijing, 100084, P.R. China

xuye05@mails.tsinghua.edu.cn, wangling@mail.tsinghua.edu.cn,
gangzhou@126.com, wangshengyao@tsinghua.org.cn

Abstract. In this paper, an effective algorithm based on the shuffled frog leaping algorithm (SFLA) is proposed to solve the hybrid flow-shop (HFS) scheduling problem, which is a strong NP-hard combinational problem with very wide engineering background. By using a special encoding scheme and combining SFLA based memetic search and Meta-Lamarckian local search strategy, the exploration and exploitation abilities are enhanced and well balanced for solving the HFS problems. Simulation results based on some typical problems and comparisons with some existing genetic algorithm and differential evolution demonstrate that the proposed algorithm is effective and robust in solving the HFS problem.

Keywords: shuffled frog leaping algorithm, hybrid flow-shop scheduling, local search, Meta-lamarckian strategy.

1 Introduction

In hybrid flow-shop (HFS) [1] problem, there are usually a set of n jobs to be processed in s stages. Each stage has at least one machine and some stages have multiple machines while machines in each same stage are unrelated. Each job should be processed in all the stages, and each job can be processed by any one of machines in each stage. At a time, one machine can process only one operation and one job can be processed at only one machine. Once an operation is started, it cannot be interrupted. The HFS problem is of wide industrial background since many real manufacturing problems in fields of textile [2], paper [3] and electronics [4] industries can be modeled as HFS problems. In addition, the HFS problem is often strongly NP-hard [5]. So, it is of important academic significance and engineering application value to study the HFS problems, especially to develop effective solution algorithms.

Since the HFS problem was proposed in 1954 [6], many approaches have been proposed. Due to the complexity of the HFS problem, exact algorithms such as branch and bound (B&B) [7] can only be used to solve small-scaled problems. Although the heuristics such as dispatching rules [8] and divide-and-conquer strategy [9] are very efficient, the quality of solution obtained are often not satisfactory, especially for the problems with many jobs or machines or stages.

During the past two decades, meta-heuristics have gained increasing research in the field of manufacturing and scheduling, which makes it possible to achieve satisfactory schedule with reasonable computational effort for large-scaled problems. Among meta-heuristics, genetic algorithm (GA) [10], particle swarm optimization (PSO) [11], ant colony optimization (ACO) [12], tabu search (TS) [13], differential evolution (DE) [14] have already been applied to solve the HFS problems. As a comparatively new intelligent optimization algorithm, shuffled frog leaping algorithm (SFLA) has less control parameters and is easier to be implemented than other algorithms [15]. The SFLA performs its search process through the instruction of memetic intelligence produced by cooperation and competition between sub-populations and individuals among them. Meanwhile, the redistribution of the sub-population makes the searching behavior less possible to be trapped in some local minima. To the best of our knowledge, SFLA has not been applied to the HFS problem yet, which motivates us to develop the SFLA for solving the HFS problem. Moreover, it has been shown that meta-heuristics that reasonably combined with local search are of good performances in solving complex optimization problems. Thus, after considering the special encoding scheme for the HFS problem, we develop a local search based on Meta-Lamarckian learning mechanism [16] and incorporate it into SFLA. Simulation results based on some typical instances and the statistical comparisons with some typical existing algorithms verify the superiority of the proposed SFLA.

The remainder of the paper is organized as follows. The HFS problem is formulated in Section 2. In Section 3, the SFLA is introduced in brief. Then, the SFLA based algorithm for the HFS problem is presented in Section 4, including the encoding and decoding schemes and the local search. Simulation results and comparisons are given in Section 5. Finally, we end the paper with some conclusions in Section 6.

2 Problem Statement

Typically, the HFS problem is supposed that: All the n jobs are independent and available to be processed at the initial time; Buffers between stages are unlimited; one machine can process only one operation and one job can be processed at only one machine at a time; the releasing time of all machines is not considered or set as 0; For all the n jobs, the processing times in each machine are deterministic and known in advance; The time between different machines for transportation is negligible; Once an operation is started, it cannot be interrupted.

The HFS problem with makespan criterion can be formulated as follows [17]:

$$\text{Minimize} \quad C_{\max} \quad (1)$$

Subject to:

$$C_{\max} = \max(C_{ik}), \quad k = 1, \dots, s, i = 1, \dots, n \quad (2)$$

$$C_{ik} = S_{ik} + P_{ik} \quad (3)$$

$$\sum_{i=1}^{m(k)} X_{jik} = 1 \quad (4)$$

$$S_{ik} \geq C_{i,k-1}, k = 2, \dots, s \quad (5)$$

$$S_{ik} \geq C_{jk} - MY_{ijk}, \text{ for all the pairs } (i, j) \quad (6)$$

$$S_{jk} \geq C_{ik} - (1-M)Y_{ijk}, \text{ for all the pairs } (i, j) \quad (7)$$

$$S_{i1} \geq R_i, \text{ for all } i=1, \dots, n \quad (8)$$

where, n is the total number of jobs, s is the total number of stages, $m(k)$ is the number of the machines at stage k , X_{ijk} is a binary variable (it is equal to 1 if job j is assigned to machine i at stage k ; otherwise, it is equal to 0), Y_{ijk} is a binary variable (it is equal to 1 if job i precedes job j at stage k ; otherwise, it is equal to 0), R_i denotes the releasing time of job i , S_{ik} denotes the starting time of job i at stage k , P_{ik} denotes the processing time of job i at stage k , C_{ik} denotes the completing time of job i , and M is a large constant.

For the above formulation: Eq. (1) denotes the objective to minimize the makespan, i.e., the maximum completion time of all the jobs shown in Eq. (2); Eq. (3) describes the computation of C_{ik} ; Constraint (4) ensures that one job can be processed exactly on one machine at each stage; Constraints (5) and (6) ensure that one machine can process only one job at one time; Constraint (7) means that one job cannot be processed until its preceding job is finished; Constraint (8) bounds the starting time of a job. In Fig. 1, it illustrates an example of the problem with 3 stages.

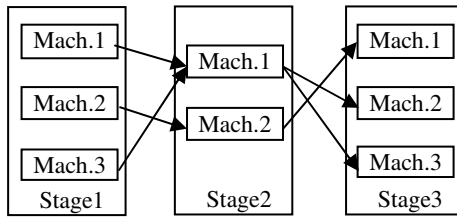


Fig. 1. An example of the HFS problem

3 Shuffled Frog Leaping Algorithm

Shuffled frog leaping algorithm is a memetic meta-heuristic algorithm proposed by Eusff and Lansey [15]. The evolution of the SFLA takes use of the cultural environment of the individuals in the population, which is called the “meme”. In the SFLA, the population is divided into several groups, i.e., sub-populations. Each

sub-population described as a memplex consists some frogs, and local search is performed respectively in each memeplex. A frog has its own behavior and is influenced by other frogs in one memeplex. After several local search steps, the frogs in the population will be mixed together and then partitioned into several sub-populations again to exchange the information among the memeplexes. After this stage named “shuffling”, the local search between frogs in each memeplex is implemented. The algorithm continues iteration until the stop criteria is satisfied.

The standard process of SFLA algorithm is described as follows.

Consider that the population consists of p memeplexes and each memeplex contains q frogs which are selected randomly from the population. Within each memeplex, Pb and Pw denote the best frog and the worst frog according to their objective values respectively. In each evolution, the worst frog Pw will leap to a new position with the distance Dis according to Eq. (9) and Eq. (10).

$$Dis = \text{rand} \bullet (Pb - Pw) \quad (9)$$

$$Pw' = \begin{cases} Pw + Dis, & \text{if } \min Dis < Dis < \max Dis \\ Pw + \min Dis, & \text{if } Dis \leq \min Dis \\ Pw + \max Dis, & \text{if } Dis \geq \max Dis \end{cases} \quad (10)$$

If the frog can reach a better position, then it accepts Pw' ; else, it uses the best frog among the whole population Pg instead of Pb in Eq. (9) to generate another new frog Pw'' . If Pw'' is still worse, then a new random solution is generated to replace the frog Pw . After sn steps, all frogs in the population are mixed together and then divided into p new memeplexes. The procedure of SFLA is summarized as follows:

Step 1: Randomly generate initial population, let $step = 0$;

Step 2: Divide the population into p memeplexes and each memeplex contains q frogs, calculate the new position of Pw , Pb and Pg ;

Step 3: Generate Pw' with Eq.(9) and Eq. (10);

If Pw' is better than Pw , let $Pw = Pw'$;

Else, generate Pw'' with Eq.(9) and Eq. (10);

If Pw'' is better than Pw , let $Pw = Pw''$;

Else, replace Pw with a random frog Pn ;

Step 4: Shuffle the whole population, and $step = step + 1$;

Step 5: If $step < sn$, go to Step 2; Else, stop algorithm.

4 The SFLA Based Algorithm for HFS Problem

4.1 Encoding and Decoding

Classically, SFLA is used to solve continuous optimization. However, the HFS problem is a typical combinatorial optimization problem. To apply the standard SFLA to solve the HFS problem, special encoding and decoding schemes should be devised. In this paper, a real number matrix is used to encode a solution.

Considering a following $s \times n$ real value matrix:

$$M_{s \times n} = \begin{bmatrix} m_{11} & m_{12} & \cdots & m_{1n} \\ m_{21} & m_{22} & \cdots & m_{2n} \\ \cdots & \cdots & \cdots & \cdots \\ m_{s1} & m_{s2} & \cdots & m_{sn} \end{bmatrix} \quad (11)$$

where m_{ij} is a real number between 1 and $m(i)+1$ that means job j is processed on machine $\text{floor}(m_{ij})$ at stage i , and $\text{floor}(m_{ij})$ is the floor of number m_{ij} .

With the meaning of every element of the matrix, it can be decoded to a schedule of the HFS problem. It may happen that $\text{floor}(m_{ij}) = \text{floor}(m_{kj})$ since two or more jobs may be processed on one machine at one stage. If $\text{floor}(m_{ij}) = \text{floor}(m_{kj})$, then the machine processes the jobs in the decent order of the numbers, that is, if $m_{ij} \geq m_{kj}$, then the machine will process m_{ij} preferentially, otherwise m_{kj} will be processed preferentially. To conveniently perform the SFLA based search, we convert the matrix to the following vector to represent an individual:

$$\bar{M} = [m_{11}, \dots, m_{1n}, \dots, m_{k1}, \dots, m_{kn}] \quad (12)$$

Consider the instance with 3 jobs as showed in Fig. 1. Suppose $\bar{M} = [2.3, 1.7, 3.1, 1.0, 2.4, 1.1, 1.3, 2.7, 3.8]$. Clearly, it is corresponding to the

encoding matrix $M = \begin{bmatrix} 2.3 & 1.7 & 3.1 \\ 1.0 & 2.4 & 1.1 \\ 1.3 & 2.7 & 3.8 \end{bmatrix}$. According to value of each element, the

individual can be decoded as the following feasible schedule: the first column of the matrix illustrates that job 1 is processed on machine 2, 1, 1 at stage 1, 2, 3, respectively; the second column shows that job 2 is processed on machine 1, 2, 2 at the three stages, respectively; the third column tells that job 3 is processed on machine 3, 1, 3 at the three stages, respectively. Seen from the processing paths of the 3 jobs, it can be found that both job 1 and job 3 are processed on machine 1 at stage 2. As $1.0 < 1.1$, machine 1 at stage 2 will process job 3 preferentially. With the help of the above encoding and decoding schemes, the standard SFLA can be directly generalized to solve the HFS problem without changing its main searching operators.

4.2 Local Search Scheme

To accelerate the searching speed and improve the searching quality of SFLA, a local search is proposed and incorporated into the algorithm. Suppose the local search is applied to the following solution S . The local search methods include Swap, Insert and Inverse. The operator of each method is as follows. Randomly choose an integer u between 1 and s and two different integers v and w between 1 and n .

$$S = \begin{bmatrix} s_{11} & s_{12} & \cdots & s_{1n} \\ s_{21} & s_{22} & \cdots & s_{2n} \\ \cdots & \cdots & \cdots & \cdots \\ s_{k1} & s_{k2} & \cdots & s_{kn} \end{bmatrix} \quad (13)$$

Swap: Exchange the number s_{uv} and s_{uw} to generate a new individual S' . Only if the objective value of S' is better than S , then let $S=S'$.

Insert: Insert the number s_{uv} in front of the number s_{uw} to generate a new individual S' . Only if the objective value of S' is better than S , then let $S=S'$.

Inverse: Inverse the sub-sequence from s_{uv} till s_{un} to generate a new individual S' . Only if the objective value of S' is better than S , then let $S=S'$.

4.3 Meta-Lamarckian Learning Strategy

The Meta-Lamarckian learning strategy is used to adaptively decide which local search to be chosen. In this paper, this strategy is adopted to determine the special local search at each generation. At the beginning all the local searches are assigned an equal probability to be chosen, and then the probability for each local search is adjusted according to the solution improvement via the local search.

At the beginning, all the local searches are applied to the initial global best solution P_g for the same number of evaluations, and then the reward η_i of the i th local search is determined as follows [16]:

$$\eta_i = \begin{cases} c_p - c_c, & c_p > c_c \\ 0 & \end{cases} \quad i=1,2,\dots,h \quad (14)$$

where c_p denotes the makespan of the global best solution; c_c denotes the makespan of the solution after performing the i th local search; h denotes the number of local searches used. To reduce the effect of initial randomness, all the rewards are set as the average reward. Then the utilizing probability p_i for the i th

local search is calculated as $p_i = \eta_i / \sum_{j=1}^h \eta_j$.

During the searching process, different local searches are applied for a certain number of times t_p . Every time a roulette wheel rule is used to decide which local search to be used according to the utilizing probability of each neighborhood. If the i th local search is used, then its reward will be updated after applying this local search. That is, $\eta_i = \eta_i + \Delta\eta_i$, where $\Delta\eta_i$ denotes the sum of all the improvement on the makespan by using the i th local search.

The above process will be repeated t_p times. After that, if P_g is updated due to any of local search, then the utilizing probability of each local search will be updated; else, keep the utilizing probability. If the P_g is improved by the SFLA but not local

search, then reward of each local search will be re-initialized according to Eq. (14) in the next generation.

5 Simulation and Comparison

In this section, two problems with different scales [17, 18] are used for testing and comparison. Problem 1 has 12 jobs and 3 stages, and the number of machines in each stage is 3, 2 and 4, respectively. Problem 2 has 12 jobs and 4 stages, and the number of machines in each stage is 3, 3, 2 and 2, respectively. Please refer the literature for the detailed processing time of each job in every machine.

Set the following parameters: $p = 10$, $q = 10$, $t_p = 40$, $sn = 10000$ for Problem 1 and $sn = 18000$ for Problem 2. The SFLA algorithm is run 10 times independently, and the results are listed in Table 1-2, where the results of genetic algorithm (GA) [18, 19] and differential evolution (DE) [14] are directly from literature.

Table 1. Comparison with GA and DE for Problem 1

Test No.	1	2	3	4	5	6	7	8	9	10
GA [18]	30	27	26	27	29	27	26	27	26	28
DE [14]	24	24	24	24	24	25	24	24	24	25
SFLA	24	24	24	24	24	24	24	24	24	24

Table 2. Comparison with DE for Problem 2

Test No.	1	2	3	4	5	6	7	8	9	10	Best
GA [19]	-	-	-	-	-	-	-	-	-	-	347
DE [14]	313	319	313	302	302	315	315	319	302	299	299
SFLA	297	313	297	297	313	310	313	311	316	306	297

It can be seen from Table 1 and 2 that SFLA based algorithm outperforms GA and DE with the same evaluation times. For Problem 1, the SFLA algorithm can consistently obtain the optimal solution while GA and DE cannot. For Problem 2, the result of the SFLA is better than that of GA, even the worst result of the 10 tests is better than the result of GA. Besides, it can be seen that the results of the SFLA are better than those of DE in statistical sense. So, the proposed SFLA is more effective and robust than the existing GA and DE with the same computational effort.

6 Conclusion

In this paper, a SFLA based algorithm was proposed for solving the HFS problem. By using the special encoding and decoding schemes as well as by combining the Meta-Lamarckian learning strategy with the memetic search of SFLA, the proposed algorithm was effective and robust in solving the HFS problem. Numerical simulation and comparison showed that the SFLA was superior to the existing DE and GA. The future work is to develop SFLA for flexible job shop scheduling and batch process.

Acknowledgements. This work was supported by the National NSFC (60774082, 70871065, 60834004), Program for NCET-10-0505 and Doctoral Program Foundation of Institutions of Higher Education of China (20100002110014).

References

1. Ruiz, R.: The Hybrid Flow Shop Scheduling Problem. *European J. of Operational Research* 205(1), 1–18 (2010)
2. Grabowski, J., Pempera, J.: Sequencing of Jobs in Some Production System. *European J. of Operational Research* 125(3), 535–550 (2000)
3. Sheralli, H.D., Sarin, S.C., Kodialam, M.S.: Models and Algorithms for A Two-stage Production Process. *Production Planning and Control* 1(1), 27–39 (1990)
4. Liu, C.Y., Chang, S.C.: Scheduling Flexible Flow Shops with Sequence Dependent Setup Effects. *IEEE Transactions on Robotics and Automation* 16(4), 408–419 (2000)
5. Gupta, J.N.D.: Two-stage Hybrid Flow Shop Scheduling Problem. *J. of the Operational Research Society* 39(4), 35–364 (1988)
6. Johnson, S.M.: Optimal Two and Three-stage Production Schedules with Setup Times Included. *Naval Research Logistics Quarterly* 1, 61–68 (1954)
7. Brah, S.A., Hunsucker, J.L.: Branch and bound algorithm for the flow-shop with multiple processors. *European J. of Operational Research* 51(1), 88–99 (1991)
8. Kadipasaoglu, S.N., Xiang, W., Khumawala, B.M.: A Comparison of Sequencing Rules in Static and Dynamic Hybrid Flow Systems. *Int. J. of Production Research* 35(5), 1359–1384 (1997)
9. Vairaktarakis, G., Elhafsi, M.: The Use of Flowlines to Simplify Routing Complexity in Two-stage Flowshops. *IIE Transactions* 32(8), 687–699 (2000)
10. Bertel, S., Billaut, J.C.: A Genetic Algorithm for An Industrial Multiprocessor Flow Shop Scheduling Problem with Recirculation. *European J. of Operational Research* 159(3), 651–662 (2004)
11. Tseng, C.T., Liao, C.J.: A Particle Swarm Optimization Algorithm for Hybrid Flowshop Scheduling with Multiprocessor Tasks. *Int. J. of Production Research* 46(17), 4655–4670 (2008)
12. Ying, K.C., Lin, S.W.: Multiprocessor Task Scheduling in Multistage Hybrid Flowshops: An Ant Colony System Approach. *Int. J. of Production Research* 44(16), 3161–3177 (2006)
13. Logendran, R., deSzoek, P., Barnard, F.: Sequence-dependent Group Scheduling Problems in Flexible Flow Shops. *Int. J. of Production Economics* 102(1), 66–86 (2006)
14. Xu, Y., Wang, L.: Differential Evolution Algorithm for Hybrid Flow-shop Scheduling Problem. *Journal of Systems Engineering and Electronics* (2011)
15. Eusuff, M., Lansey, K.: Optimization of Water Distribution Network Design Using The Shuffled Frog Leaping Algorithm. *J. of Water Resources Planning and Management* 129(3), 210–225 (2003)
16. Ong, Y.S., Keane, A.J.: Meta-Lamarckian Learning in Memetic Algorithms. *IEEE Transactions on Evolutionary Computation* 8(2), 99–110 (2004)
17. Paternina-Arboleda, C.D., Montoya-Torres, J.R., Acero-Dominguez, M.J., Herrera-Hernandez, M.C.: Scheduling Jobs on A k-stage Flexible Flow-shop. *Annals of Operations Research* 164(1), 29–40 (2008)
18. Zhou, H.R., Tang, W.S., Wei, Y.H.: Optimize Flexible Flow-shop Scheduling Using Genetic Algorithm. *Computer Engineering and Applications* 45(30), 224–226 (2009)
19. Cui, J.S., Li, T.K., Zhang, W.X.: Hybrid Flowshop Scheduling Model and Its Genetic Algorithm. *J. of University of Science and Technology Beijing* 27(5), 623–626 (2005)

A Hybrid Algorithm Based on Simplex Search and Differential Evolution for Resource-Constrained Project Scheduling Problem

Ling Wang, Ye Xu, and Chen Fang

Tsinghua National Laboratory for Information Science and Technology (TNList),
Department of Automation, Tsinghua University,
Beijing, 100084, P.R. China
wangling@tsinghua.edu.cn,
{xuye05,fangchen06}@mails.tsinghua.edu.cn

Abstract. In this paper, an effective hybrid algorithm is proposed to solve the resource-constrained project scheduling problem by merging Nelder-Mead (NM) simplex method and differential evolution (DE). The individuals are encoded with the priority value based method and decoded by serial schedule generate scheme (SGS). Moreover, a reasonable framework is proposed to hybridize the simplex-based geometric search and the DE-based evolutionary search, and the simplex search is modified to further improve the quality of solutions obtained by DE. By interactively using the two methods with different mechanisms, the searching behavior can be enriched and the exploration and exploitation abilities can be well balanced. Simulation results based on some benchmarks demonstrate the effectiveness of the proposed hybrid algorithm.

Keywords: Resource-constrained project scheduling, Nelder-Mead simplex search, differential evolution, hybrid algorithm.

1 Introduction

The resource-constrained project scheduling problem (RCPSP) is concerned with the scheduling of the project activities as the resource is limited during a certain time. Each activity has a resource requirement and a duration time [1]. Some precedence relationships also exist between different activities. To solve the RCPSP is to give the reasonable schedules of the activities and utilization of the resources to minimize certain objective. In recent years, the RCPSP has gained increasing interest due to its wide academic and application background [2]. Moreover, it has been proved that the RCPSP is strongly NP-hard [1]. Thus, meta-heuristics have gained attention to solve the RCPSP.

Differential evolution (DE) performs its search process under the instruction of swarm intelligence produced by cooperation and competition between individual vectors in the species [3-5]. Although it has some advantages in finding global optimum, the local search ability of DE is weak and sometimes it may be trapped in local minima [6]. Nelder-Mead simplex method is a direct search [7] which is easy to

implement and has been widely applied to the problems with low dimensions, but its performance depends on the initial simplex and especially it is difficult to achieve good results for multi-dimensional problems [8, 9]. This paper will hybridize the simplex-based geometric search and the DE-based evolutionary search to solve the RCPSP, and carry out simulation tests and comparisons to verify the effectiveness.

The remainder of the paper is organized as follows. In Section 2 the RCPSP is introduced, and in Section 3 DE and NM simplex methods are briefly introduced. Then, the hybrid algorithm is proposed in Section 4. Simulation results are provided in Section 5. Finally, we end the paper with some conclusions in Section 6.

2 Problem Statement

The classical RCPSP considers a project with J activities. The activities 1 and J are dummy activities only to represent the start and end of the project respectively without resource and time costs. Due to the constraints, there is some precedence relationship between activities. For an activity k , if its predecessor l is not finished, then k cannot be started. The precedence relationship of an activity j is given as a set P_j of predecessors, which indicates that the activity j can be started only if each of its predecessors $i \in P_j$ is completed. Once an activity is started, it cannot be interrupted and its resource cannot be deprived. Assume that J activities share K kinds of resource. Let A_t be the set of activities being processed in time interval $[t-1, t]$. The total units of the m th resource are R_m , the requirement of activity k for resource m is denoted as r_{km} . Denote the duration and start times of activity k as d_k and S_k . The problem is to schedule all the activities with resource constraints to minimize makespan S_J . In Fig. 1, an example with 7 activities is illustrated.

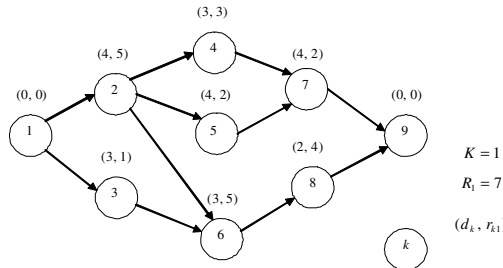


Fig. 1. An example of the RCPSP

3 DE and NM Simplex Method

3.1 Differential Evolution

DE is a population-based stochastic optimization technique [10]. According to the comprehensive study [11], DE outperforms many other methods like GA in terms of

convergence speed and robustness over some benchmark problems and real-world applications. DE differs from other evolutionary algorithms in the sense that distance and direction information from the current population is used to guide the search process [12]. The DE denoted as *DE/rand/1/bin* is adopted in this paper, whose searching power is accredited to parent choice (selection), differential operator (mutation), discrete crossover (crossover) and greedy selection (decision) [13].

Selection: All the individuals in the population have the same chance to generate candidate individuals. For each individual X_i , three other individuals are randomly selected from current population such that the four individuals are different from each other. Thus, a pool of four parents is formed.

Mutation: A mutated individual V_i is generated with the three different individuals randomly chosen by selection as $V_i = X_{r1} + F(X_{r2} - X_{r3})$, where F is a positive real number less than 1.

Crossover: A trial individual T_i is formed by recombination of the elements of X_i and V_i one by one as $t_{i,j} = \begin{cases} v_{i,j} & \text{if } r \leq cr \text{ or } j = sn \\ x_{i,j} & \text{otherwise} \end{cases} \quad j = 1, \dots, n$, where $t_{i,j}$ is the j th element of the trial individual T_i , r is a uniformly random number in $[0,1]$, cr is a real number in $[0,1]$ to control the ratio of selection between of the parent and mutated vector, and sn is an index randomly chosen to ensure that at least one element of V_i will be inherited.

Decision: Greedy selection between the trial vector T_i and X_i is applied and the one with better function value f_i will be promoted to the next generation, where f_i is the objective function of the individual i .

3.2 The Nelder-Mead Simplex Search Method

The NM simplex search method is a direct search designed for unconstrained optimization without using gradient information [3]. The procedure of this method is to rescale the simplex based on the local behavior by using four basic operators: reflection, expansion, contraction and shrink. With these operators, the simplex can successfully improve itself and get closer to the optimum. The original NM simplex procedure is outlined in [3], where all the steps are described as follows.

Initialization: To minimize a function with n variables, create $n+1$ vertex points randomly to form an initial n -dimensional simplex. Evaluate the function value at each vertex point and order the $n+1$ vertices to satisfy $f(X_1) \leq f(X_2) \dots \leq f(X_{n+1})$.

Reflection: Calculate the reflection point $X_r = \bar{X} + \alpha(\bar{X} - X_{n+1})$, where $\bar{X} = \sum_{i=1}^n X_i / n$ is the centroid of the n best points (all vertices except for X_{n+1}),

and $\alpha > 0$ is the reflection coefficient. If $f(X_1) \leq f(X_r) < f(X_n)$, then accept the reflected point X_r and terminate the iteration.

Expansion: If $f(X_r) < f(X_1)$, calculate the expansion point $X_e = \bar{X} + \beta(X_r - \bar{X})$, where $\beta > 1$ is the expansion coefficient. If $f(X_e) \leq f(X_r)$, then accept the expanded point X_e and terminate the iteration; otherwise accept X_r and terminate the iteration.

Contraction: If $f(X_r) \geq f(X_n)$, then perform a contraction between \bar{X} and the better of X_{n+1} and X_r .

(a) If $f(X_r) < f(X_{n+1})$, then perform outside contraction $X_c = \bar{X} + \gamma(X_r - \bar{X})$, where $\gamma \in (0,1)$ is the contraction coefficient. If $f(X_c) \leq f(X_r)$, then accept X_c and terminate the iteration; otherwise go to Shrink step.

(b) If $f(X_r) \geq f(X_{n+1})$, perform inside contraction $X_c = \bar{X} - \gamma(\bar{X} - X_{n+1})$. If $f(X_c) \leq f(X_{n+1})$, accept X_c and terminate the iteration; otherwise go to Shrink.

Shrink: Shrink operator is performed by $V_i = X_1 + \delta(X_i - X_1)$, $i = 2, \dots, n+1$, where $\delta \in (0,1)$ is the shrinkage coefficient. The simplex obtained by shrink is denoted as $V = \{X_1, V_1, V_2, \dots, V_{n+1}\}$ for the next iteration.

4 Hybrid NM-DE Algorithm for RCPSP

4.1 The Scheduling Generation Scheme

The serial schedule generate scheme (SGS) is used to generate a feasible schedule. SGS includes J steps, and the n th ($n=1, \dots, J$) step is corresponding to a incomplete scheduling PS_n that contains the complete part of the scheduling and a set D_n of activities to be scheduled. For each activity in D_n , all its predecessors belong to PS_n . In SGS, one activity is selected if its predecessor activity can be completed firstly and the resource constraints can be satisfied. The procedure of SGS is summarized as follows:

Step 1: Initialize $n = 1, S_1 = 0, PS_1 = \{1\}$;

Step 2: If $n \leq J$, continue; else, end the procedure;

Step 2.1: Calculate D_n , determine the total amount $R_m(r)$ of resource r ;

Step 2.2: Choose a activity k in D_n ;

Step 2.3: Calculate the earliest start time ES_k of activity k ,

$$ES_k = \max\{S_i + d_i \mid i \in P_k\};$$

Step 2.4: Calculate $S_k = \min\{t \mid t \geq ES_k, r_{km} \leq R_m(\tau), m = 1, 2, \dots, K, \tau = [t, t + d_k]\}$;

Step 2.5: Update $PS_{n+1} = PS_n \cup \{k\}$, $n = n + 1$, and go to Step 2.

4.2 The Encoding and Decoding Schemes

The RCPSP is a combinatorial optimization problem, while both simplex search and DE methods are originally used to solve continuous optimization problems. To apply the algorithms to solve the RCPSP, special encoding and decoding schemes should be devised. In this paper, a priority based method is used.

For a project that consists of n activities, the algorithm uses a real number vector \bar{X} as a solution. The number in each dimension is a real number between 0 and 1. The larger the number is, the higher priority the activity has in the scheduling process. Assume that the numbers of the first and last dummy activity all equal to 1. When arranging the schedules, activities with highest priority should be scheduled first. Consider a solution $\bar{X} = (1, 0.39, 0.54, 0.27, 0.10, 0.98, 0.77, 0.59, 1)$ for the problem in Fig. 1, the schedule generated by SGS is shown in Fig. 2.

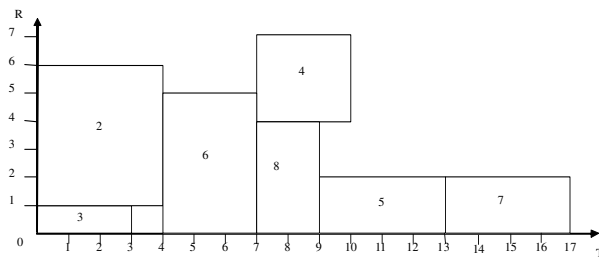


Fig. 2. A schedule generated by SGS

4.3 The NM-DE Algorithm

The hybrid framework fusing the NM and DE methods is illustrated in Fig. 3.

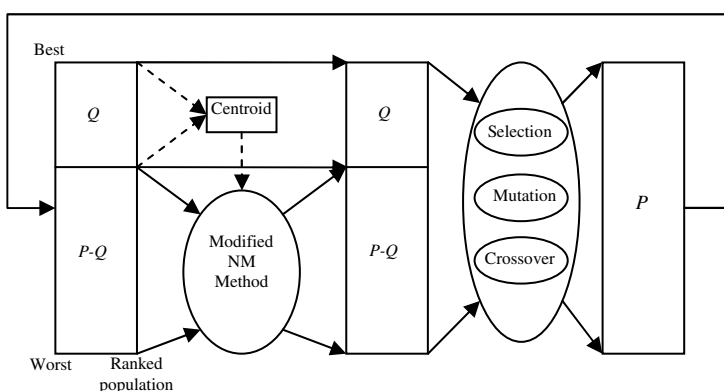


Fig. 3. Schematic framework of the NM-DE hybrid algorithm

It can be seen from Fig. 3 that NM simplex search and DE-based evolutionary search are hybridized. During each generation, the population will be improved both by differential evolution and simplex search. The information of the best individuals is well used to guide the local search of the algorithm. Thus, the advantages of these two methods could be utilized together. Moreover, the classic NM simplex search is modified, which is used to guide the search towards promising region, which can enhance the local search ability.

Suppose the population size is P , the initial P points are randomly generated from the n -dimensional space. First, the P individuals are ranked from best to worse according to the objective values. Then, the top Q individuals are used to calculate the initial simplex centroid for the NM method. For the left $P-Q$ individuals, each will perform an iteration of simplex search with the calculated centroid $\bar{X} = \sum_{i=1}^Q X_i / Q$.

When dealing with the shrink step, just shrink the single point to the best point until it reaches a better objective value while keeping the positions of the other points fixed instead of shrinking all simplex points as original NM simplex method does. For example, for the point X_j , generate the shrink point $V_j = X_1 + \delta(X_j - X_1)$. If $f(V_j) \leq f(X_j)$, then accept V_j ; otherwise, keep on shrinking operation until the termination condition is satisfied.

After performing the modified NM simplex search method, $P-Q$ new individuals are generated. Then the $P-Q$ new individuals and the original Q individuals from the initial population are merged to form the initial population of DE-based evolutionary search. Through a generation of DE-based search, P new individuals are generated. After ranking these new individuals, the modified NM simplex search is performed once again. The above interactive search process based on simplex search and DE based search is repeated until a predefined stopping criterion is satisfied.

5 Numerical Simulation and Comparisons

In this section, the proposed algorithm is tested with the well-known data sets PSPLB by using J30, J60 and J120 each with 10 testing problems. Set $P=100$, $F=0.9$, $Cr=0.9$, $\alpha=1$, $\beta=1.5$, $\gamma=0.5$, $\delta=0.5$, $Q=n+2$, where n is the problem scale. As for the stopping criterion, we set the maximum number of evaluations as 5000, 10000, 20000. The experiments are done on Intel Pentium 1600MHz / 2GB-RAM in VS 2005. For each problem, NM-DE is independently run 10 times. The results are listed in Table 1, where T is of the obtained best makespan while T^* is the best known makespan.

From Table 1, it can be seen that for J30 NM-DE can find the best schedules of problem 1~8 and 10 when the maximum number of schedules are 5000 and 10000. As the number increases, the algorithm can get all the best solutions, while the deviation rate is within 2.5% when the number is 5000 or 10000. For J60, it can be seen that when the maximum number of schedules is 5000, NM-DE can obtain 8 best solutions out of 10 instances and the deviation rate is small for instances 7 and 8. As the maximum number of schedules increases to 10000, the deviation rates for instances 7 and 8 get smaller; when the maximum number reaches 20000, the deviation rates for

instances 7 and 8 are within 1.4%. For J120, NM-DE still has certain optimization ability when the maximum number is 5000. As the number increases, the performance of NM-DE improves. When the number reaches 20000, the deviation rates are less than 8.5%.

To further test the performance of NM-DE, we compare it with some existing algorithms. Due to the limitation of paper space, we only use J30 with 480 problems for testing. The maximum numbers of schedules are set as 1000, 5000, 50000, and the average percent deviations of the obtained makespan from the optimal makespan are compared in Table 2. It can be seen that NM-DE outperforms some existing methods.

Table 1. Simulation results of NM-DE on three sets

No.	5000 schedules						10000 schedules						20000 schedules														
	J30			J60			J120			J30			J60			J120			J30			J60			J120		
	T	T*	T	T*	T	T*	T	T*	T	T*	T	T*	T	T*	T	T*	T	T*	T	T*	T	T*	T	T*	T	T*	
1	43	43	77	77	77	77	43	43	77	77	77	77	43	43	77	77	77	77	77	77	77	77	77	77	77		
2	47	47	68	68	68	68	47	47	68	68	68	68	47	47	68	68	68	68	68	68	68	68	68	68	68		
3	47	47	68	68	68	68	47	47	68	68	68	68	47	47	68	68	68	68	68	68	68	68	68	68	68		
4	62	62	91	91	91	91	62	62	91	91	91	91	62	62	91	91	91	91	91	91	91	91	91	91	91		
5	39	39	73	73	73	73	39	39	73	73	73	73	39	39	73	73	73	73	73	73	73	73	73	73	73		
6	48	48	66	66	66	66	48	48	66	66	66	66	48	48	66	66	66	66	66	66	66	66	66	66	66		
7	60	60	74	72	74	72	60	60	73	72	73	72	60	60	73	72	72	60	60	73	72	73	72	72	72		
8	53	53	78	75	78	75	53	53	77	75	77	75	53	53	76	75	76	75	76	75	76	75	76	75	75		
9	50	49	85	85	85	85	50	49	85	85	85	85	49	49	85	85	85	85	85	85	85	85	85	85	85		
10	45	45	80	80	80	80	45	45	80	80	80	80	45	45	80	80	80	80	80	80	80	80	80	80	80		

Table 2. Comparison of average deviations (%)

Algorithm	Max. No of schedules		
	1000	5000	50000
NM-DE	1.23	0.73	0.27
Sampling-random [14]	1.44	1.00	0.51
GA-priority rule [15]	1.38	1.12	0.88
Sampling-WCS [16]	1.40	1.28	-
Sampling-LFT [17]	1.40	1.29	1.13
GA-problem space [18]	2.08	1.59	-

6 Conclusion

In this paper, NM simplex method and DE were reasonably hybridized for solving the RCPSP. By using a continuous encoding scheme and a decoding scheme based on SGS, the NM-DE was applied to RCPSP conveniently. With the local search via the modified NM method and the evolutionary search via DE, NM-DE algorithm was of superior searching ability. Simulation results and comparisons demonstrated the effectiveness of the NM-DE. The future work is to design adaptive mechanisms and to apply the algorithm to the multi-mode RCPSP.

Acknowledgements. This research was supported by NSFC (70871065, 60834004) and Program for New Century Excellent Talents in University (NCET-10-0505) as well as Doctoral Program Foundation of Institutions of Higher Education of China (20100002110014).

References

1. Brucker, P., Drexl, A., Moring, R., Neumann, K., Pesch, E.: Resource-constrained Project Scheduling: Notation, Classification, Models, and Methods. *European J. of Operational Research* 112(1), 3–41 (1999)
2. Fang, C., Wang, L., Xu, Y.: An Estimation of Distribution Algorithm for Resource-constrained Project Scheduling Problem. In: Chinese Control and Decision Conference, Xuzhou, pp. 265–270 (2010)
3. Xu, Y., Wang, L., Li, L.: An Effective Hybrid Algorithm Based on Simplex Search and Differential Evolution for Global Optimization. In: Huang, D.-S., Jo, K.-H., Lee, H.-H., Kang, H.-J., Bevilacqua, V. (eds.) ICIC 2009. LNCS, vol. 5755, pp. 341–350. Springer, Heidelberg (2009)
4. Price, K., Storn, R.M., Lampinen, J.A.: Differential Evolution: A Practical Approach to Global Optimization. Springer, New York (2005)
5. Rahman, S., Tizhoosh, H.R., Salama, M.M.A.: Opposition-Based Differential Evolution. *IEEE Transactions on Evolutionary Computation* 12(1), 64–79 (2008)
6. Isaacs, A., Ray, T., Smith, W.: A Hybrid Evolutionary Algorithm with Simplex Local Search. In: IEEE CEC, pp. 1701–1708 (2007)
7. Fan, S.K.S., Zahara, E.: A Hybrid Simplex Search and Particle Swarm Optimization for Unconstrained Optimization. *European J. Operational Research* 181, 527–548 (2007)
8. Nelder, J.A., Mead, R.: A Simplex Method for Function Minimization. *Computer J.* 7(4), 308–313 (1965)
9. Lagarias, J.C., Reeds, J.A., Wright, M.H., et al.: Convergence Properties of the Nelder-Mead Simplex Method in Low Dimensions. *SIAM J. Optimization* 9(1), 112–147 (1999)
10. Ali, M.M.: Differential Evolution with Preferential Crossover. *European J. Operational Research*. 181, 1137–1147 (2007)
11. Storn, R., Price, K.: Differential evolution - A Simple and Efficient Heuristic for Global Optimization over Continuous Spaces. *J. Global Optimization* 11(4), 341–359 (1997)
12. Czajkowski, K., Fitzgerald, S., Foster, I., Kesselman, C.: Real-parameter Optimization with Differential Evolution. *Evolutionary Computation* 2(1), 506–513 (2005)
13. Omran, M.G.H., Engelbrecht, A.P., Salman, A.: Bare Bones Differential Evolution. *European J. Operational Research* 196(1), 128–139 (2009)
14. Kolisch, R.: Project Scheduling under Resource Constraints—Efficient Heuristics for Several Problem Classes. *Physica* 14 (1995)
15. Hartmann, S.: A Competitive Genetic Algorithm For Resource-constrained Project Scheduling. *Naval Research Logistics* 45, 733–750 (1998)
16. Kolisch, R.: Efficient Priority Rules for the Resource Constrained Project Scheduling Problem. *Journal of Operations Management* 14, 179–192 (1996)
17. Kolisch, R.: Serial and Parallel Resource-constrained Project Scheduling Methods Revisited: Theory and Computation. *European J. of Operational Research* 90, 320–333 (1996)
18. Leon, V.J., Ramamoorthy, B.: Strength and Adaptability of Problem-space Based Neighborhoods for Resource-constrained Scheduling. *OR Spektrum* 17, 173–182 (1995)

A Differential Evolution Algorithm for Lot-Streaming Flow Shop Scheduling Problem

Hongyan Sang^{1,2}, Liang Gao¹, and Xinyu Li^{1,*}

¹ State Key Lab. of Digital Manufacturing Equipment & Technology in Huazhong University of Science & Technology, Wuhan, 430074, P.R. China

² School of Mathematics Science, LiaoCheng University, 252059, LiaoCheng, P.R. China
lixinyu@mail.hust.edu.cn

Abstract. A differential evolution (DE) algorithm is proposed to minimize the total weighted tardiness and earliness penalties for lot-streaming flow shop scheduling problems. In the proposed DE algorithm, the largest position value (LPV) rule is used to convert a real-number DE vector to a job permutation. The DE evolution is used to perform global exploitation, and a local search procedure is used to enhance the exploration capability. Extensive computational simulations and comparisons are provided, which demonstrate the effectiveness of the proposed DE algorithm.

Keywords: lot-streaming flow shop scheduling, weighted earliness and tardiness, differential evolution algorithm, local search.

1 Introduction

This paper considers the n -job, m -machine lot-streaming flow shop scheduling problem with total weighted earliness and tardiness penalties criterion. In recent years, the problem has attracted much attention [1]. Vickson and Alfredsson [2], Sriskandarajah [3], and Marimuthu and Ponnamblam [4] researched the multi-job flow shop scheduling problem with two or three machines. Kumar et al. [5] extended the approach in Sriskandarajah [3] to an m -machine case. Marimuthu et al. [4, 6] proposed some algorithms for an m -machine flow shop with makespan and total flow time criteria. With the advent of just-in-time, the criterion involving both earliness and tardiness penalties has received significant attention [7]. Yoon and Ventura [8] presented sixteen pairwise interchange methods and a hybrid genetic algorithm (HGA) [9]. Tseng and Liao [7] developed a discrete particle swarm optimization (DPSO). Pan et al. [10] presented a discrete artificial bee colony algorithm. The experiments by the authors demonstrated the above algorithms are effective and efficient for the problem considered.

The differential evolution (DE) algorithm, introduced by Storn and Price [11], is a simple yet powerful search technique for solving complex continuous nonlinear functions. Due to its simplicity, easy implementation, and quick convergence, the

* Corresponding author.

DE algorithm has gained much attention with successful applications in mechanical engineering, data handing network, shop scheduling, communication, and etc [12-15]. In this paper, we propose a DE algorithm for the problem considered. Simulation results and comparisons demonstrate the effectiveness of the proposed DE algorithm.

The rest of the paper is organized as follows. In section 2, the problem is formulated. Section 3 describes the basic components of the proposed DE algorithm. The computational results and comparisons are described in section 4. Finally, section 5 presents the concluding remarks.

2 Problem Definition

There is a flow shop with n jobs and m machines. Each job j should be sequentially processed on m machines and the job sequence is the same on each machine i . The job j can be split into s_j smaller sublots with equal size such that s_j is the same for all the machines. Once the processing of a subplot on a machine is completed, it can be transferred to the downstream machine immediately. All the s_j sublots of job j should be processed continuously. Let π denote a processing sequence of the jobs; E_j is the earliness of job j ; and T_j is the tardiness of job j ; α_j and β_j be the earliness and tardiness penalties of job j , respectively. Then the objective is to find a sequence to minimize the total weighted earliness and tardiness penalties, which is calculated by

$$\min f(\pi) = \sum_{j=1}^n (\alpha_j E_j + \beta_j T_j) \quad (1)$$

3 The Proposed DE Algorithm

In this section, we present a DE algorithm for the problem considered, and detail its solution representation, population initialization, mutation, crossover, selection and local search procedure.

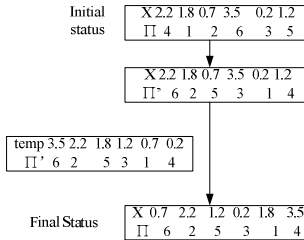
3.1 Solution Representation and Population Initialization

An individual $X_i = \{x_i(1), x_i(2), \dots, x_i(n)\}$ is represented as an n -dimensional real number vector. It is necessary to convert it to a job permutation for evaluating the objective value. Let each index of the dimensions of the vector represent a typical job from $J = \{1, 2, \dots, n\}$, and then n indexes denote n different jobs. Then the largest position value (LPV) rule is employed to obtain a job permutation $\pi = \{\pi(1), \pi(2), \dots, \pi(n)\}$ by ordering the jobs in their non-increasing position value of X_i . A simple example is illustrated in table 1.

Table 1. An example for the LPV rule

Job j	1	2	3	4	5	6
X	1	0	-	2	-	0
Job permutation	4	1	2	6	3	5

To guarantee an initial population with certain quality and diversity, it is common to use priority rules to produce a portion of good individuals and the rest are produced randomly. Since the earliest due date (EDD), the smallest slack time on the last machine (LSL), and the smallest overall slack time (OSL) rules are commonly used to produce initial sequences for the scheduling problems with total weighted earliness and tardiness criterion, this paper applies these rules to generate three initial sequences, respectively. However, due to the real number representation is adopted, it is necessary to convert the sequences to the DE individuals. The conversion process is given in Fig. 1, where X is an individual vector, Π is the corresponding job sequences, Π' is the new job sequence, and temp is a temporary array. Final status is the result after conversion.

**Fig. 1.** Job permutation convert to individual

Other individuals are produced as follows

$$x_i(j) = x_{\min}(j) + (x_{\max}(j) - x_{\min}(j)) \times r \quad j = 1, 2, \dots, n, \quad x_i(j) \in X_i \quad (2)$$

where r represents a random value uniformly generated between 0 and 1, $X_{\min} = \{x_{\min}(1), x_{\min}(2), \dots, x_{\min}(n)\}$ and $X_{\max} = \{x_{\max}(1), x_{\max}(2), \dots, x_{\max}(n)\}$ are the lower bound and upper bound of the search space, respectively.

3.2 Generation of New Individuals

The DE operators include mutation, crossover, and selection, which are given as follows.

3.2.1 Mutation

A mutant individual, $V_i = \{v_i(1), v_i(2), \dots, v_i(n)\}$, $i = 1, 2, \dots, NP$, is generated via a mutation operator. NP is the number of individuals. There are many mutation strategies in the literature [11]. We follow the commonly used DE/rand/1 below:

$$V_i = X_{best} + F \times (X_{r_1} - X_{r_2}) \quad (3)$$

where X_{best} is the best individual in the current target population, X_{r_1} and X_{r_2} are two target individuals randomly chosen such that $r_1 \neq r_2 \neq i \in \{1, \dots, NP\}$, and $F > 0$ is a mutation scale factor that affects the differential variation between two individuals. If the value of the obtained mutant individual exceeds the upper bound or lower bound, it will be set equal to the closer bound.

3.2.2 Crossover

Following the mutation operator, a crossover operator is applied to yield a trial vector $U_i = \{u_i(1), u_i(2), \dots, u_i(n)\}$ by considering the mutant individual and its corresponding target one as follows:

$$u_i(j) = \begin{cases} v_i(j) & \text{if } r_j \leq CR \text{ or } j = n_j \\ x_i(j) & \text{otherwise} \end{cases}, \quad j = 1, 2, \dots, n \quad (4)$$

where n_j refers an index randomly chosen from the set $\{1, 2, \dots, n\}$ to ensure that at least one dimension of the trial individual U_i differs from its counterpart X_i in the current generation, and CR is a crossover constant between 0 and 1, and $r_j \in [0, 1]$ is a uniformly random number.

3.2.3 Selection

After mutation and crossover phases, a one-to-one greedy selection scheme is applied to decide whether or not the trial individual U_i should become a member of the target population in next generation. The selection scheme is based on the survival of the fittest between the trial individual U_i and its target counterpart X_i . For a minimization problem, it can be formulated as follows:

$$X'_i = \begin{cases} U_i & \text{if } f(U_i) \leq f(X_i) \\ X_i & \text{otherwise} \end{cases} \quad (5)$$

where $f(U_i)$ and $f(X_i)$ are the objective values of U_i and X_i , respectively.

3.3 Local Search

To enhance the searching ability, we incorporate a local search by improving each trial individual generated in the crossover phase. Since the trial vector is a real vector, the LPV rule is first used to convert it into a job permutation. And then, an insertion heuristic [16] is applied. The insertion heuristic is based on a first-improvement type of pivoting rule. Let $\pi = \{\pi(1), \pi(2), \dots, \pi(n)\}$ be the job permutation to undergo the insertion heuristic, $\alpha = \{\alpha(1), \alpha(2), \dots, \alpha(n)\}$ be a reference job permutation

generated randomly, and $\phi = \{\phi(1), \phi(2), \dots, \phi(n)\}$ be the final sequence by the insertion heuristic. The procedure for the insertion heuristic is given as follows:

- Step 1: Set $Cnt = 0$, $j = 0$, and $\phi = \pi$.
- Step 2: Set $j = j + 1$. If $j > n$, then let $j = j - n$.
- Step 3: Remove the job that corresponds to job $\alpha(j)$ from its original position in the permutation ϕ , and insert it into all the other possible slots, respectively. Denote ω as the best obtained sequence.
- Step 4: If ω is better than ϕ , then let $\phi = \omega$ and $Cnt = 0$; Otherwise, let $Cnt = Cnt + 1$.
- Step 5: If $Cnt \leq n$, then go back to Step 2; Otherwise stop the procedure and return ϕ .

After the local search, the obtained sequence is converted to a real-number DE individual.

4 Computational Results

4.1 Experimental Setup

To test the proposed DE algorithm, we randomly generates 20 problem with the sizes $n = 10, 20, 30, 40$ and $m = 3, 5, 7, 10, 15$. The related data is given by the uniform distribution as follows: $s_j \in U(1,6)$, $\alpha_j \in U(1,6)$, $\beta_j \in U(1,6)$, $x_{\min} = 0$, $x_{\max} = 4$. We realize the algorithms in Visual C++ and conduct experiments on a Pentium PIV 3.0 GHz PC with 1G MB memory. The parameters for the proposed DE algorithm are set as: $NP=40$, $F = 0.5$, $CR = 0.7$. On the other hand, for the algorithms from the literature, their parameters were fixed at the same ones as given in their original papers. In addition, all the algorithms adopted the same termination criterion, i.e. the maximum elapsed CPU time $CT = 0.05mn$ seconds. For each instance, we carried out 30 independent replications and calculate the relative percentage increase (RPI) as follows:

$$RPI(O_i) = \frac{O_i - C^*}{C^*} \times 100 \quad (6)$$

where O_i is the objective function value generated in the i th replication, and C^* is the best objective function value found among all the algorithms. In addition, we also calculate the average relative percentage increase (ARPI) and standard deviation (SD) as statistics for the solution quality.

4.2 Computational Results

We compare our DE algorithm with several existing meta-heuristics including DPSO developed by Tseng and Liao [7], and HGA by Yoon and Ventura [9]. The results are

given in Table 2. It can be easily seen from Table 2 that the proposed DE algorithm is the winner among the compared algorithm, since it produces the lowest average percentage increase (0.28) and standard deviation (0.17). More specifically, the DE algorithm yields significantly better results for all the problem sizes when comparing to HGA. In comparison to DPSO, the DE algorithm produces significantly better results for 14 out of 20 problem sizes. The compared algorithms' convergence curves of instance 20×10 is given in Fig.2, which show that on average the proposed DE algorithm reaches lower levels than those of the HGA and DPSO. For other instances, the convergence trend of the compared algorithm is almost similar. Therefore, it is concluded that the DE algorithm outperforms both the HGA and DPSO algorithms to minimize the total weighted earliness and tardiness penalties for the lot-streaming flow shop scheduling problem with the same computational effort.

5 Conclusions

This paper aimed at minimizing total weighted earliness and tardiness penalties for the lot-streaming flow shop scheduling problems. We presented a differential evolution algorithm by combining the DE-based global search and a local search to balance the global exploration and local exploitation. Computational simulations and comparisons demonstrated the superiority of the proposed algorithms in terms of solution quality.

Table 2. Computation of the compared algorithms

n×m	DPSO		DE		HGA	
	ARPI	SD	ARPI	SD	ARPI	SD
10×3	0.11	0.26	0	0	11.12	8.49
10×5	0	0	0	0	14.11	6.07
10×7	0	0	0	0	13.23	6.23
10×10	0	0	0	0	11.50	5.18
10×15	0.13	0.43	0.1	0.3	12.76	5.80
20×3	0.00	0.00	0	0	52.16	7.01
20×5	0.15	0.17	0.14	0.11	54.65	9.18
20×7	0	0	0	0	55.57	8.83
20×10	0.23	0.25	0.21	0.21	44.56	7.87
30×15	0.00	0.00	0	0	55.63	9.89
30×3	1.74	1.94	0.08	0.08	84.67	12.23
30×5	0.75	1.83	0	0	74.65	11.11
30×7	0.86	0.85	0.63	0.54	81.07	8.01
30×10	0.15	0.16	0.06	0.04	79.26	8.09
30×15	0.38	1.45	0	0	87.07	9.06
40×3	12.65	3.41	0.75	0.80	97.20	9.37
40×5	8.98	2.77	1.59	0.78	96.16	9.21
40×7	3.48	2.21	1.36	0.15	82.08	5.56
40×10	2.01	1.79	0.27	0.18	90.26	9.67
40×15	1.08	0.89	0.38	0.12	91.21	7.88
Mean	1.64	0.92	0.28	0.17	59.45	8.24

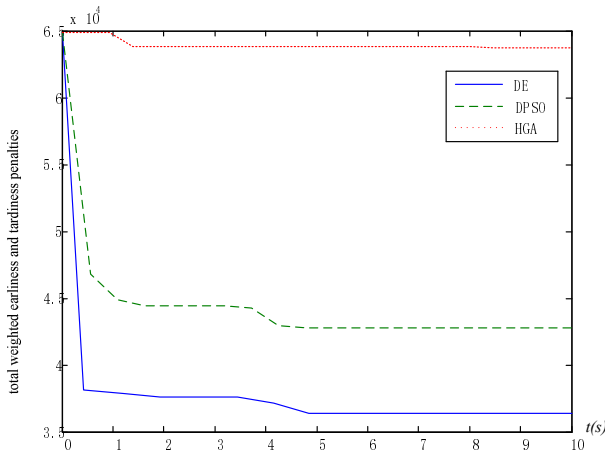


Fig. 2. The convergence curves of instance 20×10

Acknowledgments. This research is partially supported by National Science Foundation of China (Grants No. 60973085, 51005088), New Century Excellent Talents in University (Grant No. NCET-08-0232).

References

1. Chang, J.H., Chiu, H.N.: A Comprehensive Review of Lot Streaming. *International Journal of Production Research* 43(8), 1515–1536 (2005)
2. Vickson, R.G., Alfredsson, B.E.: Two- and three-machine Flow Shop Scheduling Problems with Equal Size Transfer Batches. *International Journal of Production Research* 30(7), 1551–1574 (1992)
3. Sriskandarajah, C., Wagener, E.: Lot Streaming and Scheduling Multiple Products in Two-Machine no-wait Flowsshops. *IIE Transactions* 31(8), 695–707 (1999)
4. Marimuthu, S., Ponnambalam, S.G., Jawahar, N.: Evolutionary Algorithms for Scheduling m-machine Flow Shop with Lot Streaming. *Robotics and Computer-Integrated Manufacturing* 24, 125–139 (2008)
5. Kumar, S., Bagchi, T.P., Sriskandarajah, C.: Lot Streaming and Scheduling Heuristics for m-machine No-wait Flowsshops. *Computers & Industrial Engineering* 38(1), 149–172 (2000)
6. Marimuthu, S., Ponnambalam, S.G., Jawahar, N.: Threshold Accepting and Ant-colony Optimization Algorithm for Scheduling m-machine Flow Shop with Lot Streaming. *Journal of Material Processing Technology* 209, 1026–1041 (2009)
7. Tseng, C.T., Liao, C.J.: A Discrete Particle Swarm Optimization for Lot-streaming Flowshop Scheduling Problem. *European Journal of Operational Research* 191, 360–373 (2008)
8. Yoon, S.H., Ventura, J.A.: An Application of Genetic Algorithms to Lot-streaming Flow Shop Scheduling. *IIE Transactions* 34, 779–787 (2002)

9. Yoon, S.H., Ventura, J.A.: Minimizing the Mean Weighted Absolute Deviation from Due Dates in Lot-streaming Flow Shop Scheduling. *Computers & Operations Research* 29, 1301–1315 (2002)
10. Pan, Q.K., Suganthan, P.N., Tasgetiren, M.F., Chua, T.J.: A Novel Artificial Bee Colony Algorithm for A Lot-streaming Flow Shop Scheduling Problem. *Information Sciences* 181, 2455–2468 (2011)
11. Storn, R., Price, K.V.: Differential Evolution-A Simple and Efficient Heuristic for Global Optimization over Continuous Spaces. *Journal of Global Optimization* 11, 341–359 (1997)
12. Ilonen, J., Kamarainen, J.K., Lampinen, J.: Differential Evolution Training Algorithm for Feed-forward Neural Networks. *Neural Processing Letters* 17, 93–105 (2003)
13. Joshi, R., Sanderson, A.C.: Minimal Representation Multisensor Fusion Using Differential Evolution. *IEEE Trans. Systems, Man, and Cybernetics (Part A)* 29, 63–76 (1999)
14. Onwubolu, G.C.: Design of Hybrid Differential Evolution and Group Method of Data Handling Networks for Modeling and Prediction. *Information Sciences* 178, 3616–3634 (2008)
15. Pan, Q.K., Wang, L., Qian, B.: A Novel Differential Evolution Algorithm for Bi-criteria No-wait Flow Shop Scheduling Problems. *Computers and Operations Research* 36, 2498–2511 (2009)
16. Wang, L., Pan, Q.K., Tasgetiren, M.F.: Minimizing the Total Flow Time in a Flow Shop with Blocking by Using Hybrid Harmony Search Algorithms. *Expert Systems with Applications* 37, 7929–7936 (2010)

Flexible Job Shop Scheduling Problem by Chemical-Reaction Optimization Algorithm

Junqing Li, Yuanzhen Li, Huaqing Yang, Kaizhou Gao, Yuting Wang, and Tao Sun

School of Computer, Liaocheng University, Liaocheng, 252059

Abstract. In this paper, we propose a novel discrete chemical-reaction optimization (DCRO) algorithm for solving the flexible job shop scheduling problem with three objectives. The molecule is used to represent a solution. The four elementary reactions, i.e., the on-wall ineffective collision, the decomposition, the inter-molecular ineffective collision, and the synthesis, are used as the operators for the hybrid algorithm. In the hybrid algorithm, the crossover operator is embedded to learn information among molecules. To increase the ability to escape from the local optima, the buffer is used as the energy center to share kinetic energy among molecules. Experimental results on the well-known benchmarks show the efficiency and effectiveness of the proposed algorithm.

Keywords: Flexible job shop scheduling problem, chemical-reaction optimization, multi-objective optimization.

1 Introduction

The flexible job shop scheduling problem (FJSP) is an extension version of the classical job shop scheduling problem (JSP). In literature, JSP has been verified to be an NP-hard problem. The FJSP is considered harder than JSP because of the addition of the selection of machine for each operation. Thus, heuristics and meta-heuristics has become an alterative approach for solving the FJSPs. Among these meta-heuristics, TS has been verified to be an efficient algorithm, which has been proposed and enhanced by many researchers, such as Brandimarte (1993) [1], Mastrolilli et al. (2000) [2], Li et al. (2010) [3], and Bozejko et al. (2010) [4]. In very recent years, many researchers have considered the importance of solving the FJSPs with multiple objectives. Xia and Wu (2005) [5] developed a hybrid method utilizing the PSO and the simulated annealing (SA). Gao et al. (2008) [6] provided the hGA method for the problem. Follows the above efficient algorithms, Zhang et al. (2009) [7] introduced a hybrid PSO and TS algorithm. Li et al. (2010) [8] investigated the TS algorithm with some efficient neighborhood structures for the multiple objectives FJSPs, and the results are also promising.

Chemical-reaction optimization (CRO) is proposed by Lam and Li [9] in 2010, which loosely mimics what happens to molecules in a chemical reaction system and tries to capture the energy in the reaction process. The CRO is a population based swarm intelligent algorithm. However, CRO is different with other swarm intelligent

meta-heuristics such as the particle swarm optimization (PSO), the ant colony optimization (ACO). The main difference is that the CRO is a swarm algorithm with variable population size. The CRO has a nice ability to jump out of the local optima, which makes it more suitable for solving discrete combinatorial optimization problems, such as the scheduling problems, the vehicle optimization problems. The CRO has been applied for solving many optimization problems [9, 10, 11], such as the network optimization problem, the grid scheduling problems. Experimental results have shown that the CRO is efficient for solving the optimization problems with multi-optima.

In this paper, we conduct CRO for solving the FJSP with multiple objectives. The rest of paper is organized as follows. Section 2 gives the problem description. Section 3 gives the basic concept of the CRO. In section 4, the framework of the proposed algorithm is introduced. Section 5 reports the experimental results while the last section gives the conclusion of the paper.

2 Problem Formulation

The FJSP consider n jobs to be processed on m machines. Each job i contains n_i operations. Each operation O_{ij} represents the j th operation of job J_i , which should be operated on the assigned machine (M_k) from a set of available machines (M_{ij}). The processing time (p_{ijk}) for O_{ij} being operated on M_k is determined. There are some constraints as follows: 1) each job has a predefined number of operations with a known determined sequence; 2) each job is ready at zero time; 3) each machine can only process one operation at a time, and each job can be processed on one machine at a given time; 4) each machine can process a new operation only after completing the predecessor operation; 5) each operation can be operated on an assigned machine from a set of candidate machines.

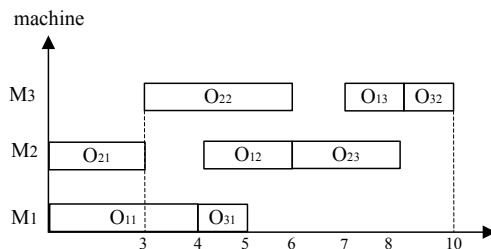


Fig. 1. Gantt chart for an example FJSP

In Fig.1, three jobs with eight operations are operated on three machines. The following objectives are to be minimized:

- (1). f_1 : Maximal completion time of all machines, i.e., the makespan;
- (2). f_2 : Total workload of all machines;
- (3). f_3 : Workload of the critical machine or the busiest machine.

The weighted sum of the above three objective values are taken as the objective function in this study:

$$F(c) = w_1 \times f_1 + w_2 \times f_2 + w_3 \times f_3$$

Where, w_1 , w_2 , w_3 represent the weight assigned to the objective f_1 , f_2 and f_3 , respectively.

3 Chemical-Reaction Optimization

3.1 The Basic Concept of the CRO

The CRO is introduced by Lam and Li [9] in 2010, which loosely mimics what happens to molecules in a chemical reaction system and tries to capture the energy in the reaction process. The molecules represent the solution for the considered problem, which have some properties. A molecule is composed of several atoms and characterized by the atom type, bond length, angle, and torsion [9]. Any change in the atom type, bond length, angle, or torsion will make the molecules different with each other. Thus, the change in molecular structure is tantamount to switching to another feasible solution. Each molecule possesses two kinds of energies, i.e., PE (potential energy) and KE (kinetic energy). PE corresponds to the objective function of a molecule while the KE of a molecule symbolized its ability of escaping from a local minimum. Therefore, the higher the KE of the molecule, the higher the possibility it can possess a new neighboring molecule with higher PE . The formulation of the PE is shown as follows.

$$PE_{\omega} = f(\omega) \quad (1)$$

Given a molecule ω , the new neighboring molecule of ω is denoted by ω' , the condition which allows the molecule replaced by ω' is as follows.

$$PE_{\omega} + KE_{\omega} \geq PE_{\omega'} \quad (2)$$

The CRO is a population based swarm intelligent algorithm. The main difference between CRO and other swarm intelligent algorithms is that the CRO is a swarm algorithm with variable population size.

3.2 Elementary Reactions of CRO

In the basic CRO, there are four elementary reactions, i.e., the on-wall ineffective collision, decomposition, inter-molecular ineffective collision, and synthesis. These elementary reactions can be categorized into single molecular reactions and multiple molecular reactions. The on-wall ineffective collision and decomposition reactions are single molecular reactions, while the inter-molecular ineffective collision and synthesis reactions are of the latter category.

3.2.1 On-wall Ineffective Collision

The on-wall ineffective collision reaction occurs when a molecule hits the wall and then bounces back. After the on-wall collision, some attributes of the molecule (ω) will change, and thus the molecule becomes a new molecule (ω') if the condition shown in the equation (2) satisfies. After the on-wall ineffective collision, the molecule ω will lose some percent of KE to the buffer. Thus, the KE for the new molecule ω' is as follows.

$$KE_{\omega'} \geq (PE_{\omega} + KE_{\omega} - PE_{\omega'}) \times q \quad (3)$$

where $q \in [KELossRate, 1]$, and $(1-q)$ represents the fraction of KE lost to the environment after the on-wall ineffective collision. $KELossRate$ is a system parameter which limits the maximum percentage of KE lost at a time. By losing kinetic energy to the environment, the molecule can improve its local search ability and enhance the convergence capability. The update of the buffer is as follows.

$$buffer = buffer + (PE_{\omega} + KE_{\omega} - PE_{\omega'}) \times (1-q) \quad (4)$$

3.2.2 Decomposition

The decomposition reaction is used to mimic the process of hitting the wall and then decomposing into two or more pieces. The kinetic energy of the resultant molecules is shown as follows.

$$KE_{\omega_1'} = (PE_{\omega} + KE_{\omega} - PE_{\omega_1'} - PE_{\omega_2'} + buffer) \times k_1 \times k_2 \quad (5)$$

$$KE_{\omega_2'} = (PE_{\omega} + KE_{\omega} - PE_{\omega_1'} - PE_{\omega_2'} + buffer) \times k_3 \times k_4 \quad (6)$$

The condition to allow the decomposition is as follows.

$$PE_{\omega} + KE_{\omega} + buffer \geq PE_{\omega_1'} + PE_{\omega_2'} \quad (7)$$

where k_1 , k_2 , k_3 , and k_4 are random numbers independently uniformly generated from the interval $[0, 1]$. Then, the buffer is updated by following formulation.

$$buffer = PE_{\omega} + KE_{\omega} - PE_{\omega_1'} - PE_{\omega_2'} + buffer - KE_{\omega_1'} - KE_{\omega_2'} \quad (8)$$

3.2.3 Inter-molecular Ineffective Collision

The process of two or more molecules to share information with each other and then produce two or more other different molecules is called inter-molecular ineffective collision. The inter-molecular ineffective collision mimics the process that two molecules collide with each other and then bounce away. The condition for the inter-molecular ineffective collision is as follows.

$$PE_{\omega_1} + KE_{\omega_1} + PE_{\omega_2} + KE_{\omega_2} \geq PE_{\omega_1'} + PE_{\omega_2'} \quad (9)$$

Then, the kinetic energy of the two new molecules are as follows.

$$KE_{\omega_1'} = (PE_{\omega_1} + KE_{\omega_1} + PE_{\omega_2} + KE_{\omega_2} - PE_{\omega_1} - PE_{\omega_2'}) \times k \quad (10)$$

$$KE_{\omega_2'} = (PE_{\omega_1} + KE_{\omega_1} + PE_{\omega_2} + KE_{\omega_2} - PE_{\omega_1'} - PE_{\omega_2}) \times (1-k) \quad (11)$$

where k is a random number independently uniformly generated from the interval $[0, 1]$.

3.2.4 Synthesis

The synthesis is the process when more than one molecule collides and combines together. Suppose two molecules ω_1 and ω_2 collide with each other, and then a new molecule ω' bounce back. The condition to allow the synthesis reaction is as follows.

$$PE_{\omega_1} + KE_{\omega_1} + PE_{\omega_2} + KE_{\omega_2} \geq PE_{\omega'} \quad (12)$$

Then the kinetic energy for the new molecule is given by following formulation.

$$KE_{\omega'} = PE_{\omega_1} + KE_{\omega_1} + PE_{\omega_2} + KE_{\omega_2} - PE_{\omega'} \quad (13)$$

4 The Hybrid DCRO

To make the basic CRO suitable for solving the FJSP, we embed the problem encoding, the neighborhood structure, the initial population approach, and the local search methods into the hybrid DCRO.

The details steps of the proposed DCRO algorithm are as follows:

Step 1: Initialization phase

Step 1.1 Set the population size P_{size} ;

Step 1.2 Initialize the population, let the central energy buffer equals 0.

Step 2: Evaluate the PE value of each molecule in the population, and then record the best molecule as the current solution.

Step 3: If the stopping criterion is satisfied, output the best solution; otherwise, Get r randomly in interval $[0, 1]$, if $r > MoleColl$, then performs step4, otherwise, performs step 5.

Step 4: Decomposition and on-wall ineffective reaction phase.

Step 4.1 Select a molecule w from the population randomly.

Step 4.2 If decomposition condition met then perform the decomposition operator to produce two molecules w_1 and w_2 around w .

Step 4.3 If the replacement condition is satisfied, then replace w with w_1 and w_2 .

Step 4.4 If the decomposition condition is not met, then perform the on-wall ineffective collision operator. That is, to produce a new molecule w_1 around w . If w_1 is allowed to replace with w , then delete w and add w_1 into the population. Meanwhile, update the central buffer.

Step 5: Synthesis and inter-molecular collision phase.

Step 5.1 Select two molecule w_1 and w_2 from the population randomly.

Step 5.2 If synthesis condition met then perform the synthesis operator to produce one new molecule w .

Step 5.3 If the replacement condition is satisfied, then delete w_1 and w_2 and add w .

Step 5.4 If the synthesis condition is not met, then perform the inter-molecular collision operator. That is, to produce two new molecule w_1' and w_2' around w_1 and w_2 . Then delete w_1 and w_2 and add w_1' and w_2' into the population.

Step 6: go to step 3.

5 Experiment Results

This section describes the computational experiments to evaluate the performance of the proposed algorithm. The current instantiation was implemented in C++ on a Pentium IV 1.8GHz with 512M memory.

5.1 Setting Parameters

Each instance can be characterized by the following parameters: number of jobs (n), number of machines (m), and the number of operations (op_num). Followings are the detail parameters value:

- Population size $P_{size}: 20$;
- $KELossRate: 0.2$;
- $MoleColl: 0.5$;
- Initial KE for each molecule: 10000;

5.2 Results Comparisons

Three present algorithms are used to make comparison with the proposed algorithm, i.e., AL+CGA from Kacem [14], PSO+TS algorithm from Zhang et al. [7], the ACO+LS algorithm by Liouane (2007 [15]), and VNS+GA algorithm from Li et al. [13].

5.2.1 4-Jobs-5-Machines Instance

This is an instance of total flexibility, in which 4 jobs with 12 operations are to be performed on 5 machines. The comparison is given in Table 1. It can be seen from Table 1 that the proposed algorithm is competitive to other algorithms.

Table 1. Comparison of results on problem 4×5 with 12 operations

	AL+CGA	PSO	VNS+GA			DCRO	
f_1	16	11	1	1	1	11	12
f_2	34	32	3	3	3	32	32
f_3	10	10	1	9	8	10	8

5.2.2 3-Jobs-6-Machines Instance

The 3-jobs-6-machines instance is taken to make a comparison with the ACO algorithm proposed by Liouane (2007 [15]). The problem is given in Table 2. The comparison of the experimental results from ACO+LS and our algorithm are given in Table 3. It can be seen from Table 3 that the DCRO algorithm is also competitive to the ACO algorithm.

Table 2. 3 jobs-6 machines instance

	M_1	M_2	M_3	M_4	M_5	M_6
J_1	O_{11}	10	7	6	13	5
	O_{12}	4	5	8	12	7
	O_{13}	9	5	6	12	6
	O_{14}	7	8	4	10	15
J_2	O_{21}	15	12	8	6	10
	O_{22}	9	5	7	13	4
	O_{23}	14	13	14	20	8
J_3	O_{31}	7	16	5	11	17
	O_{32}	9	16	8	11	6
	O_{33}	6	14	8	18	21

Table 3. Comparison of the example benchmark

	f_1	f_2	f_3
Lower Bound Value	18	45	8
ACO+LS	19	51	13
	19	50	13
	19	48	14
	19	47	14
DCRO	18	45	12

“-” denotes not given by the author

6 Conclusion

In this paper, we propose a discrete chemical-reaction optimization for multi-objective FJSP. Experimental on a well-known benchmark instance shows that the proposed algorithm is superior to several existing approaches. The future work is to apply the algorithm for solving other large scale instances.

Acknowledgments. This work supported by Science Research and Development of Provincial Department of Public Education of Shandong under Grant J08LJ20, J09LG29, J08LJ59, Soft Science Foundation of Shandong under Grant 2009RKB125.

References

1. Brandimarte, P.: Routing and Scheduling in A Flexible Job Shop by Tabu Search. *Annals of Operations Research* 41, 157–183 (1993)
2. Mastroili, M., Gambardella, L.M.: Effective Neighborhood Functions for the Flexible Job Shop Problem. *Journal of Scheduling* 3(1), 3–20 (2000)

3. Li, J.Q., Pan, Q.K., Suganthan, P.N., Chua, T.J.: A Hybrid Tabu Search Algorithm with An Efficient neighborhood structure for the flexible job shop scheduling problem. *International Journal of Advanced Manufacturing Technology* 52(5-8), 683–697 (2011)
4. Bożejko, W., Uchroński, M., Wodecki, M.: Parallel Hybrid Metaheuristics for the Flexible Job Shop Problem. *Computers & Industrial Engineering* 59, 323–333 (2010)
5. Xia, W.J., Wu, Z.M.: An Effective Hybrid Optimization Approach for Multi-objective Flexible Job-shop Scheduling Problems. *Computers and Industrial Engineering* 48(2), 409–425 (2005)
6. Gao, J., Sun, L., Gen, M.: A Hybrid Genetic and Variable Neighborhood Descent Algorithm for Flexible Job Shop Scheduling Problems. *Computers and Operations Research* 35(9), 2892–2907 (2008)
7. Zhang, G.H., Shao, X.Y., Li, P.G., Gao, L.: An Effective Hybrid Particle Swarm Optimization Algorithm for Multi-objective Flexible Job-shop Scheduling Problem. *Computers and Industrial Engineering* 56(4), 1309–1318 (2009)
8. Li, J.Q., Pan, Q.K., Liang, Y.C.: An Effective Hybrid Tabu Search Algorithm for Multi-objective Flexible Job Shop Scheduling Problems. *Computers & Industrial Engineering* 59(4), 647–662 (2010)
9. Lam, A.Y.S., Li, V.O.K.: Chemical-Reaction-Inspired Metaheuristic for Optimization. *IEEE Transactions on Evolutionary Computation* 14(3), 381–399 (2010)
10. Lam, A.Y.S., Xu, J., Li, V.O.K.: Chemical Reaction Optimization for Population Transition in Peer-to-peer Live Streaming. In: Proceeding of the IEEE Congress on Evolutionary Computation (CEC 2010), Spain, pp. 1429–1436 (July 2010)
11. Xu, J., Lam, A.Y.S., Li, V.O.K.: Chemical Reaction Optimization for the Grid Scheduling Problem. In: Proceeding of the IEEE International Conference on Communications, Hong Kong, China, pp. 1–5 (2010)
12. Pezzella, F., Morganti, G., Ciaschetti, G.: A Genetic Algorithm for the Flexible Job-shop Scheduling Problem. *Computers & Operations Research* 35, 3202–3212 (2008)
13. Li, J.Q., Pan, Q.K., Xie, S.X.: A Hybrid Variable Neighborhood Search Algorithm for Solving Multi-Objective Flexible Job Shop Problems. *ComSIS Computer Science and Information Systems* 7(4), 907–930 (2010)
14. Kacem, I., Hammadi, S., Borne, P.: Approach by Localization and Multi-objective Evolutionary Optimization for Flexible Job-shop Scheduling Problems. *IEEE Transactions on Systems, Man and Cybernetics, Part C* 32(1), 408–419 (2002)
15. Liouane, N., Saad, I., Hammadi, S., Borne, P.: Ant Systems & Local Search Optimization for Flexible Job-Shop Scheduling Production. *International Journal of Computers, Communications & Control* 2, 174–184 (2007)

Discrete Harmony Search Algorithm for the No Wait Flow Shop Scheduling Problem with Makespan Criterion

Kaizhou Gao, Shengxian Xie, Hua Jiang, and Junqing Li

Computer school of Liaocheng University, Liaocheng, China, 252059
gaokai zh@yahoo.com.cn

Abstract. This paper presents a discrete harmony search (DHS) algorithm for solving no-wait flow shop scheduling problems with makespan criterion. Firstly, a harmony is represented as a discrete job permutation and three heuristic methods are proposed to initialize the harmony memory. Secondly, by dynamically regrouping mechanism, the harmony memory is divided into several groups for sharing information reciprocally. Thirdly, to stress the balance between the global exploration and local exploration, a variable neighborhood search algorithm is developed and embedded in the DHS algorithm. Computational simulation results based on the well-known benchmarks and statistical performance comparisons are provided. Computational results and comparison show the effectiveness of the presented DHS algorithm in solving the no-wait flow shop scheduling with makespan criterion.

Keywords: no-wait flow shop, harmony search, makespan, neighborhood search.

1 Introduction

No-wait flow shop scheduling problem is a typical scheduling problem with strong engineering background, which has important applications in various industries including chemical processing, food processing, concrete production and pharmaceutical processing [1-6]. Garey and Johnson [7] proved that no-wait flow shop scheduling problems was NP-hard. In a no-wait flow shop, each job consists of m operations owning a predetermined processing time. The objective of no-wait flow shop scheduling problem is to find a job sequence to minimize the makespan. For the makespan criterion, heuristics were introduced by Bonney and Gundry [8], King and Spacins [9], Gangadharan and Rajendran [10], Rajendran [3]. With the development of computer technology, meta-heuristic for no-wait flow shop scheduling problems has grown quickly. The makespan criterion consists of simulated annealing (SA) and genetic algorithm (GA) by Aldowaisan and Allahverdi [11], hybrid GA and SA (GASA) by Schuster and Framinan [12], variable neighborhood search (VNS) by Framinan and Schuster [13], descending search (DS) and tabu search (TS) by Grabowski and Pempera [14], particle swarm optimization (PSO) and differential evolution (DE) algorithms by Pan[15,16]. In addition, a comprehensive survey of the no-wait flow shop scheduling problem can be found in Hall and Sriskandarayah [17].

Harmony search is one of the latest meta-heuristic methods presented by Geem et al [18] for solving optimization problems. During the past years, the HS algorithm has been successfully applied to various engineering problems, such as structural optimization [19], vehicle routing [20], water network design [21], multiple dam operation [22], Sudoku puzzle [23], multi-pass face-milling [24], discrete-time chaotic system [25], shop scheduling problem [26-28], and etc. However, the applications of the HS algorithm on scheduling problems with makespan criterion are still considerably limited. This paper developed a discrete HS (DHS) algorithm to solve the no-wait flow shop scheduling problem with makespan criterion.

2 The No-Wait Flow Shop Scheduling Problem

The no-wait flow shop scheduling problem considered in this paper can be described as follows: Given the processing times $P(i,j)$ for job i and machine j , each of n jobs ($i=1,2,\dots,n$) will be sequenced through m machines ($j=1,2,\dots,m$). Each job i has a sequence of m operations ($o_i,1, o_i,2, \dots, o_i, m$). To satisfy the no-wait constraint, the completion time of the operation o_i, k must be equal to the time to start of the operation $o_i, k+1$ for $k=1, 2, \dots, m-1$. That means there must be no waiting time between the processing of any operation of each job. The problem is to find a schedule such that the makespan is minimized and the processing order of jobs is the same on each machine. Suppose that the job permutation $\pi = \{\pi_1, \pi_2, \dots, \pi_n\}$ represents the schedule of jobs to be processed. Let $d(\pi_{j-1}, \pi_j)$ be the minimum delay restricted on the first machine between the start of jobs π_{j-1} and π_j by the no-wait constraint when the job π_j is directly processed after the job π_{j-1} , and $C_{j-1,j}(\pi_j, m)$ denote the makespan of jobs π_{j-1} and π_j in the $2/m/P/C_{\max}$ problem. Since the makespan for $2/m/\text{no-wait } P/C_{\max}$ and $2/m/P/C_{\max}$ is the same [29], and in the no-wait flow shop scheduling problem the difference between the completion time of a job's last operation and the starting time of its first operation is equal to the sum of its operation times on all machines [30], $d(\pi_{j-1}, \pi_j)$ can be computed as follows:

$$d(\pi_{j-1}, \pi_j) = C_{j-1,j}(\pi_j, m) - \sum_{k=1}^m p(\pi_j, k) \text{ for } j = 2, 3, \dots, n. \quad (1)$$

Then, the makespan of the job permutation $\pi = \{\pi_1, \pi_2, \dots, \pi_n\}$ can be given by

$$C_{\max} = \sum_{j=2}^n d(\pi_{j-1}, \pi_j) + \sum_{k=1}^m p(\pi_n, k) \quad (2)$$

Therefore, the no-wait flow shop scheduling problem with the makespan criterion is to find a permutation π^* in the set of all permutation Π such that

$$C_{\max}(\pi^*) \leq C_{\max}(\pi), \forall \pi \in \Pi \quad (3)$$

3 The Discrete Harmony Search Algorithm

The HS algorithm population bases on stochastic algorithm that inspired by the natural musical performance process when a musician searches for a better state of harmony. In the standard harmony search algorithm [18], the optimization procedure is as follows:

1) Initialize algorithm parameters and the optimization problem. The parameters of the HS are the harmony memory size (HMS), harmony memory considering rate (HMCR), pitch adjusting rate (PAR), the distance bandwidth (BW) and the number of improvisations (NI). 2) Initialize the harmony memory (HM). and the harmony memory (HM) is used to store, harmony, all the solution vectors. 3) Improvise a new harmony. A new harmony vector, $X' = (x'_1, x'_2, \dots, x'_N)$, is generated based on the following rules: memory consideration, pitch adjustment, and random selection. Generating a new harmony is called ‘improvisation’. The procedure works as follows:

```

for i=1,2,...,n do
if rand()<HMCR then      //memory consideration
    Xnew(i)=Xa(i), where a=1,2,..., or HMS
    if rand()<PAR then //pitch adjustment
        Xnew(i)= Xnew(i)+rand()*BW
    else // random selection
        Xnew(i)= LB(j)+rand()*(UB(j)-LB(j))

```

4) Update the HM. Evaluate the objective function value of the new harmony vector. The new harmony vector will replace the worst one in the HM, if the new harmony vector is better. 5) Repeat Step2 and Step3 until the termination criterion are meted.

3.1 Discretization of the Harmony

The job-permutation-based representation has been widely used in the literature for flow shop scheduling problems and it is easy to decode to reduce the cost of the algorithm [31]. So, in this paper, we adopt this representation. An example is given in Table 1.

3.2 Initialization Harmony Memory

In this paper, we employ the NEH [32] heuristic for initialing the harmony memory. The NEH heuristic has two phases. In phase I , jobs are ordered in descending sums of their processing times. In phase II , a job sequence is established by evaluating the partial schedules based on the initial order of the first phase. Suppose a current sequence is already determined for the first k jobs, k+1 partial sequences are constructed by inserting job k+1 in k+1 possible slots of the current sequence. Among these k+1 sequences, the one generating the minimum total flowtime is kept as the current sequence for the next iteration. Then job k + 2 from phase I is considered and so on until all jobs have been sequenced. In addition to the presented NEH heuristic, the job-pair-comparison heuristic of Edy Bertolissi [33] is also employed to initial the harmony memory.

Table 1. An example of the job permutation based representation

Dimension j	1	2	3	4	5	6	7	8	9	10
x_{ij}	7	8	6	9	3	1	2	10	4	5
Job permutation	7	8	6	9	3	1	2	10	4	5

3.3 Improvising New Harmony

Since the job permutation based representation is used in our algorithm, the improvisation of the basic HS algorithm is not suitable for producing a feasible solution. We present a new improvisation as follows:

```

for i=0 to 4 do
if rand()<HMCR //memory consideration
if  $x_j(k)$  is not included in  $x_{new}(k)$ , where  $k \in (1,2,\dots,HMS)$ 
 $x_{new}(j) = x_j(k)$ 
else
select a job from best sequence and this selected job
is no the same to  $x_j(k)$   $k \in (1,2,\dots,j)$ 
if rand()<PAR // pitch adjustment
for k=1 to j do
exchange  $x_{new}(j)$  with a randomly selected job and
evaluate the total flowtime
select the sequence with minimize total flowtime from
obtained j sequences
else // random selection
select a integer from set  $I = \{i | 1 \leq i \leq n\}$  ( $j=1$ ) or  $I'$  ( $j > 1$ )
remove  $x_{new}(j)$  from set I and obtain set  $I'$ 

```

Obviously, the above process can be used only if each dimension of x_{new} is different, that is, $x_{new}(j) \neq x_{new}(k)$ for $j,k \in \{1,2,\dots,n\} \wedge j \neq k$. Compared to basic harmony search algorithm, this improvisation can improve the quality of x_{new} .

In this way, the harmony memory is divided into four small groups and each group executes its evolution process independently. At the same time, each group can share solution information with others through regrouping. The process of regrouping is as follows:

```

for i=0 to HMS do
R=rand()%HMS; //randomly select a inteter from 0-
HMS;
for j=0 to JobNumber do
temp[j]=HM[0][j];
HM[0][j]=HM[R][j];
HM[R][j]=temp[j];

```

3.4 Local Search for Best Harmony

In this paper, we employed insert neighborhood to improve the best solution of harmony search algorithm. The insert neighborhood algorithm in this work executes as follows:

```

for i=0 to n do//insert neighborhood;
    for j=0 to n-1 do
        insert the job at the ith dimension in the jth
        dimension of X , i≠j
        if(F(X')<F(X))
            X = X';

```

The above neighborhood search is efficient and effective because the new search is based on the sequence X' but not X itself. So the neighborhood search can avoid cycling search. At the same time, X is updated only when the makespan of X' is better than that of X , so the neighborhood search can rapidly reach a local optimum.

3.5 Procedure of DHS Algorithm

Based on the above design, the procedure of HHS algorithm for the no-wait flow shop scheduling problem with makespan criteria is presented as follows:

- 1) Set the parameters HMS, HMCR, PAR, BW and NI.
- 2) Initialize harmony memory. Two harmonies of population are constructed by NEH heuristic and the job-pair-comparison heuristic, others are generated in domain randomly.
- 3) Evaluate the makespan of each harmony using the method and formula in Section 2.
- 4) Improvising new harmony. The harmonies in HM are packet into NI/4groups. Each group optimizes the total flowtime separately. All harmonies are stored in harmony memory and regrouping randomly. insert neighborhood search for the best harmony.
- 5) Output the best job sequence and its makespan.

4 Computational Results and Comparisons

To verify and demonstrate the effectiveness of the proposed algorithm, this section discusses the simulation results of the 31 benchmark for different approaches including classical NEH, Edy, HS, DHS no local search, HGA [34] and DHS. All algorithms are coded in C++ with Visio studio .net 2005 platform. For each benchmark, every algorithm independently runs on a dual core Genuine 1.6 GHz PC with 512 MB memory under the same time. In DHS, the parameters are set as follows: HMS=20, HMCR=0.95. The statistical results are reported in Table 2, where the result of each instance is the relative percentage increase (RPI) as follows:

$$RPI(O_i) = \frac{O_i - C^*}{C^*} \times 100 \quad (4)$$

where O_i is the objective function value generated in the ith algorithm, and C^* is the best objective function value found by all algorithms compared.

Table 2. Computation results of five algorithms for 31 instances

Name	Instance n xm	NEH	Edy	DHSnl	HGA	DHS
Car01	11x5	0.119	0.125	0.040	0	0
Car02	13x4,	0.156	0.122	0.122	0	0
Car03	12x5	0.124	0.124	0.124	0	0
Car04	14x4	0.225	0.205	0.171	0	0
Car05	10x6	0.100	0.102	0.100	0	0
Car06	8x9	0.032	0.008	0.008	0	0
Car07	7x7	0.090	0.114	0.090	0	0
Car08	8x8	0.112	0.087	0.041	0	0
hel1	100x10	0.011	0.040	0.011	0.004	0
hel2	20x10	0.105	0.094	0.050	0	0
Rec01	20x5	0.031	0.139	0.031	0.002	0
Rec03	20x5	0.116	0.095	0.095	0.006	0
Rec05	20x5	0.054	0.037	0.037	0.007	0
Rec07	20x10	0.089	0.065	0.015	0.003	0
Rec09	20x10	0.073	0.118	0.073	0.020	0
Rec11	20x10	0.045	0.055	0.045	0.026	0
Rec13	20x15	0.046	0.065	0.042	0.015	0
Rec15	20x15	0.069	0.054	0.020	0.009	0
Rec17	20x15	0.105	0.137	0.085	0.002	0
Rec19	30x10	0.118	0.112	0.112	0.055	0
Rec21	30x10	0.040	0.021	0.020	0.010	0
Rec23	30x10	0.048	0.032	0.032	0.010	0
Rec25	30x15	0.077	0.025	0.025	0.017	0
Rec27	30x15	0.045	0.128	0.045	0.020	0
Rec29	30x15	0.085	0.031	0.031	0.013	0
Rec31	50x10	0.050	0.019	0.019	0.008	0
Rec33	50x10	0.056	0.013	0.013	0.007	0
Rec35	50x10	0.060	0.046	0.046	0.026	0
Rec37	75x20	0.021	0.017	0.017	0.009	0
Rec39	75x20	0.015	0.018	0.015	0.006	0
Rec41	75x20	0.042	0.012	0.012	0.003	0
Mean		0.076	0.073	0.051	0.009	0

It can be seen from Table 2 that the results of DHS is best and that of HGA is followed, since the overall Mean generated by DHS and HGA are 0, 0.009, while those by the NEH, Edy, DHSnl are 0.076, 0.073 and 0.051 respectively. For instances Car1 to Car8, the HGA and DHS received the same results, but the superiority of DHS algorithm over HGA is demonstrated for the large size instances, such as Rec09, Rec11, Rec13, Rec19, Rec27, Rec35 ect al. For these reasons, it is concluded that the performance of proposed DHS algorithm is significantly better than the algorithms compared for the no-wait flow shop scheduling problem with makespan criteria.

5 Conclusion

This paper presents a discrete harmony search algorithm for solving the no-wait flow shop scheduling problem with makespan criterion. Two heuristics are used for

initialization the memory and a new method is employed for improvising the new harmony. And then, we employed the insert neighborhood for improving the solution of harmony search algorithm. Simulation experiments and comparisons demonstrated the efficiency of the discrete harmony search algorithm for no-wait flow shop scheduling with makespan criterion. In the future research, hybrid discrete harmony search algorithm will be developed for flow shop scheduling problems and multi-objective complex scheduling problems.

Acknowledgments. This research is partially supported by Science Foundation of Shandong Province in China (BS2010DX005), Postdoctoral Science Foundation of China under Grants 20100480897 .Science Research and Development of Provincial Department of Public Education of Shandong under Grant J09LG29, J10LG67; and Liaocheng University Foundation under Grant X0810013.

References

1. Qian, B., Wang, L., Hu, R., Huang, D.X., Wang, X.: A DE-based Approach to No-wait Flow Shop Scheduling. *Comput. Oper. Res.* 57, 787–805 (2009)
2. Ishibuchi, H., Yoshida, I., Murata, T.: Balance Between Genetic Search and Local Search in Memetic Algorithms for Multi-objective Permutation Flow Shop Scheduling. *IEEE T. Evolut. Comput.* 7, 204–223 (2003)
3. Rajendran, C.: A No-wait Flowshop Scheduling Heuristic to Minimize Makespan. *J. Oper. Res. Soc.* 45, 472–478 (1994)
4. Hall, N.G., Sriskandarayah, C.: A Survey of Machine Scheduling Problems with Blocking and No-wait in Process. *Oper. Res.* 44, 510–525 (1996)
5. Grabowski, J., Pempera, J.: Sequencing of Jobs in Some Production System. *Eur. J. Oper. Res.* 125, 535–550 (2000)
6. Raaymakers, W., Hoogeveen, J.: Scheduling Multipurpose Batch Process Industries with No-wait Restrictions by Simulated Annealing. *Eur. J. Oper. Res.* 126, 131–151 (2000)
7. Garey, M.R., Johnson, D.S.: Computers and Intractability, A Guide to the Theory of NP-Completeness. Freeman, San Francisco (1979)
8. Bonney, M.C., Gundry, S.W.: Solutions to the Constrained Flow Shop Sequencing Problem. *Oper. Res. Quart.* 27, 869–883 (1976)
9. King, J.R., Spachis, A.S.: Heuristics for Flow Shop Scheduling. *Int. J. Prod. Res.* 18, 343–357 (1980)
10. Gangadharan, R., Rajendran, C.: Heuristic Algorithms for Scheduling in No-wait Flow Shop. *Int. J. Prod. Econ.* 32, 285–290 (1993)
11. Rajendran, C., Chaudhuri, D.: Heuristic Algorithms for Continuous Flow-shop Problem. *Nav. Res. Log.* 37, 695–705 (1990)
12. Aldowaisan, T., Allahverdi, A.: New Heuristics for No-wait Flowshops to Minimize Makespan. *Comput. Oper. Res.* 30, 1219–1231 (2003)
13. Schuster, C.J., Framinan, J.M.: Approximative Procedure for No-wait Job Shop Scheduling. *Oper. Res. Lett.* 31, 308–318 (2003)
14. Grabowski, J., Pempera, J.: Some Local Search Algorithms for No-wait Flow-shop Problem with Makespan Criterion. *Comput. Oper. Res.* 32, 2197–2212 (2005)
15. Pan, Q.K., Fatih, T.M., Liang, Y.C.: A Discrete Particle Swarm Optimization Algorithm for the No-wait Flow Shop Scheduling Problem. *Comput. Oper. Res.* 35, 2807–2839 (2008)

16. Pan, Q.K., Wang, L., Qian, B.: A Novel Differential Evolution Algorithm for Bi-criteria No-wait Flow Shop Scheduling Problem. *Comput. Oper. Res.* 36, 2498–2511 (2009)
17. Hall, N.G., Sriskandarayah, C.: A Survey of Machine Scheduling Problems with Blocking and No-wait in process. *Oper. Res.* 44, 510–525 (1996)
18. Geem, Z.W., Kim, J.H., Loganathan, G.V.: A New Heuristic Optimization Algorithm: Harmony Search. *Simulation* 76, 60–68 (2001)
19. Lee, K.S., Geem, Z.W., Lee, S.H., Bae, K.W.: The Harmony Search Heuristic Algorithm for Discrete Structural Optimization. *Eng. Optimiz.* 37, 663–684 (2005)
20. Geem, Z.W., Lee, K.S., Park, Y.: Application of Harmony Search to Vehicle Routing. *Am. J. Appl. Sci.* 2, 1552–1557 (2005)
21. Geem, Z.W.: Optimal Cost Design of Water Distribution Networks Using Harmony Search. *Eng. Optimiz.* 38, 259–280 (2006)
22. Geem, Z.W.: Optimal Scheduling of Multiple Dam System Using Harmony Search Algorithm. In: Sandoval, F., Prieto, A.G., Cabestany, J., Graña, M. (eds.) IWANN 2007. LNCS, vol. 4507, pp. 316–323. Springer, Heidelberg (2007)
23. Geem, Z.W.: Harmony Search Algorithm for Solving Sudoku. In: Apolloni, B., Howlett, R.J., Jain, L. (eds.) KES 2007, Part I. LNCS (LNAI), vol. 4692, pp. 371–378. Springer, Heidelberg (2007)
24. Zarei, F.M., Farshi, B., Jalili, S.R., Rafar, M.R.: Optimization of Multi-pass Face-milling via Harmony Search Algorithm. *J. Mater. Process. Tech.* 209, 2386–2392 (2009)
25. Leandro, S.C.: An Improved Harmony Search Algorithm for Synchronization of Discrete-time Chaotic System. *Chaos Solitons Fract* 41, 2526–2532 (2009)
26. Wang, L., Pan, Q.K., Tasgetiren, M.F.: Minimizing the Total Flow Time in A Flow Shop with Blocking by Using Hybrid Harmony Search Algorithms. *Expert. Syst. Appl.* 37, 7929–7936 (2010)
27. Pan, Q.K., Suganthan, P.N., Liang, J.J., Tasgetiren, M.: Fatih: A Local-best Harmony Search Algorithm with Dynamic Sub-harmony Memories for Lot-streaming Flow Shop scheduling problem. *Expert. Syst. Appl.* 38, 3252–3259 (2011)
28. Gao, K.Z., Pan, Q.K., Li, J.Q.: Discrete Harmony Search Algorithm for the No-wait Flow Shop Scheduling Problem with Total Flow Time Criterion. *Int. J. Adv. Manuf. Technol.*, doi: 10.1007/s00170-011-3197-6
29. Kalcynski, P.J., Kamburowski, J.: On No-wait and No-idle Flow Shops with Makespan Criterion. *Eur. J. Oper. Res.* 178, 677–685 (2007)
30. Grabowski, J., Pempera, J.: Some Local Search Algorithms for No-wait Flow-shop Problem with Makespan Criterion. *Comput. Oper. Res.* 32, 2197–2212 (2005)
31. Wang, L., Zheng, D.Z.: An Effective Hybrid Heuristic for Flow Shop Scheduling. *Int. J. Adv. Manuf. Technol.* 21, 38–44 (2003)
32. Nawaz, M., Enscore, J., Ham, I.: A Heuristic Algorithm for the m-machine, n-job Flow Shop Sequencing Problem. *Omega* 11, 91–95 (1983)
33. Edy, B.: Heuristic Algorithm for Scheduling in the No-wait Flow Shop. *J. Mater. Process. Tech.* 107, 459–465 (2000)
34. Bassem, J.M., Eddaly, P.S.: A Hybrid Genetic Algorithm for Solving No-wait Flow Shop Scheduling Problems. *Int. J. Adv. Manuf. Technol.*, doi: 10.1007/s00170-010-3009-4

Hybrid Differential Evolution Optimization for No-Wait Flow-Shop Scheduling with Sequence-Dependent Setup Times and Release Dates

Bin Qian, Hua-Bin Zhou, Rong Hu, and Feng-Hong Xiang

Department of Automation, Kunming University of Science and Technology,
Kunming 650051, China
bin.qian@vip.163.com

Abstract. In this paper, a hybrid algorithm based on differential evolution (DE), namely HDE, is proposed to minimize the total completion time criterion of the no-wait flow-shop scheduling problem (NFSSP) with sequence-dependent setup times (SDSTs) and release dates (RDs), which is a typical NP-hard combinatorial optimization problem with strong engineering background. Firstly, to make DE suitable for solving flow-shop scheduling problem, a largest-order-value (LOV) rule is used to convert the continuous values of individuals in DE to job permutations. Secondly, a speed-up evaluation method is developed according to the property of the NFSSP with SDSTs and RDs. Thirdly, after the DE-based exploration, a problem-dependent local search is developed to emphasize exploitation. Due to the reasonable balance between DE-based global search and problem-dependent local search as well as the utilization of the speed-up evaluation, the NFSSP with SDSTs and RDs can be solved effectively and efficiently. Simulation results and comparisons demonstrate the superiority of HDE in terms of searching quality, robustness, and efficiency.

Keywords: differential evolution, no-wait flow-shop scheduling, sequence-dependent setup times, release dates, local search, speed-up evaluation.

1 Introduction

Flow-shop scheduling problems (FSSPs) have attracted much attention and wide research in both computer science and operation research fields. In many FSSPs, each job is usually required to be processed continuously from start to end without waiting either on or between machines. This type of scheduling problem is known as no-wait flow-shop scheduling problem (NFSSP) [1]. In NFSSP, usually it assumes that the setup time is part of the job processing time and the release date of each job is zero. However, in some practical applications the setup times need to be explicitly treated and the release dates are nonzero. Typical situations are encountered in metal, chemical and pharmaceutical industries. The scheduling problems with sequence-dependent setup times (SDSTs) and release dates (RDs) have gained increasing attention in recent years [2]–[4]. For the total completion time criterion, the NFSSP with SDSTs

and RDs can be classified as $Fm/no-wait, ST_{sd}, r_j / \sum C_j$, which is NP-hard because it is more complex than the NFSSP with SDSTs [2][5].

Differential evolution (DE) is a novel population-based evolutionary mechanism proposed for global optimization over continuous spaces [6]. DE searches for the global optima by utilizing differences between contemporary population members, which allows the search behaviour of each individual to self-tune. Due to its simple structure, easy implementation, quick convergence, and robustness, DE has attracted much attention and wide applications in a variety of fields. Nevertheless, due to its continuous nature, the work on DE for production scheduling problems is obviously sparser than that for continuous optimization problems. Recently, Tasgetiren et al. [7] proposed a smallest position value (SPV) rule to convert the continuous values of individuals in DE to job permutations and incorporated Interchange-based local searcher into DE to solve flow-shop scheduling problems (FSSPs) with makespan criterion. Onwubolu and Davendra [8] presented a DE-based method to minimize the objectives of makespan, mean flowtime, and total tardiness of FSSPs. Qian et al. [9] developed a hybrid DE approach for FSSPs with makespan criterion. They utilized DE to find the promising solutions over the solution space and applied a simple problem dependent local searcher to exploit the solution space from those solutions. Pan et al. [10] presented a novel discrete differential evolution algorithm with a problem-specific referenced local searcher for FSSPs, which could find several new best known makespans for Taillard benchmark instances. Wang et al. [11] developed an effective discrete differential evolution algorithm for solving blocking FSSPs. To the best of our knowledge, there is no any published paper on DE for NFSSPs with SDSTs and RDs.

This paper develops a hybrid DE (HDE) by combining DE with local search to minimize the total completion time criterion of the NFSSPs with SDSTs and RDs. In the proposed HDE, DE is used to find the promising solutions or regions over the solution space, and then a local search based on the landscape of FSSP and the speed-up evaluation is conceived to exploit the solution space from those regions.

The remaining contents are organized as follows. In Section 2, the NFSSP with SDSTs and RDs is introduced. In Section 3, a brief review of DE is provided. In Section 4, HDE is proposed after presenting solution representation, speed-up evaluation method, DE-based global search, and problem-dependent local search. In Section 5, experimental results and comparisons are presented and analyzed. Finally, in Section 6, we end the paper with some conclusions and future work.

2 Formulation of NFSSP with SDSTs and RDs

The NFSSP with SDSTs and RDs can be described as follows. There are n jobs and m machines. Each of n jobs will be sequentially processed on machine $1, 2, \dots, m$. The processing time of each job on each machine is deterministic. At any time, preemption

is forbidden and each machine can process at most one job. To satisfy the no-wait restriction, each job must be processed without interruptions between consecutive machines. Thus, all jobs are processed in the same sequence on all machines. In a flow-shop with SDSTs, setup must be performed between the completion time of one job and the start time of another job on each machine, and setup time depends on both the current and the immediately preceding jobs at each machine. In a flow-shop with RDs, if a machine is ready to process a job but the job has not been released yet, it stays idle until the release date of the job.

2.1 NFSSP with SDSTs

Let $\pi = [j_1, j_2, \dots, j_n]$ denote the schedule or permutation of jobs to be processed, $p_{j_i,l}$ the processing time of job j_i on machine l , sp_{j_i} the total processing time of job j_i on all machines, $ML_{j_i,l}$ the minimum delay on the machine l between the completion of job j_{i-1} and j_i , L_{j_{i-1},j_i} the minimum delay on the first machine between the start of job j_{i-1} and j_i , $s_{j_{i-1},j_i,l}$ the sequence-dependent setup time between job j_{i-1} and j_i on machine l . Let $p_{j_0,l} = 0$ for $l = 1, \dots, m$. Then $ML_{j_i,l}$ can be calculated as follows:

$$ML_{j_i,l} = \begin{cases} \max\{s_{j_{i-1},j_i,1} + p_{j_i,1} - p_{j_{i-1},2}, s_{j_{i-1},j_i,2}\} + p_{j_i,2}, & l = 2 \\ \max\{ML_{j_i,l-1} - p_{j_{i-1},l}, s_{j_{i-1},j_i,l}\} + p_{j_i,l}, & l = 3, \dots, m \end{cases}. \quad (1)$$

Thus, the total completion time $C_T(\pi)$ (i.e., $C_T(\pi) = \sum_j C_j$) is as follows:

$$C_T(\pi) = \sum_{i=1}^n (n+1-i)ML_{j_i,m}. \quad (2)$$

Fig. 1 shows a small example of a NFSSP with SDSTs when $n=3$ and $m=3$.

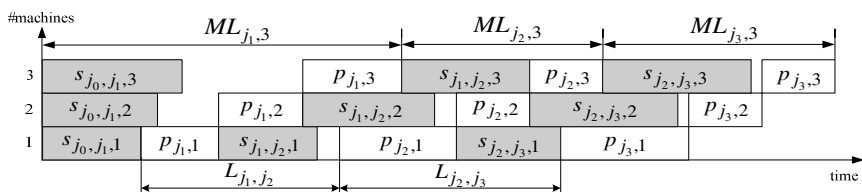


Fig. 1. NFSSP with SDSTs example when $n=3$ and $m=3$

Obviously, L_{j_{i-1},j_i} can be calculated by using the following formula:

$$L_{j_{i-1},j_i} = ML_{j_i,m} + sp_{j_{i-1}} - sp_{j_i}. \quad (3)$$

2.2 NFSSP with SDSTs and RDs

Let r_{j_i} denote the arrival time of job j_i , St_{j_i} the process start time of job j_i on machine 1, and C_{j_i} the completion time of job j_i on machine m . Then St_{j_i} can be written as follows:

$$St_{j_i} = \begin{cases} \max\{ML_{j_i,m} - sp_{j_i}, r_{j_i}\}, & i = 1 \\ St_{j_{i-1}} + \max\{L_{j_{i-1},j_i}, r_{j_i} - St_{j_{i-1}}\}, & i = 2, \dots, n \end{cases}. \quad (4)$$

Thus, C_{j_i} and $C_T(\pi)$ can be calculated as follows:

$$C_{j_i} = St_{j_i} + sp_{j_i}, i = 1, \dots, n. \quad (5)$$

$$C_T(\pi) = \sum_{i=1}^n C_{j_i}. \quad (6)$$

The aim of this paper is to find a schedule π^* in the set of all schedules Π such that

$$\pi^* = \arg\{C_T(\pi)\} \rightarrow \min \quad \forall \pi \in \Pi. \quad (7)$$

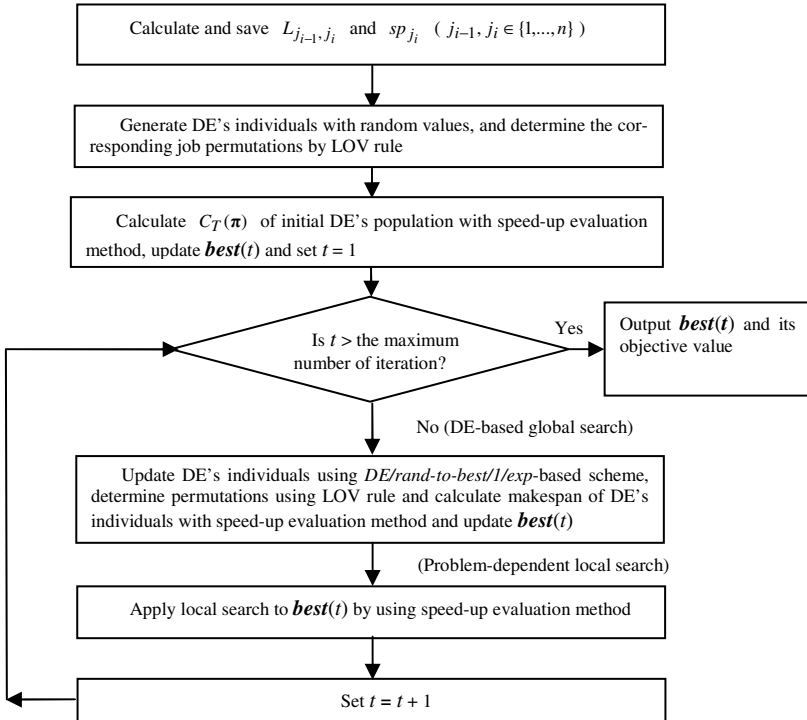
3 Brief Review of DE

DE is a branch of metaheuristic proposed by Storn and Price [6] for optimization problems over continuous domains. The basic DE algorithm aims at finding the global optima by utilizing the distance and direction information according to the differentiations among population. The theoretical framework of DE is very simple and DE is easy to be coded and implemented with computer. Thus, nowadays DE has attracted much attention and wide applications in various fields.

In DE, it starts with the random initialization of a population of individuals in the search space and works on the cooperative behaviors of the individuals in the population. The searching behavior of each individual is adjusted by dynamically altering the differentiation's direction and step length in which this differentiation performs. At each generation, the *mutation* and *crossover* operators are applied on the individuals, and a new population arises. Then, *selection* takes place, and the corresponding individuals from both populations compete to comprise the next generation. Currently, there are several variants of DE algorithm can be found in [12]. The details of DE can be found in subsection 4.3.

4 HDE for NFSSP with SDSTs and RDs

In this section, we will present HDE for NFSSP with SDSTs and RDs after explaining the solution representation, speed-up computing method, DE-based global search, problem-dependent local search.

**Fig. 2.** The procedure framework of HDE

4.1 Solution Representation

The important problem in applying DE to NFSSP is to find a suitable mapping between job sequence and individuals (continuous vectors) in DE. For the n -job and m -machine problem, each vector contains n number of dimensions corresponding to n operations. In this paper, we adopt a largest-order-value (LOV) rule in [9] to convert DE's individual $X_i = [x_{i,1}, x_{i,2}, \dots, x_{i,n}]$ to the job solution/permuation vector $\pi_i = \{j_{i,1}, j_{i,2}, \dots, j_{i,n}\}$. According to LOV rule, $X_i = [x_{i,1}, x_{i,2}, \dots, x_{i,n}]$ are firstly ranked by descending order to get the sequence $\varphi_i = [\varphi_{i,1}, \varphi_{i,2}, \dots, \varphi_{i,n}]$. Then the job permutation π_i is calculated by the following formula:

$$j_{i,\varphi_{i,k}} = k . \quad (8)$$

To better understand the LOV rule, a simple example is provided in Table 1. In this instance ($n = 6$), when $k = 1$, then $\varphi_{i,1} = 4$ and $j_{i,\varphi_{i,1}} = j_{i,4} = 1$; when $k = 2$, then $\varphi_{i,2} = 1$ and $j_{i,\varphi_{i,2}} = j_{i,1} = 2$, and so on. This representation is unique and simple in terms of finding new permutations. Moreover, according to our previous tests, this representation is more effective than the famous random key representation [13].

Table 1. Solution Representation

Dimension k	1	2	3	4	5	6
$x_{i,k}$	1.17	3.95	0.23	2.61	2.72	0.77
$\varphi_{i,k}$	4	1	6	3	2	5
$j_{i,k}$	2	5	4	1	6	3

4.2 Speed-Up Evaluation Method

In NFSSPs with SDSTs and RDs, L_{j_{i-1}, j_i} is only decided by the job j_{i-1} and j_i . According to this property, one method can be adopted to reduce the computing complexity (CC) of $C_T(\pi)$. That is, L_{j_{i-1}, j_i} , sp_{j_i} and $\sum_{i=1}^n sp_{j_i}$ can be calculated and saved in the initial phase of HDE and then can be used as constant values in the evolution phase of HDE, which can reduce the CC of $C_T(\pi)$ from $O(nm)$ to $O(n)$. The procedure of the speed-up evaluation method is given as follows:

// Suppose that L_{j_{i-1}, j_i} , sp_{j_i} and $\sum_{i=1}^n sp_{j_i}$ have already been calculated and //saved.

Step 1: Set $CT=0$;

Step 2: For $i = 1$ to n

 Calculate St_{j_i} by using (4); // L_{j_{i-1}, j_i} is a constant value in (4).

$CT = CT + St_{j_i};$ // $CT = \sum_{l=1}^i St_{j_l}$

 End For i ;

Step 3: $C_T(\pi) = CT + \sum_{i=1}^n sp_{j_i};$ // $\sum_{i=1}^n sp_{j_i}$ is a constant value.

Remark. In Step 2, CT is utilized to save the current value of $\sum_{l=1}^i St_{j_l}$ in each loop.

4.3 DE-Based Global Search

In HDE, DE-based global search is designed based on *DE/rand-to-best/1/exp* scheme [9][12] to perform parallel exploration, in which base vector is the best individual of the current population. So, those individuals performing DE-based operation will share the information of the best individual of the population. In the *mutation* and *crossover* phase, each individual can transform probabilistically to any other individual in the solution space when the evolution generation $t \rightarrow \infty$. In the *selection* phase, only the better individual can be accepted. Therefore, the DE-based search can reach enough promising regions over the solution space.

Let $\text{best}(t)$ denote the best-so-far individual found by HDE until generation t . The procedure of DE-based global search is given as follows:

- Step 1: Generate DE's individuals with random values, and determine the corresponding job permutations by LOV rule.
- Step 2: Calculate $C_T(\pi)$ of initial DE's population, update $\text{best}(t)$ and set $t = 1$.
- Step 3: Update DE's individuals using $DE/rand-to-best/I/exp$ -based scheme and determine permutations using LOV rule.
- Step 4: Calculate makespan of DE's individuals and update $\text{best}(t)$.
- Step 5: Set $t=t+1$. If $t \leq t_{\max}$ (the maximum number of iteration), then go to Step 3.
- Step 6: Output $\text{best}(t)$ and its objective value.

Because of the parallel framework of DE, local search is easy to incorporate into DE to develop effective hybrid algorithms. Next, we will present a problem-dependent local search to perform exploitation.

4.4 Problem-Dependent Local Search

For the FSSPs, two effective neighborhoods are often used in the literature. (i) remove the job at the u th dimension and insert it in the v th dimension of the job solution π ($\text{insert}(\pi, u, v)$), (ii) interchange the job at the u th dimension and the job at the v th dimension of the job solution π ($\text{interchange}(\pi, u, v)$). Thus, we employ *insert* and *interchange* here as the neighborhood for local search.

Denote $X_i(t) = [x_{i,1}, x_{i,2}, \dots, x_{i,n}]$ ($i = 1, 2, \dots, \text{popsize}$) the i th individual in the n -dimensional search space at generation t . The procedure of the local search is given as follows:

- Step 1: Convert individual $X_i(t)$ to a job permutation π_{i_0} according to the LOV rule.
- Step 2: Perturbation phase.
Randomly select u and v , where $u \neq v$; $\pi_i = \text{interchange}(\pi_{i_0}, u, v)$.
- Step 3: Exploitation phase.
Set $loop=1$;
Do
 - Randomly select u and v , where $u \neq v$;
 - $\pi_{i_1} = \text{insert}(\pi_i, u, v)$;
 - if $f(\pi_{i_1}) < f(\pi_i)$, then $\pi_i = \pi_{i_1}$;
 - $loop++$;
 - While $loop < (n \times (n-1))$.
- Step 4: If $f(\pi_i) < f(\pi_{i_0})$, then $\pi_{i_0} = \pi_i$.
- Step 5: Convert π_{i_0} back to $X_i(t)$.

As can be seen from the above procedure, step 2 is the perturbation phase, which is used to escape local optima and guide the search to a different region, and step 3 executes a thorough exploitation from the region obtained by step 2. Since the speed up computation method is adopted here, HDE has the ability to search more regions in the solution space under the same running time. So, instead of using the same neighborhood for perturbation and exploitation, the *interchange* neighborhood and the *insert* neighborhood are employed in step 2 and step 3, respectively, which can guide the search to a more different region and then improve the search ability of HDE to some extent. The effectiveness of adopting the *interchange* neighborhood as perturbation has already been validated in [14].

4.5 HDE

Based on the above solution representation, speed-up computing method, DE-based search, problem-dependent local search, the procedure framework of HDE is proposed in Fig. 2. It can be seen from Fig.2 that not only does HDE apply DE-based searching mechanism to execute exploration for all individuals to find promising regions or solutions within continuous region, but it also applies problem-dependent local search to perform exploitation for the best individual to improve the solution's quality in the permutation space. Because both exploration and exploitation are well stressed, it is expected to achieve good results for NFSSP with SDSTs and RDs. In the next section, we will investigate the performances of the proposed HDE.

5 Test and Comparisons

5.1 Experimental Setup

To test the performance of the proposed HDE for NFSSPs with SDSTs and RDs, computational simulation is carried out with 12 random instances. That is, the $n \times m$ combinations are: $\{30, 50, 70\} \times \{5, 10, 20\}$ and $\{100\} \times \{10, 20, 40\}$. The processing time $p_{j_i,l}$ and the setup time $s_{j_{i-1},j_i,l}$ are generated from a uniform distribution [1, 100] and a uniform distribution [0, 100], respectively. The job arrival time r_{j_i} is an integer that is uniformly generated in $[0, 150n\alpha]$, where the parameter α is used to control the jobs' arrival speeds. The values of α are set to 0, 0.2, 0.4, 0.6, 0.8, 1 and 1.5, respectively. Each instance at each α is independently run 30 times for every algorithm for comparison. Thus, we have a total of 84 different instances.

To evaluate the effectiveness of HDE, we carry out simulations to compare our HDE with several other scheduling algorithms, which are a modified simulated annealing algorithm with first move strategy (SAFM) [15], a hybrid DE for FSSP (HDE_FSSP) [9], HDE_FSSP with the speed-up evaluation method (HDE_FSSP_SP), and an iterated greedy heuristic (IG) [16]. According to [15], SAFM is superior to a famous simulated annealing algorithm proposed by Osman [17]. Based on our tests, SAFM is also more effective than a hybrid genetic algorithm [18]. Moreover, HDE_FSSP is an effective algorithm to address FSSPs [9] and IG is one of the state-of-the-art algorithms for solving FSSPs with SDSTs [16]. In our tests,

HDE, HDE_FSSP, and HDE_FSSP_SP use the same parameters as follows: the population size $popsize = 30$, the scaling factor $F = 0.7$, and the crossover parameter $CR = 0.1$. Thus, the difference between HDE and HDE_FSSP_SP only lies in the neighborhood used in step 2 (i.e., the perturbation phase) of local search. That is, the *interchange* neighborhood and the *insert* neighborhood are employed in the perturbation phase of HDE's and HDE_FSSP_SP's local search, respectively. We re-implement SAFM and IG according to [15] and [16], respectively. All algorithms used in the comparisons are re-implemented by ourselves and are coded in Delphi 7.0. Experiments are executed on an Intel Q8200 2.33GHz PC with 3 GB RAM.

5.2 Test Results and Comparisons

To investigate the performance of HDE, we set SAFM's maximum generation to $40 \times n$ and let all other compared algorithms run at the same time as SAFM. Denote $\pi_{ini}(\alpha)$ the permutation in which jobs are ranked by descending value of job's release date at α , $C_T(\pi(\alpha))$ the total completion time of permutation $\pi(\alpha)$ at α , $avg_C_T(\pi(\alpha))$ the average value of $C_T(\pi(\alpha))$, $best_C_T(\pi(\alpha))$ the best value of $C_T(\pi(\alpha))$, $ARI(\alpha) = (C_T(\pi_{ini}(\alpha)) - avg_C_T(\pi(\alpha))) / C_T(\pi_{ini}(\alpha)) \times 100\%$ the average percentage improvement over $C_T(\pi_{ini}(\alpha))$, $BEI(\alpha) = (C_T(\pi_{ini}(\alpha)) - best_C_T(\pi(\alpha))) / C_T(\pi_{ini}(\alpha)) \times 100\%$ the best percentage improvement over $C_T(\pi_{ini}(\alpha))$, $ET(\alpha)$ the solution evaluation times at α (i.e., the times of calculating $C_T(\pi(\alpha))$), $SD(\alpha)$ the standard deviation of $C_T(\pi(\alpha))$ at α , S_α the set of all values of α , and $|S_\alpha|$ the number of different values in S_α . Then, we define four measures to evaluate the performances of the compared algorithms, i.e.,

$$ARI = \frac{1}{|S_\alpha|} \sum_{\alpha \in S_\alpha} ARI(\alpha), \quad BEI = \frac{1}{|S_\alpha|} \sum_{\alpha \in S_\alpha} BEI(\alpha), \quad ET = \frac{1}{|S_\alpha|} \sum_{\alpha \in S_\alpha} ET(\alpha), \text{ and}$$

$$SD = \frac{1}{|S_\alpha|} \sum_{\alpha \in S_\alpha} SD(\alpha).$$

The statistical results of ARI , SD , BEI , and ET produced by

the compared algorithms are reported in Table 2 and Table 3, respectively. Furthermore, in order to show the details of the compared algorithms for solving the instance with different α , we give the test results of the instance 70×20 in Table 4. The test results of other instances with different α are similar to those in Table 4.

It can be seen from Table 2-4 that the ARI and BEI values obtained by HDE and HDE_FSSP_SP are obviously better than those obtained by SAFM, IG, and HDE_FSSP for almost all instances, which not only shows the superiority of HDE but also validates the effectiveness of utilizing speed-up evaluation method in DE. Meanwhile, the ARI and BEI values obtained by HDE are better than or very close to those obtained by HDE_FSSP_SP for all instances, which demonstrates the necessity of adopting the *interchange* neighborhood in the perturbation phase of local search. Moreover, the SD values of HDE are comparatively small, from which it is concluded that HDE is a robust algorithm. Besides, from Table 3, it is shown that the ET values of HDE and HDE_FSSP_SP increase quickly with the scale of problem, which is

helpful to search more regions/solutions and achieve better performance under the same amount of computer time. However, the local search of HDE is expensive with bigger problems, which means more effective local search method with low computing complexity needs further study.

Table 2. Comparison of *ARI* and *SD* of SAFM, IG, HDE_FSSP, HDE_FSSP_SP, HDE

Instance <i>n, m</i>	SAFM		IG		HDE_FSSP		HDE_FSSP_SP		HDE	
	<i>ARI</i>	<i>SD</i>	<i>ARI</i>	<i>SD</i>	<i>ARI</i>	<i>SD</i>	<i>ARI</i>	<i>SD</i>	<i>ARI</i>	<i>SD</i>
30, 5	17.084	1.351	20.207	0.601	20.994	0.732	20.877	0.723	20.775	0.796
30, 10	17.020	1.110	20.369	0.341	20.925	0.505	20.858	0.504	20.928	0.431
30, 20	12.903	0.804	14.851	0.433	15.412	0.412	15.452	0.396	15.534	0.378
50, 5	26.780	0.983	28.638	0.517	28.961	0.692	29.042	0.791	28.991	0.699
50, 10	22.042	0.825	23.846	0.592	24.395	0.612	24.506	0.697	24.583	0.565
50, 20	20.054	0.642	21.493	0.382	22.033	0.469	22.270	0.474	22.295	0.410
70, 5	27.512	0.741	28.036	0.509	28.920	0.646	29.412	0.605	29.492	0.564
70, 10	27.129	0.536	27.453	0.421	28.119	0.520	28.611	0.473	28.621	0.449
70, 20	22.229	0.548	22.960	0.346	23.471	0.486	24.024	0.403	24.106	0.367
100, 10	29.863	0.441	29.989	0.327	30.417	0.428	30.842	0.423	30.854	0.436
100, 20	27.196	0.423	27.328	0.350	27.828	0.451	28.147	0.371	28.225	0.326
100, 40	29.617	0.371	30.022	0.256	30.572	0.440	31.028	0.361	31.058	0.331
average	23.286	0.731	24.599	0.423	25.171	0.533	25.422	0.518	25.455	0.479

Table 3. Comparison of *BEI* and *ET* of SAFM, IG, HDE_FSSP, HDE_FSSP_SP, HDE

Instance <i>n, m</i>	SAFM		IG		HDE_FSSP		HDE_FSSP_SP		HDE	
	<i>BEI</i>	<i>ET</i>	<i>BEI</i>	<i>ET</i>	<i>BEI</i>	<i>ET</i>	<i>BEI</i>	<i>ET</i>	<i>BEI</i>	<i>ET</i>
30, 5	19.556	27743	21.225	24586	22.129	20210	22.095	19376	22.188	19316
30, 10	19.131	27624	21.316	24613	21.710	20541	21.767	21129	21.651	21146
30, 20	14.525	27444	15.753	24949	16.178	21542	16.142	25644	16.190	25708
50, 5	28.581	76496	29.608	70245	30.189	64977	30.420	69527	30.506	69693
50, 10	23.493	76239	25.045	70951	25.572	66892	25.772	80495	25.757	80424
50, 20	21.215	75975	22.126	72399	22.887	68605	23.057	106556	23.126	106615
70, 5	28.850	149504	29.071	150088	30.195	150082	30.432	312079	30.695	312148
70, 10	28.299	148997	28.386	149898	29.109	149873	29.529	371025	29.530	371279
70, 20	23.397	147924	23.599	148741	24.330	149364	24.708	499844	24.778	499659
100, 10	30.523	302329	30.577	310620	31.068	307923	31.458	763282	31.528	763471
100, 20	27.863	301525	27.810	311657	28.559	307781	28.731	1041850	28.741	1042891
100, 40	30.216	299744	30.442	305562	31.214	307356	31.589	1576192	31.567	1576145
average	24.637	138462	25.413	138692	26.095	136262	26.308	407250	26.355	407375

Table 4. Comparison of SAFM, IG, HDE_FSSP, HDE_FSSP_SP, HDE on instance 70×20

α	SAFM		IG		HDE_FSSP		HDE_FSSP_SP		HDE	
	<i>ARI</i> (α)	<i>SD</i> (α)								
0	25.759	0.566	26.957	0.275	26.876	0.413	27.476	0.419	27.618	0.395
0.2	24.024	0.393	24.403	0.242	25.247	0.434	25.716	0.277	25.856	0.309
0.4	23.522	0.527	24.440	0.146	24.499	0.465	25.333	0.456	25.389	0.306
0.6	22.702	0.611	23.671	0.329	23.702	0.693	24.205	0.431	24.258	0.400
0.8	20.416	0.628	20.209	0.563	21.845	0.476	22.368	0.445	22.468	0.351
1.0	20.622	0.560	21.684	0.231	22.105	0.514	22.619	0.462	22.669	0.475
1.5	18.560	0.549	19.358	0.637	20.020	0.405	20.449	0.334	20.481	0.335
average	22.229	0.548	22.960	0.346	23.471	0.486	24.024	0.403	24.106	0.367

In conclusion, the above comparisons show that HDE is an effective approach with excellent quality and robustness for NFSSPs with SDSTs and RDs.

6 Conclusions and Future Research

This paper presented a hybrid differential evolution (HDE) for the no-wait flow-shop scheduling problem (NFSSP) with sequence-dependent setup times (SDSTs) and release dates (RDs). To the best of the current authors' knowledge, this is the first report on the application of differential evolution (DE) approach to solve the problem considered. The developed algorithm not only applied wide scatter search guided by the evolutionary mechanism of DE, but it also applied thorough local search guided by *interchange*-based perturbation and *insert*-based exploitation. Moreover, a speed-up evaluation method was designed to reduce the computing complexity of evaluation solutions. Thus, both the effectiveness of searching solutions and the efficiency of evaluating solutions were considered. Simulation results and comparisons with some prevail algorithms demonstrated the effectiveness and robustness of our proposed algorithm. For future research, we intend to study DE for other kinds of scheduling problems, such as dynamic job shop scheduling problem.

Acknowledgements. This research is partially supported by National Science Foundation of China (Grant No. 60904081), Applied Basic Research Foundation of Yunnan Province (Grant No. 2009ZC015X), Talent Introduction Foundation of Kunming University of Science and Technology (Grant No. KKZ3200903021), and 863 High Tech Development Plan (Grant No. 2007AA04Z193).

References

1. Graham, R.L., Lawler, E.L., Lenstra, J.K., Rinnooy Kan, A.H.G.: Optimization and Approximation in Deterministic Sequencing and Scheduling: a Survey. *Annals of Discrete Mathematics* 5, 287–326 (1979)
2. Allahverdi, A., Ng, C.T., Cheng, T.C.E., Kovalyov, M.Y.: A Survey of Scheduling Problems with Setup Times or Costs. *European Journal of Operational Research* 187(3), 985–1032 (2008)
3. Oguz, C., Salman, F.S., Yalçin, Z.B.: Order Acceptance and Scheduling Decisions in Make-to-order Systems. *International Journal of Production Economics* 125(1), 200–211 (2010)
4. Urlings, T., Ruiz, R., Stützle, T.: Shifting Representation Search for Hybrid Flexible Flow-line Problems. *European Journal of Operational Research* 207(2), 1086–1095 (2010)
5. Ruiz, R., Allahverdi, A.: Some Effective Heuristics for no-wait Flowshops with Setup Times to Minimize Total Completion Time. *Annals of Operations Research* 156(1), 143–171 (2007)
6. Storn, R., Price, K.: Differential Evolution—a Simple and Efficient Heuristic for Global Optimization over Continuous Spaces. *Journal of Global Optimization* 11(4), 341–359 (1997)
7. Tasgetiren, M.F., Liang, Y.C., Sevkli, M., Gencyilmaz, G.: Differential Evolution Algorithm for Permutation Flowshop Sequencing Problem with Makespan Criterion. In: Proceedings of 4th International Symposium on Intelligent Manufacturing Systems, Sakarya, Turkey, pp. 442–452 (2004)
8. Onwubolu, G., Davendra, D.: Scheduling Flow Shops using Differential Evolution Algorithm. *European Journal of Operational Research* 171(2), 674–692 (2006)

9. Qian, B., Wang, L., Hu, R., Wang, W.L., Huang, D.X., Wang, X.: A Hybrid Differential Evolution for Permutation Flow-shop Scheduling. *International Journal of Advanced Manufacturing Technology* 38(7-8), 757–777 (2008)
10. Pan, Q.K., Tasgetiren, M.F., Liang, Y.C.: A Discrete Differential Evolution Algorithm for the Permutation Flowshop Scheduling Problem. *Computers & Industrial Engineering* 55(4), 795–816 (2008)
11. Wang, L., Pan, Q.K., Suganthan, P.N., Wang, W.H., Wang, Y.M.: A Novel Hybrid Discrete Differential Evolution Algorithm for Blocking Flow Shop Scheduling Problems. *Computers & Operations Research* 37(3), 509–520 (2010)
12. Price, K., Storn, R.: Differential Evolution (DE) for Continuous Function Optimization (2011), <http://www.icsi.berkeley.edu/%7Estorn/code.html>
13. Bean, J.C.: Genetic Algorithm and Random Keys for Sequencing and Optimization. *ORSA Journal on Computing* 6(2), 154–160 (1994)
14. Qian, B., Wang, L., Hu, R., Huang, D.X., Wang, X.: A DE-based Approach to no-wait Flow-shop Scheduling. *Computers & Industrial Engineering* 57(3), 787–805 (2009)
15. Ishibuchi, H., Misaki, S., Tanaka, H.: Modified Simulated Annealing Algorithms for the Flow Shop Sequencing Problem. *European Journal of Operational Research* 81(2), 388–398 (1995)
16. Ruiz, R., Stützle, T.: An Iterated Greedy Heuristic for the Sequence Dependent Setup Times Flowshop Problem with Makespan and Weighted Tardiness Objectives. *European Journal of Operational Research* 187(3), 1143–1159 (2008)
17. Osman, I.H., Potts, C.N.: Simulated Annealing for Permutation Flow-shop Scheduling. *Omega-Int. J. Manage. S.* 17(6), 551–557 (1989)
18. Wang, L., Zheng, D.Z.: An effective hybrid heuristic for flow shop scheduling. *International Journal of Advanced Manufacturing Technology* 21(1), 38–44 (2003)

An Improved Approximation Algorithm for a Class of Batch Scheduling Problems

Jianwei Zhang¹, Baowei Zhang², Zengyu Cai², and Zhaoyang Li²

¹ Software college, Zhengzhou University of Light Industry

² School of Computer and Communication Engineering,

Zhengzhou University of Light Industry, Zhengzhou 450002, P.R. China

{ing, bwzh, czy, lzy}@zzuli.edu.cn

Abstract. The problem of batch scheduling is discussed and the complexity of minimizing the total weighted completed time which is named the problems $1|B, r_j \in \{0, r\}|\sum \omega_j C_j$ is analyzed in this paper. On this basic the NP-completeness of the problem was proved. Then a class of special case of the problem is researched and an improved approximated algorithm is proposed. Finally the analysis and proof to the new algorithm showed that it was feasible and it decreased the computing complexity by about 0.5 times.

Keywords: batch scheduling, algorithm, class, NP-completeness.

1 Introduction

Batch scheduling problem [1] [2] [3] is an important class of scheduling problems deriving from in the final stage of semiconductor manufacturing process, and it is the promotion of the classical scheduling problem. With the development of large-scale modern production, researching batch scheduling problems have important practical significance. After several years of development, batch scheduling has been widely used in computer science, the preparation of operating plans, business management, aerospace, medical and other fields.

It can be described as: there are n work pieces $\{J_1, J_2 \dots J_n\}$ in one (or more) machine(s) to be manufactured , each work piece J_j has processing time P_j , release time r_j and due date d_j (sometimes when work piece reached, it may have not due date). Suppose that there are at most B pieces work pieces can be processed at one time and the biggest processing time of all the pieces is remarked as the processing time of the current batch ,while the completion time C_j of work piece J_j is remarked as the completion time of the current batch. In the process which does not allow interruption, how to reasonably arrange the machine and the work piece to make some of the requirements (objective function) to achieve optimal is called the batch scheduling problem.

When the work pieces arrive simultaneously and the objective function is the total completion time, Bruker gives a time complexity $O(n^{B(B-1)})$ of dynamic

programming algorithm in the literature [1], and Chandru [4] [5] gives the branch sector and several heuristic algorithms, CK Poon and Wenci Yu (2004) [6] proposed the algorithm whose complexity is $O(n^{6B})$ for sufficiently large B. In addition, Hochbaum and Laudy (1997) [7] also gave the 2 - approximation algorithm. For the situation the objective function is the total weighted completion time and the every batch has no limit to the number of pieces and the pieces have different arrival time, Deng and Zhang [8] proved $1|B=\infty, r_j| \sum \omega_j C_j$ were NP-complete, and gave a dynamic programming algorithm where the number of arrival time and the number of working hours is constant. However, in the practical application there has no such strict definition and often is a special case. For the $1|B, r_j \in \{0, r\}| \sum \omega_j C_j$ problem where the objective function is the weighted total completion time and has two arrival time, the article analyzes the computational complexity of the problem and prove its NP-completeness. And a particular type of problem $1|B, r_j \in \{0, r\}, p_j = p| \sum \omega_j C_j$ is studied, Miao Cui Xia, Zhang Yuzhong (2005) [9] gave an approximation algorithm for this problem. We studied their algorithm and proposed an improved approximation algorithm. Not only the algorithm feasibility is proved but also its performance is analyzed. Finally the results show that the algorithm effectively reduces the computational complexity.

2 Related Knowledge

2.1 Batch Scheduling

At the situation of several work pieces being processed on one machine or several machines, how to reasonably arrange the machine and the work piece to make some of the requirements (objective function) to achieve optimal is called the batch scheduling problem. After several years of development, sorting theory and algorithms has become an important branch of combinatorial optimization, Now the three-parameter representation proposed by Lawer et al (1989) is the popularly international ranking classification method, namely $\alpha|\beta|\gamma$.

α : Describe the status of the machine, if $\alpha = 1$, then it denotes a machine, if $\alpha = P$, then it denotes the case of parallel machines.

β : Describe the status of the work piece, for example, $\beta = B$ means the work piece can be processed in batches.

γ : Describe the objective function

The objective function involved in this paper are C_{\max} , $\sum C_j$, $\sum \omega_j C_j$, where C_{\max} expressed the processing time of from the first work piece to the last work piece. ω_j means the weight of the work piece. j. In general, the scheduling problem is to find a single objective function or some function of the optimal integrated to achieve the minimum order. For example: $1|B, r_j \in \{0, r\}| \sum \omega_j C_j$ is the single

machine scheduling problem of work pieces whose goal is minimizing $\sum \omega_j C_j$ at the situation of having two arrival times.

2.2 The Computational Complexity and the P and NP Problem

When we discussed the difficulty of combinatorial optimization problems, it is for some typical question. The problem is the so-called general questions to be answered, and it usually contains a number of parameters or free variables, the values of these parameters have not yet given, if given the assignment after all parameters can be an instance of the problem.

In computational complexity theory, NP is one of the most fundamental complexity classes. The abbreviation NP refers to "nondeterministic polynomial time".

Intuitively, NP is the set of all decision problems for which the instances where the answer is "yes" have efficiently verifiable proofs of the fact that the answer is indeed "yes". More precisely, these proofs have to be verifiable in polynomial time by a deterministic Turing machine. In an equivalent formal definition, NP is the set of decision problems where the "yes"-instances can be recognized in polynomial time by a non-deterministic Turing machine. The equivalence of the two definitions follows from the fact that an algorithm on such a non-deterministic machine consists of two phases, the first of which consists of a guess about the solution which is generated in a non-deterministic way, while the second consists of a deterministic algorithm which verifies or rejects the guess as a valid solution to the problem.

The complexity class P is contained in NP, but NP contains many important problems, the hardest of which are called NP-complete problems, for which no polynomial-time algorithms are known. The most important open question in complexity theory, the P = NP problem, asks whether such algorithms actually exist for NP-complete, and by corollary, all NP problems. It is widely believed that this is not the case.

Theorem 1: The decision problem $A \in NP$ is called NP-complete problem, if all other NP problems can be convert to A in deterministic polynomial time.

2.3 Approximation Algorithms

If the scheduling problem is classified by three-parameter method, there are more than 9,000 different sorts of problems, most of which is NP-complete problem, and complexity theory also makes people aware of scheduling problems can not exist unified algorithms within a wide range, so each scheduling problem must take full advantage of its structure and make different treatment. One type of solution is to reduce the original goal, not going to look for exact algorithms of solve this problem in polynomial time, and consider the polynomial time algorithm in various certain circumstance, and then find, approximation algorithm which can quickly solve the problems in most cases. If you remove the effective guarantee of performance, approximation algorithm can be regarded as heuristic ones, whose methods are effective in practice.

For a minimization problem of the objective function f , if there exists an algorithm A satisfied $f^A \leq \rho f^*$ to all instances. Where f^A express the objective function value gotten by algorithm A and f^* is the optimal objective function value. Besides ρ is called the performance index of algorithm A while the smallest such constant ρ is called the worst performance index of algorithm A.

3 The Improved Approximation Algorithm of a Particular Class of Problem

It has been proved that the problem $1|B, r_j \in \{0, r\}| \sum \omega_j C_j$ is NP-complete problem, so the research on specific issues has practical significance. In this paper, a particular type of problem is researched in this paper. Then a new improved approximation algorithm is proposed and its computational performance is analyzed.

3.1 Classical Approximation Algorithm for $1|B, r_j \in (0, r), p_j = p| \sum \omega_j C_j$

Aim at the situation that all the work pieces having same processing time and having only one same arrival time, which is called $1|B, r, p_j = p| \sum \omega_j C_j$, Miao Cuixia, Zhang Yuzhong presented an optimal algorithm FBLW at 2005 in the literature [9], and the detailed algorithm is shown as follows.

FBLW (fully batch longest weight) algorithm.

Step 1. Renumber all the work pieces according to the weight of the work ,wo got the following order $\omega_1 \geq \omega_2 \geq \dots \geq \omega_B \geq \dots \geq \omega_n$;

Step 2. Take the top B work pieces as the first group B1 and the next top B pieces as the second batch of B2, turn down;

Step 3. take each batch as a work piece and arrange those batches to be processed in turn on the machine by the order gotten in step, thus let the machines do not have any idle time.

Obviously the complexity of this algorithm is $O(n \log n)$.

Through analysis we can get that this type of sorting method contain at most $\frac{n}{B}$ batches, in which $\frac{n}{B}$ indicates the smallest integer not less than $\frac{n}{B}$. Moreover, all the batches are full except the batch containing the work piece J_n .

3.2 Improved Approximation Algorithm

On the basis of deeply researching the algorithm FBLW, aimed at solving problem $1|B, r_j \in \{0, r\}, p_j = p| \sum \omega_j C_j$, a new improved approximation algorithm

named IMFBLW is designed as follows. (Suppose that the work piece set located in the work piece set arrived at time zero is Q_0 while the one arrived at time r is Q_r).

Algorithm IMFBLW:

Step 1. Divide Q_0 into the following batches B_1, B_2, \dots, B_k ($k < n$) starting from time zero;

Step 2. If $kp \leq r$, turn to step 3, otherwise, switch to step 4;

Step 3. For Q_r , using algorithms FBLW to process the work piece in turn from time r;

Step 4. If there is j, which satisfies $1 \leq j \leq k$ and $(j-1)p \leq r \leq jp$, (suppose the start time of B_j at time $(j-1)p$), then the completion time is jp . If $(L-2)p \sum_{p_i \in B_j} \omega_i \geq \sum_{p_j \in (Q_r + Q_0)} \omega_j$, then go to step 5, else go to step 6;

Step 5. Process B_j at time $(j-1)p$ firstly, then process the remaining work pieces in Q_r and Q_0 at time jp using algorithms FBLW;

Step 6. Does not process B_j at time $(j-1)p$ while as process the remaining work pieces in Q_r and Q_0 at time jp using algorithms FBLW at time r

Where $\overline{Q_0}$ means the remaining pieces except batch B_j in Q_r and Q_0 at time r, L is the batch number located in sequence B' of the batch containing the piece having the biggest weight in batch B_j . (B' is the batch $B'_1, B'_2, \dots, B'_L \dots B'_m$ gotten by applying algorithm FBLW to the remaining pieces in Q_r and Q_0 at time r).

4 Feasibility Proof and Performance Analysis

4.1 Feasibility Proof of Algorithm IMFBLW

For algorithm IMFBLW, performance of the algorithm gotten from step 5 is better than the one gotten from step 6 as long as we prove $(L-2) \sum_{p_i \in B_j} \omega_i \geq \sum_{p_j \in (Q_r + Q_0)} \omega_j$ stands

in step 4 (Q'_0 is the pieces set having been processed at time r).

Proof:

(1) In step 5 of algorithm IMFBLW, we assume its weight sum $\sum \omega_j C_j$ is $f(a)$. If we postpone the processing time of batch B_j to time r, that is to say we process B_j at time r and process $\overline{Q_0}$ at time $r + p$, it is obviously that the weight

sum $\sum \omega_j C_j$ in this situation became bigger and we called the weight sum at this moment $f'(a)$. Based on the above analysis and assumption we have the following formula.

$$\begin{aligned}
f(a) < f'(a) &= \sum_0^{FBLW} \omega_j C_j(Q_0') + (r+p) \sum_{p_i \in B_j} \omega_i + \sum_{r+p}^{FBLW} \omega_j C_j(\overline{Q_0} + Q_1) \\
&= \sum_0^{FBLW} \omega_j C_j(Q_0') + (r+p) \sum_{p_i \in B_j} \omega_i + p \sum_{p_i \in (\overline{Q_0} + Q_1)} \omega_i \\
&\quad + \sum_r^{FBLW} \omega_j C_j(\overline{Q_0} + Q_1) \\
&= a
\end{aligned} \tag{1}$$

(2) In step 6 of algorithm IMFBLW, we assume its weight sum $\sum \omega_j C_j$ is $f(b)$. According to algorithm FBLW the batch B_j must be processed after B_{j+1}, B_j, \dots, B_k . If we put all the pieces into the batch the work piece having biggest weight belongs to, then the weight sum $\sum \omega_j C_j$ will not decrease. Set L is batch number in sequence B' the pieces having the maximum weight in B_j belongs to. Based on the above assumption we can get the following formula.

$$\begin{aligned}
f(b) &\geq \sum_0^{FBLW} \omega_j C_j(Q_0') + (r+(L-1)p) \sum_{p_i \in B_j} \omega_i + \sum_r^{FBLW} \omega_j C_j(\overline{Q_0} + Q_1) \\
&= b
\end{aligned} \tag{2}$$

From formula (1) and (2) we can get that if $b \geq a$ then $f(b) > f(a)$. In addition the following formula stands.

$$\begin{aligned}
b \geq a &\Leftrightarrow \sum_0^{FBLW} \omega_j C_j(Q_0') + (r+(L-1)p) \sum_{p_i \in B_j} \omega_i + \sum_r^{FBLW} \omega_j C_j(\overline{Q_0} + Q_1) \\
&\geq \sum_0^{FBLW} \omega_j C_j(Q_0') + (r+p) \sum_{p_i \in B_j} \omega_i + p \sum_{p_i \in (\overline{Q_0} + Q_1)} \omega_i + \sum_r^{FBLW} \omega_j C_j(\overline{Q_0} + Q_1) \\
&\Leftrightarrow (r+(L-1)p) \sum_{p_i \in B_j} \omega_i \geq (r+p) \sum_{p_i \in B_j} \omega_i + p \sum_{p_i \in (\overline{Q_0} + Q_1)} \omega_i \\
&\Leftrightarrow (L-2)p \sum_{p_i \in B_j} \omega_i \geq p \sum_{p_i \in (\overline{Q_0} + Q_1)} \omega_i \\
&\Leftrightarrow (L-2) \sum_{p_i \in B_j} \omega_i \geq \sum_{p_i \in (\overline{Q_0} + Q_1)} \omega_i \\
&\Rightarrow f(b) > f(a)
\end{aligned} \tag{3}$$

Therefore, when $(L-2) \sum_{p_i \in B_j} \omega_i \geq \sum_{p_j \in (Q_1+Q_0)} \omega_j$ the result gotten from step 5 is better than that of step 6. So algorithm IMFBLW is feasible and effective.

4.2 Performance Analysis

From the analysis we can get that algorithm IMFBLW called algorithm FBLW no more than twice and the computing time at each time is no more than $O(n \log n)$. So the computing complexity of IMFBLW is $O(n \log n)$. The main idea of classical algorithm is discussing the algorithm at different situations and select one optimal algorithm by comparing the performances in different situations, so the classical algorithm called algorithm at utmost three times. That is to say the computing complexity of the new algorithm was decreased by about 0.5 times. Therefore, comparing with the classical algorithm FBLW, algorithm IMFBLW proposed in this paper has better performance and reduces the computational complexity effectively.

5 Conclusions

In this paper problems $1|B, r_j \in \{0, r\}| \sum \omega_j C_j$ is discussed and its computational complexity of such issues is analyzed. On this basis a particular class of problems $1|B, r_j \in \{0, r\}| \sum \omega_j C_j$ is studied and an improved approximated algorithm is presented to solve the problem. Finally the feasibility is proved and performance is analyzed. The results show that the computing complexity of the improved algorithm was decreased greatly.

References

1. Brucker, P., Gladky, A., Hoogeveen, H., Kovalyov, M.Y., Tautenhahn, T.: Scheduling Batching Machine. Journal of Schedulling 1, 31–54 (1998)
2. Ahmadi, H., Ahmadi, R.H., Dasu, S., Tang, C.S.: Batching and Scheduling Job Shop on Batch and Discrete Processors. Operations Research 39(4), 750–763 (1992)
3. Albers, Brucker, P.: The Complexity of One-machine Batching Problem. Discrete Applied Mathematics 47, 87–107 (1993)
4. Chandru, V., Lee, C.Y., Uzsoy, R.: Minimizing Total Completion Time on a Batch Processing Machine. International Journal of Production Research 31, 2097–2121 (1993)
5. Chandru, V., Lee, C.Y., Uzsoy, R.: Minimizing Total Completion Time on a Batch Processing Machine with Job Families. Operations Research Letters 13, 61–65 (1993)
6. Poon, C.K., Yu, W.C.: On Minimizing Total Completion Time in Batch Machine Scheduling. International Journal of Foundations of Computer Science 15(4) (2004)
7. Hochbaum, D.S., Landy, D.: Scheduling Semiconductor Burn-in Operations to Minimize Total Flowtime. Operations Research 45(6), 874–885 (1997)
8. Deng, X., Zhang, Y.: Minimizing Mean Response Time in Batch Processing System. In: Asano, T., Imai, H., Lee, D.T., Nakano, S.-i., Tokuyama, T. (eds.) COCOON 1999. LNCS, vol. 1627, pp. 231–240. Springer, Heidelberg (1999)
9. Miao, C.X., Zhang, Y.Z.: Minimizing the Total Weighted Completed Time on Batch Processing Machines. Or Transactions 9(2), 81–86 (2005)

Exponential Stabilization for Takagi-Sugeno Fuzzy Systems with Time Delay via Impulsive Control

Qishui Zhong¹ and Shungang Xu²

¹ Institute of Astronautics & Aeronautics, University of Electronic Science and Technology of China, 611731, Chengdu, P.R. China

² School of Electrical Engineering, Southwest Jiaotong University, 610031, Chengdu, P.R. China

zhongqs@uestc.edu.cn, shungang_xu@163.com

Abstract. This paper addresses the exponential stabilization for time-delay chaotic systems based on their Takagi-Sugeno (T-S) fuzzy models via impulsive control. Using linear matrix inequality (LMI) technique and Lyapunov functional method, some exponential stability criteria are proposed. Numerical examples show that these results are effective and simple.

Keywords: T-S fuzzy system, time delay, impulsive control, exponential stability.

1 Introduction

In the real world, nonlinear dynamic systems with time-delay are common in many situations, such as long transmission lines, biological systems and communication systems. Since Mackey and Glass (M-G) [1] first found chaos in time-delay system in 1977, time-delay chaotic systems have attracted increasing attention of many researchers during the last decade (see [2, 3] and references therein). Because of nonlinear and time delay characteristics, the stability problem of these systems becomes an important issue addressed by many authors [2–6]. It is well known that the T-S fuzzy model can provide an effective representation of complex nonlinear systems in terms of fuzzy sets and fuzzy reasoning applied to a set of linear input-output submodels [7–10]. Therefore, it is widely applied to industrial control fields, especially to chaos control and synchronization [8, 11]. Recently, linear matrix inequality (LMI) technique is used to design controllers for T-S fuzzy systems, so the stability and stabilization problems are transformed to LMI problems and can be solved with ease by a convex optimization algorithm [8, 9].

At the same time, impulsive control has been widely used to stabilize and synchronize nonlinear systems [12, 14? 17], including chaotic systems [11, 15, 18]. Impulsive control scheme is discontinuous with simple structure and only small control impulses, so it is very useful in practical application. Vast endowment has

dealt with impulsive control for real world systems. [17] used the Lyapunov functionals method to analysis the exponential stability of impulsive systems with time delay, and discussed the application to second-order linear delay differential equations. In [18], a new approach to control chaotic systems is proposed combing T-S fuzzy model and impulsive control. [19] discussed the exponential stability of chaotic systems under impulsive control based on their T-S fuzzy models without delay. [19] proposed the criteria of uniform stability and uniform asymptotic stability for time-delay T-S fuzzy systems with impulse using classical analysis method and Razumikhin technique. However, the stability theory of nonlinear dynamic systems under impulsive control has not been fully developed. Furthermore, to the best of our knowledge, there are few papers deal with the exponential stability of time-delay chaotic systems under impulsive control.

Motivated by the above observations, by extending the results in [17], this paper shall establish some exponential stability criteria for time-delay chaotic systems based on their T-S fuzzy models under impulsive control and provide the corresponding procedure of the impulsive controller design.

The rest of this paper is organized as follows. In Section 2, we introduce the main problem and a definition. Some exponential stability criteria are established and the procedure of the impulsive controller design for time-delay chaotic systems is given in Section 3. Section 4 provides numerical examples to demonstrate the scheme, and Section 5 concludes this paper.

2 Problem Formulation

Throughout this paper, $A > 0 (< 0)$ means A is a symmetrical positive (negative) definite matrix. I is the identity matrix. N stand for the set of natural numbers. $\|x\|$ denotes the Euclidian norm of vector x . $\lambda_{\min}(A)$ and $\lambda_{\max}(A)$ mean the minimal and maximal eigenvalues of matrix A , respectively.

Consider a class of time-delay chaotic systems in the form of

$$\dot{x}(t) = f(x(t), x(t - \tau)), \quad (1)$$

where $x(t) \in R^n$ is the state variable, $x(t - \tau) \in R^n$ the time-delay state variable, τ the constant system delay, and $f \in C[R^n, R^n]$ an unknown nonlinear function. It is noted that a large class of chaotic systems can be represented in the form of (1), such as the time-delay Chua's circuit [3], the time-delay Logistic system and M-G system [20].

We can construct fuzzy model for (1) as follows:

Ruleⁱ: IF $z_1(t)$ is M_{i1}, \dots , and $z_p(t)$ is M_{ip}

THEN $\dot{x}(t) = A_i x(t) + B_i x(t - \tau)$

$$x(t) = \varphi(t), -\tau \leq t < 0,$$

where $i = 1, 2, \dots, r$ is the index of fuzzy rules, $z_1(l), \dots, z_p(l)$ are the premise variables, A_i and $B_i \in R^{n \times n}$ are known system matrices, $\varphi(t)$ is a differentiable function. Similar to [21], with a center-average defuzzifier, the over all fuzzy system is represented as

$$\dot{x}(t) = \sum_{i=1}^r h_i(z(t)) [A_i x(t) + B_i x(t - \tau)], \quad (2)$$

where $h_i(z(t)) = \frac{w_i(z(t))}{\sum_{i=1}^r w_i(z(t))}$, $w_i(z(t)) = \prod_{j=1}^p M_{ij}(z_j(t))$, and $M_{ij}(z_j(t))$ is the grade of membership of $z_j(t)$ in M_{ij} . Of course, $h_i(z(t)) \geq 0$ and $\sum_{i=1}^r h_i(z(t)) = 1$. Note that system (2) can locally represent system (1).

To control system (2), an impulsive control law is given by a sequence $\{t_k, I_k(x(t_k))\}$, where $0 < t_1 < t_2 < \dots < t_k < \dots$, $t_k \rightarrow \infty$ as $k \rightarrow \infty$, and $I_k \in C[R^n, R^n]$ denotes the incremental change of the state at time t_k with $I_k(0) = 0$. Thus the following impulsive differential equation is obtained

$$\begin{cases} \dot{x}(t) = \sum_{i=1}^r h_i(z(t)) [A_i x(t) + B_i x(t - \tau)], & \forall t \geq 0, t \neq t_k, \\ \Delta x(t) = I_k(x(t)), & t = t_k, k \in N, \\ x_0 = \varphi(t), & -\tau \leq t < 0, \end{cases} \quad (3)$$

in which $\Delta x(t) = x(t_k^+) - x(t_k)$, $x(t_k^+) = \lim_{t \rightarrow t_k^+} x(t_k)$, $k \in N$.

Definition 1. System (2) is impulsively stabilizable if there exists an impulsive control law $\{t_k, I_k(x(t_k))\}$ such that the trivial solution of (3) is stable.

3 Main Results

In this section, we shall establish some exponential stability criteria for impulsive time-delay system (3), and give a procedure to construct the impulsive controller.

Theorem 1. The trivial solution of system (3) is exponentially stable if there exist a matrix $P > 0$, and constants $\alpha > 0$, β , γ , $m > 0$, $l > 0$ and $d_k > 0$, $k \in N$ such that

$$\gamma \leq 2m, \quad (4)$$

$$PA_i + A_i^T P < \beta I, i = 1, \dots, r, \quad (5)$$

$$PB_i + B_i^T P < \gamma I, i = 1, \dots, r, \quad (6)$$

$$V_1(t_k, x + I_k(t_k, x)) \leq d_k V_1(t_k^-, x), \quad (7)$$

$$\tau \leq t_k - t_{k-1} \leq l, \forall k \in N, \quad (8)$$

$$\ln(d_k + m\tau) < -(\alpha + c)l, \quad (9)$$

in which $c = \frac{\beta + \frac{\gamma}{2} + m}{\lambda_{\min}(P)}$ and $V_1 \in v_0$ (see Ref. [17] for the definition of v_0).

Proof. Choose $V(t) = V_1(t) + V_2(t)$, where $V_1(t) = x^T P x$, $V_2(t) = m \int_{t-\tau}^t x(s)^T x(s) ds$. Then $\lambda_{\min}(P) \|x(t)\|^2 \leq V_1(t) \leq \lambda_{\max}(P) \|x(t)\|^2$, With the norm $\|\cdot\|_\tau$ defined by $\|\varphi\|_\tau = \sup_{-\tau \leq s \leq 0} \|\varphi(s)\|$, we have $0 \leq V_2(t) \leq m\tau \|x(t)\|_\tau^2$, which implies condition (i) of Corollary 3.1 in [17] holds with $c_1 = \lambda_{\min}(P)$, $c_2 = \lambda_{\max}(P)$, $c_3 = m\tau$, $p = 2$.

Furthermore, when $t \neq t_k$, $k \in N$, we have

$$\begin{aligned} V'_1(t, x(t)) &= 2x^T(t)x'(t) \\ &= \sum_{i=1}^r h_i(z(t)) [x^T(t)(A_i^T P + PA_i)x(t) + x^T(t)(B_i^T P + PB_i)x(t-\tau)] \\ &\leq \beta x^T(t)x(t) + \gamma x^T(t)x(t-\tau) \\ &\leq \beta x^T(t)x(t) + \frac{\gamma}{2}(x^T(t)x(t) + x^T(t-\tau)x(t-\tau)) \end{aligned} \quad (10)$$

and

$$V'_2(t, x(t)) = mx(t)^T x(t) - mx^T(t-\tau)x(t-\tau). \quad (11)$$

Recalling that $\gamma \leq 2m$ and $0 \leq V_2(t)$, it is obtained from (II) and (III) that

$$\begin{aligned} V'(t) &= V'_1 + V'_2 \\ &\leq (\beta + \frac{\gamma}{2} + m)x^T(t)x(t) + (\frac{\gamma}{2} - m)x^T(t-\tau)x(t-\tau) \\ &\leq (\beta + \frac{\gamma}{2} + m)\|x(t)\|^2 \\ &\leq \frac{\beta + \frac{\gamma}{2} + m}{\lambda_{\min}(P)} V_1(t) \leq \frac{\beta + \frac{\gamma}{2} + m}{\lambda_{\min}(P)} V(t), \end{aligned} \quad (12)$$

which implies condition (iii) of Corollary 3.1 in [17] holds with $c = \frac{\beta + \frac{\gamma}{2} + m}{\lambda_{\min}(P)}$. Conditions (ii) and (iv) of Corollary 3.1 in [17] are satisfied by (7), (8) and (9). Thus by Corollary 3.1 in [17], the trivial solution of system (3) is exponentially stable. \square

Remark 1. According to Definition 1, the trivial solution of system (3) is exponentially stable implies that system (2) is exponentially stabilizable by impulsive control law $\{t_k, I_k(x(t_k))\}$.

If $I_k(x(t_k)) = C_k x(t_k)$, $k \in N$, where each $C_k \in R^{n \times n}$ is constant matrix, then system (3) is rewrited by

$$\begin{cases} \dot{x}(t) = \sum_{i=1}^r h_i(z(t))[A_i x(t) + B_i x(t-\tau)], & \forall t \geq 0, t \neq t_k, \\ \Delta x(t) = C_k x(t), & t = t_k, k \in N, \\ x_0 = \varphi(t), & -\tau \leq t < 0. \end{cases} \quad (13)$$

Then, we have

$$V_1(t_k, x + I_k(t_k, x)) = [x(t_k) + C_k x(t_k)]^T [x(t_k) + C_k x(t_k)] = x^T(t_k)(I + C_k^T)(I + C_k)x(t_k),$$

$$\text{and } d_k V_1(t_k^-, x) = d_k x^T(t_k) I x(t_k), k \in N.$$

As a result, (7) is equivalent to

$$(I + C_k^T)(I + C_k) - d_k I \leq 0, k \in N,$$

which, by Schur complement, is equivalent to

$$\begin{bmatrix} -d_k I & I + C_k^T \\ I + C_k & -I \end{bmatrix} \leq 0, k \in N. \quad (14)$$

Therefore, we have the following theorem for system (13).

Theorem 2. The trivial solution of system (3) is exponentially stable if there exist a matrix $P > 0$, and constants $\alpha > 0, \beta, \gamma, m > 0, l > 0$ and $d_k > 0, k \in N$ and (4), (5), (6), (8), (9), (14) hold.

Remark 2. Theorem 2 provides an impulsive controller design by linear impulse, which can be easily realized, while Theorem 1 provides a general impulsive control scheme, i.e., control impulse is nonlinear with respect to the state variable $x(t)$. Although it is more involved than Theorem 2 when applied, Theorem 1 may potentially provide much more design schemes than Theorem 2.

On the basis of Theorem 2, the impulsive controller design to exponentially stabilize time-delay chaotic systems based on their T-S models is convenient and the procedure is given as follows:

Step 1. For a given T-S fuzzy system with time delay in the form of (2), figure out λ_A, λ_B .

Step 2. According to (8), compute a series of impulse times $t_k, k \in N$.

Step 3. Choose scalars $\alpha > 0, 1 \geq m > 0$, solve (9) and get $d_k, k \in N$. If $d_k > 0$, go to *Step 4*. If not, adjust the values of α and m until $d_k > 0$.

Step 4. Utilize (14) to determine $C_k, k \in N$.

4 Numerical Example

In this section, an examples are presented to show the validity of our control scheme.

Consider the T-S fuzzy model of a computer simulated truck-trailer with time delay [10]:

$$\dot{x}(t) = \sum_{i=1}^2 h_i(t)(A_i x(t) + B_i x(t - \tau)) \quad (15)$$

where

$$A_1 = \begin{bmatrix} -a \frac{v\bar{t}}{L t_0} & 0 & 0 \\ a \frac{v\bar{t}}{L t_0} & 0 & 0 \\ a \frac{v^2 \bar{t}^2}{2 L t_0} & \frac{v\bar{t}}{t_0} & 0 \end{bmatrix}, B_1 = \begin{bmatrix} -(1-a) \frac{v\bar{t}}{L t_0} & 0 & 0 \\ (1-a) \frac{v\bar{t}}{L t_0} & 0 & 0 \\ (1-a) \frac{v^2 \bar{t}^2}{2 L t_0} & 0 & 0 \end{bmatrix},$$

$$A_2 = \begin{bmatrix} -a \frac{v\bar{t}}{L t_0} & 0 & 0 \\ a \frac{v\bar{t}}{L t_0} & 0 & 0 \\ a \frac{dv^2 \bar{t}^2}{2 L t_0} & \frac{dv\bar{t}}{t_0} & 0 \end{bmatrix}, B_2 = \begin{bmatrix} -(1-a) \frac{v\bar{t}}{L t_0} & 0 & 0 \\ (1-a) \frac{v\bar{t}}{L t_0} & 0 & 0 \\ (1-a) \frac{dv^2 \bar{t}^2}{2 L t_0} & 0 & 0 \end{bmatrix},$$

$a = 0.7, L = 5.5, v = -1.0, \bar{t} = 2.0, t_0 = 0.5, \tau = 1, d = 10t_0/\pi$ and the membership functions as

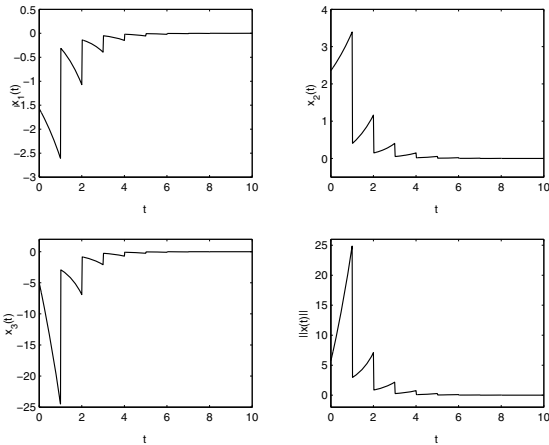


Fig. 1. State response of system (15) under impulsive control

$$h_1(\theta) = \left(1 - \frac{1}{1 + \exp(-3(\theta(t) - 0.5\pi))}\right) \left(\frac{1}{1 + \exp(-3(\theta(t) + 0.5\pi))}\right), h_2(\theta) = 1 - h_1(\theta),$$

in which, $\theta(t) = x_2(t) + a \frac{vt}{2L} x_1(t) + (1 - a) \frac{vt}{2L} x_1(t - \tau)$.

From system (15), it is obtained $\lambda_A = 0.5091$, $\lambda_B = 0.2182$. Let $m = 0.001$, $t_k - t_{k-1} = 1$, $k \in N$, $l = 1$, conditions (4) and (5) are satisfied. Choose $\alpha = 0.001$, solve (6) and get $d_k = 0.3428$, $k \in N$. Utilize the LMI (14), we get $C_k = \text{diag}(-0.8825, -0.8825, -0.8825)$, $k \in N$.

The simulation was carried out when the initial condition is $[-0.5\pi \ 0.75\pi \ -5]^T$ and exponential stabilization results are shown in Fig. 1.

5 Conclusions

A novel impulsive control scheme for T-S fuzzy systems with time delay is proposed. In terms of linear matrix inequalities, some sufficient conditions are derived to exponentially stabilize T-S fuzzy systems with time delay via impulsive control. The procedure of designing impulsive controller is also provided. Simulation results demonstrate the effectiveness of the proposed control scheme.

Acknowledgements. This work was supported by the Fundamental Research Funds for the Central Universities(Grant No. ZYGX2009J088) and Sichuan Science & Technology Plan(Grant No. 2011JY0001).

References

1. Mackey, M., Glass, L.: Oscillation and Chaos in Physiological Control System. *Science* 197, 287–289 (1977)
2. Park, J., Kwon, O.: LMI Optimization Approach to Stabilization of Time-delay Chaotic Systems. *Chaos Solitons and Fractals* 23, 445–450 (2005)

3. Guan, X., Feng, G., Chen, C., Chen, G.: A Full Delayed Feedback Controller Design Method for Time-delay Chaotic Systems. *Physica D* 227, 36–42 (2007)
4. Cao, Y., Frank, P.M.: Stability Analysis and Synthesis of Nonlinear Time-delay Systems via Linear Takagi-Sugeno Fuzzy Models. *Fuzzy Sets and Systems* 124, 213–229 (2001)
5. Zhang, X.F., Baron, L., Liu, Q.G., Boukas, E.K.: Design of Stabilizing Controllers With a Dynamic Gain for Feedforward Nonlinear Time-Delay Systems. *IEEE Transactions on Automatic Control* 56, 692–697 (2011)
6. Hua, C., Guan, X., Shi, P.: Robust Output Feedback Tracking Control for Time-delay Nonlinear Systems Using Neural Network. *IEEE Transactions on Neural Networks* 18, 495–505 (2007)
7. Takagi, T., Sugeno, M.: Fuzzy Identification of Systems and Its Application to Modeling and Control. *IEEE Transactions on Systems, Man and Cybernetics* 15, 116–132 (1985)
8. Kim, J., Park, C., Kim, E., Park, M.: Fuzzy Adaptive Synchronization of Uncertain Chaotic Systems. *Physics Letters A* 334, 295–305 (2005)
9. Lin, C., Wang, Q., Lee, T.H.: Delay-dependent LMI Conditions for Stability and Stabilization of T-S Fuzzy Systems with Bounded Time-delay. *Fuzzy Sets and Systems* 157, 1229–1247 (2006)
10. Tadeo, F., Benzaouia, A., Ait Rami, M.: Static Output-feedback for Takagi-Sugeno Systems with Delays. *International Journal of Adaptive Control and Signal Processing* 25, 295–312 (2011)
11. Liu, X., Zhong, S.: T-S Fuzzy Model-based Impulsive Control of Chaotic Systems with Exponential Decay Rate. *Physics Letters A* 370, 260–264 (2007)
12. Lakshmikantham, V., Bainov, D.D., Simeonov, P.S.: Theory of Impulsive Differential Equations. Series in Modern Applied Mathematics. World Scientific, Singapore (1989)
13. Zhong, Q., Bao, J., Yu, Y., Liao, X.: Impulsive Control for T-S Fuzzy Model-based Chaotic Systems. *Mathematics and Computers in Simulation* 79, 409–415 (2008)
14. Yang, T.: Impulsive control. *IEEE Transactions on Automatic Control* 44, 1080–1083 (1999)
15. Zhong, Q., Bao, J., Yu, Y., Liao, X.: Exponential Stabilization for Discrete Takagi-Sugeno Fuzzy Systems via Impulsive Control. *Chaos, Solitons and Fractals* 41, 2123–2127 (2009)
16. Zhong, Q., Yu, Y., Yu, J.: Fuzzy Modeling and Impulsive Control of a Memristor-based Chaotic System. *Chinese Physics Letters* 27, 020501 (2010)
17. Liu, X., Wang, Q.: The Method of Lyapunov Functionals and Exponential Stability of Impulsive Systems with Time Delay. *Nonlinear Analysis* 66, 1465–1484 (2007)
18. Jiang, H.J., Teng, Z.D.: General Impulsive Control of Chaotic Systems Based on a TS Fuzzy Model. *Fuzzy Sets and Systems* 174, 66–82 (2011)
19. Sun, J.: Stability of Takagi-Sugeno Fuzzy Delay Systems with Impulse. *IEEE Transaction on Fuzzy Systems*, doi:10.1109/TFUZZ.2006.889926
20. Guan, X., Chen, C., Peng, H., Fan, Z.: Time-delayed Feedback Control of Time-delay Chaotic Systems. *International Journal of Bifurcation and Chaos* 13, 193–205 (2003)
21. Wang, H., Griffin, M.: An Approach to Fuzzy Control of Nonlinear Systems: Stability and Design Issues. *IEEE Transactions on Fuzzy and Systems* 4, 14–23 (1996)

H_∞ Output Tracking Control for Neutral Delay System With Nonlinear Perturbations

Cuihong Wang and Huijuan Cao

Department of Mathematics and Computer Science, Shanxi Normal University,
Shanxi 041004

Abstract. This paper studies the problem of H_∞ output tracking control for neutral delay system with nonlinear perturbations. Based on a novel augmented Lyapunov functional, a sufficient condition for the existence of state-feedback controller is presented in terms of linear matrix inequality, which not only guarantees the stability of closed-loop system, but also ensure the output of the neutral system tracks the output of a given reference model in the H_∞ sense.

Keywords: H_∞ output tracking control, Neutral systems, Linear matrix inequality (LMI).

1 Introduction

During the last decades, the problem of stability and stabilization of time-delay system have been investigated by many researchers in the past years^[1–7]. Neutral delay system as a special class of time-delay system widely applies to many dynamic systems. The problem of robust stability for uncertain neutral systems using the model transformation technique is investigated in [8]. By introducing some free-weighing matrices, one can avoid employing model transformations and estimates for cross terms which have been adopted in [9]. A delay-dependent sufficient condition of the stability of uncertain neutral delay system is given in the form of linear matrix inequality in [10].

At the same time, output tracking control has found wide applications in industry, information, and biological field. In the last century, the research on the tracking control is mostly only limited to ignoring the nonlinear and uncertainty of the systems, nevertheless, the nonlinear and uncertainty exist objectively in actual system. so the problem of output tracking control with nonlinear perturbation has been widely studied in recent few years [11,12].

In this paper, we are concerned with the H_∞ output tracking control for time-varying neutral systems with nonlinear perturbation. By constructing a novel Lyapunov-Krasovskii functional, and combining with weighting matrix method, a delay-dependent criterion is derived in terms of LMI which guarantee that the output of neutral systems tracks the output of the given reference model in H_∞ sense.

2 Problem Formulation

Consider the following neutral systems with time-varying delay and nonlinear perturbations

$$\begin{cases} \dot{x}(t) = Ax(t) + Bx(t - d(t)) + C\dot{x}(t - \tau) + f_1(x(t), t) \\ \quad + f_2(x(t - d(t), t) + f_3(\dot{x}(t - \tau), t) + Du(t) + E\omega(t) \\ z(t) = C_1x(t) + C_2x(t - d(t)) + D_1u(t) \end{cases} \quad (1)$$

where $x(t) \in R^n$ is the state vector, $u(t) \in R^m$ is the control input, $z(t) \in R^p$ is the control output, $\omega(t) \in R^r$ is the disturbance input that belongs to $l_2[0, \infty)$, $\tau > 0$ is a constant neutral delay, $d(t)$ is a time-varying discrete delay satisfying $d_1 \leq d(t) \leq d_2$. $f_1(x(t), t) \in R^n$, $f_2(x(t - d(t)), t) \in R^n$, $f_3(\dot{x}(t - \tau), t) \in R^n$ are unknown nonlinear perturbations which satisfy that $f_1(0, t) = 0$, $f_2(0, t) = 0$, $f_3(0, t) = 0$, and

$$\begin{aligned} \|f_1(x(t), t)\| &\leq \alpha\|x(t)\|, \\ \|f_2(x(t - d(t)), t)\| &\leq \beta\|x(t - d(t))\|, \\ \|f_3(\dot{x}(t - \tau), t)\| &\leq \sigma\|\dot{x}(t - \tau)\|, \end{aligned}$$

where $\alpha \geq 0$, $\beta \geq 0$, $\sigma \geq 0$ are given constants. For simplicity, denote $f_1 := f_1(x(t), t)$, $f_2 := f_2(x(t - d(t)), t)$, $f_3 := f_3(\dot{x}(t - \tau), t)$.

The reference model is given as

$$\begin{cases} \dot{x}_r(t) = Gx_r(t) + r(t) \\ z_r(t) = Hx_r(t) \end{cases} \quad (2)$$

where $z_r(t)$ has the same dimension as $z(t)$, $x_r(t) \in R^r$ is the reference state input, $r(t) \in R^r$ is the energy bounded reference input, G , H are constant matrices of appropriate dimensions and G is Hurwitz.

We are interested in designing a state-feedback controller of the form

$$u(t) = K_1x(t) + K_2x_r(t). \quad (3)$$

where $K_1 \in R^{m \times n}$, $K_2 \in R^{m \times r}$ are controller gain matrices. Defining $\xi(t) = [x^T(t) \ x_r^T(t)]^T$, $v(t) = [w^T(t) \ r^T(t)]^T$, $e(t) = z(t) - z_r(t)$, $y(t) = \dot{\xi}(t)$, we can obtain the following augmented system

$$\begin{cases} \dot{\xi}(t) = \bar{A}\xi(t) + \bar{B}\xi(t - d(t)) + \bar{C}y(t - \tau) + \bar{I}f_1 + \bar{I}f_2 + \bar{I}f_3 + \bar{E}v(t) \\ e(t) = \bar{C}_1\xi(t) + \bar{C}_2\xi(t - d(t)) \end{cases} \quad (4)$$

where $\bar{A} = \begin{bmatrix} A + DK_1 & DK_2 \\ 0 & G \end{bmatrix}$, $\bar{B} = \begin{bmatrix} B & 0 \\ 0 & 0 \end{bmatrix}$, $\bar{C} = \begin{bmatrix} C & 0 \\ 0 & 0 \end{bmatrix}$, $\bar{I} = \begin{bmatrix} I \\ 0 \end{bmatrix}$, $\bar{E} = \begin{bmatrix} E & 0 \\ 0 & I \end{bmatrix}$, $\bar{C}_1 = [C_1 + D_1K_1 \ -H + D_1K_2]$, $\bar{C}_2 = [C_2 \ 0]$.

The objective of this paper is to design a state-feedback controller (3) such that the following conditions hold,

(1) The closed-loop system (4) is asymptotically stable for $v(t) = 0$.

(2) Under the assumption of zero initial condition, the controlled output $z(t)$ satisfies $\|z(t)\|_2 \leq \gamma \|v(t)\|_2$, for any non-zero $v(t) \in l_2[0, \infty)$.

In order to obtain the main results, the following lemmas are first introduced.

Lemma 1. [13] For any constant matrix $M \in R^{n \times n}$, $M = M^T > 0$, scalars r_1 and r_2 satisfying $r_1 < r_2$, and a vector function $\omega: [r_1, r_2] \rightarrow R^{n \times n}$ such that the integrations concerned are well defined, then

$$(\int_{r_1}^{r_2} \omega(s) ds)^T M (\int_{r_1}^{r_2} \omega(s) ds) \leq (r_2 - r_1) \int_{r_1}^{r_2} \omega^T(s) M \omega(s) ds.$$

Lemma 2. [14] For given matrices $A_{11}, A_{12}, A_{21}, A_{22}$ with appropriate dimensions, $\begin{bmatrix} A_{11} & A_{12} \\ A_{21} & A_{22} \end{bmatrix} < 0$, holds if and only if $A_{22} < 0$, $A_{11} - A_{12}A_{22}^{-1}A_{12}^T < 0$.

3 Main Results

3.1 H_∞ Output Tracking Performance Analysis

Theorem 1. Given nonlinear system (4) and a prescribed real number $\gamma > 0$, if there exist matrices $P > 0$, $M_1 > 0$, $M_2 > 0$, $S > 0$, U_1, V_1, U_2, V_2 and nonnegative scalars $\varepsilon_1, \varepsilon_2, \varepsilon_3$ such that the following inequality holds,

$$\Phi < 0 \quad (5)$$

with

$$\Phi = \begin{bmatrix} \varphi_{11} & \varphi_{12} & \varphi_{13} & 0 & \varphi_{15} & P\bar{I} & P\bar{I} & P\bar{I} & P\bar{E} & 0 & 0 & \bar{C}_1^T & \bar{A}^T & \bar{A}^T & \bar{A}^T \\ * & \varphi_{22} & \varphi_{23} & 0 & 0 & 0 & 0 & 0 & 0 & U_1 & 0 & 0 & 0 & 0 & 0 & 0 \\ * & * & \varphi_{33} & \varphi_{34} & 0 & 0 & 0 & 0 & 0 & U_1 & 0 & 0 & 0 & 0 & 0 & 0 \\ * & * & * & \varphi_{44} & 0 & 0 & 0 & 0 & 0 & 0 & V_2 & 0 & 0 & 0 & 0 & 0 \\ * & * & * & * & \varphi_{55} & 0 & 0 & 0 & 0 & 0 & 0 & 0 & 0 & \bar{C}^T & \bar{C}^T & \bar{C}^T \\ * & * & * & * & * & -\varepsilon_1 I & 0 & 0 & 0 & 0 & 0 & 0 & 0 & \bar{I}^T & \bar{I}^T & \bar{I}^T \\ * & * & * & * & * & * & -\varepsilon_2 I & 0 & 0 & 0 & 0 & 0 & 0 & \bar{I}^T & \bar{I}^T & \bar{I}^T \\ * & * & * & * & * & * & * & -\varepsilon_3 I & 0 & 0 & 0 & 0 & 0 & \bar{I}^T & \bar{I}^T & \bar{I}^T \\ * & * & * & * & * & * & * & * & -\gamma^2 I & 0 & 0 & 0 & 0 & \bar{E}^T & \bar{E}^T & \bar{E}^T \\ * & * & * & * & * & * & * & * & * & \varphi_{10,10} & 0 & 0 & 0 & 0 & 0 & 0 \\ * & * & * & * & * & * & * & * & * & * & \varphi_{11,11} & 0 & 0 & 0 & 0 & 0 \\ * & * & * & * & * & * & * & * & * & * & * & -I & 0 & 0 & 0 & 0 \\ * & * & * & * & * & * & * & * & * & * & * & * & \varphi_{13,13} & 0 & 0 & 0 \\ * & * & * & * & * & * & * & * & * & * & * & * & * & \varphi_{14,14} & 0 & 0 \\ * & * & * & * & * & * & * & * & * & * & * & * & * & * & * & -S^{-1} \end{bmatrix}$$

$$\varphi_{11} = P\bar{A} + \bar{A}^T P + \alpha^2 \varepsilon_1 \bar{I}\bar{I}^T - d_1^{-1} M_2, \quad \varphi_{12} = d_1^{-1} M_2, \quad \varphi_{13} = P\bar{B}$$

$$\varphi_{15} = P\bar{C}, \quad \varphi_{22} = U_1 + U_1^T - d_1^{-1} M_2, \quad \varphi_{23} = V_1^T - U_1,$$

$$\varphi_{33} = U_2 + U_2^T - V_1 - V_1^T + \beta^2 \varepsilon_2 \bar{I}\bar{I}^T, \quad \varphi_{34} = -U_2 + V_2^T,$$

$$\varphi_{44} = -V_2 - V_2^T, \quad \varphi_{55} = -S + \sigma^2 \varepsilon_3 \bar{I}\bar{I}^T, \quad \varphi_{10,10} = \varphi_{11,11} = -d_1^{-1} M_1,$$

$$\varphi_{13,13} = -d_1^{-1} M_1^{-1}, \quad \varphi_{14,14} = -d_1^{-1} M_2^{-1},$$

then the nonlinear system (4) is asymptotically stable and satisfies the H_∞ performance index.

Proof. We first establish the asymptotic stability of the augmented closed-loop system (4) with $v(t) = 0$. Choose the following Lyapunov-Krasovskii functional

$$V(t) = V_1(t) + V_2(t) + V_3(t) + V_4(t) \quad (6)$$

where

$$\begin{aligned} V_1(t) &= \xi^T(t)P\xi(t), \\ V_2(t) &= \int_{-d_2}^{-d_1} \int_{t+\theta}^t \dot{\xi}^T(s)M_1\dot{\xi}(s)dsd\theta, \\ V_3(t) &= \int_{-d_1}^0 \int_{t+\theta}^t \dot{\xi}^T(s)M_2\dot{\xi}(s)dsd\theta, \\ V_4(t) &= \int_{t-\tau}^t y^T(s)Sy(s)ds. \end{aligned}$$

Then calculating the derivative of $V(t)$ along the trajectories of system (4) yields

$$\begin{aligned} \dot{V}_1(t) &= 2\xi^T(t)P[\bar{A}\xi(t) + \bar{B}\xi(t-d(t)) + \bar{C}y(t-\tau) + \bar{I}f_1 + \bar{I}f_2 + \bar{I}f_3], \\ \dot{V}_2(t) &= d_{12}\dot{\xi}^T(t)M_1\dot{\xi}(t) - \int_{t-d_2}^{t-d(t)} \dot{\xi}^T(s)M_1\dot{\xi}(s)ds - \int_{t-d(t)}^{t-d_1} \dot{\xi}^T(s)M_1\dot{\xi}(s)ds, \\ \dot{V}_3(t) &= d_1\dot{\xi}^T(t)M_2\dot{\xi}(t) - \int_{t-d_1}^t \dot{\xi}^T(s)M_2\dot{\xi}(s)ds, \\ \dot{V}_4(t) &= \dot{\xi}^T(t)S\dot{\xi}(t) - y^T(t-\tau)Sy(t-\tau). \end{aligned} \quad (7)$$

From the Lemma 1, we can get

$$-\int_{t-d_1}^t \dot{\xi}^T(s)M_2\dot{\xi}(s)ds \leq -d_1^{-1}(\xi(t) - \xi(t-d_1))^T M_2(\xi(t) - \xi(t-d_1)) \quad (8)$$

It follows from Leibniz-Newton formula that

$$A_1 = 2 \begin{bmatrix} \xi(t-d_1) \\ \xi(t-d(t)) \end{bmatrix}^T \begin{bmatrix} U_1 \\ V_1 \end{bmatrix} (\xi(t-d_1) - \xi(t-d(t)) - \int_{t-d(t)}^{t-d_1} \dot{\xi}(s)ds) = 0 \quad (9)$$

$$A_2 = 2 \begin{bmatrix} \xi(t-d(t)) \\ \xi(t-d_2) \end{bmatrix}^T \begin{bmatrix} U_2 \\ V_2 \end{bmatrix} (\xi(t-d(t)) - \xi(t-d_2) - \int_{t-d_2}^{t-d(t)} \dot{\xi}(s)ds) = 0 \quad (10)$$

In addition, for any matrices $\begin{bmatrix} X_1 & Y_1 \\ * & Z_1 \end{bmatrix} \geq 0$, $\begin{bmatrix} X_2 & Y_2 \\ * & Z_2 \end{bmatrix} \geq 0$, we have

$$\begin{aligned} A_3 &= d_{12} \begin{bmatrix} \xi(t-d_1) \\ \xi(t-d(t)) \end{bmatrix}^T \begin{bmatrix} X_1 & Y_1 \\ * & Z_1 \end{bmatrix} \begin{bmatrix} \xi(t-d_1) \\ \xi(t-d(t)) \end{bmatrix} \\ &\quad - \int_{t-d(t)}^{t-d_1} \begin{bmatrix} \xi(t-d_1) \\ \xi(t-d(t)) \end{bmatrix}^T \begin{bmatrix} X_1 & Y_1 \\ * & Z_1 \end{bmatrix} \begin{bmatrix} \xi(t-d_1) \\ \xi(t-d(t)) \end{bmatrix} ds \geq 0 \end{aligned} \quad (11)$$

$$\begin{aligned} A_4 &= d_{12} \begin{bmatrix} \xi(t-d(t)) \\ \xi(t-d_2) \end{bmatrix}^T \begin{bmatrix} X_2 & Y_2 \\ * & Z_2 \end{bmatrix} \begin{bmatrix} \xi(t-d(t)) \\ \xi(t-d_2) \end{bmatrix} \\ &\quad - \int_{t-d_2}^{t-d(t)} \begin{bmatrix} \xi(t-d(t)) \\ \xi(t-d_2) \end{bmatrix}^T \begin{bmatrix} X_2 & Y_2 \\ * & Z_2 \end{bmatrix} \begin{bmatrix} \xi(t-d(t)) \\ \xi(t-d_2) \end{bmatrix} ds \geq 0 \end{aligned} \quad (12)$$

Combining(7)-(12), we have

$$\begin{aligned} \dot{V}(t) &\leq \dot{V}_1(t) + \dot{V}_2(t) + \dot{V}_3(t) + \dot{V}_4(t) + \varepsilon_2(\beta^2 x^T(t-d(t))x(t-d(t)) \\ &\quad - f_2^T f_2) + \varepsilon_1(\alpha^2 x^T(t)x(t) - f_1^T f_1) + \varepsilon_3(\sigma^2 \dot{x}^T(t-\tau)\dot{x}(t-\tau) \\ &\quad - f_3^T f_3) + \Lambda_1 + \Lambda_2 + \Lambda_3 + \Lambda_4 \\ &= \phi_1^T(t)(\Omega_1 + \Omega_4)\phi_1(t) + \int_{t-d(t)}^{t-d_1} \phi_2^T(t)\Omega_2\phi_2(t)ds + \int_{t-d_2}^{t-d(t)} \phi_3^T(t)\Omega_3\phi_3(t)ds. \end{aligned} \quad (13)$$

where

$$\begin{aligned} \phi_1(t) &= [\xi^T(t) \ \xi^T(t-d_1) \ \xi^T(t-d(t)) \ \xi^T(t-d_2) \ y^T(t-\tau) \ f_1^T \ f_2^T \ f_3^T]^T, \\ \phi_2(t) &= [\xi^T(t-d_1) \ \xi^T(t-d(t)) \ \dot{\xi}^T(s)]^T \\ \phi_3(t) &= [\xi^T(t-d(t)) \ \xi^T(t-d_2) \ \dot{\xi}^T(s)]^T \end{aligned}$$

and

$$\begin{aligned} \Omega_1 &= \begin{bmatrix} \varphi_{11} & \varphi_{12} & P\bar{B} & 0 & P\bar{C} & P\bar{I} & P\bar{I} & P\bar{I} \\ * & \bar{\varphi}_{22} & \bar{\varphi}_{23} & 0 & 0 & 0 & 0 & 0 \\ * & * & \bar{\varphi}_{33} & \bar{\varphi}_{34} & 0 & 0 & 0 & 0 \\ * & * & * & \bar{\varphi}_{44} & 0 & 0 & 0 & 0 \\ * & * & * & * & -S + \sigma^2 \varepsilon_3 \bar{I} \bar{I}^T & 0 & 0 & 0 \\ * & * & * & * & * & -\varepsilon_1 I & 0 & 0 \\ * & * & * & * & * & * & -\varepsilon_2 I & 0 \\ * & * & * & * & * & * & * & -\varepsilon_3 I \end{bmatrix}, \\ \Omega_2 &= \begin{bmatrix} -X_1 & -Y_1 & -U_1 \\ * & -Z_1 & -V_1 \\ * & * & -M_1 \end{bmatrix}, \quad \Omega_3 = \begin{bmatrix} -X_2 & -Y_2 & -U_2 \\ * & -Z_2 & -V_2 \\ * & * & -M_1 \end{bmatrix}, \\ \Omega_4 &= \Gamma^T(d_{12}M_1 + d_1M_2 + S)\Gamma, \quad \Gamma = [\bar{A} \ 0 \ \bar{B} \ 0 \ \bar{C} \ \bar{I} \ \bar{I} \ \bar{I}], \end{aligned}$$

with

$$\begin{aligned} \bar{\varphi}_{22} &= U_1 + U_1^T - d_1^{-1}M_2 + d_{12}X_1, \quad \bar{\varphi}_{23} = V_1^T - U_1 + d_{12}Y_1, \\ \bar{\varphi}_{33} &= U_2 + U_2^T - V_1 - V_1^T + \beta^2 \varepsilon_2 \bar{I} \bar{I}^T + d_{12}Z_1 + d_{12}X_2, \\ \bar{\varphi}_{34} &= -U_2 + V_2^T + d_{12}Y_2, \quad \bar{\varphi}_{44} = -V_2 - V_2^T + d_{12}Z_2. \end{aligned}$$

In addition, (5) is equivalent to the following inequality by using lemma 2

$$\Xi + \begin{bmatrix} 0 & 0 & 0 & 0 \\ * & \Theta_{22} & \Theta_{23} & 0 \\ * & * & \Theta_{33} & \Theta_{34} \\ * & * & * & \Theta_{44} \end{bmatrix} \begin{array}{c|c} & \mathbf{0} \\ \hline & \mathbf{0} \end{array} < 0 \quad (14)$$

where

$$\begin{aligned} \Theta_{22} &= d_{12}U_1M_1^{-1}U_1^T, \quad \Theta_{23} = d_{12}U_1M_1^{-1}V_1^T, \quad \Theta_{34} = d_{12}U_2M_1^{-1}V_2^T, \\ \Theta_{33} &= d_{12}V_1M_1^{-1}V_1^T + d_{12}U_2M_1^{-1}U_2^T, \quad \Theta_{44} = d_{12}V_2M_1^{-1}V_2^T. \end{aligned}$$

and

$$\Xi = \begin{bmatrix} \Phi_1 & \left[\begin{array}{cccc} \bar{C}_1^T & \bar{A}^T & \bar{A}^T & \bar{A}^T \\ 0 & 0 & 0 & 0 \\ \bar{C}_2^T & \bar{B}^T & \bar{B}^T & \bar{B}^T \\ 0 & 0 & 0 & 0 \\ 0 & \bar{C}^T & \bar{C}^T & \bar{C}^T \\ 0 & \bar{I}^T & \bar{I}^T & \bar{I}^T \\ 0 & \bar{I}^T & \bar{I}^T & \bar{I}^T \\ 0 & \bar{I}^T & \bar{I}^T & \bar{I}^T \\ 0 & \bar{E}^T & \bar{E}^T & \bar{E}^T \end{array} \right] \\ * & \left[\begin{array}{cccc} -I & 0 & 0 & 0 \\ * & \varphi_{13,13} & 0 & 0 \\ * & * & \varphi_{14,14} & 0 \\ * & * & * & -S^{-1} \end{array} \right] \end{bmatrix},$$

Then, there always exist matrices $\begin{bmatrix} X_1 & Y_1 \\ * & Z_1 \end{bmatrix} \geq 0, \begin{bmatrix} X_2 & Y_2 \\ * & Z_2 \end{bmatrix} \geq 0$ satisfying

$$\begin{bmatrix} U_1 M_1^{-1} U_1^T & U_1 M_1^{-1} V_1^T \\ * & V_1 M_1^{-1} V_1^T \end{bmatrix} \leq \begin{bmatrix} X_1 & Y_1 \\ * & Z_1 \end{bmatrix}, \quad \begin{bmatrix} U_2 M_1^{-1} U_2^T & U_2 M_1^{-1} V_2^T \\ * & V_2 M_1^{-1} V_2^T \end{bmatrix} \leq \begin{bmatrix} X_2 & Y_2 \\ * & Z_2 \end{bmatrix},$$

and

$$\Xi + \begin{bmatrix} 0 & 0 & 0 & 0 \\ * d_{12} X_1 & d_{12} Y_1 & 0 & \mathbf{0} \\ * & * & d_{12} Z_1 + d_{12} X_2 & d_{12} Y_2 \\ * & * & * & d_{12} Z_2 \end{bmatrix} < 0.$$

By lemma 2 we know (13)<0, therefore system(4) is asymptotically stable.

Next, we will analysis the H_∞ output tracking performance for the system (4). considering (6) and calculating the derivative of $V(t)$, we can obtain

$$\dot{V}(t) \leq \bar{\phi}_1^T(t)(\bar{\Omega}_1 + \bar{\Omega}_4)\bar{\phi}_1(t) + \int_{t-d(t)}^{t-d_1} \phi_2^T(t)\Omega_2\phi_2(t)ds + \int_{t-d_2}^{t-d(t)} \phi_3^T(t)\Omega_3\phi_3(t)ds$$

where

$$\bar{\phi}_1(t) = [\xi^T(t), \xi^T(t-d_1), \xi^T(t-d(t)), \xi^T(t-d_2), y^T(t-\tau), f_1^T, f_2^T, f_3^T, v^T(t)]^T,$$

$$\bar{\Omega}_1 = \begin{bmatrix} \varphi_{11} & \varphi_{12} & P\bar{B} & 0 & P\bar{C} & P\bar{I} & P\bar{I} & P\bar{I} & P\bar{E} \\ * & \bar{\varphi}_{22} & \bar{\varphi}_{23} & 0 & 0 & 0 & 0 & 0 & 0 \\ * & * & \bar{\varphi}_{33} & \bar{\varphi}_{34} & 0 & 0 & 0 & 0 & 0 \\ * & * & * & \bar{\varphi}_{44} & 0 & 0 & 0 & 0 & 0 \\ * & * & * & * & -S + \sigma^2 \varepsilon_3 \bar{I} \bar{I}^T & 0 & 0 & 0 & 0 \\ * & * & * & * & * & -\varepsilon_1 I & 0 & 0 & 0 \\ * & * & * & * & * & * & -\varepsilon_2 I & 0 & 0 \\ * & * & * & * & * & * & * & -\varepsilon_3 I & 0 \\ * & * & * & * & * & * & * & * & 0 \end{bmatrix},$$

$$\bar{\Omega}_4 = \bar{\Gamma}^T(d_{12}M_1 + d_1M_2 + S)\bar{\Gamma}, \quad \bar{\Gamma} = [\bar{A} \ 0 \ \bar{B} \ 0 \ \bar{C} \ \bar{I} \ \bar{I} \ \bar{I} \ \bar{E}],$$

Consider the following index

$$\rho = \int_0^\infty (e^T(s)e(s) - \gamma^2 v^T(s)v(s))ds. \quad (15)$$

Under zero initial condition, we have $V(0) = 0$ and $V(\infty) \geq 0$ which implies

$$\begin{aligned} \rho &= \int_0^\infty (e^T(t)e(t) - \gamma^2 v^T(t)v(t) + \dot{V}(t))dt - V(\infty) \\ &\leq \int_0^\infty (e^T(t)e(t) - \gamma^2 v^T(t)v(t) + \dot{V}(t))dt. \end{aligned} \quad (16)$$

Considering $e(t) = \bar{C}_1 \xi(t) + \bar{C}_2 \xi(t - d(t))$, we obtain

$$\begin{aligned} &e^T(t)e(t) - \gamma^2 v^T(t)v(t) + \dot{V}(t) \\ &\leq \bar{\phi}_1^T(t)(\tilde{\Omega}_1 + \tilde{\Omega}_4)\bar{\phi}_1(t) + \int_{t-d(t)}^{t-d_1} \bar{\phi}_2^T(t)\Omega_2\phi_2(t)ds + \int_{t-d_2}^{t-d(t)} \bar{\phi}_3^T(t)\Omega_3\phi_3(t)ds \end{aligned} \quad (17)$$

where

$$\tilde{\Omega}_1 = \bar{\Omega}_1 + \left[\begin{array}{ccc|cc} \bar{C}_1^T \bar{C}_1 & 0 & \bar{C}_1^T \bar{C}_2 & \mathbf{0} & \mathbf{0} \\ * & 0 & 0 & & \\ * & * & \bar{C}_2^T \bar{C}_2 & & \\ \hline * & & & * & \mathbf{0} \\ \hline * & & & * & -\gamma^2 I \end{array} \right].$$

Then according to (15)-(17), $\forall v(t) \in l_2[0, \infty)$, $e^T(t)e(t) - \gamma^2 v^T(t)v(t) + \dot{V}(t) < 0$. which implies that $\rho < 0$, that is $\|e\|_2 < \gamma \|v\|_2$. This completes the proof.

3.2 H_∞ Output Tracking Controller Design

In this subsection, based on the Theorem 1 we will focus on the design of H_∞ controller for the system (1). Letting $\tilde{A} = \begin{bmatrix} A & 0 \\ 0 & G \end{bmatrix}$, $\tilde{D} = \begin{bmatrix} D \\ 0 \end{bmatrix}$, $\tilde{C}_1 = [C_1 \ -H]$, $K = [K_1 \ K_2]$, we know $\bar{A} = \tilde{A} + \tilde{D}K$, $\bar{C}_1 = \tilde{C}_1 + D_1K$.

Theorem 2. Given nonlinear system (1), if there exist matrices $\bar{P} > 0$, $\bar{M}_1 > 0$, $\bar{M}_2 > 0$, $\bar{S} > 0$, \bar{U}_1 , \bar{U}_2 , \bar{V}_1 , \bar{V}_2 and nonnegative scalars $\bar{\varepsilon}_1$, $\bar{\varepsilon}_2$, $\bar{\varepsilon}_3$, such that the following inequality holds,

$$\tilde{\Phi} = [\tilde{\varphi}_{ij}] < 0 \quad (1 \leq i, j \leq 15). \quad (18)$$

where

$$\begin{aligned} \tilde{\varphi}_{11} &= \bar{P}\tilde{A}^T + \tilde{A}\bar{P} + \alpha^2\bar{\varepsilon}_1 + \tilde{D}\tilde{K} + \tilde{K}^T\tilde{D}^T + d_1^{-1}\bar{M}_2 - 2d_1^{-1}\bar{P}, \quad \tilde{\varphi}_{12} = d_1^{-1}\bar{M}_3, \\ \tilde{\varphi}_{13} &= \bar{B}\bar{P}, \quad \tilde{\varphi}_{15} = \bar{C}\bar{P}, \quad \tilde{\varphi}_{16} = \tilde{\varphi}_{17} = \tilde{\varphi}_{18} = \bar{I}\bar{I}^T\bar{P}, \quad \tilde{\varphi}_{19} = \bar{E}, \\ \tilde{\varphi}_{1,12} &= \bar{P}\tilde{C}_1^T + \tilde{K}^T\tilde{D}_1^T, \quad \tilde{\varphi}_{1,13} = \tilde{\varphi}_{1,14} = \tilde{\varphi}_{1,15} = \bar{P}\tilde{A}^T + \tilde{K}^T\tilde{D}^T, \\ \tilde{\varphi}_{22} &= \bar{U}_1 + \bar{U}_1^T + d_1^{-1}\bar{M}_2 - 2d_1^{-1}\bar{P}, \quad \tilde{\varphi}_{23} = \bar{V}_1^T - \bar{U}_1, \quad \tilde{\varphi}_{2,10} = \bar{U}_1, \\ \tilde{\varphi}_{33} &= \bar{U}_2 + \bar{U}_2^T - \bar{V}_1 - \bar{V}_1^T + \beta^2\bar{\varepsilon}_2, \quad \tilde{\varphi}_{34} = -\bar{U}_2 - \bar{V}_2^T, \quad \tilde{\varphi}_{3,10} = \bar{V}_1, \\ \tilde{\varphi}_{3,11} &= \bar{U}_2, \quad \tilde{\varphi}_{3,12} = \bar{P}\tilde{C}_2^T, \quad \tilde{\varphi}_{3,13} = \tilde{\varphi}_{3,14} = \tilde{\varphi}_{3,15} = \bar{P}\bar{B}^T, \\ \tilde{\varphi}_{44} &= -\bar{V}_2 - \bar{V}_2^T, \quad \tilde{\varphi}_{4,11} = \bar{V}_2, \quad \tilde{\varphi}_{5,13} = \tilde{\varphi}_{5,14} = \tilde{\varphi}_{5,15} = \bar{P}\bar{C}^T, \\ \tilde{\varphi}_{55} &= \bar{S} - 2\bar{P} + \sigma^2\bar{\varepsilon}_3, \quad \tilde{\varphi}_{66} = -\bar{\varepsilon}_1 I, \quad \tilde{\varphi}_{6,13} = \tilde{\varphi}_{6,14} = \tilde{\varphi}_{6,15} = \bar{P}\bar{I}\bar{I}^T, \end{aligned}$$

$$\begin{aligned}\tilde{\varphi}_{77} &= -\bar{\varepsilon}_2 I, & \tilde{\varphi}_{7,13} = \tilde{\varphi}_{7,14} = \tilde{\varphi}_{7,15} = \bar{P} \bar{I} \bar{I}^T, & \tilde{\varphi}_{88} = -\bar{\varepsilon}_3 I, \\ \tilde{\varphi}_{8,13} = \tilde{\varphi}_{8,14} &= \tilde{\varphi}_{8,15} = \bar{P} \bar{I} \bar{I}^T, & \tilde{\varphi}_{9,13} = \tilde{\varphi}_{9,14} = \tilde{\varphi}_{9,15} = \bar{E}^T, \\ \tilde{\varphi}_{99} &= -\gamma^2 I, & \tilde{\varphi}_{10,10} = \tilde{\varphi}_{11,11} = d_{12}^{-1} M_1 - 2d_{12}^{-1} \bar{P}, & \tilde{\varphi}_{12,12} = -I, \\ \tilde{\varphi}_{13,13} &= -d_{12}^{-1} \bar{M}_1, & \tilde{\varphi}_{14,14} = -d_1^{-1} M_2, & \tilde{\varphi}_{15,15} = -S,\end{aligned}$$

others, $\tilde{\varphi}_{ij} = 0$. then we can design a desired controller in the form of (3) with $K = \tilde{K} \bar{P}^{-1}$ to ensure the closed-loop system (4) is asymptotically stable and satisfies the H_∞ performance index.

The proof process of Theorem 2 is omitted due to the limitation of length.

4 Conclusion

In this paper, we are concerned with the H_∞ output tracking control for neutral systems. By constructing a suitable augmented Lyapunov functional, a delay-dependent criterion is derived in terms of LMI.

References

1. Fridman, E., Shaked, U.: An Improved Stabilization Method For Linear Time-delay Systems. *IEEE Transactions on Automatic Control* 47, 1931–1937 (2003)
2. Gu, K., Kharitonov, V.L., Chen, J.: Stability of Time-delay Systems. Birkhauser, Boston (2003)
3. Han, Q.L.: On Robust Stability of Neutral Systems with Time-varying Discrete Delay and Norm-bounded Uncertainty. *Automatica* 40, 1087–1092 (2004)
4. Jiang, X., Han, Q.L.: On H_∞ Control for Linear Systems with Interval Time-varying Delay. *Automatica* 41, 2099–2106 (2005)
5. Liu, X., Zhang, H.: New Stability Criterion of Uncertain Systems with Time-varying Delay. *Chaos Solitons and Fractals* 26, 1343–1348 (2005)
6. He, Y., Wang, Q.L., Lin, C., Wu, M.: Delay-range-dependent Stability for Systems with Time-varying Delay. *Automatica* 43, 371–376 (2007)
7. Zhang, X.M., Li, M.M., Wu, M., She, J.H.: Further Results on Stability and Stabilization of Linear Systems with State and Input Delays. *International Journal of Systems Science* 40, 1–10 (2009)
8. Han, Q.L.: Robust Stability of Uncertain Delay-differential Systems of Neutral Type. *Automatica* 38, 719–723 (2002)
9. Zhang, D., Li, Y.: H_∞ Output Tracking Control for Neutral Systems with Time-varying Delay and Nonlinear Perturbations. *Communications in Nonlinear Science and Numerical Simulation* 15, 3284–3292 (2010)
10. He, Y., Wu, M.: On Delay-dependent Robust Stability for Uncertain Neutral Systems. *Journal of Systems Engineering and Electronics* 16, 351–355 (2005)
11. Behtash, S.: Robust Output Tracking for Nonlinear Systems. *International Journal of Control* 51, 1381–1407 (1990)
12. Elmali, H., Olgac, N.: Robust Output Tracking Control of Nonlinear MIMO Systems via Sliding Node Technique. *Automatica* 28, 145–151 (1992)
13. Gu, K., Kharitonov, V.L., Chen, J.: Stability of Time-delay Systems. Birkhauser, Boston (2003)
14. Boyd, S.P., Ghaoui, L.E., Feron, E., Balakrishnan, V.: Linear Matrix Inequalities in Systems and Control Theory. SIAM, Philadelphia (1994)

Chaotic Modeling of Time-Delay Memristive System

Ju Jin¹, Yongbin Yu², Yijing Liu³, Xiaorong Pu², and Xiaofeng Liao⁴

¹ School of Life Science and Technology, University of Electronic Science and Technology of China, 611731, Chengdu, P.R. China

² School of Computer Science and Engineering, University of Electronic Science and Technology of China, 611731, Chengdu, P.R. China

³ College of Computer Science, Sichuan University, Chengdu, Sichuan, 610065, P.R.China

⁴ College of Computer Science, Chongqing University, Chongqing, 400030, P.R.China
ybyu@uestc.edu.cn

Abstract. This work considers time delay effect on memristive system. Introduced time delay in the feedback circuit of memristive system, the time-delay memristive system is presented. By the means of dynamics analysis and computer simulation, we derive chaotic model of the delayed memristive system.

Keywords: memristor, time delay, chaotic model.

1 Introduction

Traditionally, the three fundamental passive circuit elements are resistors (R), capacitors (C), and inductors (L). The behavior of each of these two-terminal elements is presented with a simple linear relationship between two of the four basic circuit variables: current (i), voltage (v), charge (q) and magnetic flux (φ). So, a resistor, an inductor and a capacitor are defined as $f_R(v, i, t) = 0$, $f_L(\varphi, i, t) = 0$ and $f_C(q, v, t) = 0$. According to the logical completeness of circuit theory, a fourth fundamental passive circuit element should be characterized by a functional relationship between charge and flux ($f_M(q, \varphi, t) = 0$), which is named as memristor (a contraction for memory resistor) by Chua (1, 2) and fabricated by a team led by R. Stanley Williams from the Hewlett-Packard Company (3). Figure 1 shows this relationship graphically. Hereby, memristor is classified as charge-controlled memristor ($M(q)$) and flux-controlled memristor ($W(\varphi)$). Memristor with charge and flux control is a passive two-terminal electronic device. Moreover, an active two-terminal memristor can be modeled by a charge-controlled memristor connected in series with a negative resistance or a flux-controlled memristor connected in parallel with a negative conductance. In fact, the notion of memristor can be generalized to capacitor and inductor whose properties depend on the state and history of the system (4). So, circuit elements with memory, including memristors, memcapacitors (a contraction for memory capacitor) and meminductors (a contraction for memory inductor), are

nanoscale devices of nanoelectronics. Combined with the general class of memory nanoscale electronic circuits and standard circuit elements, these elements and their combination open up new functionalities in electronics and are likely to find applications in neuromorphic devices to simulate learning, adaptive and spontaneous behavior.

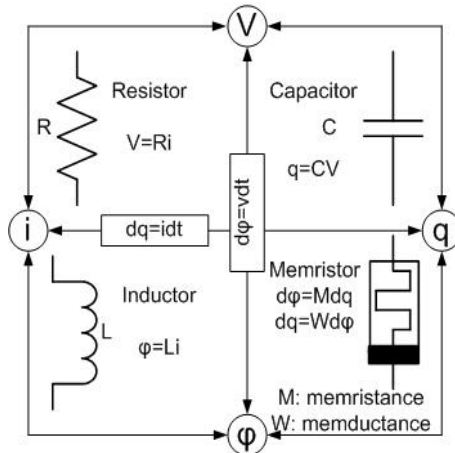


Fig. 1. The fundamental circuit elements

Time delay frequently appears in linear or nonlinear systems. Typical examples of time-delay systems are electronic networks, communication circuits, chemical processes, teleoperation systems, biosystems, underwater vehicles and so on, where the state change rate depends not only on the current state of the system but also its state at some time in the past. Delay effects may introduce instability, oscillators, chaos and other complex dynamical behaviors. Moreover, the presence of time delay makes system design and analysis much more complicated. So time-delay dynamical systems have been the subject of extensive research during the past decades [5]-[10].

In this paper, we investigate chaotic effects on memristive systems with time delay. By introducing time-delay circuit, we build mathematical model of time-delay memristive system. Furthermore, we analyze the time-delay dynamical system and present some new chaotic behaviors of the time-delay memristive system with feasible and effective simulation results. To the best of our knowledge, the proposed work in this paper on memristive systems with delayed and chaotic effects is new in the literature.

The remainder of this paper is organized as follows. In following section, we design memristive system according to memristor theory and circuit principle. In section 3, we design the time-delay circuit, and build chaotic model of memristive system with time delay, and present numerical simulation to illustrate chaos dynamical behavior of time-delay memristive system, section 4 concludes this paper.

2 Memristive System

By using passive or active memristors and the three traditional basic circuit elements, we can design a general class of memristive systems. Without loss of generality, we study the flux-controlled memristive system in figure 2, which consists of two resistors, a inductor, two capacitors, and a passive memristor or an active memristor. Replaced passive or active memristor by Chua's diodes, the memristive system is transformed into a Chua's oscillator (□).

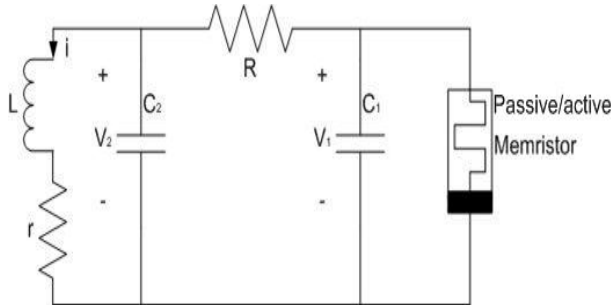


Fig. 2. Memristive system with R, L, C , and M

As for passive memristor, applying Kirchhoff's circuit laws to the nodes and the loop of the circuit in figure 2, we get

$$\begin{cases} C_1 \frac{dv_1}{dt} = \frac{v_2 - v_1}{R} - W(\varphi)v_1 \\ C_2 \frac{dv_2}{dt} = i - \frac{v_2 - v_1}{R} \\ L \frac{di}{dt} = -ri - v_2 \\ \frac{d\varphi}{dt} = v_1 \end{cases} \quad (1)$$

When a flux-controlled memristor connects in parallel with a negative conductance ($-G_M$), an active memristor is obtained. At the same time, the dynamic equations of memristive system with an active memristor is presented

$$\begin{cases} C_1 \frac{dv_1}{dt} = \frac{v_2 - v_1}{R} + G_M v_1 - W(\varphi)v_1 \\ C_2 \frac{dv_2}{dt} = i - \frac{v_2 - v_1}{R} \\ L \frac{di}{dt} = -ri - v_2 \\ \frac{d\varphi}{dt} = v_1 \end{cases} \quad (2)$$

where the nonlinear function $W(\varphi)$ given by

$$W(\varphi) = \frac{dq(\varphi)}{d\varphi} = \frac{d[b\varphi + 0.5(a-b)(|\varphi+1| - |\varphi-1|)]}{d\varphi} = \begin{cases} a, & |\varphi| < 1, \\ b, & |\varphi| > 1. \end{cases}$$

According to the above-mentioned memristive systems, time delay happens frequently because of transmitting trait of electronic signal and processing of electronic devices. Hereby, we introduce time delay to memristive system and study dynamical behaviors of time-delay memristive systems.

3 Main Results

In this section, first, we introduce time delay in the memristive system and find a way to design time-delay circuit. Then, we analyze the time-delay dynamical system, and study chaotic behaviors of the time-delay memristive system with numeral simulation.

3.1 Design of Time-Delay Memristive System

According to memristor characteristic and circuit theory, we can design time-delay memristive systems. By adding a small-amplitude voltage time-delay feedback in the memristive system, the modified memristive system is obtained. Figure 3 shows time-delay memristive system based on a passive memristor and an active memristor. When memristor is passive, The dynamics of time delay system is governed by the following state equations:

$$\left\{ \begin{array}{l} C_1 \frac{dv_1}{dt} = \frac{v_2 - v_1}{R} - W(\varphi)v_1 \\ C_2 \frac{dv_2}{dt} = i - \frac{v_2 - v_1}{R} \\ L \frac{di}{dt} = -ri - v_2 - \varepsilon \sin(\sigma v_1(t - \tau)) \\ \frac{d\varphi}{dt} = v_1 \end{array} \right. \quad (3)$$

At the same time, the corresponding form of time-delay memristive system with an active memristor is presented:

$$\left\{ \begin{array}{l} C_1 \frac{dv_1}{dt} = \frac{v_2 - v_1}{R} + G_M v_1 - W(\varphi)v_1 \\ C_2 \frac{dv_2}{dt} = i - \frac{v_2 - v_1}{R} \\ L \frac{di}{dt} = -ri - v_2 - \varepsilon \sin(\sigma v_1(t - \tau)) \\ \frac{d\varphi}{dt} = v_1 \end{array} \right. \quad (4)$$

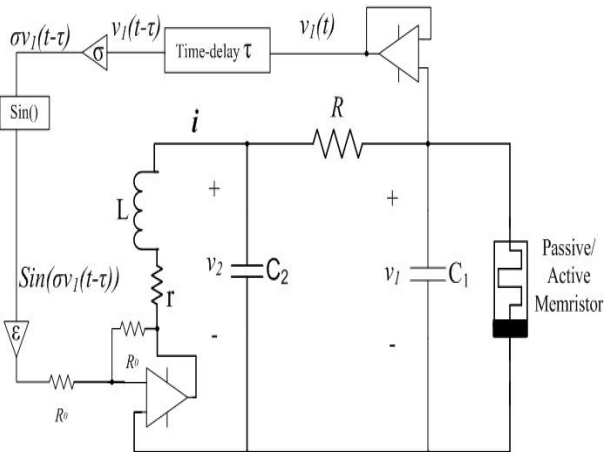


Fig. 3. Memristive system with time delay

We will show that chaotic model of memristive system with time delay can be achieved for the given parameters of $C_1, C_2, L, r, R, a, b, \sigma, \varepsilon, \tau$.

Remark 1: Time delay term is taken as $\varepsilon \sin(\sigma v_1(t-\tau))$. Obviously, the maximum amplitude of the time delay term is ε , which is an important parameter in the dynamical model.

Remark 2: In the time delay feedback circuit, time delay τ is small, which means the total delay of transmission line and circuit elements such as memristor, amplifier, and so on.

Remark 3: According to memristor theory and circuit law, we can implement circuit design of time delay.

3.2 Chaos Attractor

Combined with memristor and standard circuit elements, their combination is a typical nonlinear system for nonlinear memristor. By the means of dynamics analysis and computer simulation, we study chaotic modelling of the nonlinear memristive system with time delay.

First, we investigate the dynamical behaviors of memristive system without time delay. When $C_1 = 0.1, C_2 = 1, L = 1/18, r = 1/45, R = 1, a = -0.7$ and $b = -10$, the dynamical behavior of memristive system with a passive memristor is shown in figure 4 (left). At the same time, while $C_1 = 0.1, C_2 = 1, L = 1/13, r = 7/260, G_M = 1.5, a = 0.3$ and $b = 0.8$, the memristive system with an active memristor has a double scroll attractor as shown in figure 4 (right). Figure 4 demonstrates that chaos happens in the memristive system. Obviously, the memristive system shown in Fig.2 can be regarded as chaos generator.

Note that time delay may bring complex dynamical behaviors with memristive system. Consequently, we pay attention to the dynamics of time-delay system

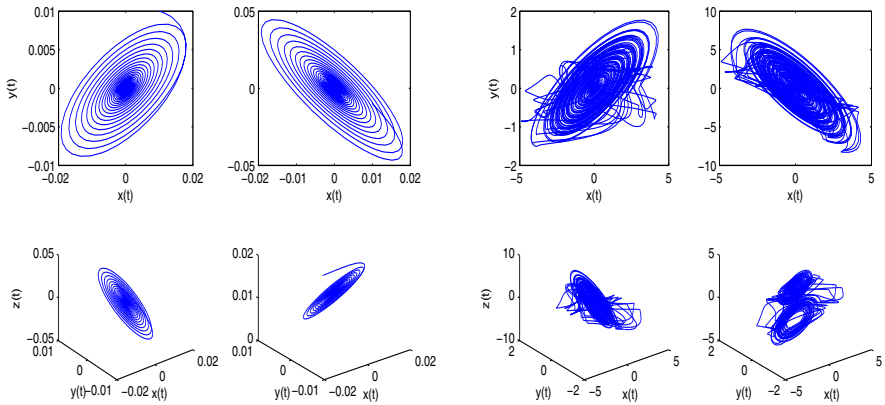


Fig. 4. The dynamical behavior of memristive system with a passive memristor (left) or an active memristor (right)

based on a passive memristor or an active memristor. If we set $C_1 = 0.0001, C_2 = 0.000001, L = 1, r = 0.01, R = 1000/3, a = 0.0004, b = 0.0005, \varepsilon = 3, \sigma = 5$ and time delay $\tau = 0.01$, our computer simulation shows that time-delay dynamical system with a passive memristor has a chaotic attractor as shown in figure 5(left). At the same time, the following parameter values of time-delay system with an active memristor are fixed for our computer simulations:

$$\begin{cases} C_1 = 0.00001, C_2 = 0.00001, L = 0.1, r = 1, R = 1, a = 0.01, b = 0.01 \\ G_M = 0.00001, \varepsilon = 10, \sigma = 1, \tau = 0.01 \end{cases}$$

and a strange chaotic attractor is obtained and shown in figure 5(right).

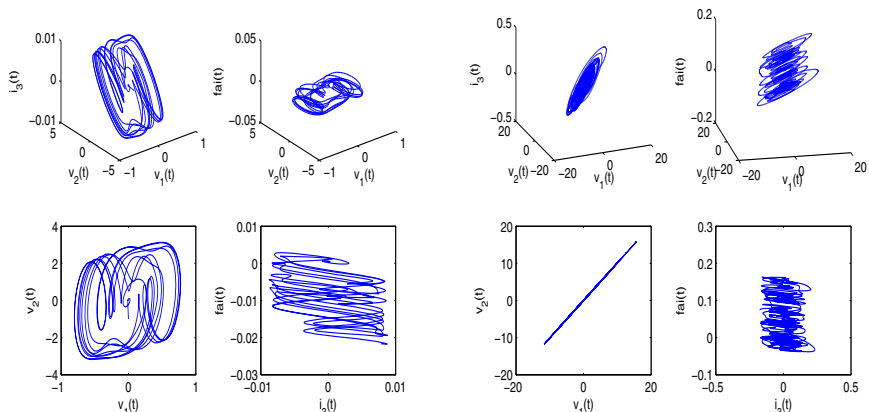


Fig. 5. The dynamical behavior of time-delay memristive system with a passive memristor (left) or an active memristor (right)

By adding the time-delay feedback with different values of σ , ε and τ , figure 5 shows distinct chaotic attractors. Firstly, figure 5 has multiple scroll attractor compared with a double scroll attractor shown in figure 4. The contour of simulation result shows that the introduced time delay may lead to dynamical complication of memristive system. Secondly, the parameters of σ , ε and τ are sensitive to chaotic behaviors of the time-delay memristive system. Finally, the intent on study chaotic model of time-delay memristive system is to probe into the nonlinear characteristic of memristor.

4 Conclusions

This paper summarizes comprehensively memristor traits and investigates memristive systems with chaotic and delayed effects. The contribution of this paper lies in the following aspects. Firstly, we find an efficient way to introduce time delay and implement time-delay circuit in memristive system. Furthermore, the proposed time delay design can be extended to other nonlinear systems. Secondly, we study chaotic behaviors of time-delay memristive system, and present a novel chaos generator based on a passive memristor and an active memristor. Finally, this work helps understand the nonlinear characteristic of memristor.

Acknowledgements. This work was supported by the National Natural Science Foundation of China (NSFC Grant No.60973070) and the Fundamental Research Funds for the Central Universities(Program No.ZYGX2010J073).

References

- Chua, L.O.: Memristor-the Missing Circuit Element. *IEEE Trans. Circuit Th.* CT-18, 507–519 (1971)
- Chua, L.O., Kang, S.M.: Memristive Devices and Systems. *Proc. IEEE* 64, 209–223 (1976)
- Strukov, D.B., Snider, G.S., Stewart, G.R., Williams, R.S.: The Missing Memristor Found. *Nature* 453, 80–83 (2008)
- Ventra, M.D., Pershin, Y.V., Chua, L.O.: Circuit Elements with Memory: Memristor, Memcapacitors, and Meminductors. *Proceedings of the IEEE* 97(10), 1717–1724 (2009)
- Wang, X.F., Zhong, G.Q., Tang, K.S., Man, K.F., Liu, Z.F.: Generating Chaos in Chua's Circuit via Time-delay Feedback. *IEEE Trans. Circuits Syst. I, Fundam. Theory Appl.* 48(2), 1151–1156 (2001)
- Mahmoud, M.S., Ismail, A.: New Results on Delay-dependent Control of Time-delay Systems. *IEEE Trans. Auto. Control* 50(1), 95–100 (2005)
- Niu, Y.G., Ho, D.W.C., Lam, J.: Robust Integral Sliding Mode Control for Uncertain Stochastic Systems with Time-varying Delay. *Automatica* 41(3), 873–880 (2005)
- Yang, Z.C., Xu, D.Y.: Stability Analysis and Design of Impulsive Control Systems with Time Delay. *IEEE Trans. Automatic Control* 52(8), 1448–1454 (2007)

9. Yu, Y.B., Zhong, Q.S., Liao, X.F., Yu, J.B.: Exponential Stability of Takagi-Sugeno Fuzzy Systems with Impulsive Effects and Time Delays. *Chinese Physics* 17(3), 842–846 (2008)
10. Yu, Y.B., Bao, J.F., Zhang, H.B., Zhong, Q.S., Liao, X.F., Yu, J.B.: Impulsive Control of Nonlinear Systems with Time-varying Delays. *Chinese Physics* 17(7), 2377–2387 (2008)
11. Makoto, I., Chua, L.O.: Memristor Oscillators. *International Journal of Bifurcation and Chaos* 18(11), 3183–3206 (2008)

Stability Analysis and Constrained Control of Positive Systems with Time-Varying Delays: A Linear Copositive Lyapunov-Krasovskii Functional Method

Yulin Song

College of Tourism Historical Culture, Southwest University for Nationalities
yulinsong8@gmail.com

Abstract. This paper considers the analysis and constrained control problems of positive systems with time-varying delays. A system is called positive system if its states keep nonnegative whenever its initial conditions and inputs are nonnegative, and the control is under positivity constraint means that the resulting closed-loop system is not only stable, but also positive. The main contribution lies in the following aspects. Firstly, based on a linear copositive Lyapunov-Krasovskii functional, some stability criteria are established for positive systems with time-varying delays. Secondly, constrained controller for a class of systems with time-varying delays is designed, which guarantees the corresponding closed-loop system is positive and asymptotically stable.

Keywords: Linear copositive Lyapunov-Krasovskii functional, positive system, polytopic uncertainty, time-varying delay, linear programming.

1 Introduction

Many physical systems involve quantities that have invariant sign. For example, population of animals, density of gas, absolute temperature, level of liquid in tanks, and concentration of substances in chemical processes are always nonnegative. They belong to the important class of systems whose states and outputs are nonnegative, whenever the initial conditions and inputs are nonnegative. In the literature [12], such systems are said to be positive. The states of positive systems are confined within a “cone” located in the positive orthant rather than in the whole space \mathbb{R}^n [3], which makes their investigation a challenging and interesting job. Much attention has been paid to this area [45].

Many researchers have been concerned with the problems of stability analysis and controller design, especially the constrained controller design, of positive systems. Ref. [6] provided a sufficient condition for stabilization of positive systems by means of Geršgorin’s theorem [7]. Refs. [8] established some necessary and sufficient conditions for the existence of a controller and supplied the controller synthesis approach for positive systems. Other relevant work can be found in Refs. [9][10] and the references therein. All the references above-mentioned were concerned with only the systems without delays.

In fact, time delays and uncertainties are common in various real systems such as biology, mechanics, society, and economics, and may cause malfunction even instability of those delayed systems. Therefore, the delayed positive systems with uncertainties are of increasing interest. Ref. [11] discussed stability of the discrete-time delayed system by means of “lifting approach” [12] which transforms an original delayed system into another equivalent system without delay but with higher dimension. [13] investigated the controller synthesis problem of the same systems by means of linear copositive Lyapunov function (see [14]) and formulated its results as linear programming(LP) problem. The copositive Lyapunov function approach relies on the following fact: a positive system is stable, if there is a function $V(\mathbf{x})$ which is positive definite and whose differential taken along the system trajectories is negative definite, when \mathbf{x} is in the positive orthant. Since linear copositive Lyapunov function captures the nature of positive systems, it has been widely used when positive systems are considered [8]. Linear copositive Lyapunov function (or functional) also works well even in the presence of delays and uncertainties, see [15] for details. All the cited references were concerned with positive systems with *constant* delays. However, time-varying delays are more important and universal in real engineering processes and have more complex impacts on system dynamics than constant ones.

On this ground, this paper addresses the problems of stability analysis and constrained control of positive systems with time-varying delays, or with polytopic uncertainties [16] in addition, by means of the linear copositive Lyapunov functional.

The remainder of this paper is organized as follows. In Section 2 notation and necessary preliminaries are presented. Subsection 3.1 treats stability analysis and constrained control of systems with time-varying delays. These results are then extended in Subsection 3.2 to the case where polytopic uncertainties occur. An examples is given in Section 4, and Section 5 concludes this paper.

2 Preliminaries

- $A \succeq 0 (\preceq 0)$: All entries of A are nonnegative (nonpositive)
- $A \succ 0 (\prec 0)$: All entries of A are positive (negative)
- $A^T(A^{-1})$: The transpose(inverse) of matrix A
- $\mathbf{R}(\mathbf{R}_+)$: The set of all nonnegative (positive) real numbers
- $\mathbb{R}^n(\mathbf{R}^n, \mathbf{R}_+^n)$: n -dimensional real (nonnegative, positive) vector space
- $\mathbb{R}^{n \times m}(\mathbf{R}^{n \times m})$: The set of all real (nonnegative) matrices of $(n \times m)$ -dimension
- \mathbf{M} : The set of Metzler matrices

The following notation of matrices will be used throughout this paper: $A = [a_{jl}]$, $A_r = \left[a_{jl}^{(r)} \right]$, $B = [b_{jl}]$, $B_i = \left[b_{jl}^{(i)} \right]$, $B_r = \left[b_{jl}^{(r)} \right]$, $B_{ir} = \left[b_{jl}^{(ir)} \right]$, $C = [c_{jk}]$. The dimensions of matrices and vectors will not be explicitly mentioned if clear from context. For simplicity, denote the sets $\{1, 2, \dots, p\}$ and $\{0, 1, \dots, p\}$ by $\underline{\mathbf{p}}$ and $\underline{\mathbf{p}}_0$, respectively, where p is a natural numbers.

Consider the following system

$$\begin{aligned}\dot{\mathbf{x}}(t) &= A\mathbf{x}(t) + B\mathbf{x}(t - \tau(t)) + C\mathbf{u}(t), \quad t \geq 0 \\ \mathbf{x}(t) &= \varphi(t), \quad t \in [-h, 0]\end{aligned}\tag{1}$$

where $\mathbf{x}(t) \in \mathbb{R}^n$ is the state variable, $\mathbf{u}(t) \in \mathbb{R}^m$ is the control input, $A, B \in \mathbb{R}^{n \times n}$ and $C \in \mathbb{R}^{n \times m}$ are system matrices, $\tau(t)$ is a time-varying delay satisfying $0 \leq \tau(t) \leq h \in \mathbf{R}_+$, and $\varphi(t) : [-h, 0] \rightarrow \mathbb{R}^n$ is an initial vector-valued smooth function.

Definition 1. System (1) is said to be positive if for any $\varphi(t) : [-h, 0] \rightarrow \mathbf{R}^n$ and $\mathbf{u}(t) \succeq 0 (t \in \mathbf{R})$, the corresponding trajectory $\mathbf{x}(t) \succeq 0$ holds for all $t \in \mathbf{R}$.

Lemma 1. System (1) is positive if and only if $A \in \mathbf{M}$, $B \succeq 0$, and $C \succeq 0$.

Proof: The approach used here is slightly similar to that in [3]. The proof is divided into two parts: necessity and sufficiency.

Necessity. Condition $A \in \mathbf{M}$, $B \succeq 0$, and $C \succeq 0$ is equivalent to

$$a_{jl} \geq 0 (j \neq l), \quad b_{jl} \geq 0, \quad c_{jk} \geq 0, \quad \forall j, l \in \underline{n}, \quad k \in \underline{m}. \tag{2}$$

We will show that if (2) does not hold, that is, at least one of $a_{jl} (j \neq l)$, b_{jl} , $c_{jk} (j, l \in \underline{n}, k \in \underline{m})$ is negative, then system (1) may not be positive.

Let $\varphi_j(0)$, the j th component of $\varphi(0)$, be zero, and represent (1) componentwise at time $t = 0$: $\dot{x}_j(0) = \sum_{l=1, l \neq j}^n a_{jl} \varphi_l(0) + \sum_{l=1}^n b_{jl} \varphi_l(-\tau(0)) + \sum_{k=1}^m c_{jk} u_k(0)$. If there exists a negative entry of $a_{jl} (l \neq j)$, b_{jl} , $c_{jk} (l \in \underline{n}, k \in \underline{m})$, then there always exist a set of $\varphi_l(0) (l \neq j)$, $\varphi_l(-\tau(0))$, $u_k(0) (l \in \underline{n}, k \in \underline{m})$, such that $\dot{x}_j(0) < 0$. Therefore, the trajectory will break out of the positive orthant. So (2) is necessary for the positivity of (1).

Sufficiency. Suppose that (2) holds. To prove $\mathbf{x}(t) \succeq 0$, it is sufficient to check that the vector $\dot{\mathbf{x}}(t)$ does not point toward the outside of positive orthant whenever $\mathbf{x}(t)$ is on its boundary. This is equivalent to verifying that the components of vector $\dot{\mathbf{x}}(t)$ corresponding to the zero components of $\mathbf{x}(t) \succeq 0$ are nonnegative. Denote t_0 the minimum of those times at which one component of $\mathbf{x}(t)$, say $x_j(t)$, equals zero. Therefore, $x_j(t_0) = 0$, and for any $t < t_0$, each component of $\mathbf{x}(t)$ is greater than zero. Since $\dot{x}_j(t_0) = \sum_{l=1, l \neq j}^n a_{jl} x_l(t_0) + \sum_{l=1}^n b_{jl} x_l(t_0 - \tau(t_0)) + \sum_{k=1}^m c_{jk} u_k(t_0)$, it can be claimed that $\dot{x}_j(t_0) \geq 0$. The proof is completed.

3 Main Results

This section discusses stability and constrained control of delayed systems, subject to the positivity constraint. The first subsection is focused on systems without uncertainties, and the second one on those with uncertainties.

3.1 Stability Analysis and Constrained Control of Delayed Systems

Consider system

$$\begin{aligned}\dot{\mathbf{x}}(t) &= A\mathbf{x}(t) + B\mathbf{x}(t - \tau(t)) + \mathbf{u}(t), \quad t \geq 0 \\ \mathbf{x}(t) &= \varphi(t), \quad t \in [-h, 0]\end{aligned}\tag{3}$$

where $\mathbf{x}(t)$, $\tau(t)$, A , and B are as in (1), $\mathbf{u}(t)$ is control input, $\tau(t)$ satisfies $\dot{\tau}(t) \leq d < 1$ with d being constant. From then on, it is always assumed that $\varphi(t): [-h, 0] \rightarrow \mathbf{R}^n$ is an initial vector-valued smooth function.

The open-loop system of system (3) is described by

$$\dot{\mathbf{x}}(t) = A\mathbf{x}(t) + B\mathbf{x}(t - \tau(t)), \quad t \geq 0 \quad (4)$$

for which the following theorem holds.

Theorem 1. System (4) is positive and asymptotically stable, if there exist vectors $\boldsymbol{\lambda}_0 \in \mathbf{R}_+^n$, $\boldsymbol{\lambda}_1 \in \mathbf{R}_+^n$ such that (5) and (6) hold.

$$a_{jl} \succeq 0, j, l \in \underline{n}, j \neq l, \quad b_{jl} \geq 0, j, l \in \underline{n} \quad (5)$$

$$A^T \boldsymbol{\lambda}_0 + \boldsymbol{\lambda}_1 \prec 0, \quad B^T \boldsymbol{\lambda}_0 + (d - 1)\boldsymbol{\lambda}_1 \prec 0. \quad (6)$$

Proof: Condition (5) implies that $A \in \mathbf{M}$, $B \succeq 0$. According to Lemma 1, system (4) is positive.

Then, let the linear copositive Lyapunov-Krasovskii functional candidate be

$$V(t) = \mathbf{x}^T(t)\boldsymbol{\lambda}_0 + \int_{t-\tau(t)}^t \mathbf{x}^T(s)\boldsymbol{\lambda}_1 ds. \quad (7)$$

Define the norm of $\mathbf{x} \in \mathbf{R}^n$ as $\|\mathbf{x}\| = \sum_{i=1}^n |x_i|$, function $f_1 : \mathbf{x} \in \mathbf{R}_+^n \rightarrow \mathbf{R}_+$ as the smallest component of \mathbf{x} , and $f_2 : \mathbf{x} \in \mathbf{R}_+^n \rightarrow \mathbf{R}_+$ as the largest one of \mathbf{x} . Denote $\alpha = f_1(\boldsymbol{\lambda}_0)$, $\beta = \max\{f_2(\boldsymbol{\lambda}_0), f_2(\boldsymbol{\lambda}_1)\}$, $\phi(s) = \mathbf{x}(t+s)$, $s \in [-h, 0]$, and $\|\phi\| = \sup_{-h \leq s \leq 0} \|\phi(s)\|$. It yields that

$$\alpha\|\phi(0)\| \leq V(t) \leq \beta(1+h)\|\phi\|.$$

The derivative of $V(t)$ along the trajectory of (4) is

$$\begin{aligned} \dot{V}(t) &= \dot{\mathbf{x}}^T(t)\boldsymbol{\lambda}_0 + \mathbf{x}^T(t)\boldsymbol{\lambda}_1 - (1 - \dot{\tau}(t))\mathbf{x}^T(t - \tau(t))\boldsymbol{\lambda}_1 \\ &\leq (\mathbf{x}^T(t)A^T + \mathbf{x}^T(t - \tau(t))B^T)\boldsymbol{\lambda}_0 + \mathbf{x}^T(t)\boldsymbol{\lambda}_1 + (d - 1)\mathbf{x}^T(t - \tau(t))\boldsymbol{\lambda}_1 \\ &= \mathbf{x}^T(t)(A^T\boldsymbol{\lambda}_0 + \boldsymbol{\lambda}_1) + \mathbf{x}^T(t - \tau(t))(B^T\boldsymbol{\lambda}_0 + (d - 1)\boldsymbol{\lambda}_1). \end{aligned} \quad (8)$$

Let $\theta = f_1(-A^T\boldsymbol{\lambda}_0 - \boldsymbol{\lambda}_1) > 0$. It follows from (6) that

$$\dot{V}(t) < -\theta\|\phi(0)\|.$$

According to Theorem 2.1, Chapter 5 in [17], system (4) is asymptotically stable. Proof is thus completed.

In the remainder part of this subsection, the constrained control is considered. In other words, a controller will be designed when it exists, which will make the corresponding closed-loop system positive and asymptotically stable.

Let $\mathbf{u}(t) = F_0 \mathbf{x}(t) + F_1 \mathbf{x}(t - \tau(t))$, where F_0 and F_1 are two gain matrices to be determined later. The closed-loop system of (3) is represented by

$$\begin{aligned}\dot{\mathbf{x}}(t) &= (A + F_0) \mathbf{x}(t) + (B + F_1) \mathbf{x}(t - \tau(t)), \quad t \geq 0, \\ \mathbf{x}(t) &= \varphi(t), \quad t \in [-h, 0].\end{aligned}\tag{9}$$

Theorem 2. System (9) is positive and asymptotically stable, if there exist vectors $\boldsymbol{\lambda}_i = [\lambda_{i1}, \lambda_{i2}, \dots, \lambda_{in}]^T \succ 0$, and $\mathbf{k}_{ij} = [k_{j1}^{(i)}, k_{j2}^{(i)}, \dots, k_{jn}^{(i)}]^T \in \mathbb{R}^n$, $i = 0, 1$, $j \in \underline{n}$, such that (I0), (II), and (I2) hold.

$$a_{jl} \lambda_{0j} + k_{jl}^{(0)} \geq 0, \quad j, l \in \underline{n}, j \neq l \tag{10}$$

$$b_{jl} \lambda_{0j} + k_{jl}^{(1)} \geq 0, \quad j, l \in \underline{n} \tag{11}$$

$$A^T \boldsymbol{\lambda}_0 + \sum_{j=1}^n \mathbf{k}_{0j} + \boldsymbol{\lambda}_1 \prec 0, \quad B^T \boldsymbol{\lambda}_0 + \sum_{j=1}^n \mathbf{k}_{1j} + (d-1)\boldsymbol{\lambda}_1 \prec 0. \tag{12}$$

Moreover, the gain matrix $F_i = [\mathbf{k}_{i1}/\lambda_{01}, \mathbf{k}_{i2}/\lambda_{02}, \dots, \mathbf{k}_{in}/\lambda_{0n}]^T$, $i = 0, 1$.

Proof: Since $\boldsymbol{\lambda}_0 \succ 0$, it follows from (I0) that $a_{jl} + \frac{k_{jl}^{(0)}}{\lambda_{0j}} \geq 0$ ($j, l \in \underline{n}, j \neq l$), and therefore $A + F_0$ is a Metzler matrix. It also follows from (II) that $B + F_1 \succeq 0$. By Lemma 1, system (9) is positive.

Note that $\sum_{j=1}^n \mathbf{k}_{ij} = [\mathbf{k}_{i1}/\lambda_{01}, \mathbf{k}_{i2}/\lambda_{02}, \dots, \mathbf{k}_{in}/\lambda_{0n}] \boldsymbol{\lambda}_0 = F_i^T \boldsymbol{\lambda}_0$. Condition (I2) is recast as

$$(A + F_0)^T \boldsymbol{\lambda}_0 + \boldsymbol{\lambda}_1 \prec 0, \quad (B + F_1)^T \boldsymbol{\lambda}_0 + (d-1)\boldsymbol{\lambda}_1 \prec 0$$

which shows, by Theorem 1, that (9) is also asymptotically stable. Proof is completed.

3.2 Extension to the Delayed Positive Systems with Polytopic Uncertainties

An important extension of the proposed results is the possibility of handling the case where the dynamics of the system are not exactly known, as it is now presented.

Consider the following uncertain system

$$\begin{aligned}\dot{\mathbf{x}}(t) &= \bar{A} \mathbf{x}(t) + \bar{B} \mathbf{x}(t - \tau(t)) + \mathbf{u}(t), \quad t \geq 0 \\ \mathbf{x}(t) &= \varphi(t), \quad t \in [-h, 0]\end{aligned}\tag{13}$$

where $\mathbf{x}(t)$, $\tau(t)$, and $\mathbf{u}(t)$ are as in (3), \bar{A} and \bar{B} are supposed to be not exactly determined. But the pair (\bar{A}, \bar{B}) is assumed to belong to the following convex set:

$$S_1 := \left\{ \sum_{r=1}^q \alpha_r (A_r, B_r) \middle| \sum_{r=1}^q \alpha_r = 1, \alpha_r \geq 0 \right\} \tag{14}$$

where $A_r \in \mathbf{M}$, $B_r \succeq 0$ are known matrices.

First, let $\mathbf{u}(t) \equiv 0$ and rewrite (13) as

$$\begin{aligned}\dot{\mathbf{x}}(t) &= \bar{A}\mathbf{x}(t) + \bar{B}\mathbf{x}(t - \tau(t)), \quad t \geq 0 \\ \mathbf{x}(t) &= \varphi(t), t \in [-h, 0].\end{aligned}\tag{15}$$

Applying Theorem 1 to system (15), we provide the following result:

Corollary 1. System (15) is positive and asymptotically stable for every $(\bar{A}, \bar{B}) \in S_1$, if there exist vectors $\lambda_0 \in \mathbf{R}_+^n, \lambda_1 \in \mathbf{R}_+^n$ such that (16) and (17) holds.

$$a_{jl}^{(r)} \geq 0, j, l \in \underline{n}, j \neq l, \quad b_{jl}^{(r)} \geq 0, j, l \in \underline{n}, r \in \underline{q} \tag{16}$$

$$A_r^T \lambda_0 + \lambda_1 \prec 0, B_r^T \lambda_0 + (d-1)\lambda_1 \prec 0, \quad r \in \underline{q}. \tag{17}$$

Proof: (16) implies that $A_r \in \mathbf{M}$ and $B_r \succeq 0$. Since (14) holds, \bar{A} is also a Metzler matrix and $\bar{B} \succeq 0$. Thus system (15) is positive.

Choose the linear copositive Lyapunov-Krasovskii functional candidate as (7), apply Theorem 1 and a simple convexity argument, and we can prove that (15) is also asymptotically stable. Proof is thus completed.

Then, let $\mathbf{u}(t) = \sum_{r=1}^q \alpha_r (F_{0r}\mathbf{x}(t) + F_{1r}\mathbf{x}(t - \tau(t)))$, where F_{0r} and F_{1r} are the gain matrices corresponding to the vertex systems $\dot{\mathbf{x}}(t) = A_r\mathbf{x}(t) + B_r\mathbf{x}(t - \tau(t))$, $r \in \underline{q}$. The closed-loop system of (13) is given by

$$\begin{aligned}\dot{\mathbf{x}}(t) &= \sum_{r=1}^q \alpha_r \{(A_r + F_{0r})\mathbf{x}(t) + (B_r + F_{1r})\mathbf{x}(t - \tau(t))\}, \quad t \geq 0 \\ \mathbf{x}(t) &= \varphi(t), t \in [-h, 0].\end{aligned}\tag{18}$$

A convexity argument based on Theorem 2 results in the following corollary.

Corollary 2. System (18) is positive and asymptotically stable, if there exist vectors $\lambda_0 = [\lambda_{01}, \lambda_{02}, \dots, \lambda_{0n}]^T \succ 0, \lambda_1 = [\lambda_{11}, \lambda_{12}, \dots, \lambda_{1n}]^T \succ 0$, and $\mathbf{k}_{irj} = [k_{j1}^{(ir)}, k_{j2}^{(ir)}, \dots, k_{jn}^{(ir)}]^T \in \mathbb{R}^n$, $i = 0, 1, j \in \underline{n}, r \in \underline{q}$, such that the following conditions hold:

$$\begin{aligned}a_{jl}^{(r)} \lambda_{0j} + k_{jl}^{(0r)} &\geq 0, j, l \in \underline{n}, j \neq l, \quad b_{jl}^{(r)} \lambda_{0j} + k_{jl}^{(1r)} \geq 0, \quad j, l \in \underline{n}, r \in \underline{q} \\ A_r^T \lambda_0 + \sum_{j=1}^n \mathbf{k}_{0rj} + \lambda_1 &\prec 0, \quad B_r^T \lambda_0 + \sum_{j=1}^n \mathbf{k}_{1rj} + (d-1)\lambda_1 \prec 0, \quad r \in \underline{q}.\end{aligned}$$

Moreover, the gain matrix $F_{ir} = [\mathbf{k}_{ir1}/\lambda_{01}, \dots, \mathbf{k}_{irn}/\lambda_{0n}]^T$, $i = 0, 1, r \in \underline{q}$.

4 Illustrative Example

Consider the following system

$$\dot{\mathbf{x}}(t) = A\mathbf{x}(t) + B\mathbf{x}(t - \tau(t)) \tag{19}$$

where $\mathbf{x}(t) = [x_1(t), x_2(t)]^T \in R^2$, $\tau(t) = 1 + 0.01 \sin^2 t$, and the system matrices are

$$A = \begin{bmatrix} -2.1 & 1.5 \\ 1 & -3 \end{bmatrix}, B = \begin{bmatrix} 0.6 & 0.91 \\ 0.51 & 0.4 \end{bmatrix}.$$

The solutions to (5) and (6) are as follows:

$$\lambda_0 = [88.0138, 85.8671]^T, \lambda_1 = [97.7163, 120.4617]^T.$$

According to Theorem 1, system (19) is positive and asymptotically stable, as shown in Fig. 1.

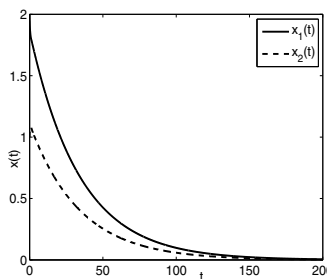


Fig. 1. Evolutions of system (19)

5 Conclusions

Addressed in this paper are the stability and constrained control problems of positive systems with time-varying delays, or with polytopic uncertainties in addition. Some sufficient stability conditions are established, and several sufficient conditions are also proposed when constrained control is considered. All the results are formulated as LP problems and therefore are computation-friendly.

References

1. Berman, A., Neumann, M., Stern, R.J.: Nonnegative Matrices in Dynamic Systems. Wiley, Chichester (1989)
2. Kaczorek, T.: Positive 1D and 2D Systems. Springer, London (2002)
3. Farina, L., Rinaldi, S.: Positive Linear Systems: Theory and Applications. John Wiley & Sons, Inc., New York (2000)
4. Kurek, J.E.: Stability of Positive 2-D System Described by the Roesser Model. IEEE Trans. on Circuits and Systems-I 49(4), 531–533 (2002)
5. Liu, X., Yu, W., Wang, L.: Stability Analysis for Continuous-time Positive Systems with Time-varying Delays. IEEE Trans. on Automatic Control 55(4), 1024–1028 (2010)
6. Kaczorek, T.: Stabilization of Positive Linear Systems by State Feedback. Pomiary, Automatyka, Kontrola 3, 2–5 (1999)
7. Horn, R.A., Johnson, C.R.: Matrix analysis. Cambridge University Press, Cambridge (1985)

8. Rami, M.A., Tadeo, F.: Controller Synthesis for Positive Linear Systems with Bounded Controls. *IEEE Trans. on Circuits and Systems-II* 54(2), 151–155 (2007)
9. Rami, M.A., Tadeo, F.: Positive Observation Problem for Linear Discrete Positive Systems. In: Proceedings of the 45th IEEE Conference on Decision & Control, CA, USA, pp. 4729–4733 (2006)
10. Rami, M.A., Tadeo, F., Benzaouia, A.: Control of Constrained Positive Discrete Systems. In: Proceedings of the 2007 American Control Conference, New York City, USA, pp. 5851–5856 (2007)
11. Busłowicz, M.: Robust Stability of Positive Discrete-time Linear Systems with Multiple Delays with Linear Unity Rank Uncertainty Structure or Non-negative Perturbation Matrices. *Bulletin of the Polish Academy of Sciences, Technical Sciences* 55(1), 1–5 (2007)
12. Xia, Y., Liu, G., Shi, P., Rees, D., Thomas, E.J.C.: New Stability and Stabilization Conditions for Systems with Time-delay. *International Journal of Systems and Science* 38(1), 17–24 (2007)
13. Liu, X., Wang, L., Yu, W., Zhong, S.: Constrained Control of Positive Discrete-time Systems with Delays. *IEEE Trans. on Circuits & Systems-II* 55(2), 193–197 (2008)
14. Mason, O., Shorten, R.: Quadratic and Copositive Lyapunov Functions and the Stability of Positive Switched Linear Systems. In: Proceedings of the 2007 American Control Conference, pp. 657–662 (2007)
15. Rami, M.A., Helmke, U., Tadeo, F.: Positive Observation Problem for Time-delays Linear Positive Systems. In: Proceedings of the 15th Mediterranean Conference on Control and Automation, Athens, Greece, pp. 1–6 (2007)
16. He, Y., Wu, M., She, J.H., Liu, G.P.: Parameter-Dependent Lyapunov Functional for Stability of Time-delay Systems with Polytopic-type Uncertainties. *IEEE Trans. on Automatic Control* 49(5), 828–832 (2004)
17. Hale, J.: Theory of Functional Differential Equations. Springer, New York (1977)

On Linear Co-positive Lyapunov Functions for a Special of Switched Linear Positive Systems

Xiuyong Ding¹, Lan Shu¹, and Changcheng Xiang²

¹ School of Mathematical Sciences, University of Electronic Science and Technology of China, 611731, Chengdu, P.R. China
dingxinzhi6489@gmail.com, shul@uestc.edu.cn

² Computer Science Department, Aba Teachers College, Aba 623000, P.R. China
yangzixia1997@yahoo.com.cn

Abstract. This paper considers a class of special of switched positive linear systems (SPLSs) composed of continuous- and discrete-time positive linear time-invariant(LTI) systems. A necessary and sufficient condition for the existence of a common linear co-positive Lyapunov function(CLCLF) for sets of positive LTI systems will be derived. This condition is characterized by some determinants which are related to system matrices. In particular, a CLCLF can be easily located according to our results.

Keywords: common linear co-positive Lyapunov functions, positive systems, switched systems.

1 Introduction

A dynamic system is called positive if any trajectory of the system starting in the non-negative orthant remains in here [1]. Positive systems play an important role in the modeling of dynamic phenomena whose variables are nonnegative. Recently, the importance of SPLSs has been highlighted by many researchers because of finding broad application in communication systems, formation flying, and systems theory (see [2–6] and references therein). When referring to the general stability, a key result in this connection is the existence of a CLCLF of sets of positive LTI systems [4]. Moreover, work discussed in [4] provided a method for determining whether or not a given SPLS is stable. Such an approach is based upon determining verifiable conditions for a CLCLF. [5] extended this result to general SPLSs. [6] presented a compact and easily verifiable conditions on SPLSs by means of the properties of geometry.

In this paper, we shall introduce a particular class of SPLSs constituting of continuous- and discrete-time subsystems and be concerned with the exponentially stable of this type of systems. A equivalent condition for the existence of a CLCLF for such systems will be derived. This condition is characterized by some determinants which be generated by system matrices.

2 Preliminaries

Throughout, \mathbb{R} denotes the set of all real numbers, \mathbb{R}^n stands for the n -dimensional real vector space and $\mathbb{R}^{n \times n}$ is the space of $n \times n$ matrices with real entries. For A in $\mathbb{R}^{n \times n}$, a_{kl} denotes the element in the (kl) position of A . $A \succeq 0 (\preceq 0)$ means that all elements of matrix A are nonnegative (nonpositive) and $A \succ 0 (\prec 0)$ means that all elements of matrix A are positive (negative). The notion $A > 0 (< 0)$ means that A is a symmetric positive (negative) definite matrix. Meanwhile, $A^T (A^{-1})$ represents the transpose (inverse) of matrix A . Let $\mathbb{N} = \{0, 1, 2, 3, \dots\}$ and $\mathbb{N}^+ = \{0\} \cup \mathbb{N}$. $\lambda(A)$ represents the eigenvalue, $\rho(A)$ denotes the spectral radius, and $\mu(A)$ stands for the maximal real part of any eigenvalue of A . Also, when referring to switched linear systems, stability shall be used to denote asymptotic stability under arbitrary switching signals.

Before proceeding, we shall recall some facts about positive systems.

Definition 1. A matrix A is called a Metzler if and only if $a_{kl} \geq 0, k \neq l$.
A matrix A is called a Hurwitz if and only if $\mu(A) < 0$.
A matrix A is called a Schur if and only if $\rho(A) < 1$.

Definition 2. The continuous-time LTI system $\Sigma_{A^c} : \dot{x} = A^c x(t), x(0) = x_0$, is positive if $x_0 \succeq 0$ implies that $x(t) \succeq 0$ for all $t \geq 0$.

The discrete-time LTI system $\Sigma_{A^d} : x(t+1) = A^d x(t), x(0) = x_0$, is positive if $x_0 \succeq 0$ implies that $x(t) \succeq 0$ for all $t \in \mathbb{N}$.

Lemma 1. [1] The continuous-time LTI system Σ_{A^c} is positive if and only if A^c is a Metzler matrix.

The discrete-time LTI system Σ_{A^d} is positive if and only if $A^d \succeq 0$.

This paper shall address the SPLS composed of a set of continuous-time positive LTI subsystems

$$\Sigma_{A_i^c} : \dot{x}(t) = A_i^c x(t), \quad x(0) = x_0, i = 1, \dots, m^c, t \geq 0. \quad (1)$$

and a set of discrete-time positive LTI subsystems

$$\Sigma_{A_j^d} : x(t+1) = A_j^d x(t), \quad x(0) = x_0, j = 1, \dots, m^d, t \in \mathbb{N}. \quad (2)$$

where $x(t) \in \mathbb{R}^n$ are the states, A_i^c are Metzler matrices and $A_j^d \succeq 0$ in $\mathbb{R}^{n \times n}$ and $m^c (m^d)$ denote the number of continuous-time(discrete-time) subsystems.

For stability of the overall SPLSs, we need to make some illustration for such type of switched systems. For simplicity, we suppose that the sampling period of all the discrete-time subsystems is τ . Since the states of the discrete-time subsystems can be viewed as piecewise constant vectors between sampling points, we can consider the value of the system states in the continuous-time domain. For example, if subsystem $\Sigma_{A_1^c}$ is activated on $[t_0, t_1]$ and then subsystem $\Sigma_{A_1^d}$ is activated for k steps and subsystem $\Sigma_{A_2^c}$ on $[t_1 + k\tau, t_2]$, the time domain is divided into

$$[t_0, t_2] = [t_0, t_1] \cup [t_1, t_1 + k\tau] \cup [t_1 + k\tau, t_2].$$

This process is repeated and ends in turning out the running status of the whole systems.

It is well known that a switched system composed of stable subsystems could be unstable if the switching is not done appropriately. When the stability of SPLSs is considered, it is natural to adopt CLCLFs. The approach of CLCLFs relies on the following fact.

Definition 3. Suppose that $A_i^c, i = 1, 2, \dots, m^c$ are Metzler and Hurwitz matrices, $A_j^d \succeq 0, j = 1, 2, \dots, m^d$ are Schur matrices. If there exists a single vector $v \succ 0$ such that $A_i^{cT}v \prec 0$ and $(A_j^d - I)v \prec 0$, then $V(x) = v^T x$ is said to be a CLCLF for sets of systems $\Sigma_{A_1^c}, \dots, \Sigma_{A_{m^c}^c}, \Sigma_{A_1^d}, \dots, \Sigma_{A_{m^d}^d}$.

In this paper, we only consider the second order cases. Our main results shall be presented in the next section.

3 Second Order SPLSs

This section addresses the existence of a CLCLF for second order positive LTI systems. Before presenting our derivation, we need to know the following technical results which are relevant to the work of this section.

Lemma 2. [7] Suppose that $A \succeq 0$ is a Schur matrix in $\mathbb{R}^{2 \times 2}$. Then $a_{11} < 1, a_{22} < 1$ and $\frac{1-a_{11}}{a_{21}} > \frac{a_{12}}{1-a_{22}}$.

We are ready to provide the following theorem.

Theorem 1. Let A^c be Metzler and Hurwitz matrix, $A^d \succeq 0$ be Schur matrix, and $A^c, A^d \in \mathbb{R}^{2 \times 2}$. Then positive LTI systems $\Sigma_{A^c}, \Sigma_{A^d}$ have a CLCLF if and only if the following conditions are satisfied.

$$\begin{vmatrix} 1 - a_{11}^d & a_{12}^c \\ a_{21}^d & -a_{22}^c \end{vmatrix} > 0, \quad \begin{vmatrix} -a_{11}^c & a_{12}^d \\ a_{21}^c & 1 - a_{22}^d \end{vmatrix} > 0.$$

Proof. Firstly, from definition 3, positive LTI systems $\Sigma_{A^c}, \Sigma_{A^d}$ have a CLCLF if and only if there is some $v \succ 0$ in \mathbb{R}^2 such that $A^{cT}v \prec 0$ and $(A^d - I)^T v \prec 0$. Let $v = (v_1, v_2)^T$, then for the following inequities

$$a_{11}^c v_1 + a_{21}^c v_2 < 0, \tag{3}$$

$$a_{12}^c v_1 + a_{22}^c v_2 < 0, \tag{4}$$

$$(a_{11}^d - 1)v_1 + a_{21}^d v_2 < 0, \tag{5}$$

$$a_{12}^d v_1 + (a_{22}^d - 1)v_2 < 0, \tag{6}$$

$$v_1 > 0, \tag{7}$$

$$v_2 > 0, \tag{8}$$

positive LTI systems $\Sigma_{A^c}, \Sigma_{A^d}$ have a CLCLF if and only if feasible solutions for (3)-(8) exist. As A^c be a Metzler matrix and $A^d \succeq 0$, in this case, it follows from Lemma 2 that $a_{kk}^c < 0, a_{kk}^d - 1 < 0$ and $a_{kl}^c \geq 0, a_{kl}^d \geq 0, k = 1, 2, k \neq l$. We thus divide the proof into four cases.

Case 1: $a_{21}^c > 0, a_{21}^d > 0$.

In this case, set up the planar rectangular coordinate $v_1 \circ v_2$. Taking into account (7) and (8), we just need to consider the first quadrant.

From (3) and (4) we can get $v_2 < -\frac{a_{11}^c}{a_{21}^c}v_1, v_2 > -\frac{a_{12}^c}{a_{22}^c}v_1$. Due to $\frac{a_{11}^c}{a_{21}^c} < 0, \frac{a_{12}^c}{a_{22}^c} < 0$, we thus know $a_{11}^c v_1 + a_{21}^c v_2 = 0$ and $a_{12}^c v_1 + a_{22}^c v_2 = 0$ lie in the first quadrant. In addition, $\frac{a_{11}^c}{a_{21}^c} < \frac{a_{12}^c}{a_{22}^c}$ results from $\det A_1^c > 0$, which ensures that the slope of $a_{11}^c v_1 + a_{21}^c v_2 = 0$ is greater than the slope of $a_{12}^c v_1 + a_{22}^c v_2 = 0$. This leads to the following fact.

$$M = \left\{ \begin{pmatrix} v_1 \\ v_2 \end{pmatrix} \middle| v_2 < -\frac{a_{11}^c}{a_{21}^c}v_1, v_1, v_2 > 0 \right\} \cap \left\{ \begin{pmatrix} v_1 \\ v_2 \end{pmatrix} \middle| v_2 > -\frac{a_{12}^c}{a_{22}^c}v_1, v_1, v_2 > 0 \right\} \neq \emptyset.$$

This fact immediately implies that the area composed of the set M is below the line $a_{11}^c v_1 + a_{21}^c v_2 = 0$ and above the line $a_{12}^c v_1 + a_{22}^c v_2 = 0$, which lies in the first quadrant.

On the other hand, from (5) and (6), we have $v_2 < \frac{1-a_{11}^d}{a_{21}^d}v_1, v_2 > \frac{a_{12}^d}{1-a_{22}^d}v_1$. Note that $\frac{1-a_{11}^d}{a_{21}^d} > 0, \frac{a_{12}^d}{1-a_{22}^d} > 0$, it easy to see that $(a_{11}^d - 1)v_1 + a_{21}^d v_2 = 0$ and $a_{12}^d v_1 + (a_{22}^d - 1)v_2 = 0$ lie in the first quadrant. Moreover, Lemma ?? ensures that the slope of $(a_{11}^d - 1)v_1 + a_{21}^d v_2 = 0$ is greater than the slope of $a_{12}^d v_1 + (a_{22}^d - 1)v_2 = 0$. From the discussion above, it is easy to check the following fact.

$$N = \left\{ \begin{pmatrix} v_1 \\ v_2 \end{pmatrix} \middle| v_2 < \frac{1-a_{11}^d}{a_{21}^d}v_1, v_1, v_2 > 0 \right\} \cap \left\{ \begin{pmatrix} v_1 \\ v_2 \end{pmatrix} \middle| v_2 > \frac{a_{12}^d}{1-a_{22}^d}v_1, v_1, v_2 > 0 \right\} \neq \emptyset.$$

Which implies that the area composed of the set N is below the line $(a_{11}^d - 1)v_1 + a_{21}^d v_2 = 0$ and above the line $a_{12}^d v_1 + (a_{22}^d - 1)v_2 = 0$, which lies in the first quadrant.

Based on the discussion above, we easily know that positive LTI systems $\Sigma_{A_1^c}, \Sigma_{A_1^d}$ have a CLCLF if and only if $M \cap N \neq \emptyset$. Hence we get

$$\begin{aligned} M \cap N \neq \emptyset &\Leftrightarrow \left(-\frac{a_{12}^c}{a_{22}^c}, -\frac{a_{11}^c}{a_{21}^c} \right) \cap \left(\frac{a_{12}^d}{1-a_{22}^d}, \frac{1-a_{11}^d}{a_{21}^d} \right) \neq \emptyset \\ &\Leftrightarrow \frac{1-a_{11}^d}{a_{21}^d} > -\frac{a_{12}^c}{a_{22}^c}, \frac{a_{12}^d}{1-a_{22}^d} < -\frac{a_{11}^c}{a_{21}^c} \\ &\Leftrightarrow \begin{vmatrix} 1-a_{11}^d & a_{12}^c \\ a_{21}^d & -a_{22}^c \end{vmatrix} > 0, \begin{vmatrix} -a_{11}^c & a_{12}^d \\ a_{21}^c & 1-a_{22}^d \end{vmatrix} > 0. \end{aligned}$$

Case 2: $a_{21}^c = 0, a_{21}^d > 0$.

In this case, $\begin{vmatrix} -a_{11}^c & a_{12}^d \\ a_{21}^c & 1-a_{22}^d \end{vmatrix} > 0$ results from $a_{11}^c < 0, a_{12}^d \geq 0$ and $a_{22}^d - 1 < 0$.

In addition, (3)-(8) exist feasible solutions if and only if

$$\left(-\frac{a_{12}^c}{a_{22}^c}, +\infty \right) \cap \left(\frac{a_{12}^d}{1-a_{22}^d}, \frac{1-a_{11}^d}{a_{21}^d} \right) \neq \emptyset \Leftrightarrow \frac{1-a_{11}^d}{a_{21}^d} > -\frac{a_{12}^c}{a_{22}^c} \Leftrightarrow \begin{vmatrix} 1-a_{11}^d & a_{12}^c \\ a_{21}^d & -a_{22}^c \end{vmatrix} > 0.$$

Case 3: $a_{21}^c > 0, a_{21}^d = 0$.

In this case, it is easy to see that $\begin{vmatrix} 1 - a_{11}^d & a_{12}^c \\ a_{21}^d & -a_{22}^c \end{vmatrix} > 0$. Moreover, the feasible solutions for (3)-(8) exist if and only if

$$\left(-\frac{a_{12}^c}{a_{22}^c}, -\frac{a_{11}^c}{a_{21}^c} \right) \cap \left(\frac{a_{12}^d}{1 - a_{22}^d}, +\infty \right) \neq \emptyset \Leftrightarrow \frac{a_{12}^d}{1 - a_{22}^d} < -\frac{a_{11}^c}{a_{21}^c} \Leftrightarrow \begin{vmatrix} -a_{11}^c & a_{12}^d \\ a_{21}^c & 1 - a_{22}^d \end{vmatrix} > 0.$$

Case 4: $a_{21}^c = 0, a_{21}^d = 0$.

In this case, $\begin{vmatrix} 1 - a_{11}^d & a_{12}^c \\ a_{21}^d & -a_{22}^c \end{vmatrix} > 0, \begin{vmatrix} -a_{11}^c & a_{12}^d \\ a_{21}^c & 1 - a_{22}^d \end{vmatrix} > 0$ are always true. This completes the proof.

Remark 1. In fact, we can easily construct a CLCLF from the process of the proof above.

Case 1: $a_{21}^c > 0, a_{21}^d > 0$.

Taking into account that $a_{kk}^c < 0, a_{kk}^d - 1 < 0$ and $a_{kl}^d \geq 0, a_{kl}^c \geq 0, k = 1, 2, k \neq l$, it is easy to check that $-\frac{a_{12}^c}{a_{22}^c}, -\frac{a_{11}^c}{a_{21}^c}, \frac{a_{12}^d}{1 - a_{22}^d}, \frac{1 - a_{11}^d}{a_{21}^d}$ are positive numbers. Without loss of generality, suppose that $-\frac{a_{12}^c}{a_{22}^c} < \frac{a_{12}^d}{1 - a_{22}^d} < -\frac{a_{11}^c}{a_{21}^c} < \frac{1 - a_{11}^d}{a_{21}^d}$. Then, a CLCLF can be defined as follows

$$V(x) = \left(1, -\frac{a_{11}^c}{2a_{21}^c} + \frac{a_{12}^d}{2(1 - a_{22}^d)} \right) (x_1, x_2)^T.$$

Case 2: $a_{21}^d = 0, a_{21}^{(d2)} > 0$.

$-\frac{a_{12}^c}{a_{22}^c}, \frac{a_{12}^d}{1 - a_{22}^d}, \frac{1 - a_{11}^d}{a_{21}^d}$ are positive numbers. Without loss of generality, assume that $-\frac{a_{12}^c}{a_{22}^c} < \frac{a_{12}^d}{1 - a_{22}^d} < \frac{1 - a_{11}^d}{a_{21}^d}$. Then, a CLCLF can be defined as follows

$$V(x) = \left(1, \frac{a_{12}^d}{2(1 - a_{22}^d)} + \frac{1 - a_{11}^d}{2a_{21}^d} \right) (x_1, x_2)^T.$$

Case 3: $a_{21}^d > 0, a_{21}^{(d2)} = 0$.

Since $-\frac{a_{12}^c}{a_{22}^c}, -\frac{a_{11}^c}{a_{21}^c}, \frac{a_{12}^d}{1 - a_{22}^d}$ are positive numbers. Without loss of generality, we assume that $-\frac{a_{12}^c}{a_{22}^c} < \frac{a_{12}^d}{1 - a_{22}^d} < -\frac{a_{11}^c}{a_{21}^c}$. Then, we can get a CLCLF

$$V(x) = \left(1, -\frac{a_{11}^c}{2a_{21}^c} + \frac{a_{12}^d}{2(1 - a_{22}^d)} \right) (x_1, x_2)^T.$$

Case 4: $a_{21}^d = 0, a_{21}^{(d2)} = 0$.

Consider the four positive numbers $-\frac{a_{12}^c}{a_{22}^c}, \frac{a_{12}^d}{1 - a_{22}^d}$. Without loss of generality, we assume that $\frac{a_{12}^d}{1 - a_{22}^d} < -\frac{a_{12}^c}{a_{22}^c}$. Then, we can get a CLCLF

$$V(x) = \left(1, -\frac{a_{12}^c}{a_{22}^c} - 1 \right) (x_1, x_2)^T.$$

Remark 2. The importance of the above result is relevant, because it provides checkable necessary and sufficient conditions for the CLCLF existence of pairs of systems composed of both continuous-time positive LTI system Σ_{A^c} and discrete-time positive LTI system Σ_{A^d} . In addition, based on the same formulation we can take into account a finite set composed of both positive LTI systems (1) and (2). This will be shown in the following result, which is straightforward from Theorem 1.

Corollary 1. Let $A_1^c, \dots, A_{m^c}^c$ be Metzler and Hurwitz matrices, $A_1^d, \dots, A_{m^d}^d \succeq 0$ be schur matrices in $\mathbb{R}^{2 \times 2}$. Then a finite of positive LTI systems $\Sigma_{A_1^c}, \dots, \Sigma_{A_{m^c}^c}, \Sigma_{A_1^d}, \dots, \Sigma_{A_{m^d}^d}$ have a CLCLF if and only if the following conditions are satisfied.

$$\left[\bigcap_{i=1}^{m^c} \left(-\frac{a_{i12}^c}{a_{i22}^c}, b_i^c \right) \right] \cap \left[\bigcap_{j=1}^{m^d} \left(\frac{a_{j12}^d}{1 - a_{j22}^d}, b_j^d \right) \right] \neq \emptyset,$$

where $i = 1, \dots, m^c, j = 1, \dots, m^d$ and

$$b_i^c = \begin{cases} -\frac{a_{i11}^c}{a_{i21}^c}, & a_{i21}^c > 0 \\ +\infty, & a_{i21}^c = 0 \end{cases}, \quad b_j^d = \begin{cases} \frac{1 - a_{j11}^d}{a_{j21}^d}, & a_{j21}^d > 0 \\ +\infty, & a_{j21}^d = 0 \end{cases}.$$

Remark 3. In fact, corollary (1) provides the simple checkable necessary and sufficient conditions for the existence of a CLCLF for the sets of sytems composed of (1) and (2).

Remark 4. It is easy to see that the above discussion for the sets of sytems composed of (1) and (2) is under arbitrary switching. The similar results can be easily obtained by the essentially same approach when we only activate the continue-time subsystems or only activate the discrete-time subsystems in time domain.

4 Example

In this section, a numerical example will be presented to show the validity of the main results derived in this paper.

Consider the second order SPLS composed of Σ_{A^c} and Σ_{A^d} with

$$A^c = \begin{pmatrix} -0.5 & 0.1 \\ 0.2 & -0.6 \end{pmatrix}, \quad A^d = \begin{pmatrix} 0.4 & 0.3 \\ 0.2 & 0.2 \end{pmatrix}. \quad (9)$$

It is easy to check that A^c is Hurwitz and Metzler matrix, $A^d \succeq 0$ is schur matrix. This means that the SPLS is positive and the subsystems are stable. See Figure 1. Furthermore, since

$$\begin{vmatrix} 1 - a_{11}^d & a_{12}^c \\ a_{21}^d & -a_{22}^c \end{vmatrix} = \begin{vmatrix} 0.6 & 0.3 \\ 0.2 & 0.6 \end{vmatrix} > 0, \quad \begin{vmatrix} -a_{11}^c & a_{12}^d \\ a_{21}^c & 1 - a_{22}^d \end{vmatrix} = \begin{vmatrix} 0.5 & 0.1 \\ 0.2 & 0.8 \end{vmatrix} > 0.$$

Then, according to Theorem II which is equivalent to that Σ_{A^c} and Σ_{A^d} have a CLCLF. In particular, based on the process of the proof in Remark 3.1, we can construct a CLCLF $V(x) = x_1 + \frac{17}{16}x_2$. Figure 2 and Figure 3 show the uniform asymptotical stability of the SPLS (9), where the switching signal is generated randomly. The initial state is $[15 \ 20]^T$, and the mark '*' in the Figure 2 indicates the state change when the discrete-time subsystem Σ_{A^d} is activated. Figure 3 connects all the sampling points of the subsystem Σ_{A^d} into a continuous trajectory.

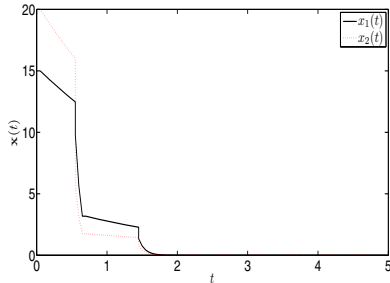


Fig. 1. The state variables of system (9)

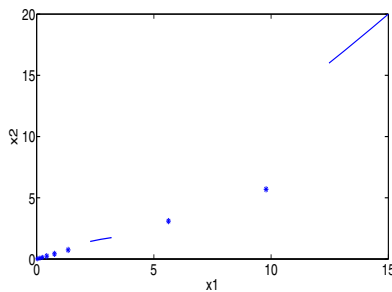


Fig. 2. The trajectory of system (9)

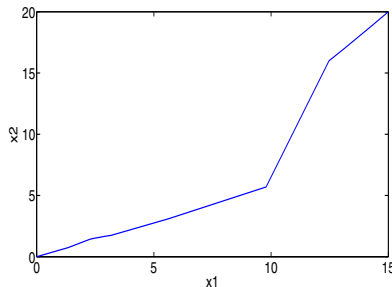


Fig. 3. The trajectory of system (9)

5 Conclusions

This paper introduced a special class of SPLSs which are constituting of continuous- and discrete-time subsystems. We investigated the existence of a CLCLF for such systems. Namely, we established the relations between the existence of a CLCLF and the properties of some determinants. Finally, a example shows that our results are very checkable.

Acknowledgements. This work was supported by the Foundation of National Nature Science of China(Grant No.11071178) and the Fostering Plan for Young and Middle Age Leading Research of UESTC(Grant No.Y02018023601033).

References

1. Farina, L., Rinaldi, S.: Positive Linear Systems: Theory and Applications. Wiley, New York (2000)
2. Liu, X., Yu, W., Wang, L.: Stability Analysis for Continuous-time Positive Systems with Time-varying Delays. *IEEE Trans. Automat. Contr.* 55(4), 1024–1028 (2010)
3. Liu, X.: Constrained Control of Positive Systems with Delays. *IEEE Trans. Automat. Contr.* 54(4), 1596–1600 (2009)
4. Mason, O., Shorten, R.: On Linear Copositive Lyapunov Functions and the Stability of Switched Positive Linear Systems. *IEEE Trans. Automat. Contr.* 52(7), 1346–1349 (2007)
5. Knorn, F., Mason, O., Shorten, R.: On Linear Co-positive Lyapunov Functions for Sets of Linear Positive Systems. *Automatica* 45(8), 1943–1947 (2009)
6. Chen, Z., Gao, Y.: On Common Linear Copositive Lyapunov Functions for Pairs of Stable Positive Linear Systems. *Nonlinear Anal. Theor. Meth. Appl.* 3, 467–474 (2009)
7. Ding, X., Shu, L., Wang, Z.: On Stability for Switched Linear Positive Systems. *Math. Comput. Model.* 53, 1044–1055 (2011)

Induction Motor Speed-Regulating Control System Based on Nonlinear Kernel Ridge Regression

Feng Wang, Jinlin Ding, and Zhifeng Hu

Department of Electronic Information Engineering, Suzhou vocational university,
Suzhou 215104, Jiangsu, China
{wf,djinlin,huzf}@jssvc.edu.cn

Abstract. To deal with the inverse model identification problem in motor variable frequency speed-regulating system, a new control method based on nonlinear kernel ridge regression is proposed. On the basis of reversible analysis of the original system, the- α order reversible model approximated by kernel ridge regression is connected with original system, and the pseudo-linear combined system is constructed. Experimental results show that the combined method can realize the linearization of the induction motor control system successfully, and high performance of speed control can be ensured for systems with inverse model identification errors and changeable load.

Keywords: Nonlinear, linearization, kernel ridge regression, reversible system, Speed-regulating.

1 Introduction

Aimed at nonlinear control system, neural network is one kind of common intelligent algorithm. But the traditional neural network control system is based on empirical risk minimization principle, and it has some problems, for example, long training time, over-fit phenomena and global optimization and so on, which reduces generalization of neural network, increases estimated error of inverse system, influence performance of control system. Kernel ridge regression (KRR) [1~4] based on structural risk minimization principle, comparing with neural network, has higher generalization ability and modeling precision in training samples with finite and noises. Therefore inverse control based on KRR is put forward, reduces steady error, can realize nonlinear system identification, this way can apply in pseudo-linear control of AC motor.

2 Nonlinear Kernel Ridge Regression

About linear regression, minimum mean-square error is adopted generally. But this method can not solve multi-collinearity, the ridge regression give reasonable results when multi-collinearity exists.

Linear ridge regression has excellent stability and generalization, but it has essential limitation in nonlinear identification. In order to solve the problem, kernel analysis is used, which can realize nonlinear mapping of sampling data from input space to

higher feature space. As for processed data which can not realize in sampling space, they are modeled in the feature space through linear regression. The method can be applied in nonlinear control system. Considered this problem, the direct optimization method for KRR is proposed in the paper.

Assumed that the training set is denoted by $\{x_i, y_i\}_{i=1}^l$, $x_i \subseteq X \subseteq R^n$, $y_i \subseteq Y \subseteq R^n$, and the mapping $x = (x_1, \dots, x_n) \rightarrow \phi(x) = (\phi_1(x), \dots, \phi_n(x))$ about nonlinear regression is proposed, which is from input space R^n to higher feature space $F = \{\phi(x) | x \subseteq X\}$.

Linear learning process in feature space is described by the following equation

$$y = f(x) = \sum_{i=1}^l w_i \phi_i(x) = \langle w, \phi(x) \rangle \quad (1)$$

The loss function is given by:

$$L(w) = \lambda \langle w, w \rangle + \sum_{i=1}^l (y_i - \langle w, \phi(x_i) \rangle)^2 = \lambda w^T w + (Y - Xw)^T (Y - Xw) \quad (2)$$

By computing partial derivatives of Eqn (2), weight factor w is obtained:

$$w = (X^T X + \lambda I_l)^{-1} X^T Y \quad (3)$$

where $X = [\phi(x_1) \dots \phi(x_l)]^T$, $Y = [y_1 \dots y_l]^T$, I_l is 1-by-1 identity matrix. In feature space, according to Mercer, inner product is described by the following equation

$$K_{ij} = K(x_i, x_j) = \phi(x_i) \cdot \phi(x_j), \quad k = \langle \phi(x_i), \phi(x_j) \rangle \quad (4)$$

So regression function is updated according to the rule:

$$y = f(x) = \langle w, \phi(x) \rangle = Y^T (K_{ij} + \lambda I_l)^{-1} k \quad (5)$$

Different kernel functions can construct different KRR model. The type of common kernel has polynomial kernel, gauss radial basis kernel, sigmoid kernel, and so on. Here, Gauss radial basis kernel function given by:

$$K_{ij} = \exp\left(-\frac{\|x_j - x_i\|^2}{2p^2}\right) \quad (6)$$

3 Motor Mathematical Model and Reversibility Analysis

Under α - β stationary frame, the mathematical model of voltage-control asynchronous machine is analyzed [5,6]. The converter worked on the constant ratio of voltage and frequency (i.e. u/f) control pattern, synchronous angular frequency ω_1 and voltage amplitude U are input variants, the rotational speed ω_r and stator flux denoted by ψ^2_{sa} plus ψ^2_{sb} are output variants. Because $\psi^2_{sa} + \psi^2_{sb}$ is constant and $U = k\omega_1 + C$, the system becomes single-input and single-output. Input variable u equates ω_1 ,

output variable y equates ω_r , and state variable is described by the following equation

$$\dot{x} = [\omega_r \ \psi_{s\alpha} \ \psi_{s\beta} \ i_{s\alpha} \ i_{s\beta}]^T = [x_1 \ x_2 \ x_3 \ x_4 \ x_5]^T \quad (7)$$

Simplified mathematical model is described as follows:

$$\dot{x} = f(x, u) = \begin{cases} \frac{n_p^2}{J}(x_2 x_5 - x_3 x_4) - \frac{n_p}{J} T_L \\ (ku + C)Cosut - R_s x_4 \\ (ku + C)Sinut - R_s x_5 \\ \frac{R_r}{L_s L_r - L_m^2} x_2 + \frac{L_r}{L_s L_r - L_m^2} x_1 x_3 - x_1 x_5 \\ - \frac{R_r L_s + L_r R_s}{L_s L_r - L_m^2} i_{s\alpha} + \frac{L_r (ku + C)}{L_s L_r - L_m^2} Cosut \\ \frac{R_r}{L_s L_r - L_m^2} x_3 - \frac{L_r}{L_s L_r - L_m^2} x_1 x_2 \\ - \frac{R_s L_r + L_s R_r}{L_s L_r - L_m^2} x_5 + x_1 x_4 + \frac{L_r (ku + C)}{L_s L_r - L_m^2} Sinut \end{cases} \quad (8)$$

where ω_r is rotor angular-rate, $i_{s\alpha}$ and $i_{s\beta}$ are stator current of α and β axis independently, $\psi_{s\alpha}$ and $\psi_{s\beta}$ is stator flux of α and β axis independently, R_s is stator resistance, R_r is rotor resistance, L_s is stator inductor, L_r is rotor inductor, p_n is motor pole pairs, T_e is electrical torque, T_L is load torque, J is rotary inertia, and L_m is mutual-inductance.

The reversibility of the system is analyzed. Relative degree is $\alpha=2$, inverse-system is the form of $u = \zeta(x_4, x_5, y, \dot{y}, \ddot{y})$. The α th-order inverse system was constructed by using PI regulator. The block diagram of the α th-order inverse system is plotted in Fig.1.

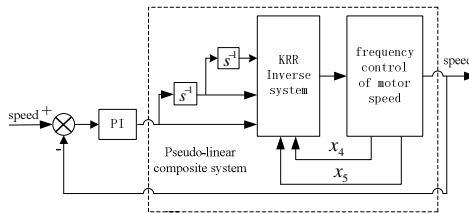


Fig. 1. The block diagram of the α th-order inverse system

4 System Testing

4.1 System Structure

The control system is made up of one induction motor with 1.1 kilo-watt, converter, industrial personal computer (IPC), programmable logic controller (PLC), photoelectric

coder and Hall sensors. The block diagram of the control system is plotted in Fig.2. Under constant u/f , PLC controls the induction motor through converter. Speed signal is gathered by counting model through photoelectric coder, and current signal is gained by Hall sensors. The acquisition is processed through off-line training of KRR by industrial personal computer, and the result of simulation is transmitted to PLC, finally the inverse system based on KRR is constructed by PLC.

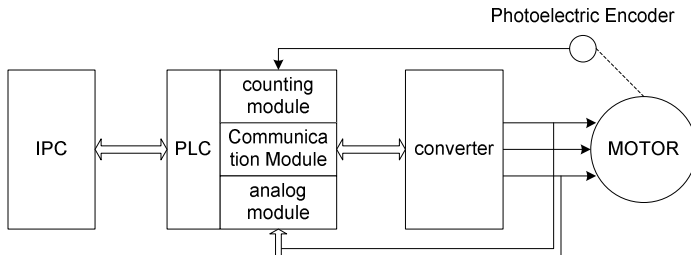


Fig. 2. Diagram of experiment system

4.2 The Implement and Synthesis of KRR

KKR is simulated in matlab. Construct model of given data, simulate time is 800 second, sample time is 0.1 second, set random model parameter, generic data is divided four groups.

Under the random variable of given 10~40 hz, sample and save ω_r , i_{sa} and $i_{s\beta}$ respectively when the open-loop control is adopted, then save sample data when system worked on the PI closed-loop control, PI modulator parameter $K_p = 0.4$, $T_I = 1$. Leave out the beginning and the end of sampling data, and compute first and second order differential of ω_r , then normalize the data. Sampling data set $\{i_{sa}, i_{s\beta}, \omega_r, \dot{\omega}_r, \ddot{\omega}_r\}$ is the input of KRR training, data set $\{\omega\}$ is the output of KKR training, train inverse model based on KRR under certain kernel parameter $p = 2$, the regularization coefficient λ is 0.002 when MSE is smaller than 10^{-3} . The fitting curve is shown by Fig.3. It demonstrated that the model based on KRR has good data fitting ability.

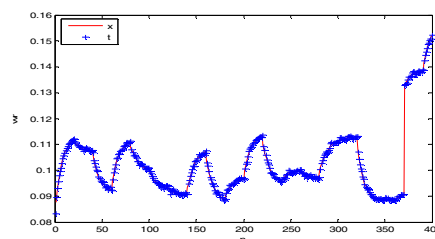


Fig. 3. The graph of KRR fitting curve

4.3 Testing

According to parameter p and λ , the- α order inverse model approximated by KRR was constructed, the inverse system is connected with original system, and the pseudo-linear combined system is constructed as Fig.1. Set PI modulator parameter $K_p = 0.008$, $T_i = 0.8$, closed-loop control system based on KRR compared with PI control.

1. Start-up testing

No-load start-up and load start-up from 0 to 20 Hz, the load is 0.3 ampere, experimental results are shown in Figure 4.

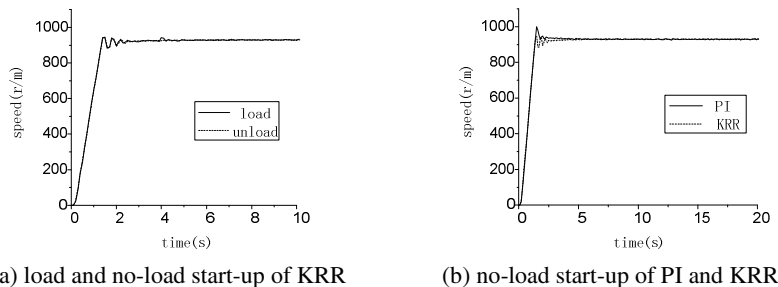


Fig. 4. The graph of start-up experiment

The results demonstrated that the system based on KRR has fast start-up ability under load and no-load. In addition, it has better start-up ability than general PI.

2. The test of increasing and decreasing the load

The frequency is 30 Hz, after load start-up under 0.2 ampere for 25 seconds, abrupt change of increasing load could reach to 0.4 ampere, then abrupt change of decreasing load at 40 second reduced to 0.3 ampere.

The experiment results were showed in Fig.5. The results demonstrate that the speed has good stabilization under abrupt change of increasing and decreasing load, and the system has strong adaptability to different load.

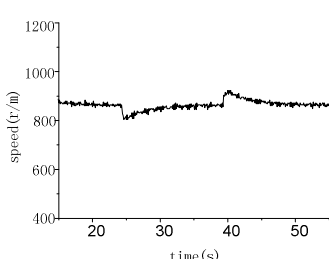


Fig. 5. Response under abrupt change

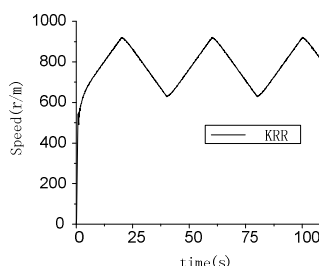


Fig. 6. Response of triangular-wave input

3. Tracking Experiment

When the input signal is triangular-wave, the graph of speed response is shown in Fig.6. The results demonstrate that the system has strong tracking ability.

5 Conclusions

The pseudo-linear combined system based on KRR and the- α order inverse model is proposed. The inverse system is modeled by Kernel Ridge Regression in detail, and applied in induction motor variable frequency speed-regulating control. Through the analysis of start-up experiment, experiment of increase or decrease the load suddenly and tracking experiment, the system showed good inhibition ability, and nonlinear factor and parameter showed good adaptability and robust stability. The inverse model based on KRR has excellent nonlinear identification ability, and can be applied in nonlinear control.

References

1. Jiang, D., Hu, M., et al.: Adaptive Bluetooth Location Method Based on Kernel Ridge Regression. Application Research of Computers 27, 3487–3489, 3492 (2010)
2. Li, Y., Luo, D., et al.: Face Recognition Using Neighborhood Preserving Maximal Margin Analysis of Kernel Ridge Regression. Pattern Recognition and Artificial Intelligence 23, 23–28 (2010)
3. Li, Q., Shao, C.: Nonlinear Systems Identification Based on Kernel Ridge Regression and Its Application. Journal of System Simulation 21, 2152–2155, 2194 (2009)
4. Quan, Y., Yang, J.: A Decoupling Control System Using Kernel Ridge Regression. Journal of Shanghai Jiaotong University 37, 1421–1425 (2003)
5. Liu, G., Dong, B., et al.: Model reference adaptive control of PMSM based on support vector machines generalized inverse. Journal of Southeast University (Natural Science Edition) 40, 13–18 (2010)
6. Wang, X., Dai, X.: Improved Method of Induction Motor s FOC based on ANN Inverse. Power Electronics 42, 48–50 (2008)

Parallel Robotics Control Strategy Study Based on Fuzzy-PID

Caihong Zhu and Hongtao Zhang

Department of Electronic Engineering, Suzhou Vocational University,
Suzhou 215104, Jiangsu, China
zch@jssvc.edu.cn

Abstract. Compared with the serial robot, the parallel robot has the stiffness, load capacity, high precision, compact structure, and can be widely used in industrial, aviation, military and other fields. Control system of the parallel robot based on the limb model is established. The PID control algorithm and the fuzzy control algorithm are compared, the Fuzzy-PID control strategy is determined, the control algorithm confirmation procedure using VC++ is designed, and then a simulative experiment is made on the Matlab/Simulink. The results show that the Fuzzy-PID control algorithm achieves high precision real-time control on this parallel robot.

Keywords: Parallel robot, control strategy, Fuzzy control, Fuzzy-PID Control.

1 Introduction

Parallel robot is one kind of new mechanism. It has the merit which the traditional series robot is unable to compare. It is the supplement and the expansion of the series robot. It has the influential role regarding the engine bed technology and the robot technology's development. Parallel robot possesses the characteristics of large rigidity, strong load bearing capacity, small error, high precision, small dead weight load, good dynamic performance, and easy control. Parallel robot is a complex, multi-variable, multi-degree of freedom, multi-parameter nonlinear coupling system, and the control strategy is extremely complex. When the control system originally is designed, mostly, the various branches of the parallel manipulator are taken as a completely independent control system [1], the control strategy is the traditional PID control strategy for the control, and the control results are not very satisfactory. The parallel robot based on limb model control system is adopted in this paper, the Fuzzy-PID controller is designed to determine, the good control effect is achieved, the control strategies on parallel robot for the promotion of theoretical research and practical application of development has played a promotional role.

2 Control System Establishment

The full Lagrange robot dynamics model can be expressed as the following form:

$$M(q)\ddot{q} + C(q, \dot{q})\dot{q} + G(q) = \tau \quad (1)$$

Here, q and \dot{q} represent the robot position and velocity of each joint, τ is the torque vector. M , C , G are the order function matrix of $n \times n$, $n \times n$ and $n \times 1$ determined by the specific structure of the robot. τ is a vector-order moment of $n \times 1$. It looks more concise as the style has been written in the form to be linear. In fact, the system started in the form of fairly complex. The distributed control system based on joint or slip on the robot model is one of the most designing applied widely in the actual process, and in industrial engineering, most systems used this type of robot design.

The parallel manipulator closed-loop control system is shown in Figure 1. The controller of the branch is actually a mini-computer. Motor is a drive unit. Electric push rod and the harmonic reducer is the executing agency. The output is feedback from the displacement sensor. In the figure, the $r(t)$ is the location in the given, $c(t)$ is the position feedback, $y(t)$ is the displacement output, $u(t)$ is the speed drive voltage, the deviation is $e(t) = r(t) - c(t)$. The $e(t)$ of the controller is based on the size of the value of regulation $u(t)$, it takes the output displacement to continue to follow the given position.

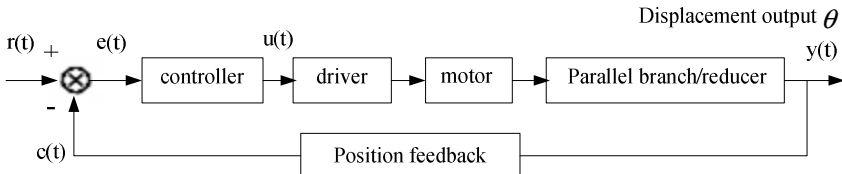


Fig. 1. The closed-loop control diagram of the limb

3 Control Algorithms and Authentication Methods to Determine

3.1 Control Algorithm to Determine

PID control is a more mature control [2], and because of its simple, it is effective and widely used. But, before the PID control is applied, it must be charged tuning PID parameters of objects. Because the charged object can not be accurately determined, there is a big part of the delay, the object controlled by temperature, component parameter changes and other reasons, PID control can not achieve the desired quality control.

Fuzzy control is a kind of intelligent control [3]. In essence, it is a simulation of the human brain. It is demonstrated the superior performance in a complex, large delay, difficult to establish accurate mathematical model of the nonlinear control process. It has many advantages of not depending on the control object with the mathematical model, good robustness, simple and practical merit. However, in fuzzy and fuzzy reconciliation process, because of the error signal and control amount classifying, the control system has a larger steady state error, so fuzzy control is limited of the high-precision control.

The two control algorithms both have their advantages and disadvantages. Therefore, the introduction of PI control to Fuzzy control strategy control, constitute

the Fuzzy-PI (or PID) compound control is a way to improve the controller performance. Fuzzy-PID control is combined the adaptive Fuzzy control and the advantages of small steady-state error of PID control, and become a new control algorithm and concern by many scholars [4]. At present, the current controller has a variety of complex composition in the form, and there are differences in how it works. The Fuzzy-PID mixture control is one kind of simple structure, and easy to realize compound controller.

3.2 Authentication Method of the Control Algorithm

The control system must be stable, in addition, the system requires good speed and accuracy. Speed and accuracy is reflected in the system which is increased the role of external response [5]. In order to facilitate analysis and comparison of different systems, some typical input signal must be selected. Typically, the more common step signal is used to study the performance in time domain. Commonly the step response performance is used in the following:

(1) Delay time t_d ;(2) Rise time t_r ;(3) Peak time t_p ;(4) Maximum overshoot $\sigma\%$;(5) Adjustment time t_s ;(6) Oscillation frequency N ;(7) Steady-state error e_{ss} .

Under the step input signal, time response curves directly reflect the performance index of the step response of the system, these performance indicators provide the most direct basis for the selection of control parameters and improving control scheme. Therefore, the output of the controlled system response data collection procedures were design in this paper, and program design using C ++ language based on VC ++ development tool. The application of program controlled system can easily obtain the output response sequence [6], the data will be processed to draw the corresponding curves, which is the time response curve of the controlled system under the step input signal.

4 Controller Design and Simulation Analysis

The control principle diagram is shown in Figure 2. The basic idea is to control the range of large deviations by Fuzzy control, and within a small deviation into a PID control. The conversion between the above two controls is realized automatically by the computer according to the deviation of the range given in advance.

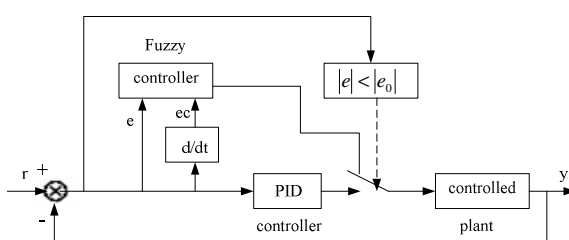


Fig. 2. Fuzzy-PID control block diagram of two-way switch

The unit step response curve under the Fuzzy-PID control algorithm for θ is in Figure 3. The curve is obtained by experiment, and the performance indicators are shown in Table 1. The sampling time is $T=20ms$, the deviation range is $|e_0|=1.2$, the control algorithm design is using C ++ Language.

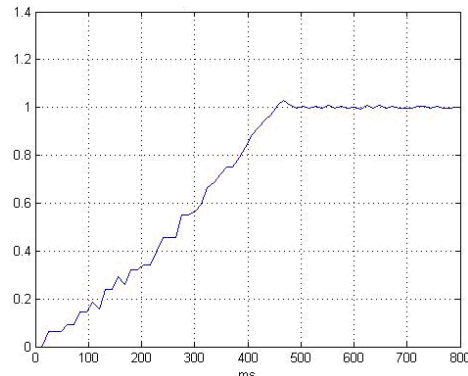


Fig. 3. The step response curves under Fuzzy-PID control algorithm of θ

Table 1. Fuzzy-PID algorithm for step response performance

Parameters	Value
Delay time t_d	260ms
Rise time t_r	450 ms
Peak time t_p	460 ms
Maximum overshoot $\sigma\%$	2%
Adjustment time t_s	480 ms
Oscillation frequency N	1
Steady-state error e_{ss}	< 0.01mm

However, the step response curves and step response performances under the PID algorithm and Fuzzy algorithm are shown in following figures and tables.

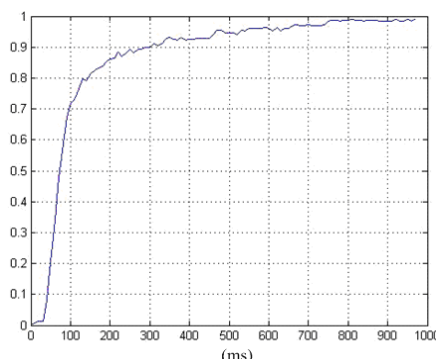
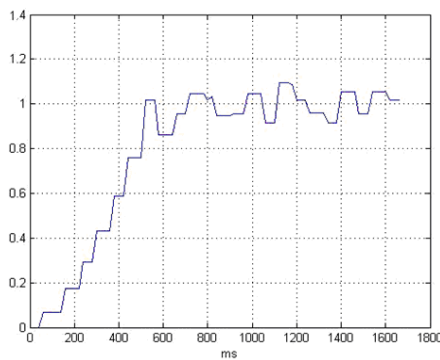


Fig. 4. The step response curves under PID control algorithm of θ

Table 2. PID algorithm for step response performance

Parameters	Value
Delay time t_d	75ms
Rise time t_r	800 ms
Peak time t_p	-
Maximum overshoot $\sigma\%$	0
Adjustment time t_s	800 ms
Oscillation frequency N	0
Steady-state error e_{ss}	< 0.01mm

**Fig. 5.** The step response curves under Fuzzy control algorithm of θ **Table 3.** Fuzzy algorithm for step response performance

Parameters	Value
Delay time t_d	370ms
Rise time t_r	520 ms
Peak time t_p	530 ms
Maximum overshoot $\sigma\%$	9%
Adjustment time t_s	> 1600 ms
Oscillation frequency N	> 6
Steady-state error e_{ss}	< 0.06mm

It can be drawn from the table: Fuzzy-PID mixture control can effectively combine the dynamic characteristics of the Fuzzy control and steady state performance of the PID control. Compared with the traditional PID and the Fuzzy control, Fuzzy-PID mixture control can improve the response speed and obtain a better accuracy of the steady state.

5 Conclusion

Currently, there is a variety of advanced robot control algorithm the some scholars studied at home and abroad. But most results were only theoretical simulation. Real

parallel robot system used little on the actual control. The Fuzzy-PID control algorithm designed in this paper achieved the ideal control effect in the actual control. The robot can successfully complete the given trajectory in its work space, and have some control over the accuracy. The future complex nonlinear control system of the parallel robot should be the composite control composed of the robust control decentralized control, the adaptive control, and the intelligent control, it can achieve simple, high-speed, high-precision control on parallel robot.

Acknowledgments. At the point of finishing this thesis, I'd like to express my sincere thanks to all those who have lent me hands in the course of my writing this thesis.

References

1. Wu, B., Wu, S.L., et al.: Current Status and Development Trend of Stewart Platform Control Strategy. *Machine Tool & Hydraulics* (10), 5–8 (2005)
2. Li, F.M.: The Research of Controlling Arithmetic for Figure PID. *Journal of Liaoning University: Natural Science Edition* 32(04), 367–370 (2005)
3. Sun, D.S., Wang, Y.: *Control Technology of Robot*. Mechanical industry publishing house, China (1998)
4. Xiong, Y.L.: *Robotics*. Mechanical industry publishing house, China (1993)
5. Zhu, J.: *Fuzzy Control Theory and System Theory*. Mechanical industry publishing house, China (2005)
6. Chen, J., Xue, B.: Present Research Situation and Prospect of the Fuzzy Control. *Automation & Instrumentation* 128(06), 1–3 (2006)

Embedded Remote Controller with Two Cameras Intelligent Orientation and Bi-direction Wireless Communication

Xueguang Zhu

The Institute of Mechanical & Electrical Engineering of Anhui
Institute of Architecture & Industry, Hefei, Anhui, China
Zhuxg_00@126.com

Abstract. A design of remote controller based on embedded platform is proposed, which adopts two patents related to machine vision. This remote controller not only has learning and wireless communication functions, but also has spatial self-orientation function. The scheme is implemented from the theory of two cameras' machine vision. Two cameras mounted on the controller can obtain the space coordinates of any corresponding point. When the remote controller is moved, and some known stationary points' picture coordinates are changed, so we can evaluate the direction and velocity of handheld remote controller. In this way it can be used as ideal baton. It not only has abundant technical contents, but also has a good market prospects.

Keywords: machine vision, moving orientation, embedded Linux, intelligent remote controller, bi-direction wireless communication.

1 Introduction

A remote controller based on embedded platform and Linux operating system with liquid crystal display touch panel and bi-direction wireless communication module is proposed in this paper. The embedded platform consists of S3C2410 microprocessor hardware which is designed to provide hand-held devices and general applications with cost-effective, low power, and high performance. The crystal panel shows text tips to simplify the learning process and dynamical buttons intelligently adapt to all kinds of devices' remote controlling.

This processor is installed with embedded Linux operating system. The embedded architecture is different from personal computer, and the operating system running on it must be properly cut down for the limited resources, and generally its function is application specific, as well as real time response should be satisfied. The driving and application program development is very important to this project. The driving programs include infrared receiving and sending, liquid crystal display and touch panel, radio receiving and sending, and so on.

The application programs are made on QT platform which can work well on Linux. It is supported on many platforms including embedded Linux with frame-buffer

support. QT is a cross-platform C++ graph user interface (GUI) application framework. It provides application developers with all the functionality needed to build state-of-the-art GUI. QT is fully object oriented, easily extensible, and allows true component programming.

The infrared and wireless modules are important peripherals. The infrared unit including that HS0038A is used for receiving and TIL104 is used for sending. Wireless communication adopts nRF905 chip, and it is a single-chip radio transceiver for the 433/868/915 MHz ISM band, and consists of a frequency generator, receiver chain with demodulator, a power amplifier, a crystal oscillator and a modulator. The Burst feature automatically handles preamble and CRC. Current consumption is very low. Built in power down modes makes power saving easily realizable.

The patents related to machine vision are used in the design of this remote controller. The remote controller is equipped with two cameras. According moving machine vision theory, two cameras can calculate the coordinates of any spatial position by corresponding point matching method. In this way if the spatial target is motionless, we can evaluate the controller's moving coordinates. In the result this remote controller not only has learning, but also has spatial self-orientation function, and we can easily evaluate the direction and velocity of remote controller itself so it can be used as ideal baton. In addition, it has the advantage of low cost, beautiful shape and good-looking pictures.

2 Patents[8,9] Technology Introduction

Two practical new type patents “Remote controller with camera and touch panel[8]” and “Remote controller with camera[9]” are used in this paper. Here we first introduce the main contents of the patents. The handheld remote controller with wireless transceivers application model is shown in Fig.1, and the project screen as the handheld controller is embedded with wireless communication module. In practical application, we suppose the scene placed with known drone, and the drone has a quantity of character points. The remote controller has advanced embedded processor whose signal process ability is powerful, using the technology of moving machine vision, the controller can obtain its

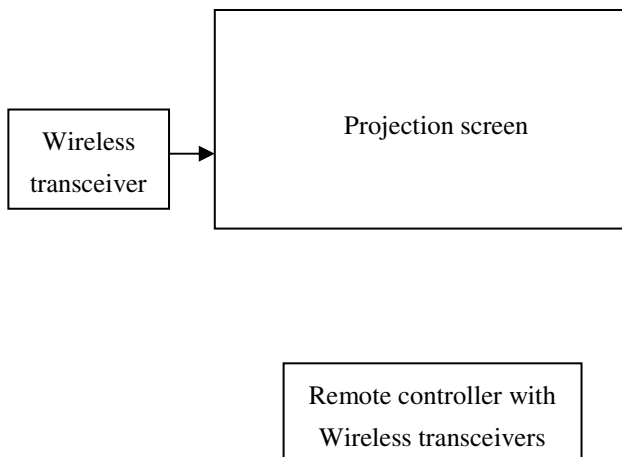


Fig. 1. Handheld remote controller with wireless transceivers application model

self spatial coordinates. The controller continuously calculates and obtains the latest spatial coordinates, and sends them to the receiver of projection screen' controller in wireless way. The receiver can use this information to change the cursor on the screen. When the operator of the handheld controller presses the dynamic button on the crystal panel, the embedded processor will send the instructing information to the receiver. This can control project screen to switch displaying contents. At the same time, the controller can show projection screen contents by communication receiving unit to get the picture information from the transceiver mounted on projection screen controller.

3 The Application of Machine Vision Theory[1,2]

Two cameras are mounted on the controller, supposing the two cameras' relative position coordinate is known beforehand. This is not difficult to satisfy, because we can use spatial drone to calibrate. When the two cameras' relative position coordinates are known, they can be expressed by known rotate matrix and displacement vector. The model of two cameras' machine vision is shown in Fig.2, on the assumption that the left camera is located on the world coordinates O-xyz origin, and its picture plane O_l - X_l Y_l parallels O-xy plane, namely the light axis is z, the effective focus is f_l , and the right camera's coordinates system is O_r - x_r y_r z_r , and its picture plane is O_r - X_r Y_r , its effective focus is f_r . by camera project model

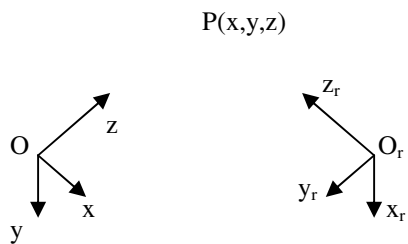


Fig. 2. The model of two cameras machine vision

$$s_l \begin{bmatrix} X_l \\ Y_l \\ 1 \end{bmatrix} = \begin{bmatrix} f_l & 0 & 0 \\ 0 & f_l & 0 \\ 0 & 0 & 1 \end{bmatrix} \begin{bmatrix} x \\ y \\ z \end{bmatrix} \quad (1)$$

$$s_r \begin{bmatrix} X_r \\ Y_r \\ 1 \end{bmatrix} = \begin{bmatrix} f_r & 0 & 0 \\ 0 & f_r & 0 \\ 0 & 0 & 1 \end{bmatrix} \begin{bmatrix} x_r \\ y_r \\ z_r \end{bmatrix} \quad (2)$$

We suppose the two cameras' relative position is expressed by rotation matrix

$$R = \begin{bmatrix} r_1 & r_2 & r_3 \\ r_4 & r_5 & r_6 \\ r_7 & r_8 & r_9 \end{bmatrix} \quad (3)$$

and displace vector

$$T = \begin{bmatrix} t_x \\ t_y \\ t_z \end{bmatrix} \quad (4)$$

So, the coordinate transformation is

$$\begin{bmatrix} x_r \\ y_r \\ z_r \end{bmatrix} = [R | T] \begin{bmatrix} x \\ y \\ z \\ 1 \end{bmatrix} \quad (5)$$

Substitute (1)-(4) into (5), we obtain

$$\rho_r \begin{bmatrix} X_r \\ Y_r \\ 1 \end{bmatrix} = \begin{bmatrix} f_r r_1 & f_r r_2 & f_r r_3 & f_r t_x \\ f_r r_4 & f_r r_5 & f_r r_6 & f_r t_y \\ r_7 & r_8 & r_9 & t_z \end{bmatrix} \begin{bmatrix} zX_l / f_l \\ zY_l / f_l \\ z \\ 1 \end{bmatrix} \quad (6)$$

So the spatial corresponding point P's coordinates are

$$\begin{cases} x = zX_l / f_l \\ y = zY_l / f_l \\ z = \frac{f_l(f_r t_x - X_r t_z)}{X_r(r_7 X_l + r_8 Y_l + f_l r_9) - f_r(r_4 X_l + r_5 Y_l + f_l r_6)} \end{cases} \quad (7)$$

If the controller is moved, the spatial corresponding point's coordinates will change. When the spatial corresponding point is motionless, due to coordinates are relative, we can find the velocity and direction of the handheld controller motion.

4 The Error Analysis

Suppose $f_l=f_r=f$, $t_x=B$, $t_y=t_z=0$, the rotation matrix is unit matrix. Then

$$z = \frac{fB}{X_r - X_l} \quad (8)$$

$$\Delta z = \frac{-fB}{(X_r - X_l)^2} \Delta X_r + \frac{fB}{(X_r - X_l)^2} \Delta X_l = \frac{z^2}{fB} (\Delta X_l - \Delta X_r) \quad (9)$$

$$\Delta x = \frac{x}{z} \Delta z + \frac{z}{f} \Delta X_l = \frac{z(z+x)}{fB} \Delta X_l - \frac{z^2}{fB} \Delta X_r \quad (10)$$

$$\Delta y = \frac{y}{z} \Delta z + \frac{z}{f} \Delta Y_l = \frac{yz}{fB} \Delta X_l + \frac{z}{f} \Delta Y_l - \frac{z^2}{fB} \Delta X_r \quad (11)$$

From (8-11), we can see that the error is smaller when B and f are larger, and the higher the cameras' accuracy the better. When ΔX_l , ΔX_r , ΔY_l and ΔY_r are all confined to the same normal distribution, and have the same covariance σ^2 . one obtains

$$|\Delta z| \propto \sqrt{2} \frac{z^2}{fB} \sigma \quad (12)$$

$$|\Delta x| \propto \frac{|z|}{fB} \sigma \sqrt{2z^2 + 2zx + x^2} \quad (13)$$

$$|\Delta y| \propto \frac{|z|}{fB} \sigma \sqrt{y^2 + B^2 + z^2} \quad (14)$$

When coordinates detection accuracy is high enough, the remote controller can take advantage of its bi-direction wireless communication module to send the real time coordinates information to the transceiver equipped on the computer controlling the projection screen. At the same time, due to the bi-direction communication character, it can display the personal computer contents, and the operator of the handheld controller can directly manipulate the interface and send various instructions. In a word, this handheld device is an ideal lecturing aiding tool.

5 Summary

The proposed intelligent remote controller has unique advantages being able to cater to satisfy market demand, for the low cost, low power consuming, simple learning procedure, facility for using, friendly interface and nice dynamical pictures developed by QT application software based on Linux operating system and ARM micro processor architecture. The Bi-direction wireless communication function greatly enlarges its application range and endows the product with novel feature. Two cameras mounted on the remote controller can obtain the remote controller self space

coordinates so as to evaluate the direction and velocity of its motion, so it can be used as ideal baton. In addition bi-direction wireless communication function enables the remote controller to obtain the projection screen picture, facilitate the operator directly manipulate the interface on the screen. It is portable and powered by rechargeable lithium battery, the patent technology' application will have a good market prospects.

References

- [1] Hartley, R.I.: In Defense of the Eight-point Algorithm. *IEEE Trans. Pattern Analysis and Machine Intelligence* 6, 580 (1997)
- [2] Longuet, H.H.: A Computer Algorithm for Reconstructing A Scene from Two Projections. *Nature* 133 (1981)
- [3] Hand, A.J.: Photonics Analyze Food Quickly, Effectively. *Photonics Spectra* 10, 114 (1998)
- [4] Haneishi, H., Miyake, Y.: Distortion Compensation of Electronic Endoscope Image. In: *IEEE Conf. Rec. Med. Image*, vol. 1717 (1993)
- [5] Hallader, M.: Research into Coil Systems Advances Remediation of Nuclear Reactors. *Society of Photo-Optical Engineering* 1, 1 (1999)
- [6] Cavallo, A., et al.: Optoelectronic Joint Angular Sensor for Robotic Fingers. *Sensors and Actuators* 1, 203 (2009)
- [7] Antonio, M., et al.: Vision-based Three-finger Grasp Synthesis Constrained by Hand Geometry. *Robotics and Autonomous System* 1, 496 (2006)
- [8] Zhu, X.G.: Remote Controller with Camera and Touch Panel. Practical New Type Patent (no. 200820147295 in Chinese) (2008)
- [9] Zhu, X.G.: Remote Controller with Camera. Practical New Type Patent (no. 200820147264 in Chinese) (2008)

Applying Answer Set Programming to Points-to Analysis of Object-Oriented Language

Bo Yang^{1,2}, Mingyi Zhang³, and Ying Zhang³

¹ College of Computer Science and Information, Guizhou University, Guiyang, China

² Department of Physics and Electronics Information Science, Guiyang University, China

99byang@163.com

³ Guizhou Academy of Science, Guiyang, China

{Zhangmingyi045, Zhangying}@yahoo.com.cn

Abstract. Points-to information is essential in software engineering, including compiler optimization, instruction-level parallelism, program verification, and so on. The propagating of points-to information along paths of a program can be viewed as the “frame problem” in a dynamic world. As a primary knowledge representing and reasoning tool in Artificial Intelligence, Answer Set Programming (ASP) provides a natural and concise way to express the frame problem. We present a collection of ASP rules to model the propagating of points-to information along paths of an object-oriented program. With these rules and basic facts of a program, points-to information at each program point can be computed easily. This makes it possible to acquire useful information for program analysis through existing ASP solvers.

Keywords: Answer Set Programming, knowledge representing and reasoning, points-to analysis, object-oriented language.

1 Introduction

Lots of efforts have been devoted to applying techniques of Artificial Intelligence on software engineering. While Mayer and Stumptner[1] give a comprehensive description about finding faults in program based on the theory of diagnosis from first principles, Dawson[2], Whaley[3] and Song[4] *et al* successfully use logic programming system for program analysis. It is shown that ideas and technologies in Artificial Intelligence are very helpful for modeling and solving some problems in software engineering.

From points-to information of references or pointer variables in a program, alias relationships between these variables can be inferred, and both of them are important in software engineering. Traditionally, in order to enhance the performance of a program, points-to information or alias information are indispensable in compiler optimization. In the context of high-performance computing, alias information can be used for instruction-level parallelism or distributed and clustering computing [5]. Furthermore, Meyer shows that the accuracy of program proving using Hoare triple will be improved with alias calculus [6], in the case of some variables refer to the same memory location—they are aliases to each other. Practically, because of

aliasing, it quite possible leads to mistaking operations on memory locations in a program, especially in those written in object-oriented language like Java. As a result, the program will end up with a wrong output. Thus it is necessary to provide points-to or alias information for debugging the failure program.

Answer Set Programming (ASP) is a paradigm based on the stable model (answer set) semantics of logic programming [7], it reduces solving of various combinatorial problems to finding the answer sets of logic programs which declaratively describe the problems. As a primary means for non-monotonic reasoning, ASP plays a significant role in commonsense knowledge representing and reasoning, which usually deals with a possibly incomplete state of knowledge. To accomplish this, *negation as failure* is used to express the closed world assumption—whenever there is no evidence showing that a property holds, it does not hold. Moreover, ASP gives a natural and simple solution to the *frame problem*, which disposes formalizing the commonsense law of inertia: Everything is presumed to remain in the state in which it is. With these expressive capacities, ASP has been applied successfully in many areas such as decision making [8,9], planning[10], e-commerce[11], and so on.

Actually, the propagation of points-to information abides by the law of inertia. To the best of our knowledge, there is not yet a non-monotonic logical mechanism dealing with points-to analysis. In this paper, we present a collection of ASP rules to model the propagating of points-to relationships along paths of an object-oriented program. With these rules and basic facts of a program, points-to information at each program point can be computed easily. Thus it is possible to acquire useful information for program analysis through existing ASP solvers.

We give an introduction about ASP and points-to analysis in object-oriented language in section 2. In section 3, effects of various statements in the language upon points-to information are modeled with ASP rules. Section 4 describes how points-to information of an example program is inferred using rules given in previous section. The last section concludes our work and presents research interests in the future.

2 Preliminaries

2.1 Syntax and Semantics of ASP

Following Lifschitz [12], *atom* is an element from a nonempty set A of symbols. A *literal* is a *positive literal* (atom) or a *negative literal* (atom preceded by the classical negation symbol \neg). Literals L and $\neg L$ are said to be *complementary*. A set of literals is *inconsistent* if it contains a pair of complementary literals, and *consistent* otherwise. By Lit we denote the set of all literals.

Generally, a *rule* r is of the form:

$$\text{Head} \leftarrow L_1, \dots, L_m, \text{not } L_{m+1}, \dots, \text{not } L_{m+k} \quad (m, k \geq 0)$$

where Head (head of r , denoted by $H(r)$) is empty or a literal L_0 , and the RHS is a finite set of two kinds of rule elements, *i.e.* literals possibly preceded by the *negation as failure* symbol *not*. We also write rule r in a brief form: $H(r) \leftarrow P(r) \cup \text{not}(N(r))$, where $P(r)=\{L_1, \dots, L_m\}$ is called *positive body*, and $N(r)=\{L_{m+1}, \dots, L_{m+k}\}$ *negative body* respectively. Especially, a rule with $H(r) \neq \emptyset$ and $P(r)=N(r)=\emptyset$ is a *basic rule*. Rule r is called a *fact* if $H(r) \neq \emptyset$ and $P(r)=N(r)=\emptyset$, and a *constraint* if $H(r)=\emptyset$.

A program Π is a set of rules, and Π is basic if every rule in it is basic.

Let X be a set of literals, X is *logically closed* if it is consistent or equals Lit , and is *closed under* a basic program Π' if for each rule $r: H(r) \leftarrow P(r)$ in Π' , $H(r) \subseteq X$ whenever $P(r) \subseteq X$. Among all sets of literals which are logically closed and closed under Π' , the smallest one is denoted by $Cn(\Pi')$. Clearly, such a set always exist, and elements of it are called the consequences of Π' . For any basic program Π' and a set X of literals, to compute $Cn(\Pi')$, a monotonic function $T_{\Pi'}$ is defined as follows:

$T_{\Pi'}X$ is $\{H(r) | H(r) \leftarrow P(r) \in \Pi', P(r) \subseteq X\}$ if X is consistent, and Lit otherwise. $Cn(\Pi')$ is the union of sets obtained by iterating $T_{\Pi'}$ on \emptyset , that is, $Cn(\Pi') = \bigcup_{n \geq 0} T_{\Pi'}^n \emptyset$.

Example 1[12]. Let $\Pi' = \{p. \neg q. r \leftarrow p, q. \neg r \leftarrow p, \neg q. s \leftarrow r. s \leftarrow p, s. \neg s \leftarrow p, \neg q, \neg r.\}$, where each rule is ended with “.”. We have: $T_{\Pi'}^0 \emptyset = \emptyset$, $T_{\Pi'}^1 \emptyset = \{p, \neg q\}$, $T_{\Pi'}^2 \emptyset = \{p, \neg q, \neg r\}$, $T_{\Pi'}^3 \emptyset = \{p, \neg q, \neg r, \neg s\}$. For every $n > 3$, $T_{\Pi'}^n \emptyset = T_{\Pi'}^3 \emptyset$. Thus $Cn(\Pi') = \bigcup_{n \geq 0} T_{\Pi'}^n \emptyset = \{p, \neg q, \neg r, \neg s\}$.

Given an arbitrary program Π and a set X of literals, the *reduct* of Π relative to X , Π^X , is derived by (i) deleting each rule $H(r) \leftarrow P(r) \cup \text{not}(N(r))$ such that $N(r) \cap X \neq \emptyset$, and (ii) replacing each remaining rule $H(r) \leftarrow P(r) \cup \text{not}(N(r))$ by $H(r) \leftarrow P(r)$.

X is an *answer set* of Π if $Cn(\Pi^X) = X$.

Example 2. Consider a simple program, let $\Pi = \{c. a \leftarrow b, \text{not } c. b \leftarrow c, \text{not } a\}$. If $X = \{b, c\}$, then $\Pi^X = \{c. b \leftarrow c\}$. So $Cn(\Pi^X) = \{b, c\} = X$, hence X is an answer set of Π .

2.2 Points-to Relationships between References and Objects

In an object-oriented programming language like Java, the *new* operator creates an *object* of a certain class in heap—a general-purpose pool of memory, then a variable of this class, called *reference*, can be defined to refer to this object. For a compositional class, some data members (fields) of it are also references that can refer to objects of other classes. Example 3 shows these notions and correlative operations.

Example 3. A Java program segment

(1) A a=new A(); //o1	(5) c=a; //assign
(2) B b=new B(); //o2	(6) a.f=b; //store
(3) A c;	(7) d=c.f; //load

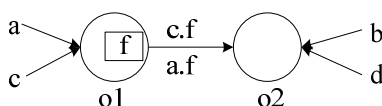


Fig. 1. Points to relationship in Example 3

Two objects $o1$ of class A and $o2$ of class B are created in statement (1) and (2) respectively, and references a and b are defined to refer to them; (5) is a simple assignment statement assigning a to c , thus c also refers to $o1$; Suppose class A is compositional and its field f can refer to an object of class B, statement (6) performs a

store operation making $a.f$ refers to $o2$; *load* operation in (7) causes d refers to $o2$ as $c.f$ does. Actually, store and load are special assignments. Fig. 1 gives corresponding points-to relationships caused by these operations.

Whenever there is a method calling statement that calls other procedure(s), it can be treated as assignment—the actual reference parameter is assigned to the formal parameter. At the calling statement, points-to information is propagated from the calling method to the called method, then probably modified by the callee, and finally passed back to the caller when the callee exits.

As mentioned in section 1, propagation of points-to information along paths of a program abides by the law of inertia. For instance, statement (5) in Example 3 makes c refer to $o1$, but points-to relationships of references a and b are not changed by (5), so they will be passed to the next statement as they are.

2.3 Control Flow Graph, Calling Graph and Data-Flow Analysis

In the context of points-to analysis, *intra-procedure analysis* within a method uses its *control flow graph*(CFG) to check the influence of assigning statements on points-to relationships, and *inter-procedure analysis* among various methods deals with calling statements by using *calling graph*(CG) and CFGs of involved methods.

Given a method m , its CFG is defined as a directed graph $\text{CFG}_m = \langle N_m, E_m, \text{entry}_m, \text{exit}_m \rangle$, where N_m is a set of nodes with entry node entry_m and exit node exit_m , and for the exit of a conditional statement, a merging node doing nothing is added to simplify our description(For example, node s in Fig. 2(b)); E_m is the set of directed edges, each $\langle n, n' \rangle \in E_m$ represents the immediate predecessor and successor relationship between n and n' . Fig.2 presents graphic representations of sequential compound, conditional statement and loop statement in CFG. In Fig.2(b) and (c), node $s0$ is a flow construct node and generally has no influence on points-to relationship.

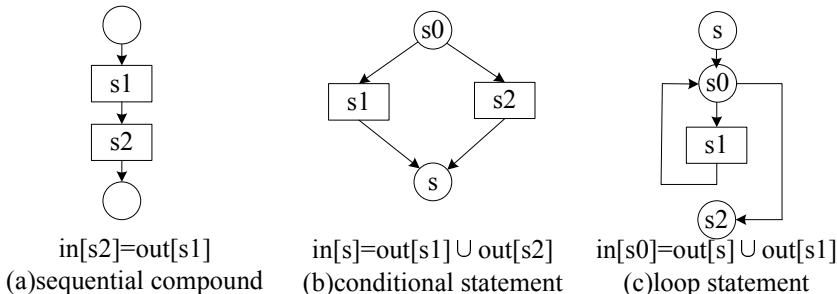


Fig. 2. Data-flow equations for basic program structures

A calling graph involving various methods is also a directed graph $\text{CG} = \langle N, E \rangle$, where each $m \in N$ represents a method, and an edge $\langle m_1, m_2 \rangle$ in CG says that m_1 is a caller *w.r.t* m_2 . To clarify changes of points-to information before and after calling m_2 , the calling statement s in m_1 is divided into two nodes— s_{pre} and s_{post} —in CFG of m_1 . While the latter “cuts” the points-to information of formal parameters and local variables of m_2 , the former deals with the assignment from actual parameters to formal parameters. More details are given in the next two sections.

Actually, points-to relationships is a kind of data-flow information, which is computed by the following data-flow equation:

$$\text{out}[s] = \text{gen}[s] \cup (\text{in}[s] - \text{kill}[s])$$

where s is a simple assigning statement or a basic block; $\text{in}[s]$ and $\text{out}[s]$ represent data-flow information before and after performing s respectively; data-flow information generated/killed by s is denoted by $\text{gen}[s]/\text{kill}[s]$. Data-flow equations for three basic program structures are presented in Fig.2. In Fig.2(b), data-flow information from different predecessors merge in node s and passes forward. In Fig.2(c), $\text{out}[s_1]$ is feed back to s_0 , this means that $\text{out}[s_0]$ is computed iteratively. In sense of points-to or alias analysis, this iteration always converges to a fixpoint[6].

In the next section, we will show how ASP is used to model propagation process of points-to information and illustrate the validity of our method.

3 Modeling Propagation of Points-to Information with ASP

Based on CFG of each method and CG among them, this section describes the propagation of points-to information with ASP rules, for intra-procedure and inter-procedure analysis.

3.1 Modeling Intra-procedure Points-to Analysis

We introduce the following notations for object-oriented programs.

- Set S of nodes: each $s \in S$ represents a node in CFG of the method;
- Set X of references: each $x \in X$ is a reference variable defined in program;
- Set F of fields: collection of fields such that each $f \in F$ is also a reference;
- Set O of objects: $o_s \in O$ represents an object defined at node s ;
- $\text{ref}(x,o,s)$: reference x refers to object o after execution of node s ;
- $\text{reff}(o,f,o',s)$: field f of object o refers to object o' after execution of s ;
- $\text{asn}(s,x,y)$: node s assigns reference y to x ;
- $\text{store}(s,x,f,y)$: node s is of the form $x.f=y$;
- $\text{load}(s,y,x,f)$: node s is a load operation $y=x.f$;
- $\text{new}(s,o_s,x)$: nodes s performs a *new* operation that creates object o_s referred by x ;
- $\text{pred}(s,s')$: node s is the immediate predecessor of node s' .

First of all, the following two ASP rules state the law of inertia—if there is no evidence showing that $\text{ref}(x,o,s')$ or $\text{reff}(o,f,o',s')$ is negated, then it holds as it is.

$$\text{ref}(x,o,s') \leftarrow \text{pred}(s,s'), \text{ref}(x,o,s), \text{not } \neg\text{ref}(x,o,s') \quad (R1)$$

$$\text{reff}(o,f,o',s') \leftarrow \text{pred}(s,s'), \text{reff}(o,f,o',s), \text{not } \neg\text{reff}(o,f,o', s') \quad (R2)$$

Within a method, *new* operation establishes initial points-to relationship between a reference and an object, and points-to relationships are influenced by execution of assignment, store or load operation. ASP rules characterizing effects of these operations are given as follows.

- $\text{ref}(x, o_s, s) \leftarrow \text{new}(s, o_s, x)$ (R3)
 $\text{ref}(x, o_y, s') \leftarrow \text{pred}(s, s'), \text{ref}(y, o_y, s), \text{asn}(s', x, y)$ (R4)
 $\neg\text{ref}(x, o_x, s') \leftarrow \text{pred}(s, s'), \text{ref}(x, o_x, s), \text{asn}(s', x, y), \text{not sp}(s')$ (R5)
 $\text{reff}(o_x, f, o_y, s') \leftarrow \text{pred}(s, s'), \text{ref}(y, o_y, s), \text{ref}(x, o_x, s), \text{store}(s', x, f, y)$ (R6)
 $\neg\text{reff}(o_x, f, o_y, s') \leftarrow \text{pred}(s, s'), \text{ref}(x, o_x, s), \text{reff}(o_x, f, o_y, s), \text{store}(s', x, f, y), \text{not sp}(s')$ (R7)
 $\text{ref}(y, o_y, s') \leftarrow \text{pred}(s, s'), \text{ref}(x, o_x, s), \text{reff}(o_x, f, o_y, s), \text{load}(s', y, x, f)$ (R8)
 $\neg\text{ref}(y, o_y, s') \leftarrow \text{pred}(s, s'), \text{ref}(y, o_y, s), \text{load}(s', y, x, f), \text{not sp}(s')$ (R9)
 $\text{sp}(s') \leftarrow \text{pred}(s, s'), \text{ref}(x, o_x, s), \text{ref}(y, o_y, s), o_x = o_y, \text{asn}(s', x, y)$ (R10)
 $\text{sp}(s') \leftarrow \text{pred}(s, s'), \text{ref}(x, o_x, s), \text{reff}(o_x, f, o_y, s), \text{ref}(y, o_y, s), o = o_y, \text{store}(s', x, f, y)$ (R11)
 $\text{sp}(s') \leftarrow \text{pred}(s, s'), \text{ref}(y, o_y, s), \text{ref}(x, o_x, s), \text{reff}(o_x, f, o_y, s), o_y = o, \text{load}(s', y, x, f)$ (R12)

If there is a statement s performing $x=y$, Rules R4 and R5 describe its influence on points-to relationship of reference x . R6~R9 are corresponding rules for store and load operations. R10 defines a predicate $\text{sp}(s')$ stating that assignment $s': x=y$ is in a special situation—before performing $x=y$, y possibly refers to one or more objects and at least one of them is also referred by x , as illustrated in Fig.3. Such situation is infrequent, but it *maybe* occur. If R5 does not mention $\text{sp}(s')$, inconsistent literals will be generated: from $\text{pred}(s, s')$, $\text{ref}(y, o1, s)$ and $\text{asn}(s', x, y)$, we get $\text{ref}(x, o1, s')$ by R4; But from $\text{pred}(s, s')$, $\text{ref}(x, o1, s)$ and $\text{asn}(s', x, y)$, $\neg\text{ref}(x, o1, s')$ will be generated. Thus, not $\text{sp}(s')$ is added into R5 to avoid generating inconsistent literals under such situation. R11 and R12 are counterparts of R10 for store and load operations.

It is needless to worry about that different immediate predecessors of a merging node probably bring inconsistent literals to it. Assume s is a merging node and it has two immediate predecessors, say $s1$ and $s2$, suppose we have $\text{ref}(x, o1, s1)$ and $\neg\text{ref}(x, o1, s2)$ before s , and s has no influence on points-to relationship of x , is it possible to generate $\text{ref}(x, o1, s)$ and $\neg\text{ref}(x, o1, s)$ after s ? Because of R1, only positive literal will be propagated forward, $\neg\text{ref}(x, o1, s2)$ is “filtered” out. Thus after s we just get $\text{ref}(x, o1, s)$.

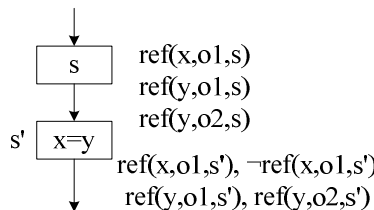


Fig. 3. Special situation for assignment

Data-flow equations for single assignment and basic program structures are well-kept by R1~R12. For single assignment, sequential compound and conditional statement, validity of these rules is obvious. As for loop structure, some explanation will be given. For simplicity of presentation, discussion is focused on simple assignment. Analyses for store and load operations are similar to that for assignment.

Fig.2(c) shows that data-flow equation for loop is $\text{in}[s0] = \text{out}[s] \cup \text{out}[s1]$, $\text{out}[s1]$ is feed back to $s0$ to generate new $\text{out}[s0]$, then $\text{out}[s1]$ is computed again. This iterative process repeats until a fixpoint is reached. As $s0$ is a merging node and does not

influence points-to relationships, thus initially points-to relationships in form of $\text{ref}(x,o,s)$ or $\text{reff}(o,f,o',s)$ are transferred unchangeably as $\text{ref}(x,o,s0)$ or $\text{reff}(o,f,o',s0)$ by R1. Because of $\text{pred}(s0,s1)$ and $\text{pred}(s1,s0)$, R4, R5 and R10 for $s1$, R1 for $s0$ are repeatedly used until no new points-to relationship is generated—a stable model for these rules on $s0$ and $s1$ occurs. Finally, $\text{out}[s0]$ is the union of results from each iteration and is propagated to $s2$.

3.2 Modeling Inter-procedure Points-to Information

To describe the propagation of points-to information among methods, more sets and predicates are needed, and they are:

- Set M of methods: each m in M is a method in a program;
- $\text{pre}(s,m)$: node s is the pre-call node of a calling statement by which method m is called;
- $\text{post}(s,m)$: node s is the post-call node of a calling statement by which method m is called;
- $\text{aP}(ap,i,m)$: reference ap is the i th actual parameter when calling m ;
- $\text{fP}(fp,i,m)$: reference fp is the i th formal parameter of method m ;
- $\text{local}(x,m)$: reference x is a local reference variable of method m .

If method m is called by statement s , then $\text{pred}(s_{\text{pre}}, \text{entry}_m)$ and $\text{pred}(\text{exit}_m, s_{\text{post}})$ hold. The following rules deal with pre-call node and post-call nodes:

$$\text{asn}(s, fp, ap) \leftarrow \text{pre}(s, m), \text{aP}(ap, i, m), \text{fP}(fp, i, m) \quad (R13)$$

$$\neg \text{ref}(fp, o, s') \leftarrow \text{post}(s', m), \text{pred}(s, s'), \text{fP}(fp, i, m), \text{ref}(fp, o, s) \quad (R14)$$

$$\neg \text{ref}(x, o, s') \leftarrow \text{post}(s', m), \text{pred}(s, s'), \text{local}(x, m), \text{ref}(x, o, s) \quad (R15)$$

R13 treats the integration of actual parameter and formal parameter as assignment from the former to the latter. R14 and R15 prevent points-to information of formal parameters and local variables from propagating forwards when m exits.

Rules R13~R15 can be used to model general method calling, as for dynamic calling in some mainstreams of object-oriented language like Java, type information should be inferred to improve precision[13,14]. It is possible to include type information in our rules, but we will not discuss it here because of limitation on space.

4 An Example

In this section a simple example is given to show how rules presented in section 3 work. This example is taken from [5] and its previous work. Consider a Java program segment shown in Example 4.

Example 4. A Java Program segment with method calling

```
(1) B c
(2) A a=new A( );      //object 2
(3) B b=new B( );      //object 3
(4) a.f=b;
(5) c=b;                (11) a.update(c);
(6) if(true) {
```

```

(7)  c=new B( ); //object 7      (12) void update(Obj i){
(8)  b.f=c;                      (13)   b=i.f;
(9)  c.f=b;                      (14) }
(10) }
```

Statement (11) is a calling statement by which method *update()* is called with *c* and *i* as actual parameter and formal parameter respectively. Calling relationship in this segment is very simple and we can give CFGs of the caller and callee, linked according to calling relationship between them, as shown in Fig.4. Nodes *s6* and *s10* are flow construct node and exit node of conditional statement respectively, calling statement (11) is divided into two nodes *s11_{pre}* and *s11_{post}*, denote pre-call node and post-call node of (11). *s12* is entry node of method *update()*, and *s14* is exit node.

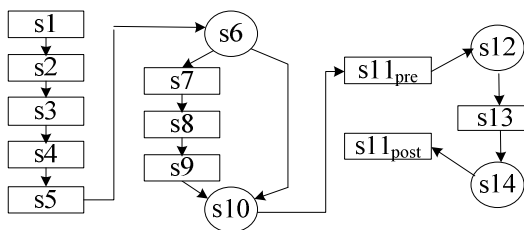


Fig. 4. Control flow graph of Example 4

According to statements presented in Example 4 and CFG in Fig.4, the following facts are obvious:

- new(*s2,o2,a*), new(*s3,o3,b*), new(*s7,o7,c*), store(*s4,a,f,b*), asn(*s5,c,b*), store(*s8,b,f,c*), store(*s9,c,f,b*), load(*s13,b,i,f*)
- pre(*s11_{pre}, update*), post(*s11_{post}, update*), aP(*c,I,update*), fP(*i,I,update*)
- pred(*s1,s2*), pred(*s2,s3*), pred(*s3,s4*), pred(*s4,s5*), pred(*s5,s6*), pred(*s6,s7*), pred(*s6,s10*), pred(*s7,s8*), pred(*s8,s9*), pred(*s9,s10*), pred(*s10,s11_{pre}*), pred(*s11_{pre},s12*), pred(*s12,s13*), pred(*s13,s14*), pred(*s13,s11_{post}*)

Using R1~R15, we get the following points-to relationships at each program points:

- ref(*a,o2,s2*)
- ref(*a,o2,s3*), ref(*b,o3,s3*)
- ref(*a,o2,s4*), ref(*b,o3,s4*), reff(*o2,f,o3,s4*)
- ref(*a,o2,s5*), ref(*b,o3,s5*), reff(*o2,f,o3,s5*), ref(*c,o3,s5*)
- ref(*a,o2,s6*), ref(*b,o3,s6*), reff(*o2,f,o3,s6*), ref(*c,o3,s6*)
- ref(*a,o2,s7*), ref(*b,o3,s7*), reff(*o2,f,o3,s7*), ref(*c,o7,s7*), !ref(*c,o3,s7*)
- ref(*a,o2,s8*), ref(*b,o3,s8*), reff(*o2,f,o3,s8*), ref(*c,o7,s8*), reff(*o3,f,o7,s8*)
- ref(*a,o2,s9*), ref(*b,o3,s9*), reff(*o2,f,o3,s9*), ref(*c,o7,s9*), reff(*o3,f,o7,s9*), reff(*o7,f,o3,s9*)
- ref(*a,o2,s10*), ref(*b,o3,s10*), reff(*o2,f,o3,s10*), ref(*c,o3,s10*), ref(*c,o7,s10*), reff(*o3,f,o7,s10*), reff(*o7,f,o3,s10*)

- $\text{ref}(a,o2,s11_{pre})$, $\text{ref}(b,o3,s11_{pre})$, $\text{reff}(o2,f,o3,s11_{pre})$, $\text{ref}(c,o3,s11_{pre})$, $\text{ref}(c,o7,s11_{pre})$, $\text{reff}(o3,f,o7,s11_{pre})$, $\text{reff}(o7,f,o3,s11_{pre})$, $\text{ref}(i,o3,s11_{pre})$, $\text{ref}(i,o7,s11_{pre})$
- $\text{ref}(a,o2,s12)$, $\text{ref}(b,o3,s12)$, $\text{reff}(o2,f,o3,s12)$, $\text{ref}(c,o3,s12)$, $\text{ref}(c,o7,s12)$, $\text{reff}(o3,f,o7,s12)$, $\text{reff}(o7,f,o3,s12)$, $\text{ref}(i,o3,s12)$, $\text{ref}(i,o7,s12)$
- $\text{ref}(a,o2,s13)$, $\text{ref}(b,o3,s13)$, $\text{ref}(b,o7,s13)$, $\text{reff}(o2,f,o3,s13)$, $\text{ref}(c,o3,s13)$, $\text{ref}(c,o7,s13)$, $\text{reff}(o3,f,o7,s13)$, $\text{reff}(o7,f,o3,s13)$, $\text{ref}(i,o3,s13)$, $\text{ref}(i,o7,s13)$
- $\text{ref}(a,o2,s14)$, $\text{ref}(b,o3,s14)$, $\text{ref}(b,o7,s14)$, $\text{reff}(o2,f,o3,s14)$, $\text{ref}(c,o3,s14)$, $\text{ref}(c,o7,s14)$, $\text{reff}(o3,f,o7,s14)$, $\text{reff}(o7,f,o3,s14)$, $\text{ref}(i,o3,s14)$, $\text{ref}(i,o7,s14)$
- $\text{ref}(a,o2,s11_{post})$, $\text{ref}(b,o3,s11_{post})$, $\text{ref}(b,o7,s11_{post})$, $\text{reff}(o2,f,o3,s11_{post})$, $\text{ref}(c,o3,s11_{post})$, $\text{ref}(c,o7,s11_{post})$, $\text{reff}(o3,f,o7,s11_{post})$, $\text{reff}(o7,f,o3,s11_{post})$, $\neg\text{ref}(i,o3,s11_{post})$, $\neg\text{ref}(i,o7,s11_{post})$

Although the result is somewhat overloaded with details, but it provides points-to information for each program point, which will be very useful when diagnosing program faults caused by aliasing.

5 Conclusion

Using Answer Set Programming, we present a natural and concise formal framework for representing and reasoning about propagation of points-to information along paths of an object-oriented program. Laws of static data-flow analysis for basic program structures are well-kept by inference rules of this framework. Especially for loop statement, no iterative algorithms are needed yet. When propagation of points-to relationships reaches a loop statement, these rules are used repeatedly and finally generate a stable model which is exactly the result of the iterative computation of the loop. Moreover, based on basic facts of an object-oriented program and inference rules, points-to information at each program point can be inferred directly by dint of existing ASP solver. There is no need of implementing a special software tool for points-to analysis, which is necessary for general points-to or alias analysis algorithms. Compared to [5] and [6], our inference framework is considerably succinct. And we can expect an improvement of computational efficiency because of increasing betterment of ASP solver. Finally, from the detailed points-to information computed by our framework, alias relationship between references can be implied. The latter is absolutely necessary for diagnosing alias-caused program faults, which is our primary concern in the future. On the other hand, in this paper only generic elements of object-oriented language are taken into consideration. The complicated elements like exception handling mechanism in Java and linked structure need to be investigated. Besides, theoretic analysis and comparison on the computational efficiency have to be taken into account next.

Acknowledgments. We wish to thank anonymous reviewers for helpful comments and suggestions. A special thanks to Professor Fangzhen Lin and Professr Zhiming Liu for their instructive advices on ASP and aliasing. This research was partially supported by the National Science Foundation of China under Grant 60963009.

References

1. Mayer, W., Stumptner, M.: Model-based Debugging-state of the Art and Future Challenges. *J. Elec. Notes in Theo. Comp. Sci.* 174, 61–82 (2007)
2. Dawson, S., Ramakrishnan, C.R., Warren, D.S.: Practical Program Analysis Using General Purpose Logic Programming System: A Case Study. In: 9th ACM SIGPLAN Conference on Programming Language Design and Implementation, pp. 117–126. ACM Press, New York (1996)
3. Whaley, J., Avots, D., Carbin, M., Lam, M.: Using Datalog with Binary Decision Diagrams for Program Analysis. In: Yi, K. (ed.) *APLAS 2005*. LNCS, vol. 3780, pp. 97–118. Springer, Heidelberg (2005)
4. Song, W.: Using Horn Clauses and Binary Decision Diagrams for Program Analysis. Ph.D. dissertation. State University of New York, Stony Brook (2010)
5. Woo, J., Gaudiot, J.L., Wendelborn, A.L.: Alias Analysis in Java with Reference-Set Representation for High-Performance Computing. *J. Para. Prog.* 32, 39–76 (2004)
6. Meyer, B.: Towards A Theory and Calculus of Aliasing. *J. Object Tech.* 9, 37–74 (2010)
7. Gelfond, M., Lifschitz, V.: The Stable Model Semantics for Logic Programming. In: 5th International Logic Programming Conference and Symposium, pp. 1070–1080. MIT Press, Cambridge (1988)
8. Nogueira, M., Balduccini, M., Gelfond, M., Watson, R., Barry, M.: An A-Prolog Decision Support System for the Space Shuttle. In: Ramakrishnan, I.V. (ed.) *PADL 2001*. LNCS, vol. 1990, pp. 169–183. Springer, Heidelberg (2001)
9. Paschke, A., Bichler, M.: Knowledge Representation Concepts for Automated SLA Management. *J. Deci. Supp. Syst.* 46, 187–205 (2008)
10. Eiter, T., Faber, W., Leone, N., Pfeifer, G., Polleres, A.: A Logic Programming Approach to Knowledge-state Planning: Semantics and Complexity. *ACM Trans. on Comp. Logic*. 5, 206–263 (2004)
11. Tiihonen, J., Soininen, T., Niemela, I., Sulonen, R.: A Practical Tool for Mass-customising Configurable Products. In: 14th International Conference on Engineering Design, pp. 1290–1299 (2003)
12. Lifschitz, V.: Foundation of Logic Programming. In: Principles of Knowledge Representation, pp. 69–128. CSLI Publications (1996)
13. Carini, P.R., Hind, M., Srinivasan, H.: Flow-Sensitive Type Analysis for C++. IBM Research Report, RC 20267 (1995)
14. Pande, H.D., Ryder, B.G.: Static Type Determination and Aliasing for C++. Technical Report, LCSR0TR-250-A. Rutgers University (1995)

Continuous Finite-Time Observer-Controller Based Speed Regulation of Permanent Magnet Synchronous Motors

Yan Yan¹, Shuanghe Yu¹, Zhenqiang Yang², and Jialu Du¹

¹ School of Information Science and Technology, Dalian Maritime University,
116026 Dalian, China

² School of Electrical Engineering, Dalian University of Technology,
116024 Dalian, China

shuanghe@dltmu.edu.cn, yangzq@dlut.edu.cn, dujl@dltmu.edu.cn

Abstract. A finite-time speed tracking control for a permanent-magnet synchronous motor (PMSM) using an unknown load torque disturbance estimation technique is presented. The proposed control scheme depends on finite-time convergence of a state observer, which estimates motor speed, acceleration and the unknown load torque. A continuous output feedback controller that can achieve global finite-time stability for a PMSM is constructed based on a “finite-time separation principle”. The simulation results show the efficiency of the method.

Keywords: Finite-time controller, finite-time observer, PMSM.

1 Introduction

During the past decades, Permanent Magnet Synchronous Motor (PMSM) has been applied in various industrial fields, such as robots, rolling mills, and machine tools. PMSM has several advantages, such as superior high power density, large torque to inertia ratio and high efficiency, compared with conventional induction motors [1]. The dynamic model of a PMSM is highly nonlinear due to the coupling between the motor speed and the d-q axis currents [2-3]. As a result, more and more nonlinear control methodologies have been applied to control of the PMSM. Zhu and Dessaint propose an exact linearization methodology to realize the speed tracking control [4]. Wang et al. introduce the backstepping method into the speed tracking control in order to simplify the system design procedure [5]. Li and Ke et al. design a finite-time control approach for PMSM [6-7]. However, one of the major difficulties in speed tracking control is the accurate knowledge of rotor acceleration is unknown. The use of an accelerometer is too expensive for industrial application. Moreover, in practice, the torque is varied with external loads, and the reference speed changes with the requirement.

Finite-time stability implies the trajectories of dynamical systems converge to an equilibrium state in finite time, as well as possesses the properties of robustness and disturbance rejection [8]. Such systems involve non-Lipschitzian dynamics since

finite-time convergence implies non-uniqueness of system solutions in backward time. The problem of output feedback finite-time stabilization of second order systems has been studied by quite a few people from different perspectives [6, 9-10]. Based on the model of PMSM, the problem of finite-time output feedback is addressed using finite-time controller and finite-time observer in this paper. As a result, the speed tracking of the PMSM can be achieved in finite time. One of the particular features of our controller design is that we use continuous a finite-time convergent observer for the model states ω , $\dot{\omega}$ and the load torque T to overcome the difficulties of measuring velocity and load disturbance of PMSM.

2 Model of PMSM

The dynamic model of a PMSM can be described in the d-q frame. Choosing $(i_d, i_q, \theta, \omega)$ as state variables, the PMSM system can be described as follows [4]

$$\begin{cases} \frac{di_d}{dt} = -\frac{R}{L}i_d + p\omega i_q + \frac{u_d}{L} \\ \frac{di_q}{dt} = -\frac{R}{L}i_q - p\omega i_d - \frac{p\phi_f}{L}\omega + \frac{u_q}{L} \\ \frac{d\omega}{dt} = \frac{3p\phi_f}{2J}i_q - \frac{B}{J}\omega - \frac{T}{J} \end{cases} \quad (1)$$

where i_d and i_q are the d-q axis currents, u_d and u_q are the d-q axis control voltages, θ is the rotor position, R is the stator resistance, L is the stator inductance, p is the number of pole pairs, ϕ_f is the rotor magnetic flux linking the stator, J is the rotor moment of inertia, B is the viscous friction coefficient and T is the load torque. In this paper, we assume the rotor position θ , the currents i_d , and i_q are the available measurements.

3 Speed Tracking Control

The objective of this section is to develop the finite-time controller which can guarantee the rotor angular speed ω tracking the desired speed ω_{ref} in finite time.

First, we design the controller on the assumption that the load torque T , the state ω and $\dot{\omega}$ are available.

3.1 Finite-Time Controller of Current i_d

Consider the subsystem of (1)

$$\frac{di_d}{dt} = -\frac{R}{L}i_d + p\omega i_q + \frac{u_d}{L} \quad (2)$$

For system (2), set

$$v_1 = -\frac{R}{L}i_d + p\omega i_q + \frac{u_d}{L} \quad (3)$$

then we have

$$\frac{di_d}{dt} = v_1 \quad (4)$$

We apply the following finite-time controller

$$v_1 = -c_1 \text{sig}(i_d)^\beta \quad (5)$$

where $\beta_1 \in (0, 1)$, c_1 is a constant and $c_1 > 0$, then system (3) can be reduced to

$$u_d = Ri_d - pL\omega i_q - Lc_1 \text{sig}(i_d)^\beta \quad (6)$$

So the state i_d can be finite-time stabilized.

3.2 Finite-Time Tracking of Speed ω

A double integrator represents a translational and rotational motion.

$$\dot{z}_1 = z_2, \quad \dot{z}_2 = u \quad (7)$$

where z_1 is the position state and z_2 is the unmeasurable velocity state. Assume both the states z_1 and z_2 are available, the following controller can stabilize the trajectories of (1) to the equilibrium in finite time [6].

$$u = -\text{sign}(z_2)|z_2|^\beta - \text{sign}(\phi_\beta(z_1, z_2))|\phi_\beta(z_1, z_2)|^{2-\beta}, \quad (8)$$

where $\alpha \in (0, 1)$, $\phi_\alpha(z_1, z_2) = z_1 + \frac{1}{2-\beta} \text{sign}(z_2)|z_2|^{2-\beta}$.

For the subsystem of (1)

$$\begin{cases} \frac{di_q}{dt} = -\frac{R}{L}i_q - p\omega i_d - \frac{p\phi_f}{L}\omega + \frac{u_q}{L} \\ \frac{d\omega}{dt} = \frac{3p\phi_f}{2J}i_q - \frac{B}{J}\omega - \frac{T}{J} \end{cases} \quad (9)$$

The new states and input are defined as

$$\begin{cases} \dot{\omega} = \frac{3p\phi_f}{2J}i_q - \frac{B}{J}\omega - \frac{T}{J} \\ \ddot{\omega} = \gamma_0 + \gamma_1\omega + \gamma_2i_q + \gamma_3\omega i_d + \gamma_4u_q \end{cases} \quad (10)$$

$$\text{where } \gamma_0 = \frac{B}{J^2}T, \gamma_1 = \frac{B^2}{J^2} - \frac{3p^2\phi_f^2}{2JL}, \gamma_2 = -\frac{3p\phi_f}{2J}\left(\frac{R}{L} + \frac{B}{J}\right), \gamma_3 = -\frac{3p^2\phi_f}{2J}, \gamma_4 = \frac{3p\phi_f}{2JL}.$$

Then a new double integrator is obtained.

$$d\omega = \dot{\omega}, \ddot{\omega} = v_2 \quad (11)$$

For (11), we use the controller (8) and the control law of (11) can be designed as

$$v_2 = -c_2 \text{sig}(\dot{\omega} - \dot{\omega}_{ref})^{\beta_2} - c_2 \text{sig}(\phi_\alpha(\omega - \omega_{ref}, \dot{\omega} - \dot{\omega}_{ref}))^{\frac{\beta_2}{2-\beta_2}} \quad (12)$$

$$\phi_{\beta_2}(\omega - \omega_{ref}, \dot{\omega} - \dot{\omega}_{ref}) = \omega - \omega_{ref} + \frac{1}{2-\beta_2} \text{sig}(\dot{\omega} - \dot{\omega}_{ref})^{2-\beta_2} \quad (13)$$

where $\beta_2 \in (0,1)$, c_2 is a constant, $c_2 > 0$, ω_{ref} expresses the reference rotor speed trajectory and it is assumed at least twice differentiable. The new defined input v_2 represents the finite-time speed tracking control.

$$u_q = -\frac{1}{\gamma_4}(v_2 - \gamma_0 - \gamma_1\omega - \gamma_2 i_q - \gamma_3 \omega i_d) \quad (14)$$

So the control laws (6) and (14) can guarantee the states of (1) converge to zero in finite time and the angular speed of (1) can track the designed speed in finite time.

4 Observer and Closed-Loop Finite-Time Stability

In this section, we design a global finite-time observer which can estimate the system states and the load disturbance torque as well.

In practice, the load torque varies slowly and we can suppose it as a constant [4]. Therefore we can consider the following extended system corresponding to (11).

Set $v_2' = v_2 - \gamma_0$, then

$$\frac{d\dot{\omega}}{dt} = v_2' + \gamma_0, \frac{d\gamma_0}{dt} = 0 \quad (15)$$

Define new state variables $x_1 = \theta, x_2 = \omega, x_3 = \dot{\omega}, x_4 = \gamma_0$. Then the subsystem (9) can be converted to the following form

$$\dot{x}_1 = x_2, \dot{x}_2 = x_3, \dot{x}_3 = x_4 + v_2', \dot{x}_4 = 0 \quad (16)$$

Theorem 1: Consider the system

$$\begin{cases} \dot{\hat{x}}_1 = \hat{x}_2 + k_1 (\text{sig}(e_1)^{\alpha_1} + m e_1) \\ \dot{\hat{x}}_2 = \hat{x}_3 + k_2 (\text{sig}(e_1)^{\alpha_2} + m e_1) \\ \dot{\hat{x}}_3 = \hat{x}_4 + k_3 (\text{sig}(e_1)^{\alpha_3} + m e_1) + v_2' \\ \dot{\hat{x}}_4 = k_4 (\text{sig}(e_1)^{\alpha_4} + m e_1) + \text{sig}(\hat{x}_4)^\mu \end{cases} \quad (17)$$

where $\alpha_i = i\alpha - (i-1)$, $i=1,\dots,4$, $\mu \in (0,1)$, $S_\infty(\eta)$ is the solution of the equation

$$\begin{cases} \eta S_\infty(\eta) + A^T S_\infty(\eta) + S_\infty(\eta)A - C^T C = 0 \\ S_\infty(\eta) = S_\infty^T(\eta) \end{cases} \quad (18)$$

where A is the anti-shift operator $A: R^4 \rightarrow R^4$, $A_{i,j} = \delta_{i,j-1}$. Define the gains $K = [k_1, \dots, k_4]^T = S_\infty^{-1}(\eta)C^T$, $C = [1 \ 0 \ 0 \ 0]$, $\rho = 0$ or $\rho = (n^2\eta^{2/3}S_1 + 1)/2$, where

$$S_1 = \max_{1 \leq i, j \leq 4} |S_\infty(1)_{i,j}| \cdot |S_\infty^{-1}(1)_{j,1}| \quad (19)$$

Then the equation (17) is a finite-time observer for (16).

Lemma 1: The matrix $S_\infty(\eta)$ and $S_\infty^{-1}(\eta)$ verify the following properties

$$S_\infty(\eta)_{i,j} = S_\infty(1)_{i,j} \frac{1}{\eta^{i+j-1}} \quad (20)$$

$$S_\infty^{-1}(\eta)_{i,j} = S_\infty^{-1}(1)_{i,j} \eta^{i+j-1} \quad (21)$$

for any $\eta > 0$ and $1 \leq i, j \leq n$. [11-13].

Proof: Subtracting (17) from (16) and the observation error $e = x - \hat{x}$ is given by

$$\begin{cases} \dot{e}_1 = e_2 - k_1 (\text{sig}(e_1)^{\alpha_1} + \rho e_1) \\ \dot{e}_2 = e_3 - k_2 (\text{sig}(e_1)^{\alpha_2} + \rho e_1) \\ \dot{e}_3 = e_4 - k_3 (\text{sig}(e_1)^{\alpha_3} + \rho e_1) \\ \dot{e}_4 = -k_4 (\text{sig}(e_1)^{\alpha_4} + \rho e_1) - \text{sig}(\hat{x}_4)^\mu \end{cases} \quad (22)$$

The proof has been made in [12] and when $\rho = 0$ the proof has been made in [14].

According to Lemma 1 and (19), we can compute $S_\infty(\eta)$ and $S_\infty^{-1}(\eta)$ as

$$S_\infty(\eta) = \begin{pmatrix} 1/\eta & -1/\eta^2 & 1/\eta^3 & -1/\eta^4 \\ -1/\eta^2 & 5/\eta^3 & -3/\eta^4 & 4/\eta^5 \\ 1/\eta^3 & -3/\eta^4 & 6/\eta^5 & -10/\eta^6 \\ -1/\eta^4 & 4/\eta^5 & -10/\eta^6 & 20/\eta^7 \end{pmatrix}, \quad S_\infty^{-1}(\eta) = \begin{pmatrix} 4\eta & 6\eta^2 & 4\eta^3 & \eta^4 \\ 6\eta^2 & 14\eta^3 & 11\eta^4 & 3\eta^5 \\ 4\eta^3 & 11\eta^4 & 15\eta^5 & 3\eta^6 \\ \eta^4 & 3\eta^5 & 3\eta^6 & \eta^7 \end{pmatrix}$$

$$K = S_\infty^{-1}(\eta)C^T = [4\eta \ 6\eta^2 \ 4\eta^3 \ \eta^4]^T, \quad S_1 = \max_{1 \leq i, j \leq 4} |S_\infty(1)_{i,j}| \cdot |S_\infty^{-1}(1)_{j,1}| = 120, \\ \rho = (n^2\eta^{2/3}S_1 + 1)/2 = (1920\eta^{2/3} + 1)/2. \text{ From (14), we get the observer equation as}$$

$$\begin{cases} \dot{\hat{x}}_1 = \hat{x}_2 + 4\eta(\text{sig}(e_1)^{\alpha_1} + ((1920\eta^{2/3} + 1)/2)e_1) \\ \dot{\hat{x}}_2 = \hat{x}_3 + 6\eta^2(\text{sig}(e_1)^{\alpha_2} + ((1920\eta^{2/3} + 1)/2)e_1) \\ \dot{\hat{x}}_3 = \hat{x}_4 + 4\eta^3(\text{sig}(e_1)^{\alpha_3} + ((1920\eta^{2/3} + 1)/2)e_1 + v_2') \\ \dot{\hat{x}}_4 = \eta^4(\text{sig}(e_1)^{\alpha_4} + ((1920\eta^{2/3} + 1)/2)e_1 + \text{sig}(\hat{x}_4)^\mu) \end{cases} \quad (23)$$

System (23) is a finite-time observer. The observer-based control scheme consists of (4) and (10), where ω , $\dot{\omega}$, and γ_0 are replaced by their estimates in (23), that is

$$u_d = Ri_d - pL\hat{\omega}i_q - Lv_1, u_q = -\frac{1}{\gamma_4}(\hat{v}_2 - \hat{\gamma}_0 - \gamma_1\hat{\omega} - \gamma_2i_q - \gamma_3\hat{\omega}i_d) \quad (24)$$

$$\hat{v}_2 = -c_2\text{sig}(\hat{\omega} - \dot{\omega}_{ref})^{\beta_2} - c_2\text{sig}(\phi_\alpha(\hat{\omega} - \omega_{ref}, \dot{\omega} - \dot{\omega}_{ref}))^{\beta_2/(2-\beta_2)} \quad (25)$$

The equilibrium of the error dynamics (15) is globally finite-time stable, then

$$u(i_d, i_q, \theta, \hat{\omega}, \dot{\hat{\omega}}) = u(i_d, i_q, \theta, \omega, \dot{\omega}), t \geq T_e(e_0) \quad (26)$$

Thus the equilibrium of (1), (14), and (26) is also finite-time stable.

5 Simulation Results

In this section, the performance of the PMSM based on the proposed controller and observer is investigated. The system parameters are $R = 2\Omega$, $T = 3N \cdot m$, $J = 0.0008kg \cdot m^2$, $p = 2$, $\phi_f = 0.3wb$, $L = 0.03H$. The system is stated with the speed reference set at $200rad/s$ and at $t = 30s$, the speed reference changes into $500rad/s$. The parameters for controller are selected as $\beta_1 = 1/3$, $\beta_2 = 2/3$, $c_1 = 1$ and $c_2 = 20$. The gains of the state observer are chosen as $\alpha = 0.8$, $\eta = 10$, $\mu = 1/3$.

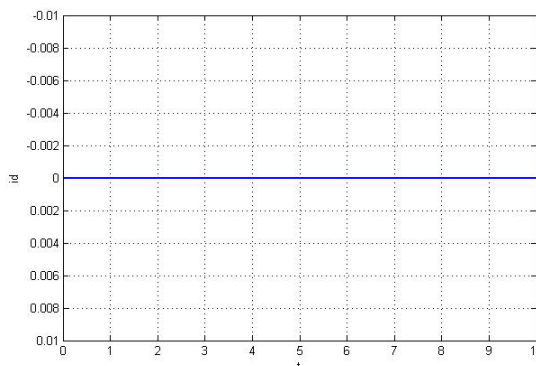


Fig. 1. The d-axis current

The simulation results are shown in Fig. 1-3. Fig. 1-2 illustrates the time response of the currents i_d and i_q . The response of the tracking speed is shown in Fig. 3. It can be seen from Fig. 1-3 that the actual control states can receive finite-time stability.

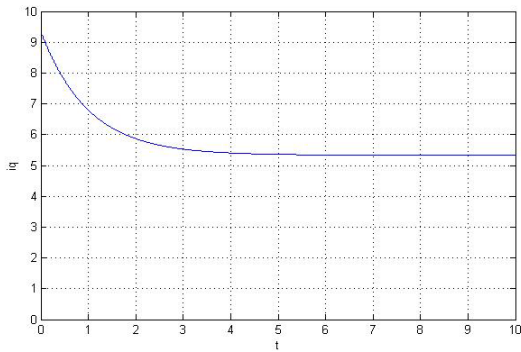


Fig. 2. The q-axis current

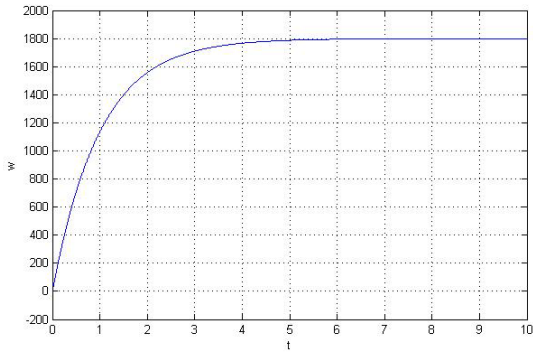


Fig. 3. The rotor speed

6 Conclusions

In this work, a finite-time control law is proposed to speed tracking control of PMSM. Assume that only the d-q axis currents and rotor position are measurable, a continuous finite-time observer is used to estimate the speed and load disturbance. Simulation results show the effectiveness of the proposed scheme. This control approach can also be used to stabilize other mechanical systems.

Acknowledgments. This work was supported by the Program for New Century Excellent Talents in University of P.R.C. and Scientific and Technological Plan fund of Liaoning Province and Dalian City of P.R.C., NSFC under grant (51079013), the Higher Education Research Fund of Education Department of Liaoning of P.R.C. under grant (LT2010013).

References

1. Leonhard, W.: Control of Electrical Drives. Springer, Heidelberg (1995)
2. Kaddouri, A., Akhrif, O., Le-huy, H., Ghribi, M.: Nonlinear Feedback Control of PMSM. Halifax (1994)
3. Azizur, M., Mahinda, D., Nasir, M., Tseng, K.: Nonlinear Control of Interior Permanent-Magnet Synchronous Motor. *IEEE Trans. on Industry Applications* 39, 408–416 (2003)
4. Zhu, G., Dessaint, L.: A Speed Tracking Control of a Permanent-Magnet Synchronous Motor with State and Load Torque Observer. *IEEE Trans. Industrial Electronics* 47, 346–355 (2000)
5. Wang, J., Zhao, G., Qi, D.: Backstepping Control of Speed for Sensorless Permanent Magnet Synchronous Motors. *Control Theory & Applications* 22, 657–660 (2005)
6. Ke, H., Zheng, C., Yang, W.: Finite-Time Tracking Control of Permanent Magnet Synchronous Motor. In: *IEEE Int. Conf. Control and Automation*, pp. 1984–1987. IEEE Press, New York (2010)
7. Li, S., Liu, H., Ding, S.: A Speed Control for a PMSM Using Finite-Time Feedback Control and Finite-Time Feedback Control and Disturbance Compensation. *Trans. Institute of Measurement and Control* 32, 170–187 (2010)
8. Yu, S., Yu, X., Bijan, S., Man, Z.: Continuous Finite-Time Control for Robotic Manipulators with Terminal Sliding Mode. *Automatica* 41, 1957–1964 (2005)
9. Davila, J., Fridman, L., Levant, A.: Second-Order Sliding-Mode Observer for Mechanical Systems. *IEEE Trans. on Automatic Control* 50, 1785–1789 (2005)
10. Moreno, J., Osorio, M.: A Lyapunov Approach to Second-Order Sliding Mode Controllers and Observers. In: *47 IEEE Conf. on Decision and Control CDC*, pp. 2856–2861 (2008)
11. Menard, T., Moulay, E., Perruquetti, W.: A Global High-gain Finite-time Observer. *IEEE Trans. on Automatic Control* 55, 1500–1506 (2010)
12. Gauthier, J., Hammouri, H., Othman, S.: A Simple Observer for Nonlinear Systems Application to Bioreactors. *IEEE Trans. on Automatic Control* 37, 875–880 (1992)
13. Shen, Y., Shen, W., Jiang, M., Huang, Y.: Semi-global Finite-time Observers for Nonlinear Systems. *Automatica* 44(12), 3152–3156 (2008)
14. Perruquetti, W., Floquet, T., Moulay, E.: Finite-Time Observers: Application to Secure Communication. *IEEE Trans. on Automatic Control* 53, 356–360 (2008)

Observer-Based Exponential Stability Analysis for Networked Control Systems with Packet Dropout

Xue Li¹, Jia-min Weng², Dajun Du^{1,*}, and Haoliang Bai¹

¹ Department of Automation, School of Mechatronical Engineering and Automation, Shanghai University, Shanghai, 200072, China

² Department of Electrical Information Engineering, Henan Institute of Engineering, Zhengzhou, 451191, China
{lixue,ddj}@shu.edu.cn,
1987baihaoliang@163.com, wjm@hntc.edu.cn

Abstract. This paper is concerned with observer-based exponential stability for networked control systems (NCSs) with data packet dropout. Firstly, the data packet dropouts both the sensor-to-controller and the controller-to-actuator are considered, which are modeled as two independent Bernoulli distributed white sequences respectively. Then an observer is designed to estimate the system state, and an augmented model for NCSs is proposed. Finally, based on Lyapunov stability theory combined with linear matrix inequalities (LMIs) techniques, a sufficient condition is derived for NCSs to be exponentially mean-square stable.

1 Introduction

Networked control systems (NCSs), with various advantages such as low cost of installation and great flexibility, have been widely used in DC motor systems and servo motor, etc. [1–3]. However, the network is inserted in the feedback control loops, which leads to data packet dropout due to the unreliability of network. This can degrade the performance of control systems even destabilize the system [4]. Therefore, the negative effects caused by communication networks must be considered in analyzing and designing NCSs.

A key issue in NCSs is data packet dropout, which have attracted significant amount of interests from the academics. Wu et al [5] described both sensor-to-controller (S/C) and controller-to-actuator (C/A) packet dropout as two independent Markov chains, and proved stochastic stability of the closed-loop systems. Zhang et al [6] modeled a discrete-time switched system with four subsystems by considering S/C and C/A packet dropouts, and sufficient conditions for the exponential stability of the closed-loop NCSs were presented in terms of nonlinear matrix inequalities. Furthermore, an iterative algorithm is proposed to design the observer-based output feedback controllers. Niu et al

* Corresponding author.

□ investigated NCSs with only S/C packet dropouts and designed the output-feedback controller which guarantees the closed-loop system is exponentially mean-square stable. Du et al □ modeled multi-input multi-output NCSs with multiple channels as a general switched system model, and a sufficient condition for the asymptotically stable was presented. According to the author's knowledge, the observer-based exponential stability analysis for NCSs with both S/C and C/A packet dropout has stimulated little research attention. Fang et al [9] firstly described S/C and C/A packet dropouts as two independent Bernoulli distributed white sequences, which were combined into the original plant model leading to a new model. Based on the new model, an observer was then designed, and exponentially mean-square stable and guaranteed cost control for NCSs were investigated. Unlike [9], S/C and C/A packet dropouts are described as two independent Bernoulli distributed white sequences, while an observer is designed based on the original plant model. An augmented model is then modeled, and a sufficient condition is derived for NCSs to be exponentially mean-square stable.

The rest of this paper is organized as follows. The problem formulation and modeling are presented in Section 2. Main results are given in Section 3. Finally, Section 4 concludes the paper.

2 Problem Formulation and Modeling

The observer-based networked control system is considered as shown in Fig.1. The communication for both the sensor-to-controller and the controller-to-actuator occur through network.

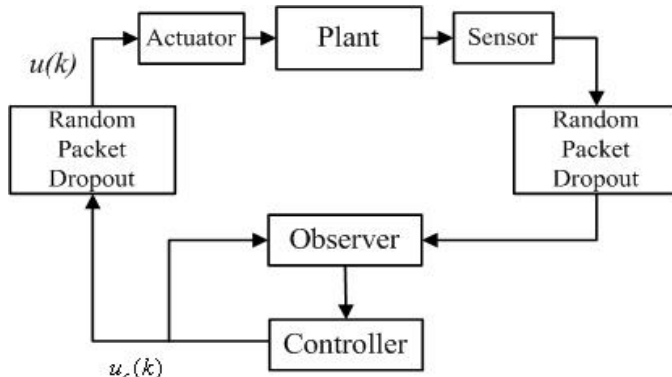


Fig. 1. Structure of observer-based networked control system with packet dropout

Consider a discrete linear time-invariant (LTI) system in the following state-space form:

$$\begin{aligned} x(k+1) &= Ax(k) + Bu(k) \\ y(k) &= Cx(k) \end{aligned} \quad (1)$$

where $x = [x_1, \dots, x_n]^T \in R^n$, $u = [u_1, \dots, u_n]^T \in R^m$, $y = [y_1, \dots, y_m]^T \in R^p$ are the plant's state, input, and output, respectively, A, C and C are known matrices with proper dimensions.

The measurement outputs are transmitted to the controller through network, data packet dropouts are inevitably introduced. Here, the data packet dropout for the sensor-to-controller is modelled as Bernoulli process θ_k with the probability distribution as follow:

$$\begin{aligned} Prob\{\theta_k = 1\} &= E\{\theta_k\} = \theta \\ Prob\{\theta_k = 0\} &= 1 - E\{\theta_k\} = 1 - \theta \\ Var\{\theta_k\} &= E\{(\theta_k - \theta)^2\} = \theta(1 - \theta) = \bar{\theta}^2 \end{aligned} \quad (2)$$

where $\theta_k = 1$ denotes the packet that will be transferred successfully, $\theta_k = 0$ denotes the packet that will be lost, the known positive constant $0 < \theta < 1$ denotes the probability that the packet will be transmitted successfully, and $\bar{\theta}$ denotes the variance of θ_k .

If the system state is not measurable, the system output is available. Further, if the system output can be successfully transferred to the observer through network, then the observer will use the data $y(k)$. Or, the most recent data $y(k-1)$ will be used. Thus, the system output can be rewritten as at the observer node

$$y_c(k) = \theta_k y(k) + (1 - \theta_k) y(k-1) \quad (3)$$

Consider the following observer-based feedback control

$$\begin{aligned} \hat{x}(k+1) &= A\hat{x}(k) + Bu_c(k) + L(y_c(k) - C\hat{x}(k)) \\ u_c(k) &= K\hat{x}(k) \end{aligned} \quad (4)$$

where L , K are the observer gain and feedback gain, respectively.

The controller signal for the controller-to-actuator will also be lost through network. Similarly, for the controller signal in the actuator node, we have

$$u(k) = \alpha_k u_c(k) + (1 - \alpha_k) u_c(k-1) \quad (5)$$

where the data packet dropout for the controller-to-actuator is also modelled as Bernoulli process α_k with the probability distribution as follow:

$$\begin{aligned} Prob\{\alpha_k = 1\} &= E\{\alpha_k\} = \alpha \\ Prob\{\alpha_k = 0\} &= 1 - E\{\alpha_k\} = 1 - \alpha \\ Var\{\alpha_k\} &= E\{(\alpha_k - \alpha)^2\} = \alpha(1 - \alpha) = \bar{\alpha}^2 \end{aligned} \quad (6)$$

where $\alpha_k = 1$ denotes the packet that will be transferred successfully, $\alpha_k = 0$ denotes the packet that will be lost, the known positive constant $0 < \alpha < 1$ denotes the probability that the packet will be transmitted successfully, and $\bar{\alpha}$ denotes the variance of α_k .

Define $e(k+1) = x(k+1) - \hat{x}(k+1)$, from (1) and (4) we obtain

$$\begin{aligned} e(k+1) &= ((1 - \theta_k)LC - (1 - \alpha_k)BK)x(k) \\ &\quad + (A - LC + (1 - \alpha_k)BK)e(k) \\ &\quad + ((1 - \alpha_k)BK - (1 - \theta_k)LC)x(k-1) \\ &\quad - (1 - \alpha_k)BKe(k-1) \end{aligned} \quad (7)$$

Further, by defining $Z(k) = [x(k)^T, e(k)^T, x(k-1)^T, e(k-1)^T]^T$, we have

$$Z(k+1) = \bar{A}_1 Z(k) + \bar{A}_2 Z(k) + \bar{A}_3 Z(k) \quad (8)$$

where

$$\bar{A}_1 = \begin{bmatrix} \Pi_1 & -\alpha\Pi_2 & \Pi_3 & -\Pi_3 \\ \Pi_4 & \Pi_5 & \Pi_6 & -\Pi_3 \\ I & 0 & 0 & 0 \\ 0 & I & 0 & 0 \end{bmatrix}, \quad \bar{A}_3 = \begin{bmatrix} 0 & 0 & 0 & 0 \\ -(\theta_k - \theta)\Pi_7 & 0 & (\theta_k - \theta)\Pi_7 & 0 \\ 0 & 0 & 0 & 0 \\ 0 & 0 & 0 & 0 \end{bmatrix},$$

$$\bar{A}_2 = \begin{bmatrix} (\alpha_k - \alpha)\Pi_2 & -(\alpha_k - \alpha)\Pi_2 & -(\alpha_k - \alpha)\Pi_2 & (\alpha_k - \alpha)\Pi_2 \\ (\alpha_k - \alpha)\Pi_2 & -(\alpha_k - \alpha)\Pi_2 & -(\alpha_k - \alpha)\Pi_2 & (\alpha_k - \alpha)\Pi_2 \\ 0 & 0 & 0 & 0 \\ 0 & 0 & 0 & 0 \end{bmatrix}$$

$$\Pi_1 = A + \alpha BK, \quad \Pi_2 = BK, \quad \Pi_3 = (1 - \alpha)BK, \quad \Pi_4 = (1 - \theta)LC - (1 - \alpha)BK, \\ \Pi_5 = A - LC + (1 - \alpha)BK, \quad \Pi_6 = (1 - \alpha)BK - (1 - \theta)LC, \quad \Pi_7 = LC.$$

3 Main Results

Definition 1: The closed-loop system (8) is said to be exponentially mean-square stable if there exist constant $\beta > 0$ and $\tau \in (0, 1)$ such that

$$E\{\|Z(k)\|^2\} \leq \beta\tau^k E\{\|Z(0)\|^2\}.$$

Lemma 1: Let $V(\psi(k))$ be a Lyapunov functional. If there exist real scalars $\rho \geq 0$, $\mu > 0$, $v > 0$, and $0 < \sigma < 1$ such that $\mu \|Z(k)\|^2 \leq V(Z(k)) \leq v \|Z(k)\|^2$ and $E\{V(Z(k+1)|Z(k))\} - V(Z(k)) \leq \rho - \sigma V(Z(k))$, then the sequence $Z(k)$ satisfies: $E\{\|Z(k)\|^2\} \leq \frac{\mu}{\mu} \|Z(0)\|^2 (1 - \sigma)^k + \frac{\rho}{\mu\sigma}$.

Lemma 2: Given matrices W , D and E of compatible dimensions with W symmetric, then $W + DFE + E^T F^T D^T < 0$ holds for all $F^T F \leq I$ if and only if there exists a constant $\varepsilon > 0$ such that $W + \varepsilon D D^T + \varepsilon^{-1} E^T E < 0$.

Theorem 1: For given packet dropout rate θ and α , if there exist symmetric positive-definite matrices P, M, N , real matrices K, L and a scalar $\varepsilon > 0$ such that (9) hold, then (8) is exponentially mean-square stable.

$$\begin{bmatrix} \Sigma_1 & * & * & * & * & * & * & * & * \\ -\varepsilon I & \Sigma_2 & * & * & * & * & * & * & * \\ -\varepsilon I & \varepsilon I & \Sigma_3 & * & * & * & * & * & * \\ \varepsilon I & -\varepsilon I & -\varepsilon I & \Sigma_4 & * & * & * & * & * \\ \Sigma_5 & -\alpha BK & \Sigma_6 & -\Sigma_6 & -P^{-1} & * & * & * & * \\ \Sigma_7 & \Sigma_8 & -\Sigma_7 & 0 & 0 & -P^{-1} & * & * & * \\ BK & -BK & -BK & BK & 0 & 0 & -2\bar{\alpha}^{-2}P^{-1} & * & * \\ -LC & 0 & LC & 0 & 0 & 0 & -\bar{\theta}^{-2}P^{-1} & * & * \\ 0 & 0 & 0 & 0 & 0 & \Sigma_6^T & 0 & 0 & -\varepsilon I \end{bmatrix} < 0 \quad (9)$$

where $\Sigma_1 = M - P + \varepsilon I$, $\Sigma_2 = N - P + \varepsilon I$, $\Sigma_3 = -M + \varepsilon I$, $\Sigma_4 = -N + \varepsilon I$, $\Sigma_5 = A + \alpha BK$, $\Sigma_6 = (1 - \alpha)BK$, $\Sigma_7 = (1 - \theta)LC$, $\Sigma_8 = A - LC$.

Proof: Choosing the following Lyapunov function

$$V(Z(k)) = x(k)^T P x(k) + e(k)^T P e(k) + x(k-1)^T M x(k-1) + e(k-1)^T N e(k-1)$$

where P, M, N are symmetric positive-definite matrices.

$$\begin{aligned} & E\{V(Z(k+1)|Z(k))\} - V(Z(k)) \\ &= E\{x^T(k+1)Px(k+1) + e^T(k+1)Pe(k+1) + x^T(k)Mx(k) + e^T(k)Ne(k)\} \\ &\quad - x^T(k)Px(k) - e^T(k)Pe(k) - x^T(k-1)Mx(k-1) - e^T(k-1)Ne(k-1) \\ &= [(A + \alpha BK)x(k) - \alpha BKe(k) + (1 - \alpha)BKx(k-1) - (1 - \alpha)BKe(k-1)]^T P \\ &\quad \times [(A + \alpha BK)x(k) - \alpha BKe(k) + (1 - \alpha)BKx(k-1) - (1 - \alpha)BKe(k-1)] \\ &\quad + E\{(\alpha_k - \alpha)^2\}[BKx(k) - BKe(k) - BKx(k-1) + BKe(k-1)]^T P \\ &\quad \times [BKx(k) - BKe(k) - BKx(k-1) + BKe(k-1)] \\ &\quad + \{[(1 - \theta)LC - (1 - \alpha)BK]x(k) + [A - LC + (1 - \alpha)BK]e(k)\} \\ &\quad \quad + [(1 - \alpha)BK - (1 - \theta)LC]x(k-1) - (1 - \alpha)BKe(k-1)\}^T P \\ &\quad \times \{[(1 - \theta)LC - (1 - \alpha)BK]x(k) + [A - LC + (1 - \alpha)BK]e(k)\} \\ &\quad \quad + [(1 - \alpha)BK - (1 - \theta)LC]x(k-1) - (1 - \alpha)BKe(k-1)\} \\ &\quad + E\{(\alpha_k - \alpha)^2\}[BKx(k) - BKe(k) - BKx(k-1) + BKe(k-1)]^T P \\ &\quad \times [BKx(k) - BKe(k) - BKx(k-1) + BKe(k-1)] \\ &\quad + E\{(\theta_k - \theta)^2\}[-LCx(k) + LCx(k-1)]^T P \\ &\quad \times [-LCx(k) + LCx(k-1)] \\ &\quad + x^T(k)Mx(k) + e^T(k)Ne(k) - x^T(k)Px(k) - e^T(k)Pe(k) \\ &\quad - x^T(k-1)Mx(k-1) - e^T(k-1)Ne(k-1) \end{aligned}$$

Noting that $E\{(\alpha_k - \alpha)^2\} = \bar{\alpha}^2$, $E\{(\theta_k - \theta)^2\} = \bar{\theta}^2$, The above formula can be rewritten as

$$E\{V(Z(k+1)|Z(k))\} - V(Z(k)) = Z(k)^T \Phi Z(k) \quad (10)$$

where

$$\begin{aligned} \Phi = & \begin{bmatrix} \Pi_1 & -\alpha\Pi_2 & \Pi_3 & -\Pi_3 \\ \Pi_4 & \Pi_5 & \Pi_6 & -\Pi_3 \\ \Pi_2 & -\Pi_2 & -\Pi_2 & \Pi_2 \\ -\Pi_7 & 0 & \Pi_7 & 0 \end{bmatrix}^T \begin{bmatrix} P & 0 & 0 & 0 \\ 0 & P & 0 & 0 \\ 0 & 0 & 2\bar{\alpha}^2 P & 0 \\ 0 & 0 & 0 & \bar{\theta}^2 P \end{bmatrix} \begin{bmatrix} \Pi_1 & -\alpha\Pi_2 & \Pi_3 & -\Pi_3 \\ \Pi_4 & \Pi_5 & \Pi_6 & -\Pi_3 \\ \Pi_2 & -\Pi_2 & -\Pi_2 & \Pi_2 \\ -\Pi_7 & 0 & \Pi_7 & 0 \end{bmatrix}^T \\ & + \begin{bmatrix} M - P & 0 & 0 & 0 \\ 0 & N - P & 0 & 0 \\ 0 & 0 & M & 0 \\ 0 & 0 & 0 & N \end{bmatrix} \end{aligned}$$

According to Schur complement, $\Phi < 0$ is equivalent to

$$\begin{bmatrix} M - P & * & * & * & * & * & * & * \\ 0 & N - P & * & * & * & * & * & * \\ 0 & 0 & -M & * & * & * & * & * \\ 0 & 0 & 0 & -N & * & * & * & * \\ \Pi_1 & -\alpha\Pi_2 & \Pi_3 & -\Pi_3 & -P^{-1} & * & * & * \\ \Pi_4 & \Pi_5 & \Pi_6 & -\Pi_3 & 0 & -P^{-1} & * & * \\ \Pi_2 & -\Pi_2 & -\Pi_2 & \Pi_2 & 0 & 0 & -2\bar{\alpha}^{-2}P^{-1} & * \\ -\Pi_7 & 0 & \Pi_7 & 0 & 0 & 0 & 0 & -\bar{\theta}^{-2}P^{-1} \end{bmatrix} < 0$$

Using the definition $\Pi_1 \Pi_7$ and the lemma 2, we can obtain (9).

According to (10), we have

$$\begin{aligned} E\{V(Z(k+1)|Z(k))\} - V(Z(k)) &= Z(k)^T \Phi Z(k) \\ &\leq -\lambda_{\min}(-\Phi) Z(k)^T Z(k) < -\gamma Z(k)^T Z(k) \end{aligned} \quad (11)$$

where $0 < \gamma < \min\{\lambda_{\min}(-\Phi), \omega\}$, $\omega = \max\{\lambda_{\max}(P), \lambda_{\max}(Q), \lambda_{\max}(M), \lambda_{\max}(N)\}$.

Hence, (11) becomes

$$E\{V(Z(k+1)|Z(k))\} - V(Z(k)) < -\gamma Z(k)^T Z(k) < -\frac{\gamma}{\omega} V(Z(k)) = -\psi V(Z(k))$$

where $0 < \psi = \frac{\gamma}{\omega} < 1$. Therefore, it is obtained from definition 1 and Lemma 1 that the closed-loop system (8) is exponentially mean-square stable. This completes the proof.

The matrix inequality (9) in Theorem 1 is not a LMI, which is difficult to solve. Without loss of generality, it is assumed that the matrix B is of full-column rank. Furthermore, the following Theorem 2 is given to convert (9) into a LMI.

Theorem 2: Under the assumption that the matrix B is of full-column rank, for given packet dropout rate θ and α , if there exist symmetric positive-definite matrices P, M, N , real matrices X, Y, P_0 and a scalar $\varepsilon > 0$ such that (12) and (13) hold, then (8) is exponentially mean-square stable.

$$\left[\begin{array}{ccccccccc} \Sigma_1 & * & * & * & * & * & * & * & * \\ -\varepsilon I & \Sigma_2 & * & * & * & * & * & * & * \\ -\varepsilon I & \varepsilon I & \Sigma_3 & * & * & * & * & * & * \\ \varepsilon I & -\varepsilon I & -\varepsilon I & \Sigma_4 & * & * & * & * & * \\ PA + \alpha BX & -\alpha BX & \hat{\alpha} BX & -\hat{\alpha} BX & -P & * & * & * & * \\ \hat{\theta} YC & PA - YC & -\hat{\theta} YC & 0 & 0 & -P & * & * & * \\ BX & -BX & -BX & BX & 0 & 0 & \Xi_1 P & * & * \\ -YC & 0 & YC & 0 & 0 & 0 & 0 & \Xi_2 P & * \\ 0 & 0 & 0 & 0 & 0 & \hat{\alpha} X^T B^T & 0 & 0 & -\varepsilon I \end{array} \right] < 0 \quad (12)$$

$$PB = BP_0 \quad (13)$$

where $\Xi_1 = -2\bar{\alpha}^{-2}$, $\Xi_2 = -\bar{\theta}^{-2}$, $\hat{\alpha} = 1 - \alpha$, $\hat{\theta} = 1 - \theta$, and the gain matrices are given as $L = P^{-1}Y$, $K = P_0^{-1}X$.

Proof: Pre- and post-multiplying both sides of (9) by $\text{diag}(I, I, I, I, P, P, P, P, I)$, and using (13), we can obtain (12). This completes the proof.

Finally, it is obvious that the linear equality condition (12) can be converted to the following LMI:

$$\begin{bmatrix} -\eta I & B^T P - P_0 B^T \\ PB - BP_0 & -I \end{bmatrix} \leq 0 \quad (14)$$

Therefore, the stability problem of the closed-loop system (8) can be solved by searching the global solution of the following minimization problem:

$$\begin{aligned} \min \eta \\ \text{s.t. } (12) \text{ and } (14) \end{aligned} \quad (15)$$

4 Conclusions

This paper has studied observer-based exponential stability for networked control systems (NCSs) with data packet dropout. Based on two independent Bernoulli distributed white sequence and an observer, an augment model has been modeled to describe NCSs with unavailable system state and data packet dropout both the sensor-to-controller and the controller-to-actuator. A sufficient condition of exponentially mean-square stable has then been derived for NCSs.

Acknowledgment. This work was supported in part by the National Science Foundation of China under Grant No. 60834002 and 61074032, Key Project Department of Science Research in Henan Province under Grant No. 112102310327, Project of Science and Technology Commission of Shanghai Municipality under Grant No. 11ZR1413100 and the Innovation Fund Project for Shanghai University.

References

1. Li, H., Chow, M., Sun, Z.: EDA-based Speed Control of a Networked DC Motor System with Time Delays and Packet Losses. *IEEE Trans. Industrial Electronics* 56(5), 1727–1735 (2009)
2. Lai, C.L., Hsu, P.L.: Design the Remote Control System with the Time-delay Estimator and the Adaptive Smith Predictor. *IEEE Trans. Industrial Informatics* 6(1), 73–80 (2010)
3. Du, D., Fei, M., Song, R.Y., Li, X.: Brief Survey and Prospect of Networked Control Systems. *Chinese Journal of Scientific Instrument* 32(3), 713–720 (2011)
4. Hespanha, J.P., Naghshtabrizi, P., Xu, Y.: A Survey of Recent Results in Networked Control Systems. *Proceedings of The IEEE* 95(1), 138–162 (2007)
5. Wu, J., Chen, T.: Design of Networked Control Systems with Packet Dropouts. *IEEE Trans. Automatic Control* 52(7), 1314–1319 (2007)
6. Zhang, W., Yu, L.: Output Feedback Stabilization of Networked Control Systems with Packet Dropouts. *IEEE Trans. Automatic Control* 52(9), 1705–1710 (2007)
7. Niu, Y., Jia, T., Wang, X., Yang, F.: Output-feedback Control Design for NCSs Subject to Quantization and Dropout. *Information Sciences* 179, 3804–3813 (2009)
8. Du, D., Fei, M., Li, K.: Stability Analysis of Multi-channel MIMO Networked Control Systems. In: Li, K., Fei, M., Jia, L., Irwin, G.W. (eds.) LSMS 2010 and ICSEE 2010. LNCS, vol. 6328, pp. 62–68. Springer, Heidelberg (2010)
9. Fang, X., Wang, J.: Stochastic Observer-based Guaranteed Cost Control for Networked Control Systems with Packet Dropouts. *IET Control Theory Appl.* 2(11), 980–989 (2008)

Modification Algorithm on Routh-Pade Model Reduction of Interval Systems

Zhi-zhen Wang, Li Li, and Xiao-fang Wang

Shanghai Normal University,
Department of Applied Mathematics, Shanghai200234, P.R. China

Abstract. By use of Routh approximation method and related reduction method to deal with the reduced-order problem, it is important to avoid or reduce the interval arithmetic expansion leading the failure of the stability criterion. Based on the feature of interval arithmetic and data consistency of Routh approximation, This note guarantees more effective calculation, and modifies interval arithmetic. The present arithmetic reduces the possibility of failure to maintain stability by interval arithmetic. A example is given to illustrate the method.

Keywords: interval system, interval arithmetic, Routh approximation, monotonicity, interval reduction.

1 Introduction

The Routh approximation method was extended to obtain a reduced order interval models for high order interval systems. The extension is based on using interval arithmetic to perform Routh stability array.

A generalization of the method for direct truncation of Routh table is propose in [1] for interval systems using interval arithmetic. However, some numerical examples show that the reduced-order models are not stable even though the original high-order systems are stable. How to overcome the disadvantage? Dolgin and Zeheb [2] modified the method given by [3] Bandypadhyay etc. [1]. Unfortunately, Shih-Feng Yang [3] points out such modification algorithm can not avoid the failure of stability.

In this note, we derive a modified algorithm of direct truncation of Routh table for interval polynomials, Which is less conservative. Examples show that using our algorithm can effective reduce the possibility of losing stability.

2 Main Result

The interval arithmetic is

$$\text{Addition: } [a, b] + [c, d] = [a + b, c + d]$$

$$\text{Subtraction: } [a, b] - [c, d] = [a - d, b - c]$$

$$\text{Multiplication: } [a, b][c, d] = [\min\{ac, ad, bc, bd\}, \max\{ac, ad, bc, bd\}]$$

Division: $\frac{[a,b]}{[c,d]} = [a,b]\left[\frac{1}{d}, \frac{1}{c}\right]$, $0 \notin [c,d]$

Consider the nth-order interval polynomial,

$$D(s) = a_n s^n + a_{n-1} s^{n-1} + \cdots + a_1 s + a_0 \quad (1)$$

where $a_i \triangleq [a_i^-, a_i^+]$, for $i = 0, 1, 2, \dots, n$.

The Routh table is generated by the following recursive algorithm:

$$\begin{aligned} a_{0,j} &= a_{n-2j} & j &= 0, 1, \dots, n_0 \\ a_{1,j} &= a_{n-2j-1} & j &= 0, 1, \dots, n_1 \\ a_{i+1,j} &= a_{i-1,j+1} - \frac{a_{i-1,0}}{a_{i,0}} a_{i,j+1} & j &= 0, 1, \dots, n_{i+1}, i = 1, \dots, n-1 \end{aligned}$$

where $n_i = [\frac{n-1}{2}]$ denotes the largest integer that does not exceed $\frac{n-i}{2}$.

The direct truncation method:

truncating the first m rows, the reduced-order interval polynomial of degree $(n-m)$ can be constructed from the first two remaining rows.

Method DZ [2]

$$a_{i+1,j} = a_{i-1,j+1} - \frac{\hat{a}_{i-1,0}}{\hat{a}_{i,0}} a_{i,j+1} \quad (2)$$

where $\hat{a}_{i-1,0}$, $\hat{a}_{i,0}$ are fixed values of $a_{i-1,0}$ and $a_{i,0}$.

Modification Method

Denote the interval Routh table as:

$$\begin{matrix} a_{0,0} & a_{0,1} & a_{0,2} & \cdots & a_{0,n_0} \\ a_{1,0} & a_{1,1} & a_{1,2} & \cdots & a_{1,n_1} \\ a_{2,0} & a_{2,1} & a_{2,2} & \cdots & a_{2,n_2} \\ \vdots & \vdots & \vdots & \cdots & \vdots \\ a_{k,0} & a_{k,1} & a_{k,2} & \cdots & a_{k,n_k} \end{matrix}$$

Algorithm:

1. $a_{2,j} = \{\nabla_{2,j} \triangleq [\nabla_{2,j}^-, \nabla_{2,j}^+], \Delta_{2,j} \triangleq [\Delta_{2,j}^-, \Delta_{2,j}^+]\}$
where,

$$\nabla_{2,j} = a_{0,j+1} - \frac{a_{0,0}^+}{a_{1,0}^-} a_{1,j+1}^+ \quad (3)$$

$$\Delta_{2,j} = a_{0,j+1} - \frac{a_{0,0}^-}{a_{1,0}^+} a_{1,j+1}^- \quad (4)$$

2. $a_{3,j} = \{\nabla_{3,j} \triangleq [\nabla_{3,j}^-, \nabla_{3,j}^+], \Delta_{3,j} \triangleq [\Delta_{3,j}^-, \Delta_{3,j}^+]\}$
where,

$$\nabla_{3,j} = a_{1,j+1}^+ - \frac{\nabla_{2,0}^-}{\nabla_{2,0}^+} a_{2,j+1}^+ \quad (5)$$

$$\Delta_{3,j} = a_{1,j+1}^- - \frac{\Delta_{2,0}^+}{\Delta_{2,0}^-} a_{2,j+1}^- \quad (6)$$

3. $a_{i,j} = \{\nabla_{i,j} \triangleq [\nabla_{i,j}^-, \nabla_{i,j}^+], \Delta_{i,j} \triangleq [\Delta_{i,j}^-, \Delta_{i,j}^+]\}, i \geq 4$

where,

$$\nabla_{i,j} = a_{i-2,j+1} - \frac{\nabla_{i-2,0}^+}{\nabla_{i-1,0}^-} a_{i-1,j+1} \quad (7)$$

$$\Delta_{i,j} = a_{i-2,j+1} - \frac{\Delta_{i-2,0}^-}{\Delta_{i-1,0}^+} a_{i-1,j+1} \quad (8)$$

and

$$\begin{cases} a_{i-2,j+1} = \nabla_{i-2,j+1} & \text{for } \nabla_{i,j}, \\ a_{i-1,j+1} = \nabla_{i-1,j+1}^+ & \\ \begin{cases} a_{i-2,j+1} = \Delta_{i-2,j+1} & \text{for } \Delta_{i,j}, \\ a_{i-1,j+1} = \Delta_{i-1,j+1}^- & \end{cases} \end{cases}$$

3 Example

Consider the nth-order interval polynomial,

$$D_7(s) = s^7 + 9s^6 + [31, 34]s^5 + 71s^4 + 111s^3 + 109s^2 + [76, 83]s + 12 \quad (9)$$

The DZ Method [2] Routh Table and modified Routh Table are thus

Table 1. Comparision between DZ Routh method and MODified Routh method

DZ Routh Table				Modified Routh Table			
[1, 1]	[31, 34]	[111, 111]	[76, 83]	[1, 1]	[31, 34]	[111, 111]	[76, 83]
[9, 9]	[71, 71]	[109, 109]	[12, 12]	[9, 9]	[71, 71]	[109, 109]	[12, 12]
[23.11, 26.11]	[98.89, 98.89]	[74.67, 81.67]		[23.11, 26.11]	[98.89, 98.89]	[74.67, 81.67]	
[34.84, 34.84]	[79.14, 81.70]	[12.00, 12.00]		[32.48, 36.91]	[77.19, 83.26]	[12, 12]	
[41.18, 42.98]	[66.19, 73.19]			[36.84, 46.76]	[65.02, 74.16]		
[18.54, 26.89]	[12.00, 12.00]			[13.69, 30.25]	[12, 12]		
[43.96, 50.96]				[32.73, 55.61]			

Remark:

The modified table maintains more effective points than DZ table, then the more exact performance of interval systems can be gained.

The reduced polynomial is thus,

$$Q(s) = [23.11, 26.11]s^5 + [32.48, 36.91]s^4 + 98.89s^3 + [77.19, 83.26]s^2 + [74.67, 81.67]s + 12$$

The reduced polynomial [2] is thus,

$$P(s) = [23.11, 26.11]s^5 + 34.84s^4 + 98.89s^3 + [79.14, 81.70]s^2 + [74.67, 81.67]s + 12$$

Figure compares the step responses of $\frac{1}{D(s)}$, $\frac{1}{P(s)}$, and $\frac{1}{Q(s)}$, showing that $\frac{1}{Q(s)}$ is an improvement on $\frac{1}{P(s)}$.

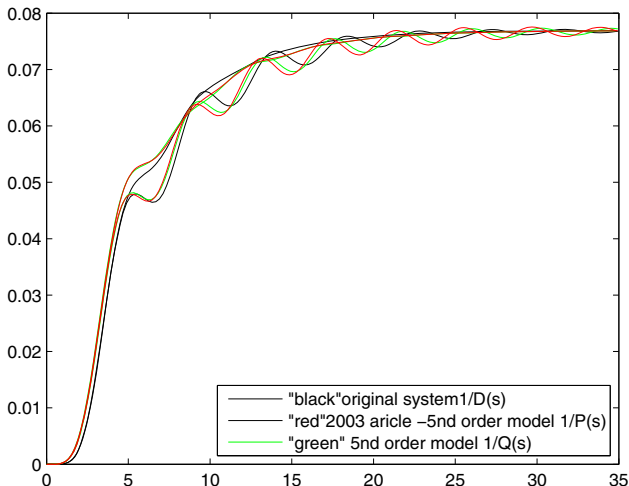


Fig. 1. Comparision of $\frac{1}{D(s)}$, $\frac{1}{P(s)}$, and $\frac{1}{Q(s)}$

4 Conclusion

In this note, a modified algorithm to test the interval system reduction is proposed. As shown in this note that the larger ideal interval range can be obtained, which assures that the original interval system has a better approximation. The promote method is very effective to reduce interval systems of the strong robustness. Because the weak robustness is greatly dependent on numerical value, we need for further research.

References

1. Bandyopadhyay, B., Ismail, O., Gorez, R.: Routh-Pade Approximation for Interval Systems. *IEEE Trans. Auto. Contr.* Vol. 39(12), 2454–2456 (1994)
2. Dolgin, Y., Zeheb, E.: On Routh-Pade Model Reduction of Interval Systems. *IEEE Trans. Automat. Contr.* 48(9), 1610–1612 (2003)
3. Yang, S.F.: Comments on “On Routh-Pade Model Reduction of Interval Systems”. *IEEE Trans. Automat. Contr.* 50(2), 273–274 (2005)

Author Index

- Agrawal, Raghav 311
Ahn, Byung Ryul 440
Aliskan, Ibrahim 218
Aminnayeri, Majid 139
Awang, Mohd Isa 108
- Bai, Haoliang 694
Bevilacqua, Vitoantonio 186, 426, 456
Bianco, Annalisa 456
- Caccia, Michele 426
Cai, Zengyu 612
Cao, Huijuan 626
Cao, Wei 33
Cascini, Egidio 456
Chen, Jie 71, 383
Chen, Wei 282
Chen, Wu 270
Chen, Xiaofeng 488
Chen, Zhigang 509, 517
Cheng, Jian 319
Cho, Sangjin 464
Choi, Jiwon 480
Chong, Uipil 464
Chong, Yanwen 270
Cui, Yuanbo 494
- Dai, Gui-Ping 290
D'Ambruoso, Dario 426
Deris, Mustafa Mat 108
Ding, Guoqiang 420
Ding, Jinlin 658
Ding, Xiuyong 650
Dinh, Tien 162
Du, Dajun 694
Du, Jialu 686
Du, Ji-Xiang 234, 242, 364
- Fan, Qiang 509, 517
Fang, Chen 568
Feng, Shoupeng 202
Ferland, Jacques 162
Fu, Zuowei 33
- Gai, Changqing 250
Gao, Jun-jun 91
Gao, Kaizhou 584, 592
Gao, Liang 576
Gavrilov, Andrey V. 210
Glotin, Hervé 276
Gulez, Kayhan 218
Guo, Yi-Lan 242
Guo, Yi-nan 319
Gupta, Phalguni 311, 327
- Ha, Jong-Eun 377
Hassan, Hasni 108
He, Yongjian 202, 303
Herawan, Tutut 108
Hou, Xin 488
Hou, Yuexian 448
Hu, Chengwei 303
Hu, Rong 600
Hu, Zhifeng 40, 658
Huai, Wen-Jun 398
Huang, Ke-Ming 282
Huang, Qinzenh 9
Huang, Yongping 432
- Janeski, Miroslav 17
Jeong, Moon-Ho 377
Jia, Wei 257
Jiang, Caigui 303
Jiang, Hua 592
Jiang, Shao-Hua 357
Jiang, Wen 116
Jin, Ju 634
Jo, Kang-Hyun 377
- Kalajdziski, Slobodan 17
Kang, Dong-Joong 377
Kang, Hee-Jun 25, 538
Kang, Myeongsu 464, 480
Katiyar, Rohit 412
Kim, Cheol-Hong 480
Kim, Jong-Myon 480
Kim, Moon-Hyun 440
Kim, Won-gy whole 440
Kim, Yongmin 480

- Kobayashi, Yoshinori 350
 Kohli, Sharad 327
 Kuno, Yoshinori 350
- Lam, William H.K. 270
 Le, Tien Dung 538
 Lee, Yang Weon 264
 Lenskiy, Artem 210
 Li, Chuan 153
 Li, Junqing 584, 592
 Li, Li 701
 Li, Peihua 226
 Li, Qingquan 270
 Li, Xinyu 576
 Li, Xue 694
 Li, Yanlai 63
 Li, Yuanzhen 584
 Li, Yu-Ge 282
 Li, Zhaoyang 612
 Li, Zhilin 270
 Liang, Xueru 47, 448
 Liang, Yun-Chia 55
 Liao, Xiaofeng 634
 Liao, Zhenjiang 91
 Lin, Che-Wei 532
 Liu, Duyu 9
 Liu, Lei 63
 Liu, Ruiming 194
 Liu, Shu-Fen 391
 Liu, Xiaoming 335
 Liu, Yijing 634
 Liu, Yue 91
 Lu, Can-Yi 83, 100
- Magarelli, Alberto 456
 Mandolino, Giovanni 426
 Mastronardi, Giuseppe 426, 456
 Mori, Satoshi 350
 Mumcu, Tarik Veli 218
- Neruda, Roman 147
- Pacelli, Vincenzo 186
 Paris, Sébastien 276
 Pathak, Vinay Kumar 412
 Pilát, Martin 147
 Pourali, Zahra 139
 Prakash, Surya 327
 Pu, Xiaorong 634
- Qi, Mei-Xing 405
 Qian, Bin 600
 Qin, Jie 502
- Ramasamy, Krishnamoorthi 370
 Ren, Shangkun 47, 448
 Ren, Wei 153
 Ren, Xingqiu 153
 Ro, Young-Shick 25
 Rose, Ahmad Nazari Mohd 108
- Saladino, Stefano 186
 Sang, Gao-Li 342
 Sang, Hongyan 576
 Santarcangelo, Vito 456
 Secmen, Mustafa 131
 Shang, Li 383, 398, 405
 Shanmugam, Sathiya Devi 370
 Shu, Lan 650
 Si, Qun 502
 Son, Mai 544
 Song, Yulin 642
 Srinivas, Badrinath 311
 Suh, Young-Soo 538
 Suma, Marco 426
 Sun, Qi 226
 Sun, Tao 584
 Sun, Yanxia 170
- Tang, Jinshan 335
 Tang, Wen-Sheng 298, 357, 517
 Tasgetiren, M. Fatih 131
 Tien, Chia-Yun 55
 Tommaso, Emanuela De 426
 Tong, Liang 553
 Trinh, Khoa 162
 Tucci, Simone 426
 Tuna, Gurkan 218
- Van, Mien 25
 Vavilin, Andrey 377
- Wang, Cuihong 626
 Wang, Fei 202, 303
 Wang, Feng 658
 Wang, Guoqiang 420
 Wang, Jeen-Shing 532
 Wang, Jianxin 178
 Wang, Jie 122, 553
 Wang, Kang 91

- Wang, Kuanquan 250
Wang, Ling 560, 568
Wang, Lingzhi 1
Wang, Min 257
Wang, Qing-Ping 364
Wang, Shengchun 298
Wang, Shengyao 560
Wang, Shu-Lin 357, 509, 517
Wang, Xiao-fang 701
Wang, Xiao-Feng 257
Wang, Yinglin 335
Wang, Yuting 584
Wang, Zenghui 170
Wang, Zhi-zhen 701
Wei, Wang 91
Weng, Jia-min 694
Wu, Jiansheng 1
Wu, Lihua 178
Wu, Qiong 202, 303
Wu, Xi 494

Xiang, Changcheng 650
Xiang, Feng-Hong 600
Xiao, Dawei 319
Xie, Shengxian 592
Xin, Jingmin 303
Xing, Yonghua 202
Xu, Shungang 619
Xu, Xin 335
Xu, Ye 560, 568
Xuan, Shi-Bin 342

Yan, Fuliang 502
Yan, Huijuan 502
Yan, Ting-Qin 391
Yan, Xiai 509, 517
Yan, Yan 686
Yang, Bo 676
Yang, Huaqing 584
Yang, Kai 234
Yang, Lei 47
Yang, Miao 194
Yang, Shixin 63
Yang, Ya-Ting C. 532
Yang, Zhenqiang 686
Yi, Myeong-Jae 544

Yu, Shuanghe 686
Yu, Won Young 440
Yu, Yongbin 634

Zakaria, Aznida Hayati 108
Zan, Hongying 472
Zeng, Anping 432
Zeng, Huanglin 257
Zhai, Chuan-Min 234, 242, 364
Zhang, Baowei 612
Zhang, Boyun 509, 517
Zhang, David 63
Zhang, Hongtao 664
Zhang, Jianhong 494
Zhang, Jianwei 612
Zhang, Jing-ling 153
Zhang, Kunli 472
Zhang, Lei 250
Zhang, Mingyi 676
Zhang, Peng 448
Zhang, Shuguo 319
Zhang, Xiaolong 335
Zhang, Xutang 488
Zhang, Ying 178, 676
Zhang, Yu 178, 405
Zhao, Bo 342
Zhao, Kong-Jin 282
Zhao, Wen-Bo 282
Zhao, Yanwei 153
Zhao, Zhong-Qiu 276
Zheng, Guang-Zheng 282
Zheng, Zeng-Guo 342
Zhong, Qishui 619
Zhou, Chang-Xiong 391
Zhou, Gang 560
Zhou, Hua-Bin 600
Zhou, Hui 33
Zhou, Lijuan 472
Zhou, Rongkun 202
Zhou, Yan 40
Zhou, Zhimin 33
Zhu, Caihong 664
Zhu, Lin 77
Zhu, Xueguang 526, 670
Zhuang, Ting 488
Zuo, Wangmeng 63, 250